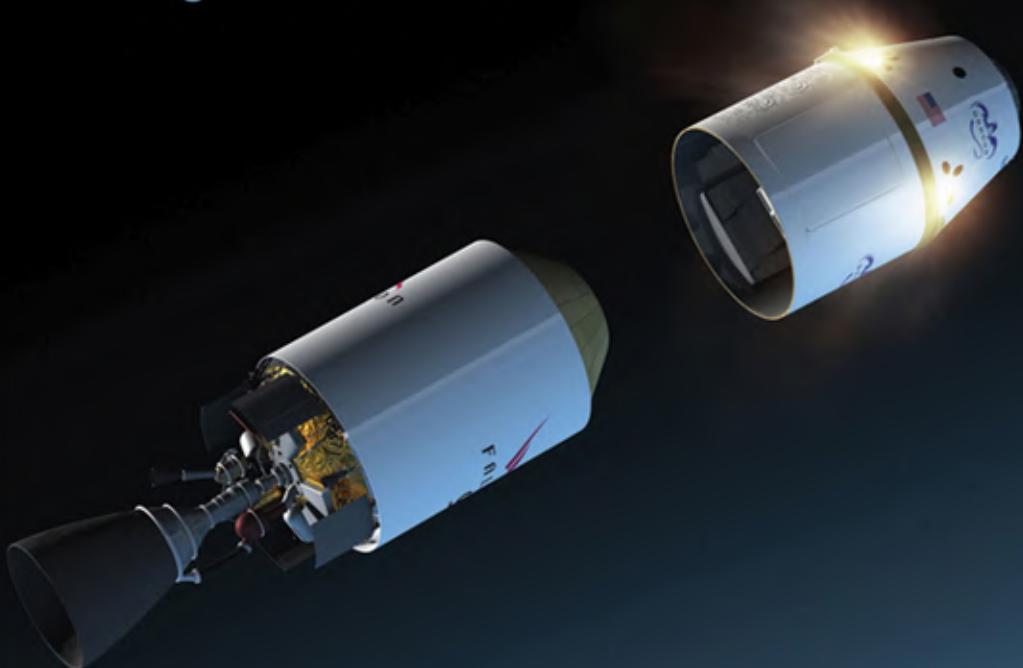


ROCKET PROPELLION ELEMENTS

Eighth Edition



GEORGE P. SUTTON
OSCAR BIBLARZ

ROCKET PROPULSION ELEMENTS

The book's cover shows a typical separation of a payload stage or satellite from an upper stage of a space flight vehicle in the vacuum of space. There are two rocket propulsion systems. The liquid propellant rocket engine on the upper stage (on the lower left) has just lifted the satellite into space and has just been shut down. The reaction control system on the payload stage has four small inclined thrusters, which can be seen during their firing operation; they are moving the payload away from the expended upper stage. A small thruster's plume (flame) has a bright, elliptically shaped, hot gas, very small core, which is visible. The hot exhaust gases disperse from this core in all directions, and this part of the plume is almost invisible.

Rocket Propulsion Elements

Eighth Edition

GEORGE P. SUTTON

Consultant

Formerly Laboratory Associate

Lawrence Livermore National Laboratory and formerly

Executive Director, Engineering

Rocketdyne Division of The Boeing Company

Now Pratt & Whitney Rocketdyne

OSCAR BIBLARZ

Professor Emeritus

Department of Mechanical and Astronautical Engineering

Naval Postgraduate School



WILEY

JOHN WILEY & SONS, INC.

This book is printed on acid-free paper.

Copyright © 2010 by John Wiley & Sons, Inc. All rights reserved

Published by John Wiley & Sons, Inc., Hoboken, New Jersey

Published simultaneously in Canada

No part of this publication may be reproduced, stored in a retrieval system, or transmitted in any form or by any means, electronic, mechanical, photocopying, recording, scanning, or otherwise, except as permitted under Section 107 or 108 of the 1976 United States Copyright Act, without either the prior written permission of the Publisher, or authorization through payment of the appropriate per-copy fee to the Copyright Clearance Center, 222 Rosewood Drive, Danvers, MA 01923, (978) 750-8400, fax (978) 646-8600, or on the web at www.copyright.com. Requests to the Publisher for permission should be addressed to the Permissions Department, John Wiley & Sons, Inc., 111 River Street, Hoboken, NJ 07030, (201) 748-6011, fax (201) 748-6008, or online at www.wiley.com/go/permissions.

Limit of Liability/Disclaimer of Warranty: While the publisher and the authors have used their best efforts in preparing this book, they make no representations or warranties with respect to the accuracy or completeness of the contents of this book and specifically disclaim any implied warranties of merchantability or fitness for a particular purpose. No warranty may be created or extended by sales representatives or written sales materials. The advice and strategies contained herein may not be suitable for your situation. You should consult with a professional where appropriate. Neither the publisher nor the authors shall be liable for any accidents or loss of profit or any other commercial damages, including but not limited to special, incidental, consequential, or other damages.

For general information about our other products and services, please contact our Customer Care Department within the United States at (800) 762-2974, outside the United States at (317) 572-3993 or fax (317) 572-4002.

Wiley also publishes its books in a variety of electronic formats. Some content that appears in print may not be available in electronic books. For more information about Wiley products, visit our web site at www.wiley.com.

Library of Congress Cataloging-in-Publication Data:

Sutton, George Paul.

Rocket propulsion elements / George P. Sutton, Oscar Biblarz. — 8th ed.
p. cm.

Includes bibliographical references and index.

ISBN 978-0-470-08024-5 (cloth)

1. Rocket engines. I. Biblarz, Oscar. II. Title.
TL782.S8 2010
629.47'5—dc22

2009042591

Printed in the United States of America

10 9 8 7 6 5 4 3 2 1

CONTENTS

| | |
|--|------|
| PREFACE | xiii |
| 1 Classification | 1 |
| 1.1. Duct Jet Propulsion / 2 | |
| 1.2. Rocket Propulsion / 4 | |
| 1.3. Applications of Rocket Propulsion / 14 | |
| References / 26 | |
| 2 Definitions and Fundamentals | 28 |
| 2.1. Definitions / 28 | |
| 2.2. Thrust / 33 | |
| 2.3. Exhaust Velocity / 36 | |
| 2.4. Energy and Efficiencies / 38 | |
| 2.5. Multiple Propulsion Systems / 40 | |
| 2.6. Typical Performance Values / 41 | |
| Problems / 43 | |
| Symbols / 45 | |
| References / 46 | |
| 3 Nozzle Theory and Thermodynamic Relations | 47 |
| 3.1. Ideal Rocket / 48 | |
| 3.2. Summary of Thermodynamic Relations / 49 | |

| | | |
|----------|--|------------|
| 3.3. | Isentropic Flow Through Nozzles / 53 | |
| 3.4. | Nozzle Configurations / 75 | |
| 3.5. | Real Nozzles / 85 | |
| 3.6. | Nozzle Alignment / 96 | |
| | Problems / 97 | |
| | Symbols / 100 | |
| | References / 101 | |
| 4 | Flight Performance | 103 |
| 4.1. | Gravity-Free Drag-Free Space Flight / 103 | |
| 4.2. | Forces Acting on a Vehicle in the Atmosphere / 107 | |
| 4.3. | Basic Relations of Motion / 110 | |
| 4.4. | Space Flight / 116 | |
| 4.5. | Flight Maneuvers / 131 | |
| 4.6. | Effect of Propulsion System on Vehicle Performance / 137 | |
| 4.7. | Flight Vehicles / 139 | |
| 4.8. | Military Missiles / 148 | |
| 4.9. | Flight Stability / 152 | |
| | Problems / 153 | |
| | Symbols / 155 | |
| | References / 157 | |
| 5 | Chemical Rocket Propellant Performance Analysis | 158 |
| 5.1. | Background and Fundamentals / 159 | |
| 5.2. | Analysis of Chamber or Motor Case Conditions / 165 | |
| 5.3. | Analysis of Nozzle Expansion Processes / 170 | |
| 5.4. | Computer-Assisted Analysis / 175 | |
| 5.5. | Results of Thermochemical Calculations / 176 | |
| | Problems / 190 | |
| | Symbols / 191 | |
| | References / 192 | |
| 6 | Liquid Propellant Rocket Engine Fundamentals | 194 |
| 6.1. | Types of Propellants / 198 | |
| 6.2. | Propellant Tanks / 201 | |
| 6.3. | Propellant Feed Systems / 208 | |
| 6.4. | Gas Pressure Feed Systems / 210 | |
| 6.5. | Tank Pressurization / 217 | |
| 6.6. | Turbopump Feed Systems and Engine Cycles / 221 | |

| | | |
|----------|--|------------|
| 6.7. | Rocket Engines for Maneuvering, Orbit Adjustments, or Attitude Control / 229 | |
| 6.8. | Engine Families / 233 | |
| 6.9. | Valves and Pipelines / 236 | |
| 6.10. | Engine Support Structure / 239 | |
| | Problems / 240 | |
| | Symbols / 242 | |
| | References / 243 | |
| 7 | Liquid Propellants | 245 |
| 7.1. | Propellant Properties / 246 | |
| 7.2. | Liquid Oxidizers / 256 | |
| 7.3. | Liquid Fuels / 259 | |
| 7.4. | Liquid Monopropellants / 263 | |
| 7.5. | Gelled Propellants / 265 | |
| 7.6. | Gaseous Propellants / 266 | |
| 7.7. | Safety and Environmental Concerns / 267 | |
| | Problems / 268 | |
| | Symbols / 269 | |
| | References / 269 | |
| 8 | Thrust Chambers | 271 |
| 8.1. | Injectors / 276 | |
| 8.2. | Combustion Chamber and Nozzle / 285 | |
| 8.3. | Low-Thrust Rocket Thrust Chambers or Thrusters / 301 | |
| 8.4. | Materials and Fabrication / 305 | |
| 8.5. | Heat Transfer Analysis / 311 | |
| 8.6. | Starting and Ignition / 323 | |
| 8.7. | Random Variable Thrust / 326 | |
| 8.8. | Sample Thrust Chamber Design Analysis / 328 | |
| | Problems / 339 | |
| | Symbols / 342 | |
| | References / 344 | |
| 9 | Liquid Propellant Combustion and Its Stability | 346 |
| 9.1. | Combustion Process / 346 | |
| 9.2. | Analysis and Simulation / 350 | |
| 9.3. | Combustion Instability / 352 | |
| | Problems / 364 | |
| | References / 364 | |

| | |
|---|------------|
| 10 Turbopumps and Their Gas Supplies | 366 |
| 10.1. Introduction / 366 | |
| 10.2. Descriptions of Several Turbopumps / 367 | |
| 10.3. Selection of Turbopump Configuration / 372 | |
| 10.4. Flow, Shaft Speeds, Power, and Pressure Balances / 376 | |
| 10.5. Pumps / 378 | |
| 10.6. Turbines / 387 | |
| 10.7. Approach to Turbopump Preliminary Design / 391 | |
| 10.8. Gas Generators and Preburners / 394 | |
| Problems / 395 | |
| Symbols / 396 | |
| References / 397 | |
| 11 Engine Systems, Controls, and Integration | 399 |
| 11.1. Propellant Budget / 399 | |
| 11.2. Performance of Complete or Multiple Rocket Propulsion Systems / 401 | |
| 11.3. Engine Design / 403 | |
| 11.4. Engine Controls / 411 | |
| 11.5. Engine System Calibration / 423 | |
| 11.6. System Integration and Engine Optimization / 430 | |
| Problems / 432 | |
| Symbols / 432 | |
| References / 433 | |
| 12 Solid Propellant Rocket Fundamentals | 435 |
| 12.1. Basic Relations and Propellant Burning Rate / 437 | |
| 12.2. Other Performance Issues / 458 | |
| 12.3. Propellant Grain and Grain Configuration / 463 | |
| 12.4. Propellant Grain Stress and Strain / 472 | |
| 12.5. Attitude Control and Side Maneuvers with Solid Propellant Rocket Motors / 483 | |
| Problems / 485 | |
| Symbols / 488 | |
| References / 489 | |
| 13 Solid Propellants | 492 |
| 13.1. Classification / 492 | |
| 13.2. Propellant Characteristics / 498 | |

| | |
|--|------------|
| 13.3. Hazards / 505 | |
| 13.4. Propellant Ingredients / 512 | |
| 13.5. Other Propellant Categories / 522 | |
| 13.6. Liners, Insulators, and Inhibitors / 526 | |
| 13.7. Propellant Processing and Manufacture / 529 | |
| Problems / 532 | |
| References / 535 | |
| 14 Solid Propellant Combustion and Its Stability | 537 |
| 14.1. Physical and Chemical Processes / 537 | |
| 14.2. Ignition Process / 541 | |
| 14.3. Extinction or Thrust Termination / 543 | |
| 14.4. Combustion Instability / 545 | |
| Problems / 553 | |
| References / 554 | |
| 15 Solid Rocket Components and Motor Design | 556 |
| 15.1. Motor Case / 556 | |
| 15.2. Nozzles / 564 | |
| 15.3. Igniter Hardware / 578 | |
| 15.4. Rocket Motor Design Approach / 583 | |
| Problems / 590 | |
| References / 592 | |
| 16 Hybrid Propellant Rockets | 594 |
| 16.1. Applications and Propellants / 596 | |
| 16.2. Interior Hybrid Motor Ballistics / 600 | |
| 16.3. Performance Analysis and Grain Configuration / 604 | |
| 16.4. Design Example / 609 | |
| 16.5. Combustion Instability / 613 | |
| Problems / 617 | |
| Symbols / 618 | |
| References / 620 | |
| 17 Electric Propulsion | 622 |
| 17.1. Ideal Flight Performance / 628 | |
| 17.2. Electrothermal Thrusters / 633 | |
| 17.3. Nonthermal Electrical Thrusters / 640 | |
| 17.4. Optimum Flight Performance / 656 | |

| | |
|--|------------|
| 17.5. Mission Applications / 661 | |
| 17.6. Electric Space-Power Supplies and Power-Conditioning Systems / 663 | |
| Problems / 667 | |
| Symbols / 669 | |
| References / 671 | |
| 18 Thrust Vector Control | 673 |
| 18.1. TVC Mechanisms with a Single Nozzle / 675 | |
| 18.2. TVC with Multiple Thrust Chambers or Nozzles / 685 | |
| 18.3. Testing / 687 | |
| 18.4. Integration with Vehicle / 687 | |
| Problems / 688 | |
| References / 689 | |
| 19 Selection of Rocket Propulsion Systems | 691 |
| 19.1. Selection Process / 693 | |
| 19.2. Criteria for Selection / 699 | |
| 19.3. Interfaces / 705 | |
| References / 709 | |
| 20 Rocket Exhaust Plumes | 710 |
| 20.1. Plume Appearance and Flow Behavior / 712 | |
| 20.2. Plume Effects / 725 | |
| 20.3. Analysis and Mathematical Simulation / 729 | |
| Problems / 730 | |
| References / 731 | |
| 21 Rocket Testing | 733 |
| 21.1. Types of Tests / 733 | |
| 21.2. Test Facilities and Safeguards / 735 | |
| 21.3. Instrumentation and Data Management / 742 | |
| 21.4. Flight Testing / 746 | |
| 21.5. Postaccident Procedures / 747 | |
| References / 748 | |

| | |
|---|------------|
| Appendix 1 Conversion Factors and Constants | 749 |
| Appendix 2 Properties of the Earth's Standard Atmosphere | 752 |
| Appendix 3 Summary of Key Equations for Ideal Chemical Rockets | 753 |
| Index | 755 |

PREFACE

This eighth edition follows earlier editions and focuses on the subject of rocket propulsion, its fundamentals, its essential technologies, and its key design rationale. It describes the various types of rocket propulsion systems, physical phenomena, and essential relationships. It aims to balance a rigorous introduction of fundamentals with tables, figures, and recent information that can be of interest to practitioners. It endeavors to provide a clearer explanation of the basic physics and chemistry of rocket propulsion and some of its design approaches.

Several chapters are devoted exclusively to liquid propellant rocket engines and also to solid propellant rocket motors (almost half the book), the two most prevalent of the rocket propulsion systems. It also has one chapter each on hybrid propulsion (with one liquid and one solid propellant) and on electrical propulsion (with several different types). The principal flight applications for these four major types of rocket propulsion systems are described. Brief discussions of nuclear thermal propulsion systems and solar thermal propulsion system are included. Our book does not contain speculative future propulsion schemes such as nuclear fusion propulsion or pulsed detonations of propellant charges, because these are as yet not considered to be practical.

The first few chapters of the book concern basic subjects. Following an introduction are definitions of the key propulsion parameters, principal thermodynamic relations, nozzle theory, vehicle flight analyses (flying inside and outside the earth's atmosphere), or thermochemical analyses of combustion gas properties. The last few chapters relate intimately to rocket propulsion systems, namely thrust vector control, selection of propulsion systems for specific missions, exhaust plumes, and the testing of rocket propulsion systems.

The book has been used for six decades in undergraduate and graduate courses of rocket propulsion in many universities, both in the United States and in other

countries. In this eighth edition many examples and problems have been revised or added for a better discussion of the principles involved and the technical issues used in preliminary design. More than 20 new homework problems have been added (and several others were deleted) for more relevance of the text material and for more practice of the key equations. Some of the problems have printed answers, so students can self-check their solutions. Many of the problems are patterned after the analyses and engineering efforts of actual propulsion systems. A solutions manual is available to selected users. Most of the book may be covered in a one- or two-semester course depending on the students' background.

Since the first edition in 1949 it has been a most popular technical rocket propulsion book and has been used by at least 75,000 students and professionals in approximately 37 countries. According to a committee of the American Institute of Aeronautics and Astronautics it is the longest living aerospace book ever, in print continuously for 60 years. It is the only aerospace book cited in two prestigious book awards of the American Institute of Aeronautics and Astronautics. Earlier editions have been translated into Russian, Chinese, and Japanese. The authors have given guest lectures on rocket propulsion subjects at several universities and a three-day course based on this book.

A number of new items and a few extensively changed sections appear in this new eighth edition. For example, this is the first edition with a separate chapter on turbopumps, an essential component of medium and large liquid propellant rocket engines. It has new or extensively revised discussions on tank pressurization, a new class of solid propellants that have been put into production, the first high-thrust large hybrid propulsion system that has flown in an experimental manned craft with nitrous oxide as the oxidizer and a rubbery fuel, a concept for integrated computer programs for modern rocket propulsion engines, health monitoring controls able to save hardware, and new flight applications for electrical propulsion systems. Almost all libraries of rocket propulsion organizations seem to have at least two editions of this book. The new edition has about three dozen new and different figures, a dozen revised or new tables, and many other clarifications, deletions, changes, or minor additions.

It is usually easier, faster, and less expensive to uprate or modify an existing proven propulsion system for a new application than to design and build a truly new one. For example, in the liquid propellant engine field with turbopump feed systems, it has been more common in the last few decades to increase the thrust or performance by modifying an existing engine than to undertake the development of a brand new engine. A revised discussion of engine families (with related engine designs) and a new table of 13 different models of the RL 10 upper-stage engine emphasized this point.

Although the United States is officially committed to convert from the English Engineering (EE) system of units (foot, pound) to the SI or metric system of units (m, kg), this has not as yet happened. The major portion of the U.S. propulsion industry for chemical rockets has been and is currently still using EE units for design and manufacturing. If a particular customer wants SI units, they will be given engineering information in SI units, but the fabrication will most likely

still be done in EE units. Many colleges and research organizations in the United States and most propulsion organizations in the other countries use the SI system of units. So this book uses both systems; the examples and problems use one or the other and some tables have both sets of units.

Computers have changed the way we do business in many fields. In rocket propulsion computer programs have been developed for many engineering analyses, computer-aided designs, computer-aided manufacturing, business and engineering transactions, test data collection, data analysis, data presentation, project management, and many others. In fact computers are used extensively in some companies to design new propulsion systems. Therefore we identify in this book the places where computer programs will be helpful and we mention this often. However, we do not discuss specific computer programs because they take up too much space, become obsolete in a short time without regular upgrading, some do not have a way to provide help to a user, and some of the better programs are company proprietary and thus not publicly available.

Propellants are hazardous materials. The authors and the publisher recommend that readers of this book do not work with them or handle them without exhaustive study of the hazards, the behavior, and properties of each propellant, and rigorous safety training including becoming familiar with protective equipment. Safety training and propellant information is given routinely to employees of organizations in this business. Neither the authors nor the publisher assume any responsibility for actions on rocket propulsion taken by the readers, either directly or indirectly. The information presented in this book is insufficient and inadequate for conducting rocket propulsion experiments or operations.

The authors acknowledge gratefully the data, suggestions, and assistance given to them while preparing the manuscript for this book. Fortunately we have had the help from a number of outstanding experts in the field, reviewers, and editors. We appreciate the reviews of solid propellant motors by David McGrath of ATK Launch Systems, Inc., and reviews of several chapters and the supply of certain propellant data by Eckart W. Schmidt, formerly of Olin Aerospace and currently a consultant in hazardous materials, is appreciated. Information on electrical propulsion was obtained from Scott Benson, of NASA Glen Research Center. Christopher Brophy of the Naval Post-Graduate School in Monterey made suggestions on hybrid propulsion. Thanks to Thomas L. Moore formerly with CPIAC (Chemical Propulsion Information Analysis Center) and now with ATK Systems for a variety of information, such as the production of a new category of solid propellant. Thanks also to Nick Heim of CPIAC for data on various motors, permissible exposure limits for toxic vapors, and gelled propellants. Frederick S. Simmons of The Aerospace Corporation reviewed the chapter on exhaust plumes and provided additional data on plumes. James H. Morehart of The Aerospace Corporation furnished precise detailed data on several rocket propulsion systems. Aerojet General Corporation of Sacramento (they elected to remain anonymous and did not single out specific deserving employees) provided data on a large solid rocket booster. Jeffrey S. Kincaid of Pratt & Whitney Rocketdyne (PWR) of Canoga Park, California, supplied the concept of integrated computer systems

and corrections to engine data, and Dennis Ramine of PWR in Canoga Park sent information on heat transfer. Vince J. Wheelock formerly of Rocketdyne furnished several key figures. Patricia Mills of PWR at West Palm Beach, Florida, collected and sent data on the RL 10 engine family. Dan Magers of John Wiley and Sons, Inc. updated references and the editors and printers of our publisher made a coarse manuscript into a useful book.

George P. Sutton
Los Angeles, California

Oscar Biblarz,
Monterey, California

CHAPTER 1

CLASSIFICATION

The word *propulsion* comes from the Latin *propulsus*, which is the past participle of the verb *propellere*, meaning to drive away. In a broad sense propulsion is the act of changing the motion of a body. Propulsion mechanisms provide a force that moves bodies that are initially at rest, changes a velocity, or overcomes retarding forces when a body is propelled through a medium. *Jet propulsion* is a means of locomotion whereby a reaction force is imparted to a device by the momentum of ejected matter.

Rocket propulsion is a class of jet propulsion that produces thrust by ejecting matter stored in a flying vehicle called the *propellant*. *Duct propulsion* is a class of jet propulsion and includes turbojets and ramjets; these engines are also commonly called air-breathing engines. Duct propulsion devices utilize mostly the surrounding medium as the “working fluid,” together with some vehicle-stored fuel. Combinations of rockets and duct propulsion devices can be attractive for some narrow applications and one is briefly described in this chapter.

The *energy source* most useful to rocket propulsion is *chemical combustion*. Energy can also be supplied by *solar radiation* and, in the past, also by *nuclear reaction*. Accordingly, the various propulsion devices can be divided into *chemical propulsion*, *nuclear propulsion*, and *solar propulsion*. Table 1–1 lists many of the important propulsion concepts according to their energy source and type of propellant or working fluid. Radiation energy can originate from sources other than the sun and theoretically can cover the transmission of energy by microwave and laser beams, electromagnetic waves, and electrons, protons, and other particle beams from a transmitter to a flying receiver. Nuclear energy is associated with the transformations of atomic particles within the nucleus of atoms and usually is created by fission or fusion. Other energy sources, both internal (in the vehicle) and external, can be considered. The energy form found in the output

TABLE 1–1. Energy Sources and Propellants for Various Propulsion Concepts

| Propulsion Device | Energy Source ^a | | | Propellant or Working Fluid |
|--------------------------------|----------------------------|---------|-------|--|
| | Chemical | Nuclear | Solar | |
| Turbojet | D/P | TFD | | Fuel + air |
| Turbo–ramjet | TFD | | | Fuel + air |
| Ramjet (hydrocarbon fuel) | D/P | TFD | | Fuel + air |
| Ramjet (H_2 cooled) | TFD | | | Hydrogen + air |
| Rocket (chemical) | D/P | TFD | | Stored propellant |
| Ducted rocket | TFD | | | Stored solid fuel + surrounding air |
| Electric rocket | D/P | TFD | D/P | Stored propellant |
| Nuclear fission rocket | | TFD | | Stored H_2 |
| Nuclear fusion rocket | | TFND | | Stored H_2 |
| Solar-heated rocket | | | TFD | Stored H_2 |
| Photon rocket (big light bulb) | | TFND | | Photon ejection (no stored propellant) |
| Solar sail | | | TFD | Photon reflection (no stored propellant) |

^aD/P, developed and/or considered practical; TFD, technical feasibility has been demonstrated, but development is incomplete; TFND, technical feasibility has not yet been demonstrated.

of a rocket is largely the kinetic energy of the ejected matter; thus the rocket converts the input from the energy source into this form. The ejected mass can be in a solid, liquid, or gaseous state. Often a combination of two or more of these is ejected. At very high temperatures it can also be a plasma, which is an electrically activated gas.

1.1. DUCT JET PROPULSION

This class, also called *air-breathing engines*, comprises devices which have a duct to confine the flow of air. They use oxygen from the air to burn fuel stored in the flight vehicle. The class includes turbojets, turbofans, ramjets, and pulsejets. This class of propulsion is mentioned primarily to provide a comparison with rocket propulsion and a background for combination rocket–duct engines, which are mentioned later. Table 1–2 compares several performance characteristics of specific chemical rockets with those of typical turbojets and ramjets. A high specific impulse, which is a measure of performance to be defined later, is directly related to a long flight range and thus indicates the superior range capability of air breather engines over chemical rockets at relatively low altitude. The uniqueness of the rocket, for example, high thrust to weight, high thrust to frontal area, and nearly thrust independence of altitude, enables extremely long flight ranges to be obtained in rarefied air and in space.

The *turbojet engine* is the most common of ducted engines. Figure 1–1 shows the basic elements.

TABLE 1–2. Comparison of Several Characteristics of a Typical Chemical Rocket and Two-Duct Propulsion Systems

| Feature | Chemical Rocket Engine or Rocket Motor | Turbojet Engine | Ramjet Engine |
|--|---|--|---|
| Thrust-to-weight ratio, typical | 75:1 | 5:1, turbojet and afterburner | 7:1 at Mach 3 at 30,000 ft |
| Specific fuel consumption (pounds of propellant or fuel per hour per pound of thrust) ^a | 8–14 | 0.5–1.5 | 2.3–3.5 |
| Specific thrust (pounds of thrust per square foot frontal area) ^b | 5000–25,000 | 2500 (low Mach at sea level) | 2700 (Mach 2 at sea level) |
| Thrust change with altitude | Slight increase | Decreases | Decreases |
| Thrust vs. flight speed | Nearly constant | Increases with speed | Increases with speed |
| Thrust vs. air temperature | Constant | Decreases with temperature | Decreases with temperature |
| Flight speed vs. exhaust velocity | Unrelated, flight speed can be greater | Flight speed always less than exhaust velocity | Flight speed always less than exhaust velocity |
| Altitude limitation | None; suited to space travel | 14,000–17,000 m | 20,000 m at Mach 3 30,000 m at Mach 5 45,000 m at Mach 12 |
| Specific impulse, typical ^c (thrust force per unit propellant or fuel weight flow per second) | 270 sec | 1600 sec | 1400 sec |

^aMultiply by 0.102 to convert to kg/(hr-N).

^bMultiply by 47.9 to convert to N/m².

^c*Specific impulse* is a performance parameter and is defined in Chapter 2.

At supersonic flight speeds above Mach 2, the *ramjet engine* (a pure duct engine) becomes attractive for flight within the atmosphere. Thrust is produced by increasing the momentum of the air as it passes through the ramjet, basically as is accomplished in the turbojet and turbofan engines but without compressors or turbines. Figure 1–2 shows the basic components of one type of ramjet. Ramjets with subsonic combustion and hydrocarbon fuel have an upper speed limit of approximately Mach 5; hydrogen fuel, with hydrogen cooling, raises this to at least Mach 16. Ramjets with supersonic combustion are known as *scramjets* and have flown in experimental vehicles. All ramjets depend on rocket boosters or some other method (such as being launched from an aircraft) for being accelerated

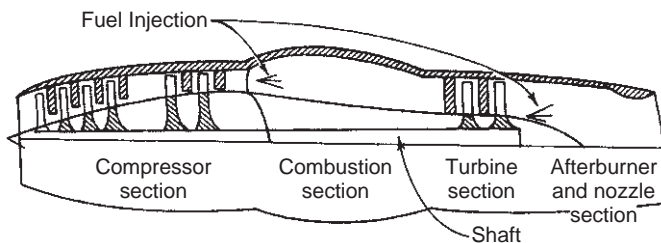


FIGURE 1–1. Simplified schematic diagram of a turbojet engine.

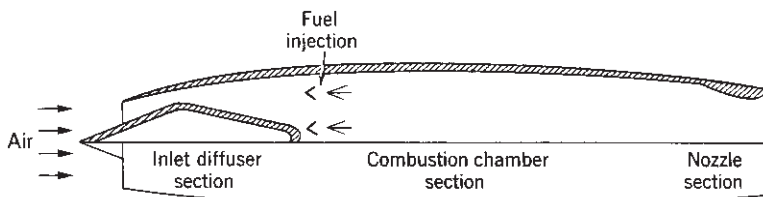


FIGURE 1–2. Simplified diagram of a ramjet with a supersonic inlet (converging and diverging flow passage).

to near their design flight speed to become functional. The primary applications of ramjets with subsonic combustion have been in shipboard and ground-launched antiaircraft missiles. Studies of a hydrogen-fueled ramjet for hypersonic aircraft look promising. The supersonic flight vehicle is a combination of a ramjet-driven high-speed airplane and a one- or two-stage rocket booster. It can travel at speeds up to a Mach number of 25 at altitudes of up to 50,000 m.

1.2. ROCKET PROPULSION

Rocket propulsion systems can be classified according to the type of energy source (chemical, nuclear, or solar), the basic function (booster stage, sustainer or upper stages, attitude control, orbit station keeping, etc.), the type of vehicle (aircraft, missile, assisted takeoff, space vehicle, etc.), size, type of propellant, type of construction, or number of rocket propulsion units used in a given vehicle.

Another way is to classify by the method of producing thrust. A thermodynamic expansion of a gas is used in the majority of practical rocket propulsion concepts. The internal energy of the gas is converted into the kinetic energy of the exhaust flow and the thrust is produced by the gas pressure on the surfaces exposed to the gas, as will be explained later. This same thermodynamic theory and the same generic equipment (nozzle) is used for jet propulsion, rocket propulsion, nuclear propulsion, laser propulsion, solar-thermal propulsion, and some types of electrical propulsion. Totally different methods of producing thrust

are used in other types of electric propulsion or by using a pendulum in a gravity gradient. As described below, these electric systems use magnetic and/or electric fields to accelerate electrically charged molecules or atoms at very low densities. It is also possible to obtain a very small acceleration by taking advantage of the difference in gravitational attraction as a function of altitude, but this method is not explained in this book.

The Chinese developed and used solid propellant in rocket missiles over 800 years ago, and military bombardment rockets were used frequently in the eighteenth and nineteenth centuries. However, the significant developments of rocket propulsion took place in the twentieth century. Early pioneers included the Russian Konstantin E. Ziolkowsky, who is credited with the fundamental rocket flight equation and his 1903 proposals to build rocket vehicles. The German Hermann Oberth developed a more detailed mathematical theory; he proposed multistage vehicles for space flight and fuel-cooled thrust chambers. The American Robert H. Goddard is credited with the first flight using a liquid propellant rocket engine in 1926. An early book on the subject was written by the Viennese engineer Eugen Sänger. For rocket history see Refs. 1–1 to 1–8.

Chemical Rocket Propulsion

The energy from a high-pressure combustion reaction of propellant chemicals, usually a fuel and an oxidizing chemical, permits the heating of reaction product gases to very high temperatures (2500 to 4100°C or 4500 to 7400°F). These gases subsequently are expanded in a nozzle and accelerated to high velocities (1800 to 4300 m/sec or 5900 to 14,100 ft/sec). Since these gas temperatures are about twice the melting point of steel, it is necessary to cool or insulate all the surfaces that are exposed to the hot gases. According to the physical state of the propellant, there are several different classes of chemical rocket propulsion devices.

Liquid propellant rocket engines use liquid propellants that are fed under pressure from tanks into a thrust chamber.* A typical pressure-fed liquid propellant rocket engine system is schematically shown in Fig. 1–3. The liquid *bipropellant* consists of a liquid oxidizer (e.g., liquid oxygen) and a liquid fuel (e.g., kerosene). A *monopropellant* is a single liquid that contains both oxidizing and fuel species; it decomposes into hot gas when properly catalyzed. A large turbopump-fed liquid propellant rocket engine is shown in Fig. 1–4. Gas pressure feed systems are used mostly on low thrust, low total energy propulsion systems, such as those used for attitude control of flying vehicles, often with more than one thrust chamber per engine. Pump-fed liquid rocket systems are used typically in applications with larger amounts of propellants and higher thrusts, such as in space launch vehicles. See Refs. 1–1 to 1–6.

*The term *thrust chamber*, used for the assembly of the injector, nozzle, and chamber, is preferred by several official agencies and therefore has been used in this book. For small spacecraft control rockets the term *thruster* (a small thrust chamber) is commonly used, and this term will be used in some sections of this book.

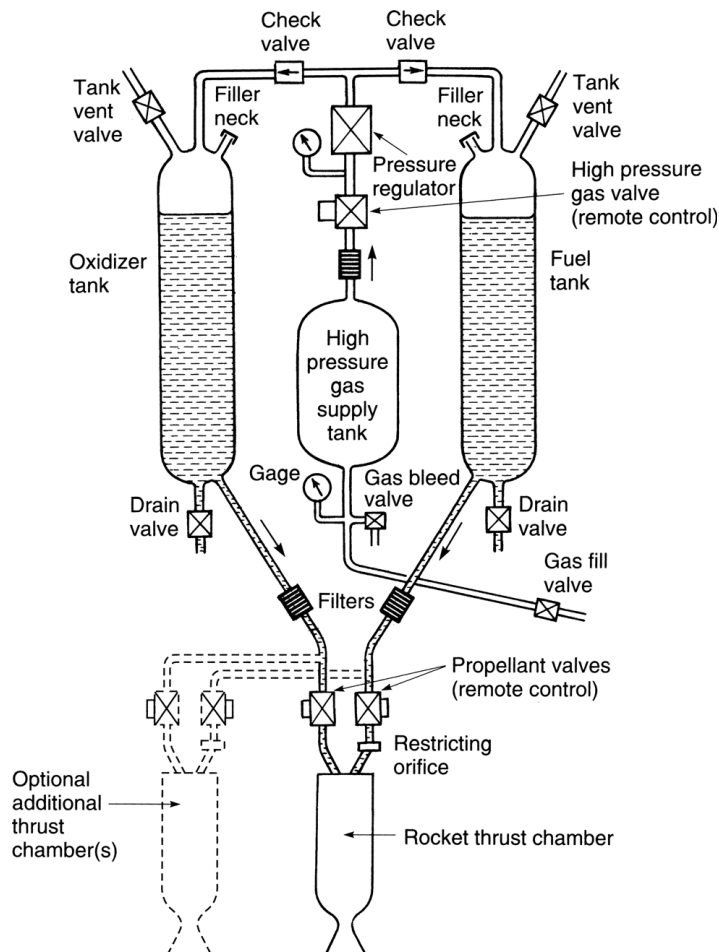


FIGURE 1–3. Schematic flow diagram of a liquid propellant rocket engine with a gas pressure feed system. The dashed lines show a second thrust chamber, but some engines have more than a dozen thrust chambers supplied by the same feed system. Also shown are components needed for start and stop, controlling tank pressure, filling propellants and pressurizing gas, draining or flushing out remaining propellants, tank pressure relief or venting, and several sensors.

In the *thrust chamber* the propellants react to form hot gases, which in turn are accelerated and ejected at a high velocity through a supersonic nozzle, thereby imparting momentum to the vehicle. A nozzle has a converging section, a constriction or throat, and a conical or bell-shaped diverging section as further described in the next two chapters.

Some liquid rocket engines permit repetitive operation and can be started and shut off at will. If the thrust chamber is provided with adequate cooling capacity, it is possible to run liquid rockets for periods exceeding 1 hour, dependent only on

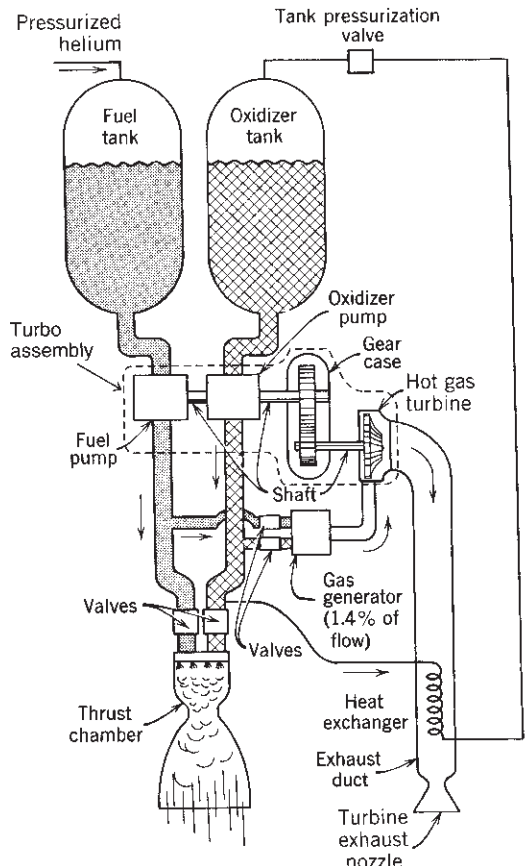


FIGURE 1–4. Simplified schematic diagram of one type of liquid propellant rocket engine with a turbopump feed system and a separate gas generator, which generates “warm” gas for driving the turbine. Not shown are components necessary for controlling the operation, filling, venting, draining, or flushing out propellants, filters or sensors. This turbopump assembly consists of two propellant pumps, a gear case, and a high speed turbine.

the propellant supply. A liquid rocket propulsion system requires several precision valves and a complex feed mechanism which includes propellant pumps, turbines, or a propellant-pressurizing device, and a relatively intricate combustion or thrust chamber.

In *solid propellant rocket motors** the propellant to be burned is contained within the combustion chamber or *case* (see Fig. 1–5). The solid propellant

*Historically, the word *engine* is used for a liquid propellant rocket propulsion system and the word *motor* is used for solid propellant rocket propulsion. They were developed originally by different groups.

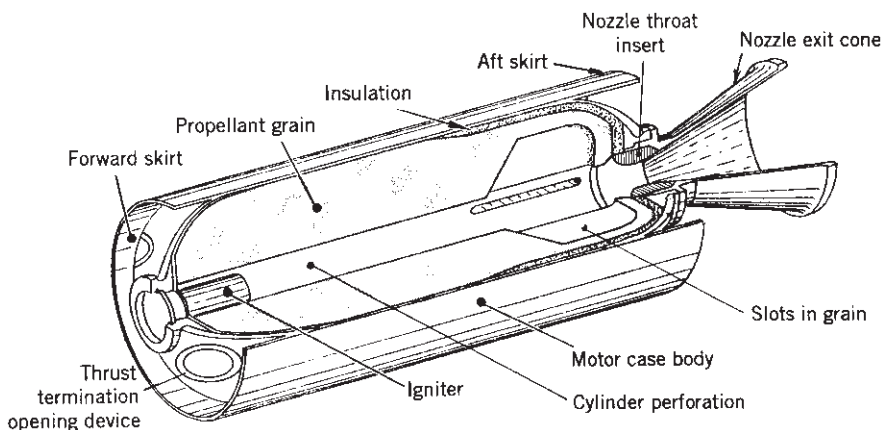


FIGURE 1–5. Simplified perspective three-quarter section of a typical solid propellant rocket motor with the propellant grain bonded to the case and the insulation layer and with a conical exhaust nozzle. The cylindrical case with its forward and aft hemispherical domes form a pressure vessel to contain the combustion chamber pressure. Adapted with permission from Ref. 12–1.

charge is called the *grain* and it contains all the chemical elements for complete burning. Once ignited, it usually burns smoothly at a predetermined rate on all the exposed internal surfaces of the grain. Initial burning takes place at the internal surfaces of the cylinder perforation and the four slots. The internal cavity grows as propellant is burned and consumed. The resulting hot gas flows through the supersonic nozzle to impart thrust. Once ignited, the motor combustion proceeds in an orderly manner until essentially all the propellant has been consumed. There are no feed systems or valves. See Refs. 1–7 to 1–10.

Liquid and solid propellants, and the propulsion systems that use them, are discussed in Chapters 6 to 11 and 12 to 15, respectively. Liquid and solid propellant rocket propulsion systems are compared in Chapter 19.

Gaseous propellant rocket engines use a stored high-pressure gas, such as air, nitrogen, or helium, as their working fluid or propellant. The stored gas requires relatively heavy tanks. These cold gas engines have been used on many early space vehicles for low thrust maneuvers and for attitude control systems and some are still used today. Heating the gas by electrical energy or by combustion of certain monopropellants improves the performance and this has often been called *warm gas propellant rocket propulsion*. Chapter 7 discusses gaseous propellants.

Hybrid propellant rocket propulsion systems use both a liquid and a solid propellant. For example, if a liquid oxidizing agent is injected into a combustion chamber filled with a solid carbonaceous fuel grain, the chemical reaction produces hot combustion gases (see Fig. 1–6). They are described further in Chapter 16. Several have flown successfully.

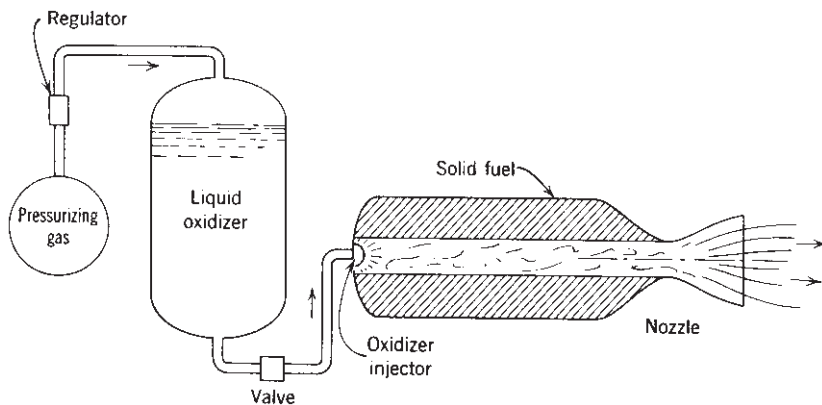


FIGURE 1–6. Simplified schematic diagram of a typical hybrid rocket engine. The relative positions of the oxidizer tank, high-pressure gas tank, and the fuel chamber with its nozzle depend on the particular vehicle design.

Combinations of Ducted Jet Engines and Rocket Engines

The Tomahawk surface-to-surface missile uses two stages of propulsion in sequence. The solid propellant rocket booster lifts the missile away from its launch platform and is discarded after its operation. A small turbojet engine sustains the low-level flight at nearly constant speed toward the target.

A *ducted rocket*, sometimes called an *air-augmented rocket*, combines the principles of rocket and ramjet engines; it gives higher performance (specific impulse) than a chemical rocket engine, while operating within the earth's atmosphere. Usually the term *air-augmented rocket* denotes mixing of air with the rocket exhaust (fuel rich for afterburning) in proportions that enable the propulsion device to retain the characteristics typifying a rocket engine, for example, high static thrust and high thrust-to-weight ratio. In contrast, the ducted rocket often is like a ramjet in that it must be boosted to operating speed and uses the rocket components more as a fuel-rich gas generator (liquid or solid).

The principles of the rocket and ramjet can be combined. An example of these two propulsion systems operating in sequence and in tandem and yet utilize a common combustion chamber volume as shown in Fig. 1–7. The low-volume configuration, known as an *integral rocket–ramjet*, can be attractive in air-launched missiles using ramjet propulsion. The transition from the rocket to the ramjet requires enlarging the exhaust nozzle throat (usually by ejecting rocket nozzle parts), opening the ramjet air inlet–combustion chamber interface, and following these two events with the normal ramjet starting sequence.

A *solid fuel ramjet* uses a grain of solid fuel that gasifies or ablates and reacts with air. Good combustion efficiencies have been achieved with a patented boron-containing solid fuel fabricated into a grain similar to a solid propellant and burning in a manner similar to a hybrid rocket propulsion system.

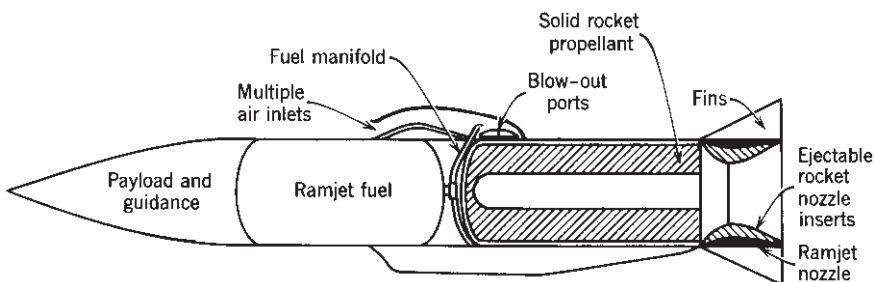


FIGURE 1–7. Elements of an air-launched missile with integral rocket–ramjet propulsion. After the solid propellant has been consumed in boosting the vehicle to flight speed, the rocket combustion chamber becomes the ramjet combustion chamber with air burning the ramjet liquid fuel.

Nuclear Rocket Engines

Two different types of nuclear energy sources have been investigated for delivering heat to a working fluid, usually liquid hydrogen, which subsequently can be expanded in a nozzle and thus accelerated to high ejection velocities (6000 to 11,000 m/sec). However, none can be considered fully developed today and none have flown. They are the *fission reactor* and the *fusion reactor*. Both are basically extensions of liquid propellant rocket engines. The heating of the gas is accomplished by energy derived from transformations within the nuclei of atoms. In chemical rockets the energy is obtained from within the propellants, but in nuclear rockets the power source is usually separate from the propellant.

In the *nuclear fission reactor rocket*, heat can be generated by the fission of uranium in the solid reactor material and subsequently transferred to the working fluid (see Refs. 1–11 to 1–13). The *nuclear fission rocket* is primarily a high-thrust engine (above 40,000 N) with specific impulse values up to 900 sec. Fission rockets were designed and tested in the 1960s in the United States and also in the Soviet Union, which today is Russia. Ground tests with hydrogen as a working fluid culminated in a thrust of 980,000 N (210,000 lb force) at a graphite core nuclear reactor power level of 4100 MW with an equivalent altitude-specific impulse of 848 sec and a hydrogen temperature of about 2500 K. There were concerns with the endurance of the materials at the high temperature (above 2600 K) and intense radiations, power level control, cooling a reactor after operation, moderating the high-energy neutrons, and designing lightweight radiation shields for a manned space vehicle. No further ground tests of nuclear fission rocket engines have been undertaken.

In recent years there has been renewed interest in nuclear fission rocket propulsion primarily for a potential manned planetary exploration mission. Studies have shown that the high specific impulse (estimated in some studies at 1100 sec) allows shorter interplanetary trip transfer times, smaller vehicles, and more flexibility in the launch time when planets are not in their optimum relative position. See Refs. 1–11 and 1–13.

Fusion is an alternate way to create nuclear energy, which can heat a working fluid. A number of different concepts have been studied. To date none are feasible or practical.

Concerns about an accident with the inadvertent spreading of radioactive materials in the earth environment and the high cost of development programs have to date prevented a renewed experimental development of a large nuclear rocket engine. Unless there are some new findings and a change in world attitude about nuclear radiation, it is unlikely that a nuclear rocket engine will be developed or flown in the next few decades. Therefore no further discussion of it is given in this book.

Electric Rocket Propulsion

In all electric propulsion the source of the electric power (nuclear, solar radiation receivers, or batteries) is physically separate from the mechanism that produces the thrust. This type of propulsion requires a heavy and inefficient power sources as discussed below. The thrust usually is low, typically 0.005 to 1 N. In order to allow a significant increase in the vehicle velocity, it is necessary to apply the low thrust and thus a small acceleration for a long time (weeks or months) (see Chapter 17 and Refs. 1–14 and 1–15).

Of the three basic types, *electrothermal* rocket propulsion most resembles the previously mentioned chemical rocket units; propellant is heated electrically (by heated resistors or electric arcs), and the hot gas is then thermodynamically expanded and accelerated to supersonic velocity through an exhaust nozzle (see Fig. 1–8). These electrothermal units typically have thrust ranges of 0.01 to 0.5 N, with exhaust velocities of 1000 to 5000 m/sec, and ammonium, hydrogen, nitrogen, or hydrazine decomposition product gases have been used as propellants.

The two other types—the *electrostatic* or *ion propulsion* engine and the *electromagnetic* or *magnetoplasma* engine—accomplish propulsion by different principles, and the thermodynamic expansion of gas in a nozzle, as such, does not apply. Both will work only in a vacuum. In an ion rocket (see Fig. 1–9) a working fluid (typically, xenon) is ionized (by stripping off electrons), and then the electrically charged heavy ions are accelerated to very high velocities (2000 to 60,000 m/sec) by means of electrostatic fields. The ions are subsequently electrically neutralized; they are combined with electrons to prevent the buildup of a space charge on the vehicle.

In the magnetoplasma rocket an electrical plasma (an energized hot gas containing ions, electrons, and neutral particles) is accelerated by the interaction between electric currents and magnetic fields and ejected at high velocity (1000 to 50,000 m/sec). There are many different types and geometries. The Hall-effect thruster, which accelerates a plasma, has a good flight record in Russia. A simple pulsed (not continuously operating) electrical propulsion unit with a solid propellant is shown in Fig. 1–10. It has had a good flight record as a spacecraft attitude control engine.

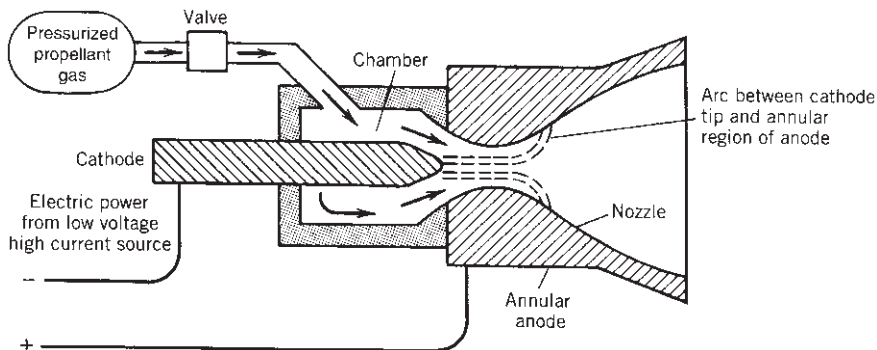


FIGURE 1–8. Simplified schematic diagram of arc-heating electric rocket propulsion system. The arc plasma temperature is very high (perhaps 15,000 K) and the anode, cathode, and chamber will get hot (1000 K) due to heat transfer.

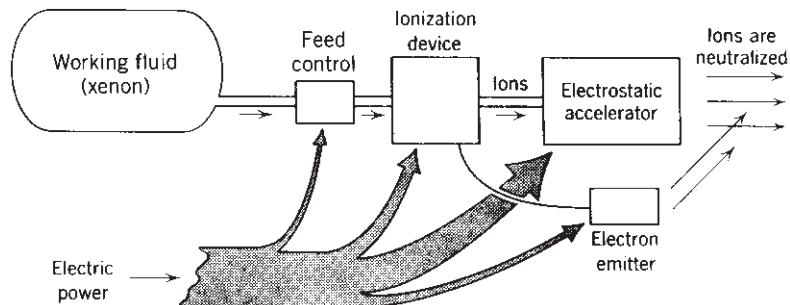


FIGURE 1–9. Simplified schematic diagram of a typical ion rocket, showing the approximate distribution of the electric power.

Other Rocket Propulsion Concepts

Several technologies exist for harnessing solar energy to provide the power for spacecraft and also to propel spacecraft using electrical propulsion. Solar cells generate electric power from the sun's radiation. They are well developed and have been successful for several decades. Most electric propulsion systems have used solar cells for their power supply. Batteries and isotope decay power sources have also been used.

One concept is the *solar thermal rocket*; it has large-diameter optics to concentrate the sun's radiation (e.g., by lightweight precise parabolic mirrors or Fresnel lenses) onto a receiver or optical cavity. Figure 1–11 shows one concept and some data is given in Table 2–1. The receiver is made of high-temperature metal (such as tungsten or rhenium) and has a cooling jacket or heat exchanger. It heats a working fluid, usually liquid hydrogen, up to perhaps 2500°C and the hot gas is controlled by hot gas valves and exhausted through one or more nozzles. The large mirror has to be pointed toward the sun, and this usually requires the mirror to be adjustable in its orientation as the spacecraft orbits around the earth.

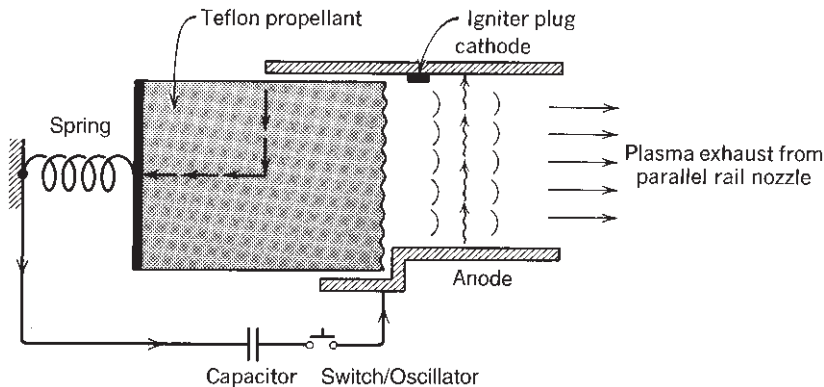


FIGURE 1–10. Simplified diagram of a rail accelerator for self-induced magnetic acceleration of a current-carrying plasma. When the capacitor is discharged, an arc is struck at the left side of the rails. The high current in the plasma arc induces a magnetic field. The action of the current and the magnetic field causes the plasma to be accelerated at right angles to both the magnetic field and the current, namely in the direction of the rails. Each time the arc is created a small amount of solid propellant (Teflon) is vaporized and converted to a small plasma cloud, which (when ejected) gives a small pulse of thrust. Actual units can operate with many pulses per second.

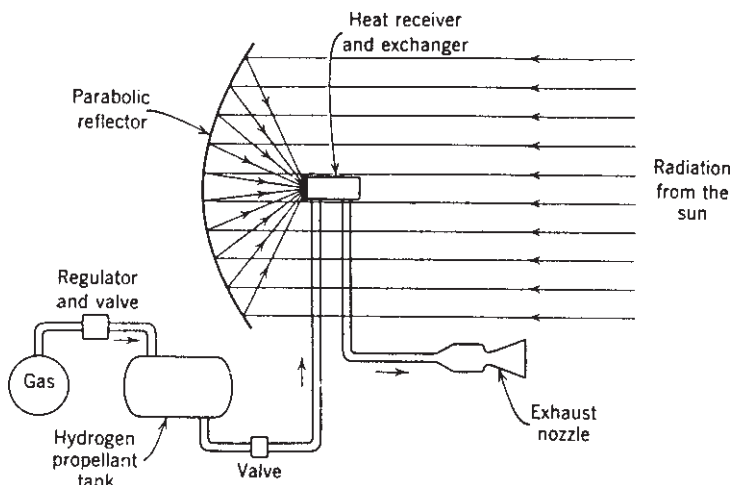


FIGURE 1–11. Simplified schematic diagram of a solar thermal rocket concept.

Performance can be two to three times higher than that of a chemical rocket and thrust levels in most studies are low (1 to 10 N). Since large lightweight optical elements cannot withstand drag forces without deformation, the optical systems are deployed outside the atmosphere. Contamination is negligible, but storage or refueling of liquid hydrogen is a challenge. Problems being investigated include

rigid, lightweight mirror or lens structures, operational life, minimizing hydrogen evaporation, and heat losses to other spacecraft components. To date the solar thermal rocket has not yet provided the principal thrust of a flying spacecraft.

The *solar sail* is another concept. It is basically a big photon reflector surface. The power source for the solar sail is the sun and it is external to the vehicle (see Ref. 1–16). Approaches using nuclear explosions and pulsed nuclear fusion have been analyzed (Refs. 1–17 and 1–18) but are not yet feasible. Concepts for transmitting radiation energy (by lasers or microwaves) from ground stations on Earth to satellites have been proposed but are not yet developed.

International Rocket Propulsion Effort

Active development or production of rocket propulsion systems was or is under way in more than 30 different countries. Some of them have made significant and original contributions to the state of the art of the technologies. There is mention in this book of a few foreign rocket units and their accomplishments and references to international rocket literature. Although most of the data in this book are taken from U.S. rocket experience, this is not intended to minimize foreign achievements.

At the time of this writing the major international program has been the *International Space Station* (ISS), a multiyear cooperative effort with major contributions from the United States and Russia and active participation by several other nations. This manned orbital space station is used for conducting experiments and observations on a number of research projects. See Ref. 1–19.

1.3. APPLICATIONS OF ROCKET PROPULSION

Because the rocket can reach a performance unequaled by other prime movers, it has its own fields of application and does not usually compete with other propulsion devices. Examples of important applications are given below and discussed further in Chapter 4.

Space Launch Vehicles

Between the first space launch in 1957 and the end of 1998 approximately 4102 space launch attempts have taken place in the world and all but about 129 were successful (see Ref. 1–20). *Space launch vehicles* or *space boosters* can be classified broadly as expendable or recoverable/reusable. Other bases of classification are the type of propellant (storable or cryogenic liquid or solid propellants), number of stages (single-stage, two-stage, etc.), size/mass of payloads or vehicles, and manned or unmanned.

Each space launch has a specific space flight objective, such as an earth orbit or a moon landing. See Ref. 1–21. It uses between two and five stages, each with its own propulsion systems, and each is usually fired sequentially after the

lower stage is expended. The number of stages depends on the specific space trajectory, the number and types of maneuvers, the energy content of a unit mass of the propellant, payload size, and other factors. The initial stage, usually called the booster stage, is the largest and it is operated first; this stage is then separated from the ascending vehicle before the second-stage rocket propulsion system is ignited and operated. As will be explained in Chapter 4, adding an extra stage permits a significant increase in the payload (such as more scientific instruments or more communications gear).

Each stage of a multistage launch vehicle is essentially a complete vehicle in itself and carries its own propellant, its own rocket propulsion system or systems, and its own control system. Once the propellant of a given stage is expended, the remaining mass of that stage (including empty tanks, cases, structure, instruments, etc.) is no longer useful in providing additional kinetic energy to the succeeding stages. By dropping off this useless mass it is possible to accelerate the final stage with its useful payload to a higher terminal velocity than would be attained if multiple staging were not used. Both solid propellant and liquid propellant rocket propulsion systems have been used for low earth orbits.

Figure 1–12 shows the Delta IV heavy-lift space launch vehicle at takeoff. Its propellants are liquid oxygen/liquid hydrogen (LOX/LH₂) in all its main engines. Its booster engine, the Pratt & Whitney Rocketdyne RS-68, is shown in Fig. 6–10 and data is in Table 11–2 and its second-stage engine, the Pratt & Whitney Rocketdyne RL 10B-2 LOX/LH₂ (24,750 lb thrust) is shown in Fig. 8–17 and data is in Table 8–1. The two liquid propellant strap-on booster pods (with the same booster engine) are removed for smaller payloads. Figure 1–13 shows the Atlas V space launch vehicle. Its booster engine is the Energomash RD-180, it has Aerojet solid propellant strap-on boosters, and the upper stage engine is the Pratt & Whitney Rocketdyne RL 10A-4-2 LOX/LH₂ engine. The Russian (Energomash) LOX/kerosene RD-180 engine is shown in Ref. 1–2 as its Figure 7.10-11 and data is in its Table 7.10-2. In both of these two launch vehicles the payload is carried on top of the second stage and it has its own propulsion system of small thrusters. Table 1–3 gives data of the larger propulsion systems of these two U.S. launch vehicles.

The *U.S. Space Shuttle* is one of the older programs and it provided the first *reusable spacecraft* that lands on a runway. Figure 1–14 shows the basic configuration of the Space Shuttle, which consists of two stages, the booster and the orbiter. It shows all the 67 rocket propulsion systems of the shuttle. The orbiter is really a reusable combination space launch vehicle, spacecraft, and glider for landing. The two solid propellant strap-on rocket motors are the largest in existence; they are equipped with parachutes for sea recovery of the burned-out motors. The large LO₂/LH₂ external tank is jettisoned and expended just before orbit insertion (see Ref. 1–22). Details of several of these Space Shuttle rocket propulsion systems are given in Table 1–4. The Space Shuttle accomplishes both civilian and military missions of placing satellites in orbit, undertaking scientific exploration, supplying a space station, and repairing, servicing, and retrieving satellites.



FIGURE 1–12. Heavy lift Delta IV space launch vehicle. The center liquid propellant booster stage has a Pratt & Whitney Rocketdyne RS-68 rocket engine (LOX/LH₂). The two strap-on stages each use the same engine. (Courtesy Pratt & Whitney Rocketdyne)



FIGURE 1–13. Atlas V space launch vehicle with three (or five) strap-on stages using Aerojet solid rocket motors and a central Energomash (Russia) RD-180 liquid propellant booster rocket engine running on LOX/kerosene. (Courtesy Lockheed Martin Corp.)

TABLE 1-3. Propulsion System Data for Two Major U.S. Launch Vehicles

| Vehicle | Designation Propulsion System | No. of Propulsion Systems per Stage | Thrust lbf/kN per Engine/Motor | Specific Impulse (sec) | Mixture Ratio, Oxidizer to Fuel Flow | Chamber Pressure psia | Nozzle Exit Area Ratio | Inert Propulsion Mass klbf/kg |
|----------|-------------------------------------|--|--|---|---|-----------------------------|------------------------------|--|
| DELTA IV | RS-68 | 1 | 1 or 3 | Full power 750,000/3.341 (vac) 655,000/2.91 (SL) ^c | 409 (vac) ^a 364 (SL) ^b | 6.0 | 1410 | 21.5:1 14,200/6,455 |
| | | | Minimum power 432,000/1.92 (vac) 337,000/1.059 (SL) ^c | 465.5 (vac) ^a | 5.88 | 633 | 285:1 | 664 |
| ATLAS V | Booster | 0 | Between 1 and 5 (SL) | 287,346/1.878 each | 279.3 (SL) ^b | N/A | N/A | 16:1 ^c 102.8 klbf loaded propellant |
| | RD-180 ^d | 1 | 1 | 933,400/4.151 kN (vac) 860,200/3.820 (SL) ^c | 310.7 (SL) ^b 337.6 (vac) ^a | 2.72 | 3722 | 36.4:1 12,081 lb/5,480 kg 5330 kg |
| | RD 10A-4-2 | 2 | 1 or 2 | 22,300/0.099 | 450.5 | 4.9-5.8 | 610 | 84:1 175 kg/367 lb |

^a(vac) means vacuum.^b(SL) means sea level.^cAt ignition.^dRD-180 has 2 gimbals mounted thrust chambers.

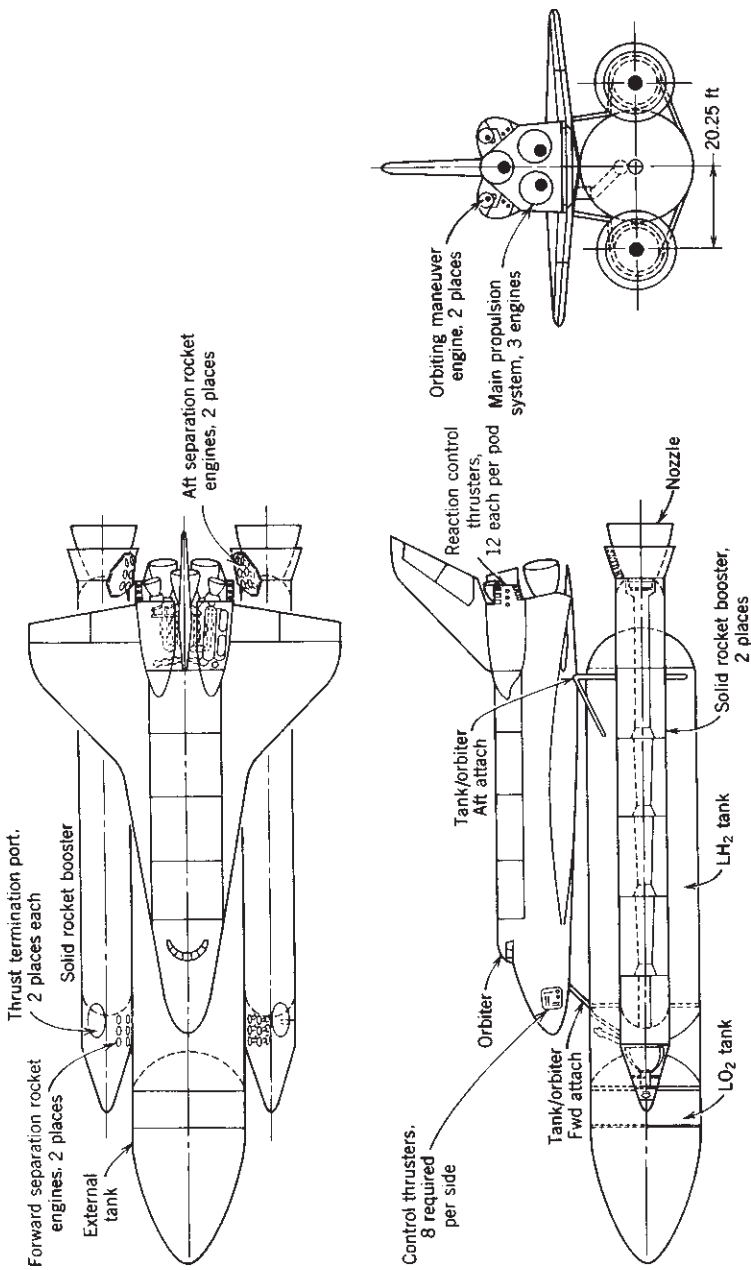


FIGURE 1–14. Simplified sketch of original version of Space Shuttle vehicle. The shuttle orbiter—the delta-winged vehicle about the size of a medium-range jet liner—is a reusable, cargo carrying, spacecraft–airplane combination that takes off vertically and lands horizontally like a glider. Each shuttle orbiter was designed for a minimum of 100 missions and can carry as much as 65,000 lb of payload to a low Earth orbit, and a crew of up to four members and 10 passengers. It can return up to 25,000 lb of payload back to earth.

TABLE 1–4. Propulsion Systems for the Space Shuttle

| Vehicle Section | Propulsion System (No. of Units) | Number of Starts and Typical Burn Time | Propellant and Specific Impulse (I_s) | Thrust | Mission |
|--|--|---|---|--|--|
| Shuttle orbiter | Space Shuttle Main Engine (3) | Start at launch 8.4 min duration Life: 55 starts and 7.5 hr | Liquid hydrogen–liquid oxygen 4464 N·sec/kg (455 sec) | 1670 kN each (375,000 lb) at sea level 2100 kN each (470,000 lbf) at space vacuum Throttled 109 to 65% of rated power | Lift orbiter off ground and accelerate to orbit velocity. Individual engines can be shut down to reduce thrust level. |
| Orbital maneuver systems (2) | | 3 to 10 starts/mission; designed for 1000 starts, 100 flights, 15 hr of cumulative time | See Note 1; $I_s = 313$ sec | Two orbiter maneuver engines; 27 kN each (6000 lbf) in vacuum | Insert orbiter vehicle into Earth orbit, correct orbit, abort, and deorbit maneuver. |
| Reaction control system, 38 primary thrusters, 6 vernier thrusters | | Multiple operations; thousands of starts; duration from a few milliseconds to seconds | See Note 1; $I_s = 280 - 304$ sec, depending on nozzle | Primary thruster 3870 N each (870 lbf), vernier thruster 106.8 N each (25 lbf) | Small vehicle velocity adjustments and attitude control during orbit insertion, on orbit corrections, rendezvous, and reentry. |
| Solid rocket boosters (SRBs) original version | Attached to external tank; multisection, 2 units | Single start at launch 2 min | See Note 2; $I_s = 292$ sec | 14,700 kN each, or 3.3 \times 10 ⁶ lbf each | Boost Shuttle vehicle to about 5500 km/hr |
| | Separation rocket motors; 16 units | 4 each at forward frustum and aft skirt; 0.66 sec, nominal | Solid propellant; $I_s = 250$ sec | 97,840 N each or 22,000 lbf | Move SRB away from vehicle after cut-off |

Notes:

1. MMH, monomethylhydrazine and NTO, nitrogen tetroxide.
2. 70% Ammonium perchlorate; 16% aluminum; 12% polybutadiene acrylic acid binder; 2% epoxy curing agent.

Table 1–4 gives propulsion system data on the Space Shuttle, which is really a combination of launch vehicle, spacecraft, and a glider. It can be seen that the thrust levels are highest for booster or first stages and are relatively high for upper stages (thousands of pounds). Only for the attitude control system of the vehicle (also called reaction control in Table 1–4) are the thrust levels low (from a fraction of a pound for small spacecraft to as high as about 1000 pounds thrust in the Space Shuttle vehicle). Frequent propulsion starts and stops are usually required in these applications.

At the time of this writing (early 2008) for this new 8th edition National Aeronautics and Space Administration (NASA) had awarded the initial contracts for a new large manned space flight vehicle identified as Ares I. It is intended to replace the aging Space Shuttle after about 2012. It is planned to use a large single 5-segment solid rocket motor as booster propulsion (being developed by ATK Launch Systems) and the second stage will use a J-2X liquid propellant rocket engine with LOX/LH₂ propellants (being developed by Pratt & Whitney Rocketdyne).

A new set of manned space flight vehicles are currently being developed by several entrepreneurial US and foreign companies, many with their own private capital. They are aimed at the future commercial market of sending tourists (for a hefty price) into space and returning them safely back to earth. All are based on reusable spacecraft, some with reusable launch vehicles, some with vertical and some with horizontal takeoff or landing. A couple of suborbital flights have already been accomplished with professional pilots using a winged vehicle. Liquid propellant rocket engines seem to be preferred and many are planned to be reusable. It is too early for determining which of these organizations will be successful in commercializing manned space flight.

The *missions* and *payloads* for space launch vehicles are many, such as military (reconnaissance satellites, command and control satellites), nonmilitary government [weather observation satellites, global positioning system (GPS) satellites], space exploration (space environment, planetary missions), or commercial (communication satellites).

A single stage-to-orbit vehicle, attractive because it avoids the costs and complexities of staging, has been expected to have improved reliability (simpler structures, fewer components). However, its payload is usually too small. A low earth orbit (say 100 miles altitude) can only be achieved with such a vehicle if the propellant performance is very high and the structure is efficient and low in mass. Liquid propellants such as liquid hydrogen with liquid oxygen were usually chosen. To date a large rocket-propelled single stage-to-orbit vehicle has not flown.

Spacecraft

Depending on their missions, *spacecraft* can be categorized as earth satellites, lunar, interplanetary, and trans-solar types, and as manned and unmanned spacecraft. Reference 1–23 lists over 20,000 satellites and categorizes them as satellites for communications, weather, navigation, scientific exploration, deep

space probes, observation (including radar surveillance), reconnaissance and other applications. Rocket propulsion is used for both primary propulsion (i.e., acceleration along the flight path, such as for orbit insertion or orbit change maneuvers) and secondary propulsion functions in these vehicles. Some of the *secondary propulsion* functions are attitude control, spin control, momentum wheel and gyro unloading, stage separation, and the settling of liquids in tanks. A spacecraft usually has a series of different rocket propulsion systems, some often very small. For spacecraft attitude control about three perpendicular axes, each in two rotational directions, the system must allow the application of pure torque for six modes of angular freedom, thus requiring a minimum of 12 thrusters. Some missions require as few as 4 to 6 thrusters, whereas the more complex manned spacecraft have 40 to 80 thrusters in all of its stages. Often the small *attitude control rockets* must give pulses or short bursts of thrust, necessitating thousands of restarts. See Section 6.7 and Ref. 1–24.

Table 1–5 presents a variety of spacecraft along with their weights, missions, and propulsion. Although only U.S. launch vehicles are listed in this table, there are also launch vehicles developed by France, the European Space Agency, Russia, Japan, China, India, and Israel that have successfully launched payloads into satellite orbits. They use rocket propulsion systems that were developed in their own countries.

The majority of spacecraft have used liquid propellant engines, a few with solid propellant boosters. Many spacecraft have operated successfully with electrical propulsion for attitude control. Electrical propulsion systems will probably also be used for some primary and secondary spacecraft propulsion missions on long-duration space flights, as described in Chapter 17.

Micropropulsion is a relatively new designation. It has been defined as any rocket propulsion system that is applicable to small spacecraft with a mass of less than 100 kg, or 220 lb. See Ref. 1–25. It encompasses a variety of different propulsion concepts, such as certain very low thrust liquid mono- and bipropellant rocket engines, small gaseous propellant rocket engines, several types of electrical propulsion systems, and emerging advanced versions of these. Many are based on fabrication of very small components (valves, thrusters, switches, insulators, or sensors) by micromachining and electromechanical processes.

Missiles and Other Applications

Military missiles can be classified as shown in Table 1–6. Rocket propulsion for new U.S. missiles uses now almost exclusively solid propellant rocket motors. They can be *strategic missiles*, such as long-range ballistic missiles (800 to 9000 km range), which are aimed at military targets within an enemy country, or *tactical missiles*, which are intended to support or defend military ground forces, aircraft, or navy ships.

Tables 1–6 and 1–7 show some parameters of rocket propulsion devices for different applications. The selection of the best rocket propulsion system type and design for any given application is a complex process involving many factors, including system performance, reliability, propulsion system size, and compatibility, as described in Chapter 19.

TABLE 1-5. Selected U.S. Spacecraft

| Name | Space Maneuver Propulsion | | | Weight (lbf) | Remarks |
|--|---|---|--|-----------------|---|
| | Thrust (lbf) | Propellants | | | |
| Mariner 69 | 50 (primary) 1.0 (secondary) | Hydrazine monopropellant Hydrazine monopropellant | | 1,100 | Flyby of Venus/Mercury |
| Pioneer 10, 11 | 50 (primary) | Hydrazine monopropellant | | 570 | Fly to Jupiter and beyond |
| Viking | 600 (primary) 5.0 (secondary) | Hydrazine monopropellant Hydrazine monopropellant | | 7,500 | Mars orbiter with soft lander |
| Nimbus 5 | 0.5 (secondary) | Hydrazine monopropellant | | | |
| Apollo command and service module | 20,500 (primary) | Stored nitrogen $\text{N}_2\text{O}_4/50\%$ and 50% UDMH and 50% N_2H_4 | | 1,700 64,500 | Weather satellite Manned lunar landing |
| Space Shuttle orbiter | 100 lbf 16 units 93 lbf 6 units (secondary) Two 6000-lbf units (primary) | $^a\text{N}_2\text{O}_4/\text{MMH}$ $\text{N}_2\text{O}_4/\text{MMH}$ $\text{N}_2\text{O}_4/\text{MMH}$ | | 150,000 | Reusable spacecraft with runway landing |
| Fleet Communications Satellite | 38 units @ 870 lbf (secondary) Six 25-lbf units (secondary) 0.1 (secondary) | $\text{N}_2\text{O}_4/\text{MMH}$ $\text{N}_2\text{O}_4/\text{MMH}$ Hydrazine monopropellant | | 1,854 | UHF communications |
| Photo Recon Intelsat V communication satellite | 4.0 (secondary) 0.10 | Hydrazine monopropellant Hydrazine | | 25,000 4,180 | Radio/photo communications Resistojet, electric propulsion for N-S station keeping |
| Deep Space 1 (DS1) | 0.02 (primary) | Xenon | | 1,070 | Ion propulsion engine for asteroid fly-by |

^a N_2O_4 , nitrogen tetroxide (oxidizer); MMH, monomethylhydrazine (fuel); 50:50 UDMH– N_2H_4 is a 50% mixture of unsymmetrical dimethylhydrazine and hydrazine.

TABLE 1–6. Selected Data for U.S. Missiles

| Mission Category | Name | Diameter (ft) | Length (ft) | Propulsion | Launch Weight (lb) |
|--|---------------------|---------------|-------------|-----------------------------|--------------------|
| Surface-to-surface (long range) | Minuteman III | 6.2 | 59.8 | 3 stages, solid | 78,000 |
| | Poseidon | 6.2 | 34 | 2 stages, solid | 65,000 |
| Surface-to-air (or to missile) | Chaparral | 0.42 | 9.5 | 1 stage, solid | 185 |
| | Improved Hawk | 1.2 | 16.5 | 1 stage, solid | 1,398 |
| Air-to-surface | Standard Missile | 1.13 | 15 or 27 | 2 stages, solid | 1,350/2,996 |
| | Redeye | 0.24 | 4 | 1 stage, solid | 18 |
| Air-to-air | Patriot | 1.34 | 1.74 | 1 stage, solid | 1,850 |
| | Maverick | 1.00 | 8.2 | 1 stage, solid | 475 |
| Antisubmarine | Shrike | 0.67 | 10 | 1 stage, solid | 400 |
| | SRAM | 1.46 | 14 | 2 staged grains | 2,230 |
| Battlefield support (surface-to-surface, short range) | Falcon | 0.6 | 6.5 | 1 stage, solid | 152 |
| | Phoenix | 1.25 | 13 | 1 stage, solid | 980 |
| Cruise missile (subsonic) | Sidewinder | 0.42 | 9.5 | 1 stage, solid | 191 |
| | Sparrow | 0.67 | 12 | 1 stage, solid | 515 |
| Cruise missile (supersonic) | Subroc | 1.75 | 22 | 1 stage, solid | 4,000 |
| | Lance | 1.8 | 20 | 2 stages, liquid | 2,424 |
| Antisubmarine | Hellfire (antitank) | 0.58 | 5.67 | 1 stage, solid | 95 |
| | Pershing II | 3.3 | 34.5 | 2 stages, solid | 10,000 |
| | Tow (antitank) | 0.58 | 3.84 | 1 stage, solid | 40 |
| | Tomahawk | 1.74 | 21 | solid booster + turbofan | 3,900 |

TABLE 1-7. Typical Propulsion Characteristics of Some Rocket Applications

| Application | Type of Propellant | Thrust Profile | Typical Firing Duration | Maximum Acceleration ^a |
|--|--|--|---|--|
| Large space launch vehicle booster | Liquid or cryogenic liquid, or solid | Nearly constant thrust | 2–8 min | 1.2–6 g_0 |
| Strap-on booster | Solid or liquid | 380,000 to 1,500,000 lbf | $\frac{1}{2}$ to 2 min 2–75 sec each | 1.2 to 3 g_0 5 to 20 g_0 , but can be up to 100 g_0 |
| Antiaircraft or antimissile-missile | Solid, some with liquid terminal divert stage | High thrust boost, decreasing thrust sustain phase | | |
| Spacecraft orbit maneuvers | Storable liquid or cryogenic liquid | Restartable in space | Up to 10 min cumulative duration | 0.2–6 g_0 |
| Air-launched guided missile | Solid | High thrust boost phase with low thrust or decreasing thrust for sustain phase; sometimes 2 pulses | Boost: 2–5 sec Sustain: 10–30 sec | Up to 25 g_0 |
| Battlefield support—surface launched | Solid | Decreasing thrust | Up to 2 min each stage | Up to 10 g_0 |
| Rocket-assisted projectile, gun launched | Solid | Constant or decreasing thrust | A few sec | Up to 20,000 g_0 in gun barrel |
| Spacecraft attitude control—large vehicles | Storable liquid (monopropellant or bipropellant); electric propulsion; xenon | Many restarts (up to several thousands); pulsing | Up to several hours cumulative duration | Less than 0.1 g_0 |
| Spacecraft attitude control—small vehicle | Electric propulsion; Cold or warm gas or storable liquid. | Same | Up to several hours cumulative | Same |
| Reusable main engines for Space Shuttle | Cryogenic liquid (O_2/H_2) | Variable thrust, many flights with same engine | 8 min, over 7 hr cumulative in several missions | |
| Lunar landing | Storable bipropellant | 10:1 thrust variation | 4 min | Several g_0 |
| Weather sounding rocket | Solid | Single burn period—often decreasing thrust | 5–50 sec | Up to 15 g_0 |
| Antitank | Solid | Single burn period | 0.2–3 sec | Up to 20 g_0 |

^a g_0 is acceleration of gravity at the Earth's surface = 9,8066 m/sec² or 32.17 ft/sec².

The term *surface launch* can mean a launch from the ground, the ocean surface (from a ship), or from underneath the sea (submarine launch). Some tactical missiles, such as the air-to-surface short-range attack missile (SRAM), have a two-pulse solid propellant motor, where two separate, insulated grains are in the same motor case; the time interval before starting the second pulse can be timed to control the flight path or speed profile. Most countries now have tactical missiles in their military inventories, and many of these countries have a capability to produce their own rocket propulsion systems that are used to propel them.

Solid propellant rocket motors are being used today in most tactical missiles, such as in surface-to-air, air-to-air, air-to-surface, and surface-to-surface applications, for the ejection of pilot aircraft seats or crew capsules, target drones, signal rockets, weather sounding rockets, antitank rockets, or for the separations of stages in a multistage flight vehicle.

Applications, which were popular 30 to 60 years ago, but are no longer active, include liquid propellant rocket engines for propelling military fighter aircraft, assisted takeoff rocket engines and rocket motors, and superperformance rocket engines for augmenting the thrust of an aircraft jet engine.

REFERENCES

- 1–1. E. C. Goddard and G. E. Pendray (Eds), *The Papers of Robert H. Goddard*, three volumes, McGraw-Hill Book Company, 1970, 1707 pages. It includes the pioneering treatise “A Method of Reaching Extreme Altitudes” originally published as Smithsonian Miscellaneous Collections, Vol. 71, No. 2, 1919.
- 1–2. G. P. Sutton, *History of Liquid Propellant Rocket Engines*, published by AIAA, 2006, 911 pages.
- 1–3. B. N. Yur'yev (Ed), *Collected Works of K. E. Tsiolkowski*, Vols. 1–3, USSR Academy of Sciences, 1951; also NASA Technical Translation F-236, April 1965.
- 1–4. H. Oberth, *Die Rakete zu den Planetenräumen* (By Rocket to Planetary Space), R. Oldenburg, Munich, 1923 (in German), a classical text.
- 1–5. E. Sänger, *Raketenflugtechnik* (Rocket Flight Technology), R. Oldenburg, Munich, 1923 (in German).
- 1–6. W. von Braun and F. Ordway, *History of Rocketry and Space Travel*, 3rd ed., Thomas Y. Crowell, New York, 1974.
- 1–7. L. H. Caveny, R. L. Geisler, R. A. Ellis, and T. L. Moore, “Solid Enabling Technologies and Milestones in the USA,” *Journal of Propulsion and Power*, Vol. 19, No. 6, Nov.–Dec. 2003, AIAA, pp. 1038–1066.
- 1–8. A. M. Lipanov, “Historical Survey of Solid Propellant Rocket Development in Russia,” *Journal of Propulsion and Power*, Vol. 19, No. 6. Nov.–Dec. 2003, pp. 1063–1088.
- 1–9. AGARD Lecture Series 150, *Design Methods in Solid Rocket Motors*, AGARD/NATO, Paris, April 1988.
- 1–10. A. Davenas, *Solid Rocket Propulsion Technology*, Pergamon Press, London (originally published in French), 1988.

- 1–11. S. V. Gunn and C. M. Ehresman, “The Space Propulsion Technology Base Established Four Decades Ago for the Thermal Nuclear Rocket Is Ready for Current Application,” AIAA paper 2003–4590, July 2003.
- 1–12. R. W. Bussard and R. D. DeLauer, *Nuclear Rocket Propulsion*, McGraw-Hill Book Company, New York, 1958.
- 1–13. D. Buden, “Nuclear Rocket Safety,” *Acta Astronautica*, Vol. 18, 30 Years of Progress in Space, 1988, pp. 217–224.
- 1–14. R. C. Finke (Ed), *Electric Propulsion and Its Application to Space Missions*, Vol. 79, Progress in Aeronautics and Astronautics Series, AIAA 1981.
- 1–15. R. G. Jahn, *Physics of Electrical Propulsion*, McGraw-Hill Book Company, New York, 1968, 339 pages.
- 1–16. T. Svitek et al., “Solar Sails as Orbit Transfer Vehicle—Solar Sail Concept Study,” Phase II Report, AIAA paper 83–1347, 1983.
- 1–17. V. P. Ageev et al., “Some Characteristics of the Laser Multi-pulse Explosive Type Jet Thruster,” *Acta Astronautica*, Vol. 8, No. 5–6, 1981, pp. 625–641.
- 1–18. R. A. Hyde, “A Laser Fusion Rocket for Interplanetary Propulsion,” Preprint UCRL 88857, Lawrence Livermore National Laboratory, Livermore, California, Sept. 1983.
- 1–19. *NASA International Space Station* (A resource on the ISS by NASA; includes operational use, wide range of background material, archives, image gallery and planned missions) www.nasa.gov/station-34k.
- 1–20. T. D. Thompson (Ed), *TRW Space Log*, Vols. 31 to 34, TRW Space and Electronics Group (today part of Northrop Grumman Corp.), Redondo Beach, CA, 1996 and 1997–1998.
- 1–21. S. J. Isakowitz, J. B. Hopkins, and J. P. Hopkins, *International Reference Guide to Space Launch Systems*, 4th ed., AIAA, 2004, 596 pages.
- 1–22. National Aeronautics and Space Administration (NASA), *National Space Transportation System Reference*, Vol. 1, *Systems and Facilities*, U.S. Government Printing Office, Washington, DC, June 1988; a description of the Space Shuttle.
- 1–23. A. R. Curtis (Ed), *Space Satellite Handbook*, 3rd ed, Gulf Publishing Company, Houston, TX, 1994, 346 pages.
- 1–24. G. P. Sutton, *History of Small Liquid Propellant Thrusters*, presented at the 52nd JANNAF Propulsion Meeting, May 2004, Las Vegas, NE, published by the Chemical Propulsion Information Analysis Center, Columbia, Maryland, June 2004.
- 1–25. M. M. Micci and A. D. Ketsdever, *Micropropulsion for Small Spacecraft*, Progress in Aeronautics and Astronautics Series, Vol. 187, AIAA, 2000, 477 pages.

CHAPTER 2

DEFINITIONS AND FUNDAMENTALS

The basic principles of rocket propulsion are essentially those of mechanics, thermodynamics, and chemistry. Propulsion is achieved by applying a force to a vehicle, that is, accelerating the vehicle or, alternatively, maintaining a given velocity against a resisting force. This propulsive force is obtained by ejecting propellant at high velocity. This chapter deals with the definitions and the basic relations of this propulsive force, the exhaust velocity, and the efficiencies of creating and converting the energy and other basic parameters. The symbols used in the equations are defined at the end of the chapter. Wherever possible the American Standard letter symbols for rocket propulsion (as given in Ref. 2-1) are used.

2.1. DEFINITIONS

The *total impulse* I_t is the thrust force F (which can vary with time) integrated over the burning time t :

$$I_t = \int_0^t F \, dt \quad (2-1)$$

For constant thrust and very short start and stop transients this reduces to

$$I_t = Ft \quad (2-2)$$

Impulse I_t is proportional to the total energy released by all the propellant in a propulsion system.

The *specific impulse* I_s is the total impulse per unit weight of propellant. It is an important figure of merit of the performance of a rocket propulsion system, similar in concept to the miles per gallon parameter used with automobiles. A higher number means better performance. Values of I_s are given in many chapters of this book, and the concept of an optimum specific impulse for a particular mission is introduced later. If the total mass flow rate of propellant is \dot{m} and the standard acceleration of gravity at sea level g_0 is 9.8066 m/sec^2 or 32.174 ft/sec^2 , then

$$I_s = \frac{\int_0^t F \, dt}{g_0 \int \dot{m} \, dt} \quad (2-3)$$

This equation will give a time-averaged specific impulse value for any rocket propulsion system, particularly where the thrust varies with time. During transient conditions (during start or the thrust buildup period, the shutdown period, or during a change of flow or thrust levels) values of I_s can be obtained by integration or by determining average values for F and \dot{m} for short time intervals. For constant thrust and propellant flow this equation can be simplified; below, m_p is the total effective propellant mass expelled through the nozzle.

$$I_s = I_t / (m_p g_0) \quad (2-4)$$

In Chapter 3 there is further discussion of the specific impulse. For constant propellant mass flow \dot{m} , constant thrust F , and negligibly short start or stop transients:

$$\begin{aligned} I_s &= F / (\dot{m} g_0) = F / \dot{w} \\ I_t / (m_p g_0) &= I_t / w \end{aligned} \quad (2-5)$$

at or near the earth's surface, the product $m_p g_0$ is the total effective propellant weight w , and the weight flow rate is \dot{w} . But in space or outer satellite orbits, the mass is just multiplied by an arbitrary constant, namely g_0 . In the *Système International* (SI) or metric system of units I_s can be expressed simply in "seconds" because of the use of the constant g_0 . In the United States today we still use the English Engineering (EE) system of units (foot, pound, second) in many of the chemical propulsion engineering, manufacturing, and test operations. In many past and current U.S. publications, data, and contracts, the specific impulse has units of thrust (1bf) divided by weight flow rate of propellants (1bf/sec), simplified as seconds. The numerical value of I_s is the same in the EE and the SI system of units. However, the units of I_s do not represent a measure of elapsed time but a thrust force per unit "weight" flow rate. In this book the symbol I_s is used for the specific impulse, as listed in Ref. 2-1. For solid propellant and several other rocket systems the symbol I_{sp} is often used, as listed in Ref. 2-2.

In a rocket nozzle the actual exhaust velocity is not uniform over the entire exit cross section and does not represent the entire thrust magnitude. The velocity profile is difficult to measure accurately. For convenience a uniform axial velocity c is assumed, which allows a one-dimensional description of the problem. This *effective exhaust velocity* c is the average equivalent velocity at which propellant is ejected from the vehicle. It is defined as

$$c = I_s g_0 = F/m \quad (2-6)$$

It is given either in meters per second or feet per second. Since c and I_s differ only by an arbitrary constant, either one can be used as a measure of rocket performance. In the Russian literature c is generally used in lieu of I_s .

In solid propellant rockets it is difficult to measure the propellant flow rate accurately. Therefore, the specific impulse is often calculated from total impulse and the propellant weight (using the difference between initial and final motor weights and Eq. 2–5). In turn the total impulse is obtained from the integral of the measured thrust with time, using Eq. 2–1. In liquid propellant units it is possible to measure thrust and instantaneous propellant flow rate and thus to use Eq. 2–3 for calculation of specific impulse. Equation 2–4 allows another definition for specific impulse, namely, the amount of impulse imparted to a vehicle per unit sea-level weight of propellant expended.

The term *specific propellant consumption* refers to the reciprocal of the specific impulse and is not commonly used in rocket propulsion. It is used in automotive and duct propulsion systems. Typical values are listed in Table 1–2.

The *mass ratio* **MR** of a vehicle or a particular vehicle stage is defined to be the final mass m_f (after rocket operation has consumed all usable propellant) divided by m_0 (before rocket operation). The various terms are depicted in Fig. 4–1.

$$\mathbf{MR} = m_f/m_0 \quad (2-7)$$

This applies to a single or a multistage vehicle; for the latter, the overall mass ratio is the product of the individual vehicle stage mass ratios. The final mass m_f is the mass of the vehicle after the rocket has ceased to operate when all the useful propellant mass m_p has been consumed and ejected. The final vehicle mass m_f includes all those components that are not useful propellant and may include guidance devices, navigation gear, payload (e.g., scientific instruments or a military warhead), flight control systems, communication devices, power supplies, tank structure, residual or unusable propellant, and all the propulsion hardware. In some vehicles it can also include wings, fins, a crew, life support systems, reentry shields, landing gears, and the like. Typical values of **MR** can range from 60% for some tactical missiles to less than 10% for some unmanned launch vehicle stages. This mass ratio is an important parameter in analyzing flight performance, as explained in Chapter 4. When **MR** is applied to a single stage, then its upper stages become the “payload.”

The *propellant mass fraction* ζ indicates the fraction of propellant mass m_p in an initial mass m_0 . It can be applied to a vehicle, a stage of a vehicle, or to a rocket propulsion system.

$$\zeta = m_p/m_0 \quad (2-8)$$

$$\zeta = (m_0 - m_f)/m_0 = m_p/(m_p + m_f) \quad (2-9)$$

$$m_0 = m_f + m_p \quad (2-10)$$

When applied to a rocket propulsion system, the mass ratio **MR** and propellant fraction ζ are different from those that apply to a vehicle as described above. Here the initial or loaded mass m_0 consists of the inert propulsion mass (the hardware necessary to burn and store the propellant) and the effective propellant mass. It would exclude masses of nonpropulsive components, such as payload or guidance devices. For example, in a liquid propellant rocket engine the final or inert propulsion mass m_f would include the propellant feed tanks, their pressurization system (with turbopump and/or gas pressure system), one or more thrust chambers, various piping, fittings and valves, an engine mount or engine structure, filters, and some sensors. The *residual or unusable remaining propellant* is usually considered to be part of the final inert mass m_f , as it will be in this book. However, some rocket propulsion manufacturers and some literature assign residuals to be part of the propellant mass m_p . When applied to a rocket propulsion system, the value of the propellant mass fraction ζ indicates the quality of the design; a value of, say, 0.91 means that only 9% of the mass is inert rocket hardware, and this small fraction contains, feeds, and burns a substantially larger mass of propellant. A high value of ζ is desirable.

The *impulse-to-weight* ratio of a complete propulsion system is defined as the total impulse I_t divided by the initial or propellant-loaded vehicle weight w_0 . A high value indicates an efficient design. Under our assumptions of constant thrust and negligible start and stop transients, it can be expressed as

$$\frac{I_t}{w_0} = \frac{I_t}{(m_f + m_p)g_0} \quad (2-11)$$

$$= \frac{I_s}{m_f/m_p + 1} \quad (2-12)$$

The *thrust-to-weight* ratio F/w_0 expresses the acceleration (in multiples of the Earth's surface acceleration of gravity) that the engine is capable of giving to its own loaded propulsion system mass. For constant thrust the maximum value of the thrust-to-weight ratio, or maximum acceleration, occurs just before termination or burnout because the vehicle mass has been diminished by the mass of useful propellant. Values of F/w are given in Table 2-1. The *thrust-to-weight ratio* is useful to compare different types of rocket systems.

TABLE 2-1. Ranges of Typical Performance Parameters for Various Rocket Propulsion Systems

| Engine Type | Specific Impulse ^a (sec) | Maximum Temperature (°C) | Thrust-to-Weight Ratio ^b | Propulsion Duration | Specific Power (kW/kg) | Typical Working Fluid | Status of Technology |
|--|--|-----------------------------|-------------------------------------|---------------------|--------------------------------|--|-------------------------|
| Chemical—solid or liquid bipropellant | 200–468 | 2500–4100 | 10^{-2} – 100 | Seconds to a few | 10^{-1} – 10^3 | Liquid or solid propellants | Flight proven |
| Liquid monopropellant | 194–223 | 600–800 | 10^{-1} – 10^{-2} | Seconds to minutes | 0.02–200 | N ₂ H ₄ | Flight proven |
| Nuclear fission | 500–860 | 2700 | 10^{-2} – 30 | Seconds to minutes | 10^{-1} – 10^3 | H ₂ | Development was stopped |
| Resistojet | 150–300 | 2900 | 10^{-2} – 10^{-4} | Days | 10^{-3} – 10^{-1} | H ₂ , N ₂ H ₄ | Flight proven |
| Arc heating—electrothermal | 280–1200 | 20,000 | 10^{-4} – 10^{-2} | Days | 10^{-3} – 1 | N ₂ H ₄ , H ₂ , NH ₃ | Flight proven |
| Electromagnetic including pulsed plasma (PP) | 700–2500 | — | 10^{-6} – 10^{-4} | Weeks | 10^{-3} – 1 | H ₂ | Flight proven |
| Hall effect | 1000–1700 | — | 10^{-4} | Weeks | 10^{-1} – 5×10^{-1} | Solid for PP | Flight proven |
| Ion—electrostatic | 1200–5000 | — | 10^{-6} – 10^{-4} | Months | 10^{-3} – 1 | Xenon | Several have flown |
| Solar heating | 400–700 | 1300 | 10^{-3} – 10^{-2} | Days | 10^{-2} – 1 | H ₂ | In development |

^aAt $p_1 = 1000$ psia and optimum gas expansion at sea level ($p_2 = p_3 = 14.7$ psia).^bRatio of thrust force to full propulsion system sea level weight (with propellants, but without payload).^cKinetic power per unit exhaust mass flow.

Example 2–1. A rocket projectile has the following characteristics:

| | |
|--|---------|
| Initial mass | 200 kg |
| Mass after rocket operation | 130 kg |
| Payload, nonpropulsive structure, etc. | 110 kg |
| Rocket operation duration | 3.0 sec |
| Average specific impulse of propellant | 240 sec |

Determine the mass ratios for the overall vehicle and for the propulsive unit, the propellant mass fraction for the propulsive unit, the effective exhaust velocity, and the total impulse. Also, sensitive electronic equipment in the payload would limit the maximum acceleration to $35g_0$'s. Is this exceeded during the flight? Assume constant thrust and neglect the short start and stop transients.

SOLUTION. From the givens, the mass of the expended propellant is 70 kg. The mass ratio (Eq. 2–8) for the vehicle is therefore $\text{MR} = m_f/m_0 = 130/200 = 0.65$, and the the propulsion unit is $(130 - 110)/(200 - 110) = 0.222$. Note that these are different. Now the propellant mass fraction of the propulsion system is

$$\zeta = 70/(200 - 110) = 0.778$$

Note that this mass fraction is acceptable for tactical missiles but might be only “fair” for spacecraft. Because the effective exhaust velocity is proportional to the specific impulse, $c = 240 \times 9.81 = 2354.4 \text{ m/sec}$. The propellant mass flow rate is $\dot{m} = 70/3 = 23.3 \text{ kg/sec}$ and the thrust becomes (Eq. 2–5)

$$F = 23.3 \times 2354.4 = 54,936 \text{ N}$$

Now the total impulse can be calculated as $I_t = 54936 \times 3 = 164,808 \text{ N-sec}$. The impulse-to-weight ratio (Eq. 2–11) for the propulsion system at the earth's surface is $I_t/w_0 = 164,808/[(200 - 110)9.81] = 187 \text{ sec}$ (this reflects only a fair design because $I_s = 240 \text{ sec}$).

For a horizontal trajectory, the maximum acceleration is found at the end of the thrusting schedule just before shutdown (because while the thrust is unchanged the mass is now at its minimum value of 130 kg).

$$\text{Final acceleration} = F/m = 54,936/130 = 422.58 \text{ m/sec}^2$$

This represents $43.08 g_0$'s, at the earth's surface and exceeds the limit of the equipment.

2.2. THRUST

The thrust is the force produced by a rocket propulsion system acting upon a vehicle. In a simplified way, it is the reaction experienced by its structure due to the ejection of matter at high velocity. It represents the same phenomenon that

pushes a garden hose backwards or makes a gun recoil. In the latter case, the forward momentum of the bullet and the powder charge is equal to the recoil or rearward momentum of the gun barrel. Momentum is a vector quantity and is defined as the product of mass times velocity. All ship propellers and oars generate their forward push at the expense of the momentum of the water or air masses, which are accelerated toward the rear. Rocket propulsion differs from these devices primarily in the relative magnitude of the accelerated masses and velocities. In rocket propulsion relatively small masses are involved that are *carried within* the vehicle and ejected at high velocities.

The thrust, due to a change in momentum, is given below. A derivation can be found in earlier editions of this book. The thrust and the mass flow are constant and the gas exit velocity is uniform and axial.

$$F = \frac{dm}{dt}v_2 = \dot{m}v_2 = \frac{\dot{w}}{g_0}v_2 \quad (2-13)$$

This force represents the total propulsion force when the nozzle exit pressure equals the ambient pressure.

The pressure of the surrounding fluid (i.e., the local atmosphere) gives rise to the second contribution that influences the thrust. Figure 2–1 shows schematically the external pressure acting uniformly on the outer surface of a rocket chamber and the changing gas pressures on the inside of a typical thermal rocket engine. The size and length of the arrows indicates the relative magnitude of the pressure

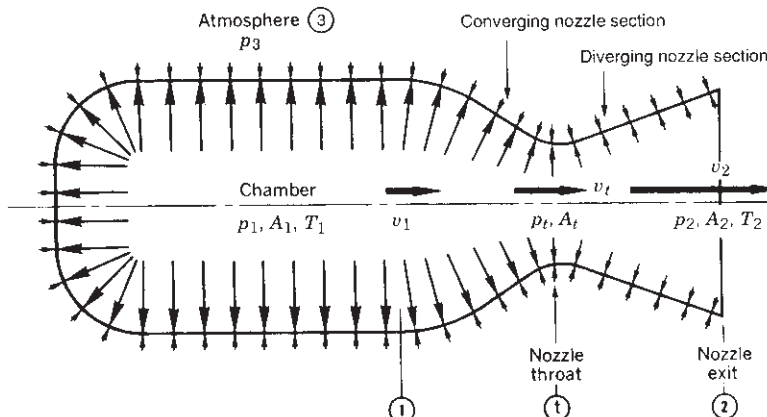


FIGURE 2–1. Pressure balance on chamber and nozzle interior walls is not uniform. The internal gas pressure (indicated by length of arrows) is highest in the chamber (p_1) and decreases steadily in the nozzle until it reaches the nozzle exit pressure p_2 . The external or atmospheric pressure p_3 is uniform. At the throat the pressure is p_t . The four subscripts (shown inside circles) refer to the quantities A , v , T , and p at specific locations.

forces. The axial thrust can be determined by integrating all the pressures acting on areas that can be projected on a plane normal to the nozzle axis. The forces acting radially outward are appreciable but do not contribute to the axial thrust because a rocket is typically an axially symmetric chamber. The conditions prior to entering the nozzle are essentially stagnation conditions.

Because of a fixed nozzle geometry and changes in ambient pressure due to variations in altitude, there can be an imbalance of the external environment or atmospheric pressure p_3 and the local pressure p_2 of the hot gas jet at the exit plane of the nozzle. Thus, for a steadily operating rocket propulsion system moving through a homogeneous atmosphere, the total thrust is equal to (this equation is arrived at using the *control volume* approach in gas dynamics; see Refs. 2–3 and 2–4):

$$F = \dot{m}v_2 + (p_2 - p_3)A_2 \quad (2-14)$$

The first term is the *momentum thrust* represented by the product of the propellant mass flow rate and its exhaust velocity relative to the vehicle. The second term represents the *pressure thrust* consisting of the product of the cross-sectional area at the nozzle exit A_2 (where the exhaust jet leaves the vehicle) and the difference between the exhaust gas pressure at the exit and the ambient fluid pressure. If the exhaust pressure is less than the surrounding fluid pressure, the pressure thrust is negative. Because this condition gives a low thrust and is undesirable, the rocket nozzle is usually so designed that the exhaust pressure is equal or slightly higher than the ambient fluid pressure.

When the ambient atmosphere pressure is equal to the exhaust pressure, the pressure term is zero and the thrust is the same as in Eq. 2–13. In the vacuum of space $p_3 = 0$ and the thrust becomes

$$F = \dot{m}v_2 + p_2A_2 \quad (2-15)$$

At the altitude where the exhaust pressure is exactly equal to the surrounding fluid pressure ($p_2 = p_3$) the pressure thrust is zero. For any nozzle this occurs only at one attitude, and this is referred to as the rocket nozzle with *optimum nozzle expansion ratio* A_2/A_t . This is further elaborated in Chapter 3.

Equation 2–14 shows that the thrust of a rocket unit is independent of the flight velocity. Because changes in ambient pressure affect the pressure thrust, there is a variation of the rocket thrust with altitude. Because atmospheric pressure decreases with increasing altitude, the thrust and the specific impulse will increase as the vehicle is propelled to higher altitudes. This change in pressure thrust due to altitude changes can amount to between 10 and 30% of the overall thrust, as is shown for a typical rocket engine in Fig. 2–2. Table 8–1 shows the sea level and high-altitude thrust for several rocket engines. Appendix 2 gives the properties of the standard atmosphere (ambient pressure p_3).

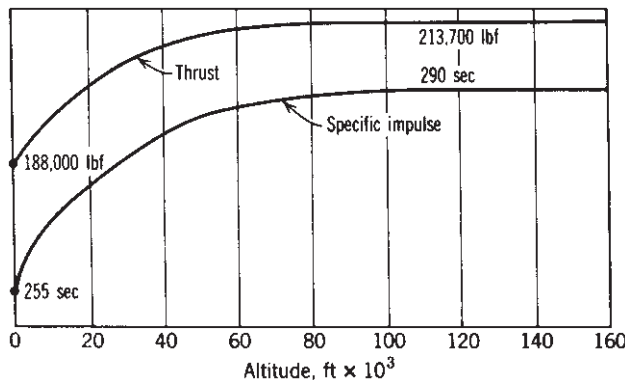


FIGURE 2–2. Altitude performance of RS 27 liquid propellant rocket engine used in early versions of the Delta launch vehicle.

2.3. EXHAUST VELOCITY

The *effective exhaust velocity* as defined by Eq. 2–6 applies to all rockets that thermodynamically expand hot gas in a nozzle and, indeed, to all mass expulsion systems. From Eq. 2–14 and for constant propellant mass flow this can be modified to

$$c = v_2 + (p_2 - p_3)A_2/\dot{m} \quad (2-16)$$

Equation 2–6 shows that c can be determined from thrust and propellant flow measurements. When $p_2 = p_3$, the effective exhaust velocity c is equal to the average actual exhaust velocity of the propellant gases v_2 . When $p_2 \neq p_3$, then $c \neq v_2$. The second term of the right-hand side of Eq. 2–16 is usually small in relation to v_2 ; thus the effective exhaust velocity is usually close in value to the actual exhaust velocity. When $c = v_2$, the thrust (from Eq. 2–14) can be rewritten as

$$F = (\dot{w}/g_0)v_2 = \dot{m}c \quad (2-17)$$

The *characteristic velocity* has been used frequently in the rocket propulsion literature. Its symbol c^* , pronounced “cee-star,” is defined as

$$c^* = p_1 A_t / \dot{m} \quad (2-18)$$

The characteristic velocity c^* is used in comparing the relative performance of different chemical rocket propulsion system designs and propellants; it is easily determined from measured data of \dot{m} , p_1 , and A_t . It relates to the efficiency of the combustion and is essentially independent of nozzle characteristics.

However, the specific impulse I_s and the effective exhaust velocity c are functions of the nozzle geometry, such as the nozzle area ratio A_2/A_t , as shown in Chapter 3. Some values of I_s and c^* are given in Tables 5–5 and 5–6.

Example 2–2. The following measurements were made a sea-level test of a solid propellant rocket motor (all cross sections are circular and unchanging):

| | |
|---------------------------------|----------|
| Burn duration | 40 sec |
| Initial propulsion system mass | 1210 kg |
| Mass of rocket motor after test | 215 kg |
| Sea-level thrust | 62,250 N |
| Chamber pressure | 7.00 MPa |
| Nozzle exit pressure | 70.0 kPa |
| Nozzle throat diameter | 8.55 cm |
| Nozzle exit diameter | 27.03 cm |

Determine \dot{m} , v_2 , c^* , and c at sea level. Also, determine the *pressure thrust* and specific impulse at sea level, 1000 m, and 25,000 m altitude. Assume the momentum thrust is invariant during the ascent, and the start and stop transients are short.

SOLUTION. The cross sections corresponding to the given diameters are $A_t = 0.00574$ and $A_2 = 0.0574 \text{ m}^2$ (i.e., an area ratio of 10). The mass flow rate for all altitudes is

$$\dot{m} = (1210 - 215)/40 = 24.88 \text{ kg/sec}$$

The desired c^* (all altitudes) and c at sea level follow (Eqs. 2–6 and 2–18):

$$c^* = p_1 A_t / \dot{m} = 7.00 \times 106 \times 0.00574 / 24.88 = 1615 \text{ m/sec}$$

$$c = F / \dot{m} = 62250 / 24.88 = 2502 \text{ m/sec}$$

The *pressure thrust* at sea level is

$$(p_2 - p_3)A_2 = (0.070 - 0.1013) \times 10^6 \times 0.0574 = -1797 \text{ N}$$

so the nozzle exit velocity becomes (all altitudes), from Eq. 2–14,

$$v_2 = (62250 - 1797) / 24.88 = 2430 \text{ m/sec}$$

The remaining answers are shown in the table below. We obtain the ambient pressures from Appendix 2.

| Altitude | p_3 (kPa) | Pressure Thrust (N) | I_s (sec) |
|-----------|-------------|---------------------|-------------|
| Sea level | 101.32 | -1798 | 248 |
| 1000 m | 89.88 | -1141 | 250 |
| 25,000 m | 2.55 | 3871 | 271 |

Further examination of the standard atmosphere table in Appendix 2 reveals that the *pressure thrust* becomes zero at an elevation of just under 3000 m.

2.4. ENERGY AND EFFICIENCIES

Although efficiencies are not commonly used directly in designing rocket units, they permit an understanding of the energy balance of a rocket system. Their definitions are arbitrary, depending on the losses considered, and any consistent set of efficiencies, such as the one presented in this section, is satisfactory in evaluating energy losses. As stated previously, two types of energy conversion processes occur in any propulsion system, namely, the generation of energy, which is really the conversion of stored energy into available energy and, subsequently, the conversion to the form in which a reaction thrust can be obtained. The kinetic energy of ejected matter is the form of energy useful for propulsion. The *power of the jet* P_{jet} is the time rate of expenditure of this energy, and for a constant gas ejection velocity v this is a function of I_s and F :

$$P_{\text{jet}} = \frac{1}{2}\dot{m}v^2 = \frac{1}{2}\dot{w}g_0I_s^2 = \frac{1}{2}Fg_0I_s = \frac{1}{2}Fv_2 \quad (2-19)$$

The term *specific power* is sometimes used as a measure of the utilization of the mass of the propulsion system including its power source; it is the jet power divided by the loaded propulsion system mass, P_{jet}/m_0 . For electrical propulsion systems that carry a heavy, relatively inefficient energy source, the specific power can be much lower than that of chemical rockets. The energy input from the energy source to the rocket propulsion system has different forms in different rocket types. For chemical rockets the energy is created by combustion. The maximum energy available per unit mass of chemical propellants is the heat of the combustion reaction Q_R ; the *power input to a chemical engine* is

$$P_{\text{chem}} = \dot{m}Q_RJ \quad (2-20)$$

where J is a conversion constant that depends on the units used. A large portion of the energy of the exhaust gases is unavailable for conversion into kinetic energy and leaves the nozzle as residual enthalpy. This is analogous to the energy lost in the hot exhaust gases of internal combustion engines.

The *combustion efficiency* for chemical rockets is the ratio of the actual and the ideal heat of reaction per unit of propellant and is a measure of the source efficiency for creating energy. Its value is high (approximately 94 to 99%), and it is defined in Chapter 3. When the power input P_{chem} is multiplied by the combustion efficiency, it becomes the power available to the propulsive device, where it is converted into the kinetic power of the exhaust jet. In electric propulsion the analogous efficiency is the power conversion efficiency. For solar cells it has a low value; it is the efficiency for converting solar radiation energy into electric power (10 to 20%).

The *power transmitted to the vehicle* at any one time is defined in terms of the thrust of the propulsion system F and the vehicle velocity u :

$$P_{\text{vehicle}} = Fu \quad (2-21)$$

The *internal efficiency* of a rocket propulsion system is an indication of the effectiveness of converting the system's energy input to the propulsion device into the kinetic energy of the ejected matter; for example, for a chemical unit it is the ratio of the kinetic power of the ejected gases expressed by Eq. 2–19 divided by the power input of the chemical reaction as given in Eq. 2–20. Internal efficiencies are used in Example 2–4. The energy balance diagram for a chemical rocket (Fig. 2–3) shows typical losses. The internal efficiency can be expressed as

$$\eta_{\text{int}} = \frac{\text{kinetic power in jet}}{\text{available chemical power}} = \frac{\frac{1}{2}\dot{m}v^2}{\eta_{\text{comb}}P_{\text{chem}}} \quad (2-22)$$

Typical values of η_{int} are listed later in Example 2–4.

An object moving through a fluid affects the fluid (i.e., stirs it) in ways that may hinder its motion and/or require extra energy expenditures. This is one consequence of skin friction and can be substantial. The *propulsive efficiency* (Fig. 2–4) reflects this energy cost for rocket vehicles. The equation that determines how much of the kinetic energy of the exhaust jet is useful for propelling a rocket vehicle is defined as

$$\begin{aligned} \eta_p &= \frac{\text{vehicle power}}{\text{vehicle power} + \text{residual kinetic jet power}} \\ &= \frac{Fu}{Fu + \frac{1}{2}\dot{m}(c-u)^2} = \frac{2u/c}{1 + (u/c)^2} \end{aligned} \quad (2-23)$$

where F is the thrust, u the absolute vehicle velocity, c the effective rocket exhaust velocity with respect to the vehicle, \dot{m} the propellant mass flow rate, and η_p the propulsive efficiency. The propulsive efficiency is a maximum when the

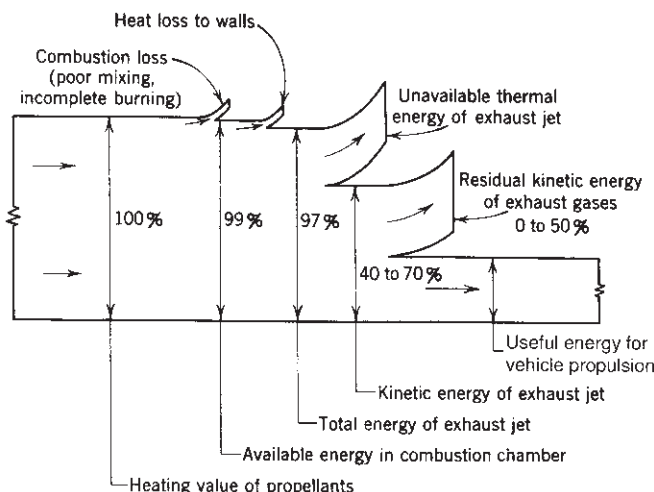


FIGURE 2–3. Typical energy balance diagram for a chemical rocket.

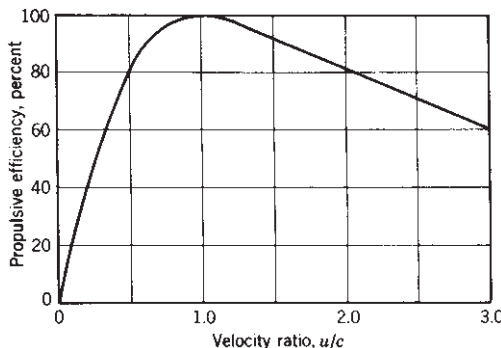


FIGURE 2–4. Propulsive efficiency at varying velocities.

forward vehicle velocity is exactly equal to the exhaust velocity. Then the residual kinetic energy and the absolute velocity of the jet are zero and the exhaust gases stand still in space.

While it is desirable to use energy economically and thus have high efficiencies, there is also the problem of minimizing the expenditure of ejected mass, which in many cases is more important than minimizing the energy. In nuclear reactor energy and some solar energy sources, for example, there is an almost unlimited amount of heat energy available; yet the vehicle can only carry a limited amount of working fluid. Economy of mass expenditures of working fluid can be obtained if the exhaust velocity is high. Because the specific impulse is proportional to the exhaust velocity, it is a measure of this propellant mass economy.

2.5. MULTIPLE PROPULSION SYSTEMS

The relationships below are for determining the overall (oa) or total thrust and the overall mass flow of propellants for a group of propulsion systems (two or more) firing in parallel (i.e., in the same direction at the same time). These relationships apply to liquid propellant rocket engines, solid propellant rocket motors, electrical propulsion systems, hybrid propulsion systems, and to any combinations of these. Many space launch vehicles and larger missiles have multiple propulsion systems. The Space Shuttle, for example, has three larger liquid engines and two large solid motors firing jointly at liftoff.

The overall thrust, F_{oa} , is needed for determining the flight path, and the overall mass flow rate, \dot{m}_{oa} , is needed for determining the vehicle's mass decrease with time. Together these two determine the overall specific impulse, $(I_s)_{\text{oa}}$:

$$F_{\text{oa}} = \sum F = F_1 + F_2 + F_3 + \dots \quad (2-24)$$

$$\dot{m}_{\text{oa}} = \sum \dot{m} = \dot{m}_1 + \dot{m}_2 + \dot{m}_3 + \dots \quad (2-25)$$

$$(I_s)_{\text{oa}} = \sum F / (g_0 \sum \dot{m}) \quad (2-26)$$

For liquid propellant rocket engines with a turbopump and a gas generator, there is a separate turbine outlet flow that is usually dumped overboard through a pipe and a nozzle (see Fig. 1–4), which needs to be included in the equations above.

Example 2–3. The MA-3 multiple liquid engine for the Atlas missile has two booster engines ($F = 165,000$ lbf at sea level and $\dot{m} = 66.7$ lbm/sec each). The turbine exhaust gas of both boosters provides an extra 2300 lbf of thrust at a propellant flow rate of about 3.3 lbm/sec. These booster engines are dropped from the vehicle after about 145 sec operation. The central sustainer rocket engine, which also starts at liftoff, continues to operate for 300 sec. It has a sea-level thrust of 57,000 lbf at a mass flow of 27.05 lbm/sec. Its turbine exhaust gases are aspirated into the nozzle of the engine. There are also two small vernier engines used for roll control of the vehicle during the sustainer-only portion of the flight. They each have a thrust of 415 lbf at sea level with a propellant flow of 0.213 lbm/sec. Determine the overall thrust F_{oa} and the overall mass flow rate \dot{m}_{oa} at liftoff, when all the nozzles are pointing vertically down.

SOLUTION. Use Eqs. 2–24 and 2–25. The thrust from the turbine must be included in 2–24.

$$F_{\text{oa}} = 165,000 \times 2 + 2300 \times 2 + 57,000 + 415 \times 2 = 390,430 \text{ lbf}$$

$$\dot{m}_{\text{oa}} = 66.7 \times 2 + 3.3 \times 2 + 27.05 + 0.213 \times 2 = 167.5 \text{ lbm/sec}$$

2.6. TYPICAL PERFORMANCE VALUES

Typical values of representative performance parameters for different types of rocket propulsion are given in Table 2–1 and in Fig. 2–5.

Chemical rockets have relatively low values of specific impulse, relatively light machinery (i.e., low engine weight), a very high thrust capability, and therefore high acceleration and high specific power. At the other extreme, the ion propulsion devices have a very high specific impulse, but they must carry a heavy electrical power source with them to deliver the power necessary for high ejection velocities. The very low acceleration potential for the electrical propulsion units and those using solar radiation energy usually requires a long period for accelerating and thus these systems are best used for missions where the flight time is long. The low thrust values of electrical systems imply that they are not useful in fields of strong gravitational gradients (for takeoff or landing) but are best used in a true space flight mission.

The chemical systems (solid and liquid propellant rockets) are fully developed and widely used for many different vehicle applications. They are described in Chapters 5 to 16. Electrical propulsion has been in operation in many space flight applications (see Chapter 17). Some of the other types are still in their exploratory or development phase, but may become useful.

Example 2–4. Compare the types of propulsion system tabulated below by computing the power input and propellant flow required for each to deliver 106.8 N (25 lbf) of thrust.

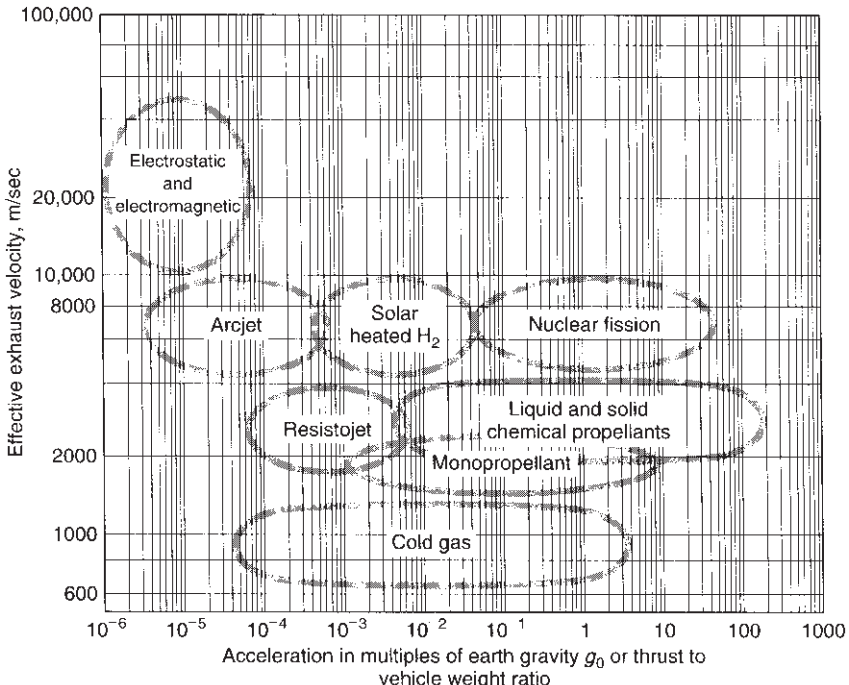


FIGURE 2–5. Exhaust velocities as a function of typical vehicle accelerations. Regions indicate approximate performance values for different types of propulsion systems. The mass of the vehicle includes the propulsion system, but the payload is assumed to be zero.

SOLUTION. From Eqs. 2–13 and 2–19 and assuming that $v_2 = c$,

$$\dot{m} = F/I_s g_0$$

$$\text{Power input} = P_{\text{jet}}/\eta_{\text{int}} = 1/2 \dot{m} v_2^2 / \eta_{\text{int}}$$

| Engine Type | η_{int} | I_s (sec) | v_2 (m/sec) | \dot{m} (kg/sec) | $P_{\text{input}}(\text{kW})$ |
|--------------------|---------------------|-------------|---------------|--------------------|-------------------------------|
| Chemical rocket | 0.70 | 300 | 2,943 | [0.0363] | [225] |
| Nuclear fission | 0.50 | 800 | 7,848 | [0.0136] | [838] |
| Arc-electrothermal | 0.40 | 600 | 5,886 | [0.0181] | [785] |
| Ion electrostatic | 0.65 | 2000 | 19,620 | [0.0054] | [1612] |

Results are shown inside square brackets in the table. More than half a megawatt input is needed for the last three propulsion systems but note that the propellant flows are small. These data are only illustrative because to date there are no single arc or ion thrusters that supply the required thrust so multiple units would be required. Electric propulsion is presently restricted to thrust levels of less than one newton in part because of the lack

of such large electrical power supplies. Nuclear propulsion units are not available at the present time so chemical propulsion would remain as the only option. Note that it would be more realistic to compare total impulse because thrust times can vary between types.

Variable Thrust

There are flight missions that require a change in thrust during flight. Some solid rocket propellant motors can have a fixed predetermined thrust usually consisting of an initial short duration high-thrust boost phase followed by a lower thrust longer sustaining phase. Details may be found in Section 12.3. Some liquid propellant rocket engines can have random variable thrust that can be adjusted during flight. Details are in Section 8.7. In small low-thrust liquid propellant attitude control thrusters, it is possible to control the number and/or timing of repeated short pulses to achieve a variable thrust effect. This concept is discussed in Section 8.3.

A predetermined thrust decrease (used in some solid propellant rocket motors) can be obtained with a special design of the grain allowing a high-thrust period (for missile acceleration) followed by a low-thrust period for maintaining the flight velocity against atmospheric drag. Alternatively, it may be a special two-pulse motor with two different grain compositions in the same combustion chamber, one for a high-thrust boost phase and one for a subsequent low-thrust sustaining phase. Both of these are discussed in Chapter 12.

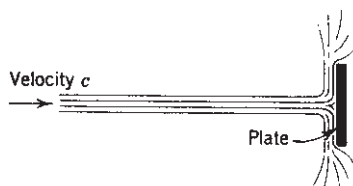
Some solid propellant and liquid propellant experimental propulsion systems have used variable nozzle throat areas (achieved with a variable position “tapered pintle” at the nozzle throat) and one experimental version has flown. To date, there has been no published information on the further production and implementation of such systems.

PROBLEMS

When solving problems, three appendixes (see end of book) may be helpful:

- Appendix 1. Conversion Factors and Constants
- Appendix 2. Properties of the Earth’s Standard Atmosphere
- Appendix 3. Summary of Key Equations

1. A jet of fluid hits a stationary flat plate in the manner shown below.



- (a) If there is 50 kg of fluid flowing per minute at an absolute velocity of 200 m/sec, what will be the force on the plate?

Answer: 167 N.

- (b) What will this force be when the plate moves in the direction of flow at $u = 50$ km/h? Explain the methodology.

Answer: 144 N.

2. The following data are given for a certain rocket unit: thrust, 8896 N; propellant consumption, 3,867 kg/sec; velocity of vehicle, 400 m/sec; energy content of propellant, 6.911 MJ/kg. Assume 100% combustion efficiency.

Determine (a) the effective velocity; (b) the kinetic jet energy rate per unit flow of propellant; (c) the internal efficiency; (d) the propulsive efficiency; (e) the overall efficiency; (f) the specific impulse; (g) the specific propellant consumption.

Answers: (a) 2300 m/sec; (b) 2.645 MJ/kg; (c) 38.3%; (d) 33.7%; (e) 13.3%; (f) 234.7 sec; (g) 0.00426 sec⁻¹.

3. A certain rocket has an effective exhaust velocity of 7000 ft/sec; it consumes 280 lbm/sec of propellant mass, each of which liberates 2400 Btu/lbm. The unit operates for 65 sec. Construct a set of curves plotting the propulsive, internal, and overall efficiencies versus the velocity ratio u/c ($0 < u/c < 1.0$). The rated flight velocity equals 5000 ft/sec. Calculate (a) the specific impulse; (b) the total impulse; (c) the mass of propellants required; (d) the volume that the propellants occupy if their average specific gravity is 0.925.

Answers: (a) 217.5 sec; (b) 3,960,000 lbf-sec; (c) 18,200 lbm; (d) 315 ft³.

4. For the rocket in Problem 2, calculate the specific power, assuming a propulsion system dry mass of 80 kg and a duration of 3 min.

5. A Russian rocket engine (RD-110) consists of four nonmoveable thrust chambers supplied by a single turbopump. The exhaust from the turbine of the turbopump then drives four vernier chamber nozzles (which can be rotated to provide some control of the flight path). Using the information below, determine the thrust, effective exhaust velocity, and mass flow rate of the four vernier thrusters.

Individual thrust chambers (vacuum):

$$F = 73.14 \text{ kN}, c = 3279 \text{ m/sec}$$

Overall engine with verniers (vacuum):

$$F = 297.93 \text{ kN}, c = 3197 \text{ m/sec}$$

Answers: 5.358 kN, 1351 m/sec, 3.965 kg/sec.

6. A certain rocket engine has a specific impulse of 250 sec. What range of vehicle velocities (u , in units of ft/sec) would keep the propulsive efficiencies at or greater than 80%. Also, how could rocket-vehicle staging be used to maintain these high propulsive efficiencies for the range of vehicle velocities encountered during launch?

Answers: 4021 to 16,085 ft/sec; design upper stages with increasing I_s .

7. Plot the variation of the thrust and specific impulse against altitude, using the atmospheric pressure information given in Appendix 2, and the data for the Minuteman first-stage rocket thrust chamber in Table 12–3. Assume that $p_2 = 8.66$ psia.
8. During the boost phase, the three Space Shuttle main engines (SSMEs) operate together with the two solid propellant rocket motors (SRBs) for the first 2 minutes. For the remaining thrust time, the SSMEs operate alone. Using Table 1–4, calculate the *overall specific impulse* for the vehicle during the 2-minute combined thrust operation.
Answer: 310 sec.
9. For the values given in Table 2–1 for the various propulsion systems, calculate the total impulse for a fixed propellant mass of 2000 kg.

SYMBOLS (English engineering units are given in parentheses)

| | |
|---------------------|--|
| A | area, $\text{m}^2(\text{ft}^2)$ |
| A_t | nozzle throat area, $\text{m}^2(\text{ft}^2)$ |
| A_2 | exit area of nozzle, $\text{m}^2(\text{ft}^2)$ |
| c | effective velocity, m/sec (ft/sec) |
| c^* | characteristic velocity, m/sec (ft/sec) |
| E | energy, J (ft-lbf) |
| F | thrust force, N (lbf) |
| F_{oa} | overall force, N (lbf) |
| g_0 | standard sea-level acceleration of gravity, $9.80665 \text{ m/sec}^2(32.174 \text{ ft/sec}^2)$ |
| I_s | specific impulse, sec |
| $(I_s)_{\text{oa}}$ | overall specific impulse, sec |
| I_t | impulse or total impulse, N-sec (lbf-sec) |
| J | conversion factor or mechanical equivalent of heat, 4.184 J/cal or 1055 J/Btu or 778 ft-lbf/Btu |
| m | mass, kg (slugs) (1 slug = mass of 32.174 lb of weight at sea level) |
| m_{oa} | overall mass, kg |
| \dot{m} | mass flow rate, kg/sec (lbm/sec) |
| m_f | final mass (after rocket propellant is ejected), kg (lbm or slugs) |
| m_p | propellant mass, kg (lbm or slugs) |
| m_0 | initial mass (before rocket propellant is ejected), kg (lbm or slugs) |
| MR | mass ratio (m_f/m_0) |
| p | pressure, pascal [Pa] or $\text{N/m}^2(\text{lbf/ft}^2)$ |
| p_3 | ambient or atmospheric pressure, Pa (lbf/ft^2) |
| p_2 | rocket gas pressure at nozzle exit, Pa (lbf/ft^2) |
| p_1 | chamber pressure, Pa (lbf/ft^2) |
| P | power, $\text{J/sec (ft-lbf/sec)}$ |
| P_s | specific power, $\text{J/sec-kg (ft-lbf/sec-lbm)}$ |

| | |
|-----------|--|
| Q_R | heat of reaction per unit propellant, J/kg (Btu/lbm) |
| t | time, sec |
| u | vehicle velocity, m/sec (ft/sec) |
| v_2 | gas velocity leaving the rocket, m/sec (ft/sec) |
| w | weight, N or kg-m/sec ² (lbf) |
| \dot{w} | weight flow rate, N/sec (lbf/sec) |
| w_0 | initial weight, N or kg-m/sec ² (lbf) |

Greek Letters

| | |
|----------------------|--------------------------|
| ζ | propellant mass fraction |
| η | efficiency |
| η_{comb} | combustion efficiency |
| η_{int} | internal efficiency |
| η_p | propulsive efficiency |

REFERENCES

- 2–1. “American National Standard Letter Symbols for Rocket Propulsion”, *ASME Publication Y 10.14*, 1959.
- 2–2. “Solid Propulsion Nomenclature Guide,” *CPIA Publication 80*, Chemical Propulsion Information Agency, Johns Hopkins University, Laurel, MD, May 1965, 18 pages.
- 2–3. P. G. Hill and C. R. Peterson, *Mechanics and Thermodynamics of Propulsion*, Addison-Wesley, Reading, MA, 1992.
- 2–4. R. D. Zucker and O. Biblarz, *Fundamentals of Gas Dynamics*, 2nd ed., John Wiley & Sons, Hoboken, NJ, 2002.

CHAPTER 3

NOZZLE THEORY AND THERMODYNAMIC RELATIONS

Thermodynamic relations of the processes inside a rocket nozzle and chamber furnish the mathematical tools needed to calculate the performance and determine several of the key design parameters of rocket propulsion systems. They are useful as a means of evaluating and comparing the performance of various rocket systems; they permit the prediction of the operating performance of any rocket unit that uses the thermodynamic expansion of a gas and the determination of several necessary design parameters, such as nozzle size and generic shape, for any given performance requirement. This theory applies to chemical rocket propulsion systems (both liquid and solid and hybrid propellant types), nuclear rockets, solar-heated and resistance or arc-heated electrical rocket systems, and to any propulsion system that uses the expansion of a gas as the propulsive mechanism for ejecting matter at high velocity.

These thermodynamic relations, which are fundamental and important in analysis and design of rocket units, are introduced and explained in this chapter. The utilization of these equations should give the reader a basic understanding of the thermodynamic processes involved in rocket gas behavior and expansion. A knowledge of elementary thermodynamics and fluid mechanics on the part of the reader is assumed (see Refs. 3–1, 3–2, and 3–3). This chapter also addresses different nozzle configurations, nonoptimum performance, energy losses, nozzle alignment, variable thrust, and four different ways for establishing nozzle performance parameters.

3.1. IDEAL ROCKET

The concept of ideal rocket propulsion systems is useful because the relevant basic thermodynamic principles can be expressed as simple mathematical relationships, which are given in subsequent sections of this chapter. These equations theoretically describe a quasi-one-dimensional nozzle flow, which corresponds to an idealization and simplification of the full two- or three-dimensional equations and the real aerothermochemical behavior. However, with the assumptions and simplifications stated below, they are very adequate for obtaining useful solutions to many rocket propulsion systems and preliminary design tasks. For chemical rocket propulsion the measured actual performance is usually between 1 and 6% below the calculated ideal value. In designing new rockets, it has become accepted practice to use ideal rocket parameters that can then be modified by appropriate corrections, such as those discussed in Section 3.5. An *ideal rocket* unit is one for which the following assumptions are valid:

1. The working substance (or chemical reaction products) is *homogeneous*.
2. All the species of the working fluid are *gaseous*. Any condensed phases (liquid or solid) add a negligible amount to the total mass.
3. The working substance obeys the *perfect gas law*.
4. There is no *heat transfer* across the rocket walls; therefore, the flow is adiabatic.
5. There is no appreciable *friction* and all *boundary layer* effects are neglected.
6. There are no *shock waves* or *discontinuities* in the nozzle flow.
7. The *propellant flow* is *steady* and *constant*. The expansion of the working fluid is uniform and steady, without vibration. Transient effects (i.e., start-up and shutdown) are of very short duration and may be neglected.
8. All exhaust gases leaving the rocket have an *axially directed velocity*.
9. The gas velocity, pressure, temperature, and density are all uniform across any section normal to the nozzle axis.
10. *Chemical equilibrium* is established within the rocket chamber and the gas composition does not change in the nozzle (frozen flow).
11. Stored propellants are at room temperature. Cryogenic propellants are at their boiling points.

These assumptions permit the derivation of a simple, quasi-one-dimensional theory as mentioned in subsequent sections. Later in this book we present more sophisticated theories or introduce correction factors for several of the items on the list, and they allow a more accurate determination of the simplified analysis. The next paragraph explains why these assumptions cause only small errors.

For a liquid bipropellant rocket the idealized theory postulates an injection system in which the fuel and oxidizer are mixed perfectly so that a homogeneous working substance results. A good rocket injector can approach this condition

closely. For a solid propellant rocket unit, the propellant must essentially be homogeneous and uniform and the burning rate must be steady. For nuclear, solar-heated or arc-heated rockets, it is assumed that the hot gases are uniform in temperature at any cross section and steady in flow. Because chamber temperatures are typically high (2500 to 3600 K for common propellants), all gases are well above their respective saturation conditions and actually follow the perfect gas law very closely. Assumptions 4, 5, and 6 above allow the use of the *isentropic expansion* relations in the rocket nozzle, thereby describing the maximum conversion of heat to kinetic energy of the jet. This also implies that the nozzle flow is thermodynamically reversible. Wall friction losses are difficult to determine accurately, but they are usually negligible in nozzles. Except for very small chambers, the energy lost as heat to the walls of the rocket is usually less than 1% (occasionally up to 2%) of the total energy and can therefore often be neglected. Short-term fluctuations of the steady propellant flow rate and pressure are usually less than 5% of the rated value; their effect on rocket performance is small and can be neglected. In well-designed supersonic nozzles, the conversion of thermal energy into directed kinetic energy of the exhaust gases proceeds smoothly and without normal shocks or discontinuities; thus the flow expansion losses are generally small.

Some companies and some authors do not include all or the same 11 items listed above in their definition of an ideal rocket. For example, instead of assumption 8 (all nozzle exit velocity is axially directed), some use a conical exit nozzle with a 15° half-angle as their base configuration in their ideal nozzle; this discounts the divergence losses, which are described later in this chapter.

3.2. SUMMARY OF THERMODYNAMIC RELATIONS

In this section we review briefly some of the basic relationships needed for the development of the nozzle flow equations. Rigorous derivations and discussions of these relations can be found in many thermodynamics or fluid dynamics texts, such as Refs. 3–1 and 3–2.

The principle of *conservation of energy* can be readily applied to the adiabatic, no shaft-work process inside the nozzle. Furthermore, without shocks or friction, the flow entropy change is zero. The concept of *enthalpy* is useful in flow systems; the enthalpy comprises the *internal thermal energy* plus the *flow work* (or work performed by the gas at a velocity v in crossing a boundary). For ideal gases the enthalpy can conveniently be expressed as the product of the specific heat c_p times the absolute temperature T (the specific heat at constant pressure is formally defined as the partial derivative of the enthalpy with respect to temperature at constant pressure). Under the above assumptions, the total or stagnation enthalpy per unit mass h_0 is constant, that is,

$$h_0 = h + v^2/2J = \text{constant} \quad (3-1)$$

In the above, J is the mechanical equivalent of heat that is inserted only when thermal units (i.e., the Btu and calorie) are mixed with mechanical units (i.e., the ft-lbf and the joule). In SI units (kg, m, sec) the value of J is one. In the EE system of units the value of the constant J is given in Appendix 1. The conservation of energy for isentropic flow between any two sections x and y shows that the decrease in enthalpy or thermal content of the flow appears as an increase of kinetic energy since any changes in potential energy may be neglected.

$$h_x - h_y = \frac{1}{2}(v_y^2 - v_x^2)/J = c_p(T_x - T_y) \quad (3-2)$$

The principle of *conservatism of mass* in a steady flow with a single inlet and single outlet is expressed by equating the mass flow rate \dot{m} at any section x to that at any other section y ; this is known in mathematical form as the continuity equation. Written in terms of the cross-sectional area A , the velocity v , and the specific volume V ,

$$\dot{m}_x = \dot{m}_y \equiv \dot{m} = Av/V \quad (3-3)$$

The *perfect gas law* is written as

$$p_x V_x = RT_x \quad (3-4)$$

where the gas constant R is found from the universal gas constant R' divided by the molecular mass \mathfrak{M} of the flowing gas mixture. The molecular volume at standard conditions becomes $22.41 \text{ m}^3/\text{kg-mol}$ or $\text{ft}^3/\text{lb-mol}$ and it relates to a value of $R' = 8314.3 \text{ J/kg-mol-K}$ or $1544 \text{ ft-lbf/lb-mol}^\circ\text{R}$. One often finds Eq. 3-3 written in terms of density ρ which is the reciprocal of the specific volume V . The specific heat at constant pressure c_p , the specific heat at constant volume c_v , and their ratio k are constant for perfect gases over a wide range of temperatures and are related:

$$k = c_p/c_v \quad (3-5a)$$

$$c_p - c_v = R/J \quad (3-5b)$$

$$c_p = kR/(k - 1)J \quad (3-6)$$

For an *isentropic flow process* the following relations hold between any points x and y :

$$T_x/T_y = (p_x/p_y)^{(k-1)/k} = (V_y/V_x)^{k-1} \quad (3-7)$$

During an isentropic nozzle expansion the pressure drops substantially, the absolute temperature drops somewhat less, and the specific volume increases. When a flow is stopped isentropically the prevailing conditions are known as *stagnation conditions* and are designated by the subscript 0. Sometimes the word

“total” is used instead of stagnation. As can be seen from Eq. 3–1 the stagnation enthalpy consists of the sum of the static or local enthalpy and the fluid kinetic energy. The stagnation temperature T_0 is found from the energy equation as

$$T_0 = T + v^2/(2c_p J) \quad (3-8)$$

where T is the absolute fluid static temperature. In adiabatic flows, the stagnation temperature remains constant. The relationship of the stagnation pressure to the local pressure in the flow can be found from the previous two equations:

$$p_0/p = [1 + v^2/(2c_p JT)]^{k/(k-1)} = (V/V_0)^k \quad (3-9)$$

When the local velocity comes close to zero, the local temperature and pressure will approach the stagnation pressure and stagnation temperature. In a combustion chamber, where the gas velocity is small, the local combustion pressure is essentially equal to the stagnation pressure. The *velocity of sound* a or the acoustic velocity in ideal gases is independent of pressure. It is defined as

$$a = \sqrt{kRT} \quad (3-10)$$

In the EE system the value of R has to be corrected and the constant g_0 is added. Equation 3–10 becomes $\sqrt{g_0 kRT}$. This correction factor must be applied wherever R is used in EE units. The *Mach number* M is a dimensionless flow parameter and is used to define the ratio of the local flow velocity v to the local acoustic velocity a :

$$M = v/a = v/\sqrt{kRT} \quad (3-11)$$

A Mach number less than one corresponds to subsonic flow and greater than one to supersonic flow. When the Mach number is equal to one, then the flow is moving at precisely the velocity of sound. It is shown later that at the throat of all supersonic nozzles the Mach number must be equal to one. The relation between stagnation temperature and Mach number can now be written from Eqs. 3–2, 3–7, and 3–10 as

$$T_0 = T \left[1 + \frac{1}{2}(k - 1)M^2 \right] \quad (3-12)$$

or

$$M = \sqrt{\frac{2}{k-1} \left(\frac{T_0}{T} - 1 \right)}$$

T_0 and p_0 designate the stagnation values of the temperature and pressure. Unlike the temperature, the stagnation pressure during an adiabatic nozzle expansion remains constant only for isentropic flows. It can be computed from

$$p_0 = p \left[1 + \frac{1}{2}(k - 1)M^2 \right]^{k/(k-1)} \quad (3-13)$$

The expansion *area ratio* for a nozzle with isentropic flow can be expressed in terms of Mach numbers for any points x and y within the nozzle. This relationship, along with those for the ratios T/T_0 and p/p_0 , is plotted in Fig. 3–1 for $A_x = A_t$ and $M_x = 1.0$. Otherwise,

$$\frac{A_y}{A_x} = \frac{M_x}{M_y} \sqrt{\left\{ \frac{1 + [(k - 1)/2]M_y^2}{1 + [(k - 1)/2]M_x^2} \right\}^{(k+1)/(k-1)}} \quad (3-14)$$

As can be seen from Fig. 3–1, for subsonic flow the chamber contraction ratio A_1/A_t can be small, with values of 3 to 6, and the passage is convergent. There is no noticeable effect from variations of k . In solid rocket motors the chamber area A_1 refers to the flow passage or port cavity in the virgin grain. With supersonic flow the nozzle section diverges and the area ratio becomes large very quickly;

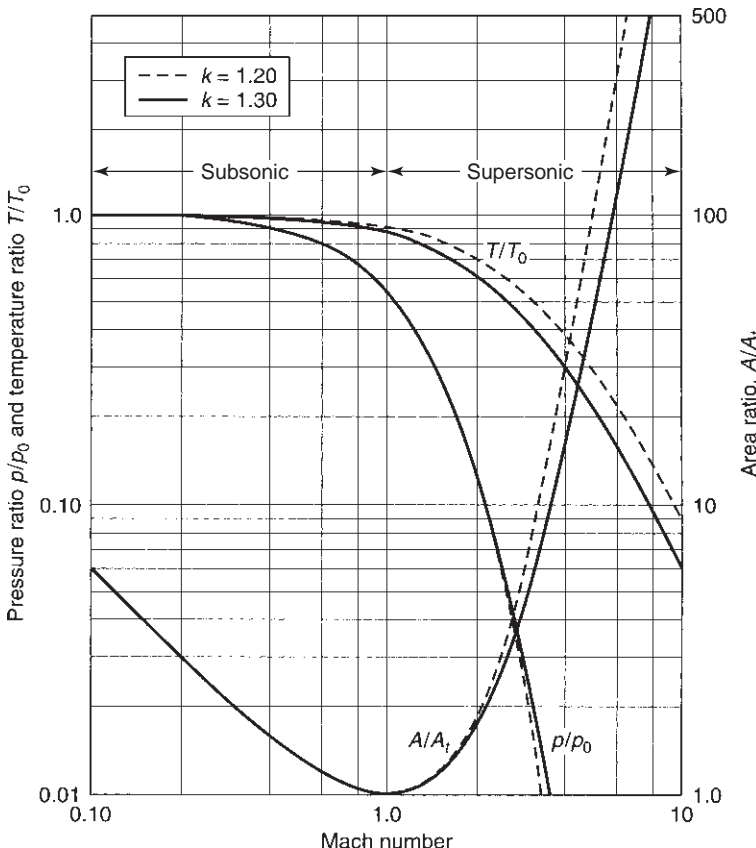


FIGURE 3–1. Relationship of area ratio, pressure ratio, and temperature ratio as functions of Mach number in a De Laval nozzle for the subsonic and supersonic nozzle regions.

the area ratio is significantly influenced by the value of k . The area ratio A_2/A_t ranges between 15 and 30 at $M = 4$, depending on the value of k . On the other hand, pressure ratios depend little on k whereas temperature ratios show more variation.

The average *molecular mass* \mathfrak{M} of a mixture of gases is the sum of all the molar fractions n_i multiplied by the molecular mass of each chemical species ($n_i\mathfrak{M}_i$) and then divided by the sum of all molar mass fractions. This is further discussed in Chapter 5. The symbol \mathfrak{M} is used to avoid confusion with M for the Mach number. In many pieces of rocket literature \mathfrak{M} is called molecular weight.

Example 3–1. An ideal rocket is designed to operate at sea level using a propellant whose products of combustion have a specific heat ratio k of 1.3. Determine the required chamber pressure if the exit Mach number is 2.52. Also determine the nozzle area ratio between the throat and exit.

SOLUTION. For optimum expansion the nozzle exit pressure must equal the local atmospheric pressure, which here has a value of 0.1013 MPa. If the chamber velocity may be neglected, then the ideal chamber pressure is the total stagnation pressure, which can be found from Eq. 3–13 as

$$\begin{aligned} p_0 &= p \left[1 + \frac{1}{2}(k - 1)M^2 \right]^{k/(k-1)} \\ &= 0.1013[1 + 0.15 \times 2.52^2]^{1.3/0.3} = 1.84 \text{ MPa} \end{aligned}$$

The ideal nozzle area is determined from Eq. 3–14 setting $M_t = 1.0$ at the throat (see also Fig. 3–1):

$$\begin{aligned} \frac{A_2}{A_t} &= \frac{1}{M_2} \left[\frac{1 + [(k - 1)/2]M_2^2}{(k + 1)/2} \right]^{(k+1)/2(k-1)} \\ &= \frac{1}{2.52} \left[\frac{1 + 0.15 \times 2.52^2}{1.15} \right]^{2.3/0.6} = 3.02 \end{aligned}$$

Note that *ideal* implies no losses, whereas *optimum* is a separate concept reflecting the best calculated performance at a particular set of given pressures. *Optimum* performance is often taken as the design condition and it occurs when $p_2 = p_3$ as will be shown in the section on the *thrust coefficient* (the peak of the curves in Figs. 3–7 and 3–8 for fixed p_1/p_3).

3.3. ISENTROPIC FLOW THROUGH NOZZLES

In a converging–diverging nozzle a large fraction of the thermal energy of the gases in the chamber is converted into kinetic energy. As will be explained, the gas pressure and temperature drop dramatically and the gas velocity can reach values in excess of 2 miles per second. This is a reversible, essentially isentropic flow process and its analysis is described here. If a nozzle inner wall has a flow obstruction or a wall protrusion (a piece of weld splatter or slag), then the kinetic

gas energy is locally converted back into thermal energy essentially equal to the stagnation temperature and stagnation pressure in the chamber. Since this would lead quickly to a local overheating and failure of the wall, nozzle inner walls have to be smooth without any protrusion. Stagnation conditions can also occur at the leading edge of a jet vane (described in Chapter 18) or at the tip of a gas sampling tube inserted into the flow.

Velocity

From Eq. 3–2 the nozzle exit velocity v_2 can be found:

$$v_2 = \sqrt{2J(h_1 - h_2) + v_1^2} \quad (3-15a)$$

This equation applies to ideal and nonideal rockets. For constant k this expression can be rewritten with the aid of Eqs. 3–6 and 3–7. The subscripts 1 and 2 apply to the nozzle inlet and exit conditions, respectively:

$$v_2 = \sqrt{\frac{2k}{k-1}RT_1 \left[1 - \left(\frac{p_2}{p_1} \right)^{(k-1)/k} \right] + v_1^2} \quad (3-15b)$$

This equation also holds for any two points within the nozzle. When the chamber section is large compared to the nozzle throat section, the chamber velocity or nozzle approach velocity is comparatively small and the term v_1^2 can be neglected. The chamber temperature T_1 is at the nozzle inlet and, under isentropic conditions, differs little from the stagnation temperature or (for a chemical rocket) from the combustion temperature. This leads to an important simplified expression of the exhaust velocity v_2 , which is often used in the analysis:

$$\begin{aligned} v_2 &= \sqrt{\frac{2k}{k-1}RT_1 \left[1 - \left(\frac{p_2}{p_1} \right)^{(k-1)/k} \right]} \\ &= \sqrt{\frac{2k}{k-1} \frac{R'T_0}{\mathfrak{M}} \left[1 - \left(\frac{p_2}{p_1} \right)^{(k-1)/k} \right]} \end{aligned} \quad (3-16)$$

It can be seen that the exhaust velocity of a nozzle is a function of the pressure ratio p_1/p_2 , the ratio of specific heats k , and the absolute temperature at the nozzle inlet T_1 , as well as the gas constant R . Because the gas constant for any particular gas is inversely proportional to the molecular mass \mathfrak{M} , the exhaust velocity or the specific impulse are a function of the ratio of the absolute nozzle entrance temperature divided by the molecular mass, as is shown in Fig. 3–2. This ratio plays an important role in optimizing the mixture ratio in chemical rockets.

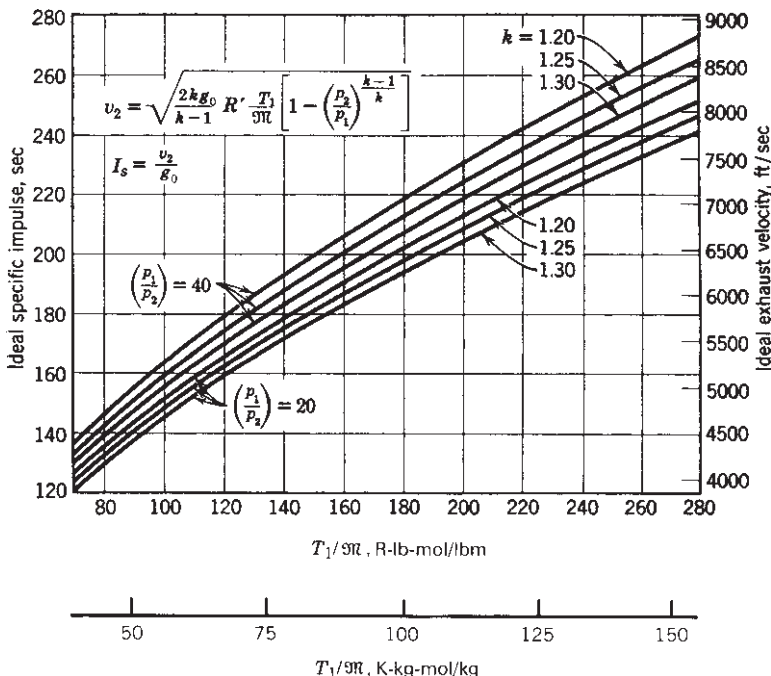


FIGURE 3–2. Specific impulse and exhaust velocity of an ideal rocket at optimum nozzle expansion as functions of the absolute chamber temperature T_1 and the molecular mass \mathfrak{M} for several values of k and p_1/p_2 .

Equations 2–14 and 2–15 give the relations between the velocity v_2 , the thrust F , and the specific impulse I_s ; it is plotted in Fig. 3–2 for two pressure ratios and three values of k . Equation 3–16 indicates that any increase in the gas temperature (usually caused by an increase in energy release) or any decrease of the molecular mass of the propellant (usually achieved by using light molecular mass gases rich in hydrogen content) will improve the performance of the rocket; that is, they will increase the specific impulse I_s or the exhaust velocity v_2 or c and, thus, the performance of the vehicle. The influences of the pressure ratio across the nozzle p_1/p_2 and of the specific heat ratio k are less pronounced. As can be seen from Fig. 3–2, performance increases with an increase of the pressure ratio; this ratio increases when the value of the chamber pressure p_1 increases or when the exit pressure p_2 decreases, corresponding to high altitude designs. The small influence of k values is fortuitous because low molecular masses are found in diatomic or monatomic gases, which have the higher values of k .

For comparing specific impulse values from one rocket system to another or for evaluating the influence of various design parameters, the value of the pressure ratio must be standardized. A chamber pressure of 1000 psia (6.894 Mpa) and an exit pressure of 1 atm (0.1013 Mpa) are generally in use today.

For *optimum expansion* $p_2 = p_3$ and the effective exhaust velocity c (Eq. 2–16) and the ideal rocket exhaust velocity are related, namely

$$v_2 = (c)_{\text{opt}} \quad (3-17)$$

and c can be substituted for v_2 in Eqs. 3–15 and 3–16. For a fixed nozzle exit area ratio, and constant chamber pressure, this optimum condition occurs only at a particular altitude where the ambient pressure p_3 happens to be equal to the nozzle exhaust pressure p_2 . At all other altitudes $c \neq v_2$.

The maximum theoretical value of the nozzle outlet velocity is reached with an infinite expansion (exhausting into a vacuum):

$$(v_2)_{\max} = \sqrt{2kRT_0/(k - 1)} \quad (3-18)$$

This maximum theoretical exhaust velocity is finite, even though the pressure ratio is infinite, because it represents the finite thermal energy content of the fluid. Such an expansion does not happen, because, among other things, the temperature of many of the working medium species will fall below their liquefaction or the freezing points; thus they cease to be a gas and no longer contribute to the gas expansion.

Example 3–2. A rocket operates near sea level with a chamber pressure of $p_1 = 2.068$ MPa or 300 psia, a chamber temperature of 2222 K, and a propellant consumption of $\dot{m} = 1.0$ kg/sec. Take $k = 1.30$ and $R = 345.7$ J/kg-K. Calculate the ideal thrust and the ideal specific impulse. Also plot the cross-section area A , the local velocity v , the specific volume V , the absolute temperature T , and the local Mach number M with respect to pressure along the nozzle.

SOLUTION. Assume that the operation of this rocket is at an optimum for expansion to sea-level pressure $p_3 = 0.1013$ MPa so that the ratio $p_2/p_1 = 0.049$ in Eq. 3–16. From this equation, the effective exhaust velocity is calculated to be 1827 m/sec since here $v_2 = c$. Hence,

$$I = c/g_0 = 1827/9.81 = 186 \text{ sec} \quad \text{and}$$

$$F = \dot{m}c = 1.0 \times 1827 = 1827 \text{ N}$$

In order to graph the desired variables as a function of pressure along the nozzle, we have to express them in analytically useful ways. In this chapter, we denote the nozzle axial location x as either the chamber (location 1) or the throat (location t) and keep the axial location y as a variable which spans the range 1 → 2 (see Fig. 2–1). The initial specific volume V_1 is calculated from the equation of state of a perfect gas (Eq. 3–4),

$$V_1 = RT_1/p_1 = 345.7 \times 2222/(2.068 \times 10^6) = 0.3714 \text{ m}^3/\text{kg}$$

Now we can write equations for the specific volume and the temperature (Eq. 3–7) as

$$V_y = V_1(p_1/p_y)^{1/k} = 0.3714(2.068/p_y)^{0.769} \text{ (m}^3/\text{kg)}$$

$$T_y = T_1(p_y/p_1)^{(k-1)/k} = 2222(p_y/2.068)^{0.231} \text{ (K)}$$

These can be plotted by inserting p_y values between 2.068 and 0.1013 in MPa. The calculations for the velocity follow from Eq. 3–16 (the derivations have been omitted in order to focus on the plotting and are left up to the interested reader),

$$v_y = 2580[1 - (p_y/2.068)^{0.231}]^{1/2} \text{ (m/sec)}$$

The cross-sectional area is found from Eq. 3–3 and the relations above:

$$\begin{aligned} A_y &= \dot{m}V_y/v_y = (1.0 \times 0.3714/2580) \times (2.068/p_y)^{0.769} \\ &\quad \times [1 - (p_y/2.068)^{0.231}]^{-1/2} \\ &= 1.44 \times 10^{-4} \times (2.068/p_y)^{0.769} [1 - (p_y/2.068)^{0.231}]^{-1/2} \text{ (m}^2\text{)} \end{aligned}$$

Finally the Mach number is obtained using Eq. 3–11 and the relations above:

$$\begin{aligned} M_y &= v_y/[kRT_y]^{1/2} = [2580/(1.30 \times 345.7 \times 2222)]^{1/2} \\ &\quad \times [1 - (p_y/2.068)^{0.231}]^{1/2} (p_y/2.068)^{-0.231} \\ &= 2.582 [1 - (p_y/2.068)^{0.231}]^{1/2} (p_y/2.068)^{-0.231} \end{aligned}$$

With the equations indicated above and graphing software such as available in MATLAB or MAPLE, the desired plots may be obtained. Figure 3–3 shows semiquantitative plots of several parameter variations and should be used for comparison. Note that in this figure the pressures are shown as decreasing to the right, representing a flow from left to right (also its units are in psia where the throat pressure is 164.4 psia and the exit pressure would be 14.7 psia).

A number of interesting deductions can be made from this example. Very *high gas velocities* (over 1 km/sec) can be obtained in rocket nozzles. The *temperature drop* of the combustion gases flowing through a rocket nozzle is appreciable. In the example given the temperature changed 1115°C in a relatively short distance. This should not be surprising, for the increase in the kinetic energy of the gases is derived from a decrease of the enthalpy, which in turn is roughly proportional to the decrease in temperature. Because the exhaust gases are still very hot (1107 K) when leaving the nozzle, they contain considerable thermal energy not available for conversion into kinetic energy of the jet.

Nozzle Flow and Throat Condition

The required nozzle area decreases to a *minimum* (at 1.130 MPa or 164 psi pressure in the previous example) and then increases again. Nozzles of this type (often called De Laval nozzles after their inventor) consist of a convergent section followed by a divergent section. From the continuity equation, the area is inversely proportional to the ratio v/V . This quantity has also been plotted in Fig. 3–3. There is a maximum in the curve of v/V because at first the velocity increases

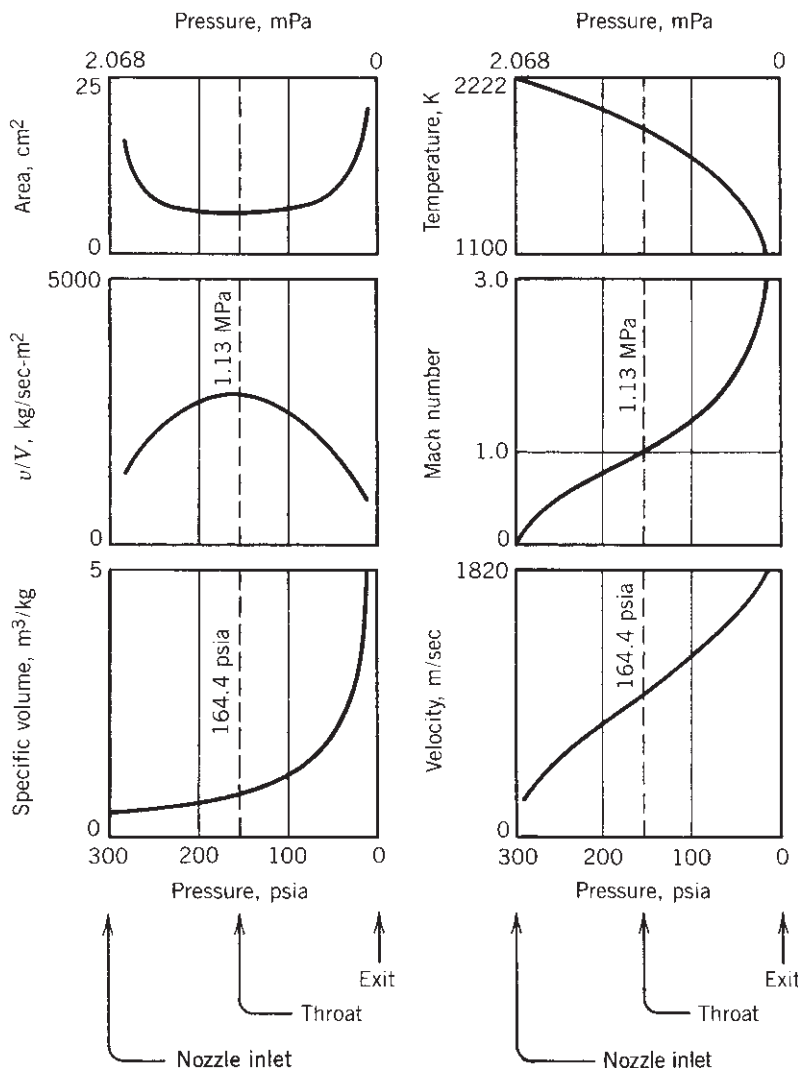


FIGURE 3–3. Typical variation of cross-sectional area, temperature, specific volume, and velocity with pressure in a rocket nozzle (from Example 3–2).

at a greater rate than the specific volume; however, in the divergent section, the specific volume increases at a greater rate.

The minimum nozzle area is called the *throat area*. The ratio of the nozzle exit area A_2 to the nozzle throat area A_t is called the nozzle expansion area ratio and is designated by the Greek letter ϵ . It is an important nozzle parameter:

$$\epsilon = A_2/A_t \quad (3-19)$$

The maximum gas flow per unit area occurs at the throat where there is a unique gas pressure ratio which is only a function of the ratio of specific heats k . This pressure ratio is found by setting $M = 1$ in Eq. 3–13:

$$p_t/p_1 = [2/(k + 1)]^{k/(k-1)} \quad (3-20)$$

The throat pressure p_t for which the isentropic mass flow rate is a maximum is called the *critical pressure*. Typical values of this critical pressure ratio range between 0.53 and 0.57 of the inlet pressure. The flow through a specified rocket nozzle with a given inlet condition is less than the maximum if the pressure ratio is larger than that given by Eq. 3–20. However, note that this ratio is not that across the entire nozzle and that the maximum flow or choking condition (explained below) is always established internally at the throat and not at the exit plane. The nozzle inlet pressure is very close to the chamber stagnation pressure, except in narrow combustion chambers where there is an appreciable drop in pressure from the injector region to the nozzle entrance region. This is discussed in Section 3.5. At the point of critical pressure, namely the throat, the Mach number is one and the values of the specific volume and temperature can be obtained from Eqs. 3–7 and 3–12:

$$V_t = V_1[(k + 1)/2]^{1/(k-1)} \quad (3-21)$$

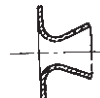
$$T_t = 2T_1/(k + 1) \quad (3-22)$$

In Eq. 3–22 the nozzle inlet temperature T_1 is very close to the combustion temperature and hence close to the nozzle flow stagnation temperature T_0 . At the critical point there is only a mild change of these properties. Take, for example, a gas with $k = 1.2$; the critical pressure ratio is about 0.56 (which means that p_t equals almost half of the chamber pressure p_1 ; the temperature drops only slightly ($T_t = 0.91T_1$), and the specific volume expands by over 60% ($V_t = 1.61V_1$)). From Eqs. 3–15, 3–20, and 3–22, the critical or throat velocity v_t is obtained:

$$v_t = \sqrt{\frac{2k}{k + 1}RT_1} = a_t = \sqrt{kRT_t} \quad (3-23)$$

The first version of this equation permits the throat velocity to be calculated directly from the nozzle inlet conditions without any of the throat conditions being known. At the nozzle throat the critical velocity is clearly also the sonic velocity. The flow in the chamber is subsonic and downstream of the nozzle throat it is supersonic. The divergent portion of the nozzle permits further decreases in pressure and increases in velocity under supersonic conditions. If the nozzle is cut off at the throat section, the exit gas velocity is sonic and the flow rate remains a maximum. The sonic and supersonic flow condition can be attained only if the critical pressure prevails at the throat, that is, if p_2/p_1 is equal to or less than the quantity defined by Eq. 3–20. There are, therefore, three different types of nozzles: subsonic, sonic, and supersonic, and these are described in Table 3–1.

TABLE 3–1. Nozzle Types

| | Subsonic | Sonic | Supersonic |
|-----------------|---|---|---|
| Throat velocity | $v_1 < a_t$ | $v_t = a_t$ | $v_t = a_t$ |
| Exit velocity | $v_2 < a_2$ | $v_2 = v_t$ | $v_2 > v_t$ |
| Mach number | $M_2 < 1$ | $M_2 = M_t = 1.0$ | $M_2 > 1$ |
| Pressure ratio | $\frac{p_1}{p_2} < \left(\frac{k+1}{2}\right)^{k/(k-1)}$ | $\frac{p_1}{p_2} = \frac{p_1}{p_t} = \left(\frac{k+1}{2}\right)^{k/(k-1)}$ | $\frac{p_1}{p_2} > \left(\frac{k+1}{2}\right)^{k/(k-1)}$ |
| Shape |  |  |  |

The supersonic nozzle is the one used for rockets. It achieves a high degree of conversion of enthalpy to kinetic energy. The ratio between the inlet and exit pressures in all rockets is sufficiently large to induce supersonic flow. Only if the absolute chamber pressure drops below approximately 1.78 atm will there be subsonic flow in the divergent portion of the nozzle during sea-level operation. This condition occurs for a very short time during the start and stop transients.

The velocity of sound is equal to the propagation speed of an elastic pressure wave within the medium, sound being an infinitesimal pressure wave. If, therefore, sonic velocity is reached at any point within a steady flow system, it is impossible for a pressure disturbance to travel past the location of sonic or supersonic flow. Thus, any partial obstruction or disturbance of the flow downstream of the nozzle throat with sonic flow has no influence on the throat or upstream of it, provided that the disturbance does not raise the downstream pressure above its critical value. It is not possible to increase the throat velocity or the flow rate in the nozzle by further lowering the exit pressure or even evacuating the exhaust section. This important condition is often described as *choking* the flow. It is always established at the throat and not the nozzle exit plane. *Choked flow* through the critical section of a supersonic nozzle may be derived from Eqs. 3–3, 3–21, and 3–23. It is equal to the mass flow at any section within the nozzle.

$$\dot{m} = \frac{A_t v_t}{V_t} = A_t p_1 k \frac{\sqrt{[2/(k+1)]^{(k+1)/(k-1)}}}{\sqrt{kRT_1}} \quad (3-24)$$

The mass flow through a rocket nozzle is therefore proportional to the throat area A_t and the chamber (stagnation) pressure p_1 ; it is also inversely proportional to the square root of T/\mathfrak{M} and a function of the gas properties. For a supersonic nozzle the *ratio between the throat and any downstream area* at which a pressure

p_y prevails can be expressed as a function of the pressure ratio and the ratio of specific heats, by using Eqs. 3–4, 3–16, 3–21, and 3–23, as follows:

$$\frac{A_t}{A_y} = \frac{V_t v_y}{V_y v_t} = \left(\frac{k+1}{2} \right)^{1/(k-1)} \left(\frac{p_y}{p_1} \right)^{1/k} \sqrt{\frac{k+1}{k-1} \left[1 - \left(\frac{p_y}{p_1} \right)^{(k-1)/k} \right]} \quad (3-25)$$

When $p_y = p_2$, then $A_y/A_t = A_2/A_t = \epsilon$ in Eq. 3–25. For low-altitude operation (sea level to about 10,000 m) the nozzle area ratios are typically between 3 and 25, depending on chamber pressure, propellant combinations, and vehicle envelope constraints. For high-altitude (100 km or higher) area ratios are typically between 40 and 200, but there have been some as high as 400. Similarly, an expression for the ratio of the velocity at any point downstream of the throat with the pressure p_y , and the throat velocity may be written from Eqs. 3–15 and 3–23:

$$\frac{v_y}{v_t} = \sqrt{\frac{k+1}{k-1} \left[1 - \left(\frac{p_y}{p_1} \right)^{(k-1)/k} \right]} \quad (3-26)$$

These equations permit the direct determination of the velocity ratio or the area ratio for any given pressure ratio, and vice versa, in ideal rocket nozzles. They are plotted in Figs. 3–4 and 3–5, and these plots allow the determination of the pressure ratios given the area or velocity ratios. When $p_y = p_2$, Eq. 3–26 describes the velocity ratio between the nozzle exit area and the throat section. When the exit pressure coincides with the atmospheric pressure ($p_2 = p_3$, see Fig. 2–1), these equations apply for optimum nozzle expansion. For rockets that operate at high altitudes, not too much additional exhaust velocity can be gained by increasing the area ratio above 1000. In addition, design difficulties and a heavy inert nozzle mass make applications above area ratios of about 350 marginal.

Appendix 2 is a table of several properties of the earth's atmosphere with agreed-upon standard values. It gives ambient pressure for different altitudes. These properties can vary somewhat from day to day (primarily because of solar activity) and between hemispheres. For example, the density of the atmosphere at altitudes between 200 and 3000 km can change by more than an order of magnitude, affecting satellite drag.

Example 3–3. Design an ideal nozzle for a rocket that operates at 25 km altitude and delivers 5000 N thrust with a chamber pressure of 2.039 MPa and a chamber temperature of 2800 K. Assuming that $k = 1.20$ and $R = 360 \text{ J/kg-K}$, determine the throat area, exit area, throat temperature, and exit velocity.

SOLUTION. At 25 km altitude the atmospheric pressure equals 2.549 kPa (in Appendix 2 the ratio is 0.025158, which must be multiplied by the pressure at sea level, 0.1013 MPa). The controlling pressure ratio is

$$p_2/p_1 = 0.002549/2.039 = 0.00125 = 1/800$$

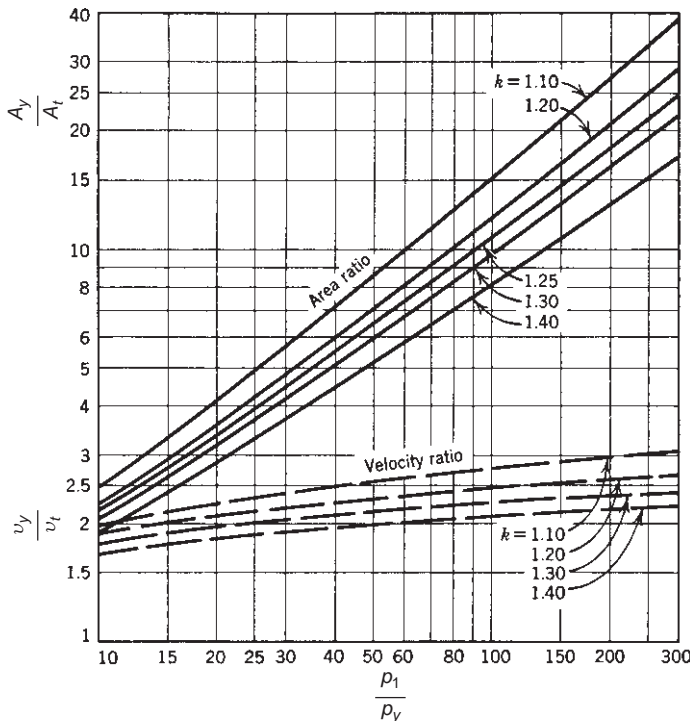


FIGURE 3-4. Area and velocity ratios as function of pressure ratio for the diverging section of a supersonic nozzle.

The area ratio can now be obtained directly from Eq. 3-25 (or Fig. 3-5) as

$$\begin{aligned} \frac{A_t}{A_2} &= \left(\frac{k+1}{2}\right)^{1/(k-1)} \left(\frac{p_2}{p_1}\right)^{1/k} \sqrt{\frac{k+1}{k-1} \left[1 - \left(\frac{p_2}{p_1}\right)^{(k-1)/k}\right]} \\ &= (1.10)^5 (0.00125)^{0.833} \sqrt{11.0 [1 - (0.00125)^{0.167}]} \\ &= 1.67 \times 10^{-2} = 1/60 \end{aligned}$$

The temperature at the throat may be found directly from Eq. 3-22:

$$T_t = 2T_1/(k+1) = 2 \times 2800/2.2 = 2545 \text{ K}$$

The ideal exit velocity is found from Eq. 3-15 as

$$\begin{aligned} v_2 &= \sqrt{\frac{2k}{k-1} RT_1 \left[1 - \left(\frac{p_2}{p_1}\right)^{(k-1)/k}\right]} \\ &= \sqrt{1.21 \times 10^7 [1 - (0.00125)^{0.167}]} \\ &= 2851 \text{ m/sec} \end{aligned}$$

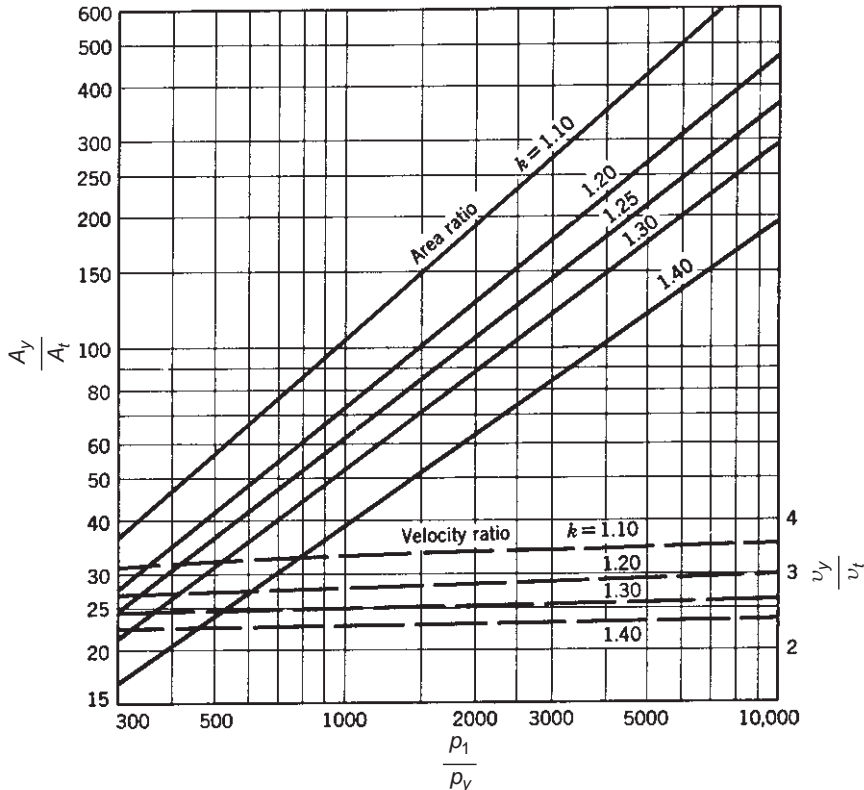


FIGURE 3–5. Continuation of prior figure of area ratios and velocity ratios, but for higher pressure ratios in a supersonic nozzle.

Next we need to find the throat area, which can be found via the mass flow rate, Eq. 3–24, $A_t = \dot{m} V_t / v_t$. To find the mass flow rate explicitly we note that $v_2 = c$ (Eq. 2–16) and from Eq. 2–17

$$\dot{m} = F/c = 5000/2851 = 1.754 \text{ kg/sec}$$

$$A_t = \frac{\dot{m}}{p_1} \sqrt{\frac{RT_1}{k[2/(k+1)]^{(k+1)/(k-1)}}}$$

$$= \frac{1.754}{2.039 \times 10^6} \sqrt{\frac{360 \times 2800}{1.2[2/2.2]^{11}}} = 13.32 \text{ cm}^2$$

And thus the exit area becomes $A_2 = 60 \times 13.32 = 799 \text{ cm}^2$. The designer would next have to modify the area ratio of the nozzle depending on the actual configuration chosen and to choose materials together with cooling methods that accommodate the high chamber and throat temperatures.

Thrust and Thrust Coefficient

The efflux of the propellant gases or the momentum flowing out causes the thrust or reaction force on the rocket structure. Because the flow is supersonic, the pressure at the exit plane of the nozzle may be different from the ambient pressure, and the pressure thrust component adds to the momentum thrust as given by Eq. 2–14, which is repeated here:

$$F = \dot{m}v_2 + (p_2 - p_3)A_2$$

The maximum thrust for any given nozzle operation is found in a vacuum where $p_3 = 0$. Between sea level and the vacuum of space, Eq. 2–14 gives the variation of thrust with altitude, using the properties of the atmosphere such as those listed in Appendix 2. Figure 2–2 shows a typical variation of thrust with altitude. To modify values calculated for optimum operating conditions ($p_2 = p_3$) for given values of p_1 , k , and A_2/A_t , the following expressions may be used. For the thrust,

$$F = F_{\text{opt}} + p_1 A_t \left(\frac{p_2}{p_1} - \frac{p_3}{p_1} \right) \frac{A_2}{A_t} \quad (3-27)$$

For the specific impulse, using Eqs. 2–5, 2–18, and 2–14,

$$I_s = (I_s)_{\text{opt}} + \frac{c^* \epsilon}{g_0} \left(\frac{p_2}{p_1} - \frac{p_3}{p_1} \right) \quad (3-28)$$

If, for example, the specific impulse for a new exit pressure p_2 corresponding to a new area ratio A_2/A_t is to be calculated, the above relations may be used.

Equation 2–14 can be expanded by modifying it and substituting v_2 , v_t , and V_t from Eqs. 3–16, 3–21, and 3–23:

$$\begin{aligned} F &= \frac{A_t v_t v_2}{V_t} + (p_2 - p_3)A_2 \\ &= A_t p_1 \sqrt{\frac{2k^2}{k-1} \left(\frac{2}{k+1} \right)^{(k+1)/(k-1)} \left[1 - \left(\frac{p_2}{p_1} \right)^{(k-1)/k} \right]} + (p_2 - p_3)A_2 \end{aligned} \quad (3-29)$$

The first version of this equation is general and applies to all rockets, the second form applies to an ideal rocket with k being constant throughout the expansion process. This equation shows that the thrust is proportional to the throat area A_t and the chamber pressure (or the nozzle inlet pressure) p_1 and is a function of the pressure ratio across the nozzle p_1/p_2 , the specific heat ratio k , and of the pressure thrust. It is called the ideal thrust equation. The thrust coefficient C_F is

defined as the thrust divided by the chamber pressure p_1 and the throat area A_t . Equations 2–14, 3–21, and 3–16 then give this relation:

$$C_F = \frac{v_2^2 A_2}{p_1 A_t V_2} + \frac{p_2 A_2}{p_1 A_t} - \frac{p_3 A_2}{p_1 A_t}$$

$$= \sqrt{\frac{2k^2}{k-1} \left(\frac{2}{k+1}\right)^{(k+1)/(k-1)} \left[1 - \left(\frac{p_2}{p_1}\right)^{(k-1)/k}\right]} + \frac{p_2 - p_3}{p_1} \frac{A_2}{A_t} \quad (3-30)$$

The thrust coefficient C_F is dimensionless. It is a key parameter for analysis and is a function of gas property k , the nozzle area ratio ϵ , and the pressure ratio across the nozzle p_1/p_2 , but independent of chamber temperature. For any fixed pressure ratio p_1/p_3 , the thrust coefficient C_F and the thrust F have a peak when $p_2 = p_3$. This peak value is known as the *optimum thrust coefficient* and is an important criterion in nozzle design considerations. The use of the thrust coefficient permits a simplification to Eq. 3–29:

$$F = C_F A_t p_1 \quad (3-31)$$

Equation 3–31 can be solved for C_F and provides the relation for determining the thrust coefficient experimentally from measured values of chamber pressure, throat diameter, and thrust. Even though the thrust coefficient is a function of chamber pressure, it is not simply proportional to p_1 , as can be seen from Eq. 3–30. However, it is directly proportional to throat area. The thrust coefficient can be thought of as representing the amplification of thrust due to the gas expanding in the supersonic nozzle as compared to the thrust that would be exerted if the chamber pressure acted over the throat area only. The thrust coefficient has values ranging from about 0.8 to 1.9. It is a convenient parameter for seeing the effects of chamber pressure or altitude variations in a given nozzle configuration, or to correct sea-level results for flight altitude conditions.

Figure 3–6 shows the variation of the *optimum expansion thrust coefficient* ($p_2 = p_3$) for different pressure ratios p_1/p_2 , values of k , and area ratio ϵ . The complete thrust coefficient is plotted in Figs. 3–7 and 3–8 as a function of pressure ratio p_1/p_3 and area ratio for $k = 1.20$ and 1.30 . These two sets of curves are useful in solving various nozzle problems for they permit the evaluation of under- and over-expanded nozzle operation, as explained below. The values given in these figures are ideal and do not consider such losses as divergence, friction, or internal expansion waves.

When p_1/p_3 becomes very large (e.g., expansion into near vacuum), then the thrust coefficient approaches an asymptotic maximum as shown in Figs. 3–7 and 3–8. These figures also give values of C_F for any mismatched nozzle ($p_2 \neq p_3$), provided the nozzle is flowing full at all times, that is, the working fluid does not separate or break away from the walls. Flow separation is discussed later in this section.

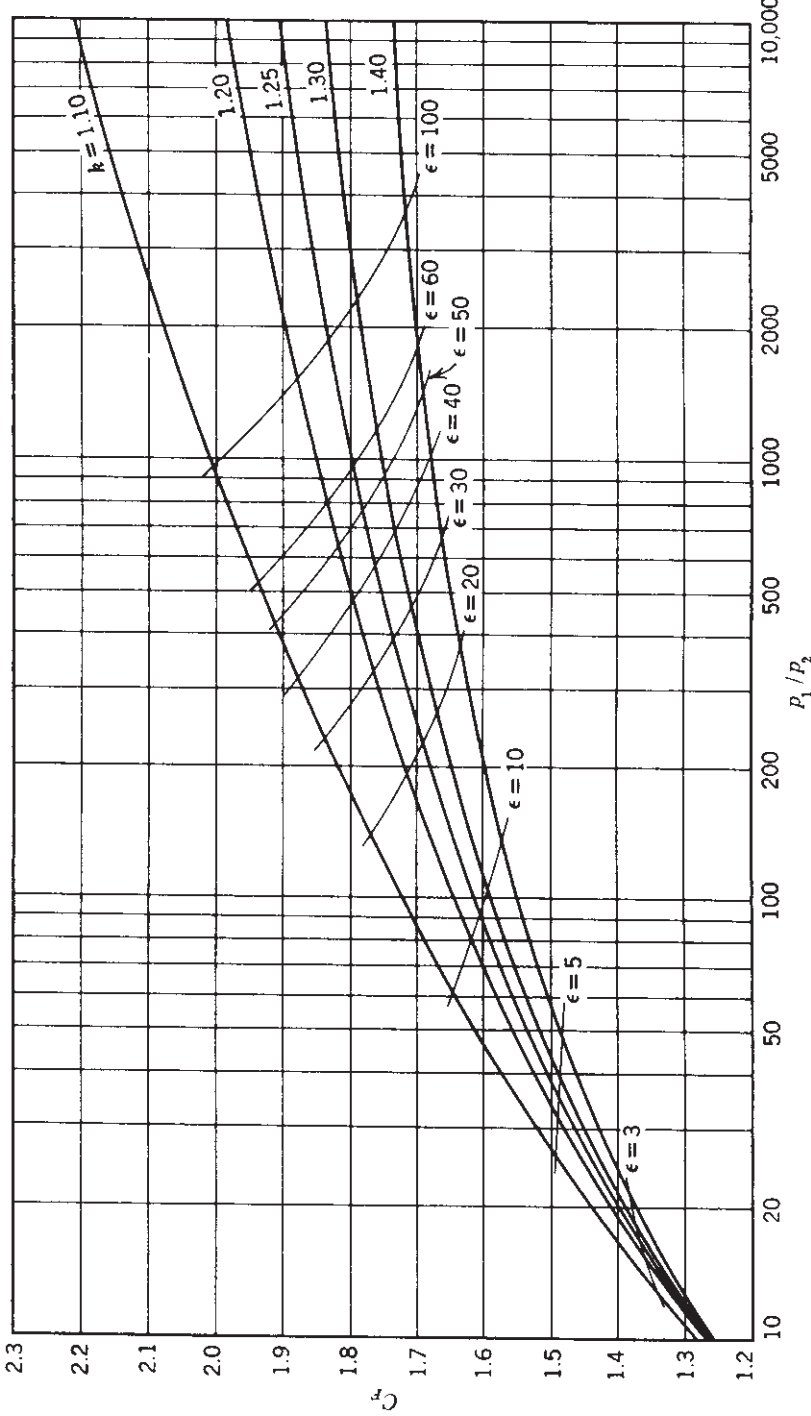


FIGURE 3–6. Thrust coefficient C_F as a function of pressure ratio, nozzle area ratio, and specific heat ratio for optimum expansion conditions ($p_2 = p_3$).

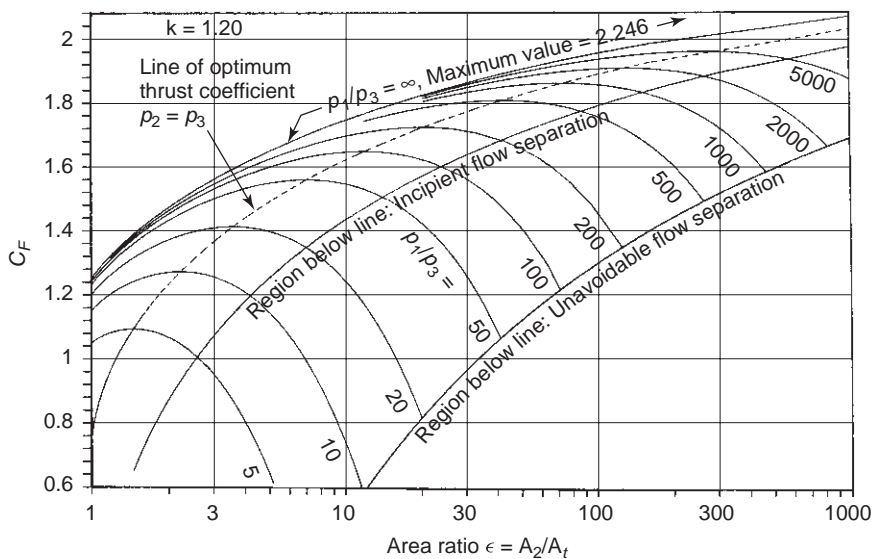


FIGURE 3–7. Thrust coefficient C_F versus nozzle area ratio for $k = 1.20$.

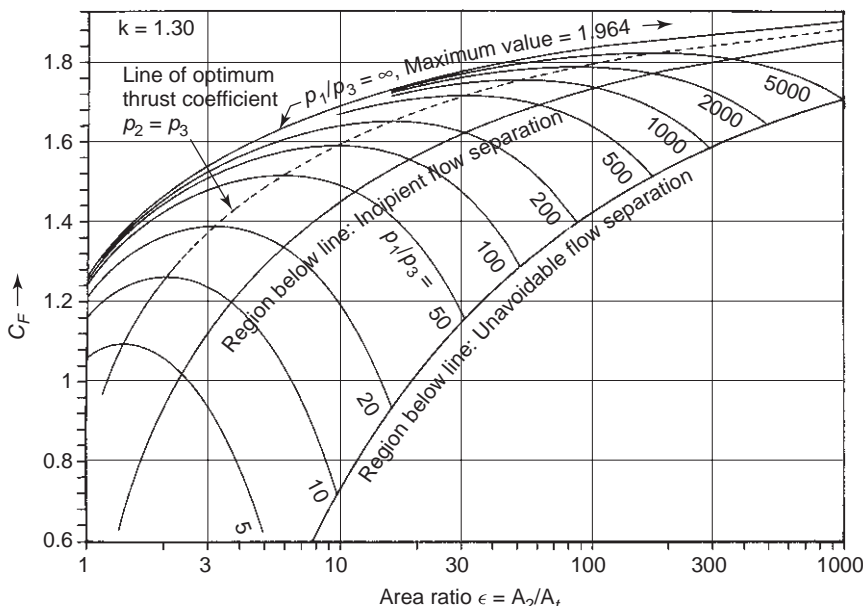


FIGURE 3–8. Thrust coefficient C_F versus nozzle area ratio for $k = 1.30$.

Characteristic Velocity and Specific Impulse

The *characteristic velocity* c^* was defined by Eq. 2–18. From Eqs. 3–24 and 3–31 it can be shown that

$$c^* = \frac{p_1 A_t}{\dot{m}} = \frac{I_s g_0}{C_F} = \frac{c}{C_F} = \frac{\sqrt{kRT_1}}{k \sqrt{[2/(k+1)]^{(k+1)/(k-1)}}} \quad (3-32)$$

It is basically a function of the propellant characteristics and combustion chamber design; it is independent of nozzle characteristics. Thus, it can be used as a figure of merit in comparing propellant combinations and combustion chamber designs. The first version of this equation is general and allows the determination of c^* from experimental data of \dot{m} , p_1 , and A_t . The last version gives the maximum value of c^* as a function of gas properties, namely k , the chamber temperature, and the molecular mass \mathfrak{M} , as determined from the theory in Chapter 5. Some values of c^* are shown in Tables 5–4 and 5–5.

The term c^* -*efficiency* is sometimes used to express the degree of completion of the energy release and the creation of high-temperature, high-pressure gas in the chamber. It is the ratio of the actual value of c^* , as determined from measurements (the first part of Eq. 3–32), and the theoretical value (last part of Eq. 3–32), and typically has a value between 92 and 99.5%.

Using Eqs. 3–31 and 3–32, the thrust itself may now be expressed as the mass flow rate times a function of the combustion chamber (c^*) times a function of the nozzle expansion C_F ,

$$F = C_F \dot{m} c^* \quad (3-33)$$

Some authors use a term called the *discharge coefficient* C_D , which is merely the reciprocal of c^* . Both C_D and the characteristic exhaust velocity c^* are used primarily with chemical rocket propulsion systems.

The influence of *variations in the specific heat ratio* k on various parameters (such as c , $c^* A_2 / A_t$, v_2/v_t , or I_s) is not as large as the changes in chamber temperature, pressure ratio, or molecular mass. Nevertheless, it is a noticeable factor, as can be seen by examining Figs. 3–2 and 3–4 to 3–8. The value of k is 1.67 for monatomic gases such as helium and argon, 1.4 for cold diatomic gases such as hydrogen, oxygen, and nitrogen, and for triatomic and beyond it varies between 1.1 and 1.3 (methane is 1.11 and ammonia and carbon dioxide 1.33). In general, the more complex the molecule the lower the value of k ; this is also true for molecules at high temperatures when their vibrational modes have been activated. The average values of k and \mathfrak{M} for typical rocket exhaust gases with several constituents depend strongly on the composition of the products of combustion (chemical constituents and concentrations), as explained in Chapter 5. Values of k and \mathfrak{M} are given in Tables 5–4, 5–5, and 5–6.

Example 3–4. What is the percentage variation in thrust between sea level and 10 km for a launch vehicle whose rocket operates with a chamber pressure of 20 atm and has

an expansion area ratio of 6? (Use $k = 1.30$.) Also, at what altitude is the performance of this rocket optimum?

SOLUTION. According to Eq. 3–33, the only component of the thrust that depends on the ambient pressure is C_F , the thrust coefficient. This coefficient can be found from Eq. 3–30 or from Fig. 3–8 by following a vertical line corresponding to $A_2/A_1 = 6.0$. We first have to find the ratio p_1/p_3 at sea level and at 10 km. Using values from Appendix 2 and solving Eq. 3–25 for $p_2/p_3 = 0.0198(p_2 = 0.396 \text{ atm})$,

$$\text{Sea level: } p_1/p_3 = 20/1.0 = 20 \quad C_F = 1.33$$

$$10 \text{ km altitude: } p_1/p_3 = 20/0.26151 = 76.5 \quad C_F = 1.56$$

$$\text{Thrust increase} = (1.56 - 1.33)/1.33 = 17.3\%$$

Note that performance at optimum nozzle expansion ($p_2 = p_3$) this nozzle delivers a thrust that is somewhat less than the maximum. From Fig. 3–6 we find that for $\epsilon = 6$ the optimum $C_F = 1.52$, which corresponds to 7.2 km elevation, whereas the maximum value is $C_F = 1.63$ in a vacuum. The thrust coefficient could be somewhat higher for larger area ratios.

Under- and Over-Expanded Nozzles

An *under-expanded nozzle* discharges the fluid at an exit pressure greater than the external pressure because the exit area is too small for an optimum area ratio. The expansion of the fluid is therefore incomplete within the nozzle, and further expansion will take place outside of the nozzle exit. The nozzle exit pressure is higher than the local atmospheric pressure.

In an *over-expanded nozzle* the fluid exists at lower pressure than the atmosphere as it has an exit area too large for optimum. The phenomenon of over-expansion for a supersonic nozzle is shown in Fig. 3–9, with typical pressure measurements of superheated steam along the nozzle axis and different back pressures or pressure ratios. Curve *AB* shows the variation of pressure with the optimum back pressure corresponding to the nozzle area ratio. Curves *AC* and *AD* show the variation of pressure along the axis for increasingly higher external pressures. The expansion within the nozzle proceeds normally for the initial portion of the nozzle. At point *I* on curve *AD*, for example, the pressure is lower than the exit pressure and a sudden rise in pressure takes place that is accompanied by the *separation* of the flow from the walls (separation is described later).

The nonideal behavior of nozzles is strongly influenced by the presence of compression waves or shock waves inside the diverging nozzle section, which are strong compression discontinuities and exist only in supersonic flow. The sudden pressure rise in the curve *ID* is such a compression wave. Expansion waves, also strictly supersonic phenomena, match the flow from a nozzle exit to lower ambient pressures. Compression and expansion waves are described in Chapter 20.

The different possible flow conditions in a supersonic nozzle are as follows:

1. When the external pressure p_3 is below the nozzle exit pressure p_2 , the nozzle will flow full but will have external expansion waves at its exit (i.e.,

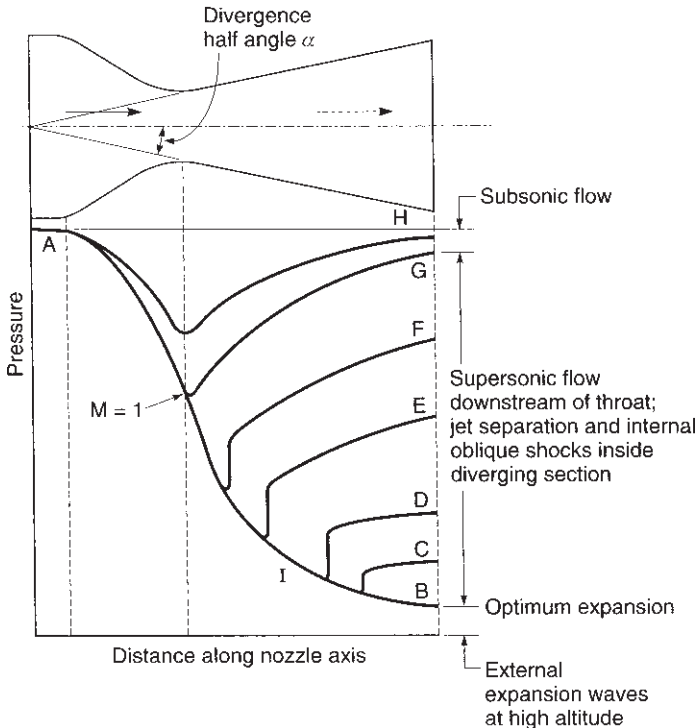


FIGURE 3–9. Distribution of pressures in a converging–diverging nozzle for different flow conditions. Inlet pressure is the same, but exit pressure changes. Based on experimental data from A. Stodala.

under-expansion). The expansion of the gas inside the nozzle is incomplete and the values of C_F and I_s will be less than at optimum expansion.

- For external pressures p_3 slightly higher than the nozzle exit pressure p_2 , the nozzle will continue to flow full. This occurs until p_2 reaches a value between about 10 and 40% of p_3 . The expansion is somewhat inefficient and C_F and I_s will have lower values than an optimum nozzle would have. Shock waves will exist outside the nozzle exit section.
- For higher external pressures, separation of the flow will begin to take place inside the divergent portion of the nozzle. The diameter of the supersonic jet will be smaller than the nozzle exit diameter. With steady flow, separation is typically axially symmetric. Figures 3–10 and 3–11 show diagrams of separated flows. The axial location of the separation plane depends on the local pressure and the wall contour. The point of separation travels downstream with decreasing external pressure. At the nozzle exit the flow in the center portion remains supersonic but is surrounded by an annular-shaped section of subsonic flow. There is a discontinuity at the separation location and the thrust is reduced, compared to a nozzle that would have

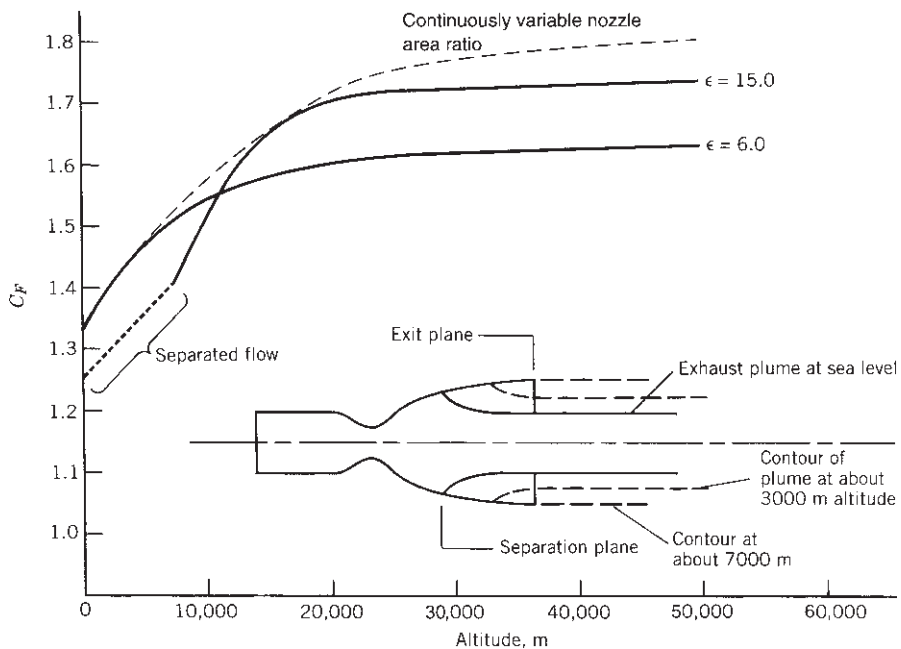


FIGURE 3–10. Thrust coefficient C_F for two nozzles with different area ratios. One has jet separation below about 7000 m altitude. The fully expanded exhaust plume at higher altitudes is not shown in the sketch.

been cut off at the separation plane. Shock waves exist outside the nozzle in the external plume.

4. For nozzles in which the exit pressure is just below the value of the inlet pressure, the pressure ratio is below the critical pressure ratio (as defined by Eq. 3–20) and subsonic flow prevails throughout the entire nozzle. This condition occurs normally in rocket nozzles for a short time during the start and stop transients.

The method for estimating pressure at the location of the separation plane inside the diverging section of a supersonic nozzle has usually been empirical. Reference 3–4 describes a variety of nozzles, their behavior, and methods used to estimate the location and the pressure at separation. Actual values of pressure for the over-expanded and under-expanded regimes described above are functions of the specific heat ratio and the area ratio (see Ref. 3–1).

The axial thrust direction is not usually altered by separation because a steady flow usually separates uniformly over a cross section in a divergent nozzle cone of conventional rocket design. During transients, such as start and stop, the separation may not be axially symmetric and may cause momentary but large side forces on the nozzle. During a normal sea-level transient of a large rocket nozzle

| Stage | A_2/A_t | During flight | | | During sea level static tests | | |
|------------------------|-----------|---------------|-------------|-----|-------------------------------|-------------|-----|
| | | h (km) | I_s (sec) | | h (km) | I_s (sec) | |
| Booster or first stage | 6 | | 0 | 267 | | 0 | 267 |
| Second stage | 10 | | 24 | 312 | | 0 | 254 |
| Third stage | 40 | | 100 | 334 | | 0 | 245 |

FIGURE 3–11. Simplified sketches of exhaust gas behavior of three typical rocket nozzles for a three-stage launch vehicle. The first vehicle stage has the biggest chamber and the highest thrust but the lowest nozzle area ratio, and the top or third stage usually has the lower thrust but the highest nozzle area ratio.

(before the chamber pressure reaches its full value), some momentary flow oscillations and nonsymmetric separation of the jet can occur during over-expanded flow operation. The magnitude and direction of transient side forces can change rapidly and erratically. The resulting side forces can be large and have caused failures of nozzle exit cone structures and thrust vector control gimbal actuators. References 3–4, 3–5, and 3–6 discuss techniques for estimating these side forces.

When the flow separates, as it does in a highly over-expanded nozzle, the thrust coefficient C_F can be estimated if the point of separation in the nozzle is known. Thus, C_F can be determined for an equivalent smaller nozzle with an exit area equal to that at the point of separation. The effect of separation is to increase the thrust and the thrust coefficient over the value that they would have if separation had not occurred. Thus, with separated gas flow, a nozzle designed for high altitude (large value of ϵ) would have a larger thrust at sea level than expected, but not as good as an optimum nozzle; in this case separation may actually be desirable. With separated flow a large and usually heavy portion of the nozzle is not utilized and the nozzle is bulkier and longer than necessary. The added engine weight and size decrease flight performance. Designers therefore select an area ratio that will not cause separation.

Because of uneven flow separation and potentially destructive side loads, sea-level static tests of an upper stage or a space propulsion system with a high area ratio over-expanded nozzle are usually avoided; instead, a sea-level test nozzle with a much smaller area ratio is substituted. However, actual and simulated altitude testing (in an altitude test facility similar to the one described in Chapter 21) would be done with a nozzle having the correct large area ratio. The ideal solution that avoids separation at low altitudes and has high values of C_F at high altitudes is a nozzle that changes area ratio in flight. This is discussed at the end of this section.

For most applications, the rocket system has to operate over a range of altitudes; for a fixed chamber pressure this implies a range of nozzle pressure ratios. The condition of optimum expansion ($p_2 = p_3$) occurs only at one altitude, and a nozzle with a fixed area ratio is therefore operating much of the time at either over-expanded or under-expanded conditions. The best nozzle for such an application is not necessarily one that gives optimum nozzle gas expansion, but one that gives the largest vehicle flight performance (say, total impulse, or specific impulse, or range, or payload); it can often be related to a time average over the powered flight trajectory.

Example 3–5. Use the data from Example 3–4 ($p_1 = 20$ atm, $k = 1.30$) and consider both the area ratio $\epsilon = 6.0$ and $\epsilon = 15.0$. Compare the performance of these two nozzles as a function of altitude by plotting C_F up to 50 km. Assume no shocks inside the nozzle.

SOLUTION. The procedures are the same as those in Example 3–4 and the resulting plot is shown in Fig. 3–10. The values of C_F can be obtained by following vertical lines for $\epsilon = 6.0$ and 15.0 in Fig. 3–8 corresponding to different pressure ratios at increasing altitudes. Alternatively, Eq. 3–30 may be used for greater accuracy. The lower area ratio gives a better performance at the lower altitudes but above about 10 km the larger area ratio gives a higher C_F . Also noted in Fig. 3–10 by the dotted line is what a continuously variable nozzle area ratio could accomplish by matching p_2 to p_3 at all altitudes.

The optimum pressure ratio always occurs when $p_1/p_3 = p_1/p_2$ and for the $\epsilon = 15.0$ case, from Fig. 3–6 or 3–8, this value is about 180; $p_3 = 20/180 = 0.111$ atm, which corresponds to about 15.5 km altitude. Below this altitude the nozzle is over-expanded. At sea level, where $p_1/p_3 = 20$, separation could occur as indicated in Fig. 3–8. For similarly shaped nozzles, it is estimated that sea-level separation begins to take place at a cross section where the local pressure is between 10 and 40% of p_3 or below 0.4 atm. Upon separation, this nozzle would not flow full downstream of an area ratio of about 6 or 7 and the gas jet would occupy only the central portion of the nozzle exit. See Figs. 3–10 and 3–11. Weak shock waves and jet contraction would then raise the exhaust jet's pressure to match the value of the surrounding atmosphere. If the jet does not separate, it would reach an exit pressure of 0.11 atm, but this is often an unstable condition. As the vehicle gains altitude, the separation plane would gradually move downstream until, at an altitude of about 700 m, the exhaust gases would occupy the full diverging section of the nozzle area.

The values of C_F can be obtained by following a vertical line for $\epsilon = 15$ and $\epsilon = 6$ in Fig. 3–8 for different pressure ratios, which correspond to different altitudes. Alternatively, Eq. 3–30 can be used for better accuracy. Results are similar to those plotted in Fig. 3–10. The lower area ratio of 6 gives a higher C_F at low altitudes but is inferior to

the area ratio of 15 at the higher altitudes. A nozzle area ratio larger than 15 would yield a higher C_F at the higher altitudes.

Figure 3–11 shows a comparison of altitude and sea-level behavior of three nozzles and their plumes at different area ratios for a typical three-stage satellite launch vehicle. When fired at sea-level conditions, the nozzle of the third stage with the highest area ratio will experience flow separation and suffer a major performance loss; the second stage will flow full but the external plume will contract; since $p_2 < p_3$, there is a loss in I_s and F . There is no effect on the first stage nozzle.

Example 3–6. A rocket engine test near sea level gives the following data: thrust $F = 53,000$ lbf, propellant mass flow rate $\dot{m} = 208$ lbm/sec, nozzle exit area ratio $A_2/A_t = 10.0$, actual local atmospheric pressure at test station $p_3 = 13.8$ psia, and chamber pressure $p_1 = 620$ psia. The test engineer also knows that for the same flow rate (and mixture ratio) the theoretical specific impulse is 289 sec at the standard reference conditions of $p_1 = 1000$ psia and $p_3 = 14.7$ psia, and that $k = 1.20$. For many propellants we may assume that the combustion temperature and k do not vary significantly with chamber pressure. Compare the test performance of this rocket with its equivalent at sea level, standard, and vacuum performance.

SOLUTION. The pressure ratio for the test condition is $620/13.8 = 44.93$; if the test would have been conducted at 14.7 psia, this pressure ratio would have been $620/14.7 = 42.18$; for the standard reference conditions the pressure ratio is $1000/14.7 = 68.03$.

Since this nozzle is operating supersonically, we find, from Eqs. 2–5, 3–24, and 3–31, that specific impulse ratios depend only on ratios of the thrust coefficient, that is, $(I_s)_b = (I_s)_a[(C_F)_b/(C_F)_a]$. From Fig. 3–7 or from Eq. 3–30 one obtains $C_F = 1.48$ for the test condition with $\epsilon = 10$, $k = 1.20$, and $p_1/p_3 = 44.9$. The corresponding specific impulse is, from Eq. 2–5, $I_s = 53000/208 = 255$ sec.

The following table shows all the results:

| | Test Results | Test for Sea Level | Standard Condition | Vacuum Condition |
|--------------|--------------|--------------------|--------------------|------------------|
| p_1 (psia) | 620 | 620 | 1,000 | 620 |
| p_3 (psia) | 13.8 | 14.7 | 14.7 | 0 |
| p_1/p_3 | 44.93 | 42.18 | 68.03 | ∞ |
| F (lbf) | 53,000 | 52,494 | 55,744 | 60,741 |
| I_s (sec) | 255 | 252 | 268 | 292 |
| C_F | 1.52 | 1.50 | 1.60 | 1.74 |

Figures 3–10 and 3–11 suggest that an ideal design for an ascending (e.g., launch) rocket vehicle would have a “rubber-like” diverging section that could be lengthened and enlarged so that the nozzle exit area could be made larger as the ambient pressure is reduced. The design would then allow the rocket vehicle to attain its maximum performance at all altitudes as it ascends. As yet we have not achieved a simple mechanical hardware design with this full altitude compensation similar to “stretching rubber.” However, there are a number of practical

TABLE 3–2. Estimated Losses for Small-Diameter Chambers

| Chamber-to-Throat Area Ratio | Throat Pressure (%) | Thrust Reduction (%) | Specific Impulse Reduction (%) |
|---------------------------------|------------------------|-------------------------|-----------------------------------|
| ∞ | 100 | 0 | 0 |
| 3.5 | 99 | 1.5 | 0.31 |
| 2.0 | 96 | 5.0 | 0.55 |
| 1.0 | 81 | 19.5 | 1.34 |

$k = 1.20; p_1/p_2 = 1000$.

nozzle configurations that can be used to alter the flow shape with altitude and obtain maximum performance at different altitudes. They are discussed in the next section.

Influence of Chamber Geometry

When the chamber has a cross section that is larger than about four times the throat area ($A_1/A_t > 4$), the chamber velocity v_1 , can be neglected, as was mentioned in explaining Eqs. 3–15 and 3–16. However, vehicle space or weight constraints often require smaller thrust chamber areas for liquid propellant engines and grain design considerations lead to small void volumes or small perforations or port areas for solid propellant motors. Then v_1 can no longer be neglected as a contribution to the performance. The gases in the chamber expand as heat is being added. The energy necessary to accelerate these expanding gases within the chamber will also cause a pressure drop and an additional energy loss. This acceleration process in the chamber is adiabatic (no heat transfer) but not isentropic. This loss is a maximum when the chamber diameter is equal to the nozzle diameter, which means that there is no converging nozzle section. This has been called a *throatless rocket motor* and has been used in a few tactical missile booster applications, where there was a premium on minimum inert mass and length. The flight performance improvement due to inert mass savings supposedly outweighs the nozzle performance loss of a throatless motor. Table 3–2 lists some of the performance penalties for three chamber area ratios.

Because of this pressure drop within narrow chambers, the chamber pressure is lower at the nozzle entrance than it would be if A_1/A_t had been larger. This causes a small loss in thrust and specific impulse. The theory of this loss is given in Ref. 3–7 and some results are listed in Table 3–2.

3.4. NOZZLE CONFIGURATIONS

A number of different proven nozzle configurations are available today. This section describes their geometries and performance. Other chapters (6, 8, 12, 15, and 18) discuss their materials, heat transfer, or application and mention

their requirements, design, construction, and thrust vector control. Nozzles and chambers are usually of circular cross section and have a converging section, a throat at the narrowest location (minimum cross section), and a diverging section. Nozzles can be seen in Figs. 1–4, 1–5, 1–8, 2–1, 3–11, 3–12, 3–14, 11–1, 12–1 to 12–3, and 15–6 to 15–8. Refs. 3–4 and 3–8 describe many nozzle configurations.

The *converging nozzle section* between the chamber and the nozzle throat has never been critical in achieving high performance. The subsonic flow in this section can easily be turned at very low pressure drop and any radius, cone angle, wall contour curve, or nozzle inlet shape is usually satisfactory. A few small attitude control thrust chambers have had their nozzle at 90° from the combustion chamber axis without any performance loss. The *throat contour* also is not very critical to performance, and any radius or other curve is usually acceptable. The pressure gradients are high in these two regions and the flow will adhere to the walls. The principal difference in the different nozzle configurations is found in the diverging supersonic-flow section, as described below. The wall surface throughout the nozzle should be smooth and shiny to minimize friction, radiation absorption, and convective heat transfer due to surface roughness. Gaps, holes, sharp edges, or protrusions must be avoided.

Six different nozzle configurations are shown in Fig. 3–12 and each will be discussed. The first three sketches show conical and bell-shaped nozzles. The other three have a center body inside the nozzle and have excellent altitude compensation. Although these last three have been ground tested, to date none of them has flown in a production space launch vehicle. The lengths of several nozzle types are compared in Fig. 3–13. The objectives of a good nozzle configuration are to obtain the highest practical I_s , minimize inert nozzle mass, and conserve length (shorter nozzles can reduce vehicle length, vehicle structure, and vehicle inert mass).

Cone- and Bell-Shaped Nozzles

The *conical nozzle* is the oldest and perhaps the simplest configuration. It is relatively easy to fabricate and is still used today in many small nozzles. A theoretical correction factor λ can be applied to the nozzle exit momentum of an ideal rocket with a conical nozzle exhaust. This factor is the ratio between the momentum of the gases in a nozzle with a finite nozzle angle 2α and the momentum of an ideal nozzle with all gases flowing in an axial direction:

$$\lambda = \frac{1}{2}(1 + \cos \alpha) \quad (3-34)$$

The variation of λ with different values of α is shown in Table 3–3 for any nozzle that has uniform mass flow per unit exit area. For ideal rockets $\lambda = 1.0$. For a rocket nozzle with a divergence cone angle of 30° (half angle $\alpha = 15^\circ$), the exit momentum and therefore the exhaust velocity will be 98.3% of the velocity calculated by Eq. 3–15b. Note that the correction factor λ only applies to the

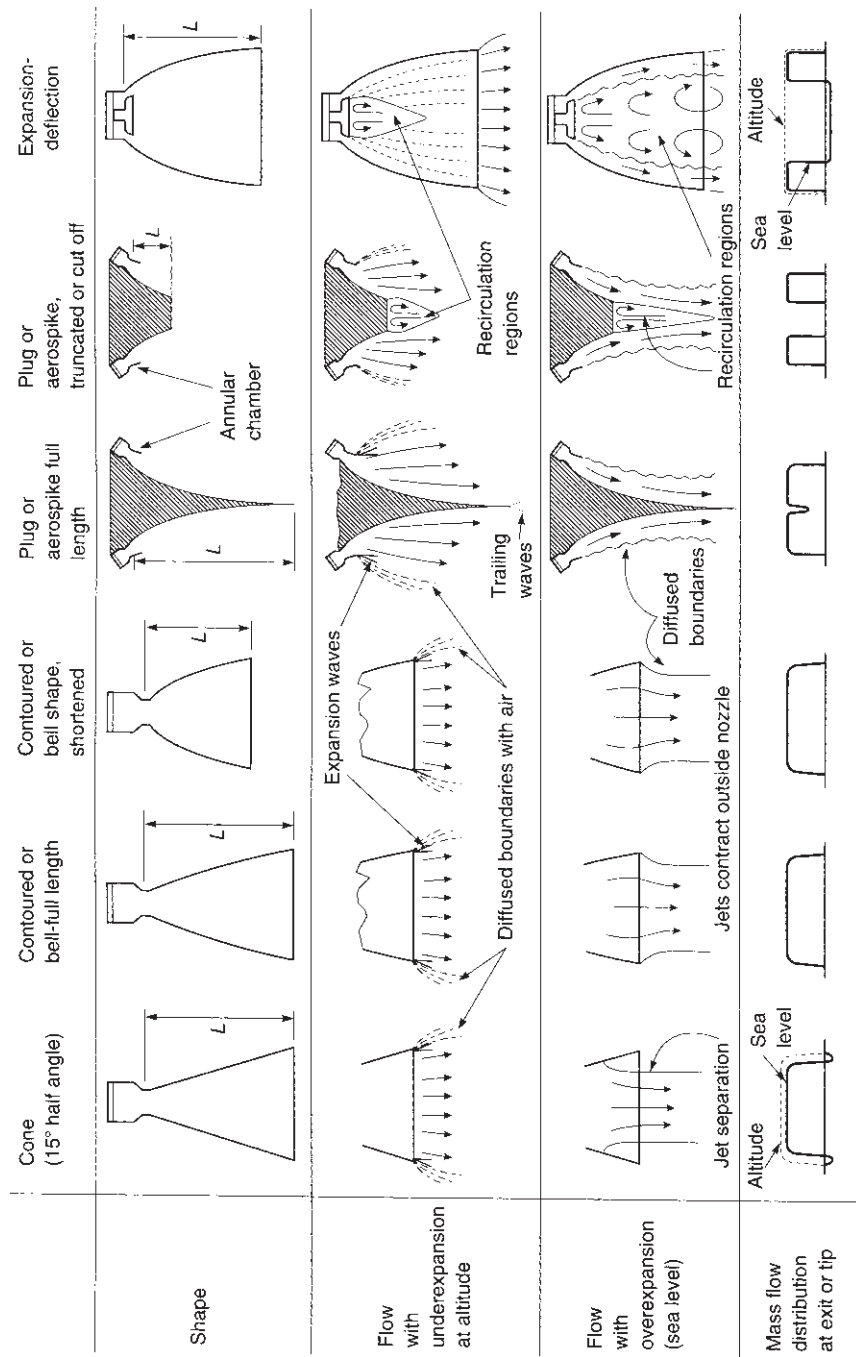


FIGURE 3–12. Simplified diagrams of several different nozzle configurations and their flow effects.

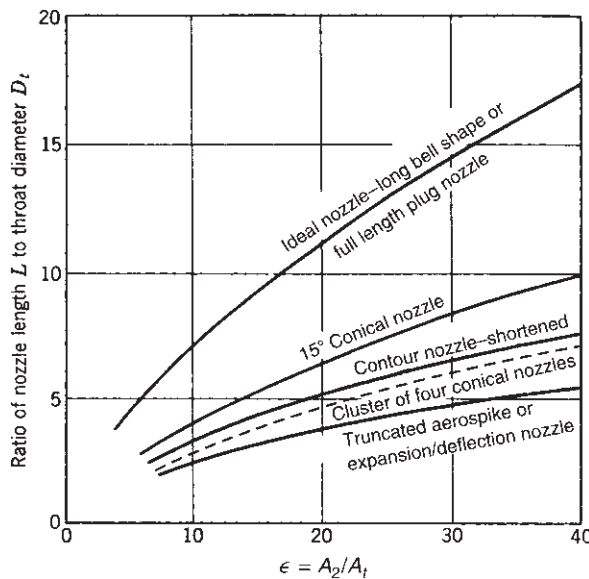


FIGURE 3–13. Length comparison of several types of nozzles. (Taken in part from Ref. 3–9.)

TABLE 3–3. Nozzle Angle Correction Factor for Conical Nozzles

| Nozzle Cone Divergence Half Angle, α (deg) | Correction Factor, λ |
|---|------------------------------|
| 0 | 1.0000 |
| 2 | 0.9997 |
| 4 | 0.9988 |
| 6 | 0.9972 |
| 8 | 0.9951 |
| 10 | 0.9924 |
| 12 | 0.9890 |
| 14 | 0.9851 |
| 15 | 0.9830 |
| 16 | 0.9806 |
| 18 | 0.9755 |
| 20 | 0.9698 |
| 22 | 0.9636 |
| 24 | 0.9567 |

first term (the momentum thrust) in Eqs. 2–14, 3–29, and 3–30 and not to the second term (pressure thrust).

A small nozzle divergence angle causes most of the momentum to be axial and thus gives a high specific impulse, but the long nozzle has a penalty in rocket propulsion system mass, vehicle mass, and also design complexity. A large

divergence angle gives short, lightweight designs, but the performance is low. There is an optimum conical nozzle shape and length (typically between 12 and 18° half angle) and it is usually a compromise which depends on the specific application and flight path.

The *bell-shaped* or *contour nozzle* (see Figs. 3–12 and 3–13) is probably the most common nozzle shape today. It has a high angle expansion section (20 to 50°) right downstream of the nozzle throat; this is followed by a gradual reversal of nozzle contour slope so that at the nozzle exit the divergence angle is small, usually less than a 10° half angle. It is possible to go to large divergence angles immediately behind the throat (20 to 50°) because the high relative pressure, the large pressure gradient, and the rapid expansion of the working fluid do not allow separation in this region unless there are discontinuities in the nozzle contour. The expansion in the supersonic bell nozzle is more efficient than in a simple straight cone of similar area ratio and length, because the wall contour is designed to minimize losses, as explained later in this section. For the past several decades most of the nozzles have been bell shaped.

A change of flow direction of a supersonic gas in an expanding wall geometry can only be achieved through *expansion waves*. An expansion wave occurs at a thin surface within the flow, where the flow velocity increases and changes its flow direction slightly, and where the pressure and temperature drop. These wave surfaces are at an oblique angle to the flow. As the gas passes through the throat, it undergoes a series of these expansion waves with essentially no loss of energy. In the bell-shaped nozzle shown in Fig. 3–14 these expansions occur internally in the flow between the throat and the inflection location *I*; the area is steadily increasing like a flare on a trumpet. The contour angle θ_i is a maximum at the inflection location. Between the inflection point *I* and the nozzle exit *E* the flow area is still increasing, but at a diminishing rate, allowing further gas expansion and additional expansion waves. However, the contour of the nozzle wall is different and the change in cross-sectional area per unit length is decreasing. The purpose of this last segment of the contoured nozzle is to have a low divergence loss as the gas leaves the nozzle exit plane. The angle at the exit θ_e is small, usually less than 10°. The difference between θ_i and θ_e is called the turn-back angle. When the gas flow is turned in the opposite direction (between points *I* and *E*) oblique compression waves will occur. These compression waves are thin surfaces where the flow undergoes a mild shock, the flow is turned, and the velocity is actually reduced slightly. Each of these multiple compression waves causes a small energy loss. By carefully determining the wall contour (by an analysis that uses a mathematical tool called the method of characteristics), it is possible to balance the oblique expansion waves with the oblique compression waves and minimize the energy loss. The analysis leading to the nozzle contour is presented in Chapter 20.33 of Ref. 3–3 and also in Refs. 3–8 to 3–11; it is based on supersonic aerodynamic flow, the method of characteristics (Ref. 3–1), and the properties of the expanding gas. Most of the rocket organizations have computer codes for this analysis. The radius of curvature or the contour shape at

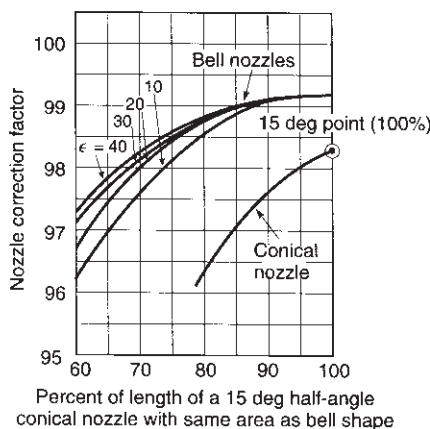
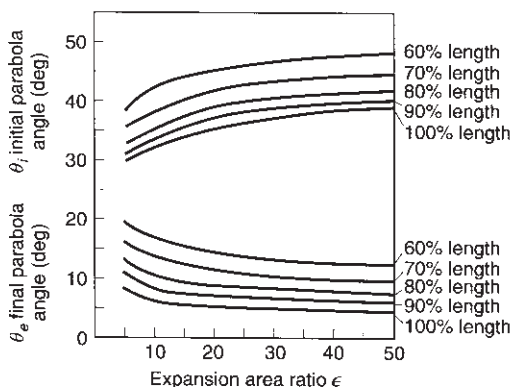
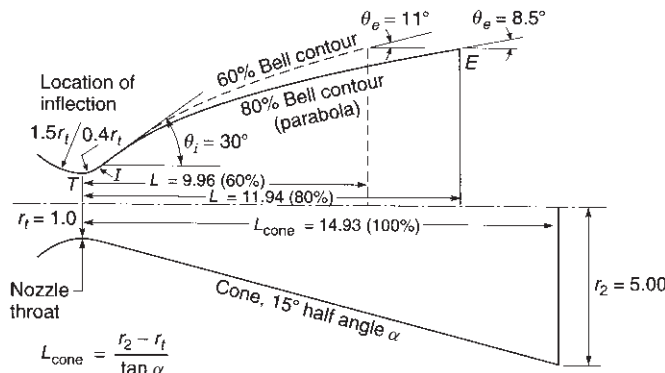


FIGURE 3–14. Top sketch shows comparison of nozzle inner wall surfaces for a 15° conical nozzle, an 80% length bell nozzle, a 60% length bell nozzle, all at an area ratio of 25. The lengths are expressed in multiples of the throat radius r_t . The middle set of curves shows the initial angle θ_i and the exit angle θ_e for bell nozzles as functions of the nozzle area ratio and percent length. The bottom curves show the nozzle losses in terms of a correction factor.

the throat region have an influence on the contour of the diverging bell-shaped nozzle section.

The length of a bell nozzle is usually given a fraction of the length of a reference conical nozzle with a 15° half angle. An 80% bell nozzle has a length (distance between throat plane and exit plane) that is 20% shorter than a comparable 15° cone of the same area ratio. Ref. 3–9 shows the original presentation by Rao of the method of characteristics applied to shorter bell nozzles. He also determined that a parabola was a good approximation for the bell-shaped contour curve (Ref. 3–3, Section 20.33), and parabolas have actually been used in some nozzle designs. The top part of Fig. 3–14 shows that the parabola is tangent (θ_i) at the inflection point I and has an exit angle (θ_e) at point E and a length L that has to be corrected for the curve TI . These conditions allow the parabola to be determined by simple geometric analysis or geometric drawing. A throat approach radius of $1.5r_t$ and a throat expansion radius of $0.4r_t$ were used. If somewhat different radii had been used, the results would have been only slightly different. The middle set of curves gives the relation between length, area ratio, and the two angles of the bell contour. The bottom set of curves gives the correction factors, equivalent to the λ factor for conical nozzles, which are to be applied to the thrust coefficient or the exhaust velocity, provided the nozzles are at optimum expansions, that is, $p_2 = p_3$.

Table 3–4 shows data for parabolas developed from this figure, which allow the reader to apply this method and check the results. The table shows two shortened bell nozzles and a conical nozzle, each for three area ratios. It can be seen that as the length has been decreased, the losses are higher for the shorter length and slightly higher for small nozzle area ratios. A 1% improvement in the correction factor gives about 1% more specific impulse (or thrust) and this difference can be significant in many applications. The reduced length is an

TABLE 3–4. Data on Several Bell-Shaped Nozzles

| Area Ratio | 10 | 25 | 50 |
|---|---------|--------|--------|
| <i>Cone (15° Half Angle)</i> | | | |
| Length (100%) ^a | 8.07 | 14.93 | 22.66 |
| Correction factor λ | 0.9829 | 0.9829 | 0.9829 |
| <i>80% Bell Contour</i> | | | |
| Length ^a | 6.45 | 11.94 | 18.12 |
| Correction factor λ | 0.985 | 0.987 | 0.988 |
| Approximate half angle at inflection point and exit (degrees) | | | |
| <i>60% Bell Contour</i> | | | |
| Length ^a | 4.84 | 9.96 | 13.59 |
| Correction factor λ | 0.961 | 0.968 | 0.974 |
| Approximate half angle at inflection point and exit (degrees) | 32.5/17 | 36/14 | 39/18 |

^aThe length is given in dimensionless form as a multiple of the throat radius.

important benefit, and it is usually reflected in an improvement of the vehicle mass ratio. The table and Fig. 3–14 show that bell nozzles (75 to 85% length) are just as efficient as or slightly more efficient than a longer 15° conical nozzle (100% length) at the same area ratio. For shorter nozzles (below 70% equivalent length) the energy losses due to internal oblique shock waves become substantial and such short nozzles are not commonly used today.

For solid propellant rocket motor exhausts with small solid particles in the gas (usually aluminum oxide), and for exhausts of certain gelled liquid propellants, there is an impingement of these solid particles against the nozzle wall in the reversing curvature section between I and E in Fig. 3–14. While the gas can be turned by oblique waves to have less divergence, the particles (particularly the larger particles) have a tendency to move in straight lines and hit the walls at high velocity. The resulting abrasion and erosion of the nozzle wall can be severe, especially with the ablative and graphite materials that are commonly used. This abrasion by hot particles increases with turn-back angle. If the turn-back angle and thus also the inflection angle θ_i are reduced, the erosion can become acceptable. Typical solid rocket motors flying today have values of inflection angles between 20 and 26° and turn-back angles of 10 to 15°. In comparison, current liquid rocket engines without entrained particles have inflection angles between 27 and 50° and turn-back angles of between 15 and 30°. Therefore the performance enhancement caused by using a bell-shaped nozzle (high value of correction factor) is somewhat lower in solid rocket motors with solid particles in the exhaust.

The ideal bell-shaped nozzle (minimum loss) is long, equivalent to a conical nozzle of perhaps 10 to 12°, as seen in Fig. 3–12. It has about the same length as a full-length aerospike nozzle. This is usually too long for reasonable vehicle mass ratios.

Two-Step Nozzles. A two-position nozzle (with different expansion area ratios) can give a better performance than a conventional nozzle with a fixed single area ratio. This can be seen in Fig. 3–10; the lower area ratio nozzle ($\epsilon = 6.0$) performs best at low altitudes and the higher area ratio nozzle performs best at higher altitudes. If these two nozzles could somehow be mechanically combined, the resulting two-position nozzle would perform closer to an ideal nozzle which adjusts continuously to the optimum area ratio, as shown by the thin dashed curve. When integrated over the flight time, the extra performance can be noticeable and it has a pay-off for high-velocity missions, such as earth-orbit injection and deep space missions. Several concepts of a bell-shaped nozzle have evolved that achieve maximum performance at more than a single altitude. Figure 3–15 shows three concepts for a two-step nozzle, one that has an initial low area ratio A_2/A_t for operation at or near the earth's surface and a larger second area ratio that improves performance at high altitudes. See Ref. 3–4.

The *extendible nozzle* requires actuators, a power supply, mechanisms for moving the extension into position during flight, and fastening and sealing devices. It has successfully flown in several solid rocket motor nozzles and in a few liquid engine applications, where it was deployed prior to ignition. Although only

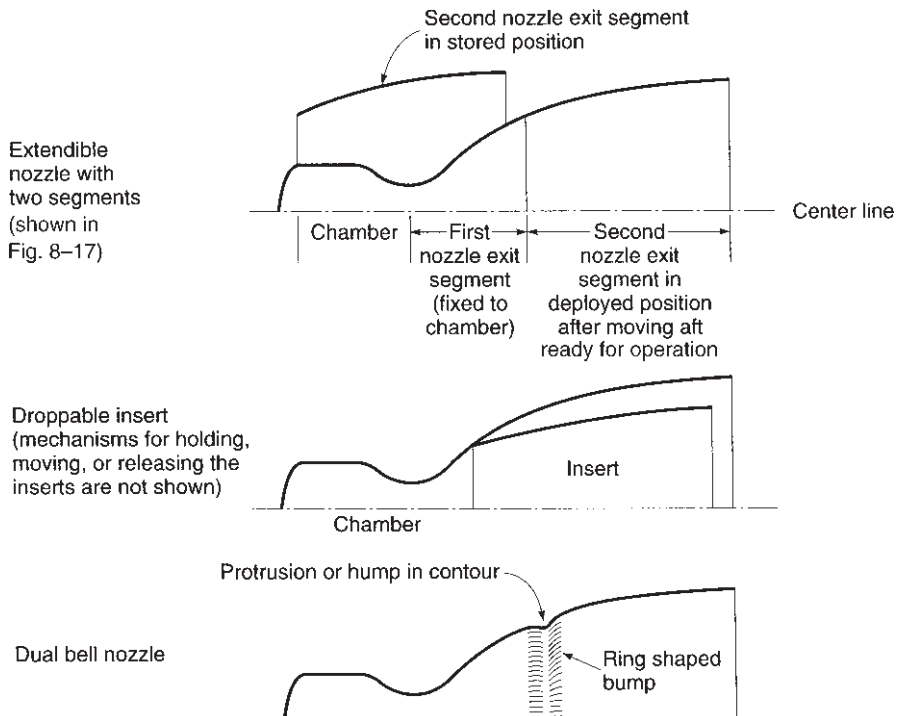


FIGURE 3–15. Simplified diagrams of three altitude-compensating two-step nozzle concepts. See Ref. 3–4.

two steps are shown, there have been versions with three steps; one is shown in Fig. 12–3. The key concerns are a reliable rugged mechanism to move the extension into position, the hot gas seal between the nozzle sections, and the extra weight involved. Its principal merit is the short length of the nozzle while stored. This reduces the length of the vehicle and a considerable part of the inert vehicle mass. A further benefit is a significant performance gain, compared to a single nozzle of a length equal to the stored length.

The *droppable insert concept* avoids the moving mechanism and gas seal but has a potential stagnation temperature problem at the joint. It requires a reliable release mechanism, and the ejected insert creates flying debris. To date it has only some actual test experience. See Refs. 3–4 and 3–12.

The *dual-bell nozzle concept* uses two shortened bell nozzles combined into one with a bump or inflection point between them, as shown in Fig. 3–15. During ascent it functions first at the lower area ratio, with separation occurring at the bump. As altitude increases and the gas expands further, the flow attaches itself downstream of this point, with the flow filling the full nozzle exit section and operating with the higher area ratio at higher performance. There is a small

performance penalty for a contour with a circular bump and concern about heat transfer. To date there has been little flight experience with this concept.

Nozzles with Aerodynamic Boundaries

These nozzles allow for nearly optimum nozzle expansion at all altitudes. The three nozzles shown on the right side of Fig. 3–12 offer full altitude compensation and are discussed next. Refs. 3–4 and 3–8 give more information. Altitude compensation means that the nozzle allows nearly optimum performance at every altitude. Complete rocket engines with either a cut-off plug nozzle or an expansion/deflection nozzle have been developed and have been ground tested. Tests with both pressurized feed systems and turbopump feed systems have been successful. However, as of 2008, none of these rocket engines with aerodynamic nozzle boundaries have flown in a production vehicle.

The *plug nozzle* or *aerospike nozzle* has an annular doughnut-shaped chamber with an annular nozzle slot. Annular nozzle throats may cause combustion problems. An alternate practical version has a number of individual small chambers (each with low area ratio short nozzles, a round throat, and a rectangular exit) arranged in a circle around a common plug or spike; see Fig. 8–12. The outside aerodynamic boundary of the gas flow in the divergent section of the nozzle is the interface between the hot gas and the ambient air; there is no outer wall as in a conical or bell-shaped nozzle. As the external or ambient pressure is reduced during the ascending flight, this gas boundary expands outward, causes a change in pressure distribution on the central spike, and allows an automatic and continuous altitude compensation. The aerospike contour with the minimum flow losses turns out to be very long, similar in length to an optimum bell nozzle as shown in Figs. 3–12 and 3–13. The mass flow per unit exit area is relatively uniform over the cross section and the divergence losses are minimal.

If the central plug is cut off or truncated and the wall contour is slightly altered, then the nozzle will be very short, as shown in Figs. 3–12, 3–13, and 3–14. It will have some internal supersonic waves and will show a small but real loss in thrust compared to a nozzle with a full length central spike. There is a small performance loss due to shock waves generated by the impingement of gases from the adjacent small chambers. The pressure distribution and the heat transfer intensity vary on the inner contoured spike wall surface and vary with altitude. Figure 8–12 shows a typical pressure distribution over the contoured spike surface at high and low altitudes.

The pressure in the recirculating trapped gas of the subsonic region below the bottom plate also exerts a thrust force. The losses caused by the cut-off spike can be largely offset by injecting a small amount of the gas flow (about 1% of total flow) through this base plate into the recirculating region, thus enhancing the back pressure on the base plate. The advantages of the truncated aerospike are short length (which helps to reduce the length and mass of the flight vehicle), full altitude compensation, no flow separation from the wall at lower altitudes, and ease of vehicle/engine integration for certain vehicle configurations.

The *linear aerospike nozzle* is a variation of the round axisymmetric aerospike nozzle. Basically, it is an unrolled version of the circular configuration. It is explained further in Section 8.2.

In the *expansion deflection nozzle* (Fig. 3–12) the flow from the chamber is directed radially outward away from the nozzle axis. The flow is turned on a curved contour outer diverging nozzle wall. The nozzle has been shortened and has some internal oblique shock wave losses. The hot gas flow leaving the chamber expands around a central plug. The aerodynamic interface between the ambient air and gas flow forms an inner boundary of the gas flow in the diverging nozzle section. As the ambient pressure is reduced, the hot gas flow fills more and more of the nozzle diverging section. Altitude compensation is achieved by this change in flow boundary and by changes in the pressure distribution on the outer walls. Actual ground tests with both liquid engines and solid motors have not yet led to routine flight tests.

Multiple Nozzles. If a single large nozzle is replaced by a cluster of smaller nozzles on a solid motor (with the same total thrust), then it is possible to reduce the nozzle length. Similarly, if a single large thrust chamber of a liquid engine is replaced by several smaller thrust chambers, the nozzle length will be shorter, reducing the vehicle length and thus the vehicle structure and inert mass. Reaction Motors, Inc. (RMI), in their first aircraft-rocket engine, and the Soviets pioneered a set of four thrust chambers, each with 25% of the total thrust, assembled next to each other and fed from the same liquid propellant feed system. This quadruple thrust chamber arrangement has been used effectively on many large Russian space launch vehicles and missiles. As seen in Fig. 3–13, the nozzle length of this cluster is about 30% shorter than a single nozzle of an equivalent larger thrust chamber. The vehicle diameter at the cluster nozzle exit is somewhat larger, the vehicle drag is higher, and there is additional engine complexity and often more engine mass.

3.5. REAL NOZZLES

The assumptions and simplifications listed in Section 3.1 are only approximations that allow relatively simple algorithms and simple mathematical solutions to the analysis of real rocket nozzle phenomena. For most of these assumptions it is possible either (1) to use an empirical correction factor (based on experimental data) or (2) to develop or use a more accurate algorithm, which involves more detailed understanding and simulation of energy losses, the physical or chemical phenomena, and also often a more complex theoretical analysis and mathematical treatment. Some of these approaches are mentioned briefly in this section.

Compared to an ideal nozzle, the real nozzle has energy losses and energy that is unavailable for conversion into kinetic energy of the exhaust gas. The principal losses are listed below and several of these are discussed in more detail.

1. The *divergence of the flow* in the nozzle exit sections causes a loss, which varies as a function of the cosine of the divergence angle as shown by Eq. 3–34 and Table 3–3 for conical nozzles. The losses can be reduced for bell-shaped nozzle contours.
2. Small chamber or port area cross sections relative to the throat area or *low nozzle contraction ratios* A_1/A_t cause pressure losses in the chamber and reduce the thrust and exhaust velocity slightly. See Table 3–2.
3. Lower flow velocity in the *boundary layer* or wall friction can reduce the effective exhaust velocity by 0.5 to 1.5%.
4. *Solid particles* or *liquid droplets* in the gas can cause losses perhaps up to 5%, as described below.
5. *Unsteady combustion* and oscillating flow can account for a small loss.
6. *Chemical reactions in nozzle flow* change gas composition and gas properties and gas temperatures, giving typically a 0.5% loss. See Chapter 5.
7. There is lower pressure and lower performance during *transient operation*, for example, during start, stop, or pulsing.
8. For uncooled nozzle materials, such as fiber-reinforced plastics or carbon, the gradual *erosion* of the *throat region* increases the throat diameter by perhaps 1 to 6% during operation. In turn this will reduce the chamber pressure and thrust by about 1 to 6%. This enlargement of the throat area causes a drop in chamber compression and a slight reduction in specific impulse usually less than 0.7%.
9. *Nonuniform gas composition* can reduce performance (due to incomplete mixing, turbulence, or incomplete combustion).
10. Using *real gas properties* can at times change the gas composition, the values of k and \mathfrak{M} , and this can cause a small loss in performance, say 0.2 to 0.7%.
11. Operation at nonoptimum nozzle expansion area ratio reduces thrust and specific impulse. There is no loss if the vehicle only flies at the altitude for optimum nozzle expansion ($p_2 = p_3$). If it flies with a fixed nozzle area ratio at higher or lower altitudes, then there is a loss (during a portion of the flight) by up to 15% in thrust compared to a nozzle with altitude compensation, as can be seen in Figs. 3–7 and 3–8. It also reduces performance by 1 to 5%.

Boundary Layer

Real nozzles have a viscous *boundary layer* next to the nozzle walls, where the gas velocities are much lower than the free-stream velocities in the inviscid flow regions. An enlarged schematic view of a boundary layer is shown in Fig. 3–16. Immediately next to the wall the flow velocity is zero and then the boundary layer can be considered as being built up of successive annular-shaped thin layers of increasing velocity until the free-stream velocity is reached. The low-velocity

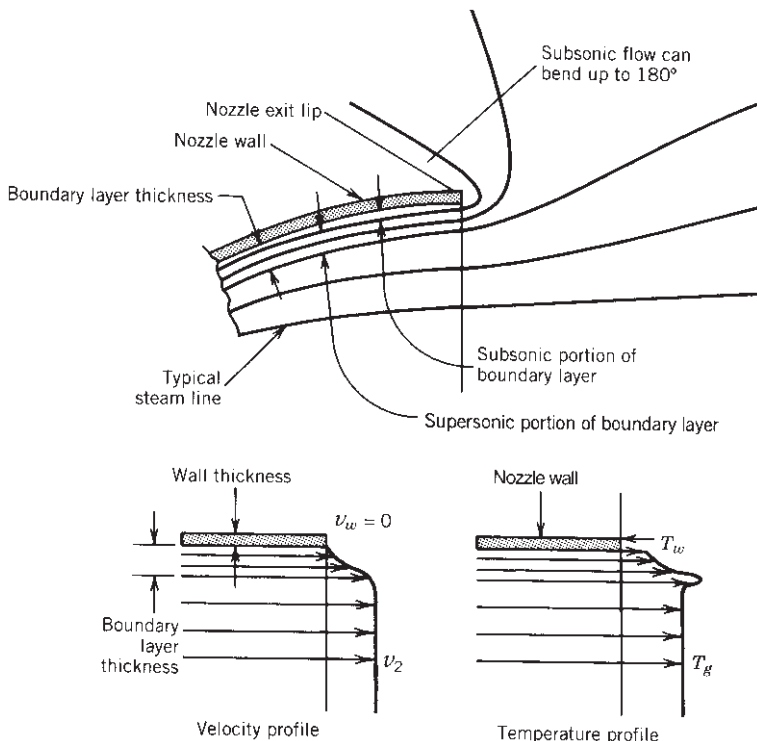


FIGURE 3–16. Flow conditions at a nozzle exit lip at high altitude, showing streamlines, boundary layer, velocity, and temperature profiles.

flow close to the wall is laminar and subsonic, but in the higher-velocity regions of the boundary layer the flow is supersonic and can become turbulent. The local temperature in part of the boundary layer can be substantially higher than the free-stream temperature because of the conversion of kinetic energy into thermal energy as the local velocity is slowed down and as heat is created by viscous friction. The layer right next to the wall will be cooler because of heat transfer to the wall. The gaseous boundary layer has a profound effect on the overall heat transfer to nozzle and chamber walls. It also has an effect on the rocket performance, particularly in applications with relatively long nozzles with high nozzle area ratios, where a relatively high proportion of the total mass flow (2 to 25%) can be in the lower-velocity region of the boundary layer. The high gradients in pressure, temperature, or density and the changes in local velocity (direction and magnitude) influence the boundary layer. Scaling laws for boundary layer phenomena have not been reliable.

Theoretical approaches to boundary layer performance effects can be found in Chapters 26 to 28 of Ref. 3–1 and in Ref. 3–17. A truly satisfactory theoretical analysis of boundary layers in rocket nozzles has not yet been developed. Fortunately, the overall effect of boundary layers on rocket performance has been small. For most rocket nozzles the loss seldom exceeds 1% of specific impulse.

Multiphase Flow

In some propulsion systems the gaseous working fluid contains small liquid droplets and/or solid particles that must be accelerated by the gas. They give up heat to the gas during the expansion in a nozzle. This, for example, occurs with solid propellants (see Chapter 13) or some gelled liquid propellants (Section 7.5), which contain aluminum powder that forms small oxide particles in the exhaust. It can also occur with iron oxide catalysts, or propellants containing beryllium, boron, or zirconium.

In general, if the particles are very small (typically with diameters of 0.005 mm or less), they will have almost the same velocity as the gas and will be in thermal equilibrium with the nozzle gas flow. Thus, as the gases give up kinetic energy to accelerate the particles, they gain thermal energy from the particles. As the particle diameters become larger, the mass (and thus the inertia) of the particle increases as the cube of its diameter; however, the drag force increases only as the square of the diameter. Larger particles therefore do not move as fast as the gas and do not give heat to the gas as readily as do smaller particles. The larger particles have a lower momentum than an equivalent mass of smaller particles and they reach the nozzle exit at a higher temperature than the smaller particles, thus giving up less thermal energy.

It is possible to derive a simple theoretical approach for correcting the performance (I_s , c , or c^*) as shown below and as given in Refs. 3–13 and 3–14. It is usually based on the following assumptions: specific heats of the gases and the particles are constant throughout the nozzle flow, the particles are small enough to move at essentially the same velocity as the gas and are in thermal equilibrium with the gas, and that particles do not exchange mass with the gas (no vaporization or condensation). Expansion and acceleration occur only in the gas, and the volume occupied by the particles is negligibly small compared to the gas volume. If the amount of particles is small, the energy needed to accelerate the particles can also be neglected. There are no chemical reactions.

The enthalpy h , the specific volume V , the specific heat notes k , and the gas constant R can be expressed as functions of the particle fraction β , which is the mass of particles (liquid and/or solid) divided by the total mass. Using the subscripts g and s to refer to the gas or solid state, the following relationships then apply:

$$h = (1 - \beta)(c_p)_g T + \beta c_s T \quad (3-35)$$

$$V = V_g(1 - \beta) \quad (3-36)$$

$$p = R_g T / V_g \quad (3-37)$$

$$R = (1 - \beta)R_g \quad (3-38)$$

$$k = \frac{(1 - \beta)c_p + \beta c_s}{(1 - \beta)c_v + \beta c_s} \quad (3-39)$$

These relations are then used in the formulas for simple one-dimensional nozzle flow, such as Eq. 2–16, 3–15, or 3–32. The values of specific impulse or characteristic velocity will decrease as β , the percent of particles, is increased. For very small particles (less than 0.01 mm in diameter) and small values of β (less than 6%) the loss in specific impulse is often less than 2%. For larger particles (over 0.015 mm diameter) and larger values of β this theory is not helpful and the specific impulse can be 10 to 20% less than the I_s value without flow lag. The actual particle sizes and distribution depend on the specific propellant, the combustion, the particular particle material, and the specific rocket propulsion system, and usually have to be measured (see Chapters 13 and 20). Thus adding a metal, such as aluminum, to a solid propellant will increase the performance only if the additional heat release can increase the combustion temperature T_1 sufficiently so that it more than offsets the decrease caused by the nonexpanding mass of the particles in the exhaust.

With very high area ratio nozzles and a low nozzle exit pressure (high altitude or space vacuum) it is possible to condense some of the propellant ingredients that are normally gases. As the temperature drops sharply in the nozzle, it is possible to condense gaseous species such as H_2O , CO_2 , or NH_3 and form liquid droplets. This causes a decrease in the gas flow per unit area and the transfer of the latent heat of vaporization to the remaining gas. The overall effect on performance is small if the droplet size is small and the percent of condensed gas mass is moderate. It is also possible to form a solid phase and precipitate fine particles of snow (H_2O) or frozen fog of other species.

Other Phenomena and Losses

The *combustion process* is really not steady. Low- and high-frequency oscillations in chamber pressure of up to perhaps 5% of rated value are usually considered as smooth-burning and relatively steady flow. Gas properties (k, \mathfrak{M}, c_p) and flow properties (v, V, T, p , etc.) will also oscillate with time and will not necessarily be uniform across the flow channel. These properties are therefore only “average” values, but it is not always clear what kind of an average they are. The energy loss due to nonuniform unsteady burning is difficult to assess theoretically. For smooth-burning rocket systems they are negligibly small, but they become significant for larger-amplitude oscillations.

The *composition of the gas* changes somewhat in the nozzle, chemical reactions occur in the flowing gas, and the assumption of a uniform or “frozen” equilibrium gas composition is not fully valid. A more sophisticated analysis for determining performance with changing composition and changing gas properties is described in Chapter 5. The thermal energy that is carried out of the nozzle ($\dot{m}c_pT_2$) is unavailable for conversion to useful propulsive (kinetic) energy, as is shown in Fig. 2–3. The only way to decrease this loss is to reduce the nozzle exit temperature T_2 (larger nozzle area ratio), but even then it is a large loss.

When the operating durations are short (as, e.g., with antitank rockets or pulsed attitude control rockets which start and stop repeatedly), the start and

stop *transients* are a significant portion of the total operating time. During the transient periods of start and stop the average thrust, chamber pressure, or specific impulse will be lower in value than those same parameters at steady full operating conditions. This can be analyzed in a step-by-step process. For example, during startup the amount of propellant reacting in the chamber has to equal the flow of gas through the nozzle plus the amount of gas needed to fill the chamber to a higher pressure; alternatively, an empirical curve of chamber pressure versus time can be used as the basis of such a calculation. The transition time is very short in small, low-thrust propulsion systems, perhaps a few milliseconds, but it can be longer (several seconds) for large propulsion systems.

Performance Correction Factors

Additional to the theoretical cone- and bell-shaped nozzle correction factors discussed in Section 3.4., we discuss here a set of empirical correction factors. These factors represent a variety of nonideal phenomena (such as friction, imperfect mixing and combustion, heat transfer, chemical nonequilibrium, and two- and three-dimensional effects) which are unavoidably present; refer to Fig. 2–3 and Ref. 3–4. Correction factors are defined for convenience in rocket analysis and may differ from the more conventional efficiencies—there are no “universal performance correction factors.” For specific propulsion systems, where accurately measured data are available, they allow for simple predictions of the actual performance. For example, a velocity correction factor of 0.942 means that the velocity or the actual specific impulse is about 94% of theoretical (the commonly accepted value might be closer to 0.92).

Corrections factors are used by engineers to predetermine performance ahead of testing, and for preliminary designs, informal proposals, and in health monitoring systems. For all these, a set of *accepted* or *nominal values* is needed to estimate performance together with some useful formula-recipes. For the most accurate calculations, the industry relies extensively on sophisticated computer programs which are largely proprietary.

Correction factors are ratios of the measured or *actual* (subscript “*a*”) to the formulated or *ideal* (subscript “*i*”) values. In the testing of propulsion systems, the combustion chamber pressure, the propellant mass flow rates, the thrust force, and the throat and exit areas are typically measured. These measurements yield two direct ratios, namely the *thrust correction factor* ($\zeta_F = F_a/F_i$) and the *discharge correction factor* ($\zeta_d = \dot{m}_a/\dot{m}_i$), and as well the product $[(p_1)_a(A_t)_a]$ which has the units of force. This product enters into the formulation of two other correction factors discussed below. The *nozzle area ratio* [$\epsilon_a = (A_2)_a/(A_t)_a$] in real nozzles may be found from their measured dimensions and this ratio will differ from the ideal calculated value as will be shown in Example 3–7.

The thrust correction factor (ζ_F) is found from the ratio of thrust measurements with the corresponding ideal values of Eq. 3–29. The discharge correction factor (ζ_d) can be determined from the ratio of mass-flow-rate measurements with the corresponding theoretical values of Eq. 3–24. Unlike incompressible flows, in

rocket propulsion systems the value of ζ_d is always somewhat larger than 1.0 (up to 1.15). The actual flow rate may be larger than the ideal flow rate for the following reasons:

1. Incomplete combustion (a lower combustion temperature) which results in increases of the exhaust gas densities.
2. Cooling at the walls which reduces the boundary layer temperature and thus the average gas temperature, especially in small thrust chambers.
3. Changes in the specific heat ratio and molecular mass in an actual nozzle which affect the flow rate and thus the discharge correction factor (see Eq. 3-24).

The c^* efficiency or ζ_{c^*} correction factor represents the combined effectiveness of the combustion chamber and the injector design. It can be determined from the ratio of measured values of $[(p_1)_a(A_t)_a]/\dot{m}_a$ (from Eq. 2-18) with the corresponding ideal value of the right-hand side of Eq. 3-32. In well-designed combustion chambers, the value of ζ_{c^*} correction factor is over 95%. The ζ_{C_F} correction factor, also known as the C_F efficiency, represents the effectiveness of the nozzle design at the operating conditions. It can be determined using measured values (from Eq. 3-31) of $F_a/[(p_1)_a(A_t)_a]$ with the corresponding ideal value of Eq. 3-30. In well-designed nozzles, the value of the ζ_{C_F} correction factor is above 90%.

An effective exhaust velocity correction factor [$\zeta_v \equiv (F_a/\dot{m}_a)/c_i$] may now be introduced using that velocity's definition given in Eq. 2-17 (or from Eq. 3-32, $c = c^* C_F$) as

$$\zeta_v = \zeta_F / \zeta_d = \zeta_{c^*} \zeta_{C_F} \quad (3-40)$$

This further suggests a correction factors relation, a form equivalent to Eq. 3-33, written as $\zeta_F = \zeta_d \zeta_{c^*} \zeta_{C_F}$ which must hold only within experimental uncertainties.

Additional useful relations may now be written. The actual specific impulse, from Eq. 2-5, may now be calculated from

$$(I_s)_a = (I_s)_i (\zeta_v) \quad (3-41)$$

The thermodynamic nozzle efficiency η_n which is defined as the ratio of ideal to the actual enthalpy changes (see Eqs. 3-15a and 3-16) under a given pressure ratio becomes

$$\eta_n = (\Delta h)_a / (\Delta h)_i = \frac{1}{2}(v_2^2)_a / \frac{1}{2}(v_2^2)_i \approx (\zeta_v)^2 \quad (3-42)$$

The approximation sign becomes an equality when $p_2 = p_3$. This nozzle efficiency will be always less than one and represents losses inside the nozzle (Ref. 3-17). Small nozzles being used in *micropulsion* can be quite inefficient because of their relatively larger frictional effects which are in proportion

to the surface-to-volume ratio (some being rectangular thus having additional sharp-corner losses).

Under strictly *frozen-flow* assumptions, the right-hand side of Eq. 3–32 leads to a useful relation between the ideal and actual stagnation temperatures [where $(T_0)_i \equiv T_1$] :

$$(T_0)_a / (T_0)_i \approx (\zeta_{c^*})^2 \quad (3-43)$$

With conditions at the inlet of the nozzle readily calculable, one task is to determine the actual throat area required to pass a specified mass flow rate of gaseous propellant and also to determine the area and the flow properties at the nozzle exit plane. Across the nozzle heat losses modify the local stagnation temperatures and, together with friction, the stagnation pressures (which begin as $(p_0)_1 = p_1$ and T_1 in the combustion chamber). Because ideal formulations are based on the *local stagnation* values at any given cross section, the challenge is to work with the appropriate flow assumptions as shown below.

When the applicable correction factors values are available, the overall ratio of the product of the stagnation pressure with the throat area may be inferred using

$$[(A_t)_a (p_1)_a] / [(A_t)_i (p_1)_i] = \zeta_F / \zeta_{CF} \quad \text{or} \quad \zeta_d \zeta_{c^*} \quad (3-44)$$

In order to arrive at the actual nozzle throat area from such available parameters additional information is needed. The key question is how to relate stagnation pressure ratios to their corresponding temperature ratios across the nozzle. When known, a *polytropic index* “ n ” providing a relation between gas properties is useful (Ref. 3–17); otherwise, we may apply the isentropic relation given as Eq. 3–7 because nozzle efficiencies are typically high (around 90%). Real nozzle flows are not isentropic but the *net entropy* change along the nozzle may be insignificant, though noticeable decreases of the stagnation pressure and temperature do exist as Example 3–7 will detail next. When dealing with real nozzles with given expansion ratios, increases of stagnation pressure over $(p_1)_i$ would be necessary to achieve a desired performance.

Example 3–7. Design a rocket nozzle to conform to the following conditions:

| | |
|------------------------------|-----------------------------------|
| Chamber pressure | 20.4 atm = 2.067 MPa |
| Atmospheric pressure | 1.0 atm |
| Mean molecular mass of gases | 21.87 kg/kg-mol |
| Specific heat ratio | 1.23 |
| Ideal specific impulse | 230 sec (at operating conditions) |
| Desired thrust | 1300 N |
| Chamber temperature | 2861 K |

Determine the actual exhaust velocity, the actual specific impulse, and the nozzle throat and exit areas. Also calculate the discharge correction factor and nozzle efficiency implied by the following correction factors which are applicable to this problem: $\zeta_F = 0.96$, $\zeta_{c^*} = 0.98$, and $\zeta_{CF} = 0.97$.

SOLUTION. The theoretical thrust coefficient can be calculated from Eq. 3–30. For optimum conditions, $p_2 = p_3$. By substituting $k = 1.23$ and $p_1/p_2 = 20.4$, the thrust coefficient is $(C_F)_i = 1.405$ and $(A_t)_i = 4.48 \text{ cm}^2$. These calculated values may be checked by interpolation between the values shown in Fig. 3–6.

An *actual effective exhaust velocity* is not measured, but for this problem it may be calculated from

$$c_a = (c_i)(\zeta_v) = (230 \times 9.81)(0.98 \times 0.97) = 2145 \text{ m/sec}$$

The actual specific impulse is $(I_s)_a = 2145/9.81 = 219 \text{ sec}$ and the discharge correction factor from Eq. 3–40

$$\zeta_d = \zeta_F/\zeta_{c^*}\zeta_{CF} = 0.96/(0.98 \times 0.97) = 1.01$$

Because for this problem, $v_2 = c$, the nozzle efficiency is found from $\eta_n = (\zeta_v)^2 = 90\%$.

An approximate exit stagnation temperature may be found using Eq. 3–43, $(T_0)_a \approx T_1(\zeta_{c^*})^2 = 2748 \text{ K}$. Now, an estimate of the stagnation pressure at the throat is needed but correction factors only apply to the overall nozzle. Because the nozzle efficiency is only 10% less than ideal, a sufficient approximation is to assign half of the *stagnation temperature* drop to the region upstream of the throat, or $(T_0)_t \approx 2804 \text{ K}$. Thus,

$$(p_0)_t \approx p_1[2804/2861]^{(k/k-1)} = 1.86 \text{ MPa}$$

The throat area may now be computed from Eq. 3–44:

$$(A_t)_a/(A_t)_i = (\zeta_F/\zeta_{CF})(p_1/(p_0)_t) = 1.10$$

As may have been expected, the actual throat area is about 10% larger than the ideal for the same flow conditions. The actual exit area may be obtained going back to the mass flow rate:

$$\dot{m} = \zeta_F F/c_a = 0.582 \text{ kg/sec} = p_2 A_2 c / RT_2$$

Now, $p_2 = p_3$ is given and T_2 is found from

$$T_2 \approx 2748 \times (0.1013/1.67)^{(0.229/1.229)} = 1631 \text{ K}$$

where $(p_0)_a \approx 1.67 \text{ MPa}$ is an actual stagnation pressure applicable to the exit of the real nozzle. Finally, the exit area and area ratio are found to be. $(A_2)_a \approx 16.61 \text{ cm}^2$ and $\epsilon_a \approx 3.37$, which may be compared to the value from Fig. 3–4.

Four Performance Parameters

When using values or quoting of thrust, specific impulse, propellant flow, and other performance parameters, one must be careful to specify or qualify the conditions under which a specific number is presented. There are at least four sets of performance parameters and they are different in concept and value, even when referring to the same rocket propulsion system. Each performance parameter, such as F , I_s , c , v_2 , and/or \dot{m} , should be accompanied by a clear definition of the conditions under which it applies. Not all the items below apply to every one of the parameters.

- (a) Chamber pressure; also, for slender chambers, the location where this pressure prevails or is measured (e.g., at nozzle entrance).
- (b) Ambient pressure or altitude or space (vacuum).
- (c) Nozzle expansion area ratio and whether this is an optimum.
- (d) Nozzle shape and exit angle (see Table 3–3 and Fig. 3–12).
- (e) Propellants, their composition or mixture ratio.
- (f) Key assumptions and corrections made in the calculations of the theoretical performance: for example, was frozen or shifting equilibrium used in the analysis? (This is described in Chapter 5.)
- (g) Initial ambient temperature of propellants, prior to start.

1. *Theoretical performance values* are defined in Chapters 2, 3, and 5 and generally apply to ideal rockets. The conditions for an ideal nozzle were given in Section 3.1. The theoretical performance of an ideal nozzle per se is not used, but one that includes theoretical corrections is used. Analyses of one or more losses can be included, and these will yield a lower theoretical performance and also an assessment in the correction factors described in the previous section. Most are two dimensional and correct for the chemical reactions in the nozzle using real gas properties, and most correct for divergence. Many also correct for one or more of the other losses mentioned above. For example, programs for solid propellant motor nozzles can include losses for throat erosion and multiphase flow; for liquid propellant engines it may include two or more concentric zones, each at different mixture ratios and thus with different gas properties. Nozzle wall contour analysis with expansion and compression waves may use a finite element analysis and/or a method of characteristics approach. Some of the more sophisticated programs include analyses of viscous boundary layer effects and heat transfer to the walls. Typically these computer simulation programs are based on computer fluid dynamics finite element analyses and on the basic Navier–Stokes relationships. Most organizations doing nozzle design have their own computer programs, often different programs for different nozzle designs, different thrust levels, or operating durations. Many also have simpler,

one-dimensional computer programs which may include one or more of the above corrections; they are used frequently for preliminary estimates or informal proposals.

2. *Delivered*, that is, *actually measured, performance values* are obtained from static tests or flight tests of full-scale propulsion systems. Again, the conditions should be explained (e.g., define $p_1, A_2/A_t, p_3$, etc.) and the measured values should be corrected for instrument deviations, errors, or calibration constants. Flight test data need to be corrected for aerodynamic effects, such as drag. Often empirical coefficients, such as the thrust correction factor, the velocity correction factor, and the mass discharge flow correction factors are used to convert the theoretical values of item 1 above to approximate actual values and this is often satisfactory for preliminary estimates. Sometimes subscale thrust chambers have been used in the development of new thrust chambers and then scale factors are used to correct the measured data to full-scale values.

3. *Performance values at standard conditions* are corrected values of items 1 and 2 above. These standard conditions are generally rigidly specified by the customer and by commonly accepted industrial practice. Usually they refer to conditions that allow ready evaluation or comparison with reference values and often they refer to conditions that can be easily measured and/or corrected. For example, to allow a good comparison of specific impulse for several propellants or rocket propulsion systems, the values are often corrected to the following standard conditions (see Example 3–6):

- (a) $p_1 = 1000$ psia or 6.894×10^6 Pa.
- (b) $p_2 = p_3 = 14.69$ psia (sea level) or 1.0132×10^5 Pa or 0.10132 Mpa.
- (c) Nozzle exit area ratio is optimum, $p_2 = p_3$.
- (d) Nozzle divergence half angle $\alpha = 15^\circ$ for conical nozzles, or some agreed-upon value.
- (e) Specific propellant, its design mixture ratio, and/or propellant composition.
- (f) Propellant initial ambient temperature: 21°C (sometimes 20 or 25°C) or boiling temperature, if cryogenic.

A rocket propulsion system is generally designed, built, tested, and delivered in accordance with some predetermined requirements or *specifications*, usually in formal documents often called the *rocket engine or rocket motor specifications*. They may define the performance as shown above and they also define many other requirements. More discussion of these specifications is given as a part of the selection process for propulsion systems in Chapter 19.

4. Rocket manufacturers are often required by their customers to deliver rocket propulsion systems with a *guaranteed minimum performance*, such as minimum F or minimum I_s and/or both. The determination of this value can be based on a nominal value (items 1, 2, or 3 above) diminished by all likely losses, including changes in chamber pressure due to variation of pressure drops in injector or pipelines, a loss due to nozzle surface roughness, propellant initial

ambient temperatures, ambient pressure variations, and manufacturing variations from rocket to rocket (e.g., in grain volume, nozzle dimensions, or pump impeller diameters, etc.). This minimum value can be determined by a probabilistic evaluation of these losses and is then usually validated by actual full-scale static and flights tests.

3.6. NOZZLE ALIGNMENT

When the thrust line or direction does not intersect the center of mass of a flying vehicle, a turning moment will tend to rotate a vehicle in flight. Turning moments are desirable and necessary for the controlled turning or attitude control of a vehicle as is routinely done by means of the deflection of the thrust vector, aerodynamic fins, or by separate attitude control rocket engines. However, this turning is undesirable when its magnitude or direction is not known; this happens when a fixed nozzle of a major propulsion system has its thrust axis misaligned. A large high-thrust booster rocket system, even if misaligned by a very small angle (less than 0.50°), can cause major upsetting turning moments for the firing duration. If not corrected or compensated, such a small misalignment can cause the flight vehicle to tumble and/or deviate from the intended flight path. For this moment not to exceed the vehicle's compensating attitude control capability, it is necessary to align the nozzle axis of all propulsion systems with fixed (nongimbal) nozzles very accurately. Normally, the geometric axis of the nozzle diverging exit surface geometry is taken to be the thrust axis. Special alignment fixtures are usually needed to orient the nozzle axis to be within less than $\pm 0.25^\circ$ of the intended line to the vehicle's center of gravity and to position the center of a large nozzle throat to be on the vehicle centerline, say within 1 or 2 mm. See Ref. 3–16.

There are other types of misalignments: (1) irregularities in the nozzle geometry (out of round, protuberances, or unsymmetrical roughness in the surface); (2) transient flow misalignments during start or stop; (3) uneven deflection of the propulsion system or vehicle structure under load; and (4) irregularities in the gas flow (faulty injector, uneven burning rate in solid propellants). For simple unguided rocket vehicles it has been customary to rotate or spin the vehicle to prevent the misalignment from being in one direction only or to even out the misalignment during powered flight.

In the cramped volume of spacecraft or upper stage launch vehicles, it is sometimes not possible to accommodate the full length of a large-area-ratio nozzle within the available vehicle envelope. In this case the nozzles are cut off at an angle at the vehicle surface, which allows a more compact installation. Figure 3–17 shows a diagram of two (out of four) roll control thrusters whose nozzle exit conforms to the vehicle contour. The thrust direction of a *scarfed nozzle* is no longer on the nozzle axis centerline, as it is with fully symmetrical nozzles, and the nozzle exit flow will not be axisymmetric. Reference 3–16 shows how to estimate the performance and thrust direction of scuffed nozzles.

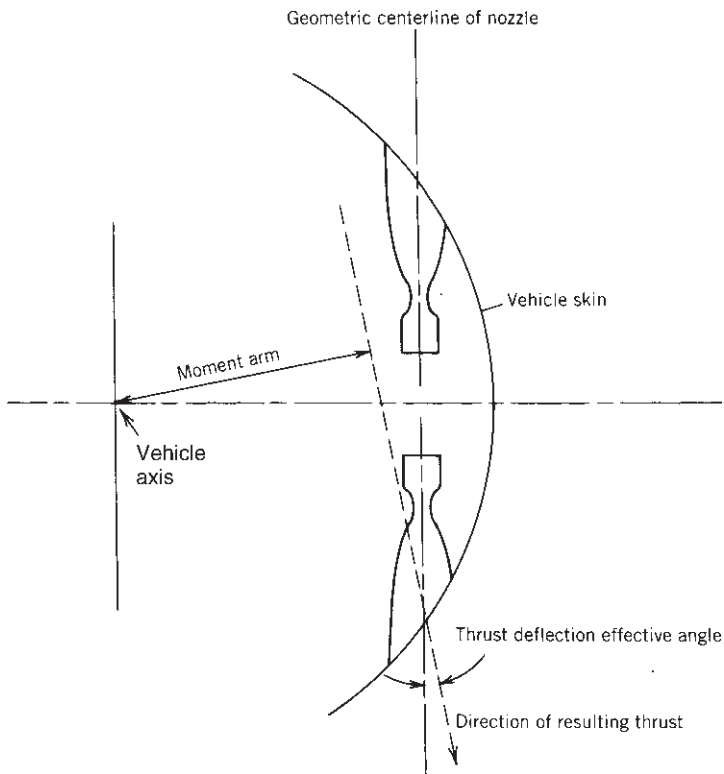


FIGURE 3–17. Simplified partial section of a flight vehicle showing two attitude control thrusters with scarfed nozzles to fit a cylindrical vehicle envelope.

PROBLEMS

1. Certain experimental results indicate that the propellant gases of a liquid oxygen–gasoline reaction have a mean molecular mass of 23.2 kg/kg-mol and a specific heat ratio of 1.22. Compute the specific heat at constant pressure and at constant volume, assuming a perfect gas.
2. The actual conditions for an optimum expansion nozzle operating at sea level are given below. Calculate v_2 , T_2 , and C_F . The mass flow $\dot{m} = 3.7 \text{ kg/sec}$; $p_1 = 2.1 \text{ MPa}$; $T_1 = 2585 \text{ K}$; $\mathfrak{M} = 18.0 \text{ kg/kg-mol}$; and $k = 1.30$.
3. A certain nozzle expands a gas under isentropic conditions. Its chamber or nozzle entry velocity equals 90 m/sec, its final velocity 1500 m/sec. What is the change in enthalpy of the gas? What percentage of error is introduced if the initial velocity is neglected?
4. Nitrogen at 500°C ($k = 1.38$, molecular mass is 28.00) flows at a Mach number of 2.73. What are its actual and its acoustic velocity?

5. The following data are given for an optimum rocket:

| | |
|------------------------|------------------------|
| Average molecular mass | 24 kg/kg-mol |
| Chamber pressure | 2.533 MPa |
| External pressure | 0.090 MPa |
| Chamber temperature | 2900 K |
| Throat area | 0.00050 m ² |
| Specific heat ratio | 1.30 |

Determine (a) throat velocity; (b) specific volume at throat; (c) propellant flow and specific impulse; (d) thrust; (e) Mach number at throat.

6. Determine the ideal thrust coefficient for Problem 5 by two methods.
7. A certain ideal rocket with a nozzle area ratio of 2.3 and a throat area of 5 in.² delivers gases at $k = 1.30$ and $R = 66 \text{ ft-lbf/lbm}^{\circ}\text{R}$ at a chamber pressure of 300 psia and a constant chamber temperature of 5300°R against a back atmospheric pressure of 10 psia. By means of an appropriate valve arrangement, it is possible to throttle the propellant flow to the thrust chamber. Calculate and plot against pressure the following quantities for 300, 200, and 100 psia chamber pressure: (a) pressure ratio between chamber and atmosphere; (b) effective exhaust velocity for area ratio involved; (c) ideal exhaust velocity for optimum and actual area ratio; (d) propellant flow; (e) thrust; (f) specific impulse; (g) exit pressure; (h) exit temperature.
8. For an ideal rocket with a characteristic velocity $c^* = 1500 \text{ m/sec}$, a nozzle throat diameter of 20 cm, a thrust coefficient of 1.38, and a mass flow rate of 40 kg/sec, compute the chamber pressure, the thrust, and the specific impulse.
9. For the rocket unit given in Example 3-2 compute the exhaust velocity if the nozzle is cut off and the exit area is arbitrarily decreased by 50%. Estimate the losses in kinetic energy and thrust and express them as a percentage of the original kinetic energy and the original thrust.
10. What is the maximum velocity if the nozzle in Example 3-2 was designed to expand into a vacuum? If the expansion area ratio was 2000?
11. Construction of a variable-area conventional axisymmetric nozzle has often been considered to make the operation of a rocket thrust chamber take place at the optimum expansion ratio at any altitude. Because of the enormous design difficulties of such a mechanical device, it has never been successfully realized. Assuming that such a mechanism can eventually be constructed, what would have to be the variation of the area ratio with altitude (plot up to 50 km) if such a rocket had a chamber pressure of 20 atm? Assume that $k = 1.20$.
12. Design a supersonic nozzle to operate at 10 km altitude with an area ratio of 8.0. For the hot gas take $T_0 = 3000 \text{ K}$, $R = 378 \text{ J/kg-K}$, and $k = 1.3$. Determine the exit Mach number, exit velocity, and exit temperature, as well as the chamber pressure. If this chamber pressure is doubled, what happens to the thrust and the exit velocity? Assume no change in gas properties. How close to optimum nozzle expansion is this nozzle?

- 13.** The German World War II A-4 propulsion system had a sea-level thrust of 25,400 kg and a chamber pressure of 1.5 MPa. If the exit pressure is 0.084 MPa and the exit diameter 740 mm, what is the thrust at 25,000 m?
- 14.** Derive Eq. 3–34. (*Hint:* Assume that all the mass flow originates at the apex of the cone.) Calculate the nozzle angle correction factor for a conical nozzle whose divergence half angle is 13° .
- 15.** For Example 3–2, determine **(a)** the actual thrust; **(b)** the actual exhaust velocity; **(c)** the actual specific impulse; **(d)** the velocity correction factor. Assume that the thrust correction factor is 0.985 and the discharge correction factor is 1.050.
- 16.** An ideal rocket has the following characteristics:

| | |
|------------------------|-----------------|
| Chamber pressure | 27.2 atm |
| Nozzle exit pressure | 3 psia |
| Specific heat ratio | 1.20 |
| Average molecular mass | 21.0 lbm/lb-mol |
| Chamber temperature | 4200°F |

Determine the critical pressure ratio, the gas velocity at the throat, the expansion area ratio, and the theoretical nozzle exit velocity.

Answers: 0.5645; 3470 ft/sec; 14.8; and 8570 ft/sec.

- 17.** For an ideal rocket with a characteristic velocity c^* of 1220 m/sec, a mass flow rate of 73.0 kg/sec, a thrust coefficient of 1.50, and a nozzle throat area of 0.0248 m^2 , compute the effective exhaust velocity, the thrust, the chamber pressure, and the specific impulse.

Answers: 1830 m/sec; 133,560 N; $3.590 \times 10^6 \text{ N/m}^2$; 186.7 sec.

- 18.** Derive Eqs. 3–24 and 3–25.
- 19.** An upper stage of a launch vehicle propulsion unit fails to meet expectations during sea-level testing. This unit consists of a chamber at 4.052 MPa feeding hot propellant to a supersonic nozzle of area ratio $\epsilon = 20$. The local atmospheric pressure at the design condition is 20 kPa. The propellant has a $k = 1.2$ and the throat diameter of the nozzle is 9 cm.

- (a)** Calculate the ideal thrust at the design condition.
(b) Calculate the ideal thrust at the sea-level condition.
(c) State the most likely source of the observed nonideal behavior.

Answers: **(a)** 44.4 kN, **(b)** 34.1 kN, **(c)** separation in the nozzle

- 20.** Assuming ideal flow within the propulsion unit:

- (a)** State all necessary conditions (realistic or not) for

$$c^* = c = v_2$$

- (b)** Do the above conditions result in an *optimum* thrust for a given p_1/p_3 ?

- (c) For a launch vehicle designed to operate at some intermediate earth altitude, sketch (in absolute or relative values) how c^* , c , and v_2 would vary with altitude.
21. A rocket nozzle has been designed with $A_t = 19.2 \text{ in.}^2$ and $A_2 = 267 \text{ in.}^2$ to operate optimally at $p_3 = 4 \text{ psia}$ and produce 18,100 lbf of ideal thrust with a chamber pressure of 570 psia. It will be attached to a previously built thrust chamber that operates at $T_1 = 6000^\circ\text{R}$ with $k = 1.25$ and $R = 68.75 \text{ ft-lbf/lbm}^\circ\text{R}$, with a c^* efficiency of 95%. But test measurements on this thrust system, at the stated pressure conditions, yield a thrust of only 16,300 lbf when the measured flow rate is 2.02 lbm/sec. Find the applicable correction factors (ζ_F , ζ_d , ζ_{C_F}) and the actual specific impulse assuming frozen flow throughout.

Answers: $\zeta_F = 0.90$; $\zeta_d = 1.02$; $\zeta_{C_F} = 0.929$; $(I_S)_a = 250 \text{ sec}$.

SYMBOLS

| | |
|----------------|---|
| A | area, $\text{m}^2(\text{ft}^2)$ |
| c | effective exhaust velocity, m/sec (ft/sec) |
| c_p | specific heat at constant pressure, $\text{J/kg-K (Btu/lbm}^\circ\text{R)}$ |
| c_s | specific heat of solid, $\text{J/kg-K (Btu/lbm}^\circ\text{R)}$ |
| c_v | specific heat at constant volume, $\text{J/kg-K (Btu/lbm}^\circ\text{R)}$ |
| c^* | characteristic velocity, m/sec (ft/sec) |
| C_F | thrust coefficient |
| C_D | discharge coefficient ($1/c^*$), sec/m (sec/ft) |
| d | total derivative |
| D | diameter, m (ft) |
| F | thrust, N (lbf) |
| g_0 | standard sea-level gravitational acceleration, $9.8066 \text{ m/sec}^2(32.174 \text{ ft/sec}^2)$ |
| h | enthalpy per unit mass, J/kg (Btu/lbm) (or altitude, km) |
| I_S | specific impulse, $\text{sec or N-sec}^3/\text{kg-m (lbf-sec/lbm)}$ |
| J | mechanical equivalent of heat; $J = 4.186 \text{ J/cal}$ in SI units or 1 Btu = 777.9 ft-lbf |
| k | specific heat ratio |
| L | length of nozzle, m (ft) |
| \dot{m} | mass flow rate, kg/sec (lbf/sec) |
| M | mach number |
| \mathfrak{M} | molecular mass, kg/kg-mol (or molecular weight, lbf/lb-mol) |
| n_i | molar fraction of species i |
| p | pressure, $\text{N/m}^2(\text{lbf/ft}^2 \text{ or lbf/in.}^2)$ |
| R | gas constant per unit weight, $\text{J/kg-K (ft-lbf/lbm}^\circ\text{R)}$ ($R = R'/\mathfrak{M}$) |
| R' | universal gas constant, $8314.3 \text{ J/kg mol-K (1544 ft-lb/lb mol}^\circ\text{R)}$ |
| T | absolute temperature, $\text{K} (\text{R})$ |
| v | velocity, m/sec (ft/sec) |
| V | specific volume, $\text{m}^3/\text{kg (ft}^3/\text{lbf)}$ |
| \dot{w} | propellant weight flow rate, N/sec (lbf/sec) |

Greek Letters

| | |
|---------------|--|
| α | half angle of divergent conical nozzle section |
| β | mass fraction of solid particles |
| ϵ | nozzle expansion area ratio A_2/A_t |
| ζ_{C_F} | thrust coefficient correction factor |
| ζ_{c^*} | c^* correction factor |
| ζ_d | discharge correction factor |
| ζ_F | thrust correction factor |
| ζ_v | velocity correction factor |
| λ | divergence angle correction factor for conical nozzle exit |
| η_n | nozzle efficiency |

Subscripts

| | |
|-----|---|
| a | actual |
| g | gas |
| i | ideal, or a particular species in a mixture |
| max | maximum |
| opt | optimum nozzle expansion |
| s | solid |
| sep | point of separation |
| t | throat |
| x | any plane within rocket nozzle |
| y | any plane within rocket nozzle |
| 0 | stagnation or impact condition |
| 1 | nozzle inlet or chamber |
| 2 | nozzle exit |
| 3 | atmospheric or ambient |

REFERENCES

- 3–1. A. H. Shapiro, *The Dynamics and Thermodynamics of Compressible Fluid Flow*, Vols. 1 and 2, Ronald Press Company, New York, 1953; and M. J. Zucrow and J. D. Hoffman, *Gas Dynamics*, Vols. I and II, John Wiley & Sons, New York, 1976 (has section on nozzle analysis by method of characteristics).
- 3–2. M. J. Moran and H. N. Shapiro, *Fundamentals of Engineering Thermodynamics*, 3rd ed., John Wiley & Sons, New York, 1996; also additional text, 1997.
- 3–3. H. H. Koelle (Ed), *Handbook of Astronautical Engineering*, McGraw-Hill Book Company, New York, 1961.
- 3–4. G. Hagemann, H. Immich, T. Nguyen, and G. E. Dummov, “Rocket Engine Nozzle Concepts,” Chapter 12 of *Liquid Rocket Thrust Chambers: Aspects of Modeling, Analysis and Design*, V. Yang, M. Habiballah, J. Hulkka, and M. Popp (Eds), Progress in Astronautics and Aeronautics, Vol. 200, AIAA, 2004.

- 3–5. P. Vuillermoz, C. Weiland, G. Hagemann, B. Aupoix, H. Grosdemange, and M. Bigert, “Nozzle Design Optimization,” Chapter 13 of *Liquid Rocket Thrust Chambers: Aspects of Modeling, Analysis and Design*, V. Yang, M. Habiballah, J. Hulkka, and M. Popp (Eds), Progress in Astronautics and Aeronautics, Vol. 200, AIAA, 2004.
- 3–6. “Liquid Rocket Engine Nozzles”, NASA SP-8120, 1976.
- 3–7. G. P. Sutton, “Flow through a Combustion Zone,” Section of Chapter 3, *Rocket Propulsion Elements*, John Wiley & Sons, New York, 1956, 1963, and 1976.
- 3–8. J. A. Muss, T. V. Nguyen, E. J. Reske, and D. M. McDaniels, “Altitude Compensating Nozzle Concepts for RLV,” AIAA Paper 97-3222, July 1997.
- 3–9. G. V. R. Rao, “Recent Developments in Rocket Nozzle Configurations,” *ARS Journal*, Vol. 31, No. 11, November 1961, pp. 1488–1494; and G. V. R. Rao, “Exhaust Nozzle Contour for Optimum Thrust,” *Jet Propulsion*, Vol. 28, June 1958, pp. 377–382.
- 3–10. J. M. Farley and C. E. Campbell, “Performance of Several Method-of-Characteristics Exhaust Nozzles,” *NASA TN D-293*, October 1960.
- 3–11. J. D. Hoffman, “Design of Compressed Truncated Perfect Nozzles,” *Journal of Propulsion and Power*, Vol. 3, No. 2, March–April 1987, pp. 150–156.
- 3–12. G. P. Sutton, Stepped Nozzle, U.S. Patent 5,779,151, 1998.
- 3–13. F. A. Williams, M. Barrère, and N. C. Huang, “Fundamental Aspects of Solid Propellant Rockets,” *AGARDograph 116*, Advisory Group for Aerospace Research and Development, NATO, October 1969, 783 pages.
- 3–14. M. Barrère, A. Jaumotte, B. Fraeijis de Veubeke, and J. Vandekerckhove, *Rocket Propulsion*, Elsevier Publishing Company, Amsterdam, 1960.
- 3–15. R. N. Knauber, “Thrust Misalignments of Fixed Nozzle Solid Rocket Motors,” AIAA Paper 92-2873, 1992.
- 3–16. J. S. Lilley, “The Design and Optimization of Propulsion Systems Employing Scarfed Nozzles,” *Journal of Spacecraft and Rockets*, Vol. 23, No. 6, November–December 1986, pp. 597–604; and J. S. Lilley, “Experimental Validation of a Performance Model for Scarfed Nozzles,” *Journal of Spacecraft and Rockets*, Vol. 24, No. 5, September–October 1987, pp. 474–480.
- 3–17. R. D. Zucker and O. Biblarz, *Fundamentals of Gas Dynamics*, 2nd ed., John Wiley & Sons, Hoboken, NJ, 2002.

CHAPTER 4

FLIGHT PERFORMANCE

This chapter is an introduction to the flight performance of rocket-propelled vehicles such as spacecraft, space launch vehicles, missiles, or projectiles. It presents the subjects from a rocket propulsion point of view. Rocket propulsion systems provide forces to a flight vehicle and cause it to accelerate (or sometimes to decelerate), overcome drag forces, or change flight direction. Some propulsion systems provide also torques to the flight vehicles for rotation or maneuvers. The flight missions can be classified into several flight regimes: (1) flight within the earth's atmosphere (air-to-surface missiles, surface-to-surface short-range missiles, surface-to-air missiles, air-to-air missiles, assisted takeoff units, sounding rockets, or aircraft rocket propulsion systems), Refs. 4–1 and 4–2; (2) near space environment (earth satellites, orbital space stations, or long-range ballistic missiles), Refs. 4–3 to 4–9; (3) lunar and planetary flights (with or without landing or earth return), Refs. 4–5 to 4–12; and (4) deep space exploration and sun escape. Each is discussed in this chapter. The chapter begins with the analysis of simple one-dimensional space flight and then treats more complex flight path scenarios and various flying rocket-propelled vehicles. The appendices give conversion factors, atmosphere properties, and a summary of key equations.

4.1. GRAVITY-FREE DRAG-FREE SPACE FLIGHT

This first simple rocket flight analysis applies to an outer space environment, far away from any star, where there is no air (thus no drag) and essentially no significant gravitational attraction. The flight direction is the same as the thrust direction (along the axis of the nozzle), namely, a one-dimensional, straight-line acceleration path; the propellant mass flow \dot{m} and thus the propulsive thrust F

remain constant for the propellant burning duration t_p . The thrust force F has been defined in Eq. 2–17. For a constant propellant flow the flow rate \dot{m} is m_p/t_p , where m_p is the total usable propellant mass. From Newton's second law and for an instantaneous vehicle mass m and a vehicle flight velocity u

$$F = m \ du/dt \quad (4-1)$$

For a rocket where the propellant flow rate is constant and the start or shut-off periods are very brief, the instantaneous mass of the vehicle m can be expressed as a function of the initial mass of the full vehicle m_0 , the propellant mass m_p , the time at power cutoff t_p , and the instantaneous time t :

$$m = m_0 - \frac{m_p}{t_p} t = m_0 \left(1 - \frac{m_p}{m_0 t_p} t \right) \quad (4-2)$$

$$= m_0 \left(1 - \zeta \frac{t}{t_p} \right) = m_0 \left[1 - (1 - \mathbf{MR}) \frac{t}{t_p} \right] \quad (4-3)$$

Equation 4–3 expresses the vehicle mass in a form useful for trajectory calculations. The vehicle mass ratio **MR** (final mass/initial mass or m_f/m_0) and the propellant mass fraction ζ have been defined by Eqs. 2–7 and 2–8. They are related by

$$\zeta = 1 - \mathbf{MR} = 1 - m_f/m_0 = m_p/m_0 \quad (4-4)$$

A definition of the various masses is shown in Fig. 4–1. The initial mass at takeoff m_0 equals the sum of the useful propellant mass m_p plus the empty or final vehicle mass m_f ; m_f in turn equals the sum of the inert masses of the engine system (such as nozzles, tanks, cases, or unused, residual propellant) plus the guidance, control, electronics, and related equipment and the payload. The *residual propellant* remaining in the propulsion system after thrust termination is not available for combustion and is usually considered to be a part of the final engine mass after operation. This is the liquid propellant trapped in pipe pockets, valve cavities, and pumps or wetting the tank and pipe walls. For solid propellant rocket motors it is the remaining unburned solid propellant, also called slivers, and sometimes also unburned insulation.

For constant propellant mass flow \dot{m} and a finite propellant burning time t_b the total propellant mass m_p is $\dot{m}t_p$ and the instantaneous vehicle mass $m = m_0 - \dot{m}t$. Equation 4–1 can be written as

$$\begin{aligned} du &= (F/m) dt = (c\dot{m}/m) dt \\ &= \frac{(c\dot{m})dt}{m_0 - m_p t / t_p} = \frac{c(m_p/t_p)dt}{m_0(1 - m_p t / m_0 t_p)} = \frac{c\zeta/t_p}{1 - \zeta t/t_p} dt \end{aligned}$$

The start period and the shutdown period are very short and can be neglected. Integration leads to the maximum vehicle velocity at propellant burnout u_p that

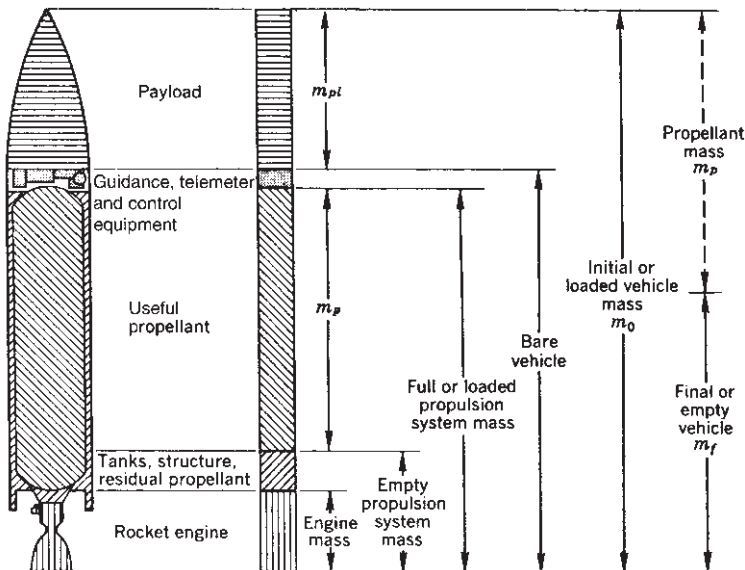


FIGURE 4-1. Definitions of various vehicle masses. For solid propellant rocket motors the words “rocket engine, tanks, and structures” are to be replaced by “rocket motor nozzle, thermal insulation, and case.”

can be attained in a gravity-free vacuum. When the initial flight velocity u_0 is not zero ($u_0 \neq 0$) it is often called the velocity increment Δu :

$$\Delta u = -c \ln(1 - \zeta) + u_0 = c \ln(m_0/m_f) + u_0 \quad (4-5)$$

If the initial velocity u_0 is assumed to be zero, then the velocity at thrust termination

$$\begin{aligned} u_p &= \Delta u = -c \ln(1 - \zeta) = -c \ln[m_0/(m_0 - m_p)] \\ &= -c \ln \mathbf{MR} = c \ln(1/\mathbf{MR}) \\ &= c \ln(m_0/m_f) \end{aligned} \quad (4-6)$$

The symbol \ln stands for the natural logarithm. This u_p is the maximum velocity increment Δu that can be obtained in a gravity-free vacuum with constant propellant flow, starting from rest with $u_0 = 0$. The effect of variations in c , I_s , and ζ on the flight velocity increment is shown in Fig. 4-2. An alternate way to write Eq. 4-6 uses e , the base of the natural logarithm:

$$e^{\Delta u/c} = 1/\mathbf{MR} = m_0/m_f \quad (4-7)$$

The concept of the maximum attainable flight velocity increment Δu in a gravity-free vacuum is useful in understanding the influence of the basic parameters. It is used in comparing one propulsion system or vehicle with another,

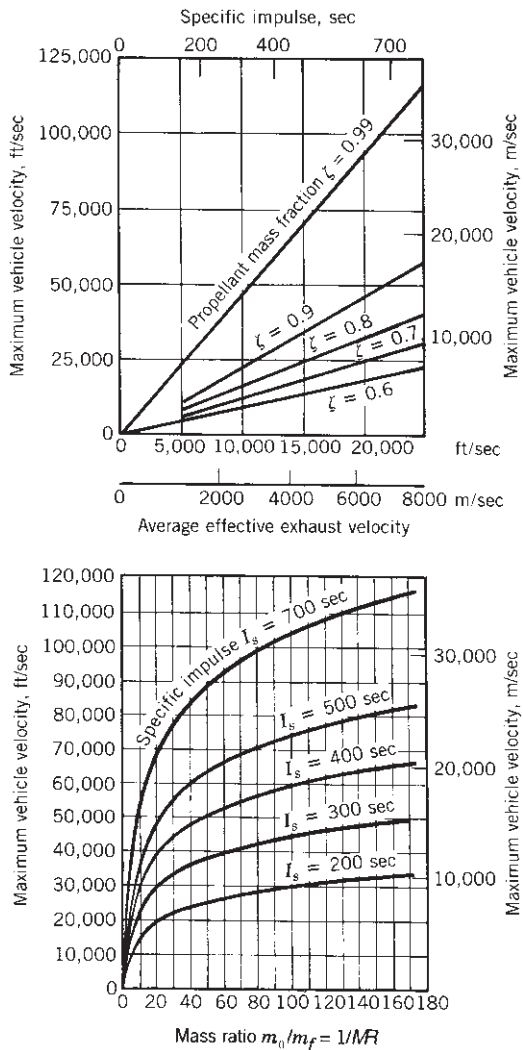


FIGURE 4-2. Maximum vehicle flight velocity in a gravitationless, drag-free space for different mass ratios and specific impulses (plot of Eq. 4-6). Single-stage vehicles can have values of MR up to about 20 and multistage vehicles can exceed 200.

one flight mission with another, or one proposed upgrade with another possible design improvement.

From Eq. 4-6 it can be seen that the vehicle's *propellant mass fraction* has a logarithmic effect on the vehicle velocity. By increasing this ratio from 0.80 to 0.90, the interplanetary maximum vehicle velocity in gravitationless vacuum is increased by 43%. A mass fraction of 0.80 would indicate that only 20% of the total vehicle mass is available for structure, skin, payload, propulsion hardware,

radios, guidance system, aerodynamic lifting surfaces, and so on; the remaining 80% is useful propellant. It requires careful design to exceed 0.85; mass fraction ratios approaching 0.95 appear to be the probable practical limit for single-stage vehicles and currently known materials. When the mass fraction is 0.90, then $1/\mathbf{MR} = 0.1$ and $\mathbf{MR} = 10.0$. This marked influence of mass fraction or mass ratio on the velocity at power cutoff, and therefore also the range, not only is true of interplanetary spaceships in a vacuum but applies to almost all types of rocket-powered vehicles. For this reason, importance is placed on saving inert mass on every vehicle component, including the propulsion system.

Equation 4–6 can be modified and solved for the effective propellant mass m_p required to achieve a desired velocity increment for a given initial takeoff mass or a final burnout mass of the vehicle. The final mass consists of the payload, the structural mass of the vehicle, the empty propulsion system mass (which includes residual propellant), plus a small additional mass for guidance, communications, and control devices. Here $m_p = m_0 - m_f$:

$$m_p = m_f(e^{\Delta u/c} - 1) = m_0(1 - e^{(-\Delta u/c)}) \quad (4-8)$$

The flight velocity increment u_p is proportional to the effective exhaust velocity c and, therefore, to the specific impulse. Thus any improvement in I_s (such as better propellants, more favorable nozzle area ratio, or higher chamber pressure) reflects itself in improved vehicle performance, provided that such an improvement does not also cause an excessive increase in rocket propulsion system inert mass, which causes a decrease in the effective propellant fraction.

4.2. FORCES ACTING ON A VEHICLE IN THE ATMOSPHERE

The external forces commonly acting on vehicles flying in the earth's atmosphere are thrust, aerodynamic forces, and gravitational attractions. Other forces, such as wind or solar radiation pressure, are usually small and generally can be neglected for many simple calculations.

The *thrust* is the force produced by the power plant, such as a propeller or a rocket. It usually acts in the direction of the axis of the power plant, that is, along the propeller shaft axis or the rocket nozzle axis. The thrust force of a rocket with constant mass flow has been expressed by Eq. 2–6 as a function of the effective exhaust velocity c and the propellant flow rate \dot{m} . In many rockets the mass rate of propellant consumption \dot{m} is essentially constant, and the starting and stopping transients are usually very short and can be neglected. Therefore, the thrust is defined by Eq. 2–13 and is restated here with different parameters:

$$F = c\dot{m} = cm_p/t_p \quad (4-9)$$

As explained in Chapter 3, for a given propellant the value of the effective exhaust velocity c or specific impulse I_s depends in part on the nozzle area

ratio and the altitude. The value of c can increase by a relatively small factor of between 1.2 and 1.6 as altitude is increased with a maximum value in space (vacuum).

The *drag* D is the *aerodynamic force* in a direction opposite to the flight path due to the resistance of the body to motion in a fluid. The *lift* L is the aerodynamic force acting in a direction normal to the flight path. They are expressed as functions of the flight speed u , the mass density of the fluid (air) in which the vehicle moves ρ , and a typical surface area A :

$$L = C_L \frac{1}{2} \rho A u^2 \quad (4-10)$$

$$D = C_D \frac{1}{2} \rho A u^2 \quad (4-11)$$

where C_L and C_D are lift and drag coefficients, respectively. For airplanes and winged missiles the area A is the wing area. For wingless missiles or space launch vehicles it is the maximum cross-sectional area normal to the missile axis. The lift and drag coefficients are primarily functions of the vehicle configuration, flight Mach number, and angle of attack, which is the angle between the vehicle axis (or the wing plane) and the flight direction. For low flight speeds the effect of Mach number may be neglected, and the drag and lift coefficients are functions of the angle of attack. A typical variation of the drag and lift coefficients for a typical supersonic missile is shown in Fig. 4-3. The values of these coefficients reach a maximum near a Mach number of unity. For wingless vehicles the angle of attack α is usually very small ($0 < \alpha < 1^\circ$). The density and other properties of the atmosphere are listed in Appendix 2. The local density of the earth's atmosphere can vary day by day by a factor up to 2 (for altitudes of 300 to 1200 km) depending on solar activity and night-to-day temperature variations. This introduces a major unknown in the drag. The aerodynamic forces are affected by the flow and pressure distribution of the rocket exhaust gases, as explained in Chapter 20.

The flight regime in the neighborhood of Mach 1 is called the transonic phase of flight. Here strong unsteady aerodynamic forces can develop (due to buffeting) which are reflected in the steep rise and decrease of the coefficients seen in Fig. 4-3. Marginal transonic load capabilities have led to structural failures of flight vehicles.

For space launch vehicles and ballistic missiles the integrated drag loss, when expressed in terms of Δu , is typically 5 to 10% of the final ideal vehicle velocity. This relatively low value is due to the fact that the air density is low at high altitudes, when the velocity is high, and at low altitudes the air density is high but the flight velocity and thus the dynamic pressure are low.

Gravitational attraction is exerted upon a flying space vehicle by all planets, stars, the moon, and the sun. Gravity forces pull the vehicle in the direction of the center of mass of the attracting body. Within the immediate vicinity of the earth, the attraction of other planets and bodies is negligibly small compared to the earth's gravitational force. This force is the *weight*.

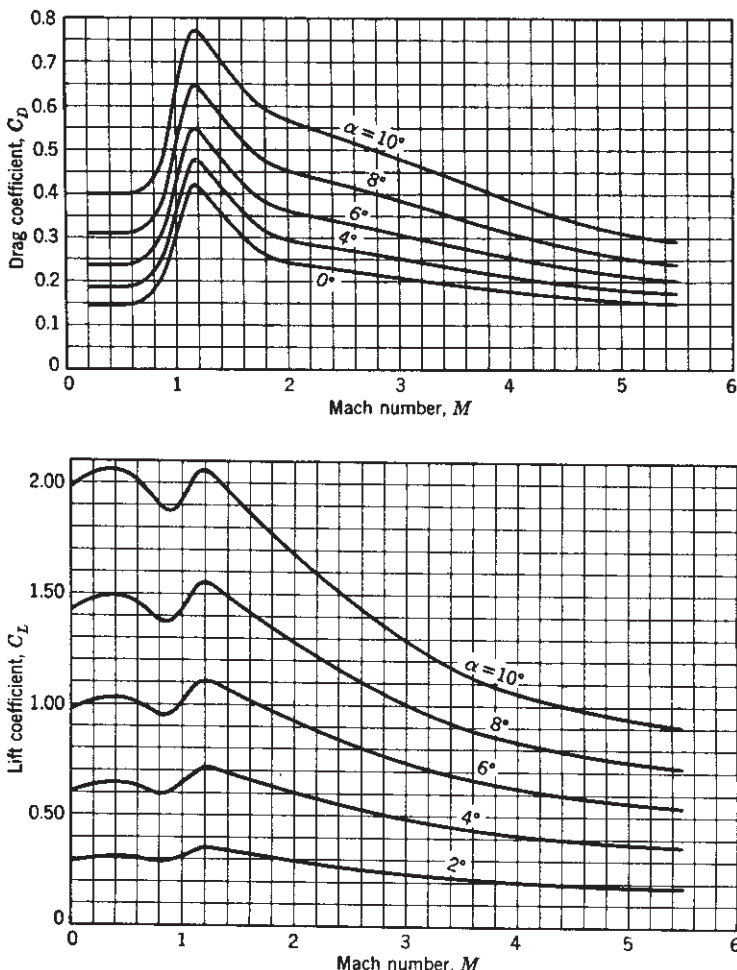


FIGURE 4–3. Variation of lift and drag coefficient with Mach number of the German V-2 missile based on body cross-sectional area with jet off and without exhaust plume effects at several angles of attack α .

If the variation of gravity with the geographical features and the oblate shape of the earth are neglected, the acceleration of gravity varies inversely as the square of the distance from the earth's center. If R_0 is the mean radius of the spherical earth's surface and g_0 the acceleration on the earth's surface at the earth's effective radius R_0 , the gravitational attraction g changes with altitude,

$$\begin{aligned} g &= g_0(R_0/R)^2 \\ &= g_0[R_0/(R_0 + h)]^2 \end{aligned} \quad (4-12)$$

where h is the altitude. At the equator the spherical earth's radius is 6378.388 km and the standard value of g_0 is 9.80665 m/sec^2 . At a distance as far away as the moon, the earth's gravity acceleration is only about $3.3 \times 10^{-4} g_0$. In a more accurate analysis the value of g will vary locally with the earth's bulge at the equator, the high mountains, and the difference of densities of specific earth regions.

4.3. BASIC RELATIONS OF MOTION

For a vehicle that flies within the proximity of the earth, the gravitational attraction of all other heavenly bodies may usually be neglected. Let it be assumed that the vehicle is moving in rectilinear equilibrium flight and that all control forces, lateral forces, and moments that tend to turn the vehicle are zero. The trajectory is two dimensional and is contained in a fixed plane. The vehicle has wings that are inclined to the flight path at an angle of attack α and that give a lift in a direction normal to the flight path. The direction of flight does not necessarily coincide with the direction of thrust. Figure 4-4 shows these conditions schematically.

Let θ be the angle of the flight path with the horizontal and ψ the angle of the direction of thrust with the horizontal. In the direction of the flight path the product of the mass and the acceleration has to equal the sum of all forces, namely the propulsive, aerodynamic, and gravitational forces:

$$m(du/dt) = F \cos(\psi - \theta) - D - mg \sin \theta \quad (4-13)$$

The acceleration perpendicular to the flight path is $u(d\theta/dt)$; for a constant value of u and the instantaneous radius R of the flight path it is u^2/R . The equation of motion in a direction normal to the flight velocity is

$$mu(d\theta/dt) = F \sin(\psi - \theta) + L - mg \cos \theta \quad (4-14)$$

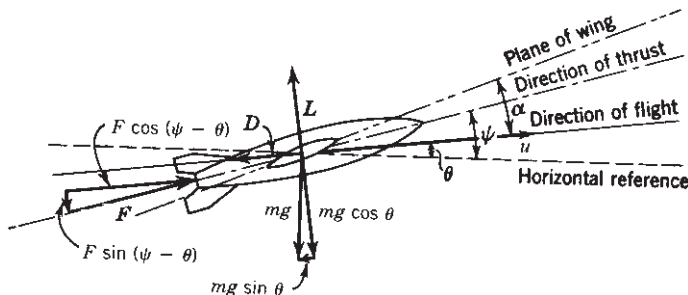


FIGURE 4-4. Two-dimensional free-body force diagram for flying vehicle with wings and fins.

By substituting from Eqs. 4–10 and 4–11, these two basic equations can be solved for the accelerations as

$$\frac{du}{dt} = \frac{F}{m} \cos(\psi - \theta) - \frac{C_D}{2m} \rho u^2 A - g \sin \theta \quad (4-15)$$

$$u \frac{d\theta}{dt} = \frac{F}{m} \sin(\psi - \theta) + \frac{C_L}{2m} \rho u^2 A - g \cos \theta \quad (4-16)$$

No general solution can be given to these equations, since t_p , u , C_D , C_L , ρ , θ , or ψ can vary independently with time, mission profile, or altitude. Also, C_D and C_L are functions of velocity or Mach number. In a more sophisticated analysis other factors may be considered, such as the propellant used for nonpropulsive purposes (e.g., attitude control or flight stability). See Refs. 4–1, 4–8, 4–11, and 4–12 for a background of flight performance in some of the flight regimes. Different flight performance parameters are maximized or optimized for different rocket flight missions or flight regimes, such as Δu , range, orbit height and shape, time-to-target, or altitude. Rocket propulsion systems are usually tailored to fit specific flight missions.

Equations 4–15 and 4–16 are general and can be further simplified for various special applications, as shown in subsequent sections. Results of such iterative calculations of velocity, altitude, or range using the above two basic equations often are adequate for rough design estimates. For actual trajectory analyses, navigation computation, space flight path determination, or missile-firing tables, this two-dimensional simplified theory does not permit sufficiently accurate results. The perturbation effects, such as those listed in Section 4.4, must then be considered in addition to drag and gravity, and digital computers are necessary to handle the complex relations. An arbitrary division of the trajectory into small elements and a step-by-step or numerical integration to define a trajectory are usually indicated. The more generalized three-body theory includes the gravitational attraction among three masses (for example, the earth, the moon, and the space vehicle) and is considered necessary for many space flight problems (see Refs. 4–2 to 4–5). When the propellant flow and the thrust are not constant, when the flight path is three dimensional, the form and the solution to the equations above become more complex.

A form of Eqs. 4–15 and 4–16 can also be used to determine the actual thrust or actual specific impulse during actual vehicle flights from accurately observed trajectory data, such as from optical or radar tracking data. The vehicle acceleration (du/dt) is essentially proportional to the net thrust and, by making an assumption or measurement on the propellant flow (which usually varies in a predetermined manner) and an analysis of aerodynamic forces, it is possible to determine the rocket propulsion system's actual thrust under flight conditions.

For each mission of flight one can obtain actual histories of velocities and distances traveled and thus complete trajectories when integrating Eqs. 4–15 and 4–16. The more general case requires six equations; three for translation along each of three perpendicular axes and three for rotation about these axes. The

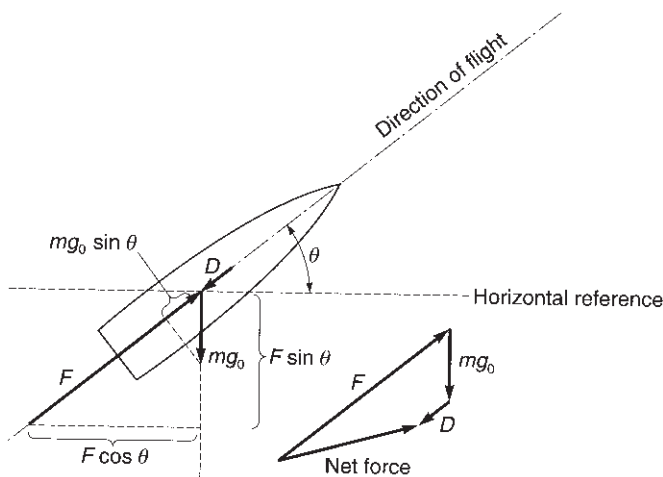


FIGURE 4–5. Simplified free-body force diagram for vehicle without wings or fins. The force vector diagram shows the net force on the vehicle.

choice of coordinate systems and the reference points can simplify the mathematical solutions (see Refs. 4–3 and 4–5).

For a wingless rocket projectile, a space launch vehicle, or a missile with constant thrust and propellant flow, these equations can be simplified. In Fig. 4–5 the flight direction θ is the same as the thrust direction and lift forces for a symmetrical, wingless, stably flying vehicle can be assumed to be zero at zero angle of attack. For a two-dimensional trajectory in a single plane (no wind forces) and a stationary earth, the acceleration in the direction of flight is as follows:

$$\frac{du}{dt} = \frac{c\xi/t_p}{1 - \xi t/t_p} - g \sin \theta - \frac{C_D \frac{1}{2} \rho u^2 A / m_0}{1 - \xi t/t_p} \quad (4-17)$$

A force vector diagram in Fig. 4–5 shows the net force (by adding thrust, drag, and gravity vectors) to be at an angle to the flight path, which will be curved. These types of diagram form the basis for iterative trajectory numerical solutions.

The relationships in this section are for a two-dimensional flight path, one that lies in a single plane. If maneuvers out of that plane are also made (e.g., due to solar attraction, thrust misalignment, or wind), then the flight paths become three dimensional and another set of equations will be needed to describe these flights. Reference 4–1 describes equations for the motion of rocket projectiles in the atmosphere in three dimensions. It requires energy and forces to push a vehicle out of its flight plane. Trajectories have to be calculated accurately in order to reach the intended flight objective and today all are done with the aid of a computer. A good number of *computer programs* for analyzing flight trajectories exist and are maintained by aerospace companies or government agencies.

Some are two dimensional, relatively simple, and used for making preliminary estimates or comparisons of alternative flight paths, alternative vehicle designs, or alternative propulsion schemes. Several use a stationary flat earth, while others use a rotating curved earth. Three-dimensional programs also exist, are used for more accurate flight path analyses, and include some or all significant perturbations, orbit plane changes, or flying at angles of attack. As explained in Ref. 4-4, they are more complex.

If the flight trajectory is vertical (as for a sounding rocket), then $\sin \theta = 1.0$ and $\cos \theta = 0$. Equation 4-17 can be modified:

$$\frac{du}{dt} = \frac{c\zeta/t_p}{1 - \zeta t/t_p} - g - \frac{C_D \frac{1}{2} \rho u^2 A / m_0}{1 - \zeta t/t_p} \quad (4-18)$$

The velocity at the end of burning can be found by integrating between the limits of $t = 0$ and $t = t_p$ when $u = u_0$ and $u = u_p$. The first two terms can readily be integrated. The last term is of significance only if the vehicle spends a considerable portion of its time within the atmosphere. It can be integrated graphically or by numerical methods, and its value can be designated as $BC_D A/m_0$ such that

$$B = \int_0^{t_p} \frac{\frac{1}{2} \rho u^2}{1 - \zeta t/t_p} dt$$

The cutoff velocity or velocity at the end of propellant burning u_p is then

$$u_p = -\bar{c} \ln(1 - \zeta) - \bar{g} t_p - \frac{BC_D A}{m_0} + u_0 \quad (4-19)$$

where u_0 is the initial velocity, such as may be given by a booster, \bar{g} is an average gravitational attraction evaluated with respect to time and altitude from Eq. 4-12, and \bar{c} is a time average of the effective exhaust velocity, which is a function of altitude.

There are always a number of trade-offs in selecting the best trajectory for a rocket projectile. For example, for a fixed thrust there is a trade-off between burning time, drag, payload, maximum velocity, and maximum altitude (or range). Reference 4-2 describes the trade-offs between payload, maximum altitude, and flight stability for a sounding rocket.

If aerodynamic forces outside the earth's atmosphere are neglected (operate in a vacuum) and no booster or means for attaining an initial velocity ($u_0 = 0$) is assumed, the velocity at the end of the burning reached in a vertically ascending trajectory will be

$$\begin{aligned} u_p &= -\bar{c} \ln(1 - \zeta) - \bar{g} t_p \\ &= -\bar{c} \ln \mathbf{MR} - \bar{g} t_p \\ &= \bar{c} \ln(1/\mathbf{MR}) - \bar{g} t_p \end{aligned} \quad (4-20)$$

The first term on the right side is usually the largest and is identical to Eq. 4–6. It is directly proportional to the effective rocket exhaust velocity and is very sensitive to changes in the mass ratio. The second term is related to the earth's gravity and is always negative during ascent, but its magnitude is small if the burning time t_p is short or if the flight takes place in high orbits or in space where \bar{g} is comparatively small.

For a flight that is not following a vertical path, the gravity loss is a function of the angle between the flight direction and the local horizontal; more specifically, the gravity loss is the integral of $g \sin \theta dt$.

For the simplified two-dimensional case the net acceleration a for vertical takeoff at sea level is

$$a = (F_0 g_0 / w_0) - g_0 \quad (4-21)$$

$$a/g_0 = (F_0/w_0) - 1 \quad (4-22)$$

where a/g_0 is the *initial takeoff acceleration* in multiples of the sea-level gravitational acceleration g_0 , and F_0/w_0 is the thrust-to-weight ratio at takeoff. For large surface-launched vehicles, this initial-thrust-to-initial-weight ratio typically has values between 1.2 and 2.2; for small missiles (air-to-air, air-to-surface, and surface-to-air types) this ratio is usually larger, sometimes even as high as 50 or 100. The *final or terminal acceleration* a_f of a vehicle in vertical ascent usually occurs just before the rocket engine is shut off and/or before the propellant is completely consumed. If drag is neglected, then

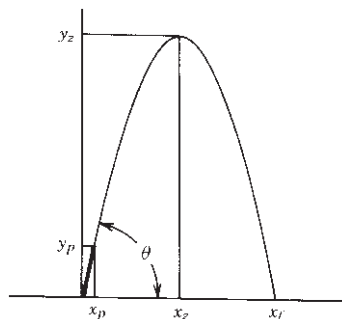
$$\begin{aligned} a_f/g_0 &= (F_f/w_f) - 1 \\ &= (F_f/m_f)g_0 - g/g_0 \end{aligned} \quad (4-23)$$

The second version of this equation applies if the powered flight path traverses a substantial change in altitude and thus a change in the value of g . In a gravity-free environment this equation becomes $a_f/g_0 = F_f/w_f$. In rockets with constant propellant flow the final acceleration is usually also the maximum acceleration, because the vehicle mass to be accelerated has its minimum value just before propellant exhaustion, and for ascending rockets the thrust usually increases with altitude. If this terminal acceleration is too large (and causes overstressing of the structure, thus necessitating an increase in structure mass), then the thrust can be designed to a lower value for the last portion of the burning period. In manned flights the maximum acceleration is limited to the maximum g loading that can be withstood by the crew.

Example 4–1. A simple single-stage rocket for a rescue flare has the following characteristics. Its flight path nomenclature is shown in the accompanying sketch.

| | |
|--|------------|
| Launch weight | 4.0 lbf |
| Useful propellant weight | 0.4 lbf |
| Effective specific impulse | 120 sec |
| Launch angle θ (relative to horizontal) | 80° |
| Burn time t_p (with constant thrust) | 1.0 sec |

The heavy line in the ascending trajectory designates the powered portion of the flight.



Drag may be neglected since the flight velocities are low. Assume that the acceleration of gravity is unchanged from its sea-level value g_0 , which then makes the propellant mass numerically equal to the propellant weight in the EE system, or 0.4 lbm. Also assume that start and stop transients are short and can be ignored.

Solve for the initial and final acceleration of powered flight, the maximum trajectory height and the time to reach maximum height, the range or horizontal distance to impact, and the angle at propulsion cutoff.

SOLUTION. We divide the flight path into three portions: the powered flight for 1 sec, the unpowered ascent after cutoff, and the free-fall descent. The thrust is obtained from Eq. 2-5:

$$F = I_s \dot{w} / t_p = 120 \times 0.4 / 1.0 = 48 \text{ lbf}$$

The initial accelerations along the x and y horizontal and vertical directions are, from Eq. 4-22,

$$(a_0)_y = g_0[(F \sin \theta/w) - 1] = 32.17[(48/4.0) \sin 80^\circ - 1] = 348 \text{ ft/sec}^2$$

$$(a_0)_x = g_0(F \cos \theta/w) = 32.17(48/4.0) \cos 80^\circ = 67.03 \text{ ft/sec}^2$$

At thrust termination the initial flight acceleration becomes

$$a_0 = \sqrt{(a_0)_x^2 + (a_0)_y^2} = 354.4 \text{ ft/sec}^2$$

The vertical and horizontal components of the velocity u_p at the end of powered flight are obtained from Eq. 4-20. Note that the vehicle mass has been diminished by the propellant that has been consumed:

$$\begin{aligned} (u_p)_y &= c \ln(m_0/m_f) \sin \theta - g_0 t_p = 32.17 \times 120 \times \ln(4/3.6) \times 0.984 - 32.17 \times 1.0 \\ &= 368 \text{ m/sec} \end{aligned}$$

$$(u_p)_x = c \ln(m_0/m_f) \cos \theta = 32.17 \times 120 \times \ln(4/3.6) \times 0.1736 = 70.6 \text{ m/sec}$$

The trajectory angle with the horizontal at rocket cutoff for a dragless flight is

$$\tan^{-1}(368/70.6) = 79.1^\circ$$

The final acceleration is found, using Eq. 4-22 with the final mass, as $a_f = 400 \text{ m/sec}^2$.

For the powered flight, the coordinates at propulsion burnout y_p and x_p can be calculated from the time integration of their respective velocities. The results are

$$\begin{aligned} y_p &= ct_p [1 - \ln(m_0/m_f)/(m_0/m_f - 1)] \sin \theta - 1/2 g_0 t_p^2 \\ &= 32.17120 [1 - \ln(4/3.6)/(4/3.6 - 1)] \times 0.984 - \frac{1}{2} \times 32.17 \times (1.0)^2 \\ &= 181 \text{ ft} \\ x_p &= ct_p [1 - \ln(m_0/m_f)/(m_0/m_f - 1)] \cos \theta \\ &= 32.17120 [1 - \ln(4/3.6)/(4/3.6 - 1)] \times 0.173 \\ &= 34.7 \text{ ft} \end{aligned}$$

The unpowered part of the trajectory reaches zero vertical velocity at its zenith. The height gained in unpowered free flight may be obtained by equating the vertical kinetic energy at power cutoff to its equivalent potential energy,

$$g_0(y_z - y_p) = \frac{1}{2}(u_p)_y^2$$

so that

$$(y_z - y_p) = \frac{1}{2}(u_p)_y^2/g_0 = \frac{1}{2}(368)^2/32.17 = 2105 \text{ ft}$$

The maximum height or zenith location thus becomes $y_z = 2105 + 181 = 2259$ ft. What remains now is to solve the free-flight portion of vertical descent. The time for descent from the zenith is $t_z = \sqrt{2y_z/g_0} = 11.85$ sec and the final vertical or impact vertical velocity $(u_f)_y - g_0 t_z = 381$ ft/sec.

The total horizontal range to the zenith is the sum of the powered and free-flight contributions. During free flight the horizontal velocity remains unchanged at 70.6 ft/sec because there are no accelerations (i.e., no drag, wind, or gravity component). We now need to find the free-flight time from burnout to the zenith, which is $t = (u_p)_y/g_0 = 11.4$ sec. The total free-flight time becomes $t_{ff} = 11.4 + 11.85 = 23.25$ sec.

Now, the horizontal or total range becomes $\Delta x = 34.7 + 70.6 \times 23.25 = 1676$ ft.

The impact angle would be around 79° . If drag had been included, solving this problem would have required information on the drag coefficient (C_D) and a numerical solution using Eq. 4-18. All resulting velocities and distances would turn out somewhat lower in value. A set of flight trajectories for sounding rockets has been worked out in Ref. 4-3.

4.4. SPACE FLIGHT

Newton's law of gravitation defines the attraction of gravitational force F_g between two bodies in space as follows:

$$F_g = Gm_1m_2/R^2 = \mu m_2/R^2 \quad (4-24)$$

Here G is the universal gravity constant ($G = 6.670 \times 10^{-11} \text{m}^3/\text{kg}\cdot\text{sec}^2$), m_1 and m_2 are the masses of the two attracting bodies (such as the earth and the moon, the earth and a spacecraft, or the sun and a planet), and R is the distance between their centers of mass. The earth's gravitational constant μ is the product of Newton's universal constant G and the mass of the earth, $m_1(5.974 \times 10^{24} \text{kg})$. It is $\mu = 3.98600 \times 10^{14} \text{m}^3/\text{sec}^2$.

The rocket offers a means for escaping the earth for lunar and interplanetary travel, for escaping our solar system, and for creating a stationary or moving station in space. The flight velocity required to escape from the earth can be found by equating the kinetic energy of a moving body to the work necessary to overcome gravity, neglecting the rotation of the earth and the attraction of other celestial bodies:

$$\frac{1}{2}mu^2 = m \int g \, dR$$

By substituting for g from Eq. 4-12 and by neglecting air friction the following relation for the escape velocity v_e is obtained:

$$v_e = R_0 \sqrt{\frac{2g_0}{R_0 + h}} = \sqrt{\frac{2\mu}{R}} \quad (4-25)$$

Here R_0 is the effective earth mean radius (6374.2 km), h is the orbit altitude above sea level, and g_0 is the acceleration of gravity at the earth surface (9.806 m/sec). The satellite flight radius R measured from the earth's center is $R = R_0 + h$. The velocity of escape at the earth's surface is 11,179 m/sec or 36,676 ft/sec and does not vary appreciably within the earth's atmosphere, as shown by Fig. 4-6. Escape velocities for surface launch are given in Table 4-1 for the sun, the planets, and the moon. Launching from the earth's surface at escape velocity is not practical. As a vehicle ascends through the earth's atmosphere, it is subject to severe aerodynamic heating and dynamic pressures. A practical launch vehicle has to traverse the atmosphere at relatively low velocity and accelerate to the high velocities beyond the dense atmosphere. For example, during a portion of the Space Shuttle's ascent, its main engines are actually throttled to a lower thrust to avoid excessive pressure and heating. Alternatively, an escape vehicle can be launched from an orbiting space station or from an orbiting Space Shuttle.

A rocket spaceship can become a *satellite* of the earth and revolve around the earth in a fashion similar to that of the moon. Satellite orbits are usually elliptical and some are circular. Low earth orbits, typically below 500 km altitude, are designated by the letters LEO. The altitude of the orbit is usually above the earth's atmosphere, because this minimizes the expending of energy to overcome the small drag which pulls the vehicle closer to the earth. The effects of the radiation in the Van Allen belt on human beings and sensitive equipment sometimes necessitate the selection of an earth orbit at low altitude.

For a circular trajectory the velocity of a satellite must be sufficiently high so that its centrifugal force balances the earth's gravitational attraction:

$$mu_s^2/R = mg$$

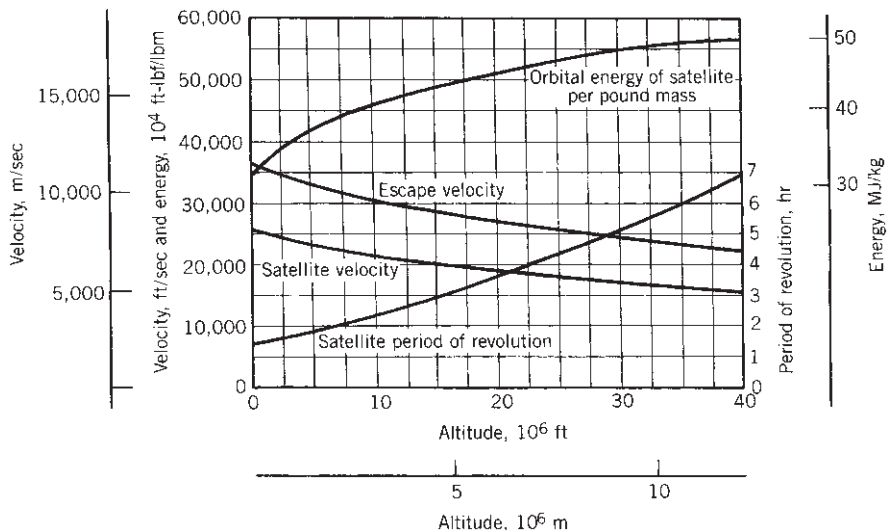


FIGURE 4–6. Orbital energy, orbital velocity, period of revolution, and earth escape velocity of a space vehicle as a function of altitude for circular satellite orbits. It is based on a spherical earth and neglects the earth's oblate shape, rotation, and atmospheric drag.

For a circular orbit, the satellite velocity u_s is found by using Eq. 4–12,

$$u_s = R_0 \sqrt{g_0/(R_0 + h)} = \sqrt{\mu/R} \quad (4-26)$$

which is smaller than the escape velocity by a factor of $\sqrt{2}$. The period τ in seconds of one revolution for a circular orbit relative to a stationary earth is

$$\tau = 2\pi(R_0 + h)/u_s = 2\pi(R_0 + h)^{3/2}/(R_0\sqrt{g_0}) \quad (4-27)$$

The energy E necessary to bring a unit of mass into a circular satellite orbit neglecting drag consists of kinetic and potential energy, namely,

$$\begin{aligned} E &= \frac{1}{2}u_s^2 + \int_{R_0}^R g \, dR \\ &= \frac{1}{2}R_0^2 \frac{g_0}{R_0 + h} + \int_{R_0}^R g_0 \frac{R_0^2}{R^2} dR = \frac{1}{2}R_0 g_0 \frac{R_0 + 2h}{R_0 + h} \end{aligned} \quad (4-28)$$

The escape velocity, satellite velocity, satellite period, and satellite orbital energy are shown as functions of altitude in Fig. 4–6.

A satellite circulating around the earth at an altitude of 300 miles or 482.8 km has a velocity of about 7375 m/sec or 24,200 ft/sec, circles a stationary earth in 1.63 hr, and ideally requires an energy of 3.35×10^7 J to place 1 kg of spaceship mass into its orbit. An equatorial satellite in a circular orbit at an altitude of

TABLE 4-1. Characteristic Data for Several Heavenly Bodies

| Name | Mean Radius of Orbit (million km) | Period of Revolution | Mean Diameter (km) | Relative Mass (Earth = 1.0) | Specific Gravity | Acceleration of Gravity at Surface (m/sec ²) | Escape Velocity at Surface (m/sec) |
|---------|---|-------------------------|--------------------------|-----------------------------------|---------------------|---|---|
| Sun | — | — | 1,393,000 | 332,950 | 1.41 | 273.4 | 616,000 |
| Moon | 0.383 | 27.3 days | 3475 | 0.012 | 3.34 | 1.58 | 2,380 |
| Mercury | 57.87 | 87.97 days | 4670 | 0.06 | 5.5 | 3.67 | 4,200 |
| Venus | 108.1 | 224.70 days | 12,400 | 0.86 | 5.3 | 8.67 | 10,300 |
| Earth | 149.6 | 365.256 days | 12,742 | 1.00 ^a | 5.52 | 9.806 | 11,179 |
| Mars | 227.7 | 686.98 days | 6760 | 0.15 | 3.95 | 3.749 | 6,400 |
| Jupiter | 777.8 | 11.86 year | 143,000 | 318.4 | 1.33 | 26.0 | 59,700 |
| Saturn | 1486 | 29.46 year | 121,000 | 95.2 | 0.69 | 11.4 | 35,400 |
| Uranus | 2869 | 84.0 year | 47,100 | 15.0 | 1.7 | 10.9 | 22,400 |
| Neptune | 4475 | 164.8 year | 50,700 | 17.2 | 1.8 | 11.9 | 31,000 |
| Pluto | 5899 | 284.8 year | 5950 | 0.90 | 4 | 7.62 | 10,000 |

Source: in part from Refs 4-3 and 4-4.^aEarth mass is 5.976×10^{24} kg.

6.611 earth radii (about 26,200 miles, 42,200 km, or 22,700 nautical miles) has a period of revolution of exactly 24 hr. It will appear stationary to an observer on earth. This is known as a *synchronous* satellite in *geo synchronous earth orbit*, usually abbreviated as GEO. It is used extensively for communications satellite applications. In Section 4.7 on launch vehicles we will describe how the payload of a given space vehicle diminishes as the orbit circular altitude is increased and as the inclination (angle between orbit plane and earth equatorial plane) is changed. See Refs. 4-3, 4-4, 4-5, 4-6, and 4-9.

Elliptical Orbits

The circular orbit described above is a special case of the more general elliptic orbit shown in Fig. 4-7; here the earth (or any other heavenly body around which another body is moving) is located at one of the focal points of this ellipse. The equations of motion may be derived from Kepler's laws, and the elliptical orbit can be described as follows, when expressed in polar coordinates:

$$u = \left[\mu \left(\frac{2}{R} - \frac{1}{a} \right) \right]^{1/2} \quad (4-29)$$

where u is the velocity of the body in the elliptical orbit, R is the instantaneous radius from the center of the attracting body (a vector quantity, which changes direction as well as magnitude), a is the major axis of the ellipse, and μ is the earth's gravitational constant with a value of $3.986 \times 10^{14} \text{ m}^3/\text{sec}^2$. The symbols are defined in Fig. 4-7. From this equation it can be seen that the velocity u_p is a maximum when the moving body comes closest to its focal point at the orbit's *perigee* and that its velocity u_a is a minimum at its *apogee*. By substituting for R

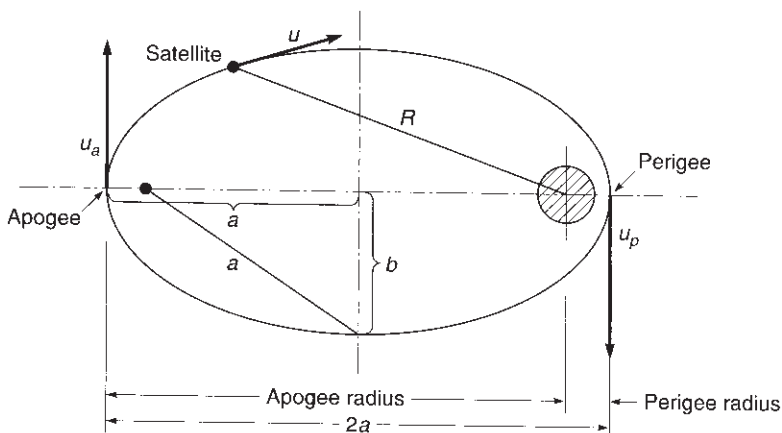


FIGURE 4-7. Elliptical orbit; the attracting body is at one of the focal points of the ellipse.

in Eq. 4–29, and by defining the ellipse's shape factor e as the *eccentricity of the ellipse*, $e = \sqrt{a^2 - b^2}/a$, the apogee and perigee velocities can be expressed as

$$u_a = \sqrt{\frac{\mu(1-e)}{a(1+e)}} \quad (4-30)$$

$$u_b = \sqrt{\frac{\mu(1+e)}{a(1-e)}} \quad (4-31)$$

Another property of an elliptical orbit is that the product of velocity and instantaneous radius remains constant for any location x or y on the ellipse, namely, $u_x R_x = u_y R_y = uR$. The exact path that a satellite takes depends on the velocity (magnitude and vector orientation) with which it is started or injected into its orbit.

For *interplanetary transfers* the ideal mission can be achieved with minimum energy in a simple transfer ellipse, as suggested originally by Hohmann (see Ref. 4–6). Assuming the planetary orbits about the sun to be circular and coplanar, it can be demonstrated that the path of minimum energy is an ellipse tangent to the planetary orbits as shown in Fig. 4–8. This operation requires a velocity increment (relatively high thrust) at the initiation (planet A at t_1) and another at termination (planet B at t_2): both increments are the velocity differences between the respective circular planetary velocities and the perigee and apogee velocities which define the transfer ellipse. The thrust levels at the beginning and end maneuvers of the Hohmann ellipse must be high enough to give a short operating time and the acceleration of at least $0.01 g_0$, but preferably more. With electrical propulsion these accelerations would be about $10^{-5} g_0$, the operating time would be weeks or months, and the best transfer trajectories would be very different from a Hohmann ellipse; they are described in Chapter 17.

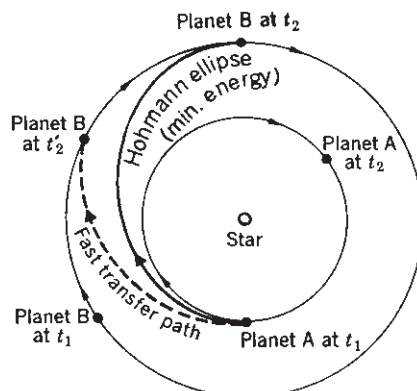


FIGURE 4–8. Schematic diagram of interplanetary transfer paths. These same transfer maneuvers apply when going from a low-altitude earth satellite orbit to a higher orbit.

The departure date or the *relative positions of the launch planet and the target planet* for a planetary transfer mission are critical, because the spacecraft has to meet with the target planet when it arrives at the target orbit. The transfer time ($t_2 - t_1$) for a Hohmann ellipse flight starting on earth is about 116 hr to go to the moon and about 259 days to Mars. If a faster orbit (shorter transfer time) is desired (see dashed lines in Fig. 4-8), it requires more energy than a Hohmann transfer ellipse. This means a larger vehicle with more propellant and a larger propulsion system or more total impulse. There also is a *time window* for a launch of a spacecraft that will make a successful rendezvous. For a Mars mission an earth-launched spacecraft may have a launch time window of more than two months. A Hohmann transfer ellipse or a faster transfer path applies not only to planetary flight but also to earth satellites, when an earth satellite goes from one circular orbit to another (but within the same plane). Also, if one spacecraft goes to a rendezvous with another spacecraft in a different orbit, the two spacecraft have to be in the proper predetermined positions prior to the launch to simultaneously reach their rendezvous location.

When the launch orbit (or launch planet) is not in the same plane as the target orbit, then additional energy will be needed by applying thrust in a direction normal to the launch orbit plane. More information is in Refs. 4-3, 4-4, 4-6, and 4-10.

Example 4-2. A satellite is launched from a circular equatorial parking orbit at an altitude of 160 km into a coplanar circular synchronous orbit by using a Hohmann transfer ellipse. Assume a homogeneous spherical earth with a radius of 6371 km. Determine the velocity increments for entering the transfer ellipse and for achieving the synchronous orbit at 42,200 km altitude. See Fig. 4-8 for the terminology of the orbits.

SOLUTION. The orbits are $R_A = 6.531 \times 10^6$ m; $R_B = 48.571 \times 10^6$ m. The major axis a of the transfer ellipse is

$$a_{te} = \frac{1}{2}(R_A + R_B) = 27.551 \times 10^6 \text{ m}$$

The orbit velocities of the two satellites in the two orbits are

$$\begin{aligned} u_A &= \sqrt{\mu/R_A} = [3.986005 \times 10^{14}/6.531 \times 10^6]^{1/2} = 7788 \text{ m/sec} \\ u_B &= \sqrt{\mu/R_B} = 2864.7 \text{ m/sec} \end{aligned}$$

The velocities needed to enter and exit the transfer ellipse are

$$\begin{aligned} (u_{te})_A &= \sqrt{\mu}[(2/R_A) - (1/a)]^{1/2} = 10,337 \text{ m/sec} \\ (u_{te})_B &= \sqrt{\mu}[(2/R_B) - (1/a)]^{1/2} = 1394 \text{ m/sec} \end{aligned}$$

The changes in velocity going from parking orbit to ellipse and from ellipse to final orbit are

$$\Delta u_A = |(u_{te})_A - u_A| = 2549 \text{ m/sec}$$

$$\Delta u_B = |u_B - (u_{te})_B| = 1471 \text{ m/sec}$$

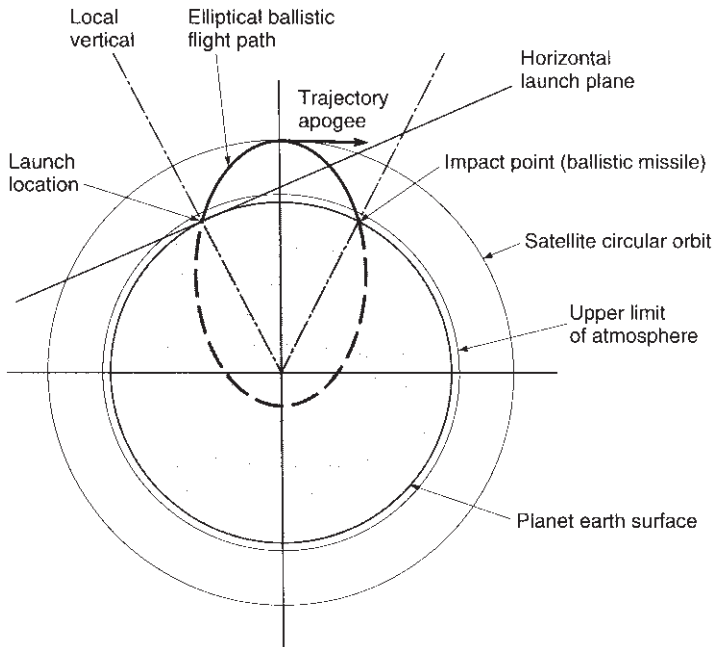


FIGURE 4–9. Long-range ballistic missiles follow an elliptical free flight trajectory, which is drag free, with the earth's center as one of the focal points. The surface launch is usually vertically up (not shown here) but the flight path is quickly tilted during the early powered flight to enter into an elliptic trajectory. The ballistic range is the arc distance on the earth's surface. The same elliptical flight path can be used by launch vehicles for satellites; another powered flight period occurs (called orbit injection) just as the vehicle is at its elliptical apogee (as indicated by the arrow), causing the vehicle to enter an orbit.

The total velocity change for the transfer maneuvers is

$$\Delta u_{\text{total}} = \Delta u_A + \Delta u_B = 4020 \text{ m/sec}$$

Figure 4–9 shows the elliptical transfer trajectory of a ballistic missile or a satellite ascent vehicle. During the initial powered flight the trajectory angle is adjusted by the guidance system to an angle that will allow the vehicle to reach the apogee of its elliptical path exactly at the desired orbit altitude. For the ideal satellite the simplified theory assumes that orbit injection is an essentially instantaneous application of the total impulse as the ballistic trajectory reaches its apogee or zenith. In reality the rocket propulsion system operates over a finite time, during which gravity losses and changes in altitude occur.

Deep Space

Lunar and *interplanetary* missions include circumnavigation, landing, and return flights to the moon, Venus, Mars, and other planets. The energy necessary to

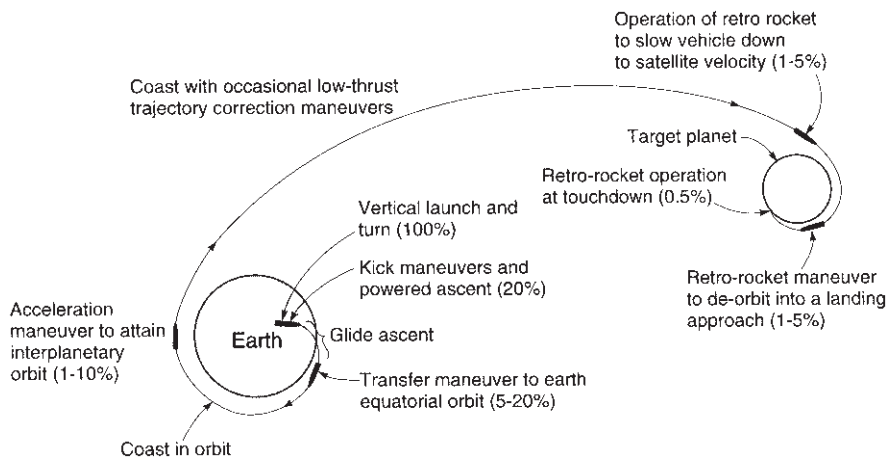


FIGURE 4–10. Schematic diagram of typical powered flight maneuvers during a hypothetical two-dimensional interplanetary mission with a landing. The numbers indicate typical thrust magnitudes of the maneuvers in percent of launch takeoff thrust. This is not drawn to scale. Heavy lines show powered flight path segments.

escape from the earth can be calculated as $\frac{1}{2}mv_e^2$ from Eq. 4–25. It is 6.26×10^7 J/kg, which is more than that required for a satellite. The gravitational attraction of various heavenly bodies and their respective escape velocities depends on their masses and diameters; approximate values are listed in Table 4–1. An idealized diagram of an interplanetary landing mission is shown in Fig. 4–10.

The *escape from the solar system* requires approximately 5.03×10^8 J/kg. This is eight times as much energy as is required for escape from the earth. There is technology to send small, unmanned probes away from the sun to outer space; as yet there needs to be an invention and demonstrated proof of a long-duration, novel, rocket propulsion system before a mission to the nearest star can be achieved. The trajectory for a spacecraft to escape from the sun is either a parabola (minimum energy) or a hyperbola. See Refs. 4–6 and 4–10.

Perturbations

This section gives a brief discussion of the disturbing torques and forces which cause perturbations or deviations from any intended space flight path or any satellite's flight orbit. For a more detailed treatment of flight paths and their perturbations, see Refs. 4–3, 4–4, and 4–13. A system is needed to measure the satellite's position and deviation from the intended flight path, to determine the needed periodic correction maneuver, and then to counteract, control, and correct them. This is called *orbit maintenance*; it corrects the perturbed or altered orbit by periodically applying small rocket propulsion forces in predetermined directions. Typically, the corrections are performed by a set of small reaction control thrusters which provide predetermined total impulses into the desired

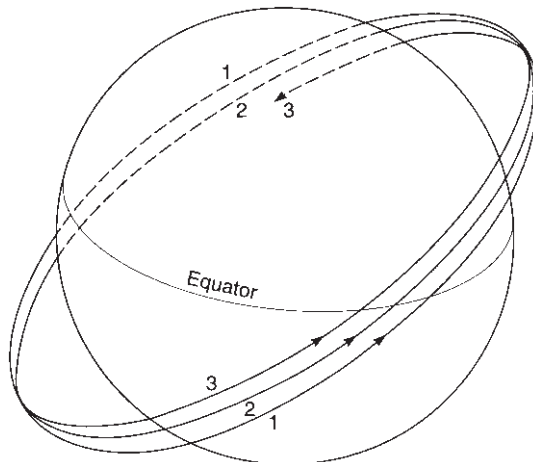


FIGURE 4–11. The regression of nodes is shown as a rotation of the plane of the orbit. The direction of the movement will be opposite to the east–west components of the earth’s satellite motion.

directions. These corrections are needed throughout the life of the spacecraft (for 1 to 20 years or sometimes more) to overcome the effects of the disturbances and maintain the intended flight regime.

Perturbations can be categorized as short term and long term. The daily or orbital period oscillating forces are called *diurnal* and those with long periods are called *secular*.

High-altitude earth satellites (36,000 km and higher) experience perturbing forces primarily as gravitational pull from the sun and the moon, with the forces acting in different directions as the satellite flies around the earth. This third-body effect can increase or decrease the velocity magnitude and change its direction. In extreme cases the satellite can come very close to the third body, such as a planet or one of its moons, and undergo what is called a hyperbolic maneuver that will radically change the trajectory. This encounter can be used to increase or decrease the energy of the satellite and intentionally change the velocity and the shape of the orbit.

Medium- and low-altitude satellites (500 to 35,000 km) experience perturbations because of the earth’s oblateness. The earth bulges in the vicinity of the equator and a cross section through the poles is not entirely circular. Depending on the inclination of the orbital plane to the earth equator and the altitude of the satellite orbit, two perturbations result: (1) the regression of the nodes and (2) shifting of the apsidal line (major axis). Regression of the nodes is shown in Fig. 4–11 as a rotation of the plane of the orbit in space, and it can be as high as 9° per day at relatively low altitudes. Theoretically, regression does not occur in equatorial orbits.

Figure 4–12 shows an exaggerated shift of the apsidal line, with the center of the earth remaining as a focus point. This perturbation may be visualized as the

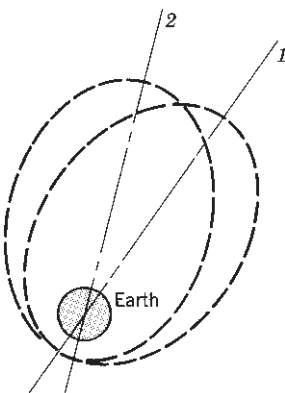


FIGURE 4–12. Shifting of the apsidal line of an elliptic orbit from position 1 to 2 because of the oblateness of the earth.

movement of the prescribed elliptical orbit in a fixed plane. Obviously, both the apogee and perigee points change in position, the rate of change being a function of the satellite altitude and plane inclination angle. At an apogee altitude of 1000 nautical miles (n.m.) and a perigee of 100 n.m. in an equatorial orbit, the apsidal drift is approximately 10° per day.

Satellites of modern design, with irregular shapes due to protruding antennas, solar arrays, or other asymmetrical appendages, experience torques and forces that tend to perturb the satellite's position and orbit throughout its orbital life. The principal torques and forces result from the following factors:

1. *Aerodynamic drag.* This factor is significant at orbital altitudes below 500 km and is usually assumed to cease at 800 km above the earth. Reference 4–8 gives a detailed discussion of aerodynamic drag, which, in addition to affecting the attitude of unsymmetrical vehicles, causes a change in elliptical orbits known as apsidal drift, a decrease in the major axis, and a decrease in eccentricity of orbits about the earth. See Refs. 4–6, –8, –12, and –13.
2. *Solar radiation.* This factor dominates at high altitudes (above 800 km) and is due to impingement of solar photons upon satellite surfaces. The solar radiation pressure p (N/m^2) on a given surface of the satellite in the vicinity of the earth exposed to the sun can be determined as

$$p = 4.5 \times 10^{-6} \cos \theta [(1 - k_s) \cos \theta + 0.67 k_d] \quad (4-32)$$

where θ is the angle (degrees) between the incident radiation vector and the normal to the surface and k_s and k_d are the specular and diffuse coefficients of reflectivity. Typical values are 0.9 and 0.5, respectively, for k_s and k_d on the body and antenna and 0.25 and 0.01, respectively, for k_s and k_d with solar array surfaces. The radiation intensity varies as the square of

the distance from the sun (see Refs. 4–4 and 4–14). The torque T on the vehicle is given by $T = pAl$, where A is the projected area and l is the offset distance between the spacecraft's center of gravity and the center of solar pressure. For a nonsymmetrical satellite with a large solar panel on one side the radiation will cause a small torque, which will rotate the vehicle.

3. *Gravity gradients.* Gravitational torque in spacecraft results from a variation in the gravitational force on the distributed mass of a spacecraft. Determination of this torque requires knowledge of the gravitational field and the distribution of spacecraft mass. This torque decreases as a function of the orbit radius and increases with the offset distances of masses within the spacecraft (including booms and appendages); it is most significant in large spacecraft or space stations operating in relatively low orbits (see Refs. 4–4 and 4–15).
4. *Magnetic field.* The earth's magnetic field and any magnetic moment within the satellite interact to produce torque. The earth's magnetic field precesses about the earth's axis but is very weak (0.63 and 0.31 gauss at poles and equator, respectively). This field is continually fluctuating in direction and intensity because of magnetic storms and other influences. Since the field strength decreases with $1/R^3$ with the orbital altitude, magnetic field forces are often neglected in the preliminary analysis of satellite flight paths (see Ref. 4–16).
5. *Internal accelerations.* Deployment of solar array panels, the shifting of liquid propellant, the movement of astronauts or other masses within the satellite, or the "unloading" of reaction wheels can produce torques and forces.
6. For precise low earth orbits the *oblateness* of the earth (diameter at equator is slightly larger than diameter between poles), high mountains, or earth surface areas of different densities will perturb these orbits.

We can categorize satellite propulsion needs according to function as listed in Table 4–2, which shows the total impulse "budget" applicable to a typical high-altitude, elliptic orbit satellite. The control system designer often distinguishes two different kinds of station-keeping orbit corrections needed to keep the satellite in a synchronous position. The east–west correction refers to a correction that moves the point at which a satellite orbit intersects the earth's equatorial plane in an east or west direction; it usually corrects forces caused largely by the oblateness of the earth. The north–south correction counteracts forces usually connected with the third-body effects of the sun and the moon.

In many satellite missions the gradual changes in orbit caused by perturbation forces are not of concern. However, in certain missions it is necessary to compensate for these perturbing forces and maintain the satellite in a specific orbit and in a particular position in that orbit. For example, a synchronous communications satellite in a Geo-Synchronous Earth Orbit or GEO needs to maintain its position and its orbit, so it will be able to (1) keep covering a specific area of the

TABLE 4-2. Propulsion Functions and Total Impulse Needs of a 2000-lbm Geosynchronous Satellite with a 7-Year Life

| Function | Total Impulse (N-sec) |
|---|--------------------------|
| Acquisition of orbit | 20,000 |
| Attitude control (rotation) | 4,000 |
| Station keeping, E-W | 13,000 |
| Station keeping, N-S | 270,000 |
| Repositioning (Δu , 200 ft/sec) | 53,000 |
| Control apsidal drift (third-body attraction) | 445,000 |
| Deorbit | 12,700 |
| Total | 817,700 |

earth or communicate with the same stations on earth within its line of sight and (2) not become a hazard to other satellites in this densely occupied synchronous equatorial orbit. Another example is a Low Earth Orbit or LEO communications satellite system with several coordinated satellites; here at least one satellite has to be in a position to receive and transmit radio-frequency (RF) signals to specific points on the earth. Their orbits, and the relative positions of these several satellites with respect to each other, need to be controlled and maintained (see Ref. 4-3).

Orbit maintenance means applying small correcting forces and torques periodically to compensate for perturbation effects; for GEO it is typically every few months. Typical velocity increments for the orbit maintenance of synchronous satellites require a Δu between 10 and 50 m/sec per year. For a satellite mass of about 2000 kg a 50-m/sec correction for a 10-year orbit life would need a total impulse of about 100,000 N-sec, which corresponds to a propellant mass of 400 to 500 kg (about a quarter of the satellite mass) if done by a small monopropellant or bipropellant thrust. It would require much less propellant if electrical propulsion were used, but in some spacecraft the inert mass of the power supply would increase. See Refs. 4-6, 4-13, and 4-14.

Mission Velocity

A convenient way to describe the magnitude of the energy requirement of a space mission is to use the concept of the *mission velocity*. It is the sum of all the flight velocity increments needed (in all the vehicle's stages) to attain the mission objective even though these increments are provided by different propulsion systems. In the simplified sketch of a planetary landing mission of Fig. 4-10, it is the sum of all the Δu velocity increments shown by the heavy lines (rocket-powered flight segments) of the trajectories. Even through some of the velocity increments were achieved by retro-action (a negative propulsion force to decelerate the flight velocity), these maneuvers required energy and their absolute magnitude is counted in the mission velocity. The initial velocity from

TABLE 4–3. Typical Estimated Space Shuttle Incremental Flight Velocity Breakdown

| | |
|--|------------|
| Ideal satellite velocity | 7790 m/sec |
| Δu to overcome gravity losses | 1220 m/sec |
| Δu to turn the flight path from the vertical | 360 m/sec |
| Δu to counteract aerodynamic drag | 118 m/sec |
| Orbit injection | 145 m/sec |
| Deorbit maneuver to re-enter atmosphere and aerodynamic braking | 60 m/sec |
| Correction maneuvers and velocity adjustments | 62 m/sec |
| Initial velocity provided by the earth's rotation at 28.5° latitude | −408 m/sec |
| Total required mission velocity | 9347 m/sec |

the earth's rotation (464 m/sec at the equator and 408 m/sec at a launch station at 28.5° latitude) does not have to be provided by the vehicle's propulsion systems. For example, the required mission velocity for launching at Cape Kennedy, bringing the space vehicle into an orbit at 110 km, staying in orbit for a while, and then entering a deorbit maneuver has the Δu components shown in Table 4–3.

The required mission velocity is the sum of the absolute values of all translation velocity increments that have forces going through the center of gravity of the vehicle (including turning maneuvers) during the flight of the mission. It is the theoretical hypothetical velocity that can be attained by the vehicle in a gravity-free vacuum, if all the propulsive energy of the momentum-adding thrust chambers in all stages were to be applied in the same direction. It is useful for comparing one flight vehicle design with another and as an indicator of the mission energy.

The required mission velocity has to be equal to the “supplied” mission velocity, that is, the sum of all the velocity increments provided by the propulsion systems of each of the various vehicle stages. The total velocity increment to be “supplied” by the shuttle's propulsion systems for the shuttle mission described below (solid rocket motor strap-on boosters, main engines and, for orbit injection, also the increment from the orbital maneuvering system—all shown in Fig. 1–14) has to equal or exceed 9347 m/sec. If reaction control system propellant and an uncertainty factor are added, it will need to exceed 9621 m/sec. With chemical propulsion systems and a single stage, we can achieve a space mission velocity of 4000 to 13,000 m/sec, depending on the payload, mass ratio, vehicle design, and propellant. With two stages it can be between perhaps 12,000 and 22,000 m/sec.

Rotational maneuvers, described later, do not change the flight velocity and some analysts do not add them to the mission velocity requirements. Also, maintaining a satellite in orbit against long-term perturbing forces (see prior section) is often not counted as part of the mission velocity. However, the designers need to provide additional propulsion capability and propellants for these purposes. These are often separate propulsion systems, called reaction control systems.

Typical vehicle velocities required for various interplanetary missions have been estimated as shown in Table 4–4. By starting interplanetary journeys from

TABLE 4-4. Approximate Vehicle Mission Velocities for Typical Interplanetary Missions

| Mission | Ideal Velocity (km/sec) | Approximate Actual Velocity (km/sec) |
|---|----------------------------|--|
| Satellite orbit around earth (no return) | 7.9–10 | 9.1–12.5 |
| Escape from earth (no return) | 11.2 | 12.9 |
| Escape from moon | 2.3 | 2.6 |
| Earth to moon (soft landing on moon, no return) | 13.1 | 15.2 |
| Earth to Mars (soft landing) | 17.5 | 20 |
| Earth to Venus (soft landing) | 22 | 25 |
| Earth to moon (landing on moon and return to earth ^a) | 15.9 | 17.7 |
| Earth to Mars (landing on Mars and return to earth ^a) | 22.9 | 27 |

^a Assumes air braking within atmospheres.

TABLE 4-5. Approximate Relative Payload-Mission Comparison Chart for Typical High-Energy Chemical Multistage Rocket Vehicles

| Mission | Relative Payload ^a (%) |
|---------------------------------------|-----------------------------------|
| Earth satellite | 100 |
| Earth escape | 35–45 |
| Earth 24-hr orbit | 10–25 |
| Moon landing (hard) | 35–45 |
| Moon landing (soft) | 10–20 |
| Moon circumnavigation (single fly-by) | 30–42 |
| Moon satellite | 20–30 |
| Moon landing and return | 1–4 |
| Moon satellite and return | 8–15 |
| Mars flyby | 20–30 |
| Mars satellite | 10–18 |
| Mars landing | 0.5–3 |

^a 300 nautical miles (555.6 km) earth orbit is 100% reference.

a space satellite station, a considerable saving in this vehicle velocity can be achieved, namely, the velocity necessary to achieve the earth-circling satellite orbit. As the space flight objective becomes more ambitious, the mission velocity is increased. For a given single or multistage vehicle it is possible to increase the vehicle's terminal velocity, but usually only at the expense of payload. Table 4-5 shows some typical ranges of payload values for a given multistage vehicle as a percentage of a payload for a relatively simple earth orbit. Thus a vehicle capable of putting a substantial payload into a near-earth orbit can only land a

very small fraction of this payload on the moon, since it has to have additional upper stages, which displace payload mass. Therefore, much larger vehicles are required for space flights with high mission velocities if compared to a vehicle of less mission velocity but identical payload. The values listed in Tables 4–4 and 4–5 are only approximate because they depend on specific vehicle design features, the propellants used, exact knowledge of the trajectory–time relation, and other factors that are beyond the scope of this short treatment.

4.5. FLIGHT MANEUVERS

In this section we describe different flight maneuvers and relate them to specific propulsion system types. See Refs. 4–5, 4–11, 4–12, 4–13, and 4–14. The three categories of *maneuvers* are:

1. In *translation maneuvers* the rocket propulsion thrust vector goes through the center of gravity of the vehicle. The vehicle momentum is changed in the direction of the flight velocity. An example of several powered (translational maneuvers) and unpowered (coasting) segments of a complex space flight trajectory is shown in schematic, simplified form in Fig. 4–10. To date, most maneuvers have used chemical propulsion systems.
2. In *truly rotational maneuvers* there is no net thrust acting on the vehicle. These are true force couples that apply only torque. It requires four thrusters to be able to rotate the vehicle in either direction about any one axis (two thrusters apart, firing simultaneously, but in opposite rotational directions). These types of maneuver are usually provided by reaction control systems. Most have used multiple liquid propellant thrusters, but in recent years selected space missions have used electrical propulsion.
3. A combination of categories 1 and 2, such as a misaligned thrust vector of a large thrust chamber that does not go exactly through the center of gravity of the vehicle. The misalignment can be corrected by changing the vector direction of the main propulsion system (thrust vector control) during powered flight or by applying a simultaneous compensating torque from a separate reaction control system.

The following types of *space flight maneuvers and vehicle accelerations* use rocket propulsion. All propulsion operations are usually controlled (started, monitored, and stopped) by the vehicle's guidance and control system.

- a. *First stage, its upper stage propulsion systems* and strap-on boosters add momentum during launch and ascent. They require rocket propulsion of high or medium thrusts and limited durations (typically 0.7 to 8 min). To date all have used chemical propulsion systems. They constitute the major mass of the space vehicle and are discussed further in the next section.

- b. *Orbit injection or transferring from one orbit to another* requires accurately predetermined total impulses. It can be performed by the main propulsion system of the top stage of the launch vehicle. More often it is done by a separate propulsion system at lower thrust levels than the upper stages in item (a) above. Orbit injection can be a single thrust operation after ascent from an earth launch station. If the flight path is a Hohmann transfer ellipse (minimum energy) or a faster transfer orbit, then two thrust application periods are necessary, one at the beginning and one at the end of the transfer path. For injection into earth orbit, the thrust levels are typically between 200 and 45,000 N or 50 and 11,000 lbf, depending on the payload size, transfer time, and specific orbit. If the new orbit is higher, then the thrusts are applied in the flight direction. If the new orbit is at a lower altitude, then the thrusts must be applied in a direction opposite to the flight velocity vector. The transfer orbits can also be achieved with a very low thrust level (0.001 to 1 N) using an electric propulsion system, but the flight paths will be very different (multiloop spiral) and the transfer duration will be much longer. This is explained in Chapter 17. Similar maneuvers are also performed with lunar or interplanetary flight missions, like the planetary landing mission shown schematically in Fig. 4-10.
- c. *Velocity vector adjustment and minor in-flight correction maneuvers* are usually performed with low-thrust, short-duration, and intermittent (pulsing) operations, using a reaction control system with multiple small liquid propellant thrusters, both for translation and rotation. The vernier rockets on a ballistic missile are used to accurately calibrate the terminal velocity vector for improved target accuracy. The reaction control rocket systems in a space launch vehicle will allow accurate orbit injection adjustment maneuvers after it is placed into orbit by another, less accurate propulsion system. Midcourse guidance-directed *correction maneuvers* for the trajectories of deep space vehicles fall also into this category. Propulsion systems for *orbit maintenance maneuvers*, also called *station-keeping maneuvers* (to overcome perturbing forces), keep a spacecraft in its intended orbit and orbital position and are also considered to be part of this category.
- d. *Reentry and landing maneuvers* can take several forms. If the landing occurs on a planet that has an atmosphere, then the drag of the atmosphere will slow down the reentering vehicle. For a multiple elliptical orbit the drag will progressively reduce the perigee altitude and the perigee velocity on every orbit. Landing at a precise, preplanned location requires a particular velocity vector at a predetermined altitude and distance from the landing site. The vehicle has to be rotated into the right position and orientation, so as to use its heat shield correctly. The precise velocity magnitude and direction prior to entering the denser atmosphere are critical for minimizing the heat transfer (usually to the vehicle's heat shield) and to achieve touchdown at the intended landing site or, in the case of ballistic missiles, the intended target. This usually requires a relatively minor maneuver (low total impulse). If there is very little or no atmosphere (for instance, landing

on the moon or Mercury), then a reverse thrust has to be applied during descent and touchdown. The rocket propulsion system usually has variable thrust to assure a soft landing and to compensate for the decrease in vehicle mass as propellant is consumed during descent. The U.S. lunar landing rocket engine, for example, had a 10 to 1 thrust variation.

- e. *Rendezvous and docking* involve both rotational and translational maneuvers of small reaction control thrusters. Rendezvous and its time windows were discussed on page xxx. Docking (sometimes called lockon) is the linking up of two spacecraft and requires a gradual gentle approach (low thrust, pulsing node thrusters) so as not to damage the spacecraft.
- f. *Simple rotational maneuvers* rotate the vehicle on command into a specific angular position so as to orient or point a telescope, instrument, solar panel, or antenna for purposes of observation, navigation, communication, or solar power reception. Such a maneuver is also used to keep the orientation of a satellite in a specific direction; for example, if an antenna needs to be continuously pointed at the center of the earth, then the satellite needs to be rotated around its own axis once every satellite revolution. Rotation is also used to point a nozzle of the primary propulsion system into its intended direction just prior to its start. It can also provide pulsed thrust for achieving flight stability, or for correcting angular oscillations, that would otherwise increase drag or cause tumbling of the vehicle. Spinning or rolling a vehicle about its axis will improve flight stability but will also average out the misalignment in a thrust vector. If the rotation needs to be performed quickly, then a chemical multithruster reaction control system is used. If the rotational changes can be done over a long period of time, then an electrical propulsion system with multiple thrusters is often preferred.
- g. *A change of plane of the flight trajectory* requires the application of a thrust force (through the vehicle center of gravity) in a direction normal to the original plane of the flight path. This is usually performed by a propulsion system that has been rotated (by the reaction control system) into the proper nozzle orientation. This maneuver is done to change the plane of a satellite orbit or when going to a planet, such as Mars, whose orbit is inclined to the plane of the earth's orbit.
- h. *Deorbiting and disposal of used or spent spacecraft* is required today to remove space debris. The spent spacecraft should not become a hazard to other spacecraft. A relatively small thrust will cause the vehicle to go to a low enough elliptical orbit so that atmospheric drag will cause further slowing. In the dense regions of the atmosphere the reentering, expended vehicle will typically break up or overheat (burn up).
- i. *Emergency or alternative mission.* If there is a malfunction in a spacecraft and it is decided to abort the mission, such as a premature quick return to the earth without pursuing the originally intended mission, then some of the rocket engines can be used for an alternate mission. For example, the

main rocket engine in the Apollo lunar mission service module is normally used for retroaction to attain a lunar orbit and for return from lunar orbit to the earth; it can be used for emergency separation of the payload from the launch vehicle and for unusual midcourse corrections during translunar coast, enabling an emergency earth return.

Table 4–6 lists the maneuvers that have just been described, together with some others, and shows the various types of rocket propulsion system (as mentioned in Chapter 1) that have been used for each of these maneuvers. The items with a double mark “ $\times \times$ ” have been the preferred methods in recent years. The table omits several propulsion systems, such as solar thermal or nuclear rocket propulsion, because these have not yet flown in a routine space mission. The three propulsion systems on the right of Table 4–6 are electrical propulsion systems and they have very high specific impulse (see Table 2–1), which makes them very attractive for deep space missions and for certain station-keeping jobs (orbit maintenance). However, they can be applied only to missions with sufficiently long thrust action time for reaching the desired vehicle velocity or rotation positions with very small acceleration.

Reaction Control System

The functions of a reaction control system have been described in the previous section on flight maneuvers. They are used for the maneuvers identified by paragraphs c, e, and g. In some vehicle designs they are also used for tasks described in b, part of d, and f, if the thrust levels are low.

A *reaction control system* (RCS), often called an *auxiliary rocket propulsion system*, is needed to provide for trajectory corrections (small Δu additions) as well as correcting the rotational or attitude position of almost all spacecraft and all major launch vehicles. If only rotational maneuvers are made, it has been called an *attitude control system*. The nomenclature has not been consistent throughout the industry or the literature.

An RCS can be incorporated into the payload stage and each of the stages of a multiple-stage vehicle. In some missions and designs the RCS is built into only the uppermost stage; it operates throughout the flight and provides the control torques and forces for all the stages. For large vehicle stages the thrust level of multiple thrusters of an RCS can be large (500 to 15,000 lbf) and for terminal stages in small satellites they can be small (0.01 to 10.0 lbf) and they can be pulsed as often as commanded by the vehicle flight control system. Liquid propellant rocket engines with multiple thrusters have been used for almost all launch vehicles and the majority of all spacecraft. Cold gas systems were used with early spacecraft design. In the last decade an increasing number of electrical propulsion systems have been used, primarily on spacecraft, as described in Chapter 17. The life of an RCS may be short (when used on an individual vehicle stage), or it may see use throughout the mission duration (perhaps more than 10 years) when part of an orbiting spacecraft.

TABLE 4–6. Types of Rocket Propulsion System Commonly Used for Different Flight Maneuvers or Application

| Flight Maneuvers and Applications ↓ | Propulsion System → | Liquid Propellant Rocket Engines | Solid Propellant Rocket Motors | Electrical Propulsion |
|---|---------------------------|--|--|--|
| Launch vehicle booster | × × | High Thrust, Liquid Propellant Rocket Engine, with Turbopump | × × | Arc Jet, Resisto Jet |
| Strap-on motor/engine | × × | Medium to Low Thrust, Liquid Propellant Rocket Engine | × × | Ion Propulsion, Electromagnetic Propulsion |
| Upper stages of launch vehicle | × × | Pulsing Liquid Propellant, Multiple Small Thrusters | Large Solid Propellant Rocket Motor, Often Segmented | Pulsed Plasma Jet |
| Satellite orbit injection and transfer orbits | × × | | × × | × × |
| Flight velocity adjustments, flight path corrections, orbit changes | × | × × | | × × |
| Orbit/position maintenance, rotation of spacecraft | | × × | | × × × |
| Docking of two spacecraft | | × × | | × |
| Reentry and landing, emergency maneuvers | × | × | | × × × |
| Deorbit | × | × | × | × |
| Deep space, sun escape | × | × | × × | × |
| Tactical missiles | × | × | × × | |
| Strategic missiles | × | × | × × | |
| Missile defense | × | × | × × | × |

Legend : × = in use : × × = preferred for use.

The vehicle attitude has to be controlled about three mutually perpendicular axes, each with two degrees of freedom (clockwise and counterclockwise rotation), giving a total of six degrees of rotational freedom. *Pitch* control raises or lowers the nose of the vehicle, *yaw* torques induce a motion to the right or the left side, and *roll* torques will rotate the vehicle about its axis, either clockwise or counterclockwise. In order to apply a true torque it is necessary to use two thrust chambers of exactly equal thrust and equal start and stop times, placed an equal distance from the center of mass. Figure 4–13 shows a simple spherical

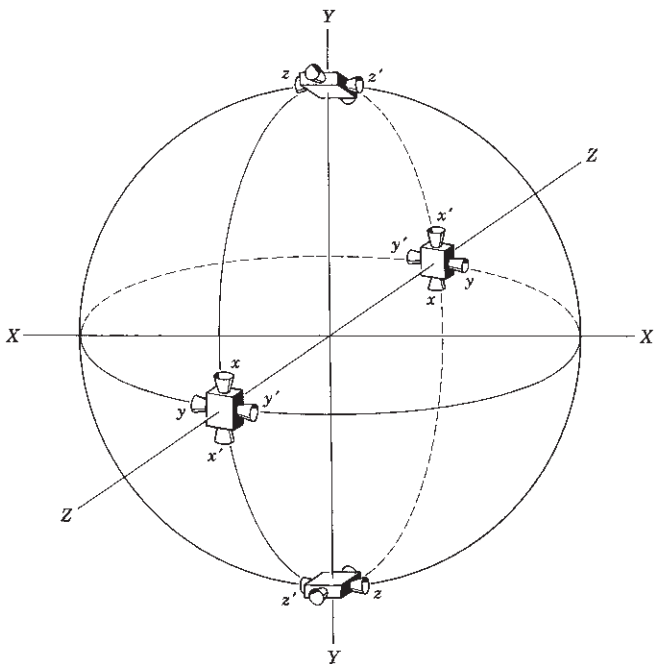


FIGURE 4–13. Simplified attitude control system diagram for spacecraft. It requires 12 thrusters (identified as x , y , z) to allow the application of pure torques about three perpendicular axes. The four unlabeled thrusters are needed for translation maneuvers along the z axis. They are shown here in four clusters.

spacecraft attitude control system; thrusters $x - x'$ or $x' - x$ apply torques that rotate about the X axis. There is a minimum of 12 thrusters in this system, but some spacecraft with geometrical or other limitations on the placement of these nozzles or with provisions for redundancy may actually have more than 12. The same system can, by operating a different set of nozzles, also provide translation forces; for example, if one each of the thrust units x and x' were operated simultaneously, the resulting forces would propel the vehicle in the direction of the Y axis. With clever design it is possible to use fewer thrusters, but they will usually not provide a pure torque.

An RCS usually contains the following major subsystems: (1) sensing devices for determining the attitude, velocity, and position of the vehicle with respect to a reference direction at any one time, such as provided by gyroscopes, star-trackers, or radio beacons; (2) a control-command system that compares the actual space and rotary position with the desired or programmed position and issues command signals to change the vehicle position within a desired time period; and (3) devices for changing the angular position, such as a set of high-speed gyroscopic wheels or a set of attitude control thrust-providing devices. See Refs. 4–13 and 4–14.

A precise attitude angular correction can also be achieved by the use of an inertial or high-speed rotating reaction wheel, which applies torque when its rotational speed is increased or decreased. While these wheels are quite simple and effective, the total angular momentum change they can supply is generally small. By using a pair of supplementary attitude control thrust rocket units it is possible to unload or respin each wheel so it can continue to supply small angular position corrections as needed.

The torque T of a pair of thrust chambers of thrust F and a separation distance l is applied to give the vehicle with an angular or rotational moment of inertia M_a an angular acceleration of magnitude α :

$$T = Fl = M_a\alpha \quad (4-33)$$

For a cylinder of equally distributed mass $M_a = \frac{1}{2}mr^2$ and for a homogeneous sphere it is $M_a = \frac{2}{5}mr^2$. The largest possible practical value of moment arm l will minimize the thrust and propellant requirements. If the angular acceleration is constant over a time period t , the vehicle will move at an angular speed ω and through a displacement angle θ , namely

$$\omega = \alpha t \quad \text{and} \quad \theta = \frac{1}{2}\alpha t^2 \quad (4-34)$$

Commonly a control system senses a small angular disturbance and then commands an appropriate correction. For this detection of an angular position change by an accurate sensor it is actually necessary for the vehicle to undergo a slight angular displacement. Care must be taken to avoid overcorrection and hunting of the vehicle position or the control system. This is one of the reasons many spacecraft require extremely short multiple pulses (0.010 to 0.030 sec) and low thrust (0.01 to 100 N) (see Refs. 4-11, 4-13, and 4-14).

Reaction control systems can be characterized by the magnitude of the total impulse, the number, thrust level, and direction of the thrusters, and their duty cycles. The *duty cycle* refers to the number of thrust pulses, their operating times, the times between thrust applications, and the timing of these short operations during the mission operating period. For a particular thruster, a 30% duty cycle means an average active cumulative thrust period of 30% during the propulsion system's flight duration. These propulsion parameters can be determined from the mission, the guidance and control approach, the desired accuracy, flight stability, the likely thrust misalignments of the main propulsion systems, the three-dimensional flight path variations, the perturbations to the trajectory, and several other factors. Some of these parameters are often difficult to determine.

4.6. EFFECT OF PROPULSION SYSTEM ON VEHICLE PERFORMANCE

This section gives several methods for improving flight vehicle performance. Most of these enhancements, listed below, are directly influenced by the flight

mission and by the selection or design of the propulsion system. A few of the flight vehicle performance improvements do not depend on the propulsion system. Most of those listed below apply to all missions, but some are peculiar to some missions only.

1. The *effective exhaust velocity* c and the *specific impulse* I_s usually have a direct effect on the vehicle's flight performance. The vehicle's final velocity increment Δu can be increased by a higher I_s . This can be done by using a more energetic chemical propellant (see Chapters 7 and 12), by a higher chamber pressure, and, for upper stages operating at high altitudes, also by a larger nozzle area ratio. Electrical propulsion (higher I_s) can enhance vehicle performance, but, as explained later, the very low thrusts do limit this type to certain space missions. See Chapter 17.
2. The mass ratio m_0/m_f has a logarithmic effect. It can be increased in several ways. One way is by reducing the final mass m_f , which consists of the inert hardware plus the nonusable, residual propellant mass. Reducing the inert mass implies lighter structures, smaller payloads, lighter guidance/control devices, or less unavailable residual propellant; this means going to stronger structural materials at higher stresses, more efficient power supplies, or smaller electronic packages. During design there is always great emphasis to reduce all hardware masses and the residual propellants to their practical minima. Another way is to increase the initial vehicle mass, and use a higher thrust and more propellant, but with a smaller increase in the structure or inert propulsion system masses.
3. Reducing the burning time (i.e., increasing the thrust level) will reduce the gravitational loss in some applications. However, the higher acceleration usually requires more structural and propulsion system mass, which in turn causes the mass ratio to be less favorable.
4. The *drag*, which can be considered as a negative thrust, can be reduced in at least four ways. The drag has several components: (a) The form drag depends on the aerodynamic shape. A slender pointed nose or sharp, thin leading edges of fins or wings have less drag than a stubby, blunt shape. (b) A vehicle with a small cross-sectional area has less drag. A propulsion design that can be packaged in a long, thin shape will be preferred. (c) The drag is proportional to the cross-sectional or frontal vehicle area. A higher propellant density will decrease the propellant volume and therefore will allow a smaller cross section. (d) The skin drag is caused by the friction of the air flowing over all the vehicle's outer surfaces. A smooth contour and a polished surface are usually better. The skin drag is also influenced by the propellant density, because it gives a smaller volume and thus a lower surface area. (e) The base drag is the fourth component; it is a function of the local ambient air pressure acting over the surface of the vehicle's base or bottom plate. It is influenced by the nozzle exit design (exit pressure), the discharge of turbine exhaust gases, and the geometry of the vehicle base design. It is discussed further in Chapter 20.

5. The length of the propulsion nozzle often is a significant part of the overall vehicle or stage length. As was described in Chapter 3, there is an optimum nozzle contour and length, which can be determined by trade-off analysis. A shorter nozzle length or multiple nozzles on the same propulsion system allow a somewhat shorter vehicle; on many designs this implies a somewhat lighter vehicle structure and a slightly better vehicle mass ratio.
6. The final vehicle velocity at propulsion termination can be increased by increasing the initial velocity u_0 . By launching a satellite in an eastward direction the rotational speed of the earth is added to the final satellite orbital velocity. This tangential velocity of the earth is about 464 m/sec or 1523 ft/sec at the equator and the Sea Launch from a ship on the equator takes full advantage of this velocity increment. For an easterly launch at John F. Kennedy Space Center (latitude of 28.5° north) this extra velocity is about 408 m/sec or 1340 ft/sec. Conversely, a westerly satellite launch has a negative initial velocity and thus requires a higher-velocity increment. Another way to increase u is to launch a spacecraft from a satellite or an aircraft, which increases the initial vehicle velocity and allows launching in the desired direction, or to launch an air-to-surface missile from an airplane. An example is the Pegasus three-stage space launch vehicle, which is launched from an airplane.
7. For vehicles that fly in the atmosphere it is possible to increase the range when aerodynamic lift is used to counteract gravity and reduce gravity losses. Using a set of wings or flying at an angle of attack increases the lift, but it also increases the drag. This lift can also be used to increase the maneuverability and trajectory flexibility.
8. When the flight velocity u is close to the rocket's effective exhaust velocity c , the propulsive efficiency is the highest (Eq. 2–23) and more of the rocket exhaust gas energy is transformed into the vehicle's flight energy. Trajectories where u is close in value to c for a major portion of the flight therefore need less propellant.

Several of these influencing parameters can be optimized. Therefore, for every mission or flight application there is an optimum propulsion system design and the propulsion parameters that define the optimum condition are dependent on vehicle or flight parameters.

4.7. FLIGHT VEHICLES

As mentioned, the vast majority of rocket-propelled vehicles are simple, single stage, and use solid propellant rocket motors. Most are used in military applications, as described in the next section. This section discusses more sophisticated multistage space launch vehicles and mentions others, such as large ballistic missiles (often called strategic missiles) and some sounding rockets. All have some

intelligence in their guidance and navigation system. The total number of multistage rocket vehicles produced worldwide in the last few years has been between 100 and 220 per year.

A single stage to orbit (LEO) is limited in the payload it can carry. Figure 4–2 shows that a high-performance single-stage vehicle with a propellant fraction of 0.95 and an average I_s of 400 sec can achieve an ideal terminal velocity of about 12,000 m/sec without payload. If the analysis includes drag and gravity forces, a somewhat higher value of I_s , maneuvers in the trajectory, and an attitude control system, it is likely that the payload would be between 0.2 and 1.4% of the gross takeoff mass, depending on the design. For a larger percentage of payload, and for ambitious missions, we use vehicles with two or more stages as described here.

Multistage Vehicles

Multistep or *multistage rocket vehicles* permit higher vehicle velocities, more payload for space vehicles, and improved performance for long-range ballistic missiles. After the useful propellant is fully consumed in a particular stage, the remaining empty mass of that expended stage is dropped from the vehicle and the operation of the propulsion system of the next step or stage is started. The last or top stage, which is usually the smallest, carries the payload. The empty mass of the expended stage or step is separated from the remainder of the vehicle, because it avoids the expenditure of additional energy for further accelerating a useless mass. As the number of steps is increased, the initial takeoff mass can be decreased; but the gain in a smaller initial mass becomes less apparent when the total number of steps is large. Actually, the number of steps chosen should not be too large, because the physical mechanisms become more numerous, complex, and heavy. The most economical number of steps is usually between two and six, depending on the mission. Several different multistage launch vehicle configurations have been used successfully and four are shown in Fig. 4–14. Most are launched vertically, but a few have been launched from an airplane, such as the three-stage Pegasus space vehicle. See Example 4–3.

The payload of a multistage rocket is essentially proportional to the takeoff mass, even though the payload is only a very small portion of the initial mass. If a payload of 50 kg requires a 6000-kg multistage rocket, a 500-kg payload would require a 60,000-kg rocket unit with an identical number of stages and a similar configuration with the same payload fraction and the same propellants. When the operation of the upper stage is started, immediately after thrust termination of the lower stage, then the total ideal velocity of a multistage vehicle of tandem or series-stage arrangement is simply the sum of the individual stage velocity increments. For n stages in series (one on top of each other) the final velocity increment Δu_f is

$$\Delta u_f = \sum_1^n \Delta u = \Delta u_1 + \Delta u_2 + \Delta u_3 + \dots \quad (4-35)$$

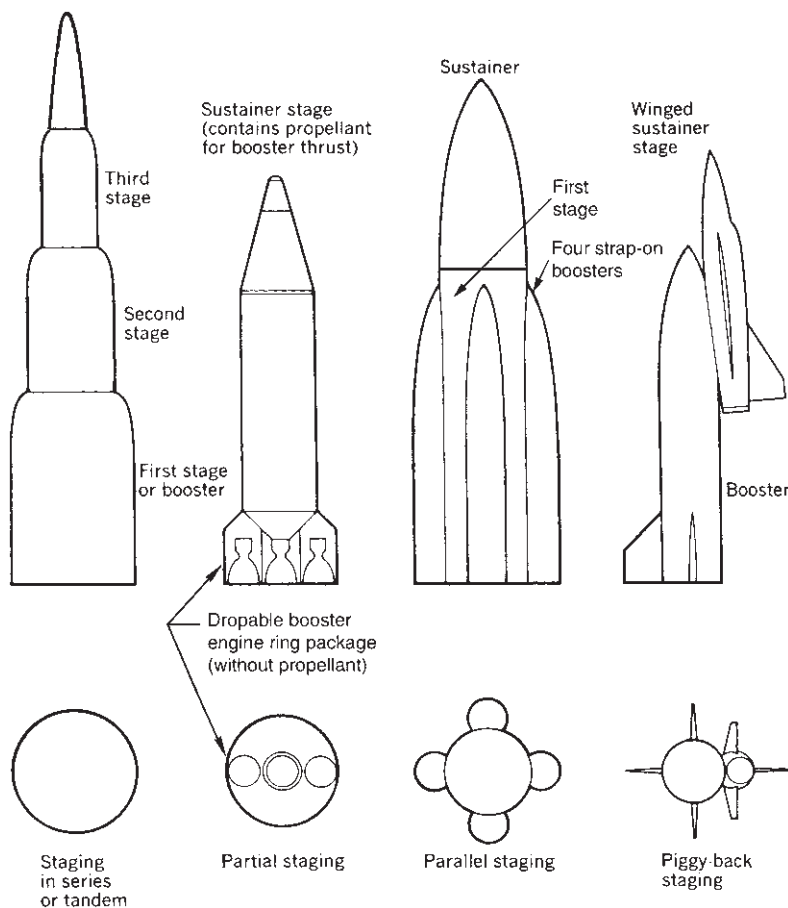


FIGURE 4-14. Simplified schematic sketches of four geometric configurations for assembling individual stages into a launch vehicle.

The individual velocity increments are given by Eq. 4-6. For the simplified case of a vacuum flight in a gravity-free field this can be expressed as

$$\Delta u_f = c_1 \ln(1/\mathbf{M}\mathbf{R}_1) + c_2 \ln(1/\mathbf{M}\mathbf{R}_2) + c_3 \ln(1/\mathbf{M}\mathbf{R}_3) + \dots \quad (4-36)$$

This equation defines the maximum velocity an ideal tandem multistage vehicle can attain in a gravity-free vacuum environment. For more accurate actual trajectories the individual velocity increments can be determined by integrating Eqs. 4-15 and 4-16, which consider drag and gravity losses. Other losses or trajectory perturbations can also be included, as mentioned earlier in this chapter. Such an approach requires numerical solutions.

For two- or three-stage vehicles the overall vehicle mass ratio (initial mass at takeoff to final mass of last stage) can reach values of over 100 (corresponding

to an equivalent single-stage propellant mass fraction ζ of 0.99). Figure 4–2 can be thus divided into regions for single- and tandem multistage vehicles. Equation 4–36 does not apply to parallel or partial staging as identified in Fig. 4–14. For stages where more than one propulsion system is operating at the same time and producing thrust in the same direction, the effective specific impulse and nozzle exhaust velocity is given by Eqs. 10–12 to 10–14.

The first sketch in Fig. 4–14 depicts a very common configuration and the stages are stacked vertically on top of each other, as in the Minuteman long-range missile or the Russian Zenit (Zenith) launch vehicle.* Partial staging was used on the early versions of the U.S. Atlas vehicle. It allows all engines to be started at launching, thus avoiding an altitude start of the sustainer engine, which was unknown in those early days. Liquid propellant rocket engines can be shut off on the launch stand if a failure is sensed prior to lift-off. The two Atlas booster engines arranged in a doughnut-shaped assembly are dropped off in flight. The third sketch has two or more separate booster “strap-on” stages attached to the bottom stage of a vertical configuration (they can be either solid or liquid propellants) and this allows an increase in vehicle performance. The piggy-back configuration concept on the right is used on the Space Shuttle. The two large solid rocket motor boosters are not shown.

Stage Separation

It usually takes a finite time for the termination of the lower stage propulsion system to go from full thrust to essentially zero thrust (typically 1 to 3 sec for large thrust values). In some multistage flight vehicles (with stage separation devices) there often was a further short delay (say 4 to 10 sec) to achieve a respectable separation distance between the upper and the lower stage, before the firing of the upper stage propulsion system was initiated. This was done in order to prevent blow-back of damaging hot flames onto the upper stage. Also the upper stage engine start-up was not instantaneous but required one or more seconds. During this cumulative delay of several seconds the earth’s gravity pull continues to diminish the vehicle’s upward velocity, causing a reduction of the flight velocity by perhaps 20 to 500 ft/sec (7 to 160 m/sec). A scheme called *hot staging* has been used to diminish this velocity loss and shorten the staging time interval. The upper stage propulsion system is actually started at low but increasing thrust before the lower stage propulsion system has been fully shut off or well before it reaches essentially zero thrust. There are special flame-resistant ducts in the interstage structure to allow the flame or hot exhaust gases of the upper stage engine to be safely discharged and deflected symmetrically prior to and immediately after the actual separation of the stages without harming the functional hardware of the vehicle. This hot staging scheme has been used on large multistage vehicles, such as the Titan II in the United States and certain

*The three-stage Zenit space launch vehicle is assembled in the Ukraine with Russian rocket engines. It is transported to the United States, loaded on a special floating launch platform (Sea Launch Program), and launched by a team that is headed by the Boeing Company.

launch vehicles in China and the Soviet Union, because it does improve the flight performance.

For multistage vehicles the stage mass ratios, thrust levels, propulsion durations, and location or travel of the center of gravity of the stages are usually optimized, often using a complex trajectory computer program. The high specific impulse rocket engine (e.g., using hydrogen–oxygen propellants) is normally employed in upper stages of space launch vehicles, because a small increase in specific impulse can be more effective there than in lower stages.

Example 4-3. A two-stage exploration vehicle is launched from a high-orbit satellite into a gravity-free vacuum trajectory. The following notation is used and explained in the accompanying diagram as well as in Fig. 4-1:

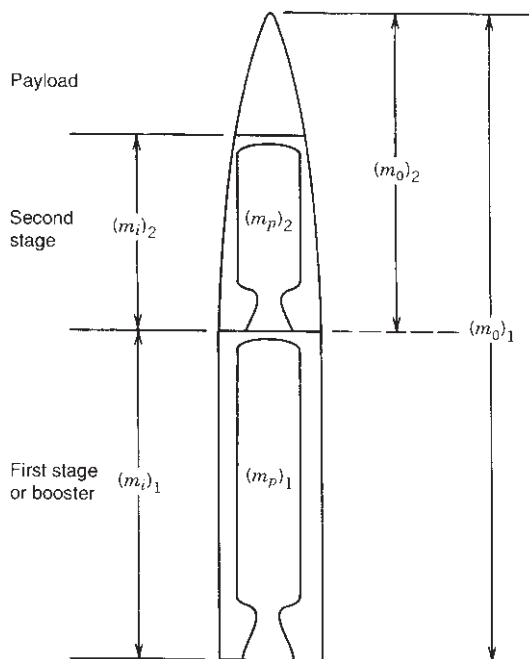
m_0 = initial mass of vehicle (or stage) at launch

m_p = useful propellant mass of stage

m_i = initial mass of stage(s)

m_f = final mass after rocket operation; it includes the empty propulsion system with its residual propellant, the vehicle structures plus the propulsion system with control, guidance and payload masses

m_{pl} = payload mass; it can include guidance, control and communications equipment, antennas, scientific instruments, military equipment, research apparatus, power supply, solar panels, sensors, etc.



Subscripts 1 and 2 refer to the first and second stages. The following data are given:

| | |
|--|------------|
| Flight velocity increment in gravity-free vacuum | 4700 m/sec |
| Specific impulse (each stage) | 310 sec |
| Initial takeoff launch vehicle mass | 4500 kg |
| Propellant mass fraction, ζ (each stage) | 0.88 |

Determine the payload for the following cases:

- When the two propulsion system or stage masses are equal [$(m_i)_1 = (m_i)_2$].
- When the mass ratios of the two stages are equal [$(m_f/m_0)_1 = (m_f/m_0)_2$].

SOLUTION. The following relationships apply to both cases. The takeoff mass or launch mass can be divided into three parts, namely, the two propulsion stages and then payload

$$(m_0) = (m_i)_1 + (m_i)_2 + (m_{pl})$$

The propellants are 88% of their propulsion system mass, and this is representative of a number of stages.

$$(m_p)_1 = 0.88(m_i)_1 \quad \text{and} \quad (m_p)_2 = 0.88(m_i)_2$$

The nozzle exit area ratio and the chamber pressure are the same in both stages and both cases. Thus the exhaust velocities are the same,

$$c_1 = c_2 = c = I_s g_0 = 310 \times 9.807 = 3040 \text{ m/sec}$$

Case 1. The stage masses and sizes are the same, or

$$(m_i)_1 = (m_i)_2 = m_i$$

Equation 4-36 can be rewritten

$$\begin{aligned} e^{\Delta u/c} &= (1/\mathbf{MR}_1)(1/\mathbf{MR}_2) = \{[m_o - (m_p)_1]/m_o\}[(m_i)_2 + m_{pl} - (m_{pl})] \\ e^{5500/3040} &= [(4500 - 0.88m_i)/4500][(m_i) + m_{pl} - 0.88m_i]/(m_i + m_{pl}) = 6.105 \end{aligned}$$

From the equation above $m_i = \frac{1}{2}(4500 - m_{pl})$.

These two equations have two unknowns: m_i and m_{pl} . The solution requires a quadratic equation, and the value of the payload can be determined as $m_{pl} \cong 480 \text{ kg}$.

Case 2. The mass ratios for the two stages are equal, or

$$\mathbf{MR}_1 = \mathbf{MR}_2 = \mathbf{MR} = m_o/m_f$$

$$1/\mathbf{MR} = [4500 - (m_p)_1]/4500 = [(m_i)_2 + m_{pl} - (m_p)_2]/[(m_i)_2 + m_{pl}]$$

$$e^{\Delta u/c} = \frac{4500 - 0.88(m_i)_1}{4500} \frac{0.12(m_i)_2 + m_{pl}}{(m_i)_2 + m_{pl}} = e^{5500/3040} = 6.105$$

These two equations (and the first equation of the example makes a third) have three variables: $(m_i)_1$, $(m_i)_2$, and m_{pl} . The solution is possible and requires quadratic equations and natural logarithms. The result is a payload of approximately 600 kg.

If a three-stage vehicle had been used in Example 4–3 instead of a two-stage version, the payload would have been even larger. However, the theoretical payload increase will only be about 8 or 10%. A fourth stage gives an even smaller theoretical improvement; it would add only 3 to 5% to the payload. The amount of potential performance improvement diminishes with each added stage. Each additional stage means extra complications in an actual vehicle (such as a reliable separation mechanism, an interstage structure, more propulsion systems, joints or couplings in connecting pipes and cables, etc.), requires additional inert mass (increasing the mass ratio **MR**), and compromises the overall reliability. Therefore, the minimum number of stages that will meet the payload and the Δu requirements is usually selected.

The flight paths taken by the vehicles in the two simplified cases of Example 4–3 are different, since the time of flight and the acceleration histories are different. One conclusion from this example applies to all multistage rocket-propelled vehicles; for each mission there is an optimum number of stages, an optimum distribution of the mass between the stages, and usually also an optimum flight path for each design, where a key vehicle parameter such as payload, velocity increment, or range is a maximum.

Launch Vehicles

Usually the *first or lowest stage*, often called a *booster stage*, is the largest and it requires the largest thrust and largest total impulse. For earth surface launch all stages now use chemical propulsion to achieve the desired thrust-to-weight ratio. These thrusts usually become smaller with each subsequent stage, also known as *upper stage* or *sustainer stage*. The thrust magnitudes depend on the mass of the vehicle, which in turn depends on the mass of the payload and the mission. Typical actual configurations are shown by simple sketches in Fig. 4–14. There is an optimum size and thrust value for each stage in a multistage vehicle and the analysis to determine these optima can be quite complex.

Many launch vehicles with heavy payloads have one to six large *strap-on stages*, also called zero stages or half stages. They augment the thrust of the booster stage, which is started at about the same time. A schematic diagram is shown in the third sketch of Fig. 4–14. Solid propellant strap-on stages are common, such as the Atlas V shown in Fig. 1–13 or the Space Shuttle shown in Fig. 1–14. They are usually smaller in size than the equivalent liquid propellant strap-on (due to higher propellant density) and have less drag and usually a very toxic exhaust. Liquid propellant strap-on stages are used in the Delta IV heavy lift launch vehicle (see Fig. 1–12), in the first Soviet ICBM (intercontinental ballistic missile, 1950s), and several Soviet/Russian space launch vehicles. They

deliver higher specific impulse, which enhances vehicle performance, and require propellant filling at the launch site.

There is a variety of existing launch vehicles. The smaller ones are for low payloads and low orbits; the larger ones usually have more stages, are heavier and more expensive, and have larger payloads or higher mission velocities. The vehicle cost increases with the number of stages and the initial vehicle launch mass. Once a particular launch vehicle has been proven to be reliable, it is usually modified and uprated to allow improvements in its capability or mission flexibility. Each of the stages of a space launch vehicle can have several rocket engines, each for specific missions or maneuvers. The Space Shuttle system has 67 different rockets which are shown schematically in Fig. 1–14. In most cases each rocket engine is used for a specific maneuver, but in many cases the same engine is used for more than one specific purpose; the small reaction control thrusters in the Shuttle serve, for example, to give attitude control (pitch, yaw, and roll) during orbit insertion and reentry, for counteracting internal shifting of masses (astronaut movement, extendible arm), small trajectory corrections, minor flight path adjustments, docking, and precise pointing of scientific instruments.

The *spacecraft* is that part of a launch vehicle that carries the payload. It is the only part of the vehicle that goes into orbit or deep space and some are designed to return to earth. The final major space maneuver, such as orbit injection or planetary landing, often requires a substantial velocity increment; the propulsion system, which provides the force for this maneuver, may be integrated with the spacecraft or it may be part of a discardable stage, just below the spacecraft. Several of the maneuvers described in Section 4.5 can often be accomplished by propulsion systems located in two different stages of a multistage vehicle. The selection of the most desirable propulsion systems, and the decision of which of the several propulsion systems will perform specific maneuvers, will depend on optimizing performance, cost, reliability, schedule, and mission flexibility as described in Chapter 19.

When a space vehicle is launched from the earth's surface into an orbit, it flies through three distinct trajectory phases. (1) Most are usually launched vertically and then undergo a turning maneuver while under rocket power to point the flight velocity vector into the desired direction. (2) The vehicle then follows a free-flight (unpowered) ballistic trajectory (usually elliptical), up to its apex. Finally (3) a satellite needs an extra push from a chemical rocket system to add enough total impulse or energy to accelerate it to orbital velocity. This last maneuver is also known as *orbit insertion* or sometimes as a *kick maneuver*. During the initial powered flight the trajectory angle and the thrust cutoff velocity of the last stage are adjusted by the guidance system to a velocity vector in space that will allow the vehicle to reach the apogee of its elliptic path exactly at the desired orbit altitude. As shown in Fig. 4–9, a *multistage ballistic missile* follows the same two ascent flight phases mentioned above, but it then continues its elliptical ballistic trajectory all the way down to the target.

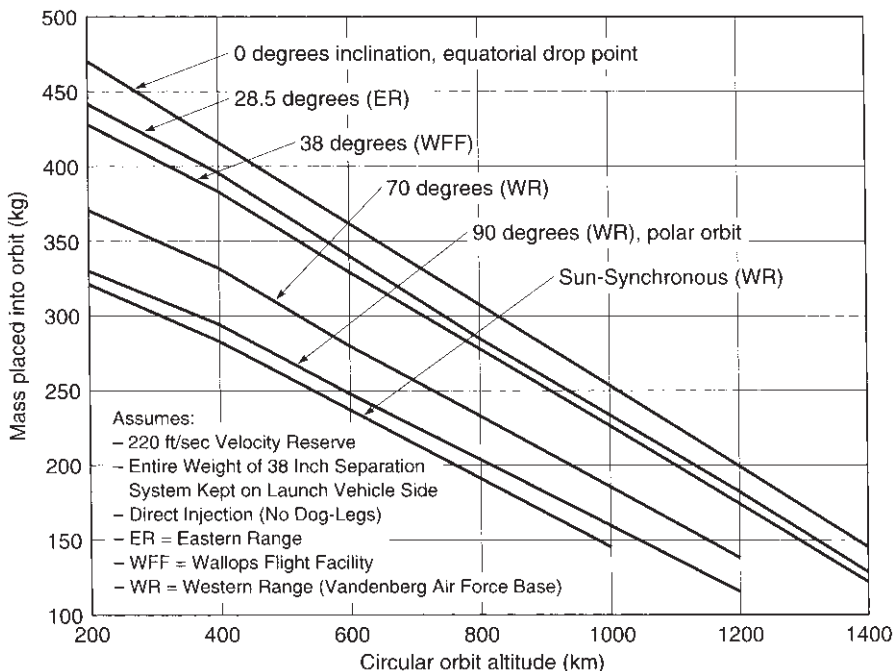


FIGURE 4–15. Decrease of payload with circular orbit altitude and orbit inclination for early version of the Pegasus launch vehicle. This is an air-launched, relatively simple, three-stage launch vehicle of 50 in. diameter driven by a solid propellant rocket motor in each stage. (Courtesy Orbital Sciences Corporation.)

Historically successful launch vehicles have been modified, enlarged, and improved in performance. The newer versions retain most of the old, proven, reliable components, materials, and subsystems. This reduces development effort and cost. Upgrading a vehicle allows an increase in mission energy (more ambitious mission) or payload or both. Typically, it is done by one or more of these types of improvement: increasing the mass of propellant without an undue increase in tank or case mass; uprating the thrust and strengthening the engine; more specific impulse; or adding successively more or bigger strap-on boosters. It also usually includes a strengthening of the structure to accept higher loads.

Figure 4–15 shows the effects of orbit inclination and altitude on the payload. The inclination is the angle between the equatorial plane of the earth and the trajectory. An equatorial orbit has zero inclination and a polar orbit has 90° inclination. Since the earth's rotation gives the vehicle an initial velocity, a launch from the equator in an eastward direction will give the highest payload. For the same orbit altitude other trajectory inclinations have a lower payload. For the same inclination the payload decreases with orbit altitude, since more energy has to be expended to overcome gravitational attraction.

The Space Shuttle has its maximum payload when launched due east into an orbit with 28.5° inclination from Kennedy Space Flight Center in Florida, namely about 56,000 lb (or 25,455 kg) at a 100-nautical-mile (185-km) orbit altitude. The payload decreases by about 100 lb (45.4 kg) for every nautical mile increase in altitude. If the inclination is 57° , the payload diminishes to about 42,000 lb (or 19,090 kg). If launched in a southerly direction from Vandenberg Air Force Base on the west coast in a 98° inclination into a circular, nearly polar orbit, the payload will be only about 30,600 lb or 13,909 kg.

The dramatic decrease of payload with circular orbits of increasing altitude and with different inclination is shown for the Pegasus, a relatively small, air-launched space launch vehicle, in Fig. 4-15. The payload is a maximum when launching from the earth equator in the east direction, that is, at 0° inclination. The figure shows that a practical payload becomes too small for orbits higher than about 1200 km. To lift heavier payloads and to go to higher orbits requires a larger launch vehicle than this Pegasus. Figure 4-15 is based on the assumption of a particular payload separation mechanism (38 in.) and a specific Δu vehicle velocity reserve (220 ft/sec) for items such as the normal changes in atmospheric density (which can double the drag) or mass tolerances of the propulsion systems. Similar curves can usually be provided by the makers of all launch vehicles.

4.8. MILITARY MISSILES

The majority of all rocket propulsion systems built today are for military purposes. There is a large variety of missiles and military missions and therefore many different propulsion systems. All are chemical propulsion systems. They range from simple, small, unguided, fin-stabilized single-stage rocket projectiles (used in air-to-surface missions and surface-to-surface bombardment) up to complex, sophisticated, expensive, long-range, multistage ballistic missiles, which are intended for faraway military or strategic targets. The term "surface" means land surface (ground launch or ground target), ocean surface (ship launched), or below the ocean surface (submarine launched). A *tactical missile* is used for attacking or defending ground troops, nearby military or strategic installations, military aircraft, or war missiles. The armed forces also use *military satellites* for missions such as reconnaissance, early warning of impending attack, secure communication, or navigation.

Strategic missiles with a range of 3000 km or more have been two- or three-stage surface-to-surface rocket-propelled missiles. Early designs used liquid propellant rocket engines and some are still in service in certain countries. Beginning about 37 years ago, newer strategic missiles have used solid propellant rocket motors in the United States and France. Both types usually also have a liquid propellant RCS for accurately adjusting the final payload flight velocity (in magnitude, direction, and position in space) at the cutoff of the propulsion system of the last stage. A solid propellant RCS version also exists. The flight analysis and ballistic trajectories of the long-range missiles are similar in many ways to those described for launch vehicles in this chapter.

Solid propellant rocket motors are preferred for most tactical missile missions, because they allow simple logistics and can be launched quickly. If altitudes are low and flight durations are long, such as with a cruise missile, an air-breathing jet engine and a winged vehicle, which provides lift, will usually be more effective than a long-duration rocket. However, a large solid propellant rocket motor may still be needed as a booster to launch the cruise missile and bring it up to speed.

For each of the tactical missile applications, there is an optimum rocket propulsion system and almost all of them use solid propellant rocket motors. Liquid propellant rocket engines have recently been used for the upper stages of two-stage anti-aircraft missiles and ballistic defense missiles, because they can be pulsed for different durations and can be randomly throttled. For each application there is an optimum total impulse, an optimum thrust time profile, an optimum nozzle configuration (single or multiple nozzles, with or without thrust vector control, optimum area ratio), optimum chamber pressure, and a favored solid propellant grain configuration. Low exhaust plume gas radiation emissions in the visible, infrared, or ultraviolet spectrum and certain safety features (making the system insensitive to energy stimuli) can be very important in some of the tactical missile applications; these are discussed in Chapters 13 and 20.

Short-range, uncontrolled, unguided, single-stage rocket vehicles, such as military rocket projectiles (ground and air launched) and rescue rockets, are usually quite simple in design. Their general equations of motion are derived in Section 4.3, and a detailed analysis is given in Ref. 4–1.

Unguided military rocket-propelled missiles are today produced in larger numbers than any other category of rocket-propelled vehicles. The 2.75-in.-diameter, folding fin unguided solid propellant rocket missile has recently been produced in the United States in quantities of almost 250,000 per year. Guided missiles for anti-aircraft, antitank, or infantry support have been produced in annual quantities of hundreds and sometimes over a thousand. Table 1–6 lists several guided missiles.

Because these rocket projectiles are essentially unguided missiles, the accuracy of hitting a target depends on the initial aiming and the dispersion induced by uneven drag, wind forces, oscillations, and misalignment of nozzles, body, and fins. Deviations from the intended trajectory are amplified if the projectile is moving at a low initial velocity, because the aerodynamic stability of a projectile with fins is small at low flight speeds. When projectiles are launched from an aircraft at a relatively high initial velocity, or when projectiles are given stability by spinning them on their axis, their accuracy of reaching a target is increased 2- to 10-fold, compared to a simple fin-stabilized rocket launched from rest.

In guided *air-to-air* and *surface-to-air* rocket-propelled missiles the time of flight to a given target, usually called the *time to target* t_t , is an important flight performance parameter. With the aid of Fig. 4–16 it can be derived in a simplified form by considering the distance traversed by the rocket (called the range) to be the integrated area underneath the velocity–time curve. This simplification assumes no drag, no gravity effect, horizontal flight, a relatively small distance traversed during powered flight compared to the total range, and a linear increase

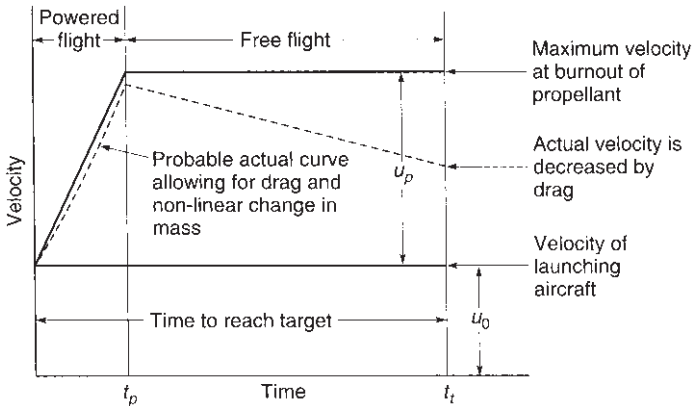


FIGURE 4–16. Simplified trajectory for an unguided, nonmaneuvering, air-launched rocket projectile. Solid line shows ideal flight velocity without drag or gravity and dashed curve shows likely actual flight.

in velocity during powered flight:

$$t_t = \frac{S + \frac{1}{2}u_p t_p}{u_0 + u_p} \quad (4-37)$$

Here S is the flight vehicle's range to the target and it is the integrated area under the velocity-time curve. Also u_p is the velocity increase of the rocket during powered flight up to the time of burnout, t_p is the time of rocket burning, and u_0 is the initial velocity of the launching aircraft. For the same flight time the range of the actual vehicle (dashed line) is less than for the ideal dragless vehicle. For more accurate values, the velocity increase u_p is given by Eq. 4–19. More accurate values can also be obtained through a detailed step-by-step trajectory analysis that considers the effects of drag and gravity.

In unguided air-to-air or air-to-surface rocket-powered projectiles the aiming at the target is done largely by orienting the launching aircraft into the direction of the target. A relatively simple solid propellant rocket motor is the most common choice for the propulsion. In guided missiles, such as air-to-air, air-to-ground, or ground-to-air, the flight path to the target has to be controlled and this can be achieved by controlling aerodynamic control surfaces and/or propulsion systems, which can be pulsed (repeated start and stop) and/or throttled to a lower thrust. The guidance system and the target seeker system of a guided missile will sense and track the flight path of a flying target, a computer will calculate a predicted impact point, and the missile's flight control will change the flight path of the guided missile to achieve the impact with the intended target. The control system will command the propulsion system to operate or fire selected liquid propellant thrusters of an engine with multiple thrusters (or to selectively provide thrust through multiple nozzles with hot-gas shut-off valves in solid motors). A similar set of events can occur in a defensive ground-to-incoming-ballistic-missile

scenario. It requires propulsion systems capable of pulsing or repeated starts, possibly with some throttling and side forces. Rocket engines with these capabilities are discussed in Section 6.8.

In both the unguided projectile and the guided missile the hit probability increases as the time to target t_t is reduced. In one particular air-to-air combat situation, the effectiveness of the rocket projectile varied approximately inversely as the cube of the time to target. The best results (e.g., best hit probability) are usually achieved when the time to target is as small as practically possible.

The analysis of the missile and propulsion configuration that gives the minimum time to target over all the likely flight scenarios can be complex. The following rocket propulsion features and parameters will help to reduce the time to target, but their effectiveness will depend on the specific mission, range, guidance and control system, and particular flight conditions.

1. *High initial thrust* or *high initial acceleration* for the missile to quickly reach a high-initial-powered flight velocity.
2. Application of additional *lower thrust* to counteract drag and gravity losses and thus maintain a high flight velocity. This can be a single rocket propulsion system that has a short high initial thrust and a smaller (10 to 25%) sustaining thrust of longer duration.
3. For higher supersonic flight speeds, a *two-stage missile* can be more effective. Here the first stage is dropped off after its propellant has been consumed, thus reducing the inert mass of the next stage and improving its mass ratio and thus its flight velocity increase.
4. If the target is highly maneuverable and if the closing velocity between missile and target is large, it may be necessary not only to provide an axial thrust but also to apply large *side forces* or side accelerations to a defensive tactical missile. This can be accomplished either by aerodynamic forces (lifting surfaces or flying at an angle of attack) or by multiple-nozzle propulsion systems with variable or pulsing thrusts; the rocket engine then would have an axial thruster and one or more side thrusters. The side thrusters have to be so located that all the thrust forces are essentially directed through the center of gravity of the vehicle in order to minimize turning moments. The thrusters that provide the side accelerations have also been called *divert* thrusters, since they divert the vehicle in a direction normal to the axis of the vehicle.
5. *Drag losses* can be reduced if the missile has a large L/D ratio (or a small cross-sectional area) and if the propellant density is high, allowing a smaller missile volume. The drag forces can be high if the missile travels at low altitude and high speed. A long and thin propulsion system geometry and a high-density propellant will help to reduce drag.

A unique military application is *rocket-assisted gun-launched projectiles* for attaining longer artillery ranges. Their small rocket motors withstand very high

accelerations in the gun barrel (5000 to 10,000 g_0 is typical). They have been in production.

4.9. FLIGHT STABILITY

Stability of a vehicle is achieved when the vehicle does not rotate or oscillate in flight. Unstable flights are undesirable, because pitch or yaw oscillations increase drag (flying at an angle of attack most of the time) and cause problems with instruments and sensors (target seekers, horizon scanners, sun sensors, or radar). Instability often leads to tumbling (uncontrolled turning) of vehicles, which causes missing of orbit insertion, missing targets, or sloshing of liquid propellant in tanks.

Stability can be built in by proper design so that the flying vehicle will be inherently stable, or stability can be obtained by appropriate controls, such as the aerodynamic control surfaces on an airplane, a reaction control system, or hinged multiple rocket nozzles.

Flight stability exists when the overturning moments (e.g., those due to a wind gust, thrust misalignment, or wing misalignment) are smaller than the stabilizing moments induced by thrust vector controls or by aerodynamic control surfaces. When the destabilizing moments exceed the stabilizing moments about the center of gravity, the vehicle turns or tumbles. In unguided vehicles, such as low-altitude rocket projectiles, stability of flight in a rectilinear motion is achieved by giving a large stability margin to the vehicle by using tail fins and by locating the center of gravity ahead of the center of aerodynamic pressure. In a vehicle with an active stability control system, a nearly neutral inherent stability is desired, so that the applied control forces are small, thus requiring small control devices, small RCS thrusters, small actuating mechanisms, and structural mass. Neutral stability is achieved by locating aerodynamic surfaces and the mass distribution of the components within the vehicle in such a manner that the center of gravity is only slightly above the center of aerodynamic pressure. Because the aerodynamic moments change with Mach number, the center of pressure does not necessarily stay fixed during accelerating flight but shifts, usually along the vehicle axis. The center of gravity also changes its position as propellant is consumed and the vehicle mass decreases. Thus it is usually very difficult to achieve neutral missile stability at all altitudes, speeds, and flight conditions.

Stability considerations affect rocket propulsion system design in several ways. By careful nozzle design and careful installation it is possible to minimize thrust misalignment and thus to minimize undesirable torques on the vehicle and the reaction control propellant consumption. It is possible to exercise considerable control over the travel of the center of gravity by judicious design. In liquid propellant rockets, special design provisions, special tank shapes, and a careful selection of tank location in the vehicle afford this possibility. By using nozzles at the end of a blast tube, as shown in Fig. 15-6, it is possible to place the solid propellant mass close to the vehicle's center of gravity. Attitude control liquid

propellant engines with multiple thrusters have been used satisfactorily to obtain control moments for turning vehicles in several ways, as described in Section 4.5 and in Chapter 6.

Unguided rocket projectiles and missiles are often given a roll or rotation by inclined aerodynamic fins or inclined multiple rocket exhaust gas nozzles to improve flight stability and accuracy. This is similar to the rotation given to bullets by spiral-grooved barrels. This *spin stability* is achieved in part by gyroscopic effects, where an inclination of the spin axis is resisted by torques. The centrifugal effects cause problems in emptying liquid propellant tanks and extra stresses on solid propellant grains. In some applications a low-speed roll is applied not for spin stability but to assure that any effects of thrust vector deviations or aerodynamic vehicle shape misalignments are minimized and canceled out.

PROBLEMS

- For a vehicle in gravitationless space, determine the mass ratio necessary to boost the vehicle velocity by (a) 1600 m/sec and (b) 3400 m/sec; the effective exhaust velocity is 2000 m/sec. If the initial total vehicle mass is 4000 kg, what are the corresponding propellant masses?

Answers: (a) 2204 kg.

- Determine the burnout velocity and burnout altitude for a dragless projectile with the following parameters for a simplified vertical trajectory: $\bar{c} = 2209$ m/sec; $m_p/m_0 = 0.57$; $t_p = 5.0$ sec; and $u_0 = 0$; $h_0 = 0$. Select a relatively small diameter missile with L/D of 10 and an average vehicle density of 1200 kg/m³.
- Assume that this projectile had a drag coefficient essentially similar to the 0° curve in Fig. 4-3 and redetermine the answers of Problem 3 and the approximate percentage errors in u_p and h_p . Use a step-by-step or a numerical method.
- A research space vehicle in gravity-free and drag-free outer space launches a smaller spacecraft into a meteor shower region. The 2-kg sensitive instrument package of this spacecraft (25 kg total mass) limits the maximum acceleration to no more than 50 m/sec². It is launched by a solid propellant rocket motor ($I_s = 260$ sec and $\zeta = 0.88$). Assume instant start and stop of rocket motor.

- (a) Determine the maximum allowable burn time, assuming steady constant propellant mass flow;
- (b) Determine the maximum velocity relative to the launch vehicle.
- (c) Solve for (a) and (b) if half of the total impulse is delivered at the previous propellant mass flow rate, with the other half at 20% of this mass flow rate.

- For a satellite cruising in a circular orbit at an altitude of 500 km, determine the period of revolution, the flight speed, and the energy expended to bring a unit mass into this orbit.

Answers: 1.58 hr, 7613 m/sec, 33.5 MJ/kg.

- A large ballistic rocket vehicle has the following characteristics: propellant mass flow rate: 12 slugs/sec (1 slug = 32.2 lbm = 14.6 kg); nozzle exit velocity: 7100 ft/sec;

nozzle exit pressure: 5 psia (assume no separation); atmospheric pressure: 14.7 psia (sea level); takeoff weight: 12.0 tons (1ton = 2000 lbf); burning time: 50 sec; nozzle exit area: 400 in.² Determine (a) the sea-level thrust; (b) the sea-level effective exhaust velocity; (c) the initial thrust-to-weight ratio; (d) the initial acceleration; (e) the mass inverse ratio m_0/m_f .

Answers: 81,320 lbf; 6775 ft/sec; 3.38; 2.38g₀.

7. In Problem 5 compute the altitude and missile velocity at the time of power plant cutoff, neglecting the drag of the atmosphere and assuming a simple vertical trajectory.
8. A spherical satellite has 12 identical monopropellant thrust chambers for attitude control with the following performance characteristics: thrust (each unit): 5 lbf; I_s (steady state or more than 2 sec): 240 sec; I_s (pulsing duration 20 msec): 150 sec; I_s (pulsing duration 100 msec): 200 sec; satellite weight: 3500 lbf; satellite diameter: 8 ft; satellite internal density distribution is essentially uniform; disturbing torques, Y and Z axes: 0.00005 ft-lbf average; disturbing torque, for X axis: 0.001 ft-lbf average; distance between thrust chamber axes: 8 ft; maximum allowable satellite pointing position error: $\pm 1^\circ$. Time interval between pulses is 0.030 sec.
 - (a) What would be the maximum and minimum vehicle angular drift per hour if no correction torque were applied?
- Answers: 0.466 and 0.093 rad/hr.
- (b) What is the frequency of pulsing action (how often does an engine pair operate?) at 20-msec, 100-msec, and 2-sec pulses in order to correct for angular drift? Discuss which pulsing mode is best and which is impractical.
9. For an ideal multistage launch vehicle with several stages in series, discuss the following: (a) the effect on the ideal mission velocity if the second and third stages are not started immediately but are each allowed to coast for a short period after shutdown and separation of the expended stage before rocket engine start of the next stage; (b) the effect on the mission velocity if an engine malfunctions and delivers a few percent less than the intended thrust but for a longer duration and essentially the full total impulse of that stage.
10. Given a cylindrically shaped space vehicle ($D = 1\text{m}$, height is 0.7 m, average density is 1.1 g/cm³) with a flat solar cell panel on an arm (mass of 32 kg, effective moment arm is 1.5 m, effective average area facing normally toward sun is 0.6 m²) in a set of essentially frictionless bearings and in a low circular orbit at 160 km altitude with sunlight being received, on the average, about 54% of the time. The top surface of the cylinder and the surface of the solar panel have solar cells. The satellite is maneuvered so that these two surfaces are always perpendicular to the sun's rays. The articulated arm between the cylinder and the solar panel is small and its mass and force, due to solar radiation pressure, are also small and can be neglected.
 - (a) Compute the maximum solar pressure-caused torque and the angular displacement this would cause during 1 day if not corrected.
 - (b) Using the data from the atmospheric table in Appendix 2 and an arbitrary average drag coefficient of 1.0 for both the body and the flat plate, compute the drag force and torque.

- (c) Using stored high-pressure air at $14 \times 10^6 \text{ N/m}^2$ initial pressure as the propellant for attitude control, design an attitude control system to periodically correct for these two disturbances (F, I_s, t, I_t , etc.).
11. Determine the payload for a single-stage vehicle in Example 4–3. Using the data from this example compare it with the two-stage vehicle.
12. An earth satellite is in an elliptical orbit with the perigee at 600 km altitude and an eccentricity of $e = 0.866$. Determine the parameters of the new satellite trajectory, if a rocket propulsion system is fired in the direction of flight giving an incremental velocity of 200 m/sec when (a) fired at apogee, (b) fired at perigee, and (c) fired at perigee, but in the opposite direction, reducing the velocity.
13. A sounding rocket (75 kg mass, 0.25 m diameter) is speeding vertically upward at an altitude of 5000 m and a velocity of 700 m/sec. What is the deceleration in multiples of g due to gravity and drag? (Use C_D from Fig. 4–3 and use Appendix 2.)
14. Derive Eq. 4–37; state all your assumptions.

SYMBOLS

| | |
|-----------|--|
| a | major axis of ellipse, m, or acceleration, m/sec^2 (ft/sec^2) |
| A | area, $\text{m}^2(\text{ft}^2)$ |
| b | minor axis of ellipse, m |
| B | numerical value of drag integral |
| c | effective exhaust velocity, m/sec (ft/sec) |
| \bar{c} | average effective exhaust velocity, m/sec |
| C_D | drag coefficient |
| C_L | lift coefficient |
| d | total derivative |
| D | drag force, N (lbf) |
| e | eccentricity of ellipse, $e = \sqrt{1 - b^2/a^2}$ |
| e | base of natural logarithm (2.71828) |
| E | energy, J |
| F | thrust force, N (lbf) |
| F_f | final thrust, N |
| F_g | gravitational attraction force, N |
| F_0 | initial thrust force, N |
| g | gravitational acceleration, m/sec^2 |
| g_0 | gravitational acceleration at sea level, 9.8066 m/sec^2 |
| \bar{g} | average gravitational attraction, m/sec^2 |
| G | universal or Newton's gravity constant, $6.6700 \times 10^{11} \text{ m}^3/\text{kg}\cdot\text{sec}^2$ |
| h | altitude, m (ft) |
| h_p | altitude of rocket at power cutoff, m |
| I_s | specific impulse, sec |
| k_d | diffuse coefficient of reflectivity |
| k_s | specular coefficient of reflectivity |
| l | distance of moment arm, m |

| | |
|----------------------|--|
| <i>L</i> | lift force, N (lbf) |
| <i>m</i> | instantaneous vehicle mass, kg (lbm) |
| <i>m_f</i> | final vehicle mass after rocket operation, kg |
| <i>m_p</i> | useful propellant mass, kg |
| <i>m₀</i> | initial vehicle launching mass, prior to rocket operation, kg |
| <i>ṁ</i> | mass flow rate of propellant, kg/sec |
| <i>M_a</i> | angular moment of inertia, kg-m ² |
| MR | mass ratio of vehicle = m_f/m_0 |
| <i>n</i> | number of stages |
| <i>p</i> | pressure, N/m ² or Pa (psi) |
| <i>r</i> | radius, m, or distance between the centers of two attracting masses, m |
| <i>R</i> | instantaneous radius from vehicle to center of earth, m |
| <i>R₀</i> | effective mean earth radius, 6.3742×10^6 m |
| <i>S</i> | range, m |
| <i>t</i> | time, sec |
| <i>t_p</i> | time from launching to power cutoff or time from propulsion start to thrust termination, sec |
| <i>t_t</i> | time to target, sec |
| <i>T</i> | torque, N-m (ft-lbf) |
| <i>u</i> | vehicle flight velocity, m/sec (ft/sec) |
| <i>u_a</i> | orbital velocity at apogee, m/sec |
| <i>u_p</i> | velocity at power cutoff, m/sec, or orbital velocity at perigee, m/sec |
| <i>u₀</i> | initial or launching velocity, m/sec |
| <i>v_e</i> | escape velocity, m/sec |
| <i>w</i> | weight, N (in some problems, lbf) |
| <i>x, y</i> | any points on an elliptical orbit |

Greek Letters

| | |
|----------|---|
| α | angle of attack, deg or rad, or angular acceleration, angle/sec ² |
| ζ | propellant mass fraction ($\zeta = m_p/m_0$) |
| θ | angle between flight direction and horizontal, or angle of incident radiation, deg or rad |
| μ | gravity constant for earth, 3.98600×10^{14} m ³ /sec ² |
| ρ | mass density, kg/m ³ |
| τ | period of revolution of satellite, sec |
| ψ | angle of thrust direction with horizontal |
| ω | angular speed, deg/sec (rad/sec) |

Subscripts

| | |
|----------|--|
| <i>e</i> | escape condition |
| <i>f</i> | final condition at rocket thrust termination |
| <i>i</i> | initial condition |

| | |
|----------|---|
| max | maximum |
| <i>p</i> | condition at power cutoff or propulsion termination |
| pl | payload |
| <i>s</i> | satellite |
| <i>z</i> | zenith |
| 0 | initial condition or takeoff condition |

REFERENCES

- 4–1. J. B. Rosser, R. R. Newton, and G. L. Gross, *Mathematical Theory of Rocket Flight*, McGraw-Hill Book Company, New York, 1947; or F. R. Gantmakher and L. M. Levin, *The Flight of Uncontrolled Rockets*, Macmillan, New York, 1964.
- 4–2. R. S. Wolf, “Development of a Handbook for Astrobee F (Sounding rocket) Flight Performance Predictions,” *Journal of Spacecraft and Rockets*, Vol. 24, No. 1, January–February 1987, pp. 5–6.
- 4–3. *Orbital Flight Handbook*, NASA SP33, 1963, Part 1: Basic Techniques and Data. Part 2: Mission Sequencing Problems. Part 3: Requirements.
- 4–4. V. A. Chobotov (Ed) *Orbital Mechanics*, 3rd ed., Educational Series, AIAA, Reston, VA., 2002; and T. Logsdon, *Orbital Mechanics and Application*, John Wiley & Sons, New York, October 1997.
- 4–5. J. W. Cornelisse, H. F. R. Schöyer, and K. F. Wakker, *Rocket Propulsion and Space Flight Dynamics*, Pitman Publishing, Londn, 1979.
- 4–6. J. P. Vinti, G. J. Der, and L. Bonavito, *Orbits and Celestial Mechanics*, Vol. 177 of Progress in Aeronautics and Astronautics Series, AIAA, Reston, VA, 1998, 409 pages.
- 4–7. W. Hohmann, *Die Erreichbarkeit der Himmelskörper (Accessibility of Celestial Bodies)*, Oldenburg, Munich, 1925.
- 4–8. W. J. Larson and J. R. Wertz, *Space Mission Analysis and Design*, 3rd ed., published jointly by Microcosm, Inc. and Kluwer Academic Press, 1999.
- 4–9. J. J. Pocha, *An Introduction to Mission Design for Geostationary Satellites*, Kluwer Academic Publishers, Hingham, MA, 1987, 222 pages.
- 4–10. M. H. Kaplan, *Orbital Spacecraft Dynamics and Control*, John Wiley & Sons, New York, 1976.
- 4–11. R. W. Humble, G. N. Henry, and W. J. Larson, *Space Propulsion Analysis and Design*, McGraw-Hill, New York, 1995, 748 pages.
- 4–12. J. P. Vinti, G. J. Der, and L. Bonavito, *Orbit and Celestial Mechanics*, Vol. 177 of Progress in Astronautics and Aeronautics Series, AIAA, Reston, VA, 1998, 409 pages.
- 4–13. C-C. G. Chao, *Applied Orbit Perturbations and Maintenance*, Aerospace Press, 2005, 264 pages.
- 4–14. “Spacecraft Aerodynamic Torques,” *NASA SP 8058*, January 1971 (N 71-25935).
- 4–15. “Spacecraft Radiation Torques,” *NASA SP 8027*, October 1969 (N 71-24312).
- 4–16. “Spacecraft Gravitational Torques,” *NASA SP 8024*, May 1964 (N 70-23418).
- 4–17. “Spacecraft Magnetic Torques,” *NASA SP 8018*, March 1969 (N 69-30339).

CHAPTER 5

CHEMICAL ROCKET PROPELLANT PERFORMANCE ANALYSIS

In Chapter 3, simplified one-dimensional performance relations were developed. They require a knowledge of the composition of the hot rocket gas and the properties of the propellant reaction products, such as their combustion temperature T_1 , average molecular mass \bar{M} , and the specific heat ratio or the enthalpy change ($h_1 - h_2$). This chapter discusses several approaches to determine these theoretical thermochemical properties for a given composition or mixture of propellant, chamber pressure, nozzle shape, and nozzle exit pressure. This then allows the determination of performance parameters, such as theoretical specific impulse or exhaust velocity for chemical rockets.

By knowing the calculated gas temperature, pressure, and gas composition it is possible to calculate other gas properties. This knowledge also allows the analysis and selection of materials for chamber and nozzle structures. Heat transfer analyses require the determination of the specific heats, thermal conductivity, and specific heat ratio for the gas mixture. The calculated exhaust gas composition forms the basis for estimating environmental effects, such as the potential spreading of a toxic cloud near a launch site, as discussed in Chapter 21. The exhaust gas parameters also form the basis for the analysis of exhaust plumes (Chapter 20) or flames external to the nozzle.

With the advent of digital computers it has been possible to solve the set of equations involving mass balance, energy balance, together with thermodynamic and chemical equilibria of complex systems with a variety of propellant ingredients. This chapter is intended to introduce the background to this theoretical analysis, so the reader can understand the thermodynamic and chemical basis of the several computer programs that are in use today. This chapter does not describe any specific computer analysis programs. However, it discusses which

of the physical phenomena or chemical reactions can or cannot be adequately simulated by computer analysis.

The reader is referred to Refs. 5–1 to 5–5 for general chemical and thermodynamic background and principles. For a detailed description of the properties of each of the possible reactant and reaction products, see Refs. 5–6 to 5–12.

All of these theoretical analyses are only approximations of what really happens in rocket combustion and nozzle flow, since they all require some simplifying assumptions. As more of the different phenomena are understood and mathematically simulated, the analysis approach and the computer implementation become more realistic but also more complex. The 11 assumptions made in Section 3.1 for an ideal rocket are valid here also but only for a quasi-one-dimensional flows. However, more sophisticated analyses can make one or more of these assumptions unnecessary. The analysis is usually divided into two somewhat separate sets of calculations:

1. The *combustion process* is the first part. It usually occurs in the combustion chamber at essentially constant chamber pressure (isobaric) and the resulting gases follow Dalton's law, which is discussed in this chapter. The chemical reactions or the combustions occur very rapidly. The chamber volume is assumed to be large enough and the residence time in the chamber long enough for attaining chemical equilibrium in the chamber.
2. The *nozzle gas expansion process* constitutes the second set of calculations. The fully reacted, equilibrated gas combustion products enter the nozzle and undergo an adiabatic expansion in the nozzle. The entropy remains constant during a reversible (isentropic) nozzle gas expansion, but in real nozzles it increases slightly.

The principal chemical reactions occur inside the combustion chamber of a liquid propellant rocket engine or inside the grain cavity of a solid propellant rocket motor, usually within a short distance from the burning surface. These chamber combustion analyses are discussed further in Chapters 9 and 14. However, some chemical reactions also occur in the nozzle as the gases expand; the composition of the reaction products can therefore change in the nozzle, as described in this chapter. A further set of chemical reactions can occur in the exhaust plume outside the nozzle, as described in Chapter 20; many of the same basic thermochemical analysis approaches described in this chapter also apply to exhaust plumes.

5.1. BACKGROUND AND FUNDAMENTALS

The analytical description of chemical reaction or combustion of one or more fuels with one or more oxidizing reactants is the basis of chemical rocket propulsion. The heat liberated in this reaction transforms the propellants (reactants) into

hot gaseous products, which in turn are thermodynamically expanded in a nozzle to produce thrust.

The chemical reactants or propellants can initially be either liquid or solid and occasionally also gaseous. The reaction products are usually gaseous, but with some propellants one or more reactant species remain in the solid or liquid phase. For example, with aluminized solid propellants, the chamber reaction gases contain liquid aluminum oxide and the colder gases in the nozzle exhaust contain solid, condensed aluminum oxide particles. For some of the chemical species, therefore, the analysis must consider as many as all three phases and the energy changes for the phase transitions must be included. When the amount of solid or liquid in the exhaust is small and the particles are small, to assume a perfect gas introduces only small errors.

It is necessary to accurately know the chemical composition of the propellants and their relative proportion. In liquid propellant this means the mixture ratio and the major propellant impurities; in gelled or slurried liquid propellants it also includes suspended or dissolved solid materials; and in solid propellants it means all the ingredients, their proportions and impurities, and phase (some ingredients, such as plasticizers, can be in a liquid state).

Dalton's law applies to the gas resulting from the combustion. It states that a mixture of gases at equilibrium exerts a pressure that is the sum of the partial pressures of the individual gases, all at a common volume and a common temperature. The subscripts a, b, c , and so on refer to individual gas constituents:

$$p = p_a + p_b + p_c + \dots \quad (5-1)$$

$$T = T_a = T_b = T_c = \dots \quad (5-2)$$

The perfect gas equation $pV = RT$ applies very closely to high-temperature gases. Here V is the specific volume or the volume per unit mass of gas mixture, and the gas constant R for the mixture is obtained by dividing the universal gas constant R' (8314.3 J/kg-mol-K) by the average molecular mass \bar{M} (often erroneously called the molecular weight) of the gas mixture. Using Dalton's law, Eq. 5-1 can be rewritten

$$p = R_a T/V_a + R_b T/V_b + R_c T/V_c + \dots = R' T / (\bar{M} V_{\text{mix}}) \quad (5-3)$$

The volumetric proportions of gas species in a gas mixture are determined from the *molar concentration* or *molar fractions*, n_j , expressed as kg-mol for a particular species j per kg of mixture. If n is the total number of kg-mol of all species per kilogram of uniform gas mixture, then the mole fraction X_j

$$X_j = \frac{n_j}{n} \quad \text{since} \quad n = \sum_{j=1}^{j=m} n_j \quad (5-4)$$

where n_j is the kg-mol of species j per kilogram of mixture, m is the number of different gaseous species present in the equilibrium combustion gas products. The effective average molecular mass \bar{M} of a gas mixture is then

$$\bar{M} = \frac{\sum_{j=1}^m n_j M_j}{\sum_{j=1}^m n_j} \quad (5-5)$$

There are n possible species which enter into the relationship and of these only m are gases, so $n - m$ represents the number of condensed species. The *molar specific heat* for a gas mixture at constant pressure C_p can be determined from the individual gas molar fractions n_j and their molar specific heats as shown by Eq. 5–6. The specific heat ratio k of the mixture follows from Eq. 5–7:

$$(C_p)_{\text{mix}} = \frac{\sum_{j=1}^m n_j (C_p)_j}{\sum_{j=1}^m n_j} \quad (5-6)$$

$$k_{\text{mix}} = \frac{(C_p)_{\text{mix}}}{(C_p)_{\text{mix}} - R'} \quad (5-7)$$

When a chemical reaction goes to completion, that is, all of the reactants are consumed and transformed into reaction products, the reactants are in *stoichiometric* proportions. For example, consider this reaction:



All the hydrogen and oxygen are fully consumed to form the single product—water vapor—without any reactant residue of either hydrogen or oxygen. In this case it requires 1 mol of the H_2 and $\frac{1}{2}$ mole of the O_2 to obtain 1 mol of H_2O . On a mass basis this *stoichiometric mixture* requires half of 32.0 kg of O_2 and 2 kg of H_2 , which are in the stoichiometric mixture mass ratio of 8:1. The release of energy per unit mass of propellant mixture and the combustion temperature are highest at or near the stoichiometric mixture.

Rocket propulsion systems usually do not operate with the proportion of their oxidizer and fuel in the stoichiometric mixture ratio. Instead, they usually operate fuel rich because this allows lightweight molecules such as hydrogen to remain unreacted; this reduces the average molecular mass of the reaction products, which in turn increases the specific impulse (see Eq. 3–16). For rockets using H_2 and O_2 propellants the best operating mixture mass ratio for high-performance rocket engines is typically between 4.5 and 6.0, not at the stoichiometric value of 8.0, because the drop in combustion temperature is small and there is more H_2 gas (low molecular mass) in the exhaust.

Equation 5–8 is a reversible chemical reaction; by adding energy to the H_2O the reaction can be made to go backward to create H_2 and O_2 and the arrow in the equation would be reversed. The decompositions of solid propellants into reaction product gases are irreversible chemical reactions, as is the reaction of

liquid propellants burning to create gases. However, reactions among combustion product gases are usually reversible.

Chemical equilibrium exists in reversible chemical reactions when the rate of forming products is exactly equal to the reverse reaction of forming reactants from the products. Once this equilibrium is reached, no further changes in concentration can take place. In Equation 5–8 all three gases would be present and their relative proportions would depend on the pressure, temperature, and initial mixture.

The *heat of formation* $\Delta_f H^0$ is the energy released (or absorbed), or the value of enthalpy change, when 1 mol of a chemical compound is formed from its constituent atoms or elements at 1 bar (100,000 Pa) and isothermally at 298.15 K or 25°C. The Δ implies that it is an energy change. The subscript f refers to formation and the superscript 0 means that each product or reactant substance is at its thermodynamic standard state and at the reference pressure and temperature. By convention, the heat of formation of the gaseous elements (e.g., H₂, O₂, Ar, Xe, etc.) is set to zero at these standard conditions of temperature and pressure. Typical values of $\Delta_f H^0$ and other properties are given in Table 5–1 for selected species. When heat is absorbed in the formation of a product, then $\Delta_f H^0$ has a positive value. Earlier analyses have been made with the standard temperature at other values, such as 273.15 K and a slightly higher standard reference pressure of 1 atm (101,325 Pa).

The *heat of reaction* $\Delta_r H^0$ is the energy released or absorbed when products are formed from its reactants at standard reference conditions, namely at 1 bar and 25°C. The heat of reaction can be negative or positive, depending on whether the reaction is *exothermic* or *endothermic*. The heat of reaction at other temperatures or pressures has to be corrected in accordance with the change in enthalpy. When a species changes from one state to another (e.g., liquid becomes gas or vice versa), it may lose or gain energy. In most rocket propulsion the heat of reaction is determined for a constant-pressure combustion process. In general the heat of reaction can be determined from sums of the heats of formation of the products and the reactants, namely

$$\Delta_r H^0 = \sum [n_j (\Delta_f H^0)_j]_{\text{products}} - \sum [n_j (\Delta_f H^0)_j]_{\text{reactants}} \quad (5-9)$$

Here n_j is the molar fraction of each particular species j . In a typical rocket propellant there are a number of different chemical reactions going on simultaneously; Eq. 5–9 provides the heat of reaction for all of these simultaneous reactions. For data on heats of formation and heats of reaction, see Refs. 5–7 to 5–13.

Various thermodynamic criteria that represent the necessary and sufficient conditions for an equilibrium to be stable were first advanced by J. W. Gibbs early in the 20th century; they are based on minimizing the free energy. The Gibbs *free energy* G (often called the *chemical potential*) is a convenient derived function or property of the state of a chemical material describing its thermodynamic potential and is directly related to the internal energy U , the pressure p , molar volume V , enthalpy h , temperature T , and entropy S . For a single species j the

TABLE 5–1. Chemical Thermodynamic Properties of Selected Substances at 298.15 K (25°C) and 0.1 MPa (1 bar)

| Substance | Phase ^a | Molar Mass (g/mol) | $\Delta_f H^0$ (kJ/mol) | $\Delta_f G^0$ (kJ/mol) | S^0 (J/mol-K) | C_p (J/mol-K) |
|----------------------------------|--------------------|-----------------------|----------------------------|----------------------------|--------------------|--------------------|
| Al (crystal) | s | 29.9815 | 0 | 0 | 28.275 | 24.204 |
| Al ₂ O ₃ | l | 101.9612 | -1620.567 | -1532.025 | 67.298 | 79.015 |
| C (graphite) | s | 12.011 | 0 | 0 | 5.740 | 8.517 |
| CH ₄ | g | 16.0476 | -74.873 | -50.768 | 186.251 | 35.639 |
| CO | g | 28.0106 | -110.527 | -137.163 | 197.653 | 29.142 |
| CO ₂ | g | 44.010 | -393.522 | -394.389 | 213.795 | 37.129 |
| H ₂ | g | 2.01583 | 0 | 0 | 130.680 | 28.836 |
| HCl | g | 36.4610 | -92.312 | -95.300 | 186.901 | 29.136 |
| HF | g | 20.0063 | -272.546 | -274.646 | 172.780 | 29.138 |
| H ₂ O | l | 18.01528 | -285.830 | -237.141 | 69.950 | 75.351 |
| H ₂ O | g | 18.01528 | -241.826 | -228.582 | 188.834 | 33.590 |
| N ₂ H ₄ | l | 32.0451 | +50.626 | 149.440 | 121.544 | 98.840 |
| N ₂ H ₄ | g | 32.0451 | +95.353 | +159.232 | 238.719 | 50.813 |
| NH ₄ ClO ₄ | s | 117.485 | -295.767 | -88.607 | 184.180 | 128.072 |
| ClF ₅ | g | 130.4450 | -238.488 | -146.725 | 310.739 | 97.165 |
| ClF ₃ | g | 92.442 | -158.866 | -118.877 | 281.600 | 63.845 |
| N ₂ O ₄ | l | 92.011 | -19.564 | +97.521 | 209.198 | 142.509 |
| N ₂ O ₄ | g | 92.011 | 9.079 | 97.787 | 304.376 | 77.256 |
| NO ₂ | g | 46.0055 | 33.095 | 51.258 | 240.034 | 36.974 |
| HNO ₃ | g | 63.0128 | -134.306 | -73.941 | 266.400 | 53.326 |
| N ₂ | g | 28.0134 | 0 | 0 | 191.609 | 29.125 |
| O ₂ | g | 31.9988 | 0 | 0 | 205.147 | 29.376 |
| NH ₃ | g | 17.0305 | -45.898 | -16.367 | 192.774 | 35.652 |

^as = solid, l = liquid, g = gas. Several species are listed twice, as a liquid and as a gas; the difference is due to evaporation or condensation.

The molar mass can be in g/g-mol or kg/kg-mol and C_p can be in J/g-mol-K or kJ/kg-mol-K.

Source: Refs. 5–8 and 5–9.

free energy is defined as G_j ; it can be determined for specific thermodynamic conditions, for mixtures of gas as well as an individual gas species:

$$G = U + pV - TS = h - TS \quad (5-10)$$

For most materials used as rocket propellant, the free energy has been determined and tabulated as a function of temperature. It can be corrected for pressure. G_j 's units are J/kg-mol. For a series of different species the mixture free energy G is

$$G = \sum_{j=1}^n G_j n_j \quad (5-11)$$

The *free energy* is a function of temperature and pressure. It is another property of a material, just like enthalpy or density; only two such independent parameters are required to characterize a gas condition. The free energy may be thought of as the tendency or driving force for a chemical material to enter into a chemical (or physical) change. Although it cannot be measured directly, differences in chemical potential can be measured. When the chemical potential of the reactants is higher than that of the likely products, a chemical reaction can occur and the chemical composition can change. The change in free energy ΔG for reactions at constant temperature and pressure is the chemical potential of the products less that of the reactants:

$$\Delta G = \sum_{j=1}^m [n_j (\Delta_f G^0)_j]_{\text{products}} - \sum_{j=1}^n [n_j (\Delta_f G^0)_j]_{\text{reactants}} \quad (5-12)$$

Here the superscript m gives the number of gas species in the combustion products, the superscript n gives the number of gas species in the reactants, and the ΔG represents the maximum energy that can be “freed” to do work on an “open” system where mass enters and leaves the system. At equilibrium the free energy is a minimum; at its minimum a small change in mixture fractions causes almost no change in ΔG , and the free energies of the products and the reactants are essentially equal. Then

$$d\Delta G/dn = 0 \quad (5-13)$$

and a curve of molar concentration n versus ΔG would have a minimum.

If reacting propellants are liquid or solid materials, energy will be needed to change phase, vaporize them, or break them down into other gaseous species. This energy has to be subtracted from the heat or the energy available to heat the gases from the reference temperature to the combustion temperature. Therefore, the values of ΔH^0 and ΔG^0 for liquid and solid species are different from those of the same species in a gaseous state. The standard *free energy of formation* $\Delta_f G^0$ is the increment in free energy associated with the reaction of forming a given compound or species from its elements at their reference state. Table 5–2 gives values of $\Delta_f H^0$ and $\Delta_f G^0$ and other properties of carbon monoxide as a function of temperature. Similar data for other species can be obtained from Refs. 5–7 and 5–13. The *entropy* is another thermodynamic property of matter that is relative, which means that it is determined as a change in entropy. In the analysis of isentropic nozzle flow, it is assumed that the entropy remains constant. It is defined as

$$dS = \frac{dU}{T} + \frac{p \, dV}{T} = C_p \frac{dT}{T} - R \frac{dp}{p} \quad (5-14)$$

and the corresponding integral is

$$S - S^0 = C_p \ln \frac{T}{T_0} - R \ln \frac{p}{p_0} \quad (5-15)$$

TABLE 5–2. Variation of Thermochemical Data with Temperature for Carbon Monoxide (CO) as an Ideal Gas

| Temp. (K) | C_p^0 (J/mol-K) | S^0 | $H^0 - H^0(T)$ (kJ/mol) | $\Delta_f H^0$ (kJ/mol) | $\Delta_f G^0$ (kJ/mol) |
|--------------|----------------------|---------|----------------------------|----------------------------|----------------------------|
| 0 | 0 | 0 | -8.671 | -113.805 | -113.805 |
| 298.15 | 29.142 | 197.653 | 0 | 110.527 | -137.163 |
| 500 | 29.794 | 212.831 | 5.931 | -110.003 | -155.414 |
| 1000 | 33.183 | 234.538 | 21.690 | -111.983 | -200.275 |
| 1500 | 35.217 | 248.426 | 38.850 | -115.229 | -243.740 |
| 2000 | 36.250 | 258.714 | 56.744 | -118.896 | -286.034 |
| 2500 | 36.838 | 266.854 | 74.985 | -122.994 | -327.356 |
| 3000 | 37.217 | 273.605 | 93.504 | -127.457 | -367.816 |
| 3500 | 37.493 | 279.364 | 112.185 | -132.313 | -407.497 |
| 4000 | 37.715 | 284.386 | 130.989 | -137.537 | -446.457 |

Source: Refs. 5–8 and 5–9.

where the zero applies to the reference state. In an isentropic process, entropy is constant. For a mixture the entropy is

$$S = \sum_{j=1}^n S_j n_j \quad (5-16)$$

Here entropy S_j is in J/kg-mol-K. The entropy for each gaseous species is

$$S_j = (S_T^0)_j - R \ln \frac{n_j}{n} - R \ln p \quad (5-17)$$

For solid and liquid species the last two terms are zero. Here $(S_T^0)_j$ refers to the standard state entropy at temperature T . Typical values for entropy are listed in Tables 5–1 and 5–2.

5.2. ANALYSIS OF CHAMBER OR MOTOR CASE CONDITIONS

The objectives here are to determine the theoretical combustion temperature and the theoretical composition of the resulting reaction products, which in turn will allow the determination of the physical properties of the combustion gases (C_p , k , ρ , or other). Before we can make this analysis, some basic data (e.g., propellants, their ingredients, desired chamber pressure, or all likely reaction products) have to be known or postulated. Although the combustion process really consists of a series of different chemical reactions that occur almost simultaneously and includes the breakdown of chemical compounds into intermediate and subsequently into final products, the analysis is only concerned with the initial and final conditions, before and after combustion. We will mention several

approaches to the analysis of chamber conditions. In this section we will first give some definitions of key terms and explain some concepts and principles.

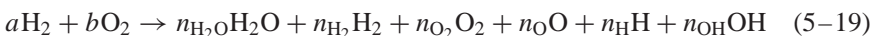
The first principle concerns the *conservation of energy*. The heat created by the combustion is equal to the heat necessary to raise the resulting gases adiabatically to their final combustion temperature. The heat of reaction of the combustion $\Delta_r H$ has to equal the enthalpy change ΔH of the reaction product gases. The *energy balance* can be thought of as a two-step process. The chemical reaction occurs instantaneously but isothermally at the reference temperature, and the resulting energy release then heats the gases from this reference temperature to the final combustion temperature. The heat of reaction, Equation 5–9, becomes

$$\Delta_r H = \sum_1^n n_j \int_{T_{\text{ref}}}^{T_1} C_p dT = \sum_1^n n_j \Delta h_j \Big|_{T_{\text{ref}}}^{T_1} \quad (5-18)$$

Here Δh is the increase in enthalpy for each species multiplied by its molar fraction, and C_p is the molar specific heat at constant pressure.

The second principle is the *conservation of mass*. The mass of any of the atomic species present in the reactants before the chemical reaction must be equal to the mass of the same species in the products. This can be illustrated by a more general case of the reaction of Equation 5–8. In this case the reactants are not in stoichiometric proportion.

In the combustion of hydrogen with oxygen it is possible to form six products: water, hydrogen, oxygen, hydroxyl, atomic oxygen, and atomic hydrogen. In this case all the reactants and products are gaseous. Theoretically, there could be two additional products: ozone O_3 and hydrogen peroxide H_2O_2 ; however, these are unstable materials that do not readily exist at high temperature, and they can be ignored. In chemical notation this can be stated by



The left side shows the condition before and the right side the condition after the reaction. Since H_2 and O_2 can be found on both sides, it means that not all of these species are consumed and a portion, namely n_{H_2} and n_{O_2} , will remain unreacted. With chemical equilibrium at a particular temperature and pressure the molar concentrations on the right side will remain fixed. Here a , b , $n_{H_2}O$, n_{H_2} , n_{O_2} , n_O , n_H , and n_OH are the respective molar quantities of these substances before and after the reaction, and they can be expressed in kg-mol per kilogram of propellant reactants or reaction products. The initial proportions of a and b are usually known. The number of kg-mol per kilogram of mixture of each element can be established from this initial mix of oxidizer and fuel ingredients. For the hydrogen–oxygen relation above, the mass balances would be

$$\begin{aligned} \text{for hydrogen: } & 2a = 2n_{H_2}O + 2n_{H_2} + n_H + n_OH \\ \text{for oxygen: } & 2b = n_{H_2}O + 2n_{O_2} + n_O + n_OH \end{aligned} \quad (5-20)$$

The *mass balance* of Eq. 5–20 provides two more equations for this reaction (one for each atomic species) in addition to the energy balance equation. There are six unknown product percentages and an unknown combustion or equilibrium temperature. However, three equations provide a solution for only three unknowns, say the combustion temperature and the molar fractions of two of the species. If, for example, it is known that the initial mass mixture ratio of b/a is fuel rich, so that the combustion temperature will be relatively low, the percentage of remaining O_2 and the percentage of the dissociation products (O , H , and OH) would all be very low and can be neglected. Thus n_O , n_H , n_{OH} , and n_{O_2} are set to be zero. The solution requires knowledge of the enthalpy change of each of the species, and that information can be obtained from existing tables, such as Table 5–2 or Refs. 5–8 and 5–9.

In more general form, the mass for any given element must be the same before and after the reaction. The number of kg-mol of a given element per kilogram of reactants and product is equal, or their difference is zero. For any one atomic species, such as the H or the O in Eq. 5–20,

$$\left[\sum_{j=1}^m a_{ij} n_j \right]_{\text{products}} - \left[\sum_{j=1}^n a_{ij} n_j \right]_{\text{propellants}} = 0 \quad (5-21)$$

Here the atomic coefficients a_{ij} are the number of kilogram atoms of element i per kg-mol of species j , and m and n are as defined above. The average molecular mass of the products from Eq. 5–5 would be

$$\bar{M} = \frac{2n_{H_2} + 32n_{O_2} + 18n_{H_2O} + 16n_O + n_H + 17n_{OH}}{n_{H_2} + n_{O_2} + n_{H_2O} + n_O + n_H + n_{OH}} \quad (5-22)$$

The approach used in Ref. 5–13 is commonly used today for thermochemical analysis. It relies on the minimization of the Gibbs free energy and on mass balance and energy balance equations. As was explained in Eq. 5–12, the change in the Gibbs free energy function is zero at equilibrium ($\Delta G = 0$): the chemical potential of the gaseous propellants has to equal that of the gaseous reaction products, which is Eq. 5–12:

$$\Delta G = \sum (n_j \Delta G_j)_{\text{products}} - \sum (n_j \Delta G_j)_{\text{reactants}} = 0 \quad (5-23)$$

To assist in solving this equation a Lagrangian multiplier or a factor of the degree of the completion of the reaction is often used. An alternative method for solving for the gas composition, temperature, and gas properties is to use the energy balance (Eq. 5–18) together with several mass balances (Eq. 5–21) and equilibrium constant relationships.

After assuming a chamber pressure and setting up the energy balance, mass balances, and equilibrium relations, one method of solving all the equations is to estimate a combustion temperature and then solve for the various values of n_j .

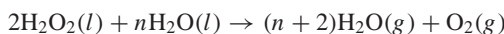
Then a balance has to be achieved between the heat of reaction $\Delta_r H^0$ and the heat absorbed by the gases, $H_T^0 - H_0^0$, to go from the reference temperature to the combustion temperature. If they do not balance, another value of the combustion temperature is chosen until there is convergence and the energy balances.

The *energy release efficiency*, sometimes called the *combustion efficiency*, can now be defined as the ratio of the actual change in enthalpy per unit propellant mixture to the calculated change in enthalpy necessary to transform the propellants from the initial conditions to the products at the chamber temperature and pressure. The actual enthalpy change can be evaluated if the initial propellant condition and the actual composition and the temperature of the combustion gases are measured. Experimental measurements of combustion temperature and gas composition are difficult to perform accurately, and the combustion efficiency is therefore actually evaluated only in rare instances. The combustion efficiency in liquid propellant rocket thrust chambers depends on the method of injection and mixing and increases with increased combustion temperature. In solid propellants the combustion efficiency is a function of the grain design, the propellant, and the degree of mixing between the several solid constituents. Actual measurements on well-designed rocket propulsion systems indicate efficiency values of 94 to 99%. These high values indicate that the combustion is essentially complete, that very little, if any, unreacted propellant remains, and that chemical equilibrium is indeed established.

The number of compounds or species in the exhaust can be 50 or more with solid propellants or with liquid propellants that have certain additives. The number of nearly simultaneous chemical reactions that have to be considered can easily exceed 150. Fortunately, many of these chemical species are present only in very small amounts and can usually be neglected.

Example 5–1. Hydrogen peroxide is used both as a monopropellant and as an oxidizer in bipropellant systems. It is stored in liquid form and available in various degrees of dilution with liquid water. For rocket applications, concentrations (70 to 98+%), known as high-test peroxide (HTP) are used. For a monopropellant application, calculate the *adiabatic flame temperature* as a function of water content based on an initial mixture temperature of 298.15 K (the standard condition).

SOLUTION. In this usage, hydrogen peroxide dissociates while passing through a catalyst and releases energy which goes to increase the propellant temperature in the absence of any heat transfer losses. But some of this heat will be required to evaporate the diluent water. The mass balance, Eq. 5–21, is satisfied by 2 mol of hydrogen peroxide in n moles of liquid water, producing $n + 2$ mol of water vapor plus 1 mol of oxygen gas. Since the reaction goes to completion, no equilibrium constant is needed:



The symbols (*l*) and (*g*) refer to the liquid state and the gaseous state, respectively. The heats of formation from the standard state, $\Delta_f H^0$ and molar specific heats C_p are shown below (see Table 5–1 and other common sources such as the NIST Chemistry

web-book, <http://webbook.nist.gov/chemistry/>). For these calculations the heat of mixing may be ignored.

| Species | $\Delta_f H^0$ (kJ/kg-mol) | C_p (J/kg-mol-k) | \mathfrak{M} (kg/kg-mol) |
|---------------------------|----------------------------|--------------------|----------------------------|
| $\text{H}_2\text{O}_2(l)$ | -187.69 | | 34.015 |
| $\text{H}_2\text{O}(l)$ | -285.83 | | 18.015 |
| $\text{H}_2\text{O}(g)$ | -241.83 | 0.03359 | 18.015 |
| $\text{O}_2(g)$ | 0 | 0.02938 | 31.999 |

The energy balance, Eq. 5–9, for 2 mol of decomposing hydrogen peroxide becomes

$$\begin{aligned}\Delta_r H^0 &= [n \Delta_f H^0]_{\text{H}_2\text{O}} - [n \Delta_f H^0]_{\text{H}_2\text{O}_2} \\ &= 2 \times (-241.83) - 2 \times (-187.69) \\ &= -108.28 \text{ kJ}\end{aligned}$$

The reaction is exothermic but as stated some of this energy is used up in vaporizing the diluent liquid water, namely $285.83 - 241.83 = 44.0$ kJ/kg-mol (at standard conditions). The net available heat release thus becomes $108.28 - 44.0n$ (kJ). In order to calculate the *adiabatic temperature*, we assume ideal-gas heating at constant pressure, Eq. 5–18 (values for the molar specific heats are from Table 5–1 and are taken as constant):

$$\int (n_{\text{H}_2\text{O}} C_{p,\text{H}_2\text{O}} + n_{\text{O}_2} C_{p,\text{O}_2}) dT = [(2+n) C_{p,\text{H}_2\text{O}} + C_{p,\text{O}_2}] \Delta T = 108.28 - 44.0n$$

It will be more convenient to give results in terms of a *mass fraction* z of the diluent water in the original mixture, and for this the molecular masses need to be inserted (also shown in Table 5–1):

$$\begin{aligned}z &= m_{\text{H}_2\text{O}} / (m_{\text{H}_2\text{O}_2} + m_{\text{H}_2\text{O}}) = n \mathfrak{M}_{\text{H}_2\text{O}} / (2 \mathfrak{M}_{\text{H}_2\text{O}_2} + n \mathfrak{M}_{\text{H}_2\text{O}}) \\ &= 18.015n / (2 \times 34.015 + 18.015n)\end{aligned}$$

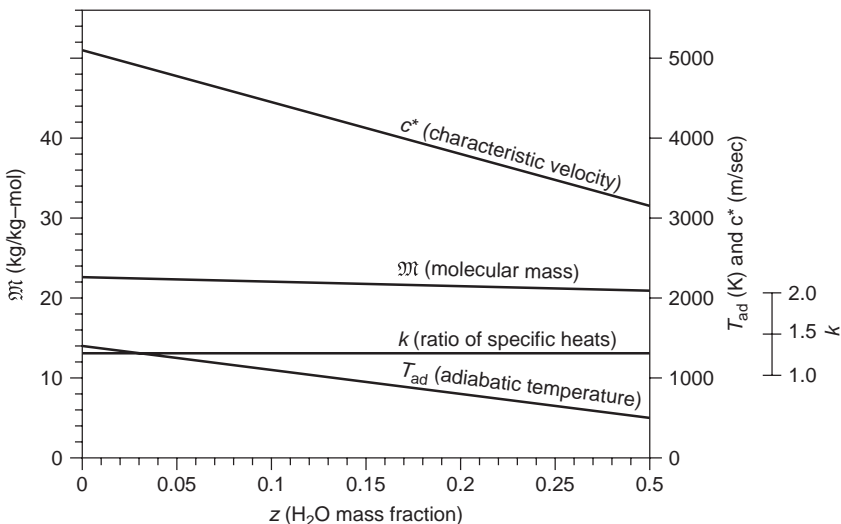
Now solve for n

$$n = 3.78z / (1 - z)$$

and substitute it in the relation for the temperature. The resulting value (the adiabatic temperature, T_{ad}) may then be plotted in terms of the mass fraction z with the initial temperature as given:

$$\begin{aligned}T_{\text{ad}} &= [108.28 - 44 \times 3.78z / (1 - z)] / [0.03359 \times (2 + 3.78z / (1 - z))] \\ &\quad + 0.02838] + 298.15d\end{aligned}$$

The figure also displays the values of c^* (where $T_1 = T_{\text{ad}}$), \mathfrak{M} , and k , which are calculated according to Eqs. 3–32 and 5–5 and 5–7.



5.3. ANALYSIS OF NOZZLE EXPANSION PROCESSES

There are several methods for analyzing the nozzle flow, depending on the assumptions made for chemical equilibrium, nozzle expansion, particulates, or energy losses. Several are outlined in Table 5-3.

Once the gases reach the nozzle, they experience an adiabatic, reversible expansion process which is accompanied by a major drop in temperature and pressure and a conversion of thermal energy into kinetic energy. Several increasingly more complicated methods have been used for the analysis of the process. For the simple case of frozen equilibrium and one-dimensional flow the state of the gas throughout expansion in the nozzle is fixed by the entropy of the system, which is presumed to be invariant as the pressure is reduced to the value assigned to the nozzle exit plane. All the assumptions listed in Chapter 3 for an ideal rocket would be valid here. Again, the effects of friction, divergence angle, heat losses, shock waves, or nonequilibrium are neglected in the simple cases but are considered in the more sophisticated solutions. The condensed (liquid or solid) phases are similarly assumed to have zero volume and to be in kinetic as well as thermal equilibrium with the gas flow. This implies that particles or droplets are very small in size, move at the same velocity as the gas stream, and have the same temperature as the gas at all places in the nozzle.

The chemical equilibrium during expansion in the nozzle can be analytically regarded in the following ways:

1. When the composition is invariant throughout the nozzle, there are no chemical reactions or phase changes and the product composition at the nozzle exit is identical to that of its chamber condition. The results are known as *frozen equilibrium* rocket performance. This method usually is simple, but underestimates the performance, typically by 1 to 4%.

2. Instantaneous chemical equilibrium among all molecular species is maintained under the continuously variable pressure and temperature conditions of the nozzle expansion process. Thus the product composition shifts; similarly, instantaneous chemical reactions, phase changes or equilibria occur between gaseous and condensed phases of all species in the exhaust gas. The results so calculated are called *shifting equilibrium* performance. The gas composition mass percentages are different in the chamber and the nozzle exit. This method usually overstates the performance values, such as c^* or I_s , typically by 1 to 4%. Here the analysis is more complex.
3. Chemical reactions do not occur instantaneously; even though the reactions occur rapidly, they require a finite time. Reaction rates of specific reactions can be estimated; the rates are usually a function of temperature, the magnitude of deviation from the equilibrium molar composition, and the nature of the chemicals or reactions involved. The values of T , c^* , or I_s for these types of equilibrium analysis usually are between those of frozen and instantaneously shifting equilibria. This approach is almost never used because of the lack of good data on reaction rates with multiple simultaneous chemical reactions.

For an axisymmetric nozzle, both one-and two-dimensional analyses can be used. The simplest nozzle flow analysis is one dimensional, which means that all velocities and temperatures or pressures are equal at any normal cross section of an axisymmetric nozzle. It is often satisfactory for preliminary estimates. In a two-dimensional analysis the velocity, temperature, density, and/or Mach number do not have a flat profile and vary somewhat over the cross sections. For nozzle shapes that are not bodies of revolution (e.g., rectangular, scarfed, or elliptic) a three-dimensional analysis should be performed.

If solid particles or liquid droplets are present in the nozzle flow and if the particles are larger than about 0.1 μm average diameter, there will be a thermal lag and velocity lag. The solid particles or liquid droplets do not expand like a gas; their temperature decrease depends on losing energy by convection or radiation, and their velocity depends on the drag forces exerted on the particle. Larger-diameter droplets or particles are not accelerated as rapidly as the smaller ones and flow at a velocity lower than that of the adjacent accelerating gas. Also, the particulates are hotter than the gas and provide heat to the gas. While these particles contribute to the momentum of the exhaust mass, they are not as efficient as an all-gaseous exhaust flow. For composite solid propellants with aluminum oxide particles in the exhaust gas, the loss due to particles could typically be 1 to 3%. The analysis of a two- or three-phase flow requires knowledge of an assumption about the nongaseous matter, the sizes (diameters), size distribution, shape (usually assumed to be spherical), optical surface properties (for determining the emission/absorption or scattering of radiant energy), and their condensation or freezing temperatures. Some of these parameters are not well known. Performance estimates of flows with particles are explained in Section 3.5.

TABLE 5–3. Typical Steps and Alternatives in the Analysis of Rocket Thermochemical Processes in Nozzles

| Step | Process | Method/Implication/Assumption |
|--|---|--|
| Nozzle inlet condition | Same as chamber exit; need to know $T_1, p_1, v_1, H, c^*, \rho_1$, etc. | For simpler analyses assume the flow to be uniformly mixed and steady. |
| Nozzle expansion | An adiabatic process, where flow is accelerated and thermal energy is converted into kinetic energy. Temperature and pressure drop drastically. Several different analyses have been used with different specific effects. Can use one-, two-, or three-dimensional flow pattern. | <p>1. Simplest method is inviscid isentropic expansion flow with constant entropy.</p> <p>2. Include internal weak shock waves; no longer a truly isentropic process.</p> <p>3. If solid particles are present, they will create drag, thermal lag, and a hotter exhaust gas. Must assume an average particle size and optical surface properties of the particulates. Flow is no longer isentropic.</p> <p>4. Include viscous boundary layer effects and/or nonuniform velocity profile.</p> |
| Chemical equilibrium during nozzle expansion | Due to rapid decrease in T and p , the equilibrium composition can change from that in the chamber. The four processes listed in the next column allow progressively more realistic simulation and require more sophisticated techniques. | <p>1. Frozen equilibrium; no change in gas composition; usually gives low performance.</p> <p>2. Shifting equilibrium or instantaneous change in composition; usually overstates the performance slightly.</p> <p>3. Use reaction time rate analysis to estimate the time to reach equilibrium for each of the several chemical reactions; some rate constants are not well known; analysis is more complex.</p> <p>4. Use different equilibrium analysis for boundary layer and main inviscid flow; will have nonuniform gas temperature, composition, and velocity profiles.</p> |

TABLE 5–3. (Continued)

| Step | Process | Method/Implication/Assumption |
|----------------------------|---|--|
| Heat release in nozzle | Recombination of dissociated molecules (e.g., $H + H = H_2$) and exothermic reactions due to changes in equilibrium composition cause an internal heating of the expanding gases. Particulates release heat to the gas. | Heat released in subsonic portion of nozzle will increase the exit velocity. Heating in the supersonic flow portion of nozzle can increase the exit temperature but reduce the exit Mach number. |
| Nozzle shape and size | Can use straight cone, bell-shaped, or other nozzle contour; bell can give slightly lower losses. Make correction for divergence losses and nonuniformity of velocity profile. | Must know or assume a particular nozzle configuration. Calculate bell contour by method of characteristics. Use Eq. 3–34 for divergence losses in conical nozzle. Most analysis programs are one- or two-dimensional. Unsymmetrical nonround nozzles may need three-dimensional analysis. |
| Gas properties | The relationships governing the behavior of the gases apply to both nozzle and chamber conditions. As gases cool in expansion, some species may condense. | Either use perfect gas laws or, if some of the gas species come close to being condensed, use real gas properties. |
| Nozzle exit conditions | Will depend on the assumptions made above for chemical equilibrium, nozzle expansion, and nozzle shape/contour. Assume no jet separation. Determine velocity profile and the pressure profile at the nozzle exit plane. If pressure is not uniform across a section it will have some cross flow. | Need to know the nozzle area ratio or nozzle pressure ratio. For quasi-one-dimensional and uniform nozzle flow, see Eqs. 3–25 and 3–26. If v_2 is not constant over the exit area, determine effective average values of v_2 and p_2 . Then calculate profiles of T , ρ , etc. For nonuniform velocity profile, the solution requires an iterative approach. Can calculate the gas conditions (T , p , etc.) at any point in the nozzle. |
| Calculate specific impulse | Can be determined for different altitudes, pressure ratios, mixture ratios, nozzle area ratios, etc. | Can be determined for average values of v_2 , p_2 , and p_3 based on Eqs. 2–6 or 2–14. |

The viscous boundary layer next to the nozzle wall has velocities substantially lower than that of the inviscid free stream. The slowing down of the gas flow near the wall due to the viscous drag actually causes the conversion of kinetic energy back into thermal energy, and thus some parts of the boundary layer can be hotter than the local free-stream static temperature. A diagram of a two-dimensional boundary layer is shown in Figure 3–16. With turbulence this boundary layer can be relatively thick in large-diameter nozzles. The boundary layer is also dependent on the axial pressure gradient in the nozzle, the nozzle geometry, particularly in the throat region, the surface roughness, or the heat losses to the nozzle walls. Theoretical boundary layer analyses with unsteady flow are only approximations, but are expected to improve in the future as our understanding of the phenomena and computational fluid dynamics (CFD) techniques are validated. The net effect is a nonuniform velocity and temperature profile, an irreversible friction process in the viscous layers, and therefore an increase in entropy and a slight reduction (usually less than 5%) of the kinetic exhaust energy. The layers immediately adjacent to the nozzle walls have laminar and subsonic flow.

At the high combustion temperatures a small portion of the combustion gas molecules dissociate (split into simpler species); in this *dissociation* process some energy is absorbed. When energy is released during reassociation (at lower pressures and temperatures in the nozzle), this reduces the kinetic energy of the exhaust gas at the nozzle exit. This is discussed further next.

For propellants that yield only gaseous products, extra energy is released in the nozzle, primarily from the recombination of free-radical and atomic species, which become unstable as the temperature is decreased in the nozzle expansion process. Some propellant products include species that condense as the temperature drops in the nozzle expansion. If the heat release on condensation is large, the difference between frozen and shifting equilibrium performance can be substantial.

In the simplest method the exit temperature T_2 is determined for an isentropic process (frozen equilibrium) by considering the entropy to be constant. The entropy at the exit is the same as the entropy in the chamber. This determines the temperature at the exit and thus the gas condition at the exit. From the corresponding change in enthalpy it is then possible to obtain the exhaust velocity and the specific impulse. For those analysis methods where the nozzle flow is not really isentropic and the expansion process is only partly reversible, it is necessary to include the losses due to friction, shock waves, turbulence, and so on. The result is a somewhat higher average nozzle exit temperature and a slight loss in I_s . A possible set of steps used for the analysis of nozzle processes is given in Table 5–3.

When the contraction between the combustion chamber (or the port area) and the throat area is small ($A_p/A_t \leq 3$), the acceleration of the gases in the chamber causes a drop in the effective chamber pressure at the nozzle entrance. This pressure loss in the chamber causes a slight reduction of the values of c and I_s . The analysis of this chamber configuration is treated in Ref. 5–14 and some data are briefly shown in Table 3–2.

5.4. COMPUTER-ASSISTED ANALYSIS

All the analyses discussed in this chapter are done today with computer programs. Most are based on minimizing the free energy. This is a simpler approach than relying on equilibrium constants, which was used some years ago. Once the values of n_j and T_1 are determined, it is possible to calculate the molecular mass of the gases (Eq. 5–5), the average molar specific heats C_p by a similar formula, and the specific heat ratio k from Eqs. 3–6 and 5–7. This then characterizes the thermodynamic conditions in the combustion chamber. With these data we can calculate c^* , R , and other mixture parameters of the chamber combustion. The nozzle expansion process simulated with computers give the performance (such as I_s , c , or A_2/A_t) and the gas conditions in the nozzle; it usually includes several of the corrections mentioned in Chapter 3. Programs exist for one-, two-, and three-dimensional flow patterns.

More sophisticated solutions include a supplementary analysis of combustion chamber conditions where the chamber velocities are high (see Ref. 5–14), a boundary layer analysis, a heat transfer analysis, or a two-dimensional axisymmetric flow with nonuniform flow properties across any cross section of the nozzle. Time-dependent chemical reactions in the chamber are usually neglected, but they can be analyzed by estimating the time rate at which the reaction occurs. This is described in Ref. 5–3.

A commonly used computer program, based on equilibrium compositions, has been developed at the NASA Glenn Laboratories and is known as the *NASA CEA* code (Chemical Equilibrium with Applications). It is described in Ref. 5–13, Vols. 1 and 2. Key assumptions for this program are one-dimensional forms of the continuity, energy and momentum equations, negligible velocity at the forward end of the combustion chamber, isentropic expansion in the nozzle, ideal gas behavior, and chemical equilibrium in the combustion chamber. It includes options for frozen flow and for narrow chambers (for liquid propellant combustion) or port areas with small cross sections (for solid propellant grains), where the chamber flow velocities are relatively high, resulting in extra pressure losses and a slight loss in performance. NASA's CEA code has recently become part of a commercial code named CequelTM, which extends the code's original capabilities.

Other relatively common computer codes used in the United States for analyzing the converging–diverging nozzle flow include:

ODE (*one-dimensional equilibrium code*) which features infinitely fast chemical reactions (shifting equilibrium) and includes all gaseous constituents.

ODK (*one-dimensional kinetics*) which incorporates finite chemical reaction kinetic rates for temperature-dependent composition changes in the flow direction with uniform flow properties across any nozzle section. It is used as a module in more complex codes and has no provision for particles.

TDK (*two-dimensional kinetic code*) which incorporates finite kinetic chemical reaction rates and radial variance in flow properties. It has no provision for particles.

VIPERP (*viscous interaction performance evaluation routine for two-phased flows*) a parabolized Navier–Stokes code for internal two-phased nozzle flow with turbulent and nonequilibrium reacting gases. It can be used with solid particles but requires data (or assumptions) on the amount of solids, particle size distribution, or their shape (see, e.g., pp. 503 to 505 in 7th Edition).

More information on these computer codes may be obtained from the appropriate government offices and/or from small companies (who actually run the nozzle codes for their customers). Some of the more sophisticated codes are proprietary to propulsion organizations and not publicly available.

5.5. RESULTS OF THERMOCHEMICAL CALCULATIONS

Extensive computer results of these machine calculations are available and only a few samples are indicated here to illustrate typical effects of the variations of key parameters. In general, high specific impulse or high values of c^* can be obtained if the average molecular mass of the reaction products is low (usually this implies a formulation rich in hydrogen) and/or if the available chemical energy (heat of reaction) is large, which means high combustion temperatures (see Eq. 3–16).

Table 5–4 shows calculated results for a liquid oxygen, liquid hydrogen thrust chamber taken from an example of this reference. It has shifting equilibrium in the nozzle flow. The narrow chamber has a cross section that is only a little larger than the throat area. The large pressure drop in the chamber (approximately 126 psi) is due to the energy needed to accelerate the gas, as discussed in Section 3.3 and Table 3–2.

Values of calculated specific impulse will be higher than those obtained from firing actual propellants in rocket units. In practice it has been found that the experimental values are about 3 to 12% lower than those calculated by the method explained in this chapter. Because the nozzle inefficiencies explained in Chapter 3 must be considered, only a portion of this correction (perhaps 1 to 4%) is due to combustion inefficiencies.

Figures 5–1 to 5–6 indicate the results of performance calculations for the liquid propellant combination, liquid oxygen-RP-1. These data are taken from Refs. 5–7 and 5–8. The RP-1 fuel is a narrow-cut hydrocarbon similar to kerosene with an average of 1.953 mol of hydrogen for each mole of carbon; thus it has a nominal formula of $\text{CH}_{1.953}$. The calculations are limited to a chamber pressure of 1000 psia. Most of the curves are for optimum area ratio expansion to atmospheric pressure, namely 1 atm or 14.696 psia, and for a limited range of oxidizer-to-fuel mixture ratios.

For maximum specific impulse, Figs. 5–1 and 5–4 show an *optimum mixture ratio* of approximately 2.3 (kg/sec of oxidizer flow divided by kg/sec of fuel flow) for frozen equilibrium expansion and 2.5 for shifting equilibrium with gas expansion to sea-level pressure. The maximum values of c^* are at slightly

TABLE 5–4. Calculated Parameters for Liquid Oxygen and Liquid Hydrogen Rocket Engine for Four Different Nozzle Expansions

Chamber pressure at injector 773.3 psia or 53.317 bar; $c^* = 2332.1\text{ m/sec}$; shifting equilibrium nozzle flow mixture ratio $O_2/H_2 = 5.551$; chamber to throat area ratio $A_1/A_t = 1.580$.

| Location | Injector face | Comb. end | Parameters | | | Exit | Exit | Exit |
|--------------------------------------|--------------------|--------------------|-------------------|---------|---------|---------|---------|------|
| | | | Throat | Exit | Exit | | | |
| p_{inj}/p | 1.00 | 1.195 | 1.886 | 10.000 | 100.000 | 282.15 | 709.71 | |
| T (K) | 3389 | 3346 | 3184 | 2569 | 1786 | 1468 | 1219 | |
| \mathfrak{M} (molec. mass) | 12.7 | 12.7 | 12.8 | 13.1 | 13.2 | 13.2 | 13.2 | |
| k (spec. heat ratio) | 1.14 | 1.14 | 1.15 | 1.17 | 1.22 | 1.24 | 1.26 | |
| C_p (spec. heat, kJ/kg-K) | 8.284 | 8.250 | 7.530 | 4.986 | 3.457 | 3.224 | 3.042 | |
| M (Mach number) | 0.00 | 0.413 | 1.000 | 2.105 | 3.289 | 3.848 | 4.379 | |
| A_2/A_t | 1.580 ^a | 1.580 ^a | 1.000 | 2.227 | 11.52 | 25.00 | 50.00 | |
| c (m/sec) | NA | NA | 2879 ^b | 3485 | 4150 | 4348 | 4487 | |
| v_2 (m/sec) | NA | NA | 1537 ^b | 2922 | 3859 | 4124 | 4309 | |
| <i>Mole fractions of gas mixture</i> | | | | | | | | |
| H | 0.03390 | 0.03336 | 0.02747 | 0.00893 | 0.00024 | 0.00002 | 0.00000 | |
| HO_2 | 0.00002 | 0.00001 | 0.00001 | 0.00000 | 0.00000 | 0.00000 | 0.00000 | |
| H_2 | 0.29410 | 0.29384 | 0.29358 | 0.29659 | 0.30037 | 0.30050 | 0.30052 | |
| H_2O | 0.63643 | 0.63858 | 0.65337 | 0.68952 | 0.69935 | 0.69948 | 0.69948 | |
| H_2O_2 | 0.00001 | 0.00001 | 0.00000 | 0.00000 | 0.00000 | 0.00000 | 0.00000 | |
| O | 0.00214 | 0.00204 | 0.00130 | 0.00009 | 0.00000 | 0.00000 | 0.00000 | |
| OH | 0.03162 | 0.03045 | 0.02314 | 0.00477 | 0.00004 | 0.00000 | 0.00000 | |
| O_2 | 0.00179 | 0.00172 | 0.00113 | 0.00009 | 0.00000 | 0.00000 | 0.00000 | |

^aChamber contraction ratio A_1/A_t .

^bIf cut off at throat.

c is the effective exhaust velocity in a vacuum.

v_2 is the nozzle exit velocity at optimum nozzle expansion.

NA means not applicable.

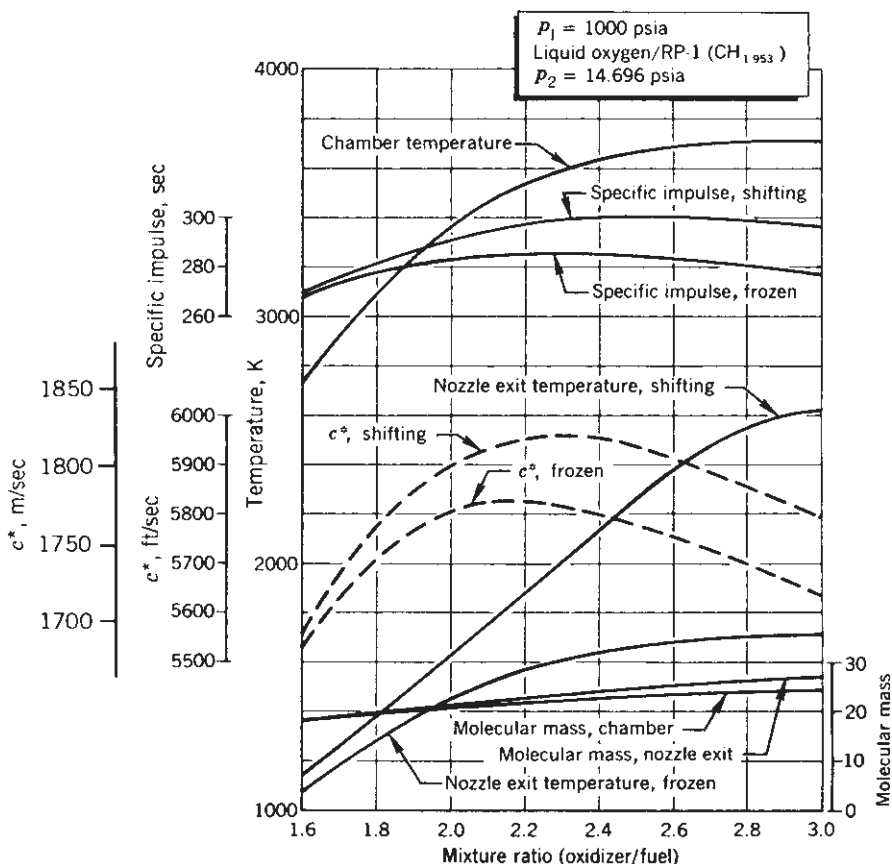


FIGURE 5-1. Calculated performance analysis of liquid oxygen and hydrocarbon fuel as a function of mixture ratio.

different mixture ratios. This optimum mixture ratio is not the value for highest temperature, which is usually fairly close to the stoichiometric value. The stoichiometric mixture ratio is more than 3.0 where much of the carbon is burned to CO_2 and almost all of the hydrogen to H_2O .

Because shifting equilibrium makes more enthalpy available for conversion to kinetic energy, it gives higher values of performance (higher I_s or c^*) and higher values of nozzle exit temperature for the same exit pressure (see Fig. 5-1). The influence of mixture ratio on chamber gas composition is evident from Fig. 5-2. A comparison with Fig. 5-3 indicates the marked changes in the gas composition as the gases are expanded under shifting equilibrium conditions. The influence of the degree of expansion, or of the nozzle exit pressure on the gas composition, is shown in Fig. 5-6. As the gases are expanded to higher area ratios and lower exit pressure (or higher pressure ratios) the performance increases; however,

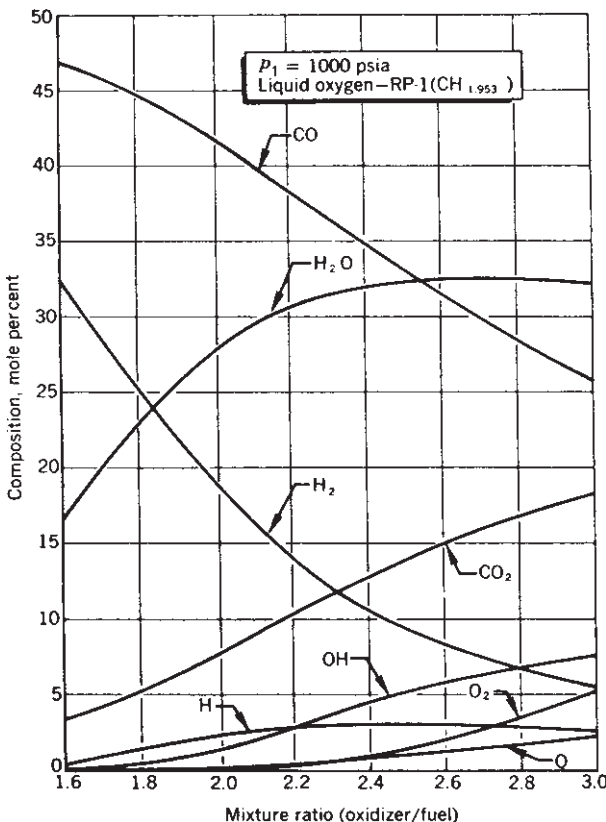


FIGURE 5–2. Calculated chamber gas composition for liquid oxygen and hydrocarbon fuel as a function of mixture ratio. Aggressive gases, such as O_2 , O , or OH , can cause oxidation of the wall materials in the chamber and the nozzle.

the relative increase diminishes as the pressure ratio is further increased (see Figs. 5–5 and 5–6).

Dissociation of molecules absorbs considerable energy and causes a decrease in the combustion temperature, which in turn can reduce the specific impulse. Dissociation of the reaction products increases as the chamber temperature rises, and decreases with increasing chamber pressure. Atoms or radicals such as monatomic O or H and OH are formed, as can be seen from Fig. 5–2; some unreacted O_2 also remains at the higher mixture ratios and very high combustion temperatures. As the gases are cooled in the nozzle expansion, the dissociated species react again to form molecules and release heat into the flowing gases. As can be seen from Fig. 5–3, only a small percentage of dissociated species persists at the nozzle exit and only at the high mixture ratio, where the exit temperature is relatively high. (See Fig. 5–1 for exit temperatures with shifting equilibria). Heat released in a supersonic flow actually reduces the Mach number.

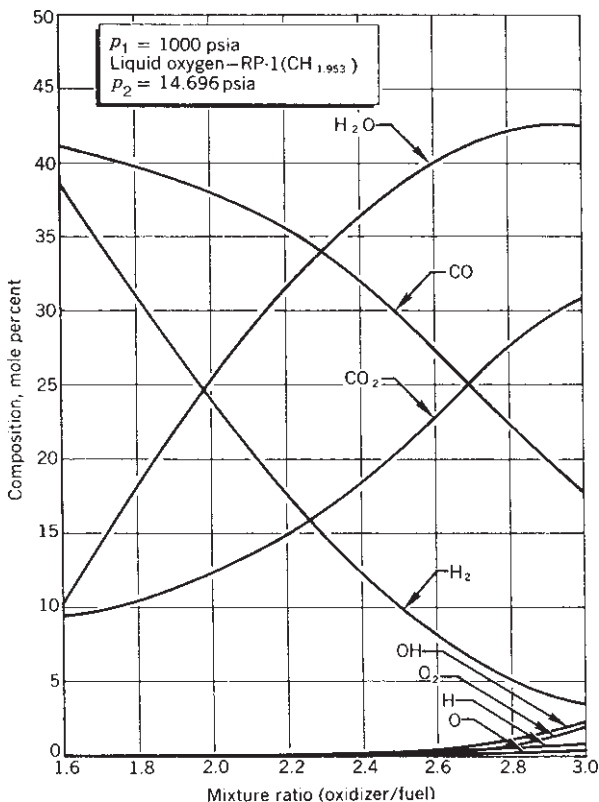


FIGURE 5-3. Calculated nozzle exit gas composition for shifting equilibrium conditions as a function of mixture ratio. Breakdown into O, OH, or H and free O₂ occurs only at the higher temperatures or higher mixture ratios.

Results of calculations for several different liquid and solid propellant combinations are given in Tables 5-5 and 5-6. For the liquid propellant combinations, the listed mixture ratios are optimum and their performance is a maximum. For solid propellants, practical considerations (such as propellant physical properties) do not always permit the development of a satisfactory propellant grain when the ingredients are mixed in optimum performance proportions (insufficient binder); therefore the values listed for solid propellants in Table 5-6 correspond in part to practical formulations with reasonable physical and ballistic properties.

Calculated data obtained from Ref. 5-13 are presented in Tables 5-7 to 5-9 for a specific solid propellant to indicate typical variations in performance or gas composition. This particular propellant consists of 60% ammonium perchlorate (NH_4ClO_4), 20% pure aluminum powder, and 20% of an organic polymer of an assumed chemical composition, namely $\text{C}_{3.1}\text{ON}_{0.84}\text{H}_{5.8}$. Table 5-7 shows

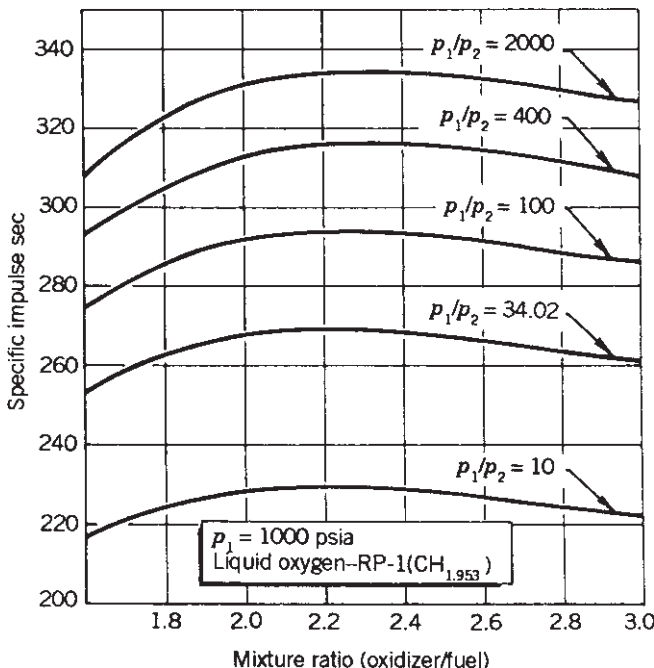


FIGURE 5–4. Variation of theoretical specific impulse with mixture ratio and pressure ratio, calculated for frozen equilibrium.

the variation of several performance parameters with different chamber pressures expanding to atmospheric exit pressure. The area ratios listed are optimum for this expansion with shifting equilibrium. The exit enthalpy, exit entropy, thrust coefficient, and the specific impulse also consider shifting equilibrium conditions. The characteristic velocity c^* and the chamber molecular mass are functions of chamber conditions only. Table 5–8 shows the variation of gas composition with chamber pressure. Some of the reaction products are in the liquid phase, such as Al_2O_3 . Table 5–9 shows the variation of nozzle exit characteristics and composition for shifting equilibria as a function of exit pressure or pressure ratio for a fixed value of chamber pressure. Table 5–9 shows how the composition is shifted during expansion in the nozzle and how several of the species present in the chamber have disappeared at the nozzle exit. These three tables show theoretical results calculated on a computer; some of the thermodynamic properties of the reactants and reaction products probably do not warrant the indicated high accuracy of five significant figures. In the analysis for chemical ingredients of this solid propellant, approximately 76 additional reaction products were considered

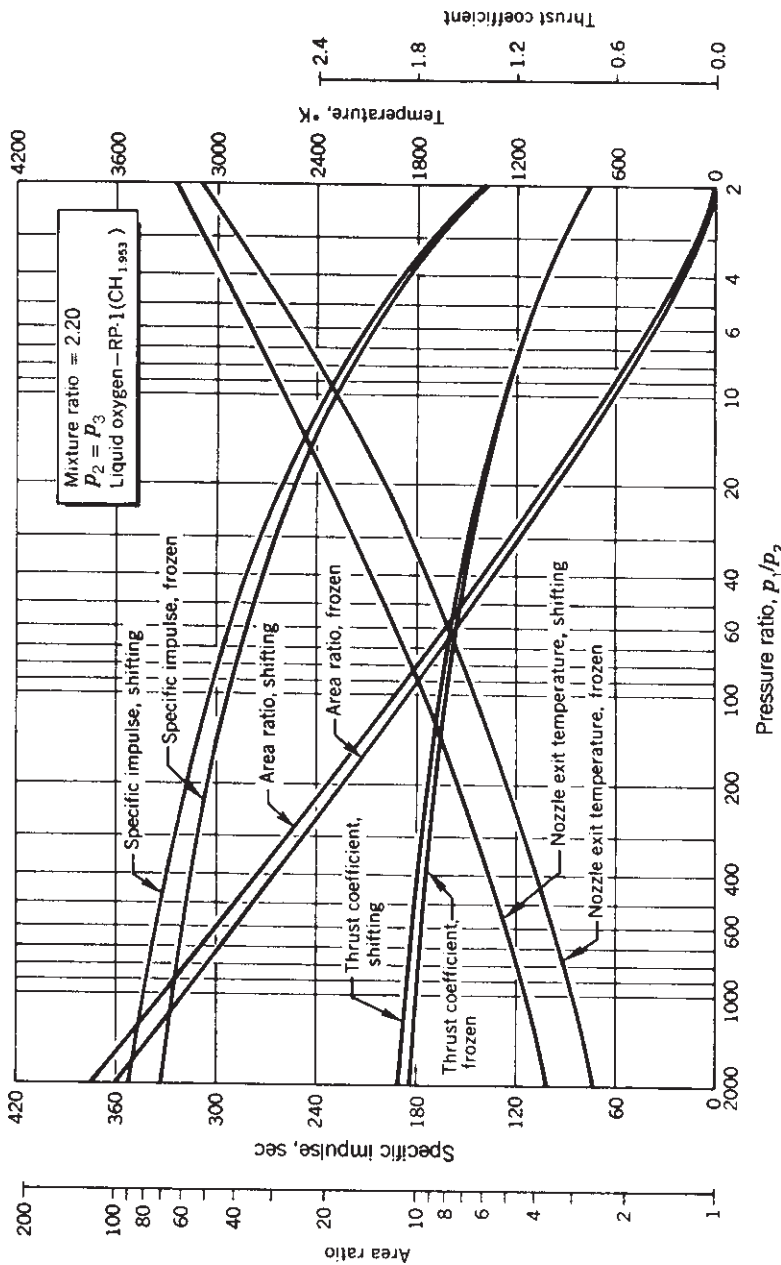


FIGURE 5-5. Variation of calculated parameters with pressure ratio for liquid oxygen-hydrocarbon propellant at a mixture ratio of 2.20. An increase in pressure ratio is due to an increase in chamber pressure, a decrease of nozzle exit pressure (larger area ratio and higher altitude), or both.

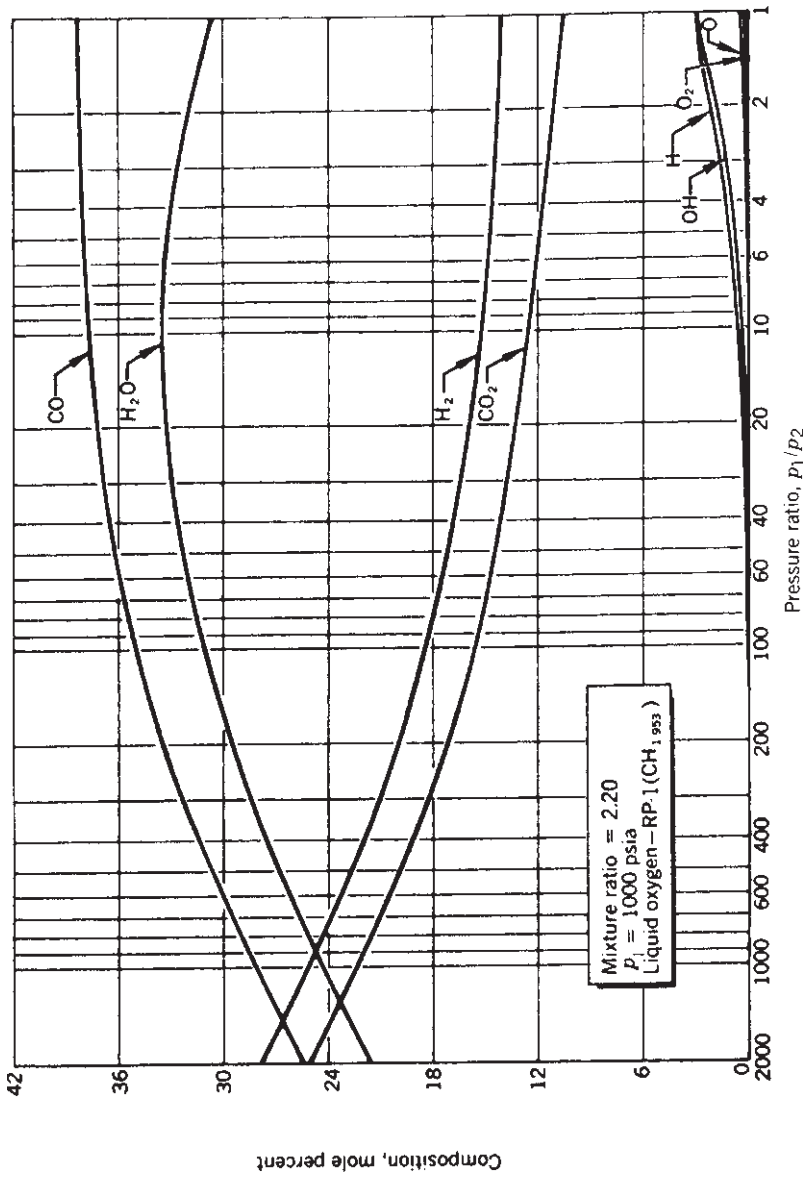


FIGURE 5-6. Variation of exhaust gas composition at nozzle exit with pressure ratio at a fixed mixture ratio and for shifting equilibrium. For frozen equilibrium the composition would be the same as in the chamber, as shown in Fig. 5-2.

TABLE 5-5. Theoretical Performance of Liquid Rocket Propellant Combinations

| Oxidizer | Fuel | Mixture Ratio | | Average Specific Gravity | Chamber Temp.(K) | (m/sec) | \bar{m} (kg/mol) | Shifting | I_s (sec) | k |
|-------------------------|------------------------|---------------|-----------|--------------------------|------------------|---------|--------------------|----------|-------------|-----|
| | | By Mass | By Volume | | | | | | | |
| Oxygen | Methane | 3.20 | 1.19 | 0.81 | 3526 | 1835 | 20.3 | 296 | 1.20 | |
| | Hydrazine | 3.00 | 1.11 | 0.80 | 3526 | 1853 | 311 | 301 | 1.25 | |
| | Hydrogen | 0.74 | 0.66 | 1.06 | 3285 | 1871 | 18.3 | 313 | 1.26 | |
| | RP-1 | 0.90 | 0.80 | 1.07 | 3404 | 1892 | 19.3 | 386 | 1.24 | |
| Fluorine | Hydrazine | 3.40 | 0.21 | 0.26 | 2959 | 2428 | 8.9 | 389.5 | 1.24 | |
| | Hydrogen | 4.02 | 0.25 | 0.28 | 2999 | 2432 | 10.0 | 285.4 | 1.24 | |
| | UDMH | 2.24 | 1.59 | 1.01 | 3571 | 1774 | 21.9 | 300 | 1.25 | |
| | RP-1 | 2.56 | 1.82 | 1.02 | 3677 | 1800 | 23.3 | 295 | 1.25 | |
| Nitrogen tetroxide | Hydrazine | 1.39 | 0.96 | 0.96 | 3542 | 1835 | 19.8 | 310 | 1.33 | |
| | Hydrogen | 1.65 | 1.14 | 0.98 | 3594 | 1864 | 21.3 | 334 | 1.33 | |
| | MMH | 1.83 | 1.22 | 1.29 | 4553 | 2128 | 18.5 | 365 | 1.33 | |
| | RP-1 | 2.30 | 1.54 | 1.31 | 4713 | 2208 | 19.4 | 389 | 1.33 | |
| Red fuming nitric acid | Hydrazine | 4.54 | 0.21 | 0.33 | 3080 | 2534 | 8.9 | 410 | 1.26 | |
| | Hydrogen | 7.60 | 0.35 | 0.45 | 3900 | 2549 | 11.8 | 283 | 1.26 | |
| | MMH | 1.08 | 0.75 | 1.20 | 3258 | 1765 | 19.5 | 297 | 1.24 | |
| | RP-1 | 1.34 | 0.93 | 1.22 | 3152 | 1782 | 20.9 | 278 | 1.24 | |
| Hydrogen peroxide (90%) | 50% UDMH-50% hydrazine | 1.62 | 1.01 | 1.18 | 3242 | 1652 | 21.0 | 289 | 1.22 | |
| | RP-1 | 2.00 | 1.24 | 1.21 | 3372 | 1711 | 22.6 | 269 | 1.22 | |
| | MMH | 3.4 | 1.05 | 1.23 | 3290 | 24.1 | 22.3 | 272 | 1.22 | |
| | RP-1 | 2.15 | 1.30 | 1.20 | 3396 | 1747 | 21.7 | 279 | 1.19 | |

Notes:

Combustion chamber pressure—1000 psia (6895 kN/m²); nozzle exit pressure—14.7 psia (1 atm); optimum expansion.

Adiabatic combustion and isentropic expansion of ideal gas.

The specific gravity at the boiling point was used for those oxidizers or fuels that boil below 20°C at 1 atm pressure.

Mixture ratios are for approximate maximum value of I_s .

TABLE 5–6. Theoretical Performance of Typical Solid Rocket Propellant Combinations

| Oxidizer | Fuel | ρ (g/cm ³) ^a | T_1 (K) | C^* (m/sec) ^b | \mathfrak{M} (kg/mol) | I_s (sec) ^b | k |
|--------------------------------|---|---|--------------|-------------------------------|----------------------------|-----------------------------|------|
| Ammonium nitrate | 11% binder and 7% additives | 1.51 | 1282 | 1209 | 20.1 | 192 | 1.26 |
| Ammonium perchlorate 78–66% | 18% organic polymer binder and 4–20% aluminum | 1.69 | 2816 | 1590 | 25.0 | 262 | 1.21 |
| Ammonium perchlorate 84–68% | 12% polymer binder and 4–20% aluminum | 1.74 | 3371 | 1577 | 29.3 | 266 | 1.17 |

^aAverage specific gravity of solid propellant.

^bConditions for I_s and c^* : Combustion chamber pressure: 1000 psia; nozzle exit pressure: 14.7 psia; optimum nozzle expansion ratio; frozen equilibrium.

in addition to the major product species. This includes, for example, CN, CH, CCl, Cl, NO, and so on. Their calculated mole fractions were very small and therefore they have been neglected and are not included in Table 5–8 or 5–9.

Calculations of this type are useful in estimating performance (I_s , c^* , C_F , ϵ , etc.) for a particular chamber pressure and nozzle exit pressure, and knowledge of the gas composition, as indicated by the previous figures and tables, permits a more detailed estimate of other design parameters, such as gas–film properties for heat transfer determination, radiation characteristics of the flame inside and outside the thrust chambers, and the acoustic characteristics of the gases. Performance data relevant to hybrid propellants are presented briefly in Chapter 16.

The thermochemical analysis of this chapter can also be applied to gas generators; the results (such as gas temperature T_1 , the specific heat c_p , specific heat ratio k , or composition) are used for estimating turbine inlet conditions or turbine power. In gas generators and preburners for staged combustion cycle rocket engines (explained in Section 6.6) the gas temperatures are much lower, to avoid damage to the turbine blades. Typically, the combustion reaction gases are at 800 to 1200 K, which is lower than the gas in the thrust chamber (2900 to 3600 K). Examples are listed in Table 5–10 for a chamber pressure of 1000 psia. Some species in the gases will not be present (such as atomic oxygen or hydroxyl), and often real gas properties will need to be used because some of these gases do not behave as a perfect gas at these temperatures.

TABLE 5-7. Variation of Calculated Performance Parameters for an Aluminized Ammonium Perchlorate Propellant as a Function of Chamber Pressure for Expansion to Sea Level (1 atm) with Shifting Equilibrium

| | 1500 | 1000 | 750 | 500 | 200 |
|--|----------|----------|----------|---------|---------|
| Chamber pressure (psia) | 102.07 | 68.046 | 51.034 | 34.023 | 13.609 |
| Chamber pressure (atm) or pressure ratio p_1/p_2 | 3346.9 | 3322.7 | 3304.2 | 3276.6 | 3207.7 |
| Chamber temperature (K) | 2007.7 | 2135.6 | 2226.8 | 2327.0 | 2433.6 |
| Nozzle exit temperature (K) | -572.17 | -572.17 | -572.17 | -572.17 | -572.17 |
| Chamber enthalpy (cal/g) | -1382.19 | -1325.15 | -1282.42 | -1219.8 | -1071.2 |
| Exit enthalpy (cal/g) | 2.1826 | 2.2101 | 2.2297 | 2.2574 | 2.320 |
| Entropy (cal/g-K) | 29.303 | 29.215 | 29.149 | 29.050 | 28.908 |
| Chamber molecular mass (kg/mol) | 29.879 | 29.853 | 29.820 | 29.763 | 29.668 |
| Exit molecular mass (kg/mol) | 3.20 | 3.00 | 2.86 | 2.89 | 2.32 |
| Exit Mach number | 1.1369 | 1.1351 | 1.1337 | 1.1318 | 1.1272 |
| Specific heat ratio—chamber, k | 287.4 | 280.1 | 274.6 | 265.7 | 242.4 |
| Specific impulse, vacuum (sec) | 265.5 | 256.0 | 248.6 | 237.3 | 208.4 |
| Specific impulse, sea-level expansion (sec) | 1532 | 1529 | 1527 | 1525 | 1517 |
| Characteristic velocity, c^* (m/sec) | 14.297 | 10.541 | 8.507 | 8.531 | 6.300 |
| Nozzle area ratio, A_2/A_1^a | 1.700 | 1.641 | 1.596 | 1.597 | 1.529 |
| Thrust coefficient, C_F^a | | | | | |

^aAt optimum expansion.
Source: From Ref. 5-13.

TABLE 5–8. Mole Fraction Variation of Chamber Gas Composition with Combustion Chamber Pressure for a Solid Propellant

| Pressure (psia) | 1500 | 1000 | 750 | 500 | 200 |
|---|---------|---------|---------|---------|---------|
| Pressure (atm) or pressure ratio | 102.07 | 68.046 | 51.034 | 34.023 | 13.609 |
| Ingredient | | | | | |
| Al | 0.00007 | 0.00009 | 0.00010 | 0.00012 | 0.00018 |
| AlCl | 0.00454 | 0.00499 | 0.00530 | 0.00572 | 0.00655 |
| AlCl ₂ | 0.00181 | 0.00167 | 0.00157 | 0.00142 | 0.00112 |
| AlCl ₃ | 0.00029 | 0.00023 | 0.00019 | 0.00015 | 0.00009 |
| AlH | 0.00002 | 0.00002 | 0.00002 | 0.00002 | 0.00002 |
| AlO | 0.00007 | 0.00009 | 0.00011 | 0.00013 | 0.00019 |
| AlOCl | 0.00086 | 0.00095 | 0.00102 | 0.00112 | 0.00132 |
| AlOH | 0.00029 | 0.00032 | 0.00034 | 0.00036 | 0.00041 |
| AlO ₂ H | 0.00024 | 0.00026 | 0.00028 | 0.00031 | 0.00036 |
| Al ₂ O | 0.00003 | 0.00004 | 0.00004 | 0.00005 | 0.00006 |
| Al ₂ O ₃ (solid) | 0.00000 | 0.00000 | 0.00000 | 0.00000 | 0.00000 |
| Al ₂ O ₃ (liquid) | 0.09425 | 0.09378 | 0.09343 | 0.09293 | 0.09178 |
| CO | 0.22434 | 0.22374 | 0.22328 | 0.22259 | 0.22085 |
| COCl | 0.00001 | 0.00001 | 0.00001 | 0.00001 | 0.00000 |
| CO ₂ | 0.00785 | 0.00790 | 0.00793 | 0.00799 | 0.00810 |
| Cl | 0.00541 | 0.00620 | 0.00681 | 0.00772 | 0.01002 |
| Cl ₂ | 0.00001 | 0.00001 | 0.00001 | 0.00001 | 0.00001 |
| H | 0.02197 | 0.02525 | 0.02776 | 0.03157 | 0.04125 |
| HCl | 0.12021 | 0.11900 | 0.11808 | 0.11668 | 0.11321 |
| HCN | 0.00003 | 0.00002 | 0.00001 | 0.00001 | 0.00000 |
| HCO | 0.00003 | 0.00002 | 0.00002 | 0.00002 | 0.00001 |
| H ₂ | 0.32599 | 0.32380 | 0.32215 | 0.31968 | 0.31362 |
| H ₂ O | 0.08960 | 0.08937 | 0.08916 | 0.08886 | 0.08787 |
| NH ₂ | 0.00001 | 0.00001 | 0.00001 | 0.00000 | 0.00000 |
| NH ₃ | 0.00004 | 0.00003 | 0.00002 | 0.00001 | 0.00001 |
| NO | 0.00019 | 0.00021 | 0.00023 | 0.00025 | 0.00030 |
| N ₂ | 0.09910 | 0.09886 | 0.09867 | 0.09839 | 0.09767 |
| O | 0.00010 | 0.00014 | 0.00016 | 0.00021 | 0.00036 |
| OH | 0.00262 | 0.00297 | 0.00324 | 0.00364 | 0.00458 |
| O ₂ | 0.00001 | 0.00001 | 0.00002 | 0.00002 | 0.00004 |

Source: From Ref. 5–13.

TABLE 5–9. Calculated Variation of Thermodynamic Properties and Exit Gas Composition for an Aluminized Perchlorate Propellant with $p_1 = 1500$ psia and Various Exit Pressures at Shifting Equilibrium and Optimum Expansion

| | Chamber | Throat | Nozzle Exit |
|---|---------|---------|-------------|
| Pressure (atm) | 102.07 | 58.860 | 0.1276 |
| Pressure (MPa) | 10.556 | 5.964 | 0.0132 |
| Nozzle area ratio | >0.2 | 1.000 | 70.888 |
| Temperature (K) | 3346.9 | 3147.3 | 41.111 |
| Ratio chamber pressure/local pressure | 1.000 | 1.7341 | 1443.1 |
| Molecular mass (kg/mol) | 29.303 | 29.453 | 800.00 |
| Composition (mol %) | | | |
| Al | 0.00007 | 0.00003 | 0.00000 |
| AlCl | 0.00454 | 0.00284 | 0.00008 |
| AlCl ₂ | 0.00181 | 0.00120 | 0.00002 |
| AlCl ₃ | 0.00029 | 0.00023 | 0.00002 |
| AlOCl | 0.00086 | 0.00055 | 0.00001 |
| AlOH | 0.00029 | 0.00016 | 0.00000 |
| AlO ₂ H | 0.00024 | 0.00013 | 0.00000 |
| Al ₂ O | 0.00003 | 0.00001 | 0.00000 |
| Al ₂ O ₃ (solid) | 0.00000 | 0.09955 | 0.09976 |
| Al ₂ O ₃ (liquid) | 0.09425 | 0.09608 | 0.00000 |

| | | | | | | | |
|------------------|----------|---------|---------|---------|---------|---------|---------|
| CO | 0.22434 | 0.22511 | 0.22553 | 0.22416 | 0.22008 | 0.21824 | 0.21671 |
| CO ₂ | 0.00785 | 0.00787 | 0.00994 | 0.01126 | 0.01220 | 0.01548 | 0.01885 |
| Cl | 0.00541 | 0.00441 | 0.00074 | 0.00028 | 0.00009 | 0.00002 | 0.00000 |
| H | 0.02197 | 0.01722 | 0.00258 | 0.00095 | 0.00030 | 0.00007 | 0.00001 |
| HCl | 0.12021 | 0.12505 | 0.13635 | 0.13707 | 0.13734 | 0.13743 | 0.13746 |
| H ₂ | 0.32599 | 0.33067 | 0.34403 | 0.34630 | 0.34842 | 0.35288 | 0.35442 |
| H ₂ O | 0.08960 | 0.08704 | 0.08091 | 0.07967 | 0.07796 | 0.07551 | 0.07214 |
| NO | 0.00019 | 0.00011 | 0.00001 | 0.00000 | 0.00000 | 0.00000 | 0.00000 |
| N ₂ | 0.09910 | 0.09950 | 0.10048 | 0.10058 | 0.10063 | 0.10064 | 0.10065 |
| O | 0.00010 | 0.00005 | 0.00000 | 0.00000 | 0.00000 | 0.00000 | 0.00000 |
| OH | 0.000262 | 0.00172 | 0.00009 | 0.00005 | 0.00002 | 0.00000 | 0.00000 |

Source: From Ref. 5–13.

TABLE 5–10. Typical Gas Characteristics for Fuel-Rich Liquid Propellant Gas Generators

| Propellant | T_1 (K) | k | Gas Constant R (ft-lbf/lbm-°r) | Oxidizer-to-Fuel Ratio | Specific Heat c_p (kcal/kg-K) |
|---|-----------|-------|-----------------------------------|------------------------|------------------------------------|
| Liquid oxygen and liquid hydrogen | 900 | 1.370 | 421 | 0.919 | 1.99 |
| | 1050 | 1.357 | 375 | 1.065 | 1.85 |
| | 1200 | 1.338 | 347 | 1.208 | 1.78 |
| Liquid oxygen and kerosene | 900 | 1.101 | 45.5 | 0.322 | 0.639 |
| | 1050 | 1.127 | 55.3 | 0.423 | 0.654 |
| | 1200 | 1.148 | 64.0 | 0.516 | 0.662 |
| Nitrogen tetroxide and dimethyl hydrazine | 1050 | 1.420 | 87.8 | 0.126 | 0.386 |
| | 1200 | 1.420 | 99.9 | 0.274 | 0.434 |

PROBLEMS

- Explain the physical or chemical reasons for a maximum value of specific impulse at a particular mixture ratio of oxidizer to fuel.
- Explain why, in Table 5–8, the relative proportion of monatomic hydrogen and monatomic oxygen changes markedly with different chamber pressures and exit pressures.
- This chapter contains several charts for the performance of liquid oxygen and RP-1 hydrocarbon fuel. By mistake the next shipment of cryogenic oxidizer contains at least 15% liquid nitrogen. Explain what general trends should be expected in the results of the next test in the performance values, the likely composition of the exhaust gas under chamber and nozzle conditions, and the optimum mixture ratio.
- A mixture of perfect gases consists of 3 kg of carbon monoxide and 1.5 kg of nitrogen at a pressure of 0.1 MPa and a temperature of 298.15 K. Using Table 5–1, find (a) the effective molecular mass of the mixture, (b) its gas constant, (c) specific heat ratio, (d) partial pressures, and (e) density.

Answers: (a) 28 kg/kg-mol, (b) 297 J/kg-K, (c) 1.40, (d) 0.0666 and 0.0333 MPa, (e) 1.13 kg/m³.

- Using information from Table 5–2, plot the value of the specific heat ratio for carbon monoxide (CO) as a function of temperature. Notice the trend of this curve; it is typical of the temperature behavior of other diatomic gases.

Answers: $k = 1.28$ at 3500 K, 1.30 at 2000 K, 1.39 at 500 K.

- Modify and tabulate two entries in Table 5–5 for operation in the vacuum of space, namely oxygen/hydrogen and nitrogen tetroxide/hydrazine. Assume the data in the table represents the design condition.

7. Various experiments have been conducted with a liquid monopropellant called nitromethane (CH_3NO_2), which can be decomposed into gaseous reaction products. Determine the values of T , \mathfrak{M} , k , c^* , C_F , and I_s using the water–gas equilibrium conditions. Assume no dissociations and no O_2 .

Answers: 2470 K, 20.3 kg/kg-mol, 1.25, 2394 m/sec, 1.57, 244 sec.

8. The figures in this chapter show several parameters and gas compositions of liquid oxygen burning with RP-1, which is a kerosene-type material. For a mixture ratio of 2.0, use the compositions to verify the molecular mass in the chamber and the specific impulse (frozen equilibrium flow in nozzle) in Fig. 5–1.

SYMBOLS

(Symbols referring to chemical elements, compounds, or mathematical operators are not included in this list.)

| | |
|----------------|--|
| a | number of kilogram atoms |
| A_t | throat area, m^2 |
| c^* | characteristic velocity, m/sec |
| c_p | specific heat per unit mass, J/kg-K |
| C_p | molar specific heat at constant pressure of gas mixture, J/kg-mol-K |
| g_0 | acceleration of gravity at sea level, 9.8066 m/sec^2 |
| G | Gibbs free energy for a propellant combustion gas mixture, J/kg |
| $\Delta_f G^0$ | change in free energy of formation at 298.15 K and 1 bar |
| G_j | free energy for a particular species j , J/kg |
| ΔH | overall enthalpy change, J/kg or J/kg-mol |
| ΔH_j | enthalpy change for a particular species j , J/kg |
| $\Delta_r H^0$ | heat of reaction at reference 298.15 K and 1 bar, J/kg |
| $\Delta_f H^0$ | heat of formation at reference 298.15 K and 1 bar, J/kg |
| h | enthalpy for a particular species, J/kg or J/kg-mol |
| I_s | specific impulse, sec |
| k | specific heat ratio |
| m | number of gaseous species |
| \dot{m} | mass flow rate, kg/sec |
| \mathfrak{M} | molecular mass (also called molecular weight) of gas mixture, kg/mol |
| n | total number of moles per unit mass (kg-mol/kg) of mixture |
| n_j | moles of species j , kg-mol/kg |
| P | pressure of gas mixture, N/m ² |
| R | gas constant, J/kg-K |
| R' | universal gas constant, 8314.3 J/kg mol-K |
| S | entropy, J/kg mol-K |
| T | absolute temperature, K |
| T_{ad} | adiabatic temperature, K |
| U | internal energy, J/kg-mol |

| | |
|-------|---|
| v | gas velocity, m/sec |
| V | specific volume, m^3/kg |
| X_j | mole fraction of species j |

Greek Letters

| | |
|--------|---------------------------------|
| ρ | density, kg/m^3 |
|--------|---------------------------------|

Subscripts

| | |
|--------|--|
| a, b | molar fractions of reactant species A or B |
| c, d | molar fractions of product species C or D |
| i | atomic species in a specific propellant |
| j | constituents or species in reactants or products |
| mix | mixture of gases |
| ref | at reference condition (also superscript 0) |
| 1 | chamber condition |
| 2 | nozzle exit condition |
| 3 | ambient atmospheric condition |

REFERENCES

- 5–1. F. Van Zeggeren and S. H. Storey, *The Computation of Chemical Equilibria*, Cambridge University Press, Cambridge, 1970.
- 5–2. S. S. Penner, *Thermodynamics for Scientists and Engineers*, Addison-Wesley Publishing, Reading, MA, 1968.
- 5–3. S. I. Sandler, *Chemical and Engineering Thermodynamics*, John Wiley & Sons, New York, 1999.
- 5–4. R. H. Dittman and M. W. Zemansky *Heat and Thermodynamics*, 7th ed., McGraw-Hill Book Company, New York, 1996.
- 5–5. K. Denbigh, *The Principles of Chemical Equilibrium*, 4th ed., Cambridge University Press, Cambridge, 1981.
- 5–6. K. K. Kuo, *Principles of Combustion*, 2nd ed., John Wiley & Sons, Hoboken, NJ, 2005.
- 5–7. *JANAF Thermochemical Tables*, Dow Chemical Company, Midland, MI, Series A (June 1963) through Series E (January 1967).
- 5–8. M. W. Chase, C. A. Davies, J. R. Downey, D. J. Frurip, R. A. McDonald, and A. N. Syverud, *JANAF Thermochemical Tables*, 3rd ed., Part I, *Journal of Physical and Chemical Reference Data*, Vol. 14, Supplement 1, American Chemical Society, American Institute of Physics, and National Bureau of Standards, 1985.

- 5-9. D. D. Wagman et al., "The NBS Tables of Chemical Thermodynamic Properties," *Journal of Physical and Chemical Reference Data*, Vol. 11, Supplement 2, American Chemical Society, American Institute of Physics, and National Bureau of Standards, 1982.
- 5-10. J. B. Pedley, R. D. Naylor, and S. P. Kirby, *Thermochemical Data of Organic Compounds*, 2nd ed., Chapman & Hall, London, 1986.
- 5-11. B. J. McBride, S. Gordon, and M. Reno, "Thermodynamic Data for Fifty Reference Elements," *NASA Technical Paper 3287*, January 1993.
- 5-12. B. J. McBride and S. Gordon, "Computer Program for Calculating and Fitting Thermodynamic Functions," *NASA Reference Publication 1271*, November 1992.
- 5-13. S. Gordon and B. J. McBride, "Computer Program for Calculation of Complex Chemical Equilibrium Compositions and Applications, Vol. 1: Analysis" (October 1994) and "Vol. 2: User Manual and Program Description" (June 1996), *NASA Reference Publication 1311*.
- 5-14. S. Gordon and B. J. McBride, "Finite Area Combustor Theoretical Rocket Performance," *NASA TM 100785*, April 1988.

CHAPTER 6

LIQUID PROPELLANT ROCKET ENGINE FUNDAMENTALS

This chapter gives an overview of liquid propellant rocket engines. It is the first of six chapters devoted to this subject. It identifies the types of liquid rocket engines, their key components, different propellants, and tank configurations. It also discusses two types of feed systems, engine cycles, propellant tanks, their pressurization subsystems, engine controls, valves, piping, and structure. Chapter 7 covers liquid propellants in more detail. Chapter 8 describes thrust chambers (and their nozzles), small thrusters, and heat transfer. Chapter 9 is about the combustion process and Chapter 10 discusses turbopumps. Chapter 11 discusses engine design, engine controls, propellant budgets, engine balance and calibration, and overall engine systems.

In this book a *liquid propellant rocket propulsion system* consist of a *rocket engine* and a set of *tanks* for storing and supplying propellants. It has all the hardware components and the propellants necessary for its operation, that is, for producing thrust. See Refs. 6–1 and 6–2. They are described in this chapter. A *rocket engine* consists of one or more *thrust chambers*, a *feed mechanism* for feeding the propellants from their tanks into the thrust chamber(s), a *power source* to furnish the energy for the feed mechanism, suitable *plumbing* or *piping* to transfer the liquid propellants, a *structure* to transmit the thrust force, and *control devices* (including valves) to start and stop and sometimes also vary the propellant flow and thus the thrust. Propellants are either pushed out of their tanks by high-pressure gas or they are pumped by pumps to the thrust chambers. Figure 6–1 shows the Space Shuttle main engine, a large sophisticated high-performance liquid propellant rocket engine. The index lists the pages where information on the Space Shuttle, its main rocket engine, and various components can be found.

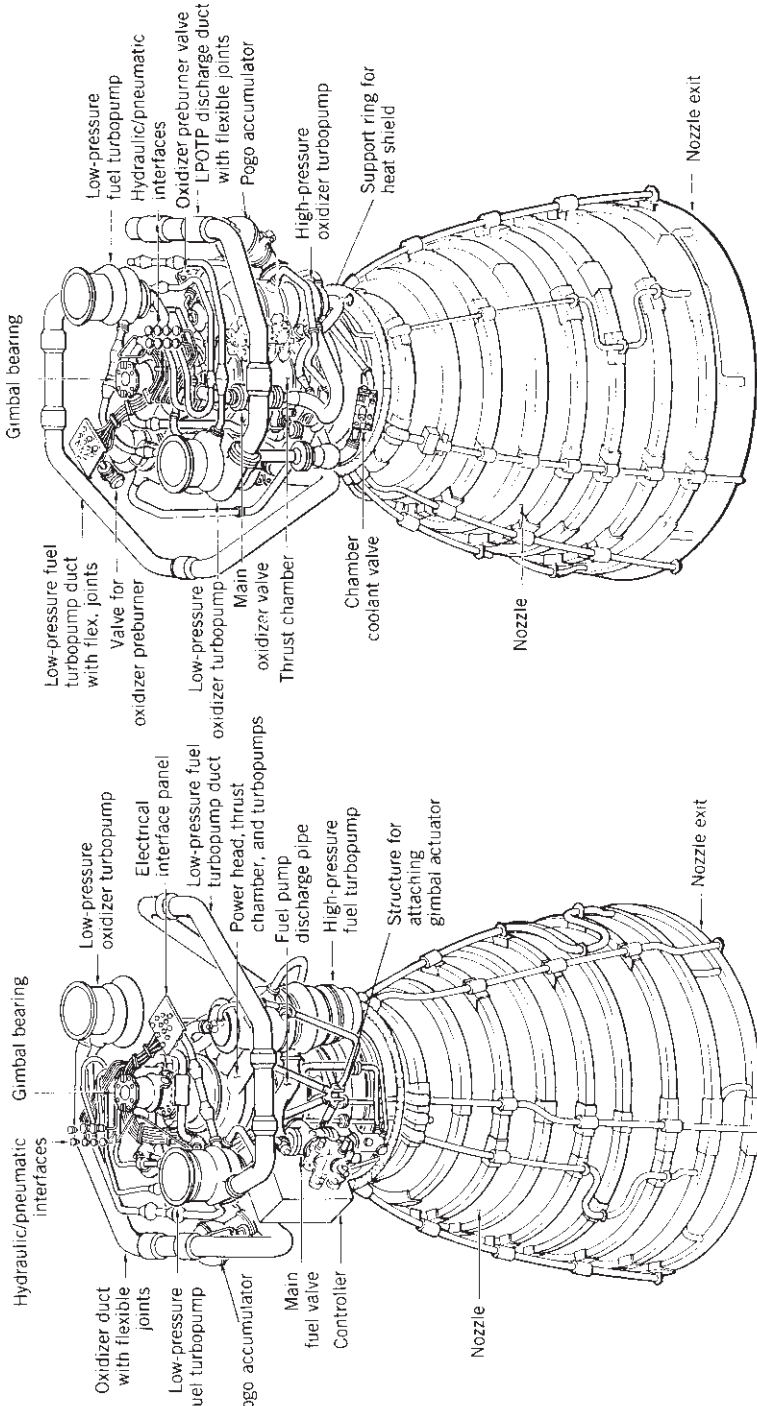


FIGURE 6-1. Two views of the Space Shuttle Main Engine (SSME). Its flowsheet is in Figure 6-12 and some component data are in Chapter 10. (Courtesy of Pratt & Whitney Rocketdyne and NASA.)

In some applications rocket engines may also include a *thrust vector control* system (explained in Chapter 18), a random *variable thrust* feature (see Section 8.5), an engine *condition monitoring* or engine *health monitoring* subsystem (see Section 11.4), and various *instrumentation/measuring* devices (see Chapter 21). The *tanks*, which store the propellants, and the subsystem for *pressurizing the tanks with gas* are in this chapter and are considered in this book to be part of the *rocket propulsion system*.*

The design of any propulsion system is tailored to fit a specific *mission requirement* as explained in Chapter 19. These requirements are usually stated in terms of the application, such as anti-aircraft missile or second stage of a space launch vehicle, flight velocity increment, flight path and flight maneuvers, launch sites, minimum life (in storage or in orbit), or number of vehicles to be delivered. The requirement usually include constraints of the inert engine weight, cost, or safety provisions. Other criteria, constraints and the selection process are in Chapter 19.

From the *mission requirements* and *definition* one can derive the *propulsion system* and the *engine requirements*, which include the thrust–time profile, the minimum specific impulse, number of thrust chambers, total impulse, number of restarts, if any, likely propellants, or constraints of engine masses or engine sizes. Some engine parameters, such as thrust, chamber pressure, mixture ratio, or nozzle exit area ratio, can be analytically optimized for a specific mission. Other engine parameters can be selected based on experience and/or design studies, including the feed system, the arrangement of the engine components, engine cycle, thrust modulation, or alternate methods of thrust vector control. Two or more preliminary or conceptual designs can be compared with the objective of arriving at a selected propulsion design for the mission.

Tables 1–3, 11–2, and 11–3 give typical data for selected rocket engines. Many different types of rocket engines have been studied, built, and flown, ranging in thrust size from less than 0.01 lbf to over 1.75 million pounds, with one-time operation or multiple starts (some have over 150,000 restarts), with or without thrust modulation (called throttling), single use or reusable, arranged as single engines, or in clusters of multiple units.

One way to categorize liquid propellant rocket engines is described in Table 6–1. There are two categories, namely those used for *boosting* a payload and imparting a significant velocity increase to a payload and *auxiliary propulsion* for *trajectory adjustments* and *attitude control*. Liquid propellant

*The responsibilities for the design, development, fabrication, and operation of a propulsion system are usually shared between a rocket engine organization and a flight vehicle organization. However, the allocations of the responsibilities for components or subsystems have not been rigid or consistent in the literature and in actual industry practice. For example, some vehicle design/development organizations have considered the tanks and parts of the engine structure to be really a part of their vehicle. The tank pressurization system has in various scenarios been considered to be part of either the engine, the propulsion system, or the vehicle. For some reaction control systems the vehicle developer often assumed the responsibility for the propulsion systems and obtained only the small thrusters and their small propellant valves from a rocket engine company. In some programs, such as the peacekeeper missile fourth stage, the rocket engine developer has developed not only the engine, but also much of the vehicle stage with its propellant tanks and pressurization system.

TABLE 6–1. Characteristics of Two Categories of Liquid Propellant Rocket Engines

| Purpose | Boost Propulsion | Auxiliary Propulsion |
|--|---|--|
| Mission | Impart significant velocity to propel a vehicle along its flight path | Attitude control, minor space maneuvers, trajectory corrections, orbit maintenance |
| Applications | Booster stage and upper stages of launch vehicles, large missiles | Spacecraft, satellites, top stage of antiballistic missile, space rendezvous |
| Total impulse | High | Low |
| Number of thrust chambers per engine | Usually 1; sometimes 4, 3, or 2 | Between 4 and 24 |
| Thrust level | High; 4500 N up to 7,900,000 N or 1000–1,770,000 lbf | Small; 0.001 up to 4500 N, a few go up to 1000 lbf |
| Feed system, typical | Mostly turbopump type; occasionally pressurized feed system for smaller thrusts | Pressurized feed system with high-pressure gas supply |
| Tank pressure range | 0.138–0.379 MPa or 20–55 psi | 0.689–17.23 MPa or 100–2500 psi |
| Most common cooling method | Propellant cooled | Radiation cooled |
| Propellants (see next section) | Cryogenic and storable liquids | Storable liquids, monopropellants, and/or stored cold gas |
| Chamber pressure | 2.4–21 MPa or 350–3600 psi | 0.14–2.1 MPa or 20–300 psi |
| Number of starts during a single mission | Usually no restart; sometimes one, but up to four in some cases | Several thousand starts are typical for small thrusters |
| Cumulative duration of firing | Up to a few minutes | Up to several hours |
| Shortest firing duration | Typically 5–40 sec | 0.02 sec typical for small thrusters |
| Time elapsed to reach full thrust | Up to several seconds | Usually very fast, 0.004–0.080 sec |
| Life in space | Hours, days, or months | 10 years or more in space |

rocket engine systems can be *classified* in several other ways. They can be *reusable* (like the Space Shuttle main engine or a rocket engine for quick ascent or maneuvers of fighter aircraft) or suitable for a *single flight* only (as the engines in other launch vehicles), and they can be *restartable*, like a reaction control engine, or *single firing*, as in space launch vehicle boosters. They can also be categorized by their *propellants*, *application*, or *stage*, such as an upper stage or booster stage, their *thrust level*, and by the *feed system type* (*pressurized* or *turbopump*).

The *thrust chamber* or *thruster* is the combustion device where the liquid propellants are metered, injected, atomized, mixed, and burned to form hot gaseous reaction products, which in turn are accelerated and ejected at a high velocity to impart a thrust force. A thrust chamber has three major parts: an *injector*, a *combustion chamber*, and a *nozzle*. In a *cooled thrust chamber*, one of the propellants (usually the fuel) is circulated through cooling jackets or a special cooling passage to absorb the heat that is transferred from the hot reaction gases to the thrust chamber walls (see Figs. 8–2 and 8–9). A *radiation-cooled* thrust chamber uses a special high-temperature material, such as niobium metal, which can radiate away its excess heat. There are *uncooled* or *heat-absorbing* thrust chambers, such as those using *ablative* materials. Thrust chambers are discussed in Chapter 8.

There are two types of feed systems used for liquid propellant rocket engines: those that use pumps for moving the propellants from their flight vehicle tanks to the thrust chamber and those that use high-pressure gas for expelling or displacing their propellants from their tanks. They are discussed further in Chapter 10 and in Section 6.3.

Tables 19–1 to 19–4 compare the advantages and disadvantages of liquid propellant rocket engines and solid propellant rocket motors.

6.1. TYPES OF PROPELLANTS

The liquid propellants, which are the working substance of rocket engines, constitute the fluid that undergoes chemical and thermodynamic changes. The term *liquid propellant* embraces all the various liquids used and may be one of the following:

1. Oxidizer (liquid oxygen, nitric acid, nitrogen tetroxide, etc.)
2. Fuel (kerosene, alcohol, liquid hydrogen, etc.)
3. Chemical compound or mixture of oxidizer and fuel ingredients, capable of self-decomposition, such as hydrazine
4. Any of the above, but with a gelling agent. Used only rarely.

All are described in Chapter 7.

A *bipropellant* has two separate liquid propellants, an oxidizer and a fuel. They are the most common type. They are stored separately and are not mixed outside the combustion chamber. A *hypergolic* bipropellant combination is *self-igniting* upon contact between the oxidizer and the fuel. A *nonhypergolic* bipropellant combination needs energy to start its combustion (e.g., heat or electric discharge) and its engine needs an ignition system.

A *monopropellant* contains an oxidizing agent and combustible matter in a single substance. It may be a mixture of several compounds or it may be a homogeneous material, such as hydrogen peroxide or hydrazine. Monopropellants are stable at ordinary atmospheric conditions but decompose and yield hot combustion gases when heated or catalyzed.

A *cold gas propellant* (e.g., gaseous nitrogen or air) is stored at ambient temperature but at very high pressure, gives a low performance, allows a simple system, and is usually very reliable. It has been used for roll control and attitude control.

A *cryogenic propellant* is liquified gas at low temperature, such as liquid oxygen (-183°C) or liquid hydrogen (-253°C). Provisions for venting the storage tank and minimizing vaporization losses are necessary with this type.

Storable propellants (e.g., nitric acid or gasoline) are liquid at ambient temperature and at modest pressure and can be stored for long periods in sealed tanks. *Space-storable propellants* are liquid in the environment of space; this storability depends on the specific tank design, thermal conditions, and tank pressure. An example is ammonia.

A *gelled propellant* is a thixotropic liquid with a gelling additive. It behaves like a jelly or thick paint. It will not spill or leak readily, can flow under pressure, will burn, and is safer in some respects. It is described at the end of Chapter 7. Gelled propellants have been used in a few experimental rocket engines.

A *hybrid propellant* usually has a liquid oxidizer and a solid fuel. It is discussed in Chapter 16.

The propellant *mixture ratio* for a bipropellant is the ratio at which the oxidizer and fuel are mixed and react to give hot gases. The mixture ratio r is defined as the ratio of the oxidizer mass flow rate \dot{m}_o and the fuel mass flow rate \dot{m}_f or

$$r = \dot{m}_o / \dot{m}_f \quad (6-1)$$

As explained in Chapter 5 the mixture ratio defines the composition and temperature of the combustion or reaction products. It is usually chosen to give a maximum value of specific impulse or T_1/\mathfrak{M} , where T_1 is the absolute combustion temperature and \mathfrak{M} is the average molecular mass of the reaction gases (see Eq. 3-16 or Fig. 3-2). For a given thrust F and a given effective exhaust velocity c , the total propellant flow is given by Eq. 2-6; namely, $\dot{m} = \dot{w}/g_0 = F/c$. The relationships between r , \dot{m} , \dot{m}_o , and \dot{m}_f are

$$\dot{m}_o + \dot{m}_f = \dot{m} \quad (6-2)$$

$$\dot{m}_o = r\dot{m}/(r + 1) \quad (6-3)$$

$$\dot{m}_f = \dot{m}/(r + 1) \quad (6-4)$$

These same four equations are valid when w and \dot{w} (weight and weight flow rate) are substituted for m and \dot{m} . Calculated performance values for a number

of different propellant combinations are given for specific mixture ratios in Table 5–5. Physical properties and a discussion of several common liquid propellants and their safety concerns are described in Chapter 7.

Example 6–1. A liquid oxygen–liquid hydrogen rocket thrust chamber of 10,000-lbf thrust operates at a chamber pressure of 1000 psia, a mixture ratio of 3.40, has exhaust products with a mean molecular mass of 8.90 lbm/lb-mol, a combustion temperature of 4380°F, and a specific heat ratio of 1.26. Determine the nozzle throat area, nozzle exit area for optimum operation at an altitude where $p_3 = p_2 = 1.58$ psia, the propellant weight and volume flow rates, and the total propellant requirements for 2.5 min of operation. Assume that the actual specific impulse is 97% of the theoretical value and that the thrust coefficient is 98% of ideal value for this problem.

SOLUTION. The exhaust velocity for an optimum nozzle is determined from Eq. 3–16, but with a correction factor of g_0 for the foot-pound system:

$$\begin{aligned} v_2 &= \sqrt{\frac{2g_0 k}{k-1} \frac{R' T_1}{\mathfrak{M}} \left[1 - \left(\frac{p_2}{p_1} \right)^{(k-1)/k} \right]} \\ &= \sqrt{\frac{2 \times 32.2 \times 1.26}{0.26} \frac{1544 \times 4840}{8.9} (1 - 0.00158^{0.205})} = 13,890 \text{ ft/sec} \end{aligned}$$

The theoretical specific impulse is c/g_0 , or in this optimum expansion case v_2/g_0 or $13,890/32.2 = 431$ sec. The actual specific impulse is $0.97 \times 431 = 418$ sec. The theoretical or ideal thrust coefficient can be found from Eq. 3–30 or from Fig. 3–6 ($p_2 = p_3$) and for a pressure ratio $p_1/p_2 = 633$ to be $C_F = 1.76$. The actual thrust coefficient is slightly less, say 98% or $C_F = 1.72$. The throat area required is found from Eq. 3–31.

$$A_t = F/(C_F p_1) = 10,000/(1.72 \times 1000) = 5.80 \text{ in.}^2 \quad (\text{2.71 in. diameter})$$

The optimum area ratio can be found from Eq. 3–25 or Fig. 3–5 to be 42. The exit area is $5.80 \times 42 = 244 \text{ in.}^2$ (17.6 in. diameter). The weight density of oxygen is 71.1 lbf/ft^3 and of hydrogen is 4.4 lbf/ft^3 . The propellant weight flow rates (Eqs. 2–5, 6–3, and 6–4) are

$$\dot{w} = F/I_s = 10,000/418 = 24.0 \text{ lbf/sec}$$

$$\dot{w}_o = \dot{w} r / (r + 1) = 24.0 \times 3.40 / 4.40 = 18.55 \text{ lbf/sec}$$

$$\dot{w}_f = \dot{w} / (r + 1) = 24 / 4.40 = 5.45 \text{ lbf/sec}$$

The volume flow rates are determined from the densities and the weight flow rates:

$$\dot{V}_o = \dot{w}_o / \rho_o = 18.55 / 71.1 = 0.261 \text{ ft}^3/\text{sec}$$

$$\dot{V}_f = \dot{w}_f / \rho_f = 5.45 / 4.4 = 1.24 \text{ ft}^3/\text{sec}$$

For 150 sec of operations (arbitrarily allow the equivalent of two additional seconds for start and stop transients and unavailable residual propellant), the weight and volume of required propellant are

$$w_o = 18.55 \times 152 = 2820 \text{ lbf of oxygen}$$

$$w_f = 5.45 \times 152 = 828 \text{ lbf of hydrogen}$$

$$V_o = 0.261 \times 152 = 39.7 \text{ ft}^3 \text{ of oxygen}$$

$$V_f = 1.24 \times 152 = 188.5 \text{ ft}^3 \text{ of hydrogen}$$

Note that, with the low-density fuel, the volume flow rate and therefore the tank volume of hydrogen are 5 times as large compared to the oxidizer. Hydrogen is unique and in its liquid state has a very low density.

6.2. PROPELLANT TANKS

In liquid bipropellant rocket engine systems the propellants are usually stored in an oxidizer tank and a fuel tank within the flying vehicle. Monopropellant rocket engine systems have, of course, only one propellant tank. There are usually also one or more high-pressure gas tanks, the gas being used to pressurize the propellant tanks. However, as will be discussed in Section 6.5, there are tank pressurization schemes using heated gas from the engine without the need for a high-pressure heavy gas storage tank. Tanks can be arranged in a variety of ways, and the tank design, shape, and location can be used to exercise some control over the change in the location of the vehicle's center of gravity. Typical arrangements are shown in Fig. 6-2. Because the propellant tank has to fly, its mass is at a premium and the tank material is therefore highly stressed. Common tank materials are aluminum, stainless steel, titanium, alloy steel, and fiber-reinforced plastics with an impervious thin inner liner of metal to prevent leakage through the pores of the fiber-reinforced walls. Chapter 8 of Ref. 6-1 describes the design of propellant tanks.

The extra volume of gas above the propellant in sealed tanks is called *ullage*. It is necessary space that allows for thermal expansion of the propellant liquids, for the accumulation of gases that were originally dissolved in the propellant, or for gaseous products from slow reactions within the propellant during storage. Depending on the storage temperature range, the propellants' coefficient of thermal expansion, and the particular application, the ullage volume is usually between 3 and 10% of the tank volume. Once propellant is loaded into a tank, the ullage volume (and, if it is sealed, also its pressure) will change as the bulk temperature of the propellant varies.

The *expulsion efficiency* of a tank and/or propellant piping system is the amount of propellant expelled or available for propulsion divided by the total amount of propellant initially present. Typical values are 97 to 99.7%. The losses

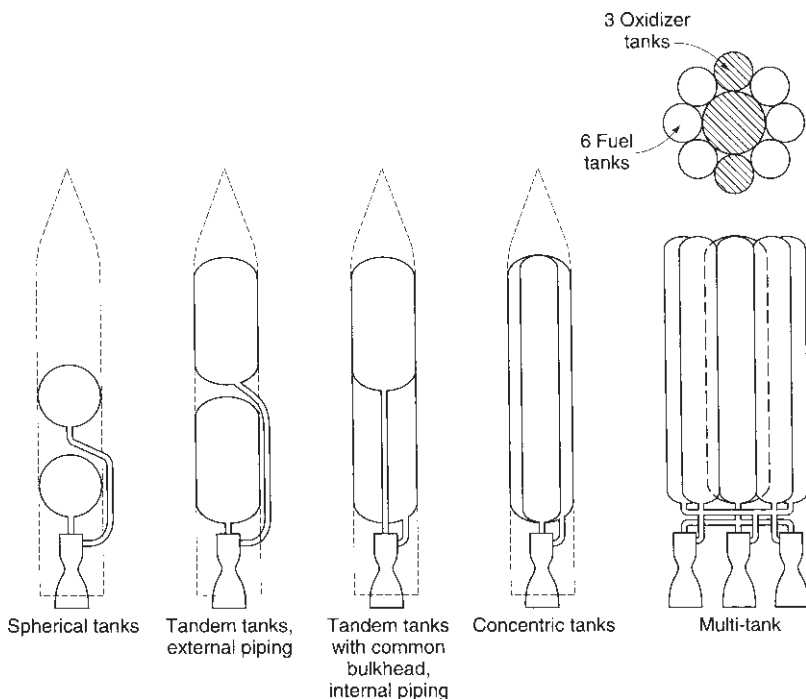


FIGURE 6–2. Simplified sketches of typical tank arrangements for large turbopump-fed liquid propellant rocket engines.

are unavailable propellants that are trapped in grooves or corners of pipes, fittings, and valves, are wetting the walls, retained by surface tension, or caught in instrument taps. This *residual propellant* is not available for combustion and must be treated as inert mass, causing the vehicle mass ratio to decrease slightly. In the design of tanks and piping systems, an effort is made to minimize the residual propellant.

The optimum shape of a propellant tank (and also a gas pressurizing tank) is spherical because for a given volume it results in a tank with the least weight. Small spherical tanks are often used with reaction control engine systems, where they can be packaged with other vehicle equipment. Unfortunately, the larger spheres, which are needed for the principal propulsion systems, are not very efficient for using the space in a flight vehicle. These larger tanks are often made integral with the vehicle fuselage or wing. Most are cylindrical with half ellipses at the ends, but they can be irregular in shape. A more detailed discussion of tank pressurization is given in Section 6.5.

Cryogenic propellants cool the tank wall temperature far below the ambient air temperature. This causes condensation of moisture from the air on the outside of the tank and usually also formation of ice during the period prior to launch. The ice is undesirable because it increases the vehicle inert mass. Also, as pieces

of ice are shaken off or break off during the initial flight, these pieces can damage the vehicle; for example, the ice from the Shuttle's cryogenic tank can hit the orbiter vehicle.

For an extended storage period, cryogenic tanks are usually thermally insulated; porous external insulation layers have to be sealed to prevent moisture from being condensed inside the insulation layer. With liquid hydrogen it is possible to liquify or solidify the ambient air on the outside of the fuel tank. Even with heavy insulation and low-conductivity structural tank supports, it is not possible to prevent the continuous evaporation of the cryogenic fluid. Even with good thermal insulation, all cryogenic propellants evaporate slowly during storage and therefore cannot be kept in a vehicle for more than perhaps a week without refilling of the tanks. For vehicles that need to be stored or to operate for longer periods, a storable propellant combination is preferred.

Prior to loading very cold cryogenic propellant into a flight tank, it is necessary to remove or evacuate the air to avoid forming solid air particles or condensing any moisture as ice. These frozen particles would plug up injection holes, cause valves to freeze shut, or prevent valves from being fully closed. Tanks, piping, and valves need to be chilled or cooled down before they can contain cryogenic liquid without excessive bubbling. This is usually done by letting an initial amount of cryogenic liquid absorb the heat from the relatively warm hardware prior to engine start. This initial cool-down propellant is vaporized and vented through appropriate vent valves and cannot be used for propulsion.

If the tank or any segment of piping containing low-temperature cryogenic liquid is sealed for an extended period of time, heat from ambient-temperature hardware will result in evaporation, and this will greatly raise the pressure until it exceeds the strength of the container (see Ref. 6-3). Controlled self-pressurization can be difficult to achieve. Uncontrolled self-pressurization will cause a failure, usually a major leak or even a tank explosion. All cryogenic tanks and piping systems are therefore vented during storage on the launch pad, equipped with pressure safety devices (such as burst diaphragms or relief valves), and the evaporated propellant is allowed to escape from its container. For long-term storage of cryogenic propellants in space vacuum (or on the ground) some form of a powered refrigeration system is needed to recondense the vapors and minimize evaporation losses. The tanks are usually refilled or topped off just before launch to replace the evaporated and vented cool-down propellant. When the tank is pressurized, just before launch, the boiling point is usually raised slightly and the cryogenic liquid can usually absorb the heat transferred to it during the several minutes of rocket firing.

There are several categories of tanks in liquid propellant propulsion systems. There are a few exceptions to the pressure values listed below.

1. For *pressurized feed systems* the *propellant tanks* typically operate at an average pressure between 1.3 and 9 MPa or about 200 to 1800 lbf/in.² These tanks have thick walls and are heavy.

2. For *high-pressure gas* (used to expel the propellants) the tank pressures are much higher, typically between 6.9 and 69 MPa or 1000 to 10,000 lbf/in.². These tanks are usually spherical for minimum inert mass. Several small spherical tanks can be connected together, and then they are relatively easy to place within the confined space of a vehicle.
3. For *turbopump feed systems* it is necessary to pressurize the propellant tanks slightly (to suppress pump cavitation as explained in Sections 10.3 and 10.4) to average values of between 0.07 and 0.34 MPa or 10 to 50 lbf/in². These low pressures allow thin tank walls, and therefore turbopump feed systems have relatively low inert tank weights.

Liquid propellant tanks can be difficult to empty under side accelerations, zero-*g*, or negative-*g* conditions during flight. Special devices and special types of tanks are needed to operate under these conditions. Some of the effects that have to be overcome are described below.

The oscillations and side accelerations of vehicles in flight can cause *sloshing* of the liquid in the tank, very similar to a glass of water that is being jiggled. In an anti-aircraft missile, for example, the side accelerations can be large and can initiate severe sloshing. Typical analysis of sloshing can be found in Refs. 6–4 and 6–5. When the tank is partly empty, sloshing can uncover the tank outlet and allow gas bubbles to enter into the propellant discharge line. These bubbles can cause major combustion problems in the thrust chambers; the aspirating of bubbles or the uncovering of tank outlets by liquids therefore needs to be avoided. Sloshing also causes shifts in the vehicle's center of gravity and makes flight control difficult.

Vortexing can also allow gas to enter the tank outlet pipe; this phenomenon is similar to the Coriolis force effects in bath tubs being emptied and can be augmented if the vehicle spins or rotates in flight. Typically, a series of internal baffles is often used to reduce the magnitude of sloshing and vortexing in tanks with modest side accelerations. A positive expulsion mechanism can prevent gas from entering the propellant piping under multidirectional major accelerations or spinning (centrifugal) acceleration. Both the vortexing and sloshing can also greatly increase the unavailable or residual propellant, and thus cause a reduction in vehicle performance.

In the gravity-free environment of space, the stored liquid will float around in a partly emptied tank and may not always cover the tank outlet, thus allowing gas to enter the tank outlet or discharge pipe. Figure 6–3 shows that gas bubbles have no orientation. Various devices have been developed to solve this problem: namely, *positive expulsion devices* and *surface tension devices*. The positive expulsion tank design includes movable pistons, inflatable flexible bladders, or thin movable, flexible metal diaphragms. Surface tension devices rely on surface tension forces to keep the outlet covered with liquid.

Several basic types of *positive expulsion devices* have been used successfully in propellant tanks of pressurized feed systems. They are compared in Table 6–2

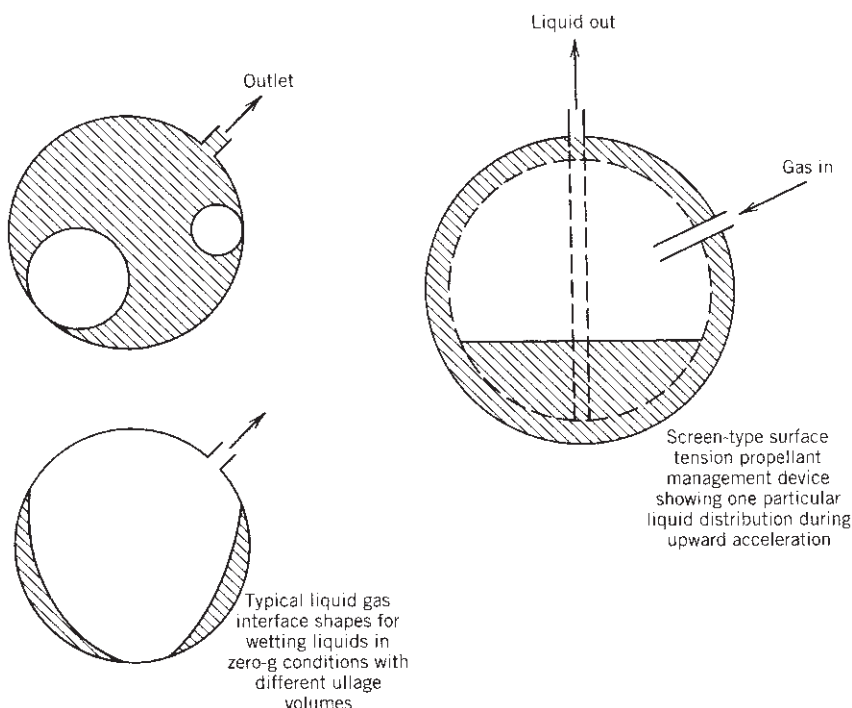


FIGURE 6–3. Ullage bubbles can float around in a zero-gravity environment; surface tension device can keep tank outlet covered with liquid.

and shown in Fig. 6–4 for simple tanks. These devices mechanically separate the pressurizing gas from the liquid propellant in the propellant tank. Separation is useful for these reasons:

1. It prevents pressurizing gas from dissolving in the propellant and propellant from evaporating. Dissolved pressurizing gas dilutes the propellant, reduces its density as well as its specific impulse, and makes the pressurization inefficient.
2. It allows moderately hot and reactive gases (such as gas generated by gas generators) to be used for pressurization, and this permits a reduction in pressurizing system mass and volume. The mechanical separation prevents a chemical reaction between the hot gas and the propellant, prevents gas from being dissolved in the propellant, and reduces the heat transfer to the liquid.
3. In some cases tanks containing toxic propellant must be vented without spilling any toxic liquid propellant or its vapor. For example, in servicing a reusable rocket, the tank pressure needs to be relieved without venting or spilling potentially hazardous material.

TABLE 6-2. Comparison of Propellant Expulsion Methods for Spacecraft Hydrazine Tanks

| | | Positive Expulsion Devices | | | | | |
|------------------------------|------------------------|--|---|---|--|------------------------------|-------------------------|
| Selection Criteria | Application history | Single | Inflatable Dual | Foldable | Piston or Bellows | Rolling Diaphragm | Surface Tension Screens |
| | | Elastomeric Diaphragm (Hemispherical) | Elastomeric Bladder (Spherical) | Diaphragm (Hemispherical) | | | |
| Weight (normalized) | 1.0 | | 1.1 | 1.25 | | 1.0 | 0.9 |
| Expulsion efficiency | Excellent | Very good | Good | Excellent | Very good | Good | Good or fair |
| Maximum side acceleration | Low | Low | Medium | High | Medium | | Lowest |
| Control of center of gravity | Poor | Limited | Good | Excellent | Good | Poor | |
| Long service life | Excellent | Excellent | Excellent | Very good | Good | Excellent | |
| Preflight check | Leak test | Leak test | Leak test | Leak test | Leak test | None | |
| Dissadvantages | Chemical deterioration | Chemical deterioration; fits only into a few tank geometries | High-pressure drop; fits only into a certain tank geometries; high weight | Potential seal failure; critical tolerances on piston seal; heavy | Weld inspection is difficult; adhesive (for bonding to wall) can deteriorate | Limited to low accelerations | |

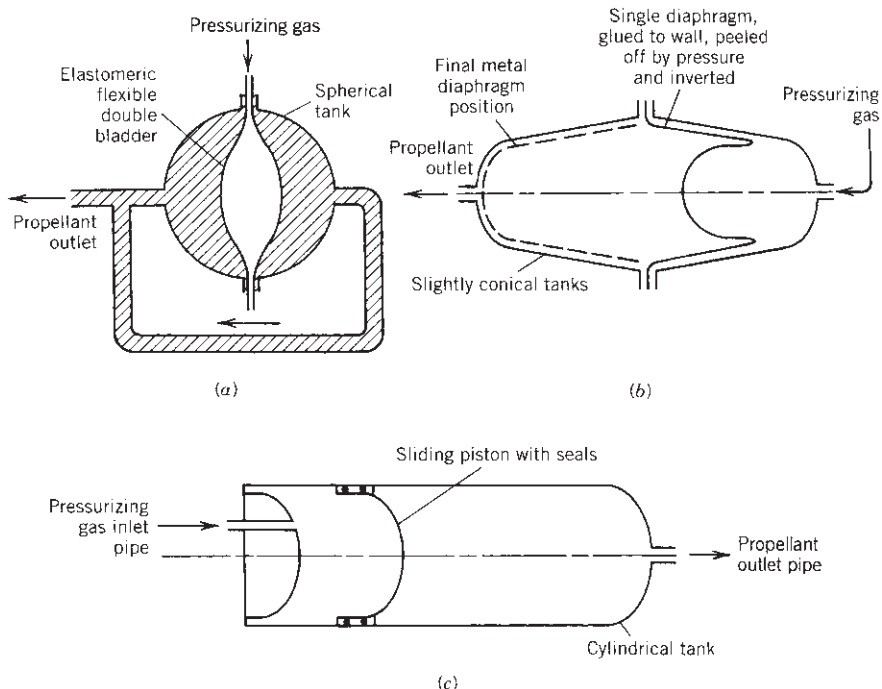


FIGURE 6–4. Three concepts of propellant tanks with positive expulsion: (a) inflatable dual bladder; (b) rolling, peeling diaphragm; (c) sliding piston. As the propellant volume expands or contracts with changes in ambient temperature, the piston or diaphragm will also move slightly and the ullage volume will change during storage.

A *piston expulsion* device permits the center of gravity (CG) to be accurately controlled and its location to be known during the engine operation. This is important in rockets with high side accelerations such as anti-aircraft missiles or space defense missiles, where the thrust vector needs to go through the vehicle's CG; if the CG is not well known, unpredictable turning moments may be imposed on the vehicle. A piston also prevents sloshing or vortexing.

Surface tension devices use capillary attraction for supplying liquid propellant to the tank outlet pipe. These devices (see Fig. 6–3) are often made of very fine (300 mesh) stainless steel wire woven into a screen and formed into tunnels or other shapes (see Refs. 6–6 and 6–7). These screens are located near the tank outlet and, in some tanks, the tubular galleries are designed to connect various parts of the tank volume to the outlet pipe sump. These devices work best in a relatively low-acceleration environment, when surface tension forces can overcome the inertia forces.

The combination of surface tension screens, baffles, sumps, and traps is called a *propellant management device*. Although not shown in any detail, they are included inside the propellant tanks of Figs. 6–3 and 6–13.

High forces can be imposed on the tanks and thus on the vehicle by strong sloshing motions of the liquid and also by sudden changes in position of liquid mass in a partly empty tank during a gravity-free flight when suddenly accelerated by a relatively large thrust. These forces can be large and can cause tank failure. The forces will depend on the tank geometry, baffles, ullage volume, and its initial location and the acceleration magnitude and direction.

6.3. PROPELLANT FEED SYSTEMS

The propellant feed system has two principal functions: to raise the pressure of the propellants and to feed them at predicted mass flow rates to one or more thrust chambers. The energy for these functions comes either from a high-pressure gas, centrifugal pumps, or a combination of the two. The selection of a particular feed system and its components is governed primarily by the application of the rocket, the requirements mentioned at the beginning of this chapter, duration, number or type of thrust chambers, past experience, mission, and by general requirements of simplicity of design, ease of manufacture, low cost, and minimum inert mass. A classification of several of the more important types of feed system is shown in Fig. 6–5, and some are discussed in more detail in other parts of this book. All feed systems have piping, a series of valves, provisions for filling and usually also

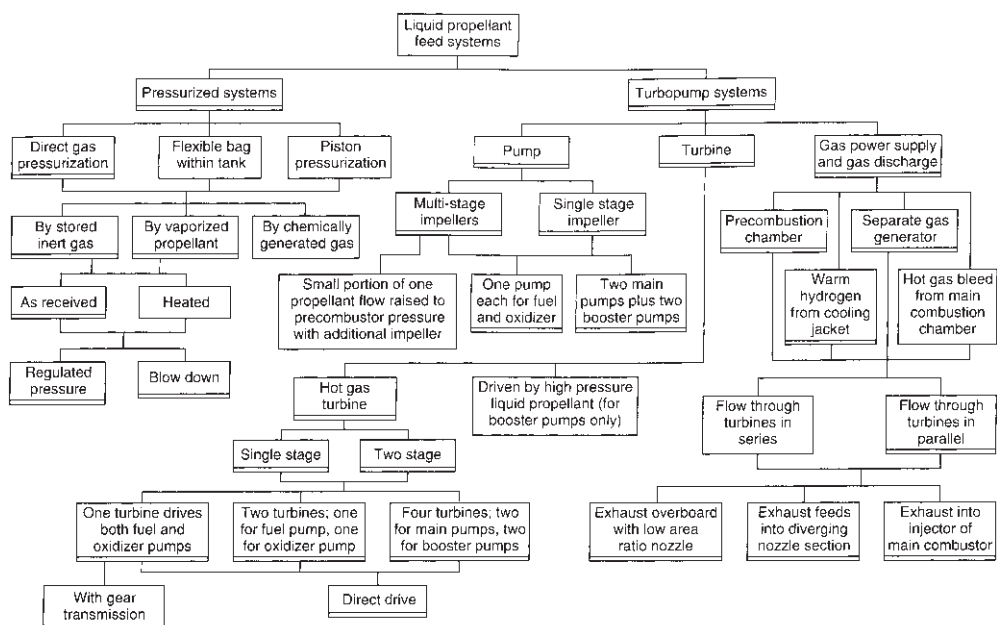


FIGURE 6–5. Design options of feed systems for liquid propellant rocket engines. The more common types are designated with a double line at the bottom of the box.

for removing (draining and flushing) the liquid propellants, and control devices to initiate, stop, and regulate their flow and operation. See Ref. 6-1.

In general, a *gas pressure feed system* gives a vehicle performance superior to a turbopump system when the total impulse or the mass of propellant is relatively low, the chamber pressure is low, the engine thrust-to-weight ratio is low (usually less than 0.6), and when there are repeated short-duration thrust pulses; the heavy-walled tanks for the propellant and the pressurizing gas usually constitute the major inert mass of the engine system. In a *turbopump feed system* the propellant tank pressures are much lower (by a factor of 10 to 40) and thus the vehicle's tank masses are much lower (again by a factor of 10 to 40). Turbopump systems usually give a superior vehicle performance when the total impulse is large (higher Δu) and the chamber pressure is higher.

Local Pressures and Flows

Key parameters of any feed system and any liquid propellant rocket engine are the flow magnitudes and the local pressures of the pressurizing gas subsystem, the oxidizer, and the fuel flow subsystem including the flow passages of thrust chambers. An inspection of the flow diagram of a relatively simple rocket engine with a pressurized feed system, similar to Fig. 1-3, shows that the gas flow splits into two branches, and the propellant flow splits into pipes leading to each of the thrust chambers. The highest pressure is in the high-pressure gas supply tank. The pressure drops in the pressurizing gas subsystem (pipes, valves, regulator) and then drops further in the liquid propellant flow subsystems (more pipes, valves, filters, injector, or cooling jacket) and the flows go into the thrust chamber, where the propellants burn at chamber pressure. The pressure reaches a minimum at the nozzle exit. If enough information is known about the geometric details and functions of the components and their flow passages, then it has been possible to use computer programs to obtain these pressure drops and flow distributions. If this analysis can be validated by data from previous pertinent tests, it will be more useful. Many rocket engine design organizations have developed their own computer programs for estimating pressures and flows in different parts of an engine.

Analyzing and knowing the local branch flows and local pressures is important for the following reasons:

1. They are used in the *stress analysis* and sometimes in the thermal analysis of components and subsystems.
2. They are needed in the *calibration of the rocket engine*, so that this engine will operate at the intended mixture ratio, chamber pressure, or thrust. This is accomplished by using control devices or simple orifices to adjust the pressures. This calibration also requires the proper balance of flows and pressures. For a feed system with one or more turbopumps, such as the one in Fig. 1-4, one needs to also include the rise in pressure as propellants flow through a pump. Furthermore there is another combustion

device (gas generator or preburner) or alternatively the evaporation of a cryogenic propellant in a cooling jacket, and this makes the feed system with turbopumps more complex. A more detailed discussion of engine calibration is given in Section 11.5.

3. Measuring the actual flows and several key local pressures during engine ground tests or actual flight operation and then comparing these actual values with the calculated or predicted values makes it possible to identify discrepancies between practice and theory. Such discrepancies give clues to possible malfunction, inadequate design, or poor fabrication, which can then be identified and probably corrected. If the real measured values can be compared with the analysis values in real time, some experimental test hardware can be saved from self-destruction. This can be the basis for a real-time engine health monitoring system, which is discussed in Section 11.4.

Some of the analyses are aimed at transient conditions, such as during the start period, the shutdown period, or the change in thrust value (throttling). These transient analyses provide for the filling of empty propellant passages with propellant, for different propellant temperatures, water hammer, valve reaction time, and the like.

6.4. GAS PRESSURE FEED SYSTEMS

One of the simplest and most common means of pressurizing the liquid propellants is to force them out of their respective tanks by displacing them with high-pressure gas. Rocket engines with pressurized gas feed systems can be very reliable. References 6–1, 6–8, and 6–9 give additional information. A rocket engine with a gas-pressurized feed system was the first to be tested and flown (1926). Since then there have been two common types of pressurized feed systems and both are still used often today. The first uses a *gas pressure regulator* in the gas feed line and its engine operates at essentially constant tank pressure and nearly constant thrust.

It is shown schematically in Fig. 1–3 and consists of a high-pressure gas tank, a gas starting valve, a pressure regulator, propellant tanks, propellant valves, and feed lines. Additional components, such as filling and draining provisions, check valves, filters, flexible elastic bladders for separating the liquid from the pressurizing gas, and pressure sensors or gauges, are also often incorporated. After all tanks are filled, the high-pressure gas valve in Fig. 1–3 is remotely actuated and admits gas through the pressure regulator at a constant pressure to the propellant tanks. The check valves prevent mixing of the oxidizer with the fuel, particularly when the unit is not in an upright position. The propellants are fed to the thrust chamber by opening appropriate valves. When the propellants are completely consumed, the pressurizing gas can also scavenge and clean lines and valves of much of the liquid propellant residue. The variations in this system, such as the combination of several valves into one or the elimination and addition

of certain components, depend to a large extent on the application. If a unit is to be used and flown repeatedly, such as a space-maneuver rocket, it will include several additional features such as, possibly, a thrust-regulating device and a tank level gauge; they will not be found in an expendable, single-shot unit, which may not even have a tank-drainage provision.

The second common type of gas pressure feed system is called a *blow-down feed system*. It is shown in Fig. 6–6 and discussed in Ref. 6–10. Here the propellant tanks are enlarged because they store not only the propellants but also the pressurizing gas at the initial maximum propellant tank pressure. There is no separate high-pressure gas tank and no pressure regulator. The expansion of the gas already in the tanks provides for the expulsion of the propellants from their tanks. The blow-down system can be lighter than a regulated pressure system, but the thrust and the pressures decrease steadily as the propellants are consumed. A comparison of these two common types is shown in Table 6–3.

Different bipropellant pressurization concepts are evaluated in Refs. 6–1, 6–8, 6–9, and 6–10. Table 6–4 lists various optional features aimed at satisfying particular design goals. Many of these features also apply to pump-fed systems, which are discussed in Section 6.6. Many feed systems or engines have some, but certainly not all, of the features listed in Table 6–4. With monopropellants the gas pressure feed system becomes simpler since there is only one propellant and not two, reducing the number of pipes, valves, and tanks.

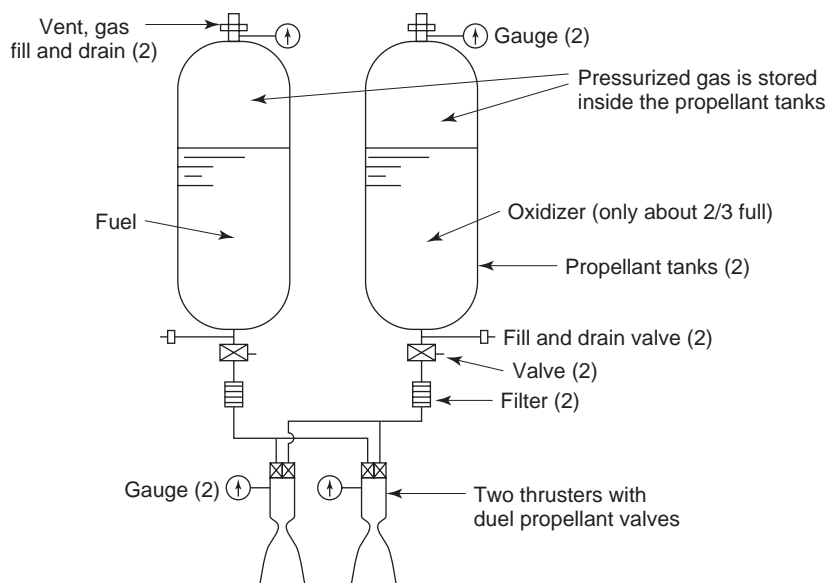


FIGURE 6–6. Simplified schematic diagram of a bipropellant blow-down pressurized gas feed system with two thrusters.

TABLE 6–3. Comparison of Two Types of Gas Pressurization Systems

| Type | Regulated Pressure | Blowdown |
|--------------------------------|---|---|
| Pressure/thrust Gas storage | Stays essentially constant In separate high-pressure tanks | Decreases as propellant is consumed Gas is stored inside propellant tank with large ullage volume (30–60%) |
| Required components | Needs regulator, filter, gas valve, and gas tank | Larger, heavier propellant tanks |
| Advantages | Constant-pressure feed gives essentially constant propellant flow and approximately constant thrust, constant I_s and r | Simpler system. Less gas required Can be less inert mass |
| Disadvantages | Better control of mixture ratio Slightly more complex Regulator introduces a small pressure drop Gas stored under high pressure Shorter burning time | Thrust decreases with burn duration Somewhat higher residual propellant due to less accurate mixture ratio control Thruster must operate and be stable over wide range of thrust values and modest range of mixture ratio Propellants stored under pressure; slightly lower I_s toward end of burning time |

An example of a complex man-rated pressurized feed system, the combined *Space Shuttle Orbital Maneuver System* (OMS) and the *Reaction Control System* (RCS), is described in Figs. 6–7 and 6–8, and Ref. 6–11. There are three locations on the Space Shuttle for the RCS, as shown in Fig. 1–14: a forward pod and a right and left aft pod. Figures 6–7 and 6–8 and Table 6–5 refer to one of the aft pods only and show a combined OMS and RCS arrangement. The OMS provides thrust for orbit insertion, orbit circularization, orbit transfer, rendezvous, deorbit, and abort. The RCS provides thrust for attitude control (in pitch, yaw, and roll) and for small-vehicle velocity corrections or changes in almost any direction (translation maneuvers), such as are needed for rendezvous and docking; it can operate simultaneously with or separate from the OMS.

The systems feature various redundancies, an automatic RCS thruster selection system, various safety devices, automatic controls, sensors to allow a display to the shuttle's crew of the system's status and health, and manual command overrides. The reliability requirements are severe. Several key components, such as all the helium pressure regulators, propellant tanks, some valves, and about half the thrusters are duplicated and redundant; if one fails, another can still complete the mission. It is possible to feed up to 1000 lbm of the liquid from the large OMS propellant tanks to the small RCS ones, in case it is necessary to run one or more of the small reaction control thrusters for a longer

TABLE 6–4. Typical Features of Liquid Propellant Feed Systems

| <i>Enhance Safety</i> |
|--|
| Check valves to prevent backflow of propellant into the gas tank and inadvertent mixing of propellants inside flow passages |
| Pressurizing gas should be inert, clean, and insoluble in propellant |
| Burst diaphragms or isolation valves to isolate the propellants in their tanks and positively prevent leakage into the thrust chamber or into the other propellant tank during storage |
| Isolation valves to shut off a section of a system that has a leak or malfunction |
| Sniff devices to detect leak of hazardous vapor; used on some versions of Space Shuttle Orbiter |
| Features that prevent an unsafe condition to occur or persist and shut down engine safely, such as relief valves or relief burst diaphragms to prevent tank overpressurization), or a vibration monitor to shut off operation in the case of combustion instability |
| <i>Provide Control</i> |
| Valves to control pressurization and flow to the thrust chambers (start/stop/throttle) |
| Sensors to measure temperatures, pressures, valve positions, thrust, etc., and computers to monitor/analyze system status. Compare measured values with analytical estimates, issue command signals, and correct if sensed condition is outside predetermined limits |
| Manned vehicle can require system status display and command signal override |
| Fault detection, identification, and automatic remedy, such as shut-off isolation valves in compartment in case of fire, leak, or disabled thruster |
| Control thrust (throttle valve) to fit a desired thrust–time flight profile |
| <i>Enhance Reliability</i> |
| Fewest practical number of components/subassemblies |
| Filters to catch dirt in propellant lines, which could prevent valve from closing or small injector holes from being plugged up or bearings from galling |
| Duplication of key components, such as redundant small thrusters, regulators, or check valves. If malfunction is sensed, then remedial action is to use the redundant spare component |
| Heaters to prevent freezing of moisture or low-melting-point propellant |
| Long storage life—use propellants with little or no chemical deterioration and no reaction with wall materials |
| <i>Provide for Reusability</i> |
| Provisions to drain propellants or pressurants remaining after operation |
| Provision for cleaning, purging, flushing, and drying the feed system and refilling propellants and pressurizing gas |
| Devices to check functioning of key components prior to next operation |
| Features to allow checking of engine calibration and leak testing after operation |
| Access for inspection devices for visual inspection of internal surfaces or components for damage or failure |
| <i>Enable Effective Propellant Utilization</i> |
| High tank expulsion efficiency with minimum residual, unavailable propellant |
| Lowest possible ambient temperature variation and/or matched propellant property variation with temperature so as to minimize mixture ratio change and residual propellant |
| Alternatively, measure remaining propellant in tanks (using a special gauge) and automatically adjust mixture ratio (throttling) to minimize residual propellant |
| Minimize pockets in the piping and valves that cannot be readily drained or flushed |

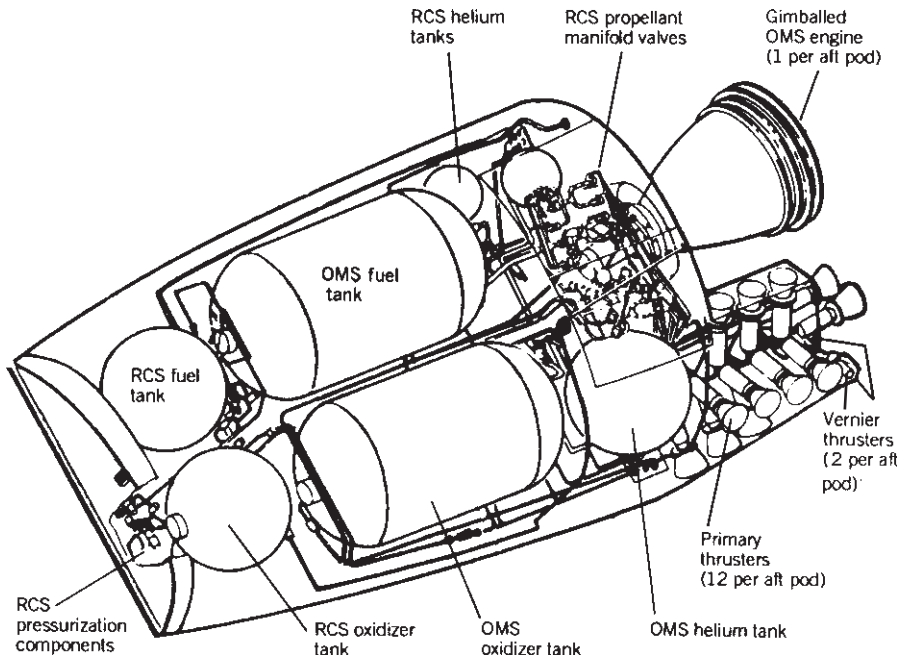


FIGURE 6-7. Simplified sketch at the left aft pod of the Space Shuttle's Orbiting Maneuvering System (OMS) and the Reaction Control System (RCS). (Source: NASA.)

period and use more propellant than the smaller tanks allow; it is also possible to feed propellant from the left aft system to the one on the vehicle's right side, and vice versa. These features allow for more than nominal total impulse in a portion of the thrusters, in case it is needed for a particular mission mode or an emergency mode.

The compartmented steel propellant tanks with antislosh and antivortex baffles, sumps, and a surface tension propellant retention device allow propellant to be delivered independent of the propellant load, the orientation, or the acceleration environment (some of the time in zero-g). Gauges in each tank allow a determination of the amount of propellant remaining, and they also indicate a leak. Safety features include sniff lines at each propellant valve actuator to sense leakage. Electrical heaters are provided at propellant valves, certain lines, and injectors to prevent fuel freezing or moisture forming into ice.

Some pressure feed systems can be prefilled with storable propellant and pressurizing agent at the factory and stored in readiness for operation. Compared to a solid propellant rocket unit, these storable prepackaged liquid propellant pressurized feed systems offer advantages in long-term storability, random restarts, and resistance to transportation vibration or shock.

TABLE 6–5. Characteristics of the Orbital Maneuver System (OMS) and the Reaction Control System (RCS) of the Space Shuttle in one of the Aft Side Pods

| Item | OMS | Primary RCS | Vernier RCS |
|--|----------------------------|--------------------|--------------------|
| Thrust (per nozzle) (lbf) | 6000 | 870 | 25 |
| Number of thrusters per pod | 1 | 12 | 2 |
| Thrust chamber cooling | Regenerative and radiation | Radiation cooling | |
| Chamber pressure, nominal (psi) | 125 | 152 | 110 |
| Specific impulse (vacuum nominal) (sec) | 313 | 280 ^a | 265 ^a |
| Nozzle area ratio | 55 | 22–30 ^a | 20–50 ^a |
| Mixture ratio (oxide/fuel mass flow) | 1.65 | 1.6 | 1.6 |
| Burn time, minimum (sec) | 2 | 0.08 | 0.08 |
| Burn time, maximum (sec) | 160 | 150 | 125 |
| Burn time, cumulative (sec) | 54,000 | 12,800 | 125,000 |
| Number of starts, cumulative (sec) | 1000 | 20,000 | 330,000 |
| Oxidizer (N_2O_4) weight in tank (lb) | 14,866 | | 1464 |
| Fuel (MMH) weight in tank (lb) | 9010 | | 923 |
| Number of oxidizer/fuel tanks | 1/1 | | 1/1 |
| Propellant tank volume, each tank (ft^3) | 90 | | 17.9 |
| Ullage volume, nominal (full tank) (ft^3) | 7.8 | | 1.2–1.5 |
| Tank pressure, nominal (psi) | 250 | | 280 |
| Helium storage tank pressure (psi) | 4700 | | 3600 |
| Number of helium tanks | 1 | | 2 |
| Volume of helium tanks (ft^3) | 17 | | 1.76 |

^aDepends on specific vehicle location and scarfing of nozzle.

Sources: NASA, Aerojet General Corporation.

The *thrust* level of a rocket propulsion system with a pressurized gas feed system is determined by the magnitude of the propellant flows which, in turn, is determined by the gas pressure regulator setting. The propellant *mixture ratio* in this type of feed system is controlled by the hydraulic resistance of the liquid propellant lines, cooling jacket, and injector, and can usually be adjusted by means of variable restrictors or fixed orifices. Further discussion of the adjusting of thrust and mixture ratio can be found in Sections 11.5 and 11.6 and in Example 11–2.

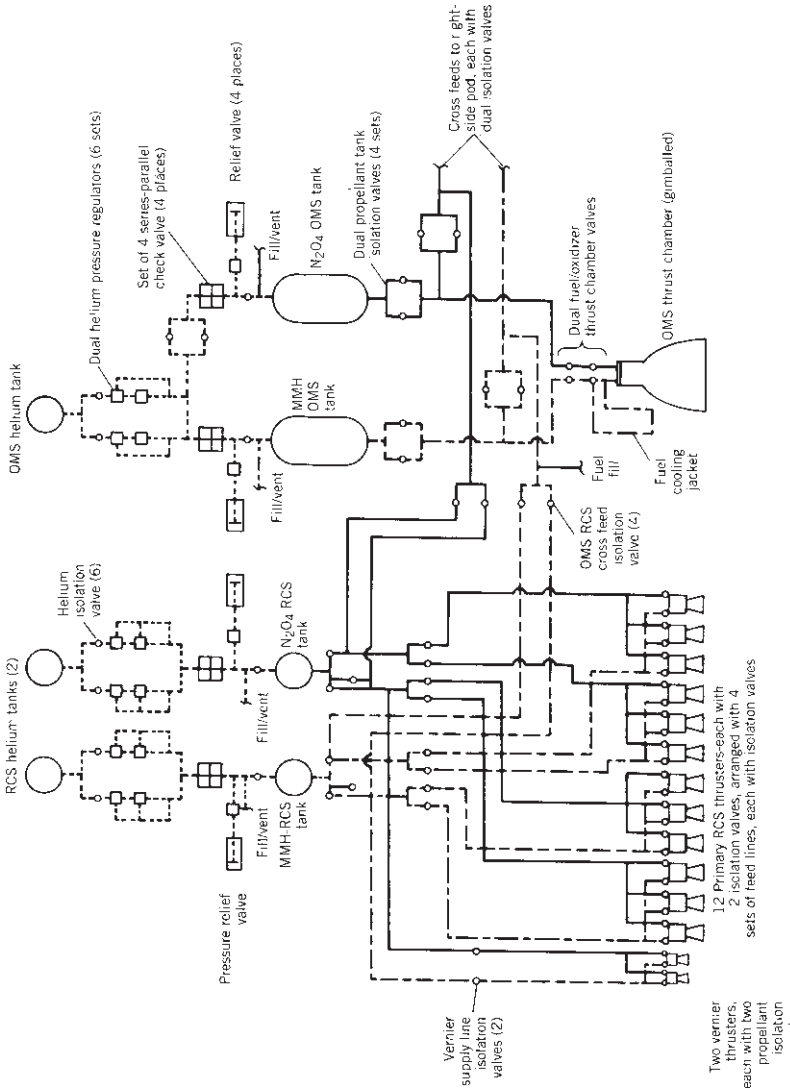


FIGURE 6-8. Simplified flow diagram of the propellant feed system flow for the left aft pod of the Orbital Maneuvering System (OMS) and Reaction Control System (RCS) of the Space Shuttle orbiter vehicle. Solid lines: nitrogen tetroxide (N_2O_4); dash-dot lines: monomethylhydrazine (MMH); short dashed lines: high-pressure helium. (Source: NASA.)

6.5. TANK PRESSURIZATION

As was stated before the objective of *feed systems* is to move the propellants under pressure from the propellant tanks to the thrust chamber(s). The *tank pressurization system* is that part of the feed system that provides a gas to expel propellants from the tanks. See Refs. 6–1, 6–8, 6–9, and 6–10. As was described in Section 6.3 there are two types: (1) in a pressurized gas feed system a relatively high pressure gas displaces the propellants from the tanks and (2) in a pumped feed system (described in the next section) the main energy for feeding the propellants comes from one or more pumps, but it requires a low gas pressure in the tanks to move the propellants to the pump inlet in order to avoid pump cavitation.

There are several *sources of pressurizing gas* commonly used in tank pressurization systems.

1. *High-pressure inert gas* stored at ambient temperature is the most common. Typical gases are helium, nitrogen, or air. Table 6–3 shows a comparison of the regulated pressure system (see Fig. 1–3) and the blow-down system (see Fig. 6–6). It is discussed further in this section. As the gas expands, its temperature drops.
2. *Heated high-pressure inert gas* (typically 200 to 800°F or 93 to 427°C) reduces the amount of required gas mass and thus the inert mass of the pressurizing system. Examples are gas heated by a heat exchanger with warm gas from a gas generator, with warm gas from turbine exhaust, or with electrical heaters inside the gas tank. Reference 6–12.
3. *Gas is created by a chemical reaction* by using either liquid bipropellants or a monopropellant and alternatively by a solid propellant, all at mixture ratios that allow a low enough or “warm” gas reaction temperature, so uncooled hardware can be used. The term “warm gas” (say 400 to 1600°F or 204 to 871°C) is used here to distinguish it from the hot gas (4000 to 6000°F, or 2204 to 3319°C) in the main combustion chamber. This chemically generated warm gas usually results in a lighter tank pressurization system than the heated inert gas system, particularly for applications with a high total impulse. This gas can come from two separate small gas generators for tank pressurization; one produces fuel-rich gas for pressurizing the fuel tank and the other feeds oxidizer-rich pressurizing gas into the oxidizer tank. This scheme was first used in the United States on the Bomarc rocket engine around 1952 and on the Russian RD-253 around 1961. The other common warm-gas scheme is to bleed a small amount of warm gas from the engine’s gas generator or preburner. If this gas is fuel rich, then it can only be used for pressurizing the fuel tank, and it may need to be cooled. These chemical reaction gases typically are at 1200 to 1700°F or 649 to 921°C, which are within the gas temperatures allowable for most alloy turbines and steel tanks. Catalyzed decomposed hydrazine warm gaseous reaction products have successfully pressurized liquid hydrazine tanks. With aluminum

propellant tanks it is necessary to cool the warm gas further. Many aluminum alloys melt around 1100°F (593°C). This cooling of gas has been accomplished by using a heat exchanger with one of the propellants. Solid propellant gas generators have been used on experimental liquid propellant rocket engines, but as far as the author can determine, none have been adapted for a production flight vehicle. One clever system developed in the former Soviet Union uses two rocket engines operating simultaneously on the same vehicle. The larger engine has a bleed of oxidizer-rich gases from an oxidizer-rich preburner for pressurizing the common oxidizer tank. The second engine feeds four smaller hinge-mounted vernier thrust chambers, which have been used for attitude control and also for extra thrust; its fuel-rich gas generator has a bleed of gas for pressurizing the common fuel tank. See Ref. 6–12.

4. *Evaporate a flow of a cryogenic liquid propellant*, usually liquid hydrogen, by applying heat usually taken from a thrust chamber cooling jacket and then use a part or all of this evaporated flow for tank pressurization. Orifices or pressure regulators may be needed to control the desired tank pressure. This scheme is used for the fuel tank of the Space Shuttle Main Engine and the tap-off stub for pressurizing gas can be seen in Fig. 6–12 in the turbine exhaust manifold of the fuel booster pump. The oxygen tank is pressurized by gasified liquid oxygen, which was tapped off the discharge side of the main oxygen pump and heated in a heat exchanger around the turbine of the main oxygen pump, as shown in Figure 6–12. See Ref. 6–12.
5. *Direct injection* of a small stream of hypergolic fuel into the main oxidizer tank and a small flow of oxidizer into the fuel tank has been tried in several countries without success. It is really a form of chemical gas generation. The only successful flight application is reported to be with a Russian ICBM upper stage engine using hypergolic propellants. See Refs. 6–1 and 6–12.
6. *Self-pressurization of cryogenic propellants* by evaporation is feasible but can be difficult to control (see Ref. 6–3). Experience is limited.

In order to design or analyze a pressurizing system it is necessary to know or to assume certain data about the tank and the engine. This can include the basic engine parameters, such as the propellant flow, thrust, duration, pulse width, propellant tank volume, percent ullage of that volume, storage temperature range, propellant and pressurizing gas properties, propellant tank pressure, gas tank pressure, or amount of unavailable residual propellant. For many of these the nominal, maximum, and minimum values may be needed.

Factors Influencing the Required Mass of Pressurizing Gas

A key task in the analysis and design of tank pressurization systems is determining the required mass of pressurizing gas. Many different factors influence this gas mass, and some of them can be quite complex as shown in Ref. 6–1. Therefore

a basic analysis of the amount of pressurizing gas for a new propulsion system is usually not accurate or fully useful. The mass of gas can be estimated using simplifying assumptions, but it is more accurate if it is based on actual test results and/or data from similar proven pressurizing systems. These are some of the *influencing factors*:

1. *Evaporation of propellant* at the interface between the pressurizing gas and the liquid propellant is a key phenomenon. The evaporated propellant dilutes the gas and changes its properties and expansion behavior. It depends on the temperature difference between the gas and the liquid, sloshing, vapor pressure of the propellant, turbulence, and local velocities of the gas. Furthermore the film of propellant on those portions of the tank walls and baffles, which are above the liquid level, will also evaporate. "Warm" gases (e.g., a bleed from a gas generator) will cause heating of the top layer of the liquid propellant and increase propellant evaporation. With cryogenic propellants the gas is always warmer than the liquid. The gas is cooled and more liquid evaporates.
2. The temperature of those walls of the propellant tanks, which are part of the exterior vehicle surface, can be affected by *aerodynamic heating*, which varies during the flight. This heat can increase the gas temperature as well as the liquid propellant temperature, and can augment the liquid evaporation.
3. The *solubility of the gas in the liquid* is affected by temperature and pressure. For example, nitrogen gas is soluble in liquid oxygen. It requires four times as much nitrogen gas to pressurize liquid oxygen as an equivalent volume of water. This dilutes the oxygen and causes a small performance loss. Helium is not very soluble in oxygen.
4. *Condensation* of certain species of the gas can dilute the propellant. Water vapor in warm gases is an example. Condensation can also occur on the exposed wetted inner walls of the propellant tanks and this requires more pressurizing gas.
5. *Changes in the gas temperature* take place during the operation. The compressed gas undergoes an expansion that can cause a dramatic cooling of the gas. Temperatures as low as 160 to 200 K (-228 to -100°F) have been recorded with helium. The cold gas absorbs heat from the propellants and the engine hardware. The particular expansion process will depend largely on the time of rocket operation. For large liquid propellant rocket engines, which run only for a few minutes, the expansion process will be close to adiabatic, which means little heat transfer from the hardware to the gas. For satellites, which stay in orbits for years and where the thrusters operate only occasionally for short operating periods, heat will be transferred from the vehicle hardware to the gas and the process will be close to an isothermal expansion (no change in temperature).
6. *Chemical reactions* of some species of the pressurizing gas with the liquid propellant have occurred and some can generate heat. Inert gases, such as helium, have no chemical reactions with the propellants.

7. *Turbulence and irregular flow distribution* of the entering gas will increase the heat transfer between the liquid and the gas. Depending on the temperature difference, it can cause additional heating or cooling of the top liquid layers.

8. *Vigorous sloshing* can quickly change the gas temperature. In some of the experimental flights of the Bomarc missile the side accelerations induced sloshing, which caused a sudden cooling of the warm tank pressurizing gas and caused a sudden reduction of tank pressure and propellant flow. See Refs. 6–4 and 6–5.

9. In many rocket engines some of the pressurizing gas is used for purposes other than tank pressurization, such as actuation of valves or controls. The amount required has to be determined and added to the total needed gas mass.

Simplified Analysis for the Mass of Pressurizing Gas

This is one example for a pressurizing system using a compressed gas initially in a separate tank at ambient temperature. It is the first category of pressurizing systems discussed above and it is perhaps the most common type. It assumes an adiabatic expansion of the gas (implies no heat transfer to or from the system hardware), the gas behaves like an ideal gas (obeys the gas laws), and the conservation of energy can be applied. Since the tank often has some insulation and since the operation of the rocket engines is short, the expansion process will be close to an adiabatic one. The expansion of the gas in the storage tank causes a significant drop in gas temperature and an increase in gas density. Furthermore it assumes that there is no evaporation of the liquid propellant (usually valid for a propellant with low vapor pressure), the gas is inert, does not dissolve in the liquid propellant, and there is no sloshing or vortexing.

Let the initial condition in the gas tank be given by subscript 0 and the instantaneous conditions in the gas tank by subscript g and in the propellant tank by subscript p . The gas energy after and before propellant expulsion is

$$m_g c_v T_g + m_p c_v T_p + p_p V_p = m_0 c_v T_0 \quad (6-5)$$

The work done by the gas in displacing the propellants is given by $p_p V_p$. Using Eqs. 3–3 to 3–6, the initial storage gas mass m_0 may be found:

$$\begin{aligned} c_v P_g V_0 / R + c_v p_p V_p / R + p_p V_p &= m_0 c_v T_0 \\ m_0 &= (p_g V_0 + p_p V_p k) / (R T_0) \end{aligned} \quad (6-6)$$

Here c_v is the specific heat at constant volume, R is the gas constant per unit mass, and k is the specific heat ratio. This equation may be expressed as

$$m_0 = \frac{p_g m_0}{p_0} + \frac{p_p V_p}{R T_0} k = \frac{p_p V_p}{R T_0} \left(\frac{k}{1 - p_g / p_0} \right) \quad (6-7)$$

The first term in this equation expresses the mass of gas required to empty a completely filled propellant tank if the gas temperature is maintained at the initial storage temperature T_0 . The second term expresses the availability of the storage gas as a function of the pressure ratio through which the gas expands.

Example 6–2. Determine the approximate mass and volume of air needed to pressurize a tank of 250 kg of 90% hydrogen peroxide for an initial gas tank pressure p_0 of 14 MPa and a required propellant tank pressure of 3.40 MPa. The density of this propellant is 1388 kg/m³, the gas constant R is 289 J/kg-K, the ambient temperature is 292 K, and for air $k = 1.40$.

SOLUTION. Since the vapor pressure of 90% hydrogen peroxide is low, the amount of liquid propellant that would evaporate is very small and the assumption of no evaporation can apply. The propellant volume is $250/1388 = 0.180 \text{ m}^3$. Allow 5% more gas to compensate for the ambient temperature changes of the liquid propellant and the stored gas, and for geometric variations of the hardware. From Eq. 6–7 the initial mass of air m_0 is

$$\begin{aligned} m_0 &= \frac{p_p V_p}{RT_0} \frac{k}{1 - (p_g/p_0)} \\ &= \frac{3.4 \times 10^6 \times 0.180 \times 1.05 \times 1.40}{289 \times 298 \times [1 - (3.4/14)]} \\ &= 13.8 \text{ kg of compressed air} \end{aligned}$$

The volume of the gas tank is from Eq. 3–4:

$$V_0 = m_0 RT_0 / p_0 = 13.8 \times 289 \times 298 / (14 \times 10^6) = 0.0847 \text{ m}^3$$

The high-pressure gas tank volume is almost half of the propellant tank volume.

6.6. TURBOPUMP FEED SYSTEMS AND ENGINE CYCLES

The principal components of a rocket engine with one type of turbopump system are shown in the simplified diagram of Fig. 1–4. Here the propellants are pressurized by means of *pumps*, which in turn are driven by *turbines*. These turbines derive their power from the expansion of warm gases.

Figures 10–1, 10–2, and 10–3 show examples of turbopumps and Chapter 10 is devoted exclusively to the turbopump. It is a high precision accurately balanced piece of high shaft speed (rpm) rotating machinery. It has usually two or one centrifugal pump and a turbine. Its high-speed high-load bearings support the shaft(s) on which the pump(s) and turbine are mounted. It has shaft seals to prevent leakage of propellants and also to prevent the two propellants from mixing with each other inside the turbopump. Some turbopumps also have a gear transmission, which allows the pumps or turbine to rotate at a different, usually more

efficient, shaft speed. Chapter 10 describes the design of turbopumps, the several arrangements of the key components, the design of its major components, and alternate configurations. While pressurized feed systems can be started relatively quickly, the starting of turbopump feed systems usually takes longer, because it takes some time for the rotating components (pumps, turbines) to accelerate to operating shaft speed. Starting is discussed in Section 11.4.

Engines with turbopumps are preferred for booster and sustainer stages of space launch vehicles, long-range missiles, and in the past also for aircraft performance augmentation. They are usually lighter than other types for these high-thrust, long-duration applications. The inert hardware mass of the rocket engine (without tanks) is essentially independent of duration. Examples can be seen in Figs. 6–1 and 6–9 and also in Refs. 6–1, and 6–2. For aircraft performance augmentation the rocket pump was driven directly by the jet engine, as in Ref. 6–13. From the turbopump feed system options depicted in Chapter 10, the designer can select the most suitable concept for a particular application.

As stated elsewhere in this book turbopump feed systems are usually preferred when the engine has a relatively high total impulse, which means high thrust and long duration. Pressurized feed systems are best for rocket engines with relatively low total impulse, that is, low thrust and often low cumulative firing durations.

Engine Cycles

Engine cycles apply only to liquid propellant rocket engines with a turbopump feed system. The three most common engine cycles are shown in Fig. 6–9 and many of each of these have flown. Reference 6–14 shows variations of these three cycles and other feasible cycles; some of them have not yet flown and some have not yet even been built.

An *engine cycle* for turbopump-fed engines describes the specific propellant flow paths through the major engine components, the method of providing the hot gas to one or more turbines, and the method of handling the turbine exhaust gases. There are *open cycles* and *closed cycles*. *Open* denotes that the working fluid exhausting from the turbine is discharged overboard, usually after having been expanded in a separate nozzle of its own as in Figs. 1–4 and 6–10, or discharged into the nozzle exit section of the thrust chamber at a point in the expanding section far downstream of the nozzle throat as shown in Fig. 6–9. In *closed cycles* or *topping cycles* all the working fluid from the turbine is injected into the engine combustion chamber to make the most efficient use of its remaining energy. In closed cycles the turbine exhaust gas is fed into the injector of the thrust chamber and is expanded through the full pressure ratio of the main thrust chamber nozzle, thus giving a little more performance than the open cycles, where these exhaust gases expand only through a relatively small pressure ratio.

Table 6–6 shows key parameters for each of the three common cycles and it describes the differences between them. The schematic diagrams of Fig. 6–9 show each cycle with a separate turbopump for fuel and for oxidizer. However, an arrangement with the fuel and oxidizer pump driven by the same turbine is

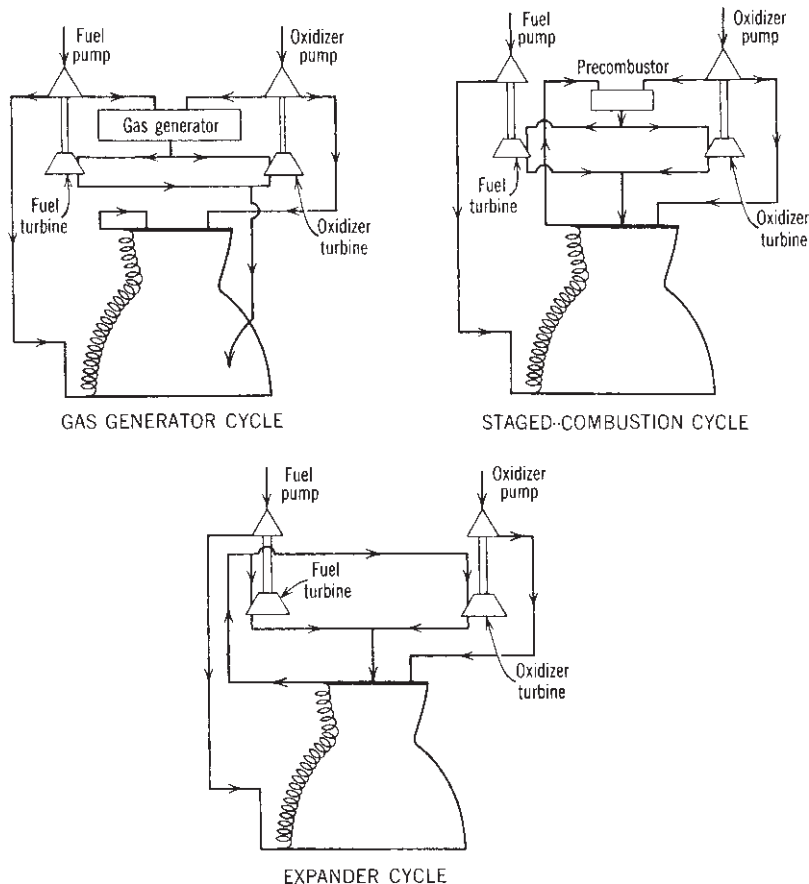


FIGURE 6–9. Simplified diagrams of three engine cycles for liquid propellant rocket engines. The spirals are a symbol for an axisymmetric cooling jacket where heat is absorbed.

also feasible and sometimes reduces the hardware mass, volume, and cost. The “best” cycle has to be selected on the basis of the mission, the suitability of existing engines, and the criteria established for the particular vehicle. There is an optimum chamber pressure and an optimum mixture ratio for each application, engine cycle, or optimization criterion, such as maximum range, lowest cost, or highest payload.

The *gas generator cycle* has been the most common. Compared to other engine cycles, it is relatively simple, pressures are usually lower, generally has a lower inert mass, and its engine cost is usually lower. However, its performance (specific impulse) is lower by a few percent. Its performance is adequate for many space flight and military missions.

TABLE 6-6. Qualitative Characteristics for Three Different Engine Cycles

| Engine Cycle | Gas Generator Cycle | Expander Cycle | Staged Combustion Cycle |
|--|---|--|---|
| Engine specific impulse, as % of gas gen. cycle | Set to 100% | 102–106% | 102–108% |
| Turbine flow, as % of total propellant flow | 1.5–7% | 75–96% of the fuel flow or 12–20% of total | 60–80% |
| Typical pressure drop, across turbine as % of chamber pressure | 50–90 | 5–30 | 60–100 |
| Propellant type | All types | Cryogenic fuel for cooling | All types |
| Pump discharge pressure, % of chamber pressure | 135–180 | 150–200 | 170–250 |
| Turbine exhaust gas | Dumped overboard through a separate nozzle or aspirated into main nozzle exit section | Fed into main thrust chamber injector | Fed into main thrust chamber injector |
| Relative inert mass of engine | Relatively low | Higher | Highest |
| Thrust control, typical | Regulate flow and/or mixture ratio in gas generator | Control bypass of some gasified fuel flow around turbine | Regulate preburner mixture ratio and propellant flows |
| Maximum pressure in feed system | Relatively low | Higher | Highest |
| First ground tests | Goddard, USA, 1934 Hellmuth Walter Comp., Germany, 1939 | Pratt & Whitney Rocketdyne, 1960 Pratt & Whitney Rocketdyne, 1963 | RNII ^a , Russia, 1958 Korolev Design Bureau, 1961 |
| First flight operation | | | |

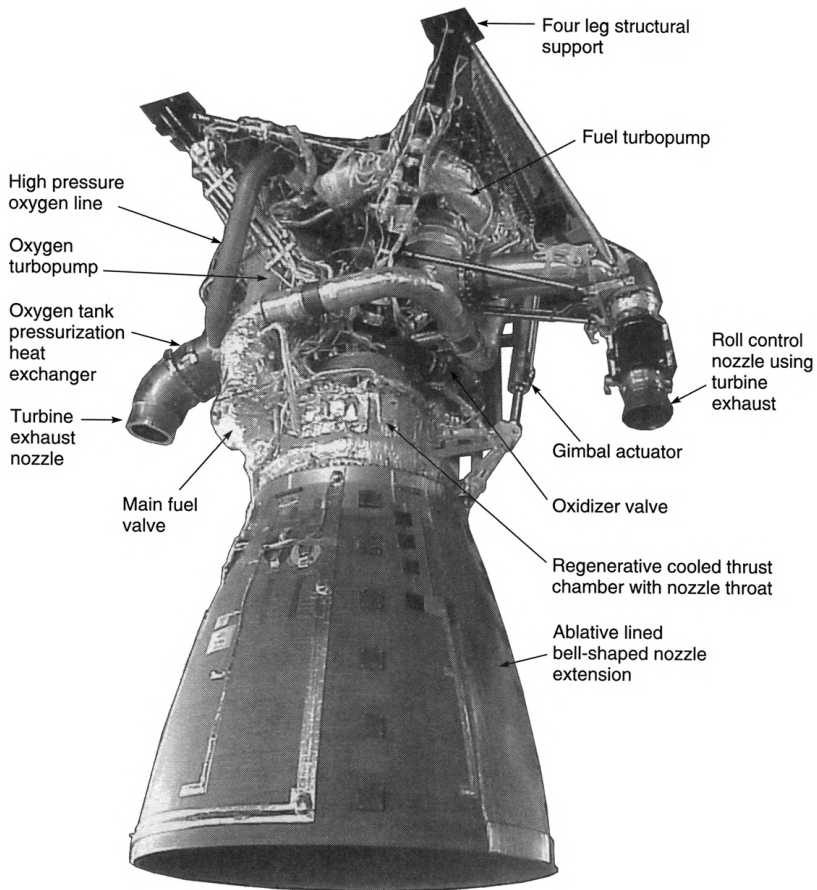
^aRossiyskiy Nauchno Issledovatel'skiy Institut (Reaction Propulsion Research Institute).

In the gas generator cycle the turbine inlet gas comes from a separate gas generator. Its propellants can be supplied from two separate propellant tanks or can be bled off the main propellant feed system tanks. Some early engines used a separate monopropellant for creating the generator gas. The German V-2 missile engine used hydrogen peroxide, which was decomposed by a catalyst. Typically, the turbine exhaust gas is discharged overboard through one or two separate small low-area-ratio nozzles (at relatively low specific impulse), as shown schematically in Fig. 1–4 and in the Vulcain engine or RS-68 engine listed in Table 11–2. See Ref. 6–15. Alternatively, this turbine exhaust can be aspirated into the main flow through multiple openings in the diverging nozzle section, as shown schematically in Fig. 6–9 for a gas generator engine cycle. This gas then protects the walls near the nozzle exit from high temperatures. Both methods can provide a small amount of additional thrust. The gas generator mixture ratio is usually fuel rich (in some engines it is oxidizer rich) so that the gas temperatures are low enough (typically 900 to 1350 K) to allow the use of uncooled turbine blades and uncooled nozzle exit segments. The RS-68 rocket engine, shown in Fig. 6–10, has a simple gas generator cycle. As can be seen from the data under the figure, with a gas generator cycle the specific impulse of the thrust chamber by itself is always a little higher than that of the engine, and the thrust of the thrust chamber is always slightly lower than that of the engine. The thrust of the RS-68 can be reduced or throttled to less than 60% of full thrust. See Ref. 6–15.

The *expander cycle* and the *staged combustion cycle* are both closed cycles, and they offer several percent higher performance than the gas generator cycle; this small improvement makes a substantial difference in payload for flight missions with high mission velocities. Alternatively they allow a somewhat smaller flight vehicle. However, the engines are usually more complex, heavier, and more expensive.

A flow diagram of an *expander cycle* is shown in Fig. 6–11. The engine coolant (usually hydrogen fuel) is evaporated, heated, and then fed to low-pressure-ratio turbines after having passed through the cooling jacket where it picked up energy. Part of the coolant, perhaps 5 to 15%, bypasses the turbine (shown in Fig. 6–11) and rejoins the turbine exhaust flow before the entire coolant flow is injected into the engine combustion chamber where it mixes and burns with the oxidizer (see Refs. 6–14 and 6–16). The primary advantages of the expander cycle are good specific impulse, relative engine simplicity, no gas generator, and relatively low engine mass. In the expander cycle all the propellants are fully burned in the engine combustion chamber and expanded efficiently in the exhaust nozzle of the thrust chamber.

This cycle is used in the RL10 hydrogen/oxygen rocket engine, and different versions of this engine have flown successfully in the upper stages of several space launch vehicles. Data on the RL10 engines are given in Tables 6–8, 8–1, and 11–2. A modification of this engine, the RL10B-2 with an extendible nozzle skirt, can be seen in Fig. 8–17. The RL10B-2 flow diagram in Fig. 6–11 shows



| Parameter | Thrust chamber | Engine |
|---|----------------|---------|
| Specific impulse at sea level (max.), sec | 363 | 357 |
| Specific impulse in vacuum (max.), sec | 415 | 409 |
| Thrust, at sea level, lbf | 640,700 | 656,000 |
| Thrust in vacuum lbf | 732,400 | 751,000 |
| Mixture ratio | 6.74 | 6.0 |

FIGURE 6–10. Simplified view of the RS-68 rocket engine with a gas generator cycle. For engine data see Table 10–3. (Courtesy of Pratt & Whitney, Rocketdyne.)

its expander cycle. The turbine drives a single-stage liquid oxygen pump (through a gear case) and a two-stage liquid hydrogen pump. The cooling down of the hardware to cryogenic temperatures is accomplished by flowing (prior to engine start) cold propellant through cool-down valves. The pipes for discharging the cooling propellants overboard are not shown here but can be seen in Fig. 8–17.

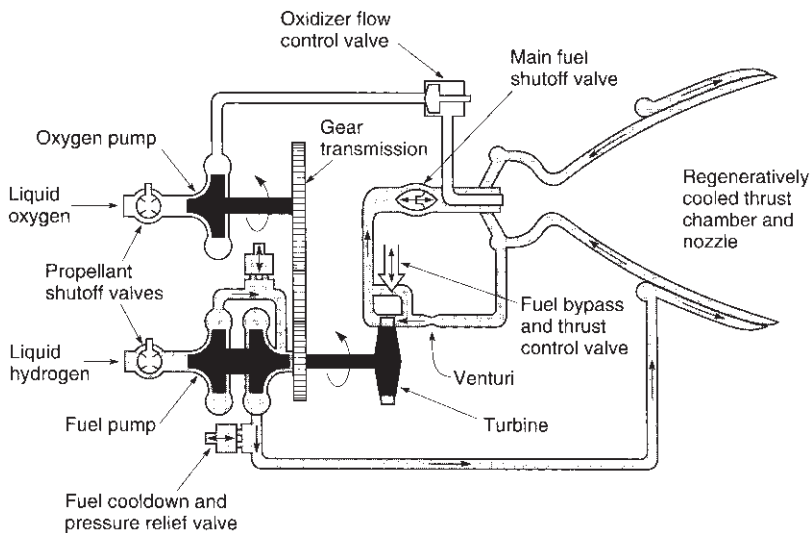


FIGURE 6–11. Simplified schematic flow diagram of the RL10B-2 upper-stage rocket engine is an example of an expander engine cycle. For data see Tables 6–8 and 8–1. (Courtesy of Pratt & Whitney Rocketdyne.)

Thrust is regulated by controlling the flow of hydrogen gas to the turbine, using a bypass to maintain constant chamber pressure. Helium is used as a means of power boost by actuating several of the larger valves through solenoid-operated pilot valves.

In the *staged combustion cycle*, the coolant flow path through the cooling jacket is the same as that of the expander cycle. Here a high-pressure preburner (a high-pressure gas generator) burns all the fuel with part of the oxidizer to provide high-energy gas to the turbines. The total turbine exhaust gas flow is injected into the main combustion chamber where it burns with the remaining oxidizer. This cycle lends itself to high-chamber-pressure operation, which allows a small thrust chamber size. The extra pressure drop in the preburner and turbines causes the pump discharge pressures of both the fuel and the oxidizer to be higher than with open cycles, requiring heavier and more complex pumps, turbines, and piping. The turbine flow is relatively high and the turbine pressure drop is low, when compared to other cycles. The staged combustion cycle gives high specific impulse, but it is more complex and heavy. A variation of the staged combustion cycle is used in the Space Shuttle Main Engine, as shown in Figs. 6–1 and 6–12. This engine actually uses two separate preburner chambers, each mounted directly on a separate main turbopump. In addition, there are two more turbopumps for providing a boost pressure to the main pumps, but their turbines are not driven by combustion gases; instead, high-pressure liquid oxygen drives one booster pump and evaporated hydrogen drives the other. The injector of this reusable liquid propellant high-pressure engine is shown in Fig. 9–6 and performance data are

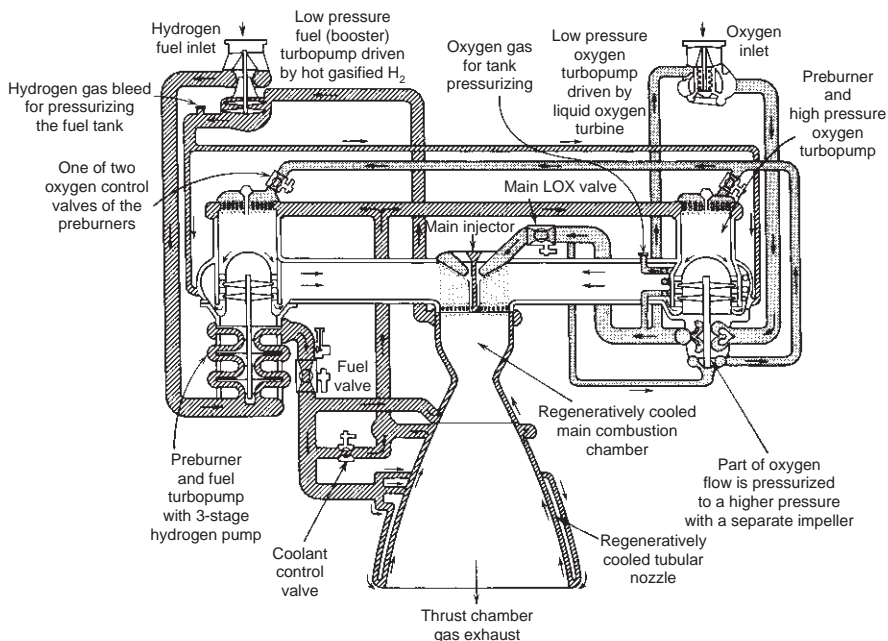


FIGURE 6–12. Flow diagram illustrating the staged combustion cycle of the Space Shuttle Main Engine (SSME) using liquid oxygen and liquid hydrogen fuel. (Courtesy of Pratt & Whitney Rocketdyne and NASA.)

given in Tables 10–1 and 11–2. While the Space Shuttle Main Engine (burning hydrogen with oxygen) has fuel-rich preburners, oxidizer-rich preburners are used in the Energomash RD-170 and RD-120 engines (kerosene/oxygen) and other Russian staged combustion rocket engines. See Table 11–3. Another example of a staged combustion cycle is the Russian engine RD-253; all of the nitrogen tetroxide oxidizer and some of the unsymmetrical dimethyl hydrazine fuel are burned in the preburner, and the remaining fuel is injected directly into the main combustion chamber.

In an engine with a gas generator cycle the thrust of the thrust chamber is always slightly less than the Thrust of the engine, because the exhaust from the turbine provides a little extra thrust. Also the thrust chamber specific impulse is a little higher than the rocket engine specific impulse, because the low-flow gas exhausted from the turbine has a very low specific impulse. For closed cycles, namely the expander cycle and the staged combustion cycle, the values of the thrust and the specific impulse are the same for the engine and its thrust chamber(s).

6.7. ROCKET ENGINES FOR MANEUVERING, ORBIT ADJUSTMENTS, OR ATTITUDE CONTROL

These engines have usually a set of small thrusters that are installed at various places in a vehicle and a common pressurized feed system, similar to Figs. 1–3, 4–13, or 6–13. They are called *reaction control systems* or *auxiliary rocket propulsion systems* as contrasted to higher-thrust *primary or boost propulsion systems*. Most have low thrust, use storable liquid propellants, require accurate repeatable pulsing, a long life in space, and/or a long-term storage with loaded propellants in flight tanks. Typical thrust levels of a small thruster are between 0.1 and 1000 lbf. Figure 4–13 shows that it requires 12 thrusters for the application of pure torques about three vehicle axes. If a three-degree-of-rotation freedom is not a requirement, or if torques can be combined with some translation maneuvers, fewer thrusters will be needed. These *auxiliary rocket engines* are commonly used in spacecraft or missiles for the accurate *control of flight trajectories, orbit adjustments, or attitude control* of the vehicle. References 6–1 and 6–17 give information on several of these. Figure 6–13 shows a simplified flow diagram for a postboost control rocket engine, with one larger rocket thrust chamber for changing the velocity vector and eight small thrusters for attitude control.

Section 4.5 describes various space trajectory correction maneuvers and satellite station-keeping maneuvers that are typically performed by these small auxiliary liquid propellant rocket engines with multiple thrusters. Table 6–7 lists typical applications for rocket engines with small thrusters.

Attitude control can be provided both while a primary propulsion system (of a vehicle or of a stage) is operating and while its small thruster rocket system operates by itself. For instance, this is done to point satellite's telescope into

TABLE 6–7. Typical Applications for Small Thrusters

| |
|---|
| Flight path (or orbit) corrections or changes |
| Minor flight velocity adjustments |
| Station keeping (correcting for deviations from orbit) |
| Orbit injection for small satellites |
| Deorbit maneuver for small satellites |
| Divert maneuvers of terminal interceptors |
| Attitude control for: |
| Satellites, stages of space launch vehicles, space stations, missiles |
| Roll control for a single gimbaled rocket engine |
| Pointing/orienting antennas, solar cells, mirrors, telescopes, etc. |
| Correct the misalignment of principal, larger thrust chamber |
| Velocity tuning of war heads (postboost control system) for accurate targeting |
| Settling of liquid propellants prior to gravity-free start of main upper stage engine |
| Flywheel desaturation |

Source: Mostly from Ref. 6–17.

a specific orientation or to rotate a spacecraft's main thrust chamber into the desired direction for a vehicle turning maneuver.

A common method for achieving accurate velocity corrections or precise angular positions is to operate or fire some of the thrusters in a *pulsing mode* (e.g., fire repeatedly for 0.020 sec, each time followed by a pause of perhaps 0.020 to 0.100 sec). The guidance system determines the maneuver to be undertaken and the vehicle control system sends command signals to specific thrusters for the number of pulses needed to accomplish this maneuver. Small liquid propellant engine systems are uniquely capable of these pulsing operations. Some small thrusters have been tested for more than 300,000 pulses. For very short pulse durations the specific impulse is degraded by 5 to 25%, because the performance during the thrust buildup and thrust decay period (at lower chamber pressure) is inferior to operating only at the rated chamber pressure and the transient time becomes a major portion of the total pulse time.

Ballistic missile defense vehicles usually have highly maneuverable upper stages. These require substantial side forces also called divert forces (200 to 6000 N) during the final closing maneuvers just prior to reaching the target. In concept the system is similar to that of Fig. 6-13, except that the larger thrust chamber would be at right angles to the vehicle axis. A similar system for terminal maneuvers, but using solid propellants, is shown in Figs. 12-27 and 12-28.

The Space Shuttle performs its reaction control with 38 different thrusters, as shown schematically in Figs. 1-14 and 6-8; this includes several duplicate (spare or redundant) thrusters. Selected thrusters are used for different maneuvers, such as space orbit corrections, station keeping, or positioning the Space Shuttle for reentry or visual observations. These small restartable rocket engines are also used for space *rendezvous* or *docking maneuvers*, where one spacecraft slowly approaches another and locks itself to the other, without causing excessive impact forces during this docking maneuver. This docking operation requires rotational and translational maneuvers from a series of rocket engines.

The application of pure torque to spacecraft can be divided into two classes, *mass expulsion* types (rockets) and *nonmass expulsion* types. Nonmass expulsion types include momentum storage, gravity gradient, solar radiation, and magnetic systems. Some space satellites are equipped with both the mass and nonmass expulsion types. *Reaction wheels* or flywheels, a momentum storage device, are particularly well suited to obtaining vehicle angular position control with high accuracies of less than 0.01° deviation and low vehicle angular rates of less than 10^{-5} degrees/sec with relatively little expenditure of energy. The vehicle angular momentum is changed by accelerating (or decelerating) the wheel. Of course, when the wheel speed reaches the maximum (or minimum) permissible, no further electrical motor torquing is possible; the wheel must be decelerated (or accelerated) to have its momentum removed (or augmented), a function usually accomplished through the simultaneous use of two small attitude control rocket thrusters, which apply a torque to the vehicle in the opposite direction. This has been called desaturation of the fly wheel.

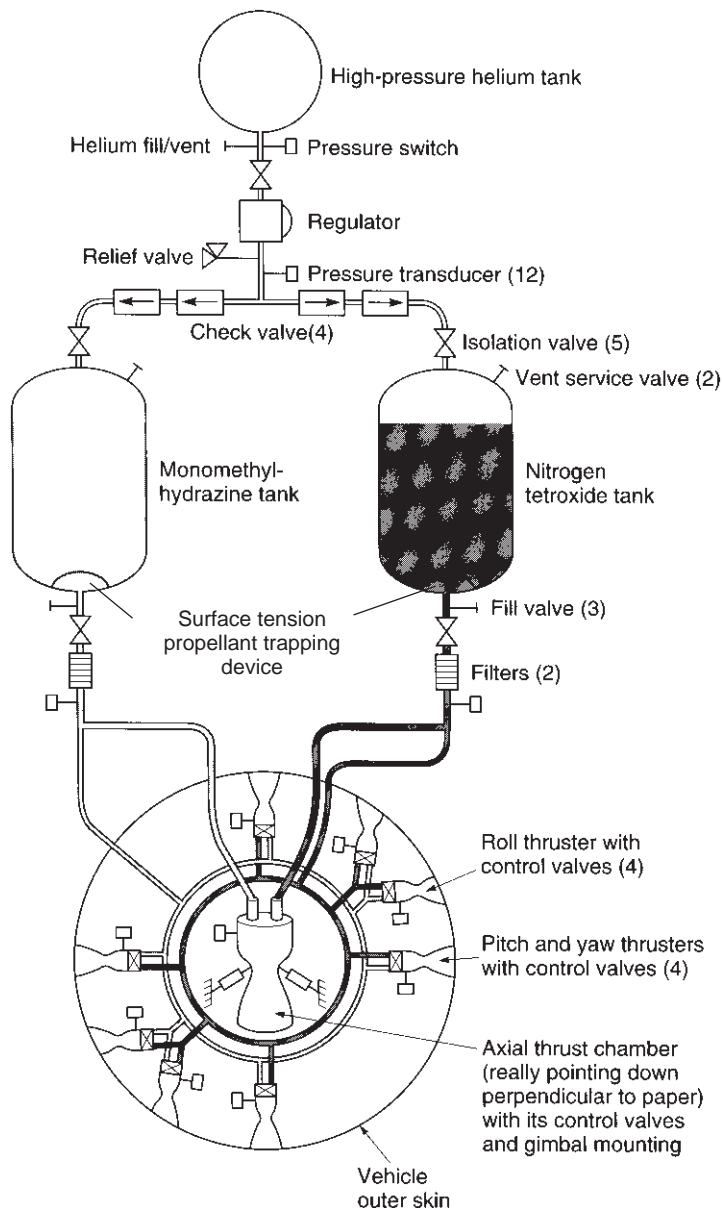


FIGURE 6–13. Schematic flow diagram of the helium-pressurized, bipropellant rocket engine system of the fourth stage of the Peacekeeper ballistic missile, which provides the terminal velocity (in direction and magnitude) to each of several warheads. It has one larger gimballed thrust chamber for trajectory translation maneuvers and eight small thrusters (with scarfed nozzles) for attitude control in pitch, yaw, and roll. For clarity the tanks and feed system are shown outside the vehicle skin; really they are located within the vehicle. (Courtesy of USAF.)

The propellants for *auxiliary rockets* fall into three categories: *cold gas jets* (also called inert gas jets), *warm or heated gas jets*, and *chemical combustion rockets*, such as bipropellant liquid propellant rockets. The specific impulse is typically 50 to 120 sec for various cold gas systems and 105 to 250 sec for warm gas systems. Warm gas systems can use inert gas with an electric heater or a monopropellant which is catalytically and/or thermally decomposed. Bipropellant attitude control thrust chambers allow an I_s of 220 to 325 sec and have varied from 5 to 4000 N thrust; the highest thrusts apply to large spacecraft. All basically use pressurized feed systems with multiple thrusters or thrust chambers equipped with fast-acting, positive-closing precision valves. Many systems use small, uncooled, metal-constructed thrusters with supersonic exhaust nozzles, and they are strategically located on the periphery of the spacecraft pointing in different directions. Gas jets are used typically for low thrust (up to 10 N) and low total impulse (up to 4000 N-sec). They have been used on smaller satellites and often only for roll control. See Ref. 6-17 and Section 7.6.

Small liquid monopropellant and liquid bipropellant rocket units are common in auxiliary rocket systems for thrust levels typically above 2 N and total impulse values above 3000 N-sec. Hydrazine is the most common monopropellant used in auxiliary control rockets; nitrogen tetroxide and monomethylhydrazine is a common bipropellant combination. The next chapter contains data on all three categories of these propellants, and Chapter 8 shows diagrams of small thrusters.

Combination systems are also in use. Here a bipropellant with a relatively high value of I_s , such as N_2O_4 and N_2H_4 , is used in the larger thrusters, which consume most of the propellant; then several simple monopropellant thrusters (with a lower I_s), used for attitude control pulsing, usually consume a relatively small fraction of the total fuel. Another combination system is to employ bipropellant or monopropellant thrusters for adding a velocity increment to a flight vehicle or to bleed or pulse some of the pressurizing gas, such as helium, through small nozzles controlled by electromagnetic valves to provide roll control. The specific mission requirements need to be analyzed to determine which type or combination is most advantageous for a particular application.

Special thruster designs exist that can be used in a bipropellant mode at higher thrust and also in a monopropellant mode for lower thrust. This can offer an advantage in some spacecraft applications. An example is the Northrop-Grumman secondary combustion augmented thruster (SCAT), which uses hydrazine and nitrogen tetroxide, is restartable, vaporizes the propellants prior to injection and therefore has very efficient combustion (over 99%), can operate over a wide range of mixture ratios, and can be throttled from 5 to 15 lbf thrust. From Ref. 6-12.

6.8. ENGINE FAMILIES

An engine family is a series of related rocket engines, which have evolved over a period of many years. They come from the same rocket engine organization and each engine has been tailored to a specific application. The engines in the family have a strong resemblance to each other, use the same engine concept, usually the same propellants, and some identical or somewhat modified components of the same type. When an existing proven liquid propellant rocket engine can be modified and/or up-rated to fit a new application, the newer modified engine can use a lot of the proven hardware, test data, and software of the original earlier engines.

An example is the RL 10 rocket engine family of upper-stage engines. It was developed by Pratt & Whitney Rocketdyne over a period of about 46 years and is shown in Table 6–8. Data is from Refs. 6–12 and 6–16. Each engine is for a specific application and is a modification and/or uprating of an earlier model. The principal changes from one engine model to the next included increases in thrust, increases in performance (somewhat higher specific impulse) by using higher chamber pressure, improved injector designs, and increases in nozzle exit area ratios. All use LOX/LH₂ propellants, the same basic engine concept with an expander engine cycle, the same tubular cooling jacket approach for the chamber and nozzle throat region, the same generic geared turbopump arrangement, often the same or similar valves, and power level control by a bypass of hydrogen gas around the turbine. In the turbopump the fuel pump and turbine are on the same high-speed shaft and the LOX pump is driven efficiently through a gear train at a lower speed. All engines are gimbal mounted (most at 4° maximum deflection) and most have space restart capability. Figure 8–17 shows the extendable nozzle of the RL 10B-2. In the RL 10A-3-3A thrust chamber a high-conductivity silver ring was brazed with silver into the nozzle throat, thus enabling a higher chamber pressure. The cooling jacket tubes were brazed with silver and were compatible. Figure 6–11 shows a flow sheet of an RL 10 expander engine cycle.

It is interesting to see how thrust or specific impulse changed with time and with the model. Incidentally the specific impulse listed in Table 6–8 for the RL 10B-2 is the highest of any flying liquid propellant rocket engine in the world and the extendable nozzle exit segment of the RL 10A-4 was the first for liquid propellant rocket engines.

When compared to a brand new engine, the principal benefits of adopting a modified engine, which is based on an earlier family of proven engines, are savings in costs (costs of design, development, less fabrication, less testing, qualification, and operation), attaining a high engine reliability more quickly, and often also a shorter schedule. The heritage of earlier proven similar engines allows the use of old engine or component data, having trained experienced personnel, proven subcontractors, a higher confidence level of reliability, and often, but not

TABLE 6-8. The RL 10 Engine Family^a

| Engine Model | Qualification Year | Vehicle | p_1 psia | Thrust lbf | Mixture Ratio | Weight I_{f} (vac) lbf sec | Nozzle Area Ratio | No. Engines per Stage | Comments |
|--------------|--------------------|------------------------------------|---------------|---------------|---------------|--|-------------------|-----------------------|---|
| RL 10A-1 | 1961 | Atlas Centaur | 300 | 15,000 | 5.0:1 | 300 424 | 40.0:1 | 2 | Never fired in space. Two were on the 1st Centaur vehicle launch attempt that had a booster failure. |
| RL 10A-3C | 1962 | Atlas Centaur | 292 | 15,000 | 5.0:1 | 292 427 | 40.0:1 | 2 | Early Centaur missions. Improved injector incorporated. |
| RL 10A-3S | 1962 | Saturn IV | 292 | 15,000 | 5.0:1 | 296 427 | 40.0:1 | 6 | Saturn IV upper stage. Separate solenoid added to separate LOX cooldown from fuel cooldown. |
| RL 10A-3-1 | 1964 | Atlas Centaur | 292 | 15,000 | 5.0:1 | 291 433 | 40.0:1 | 2 | Improved injector incorporated. Early Surveyor missions. |
| RL 10A-3-3 | 1966 | Atlas & Titan Centaur | 396 | 15,000 | 5.0:1 | 282 442.4 | 57.0:1 | 2 | New chamber/nozzle and turbopump incorporated. Used on Centaur for both Atlas & Titan. Used for Surveyor, Mariner, Pioneer, Helios, Viking, and Voyager missions. |
| RL 10A-3-3A | 1981 | Atlas & Titan & Shuttle Centaur | 475 | 16,500 | 5.0:1 | 310 444.4 | 61.0:1 | 2 | Engine modified to operate with reduced propellant inlet pressures (cooldown valve changes) because of boost pump removal from the vehicle. Silver throat insert incorporated in chamber. |
| RL 10A-3-3B | 1986 | Shuttle Centaur | 425 | 15,000 | 6.0:1 | 310 436 | 61.0:1 | 2 | RL 10A-3-3A modified to handle long space stay time for AF version of Shuttle/Centaur. Mixture ratio increased to 6.0 and cooldown components changed. Never flew. |

| | | | | | | | | | | |
|-------------|------|---------------|-----|--------|--------|-----|-------|---------|--------|---|
| RL 10A-4 | 1991 | Atlas Centaur | 570 | 20,800 | 5.5:1 | 370 | 448.9 | 84.0:1 | 2 | New thrust chamber with no silver throat. Turbopump modified for increased thrust and chamber pressure. Extendible radiation cooled columbiurn nozzle incorporated. |
| RL 10A-4-1 | 1994 | Atlas Centaur | 610 | 22,300 | 5.5:1 | 370 | 450.5 | 84.0:1 | 1 or 2 | Improved injector incorporated. |
| RL 10A-4-1A | 1999 | Titan Centaur | 580 | 20,500 | 5.0:1 | 321 | 444.4 | 61.0:1 | 2 | Derivative of RL 10A-4-1 derated to 20.5K thrust and 5.0 O/F. Only 2 engines flown. No nozzle extension. |
| RL 10A-4-2 | 2000 | Atlas Centaur | 610 | 22,300 | 5.5:1 | 370 | 450.5 | 84.0:1 | 1 or 2 | Dual spark plugs and igniter flow path modifications incorporated. Can use fixed or translating nozzle extension. |
| RL 10A-5 | 1993 | DC-X | 470 | 13400 | 6.0:1 | 316 | 365.1 | 13.0:1 | 4 | Chamber modified for sea-level operation and controls modified to enable 3 to 1 throttling. Delta Clipper Experimental vehicle. |
| RL 10B-2 | 1998 | DELTA | 633 | 24,750 | 5.88:1 | 664 | 465.5 | 285.0:1 | 1 | New chamber/nozzle and high area ratio extendable composite nozzle incorporated. Used on Delta III and IV upper stages. |

^a As of April 2008, 385 RL10 engines have flown in space with 731 engine firings. Courtesy Pratt & Whitney Rocketdyne.

always, the use of the same debugged materials, fabrication, and test facilities. An intangible benefit is that the vehicle developer or prime contractor, who plans to use one of these engines, will have more confidence in the engine. A brand new engine may have slightly better performance and/or a somewhat lower inert engine mass and some other improvements, but it will usually be more costly, take longer to develop, and take more time to reach an equivalent high level of reliability.

6.9. VALVES AND PIPELINES

Valves control the flows of liquids and gases and pipes conduct these fluids to the intended components. There are no rocket engines without them. There are many different types of valves. All have to be reliable, lightweight, leakproof, and must withstand intensive vibrations and very loud noises. Table 6–9 gives several key classification categories for rocket engine valves. Any one engine will use only some of the valves listed here.

The art of designing and making valves is based, to a large extent, on experience. A single chapter cannot do justice to it by describing valve design and operation. References 6–1 and 6–2 describe the design of specific valves, lines, and joints. Often the design details, such as clearance, seat materials, or opening time delay present development difficulties. With many of these valves, any significant leakage or valve failure can cause a failure of the engine itself. All valves are tested for two qualities prior to installation; they are tested for leaks—through the seat and also through the glands—and for functional soundness or performance.

The propellant valves in high-thrust units handle relatively large flows at high service pressures. Therefore, the forces necessary to actuate the valves are large. Hydraulic or pneumatic pressure, controlled by pilot valves, operates the larger valves; these pilot valves are in turn actuated by a solenoid or a mechanical linkage. Essentially this is a means of power boost.

Two valves commonly used in pressurized feed systems are *isolation valves* (when shut, they isolate or shut off a portion of the propulsion system) and *latch valves*; they require power for brief periods during movements, such as to open or shut, but need no power when latched or fastened into either an open or a closed position.

A very simple and very light valve is a *burst diaphragm*. It is essentially a circular disk of material that blocks a pipeline and is designed so that it will fail and burst at a predetermined pressure differential. Burst diaphragms are positive seals and prevent leakage, but they can be used only once. The German *Wasserfall* anti-aircraft missile, an early application, used four burst disks; two were in high-pressure air lines and two were in the propellant lines.

TABLE 6–9. Classification of Valves Used in Liquid Propellant Rocket Engines^a

-
1. *Fluid*: fuel; oxidizer; cold or heated pressurized gas; hot turbine gas
 2. *Application or Use*: main propellant control; thrust chamber valve (dual or single); bleed; vent; drain; fill; by-pass; preliminary stage flow; pilot valve; safety valve; overboard dump; regulator; gas generator or preburner control; sequence control; prevent back flow; isolation of propellant or, latch valve
 3. *Mode of Actuation*: automatically operated (by solenoid, pilot valve, trip mechanism, pyrotechnic, etc.); manually operated; pressure-operated by air, gas, propellant, or hydraulic fluid (e.g., check valve, tank vent valve, pressure regulator, relief valve), with or without position feedback, rotary or linear actuator
 4. The *Flow* magnitude determines the *size* of the valve
 5. *Duty cycle*: single operation or multiple operation during the same flight, short duration pulse operation; reusable for other flights; long or short life
 6. *Valve Type*: normally open; normally closed; normally partly open; two-way; three-way, with/without valve position feedback; ball valve, gate valve, butterfly type, spring loaded, low pressure drops
 7. *Temperature and pressure* allow classification by high, low, or cryogenic temperature fluids, or high or low pressure or vacuum capability
 8. *Accessible or not accessible* to inspection, servicing, or replacement of valve or its seal
-

^aThis list is not comprehensive or complete.

Figure 6–14 shows a large main liquid oxygen valve. It is normally closed, rotary actuated, cryogenic, high pressure, high flow, reusable ball valve with a low-pressure loss in the open position, allowing continuous throttling, a controlled rate of opening through a crank and hydraulic piston (not shown), with a position feedback and anti-icing controls.

Pressure regulators are special valves that are used frequently to regulate gas pressures. Usually the discharge pressure is regulated to a predetermined standard pressure value by continuously throttling the flow, using a piston, flexible diaphragm, or electromagnet as the actuating mechanism. Regulators can be seen in the flow sheets of Figs. 1–3 and 6–13.

The various fluids in a rocket engine are usually transported by *pipes* or *lines*, usually made of metal and joined by fittings or welds. Their design must provide for thermal expansion and provide support to minimize vibration effects. For gimballed thrust chambers it is necessary to provide flexibility in the piping to allow the thrust axis to be rotated through a small angle, typically ± 3 to $\pm 10^\circ$. This flexibility is provided by flexible pipe joints and/or by allowing pipes to deflect slightly when using two or more right-angle turns in the lines. The high-pressure propellant feed lines of the SSME have both flexible joints and right-angle bends, as shown in Figs. 6–1 and 6–15. This joint has flexible bellows as a seal and a universal joint-type mechanical linkage with two sets of bearings for carrying the separating loads imposed by the high pressure.

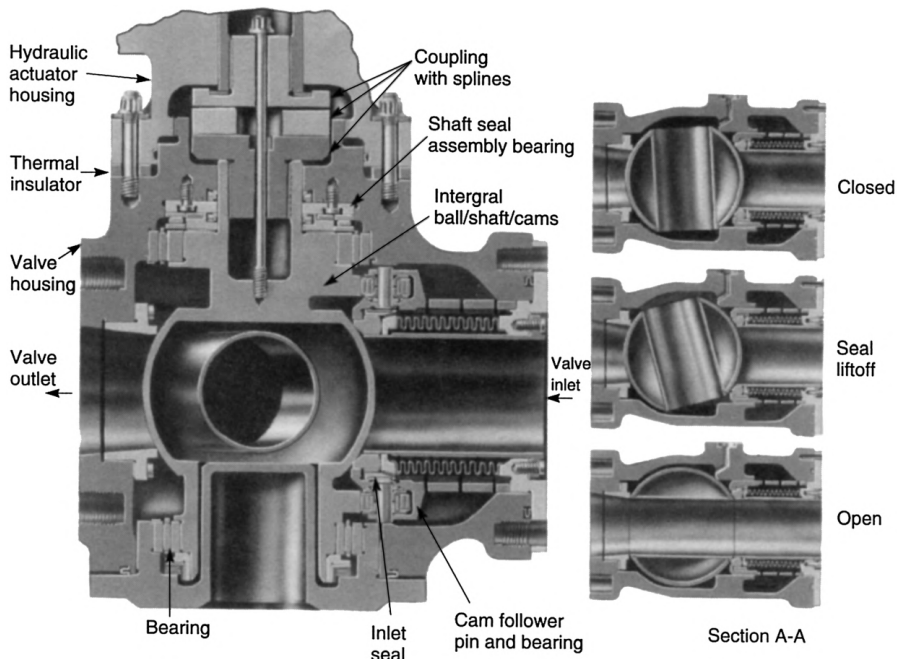


FIGURE 6-14. The SSME main oxidizer valve is a low-pressure drop ball valve representative of high-pressure large valves used in rocket engines. The ball and its integral shaft rotate in two bearings. The seal is a machined plastic ring spring-loaded by a bellows against the inlet side of the ball. Two cams on the shaft lift the seal a short distance off the ball within the first few degrees of ball rotation. The ball is rotated by a precision hydraulic actuator (not shown) through an insulating coupling. (Courtesy of Pratt & Whitney Rocketdyne.)

Sudden closing of valves can cause *water hammer* in the pipelines, leading to unexpected pressure rises that can be destructive to propellant system components. An analysis of this water hammer phenomenon will allow determination of the approximate maximum pressure (Ref. 6-18). The friction of the pipe and the branching of pipelines reduce this maximum pressure. Water hammer can also occur when admitting the initial flow of high-pressure propellant into evacuated pipes. The pipes are under vacuum to remove air and prevent the forming of gas bubbles in the propellant flow, which can cause combustion problems.

Many liquid rocket engines have *filters* in their lines. This is necessary to prevent dirt, particles, or debris, such as small pieces from burst diaphragms, from entering precision valves or regulators (where debris can cause a malfunction) or from plugging small injection holes, which could cause hot streaks in the combustion gases, in turn causing a thrust chamber failure.

Occasionally, a convergent-divergent *venturi section*, with a sonic velocity at its throat, is placed into one or both of the liquid propellant lines. It has also been called a *cavitating venturi*, when the local throat pressure goes below

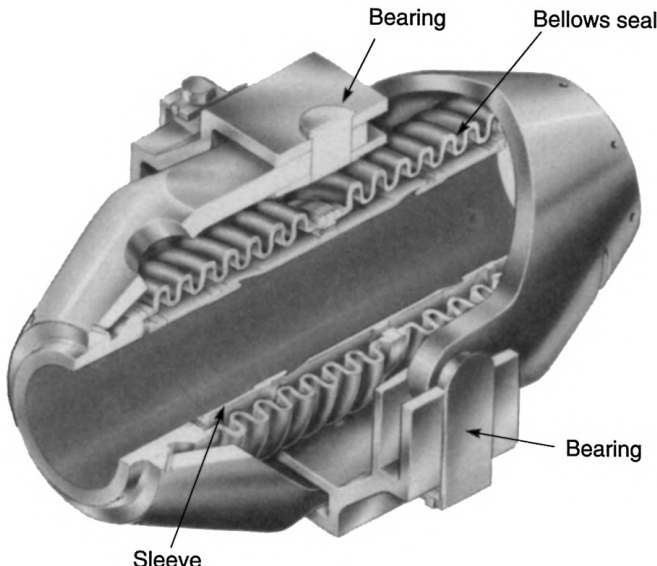


FIGURE 6–15. Flexible high-pressure joint with external gimbal rings for a high-pressure hot turbine exhaust gas. (Courtesy of Pratt & Whitney Rocketdyne)

the vapor pressure. The merits are that it maintains constant flow and prevents pressure disturbances from traveling upstream. This can prevent the propagating of chamber pressure oscillations or coupling with thrust chamber combustion instabilities. The venturi section can also help in minimizing some water hammer effects in a system with multiple banks of thrust chambers.

6.10. ENGINE SUPPORT STRUCTURE

Most of the larger rocket engines have their own mounting structure or support structure. On it the major components are mounted. It also transmits the thrust force to the vehicle. Welded tube structures or metal plate/sheet metal assemblies have been used. In some large engines the thrust chamber is used as a structure and the turbopump, control boxes, or gimbal actuators are attached to it.

In addition to the thrust load, an engine structure has to withstand forces imposed by vehicle maneuvers (in some cases a side acceleration of $10 g_0$), vibration forces, actuator forces for thrust vector control motions, and loads from transportation over rough roads.

In low-thrust engines with multiple thrusters there often is no separate engine mounting structure; the major components are in different locations of the vehicle, connected by tubing, wiring, or piping, and each is usually mounted directly to the vehicle or spacecraft structure.

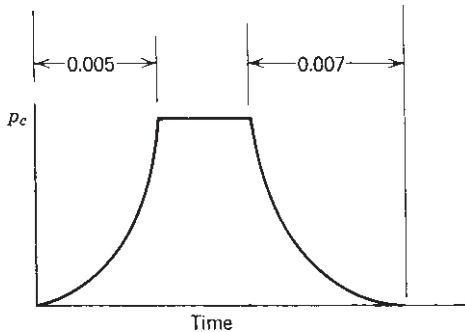
PROBLEMS

- In an engine with a gas generator engine cycle, the turbopump has to do more work in the pumps, if the thrust chamber operating pressure is raised. This of course requires an increase in turbine gas flow which, when exhausted, adds little to the engine specific impulse. If the chamber pressure is raised too much, the decrease in performance due to an excessive portion of the total propellant flow being sent through the turbine and the increased mass of the turbopump will outweigh the gain in specific impulse that can be attained by increased chamber pressure and also by increased thrust chamber nozzle exit area. Outline in detail a method for determining the optimum chamber pressure where the sea-level performance will be a maximum for a rocket engine that operates in principle like the one shown in Fig. 1-4.
- The engine performance data for a turbopump rocket engine system are as follows:

| | |
|---|-------------------------------|
| Propellants | Liquid oxygen/kerosene |
| Engine system specific impulse (steady state) | 272 sec |
| Engine system mixture ratio | 2.52 |
| Rated engine system thrust | 40,000 N |
| Oxidizer vapor flow to pressurize oxidizer tank | 0.003% of total oxidizer flow |
| Propellant flow through turbine at rated thrust | 2.1% of total propellant flow |
| Gas generator mixture ratio | 0.23 |
| Specific impulse of turbine exhaust | 85 sec |

Determine performance of the thrust chamber I_s , r , F (see Section 11.2).

- For a pulsing rocket engine, assume a simplified parabolic pressure rise of 0.005 sec, a steady-state short period of full chamber pressure, and a parabolic decay of 0.007 sec approximately as shown in the sketch. Plot curves of the following ratios as a function of operating time t from $t = 0.013$ to $t = 0.200$ sec: (a) average pressure to ideal steady-state pressure (with zero rise or decay time); (b) average I_s to ideal steady-state I_s ; (c) average F to ideal steady-state F .



4. For a total impulse of 100 lbf-sec compare the volume and approximate system weights of a pulsed propulsion system using different gaseous propellants, each with a single spherical gas storage tank (at 3500 psi and 0°C). A package of small thrust nozzles with piping, valves, and controls is provided which weighs 3.2 lb. The gaseous propellants are hydrogen, nitrogen, or argon (see Table 7-3).
5. Compare several systems for a potential roll control application which requires four thrusters of 1 lbf each to operate for a cumulative duration of 2 min each over a period of several days, which allows a constant gas temperature. Include the following:

| | |
|---|--------------------------|
| Pressurized helium | 70°F temperature |
| Pressurized nitrogen | 70°F Ambient temperature |
| Pressurized krypton | 70°F Ambient temperature |
| Pressurized helium at 300°F (electrically heated) | |

The pressurized gas is stored at 5000 psi in a single spherical fiber-reinforced plastic tank; use a tensile strength of 150,000 psi and a density of 0.050 lbm/in.³ with a 0.012-in.-thick aluminum inner liner as a seal against leaks. Neglect the gas volume in the pipes, valves, and thrusters, but assume the total hardware mass of these to be about 1.3 lbm. Use Table 7-3. Make estimates of the tank volume and total system weight. Discuss the relative merits of these systems.

6. A sealed propellant tank contains hydrazine. It is stored for long periods of time, and therefore the propellant and the tank will reach thermal equilibrium with the environment. At an ambient temperature of 20°C and an internal pressure of 1.2 atm the liquid occupies 87% of the tank volume and the helium pressurizing gas occupies 13%. Assume no evaporation of the propellant, no dissolving of the gas in the liquid, and no movement of the tank. Use the hydrazine properties from Figs. 7-1 and 7-2 and Table 7-1. What will be the approximate volume percentages and the gas pressure at the extreme storage temperatures of 4 and 40°C?
7. A liquid hydrogen/liquid oxygen thrust chamber has a constant bipropellant flow rate of 347 kg/sec at a mixture ratio of 6.0. It operates at full thrust for exactly 2 min. The propellant in the tanks are initially at the propellant boiling points and are assumed to be of uniform initial temperature at start. Use data from Table 7-1 for the propellant specific gravities. Assuming no losses, find the masses of (a) fuel and (b) of oxidizer used to produce the thrust for the nominal duration. (c) What was the volume of the liquid hydrogen actually used? (d) Assuming 4.0% extra fuel mass (for unusable propellant residual, evaporation, hardware cooling, or venting just prior to start, or propellant consumed inefficiently during startup and shutdown) and a 10% ullage volume (the void space above the liquid in the tank), what will be the volume of the fuel tank? Assume other losses can be neglected.
- Answers: (a) 5941 kg, (b) 35,691 kg, (c) 83.83 m³ (d) 95.6 m³.
8. Prepare dimensioned rough sketches of the four propellant tanks needed for operating a single gimbal-mounted RD 253 engine (Table 11-3) for 80 sec at full thrust and

an auxiliary rocket system with a separate pressurized feed system using the same propellants, with two gimbal-mounted small thrust chambers, each of 150 kg thrust, a duty cycle of 12% (fires only 12% of the time), but for a total flight time of 1.00 hr. For propellant properties Table 7–1. Describe any assumptions that were made with the propellant budget, the engines, or the vehicle design, as they affect the amount of propellant.

9. Table 10–5 shows that the RD 120 rocket engine can operate at thrusts as low as 85% of full thrust and with a mixture ratio variation of $\pm 10.0\%$. Assume a 1.0% unavailable residual propellant. The allowance for operational factors, loading uncertainties, off-nominal rocket performance, and a contingency is 1.27% for the fuel and 1.15% for the oxidizer.
- In a particular flight the average main thrust was 98.0% of nominal and the mixture ratio was off by +2.00% (oxidizer rich). What percent of the total fuel and oxidizer loaded into the vehicle will remain unused at thrust termination?
 - If we want to run at a fuel-rich mixture in the last 20% of the flight duration (in order to use up all the intended flight propellant), what would the mixture ratio have to be for this last period?
 - In the worst possible scenario with maximum throttling and extreme mixture ratio excursion ($\pm 3.00\%$, but operating for the nominal duration), what is the largest possible amount of unused oxidizer or unused fuel in the tanks?

SYMBOLS

| | |
|------------|---|
| c | effective exhaust velocity, m/sec (ft/sec) |
| c_v | specific heat at constant volume, J/kg-K (Btu/lbm-°R) |
| C_F | thrust coefficient |
| F | thrust force, N (lbf) |
| g_0 | acceleration of gravity at sea level, 9.8066 m/sec ² |
| I_s | specific impulse, sec |
| k | specific heat ratio |
| m | propellant mass, kg (lbm) |
| \dot{m} | mass flow rate, kg/sec (lb/sec) |
| p | pressure, N/m ² (psi) |
| Δp | pressure difference, N/m ² (psi) |
| r | mixture ratio (oxidizer to fuel mass flow rates) |
| R | gas constant per unit mass, J/kg-K (ft-lbf/lbm-°R) |
| T | absolute temperature, K |
| V | volume flow rate, m ³ /sec (ft ³ /sec) |
| w | total propellant weight, N (lbf) |
| \dot{w} | weight flow rate, N/sec (lbf/sec) |

Subscripts

| | |
|----------|---|
| <i>f</i> | fuel |
| 0 | initial condition or stagnation condition |
| <i>g</i> | gas tank |
| <i>o</i> | oxidizer |
| <i>p</i> | propellant tank or power cutoff |

REFERENCES

- 6–1. D. K. Huzel and D. H. Huang, *Design of Liquid Propellant Rocket Engines*, rev. ed., AIAA, Reston, VA, 1992.
- 6–2. G. G. Gakhun, V. I. Baulin, et al. *Construction and Design of Liquid Propellant Rocket Engines* (in Russian), *Konstruksiya i Proyektirovaniye Zhidkostniy Raketnykh Dvigateley*, Mashinostroyeniye, Moscow, 1989.
- 6–3. J. I. Hochsten, H.-C. Ji, and J. Ayelott, “Prediction of Self-Pressurization Rate of Cryogenic Propellant Tankage,” *Journal of Propulsion and Power*, Vol. 6, No. 1, January–February 1990, pp. 11–17.
- 6–4. B. Morton, M. Elgersma, and R. Playter, “Analysis of Booster Vehicle Slosh Stability During Ascent to Orbit,” AIAA Paper 90–1876, July 1990.
- 6–5. J. J. Pocha, “Propellant Slosh in Spacecraft and How to Live with It,” *Aerospace Dynamics*, Vol. 20, Autumn 1986, pp. 26–31.
- 6–6. G. P. Purohit and L. D. Loudenback, “Application of Etched Disk Stacks in Surface Tension Propellant Management Devices,” *Journal of Propulsion and Power*, Vol. 7, No. 1, January–February 1991, pp. 22–30.
- 6–7. J. R. Rollins, R. K. Grove, and D. R. Walling, Jr. “Design and Qualification of a Surface Tension Propellant Tank for an Advanced Spacecraft,” AIAA Paper 88–2848, 24th Joint Propulsion Conference, 1988.
- 6–8. *Design Guide for Pressurized Gas Systems*, Vols. I and II, prepared by IIT Research Institute, NASA Contract NAS7-388, March 1966.
- 6–9. H. C. Hearn, “Evaluation of Bipropellant Pressurization Concepts for Spacecraft,” *Journal of Spacecraft and Rockets*, Vol. 19, July 1982, pp. 320–325.
- 6–10. H. C. Hearn, “Design and Development of a Large Bipropellant Blowdown Propulsion System,” *Journal of Propulsion and Power*, Vol. 11, No. 5, September–October 1995.
- 6–11. *National Space Transportation System Reference*, Vol. 1, National Aeronautics and Space Administration, Washington, DC, June 1988 (description of Space Shuttle system and operation).
- 6–12. Personal communications from Jim Morehart, The Aerospace Corp., Vince Whee- lock, Pat Mills, and Randy Parsley of Pratt & Whitney Rocketdyne, and Gordon Dressler, Northrop Grumman Corp.

- 6–13. H. Grosdemange and G. Schaeffer, “The SEPR 844 Reuseable Liquid Rocket Engine for Mirage Combat Aircraft,” AIAA Paper 90–1835, July 1990.
- 6–14. D. Manski, C. Goertz, H. D. Sassinick, J. R. Hulk, B. D. Goracke, and D. J. H. Levack, “Cycles for Earth to Orbit Propulsion,” *Journal of Propulsion and Power*, AIAA, Vol. 14, No. 5, September–October 1998.
- 6–15. D. Conley, N. Y. Lee, P. L. Portanova and B. K. Wood, “Evolved Expendable Launch Vehicle System: RS-68 Main Engine Development,” Paper IAC-02.S.1.01, 53rd International Astronautical Congress, 10–19 Oct. 2002, Houston, Texas.
- 6–16. J. R. Brown, “Expander Cycle Engines for Shuttle Cryogenic Upper Stages,” AIAA Paper 83–1311, 1983.
- 6–17. G. P. Sutton, “History of Small Liquid Propellant Thrusters,” presented at 52nd JANNAF Propulsion Meeting, 12 May 2004, Las Vegas, Nevada; published by Chemical Propulsion Information Analysis Center, Columbia, MD.
- 6–18. R. P. Prickett, E. Mayer, and J. Hermel, “Waterhammer in Spacecraft Propellant Feed Systems,” *Journal of Propulsion and Power*, Vol. 8, No. 3, May–June 1992.

CHAPTER 7

LIQUID PROPELLANTS

Section 6.1 gave the classification of liquid propellants. In this chapter we discuss properties, performance, hazards, and characteristics of selected common liquid propellants. These characteristics affect the engine and vehicle design, test facilities, and propellant storage and handling. Today we commonly use three liquid bipropellant combinations. Each of these propellants will be described further in this chapter. They are: (1) the cryogenic *oxygen–hydrogen propellant system*, used in upper stages and sometimes booster stages of space launch vehicles; it gives the highest specific impulse for a nontoxic propellant combination, which makes it best for high vehicle velocity missions; (2) the *liquid oxygen–hydrocarbon propellant combination*, used for booster stages (and a few second stages) of space launch vehicles; its higher average density allows a more compact booster stage, when compared to the first combination; also, historically, it was developed before the first combination and was originally used for ballistic missiles; (3) not a single propellant combination, but several *storable propellant combinations*, are used in large rocket engines for first and second stages of ballistic missiles and in almost all bipropellant low-thrust, auxiliary or reaction control rocket engines (this term is defined below); they allow long-term storage and almost instant readiness to start without the delays and precautions that come with cryogenic propellants. There also were fuel mixtures of several storable propellant such as alcohol and hydrazine. In Russia the nitric acid–hydrocarbon combination was used in ballistic missiles many years ago. Today Russia and China favor nitrogen tetroxide as the oxidizer–unsymmetrical dimethylhydrazine, or UDMH, as the fuel for ballistic missiles and auxiliary engines. The United States started with nitrogen tetroxide and a fuel mixture of 50% UDMH with 50% hydrazine in the large engines for the Titan II missile. For auxiliary engines in many satellites and upper stages the United States has used, and is still using, the

bipropellant of nitrogen tetroxide with monomethylhydrazine. The orbit maneuvering system of the Space Shuttle uses it. Alternatively many U.S. satellites have used, and are still using monopropellant hydrazine for low-thrust auxiliary engines.

In the last 30 years there has not been a truly new propellant used in a rocket engine for an operational flight vehicle. Some new propellants, such as hydroxyl ammonium nitrate, have been synthesized, manufactured, and ground tested in thrust chambers in the last decade, but they have not found their way into an operational rocket engine. Between 1942 and 1975 a number of other propellants (not the ones commonly used today) were successfully flown; this includes ammonia (X-15 Research test aircraft), ethyl alcohol (German V-2 or U.S. Redstone), or aniline (WAC Corporal). They each had some disadvantages and they are no longer used for operational flights today. The liquid oxidizer nitrous oxide (N_2O), also known as laughing gas, has found a new application in a hybrid propulsion system (with a solid fuel) and it is discussed further in Chapter 16 on hybrid propulsion systems. Most of the commonly used liquid oxidizers for liquid propellant rocket engines are listed and described briefly in this chapter.

A comparative listing of various performance quantities for a number of propellant combinations is given in Table 5-5 and in Ref. 7-1. Some important physical properties of selected common propellants are given in Table 7-1. For comparison water is also listed. Specific gravities and vapor pressures are shown in Figs. 7-1 and 7-2.

7.1. PROPELLANT PROPERTIES

It is important to distinguish between the characteristics and properties of the *liquid propellants* (the fuel and oxidizer liquids in their unreacted condition) and those of the *hot gas mixture*, which results from the reaction in the combustion chamber. The chemical nature of the liquid propellants and their mixture ratio determines the properties and characteristics of both of these types. Unfortunately, none of the practical, known propellants have all the desirable properties, and the selection of the propellant combination is usually a compromise of various factors, such as those listed below.

Economic Factors

Availability in quantity and a *low cost* are very important considerations in the selection of a propellant. In military applications, consideration has to be given to *logistics* of production, supply, storage, and other factors. The production process should be simple, requiring only ordinary chemical equipment and available raw materials. It is usually more expensive to use a toxic or cryogenic propellant than a storable, nontoxic one, because it requires additional steps in the operation, more safety provisions, additional design features, longer check-out procedures prior to launch, and often better trained personnel.

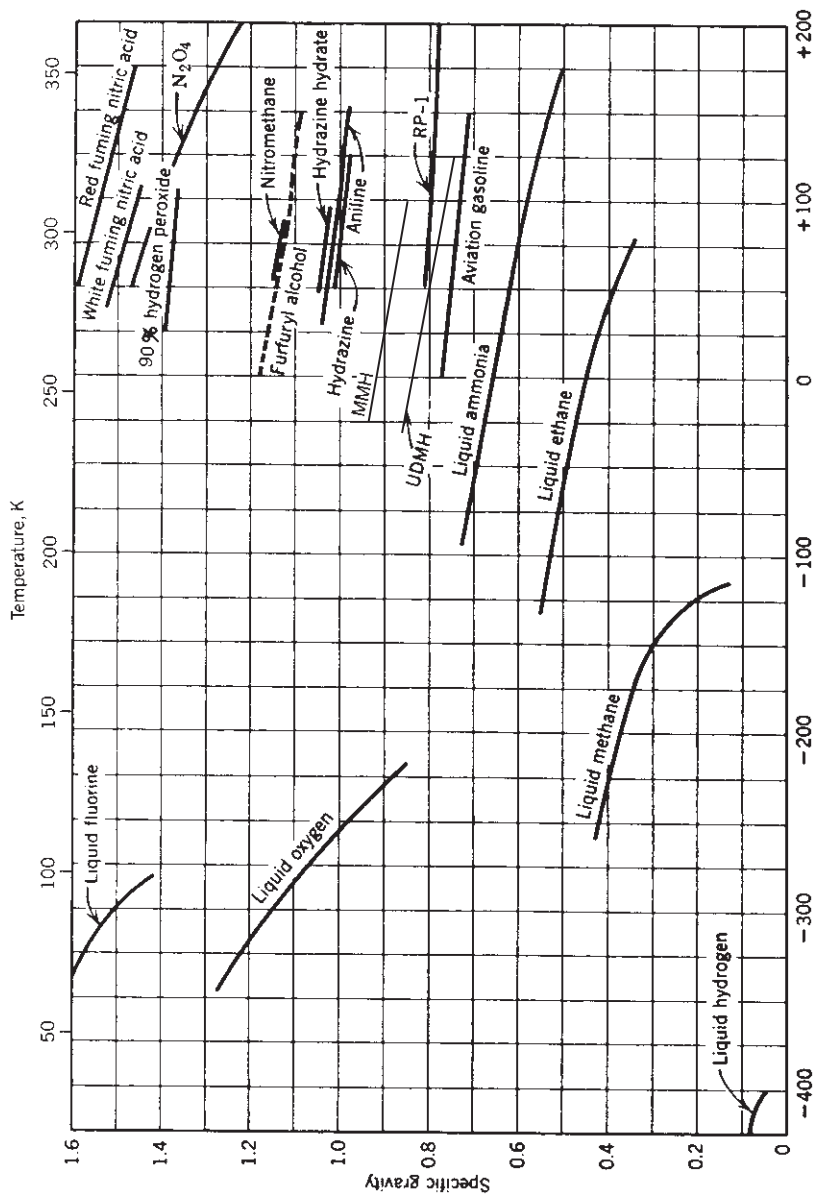


FIGURE 7-1. Specific gravities of several liquid propellants as a function of temperature.

TABLE 7–1. Physical Properties of Several Common Liquid Propellants

| Propellant | Liquid Fluorine | Hydrazine | Liquid Hydrogen | Methane | Monomethylhydrazine |
|-------------------------------|---------------------------------------|---------------------------------------|--|---------------------------------------|---------------------------------------|
| Chemical formula | F ₂ | N ₂ H ₄ | H ₂ | CH ₄ | CH ₃ NHNH ₂ |
| Molecular mass | 37.997 | 32.045 | 2.016 | 16.03 | 46.072 |
| Melting or freezing point (K) | 53.54 | 275.16 | 14.0 | 90.5 | 220.7 |
| Boiling point (K) | 85.02 | 387.46 | 20.4 | 111.6 | 360.8 |
| Heat of vaporization (kJ/kg) | 172.2 ^b | 1219 ^b | 446 | 510 ^b | 808 |
| Specific heat (kcal/kg-K) | 0.368 (85 K) 0.357 (69.3 K) | 0.736 (293 K) 0.758 (338 K) | 1.75 ^b (20.4 K) — | 0.835 ^b (298 K) — | 0.700 (393 K) |
| Specific gravity ^c | 1.636 (66 K) 1.440 (93 K) | 1.0037 (298 K) 0.952 (350 K) | 0.071 (20.4 K) 0.076 (14 K) | 0.424 (111.5 K) — | 0.8702 (298 K) 0.857 (311 K) |
| Viscosity (centipoise) | 0.305 (77.6 K) 0.397 (70 K) | 0.97 (298 K) 0.913 (330 K) | 0.024 (14.3 K) 0.013 (20.4 K) | 0.12 (111.6 K) 0.22 (90.5 K) | 0.775 (298 K) 0.40 (344 K) |
| Vapor pressure (MPa) | 0.037 (77 K) 0.0065 (66.5 K) | 0.0019 (298 K) 0.016 (340 K) | 0.2026 (23 K) 0.87 (30 K) | 0.033 (100 K) 0.101 (117 K) | 0.0066 (298 K) 0.638 (428 K) |

^aRed fuming nitric acid (RFNA) has 5 to 20% dissolved NO₂ with an average molecular mass of about 60, and a density and vapor pressure somewhat higher than those of pure nitric acid.

^bAt boiling point.

^cReference for specific gravity ratio: 10³ kg/m³ or 62.42 lbm/ft³.

Performance of Propellants

The rocket engine performance can be compared on the basis of the *specific impulse*, the *exhaust velocity*, the *characteristic velocity*, or other engine parameters. They have been explained in Chapters 3, 5, and 6. The specific impulse and exhaust velocity are functions of pressure ratio, specific heat ratio, combustion temperature, mixture ratio, and molecular mass. Values of performance parameters for various propellant combinations can be calculated with a high degree of accuracy and several are listed in Table 5–5. Very often the performance is expressed in terms of *flight performance parameters* for a given rocket

| Nitric Acid ^a (99% pure) | Nitrogen Tetroxide | Liquid Oxygen | Rocket Fuel RP-1, RP-2 | Unsymmetrical Dimethyl- hydrazine (UDMH) | Water |
|--|-------------------------------|------------------|-----------------------------------|---|-------------------|
| HNO ₃ | N ₂ O ₄ | O ₂ | Hydrocarbon CH _{1.97} | (CH ₃) ₂ NNH ₂ | H ₂ O |
| 63.016 | 92.016 | 31.988 | ~ 175 | 60.099 | 18.02 |
| 231.6 | 261.95 | 54.4 | 225 | 216 | 273.15 |
| 355.7 | 294.3 | 90.0 | 460–540 | 335.5 | 373.15 |
| 480 | 413 ^b | 213 | 246 ^b | 543 | 2253 ^b |
| 0.042 | 0.374 | 0.4 | 0.45 | 0.704 | 1.008 |
| (311 K) | (290 K) | (65 K) | (298 K) | (298 K) | (273.15 K) |
| 0.163 | 0.447 | | | 0.715 | |
| (373 K) | (360 K) | | | (340 K) | |
| 1.549 | 1.447 | 1.14 | 0.58 | 0.7861 | 1.002 |
| (273.15 K) | (293 K) | (90.4 K) | (422 K) | (298 K) | (373.15 K) |
| 1.476 | 1.38 | 1.23 | 0.807 | 0.784 | 1.00 |
| (313.15 K) | (322 K) | (77.6 K) | (289 K) | (244 K) | (293.4 K) |
| 1.45 | 0.47 | 0.87 | 0.75 | 0.492 | 0.284 |
| (273 K) | (293 K) | (53.7 K) | (289 K) | (298 K) | (373.15 K) |
| 0.33 | 0.19 | 0.21 | | 0.48 | 1.000 |
| | (315 K) | (90.4 K) | (366 K) | (300 K) | (277 K) |
| 0.0027 | 0.01014 | 0.0052 | 0.002 | 0.0223 | 0.00689 |
| (273.15 K) | (293 K) | (88.7 K) | (344 K) | (298 K) | (312 K) |
| 0.605 | 0.2013 | | 0.023 | 0.1093 | 0.03447 |
| (343 K) | (328 K) | | (422 K) | (339 K) | (345 K) |

application, as explained in Chapter 4. Here the average density, the total impulse, and the engine mass ratio usually enter into a complex flight relation equation.

For high performance a *high content of chemical energy* per unit of propellant mixture is desirable because it permits a high chamber temperature. A *low molecular mass* of the product gases of the propellant combination is also desirable. It can be accomplished by using fuels rich in combined hydrogen, which is liberated to become gas during the reaction. A low molecular mass is obtained if a large portion of the hydrogen gas produced does not combine with oxygen. In general, therefore, the best mixture ratio for many bipropellants is not necessarily the stoichiometric one (which results in complete oxidation and yields a high flame temperature) but usually a fuel-rich mixture containing a large portion of low-molecular-mass reaction products, as shown in Chapter 5.

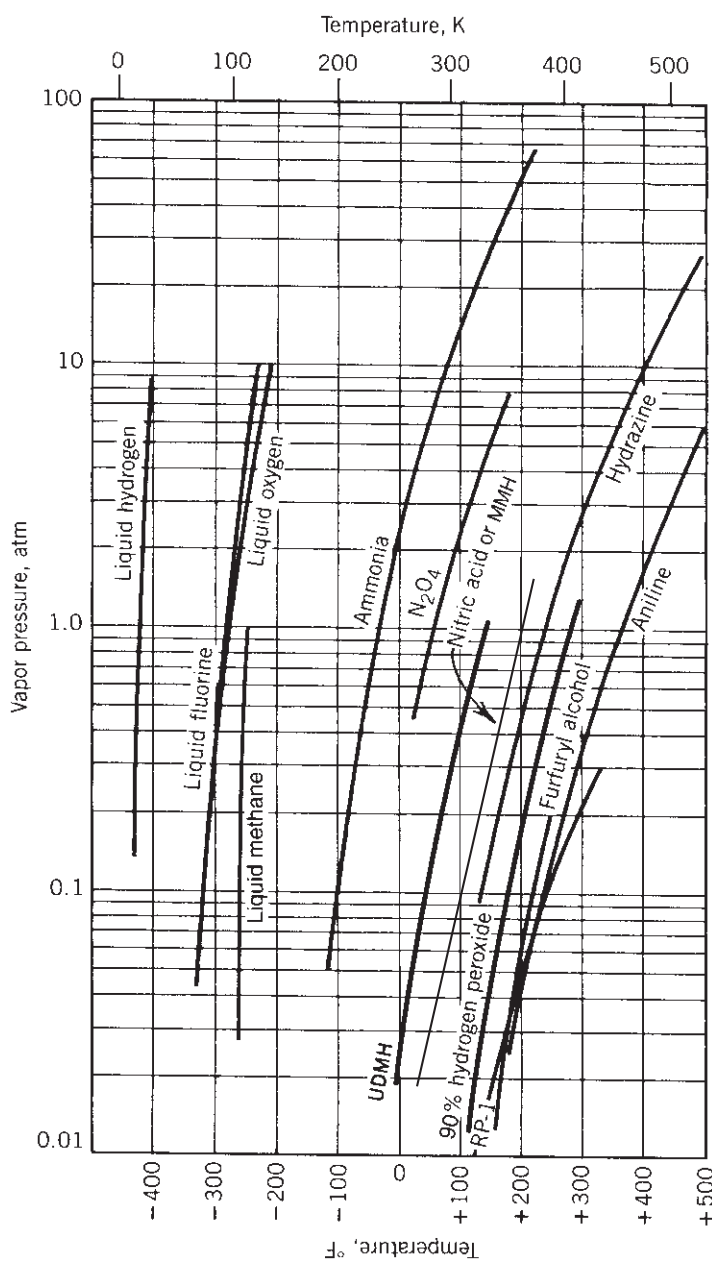


FIGURE 7-2. Vapor pressures of several liquid propellants as a function of temperature.

If very small metallic fuel particles of beryllium or aluminum are suspended in the liquid fuel, it is theoretically possible to increase the specific impulse by between 9 and 18%, depending on the particular propellant combination, its mixture ratio, and the metal powder additive. Gelled propellants with suspended small solid particles have been ground tested successfully with storable fuels. For gelled propellants, see Section 7.5.

The chemical propellant combination that has the highest potential specific impulse (approximately 480 sec at 1000 psia chamber pressure and expansion to sea-level atmosphere, and 565 sec in a vacuum with a nozzle area ratio of 50) uses a toxic liquid fluorine oxidizer with hydrogen fuel plus suspended toxic solid particles of beryllium; as yet a practical means for storing these propellants and a practical rocket engine have not been developed.

Common Physical Hazards

Although the several categories of hazards are described below, they do not all apply to every propellant or every bipropellant combination. The hazards are different for each specific propellant and must be carefully understood before working with that propellant. The consequences of unsafe operation or unsafe design are usually also unique to several propellants.

Corrosion. Various propellants, such as nitrogen tetroxide, nitric acid, or hydrogen peroxide, have to be handled in containers and pipelines of special materials. If the propellant were permitted to become contaminated with corrosion products, its physical and chemical properties could change sufficiently to make it unsuitable for rocket operation. The corrosion of the gaseous reaction products is important in applications in which the reaction products are likely to damage structure and parts of the vehicle or affect communities and housing near a test facility or launch site.

Explosion Hazard. Some propellants, such as hydrogen peroxide and nitromethane, are unstable and tend to detonate under certain conditions of impurities, temperature, and shock. If liquid oxidizers (e.g., liquid oxygen) and fuels are mixed together, they can be detonated. Unusual, rare flight vehicle launch or transport accidents have caused such mixing to occur (see Refs. 7-2 and 7-3).

Fire Hazard. Many oxidizers will start chemical reactions with a large variety of organic compounds. Nitric acid, nitrogen tetroxide, fluorine, or hydrogen peroxide react spontaneously with many organic substances, resulting in a conflagration. Most of the fuels are readily ignitable when exposed to air and heat. Also some household dusts, certain paints, or smoke particles can be oxidized.

Accidental Spills. Unforeseen mishaps during engine operation and traffic accidents on highways or railroads while transporting hazardous materials, including propellants, have on occasion caused spills, which expose people to unexpected

fires or potential health hazards. The U.S. Department of Transportation has rules for marking and containing hazardous materials during transport and also guidelines for emergency action (see Ref. 7–4).

Health Hazards. Many propellants are toxic or poisonous, and special precautions have to be taken to protect personnel. Fluorine, for example, is very poisonous. Toxic propellant chemicals or poisonous exhaust species can enter the human body in several ways. The resulting health disorders are propellant specific. Nitric acid can cause severe skin burns and tissue disintegration. Skin contact with aniline or hydrazine can cause nausea and other adverse health effects. Hydrazine, monomethylhydrazine, unsymmetrical dimethylhydrazine, or hydrazine hydrate are known animal carcinogens (cancer-causing substances) and suspected human carcinogens. Many propellant vapors cause eye irritation, even in very small concentration. Inadvertent ingestion (swallowing) of many propellants can also cause severe health degradation.

The inhalation of certain toxic exhaust gases or gaseous or vaporized propellants is perhaps the most common health hazard. It can cause severe damage if the exposure is for long duration or in concentrations that exceed established maximum threshold values. In the United States the Occupational Safety and Health Administration (OSHA) has established limits or thresholds on the allowable exposure and concentration for most propellant chemicals. Several of these threshold limits are mentioned later in this chapter. Toxic gases in the exhaust could include hydrofluoric acid (HF) gas; its OSHA 8-hr personnel exposure limit is 3 ppm (volumetric parts per million) and its short-term (typically, 15 min) exposure limit is 6 ppm. A concentration of 3000 ppm or 0.3% can be fatal within a few seconds. References 7–2 and 7–5 give more information on toxic effects.

The corrosion, explosion, and fire hazards of many propellants put severe limitations on the materials, the handling, and the design of rocket-propelled vehicles and their vehicle's engine compartments. Not only is the rocket system itself exposed to the hazardous propellant, but adjacent personnel, structural parts, electrical and other vehicle equipment, and test and launch facilities have to be properly protected against the effects of possible leaks, fumes, and fires or explosions from propellant accumulations.

Material Compatibility. Several liquid propellants have only a limited number of truly compatible materials, both metals and nonmetals, such as gaskets or O-rings. There have been unfortunate failures (causing fires, leakage, corrosion, or malfunctions) when an improper or incompatible material was used in the hardware of a rocket engine. Depending on the specific component and loading conditions, these structural materials have to withstand high stresses, stress corrosion, and in some versions high temperatures or abrasion. Several specific material limitations are mentioned in the next section. Certain materials catalyze a self-decomposition of stored hydrogen peroxide into water and oxygen, making long-term storage difficult and, if confined, causing its closed container to

explode. Many structural materials, when exposed to cold, cryogenic propellants, can become very brittle.

Desirable Physical Properties

Low Freezing Point. This permits operation of rockets in cold weather. The addition of small amounts of freezing point depressant has been found to help lower the freezing point of some liquid propellants which otherwise might solidify at relatively high temperature.

High Specific Gravity. A denser propellant will provide a larger mass of propellants in a given vehicle tank volume. It permits a smaller tank volume and, consequently, a lower structural vehicle mass and lower aerodynamic drag. Propellant specific gravity, therefore, has an important effect on the maximum flight velocity and range of any rocket-powered vehicle or missile, particularly when flying within the Earth's atmosphere, as explained in Chapter 4. Specific gravities for various propellants are plotted in Fig. 7-1. A variation of the temperature of stored propellant will cause a change of the liquid level in the tank.

For any given mixture ratio r , the *average specific gravity* of a propellant combination δ_{av} can be determined from the specific gravities of the fuel δ_f and of the oxidizer δ_o . The average specific gravity is defined as the mass of the fuel and oxidizer, divided by the sum of their volumes. Here the mixture ratio is defined as the oxidizer mass flow rate divided by the fuel mass flow rate. (Eq. 6-1):

$$\delta_{av} = \frac{\delta_o \delta_f (1 + r)}{r \delta_f + \delta_o} \quad (7-1)$$

Values of δ_{av} for various propellant combinations are listed in Table 5-5. The value of δ_{av} can be increased by adding heavy materials to the propellants, either by solution or colloidal suspension. The identical type of equation can be written for the average density ρ_{av} in terms of the fuel density and the oxidizer density:

$$\rho_{av} = \frac{\rho_o \rho_f (1 + r)}{\rho_f r + \rho_o} \quad (7-2)$$

In the SI system of units the specific gravity has the same numerical value as the density expressed in units of grams per cubic centimeter or kg/liter. In some performance comparisons the parameter *density specific impulse* I_d is used. It is defined as the product of the average specific gravity δ and the specific impulse I_s :

$$I_d = \delta_{av} I_s \quad (7-3)$$

Stability. No deterioration and no decomposition with long-term (over 15 years) storage and minimal reaction with the atmosphere have been attained with many propellants. Good *chemical stability* means no decomposition of the liquid propellant during operation or storage, even at elevated temperature. A good liquid

propellant should also have no *chemical deterioration* when in contact with tubing pipes, tank walls, valve seats, and gasket materials, even at relatively high ambient temperatures. No appreciable *absorption of moisture* and no adverse effects of small amounts of *impurities* are desirable properties. There should be no chemical deterioration when liquid flows through the hot cooling jacket passages of a regeneratively cooled thrust chamber. Some hydrocarbons (e.g., some olefins) decompose and form carbonaceous deposits on the hot inside surfaces of the cooling passage. These deposits can become hard, reduce the heat flow, increase the local metal temperatures, and thus can cause the metal to weaken and fail. About 1% per year of stored 90% concentrated hydrogen peroxide decomposes even in clean storage tanks. Between 1 and 20% of a cryogenic propellant (stored in a flight vehicle) evaporates every day in an insulated tank.

Heat Transfer Properties. *High specific heat, high thermal conductivity, and a high boiling or decomposition temperature* are desirable for propellants that are used for thrust chamber cooling (see Section 8.5).

Pumping Properties. A low *vapor pressure* permits not only easier handling of the propellants, but also a more effective pump design in applications where the propellant is pumped. This reduces the potential for cavitation, as explained in Chapter 10. If the *viscosity* of the propellant is too high, then pumping and engine-system calibration become difficult. Propellants with high vapor pressure, such as liquid oxygen, liquid hydrogen, and other liquefied gases, require special design provisions, unusual handling techniques, and special low-temperature materials.

Temperature Variation of Physical Properties. The *temperature variation* of the physical properties of the liquid propellant should be small and should be very similar for the fuel and for the oxidizer. For example, a wide temperature variation in vapor pressure and density (*thermal coefficient of expansion*) or an unduly high change in viscosity with temperature makes it difficult to accurately calibrate a rocket engine flow system or predict its performance over any reasonable range of operating temperatures.

Ignition, Combustion, and Flame Properties

If the propellant combination is *spontaneously ignitable*, it does not require an ignition system. This means that burning is initiated as soon as the oxidizer and the fuel come in contact with each other. Spontaneously or self-ignitable propellant combinations are often termed *hypergolic* propellants. Although an ignition system is not a very objectionable feature, its elimination is usually desirable because it simplifies the propulsion system. All rocket propellants should be readily ignitable and have only a very short ignition time delay in order to reduce the potential explosion hazard during starting. Starting and ignition problems are discussed further in Section 8.6.

Nonspontaneously ignitable propellants have to be heated by external means before ignition can begin. Igniters are devices that accomplish an initial slight

pressurization of the chamber and the initial heating of the propellant mixture to the point where steady flow combustion can be self-sustained. The amount of energy added by the igniter to activate the propellants should be small so that low-power ignition systems can be used. The energy required for satisfactory ignition usually diminishes for increasing ambient temperature of the propellant. At low ambient temperatures ignition can be very slow (0.05 to 0.02 sec).

Certain propellant combinations burn very smoothly without combustion vibration which are gas pressure oscillations. Other propellant combinations do not demonstrate this *combustion stability* and, therefore, are less desirable. Combustion is treated in Chapter 9.

Smoke formation is objectionable in many applications because of the smoke deposits on the surrounding equipment and parts. *Smoke* and brilliantly *luminous exhaust flames* are objectionable in certain military applications because they can be easily detected. In some applications the condensed species in the exhaust gas can cause *surface contamination* on spacecraft windows or optical lenses, and the electrons in the flame can cause undesirable *interference* or *attenuation of communications radio signals*. See Chapter 20 for information on exhaust plumes.

Property Variations and Specifications

The propellant properties and quality must not vary from batch to batch, because this can affect engine performance, combustion, and physical or chemical properties. The same propellant must have the same composition, properties, and storage or rocket operating characteristics if manufactured at different times or if made by different manufacturers. For these reasons propellants are purchased against specifications which define ingredients, maximum allowable impurities, packaging methods or compatible materials, allowable tolerances on physical properties (such as density, boiling point, freezing point, viscosity, or vapor pressure), quality control requirements, cleaning procedures for containers, documentation of inspections, laboratory analyses, or test results. A careful chemical analysis of the composition and impurities is necessary. Reference 7-6 describes some of these methods of analysis.

Additives

Altering and tailoring propellant properties can be achieved with additives. For example, to make a nonhypergolic fuel become hypergolic (readily ignited), a reactive ingredient has been added. To desensitize concentrated hydrogen peroxide and reduce self-decomposition, it is diluted with 3 to 15% of clean water. To increase density or to alleviate certain combustion instabilities, a fine powder of a heavy solid material, such as aluminum, can be suspended in the fuel. The use of additives to lower the freezing point temperature has already been mentioned.

7.2. LIQUID OXIDIZERS

The most energetic oxidizer with the highest specific impulse is liquid fluorine. It has a high density and is extremely corrosive and toxic. It has been tested in several complete rocket engines but has been abandoned because of its hazards. Many different types of new storable and cryogenic liquid oxidizer propellants have been synthesized, tested in small thrust chambers, or proposed. For high specific impulse this includes boron–oxygen–fluorine compounds, oxygen–fluorine compounds, nitrogen–fluorine formulations, and fluorinated hydrocarbons; however, they all have some undesirable characteristics and these synthetic oxidizers have not been proven to be practical. Oxidizer liquids that have been used in experimental liquid rocket engines include mixtures of liquid oxygen and liquid fluorine, oxygen difluoride (OF_2), chlorine trifluoride (ClF_3), or chlorine pentafluoride (ClF_5). All of these are highly toxic, very corrosive, and are not used today. Several commonly used oxidizers are listed below.

Liquid Oxygen (O_2)

Liquid oxygen, often abbreviated as LOX, boils at 90 K at atmospheric pressure; at these conditions it has a specific gravity of 1.14 and a heat of vaporization of 213 kJ/kg. It is widely used as an oxidizer and burns with a bright white-yellow flame with most hydrocarbon fuels. It has been used in combination with alcohols, jet fuels (kerosene-type), gasoline, and hydrogen. As shown in Table 5–5, the attainable performance is relatively high, and liquid oxygen is therefore a desirable and commonly used propellant in large rocket engines. The following missiles and space launch vehicles use oxygen: (1) with jet fuel or RP-1 (kerosene)—Atlas V and Soyuz (Russia); (2) with hydrogen—Space Shuttle, Ariane-V (France), Delta IV, and Centaur upper stage; (3) with alcohol—some amateur rocket engines, Figs. 1–4 and 6–1 show units that use oxygen. Figures 5–1 to 5–6 give theoretical performance data for liquid oxygen with a kerosene-type fuel.

Although it usually does not burn spontaneously with organic materials at ambient pressures, combustion or explosions can occur when a confined mixture of oxygen and organic matter is suddenly pressurized. Impact tests show that mixtures of liquid oxygen with many commercial oils or organic materials will detonate. Liquid oxygen supports and accelerates the combustion of other materials. Handling and storage are safe when contact materials are clean. Liquid oxygen is a noncorrosive and nontoxic liquid and will not cause the deterioration of clean container walls. When in prolonged contact with human skin, the cryogenic propellant causes severe frostbite. Because liquid oxygen evaporates rapidly, it cannot be stored readily for any great length of time. If liquid oxygen is used in large quantities, it is often produced very close to its geographical point of application. Liquid oxygen can be obtained in several ways, such as by fractionated distillation of liquid nitrogen out of liquid air.

It is necessary to insulate all lines, tanks, valves, and so on that contain liquid oxygen in order to reduce the evaporation loss. Rocket propulsion systems which

remain filled with liquid oxygen for several hours and liquid oxygen storage systems have to be well insulated against absorbing heat from the surroundings. External drainage provisions have to be made on all liquid oxygen tanks and lines to eliminate the water that condenses on the walls.

Example 7-1. Estimate the approximate temperature and volume change of liquid oxygen if an oxygen tank is pressurized to 8.0 atm for a long time before engine start. Assume the tank is 60% full and the evaporated oxygen is caught, refrigerated, and recondensed (constant mass).

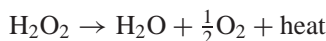
SOLUTION. Using Table 7-1 and Figs. 7-1 and 7-2, the vapor pressure goes from 1.0 atm (0.1 MPa) to 8 atm (about 0.8 MPa) and the equilibrium temperature goes from the boiling point of 90 K at 1.0 atm to about 133 K at 8 atm. The corresponding specific gravities are 1.14 and 0.88, respectively. This is an increase of $1.14/0.88 = 1.29$. (29% more volume). The tank would be 77% full.

In tanks with turbopump feed systems the actual tank pressures are lower (typically 2 to 4 atm) and the evaporated oxygen is vented, causing a cooling effect on the liquid surface. So the numbers calculated above are too large (8 atm was selected to clearly show the effect). The warming occurs when there is a long hold period of a pressurized cryogenic propellant tank and is most pronounced when the final portion of the propellant is being emptied. Nevertheless the higher temperature, higher vapor pressure, and lower density can cause changes in mixture ratio, required tank volume, and pump suction condition (see Section 10.5). Therefore tanks with cryogenic propellant are insulated (to minimize heat transfer and density changes) and are pressurized only shortly before engine start, so as to keep the propellant at its lowest possible temperature and highest density.

Hydrogen Peroxide (H_2O_2)

This propellant is not only a powerful liquid oxidizer but also a clean-burning monopropellant. In rocket applications, hydrogen peroxide has been used in a highly concentrated form of 70 to 99%; the remainder is mostly water. Commercial peroxide is approximately 30% concentrated. For many paper and pulp mills it is 70% concentrated hydrogen peroxide. It was used in gas generators and rocket applications between 1938 and 1965 (X-1 and X-15 research aircraft). Today 90% hydrogen peroxide is the most common.

As a monopropellant it decomposes according to the following chemical reaction, forming superheated steam and gaseous oxygen:



This decomposition is brought about by the action of catalysts such as silver screens, various liquid permanganates, solid manganese dioxide, platinum, and iron oxide. In fact, most impurities act as a catalyst. H_2O_2 is hypergolic with hydrazine and will burn well with kerosene. The theoretical specific impulse of 90% hydrogen peroxide is 154 sec, when used as a monopropellant with a solid catalyst bed.

Even under favorable conditions H_2O_2 will often decompose at a slow rate during storage, about 1% per year for 90 to 95%, and gas will bubble out of the liquid. Contaminated liquid peroxide must be disposed of before it reaches about 448 K, when an explosion may occur. Concentrated peroxide causes severe burns when in contact with human skin and may ignite and cause fires when in contact with wood, oils, and many other organic materials. In the past rocket engines with hydrogen peroxide as the oxidizer have been used for aircraft boost (German Me 163, and U.S. F 104) and a satellite launcher (Britain: Black Arrow). As a monopropellant it was used for attitude control thrusters and for gas generators. It has not been used for a long time, partly because of its long-term storage stability. However, there has been some improvement and some renewed interest in this dense oxidizer, which produces a nontoxic exhaust.

Nitric Acid (HNO_3)

There are several types of nitric acid mixtures that have been used as oxidizers between 1940 and 1965; they are not used extensively today in the United States. The most common type, *red fuming nitric acid* (RFNA), consists of concentrated nitric acid (HNO_3) that contains between 5 and 27% dissolved nitrogen dioxide (NO_2). The evaporating red-brown fumes are exceedingly annoying and poisonous. Compared to concentrated nitric acid (also called *white fuming nitric acid*), RFNA is more energetic, more stable in storage, and slightly less corrosive to many tank materials.

Nitric acid is highly corrosive. Only certain types of stainless steel, gold, and a few other materials are satisfactory as storage containers or tubing materials. A small addition of fluoride ion (less than 1% of hydrofluoric acid, or HF) inhibits the nitric acid, causes a protective fluoride layer to form on the wall, and reduces the corrosion with many metals. It is called *inhibited red fuming nitric acid* (IRFNA). Even with an inhibitor, nitric acid reacts with the wall materials and forms dissolved nitrates and sometime insoluble nitrates. This changes the properties of the acid and may cause blocking of valve and injector orifices. In case of accidental spilling, the acid should be diluted with water or chemically deactivated. Lime and alkali metal hydroxides and carbonates are common neutralizing agents. However, nitrates formed by the neutralization are also oxidizing agents and must be handled accordingly.

Nitric acid has been used with gasoline, various amines, hydrazine, dimethylhydrazine, and alcohols. It ignites spontaneously with hydrazine, furfuryl alcohol, aniline, and other amines. The specific gravity of nitric acid varies from 1.5 to 1.6, depending on the percentages of nitrogen dioxide, water, and impurities. This high density permits compact vehicle construction.

Vapors from nitric acid or red fuming nitric acid have an OSHA 8-hr personnel exposure limit or a threshold work allowance of 2 ppm (parts per million or about 5 mg/m³) and a short-term exposure limit of 4 ppm. Droplets on the skin cause burns and sores which do not heal readily.

Nitrogen Tetroxide (N_2O_4), Often Abbreviated as NTO

This is a high-density yellow-brown liquid (specific gravity of 1.44). It is commonly used with the hypergolic fuels hydrazine, monomethylhydrazine (MMH), and unsymmetrical dimethylhydrazine (UDMH). Although it is the most common storable oxidizer today, its liquid temperature range is narrow and it is easily frozen or vaporized. It is only mildly corrosive when pure, but forms strong acids when moist or allowed to mix with water. It readily absorbs moisture from the air. It can be stored indefinitely in sealed containers made of compatible material. It is hypergolic with many fuels and can cause spontaneous ignition with many common materials, such as paper, grease, leather, or wood. The NO_2 fumes are reddish brown and are extremely toxic. Because of its high vapor pressure it must be kept in relatively heavy tanks. The freezing point of N_2O_4 can be lowered (for example, by adding a small amount of nitric oxide or NO) but at the penalty of a higher vapor pressure and slightly reduced performance. This mixture of NO and N_2O_4 is called mixed oxides of nitrogen (MON) and different grades have between 2 and 30% by weight NO content.

Nitrogen tetroxide oxidizer is used with UDMH in many Russian engines and almost all their small thrusters. It is also used with monomethylhydrazine fuel in the Space Shuttle orbital maneuver system, multithruster reaction control system, and in many U.S. spacecraft propulsion systems. In many of these applications care must be taken to avoid freezing this nitrogen tetroxide. The OSHA 8-hr personnel exposure limit is 5 ppm or 9 mg/m^3 .

7.3. LIQUID FUELS

Again, many different chemicals have been proposed, investigated, and tested as fuels. Only a few have been used in production rocket engines. Liquid fuels other than those listed in this chapter have been used in experimental rocket engines, in older experimental designs, and in some older production engines. These include aniline, furfuryl alcohol, xylidine, gasoline, hydrazine hydrate, borohydrides,-methyl and/or ethyl alcohol, ammonia, and mixtures of some of these.

Hydrocarbon Fuels

Petroleum derivatives encompass a large variety of different hydrocarbon chemicals, most of which can be used as a rocket fuel. Most common are those types that are in use with other applications and engines, such as gasoline, kerosene, diesel oil, and turbojet fuel. Their physical properties and chemical composition vary widely with the type of crude oil from which they were refined, with the chemical process used in their production, and with the accuracy of control exercised in their manufacture. Typical values are listed in Table 7-2.

In general, these petroleum fuels form yellow-white, brilliantly radiating flames and give good performance. They are relatively easy to handle, and there

TABLE 7–2. Properties of Some Typical Hydrocarbon Fuels Made from Petroleum

| | Jet Fuel | Kerosene | Aviation Gasoline 100/130 | RP-1 | RP-2 |
|-----------------------------------|-------------|----------|---------------------------------|-----------------|-----------------|
| Specific gravity at 289 K | 0.78 | 0.81 | 0.73 | 0.80–0.815 | 0.80–0.815 |
| Freezing point (K) | 213 (max.) | 230 | 213 | 213 (max.) | 213 (max.) |
| Viscosity at 289 K (cP) | 1.4 | 1.6 | 0.5 | 16.5 (at 239 K) | 16.5 (at 239 K) |
| Flash point ^a (K) | 269 | 331 | 244 | 333 | 333 |
| ASTM distillation (K) | | | | | |
| 10% evaporated | 347 | — | 337 | 458–483 | 458–483 |
| 50% evaporated | 444 | — | 363 | — | — |
| 90% evaporated | 511 | — | 391 | — | — |
| Reid vapor pressure (psia) | 2 to 3 | Below 1 | 7 | — | — |
| Specific heat (cal/kg-K) | 0.50 | 0.49 | 0.53 | 0.50 | 0.50 |
| Average molecular mass (g/mol) | 130 | 175 | 90 | — | — |
| Sulfur, total mg/kg | — | — | — | 30 (max) | 1 (max) |

^aTag closed cup method.

is an ample supply of these fuels available at relatively low cost. A specifically refined petroleum product particularly suitable as a rocket propellant has been designated RP-1 (Rocket Propellant number 1). It is basically a kerosene-type fuel mixture of hydrocarbons with a somewhat narrow range of densities and vapor pressure. Several hydrocarbon fuels can form carbon deposits on the inside of cooling passages, impeding the heat transfer and raising wall temperatures. Ref. 7–7 indicates that this carbon formation depends on fuel temperature in the cooling jacket, the particular fuel, the heat transfer, and the chamber wall material. RP-1 is low in olefins and aromatics, which can cause carbonaceous deposits inside fuel cooling passages. RP-1 has been used with liquid oxygen in many early rocket engines (see Figs. 5–1 to 5–6 and Ref. 7–8). A very similar kerosene-type fuel is used in Russia today. A few years ago RP-2 was substituted for RP-1 in U.S. rocket applications. The principal difference is a reduced sulphur content (see Table 7–2), because this impurity was believed to have caused corrosion in cooling jackets of certain thrust chambers. See Ref. 7–8.

Methane (CH_4) is a cryogenic hydrocarbon fuel. It is denser than liquid hydrogen and relatively low in cost. Compared to petroleum-refined hydrocarbons, it has highly reproducible properties. With liquid oxygen it is a candidate propellant combination for launch vehicle booster rocket engines and also reaction

control engines when oxygen is available from the main engines. Experimental oxygen–methane engines have been tested, but they have not yet flown.

Liquid Hydrogen (H_2)

Liquid hydrogen, when burned with liquid fluorine or liquid oxygen, gives a high performance, as shown in Table 5–5. It also is an excellent regenerative coolant. With oxygen it burns with a colorless flame; however, the shock waves in the plume may be visible. Of all known fuels, liquid hydrogen is the lightest and the coldest, having a specific gravity of 0.07 and a boiling point of about 20 K. The very low fuel density requires bulky fuel tanks, which necessitate very large vehicle volumes. The extremely low temperature limits the selection of materials for pumps, cooling jackets, tanks, and piping because many metals become brittle at low temperatures.

Because of its low temperature, liquid hydrogen tanks and lines have to be well insulated to minimize the evaporation of hydrogen or the condensation of moisture or air on the outside with the subsequent formation of liquid or solid air or ice. A vacuum jacket often has been used in addition to insulating materials. All common liquids and gases solidify in liquid hydrogen. These solid particles in turn plug orifices and valves. Therefore, care must be taken to purge all lines and tanks of air and moisture (flush with helium or pull vacuum) before introducing the propellant. Mixtures of liquid hydrogen and solid oxygen or solid air can be explosive.

Liquid hydrogen has two isomers, namely, orthohydrogen and parahydrogen, which differ in the orientation of their nuclear spin state. As hydrogen is liquefied and cooled to lower and lower temperatures, the relative equilibrium composition of ortho- and parahydrogen changes. The transformation from orthohydrogen to parahydrogen is exothermic and results in excessive boiloff, unless complete conversion to parahydrogen is achieved during liquefaction. Liquid hydrogen is manufactured from gaseous hydrogen by successive compression, cooling, and expansion processes.

Hydrogen gas, when mixed with air, is highly flammable and explosive over a wide range of mixture ratios. To avoid this danger, escaping excess hydrogen gas (at tank vent lines) is often intentionally ignited and burned or “flared” in air. Liquid hydrogen is used with liquid oxygen in the Delta IV launcher, Centaur upper stage, the Space Shuttle main engine, and upper stage space engines developed in Japan, Russia, Europe, India, and China.

Hydrogen burning with oxygen forms a nontoxic almost invisible exhaust gas. This propellant combination has been applied successfully to space launch vehicles because of its high specific impulse. Here the payload capability usually increases greatly for relatively small increases in specific impulse. However, the low density of hydrogen makes for a very large fuel tank, a large vehicle, and a relatively high drag.

Some studies have shown that, when burned with liquid oxygen, a hydrocarbon (such as methane or RP-1) can give a small advantage in space launch vehicle first

stages. Here the higher average propellant density allows a smaller vehicle with lower drag, which compensates for the lower specific impulse of the hydrocarbon when compared to a hydrogen fuel. Also, there are some concepts for operating the booster-stage rocket engine initially with hydrocarbon fuel and then switching during flight to hydrogen fuel. Engines using LOX and these two fuels, namely hydrocarbon and hydrogen, have been called *tripropellant* engines. They have not yet been fully developed or flown. Some work on experimental engines was done in Russia, but there is no known current effort.

Hydrazine (N_2H_4)

Reference 7–9 gives a good discussion of this propellant, which is used as a bipropellant fuel as well as a monopropellant. Hydrazine, monomethylhydrazine (MMH), and unsymmetrical dimethylhydrazine (UDMH) have similar physical and thermochemical properties. Hydrazine is a toxic, colorless liquid with a high freezing point (274.3 K or 34°F). Hydrazine tanks, pipes, injectors, catalysts, and valves are usually electrically heated to prevent freezing in cool weather or in outer space. Hydrazine has a short ignition delay and is spontaneously ignitable with nitric acid, nitrogen tetroxide, and concentrated hydrogen peroxide.

Its vapors may form explosive mixtures with air. If hydrazine is spilled on a porous surface or a cloth, a spontaneous ignition with air can occur.

Pure anhydrous hydrazine is a stable liquid; it has been safely heated above 480 K. It has been stored in sealed tanks for over 15 years. With impurities or at higher temperatures it decomposes and releases energy. Under pressure shock (blast wave or adiabatic compression) hydrazine vapor or hydrazine mist can decompose at temperatures as low as 367 K. Under some conditions this decomposition can be a violent detonation, and this has caused problems in cooling passages of experimental injectors and thrust chambers. Harmful effects to personnel may result from ingestion, inhalation of vapors, or prolonged contact with skin. The American Conference of Government Industrial Hygienists (ACGIH) recommended 8-hr personnel exposure limit is 0.01 ppm or 0.013 mg/m³. Hydrazine is a known animal carcinogen and a suspected carcinogen for people.

Hydrazine reacts with many materials, and care must be exercised to avoid storage contact with materials that cause a decomposition (see Refs. 7–9 and 7–10). Tanks, pipes, injectors, catalysts, or valves must be cleaned and free of impurities. Compatible materials include certain stainless steels (303, 304, 321, or 347), nickel, and 1100 and 3003 series of aluminum. Iron, copper, and its alloys (such as brass or bronze), monel, magnesium, zinc, and some types of aluminum alloy must be avoided.

Unsymmetrical Dimethylhydrazine [$(CH_3)_2NNH_2$]

A derivative of hydrazine, namely UDMH, is often used instead of or in mixtures with hydrazine because it forms a more stable liquid, particularly at higher temperatures. Furthermore, it has a lower freezing point (215.9 K) and a lower

boiling point (336.5 K) than hydrazine. When UDMH is burned with an oxidizer it gives only slightly lower values of I_s than pure hydrazine. UDMH is often used when mixed with 30 to 50% hydrazine or with 25% hydrazine hydrate. UDMH is used in Russian and Chinese rocket engines and small thrusters. The ACGIH recommended 8-hr personnel exposure limit for vapor is 0.01 ppm, and UDMH is a suspected carcinogen.

Monomethylhydrazine (CH_3NHNH_2)

This fuel abbreviated as MMH has been used extensively in U.S. spacecraft rocket engines, particularly in small attitude control engines, usually with N_2O_4 as the oxidizer. It has a better shock resistance to blast waves and a better liquid temperature range than pure hydrazine. Like hydrazine, its vapors are easily ignited in air; the flammability limits are from 2.5 to 98% by volume at atmospheric sea-level pressure and ambient temperature. The materials compatible with hydrazine are also compatible with MMH. The specific impulse with storable oxidizers usually is 1 or 2% lower with MMH than with N_2H_4 .

Both MMH and UDMH are soluble in many hydrocarbons; hydrazine is not. All hydrazines are toxic materials, but MMH is the most toxic when inhaled. Atmospheric concentrations of all hydrazines should be kept below 0.1 ppm for long periods of personnel exposure.

Monomethylhydrazine, when added in relatively small quantities of 3 to 15% to hydrazine, has a substantial quenching effect on the explosive decomposition of hydrazine. Monomethylhydrazine decomposes at 491 K, whereas hydrazine can explode at 369 K when subjected to certain pressure shocks. MMH is a known animal carcinogen and the ACGIH recommended personnel 8-hour exposure limit is 0.01 ppm.

7.4. LIQUID MONOPROPELLANTS

The propellant-feed and control-system simplicity associated with a monopropellant makes this type of propellant attractive for certain applications. Hydrazine is being used extensively as a monopropellant in small attitude and trajectory control rockets for the control of satellites and other spacecraft and also as a hot gas generator. (It is discussed in the preceding section.) Other monopropellants (ethylene oxide or nitromethane) were tried experimentally, but are no longer used today. Concentrated hydrogen peroxide was used for small thrusters between 1945 and 1965 and for monopropellant gas generation in the United States, Russia, United Kingdom or Britain, and Germany.

Ignition of monopropellants can be achieved thermally (electrical or flame heat) or by a catalytic material. A monopropellant must be chemically and thermally stable to ensure good liquid storage properties, and yet it must be easily decomposed and reactive to quickly give good combustion.

Hydrazine as a Monopropellant

Hydrazine is not only an excellent storable fuel but also an excellent monopropellant when decomposed by a suitable solid catalyst; this catalyst often needs to be preheated for fast startup or for extending the useful catalyst life. Iridium on porous alumina base is an effective catalyst at room temperature. At elevated temperature (about 450 K) many materials decompose hydrazine, including iron, nickel, and cobalt. See Ref. 7–9. Different catalysts and different catalyst configurations make the decomposition reaction go to different products, resulting in gases varying in composition or temperature. As a monopropellant, it is used in gas generators or in space engine attitude control rockets. A typical

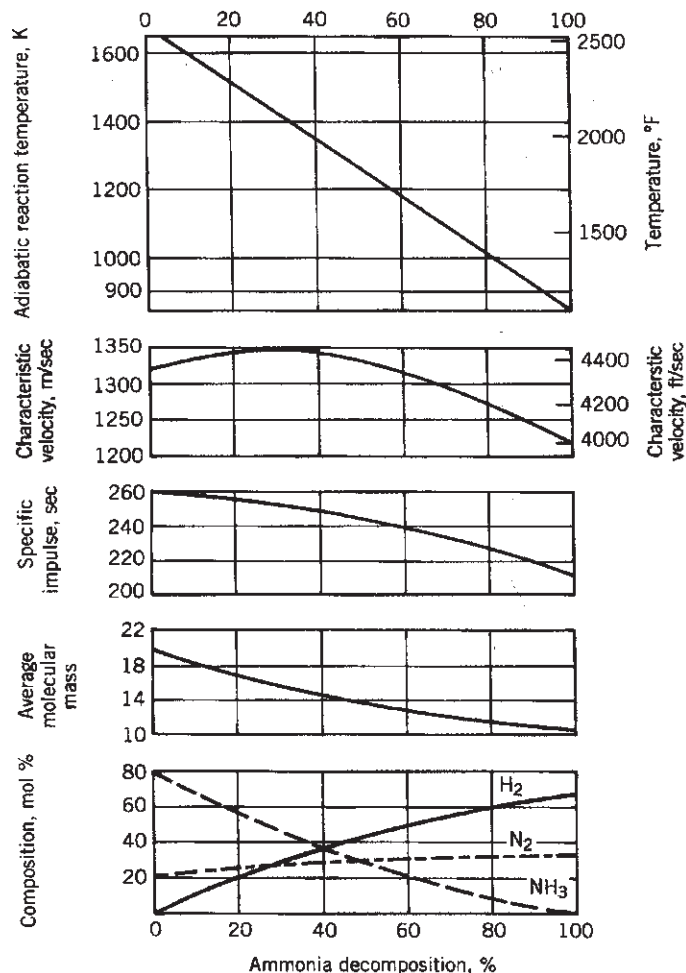
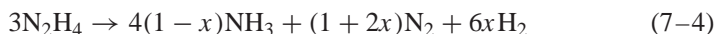


FIGURE 7-3. Operating parameters for decomposed hydrazine at the exit of a catalytic reactor as a function of the ammonia dissociation fraction. Adapted with permission from Ref. 7–9.

hydrazine monopropellant thrust chamber, its injection patterns, and its decomposition reaction are described in Fig. 8–14. Typical operating parameters are shown in Fig. 7–3.

The catalytic decomposition of hydrazine can be described ideally as a two-step process; this ignores other steps and intermediate products. First, hydrazine (N_2H_4) decomposes into gaseous ammonia (NH_3) and nitrogen (N_2); this reaction is highly exothermic, that is, it releases heat. Second, the ammonia decomposes further into nitrogen and hydrogen gases, but this reaction is endothermic and absorbs heat. These simplified reactions can be written as



Here x is the degree of ammonia dissociation; it is a function of the catalyst type, size, and geometry, the chamber pressure, and the dwell time within the catalyst bed. Figure 7–3 shows several ideal rocket engine parameters for hydrazine monopropellant as a function of x , the fraction of ammonia that is decomposed. The values are for an ideal thruster at 1000 psia chamber pressure with a nozzle area ratio of 50 expanding at high altitude. The best specific impulse is attained when little ammonia is allowed to dissociate.

7.5. GELLED PROPELLANTS

Gelled propellants have additives that make them thixotropic materials. They have the consistency of thick paint or jelly when at rest, but they liquefy and flow through pipes, valves, pumps, or injectors when an adequate shear stress is applied. They offer these *advantages*: (1) Small aluminum fuel particles can be suspended in the fuels. Inert solid particles can be suspended in oxidizer liquids. This increases propellant density, density impulse, and thus reduces the size of tanks and vehicles. (2) There is no plugging of injector orifices or valve passages and good flow control has been demonstrated. (3) Most gelled fuel propellants are essentially nonflammable and will not usually sustain an open fire. (4) There is reduced susceptibility of leakage or spill, reduced sloshing of liquids in the tanks, and the boil-off rate is reduced. (5) Long-term storage of 10 years or more without settling or separation of the solid particles has been demonstrated. (6) Explosions or detonations, which happen when a vehicle accident causes liquid propellants to become inadvertently mixed, are much less likely with gelled propellants, which are difficult to mix. (7) Short-duration pulsing has been tested. (8) Most storable oxidizers, a few cryogenic propellants, and most liquid storable fuels can be gelled. (9) Explosions are much less likely when a propellant tank is penetrated by a bullet or when a missile is exposed to an external fire or a nearby detonation.

These are some of the *disadvantages*: (1) There is a small decrease in specific impulse due to dilution with a gelling agent, and less efficient atomization into small droplets (due to high viscosity) or less efficient combustion. For example, the characteristic velocity c^* of oxygen–kerosene propellant is decreased by

4 to 6% when the kerosene is gelled and aluminum is suspended in the fuel. (2) Bubble-free loading or unloading of propellants is somewhat more complex and may take longer. Residual propellant quantity will be slightly higher because the thixotropic fluid layer on the walls of the tanks and pipes will be thicker. (3) Changes in ambient temperature will cause slight changes in propellant density and viscosity and therefore also in mixture ratio; this can result in more leftover or residual propellant and thus in a slight reduction of available total impulse. Suspended metals can make the exhaust plume smoky and visible.

Experimental rocket engines have shown these gelled propellants to be generally safer than ordinary liquid propellants and to have adequate performance and operational characteristics (see Refs. 7–11 and 7–12). This makes them less susceptible to field accidents. A variety of different organic and inorganic gelling agents have been explored with a number of different liquid propellants.

Experimental thrust chambers and rocket engine systems have been satisfactorily demonstrated with several gelled propellant combinations. One experimental engine has flown. As far as is known, no such rocket engine has yet been put into production or flight operation.

7.6. GASEOUS PROPELLANTS

Cold gas propellants have been used successfully for reaction control systems (RCS) for more than 60 years. The words “cold gas” (stored at ambient temperature) is distinguished from a “warm gas,” which has been heated. The engine system is simple, consisting of one or more high-pressure gas tanks, multiple simple nozzles (often aluminum or plastic), an electrical control valve with each nozzle, a pressure regulator, and provisions for filling and venting the gas. The tank size will be smaller if the tank pressures are high. Pressures are typically between 300 and 1000 MPa (about 300 to 10,000 psi), and these gas tanks have thick walls and are heavy.

Typical cold gas propellants and some of their properties and characteristics are listed in Table 7–3. Nitrogen, argon, dry air, krypton and Freon 14 have been employed in spacecraft RCS. With high-pressure hydrogen or helium as cold gas, the specific impulse is much higher, but the densities of these gases are much lower. This requires a much larger gas storage volume and heavier high-pressure tanks. In most applications the extra inert mass outweighs the advantage of better performance. In a few applications the gas (and its storage tank) are heated electrically or chemically. This improves the specific impulse and allows a smaller tank, but it also introduces complexity.

The selection of the gas propellant, the storage tanks, and RCS design depend on many factors, such as volume and mass of the storage tanks, the maximum thrust and total impulse, the gas density, required maneuvers, duty cycle, and flight duration. Cold gas systems have been used for total impulses of perhaps 22,200 N-sec or 5000 lbf-sec. Higher values usually employ liquid propellants.

If the operation is short (most of the gas consumed in a few minutes, while the main engine is running), the gas expansion will be close to adiabatic (no heat

TABLE 7–3. Properties of Gaseous Propellants Used for Auxiliary Propulsion

| Propellant | Molecular Mass | Density ^a (lb/ft ³) | Specific heat ratio <i>k</i> | Theoretical Specific Impulse ^b (sec) |
|------------|----------------|---|------------------------------|---|
| Hydrogen | 2.0 | 1.77 | 1.40 | 284 |
| Helium | 4.0 | 3.54 | 1.67 | 179 |
| Methane | 16.0 | 14.1 | 1.30 | 114 |
| Nitrogen | 28.0 | 24.7 | 1.40 | 76 |
| Air | 28.9 | 25.5 | 1.40 | 74 |
| Argon | 39.9 | 35.3 | 1.67 | 57 |
| Krypton | 83.8 | 74.1 | 1.63 | 50 |

^aAt 5000 psia and 20°C.

^bIn vacuum with nozzle area ratio of 50:1 and initial temperature of 20°C.

absorption by gas) and often is analyzed as isentropic. The temperature of the gas, the pressure, and specific impulse will drop as the gas is consumed. For long intermittent operations (months or years in space) the heat from the spacecraft is transferred to the gas and the tank temperature stays essentially constant; the expansion will be nearly isothermal.

The advantages and disadvantages of cold gas thrusters and systems are described in Section 8.3 in the discussion of low thrust.

7.7. SAFETY AND ENVIRONMENTAL CONCERNS

To minimize the hazards and potential damage inherent in reactive propellant materials, it is necessary to be very conscientious about the likely risks and hazards (see Refs. 7–4, 7–13, and 7–14). This concerns toxicity, explosiveness, fire or spill danger, and others mentioned in Section 7.1. Before an operator, assembler, maintenance mechanic, supervisor, or engineer is allowed to transfer or use a particular propellant, he or she should receive safety training in the particular propellant, its characteristics, its safe handling or transfer, potential damage to equipment or the environment, and the countermeasures for limiting the consequences in case of an accident. They must also understand the potential hazards to the health of personnel, first aid, remedies in case of contact exposure of the skin, ingestion, or inhaling, and the use of safety equipment. Examples of safety equipment are protective clothing, face shields, detectors for toxic vapors, remote controls, warning signals, or emergency water deluge. The personnel working with or being close to highly toxic materials usually have to undergo periodic health monitoring. Also rocket engines need to be designed for safety to minimize the occurrence of a leak, an accidental spill, an unexpected fire, or other potentially unsafe conditions. Most organizations have one or more safety specialists who review the safety of the test plans, manufacturing operations, designs, procedures, or safety equipment. With the proper training, equipment, precautions, and design safety features, all propellants can be handled safely.

If a safety violation occurs or if an operation, design, procedure, or practice is found to be (or appears to be) unsafe, then a thorough investigation of the particular item or issue should be undertaken, the cause of the lack of safety should be investigated and identified, and an appropriate remedial action should be selected and initiated as soon as possible.

The discharge of toxic exhaust gases to the environment and their dispersion by the wind can cause exposure of operating personnel as well as the people in nearby areas, and can cause damage to plants and animals. This is discussed in Section 20.2. The dumping or spilling of toxic liquids can contaminate subterranean aquifers and surface waters, and their vapors can pollute the air. Today the type and amount of gaseous and liquid discharges are regulated and monitored by government authorities. These discharge quantities must be controlled or penalties will be assessed against violators. Obtaining a permit to discharge can be a lengthy and involved procedure.

PROBLEMS

- Plot the variation of the *density specific impulse* (product of average specific gravity and specific impulse) with mixture ratio and explain the meaning of the curve. Use the theoretical shifting specific impulse values of Fig. 5–1 and the specific gravities from Fig. 7–1 or Table 7–1 for the liquid oxygen–RP-1 propellant combination.
Answers: Check point at $r = 2.0$; $I_s = 290$; $I_d = 303$; $\delta_{av} = 1.01$.
- Prepare a table comparing the relative merits of liquid oxygen and nitrogen tetroxide as rocket engine oxidizers.
- Derive Eq. 7–1 for the average specific gravity.
- A rocket engine uses liquid oxygen and RP-1 as propellants at a design mass mixture ratio of 2.40. The pumps used in the feed system are basically constant-volume flow devices. The RP-1 hydrocarbon fuel has a nominal temperature of 298 K and it can vary at about $\pm 25^\circ\text{C}$. The liquid oxygen is nominally at its boiling point (90 K), but, after the tank is pressurized, this temperature can increase by up to 30 K during long time storage. What are the extreme mixture ratios under unfavorable temperature conditions? If this engine has a nominal mass flow rate of 100 kg/sec and a duration of 100 sec, what is the maximum residual propellant mass when the other propellant is fully consumed? Use the curve slopes of Fig. 7–1 to estimate changes in density. Assume that the specific impulse is constant for the relatively small changes in mixture ratio, that small vapor pressure changes have no influence on the pump flow, that there is no evaporation of the oxygen in the tank, and that the engine has no automatic control for mixture ratio. Assume zero residual propellant.
- The vehicle stage propelled by the rocket engine in Problem 4 has a design mass ratio m_f/m_0 of 0.50 (see Eq. 4–6). For the specific impulse please use a value half way between the shifting and the frozen equilibrium curves of Fig. 5–1. How much will the worst combined changes in propellant temperatures affect the mass ratio and the ideal gravity-free vacuum velocity?

6. (a) What should be the approximate percent ullage volume for nitrogen tetroxide tank when the vehicle is exposed to ambient temperatures between about 50°F and about 150°F?

(b) What is maximum tank pressure at 150°F.

(c) What factors should be considered in part (b)?

Answers: (a) 15 to 17%; the variation is due to the nonuniform temperature distribution in the tank; (b) 6 to 7 atm; (c) vapor pressure, nitrogen monoxide content in the oxidizer, chemical reactions with wall materials, or impurities that result in largely insoluble gas products.

7. An insulated, long vertical, vented liquid oxygen tank has been sitting on the sea-level launch stand for a period of time. Assume no heat loss to the tank walls. The surface of the liquid is at atmospheric pressure and is 10.2 m above the closed outlet at the bottom of the tank. If there is no circulation, what will be the temperature, pressure, and density of the oxygen at the tank outlet?

SYMBOLS

| | |
|-------|--|
| I_d | density specific impulse, sec |
| I_s | specific impulse, sec |
| k | ratio of specific heats |
| r | mixture ratio (mass flow rate of oxidizer to mass flow rate of fuel) |

Greek Letters

| | |
|-----------------------------|---|
| δ_{av} | average specific gravity of mixture |
| δ_f | specific gravity of fuel |
| δ_o | specific gravity of oxidizer |
| $\rho_{av}, \rho_f, \rho_o$ | densities average, fuel, and oxidizer, kg/m ³ (lbm/ft ³) |

REFERENCES

- 7-1. S. F. Sarner, *Propellant Chemistry*, Reinhold Publishing, New York, 1966.
- 7-2. *Chemical Rocket Propellant Hazards*, Vol. 1, *General Safety Engineering Design Criteria*, Chemical Propulsion Information Agency (CPIA) Publication 194, October 1971.
- 7-3. L. C. Sutherland, "Scaling Law for Estimating Liquid Propellant Explosive Yields," *Journal of Spacecraft and Rockets*, March–April 1978, pp. 124–125.
- 7-4. *NIOSH Pocket Guide to Chemical Hazards*, DHHS (NIOSH) Publication No. 2005-149, Department of Health and Human Services, Washington DC, September 2005.
- 7-5. 1990–1991 *Threshold Limit Values for Chemical Substances and Physical Agents and Biological Exposure Indices*, American Conference of Government Industrial Hygienists, Cincinnati, OH, 1990 (revised periodically).

- 7-6. H. E. Malone, *The Analysis of Rocket Propellants*, Academic Press, New York, 1976.
- 7-7. K. Liang, B. Yang, and Z. Zhang, "Investigation of Heat Transfer and Coking Characteristics of Hydrocarbon Fuels," *Journal of Propulsion and Power*, Vol. 14, No. 5, September–October 1998.
- 7-8. *Detail Specification—Propellant Rocket Grade Kerosene*, Department of Defense, Washington DC, MIL-DTL-25576D, 20 May 2005.
- 7-9. E. W. Schmidt, *Hydrazine and Its Derivatives, Preparation, Properties, Applications*, 2nd ed., John Wiley & Sons, New York, 2001.
- 7-10. O. M. Morgan and D. S. Meinhardt, "Monopropellant Selection Criteria—Hydrazine and other Options," AIAA Technical Paper 99-2595, June 1999.
- 7-11. K. F. Hodge, T. A. Crofoot, and S. Nelson, "Gelled Technical Propellants for Tactical Missile Application," AIAA Technical Paper 99-2976, June 1999.
- 7-12. B. D. Allen, "History, Development and Testing of Thixotropic Gels for Advanced Systems," AIAA Propulsion Conference, July 1985.
- 7-13. *Hazards of Chemical Rockets and Propellants*, Vol. I, *Safety, Health and the Environment*, and Vol. III, *Liquid Propellants*, Chemical Propulsion Information Analysis Center, CPIA Publication 394, 1984.
- 7-14. *Emergency Response Guidebook*, National Institute for Occupational Safety and Health (NIOSH), Department of Health and Human Services, Washington, DC, rev. ed., 2004.

CHAPTER 8

THRUST CHAMBERS

This chapter describes *thrust chambers*, their components, cooling, ignition, and heat transfer. The thrust chamber is the key subassembly of a rocket engine. Here the liquid propellants are metered, injected, atomized, vaporized, mixed, and burned to form hot reaction gas products, which in turn are accelerated and ejected at supersonic velocity (see Refs. 6–1, 6–2, and 8–1). A rocket thrust chamber assembly (Figs. 8–1 and 8–2) has an *injector*, a *combustion chamber*, a *supersonic nozzle*, and *mounting provisions*. All have to withstand the extreme heat of combustion and the various forces, including the transmission of the thrust force to the vehicle. There also is an ignition system if nonspontaneously ignitable propellants are used. Some thrust chamber assemblies also have integrally mounted propellant valves and sometimes a thrust vector control device, as described in Chapter 18. Table 8–1 gives various data about five different thrust chambers with different kinds of propellants, cooling methods, injectors, feed systems, thrust levels, or nozzle expansions. Some engine parameters are also listed. Some of the terms used in this table will be explained later in this chapter.

The basic analyses for thrust chamber specific impulse and combustion temperature are given in Chapter 5, the basic design parameters (thrust, flow, chamber pressure, or throat area) are in Chapter 3, and the combustion phenomena in Chapter 9.

Although we use the word *thrust chamber* in this book (for rocket engines generally larger than 1000 lbf thrust), some technical publications use the terms *thrust cylinder*, *thrust cell*, or *rocket combustor*. We will also use the term *thruster* for small thrust units, such as attitude control thrusters, and for electrical propulsion systems.

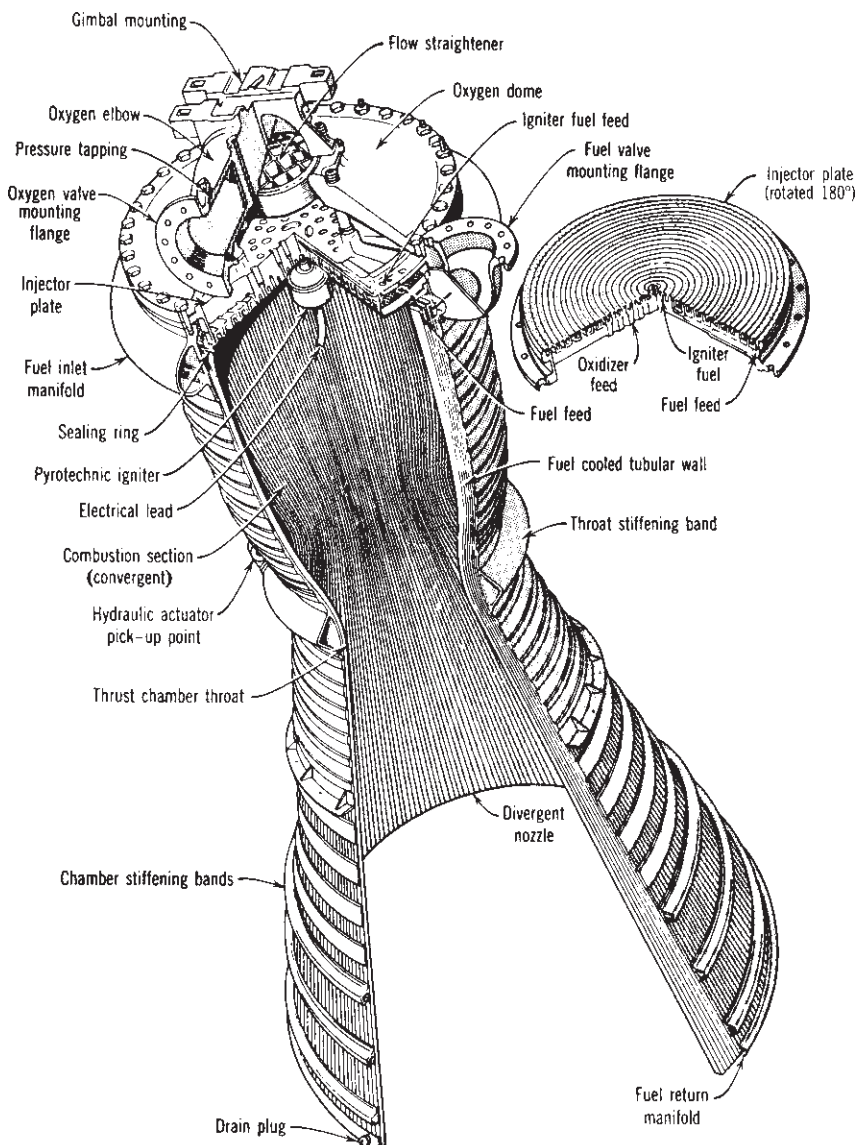


FIGURE 8–1. Construction of an early regeneratively cooled tubular thrust chamber using a kerosene-type fuel and liquid oxygen, as originally used in the Thor missile. The nozzle throat inside diameter is about 15 in. The sea-level thrust was originally 120,000 lbf, but was uprated to 135,000, then 150,000, and finally to 165,000 lbf by increasing the flow and chamber pressure and strengthening and modifying the hardware. The cone-shaped nozzle exit was replaced by a bell-shaped nozzle exit. Figure 8–9 shows how the fuel flows down through every other tube and returns through the adjacent tube before flowing into the injector. Figure 8–5 shows the flow passages in a similar injector. (Courtesy of Rolls Royce, England.)

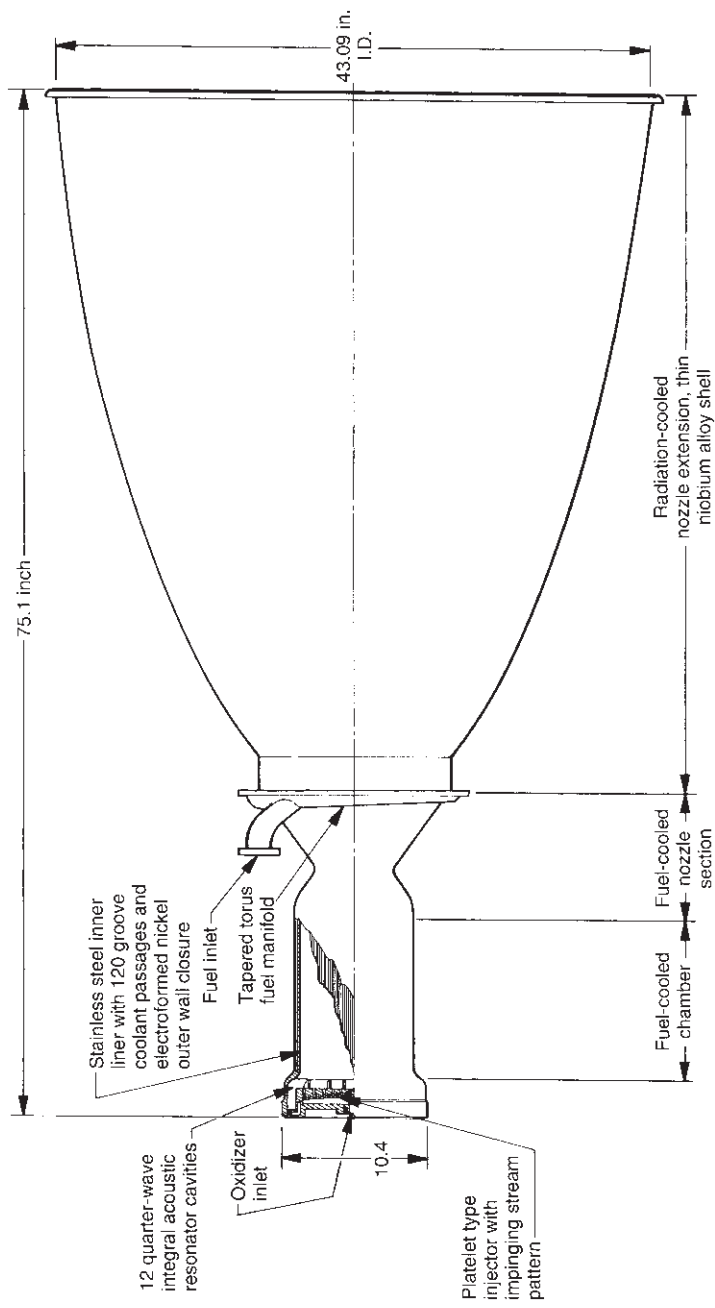


FIGURE 8–2. Simplified half-section of one of the two thrust chambers of the orbital maneuvering engines used on the Space Shuttle Orbiter. Each develops a vacuum thrust of 6000 lbf (26,689 N) and delivers a minimum vacuum specific impulse of 31.0 sec, using nitrogen tetroxide and monomethyl hydrazine propellants at a nominal mixture ratio of 1.65 and a nominal chamber pressure of 128 psia. It is designed for 100 flight missions, a service life of 10 years, and a minimum of 500 starts. These engines provide the thrust for final orbit attainment, orbit circularization, orbit transfer, rendezvous, and deorbit maneuvers. The nozzle area ratio is 55:1. (Courtesy of Aerojet Propulsion Company.)

TABLE 8-1. Thrust Chamber Characteristics

| | Engine Designation | | | |
|--|---|---------------------------------|-------------------------------|---|
| | RL 10B-2 | LE-7 (Japan) | RCS | RS-27 |
| Application | Delta-III and IV upper stage | Booster stage for H-II launcher | Altitude control | Delta II Space |
| Manufacturer | Pratt & Whitney Rocketdyne, United Technologies Corporation | Mitsubishi Heavy Industries | Aerojet Propulsion Company | Launch booster Pratt & Whitney, Rockordyne, United Technologies Corp. |
| <i>Thrust Chamber</i> | | | | Delta II Second stage Aerojet Propulsion Company |
| Fuel | Liquid H ₂ | Liquid H ₂ | MMH | RP-1 (kerosene) |
| Oxidizer | Liquid O ₂ | Liquid O ₂ | N ₂ O ₄ | Liquid oxygen |
| Thrust chamber thrust at sea level (lbf) | No sea-level firing 24,750 | 190,400 242,500 | 12 18 | 164,700 207,000 |
| in vacuum (lbf) | 5.88 | 6.0 | 2.0 | 2.35 |
| Thrust chamber mixture ratio | | | | NA |
| Thrust chamber specific impulse at sea level (sec) | NA | 349.9 | 200 | 257 |
| in vacuum (sec) | 466 | 445.6 | 290 | 294 |
| Characteristic exhaust velocity, <i>c</i> * (ft/sec) | 7578 | 5594.8 | 5180 | 5540 |
| Thrust chamber propellant flow (lb/sec) | 53.2 | 346.9 | 0.062 | 640 |
| Injector end chamber pressure (psia) | 640 | — | 70 | 576 |
| Nozzle end stagnation pressure (psia) | NA | 1917 | 68 | 534 |
| Thrust chamber sea-level weight (lbf) | < 150 | 1560 | 7 | 730 |
| Gimbal mount sea-level dry weight (lbf) | < 10 | 57.3 | NA | 70 |
| Chamber diameter (in.) | — | 15.75 | 1.09 | 21 |
| Nozzle throat diameter (in.) | 5.2 | 9.25 | 0.427 | 16.2 |
| Nozzle exit diameter (in.) | 88 | 68.28 | 3.018 | 45.8 |
| Nozzle exit area ratio | 285 | 54:1 | 50:1 | 8:1 |
| | | | | 65:1 |

| | | | | | |
|--|---|---|---|--|---|
| Chamber contraction area ratio | — | 2.87 | 6:1 | 1.67:1 | 2.54:1 |
| Characteristic chamber length L^* (in.) | — | 30.7 | 18 | 38.7 | 30.5 |
| Thrust chamber overall length (in.) | 90 | 14.8 | 11.0 | 86.15 | 18.7 |
| Fuel jacket and manifold volume (ft ³) | — | 3.5 | — | 2.5 | — |
| Nozzle extension | Carbon–carbon $>360^a$ | None ^a | None ^a | None ^a | None >150 |
| Cumulative firing duration (sec) | Yes | No | Yes | No | Yes |
| Restart capability | Stainless steel tubes, $1\frac{1}{2}$ passes | Regenerative (fuel) cooled, stainless steel tubes 0.05 (channel) | Radiation cooled, niobium NA | Stainless steel tubes, single pass, regenerative cooling 0.45 | Ablative layer is partly consumed |
| Cooling system | regenerative cooled NA | 288 540 | 0 NA | NA | Ablative material: Silica phenolic 0 |
| Tube diameter/channel width (in.) | Number of tubes NA 253 | Concentric annular swirl and resonator cavities | Hollow post/sleeve elements; baffle and acoustic cavities | Flat plate, drilled holes | Outer row: shower head; triplets & doublets, with dual tuned resonator 40 |
| Number of tubes | 100 | 704 | 50 | 292 | NA |
| Jacket pressure drop (psi) | 54 | 154 | 50 | 100 | NA |
| Injector type | 216 | 452 (coaxial) | 1 | 1145 | 1050 |
| Injector pressure drop—oxidizer (psi) | 216 | 452 (coaxial) | 1 | 1530 | 1230 |
| Injector pressure drop—fuel (psi) | 100 | 704 | 50 | 156 | 40 |
| Number of oxidizer injector orifices | 54 | 154 | 50 | 140 | 40 |
| Number of fuel injector orifices | 216 | 452 (coaxial) | 1 | 1145 | 1050 |
| <i>Engine Characteristics</i> | | | | | |
| Feed system | Turbopump with expander cycle NA | Turbopump | Pressure fed tanks | Turbopump with gas generator | Pressure fed tanks |
| Engine thrust (at sea level) (lb) | 24,750 | 190,400 242,500 | 12 18 | 165,000 207,700 | NA 9850 |
| Engine thrust (altitude) (lb) | NA | 349.9 | 200 | 253 | 320 |
| Engine specific impulse at sea level | 462 | 445.6 | 290 | 288 | 320 |
| Engine specific impulse at altitude | | 5.88 | 2.0 | 2.27 | 1.90 |

^aLimited only by available propellant.
Sources: Companies listed above and NASA.

8.1. INJECTORS

The functions of an injector are similar to those of a carburetor of an internal combustion engine. The injector has to introduce and meter the flow of liquid propellants to the combustion chamber, cause the liquids to be broken up into small droplets (a process called atomization), and distribute and mix the propellants in such a manner that a correctly proportioned mixture of fuel and oxidizer will result, with uniform propellant mass flow and composition over the chamber cross section.

There are two design approaches for admitting propellants into the combustion chamber. The individual locations on the injector face are called injector elements. The older types use a set of propellant jets going through a set of holes in a pattern on the injector face. Different hole arrangements are shown in Figure 8–3. Many of the rocket injectors developed in the United States used this type for large and small thrust chambers. The second type has cylindrical injection elements, which are inserted and fastened (welded, brazed, or soldered) into the injector face and each element delivers a conically shaped spray of propellants into the combustion chamber. Figure 8–4 shows several spray injection elements with conical sheets of propellant coming from a slot or from the internal edge of a hollow cylinder in the injection element. It has been used with LOX/LH₂ thrust chamber worldwide including the Space Shuttle thrust chamber. Also it has been the preferred approach in Russia (and its predecessor the Soviet Union), where it was used with most propellants and all thrust chamber sizes. There are also some combination types that use jets and sprays together. Typical injectors with hole patterns can be seen in Figs. 8–1 and 8–5.

The *injection pattern* on the face of the injector is closely related to the internal manifolds or feed passages within the injector. These provide for the distribution of the propellant from the injector inlet to all the injection holes or spray elements. A large complex manifold volume allows low passage velocities and good distribution of flow over the cross section of the chamber. A small manifold volume allows for a lighter weight injector, a faster start, and reduces the amount of “dribble” flow after the main valves are shut. The higher passage velocities usually cause a more uneven flow through different identical injection holes and thus a poorer distribution and wider local gas composition variation. Dribbling results in after-burning, which is an inefficient irregular combustion that gives a little “cutoff” thrust after valve closing. For applications with very accurate terminal vehicle velocity requirements, the cutoff impulse has to be very small and reproducible and often valves are built into the injector to minimize passage volume.

Doublet *impinging-stream-type, multiple-hole injectors* are commonly used with oxygen–hydrocarbon and storables propellants, as seen in Fig. 8–3. For *unlike doublet* patterns the propellants are injected through a number of separate small holes in such a manner that the fuel and oxidizer streams impinge upon each other. Impingement forms thin liquid fans and aids atomization of the liquids into droplets, also aiding distribution. Characteristics of specific injector orifices

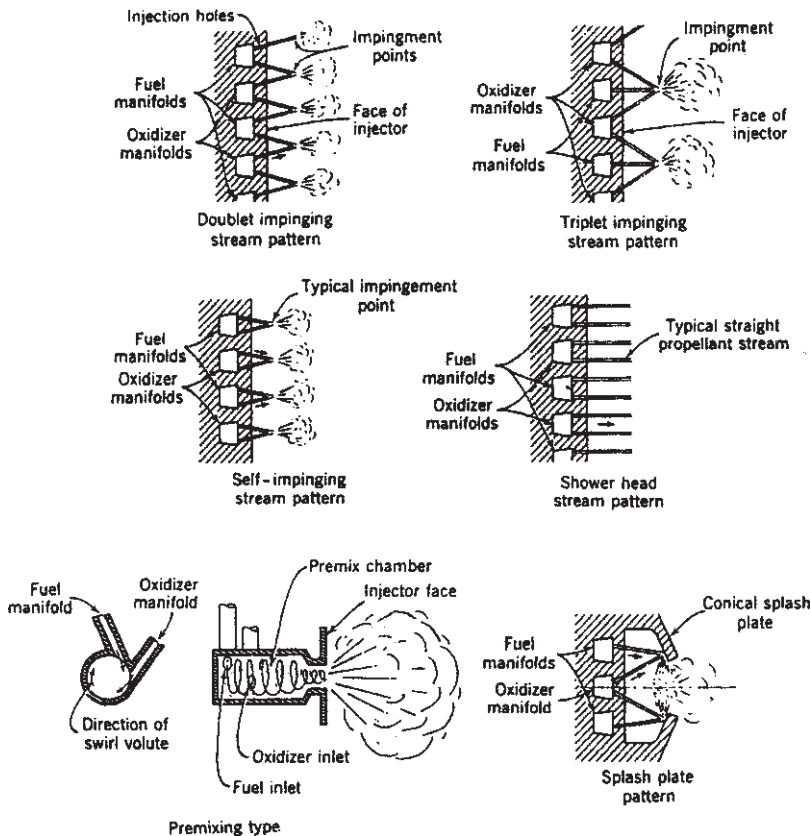


FIGURE 8–3. The upper four simplified sketches show common injection designs using holes. The premix chamber-type (its igniter is not shown) is used today on a few large LOX/LH₂ thrust chambers. The splash plate-type was popular in the late 1940s and 1950s but is not used today. (Used with permission from Ref. 8–1.)

are given in Table 8–2. Impinging hole injectors are also used for *like-on-like* or *self-impinging patterns* (fuel-on-fuel and oxidizer-on-oxidizer). The two liquid streams then form a fan which breaks up into droplets. Unlike doublets work best when the hole size (more exactly, the volume flow) of the fuel is about equal to that of the oxidizer and the ignition delay is long enough to allow the formation of fans. For uneven volume flow the triplet pattern often seems to be more effective.

The *nonimpinging* or *shower head* injector employs nonimpinging streams of propellant usually emerging normal to the face of the injector. It relies on turbulence and diffusion to achieve mixing. The German World War II V-2 rocket used this type of injector. This type is no longer used because it requires a large chamber volume for good combustion.

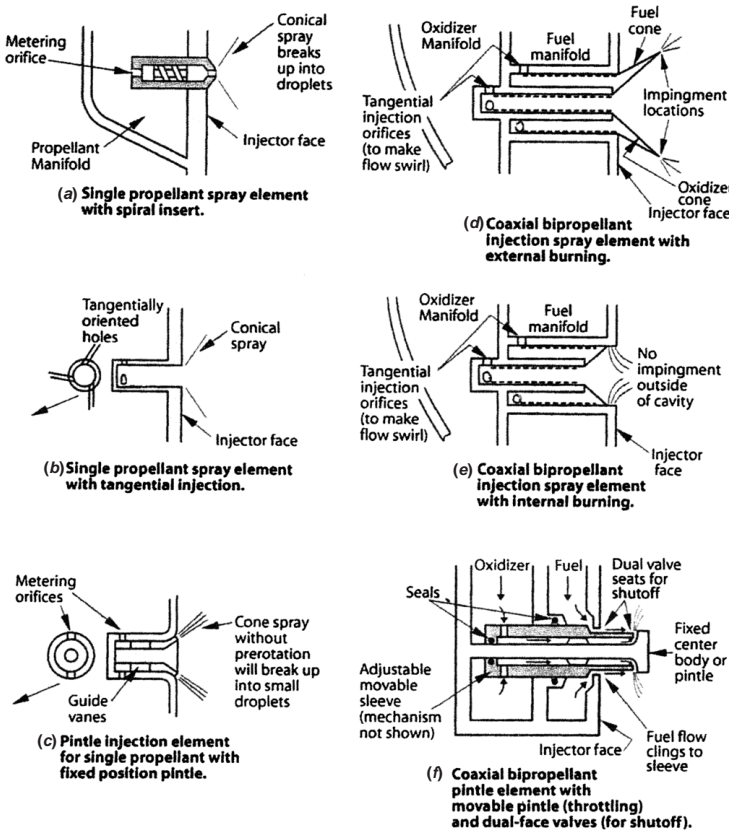


FIGURE 8–4. Simplified cross-section sketches of several common types of spray injection elements. (Used with permission from Ref. 8–1.)

Sheet or spray-type injectors give cylindrical, conical, or other types of spray sheets; these sprays generally intersect and thereby promote mixing and atomization. See Fig. 8–4. The conical sheets break up into droplets, which are then vaporized. The size distribution of droplets from spray injection elements is usually more uniform than with impinging streams from holes. By changing some of the internal dimensions of the spray elements (change size or number of tangential feed holes, the length/protrusion of an internal cylinder, or the angle of an internal spiral rib), it is possible to change the angle of the conical sheet or the location of the impingement of fuel and oxidizer spray sheets, and to affect the combustion efficiency. By varying the width of the sheet (through an axially movable sleeve), it is possible to throttle the propellant flow over a wide range without excessive reduction in injector pressure drop. This type of variable area concentric tube injector was used on the descent engine of the Apollo lunar excursion module and throttled over a 10:1 range of flow with only a very small change in mixture ratio or performance.

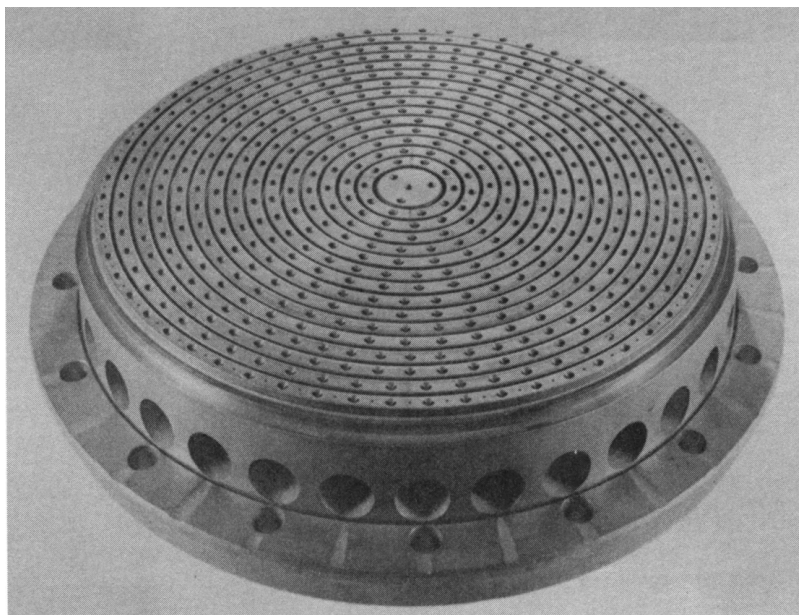


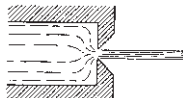
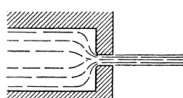
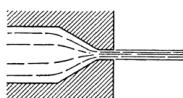
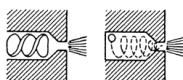
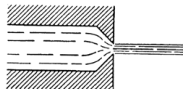
FIGURE 8–5. Injector with 90° self-impinging (fuel-against-fuel and oxidizer-against-oxidizer)-type countersunk doublet injection pattern. Large holes are inlets to fuel manifolds. Predrilled rings are brazed alternately over an annular fuel manifold or groove and a similar adjacent oxidizer manifold or groove. A section through a similar but larger injector is shown in Fig. 8–1.

The *coaxial hollow post or spray injector* has been used for liquid oxygen and gaseous hydrogen injectors by most domestic and foreign rocket designers. It is shown in sketches **d** and **e** of Fig. 8–4. It works well when the liquid hydrogen has absorbed heat from cooling jackets and has been gasified. This gasified hydrogen flows at high speed (typically 330 m/sec or 1000 ft/sec); the liquid oxygen flows far more slowly (usually at less than 33 m/sec or 100 ft/sec), and the differential velocity causes a shear action, which helps to break up the oxygen stream into small droplets. The injector has a multiplicity of these coaxial elements on its face. In Russia and in Germany the spray injector elements have also been used with storable propellants.

The SSME injector shown in Fig. 9–6 uses 600 of these concentric sleeve injection elements; 75 of them have been lengthened beyond the injector face to form cooled baffles, which reduce the incidence of combustion instability.

The original method of making injection holes was to carefully drill them and round out or chamfer their inlets. This is still being done today. It is difficult to align these holes accurately (for good impingement) and to avoid burrs and surface irregularities. One method that avoids these problems and allows a large number of small accurate injector orifices is to use multiple etched, very thin plates (often called platelets) that are then stacked and diffusion bonded together

TABLE 8-2. Injector Discharge Coefficients

| Orifice Type | Diagram | Diameter (mm) | Discharge Coefficient |
|--|--|------------------------|-----------------------|
| Sharp-edged orifice |  | Above 2.5 | 0.61 |
| | | Below 2.5 | 0.65 approx. |
| Short-tube with rounded entrance $L/D > 3.0$ |  | 1.00 | 0.88 |
| | | 1.57 | 0.90 |
| | | 1.00 | |
| | | (with $L/D \sim 1.0$) | 0.70 |
| Short tube with conical entrance |  | 0.50 | 0.7 |
| | | 1.00 | 0.82 |
| | | 1.57 | 0.76 |
| | | 2.54 | 0.84–0.80 |
| | | 3.18 | 0.84–0.78 |
| Short tube with spiral effect |  | 1.0–6.4 | 0.2–0.55 |
| Sharp-edged cone |  | 1.00 | 0.70–0.69 |
| | | 1.57 | 0.72 |

to form a monolithic structure as shown in Fig. 8-6. The photo-etched pattern on each of the individual plates or metal sheets then provides not only for many small injection orifices at the injector face but also for internal distribution or flow passages in the injector and sometimes also for a fine-mesh filter inside the injector body. The platelets can be stacked parallel to or normal to the injector face. The finished injector has been called the platelet injector and has been patented by the Aerojet Propulsion Company.

Injector Flow Characteristics

The differences of the various injector element configurations shown in Figs. 8-3 and 8-4 reflect themselves in different hydraulic flow–pressure relationships, different starting characteristics, atomization, resistance to self-induced vibrations, and combustion efficiency.

The *hydraulic injector characteristics* can be evaluated accurately and can be designed for orifices with the desired injection pressures, injection velocities, flows, and mixture ratio. For a given thrust F and a given effective exhaust

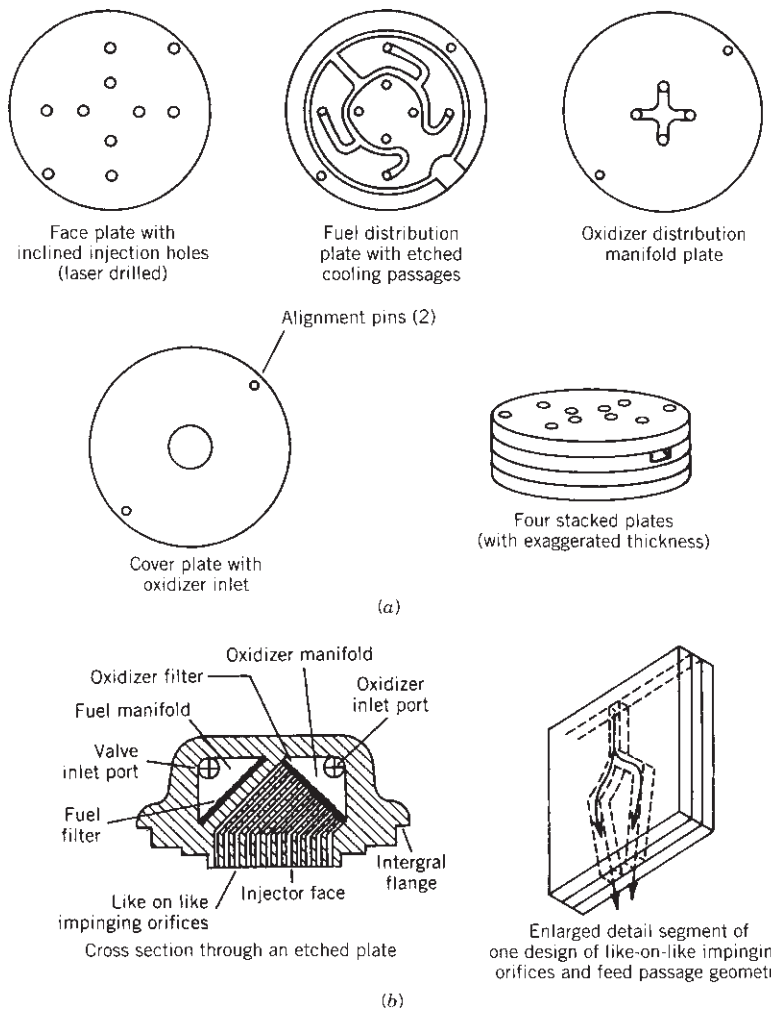


FIGURE 8–6. Simplified diagrams of two types of injector using a bonded platelet construction technique: (a) injector for low thrust with four impinging unlike doublet liquid streams; the individual plates are parallel to the injector face; (b) like-on-like impinging stream injector with 144 orifices; plates are perpendicular to the injector face. (Courtesy of Aerojet Propulsion Company).

velocity c , the total propellant mass flow \dot{m} is given by $\dot{m} = F/c$ from Eq. 2–6. The relations between the mixture ratio, the oxidizer, and the fuel flow rates are given by Eqs. 6–1 to 6–4. For the flow of an incompressible fluid through hydraulic orifices,

$$Q = C_d A \sqrt{2\Delta p / \rho} \quad (8-1)$$

$$\dot{m} = Q\rho = C_d A \sqrt{2\rho \Delta p} \quad (8-2)$$

where Q is the volume flow rate, C_d the dimensionless discharge coefficient, ρ the propellant mass density, A the cross-sectional area of the orifice, and Δp the pressure drop. These relationships are general and can be applied to any one section of the propellant feed system, to the injector, or to the overall liquid flow system.

For any given pressure drops the injection orifices usually determine the *mixture ratio* and the *propellant flows* of the rocket unit. From Eqs. 6-1 and 8-2 the mixture ratio r is

$$r = \dot{m}_o / \dot{m}_f = [(C_d)_o / (C_d)_f] (A_o / A_f) \sqrt{(\rho_o / \rho_f) (\Delta p_o / \Delta p_f)} \quad (8-3)$$

The quantities in the preceding equations have to be chosen so that the correct design mixture ratio is attained. Orifices whose discharge coefficients are constant over a large range of Reynolds numbers and whose ratio $(C_d)_o / (C_d)_f$ remains essentially invariant should be selected. For a given injector it is usually difficult to maintain the mixture ratio constant at low flows or thrusts, such as in starting.

The quality of the injector can be checked by performing cold tests with inert simulant liquids instead of reactive propellant liquids. Often water is used to confirm pressure drops through the fuel or oxidizer side at different flows, and this allows determination of the pressure drops with propellants and the discharge coefficients. Nonmixable inert liquids are used with a special apparatus to determine the local cold flow mixture ratio distribution over the chamber cross section. The simulant liquid should be of approximately the same density and viscosity as the actual propellant. New injectors are usually hot fired and tested with actual propellants.

The actual mixture ratio can be estimated from cold flow test data, the measured hole areas, and discharge coefficients by correcting by the square root of the density ratio of the simulant liquid and the propellant. When water at the same pressure is fed alternately into both the fuel and the oxidizer sides, $\Delta p_f = \Delta p_o$ and $\rho_f = \rho_o$ and the water mixture ratio will be

$$r = [(C_d)_o / (C_d)_f] A_o / A_f \quad (8-4)$$

Therefore, the mixture ratio measured in water tests can be converted into the actual propellant mixture ratio by multiplying it by the square root of the density ratio of the propellant combination and the square root of the pressure drop ratio. The mechanism of propellant atomization with simultaneous vaporization, partial combustion, and mixing is difficult to analyze, and performance of injectors has to be evaluated by experiment within a burning rocket thrust chamber. The *injection velocity* is given by

$$v = Q/A = C_d \sqrt{2\Delta p/\rho} \quad (8-5)$$

Values of discharge coefficients for various types of injection orifices are shown in Table 8–2. The velocity is a maximum for a given injection pressure drop when the discharge coefficient approaches 1. Smooth and well-rounded entrances to the injection holes and clean bores give high values of the discharge coefficient, and this hole entry design is the most common. Small differences in chamfers, hole entry radius, or burrs at the edge of a hole can cause significant variations in the discharge coefficient and the jet flow patterns, and these in turn can alter the quality and distribution of the atomized small droplets, the local mixture ratio, and the local heat transfer rates. An improperly manufactured hole can cause local chamber or injector burnout.

When an oxidizer and a fuel jet impinge, the *resultant momentum* can be calculated from the following relation, based on the principle of conservation of momentum. Figure 8–7 illustrates a pair of impinging jets and defines γ_0 as the angle between the chamber axis and the oxidizer stream, γ_f as the angle between the chamber axis and the fuel stream, and δ as the angle between the chamber axis and the average resultant stream. If the total momentum of the two jets before and after impingement is equal,

$$\tan \delta = \frac{\dot{m}_o v_o \sin \gamma_o - \dot{m}_f v_f \sin \gamma_f}{\dot{m}_o v_o \cos \gamma_o + \dot{m}_f v_f \cos \gamma_f} \quad (8-6)$$

Good performance is often obtained when the resultant momentum of impinging streams is approximately axial. If the resultant momentum is along the chamber axis, $\delta = 0$, $\tan \delta = 0$, and the angular relation for an axially directed jet momentum is given by

$$\dot{m}_o v_o \sin \gamma_0 = \dot{m}_f v_f \sin \gamma_f \quad (8-7)$$

From these equations the relation between γ_f , γ_0 , and δ can be determined. A sample injector analysis is shown in Section 8.8.

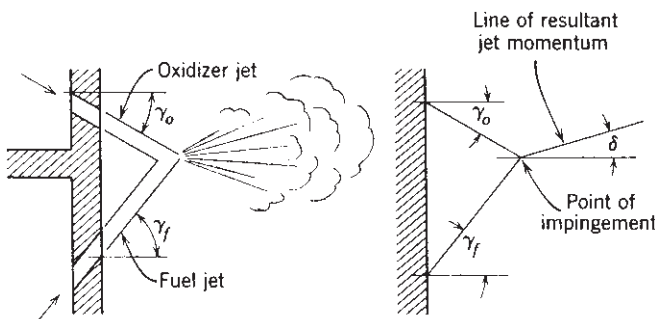


FIGURE 8–7. Angular relation of doublet impinging-stream injection pattern.

Factors Influencing Injector Behavior

A complete theory relating injector design parameters to rocket performance and combustion phenomena has not yet been devised, and therefore the approach to the design and development of liquid propellant rocket injectors has been largely empirical. Some of the analyses (see Ref. 8-2) has been useful in understanding the phenomenology and in indicating the directions for injector development. The available data indicate several important factors that affect the performance and operating characteristics of injectors; some of these are briefly enumerated here. These factors are different for injectors where both propellants are liquid (such as nitrogen tetroxide and hydrazine) or where one propellant is liquid and the other is gaseous as with LOX/gasified liquid hydrogen. Monopropellant injectors feed propellants into a catalyst bed and they are different and described in Section 8.3.

Propellant Combination. The particular combination of fuel and oxidizer affects such characteristics as the relative chemical reactivity, the ease and speed of vaporization, the ignition temperature, the diffusion of hot gases, the volatility, or the surface tension. Hypergolic (self-igniting) propellants generally require injector designs somewhat different from those required by propellants that must be ignited. Injector designs that perform efficiently with one combination do not necessarily work too well with a different propellant combination.

Injection, Element Pattern, and Orifice Size. With individual elements of holes or sprays in the injector plate, there appears to be an optimum performance and/or heat transfer condition for each of the following parameters: orifice size, angle of impingement, angle of resultant momentum, distance of the impingement locus from the injector face, number of injection orifices per unit of injector face surface, flow per unit of injection orifice, and distribution of orifices over the injector face. These parameters are largely determined experimentally or from similar earlier successful injectors.

Transient Conditions. Starting and stopping may require special provisions (temporary plugging of holes, accurate valve timing, insertion of paper cups over holes to prevent entry of one propellant into the manifold of the other propellant as was done on the German A-4 or V-2 thrust chamber, or check valves) to permit satisfactory transient operation.

Hydraulic Characteristics. The orifice type and the pressure drop across the injection orifice determine the injection velocity. A low pressure drop is desirable to minimize the weight of the feed system or the pumping power. High-pressure drops are used often to increase the rocket's resistance to combustion instability and enhance atomization of the liquids and improve performance.

Heat Transfer. Injectors influence the performance and the heat transferred in rocket thrust chambers. Low heat transfer rates have been obtained when the injection pattern resulted in an intentionally rich mixture near the chamber walls and when the chamber pressure is low. In general, the higher performance injectors have a higher heat transfer rate to the walls of the combustion chamber, the nozzle, and the injector face.

Structural Design. The injector is highly loaded by pressure forces from the combustion chamber and the propellant manifolds. During transition (starting or stopping) these pressure conditions can cause internal transient structural stresses which sometimes exceed the steady-state operating conditions. The faces of most modern injectors are flat and must be reinforced by suitable structures which nevertheless should provide no obstructions to the hydraulic manifold passages; the structure must also be sufficiently flexible to allow thermal deformations caused by heating the injector face with hot combustion gases or cooling of certain flow passages by cryogenic propellants. The injector design must also provide for positive seals between fuel and oxidizer manifolds (an internal leak can cause manifold explosions or internal fires) and a sealed attachment of the injector to the chamber. In large, gimbal-mounted thrust chambers the injector also often carries the main thrust load, and a gimbal mount is often directly attached to the injector, as shown in Figs. 6–1 and 8–1.

Combustion Stability. The injection hole or spray pattern, impingement pattern, hole or spray element distribution, and pressure drop have a strong influence on combustion stability; some types are much more resistant to pressure disturbances. As explained in Section 9.3, the resistance to vibration is determined experimentally, and often special antivibration devices, such as baffles or resonance cavities, are designed directly into the injector.

8.2. COMBUSTION CHAMBER AND NOZZLE

The *combustion chamber* is that part of a thrust chamber where the combustion or burning of the propellant takes place. The combustion temperature is much higher than the melting points of most chamber wall materials. Therefore it is necessary either to cool these walls (as described in a later section of this chapter) or to stop rocket operation before the critical wall areas become too hot. If the heat transfer is too high and thus the wall temperatures become locally too high, the thrust chamber will fail. Heat transfer to thrust chambers will be described later in this chapter. Section 8.8 gives a sample analysis of a thrust chamber and Ref. 8–2 describes the analyses for design and development.

Volume and Shape

Spherical chambers give the least internal surface area and inert mass per unit chamber volume; they are expensive to build and several have been tried. Today

we prefer a cylindrical chamber (or slightly tapered cone frustum) with a flat injector and a converging–diverging nozzle. The chamber volume is defined as the volume up to the nozzle throat section, and it includes the cylindrical chamber and the converging cone frustum of the nozzle. Neglecting the effect of the corner radii, the chamber volume V_c is

$$V_c = A_1 L_1 + A_1 L_c (1 + \sqrt{A_t/A_1} + A_t/A_1) \quad (8-8)$$

Here L_1 is the cylinder length, A_t/A_1 is the chamber contraction ratio, and L_c is the length of the conical frustum. The chamber surfaces exposed to heat transfer from hot gas are the injector face, the inner surface of the cylinder chamber, and the inner surface of the converging cone frustum. The *volume and shape* are selected after evaluating these parameters:

1. The volume has to be large enough for adequate *atomization, mixing, evaporation*, and *complete combustion* of propellants. Chamber volumes vary for different propellants with the time delay necessary to vaporize and activate the propellants and with the speed of combustion reaction of the propellant combination. When the chamber volume is too small, combustion is incomplete and the performance is poor. With higher chamber pressures or with highly reactive propellants, and with injectors that give improved mixing, a smaller chamber volume is usually permissible.
2. The chamber diameter and volume can influence the *cooling requirements*. If the chamber volume and the chamber diameter are large, the heat transfer rates to the walls will be reduced, the area exposed to heat will be large, and the walls are somewhat thicker. Conversely, if the volume and cross section are small, the inner wall surface area and the inert mass will be smaller, but the chamber gas velocities and the heat transfer rates will be increased. For the same thrust chamber there is an optimum chamber volume and diameter where the total heat absorbed by the walls will be a minimum. This is important when the available cooling capacity of the coolant is limited (e.g., oxygen–hydrocarbon at high mixture ratios) or if the maximum permissive coolant temperature has to be limited (for safety reasons with hydrazine cooling). The total heat transfer can also be further reduced by going to a rich mixture ratio or by adding film cooling (discussed below).
3. All inert components should have *minimum mass*. The thrust chamber mass is a function of the chamber dimensions, chamber pressure, and nozzle area ratio, and the method of cooling.
4. Manufacturing considerations favor a simple chamber geometry, such as a cylinder with a double cone bow-tie-shaped nozzle, low-cost materials, and simple fabrication processes.
5. In some applications the *length* of the chamber and the nozzle relate directly to the overall length of the vehicle. A large-diameter but short chamber and/or a short nozzle can allow a somewhat shorter vehicle with a lower structural inert vehicle mass.

6. The *gas pressure drop* for accelerating the combustion products within the chamber should be a minimum; any pressure reduction at the nozzle inlet reduces the exhaust velocity and the performance of the vehicle. These losses become appreciable when the chamber area is less than three times the throat area.
7. For the same thrust the combustion volume and the nozzle throat area become smaller as the operating chamber pressure is increased. This means that the chamber length and the nozzle length (for the same area ratio) also decrease with increasing chamber pressure. The performance and the heat transfer also go up with chamber pressure.

The preceding chamber considerations conflict with each other. It is, for instance, impossible to have a large chamber that gives complete combustion but has a low mass. Depending on the application, a compromise solution that will satisfy the majority of these considerations is therefore usually selected and verified by experiment.

The *characteristic chamber length* is defined as the length that a chamber of the same volume would have if it were a straight tube and had no converging nozzle section:

$$L^* = V_c / A_t \quad (8-9)$$

where L^* (pronounced el star) is the characteristic chamber length, A_t is the nozzle throat area, and V_c is the chamber volume. The chamber includes all the volume up to the throat area. Typical values for L^* are between 0.8 and 3.0 m (2.6 to 10 ft) for several bipropellants and higher for some monopropellants. Because this parameter does not consider any variables except the throat area, it is useful only for a particular propellant combination and a narrow range of mixture ratio and chamber pressure. The parameter L^* was used about 40 years ago, but today the chamber volume and shape are chosen by using data from successful thrust chambers of prior similar designs and identical propellants.

The *stay time* t_s of the propellant gases is the average value of the time spent by each molecule or atom within the chamber volume. It is defined by

$$t_s = V_c / (\dot{m} V_1) \quad (8-10)$$

where \dot{m} is the propellant mass flow, V_1 is the average specific volume or volume per unit mass of propellant gases in the chamber, and V_c is the chamber volume. The minimum stay time at which a good performance is attained defines the chamber volume that gives essentially complete combustion. The stay time varies for different propellants and has to be experimentally determined. It includes the time necessary for vaporization, activation, and complete burning of the propellant. Stay times have values of 0.001 to 0.040 sec for different types and sizes of thrust chambers and for different propellants.

The *nozzle* dimensions and configuration can be determined from the analyses presented in Chapter 3. The converging section of the nozzle experiences a much higher internal gas pressure than the diverging section and therefore the design of the converging wall is similar to the design of the cylindrical chamber wall. The exact contour of the converging nozzle section is not critical. Most thrust chambers use a shortened bell shape for the diverging nozzle section. Nozzles with area ratios over 400 have been developed and flown.

In Chapter 3 it was stated that very large nozzle exit area ratios allow a small but significant improvement in specific impulse, particularly at very high altitudes; however, the extra length, extra nozzle mass, and extra vehicle mass necessary to house a large nozzle often make this unattractive. This disadvantage can be mitigated by a multipiece nozzle that is stored in annular pieces around the engine during the ascent of the launch vehicle and automatically assembled in space after launch vehicle separation and before firing. This concept, known as *extendible nozzle*, has been successfully employed in solid propellant rocket motors for space applications for about 27 years. The first flight with an extendible nozzle on a liquid propellant engine was performed in 1998 with a modified version of a Pratt & Whitney Rocketdyne upper stage engine. Its flight performance is listed in Table 8–1. The engine is shown later in Fig. 8–17 and its carbon–carbon extendible nozzle cone is described in the section on materials and fabrication of this chapter.

Heat Transfer Distribution

Heat is transmitted to all internal hardware surfaces exposed to hot gases, namely the injector face, the internal chamber and nozzle walls. The *heat transfer rate* or *heat transfer intensity*, that is, local wall temperatures and heat transfer per unit wall area, varies within the thrust chamber. A typical heat transfer rate distribution is shown in Fig. 8–8. Only 0.5 to 5% of the total energy generated in the gas is transferred as heat to the chamber walls. For a typical rocket of 44,820 N or 10,000 lbf thrust the heat rejection rate to the wall may be between 0.75 and 3.5 MW, depending on the exact conditions and design. See Section 8.5.

The amount of heat transferred by *conduction* from the chamber gas to the walls in a rocket thrust chamber is negligible. By far the largest part of the heat is transferred by means of *convection*. A part (usually 5 to 35%) of the transferred heat is attributable to *radiation*.

For constant chamber pressure, the chamber wall surface increases less rapidly than the volume as the thrust level is raised. Thus the cooling of chambers is generally easier in large thrust sizes, and the capacity of the wall material or the coolant to absorb all the heat rejected by the hot gas is generally more critical in smaller sizes because of the volume–surface relationship.

Higher chamber pressure leads to higher vehicle performance (higher I_s), but also to higher engine inert mass. However, the resulting *increase of heat transfer with chamber pressure* often imposes design or material limits on the maximum practical chamber pressure for both liquid and solid propellant rockets.

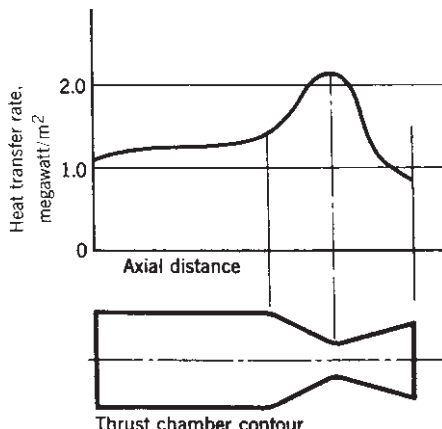


FIGURE 8–8. Typical axial heat transfer rate distribution for liquid propellant thrust chambers and solid propellant rocket motors. The peak is always at the nozzle throat or slightly upstream of the throat and the lowest value is usually near the nozzle exit.

The heat transfer intensity in chemical rocket propulsion can vary from less than 50 W/cm^2 or $0.3 \text{ Btu/in.}^2\text{-sec}$ to over 16 kW/cm^2 or $100 \text{ Btu/in.}^2\text{-sec}$. The high values are for the nozzle throat region of large bipropellant thrust chambers and high-pressure solid rocket motors. The lower values are for gas generators, nozzle exit sections, or small thrust chambers at low chamber pressures.

Cooling of Thrust Chambers

The primary objective of cooling is to prevent the chamber and nozzle walls from becoming too hot, so they will no longer be able to withstand the imposed loads or stresses, thus causing the chamber or nozzle to fail. Most wall materials lose strength and become weaker as temperature is increased. These loads and stresses are discussed in the next section. With further heating, the walls would ultimately fail or even melt. Cooling thus reduces the wall temperatures to an acceptable value.

Basically, there are two cooling methods in common use today. The first is the *steady-state method*. The heat transfer rate and the temperatures of the chambers reach *thermal equilibrium*. This includes *regenerative cooling* and *radiation cooling*. The duration is limited only by the available supply of propellant.

Regenerative cooling is done by building a cooling jacket around the thrust chamber and circulating one of the liquid propellants (usually the fuel) through it before it is fed to the injector. This cooling technique is used primarily with bipropellant chambers of medium to large thrust. It has been effective in applications with high chamber pressure and high heat transfer rates. Also, most injectors use regenerative cooling on their hot faces.

In *radiation cooling* the chamber and/or nozzle have only a single wall made of high-temperature material, such as niobium or molybdenum. When it reaches

thermal equilibrium, this wall usually glows red or white hot and radiates heat away to the surroundings or to empty space. Radiation cooling is used with bipropellant and monopropellant thrusters, bipropellant and monopropellant gas generators, and for diverging nozzle exhaust sections beyond an area ratio of about 6 to 10 in larger thrust chambers (see Fig. 8-2). A few small bipropellant thrusters are also radiation cooled. This cooling scheme has worked well with lower chamber pressures (less than 250 psi) and moderate heat transfer rates.

The second cooling method relies on *transient heat transfer* or *unsteady heat transfer*. It is also called *heat sink cooling*. The thrust chamber does not reach a thermal equilibrium, and temperatures continue to increase with operating duration. The heat-absorbing capacity of the metal hardware determines its maximum duration, which is usually short (a few seconds for an all-metal construction). The rocket combustion operation has to be stopped just before any of the exposed walls reaches a critical temperature at which it could fail. This method has mostly been used with low chamber pressures and low heat transfer rates. Heat sink cooling of thrust chambers can also be done by absorbing heat in an inner liner made of an *ablative material*, such as fiber-reinforced plastics. Ablative materials burn or erode slowly and cumulative operating durations can be minutes. Ablative materials are used extensively in solid propellant rocket motors and will be discussed further in Chapter 15. The analysis of both of these cooling methods is given in the next section of this chapter.

Film cooling and *special insulation* are supplementary techniques that are used occasionally with both methods to locally augment their cooling capability. All these cooling methods will be described further in this chapter.

Cooling also helps to reduce the oxidation of the wall material and the rate at which walls would be eaten away. The rates of chemical oxidizing reactions between the hot gas and the wall material can increase dramatically with wall temperature. This oxidation problem can be minimized not only by limiting the wall temperature but also by burning the liquid propellants at a mixture ratio where the percentage of aggressive gases in the hot gas (such as oxygen or hydroxyl) is very small, and by coating certain wall materials with an oxidation-resistant coating; for example, iridium has been coated on the inside of rhenium walls.

Cooling with Steady-State Heat Transfer. *Cooled thrust chambers* have provisions for cooling some or all metal parts coming into contact with hot gases, such as chamber walls, nozzle walls, and injector faces. Internal cooling passages, cooling jackets, or cooling coils permit the circulation of a *coolant*. Jackets can consist of separate inner and outer walls or of an assembly of contoured, adjacent tubes (see Figs. 8-1 and 8-9). The inner wall confines the gases, and the spaces between the walls serve as the coolant passage. The *nozzle throat region* is usually the location that has the highest heat transfer intensity and is therefore the most difficult to cool. For this reason the cooling jacket is often designed so that the coolant velocity is highest at the critical regions by restricting the coolant passage cross section, and so that the fresh cold coolant enters the jacket

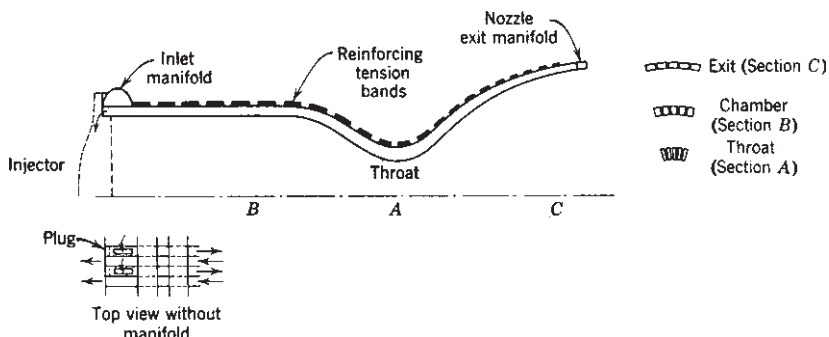


FIGURE 8–9. Diagram of a tubular cooling jacket. The tubes are bent to the chamber and nozzle contours; they are formed hydraulically to give a variable cross section to permit the same number of tubes at the throat and exit diameters. Coolant enters through the inlet manifold into every other tube and proceeds axially to the nozzle exit manifold, where it then enters the alternate tubes and returns axially to go directly to the injector.

at or near the nozzle. While the selection of the coolant velocity and its variation along the wall for any given thrust chamber design depends on heat transfer considerations, the selection of the coolant passage geometry often depends on pressure loss, stresses, and manufacturing considerations. An *axial flow cooling jacket*, or a *tubular wall*, has a low hydraulic friction loss but is practical only for large coolant flows (above approximately 9 kg/sec). For small coolant flows and small thrust units, the design tolerances of the cooling jacket width between the inner and outer walls or the diameters of the tubes, become too small, or the tolerances become prohibitive. Therefore, most small thrust chambers use radiation cooling or ablative materials.

In *regenerative cooling* the heat absorbed by the coolant is not wasted; it augments the initial energy content of the propellant prior to injection, increasing the exhaust velocity slightly (0.1 to 1.5%). This method is called regenerative cooling because of the similarity to steam regenerators. The design of the tubular chamber and nozzle combines the advantages of a thin wall (good for reducing thermal stresses and high wall temperatures) and a cool, lightweight structure. Tubes are formed to special shapes and contours (see Figs. 8–1 and 8–9), usually by hydraulic means, and then brazed, welded, or soldered together (see Ref. 8–3). In order to take the gas pressure loads in hoop tension, they are reinforced on the outside by high-strength bands or wires. While Fig. 8–9 shows alternate tubes for up and down flow, there are chambers where the fuel inlet manifold is downstream of the nozzle throat area and where the coolant flow is up and down in the nozzle exit region, but unidirectionally up in the throat and chamber regions.

Radiation cooling is another steady-state method of cooling. It is simple and is used extensively in the low heat transfer applications listed previously. Further discussion of radiation cooling is given in Section 8.4. In order for heat to be radiated into space, it is usually necessary for the bare nozzle and chamber

to stick out of the vehicle. Figure 8–16 shows a radiation-cooled thrust chamber. Since the white hot glowing *radiation-cooled* chambers and/or nozzles are potent radiators, they may cause undesirable heating of adjacent vehicle or engine components. Therefore, many have insulation (see Fig. 8–13) or simple external radiation shields to minimize these thermal effects; however, in these cases the actual chamber or nozzle wall temperatures are higher than they would be without the insulation or shielding.

Cooling with Transient Heat Transfer. *Thrust chambers with unsteady heat transfer* are basically of two types. One is a *simple metal chamber* (steel, copper, stainless steel, etc.) made with walls sufficiently thick to absorb plenty of heat energy. For short-duration testing of injectors, testing of new propellants, rating combustion stability, and very short duration rocket-propelled missiles, such as an antitank weapon, a heavy-walled simple, short-duration steel chamber is often used. The common method of *ablative cooling* or *heat sink cooling* uses a combination of endothermic reactions (breakdown or distillation of matrix material into smaller compounds and gases), pyrolysis of organic materials, counter-current heat flow and coolant gas mass flow, charring, and localized melting. An ablative material usually consists of a series of strong, oriented fibers (such as glass, Kevlar, or carbon fibers) engulfed by a matrix of an organic binder material (such as plastics, epoxy resins or phenolic resins). As shown in Fig. 15–11, the gases seep out of the matrix and form a protective film cooling layer on the inner wall surfaces. The fibers and the residues of the matrix form a hard char or porous coke-like material that preserves the wall contour shapes.

The orientation, number, and type of fiber determine the ability of the composite ablative material to withstand significant stresses in preferred directions. For example, internal pressure produces longitudinal as well as hoop stresses in the thrust chamber walls and thermal stresses produce compression on the inside of the walls and tensile stresses on the outside. We have learned how to place the fibers in two or three directions, which makes them anisotropic. We then speak of two-dimensional (2-D) and 3-D fiber orientation.

A set of strong carbon fibers in a matrix of amorphous carbon is a special, but favorite type of material. It is often abbreviated as C–C or carbon–carbon. The carbon materials lose their ability to carry loads at a high temperature of about 3700 K or 6200 F. Carbon oxidizes readily from CO or CO₂. Its best applications are with fuel-rich propellant mixtures that have little or no free oxygen or hydroxyl in their exhaust. It has also been used for nozzle throat inserts. Properties for one type of C–C are given in Table 15–5. A C–C nozzle extension is shown in Fig. 8–17. See Ref. 8–4.

Ablative cooling was first used and is still used extensively with solid propellant rocket motors. It has since been successfully applied to liquid propellant thrust chambers, particularly at low chamber pressure, where the static gas temperatures are relatively low. It is still used today as a material for nozzle extensions, such as for the RS-68 in Fig. 6–10, and it can operate for several minutes. It is also used as a chamber and nozzle liner at low chamber pressure. An example is the axial gimbaled thruster of the Peacekeeper fourth stage

which is seen in Figure 6–13. Ablative lined small thrusters (100 lbf thrust or less) have been flown extensively in the 1950s and 1960s in Apollo missions and other applications for attitude control and minor maneuvers. They are no longer used today because they are relatively heavy and because the eroded particle, droplets, or certain gases in the exhaust plume deposit condense on optical surfaces of spacecraft (mirror, solar cells, or windows).

It is often advantageous to use a different cooling method for the downstream part of the diverging nozzle section, because its heat transfer rate per unit area is usually much lower than in the chamber or the converging nozzle section, particularly with nozzles of large area ratio. There is usually a small saving in inert engine mass, a small increase in performance, and a cost saving, if the chamber and the converging nozzle section and the throat region (up to an area ratio of perhaps 5 to 10) use regenerative cooling and the remainder of the nozzle exit section is radiation cooled (or sometimes ablative cooled). See Fig. 8–2 and Ref. 8–4.

Film Cooling. This is an auxiliary method applied to chambers and/or nozzles, augmenting either a marginal steady-state or a transient cooling method. It can be applied to a complete thrust chamber or just to the nozzle, where heat transfer is the highest. Film cooling is a method of cooling whereby a relatively cool thin fluid film covers and protects exposed wall surfaces from excessive heat transfer. Figure 8–10 shows film-cooled chambers. The film can be introduced by injecting small quantities of fuel or an inert fluid at very low velocity through a large number of orifices along the exposed surfaces in such a manner that a protective relatively cool gas film or cool boundary layer is formed. In liquid propellant rocket engines extra fuel can also be admitted through extra injection holes at the outer layers of the injector; thus a propellant mixture is achieved (at the periphery of the chamber), which has a much lower combustion temperature. This differs from film cooling or transpiration cooling because there does not have to be a chamber cooling jacket or film-cooling manifolds.

Film cooling by itself (without another cooling method) has been very effective in keeping chamber and nozzle materials from becoming too hot. In fact the very first thrust chambers developed by Robert H. Goddard in the 1920s were film cooled. However, the film coolant is not burned effectively and there was a 5 to 17% reduction in specific impulse. Therefore, today, film cooling is used in small quantities (1 to 6% of fuel) to locally supplement other cooling methods and the performance loss is 0.5 to 2%. In solid propellant rocket engines this film cooling can be accomplished by inserting a ring of cool-burning propellant upstream of the nozzle, as shown in Fig. 8–10 or by wall insulation materials, whose ablation and charring will release relatively cool gases into the boundary layer.

Turbine discharge gas (400 to 800°C or 752 to 1972°F) has also been used as a film coolant for uncooled nozzle exit sections of large liquid propellant rocket engines. Of course, the injection of an annular gas layer at the periphery of the nozzle exit, at a temperature lower than the maximum possible value, causes

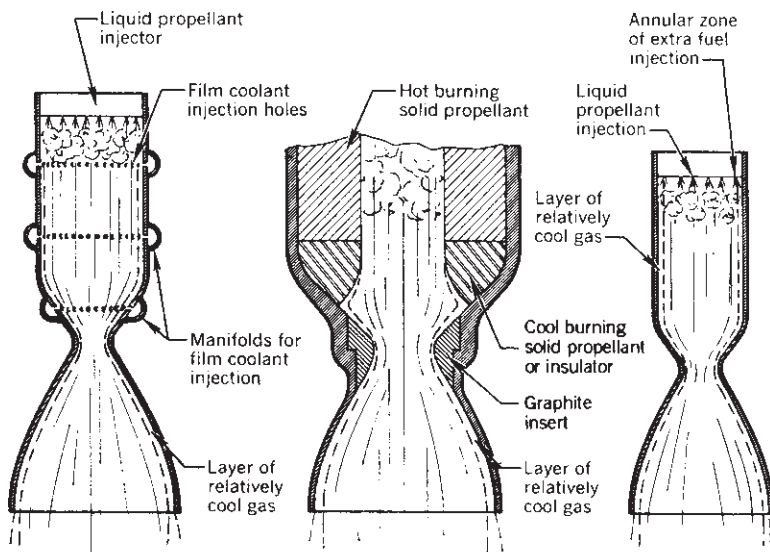


FIGURE 8-10. Simplified diagrams of three different methods of forming a cool boundary layer in the nozzle.

a decrease in a specific impulse. Therefore, it is desirable to reduce both the thickness of this cooler layer and the mass flow of cooler gas, relative to the total flow, to a practical minimum value at which cooling will still be effective.

A special type of film cooling, *sweat cooling* or *transpiration cooling*, uses a porous wall material which admits a coolant through pores uniformly over the surface. This technique has been successfully used to cool injector faces in the upper stage engine (J-2) of the moon launch vehicle and the Space Shuttle main engine (SSME) with hydrogen fuel.

Thermal Insulation. Theoretically, a good thermal insulation layer on the gas side of the chamber wall can be very effective in reducing chamber wall heat transfer and wall temperatures. However, efforts with good insulation materials such as refractory oxides or ceramic carbides have usually not been successful. They will not withstand differential thermal expansion without cracking or spalling. A sharp edge on the surface (crack or flaked-off piece of insulator) will cause a sudden rise in the stagnation temperature and most likely lead to a local wall failure. Asbestos is a good insulator and was used several decades ago; because it is a cancer-causing agent, it is no longer used. Coating development efforts with rhenium and other materials are continuing. Insulation or heat shields have been successfully applied on the exterior of radiation-cooled thrust chambers to reduce the heat transfer from the hot thrust chamber wall to adjacent sensitive equipment or structures.

With hydrocarbon fuels it is possible to form small carbon particles or soot in the hot gas and that can lead to a carbon deposit on the gas side of the chamber

or nozzle walls. If it is a thin, mildly adhesive soot, it can be an insulator, but it is difficult to reproduce such a coating. More likely it forms hard, caked deposits, which can be spalled off in localized flakes and form sharp edges, and then it is undesirable. Most designers have preferred instead to use film cooling or extra high coolant velocities in the cooling jacket with injectors that do not create adhesive soot.

Hydraulic Losses in the Cooling Passage

The cooling coil or cooling jacket should be designed so that the fluid adsorbs all the heat transferred across the inner motor wall, and so that the coolant pressure drop will be small.

A higher pressure drop allows a higher coolant velocity in the cooling jacket, will do a better job of cooling, but requires a heavier feed system, which increases the engine mass slightly and thus also the total inert vehicle mass. For many liquid propellant rockets the coolant velocity in the chamber is approximately 3 to 10 m/sec or 10 to 33 ft/sec and, at the nozzle throat, 6 to 24 m/sec or 20 to 80 ft/sec.

A cooling passage can be considered to be a hydraulic pipe, and the *friction loss* can be calculated accordingly. For a straight pipe,

$$\Delta p / \rho = \frac{1}{2} f v^2 (L/D) \quad (8-11)$$

where Δp is the friction pressure loss, ρ the coolant mass density, L the length of coolant passage, D the equivalent diameter, v the average velocity in the cooling passage, and f the friction loss coefficient. In English engineering units the right side of the equation has to be divided by g_0 , the sea-level acceleration of gravity (32.2 ft/sec²). The friction loss coefficient is a function of Reynolds number and has values between 0.02 and 0.05. A *typical pressure loss* of a cooling jacket is between 5 and 25% of the chamber pressure.

A large portion of the pressure drop in a cooling jacket usually occurs in those locations where the flow direction or the flow-passage cross section is changed. Here the sudden expansion or contraction causes a loss, sometimes larger than the velocity head $v^2/2$. This hydraulic situation exists in inlet and outlet chamber manifolds, injector passages, valves, and expansion joints.

The pressure loss in the cooling passages of a thrust chamber can be calculated, but more often it is measured. This pressure loss is usually determined in cold flow tests (with an inert fluid instead of the propellant and without combustion), and then the measured value is corrected for the actual propellant (different physical properties) and the hot firing conditions; a higher temperature will change propellant densities or viscosities and in some designs it changes the cross section of cooling flow passages.

Thrust Chamber Wall Loads and Stresses

The analysis of loads and stresses is performed on all propulsion components during their engineering design. Its purpose is to assure the propulsion designer

and the flight vehicle user that (1) the components are strong enough to carry all the loads, so that they can fulfill their intended function; (2) potential failures have been identified, together with the possible remedies or redesigns; and (3) their masses have been reduced to a practical minimum. In this section we concentrate on the loads and stresses in the walls of thrust chambers, where high heat fluxes and large thermal stresses complicate the stress analysis. Some of the information on safety factors and stress analysis apply also to all propulsion systems, including solid propellant motors and electric propulsion.

The safety factors (really margins for ignorance) are very small in rocket propulsion when compared to commercial machinery, where these factors can be 2 to 6 times larger. Several *load conditions* are considered for each rocket component; they are:

1. *Maximum expected working load* is the largest likely operating load under all likely operating conditions or transients. Examples are operating at a slightly higher chamber pressure than nominal as set by tolerances in design or fabrication (an example is the tolerance in setting the tank pressure regulator) or the likely transient overpressure from ignition shock.
2. *The design limit load* is typically 1.20 times the maximum expected working load, to provide a margin. If the variation in material composition, material properties, the uncertainties in the method of stress analysis, or predicted loads are significant, a larger factor may be selected.
3. *The damaging load* can be based on the yield load or the ultimate load or the endurance limit load, whichever gives the lowest value. The yield load causes a permanent set or deformation, and it is typically set as 1.10 times the design limit load. The endurance limit may be set by fatigue or creep considerations (such as in pulsing). The ultimate load induces a stress equal to the ultimate strength of the material, where significant elongation and area reduction can lead to failure. Typically, it is set as 1.50 times the design limit load.
4. *The proof test load* is applied to engines or their components during development and manufacturing inspection. It is often equal to the design limit load, provided this load condition can be simulated in a laboratory. Thrust chambers and other components, whose high thermal stresses are difficult to simulate, use actual hot firing tests to obtain this proof, often with loads that approach the design limit load (e.g., higher than nominal chamber pressure or a mixture ratio that results in hotter gas).

The walls of all thrust chambers are subjected to radial and axial *loads from the chamber pressure, flight accelerations* (axial and transverse), *vibration*, and *thermal stresses*. They also have to withstand a momentary *ignition pressure surge or shock*, often due to excessive propellant accumulation in the chamber. This surge can exceed the nominal chamber pressure. In addition, the chamber walls have to *transmit thrust loads* as well as forces and in some applications also moments, imposed by *thrust vector control* devices described in Chapter 18.

Walls also have to survive a “thermal shock,” namely, the initial thermal stresses at rapid starting. When walls are cold or at ambient temperature, they experience higher gas heating rates than after the walls have been heated. These loads are different for almost every design, and each unit has to be considered individually in determining the wall strengths.

A heat transfer analysis is usually done only for the most critical wall regions, such as at and near the nozzle throat, at a critical location in the chamber, and sometimes at the nozzle exit. The thermal stresses induced by the temperature difference across the wall are often the most severe stresses and a change in heat transfer or wall temperature distribution will affect the stresses in the wall. Specific failure criteria (wall temperature limit, reaching yield stress, or maximum coolant temperature, etc.) have to be established for these analyses.

The temperature differential across a chamber wall introduces a compressive stress on the inside and a tensile stress on the outside of the inner wall; the stress s can be calculated for simple cylindrical chamber walls that are thin in relation to their radius as

$$s = 2\lambda E \Delta T / (1 - \nu) \quad (8-12)$$

where λ is the coefficient of thermal expansion of the wall material, E the modulus of elasticity of the wall material, ΔT the temperature drop across the wall, and ν the Poisson ratio of the wall material. Temperature stresses frequently exceed the yield point. The materials experience a change in the yield strength and the modulus of elasticity with temperature. The preceding equation is applicable only to elastic deformations. This yielding of rocket thrust chamber wall materials can be observed by the small and gradual contraction of the throat diameter after each operation (perhaps 0.05% reduction in throat diameter after each firing) and the formation of progressive cracks of the inside wall surface of the chamber and throat after successive runs. These phenomena limit the useful life and number of starts or temperature cycles of a thrust chamber (see Refs. 8-5 and 8-6).

In selecting a working stress for the wall material of a thrust chamber, the variation of strength with temperature and the temperature stresses over the wall thickness have to be considered. The temperature drop across the inner wall is typically between 50 and 550 K, and an average temperature is sometimes used for estimating the material properties. The most severe thermal stresses can occur during the start, when the hot gases cause thermal shock to the hardware. These transient thermal gradients cause severe thermal strain and local yielding.

A picture of a typical steady-state stress distribution caused by pressure loads and thermal gradients is shown in Fig. 8-11. Here the inner wall is subjected to a compressive pressure differential caused by a high liquid pressure in the cooling jacket and a relatively large temperature gradient. In a large rocket chamber, such as is used in the Redstone missile or the German V-2, the wall thickness of the nozzle steel way may be 7 mm and the temperature differential across it may readily exceed several hundred degrees. This temperature gradient causes the hot inner wall surface to expand more than the wall surface on the coolant

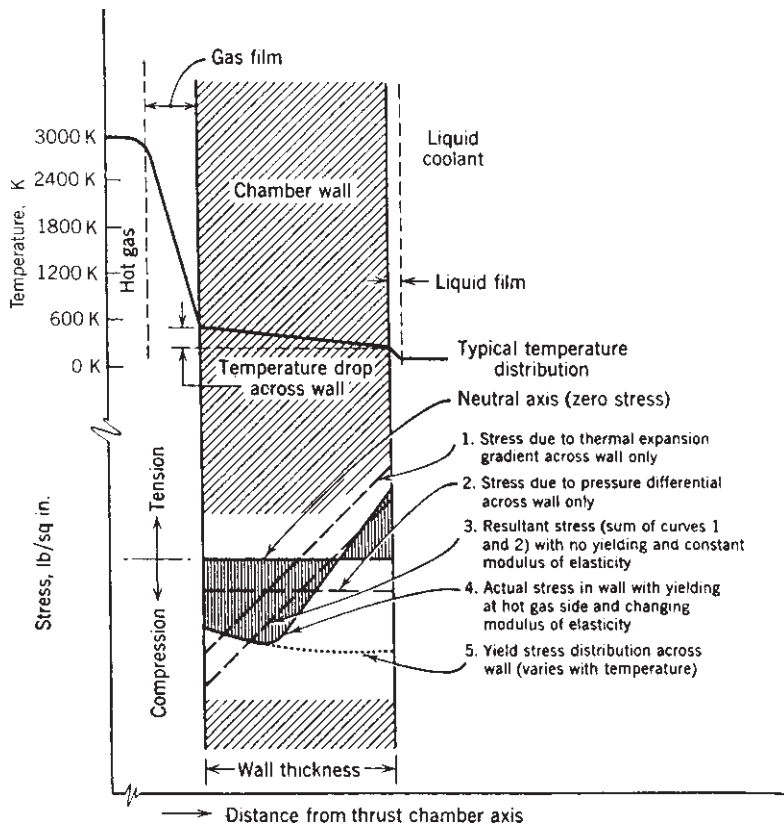


FIGURE 8–11. Typical stresses in a thrust chamber inner wall.

side and imposes a high compressive thermal stress on the inside surface and a high tensile thermal stress on the coolant side. In these thick walls the stress induced by the pressure load is usually small compared to the thermal stress. The resultant stress distribution in thick inner walls (shown shaded in the sample stress diagram of Fig. 8–11) indicates that the stress in the third of the wall adjacent to the hot gases has exceeded the yield point. Because the modulus of elasticity and the yield point diminish with temperature, the stress distribution is not linear over the yielded portion of the wall. In effect, this inner portion acts as a heat shield for the outer portion which carries the load.

Because of the differential expansion between the hot inner shell and the relatively cold outer shell, it is necessary to provide for axial *expansion joints* to prevent severe temperature stresses. This is particularly critical in larger double-walled thrust chambers. The German V-2 thrust chamber expanded over 5 mm in an axial and 4 mm in a radial direction.

Tubes for tubular wall thrust chambers are subjected to several different stress conditions. Only that portion of an individual cooling tube exposed to

hot chamber gases experiences high thermal stresses and deformation as shown in Fig. 8–15. The tubes have to hold the internal coolant pressure, absorb the thermal stresses, and contain the gas pressure in the chamber. The hottest temperature occurs in the center of the outer surface of that portion of each tube exposed to hot gas. The thermal stresses are relatively low, since the temperature gradient is small; copper has a high conductivity and the walls are relatively thin (0.5 to 2 mm). The coolant pressure-induced load on the tubes is relatively high, particularly if the thrust chamber operates at high chamber pressure. The internal coolant pressure tends to separate the tubes. The gas pressure loads in the chamber are usually taken by reinforcing bands which are put over the outside of the tubular jacket assembly (see Figs. 8–1 and 8–9). The joints between the tubes have to be gas tight and this can be accomplished by soldering, welding, or brazing.

When a high-area-ratio nozzle is operated at high ambient pressure (sea level or low altitude), the lower part of the nozzle structure experiences a compression because the pressure in the nozzle near the exit is actually below atmospheric value. Therefore, high-area-ratio nozzles usually have stiffening rings on the outside of the nozzle near the exit to maintain a circular shape and thus prevent buckling, flutter, or thrust misalignment.

Aerospike Thrust Chamber

A separate category comprises thrust chambers using a center body, such as a plug nozzle or aerospike nozzle. They have more surface to cool than ordinary thrust chambers. A circular aerospike thruster is described in Chapter 3 and shown schematically in Figs. 3–12 and 8–12 and described in Ref. 8–7. Here the diameter of the exhaust flow plume increases with altitude. Each individual small (regeneratively cooled) thrust chamber or cell has its own cylindrical combustion chamber, a circular small nozzle throat, but a rectangular nozzle exit of low area ratio. The gas from these rectangular nozzle exits is further expanded (and thus reaches a higher exhaust velocity) along the contour of the spike or ramp. The flat surface at the bottom or base is porous or full of small holes and a low-pressure gas flows through these openings. This causes a back pressure on the flat base surface. This flow can be the exhaust gas from the turbopumps of an engine with a gas generator cycle; it is typically 1 or 2% of the total flow. The gas region below this base is enclosed by gas flows from the ramps. A linear version of a truncated (shortened) aerospike engine with two opposing ramps has been developed using LOX/LH₂ propellants at a thrust level of about 200,000 lbf and the ground tests were satisfactory. It has two fuel-cooled side plates. Except for a flight of a very small, inefficient, truncated experimental aerospike, none of these liquid propellant engines have flown.

The thrust of this aerospike thrust chamber consists of (1) the axial component thrusts of each of the little chamber modules or cells, (2) the integral of the pressures acting on the ramps over the axially projected area normal to the axis of the ramps, and (3) the pressure acting over the base area.

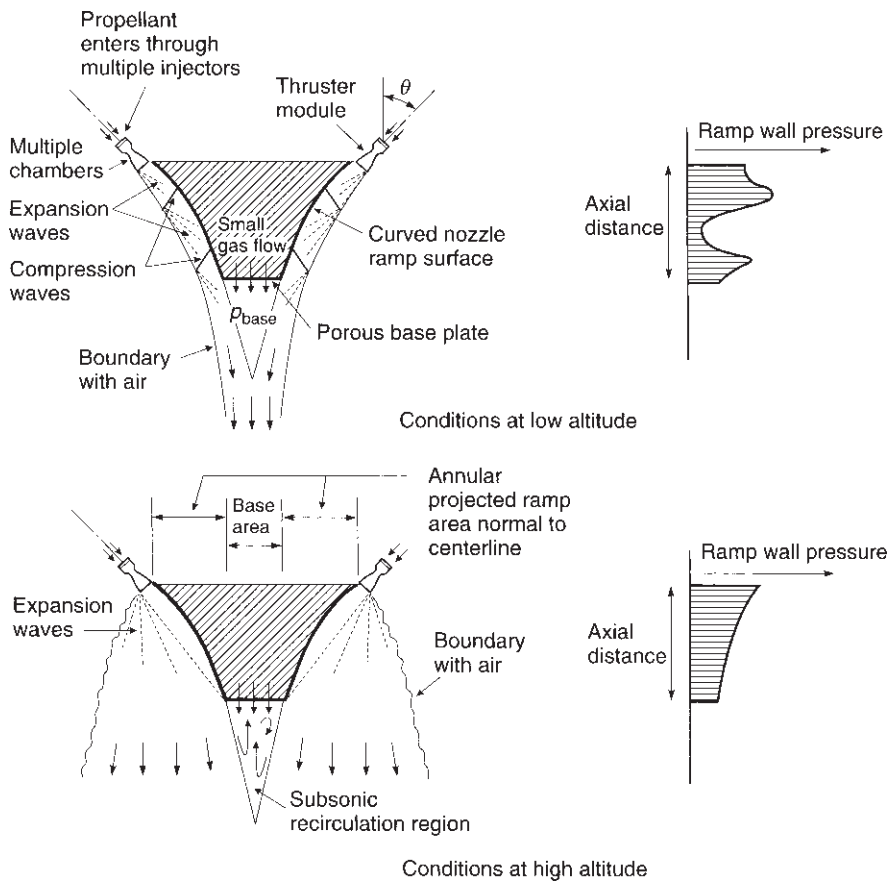


FIGURE 8–12. Pressure profile and flow pattern along the ramp of an aerospike nozzle.

The local gas pressures on the ramps are influenced by shock wave phenomena and change pressure profiles with altitude. Figure 8–12 shows a typical pressure distribution on a typical ramp surface and the flow patterns for low and high altitude. The hot gas flows coming out of the cell nozzles are turned into a nearly axial direction by multiple expansion waves (shown as dashed lines), which cause a reduction in pressure. At lower altitudes the turning causes compression shock waves (represented as solid lines), which causes local pressures to rise. The compression waves are reflected off the boundary between the hot gas jet and the ambient airstream, creating further expansion waves. At high altitude there are no compression waves emanating from the ramp and the expanding diverging flow exerts a decreasing pressure on the ramp area and behaves very similarly to the diverging nozzle flow in a bell-shaped conventional nozzle exit section. The contact locations, where the compression waves touch the ramp surface, have higher local heat transfer than other areas on the ramp surface; these

locations move downstream as the vehicle gains altitude. The wave patterns and the pressure distribution on the spike or ramp surface can be determined from computerized fluid dynamics programs or a method of characteristics program.

The *advantages* claimed for an aerospike engine are these: (1) Compared to rocket engines with conventional axisymmetric nozzles, the truncated aerospike is very short (about one third the length), and this also reduces the vehicle length and vehicle structure mass; (2) it has altitude compensation and thus operates at optimum nozzle expansion and highest possible exhaust velocity at every altitude; and (3) differential throttling of certain sets of individual thruster modules or cells allows pitch and yaw control, and with two engines it also allows roll control of the vehicle during powered flight, as explained in Chapter 18. There is no gimbal joint, no movement of the nozzle, no actuators, and no actuator power supply or strong structural locations for actuator side loads. The *disadvantages* include the lack of proven flight experience, proven reliability and performance validation, and a larger-than-usual surface area subject to high heat transfer. There are some small performance losses as the supersonic gas flow goes from a round nozzle throat of each cell into a rectangular nozzle exit of the cell, also in turning the flow on the ramp, and in combining supersonic flow from adjacent cell nozzles. The average total loss with liquid propellants is believed to be about 1% of the specific impulse. For combustion gases, which contain small particulates (e.g., gases from solid composite propellant explained in Chapter 13), the losses will be higher—up to 7%—depending on the percentage of particulates (which are tiny solid particles and/or small liquid droplets). Due to the inertia of the particulates, they can only be turned through a small angle in a high-speed gas flow and they will hit the nozzle walls. The mass flow distribution will be uneven with the heavy particulates mostly in the gas layers next to the concave curved nozzle walls. Ref. 8–8 gives an example, which did not recognize the loss from particulates.

8.3. LOW-THRUST ROCKET THRUST CHAMBERS OR THRUSTERS

Spacecraft, certain tactical missiles, missile defense vehicles, and upper stages of ballistic missiles often use special, multiple thrusters in their small, liquid propellant rocket engines. They generally have thrust levels between about 0.5 and 10,000 N or 0.1 to 2200 lbf, depending on vehicle size and mission. As mentioned in Section 4.5, they are used for trajectory corrections, attitude control, docking, terminal velocity control in spacecraft or ballistic missiles, divert or side movement, propellant settling, and other functions. Most operate with multiple restarts for relatively short durations during a major part of their duty cycle. As mentioned in Section 6.7, they can be classified into *hot gas thrusters* (high-performance bipropellant with combustion temperatures above 2600 K and vacuum I_s of 230 to 325 sec), *warm gas thrusters* such as monopropellant hydrazine (temperatures between 500 and 1600 K and I_s of 180 to 245 sec), and *cold gas thrusters* such as high-pressure stored nitrogen (200 to 320 K) with low specific impulses (40 to 120 sec).

A typical small thruster for bipropellant is shown in Fig. 8-13 and for hydrazine monopropellant in Fig. 8-14. For attitude control angular motions these thrust chambers are usually arranged in pairs as explained in Section 4.5. The same control signal activates the valves for both units of such a pair. All these small space rocket systems use a pressurized feed system, some with positive expulsion provisions, as explained in Section 6.2. The vehicle mission and the automatic control system of the vehicle often require irregular and frequent pulses to be applied by pairs of attitude control thrust chambers, which often operate for very short periods (as low as 0.01 to 0.02 sec). This type of frequent and short-duration thrust application is also known as *pulsed thrust operation*. For translation maneuvers a single thruster can be fired (often in a pulsing mode) and the thrust axis usually goes through the center of gravity of the vehicle. The resulting acceleration will depend on the thrust and the location of the thruster on the vehicle; it can be axial or at an angle to the flight velocity vector.

There is a performance degradation with decreasing pulse duration for all three types of thrusters, because propellants are used inefficiently during the buildup of thrust and the decay of thrust, when they operate below full chamber pressure and the nozzle expansion characteristics are not optimum. The specific impulse

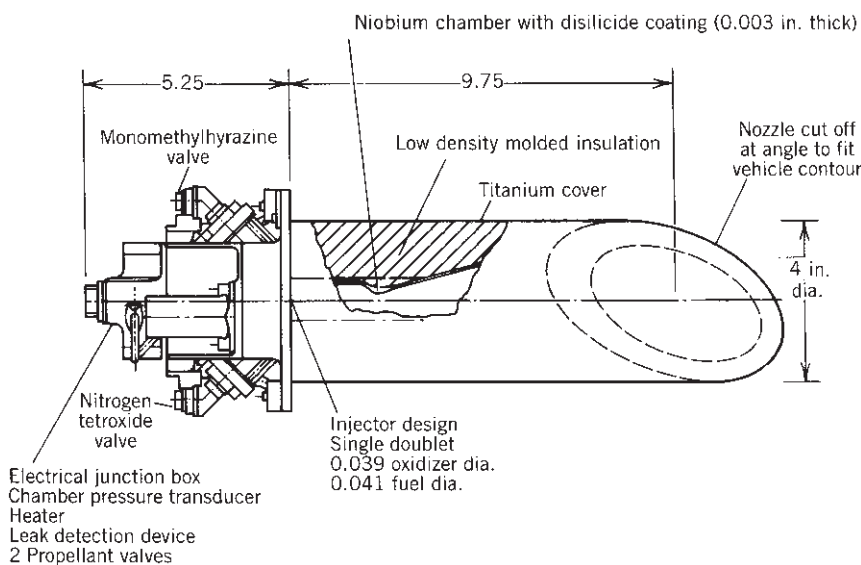


FIGURE 8-13. This radiation-cooled, insulated vernier thruster is one of several used on the reaction control system of the Space Shuttle vehicle for orbit stabilization and orientation, rendezvous or docking maneuvers, station keeping, deorbit, or entry. The nozzle is cut off at an angle to fit the contour of the vehicle. Performance data are given in Table 6-5. Operation can be in a pulse mode (firing durations between 0.08 and 0.32 sec with minimum offtime of 0.08 sec) or a steady-state mode (0.32 to 125 sec). Demonstrated life is 23 hr of operation and more than 300,000 starts. (Courtesy of Aerojet Propulsion Company and NASA.)

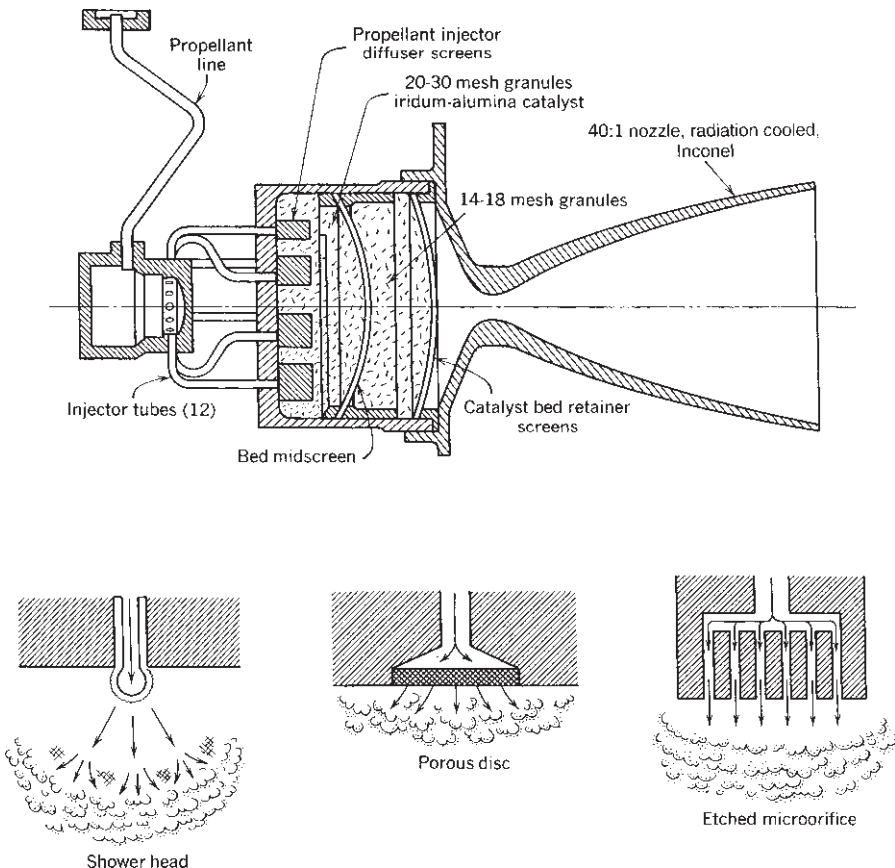


FIGURE 8-14. Typical hydrazine monopropellant small thrust chamber with catalyst bed, showing different methods of injection.

really suffers when the pulse duration becomes very short. In Section 3.5 the actual specific impulse of a rocket operating at a steady state was given at about 92% of theoretical specific impulse. With very short pulses (0.01 sec) this can be lower than 50%, and with pulses of 0.10 sec it can be around 75 to 88%. Also, the reproducibility of the total impulse delivered in a short pulse is not as high after prolonged use. A preheated monopropellant catalyst bed will allow performance improvement in the pressure rise and in short pulses.

One way to minimize the impulse variations in short pulses and to maximize the effective actual specific impulse is to minimize the liquid propellant passage volume between the control valve and the combustion chamber. The propellant flow control valves for pulsing attitude control thrust chambers are therefore often designed as an integral part of the thrust chamber-injector assembly, as shown in Fig. 8-13. Special electrically actuated leakproof, fast-acting valves with response times ranging from 2 to 25 msec for both the opening and closing

operation are used. Valves must operate reliably with predictable characteristics for perhaps 40,000 to 80,000 starts. This in turn often requires endurance proof tests of 400,000 to 800,000 cycles.

Throttling or reducing the thrust is equivalent to reducing the total impulse over the operating duration. This can be achieved by varying (1) the time between pulses (less total cumulative impulse per unit time) or (2) by limiting the total number of pulses.

Liquid storable bipropellants such as N_2O_4 -monomethylhydrazine are used when high performance is mandatory. Some have used ablative materials for thrust chamber construction, as in the Gemini command module. The Space Shuttle small thrusters use radiation cooling with refractory metals, as shown in Fig. 8-13. A radiation-cooled thruster is shown later in Fig. 8-16. Carbon materials made of woven strong carbon fibers in a matrix of carbon have also been used in radiation-cooled bipropellant thrusters.

Hydrazine monopropellant thrusters are used when system simplicity is important and moderate performance is acceptable. They have a nontoxic, clear, clean exhaust plume. Virtually all hydrazine monopropellant attitude control rockets use finely dispersed iridium or cobalt deposited on porous ceramic (aluminum oxide) substrate pellets 1.5 to 3 mm in diameter as a catalyst. Figure 8-14 shows a typical design of the catalyst pellet bed in an attitude control thruster designed for pulse and steady-state operation meeting a specific duty cycle. Each injection passage is covered with a cylindrical screen section which extends into a part of the catalyst bed and distributes the hydrazine propellant. Figure 8-14 also shows other successful types of hydrazine injector. Several arrangements of catalyst beds are employed; some have spring-loading to keep the pellets firmly packed. Hydrazine monopropellant thrust units range in size from 0.2 to 2500 N of thrust; the scaling procedure is empirical and each size and design requires testing and retesting. The amount of ammonia decomposition, shown in Fig. 7-3, can be controlled by the design of the catalyst bed and its decomposition chamber.

Mechanical, thermal, and chemical problems arise in designing a catalyst bed for igniting hydrazine, the more important of which are catalytic attrition and catalyst poisoning. *Catalytic attrition* or physical loss of catalyst material stems from motion and abrasion of the pellets, with loss of very fine particles. Crushing of pellets can occur because of thermal expansion and momentary overpressure spikes. As explained in Chapter 7, the catalyst activity can also decline because of *poisoning* by trace quantities of contaminants present in commercial hydrazine, such as aniline, MMH, UDMH, sulfur, zinc, sodium, or iron. Some of these contaminants come with the hydrazine and some are added by the materials used in the tanks, and propellant plumbing in the spacecraft. The high-purity grade hydrazine has less than 0.003% aniline and less than 0.005% carbonaceous material; it does not contaminate catalysts. Catalyst degradation, regardless of cause, produces ignition delays, overpressures, and pressure spikes, decreases the specific impulse, and decreases the impulse bit per pulse in attitude control engines.

Figure 17–4 shows a combination of chemical monopropellant and electrical propulsion. Electrical postheating of the reaction gases from catalysis allows an increase of the altitude specific impulse from 240 sec to about 290 or 300 sec. A number of these combination auxiliary thrusters have successfully flown on a variety of satellite applications and are particularly suitable for spacecraft where electrical power is available and extensive short-duration pulsing is needed.

Cold gas thrusters use stored high-pressure inert gas as the propellant; they and their performance were mentioned in Section 7.6 and their propellants and specific impulses are listed in Table 7–3. They are simple, low cost, used with pressurized feed systems, used for pulsing operations, and for low thrust and low total impulse. They can use aluminum or plastics for thrusters, valves, and piping. The early versions of the Pegasus air-launched launch vehicle used them for roll control. The advantages of cold gas systems are: (a) they are very reliable and have been proven in space flights lasting more than 10 years; (b) the system is simple and relatively inexpensive; (c) the ingredients are nontoxic; (d) no deposit or contamination on sensitive spacecraft surfaces, such as mirrors; (e) they are safe; and (f) capable of random pulsing. The disadvantages are: (a) engines are relatively heavy with poor propellant mass fractions (0.02 to 0.19); (b) the specific impulses and vehicle velocity increments are low, when compared to mono- or bipropellant systems; and (c) relatively large volumes.

8.4. MATERIALS AND FABRICATION

The choice of the material for the inner chamber wall in the chamber and the nozzle throat region, which are the critical locations, is influenced by the hot gases resulting from the burning of propellants, the maximum wall temperature, the heat transfer, and the duty cycle. A large variety of material has been used. Table 8–3 lists typical selected materials for several applications, thrust sizes, and propellants. For high-performance, high heat transfer, regeneratively cooled thrust chambers a material with high thermal conductivity and a thin-wall design will reduce the thermal stresses. Copper is an excellent conductor and it will not really oxidize in fuel-rich noncorrosive gas mixtures. It is often used with oxygen and hydrogen below a mixture ratio of 6.0. The inner walls are therefore usually made of a copper alloy (with small additions of zirconium, silver, or silicon), which has a conductivity not quite as good as pure (oxygen-free) copper but has improved high-temperature strength.

Figure 8–15 shows a partial section through five configurations of cooling jackets. All involve curved or doubly curved components and precision fits for good fastening or joining. The top configuration has an intermediate thin corrugated sheet of metal and has been used extensively in Russia and its predecessor the Soviet Union. It is soldered together under external pressure in a furnace. It is used in those locations on a thrust chamber, where the heat transfer is mild or of intermediate intensity. The milled slot design can usually accept the highest heat transfer intensities. One fabrication technique is to machine (usually on

a milling machine) nearly rectangular grooves or cooling channels of varying width and depth into the inner surface of a relatively thick contoured inner wall using a high conductivity material such as a copper alloy. The grooves are then filled with wax and by an electrolytic plating technique build an outer wall of a suitable metal (such as nickel) so as to enclose the coolant channels. The wax is then melted out. The third design shows a tubular construction; it has been used extensively in the United States for larger thrust chambers with intermediate to high heat transfer. Figure 8–9 shows that individual tubes are shaped to the contour of the thrust chamber including its nozzle; the round tube shape is altered into nearly rectangular cross sections. The formed and brazed tubes are brazed or soldered together in a furnace and the outer structural shell or outer bands are also brazed to the assembly. The corrugated outer wall concept is perhaps the simplest and often the lightest cooling jacket configuration. It has been used in locations where heat transfer is modest. The bottom shell represents a welded construction, made of stainless steel. It has a higher allowable maximum wall temperature than a brazed construction. It has been used in nozzles designed and built in Europe.

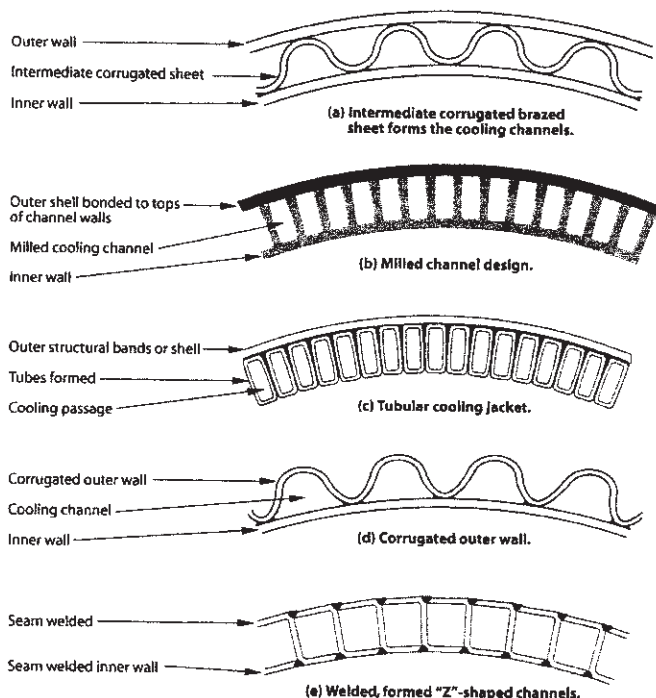


FIGURE 8–15. Simplified sketches of sections through a portion of the cooling jacket of several different cooling schemes in regeneratively cooled thrust chambers. (Used with permission from Ref. 8–1.)

TABLE 8–3. Typical Materials Used in Several Common Liquid Propellant Thrust Chambers

| Application | Propellant | Components | Cooling Method | Typical Materials |
|--|--|-------------|----------------|---|
| Bipropellant TC, cooled, high pressure (booster or upper stage) | Oxygen— hydrogen | C, N, E | F | Copper alloy |
| | | I | F | Transpiration cooled porous stainless steel face. Structure is stainless steel |
| | | Alternate E | R | Carbon fiber in a carbon matrix, or niobium |
| Bipropellant TC cooled, high pressure (booster or upper stage) | Oxygen— hydrocarbon or storable propellant ^a | Alternate E | T | Steel shell with ablative inner liner |
| | | C, N, E, I | F | Stainless steel with tubes or milled slots |
| | | Alternate E | R | Carbon fiber in a carbon matrix, or niobium |
| Experimental TC (very limited duration—only a few seconds) | All types | Alternate E | T | Steel shell with ablative inner liner |
| | | C, N, E | U | Low carbon steel |
| Small bipropellant TC | All types | C, N, E | R | Carbon fiber in carbon matrix, rhodium, niobium |
| | | | T | Steel shell with ablative inner liner |
| | | I | F | Stainless steels, titanium |
| Small monopropellant TC | Hydrazine | C, N, E, | R | Inconel, alloy steels |
| Cold gas TC | Compressed air, nitrogen | I | F | Stainless steel |
| | | C, N, E, I | U | Aluminum, steel, or plastic |

^aHNO₃ or N₂O₄ oxidizer with N₂H₄, MMH, or UDMH as fuels (see Chapter 7). TC = thrust chamber, C = chamber wall, N = nozzle converging section walls, diverging section walls, and throat region walls, E = walls at exit region of diverging section of nozzle, I = injector face, F = fuel cooled (regenerative), R = radiation cooled, U = uncooled, T = transient heat transfer or heat sink method (ablative material).

The depth and width of the cooling channels vary with the chamber profile location and the local thrust chamber diameter. At the nozzle throat region the heat transfer is the highest; therefore it is the location of the highest cooling velocity; therefore the total cooling passage area at the throat region is the smallest. Often two or sometimes three different cooling jacket constructions are designed into the same thrust chamber. Typically, the milled groove configuration is used for the nozzle throat region and other configurations are then used for the chamber and the nozzle exit regions.

The failure modes often are bulging on the hot wall on the gas side and the opening up of cracks. During hot firing, the strain at the hot surface can exceed the local yield point, thus giving it a local permanent compressive deformation. With the cooldown after operation and with each successive firing, some additional yielding and further plastic deformation will occur until cracks form. With successive firings the cracks can become deep enough for a leak of cooling propellant into the chamber or nozzle and the thrust chamber will then usually fail. The *useful life* of a metal thrust chamber is the maximum number of firings (and sometimes also the cumulative firing duration) without such a failure. The prediction of wall failures is not simple and Refs. 8–5 and 8–6 explain this in more detail. Useful life can also be limited by the storage life of soft components (O-rings, gaskets, valve stem lubricant) and, for small thrusters with many pulses, also the fatigue of valve seats. Therefore, there is a maximum limit on the number of firings that such a thrust chamber can withstand safely, and this limits its *useful life*.

For *radiation cooling*, several different carbon materials have worked in a reducing, fuel-rich rocket combustion atmosphere. At leaner gas mixtures the carbon can oxidize at the elevated temperatures when they glow red or white. They can be used at wall temperatures up to perhaps 3300 K or 6000°R. Carbon materials and ablative materials are used extensively in solid propellant rocket motors and are discussed further in Chapter 15.

For some small radiation-cooled bipropellant thrusters with storable propellants, such as those of the reaction control thrusters on the Space Shuttle orbiter, the hot walls are made of niobium coated with disilicide (up to 1120 K or 2050°R). To prevent damage, a fuel-rich mixture or film cooling is often used. For small thrusters rhenium walls protected by iridium coatings (oxidation resistant) have come into use more recently and have been used up to about 2300 K or 4100°R (see Refs. 8–1 and 8–9). Other high-temperature materials, such as tungsten, molybdenum, alumina, or tantalum, have been tried but have had problems in manufacture, cracking, hydrogen embrittlement, or excessive oxidation.

A small radiation-cooled bipropellant thruster is shown in Fig. 8–16. It uses three different nozzle and chamber materials. This thruster's injector has extra fuel injection holes (not shown in Fig. 8–16) to provide film cooling to keep wall temperatures below their failure limits. High temperature copper-nickel alloys or stainless steels are used for the radiation cooled nozzle-and chamber walls of thrusters operating with hydrazine monopropellant. See Fig. 8–14.

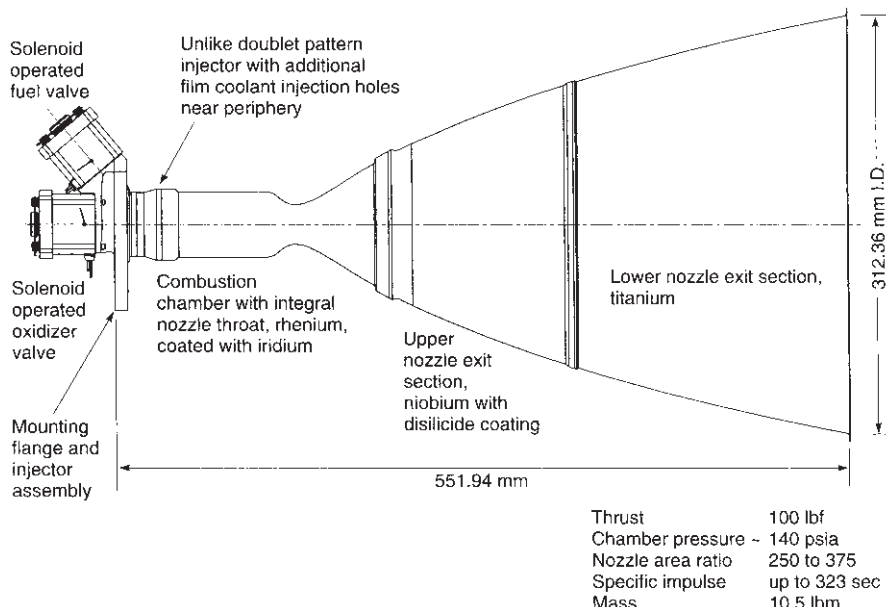
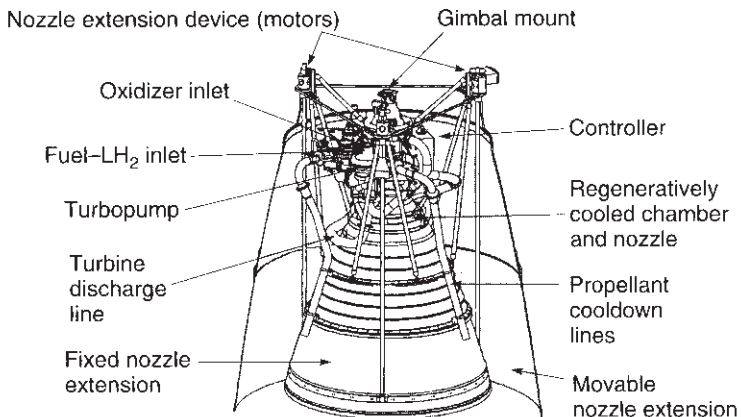


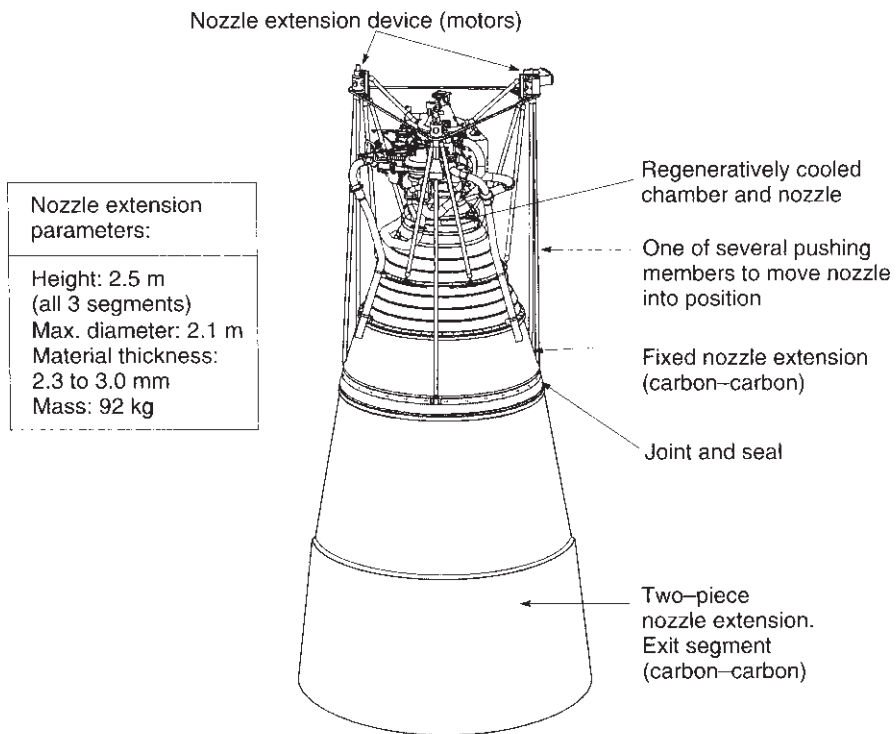
FIGURE 8–16. Radiation-cooled reaction control thruster R-4D-15 uses nitrogen tetroxide and monomethylhydrazine propellants. The large nozzle area ratio allows good vacuum performance. It has three different nozzle materials, each with a lower allowable temperature (Re 4000°F; Nb 3500°F; Ti 1300°F). Courtesy of Aerojet Propulsion Company.

Until recently it has not been possible to make large pieces of carbon–carbon material. This was one of the reasons why large nozzle sections and integral nozzle exit cone pieces in solid motors were made from carbon phenolic cloth lay-ups. Progress in manufacturing equipment and technology has now made it possible to build and fly larger pieces made of carbon fiber in a carbon matrix. A three-piece extendible carbon nozzle exit cone of 2.3 m (84 in.) diameter and 2.3 to 3 mm thickness has flown on an upper-stage engine. This thrust chamber with its movable nozzle extension is shown in Fig. 8–17, its parameters are listed in Table 8–1, its testing is reported in Ref. 8–4, and it has flown successfully many times.

The material properties have to be evaluated under all likely operating conditions, loads, start conditions, pressure variations, and the like before a material can be selected for a specific thrust chamber application. This evaluation includes physical properties, such as tensile and compressive strengths, yield strength, fracture toughness, modulus of elasticity (for determining deflections under load), thermal conductivity (a high value is best for steady-state heat transfer), coefficient of thermal expansion (some large thrust chambers grow by 3 to 10 mm when they become hot, and that can cause problems with their piping connections or structural supports), specific heat (capacity to absorb thermal energy), reflectivity (for radiation), or density (ablatives require more volume than steel).



(a) Half section of nozzle extension in stowed position



(b) Nozzle extension in deployed position

FIGURE 8-17. The RL-10B-2 rocket engine has an extendible nozzle cone or skirt, which is placed around the engine during the ascent of the Delta III and IV launch vehicles. This extension is lowered into position by electromechanical devices after the launch vehicle has been separated from the upper stage at high altitude and before firing. (Courtesy of Pratt & Whitney Rocketdyne, of United Technologies, Inc.)

These properties change with temperature (they are different when they are hot) and sometimes they change with little changes in materials composition. The temperature where a material loses perhaps 60 to 75% of its room temperature strength is often selected as the maximum allowable wall temperature, well below its melting point. Since a listing of all the key properties of a single material requires many pages, it is not possible to list them here, but they are usually available from manufacturers and other sources. Other important properties are erosion resistance, little or no chemical reactions with the propellants or the hot gases, reproducible decomposition or vaporization of ablative materials, ease and low cost of fabrication (welding, cutting, forming, etc.), the consistency of the composition (impurities) of different batches of each material (metals, organics, seals, insulators, lubricants, cleaning fluids), and ready availability and low cost of each material.

8.5. HEAT TRANSFER ANALYSIS

In actual rocket development not only is the heat transfer analyzed but the rocket units are almost always tested to assure that heat is transferred satisfactorily under all operating and emergency conditions. Heat transfer calculations are useful to guide the design, testing, and failure investigations. Those rocket combustion devices that are regeneratively cooled or radiation cooled can reach thermal equilibrium and the steady-state heat transfer relationships will apply. Transient heat transfer conditions apply not only during thrust buildup (starting) and shutdown of all rocket propulsion systems, but also with cooling techniques that never reach equilibrium, such as with ablative materials.

Sophisticated *finite element analysis* (FEA) programs of heat transfer have been available for at least 20 years, and several different FEA computer programs have been used for the analysis of thrust chamber steady-state and transient heat transfer, with different chamber geometries or different materials and with temperature-variant properties. A detailed description of this powerful analysis is beyond the scope of this book, but can be found in Refs. 8–10, 8–11, and 8–12. Major rocket propulsion organizations have developed their own versions of suitable computer programs for solving their heat transfer problems. This section gives the basic relationships that are the foundation for FEA programs. They are intended to give some understanding of the phenomena and underlying principles.

General Steady-State Heat Transfer Relations

For heat transfer *conduction* the following general relation applies:

$$\frac{Q}{A} = -\kappa \frac{dT}{dt_w} = -\kappa \frac{\Delta T}{t_w} \quad (8-13)$$

where Q is the heat transferred across a surface area A , dT/dL the temperature gradient with respect to thickness t_w at the surface A , and κ the thermal conductivity expressed as the amount of heat transferred per unit time through a unit area of surface for 1° temperature difference over a unit wall thickness. The negative sign indicates that temperature decreases as thickness increases.

The steady-state heat transfer through the chamber wall of a liquid-cooled rocket chamber can be treated as a series-type, steady-state heat transfer problem with a large temperature gradient across the gaseous film on the inside of the chamber wall, a temperature drop across the wall, and, in cases of cooled chambers, a third temperature drop across the film of the moving cooling fluid. It is a combination of convection at the boundaries of the flowing fluids and conduction through the chamber walls. It is shown schematically in Fig. 8–18.

The general steady-state heat transfer equations for regeneratively cooled thrust chambers can be expressed as follows:

$$q = h(T_g - T_l) = Q/A \quad (8-14)$$

$$= \frac{T_g - T_l}{1/h_g + t_w/\kappa + 1/h_l} \quad (8-15)$$

$$= h_g(T_g - T_{wg}) \quad (8-16)$$

$$= (\kappa/t_w)(T_{wg} - T_{wl}) \quad (8-17)$$

$$= h_l(T_{wl} - T_l) \quad (8-18)$$

where q is heat transferred per unit area per unit time, T_g the absolute chamber gas temperature, T_l the absolute coolant liquid temperature, T_{wl} the absolute wall temperature on the liquid side of the wall, T_{wg} the absolute wall temperature on

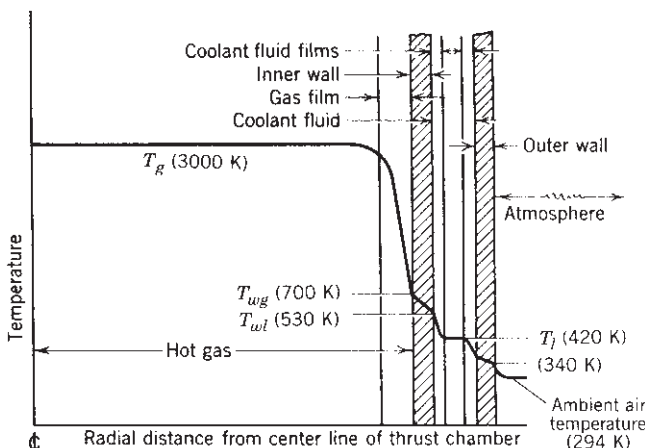


FIGURE 8–18. Temperature gradients in cooled rocket thrust chamber. The listed temperatures are typical.

the gas side of the wall, h the overall film coefficient, h_g the gas film coefficient, h_l the coolant liquid film coefficient, t_w the thickness of the chamber wall, and κ the conductivity of the wall material. The strength and thermal properties of materials are functions of temperature. Any consistent set of units can be used in these equations. These simple relations assume that the heat flow is radial. The simple quasi-one-dimensional theory also often assumes that the thermal conductivity and the film coefficients are at average values and not functions of temperature or pressure. A two- or three-dimensional finite element model would also need to be used to analyze the heat transfer in the axial directions, which usually occurs in the nozzle throat wall regions; some of the heat from the hot nozzle throat is transferred to wall regions upstream and downstream of the throat.

Because the film coefficients, the gas and liquid coolant temperatures, the wall thickness, and the surface areas usually vary with the axial distance L within a combustion chamber (assuming axial heat transfer symmetry), the *total heat transfer per unit time* Q can be found by integrating the local heat transfer over the entire internal surface area of the chamber and the nozzle:

$$Q = \int q \, dA = \pi \int Dq \, dL \quad (8-19)$$

Because both q and D are complicated functions of the thrust chamber length L , the equation usually has to be solved by dividing the rocket chamber into finite lengths. Assuming that q is given by Eqs. 8–13 to 8–19 and remains constant over the length of each element gives an approximate solution.

The important quantities for controlling the heat transfer across a rocket chamber wall are the fluid film boundaries established by the combustion products on one side of the wall and the coolant flow on the other. The gas film coefficient largely determines the numerical value of the heat transfer rate, and the liquid film largely determines the value of the wall temperatures. The determination of the film coefficients in Eqs. 8–16 and 8–18 is difficult because of the complex geometries, the nonuniform velocity profile, the surface roughness, the boundary layer behavior, and the combustion oscillations.

Conventional heat transfer theory is usually given in terms of several dimensionless parameters (Ref. 8–10, 8–11, and 8–12):

$$\frac{h_g D}{\kappa} = 0.026 \left(\frac{D v \rho}{\mu} \right)^{0.8} \left(\frac{\mu c_p}{\kappa} \right)^{0.4} \quad (8-20)$$

where h_g is the film coefficient, D the diameter of the chamber of the nozzle, v the calculated average local gas velocity, κ the conductivity of the gas, μ the absolute gas viscosity, c_p the specific heat of the gas at constant pressure, and ρ the gas density.

In Eq. 8–20 the quantity $h_g D / \kappa$ is known as the Nusselt number, the quantity $D v \rho / \mu$ as the Reynolds number, and the quantity $c_p \mu / \kappa$ as the Prandtl number

Pr. The gas film coefficient h_g can be determined from Eq. 8–21:

$$h_g = 0.026 \frac{(\rho v)^{0.8}}{D^{0.2}} \text{Pr}^{0.4} \kappa / \mu^{0.8} \quad (8-21)$$

where ρv is the local mass velocity, and the constant 0.026 is dimensionless. The boundary layer temperature gradient has effects on the various gas properties in rocket combustion. Conventional theoretical approaches, such as for Eq. 8–20 or 8–21, are usually for heated circular tubes, relatively long tubes, steady-state flow, and they reach an equilibrium velocity profile. Heat flows into the tube from all sides (360°). However, in thrust chambers the heat flow to the coolant passage is only on one side of the cooling passage and the combustion phenomena are propellant specific. The chamber length is relatively short, and an equilibrium flow profile does not exist. The actual flow in the combustion chamber is highly turbulent. There are liquid droplets, which evaporate, and there is no equilibrium. For these reasons Eqs. 8–20 and 8–21 are approximations only.

Equations where the coefficients have been validated by actual experimental data are more reliable and they are used in design. Bartz (Ref. 8–13) has surveyed the agreement between theory and experiment and developed semiempirical correction factors:

$$h_g = \frac{0.026}{D^{0.2}} \left(\frac{c_p \mu^{0.2}}{\text{Pr}^{0.6}} \right) (\rho v)^{0.8} \left(\frac{\rho_{am}}{\rho'} \right) \left(\frac{\mu_{am}}{\mu_0} \right)^{0.2} \quad (8-22)$$

The subscript 0 refers to properties evaluated at the stagnation or combustion temperature; the subscript am refers to properties at the arithmetic mean temperature of the local free-stream static temperature and the wall temperatures; and ρ' is the free-stream value of the local gas density. Again, the empirical constant 0.026 is dimensionless when compatible dimensions are used for the other terms. The gas velocity v is the local free-stream velocity corresponding to the density ρ' . Since density raised to the 0.8 power is roughly proportional to the pressure and the gas film coefficient is roughly proportional to the heat flux, it follows that the heat transfer rate increases approximately linearly with the chamber pressure. These semiempirical heat transfer equations have been modified and validated for common propellants, limited chamber pressure ranges, and specific injectors (see Ref. 8–13) and are often proprietary to specific design organizations.

The temperature drop across the inner wall and the maximum temperature are reduced if the wall is thin and is made of material of high thermal conductivity. The wall thickness is determined from strength considerations and thermal stresses, and some designs have as little as 0.025 in. thickness. The effect of changing the film coefficients is shown in Example 8–1.

Surface roughness can have a large effect on the film coefficients and thus on the heat flux. Measurements have shown that the heat flow can be increased by a factor of up to 2 by surface roughness and to higher factors when designing turbulence-creating obstructions in the cooling channels. Major surface roughness

on the gas side will cause the gas locally to come close to stagnation temperature. However, surface roughness on the liquid coolant side of the wall will enhance turbulence and the absorption of heat by the coolant and reduce wall temperatures.

Example 8–1. The effects of varying the film coefficients on the heat transfer and the wall temperatures are to be explored. The following data are given:

| | |
|---------------------------------|------------------------------|
| Wall thickness | 0.445 mm |
| Wall material | Low-carbon steel |
| Average conductivity | 43.24 W/m ² · K/m |
| Average gas temperature | 3033 K or 2760°C |
| Average liquid bulk temperature | 311.1 K or 37.8°C |
| Gas-film coefficient | 147 W/m ² ·°C |
| Liquid-film coefficient | 205,900 W/m ² ·°C |

Vary h_g (at constant h_l), then vary h_l (at constant h_g), and then determine the changes in heat transfer rate and wall temperatures on the liquid and the gas side of the wall.

SOLUTION. Use Eqs. 8–13 to 8–18 and solve for q , T_{wg} , and T_{wl} . The answers shown in Table 8–4 indicate that variations in the gas-film coefficient have a profound influence on the heat transfer rate but relatively little effect on the wall temperature. The exact opposite is true for variations in the liquid-film coefficient; here, changes in h_l produce little change in q but a fairly substantial change in the wall temperature.

TABLE 8–4. Change in Film Coefficient for Example 8–1

| Change in Film Coefficient (%) | Change in Heat Transfer | | | Wall Temperature (K) | |
|-----------------------------------|----------------------------|-------------|-----|----------------------|-----------------------|
| | Gas Film | Liquid Film | (%) | Gas Side, T_{wg} | Liquid Side, T_{wl} |
| 50 | 100 | 50 | 50 | 324.4 | 321.1 |
| 100 | 100 | 100 | 100 | 337.2 | 330.5 |
| 200 | 100 | 198 | 198 | 362.8 | 349.4 |
| 400 | 100 | 389 | 389 | 415.6 | 386.1 |
| 100 | 50 | 99 | 99 | 356.1 | 349.4 |
| 100 | 25 | 98 | 98 | 393.3 | 386.7 |
| 100 | 12.5 | 95 | 95 | 460.0 | 397.8 |
| 100 | 6.25 | 91 | 91 | 596.7 | 590.5 |

Figure 8–19 shows heat flow directions, temperature distribution, and the locations for the maximum wall temperatures for a milled cooling jacket design. This design is represented by the third sketch of Fig. 8–15. The inner wall should be thin, so that the temperature difference across this wall is low and therefore the thermal stresses are also low.

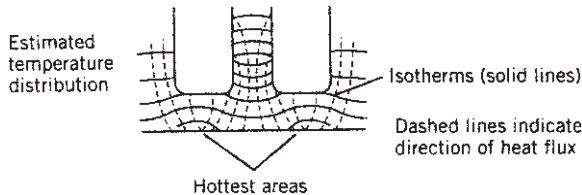


FIGURE 8–19. Results of a two-dimensional analysis of the heat transfer in two cooling channels of a milled slot cooling jacket. The outer wall and the upper parts of the channels are not shown.

Transient Heat Transfer Analysis

An uncooled (high melting point) metal thrust chamber is the simplest type to analyze because there is no chemical change. Thermal equilibrium is not reached. The uncooled walls act essentially as a heat sponge and absorb heat from the hot gases. With the aid of experimental data to determine some typical coefficients, it is possible in some cases to predict the transient heating of uncooled walls.

Heat is transferred from the hot gases to the wall, and during operation a changing temperature gradient exists across the wall. The heat transferred from the hot wall to the surrounding atmosphere, and by conduction of metal parts to the structure, is negligibly small during this transient heating. Each local point within the wall has its temperature raised as the burning process is extended in time. After the completion of the rocket's operation, the wall temperatures tend to equalize. A typical temperature-time-location history is given in Fig. 8–20. Here the horizontal line at $T = 21^\circ\text{C}$ denotes the initial equilibrium condition of the wall before the rocket operates; the various curves show the temperature profile across the wall at successive time intervals after initiation of combustion. The line at $T = 357^\circ\text{C}$ shows an equilibrium temperature of the wall a finite time after cutoff.

The heat transferred across the hot surface of the wall (and distributed within the wall by conduction) must be less than the heat-absorbing capacity of the wall material below the critical temperature. If heat transfer to the outside atmosphere and axially within the metal wall is neglected, this can be expressed in a simplified form:

$$Q \Delta t = -\kappa A (dT/dL) \Delta t = m \bar{c} \Delta T \quad (8-23)$$

where Q is the heat per second transferred across an inner wall surface area A . Equation 8–14 shows that Q/A depends on the hot gas temperature, the wall temperature, and the gas film coefficient. The heat conductivity κ depends on the material and its temperature; ΔT denotes the average wall temperature increment; dT/dL the temperature gradient of the heat flow near the hot wall surface in degrees per unit thickness; m the mass of a unit area of wall; \bar{c} the average specific heat of the wall material; and Δt is the time increment. The chamber and nozzle walls can be divided into cylindrical or conical segments, and each wall

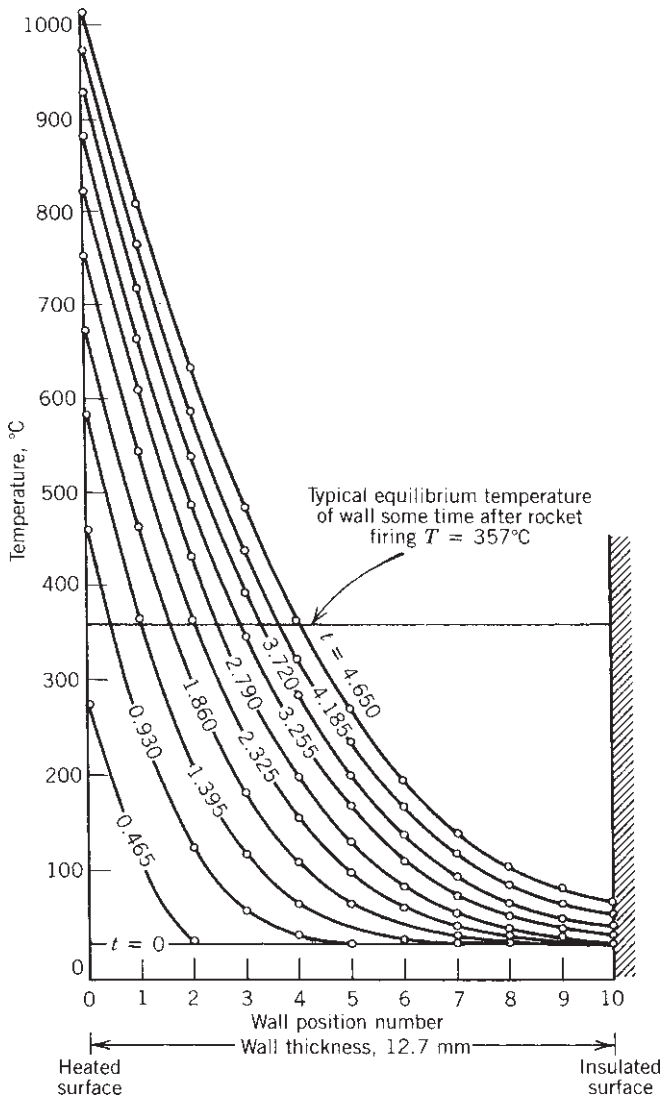


FIGURE 8–20. Typical temperature distributions through a wall of an uncooled relatively thick metal thrust chamber as a function of heating time.

segment in turn is divided into an arbitrary number of axisymmetric concentric layers, each of a finite thickness. At any given time the heat conducted from any one layer of the wall exceeds the heat conducted into the next outer layer by the amount of heat absorbed in raising the temperature of the particular layer. This iterative approach lends itself readily to two- or three-dimensional computer analysis, resulting in data similar to Fig. 8–20. It is usually sufficient to determine the heat transfer at the critical locations, such as in the nozzle throat region.

A more complex three-dimensional analysis can also be undertaken; here the wall geometry is often more complex than merely cylindrical, heat is conducted also in directions other than normal to the axis, temperature variable properties are used, boundary layer characteristics vary with time and location, and there may be more than one material layer in the wall.

A number of mathematical simulations of transient heat transfer in *ablative materials* have been derived, many with limited success. This approach should include simulation for the pyrolysis, chemical decomposition, char depth, and out-gassing effects on film coefficient, and it requires good material property data. Most simulations require some experimental data.

Steady-State Transfer to Liquids in Cooling Jacket

The term *regenerative cooling* is used for rockets where one of the propellants is circulated through cooling passages around the thrust chamber prior to the injection and burning of this propellant in the chamber. It is really forced convection heat transfer. The term *regenerative* is perhaps not altogether appropriate here, and it bears little relation to the meaning given to it in steam turbine practice. It is intended to convey the fact that the heat absorbed by the coolant propellant is not wasted but augments its initial temperature and raises its energy level before it passes through the injector. This increase in the internal energy of the liquid propellant can be calculated as a correction to the enthalpy of the propellant (see Chapter 5). However, the overall effect on rocket performance is usually very slight. With some propellants the specific impulse can be 1% larger if the propellants are preheated through a temperature differential of 100 to 200°C. In hydrogen-cooled thrust chambers and in small combustion chambers, where the wall-surface-to-chamber volume ratio is relatively large, the temperature rise in the regenerative coolant will be high, and the resulting increase in specific impulse is sometimes more than 1%.

The behavior of the *liquid film* is critical for controlling the wall temperatures in forced convection cooling of rocket devices at high heat fluxes (see Table 8–4 and Refs. 8–10, 8–14, and 8–15). At least four different types of film appear to exit, as can be interpreted from Fig. 8–21. Here the heat transfer rate per unit of wall surface q is shown as a function of the difference between the wall temperature on the liquid side T_{wl} and the bulk temperature of the liquid T_l .

1. The normal *forced convection* region at low heat flux appears to have a liquid boundary layer of predictable characteristics. It is indicated by region A–B in Fig. 8–21. Here the wall temperature is usually below the boiling point of the liquid at the cooling jacket pressure. In steady-state heat transfer analysis the liquid-film coefficient can be approximated by the usual equation (see Refs. 8–10, 8–11, and 8–12):

$$h_l = 0.023\bar{c}\frac{\dot{m}}{A} \left(\frac{Dv\rho}{\mu} \right)^{-0.2} \left(\frac{\mu\bar{c}}{\kappa} \right)^{-2/3} \quad (8-24)$$

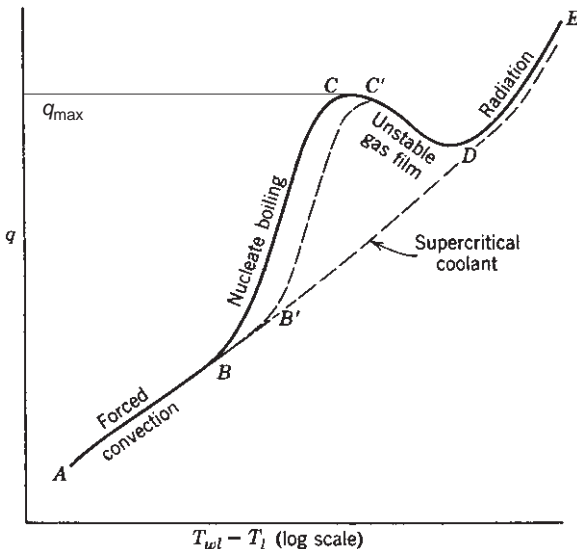


FIGURE 8–21. Regimes in transferring heat from a hot wall to a flowing liquid.

where \dot{m} is the liquid fluid mass flow rate, \bar{c} its average specific heat, A the cross-sectional cooling jacket flow area, D the equivalent diameter of the coolant passage cross section,* v the fluid velocity, ρ the coolant density, μ its absolute viscosity, and κ its conductivity. Many liquid-cooled rocket devices operate in this regime of heat transfer. Values of the physical properties of several propellants are given in Tables 8–5 and 7–1.

- When the wall temperature T_{wl} exceeds the boiling point of the liquid by perhaps 10 to 50 K, small vapor bubbles form at the hot wall surface. These small, nuclei-like bubbles cause local turbulence, break away from the wall, and collapse in the cooler liquid. This phenomenon is known as *nucleate boiling*. The turbulence induced by the bubbles changes the character of the liquid film and, augmented by the vaporization of some of the propellant, the heat transfer rate is increased without a proportional increase in the temperature drop across the film, as can be seen by the steep slope $B-C$ of the curve in Fig. 8–21. If the pressure of the fluid is raised, then the boiling point is also raised and the nucleate boiling region shifts to the right, to $B'-C'$. This boiling permits a substantial increase in the heat transfer beyond that predicted by Eq. 8–24. This phenomenon often occurs locally in the nozzle throat area, where the heat flux is high. The maximum feasible heat transfer rate (point C) is indicated as q_{\max} in Table 8–5 and

*The grooves, tubes, or coolant passages in liquid propellant rocket chambers are often of complex cross section. The *equivalent diameter*, needed for fluid-film heat transfer calculations, is usually defined as four times the hydraulic radius of the coolant passage; the hydraulic radius is the cross-sectional flow area divided by the wetted perimeter.

appears to be a function of the cooling-fluid properties, the presence of dissolved gases, the pressure, and the flow velocity. In Table 8-5 it can be seen that hydrazine is a good heat absorber, but kerosene is poor (low q_{\max} and low critical pressure).

3. As the heat transfer is increased further, the rate of bubble formation and the bubble size become so great that the bubbles are unable to escape from the wall rapidly enough. This reaction (shown as $C-D$ in Fig. 8-21) is characterized by an unstable *gas film* and is difficult to obtain reproducibly in tests. When a film consisting largely or completely of gas forms along the hot wall surface, then this film acts as an insulation layer, causing a decrease in heat flux and, usually, a rapid increase in wall temperature, often resulting in a burnout or melting of the wall material. The cooling flow system has to be designed to avoid this unstable gas film regime
4. As the temperature difference across the film is further increased, the wall temperatures reach values in which heat transfer by *radiation* becomes important. Region $D-E$ is not of interest to cooling jacket designers.

Cooling can also be accomplished by a fluid above its critical point with coolants such as hydrogen. In this case there is no nucleate boiling and the heat transfer increases with the temperature difference, as shown by the supercritical (dashed) line in Fig. 8-21. Liquid hydrogen is an excellent coolant, has a high specific heat, and leaves no residues.

Chemical changes in the liquid can seriously influence the heat transfer from hot walls to liquids. Cracking of hydrocarbon fuel, with an attendant formation of insoluble gas, tends to reduce the maximum heat flux and thus promote failure more readily. Hydrocarbon fuel coolants (methane, jet fuel) can break down and form solid, sticky carbon deposits inside the cooling channel, impeding the heat transfer. Other factors influencing steady-state coolant heat transfer are gas radiation to the wall, bends in the coolant passage, improper welds or manufacture, and flow oscillations caused by turbulence or combustion unsteadiness. Some propellants, such as hydrazine, can decompose spontaneously and explode in the cooling passage if they become too hot.

To achieve a good *heat-absorbing capacity of the coolant*, the pressure and the coolant flow velocity are selected so that boiling is permitted locally, but the bulk of the coolant does not reach this boiling condition. The total heat rejected by the hot gases to the surface of the hot walls, as given by Eq. 8-14 must be less than that permitted by the temperature rise in the coolant, namely

$$qA = Q = \dot{m}\bar{c}(T_1 - T_2) \quad (8-25)$$

where \dot{m} is the coolant mass flow rate, \bar{c} the average specific heat of the liquid, T_1 the initial temperature of the coolant as it enters the cooling jacket, and T_2 its final temperature; Q is the rate of heat absorption per unit time; q is this same rate per unit heat transfer area A ; T_2 should be below the boiling point prevailing at the cooling jacket pressure.

TABLE 8-5. Heat Transfer Characteristics of Several Liquid Propellants

| Liquid Coolant | Boiling Characteristics | | | Critical Pressure (MPa) | Temp. (K) | Nucleate Boiling Characteristics | | |
|----------------------------------|-------------------------|-------------------|--------------------|-------------------------|-----------|----------------------------------|-----------|------------------|
| | Pressure (MPa) | Boiling Temp. (K) | Critical Temp. (K) | | | Pressure (MPa) | Temp. (K) | Velocity (m/sec) |
| Hydrazine | 0.101 | 387 | 652 | 14.7 | 3222.2 | 4.13 | 10 | 22.1 |
| | 0.689 | 455 | | | 405.6 | 4.13 | 20 | 29.4 |
| | 3.45 | 540 | | | | 10 | 10 | 14.2 |
| | 6.89 | 588 | | | 297.2 | 0.689 | 20 | 21.2 |
| Kerosene | 0.101 | 490 | 678 | 2.0 | 297.2 | | 1 | 2.4 |
| | 0.689 | 603 | | | 297.2 | 1.38 | 8.5 | 6.4 |
| | 1.38 | 651 | | | | 1 | 1 | 2.3 |
| | 1.38 | 651 | | | 3222.2 | | 20 | 6.2 |
| Nitrogen tetroxide | 0.101 | 294 | 431 | 10.1 | 288.9 | 4.13 | 20 | 11.4 |
| | 0.689 | 342 | | | 3222.2 | | 9.3 | |
| | 4.13 | 394 | | | 366.7 | | | 6.2 |
| | 0.101 | 336 | 522 | 6.06 | 300 | 2.07 | 10 | 4.9 |
| Unsymmetrical dimethyl hydrazine | 1.01 | 400 | | | | | 20 | 7.2 |
| | 3.45 | 489 | | | 300 | 5.52 | 10 | 4.7 |

Radiation

Radiation heat emission is the electromagnetic radiation emitted by a gas, liquid, or solid body by the virtue of its temperature and at the expense of its internal energy. It covers the wavelength range from 10,000 to 0.0001 μm , which includes the visible range of 0.39 to 0.78 μm . Radiation heat transfer occurs most efficiently in a vacuum because there is no absorption by the intervening fluids.

The heat transmitted by the mechanism of radiation depends primarily on the temperature of the radiating body and its surface condition. The second law of thermodynamics can be used to prove that the radiant energy E is a function of the fourth power of the absolute temperature T :

$$E = f\varepsilon\sigma AT^4 \quad (8-26)$$

The energy E radiated by a body is defined as a function of the emissivity ε , which is a dimensionless factor for surface condition and material properties, the Stefan–Boltzmann constant $\sigma(5.67 \times 10^{-8} \text{ W/m}^2\text{-K}^4)$, the surface area A , the absolute temperature T , and the geometric factor f , which depends on the arrangement of adjacent parts and the shape. At low wall temperatures (below 800 K) radiation accounts for only a negligible portion of the total heat transfer in a rocket device and can usually be neglected.

In rocket propulsion there are these radiation concerns:

1. Emission of hot gases to the internal walls of a combustion chamber, and its nozzle converging section, a solid propellant grain, or a hybrid propellant grain.
2. Emission to the surroundings or to space from the external surfaces of hot hardware (radiation-cooled chambers, nozzles, or electrodes in electric propulsion).
3. Radiation from the hot plume downstream of the nozzle exit. This is described in Chapter 20.

In rocket combustion devices gas temperatures are between 1900 and 3900 K or about 3000 to 6600°F; their radiation contributes between 3 and 40% of the heat transfer to the chamber walls, depending on the reaction gas composition, chamber size, geometry, and temperature. It can be a significant portion of the total heat transfer. In solid propellant motors the radiation heating of the grain surfaces can be critical to the burning rate, as discussed in Chapter 12. The absorption of radiation on the wall follows essentially the same laws as those of emission. Metal surfaces and formed tubes reflect much of the radiant energy, whereas ablative materials and solid propellants seem to absorb most of the incident radiation. A highly reflective surface on the inside wall of a combustor tends to reduce absorption and to minimize the temperature increase of the walls.

The hot reaction gases in rocket combustion chambers are potent radiation sources. Gases with symmetrical molecules, such as hydrogen, oxygen, and

nitrogen, have been found not to show many strong emission bands in those wavelength regions of importance in radiant heat transfer. Also, they do not really absorb much radiation and do not contribute considerable energy to the heat transfer. Heteropolar gases, such as water vapor, carbon monoxide, carbon dioxide, hydrogen chloride, hydrocarbons, ammonia, oxides of nitrogen, and the alcohols, have strong emission bands of known wavelengths. The radiation of energy of these molecules is associated with the quantum changes in their energy levels of rotation and interatomic vibration. In general, the radiation intensity of all gases increases with their volume, partial pressure, and the fourth power of their absolute temperature. For small thrust chambers and low chamber pressures, radiation contributes only a small amount of energy to the overall heat transfer.

If the hot reaction gases contain small solid particles or liquid droplets, then the radiation heat transfer can increase dramatically by a factor of 2 to 10. The particulates greatly increase the radiant energy as explained in Section 20.1. For example, the reaction gas from a gelled liquid propellants contains small solid particles and many solid propellants contain fine aluminum powder. When burned to form aluminum oxide, the heat of combustion and the combustion temperature are increased (raising heat transfer), and the specific impulse is raised somewhat (giving improved performance). The oxide can be in the form of liquid droplets (in the chamber) or solid particles (in the nozzle diverging section), depending on the local gas temperature. Furthermore, the impact of these particulates with the wall will cause an additional increase in heat transfer, particularly to the walls in the nozzle throat and immediately upstream of the nozzle throat region. The particles also cause erosion or abrasion of the walls.

8.6. STARTING AND IGNITION

The starting of a thrust chamber has to be controlled so that a timely and even ignition of propellants is achieved and the flow and thrust are built up smoothly and quickly to their rated value (see Refs. 6–1, 8–16, and 8–17). The *initial propellant flow* is always less than *full flow*, and the *starting mixture ratio* is usually different from the *operating mixture ratio*. A low initial flow prevents strong water hammer, gives a low initial heat release, and for nonhypergolic propellants it prevents an excessive accumulation of unignited liquid propellants in the chamber.

The starting injection velocity is low, the initial vaporization, atomization, and mixing of propellants in a cold combustion chamber is often incomplete, and there are local regions of lean and rich mixtures. With cryogenic propellants the initial chamber temperature can be below ambient. The optimum starting mixture is therefore only an average of a range of mixture ratios, all of which should be readily ignited. Mixture ratios near the stoichiometric mixture ratio have a high heat release per unit of propellant mass and therefore permit bringing the chamber and the gases up to equilibrium faster than would be possible with other mixtures. The operating mixture ratio is usually fuel rich and is usually selected

for optimum specific impulse. One method of analytical modeling of the ignition of cryogenic propellants is given in Ref. 8–16.

The *time delay for starting* a thrust chamber ideally consists of the following time periods:

1. Time needed to fully open the propellant valves (typically 0.002 to more than 1.00 sec, depending on valve type and its size and upstream pressure).
2. Time needed to fill the liquid passage volume between the valve seat and the injector face (piping, internal injector feed holes, and cavities).
3. Time for forming discrete streams or sprays of liquid propellant (sometimes gaseous propellant, if cryogenic liquid is preheated by heat from cooling jacket) and for initial atomization into small droplets and for mixing these droplets.
4. For today's hypergolic propellant combinations at ambient initial temperatures, the combustion starts within a few milliseconds after a fuel droplet or fuel vapor comes into contact with an oxidizer droplet or oxidizer vapor. This delay can be longer at low ambient temperatures and at off-mixture ratios.
5. For nonhypergolic propellant combinations an igniter system has to provide sufficient heat to bring a flow of mixed propellant to its ignition temperature, before combustion can safely start. The igniter is usually started before any propellant is admitted to the chamber and usually before the propellant valves are opened. The time for the igniter to operate before any propellant comes in contact with the igniter flame can be one or more seconds in larger thrust chambers. If the igniter fails to operate and if this is sensed, then the engine controls can block the opening of the propellant valves.
6. Time needed for droplets to vaporize and ignite (laboratory tests show this to be short, 0.02 to 0.05 sec, but this depends on the propellants and the available heat).
7. Once ignition is achieved at a particular location in the chamber, it takes time to spread the flame or to heat all the mixed propellant that is entering into the chamber, vaporizing it, and raising it to ignition temperature.
8. Time needed to raise the chamber pressure and temperature to the point where combustion will be self-sustaining. Then it is raised to its full pressure.

There are overlaps in these delays and several of them can occur simultaneously. The delays are longer with large injectors or large-diameter chambers. Small thrusters can usually be started very quickly, in a few milliseconds, while larger units require 1 sec or more, sometimes as much as 5 sec.

In starting a thrust chamber, one propellant always reaches the chamber a short time ahead of the other; it is almost impossible to synchronize exactly the fuel and oxidizer feed systems so that the propellants reach the chamber simultaneously at all injection holes or spray elements. Frequently, a more reliable

ignition is assured when one of the propellants is intentionally made to reach the chamber first. For example, for a fuel-rich starting mixture the fuel is admitted first. Reference 8–17 describes the control of the propellant lead.

Other factors influencing the starting flows, the propellant lead or leg, and some of the delays mentioned above are the liquid pressures supplied to the injector (e.g., regulated pressure), the temperature of the propellant (some can be close to their vapor point), and the amount of insoluble gas (air bubbles) mixed with the initial quantity of propellants.

The propellant valves (and the flow passages between the valves and the injector face) are often so designed and controlled that they operate in a definite sequence, thereby assuring an intentional lead of one of the propellants and a controlled buildup of flow and mixture ratio. Often the valves are only partially opened because it is easier to ignite a small flow and it avoids an accumulation of hazardous unburned propellant mixture in the chamber. Once combustion is established, the valves are fully opened and full flow may reach the thrust chamber assembly. The initial reduced flow burning period is called the *preliminary stage*. Section 11.4 describes the starting controls.

Full flow in the larger thrust chambers is not initiated with non-self-igniting propellants until the controller received a signal of successful ignition. The verification of ignition or initial burning is often built into engine controls using visual detection (photocell), heat detection (pyrometer), a fusible wire link, or sensing of a pressure rise. If the starting controls are not designed properly, unburnt propellant may accumulate in the chamber; upon ignition it may then explode, causing sometimes severe damage to the rocket engine. Starting controls and engine calibrations are discussed in Sections 11.4 and 11.5.

Nonspontaneously ignitable propellants need to be activated by absorbing energy prior to combustion initiation. This energy is supplied by the *ignition system*. Once ignition has begun the flame is self-supporting. The igniter has to be located near the injector in such a manner that a satisfactory starting mixture at low initial flow is present at the time of igniter activation, yet it should not hinder or obstruct the steady-state combustion process. At least five different types of successful propellant ignition systems have been used.

Spark plug ignition has been used successfully on liquid oxygen–gasoline and on oxygen–hydrogen thrust chambers, particularly for multiple starts during flight. The spark plug is often built into the injector, as shown in Fig. 9–6.

Ignition by electrically heated wires has been accomplished but at times has proven to be less reliable than spark ignition for liquid propellants.

Pyrotechnic ignition uses a solid propellant squib or grain of a few seconds' burning duration. The solid propellant charge is electrically ignited and burns with a hot flame within the combustion chamber. Almost all solid propellant rockets and many liquid rocket chambers are ignited in this fashion. The igniter container may be designed to fit directly onto the injector or the chamber (see Fig. 8–1), or may be held in the chamber from outside through the nozzle. This ignition method can only be used once; thereafter the charge has to be replaced.

Ignition has been achieved in a *precombustion chamber* also called *premix chamber*; see Fig. 8-3; it is a small chamber built next to the main combustion chamber and connected through an orifice; this is similar to the precombustion chamber used in some internal combustion engines. A small amount of fuel and oxidizer is injected into the precombustion chamber and ignited. The burning mixture enters the main combustion chamber in a torchlike fashion and ignites the larger main propellant flow which is injected directly into the main chamber. This ignition procedure permits repeated starting of thrust chambers and has proved successful with the liquid oxygen–gasoline and oxygen–hydrogen thrust chambers.

Auxiliary fluid ignition is a method whereby some hypergolic liquid or gas, in addition to the regular fuel and oxidizer, is injected into the combustion chamber for a very short period during the starting operation. This fluid is hypergolic, which means it produces spontaneous combustion with either the fuel or the oxidizer. The combustion of nitric acid and some organic fuels can, for instance, be initiated by the introduction of a small quantity of hydrazine or aniline at the beginning of the rocket operation. Liquids that ignite with air (zinc diethyl or aluminum triethyl), when preloaded in the fuel piping, can accomplish a hypergolic ignition. The flow diagram of the RD 170 Russian rocket engine in Fig. 11-2 shows several cylindrical containers prefilled with a hypergolic liquid, one for each of the high-pressure fuel supply lines; this hypergolic liquid is pushed out (by the initial fuel) into the thrust chambers and into the preburners to start their ignitions.

In vehicles with multiple engines or thrust chambers it is required to start two or more together. It is often difficult to get exactly simultaneous starts. Usually the passage or manifold volumes of each thrust chamber and their respective values are designed to be the same. The temperature of the initial propellant fed to each thrust chamber and the lead time of the first quantity of propellant entering into the chambers have to be controlled. This is needed, for example, in two small thrusters when used to apply roll torques to a vehicle. It is also one of the reasons why large space launch vehicles are not released from their launch facility until there is assurance that all the thrust chambers are started and operating.

8.7. RANDOM VARIABLE THRUST

Only some applications require a randomly variable thrust from an engine. Examples are descend on a planet or the moon, combat aircraft or upper stage of an anti-ballistic missile. One of the advantages of liquid propellant rocket engines is that they can be designed to throttle or randomly vary its thrust over a wide range during flight. There have been several approaches to achieve variable or randomly reduced thrust. Essentially all the approaches to vary the thrust involve the thrust chamber and therefore this section has been placed into the thrust chamber chapter. One of the early schemes was to use multiple engines or

multiple thrust chambers on the same engine and then stop the operation of one or more of them. The Reaction Motors 6,000C-4 engine had four thrust chambers and they could be turned on or off individually; this gave a step change in thrust.

Today one can distinguish between two modes of operation and both depend on reducing the propellant flow. The first is *moderate throttling*, typically over a thrust range of two or three, and this can usually be accomplished without significant design changes to the engine. In one application the thrust is throttled during the ascent of a booster vehicle in order to prevent excessive aerodynamic heating. The other mode, often called *deep throttling*, varies the thrust by a factor of between 6 to 30 for specific engines. It applies, for example, to a planetary landing rocket engine with controlled deceleration. To achieve this deep throttling, the engine requires some special features and some of these are mentioned below.

The thrust is almost proportional to the propellant mass flow (Eq. 2-14) and therefore reducing that flow will reduce the thrust. With moderate throttling it can be achieved by simultaneously closing the main fuel valve and the main oxidizer valve (with matching flow characteristics) or alternatively by slowing down the rotary speed of the turbopumps (by reducing the gas flow to the turbine) with a hydraulically matched fuel pump and oxidizer pump. At lower flow the pressure drop across the injector and the injection velocity will be diminished, the atomization and mixing of the propellants will be somewhat less efficient and the combustion will be less complete, and the chamber pressure will be reduced. This usually causes a decrease in the specific impulse at the lower thrust levels of perhaps 1.5 to 9%, depending on the specific engine design. This method of varying the thrust is used in a number of booster engines for space launch vehicles.

With deeper throttling the oxidizer and fuel flows tend to oscillate and will usually no longer be at the original mixture ratio, the propellant injection streams or sprays and their impingement locations will wander, and the flow is likely to become erratic. To prevent these phenomena the engines have some special features as illustrated by the lunar landing rocket engine; this engine was throttled by a factor of up to 10:1, was developed by the predecessor of Northrop Grumman, and flew in the late 1960s and 1970s. Its propellant flow control valves each included a cavitating venturi with a movable tapered pintle that allowed to vary the flow area of the venturi throat of the thrust chamber valve. This assured a predetermined steady reduced flow of propellants at all thrust levels, and maintained the mixture ratio to be the same as the full thrust value. Furthermore the injection of the propellants was through a pintle injector with two annular slots of a moving sleeve and the width of these slots could be reduced by an actuator built into the injector. The lower right sketch of Fig. 8-3 shows this feature. It allows high injection velocities of the liquid propellants, giving good atomization and pretty good combustion and a relatively small loss in performance at low thrust. The highest thrust variation of 357 to 1.0 was with the sustainer engines of the Lance surface-to-surface missile. Its engine, developed by Rocketdyne (today Pratt & Whitney Rocketdyne), first flew in the late 1960s. The specific impulse at low thrust was poor (more than 15% loss).

Another approach to achieve variable thrust is to also vary the nozzle throat area. See Eq. 3–31. This scheme requires a moveable tapered pintle in the main nozzle throat area. The pintle has to be made of heat-tolerant material or has to be regeneratively cooled and the pintle position is usually hydraulically controlled. This will allow to maintain essentially constant chamber pressure at all thrust levels. Several experimental liquid propellant engines and also solid propellant motors with a random variable nozzle throat area have been built and tested. To the best of the author's knowledge, none have flown.

For small reaction control thrusters the average thrust is usually reduced by pulsing. It is accomplished by controlling the number of cycles or pulses (each has one short fixed-duration thrust pulse plus a short fixed-duration zero-thrust pause), by modulating the duration of individual pulses (with short pauses between pulses), or alternatively by lengthening the pause between pulses.

8.8. SAMPLE THRUST CHAMBER DESIGN ANALYSIS

This example shows how a thrust chamber is strongly influenced by the overall vehicle system requirements or the mission parameters and the vehicle design. As outlined in the design section of Chapter 11 and in the discussion of the selection of propulsion systems in Chapter 19, each engine goes through a series of rationalizations and requirements that define its key parameters and its design. In this example we describe one way of how the thrust chamber parameters are derived from the vehicle and engine requirements. The overall system requirements relate to the mission, its purpose, environment, trajectories, reusability, reliability, and to restraints such as allowable engine mass, or maximum dimensional envelope. We are listing some, but not all of the requirements. It shows how theory is blended with experience to arrive at the initial choices of the design parameters. This example could be different, if it would be done by a different design team.

Example 8–2. Here we define the application as a new upper stage of an existing multistage space launch vehicle that will propel a payload into deep space. This means continuous firing (no restart or reuse), operating in the vacuum of space (high nozzle area ratio), modest acceleration (not to exceed $5 g_0$), reasonably low cost, moderately high performance (specific impulse), and a thrust whose magnitude depends on the payloads, the flight path, and acceleration limits. The desired mission velocity increase of the stage is 3400 m/sec. The engine is attached to its own stage, which is subsequently disconnected and dropped from the payload stage. The payload stage (3500 kg) consists of a payload of 1500 kg (for scientific instruments, power supply, or communications and flight control equipment) and its own propulsion systems (including propellant) of 2000 kg (for trajectory changes, station keeping, attitude control, or emergency maneuvers). There are two geometric restraints: The vehicle has an outside diameter of 2.0 m, but when the structure, conduits, certain equipment, thermal insulation, fittings, and assembly are considered, it

really is only about 1.90 m. The restraint on the stage length of 4.50 m maximum will affect the length of the thrust chamber. We can summarize the key requirements:

| | |
|--------------------------------------|--|
| Application | Uppermost stage to an existing multistage launch vehicle |
| Payload | 3500 kg |
| Desired velocity increase Δu | 3400 m/sec in gravity-free vacuum |
| Maximum stage diameter | 1.90 m |
| Maximum stage length | 4.50 m |
| Maximum acceleration | 5 g_0 |

Decisions on Basic Parameters. The following engine design decisions or parameter selection should be made early in the design process:

- Propellant combination
- Chamber pressure
- Nozzle area ratio
- Feed system, using pumps or pressurized tanks
- Thrust level

From a performance point of view, the best *propellant combination* would be liquid oxygen with liquid hydrogen. However, this bipropellant would have a low average specific gravity (0.36). There is not enough volume in this upper stage to allow sufficient propellant mass for attaining the desired vehicle velocity increment Δu . The lower stages of the existing launch vehicle use liquid oxygen with RP-1 fuel with an average specific gravity of about 1.014, and the launch pad is already equipped for supplying these. The new stage is limited in volume and cross section. Because of these factors the propellant combination of liquid oxygen and RP-1 (a type of kerosene) is selected. From Fig. 5-1 we see that the theoretical specific impulse is between 280 and 300 sec, depending on the mixture ratio and whether we use frozen or shifting chemical equilibrium in the nozzle flow expansion. This figure also shows that the maximum value of the characteristic velocity c^* is reached at a mixture ratio of about 2.30, which is a fuel-rich mixture. We select this mixture ratio. Its combustion temperature is lower than the mixture ratios with higher values, and this should make the cooling of the thrust chamber easier. We will see later that cooling may present some problems. Based on universal experience, we select a value of I_s part way (about 40%) between the values for frozen and shifting equilibrium, namely 292 sec at the standard chamber pressure of 1000 psi or 6.895 MPa, and a nozzle big enough for expansion to sea level. From Fig. 5-1 and Table 5-5 we find the molecular mass to be 23 kg/kg-mol and the specific heat ratio k to be about 1.24. Later we will correct this value of I_s from this standard reference condition to the actual vacuum specific impulse of the thrust chamber with its actual nozzle exit area ratio.

Next we will select a chamber pressure, a nozzle area ratio, and a feed system concept. Historically there has been favorable experience with this propellant combination at chamber pressures between 100 and 3400 psia with nozzle area ratios up to about 40 with both gas generator cycles and staged combustion cycles, giving proof that this is feasible. The following considerations enter into this selection:

1. Higher chamber pressures allow a smaller thrust chamber and (for the same nozzle exit pressure) a shorter nozzle cone with a smaller nozzle exit diameter. The thrust chamber is small enough for a toroidal tank to be built around it, and this conserves stage length. This not only saves vehicle space but usually also some inert mass in the vehicle and the engine. Figure 8–22 shows the relative sizes of thrust chambers for three chamber pressures and two nozzle area ratios (ϵ of 100 and 300). The nozzle length and exit diameter cannot exceed the values given in the requirements, which, as can be seen, rules out low chamber pressure or a large nozzle. The dimensions shown are calculated later in this analysis.
2. The heat transfer rate, which varies with the gas-film coefficient, is almost proportional to the gas density, which is nearly proportional to the chamber pressure, as shown by Eq. 8–20 or 8–22. On some prior thrust chambers there have been problems with the formation of solid carbon layer or deposits either inside the cooling jacket (increasing wall temperatures) or on the inner walls of the combustion chamber (the solid can flake off and cause burnout). This favors a lower chamber pressure.

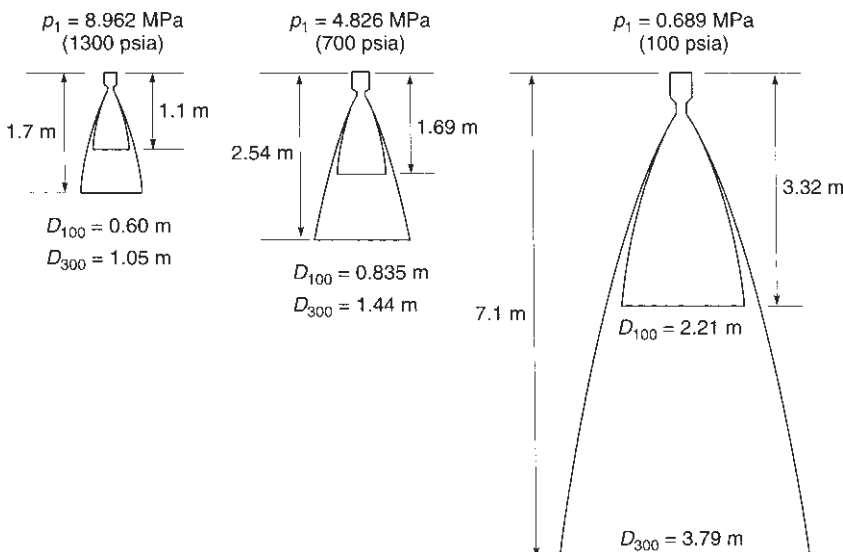


FIGURE 8–22. Comparison of thrust chamber sizes for three chamber pressures and two nozzle area ratios (100 and 300).

3. Concern over leak-free seals for both static and dynamic seals increases with chamber pressure, which in turn causes all feed pressures also to increase.
4. A feed system using pressurized gas is feasible, but its inert masses of tanks and engine are favorable only if the chamber pressure is very low, perhaps around 100 psia or less. The tanks for propellants and pressurizing gas become very heavy and the thrust chamber will be very large and exceed the dimensional restraints mentioned above. We therefore cannot use this feed system or very low chamber pressures.
5. If we use a pump feed system, the power needed to drive the pumps increases directly with chamber pressure p_1 . In a gas generator engine cycle this means a slightly reduced performance as the value of p_1 goes up. For a staged combustion cycle it means high pressures, particularly high-pressure hot gas flexible piping, and a more complex, heavier, and expensive engine. We therefore select a gas generator cycle (see Fig. 1–4) at a low enough chamber pressure so that the thrust chamber (and the other inert hardware) will just fit the geometrical constraints, and the engine inert mass and the heat transfer will be reasonable.

For these reasons we pick a *chamber pressure* of 700 psia or 4.825 MPa and an *area ratio* of 100. With further analysis we could have picked p_1 more precisely; it could be slightly lower. Next we correct the *specific impulse* to the operating conditions using a ratio of thrust coefficients. We can use Eq. 3–30 or interpolate between Figs. 3–7 and 3–8 for a value of $k = 1.24$. The reference or standard condition (see Fig. 3–6) is for a pressure ratio p_1/p_3 of $1000/14.7 = 68$, which corresponds to an area ratio of about 8. Then $(C_F)_{\text{standard}} = 1.58$. For the actual high-altitude operation the pressure ratio is close to infinity. The nozzle has an area ratio of 100; we can determine the thrust coefficient by interpolating with pressure at $k = 1.24$. The result is $(C_F)_{\text{vacuum}} = 1.90$. The new ideal specific impulse value for a chamber threshold of 700 psia and a nozzle area ratio of 100 is therefore $292 \times (1.90/1.58) = 351.1$ sec. In order to correct for losses (divergence, boundary layer, incomplete combustion, some film cooling, etc.) we use a correction factor of 0.96 giving a thrust chamber specific impulse of 337.1 sec. The engine uses a gas generator and this will reduce the engine specific impulse further by a factor of approximately 0.98 or $(I_s)_{\text{engine}} = 330.3$ sec or an effective exhaust velocity of 3237 m/sec.

Stage Masses and Thrust Level. An estimate of the stage masses will next be made. We assume that the inert hardware (tanks, gas, generator, turbopumps, etc.) is about 7% of the propellant mass, which is conservative when compared to existing engines. In a full-fledged engine design this number would be verified or corrected once an estimated but more detailed mass budget becomes available. From Eq. 4–7

$$e^{\Delta u/v} = \frac{m_o}{m_f} = \frac{m_p + 0.07m_p + 3500}{0.07m_p + 3500} = e^{3400/3237}$$

Solve for $m_p = 7483$ kg. The final and initial masses m_f and m_0 of the stage are then 4023 kg and 11,510 kg, respectively.

The maximum *thrust* is limited by the maximum allowed acceleration of $5g_0$. It is $F_{\max} = m_0a = 11,510 \times 5 \times 9.8 = 564,400$ N. This would become a relatively large and heavy thrust chamber. Considerable saving in inert mass can be obtained if a smaller thrust size (but longer firing duration) is chosen. Since this same thrust chamber is going to be used for another mission where an acceleration of somewhat less than $1.0 g_0$ is wanted, a thrust level of 50,000 N or 11,240 lbf is chosen. The maximum acceleration of the stage occurs just before cutoff; it is $a = F/m_f = 50,000/4023 = 12.4$ m/sec² or about 1.26 times the acceleration of gravity. This fits the thrust requirements.

The following have now been determined:

| | |
|--|---|
| Propellant | Liquid oxygen and liquid kerosene (RP-1) |
| Mixture ratio (O/F) | 2.30 (engine) |
| Thrust | 50,000 N or 11,240 lbf |
| Chamber pressure | 700 psia or 4.826 MPa |
| Nozzle area ratio | 100 |
| Specific impulse (engine) | 330.3 sec |
| Specific impulse (thrust chamber) | 337.1 sec |
| Engine cycle | Gas generator |
| Usable propellant mass | 7478 kg |
| Estimated nozzle exit exhaust velocity | 3237 m/sec or 10,613 ft/sec |

Propellant Flows and Dimensions of Thrust Chamber. From Eq. 2–6 we obtain the propellant mass flow:

$$\dot{m} = F/c = 50,000/3237 = 15.446 \text{ kg/sec}$$

When this total flow and the overall mixture ratio are known, then the fuel flow \dot{m}_f and oxidizer flow \dot{m}_o for the engine, its gas generator, and its thrust chamber can be determined from Eqs. 6–3 and 6–4 as shown below:

$$\dot{m}_f = \dot{m}/(r + 1) = 15.446/(2.3 + 1) = 4.680 \text{ kg/sec}$$

$$\dot{m}_o = \dot{m}r/(r + 1) = (15.446 \times 2.3)/3.30 = 10.765 \text{ kg/sec}$$

The gas generator flow \dot{m}_{gg} consumes about 2.0% of the total flow and operates at a fuel-rich mixture ratio of 0.055; this results in a gas temperature of about 890 K:

$$(\dot{m}_f)_{gg} = 0.2928 \text{ kg/sec} \quad (\dot{m}_o)_{gg} = 0.0161 \text{ kg/sec}$$

The flows through the thrust chamber are equal to the total flow diminished by the gas generator flow, which is roughly 98.0% of the total flow or 15.137 kg/sec:

$$(\dot{m}_f)_{tc} = 4.387 \text{ kg/sec} \quad (\dot{m}_o)_{tc} = 10.749 \text{ kg/sec}$$

The *duration* is the total effective propellant mass divided by the mass flow rate:

$$t_b = m_p / \dot{m}_p = 7478 / 15.446 = 484.1 \text{ sec or a little longer than 8 min}$$

The *nozzle throat area* is determined from Eq. 3–31. This neglects start and stop transients:

$$A_t = F / (P_1 C_F) = 50,000 / (4.826 \times 10^6 \times 1.90) = 0.005453 \text{ m}^2 \text{ or } 54.53 \text{ cm}^2$$

The *nozzle throat diameter* is $D_t = 8.326 \text{ cm}$. The internal diameter of the nozzle at exit A_2 is determined from the area ratio of 100 to be $D_2 = \sqrt{100} \times D_t$ or 83.26 cm. A shortened or *truncated bell nozzle* (as discussed in Section 3.4) will be used with 80% of the length of a 15° conical nozzle, but with the same performance as a 15° cone. The nozzle length (from the throat to the exit) can be determined by an accurate layout or by an equivalent 15° conical nozzle exit $L = (D_2 - D_t) / (2 \tan 15)$ as 139.8 cm. For an 80% shortened bell nozzle this length would be about 111.8 cm. The contour or shape of a shortened bell nozzle can be approximated by a parabola (parabola equation is $y^2 = 2px$). Using an analysis (similar to the analysis that resulted in Fig. 3–14), the maximum angle of the diverging section at the inflection point would be about $\theta_i = 34^\circ$ and the nozzle exit angle $\theta_e = 7^\circ$. The approximate contour consists of a short segment of radius $0.4r_t$ of a 34° included angle (between points T and I in Fig. 3–14) and a parabola with two known points at I and E . Knowing the tangent angles (34° and 7°) and the y coordinates [$y_e = r_2$ and $y_i = r_t + 0.382 r_t(1 - \cos\theta_i)$] allows the determination of the parabola by geometric analysis. Before detail design is undertaken, a more accurate contour, using the method of characteristics, is suggested.

The *chamber diameter* should be about twice the nozzle throat diameter to avoid pressure losses in the combustion chamber ($D_c = 16.64 \text{ cm}$). Using the approximate length of prior successful smaller chambers and a characteristic length L^* of about 1.1 m, the chamber length (together with the converging nozzle section) is about 11.8 in. or 29.9 cm. The overall length of the thrust chamber (169 cm) is the sum of the nozzle length (111.8 cm), chamber (29.9 cm), injector thickness (estimated at 8 cm), mounted valves (estimated at 10 cm), a support structure, and possibly also a gimbal joint. The middle sketch of the three thrust chambers in Fig. 8–22 corresponds roughly to these numbers.

We have now the stage masses, propellant flows, nozzle, and chamber configuration. Since this example is aimed at a thrust chamber, data on other engine components or parameters are given only if they relate directly to the thrust chamber or its parameters.

Next we check if there is enough available vehicle volume (1.90 m diameter and 4.50 m long) to allow making a larger nozzle area ratio and thus gain a little more performance. First we determine how much of this volume is occupied by propellant tanks and how much might be left over or be available for the

thrust chamber. This analysis would normally be done by tank design specialists. The average density of the propellant mixture can be determined from Eq. 7–1 to be 1014 kg/m^3 and the total usable propellant of 7478 kg. Using densities from Table 7–1 the fuel volume and the oxidizer volume can be calculated to be 2.797 and 4.571 m^3 , respectively. For a diameter of 1.90 m, a nearly spherical fuel tank, a separate oxidizer cylindrical tank with elliptical ends, 6% ullage, and 2% residual propellant, a layout would show an overall tank length of about 3.6 m in a space that is limited to 4.50 m. This would leave only 0.9 m for the length of the thrust chamber, and this is not long enough. Therefore we would need to resort to a more compact tank arrangement, such as using a common bulkhead between the two tanks or building a toroidal tank around the engine. It is not the aim to design the tanks in this example, but the conclusion affects the thrust chamber. Since the available volume of the vehicle is limited, it is not a good idea to try to make the thrust chamber bigger.

This diversion into the tank design shows how a vehicle parameter affects the thrust chamber design. For example, if the tank design would turn out to be difficult or the tanks would become too heavy, then one of these thrust chamber options can be considered: (1) go to a higher chamber pressure (makes the thrust chamber and nozzle smaller, but heavier), (2) go to a lower thrust engine (will be smaller and lighter), (3) store the nozzle of the upper-stage thrust chamber in two pieces and assemble them during the flight once the lower stages have been used and discarded (see extendible nozzle in Fig. 8–17; it is more complex and somewhat heavier), or (4) use more than one thrust chamber in the engine (will be heavier, but shorter and can provide roll control). We will not pursue these or other options here.

Heat Transfer. The particular computer program for estimating heat transfer and cooling parameters of thrust chambers will depend on the background and experience of specific engineers and rocket organizations. Typical computer programs divide the internal wall surface of the chamber and nozzle into incremental axial steps. Usually in a preliminary analysis the heat transfer is estimated only for critical locations such as for the throat and perhaps the chamber.

From Fig. 5–1 and Eq. 3–12 or 3–22 we determine the following gas temperatures for the chamber, nozzle throat region, and a location in the diverging exit section. They are: $T_1 = 3600 \text{ K}$, $T_t = 3214 \text{ K}$, and $T_e = 1430 \text{ K}$ at an area ratio of 6.0 in the diverging nozzle section. The chamber and nozzle down to an exit area ratio of 6 will have to be cooled by fuel. For this propellant combination and for the elevated wall temperatures a stainless steel has been successfully used for the inner wall material.

Notice that beyond this area ratio of about 6, the nozzle free-stream gas temperatures are relatively low. Uncooled high-temperature metals can be used here in this outer nozzle region. Radiation cooling, using a material such as niobium (coated to prevent excessive oxidation) or carbon fibers in a nonporous carbon matrix, is suitable between an area ratio of 6 and about 25. For the final large nozzle exit section, where the temperatures are even lower, a lower cost material

such as stainless steel or titanium is suggested. Ablative materials have been ruled out because of the long duration and the aggressive ingredients in the exhaust gas. The gas compositions of Figs. 5–2 and 5–3 indicate that some free oxygen and hydroxyl are present.

We now have identified the likely materials for key chamber components. The best way to cool the radiation-cooled exit segment of the nozzle (beyond area ratio of 6) is to let it stick out of the vehicle structure; the heat can then be freely radiated to space. One way to accomplish this is to discard the vehicle structure around the nozzle end after stage separation and before second-stage start.

As in Fig. 8–8, the maximum heat transfer rate will be at the nozzle throat region. A variety of heat transfer analysis programs are available for estimating this heat transfer. If a suitable computer program is not available, then an approximate steady-state heat transfer analysis can be made using Eqs. 8–14 to 8–18 and the physical properties (specific heat, thermal conductivity, and density) of RP-1 at elevated temperatures. The film coefficients of Eqs. 8–22 and 8–24 are also needed. This is not done in this example, in part because data tables for the physical properties would take up a lot of space and results are not always reliable. Data from prior thrust chambers with the same propellants indicate a heat transfer rate at the nozzle throat region exceeding $10 \text{ Btu/in.}^2\text{-sec}$ or $1.63 \times 10^7 \text{ W/m}^2$.

The RP-1 fuel is an unusual coolant since it does not have a distinct boiling point. Its composition is not consistent and depends on the oil stock from which it was refined and the refining process. It is distilled or evaporated gradually over a range of temperatures. The very hot wall can cause the RP-1 to locally break down into carbon-rich material and to partially evaporate or gasify. As long as the small vapor bubbles are recondensed when they are mixed with the cooler portions of the coolant flow, a steady heat transfer process will occur. If the heat transfer is high enough, then these bubbles will not be condensed, may contain noncondensable gases, and the flow will contain substantial gas bubbles and become unsteady, causing local overheating. The recondensing is aided by high cooling passage velocities (more than 10 m/sec at the throat region) and by turbulence in these passages. A coolant flow velocity of 15 m/sec is selected for the nozzle throat region (adequate to prevent big gas bubbles), 7 m/sec for the chamber region and somewhat less, 3 m/sec for the cooled nozzle exit segment.

The material for the cooling jacket will be stainless steel to resist the oxidation and erosion of the fast moving, aggressive hot gas, which contains a small amount of free oxygen and hydroxyl species. The forced cooling by fuel will assure that the temperatures of this stainless steel are well below its softening temperature of about 1050 K.

The construction of the cooling jacket can be tubular, as shown in Figs. 8–1 and 8–9, or it can consist of milled channels as shown in Figs. 8–2 and 8–15. The cross section of each tube or cooling channel will be a minimum at the throat region, gradually become larger, and be about two or more times as large at the chamber and diverging nozzle regions. The wall thickness (on the hot gas side) should be as small as possible to reduce the temperature drop across the wall

(which reduces the thermal stresses and allows a lower wall temperature) and to minimize the yielding of the material that occurs due to thermal deformation and pressure loads. Figure 8–11 shows this behavior, but for a thick wall. Practical considerations such as manufacturability, the number of test firings before flight, the deformation under pressure loads, the temperature gradient and dimensional tolerances also enter into the selection of the wall thickness. A inner wall thickness of 0.5 mm and a cooling velocity of 15 m/sec have been selected for the throat region of the cooling jacket. Milled slots (rather than tubes) have been selected for this thrust chamber.

The selection of the number of milled slots, their cross sections, and the wall thickness is a function of the coolant mass flow, its pressure, wall stresses, wall material, and the shape of the channel. Figure 8–23 and Table 8–6 describe the channel width and height for different numbers of channels and different locations. The fuel coolant flow is diminished by the gas generator fuel flow (0.293 kg/sec) and is about 4.387 kg/sec. For this flow and a cooling velocity of 15 m/sec in the throat region the cumulative cross-sectional area of all the channels is only about 3.62 cm^2 . The cooling velocity is lower in the chamber and nozzle regions and the cumulative channel flow area will be larger there. The variables are the number of channels, the thickness of the hot wall, the rib thickness between channels, the cooling velocity, the gas temperature, and the location along the thrust chamber profile. The number of channels or tubes will determine the shape of the cross section, ranging from deep and thin to almost square. The effect of varying the number of channels or channel dimensions and shape is shown in Table 8–6. The minimum inert mass of the cooling jacket and a low friction loss occur, when the shape (which varies axially throughout the jacket) is on the average close to a square. On the basis of analyses, as shown in the table, a 150-channel design has been selected for giving favorable cross section, reasonable dimensions for ease of fabrication, good cooling, and often low thermal wall stresses.

Reinforcing bands have to be put on the outside of the tubes or channels to hold the internal gas pressure during operation, to contain the coolant pressures, which cause heated walls wanting to become round, and any surge pressures during the start transient or arising from water hammer in the lines. We assume a surge pressure of 50% above chamber pressure and a steel strength of 120,000 psi. In the chamber the inside diameter is 16.7 cm (6.57 in.), the walls and channels

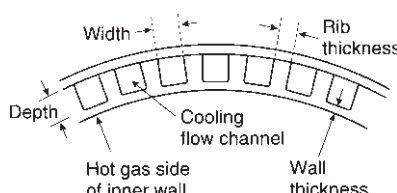


FIGURE 8–23. Segment of cooling jacket with milled channels and an electroformed outer wall.

TABLE 8–6. Alternative Milled Channel Configurations for Fuel (Cooling) Flow of 4.387 kg/sec

| <i>Throat Section</i> | | <i>Chamber Section</i> | | | |
|-----------------------|-----------------------|------------------------|-----------------------|--------------------|-------------------|
| Wall thickness | 0.05 cm | Wall thickness | 0.06 cm | | |
| Rib thickness | 0.08 cm | Rib thickness | 0.08 | | |
| Total flow area | 3.653 cm ² | Total flow area | 7.827 cm ² | | |
| Flow velocity | 15 m/sec | Flow velocity | 7.0 m/sec | | |
| Number of Channels | Channel Width, cm | Channel Depth, cm | Number of Channels | Channels Width, cm | Channel Depth, cm |
| 80 | 0.257 | 0.177 | | | |
| 100 | 0.193 | 0.189 | 100 | 0.456 | 0.171 |
| 120 | 0.145 | 0.210 | 120 | 0.367 | 0.179 |
| 140 | 0.113 | 0.231 | 140 | 0.303 | 0.184 |
| 150 | 0.100 | 0.243 | 150 | 0.277 | 0.188 |
| 160 | 0.092 | 0.247 | 160 | 0.255 | 0.192 |
| 180 | 0.070 | 0.289 | 180 | 0.218 | 0.196 |

each are 0.3 cm deep, and the pressure is 700 psia or 4.826 MPa. If one band allows the reinforcing of a length of chamber of 3.0 in., the cross-sectional area of that reinforcing band will be

$$A = pDL/(2\sigma) = [700 \times 1.5 \times (6.57 + 0.3) \times 3]/(2 \times 120,000) = 0.0902 \text{ in.}^2$$

If the bands were 1.0 in. wide, its thickness would be 0.09 in.; and if it were 3 in. wide, it would be 0.03 in. thick. Large nozzle exit sections have been observed to experience flutter or cyclic deformation, and therefore some stiffening rings may be needed near the exit.

The capacity of the fuel to absorb heat (Eq. 8–25) is approximately $c_p \dot{m}_f \Delta T = 0.5 \times 4.81 \times 200 = 278,000 \text{ J/sec}$. The maximum ΔT is established by keeping the fuel well below its chemical decomposition point. This calculated heat absorption is less than the heat transfer from the hot gases. It is therefore necessary to reduce the gas temperature near the chamber and nozzle walls or to increase the heat absorption. This can be accomplished by (1) introducing film cooling by injection into the chamber just ahead of the nozzle, by (2) modifying the injection patterns, so that a cooler, fuel-rich thick internal boundary layer is formed, or (3) by allowing some nucleate boiling in the throat region. The analysis of these three methods is not given here. Item (2), supplementary cooling, is selected because it is easy to design and build and can be based on extensive data of prior favorable experience. However, it causes a small loss of performance (up to about 1% in specific impulse). The specific impulse of the engine is then 327 sec.

Injector Design. The injector pattern can be any one of the several types shown in Figs. 8–3 and 8–4. For this propellant combination we have used both doublets (like and unlike), and triplets in the United States, and the Russians have used multiple hollow double posts with swirling or rotation of the flow in the outer annulus. Based on good experience and demonstrated combustion stability with similar designs, we select a doublet self-impinging-type stream pattern (Fig. 8–3) and an injector structure design similar to Fig 8–5. The impinging streams form fans of liquid propellant, which break up into droplets. Oxidizer and fuel fans alternate radially. We could also use a platelet design, like Fig. 8–6.

The pressure drop across the injector is usually set at values between 15 and 25% of the chamber pressure, in part to obtain high injection velocities, which aid in atomization and droplet breakup. In turn this leads to more complete combustion (and thus better performance) and to stable combustion. We will use 20% or 140 psi or 0.965 MPa for the injector pressure drop. There is a small pressure loss in the injector passages. The injection velocities are found from Eqs. 8–1 and 8–5. The equation is solved for the area A , which is the cumulative cross-section area of all the injection holes of one of the propellants in the injector face.

With rounded and clean injection hole entrances the discharge coefficient will be about 0.80 as shown in Table 8–2. Solving for the cumulative injection hole area for the fuel and the oxidizer flows gives 1.98 cm^2 for the fuel and 4.098 cm^2 for the oxidizer. A typical hole diameter in this size of injector would be about 0.5 to 2.5 mm. We will use a hole size of 1.5 mm for the fuel holes (with 90% of the fuel flow) and 2.00 mm for the oxidizer hole size, resulting in 65 doublets of oxidizer holes and 50 doublets of fuel. By using a slightly smaller fuel injection hole diameter, we can match the number of 65 doublets as used with the oxidizer holes. These injection doublets will be arranged on the injector face in concentric patterns similar to Fig. 8–5. We may be able to obtain a slightly higher performance by going to smaller hole sizes and a large number of fuel and oxidizer holes. In addition there will be extra fuel holes on the periphery of the injector face to help in providing the cooler boundary layer, which is needed to reduce heat transfer. They will use 10% of the fuel flow and, for a 0.5-mm hole diameter, the number of holes will be about 100. To make a good set of liquid fans, equal inclination angles of about 25° are used with the doublet impingements. See Fig. 8–7.

Igniter Dimensions. A pyrotechnic (solid propellant) igniter will be used. It has to have enough energy and run long enough to provide the pressure and temperature in the thrust chamber for good ignition. Its largest diameter has to be small enough to be inserted through the throat, namely 8.0 cm maximum diameter and it can be 10 to 15 cm long. The actual igniter will, most likely, be smaller than this.

Layout Drawings, Masses, Flows, and Pressure Drops. We now have enough of the key design parameters of the selected thrust chamber, so a preliminary layout drawing can be made. Before this can be done well, we will need some analysis or estimates on the thrust chamber manifolds for fuel and oxidizer, valve mounting provisions and their locations, a nozzle closure during storage, a thrust structure, and possibly an actuator and gimbal mount, if gimbaling is required by the mission. A detailed layout or CAD (computer-aided design) image (not shown in this analysis) would allow a more accurate picture and a good determination of the mass of the thrust chamber and its center of gravity both with and without propellants.

Estimates of gas pressures, liquid pressures (or pressure drops) in the flow passages, injector, cooling jacket, and the valves are needed for the stress analysis, so that various wall thicknesses and component masses can be determined. Material properties will need to be obtained from references or tests. A few of these analyses and designs may actually change some of the data we selected or estimated early in this sample analysis, and some of the calculated parameters may have to be re-analyzed and revised. Further changes in the thrust chamber design may become evident in the design of the engine, the tanks, or the interface with the vehicle. The methods, processes, and fixtures for manufacturing and testing (and the number and types of tests) will have to be evaluated and the number of thrust chambers to be built has to be decided before we can arrive at a reasonable manufacturing plan, a schedule, and cost estimates.

PROBLEMS

1. How much total heat per second can be absorbed in a thrust chamber with an inside wall surface area of 0.200 m^2 if the coolant is liquid hydrogen and the coolant temperature does not exceed 145 K in the jacket? Coolant flow is 2 kg/sec. What is the average heat transfer rate per second per unit area? Use the data from Table 7-1 and the following:

2. During a static test a certain steel thrust chamber is cooled by water in its cooling jacket. The following data are given for the temperature range and pressure of the coolant:

| | |
|-------------------------------|--|
| Average water temperature | 100°F |
| Thermal conductivity of water | 1.07×10^{-4} Btu/sec-ft ² -°F/ft |
| Gas temperature | 4500°F |
| Specific gravity of water | 1.00 |

| | |
|---------------------------------------|--|
| Viscosity of water | 2.5×10^{-5} lbf-sec/ft ² |
| Specific heat of water | 1.3 Btu/lb-°F |
| Cooling passage dimensions | $\frac{1}{4} \times \frac{1}{2}$ in. |
| Water flow through passage | 0.585 lb/sec |
| Thickness of inner wall | $\frac{1}{8}$ in. |
| Heat absorbed | 1.3 Btu/in. ² -sec |
| Thermal conductivity of wall material | 26 Btu/hr-ft ² -°F/ft |

Determine (a) the film coefficient of the coolant; (b) the wall temperature on the coolant side; (c) the wall temperature on the gas side.

- In the example of Problem 2 determine the water flow required to decrease the wall temperature on the gas side by 100°F. What is the percentage increase in coolant velocity? Assume that the various properties of the water and the average water temperature do not change.
- Determine the absolute and relative reduction in wall temperatures and heat transfer caused by applying insulation in a liquid-cooled rocket chamber with the following data:

| | |
|---------------------------|-------------------------------|
| Tube wall thickness | 0.381 mm |
| Gas temperature | 2760 K |
| Gas-side wall temperature | 1260 K |
| Heat transfer rate | 15 MW/m ² -sec |
| Liquid-film coefficient | 23 kW/m ² -K |
| Wall material | Stainless steel AISI type 302 |

A 0.2-mm-thick layer of insulating paint is applied on the gas side; the paint consists mostly of magnesia particles. The average conductivity of this magnesia paint is 2.59W/m²-K/m over the temperature range. The stainless steel has an average thermal conductivity of 140 Btu/hr-ft²-°F/in. and a specific gravity of 7.98

- A small thruster has the following characteristics:

| | |
|--------------------------------------|--|
| Propellants | Nitrogen tetroxide and monomethyl hydrazine |
| Injection individual hole size | Between 0.063 and 0.030 in. |
| Injection hole pattern | Unlike impinging doublet |
| Thrust chamber type | Ablative liner with a carbon–carbon nozzle throat insert |
| Specific gravities | 1.446 for oxidizer and 0.876 for fuel |
| Impingement point | 0.25 in. from injector face |
| Direction of jet momentum | Parallel to chamber axis after impingement |
| $r = 1.65$ (fuel rich) | $(I_s)_{\text{actual}} = 251$ sec |
| $F = 300$ lbf | $t_b = 25$ sec |
| $p_1 = 250$ psi | $A_1/A_t = 3.0$ |
| $(\Delta p)_{\text{inj}} = 50.0$ psi | $(C_d)_o = (C_d)_f = 0.86$ |

Determine the number of oxidizer and fuel injection holes and their angles. Make a sketch to show the symmetric hole pattern and the feed passages in the injector. To protect the wall, the outermost holes should all be fuel holes.

6. A large, uncooled, uninsulated, low-carbon-steel thrust chamber burned out in the throat region during a test. The wall (0.375 in. thick) had melted and there were several holes. The test engineer said that he estimated the heat transfer to have been about 15 Btu/in^2 . The chamber was repaired and you are responsible for the next test. Someone suggested that a series of water hoses be hooked up to spray plenty of water on the outside of the nozzle wall at the throat region during the next test to prolong the firing duration. The steel's melting point is estimated to be 2550°F . Because of the likely local variation in mixture ratio and possibly imperfect impingement, you anticipate some local gas regions that are oxidizer rich and could start the rapid oxidation of the steel. You therefore decide that 2150°F should be the maximum allowable inner wall temperature. Besides knowing the steel weight density (0.284 lbf/in^3), you have the following data for steel for the temperature range from ambient to 2150°F : the specific heat is $0.143 \text{ Btu/lbm-}^\circ\text{F}$ and the thermal conductivity is $260 \text{ Btu/hr-ft}^2-{}^\circ\text{F/in}$. Determine the approximate time for running the next test (without burnout) both with and without the water sprays. Justify any assumptions you make about the liquid-film coefficient of the water flow. If the water spray seems to be worth while (getting at least 10% more burning time), make sketches with notes on how the mechanic should arrange for this water flow so it will be most effective.
7. The following conditions are given for a double-walled cooling jacket of a rocket thrust chamber assembly:

| | |
|---|--|
| Rated chamber pressure | 210 psi |
| Rated jacket pressure | 290 psi |
| Chamber diameter | 16.5 in. |
| Nozzle throat diameter | 5.0 in. |
| Nozzle throat gas pressure | 112 psi |
| Average inner wall temperature at throat region | 1100°F |
| Average inner wall temperature at chamber region | 800°F |
| Cooling passage height at chamber and nozzle exit | 0.375 in. |
| Cooling passage height at nozzle throat | 0.250 in. |
| Nozzle exit gas pressure | 14.7 psi. |
| Nozzle exit diameter | 10 in. |
| Wall material | 1020 carbon steel |
| Inner wall thickness | 0.08 in. |
| Safety factor on yield strength | 2.5 |
| Cooling fluid | RP-1 |
| Average thermal conductivity of steel | $250 \text{ Btu/hr-ft}^2-{}^\circ\text{F/in.}$ |

Assume other parameters, if needed. Compute the outside diameters and the thickness of the inner and outer walls at the chamber, at the throat, and at the nozzle exit.

8. Determine the hole sizes and the angle setting for a multiple-hole, doublet impinging stream injector that uses alcohol and liquid oxygen as propellants. The resultant

momentum should be axial, and the angle between the oxygen and fuel jets ($\gamma_o + \gamma_f$) should be 60° . Assume the following:

| | | | |
|---------------------------------|-----------------------|---------------------|---------|
| $(C_d)_o$ | 0.87 | Chamber pressure | 300 psi |
| $(C_d)_f$ | 0.91 | Fuel pressure | 400 psi |
| ρ_o | 71 lb/ft ³ | Oxygen pressure | 380 psi |
| ρ_f | 51 lb/ft ³ | Number of jet pairs | 4 |
| r | 1.20 | Thrust | 250 lbf |
| Actual specific impulse 218 sec | | | |

Answers: 0.0197 in.; 0.0214 in.; 32.3° ; 27.7° .

- Table 11–6 shows that the RD-120 rocket engine can operate down to 85% of full thrust and at a mixture ratio variation of $\pm 10.0\%$. In a particular static test the average thrust was held at 96% of nominal and the average mixture ratio was 2.0% fuel rich. Assume a 1.0% residual propellant, but neglect other propellant budget allowances. What percentage of the fuel and oxidizer that have been loaded will remain unused at thrust termination? If we want to correct the mixture ratio in the last 20.0% of the test duration and use up all the available propellant, what would be the mixture ratio and propellant flows for this last period?
- Make a simple cross-section sketch approximately to scale of the thrust chamber that was analyzed in Section 8.8. The various dimensions should be close, but need not be accurate. Include or make separate detailed-section sketches of the cooling jacket and the injector. Also compile a table of all the key characteristics, similar to Table 8–1, but include gas generator flows and key materials. Make estimates or assumptions for any key data that is not mentioned in Section 8.8.

SYMBOLS

| | |
|-----------|---|
| A | area, m ² (ft ²) |
| A_a | projected area of linear aerospike ramp, m ² (ft ²) |
| c_p | specific heat at constant pressure, J/kg-K (Btu/lbm°R) |
| \bar{c} | average liquid specific heat, J/kg-K (Btu/lbm°R) |
| C_d | discharge coefficient |
| c_p | specific heat at constant pressure J/kg-K (Btu/lbm R) |
| D | diameter, m (ft) |
| E | modulus of elasticity, N/m ² (lbf/in. ²), or radiation energy, kg-m ² /sec ² |
| f | friction loss coefficient, or geometric factor in radiation or final (velocity) |
| g_0 | sea-level acceleration of gravity, 9.806 m/sec ² (32.17 ft/sec ²) |
| h | film coefficient, W/(m ² -K); (Btu/(ft ² -°R)) |
| I_s | specific impulse, sec |
| k | specific heat ratio |
| L | length, m (ft) |
| L^* | characteristic chamber length, m (ft) |
| m | mass, kg |

| | |
|------------|---|
| \dot{m} | mass flow rate, kg/sec (lb/sec) |
| p | pressure, N/m ² or Pa (lbf/in. ²) |
| Pr | Prandtl number ($c_p\mu/\kappa$) |
| q | heat transfer rate or heat flow per unit area, J/m ² -sec (Btu/ft ² -sec) |
| Q | volume flow rate, m ³ /sec (ft ³ /sec), or heat flow rate, J/sec |
| R | Reynold's number $Dv\rho/\mu$ |
| r | flow mixture ratio (oxidizer to fuel); or radius, m (ft) |
| s | stress N/m ² (lbf/in. ²) |
| t | time, sec, or thickness, m (ft) |
| t_s | stay time, sec |
| t_w | wall thickness, m (in.) |
| T | absolute temperature, K (°R) |
| Δu | flight velocity increment m/sec (lf/sec) |
| v | velocity, m/sec (ft/sec) |
| V_1 | specific volume, m ³ /kg (ft ³ /lb) |
| V_c | combustion chamber volume (volume up to throat), m ³ (ft ³) |
| x, y | coordinates of a parabola with constant p |

Greek Letters

| | |
|---------------|--|
| γ_o | angle between chamber axis and oxidizer stream |
| γ_f | angle between chamber axis and fuel stream |
| Δ | finite differential |
| δ | angle between chamber axis and the resultant stream |
| ϵ | nozzle exit area ratio ($\epsilon = A_2/A_t$) |
| ε | emmissivity of radiating surface, dimension gas less |
| θ | angle |
| κ | thermal conductivity, J/(m ² -sec-K)/m (Btu/in. ² -sec ² -°R/in.) |
| λ | coefficient of thermal expansion, m/m-K (in./in.-°R) |
| μ | absolute gas viscosity, kg/(m-sec) or lbf/ft ² -sec |
| ν | Poisson ratio |
| ρ | density, kg/m ³ (lbf/ft ³) |
| σ | Stefan-Boltzmann constant (5.67×10^{-8} W/m ² -K ⁴); also stress N/m ² (lbf/in ²) N/m ² (lbf/in ²) |

Subscripts

| | |
|----------|-------------------------|
| am | arithmetic mean |
| <i>c</i> | chamber |
| <i>f</i> | fuel or final condition |
| <i>g</i> | gas |
| gg | gas generator |

| | |
|-----------|---------------------------------|
| inj | injector |
| <i>l</i> | liquid |
| <i>o</i> | oxidizer |
| <i>t</i> | throat |
| tc | thrust chamber |
| <i>w</i> | wall |
| <i>wg</i> | wall on side of gas |
| <i>wl</i> | wall on side of liquid |
| 0 | initial condition |
| 1 | inlet or chamber condition |
| 2 | nozzle exit condition |
| 3 | atmosphere or ambient condition |

REFERENCES

- 8–1. G. P. Sutton, *History of Liquid Propellant Rocket Engines*, AIAA, Reston, VA, 2006.
- 8–2. V. Yang, M. Habiballah, J. Hulka, and M. Popp, (Eds.), *Liquid Rocket Thrust Chambers: Aspects of Modeling, Analysis, and Design*, Progress in Astronautics and Aeronautics (Series), Vol. 200, AIAA, Reston, VA, 2004.
- 8–3. R. D. McKown, “Brazing the SSME,” *Threshold, an Engineering Journal of Power Technology*, No. 1, Rocketdyne Division of Rockwell International (now Pratt & Whitney Rocketdyne.), Canoga Park, CA, March 1987, pp. 8–13.
- 8–4. R. A. Ellis, J. C. Lee, F. M. Payne, M. Lacoste, A. Lacombe, and P. Joyes, “Testing of the RL 10B-2 Carbon-Carbon Nozzle Extension,” AIAA Conference Paper 98-3363, July 1998.
- 8–5. M. Niino, A. Kumakawa, T. Hirano, K. Sumiyashi, and R. Watanabe, “Life Prediction of CIP Formed Thrust Chambers,” *Acta Astronautica*, Vol. 13, Nos. 6–7, 1986, pp. 363–369 (fatigue life prediction).
- 8–6. J. S. Porowski, W. J. O’Donnell, M. L. Badlani, B. Kasraie, and H. J. Kasper, “Simplified Design and Life Predictions of Rocket Thrustchambers,” *Journal of Spacecraft and Rockets*, Vol. 22, No. 2, March–April 1985, pp. 181–187.
- 8–7. J. S. Kinkaid, “Aerospike Evolution,” *Threshold*, The Boeing Co., Rocketdyne Propulsion and Power, No. 18, Spring 2000, pp. 4–13.
- 8–8. T. T. Bui, J. E. Murray, C. E. Rodgers, S. Bartel, A. Cesaroni, and M. Dennet, “Flight Research of an Aerospike Nozzle Using High Power Solid Rockets,” AIAA paper 2005-3797, 2005.
- 8–9. A. J. Fortini and R. H. Tuffias, “Advanced Materials for Chemical Propulsion: Oxide-Iridium/Rhenium Combustion Chambers,” AIAA Paper 99-2894, June 1999.
- 8–10. F. P. Incropera, D. P. DeWitt, T. L. Bergman, and A. S. Lavine, *Introduction to Heat Transfer*, 5th d., John Wiley & Sons, Hoboken, NJ, 2006.
- 8–11. A. A. Samarskii and P. N. Vabishchevich, *Computational Heat Transfer*, Vol. 1. *Mathematical Modeling* and Vol. 2. *The Finite Difference Methodology*, John Wiley & Sons, New York, 1995 and 1996.

- 8–12. R. W. Lewis, Perumal Nithiarasu, and Kankanhalli Seetharamu, *Fundamentals of the Finite Element Method for Heat and Fluid Flow*, John Wiley & Sons, Hoboken, NJ, 2004.
- 8–13. D. R. Bartz, “Survey of Relationships between Theory and Experiment for Convective Heat Transfer in Rocket Combustion Gases,” in *Advances in Rocket Propulsion*, S. S. Penner (Ed.), AGARD, Technivision Services, Manchester, UK, 1968.
- 8–14. E. Mayer, “Analysis of Pressure Feasibility Limits in Regenerative Cooling of Combustion Chambers for Large Thrust Rockets,” in *Liquid Rockets and Propellants*, L. E. Bollinger, M. Goldsmith, and A. W. Lemmon, Jr. (Eds.), Academic Press, New York, 1969, pp. 543–561.
- 8–15. J. M. Fowler and C. F. Warner, “Measurements of the Heat-Transfer Coefficients for Hydrogen Flowing in a Heated Tube,” *American Rocket Society Journal*, Vol. 30, No. 3, March 1960, pp. 266–267.
- 8–16. P. A. Baudart, V. Duthoit, T. Delaporte, and E. Znaty, “Numerical Modeling of the HM 7 B Main Chamber Ignition,” AIAA Paper 89-2397, 1989.
- 8–17. A. R. Casillas, J. Eninger, G. Josephs, J. Kenney, and M. Trinidad, “Control of Propellant Lead/Lag to the LEA in the AXAF Propulsion System,” AIAA Paper 98-3204, July 1998.

CHAPTER 9

LIQUID PROPELLANT COMBUSTION AND ITS STABILITY

In this chapter we treat the complex phenomena of the combustion processes in the combustion chamber of a liquid bipropellant thrust chamber. We describe in general terms the combustion behavior, the progress in analysis of combustion, the several types of combustion instability with its undesirable effects, and semiempirical remedies which avoid these. The objective is to operate at very high combustion efficiencies and to prevent 100% of all the occurrence of disruptive or destructive combustion instability. Thrust chambers should operate with stable combustion over their full range of operating conditions. For a treatment of these subjects see Refs. 9-1 to 9-7.

The combustion of liquid propellants is very efficient in well-designed thrust chambers, precombustion chambers, or gas generators. Efficiencies of 95 to 99.5% are typical compared to turbojets or furnaces, which can range from 50 to 97%. This is due to the very high reaction rates at the high combustion temperatures and the thorough mixing of fuel and oxidizer reaction species by means of good injection flow distribution and gas turbulence. The losses are largely due to incomplete burning or inadequate mixing (nonuniform mixing ratio). For very small bipropellant thrust chambers or small gas generators, where the injector has very few injection orifices or elements, the combustion efficiency can be well below 95%.

9.1. COMBUSTION PROCESS

In describing the combustion processes, it is convenient and helpful to the understanding to divide the combustion chamber into a series of discrete zones, as shown in Fig. 9-1 for a typical configuration. It has a flat injector face

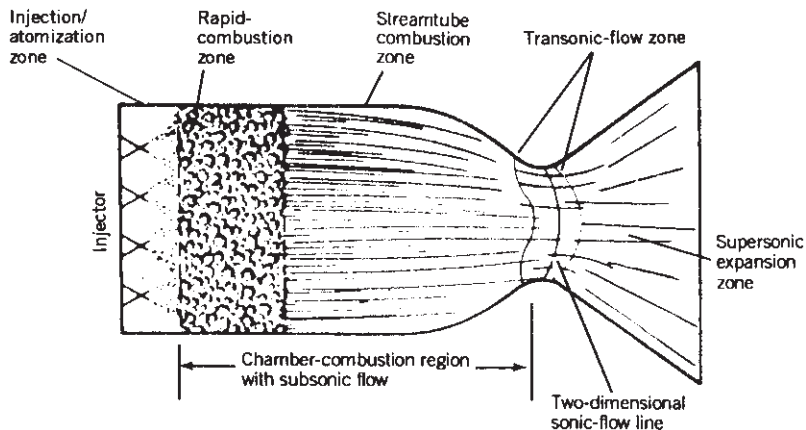


FIGURE 9–1. Division of combustion chamber into zones for analysis. (Modified from Y. M. Timnat, *Advanced Chemical Rocket Propulsion*, Academic Press, New York, 1987.)

with many small injection orifices for introducing both fuel and oxidizer liquids as many discrete individual streams, jets, or thin sprays or sheets. The relative thicknesses of these zones in the axial direction, their behavior, and their transitions are influenced by the specific propellant combination, the operating conditions (pressure, mixture ratio, etc.), the design of the injector, and chamber geometry. The boundaries between the zones shown in Fig. 9–1 are really not flat surfaces and do not display steady flow. They are undulating, dynamically movable, irregular boundaries with localized changes in velocity, temporary bulges, locally intense radiation emissions, or variable temperature. Table 9–1 shows the major interacting physical and chemical processes that occur in the chamber. This table is a modification of tables and data in Refs. 9–2, 9–3, and 9–7.

The combustion behavior is propellant dependent. If the cryogenic fuel hydrogen has been used to cool the thrust chamber, the hydrogen would be gaseous and fairly warm (60 to 240 K); there would be no liquid hydrogen droplets and no evaporation. With hypergolic propellants there is an initial chemical reaction in the liquid phase when a droplet of fuel impinges on a droplet of oxidizer. Experiments show that the contact can create local explosions and enough energy release to suddenly vaporize a thin layer of the fuel and the oxidizer locally at the droplet's contact face; there immediately follows a vapor chemical reaction and a blow-apart and breakup of the droplets. Occasionally there are small local explosions and shock wave phenomena (Refs. 9–8 and 9–9).

The combustion process is usually analyzed as a steady-flow process, but in reality it is not so. When observing any one location within the chamber, one finds a turbulent flow with local fluctuations with time in pressure, flow, temperature, density, mixture ratio, or radiation emissions. The boundaries between zones identified in Fig. 9–1 or Table 9–1 are not in a single plane, do not have steady flow, are more like an undulating changing surface, which locally moves

TABLE 9–1. Physical and Chemical Processes in the Combustion of Liquid Propellants

| Injection | Atomization | Vaporization |
|---|--|---|
| Liquid jets or sprays enter chamber at relatively low velocities | Impingement of jets or sheets | Droplet gasification and diffusion |
| Sometimes gas propellant is injected | Formation of liquid fans or spray cones | Further heat release from local chemical reactions |
| Partial evaporation of liquids | Formation of droplets | Relatively low gas velocities and some cross flow |
| Interaction of jets or sprays with high-pressure gas | Secondary breakup of drops Liquid mixing and some liquid-liquid chemical reaction Oscillations of jets or fans or spray liquid sheets as they become unstable during breakup Vaporization begins and some vapor reactions occur | Heat absorbed by radiation, convection, and conduction, from blowback of turbulent gases from the hot reaction zone Acceleration to higher velocities Vaporization rate influenced by turbulence, pressure or temperature oscillations and acoustic waves |
| Mixing and Reaction | Expansion in Chamber | |
| Turbulent mixing (three-dimensional) | Chemical kinetics causes attainment of final combustion temperature and final equilibrium reaction gas composition | |
| Multiple chemical reactions and major heat releases | Gas dynamics displays turbulence and increasing axial gas velocities | |
| Interactions of turbulence with droplets and chemical reactions | Formation of a boundary layer | |
| Temperature rise reduces densities and increases volume flow | Acceleration to high chamber velocities | |
| Local mixture ratios, reaction rates, or velocities are not uniform across chamber and vary rapidly with time | Streamlined high-velocity axial flow with very little cross flow | |
| Some tangential and radial flows, much of it near the injector | Flow toward nozzle Heat transfer to walls | |

forward and backward. Some of the processes listed in the table occur sequentially, while others occur simultaneously. Not all the listed processes happen with each propellant. Three-dimensional turbulence happens in all parts of the combustion chamber and nozzle. Most processes also create noise.

Rapid Combustion Zone

In this zone intensive and rapid chemical reactions occur at increasingly higher temperature; any remaining liquid droplets are vaporized by convective heating and gas pockets of fuel-rich and fuel-lean gases are mixed. The mixing is accomplished by local three-dimensional turbulence and diffusion of the gas species.

The further breakdown of the propellant chemicals into intermediate fractions and smaller, simpler chemicals and the oxidation of fuel fractions occur rapidly in this zone. The rate of heat release increases greatly, and this causes the specific volume of the gas mixture to increase and the local axial velocity to increase by a factor of 100 or more. The rapid expansion of the heated gases also forces a series of small local transverse gas flows (cross flow) and even some localized temporary back flow from hot high-burning-rate sites to colder low-burning-rate sites. The liquid droplets that may still persist in the upstream portion of this zone, do not follow the gas flow quickly, and are difficult to move in a transverse direction. Therefore, zones of fuel-rich or oxidizer-rich gases will persist according to the orifice spray pattern in the upstream injection zone. The gas composition and mixture ratio across the chamber section become more uniform as the gases move through this zone, but the mixture never becomes truly uniform. As the reaction product gases are accelerated, they become hotter (due to further heat releases) and the lateral velocities remain relatively small compared to the increasing axial velocities. Our understanding of the process is aided by high-speed photography See Ref. 9-7.

Injection/Atomization Zone

Two different liquids are injected, both with storable bipropellants and/or liquid oxygen–hydrocarbon combinations. They are injected through orifices or slots at velocities typically between 7 and 60 m/sec or about 20 to 200 ft/sec. The injector design has a profound influence on the combustion behavior and some seemingly minor design changes can have a major effect on instability. The pattern, sizes, number, distribution, and types of orifices influence the combustion behavior, as do the pressure drop, manifold geometry, or surface roughness in the injection orifice walls. The individual jets, streams, or sheets break up into droplets by impingement of one jet with another (or with a surface), by impingement of conical spray sheets, by the inherent instabilities of liquid jets or sprays, or by the interaction with gases at a different velocity and temperature. In this first zone the liquids are atomized into a large number of small droplets (see Refs. 9-3, 9-6, 9-7, 9-9, and 9-10). Heat is transferred to the droplets by radiation from the very hot rapid combustion zone and by convection from moderately hot gases in the first zone. The droplets evaporate and create local regions rich either in fuel vapor or oxidizer vapor.

This first zone is heterogeneous; it contains liquids and vaporized propellant as well as some burning hot gases. With the liquid being located at discrete sites, there are large gradients in all directions with respect to fuel and oxidizer mass fluxes, mixture ratio, size and dispersion of droplets, or properties of the gaseous medium. Chemical reactions begin to occur in this zone, but the rate of heat generation is relatively low, in part because the liquids and the gases are still relatively cold and in part because vaporization near the droplets causes fuel-rich and fuel-lean regions which do not burn as quickly. Some hot gases from the combustion zone are recirculated back from the rapid combustion zone, and they

can create local gas velocities that flow across the injector face. The hot gases, which can flow in unsteady vortexes or turbulence patterns, are essential to the initial evaporation of the liquids.

The injection, atomization, and vaporization processes are different if one of the propellants is a gas. For example, this occurs in liquid oxygen with gaseous hydrogen propellant in thrust chambers or precombustion chambers, where liquid hydrogen has absorbed heat from cooling jackets and has been gasified. Hydrogen gas has no droplets and does not evaporate. The gas usually has a much higher injection velocity (above 120 m/sec) than the liquid propellant. This causes shear forces to be imposed on the liquid jets, with more rapid droplet formation and gasification. The preferred injector design for gaseous hydrogen and liquid oxygen is different from the individual jet streams used with storable propellants, as shown in Chapter 8.

Stream Tube Combustion Zone

In this zone oxidation reactions continue, but at a lower rate, and some additional heat is released. However, chemical reactions continue because the mixture tends to be driven toward an equilibrium composition. Axial velocities are high (200 to 600 m/sec), and the transverse convective flow velocities are relatively small. Streamlines are formed and there is relatively little turbulent mixing across streamline boundaries. Locally the flow velocity and the pressure fluctuate somewhat. The residence time in this zone is very short compared to the residence time in the other two zones. The streamline type, inviscid flow, and the chemical reactions toward achieving chemical equilibrium persist not only throughout the remainder of the combustion chamber, but are also extended into the nozzle.

The residence time of the propellant material in the combustion chamber is very short, usually less than 10 msec. Combustion in a liquid rocket engine is very dynamic, with the volumetric heat release being approximately $370 \text{ MJ/m}^3\text{-sec}$, which is much higher than in turbojets. Further, the higher temperature in a rocket causes chemical reaction rates to be several times faster (increasing exponentially with temperature) than in turbojet.

9.2. ANALYSIS AND SIMULATION

For the purpose of analyzing the combustion process and its instabilities, it has been convenient to divide the acoustical characteristics into linear and nonlinear behavior. A number of computer simulations with linear analyses have been developed over the last 45 years and have been used to understand the combustion process with liquid propellant combustion devices and to predict combustion oscillation frequencies. The nonlinear behavior (e.g., why does a disturbance cause an apparently stable combustion to suddenly become unstable?) is not well understood and not properly simulated. Mathematical simulations require a number of assumptions and simplifications to permit feasible solutions

(see Refs. 9–1 to 9–5, 9–7, 9–11, and 9–12). Good models exist for relatively simple phenomena such as droplets of a propellant vaporizing (see Refs. 9–8 and 9–10) and burning in a gaseous atmosphere or the steady-state flow of gases with heat release from chemical reactions. The thermochemical equilibrium principles mentioned in Chapter 5 also apply here. Some programs consider turbulence and film cooling effects.

The following phenomena are usually ignored or greatly simplified: cross flows; nonsymmetrical gradients; unsteadiness of the flow; time variations in the local temperature, local velocity, or local gas composition; thermochemical reactions at local off-design mixture ratios and at different kinetic rates; enhancement of vaporization by acoustic fields (see Ref. 9–9); uncertainties in the spatial as well as the size distribution of droplets from sprays; or drag forces on droplets. It requires skilled, experienced personnel to use, interpret, and modify the more complex programs so that meaningful results and conclusions can be obtained. The outputs of these computer programs can give valuable help and confirmation about the particular design and are useful guides in interpreting actual test results, but by themselves they are not sufficient to determine the designs, select specific injector patterns, or predict the occurrence of combustion instabilities.

All the existing computer programs known to the authors are suitable for steady-state flow conditions, usually at a predetermined average mixture ratio and chamber pressure. However, during the starting, thrust change (such as throttling), and stopping transients, the mixture ratio and the pressure can change drastically. The analysis of these transient conditions is more difficult.

The combustion is strongly influenced by the injector design. The following are some of the injection parameters which influence combustion behavior: injector spray or jet pattern, their impingement, hole sizes or hole distribution, droplet evaporation, injection pressure drop, mixture ratio, pressure or temperature gradients near the injector, chamber/injector geometry, pressurant gas saturation, initial propellant temperature, and liquid injection pressure drop. Attempts to analyze these effects have met with only partial success.

Computational fluid dynamics (CFD) is a relatively new analytical tool that can provide a comprehensive description of complex fluid dynamic and thermodynamic behavior. It allows for a time history of all parameters and can even include some nonlinear effects. Numerical approaches are used to evaluate sets of equations and models that represent the behavior of the fluid. For complex geometries the information has been tracked with more than 150,000 discrete locations and can include changes in gas composition, thermodynamic conditions, equilibrium reactions, phase changes, viscous or nonviscous flow, one-, two-, or three-dimensional flow and steady-state or transient conditions. It has been applied to resonance cavities in injectors or chambers and to the flow of burning gases through turbines. A comprehensive rocket combustion model using CFD is not yet available, but could become useful in the future.

9.3. COMBUSTION INSTABILITY

If the process of rocket combustion is not controlled (by proper design), then combustion instabilities can occur which can very quickly cause excessive pressure vibration forces (which may break engine parts) or excessive heat transfer (which may melt thrust chamber parts). The aim is to prevent all occurrences of this instability and to maintain reliable operation (see Refs. 9–5 and 9–11 to 9–14). Much progress has been made in understanding and avoiding combustion instability.

References 9–1 to 9–3 and 9–5 to 9–7 describe the analysis and behavior of combustion instability in thrust chambers as practiced in the United States. References 9–13 and 9–14 present the same but as practiced in Russia and its predecessor the Soviet Union. There are some differences in the assumptions, analysis, and testing, but the basic approach is essentially similar. In both countries any new or modified thrust chamber and/or rocket engine has to be tested to demonstrate that combustion instability will not occur.

Table 9–2 lists the principal types of combustion vibrations encountered in liquid rocket thrust chambers (see Refs. 9–3 and 9–9). Admittedly, combustion in a liquid rocket is never perfectly smooth; some fluctuations of pressure, temperature, and velocity are always present. When these fluctuations interact with the natural frequencies of the propellant feed system (with and without vehicle structure) or the chamber acoustics, periodic superimposed oscillations, recognized as instability, occur. In normal rocket practice *smooth combustion* occurs when pressure fluctuations during steady operation do not exceed about $\pm 5\%$ of the mean chamber pressure. Combustion that gives greater pressure fluctuations at a chamber wall location which occur at completely random intervals is called *rough combustion*. Unstable combustion, or *combustion instability*, displays organized oscillations occurring at well-defined intervals with a pressure peak that may be maintained, may increase, or may die out. These periodic peaks, representing fairly large concentrations of vibratory energy, can be easily recognized against the random-noise background (see Fig. 9–2).

Chugging, the first type of combustion instability listed in Table 9–2, stems mostly from the elastic nature of the feed systems and structures of vehicles or the imposition of propulsion forces upon the vehicle. Chugging of an engine or thrust chamber assembly can occur in a test facility, especially with low chamber pressure engines (100 to 500 psia), because of propellant pump cavitation, gas entrapment in propellant flow, tank pressurization control fluctuations, and vibration of engine supports and propellant lines. It can be caused by resonances in the engine feed system (such as an oscillating bellows inducing a periodic flow fluctuation) or a coupling of structural and feed system frequencies.

When both the vehicle structure and the propellant liquid in the feed system have about the same natural frequency, then force coupling can occur, not only to maintain but also to strongly amplify oscillations. Propellant flow rate disturbances, usually at 10 to 50 Hz, give rise to low-frequency longitudinal combustion instability, producing a longitudinal motion of vibration in the

TABLE 9–2. Principal Types of Combustion Instability

| Type and Word Description | Frequency Range (Hz) | Cause Relationship |
|---|----------------------|--|
| Low frequency, called chugging or feed system instability | 10–400 | Linked with pressure interactions between propellant feed system, if not the entire vehicle, and combustion chamber |
| Intermediate frequency, called acoustic, ^a buzzing, or entropy waves | 400–1000 | Linked with mechanical vibrations of propulsion structure, injector manifold, flow eddies, fuel/oxidizer ratio fluctuations, and propellant feed system resonances |
| High frequency, called screaming, screeching, or squealing | Above 1000 | Linked with combustion process forces (pressure waves) and chamber acoustical resonance properties |

^aUse of the word *acoustic* stems from the fact the frequency of the oscillations is related to combustion chamber dimensions and velocity of sound in the combustion gas.

vehicle. This vehicle flight instability phenomenon has been called *pogo instability* since it is similar to pogo jumping stick motion. Pogo instabilities can occur in the large, long propellant feed lines of large vehicles such as space launch vehicles or ballistic missiles. See Refs. 9–15 to 9–17.

Avoiding objectionable engine–vehicle coupled oscillation is best accomplished at the time of initial design of the vehicle, as contrasted to applying “fixes” later as has been the case with rocket engines for the Thor, Atlas, and Titan vehicles. Analytical methods exist for understanding the vibration modes and damping tendencies of major vehicle components, including the propellant tanks, tank pressurization systems, propellant flow lines, engines, and basic vehicle structure. Figure 9–3, a simplified spring–mass model of a typical two-stage vehicle, indicates the complexity of the analytical problem. Fortunately, the vibrational characteristics of the assembly can be affected substantially by designing damping (energy absorption) into the major components or subassemblies. Techniques for damping pogo instability include the use of energy absorption devices in fluid flow lines, perforated tank liners, special tank supports, and properly designed engine, interstage, and payload support structures.

A partially gas-filled pogo accumulator has been an effective damping device; it is attached to the main propellant feed line. Such an accumulator is used in the oxidizer feed line of the Space Shuttle Main Engine (SSME) between the two oxidizer turbopumps; it can be seen in Figs. 6–1 and 6–12. The SSME fuel line does not need such a damping device because the fuel has a relatively very low density and a lower mass flow.

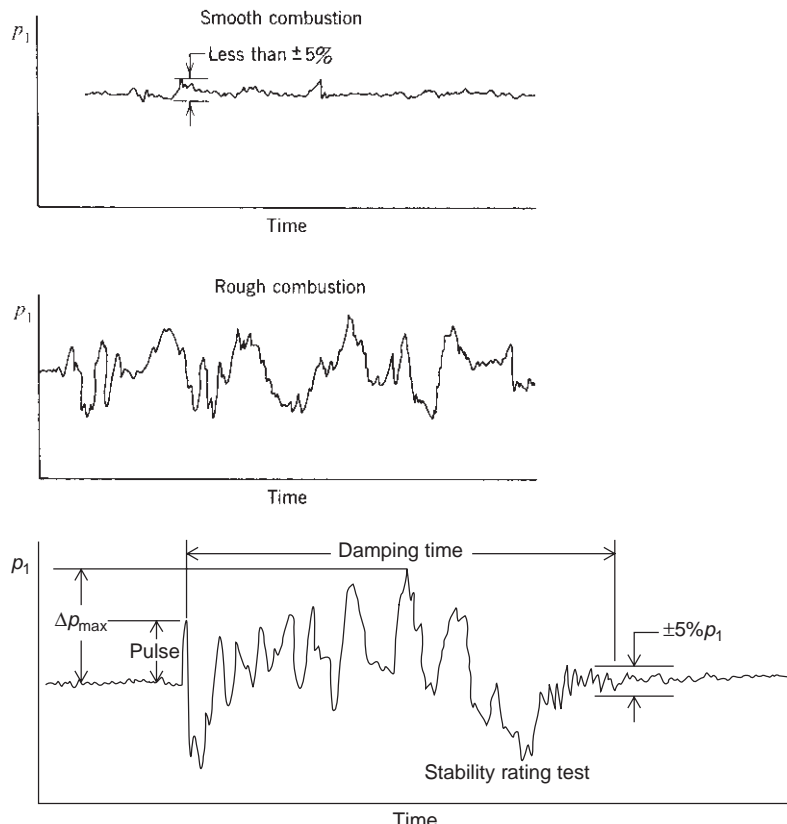


FIGURE 9-2. Typical oscillograph traces of chamber pressure p_1 with time for different combustion events.

The dynamic characteristics of a propellant pump can also have an influence on the pogo-type vibrations, as examined in Ref. 9-17. The pogo frequency will change as propellant is consumed and the remaining mass of propellant in the vehicle changes. The bending or flexing of pipes, joints or bellows, or long tanks also has an influence.

Buzzing, the intermediate type of instability, seldom represents pressure perturbations greater than 5% of the mean in the combustion chamber and usually is not accompanied by large vibratory energy. It often is more noisy and annoying than damaging, although the occurrence of buzzing may initiate high-frequency instability. Often it is characteristic of coupling between the combustion process and flow in a portion of the propellant feed system. Initiation is thought to be from the combustion process. Acoustic resonance of the combustion chamber with a critical portion of the propellant flow system, sometimes originating in a pump, promotes continuation of the phenomenon. This type of instability seems to be more prevalent in medium-size engines (2000 to 250,000 N thrust or about 500 to 60,000 lbf) than in large engines.

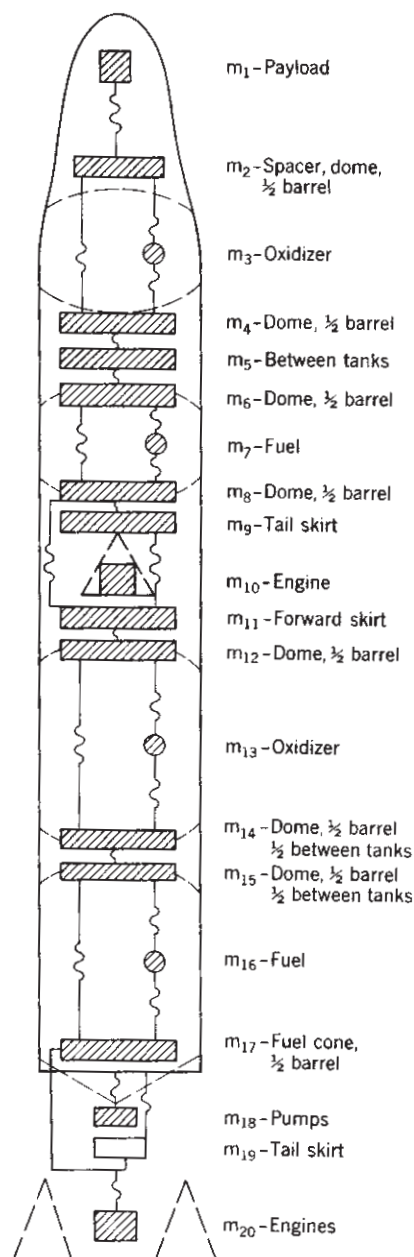


FIGURE 9–3. Typical two-stage vehicle spring–mass model used in analysis of pogo vibration in the vertical direction.

The third type, *screeching* or *screaming*, has high frequency and is most perplexing and most common in the development of new engines. Both liquid and solid propellant rockets commonly experience high-frequency instability during their development phase. Since energy content increases with frequency, this type is the most destructive, capable of destroying an engine in much less than 1 sec. Once encountered, it is the type for which it is most difficult to prove that the incorporated "fixes" or improvements render the engine "stable" under all launch and flight conditions. It can be treated as a phenomenon isolated to the combustion chamber and not generally influenced by feed system or structure.

High-frequency instability occurs in at least two modes, *longitudinal* and *transverse*. The *longitudinal mode* (sometimes called *organ pipe mode*) propagates along axial planes of the combustion chamber, and the pressure waves are reflected at the injector face and the converging nozzle cone. The *transverse modes* propagate along planes perpendicular to the chamber axis and can be broken down into *tangential* and *radial* modes. Transverse mode instability predominates in large liquid rockets, particularly in the vicinity of the injector. Figure 9-4 shows the distribution of pressure at various time intervals in a cylindrical combustion chamber (cross section) encountering transverse mode instability. Two kinds of wave form have been observed for tangential vibrations. One can be considered a *standing wave* that remains fixed in position while its pressure amplitude fluctuates. The second is a *spinning* or *traveling* tangential wave which has associated with it a rotation of the whole vibratory system. This waveform can be visualized as one in which the amplitude remains constant while the wave rotates. Combinations of transverse and longitudinal modes can also occur and their frequency can also be estimated. See Refs. 9-3 to 9-6.

Energy that drives screeching is believed to be predominantly from acoustically stimulated variations in droplet vaporization and/or mixing, local detonations, and acoustic changes in combustion rates. Thus, with favorable acoustic properties, high-frequency combustion instability, once triggered, can rapidly drive itself into a destructive mode. Invariable, a distinct boundary layer seems to disappear and heat transfer rates increase by an order of magnitude, much as with detonation, causing metal melting and wall burn-throughs, sometimes within less than 1 sec. The tangential modes appear to be the most damaging, heat transfer rates during instability often increasing 4 to 10 times. Often the instantaneous pressure peaks are about twice as high as with stable operation.

One possible source of triggering high-frequency instability is a rocket combustion phenomenon called *popping*. Popping is an undesirable random high-amplitude pressure disturbance that occurs during steady-state operation of a rocket engine with hypergolic propellants. It is a possible source for initiation of high-frequency instability. "Pops" exhibit some of the characteristics of a detonation wave. The rise time of the pressure is a few microseconds and the pressure ratio across the wave can be as high as 7:1. The elimination of popping is usually achieved by redesign of the injector rather than by the application of baffles or absorbers. They are explained later in this chapter.

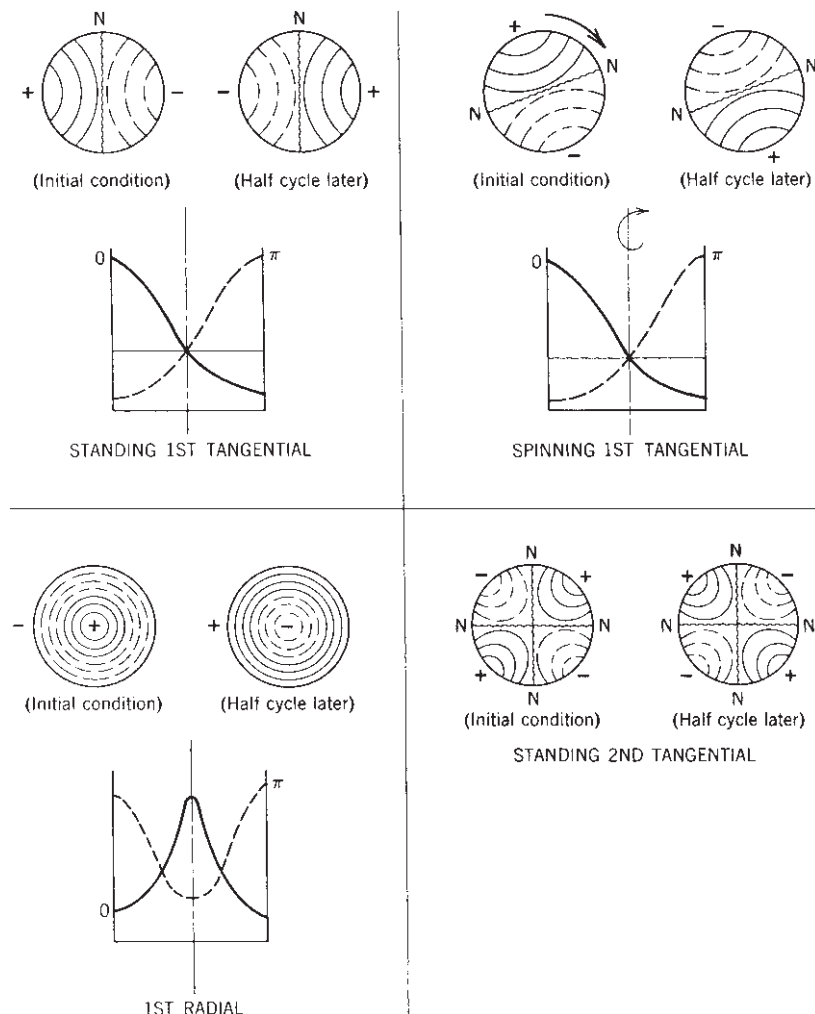


FIGURE 9-4. Simplified representation of transverse pressure oscillation modes at two time intervals in a cylindrical combustion chamber. The solid line curves indicate pressures greater than the normal or mean operating pressure and the dashed lines indicate lower pressures. The N–N lines show the node locations for these wave modes.

Some combustion instabilities can be induced by *pulsations in the liquid flow* originating in turbopumps. Unsteady liquid flow can be caused by irregular cavitation at the leading edge of the inducer impellers or of the main pump impellers (Ref. 9-18). Also, when an impeller's trailing edge passes a rib or stationary vane of the volute, a small pressure perturbation always occurs in the liquid flow that travels downstream to the injector. These two types of pressure fluctuation can be greatly amplified if they coincide with the natural frequency of combustion vibrations in the chamber.

The estimated natural frequencies can be determined from the wavelength l , or the distance traveled per cycle, and the acoustic velocity a (see Eq. 3–10). The frequency, or number of cycles per second, is

$$\text{Frequency} = a/l = (1/l)\sqrt{kTR'/\mathfrak{M}} \quad (9-1)$$

where k is the specific heat ratio, R' the universal gas constant, \mathfrak{M} the estimated molecular weight of the hot chamber gases, and T the local average absolute temperature. The length of wave travel depends on the vibrational mode, as shown in Fig. 9–4. Smaller chambers give higher frequencies.

Table 9–3 shows a list of estimated vibration frequencies for one version of the Vulcain HM 60 rocket thrust chamber; it operates with liquid hydrogen and liquid oxygen propellants at a vacuum thrust of 1008 kN, a nominal chamber pressure of 10 MPa, and a nominal mixture ratio of 5.6 (see Ref. 9–19). The data in the table are based on acoustic measurements at ambient conditions with corrections for an appropriate sonic velocity correlation; since the chamber has a shallow conical shape and no discrete converging nozzle section, the purely longitudinal vibration modes would be weak; in fact, no pure longitudinal modes were detected.

Figure 9–5 shows a series of time-sequenced diagrams of frequency–pressure–amplitude measurements taken in the oxygen injector manifold of the Vulcain HM 60 engine during the first 8 sec of a static thrust chamber test while operating at off-nominal design conditions. Chugging can be seen at low frequency (up to 500 Hz) during the first few seconds, and a natural frequency around 1500 Hz is attributed to the natural resonance frequency of the oxygen injector dome structure where the high-frequency pressure transducer was mounted. The continued oscillations observed at about 500 and 600 Hz are probably resonances associated with the feed system.

TABLE 9–3. Estimated Acoustic Hot Gas Frequencies for Nominal Chamber Operating Conditions for the Vulcain HM-60 Thrust Chamber

| Mode ^a | (L, T, R) | Frequency (Hz) | Mode ^a | (L, T, R) | Frequency (Hz) |
|-------------------|-----------|----------------|-------------------|-----------|----------------|
| T1 | (0, 1, 0) | 2424 | L1T3 | (1, 3, 0) | 6303 |
| L1T1 | (1, 1, 0) | 3579 | T4 | (0, 4, 0) | 6719 |
| T2 | (0, 2, 0) | 3856 | L2R1 | (2, 0, 1) | 7088 |
| R1 | (0, 0, 1) | 4849 | T5 | (0, 5, 0) | 8035 |
| L1T2 | (1, 2, 0) | 4987 | TR21 | (0, 2, 1) | 8335 |
| T3 | (0, 3, 0) | 5264 | R2 | (0, 0, 2) | 8774 |
| L1R1 | (1, 0, 1) | 5934 | | | |

Reprinted with AIAA permission from Ref. 9–19.

^aModes are classified as L (longitudinal), T (tangential), or R (radial), and the number refers to the first, second, or third natural frequency.

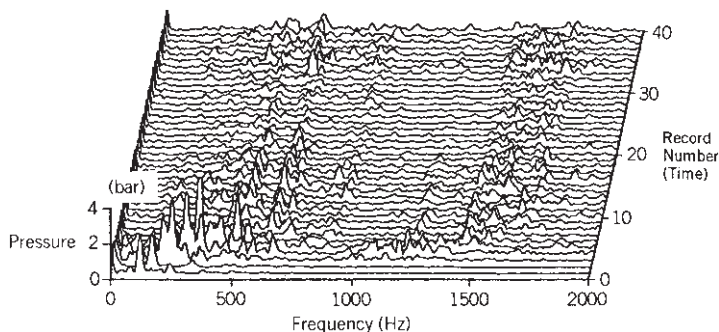


FIGURE 9-5. Graphical representation of a series of 40 superimposed frequency–amplitude diagrams taken 0.200 sec apart during the start phase (for the first 8 sec) of the Vulcain HM 60 thrust chamber. In this static hot-firing test the thrust chamber was operating at 109 bar chamber pressure and an oxidizer-to-fuel mass flow mixture ratio of 6.6. (Used with permission from Ref. 9-19.)

Rating Techniques

Semiempirical techniques exist for artificially disturbing combustion in a rocket thrust chamber during test operation and evaluating its resistance to instability (see Refs. 9-6 and 9-20). These include: (1) nondirectional “bombs” placed within the combustion chamber; (2) oriented explosive pulses from a “pulse gun” directed through the chamber sidewall; and (3) directed flows of inert gas through the sidewall into the chamber. Often heavy prototype thrust chambers are used because they are less expensive and more resistant to damage than flight-weight engines. Other techniques used less widely but which are important, especially for small engines include: (1) momentary operation at “off-mixture ratio;” (2) introduction of “slugs” of inert gas into a propellant line; and (3) a purposeful “hard start” achieved by introducing a quantity of unreacted propellant at the beginning of the operation.

The objective of these rating techniques is to measure and demonstrate the ability of an engine system to return quickly to normal or rated operation and stable combustion after the combustion process has intentionally been disturbed or perturbed.

All techniques are intended to introduce shock waves into the combustion chamber or to otherwise perturb the combustion process, affording opportunity for measuring recovery time from a predetermined overpressure disturbance, assuming stable combustion resumes. Important to the magnitude and mode of the instability are the type of explosive charge selected, the size of the charge, the location and direction of the charge, and the duration of the exciting pulse. The bottom curve in Fig. 9-2 characterizes the recovery of stable operation after a combustion chamber was “bombed.” The time interval to recover and the magnitude of explosive or perturbation pressure are then used to rate the resistance of the engine to instability.

The nondirectional bomb method and the explosive pulse-gun method are the two techniques in more common use. The bomb that can be used in large flight-weight thrust chambers without modification consists of six charges of 250 grains or 16.2 grams of explosive (PETN, RDX, or similar) encased in a Teflon, nylon, or micarta case. Detonation of the bomb is achieved either electrically or thermally. Although the pulse gun requires modification of a combustion chamber, this technique affords directional control, which is important to tangential modes of high-frequency instability and allows several data points to be observed in a single test run by installing several pulse guns on one combustion chamber. Charges most frequently used are 10, 15, 20, 40, and 80 grains of pistol powder. Pulse guns can be fired in sequence, introducing successive pressure perturbations (approximately 150 msec apart), each of increasing intensity, into the combustion chamber.

Control of Instabilities

The control or really the complete elimination of instabilities is an important task during the design and development of a rocket engine. The designer usually relies on prior experience with similar engines and tests on new experimental engines. Analytical tools are available with which to simulate and evaluate the combustion process. The design selection has to be proven in actual experiments to be free of instabilities over a wide range of transient and steady-state operating conditions. Some of the experiments can be accomplished on a subscale rocket thrust chamber that has a similar injector, but most tests have to be done on a full-scale engine.

The design features to control instabilities are different for the three types of vibrations described in Table 9–2. Chugging is usually avoided if there is no resonance in the propellant feed system or its coupling with the elastic vehicle structure. Increased injection pressure drop and the addition of artificial damping devices in the propellant feed lines have been used successfully. Chugging and acoustical instabilities sometimes relate to the natural frequency of a particular feed system component that is free to oscillate, such as a loop of piping that can vibrate an injector dome, or a bellows whose oscillations cause a pumping effect.

With the choice of the propellant combination usually fixed early in the planning of a new engine, the designer can alter combustion feedback (depressing the driving mechanism) by altering injector details (such as changing the injector hole pattern, hole sizes, or by increasing the injection pressure drop), or alternatively by increasing acoustical damping within the combustion chamber. Of the two methods, the second has been favored in recent years because it is very effective, it is better understood, and theory fits. This leads to the application of *injector face baffles*, *discrete acoustic energy absorption cavities*, and *combustion chamber liners* or *changes in injector design*, often by using a trial-and-error approach.

Injector face baffles (see Fig. 9–6) were a widely accepted design practice in the 1960s for overcoming or preventing high-frequency instability. Baffle design is predicated on the assumption that the most severe instability oscillations, along

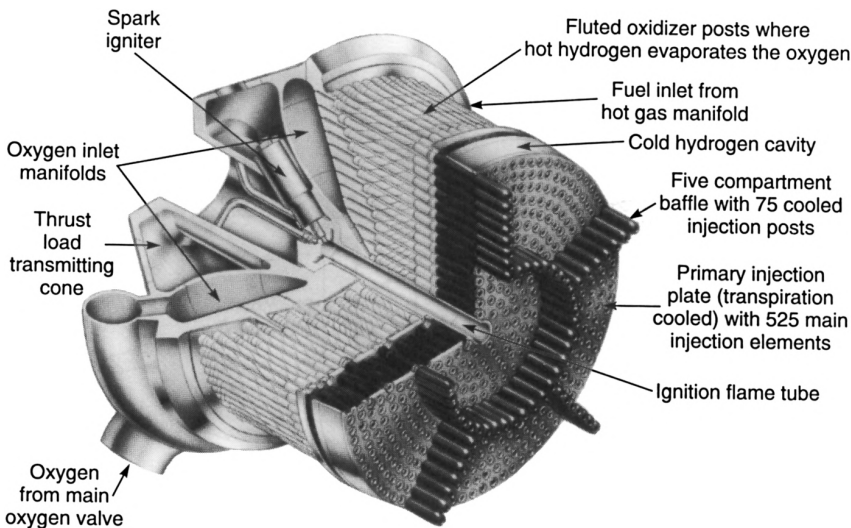


FIGURE 9–6. Main injector assembly of the Space Shuttle Main Engine showing baffle with five outer compartments. (Courtesy of Pratt & Whitney Rocketdyne.)

with the driving source, are located in or near the injector-atomization zone at the injector end of the combustion chamber. The baffles minimize influential coupling and amplification of gas dynamic forces within the chamber. Obviously, baffles must be strong, have excellent resistance to combustion temperatures (they are usually cooled by propellant), and must protrude into the chamber enough to be effective, yet not so far as to act like an individual combustion chamber with its own acoustical characteristics. The number of baffle compartments is usually odd. An even number of compartments enhances the standing modes of instability, with the baffles acting as nodal lines separating regions of relatively high and low pressure. The design and development of baffles remains largely empirical. Generally, baffles are designed to minimize acoustical frequencies below 4000 Hz, since experience has shown damaging instability is rare at frequencies above 4000 Hz.

Various mechanisms of *energy absorption* or *vibration damping* exist in a thrust chamber. Damping by wall friction in combustion chambers is not significant. The exhaust nozzle produces the main damping of longitudinal mode oscillations; the reflection of waves from the convergent nozzle entrance departs from that of an ideal closed end. The principal damping source affecting propagation in the transverse plane is combustion itself. The great volumetric change in going from liquid to burned gases and the momentum imparted to a particle (solid or liquid) both constitute damping phenomena in that they take energy from high instantaneous local pressures. Unfortunately, the combustion process can generate a great deal more pressure oscillation energy than is absorbed by its inherent damping mechanism.

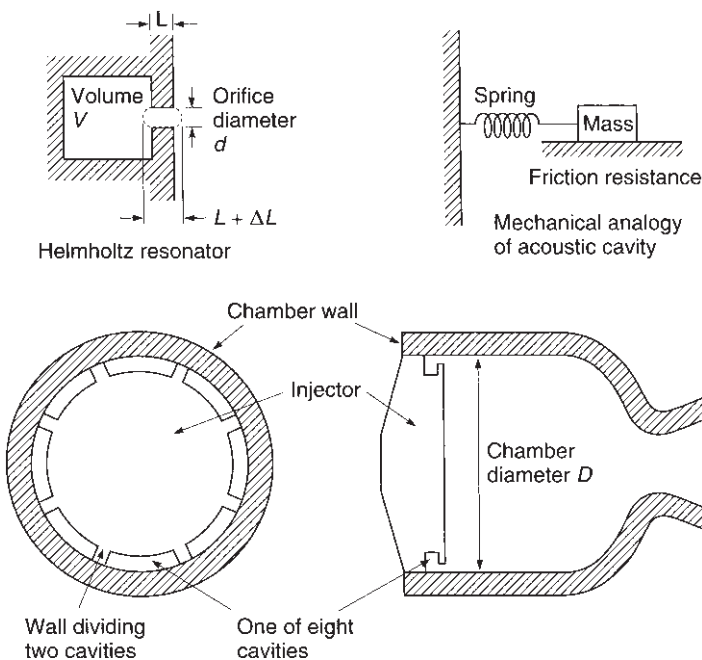


FIGURE 9-7. Diagram of acoustic energy absorber cavities at the periphery of an injector. In this thrust chamber the cavity restriction is a slot (in the shape of sections of a circular arc) and not a hole. Details of the chamber cooling channels, injector holes, or internal feed passages are not shown.

Acoustical absorbers are applied usually as discrete *cavities* along or in the wall of the combustion chamber near the injector end. Both act as a series of Helmholtz resonators that remove energy from the vibratory system which otherwise would maintain the pressure oscillations. Figure 9-7 shows the application of discrete cavities (interrupted slots) at the “corner” of the injector face. The corner location usually minimizes the fabrication problems, and it is the one location in a combustion chamber where a pressure antinode exists for all resonant modes of vibration, including longitudinal, tangential, radial, and combinations of these. Velocity oscillations are minimal at this point, which favors absorber effectiveness. Transverse modes of instability are best damped by locating absorbers at the corner location. Figure 9-7 also shows a Helmholtz resonator cavity and its working principles in simple form. Taking one resonator element, the mass of gas in the orifice with the volume of gas behind it forms an oscillatory system analogous to the spring–mass system shown (see Ref. 9-21).

Absorption cavities designed as Helmholtz resonators placed in or near the injector face offer relatively high absorption bandwidth and energy absorbed per cycle. The Helmholtz resonator (an enclosed cavity with a small passage entry) dissipates energy twice each cycle (jets are formed upon inflow and outflow). Modern design practice favors acoustic absorbers over baffles. The storable

propellant rocket engine shown in Fig. 8–2 has acoustic absorption cavities in the chamber wall at a location next to the injector.

The resonance frequency f of a Helmholtz cavity can be estimated as

$$f = \frac{a}{2\pi} \sqrt{\frac{A}{V(L + \Delta L)}} \quad (9-2)$$

Here a is the local acoustic velocity, A is the restrictor area, $A = (\pi/4)d^2$, and other symbols are as shown in Fig. 9–7. The ΔL is an empirical factor between 0.05 and 0.9L to allow for additional oscillating gas mass. It varies with the L/d ratio and the edge condition of the restricted orifice (sharp edge, rounded, chamfered). Resonators in thrust chambers are tuned or designed to perform their maximum damping at predicted frequencies.

Small changes in injector geometry or design can cause an unstable combustion to become stable and vice versa. New injectors, therefore, use the design and geometry of proven, stable prior designs with the same propellants. For example, the individual pattern of concentric tube injector elements used with gaseous hydrogen and liquid oxygen (shown in Fig. 8–4d) are likely to be more stable, if the hydrogen gas is relatively warm and the injection velocity of the hydrogen is at least 10 times larger than that of the liquid oxygen.

There are other combustion vibration remedies besides those that have already been mentioned, such as baffles or resonance cavities. This includes higher injection pressure drop, avoiding resonance with certain key engine component structures, changing critical injector dimension details, changing or modifying the propellant, or adding liners. References 9–3 and 9–6 describe several others, such as cooled flame holders, eliminating the entry of gases into the chamber during combustion, changing the locations of maximum heat release, varying critical dimensions on the injector elements, varying the number of injector elements and their distribution over the cross section of the chamber, changing the mixture ratio to be nonuniform near the face of the injector, or temporary consumable baffles, which are effective only during the start.

In summary, the designer needs to (1) use data from prior successful engines and simulation programs to establish key design features and estimate the likely resonances of the engine and its major components, (2) design the feed system and structure to avoid these resonances, (3) use a robust injector design that will provide good mixing and dispersion of propellants and be resistant to disturbances, and (4) if needed, include tuned damping devices (cavities) to overcome acoustic oscillations. To validate that a particular thrust chamber is stable, it is necessary to test it over the range of likely operating conditions without encountering instability. An analysis is needed to determine the maximum and minimum likely propellant temperatures, maximum and minimum probable chamber pressures, and the highest and lowest mixture ratios, using a propellant budget as shown in Section 11.1. These limits then establish the variations of test conditions for this test series. Because of our improved understanding, the amount of testing needed to prove stability has been reduced compared to that required 20 to 40 years ago.

PROBLEMS

1. For a particular liquid propellant thrust chamber the following data are given:

| | |
|--|--------------|
| Chamber pressure | 68 MPa |
| Chamber shape | Cylindrical |
| Internal chamber diameter | 0.270 m |
| Length of cylindrical section | 0.500 m |
| Nozzle convergent section angle | 45° |
| Throat diameter and radius of wall curvature | 0.050 m |
| Injector face | Flat |
| Average chamber gas temperature | 2800 K |
| Average chamber gas molecular weight | 20 kg/kg-mol |
| Specific heat ratio | 1.20 |

Assume the gas composition and temperature to be uniform in the cylindrical chamber section. State any other assumptions that may be needed. Determine the approximate resonance frequencies in the first longitudinal mode, radial mode, and tangential mode.

- Explain how the three frequencies from Problem 1 will change with combustion temperature, chamber pressure, chamber length, chamber diameter, and throat diameter.
- Why does heat transfer increase during combustion instability?
- Prepare a list of steps for undertaking a series of tests to validate the stability of a new pressure-fed liquid bipropellant rocket engine. State the assumptions.
- Estimate the resonant frequency of a set of each of nine cavities similar to Fig. 9-7. Here the chamber diameter $D = 0.200$ m, the slot width is 1.0 mm, and the width and height of the cavity are each 20.0 mm. The walls separating the individual cavities are 10.0 mm thick. Assume $L = 4.00$ mm, $\Delta L = 2.00$ mm, and $a = 1050$ m/sec.

REFERENCES

- R. D. Sutton, W. S. Hines, and L. P. Combs, "Development and Application of a Comprehensive Analysis of Liquid Rocket Combustion," *AIAA Journal*, Vol. 10, No. 2, February 1972, pp. 194–203.
- K. K. Kuo, *Principles of Combustion*, 2nd ed., John Wiley & Sons, Hoboken, NJ, 2005.
- V. Yang and W. Anderson (Eds.), *Liquid Rocket Engine Combustion Instability*, Vol. 169 of *Progress in Astronautics and Aeronautics*, AIAA, 1995, in particular Chapter 1, F.E.C. Culick and V. Yang, "Overview of Combustion Instabilities in Liquid Propellant Rocket Engines."
- W. Sirigano, A. Merzhanov, and L. De Luca, *Advances in Combustion Science: In Honor of Ya. B. Zel'dovich*, Progress in Astronautics and Aeronautics Series, V-173, American Institute of Aeronautics and Astronautics, 1997.
- D. T. Harrje (Ed.), "Liquid Propellant Rocket Combustion Instability," *NASA SP-194*, U.S. Government Printing Office, No. 3300–0450, 1972.
- G. P. Sutton, *History of Liquid Propellant Rocket Engines*, AIAA, 2006, Chapter 4.10 "Combustion and Vibration."

- 9–7. V. Yang, M. Habiballah, J. Hulk and M. Popp (Eds.), *Liquid Rocket Thrust Chambers: Aspects of Modeling, Analysis and Design*, Progress in Astronautics and Aeronautics (server), Vol 200, American Institute of Aeronautics and Astronautics, Reston, VA 2004.
- 9–8. B. R. Lawyer, “Photographic Observations of Reactive Stream Impingement,” *Journal of Spacecraft and Rockets*, Vol. 17, No. 2, March–April 1980, pp. 134–139.
- 9–9. M. Tanaka and W. Daimon, “Explosion Phenomena from Contact of Hypergolic Liquids,” *Journal of Propulsion and Power*, Vol. 1, No. 4, 1984, pp. 314–316.
- 9–10. R. I. Sujith, G. A. Waldherr, J. I. Jagoda, and B. T. Zinn, “Experimental Investigation of the Evaporation of Droplets in Axial Acoustic Fields,” *Journal of Propulsion and Power*, AIAA, Vol. 16, No. 2, March–April 2000, pp. 278–285.
- 9–11. P. Y. Liang, R. J. Jensen, and Y. M. Chang, “Numerical Analysis of the SSME Preburner Injector Atomization and Combustion Process,” *Journal of Propulsion and Power*, Vol. 3, No. 6, November–December 1987, pp. 508–513.
- 9–12. M. Habiballah, D. Lourme, and F. Pit, “PHEDRE—Numerical Model for Combustion Stability Studies Applied to the Ariane Viking Engine,” *Journal of Propulsion and Power*, Vol. 7, No. 3, May–June 1991, pp. 322–329.
- 9–13. M. L. Dranovsky (author), V. Yang, F. E. C. Culick, and D. G. Talley (Eds.), *Combustion Instability in Liquid Rocket Engines, Testing and Development; Practices in Russia*, Progress in Astronautics and Aeronautics, Vol. 221, AIAA, Reston, VA, 2007.
- 9–14. M. S. Natanzon and F. E. C. Culick, *Combustion Instability*, Progress in Astronautics and Aeronautics, Vol. 222, AIAA, Reston, VA, 2008.
- 9–15. B. W. Oppenheim and S. Rubin, “Advanced Pogo Analysis for Liquid Rockets,” *Journal of Spacecraft and Rockets*, Vol. 30, No. 3, May–June 1993, pp. 360–373.
- 9–16. G. About, F. Bouvert, C. Bonna, N. David, and J. C. Lemoine, “A New Approach of POGO Phenomenon Three-Dimensional Studies on the Ariane 4 Launcher,” *Acta Astronautica*, Vol. 15, Nos. 6 and 7, 1987, pp. 321–330.
- 9–17. K. W. Dotson, S. Rubin, and B. M. Sako, “Mission Specific Pogo Stability Analysis with Correlated Pump Parameters”, *Journal of Propulsion and Power*, Vol. 21, No. 4. July–August 2005, pp. 619–626.
- 9–18. T. Shimura and K. Kamijo, “Dynamic Response of the LE-5 Rocket Engine Liquid Oxygen Pump,” *Journal of Spacecraft and Rockets*, Vol. 22, No. 7, March–April 1985, pp. 195–200.
- 9–19. E. Kirner, W. Oechslein, D. Theleman, and D. Wolf, “Development Status of the Vulcain (HM 60) Thrust Chamber” AIAA Paper 90-2255, July 1990.
- 9–20. “Guidelines for Combustion Stability Specifications and Verification Procedures for Liquid Propellant Rocket Engines,” CPIA Publication 655, Chemical Propulsion Information Agency, John Hopkins University, January 1997.
- 9–21. T. L. Acker and C. E. Mitchell, “Combustion Zone–Acoustic Cavity Interactions in Rocket Combustors,” *Journal of Propulsion and Power*, Vol. 10, No 2, March–April 1994, pp. 235–243.

CHAPTER 10

TURBOPUMPS AND THEIR GAS SUPPLIES

10.1. INTRODUCTION

This is the first revised edition of this book, which has a separate chapter on turbopumps (abbreviated here as TP) and their gas supplies. A TP is a high-pressure high-precision piece of rotating high-speed power machinery usually consisting of a turbine driving one or two centrifugal propellant pumps. Its purpose is to take propellants from the vehicle's propellant tanks, raise their pressure, and deliver these propellants into the high-pressure piping system. The pressurized propellants are then fed to one or more thrust chambers, where they are burned and form hot gases. A TP is a unique key component of all larger liquid propellant rocket engines with a pumped feed system and its design, fabrication, and functions are unlike any of the other rocket engine components. This chapter discusses the various common types of TPs, outlines one design approach, describes major TP components, and mentions some of their principal design issues.

A well-designed TP delivers the intended propellant flows at the intended pump discharge pressures and mixture ratio, must have good enough reliability so that it will not malfunction or fail during the intended flight duration, and many will run at the highest practical energy efficiency of the pumps and turbines. Furthermore the TP should not stimulate or cause any significant vibration (in the engine or vehicle) or should not be adversely affected by externally caused vibrations, will function well over all operating conditions (such as different initial propellant temperatures, a range of ambient temperatures, start and stop transients, accelerations in the flight direction and other directions) at the

minimum practical inert TP mass. It is important that the pumps will not cavitate because the cavitation bubbles can reduce the steady nominal propellant flow and can cause combustion instability. Cavitation is discussed later in Section 10.5. The bearings and seals need to be adequately cooled by small secondary flows of propellant within the TP assembly to prevent their overheating and malfunctioning. There should not be any unexpected leakage in the seals and secondary flow passages within a TP; this means leaks between bipropellants, between turbine stages (gas) or pump stages (liquid), between a propellant and hot gas, or between propellant or hot gas and the outside.

The *selection of a specific TP configuration*, such as those seen later in this chapter, will depend on the propellant combination, the desired flows and pump discharge pressures, the engine cycle, the available suction pressure, the number of units to be built and delivered, and other factors. The available proven heat-resistant materials and their maximum working temperatures for turbine blades or the maximum load capacity of a bearing can influence the design selection. The best placement of a TP within a rocket engine is usually a compromise between several design considerations. For example, its inlet and outlet flanges should be placed to minimize the piping, access bearings and turbine blades for inspection on reusable engines, mounting which allows thermal expansion without high stresses, or the simplicity of the design (e.g., minimum number of TP components)—all these will influence the choice of the TP design configuration. References 10–1 to 10–5 give further information on TP selection and design.

10.2. DESCRIPTIONS OF SEVERAL TURBOPUMPS

Typical TPs can be seen in Figs. 10–1 to 10–3 and 6–10, and many key components can be identified by their callouts. Most of the part names in these figures will be discussed in subsequent paragraphs of this chapter. TPs are also seen as a component of an engine in Figs. 6–1, 6–11, 6–12, and 8–17. Figure 6–2 gives a diagram of various common feed system arrangements; many have one or more TPs. A number of different arrangements of the key TP components for several common TP assemblies are shown in Fig. 10–4. This includes different numbers of pumps and turbines, different component arrangements on TP shafts, with or without gear cases, or with and without booster pumps. All will be discussed later in this chapter. Figures 10–1 and 10–2 are experimental TPs. They were selected for this book because they clearly identify the key components. (see Ref. 10–6). Figure 10–1 shows a single-stage propellant pump; it has a screw-type axial-flow inducer impeller ahead of the main impeller, is driven by a single-stage axial-flow turbine. The hot combustion gases, which drive this turbine, are burned in a separate gas generator (or a precombustion chamber or preburner) at a mixture ratio that gives gases between 900 and 1200 K; this is sufficiently cool, so that the hot turbine hardware (blades, nozzles, manifolds, or disks) still have sufficient strength without needing forced cooling. The gases are expanded (accelerated) in an annular set of converging–diverging supersonic turbine inlet

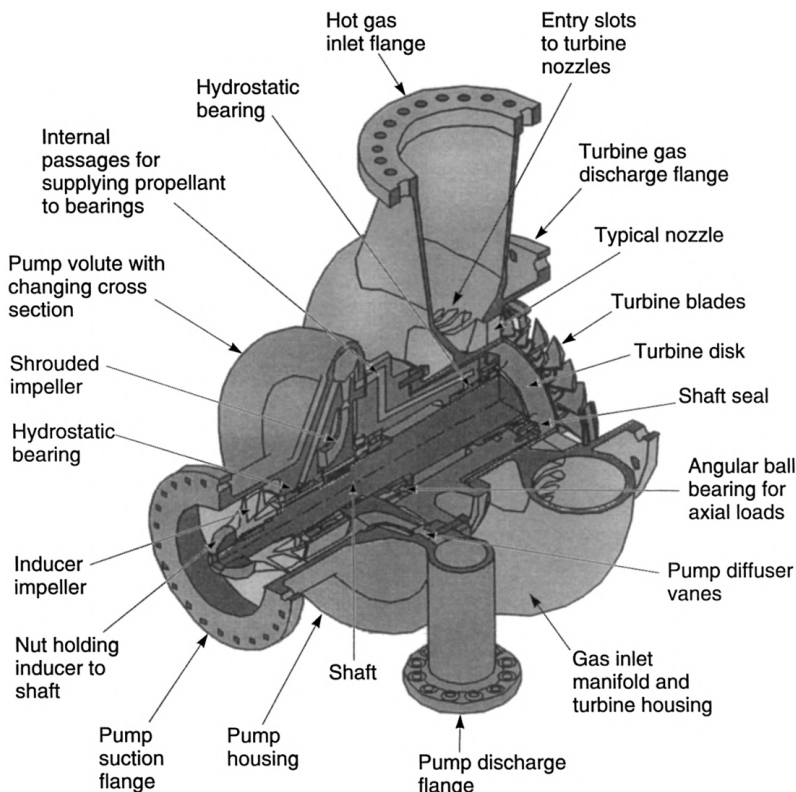


FIGURE 10–1. Cut-away view of an experimental turbopump demonstrator with a single-stage liquid oxygen pump impeller, an inducer impeller, and a single-stage turbine (one row of blades) on the same shaft. (Courtesy of Pratt & Whitney Rocketdyne.)

nozzles, which are usually cast into the cast turbine inlet housing. The gases then enter a set of rotating blades, which are mounted on a rotating wheel or turbine disk. The blades essentially remove the tangential energy of the gas flow. The exhaust gas velocity exiting from the blades is relatively low and its direction is essentially parallel to the shaft. The pump is driven by the turbine through a shaft which is supported by two experimental hydrostatic bearing. The propellant enters the pump through an *inducer*, a special impeller where the pressure of the propellant is raised only slightly (perhaps 5 to 10% of the total pressure rise). This is just enough pressure so that there will be no cavitation as the flow enters the main pump impeller. Most of the kinetic energy given to the flow by the pump impeller is converted into hydrostatic pressure in the diffusers (the diffuser vanes are not clearly visible, since they are inclined) and/or volutes of the pump. The two hydrostatic bearings support the shaft radially. All bearings and shaft seals create heat as they run. They are cooled and lubricated by small flows of propellant, which are supplied from the pump discharge through drilled passages.

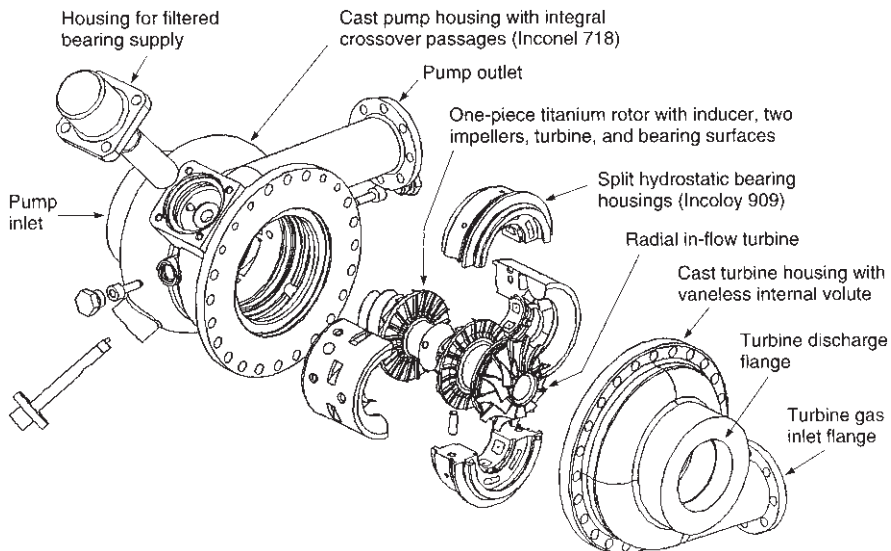


FIGURE 10–2. Exploded view of an advanced high-speed, two-stage liquid hydrogen fuel pump driven by a radial flow turbine. (Used with permission of Pratt & Whitney Rocketdyne, a part of United Technologies Corp.; adapted from Ref. 10–7.)

One bearing (near the pump) is very cold and the other is hot, since it is close to the hot turbine. The angular ball bearing accepts the axial net loads from the unbalanced hydrodynamic pressures around the shrouded impeller, the inducer, and also the turbine blades or the turbine disk.

A novel, experimental, high-speed, compact, and light weight liquid hydrogen turbopump is shown in Fig. 10–2 and in Ref. 10–6 and 10–7. It was intended to be used with an upper-stage hydrogen–oxygen rocket engine with a thrust of about 50,000 lbf (22.4 kN). The unique single-piece titanium rotor turns nominally at 166,700 rpm, has two machined sets of pump vanes, a machined inducer impeller, a set of machined radial inflow turbine blades, and radial as well as axial hydrostatic bearing surfaces. A small filtered flow of hydrogen lubricates the hydrostatic bearing surfaces. The cast pump housing has internal crossover passages between stages. The unique radial inflow turbine (3.2 in. dia.) produces about 5900 hp at an efficiency of 78%. The hydrogen pump impellers are only 3.0 in. diameter and produce a pump discharge pressure of about 4500 psi at a fuel flow of 16 lbm/sec and an efficiency of 67%. A high pump inlet pressure of about 100 psi is needed to assure cavitation-free operation. The turbopump can operate at about 50% flow (at 36% discharge pressure and 58% of rated speed). The number of pieces to be assembled is greatly reduced, compared to a more conventional turbopump, thus enhancing its inherent reliability.

The geared turbopump in Fig. 10–3 has high turbine and pump efficiencies, the rotary speed of the two-stage turbine is higher than the pump shaft speeds, and the turbine is smaller than a comparable single-shaft TP. The auxiliary power

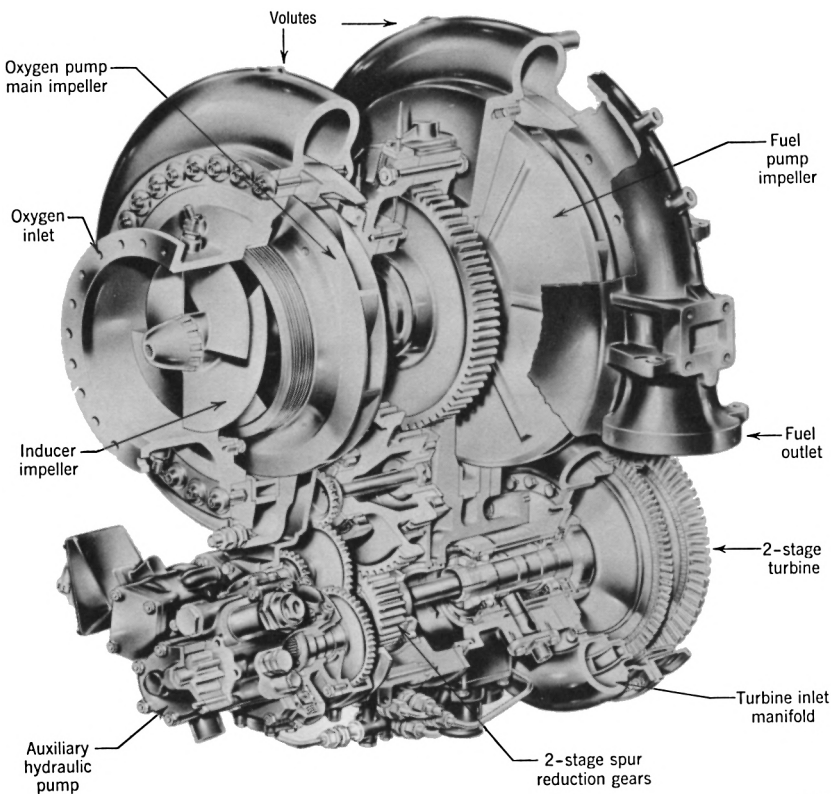


FIGURE 10–3. Typical geared turbopump assembly similar to the one used on the RS-27 engine (Delta I and II launch vehicles) with liquid oxygen and RP-1 propellants. (Courtesy of Pratt & Whitney Rocketdyne.)

package (e.g., hydraulic pump) was used in early applications. The precision ball bearings and seals on the turbine shaft can be seen, but the pump bearings and seals are not visible in this figure.

Table 10–1 gives selected data on relatively large TPs for two large LOX/LH₂ rocket engines. It shows that the main LOX pumps have single-stage impellers, while the main fuel pumps are multistage with two or three impellers in series. The Space Shuttle Main Engine (SSME) has axial-flow inducer impellers on its main pumps and also two booster pumps, which together raise the pressure of the flows going to the inlets of the respective main centrifugal pumps. The booster pump data is also listed. The Japanese LE-7 engine feed system does not use booster pumps and it features pump inducers ahead of the main impellers. The turbine blade shapes for both TPs are a combination of impulse turbines with some reaction turbines contours. These terms will be explained later.

TABLE 10–1. Turbopump Characteristics

| Engine: | Space Shuttle Main Engine ^a | | | | LE-7 ^b |
|------------------------------------|---|------------------|---------------------|-------------------|---|
| Feed System Cycle: Propellants: | Modified Staged Combustion Cycle Liquid Oxygen and Liquid Hydrogen | | | | Modified Staged Combustion Cycle Liquid Oxygen and Liquid Hydrogen |
| Pumps | | | | | |
| Designation ^c | LPOTP ^c | LPFTP | HPOTP ^c | HPFTP | HPOTP |
| Type | Axial flow | Axial flow | Dual inlet | Radial flow | Radial flow |
| No. of impeller stages | — | — | 1 + 1 ^d | 3 | 2 + 1 ^d |
| No. of aux. or inducers | 1 | 1 | — | 1 | 1 |
| Flow rate (kg/sec) | 425 | 70.4 | 509 | 70.4 | 46.7 ^d |
| Inlet pressure (MPa) | 0.6 | 0.9 | 2.70 | NA | 18.2 ^d |
| Discharge pressure (MPa) | 2.89 | 2.09 | 27.8 | 47.8 ^d | 26.7 ^d |
| Pump efficiency (%) | 68 | 75 | 72 | 75 | 78.4 ^d |
| Turbines | | | | | |
| No. of stages | 6 | 2 | 3 | 2 | Reaction-impulse |
| Type | Hydraulic LOX driven | Reaction-impulse | Reaction-impulse | Reaction-impulse | Reaction-impulse |
| Flow rate (kg/sec) | 105.5 | 264 | 756 | 1000 | 33.1 |
| Inlet temperature (K) | 26.2 | 29.0 | 32.9 | 32.9 | 20.5 |
| Inlet pressure (MPa) | NA | 1.29 | 1.54 | 1.50 | 1.43 |
| Pressure ratio | 69 | 60 | 74 | 79 | 73.2 |
| Turbine efficiency (%) | 5020 | 15,670 | 22,300 | 34,270 | 41,600 |
| Turbine speed (rpm) | 1120 | 2290 | 15,650 | 40,300 | 25,350 |
| Turbine power (kW) | LOX | only | H ₂ only | ~ 0.62 | ~ 0.88 |
| Mixture ratio, O/F | | | | | ~ 0.7 |

^aData courtesy of Pratt & Whitney Rockordyne, at flight power level of 104.5% of design thrust.

^bData courtesy of Mitsubishi Heavy Industries, Ltd.

^cLPOTP, low-pressure oxidizer turbopump; HPFTP, high-pressure fuel turbopump.

^dBoost impeller stage for oxygen flow to preburners.

10.3. SELECTION OF TURBOPUMP CONFIGURATION

The selection of the features, performance, and configuration of a specific new TP arrangement can be complex. First of all it depends on the engine requirements for the particular flight application (thrust, propellant combination, mixture ratio, chamber pressure, duration, low cost, schedule, etc.). These engine criteria have to be evaluated, weighed, and prioritized. Furthermore it depends on the engine cycle (see Section 6.6 and Fig. 6–9), propellant physical properties (such as vapor pressure, density, or viscosity), the nominal flows and pump discharge pressures (sum of chamber pressure, hydraulic losses in valves, cooling jacket, injector, and pipes), minimum practical inert TP mass, high reliability (no flight failures allowed), available suction pressure, maximum and minimum propellant and hardware initial temperatures, and the components arrangement of the assembly. It is also influenced by the size of the TP, the location of the TPs inlet and outlet flanges relative to the thrust chamber inlets and the suction pipes outlets, maximum allowable turbine gas inlet temperature (which depends on the turbine material), number of hot starts during the life time, critical speed of the rotating assembly, or the simplicity of the design (e.g., fewest number of parts). If reuse is an engine requirement, then additional factors have to be considered, such as ease of access to bearings, seals, or turbine blades for inspection of wear or cracks. With throttling of the thrust the TP has to operate efficiently over a range of speeds. There can be other TP selection criteria. Some of the preliminary selection and design criteria are explained in Refs. 10–1 to 10–3 and 10–5 and basic texts on pumps are in Refs. 10–8 and 10–9.

The *shaft speed* is related to the *TP diameter or size* and thus to the *TP mass*. The tip speed of the pump impeller blades or the speed of the turbine blades at their mean diameter can be the same at different diameters and rotational speeds. Obviously, the highest practical shaft speed gives the smallest diameter, and thus usually the lowest inert TP mass. This is often in conflict with other criteria, such as cavitation avoidance, which is likely to be more difficult if the impeller speed is increased. It will be discussed later in this section.

The *arrangements of the various key TP components* into an assembly can be an important design criteria. Figure 10–4 shows several common arrangements. The two most common are to have one turbine with two propellant pumps on the same shaft (Figs. 10–4a and 10–4b) and two smaller separate TPs, one where a turbine drives an oxidizer pump and one where another turbine drives a fuel pump (Fig. 10–4c). In Fig. 10–4a the fuel pump inlet has a shaft going through it and that will affect the suction pressure. In the TP in Fig. 10–4b the turbine requires more seals. Although not discussed here, the placement and selection of bearings and seals influences the TP selection.

Centrifugal pumps are used in all known production TPs, and these are basically constant-volume flow devices (Refs. 10–3, 10–4, 10–5, 10–8, and 10–9). If the two propellants have similar densities (say within about 40%), such as nitrogen tetroxide and UDMH or liquid oxygen and kerosene and the volume flow of oxidizer and of fuel are similar, then the same type of impeller (running

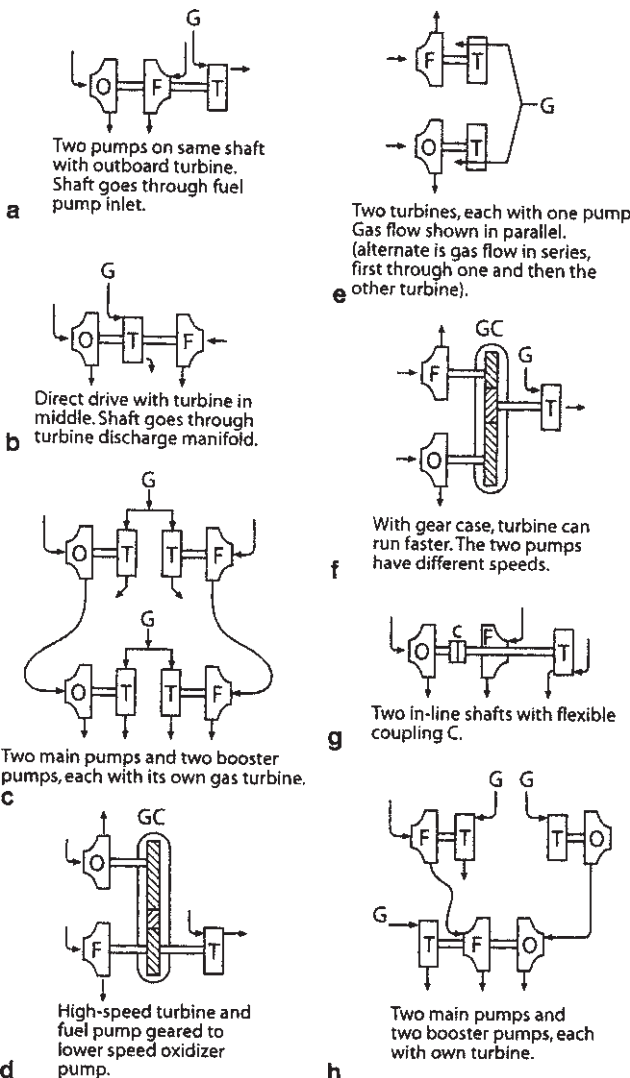


FIGURE 10–4. Simplified diagrams of several different component arrangements of turbopumps (TP); F, fuel pump; O, oxidizer pump; T, turbine; G, hot gas; C, shaft coupling; and GC, gear case. (Used with permission from Ref. 10–1.)

at the same speed) can be used on both of them on a single shaft. If the densities are quite different (e.g., liquid oxygen and liquid hydrogen), a single shaft would not be practical or efficient. Instead two separate TP's are used—rotating at high speed for the fuel pump and lower speed for the oxidizer pump—thus giving good pump efficiencies. This corresponds to Fig. 10–4e.

It is at times difficult to package a relatively large TP into an engine package. The two-TP configuration is often easier to integrate into an engine assembly,

both pumps will be able to run at a relatively high efficiency, the TP will have fewer seals, and since the shafts are shorter, they are lighter for the same shaft stiffness.

Figure 10–4g shows *two shafts, in line with each other, with a mechanical coupling* between them (Ref. 10–10). In this example the fuel pump and the turbine are on one shaft and the oxidizer pump on the other. The two shafts are connected by a flexible coupling, and this allows considerable shaft misalignment, and as a result some more generous fabrication and assembly tolerances in the TP. The first two-shaft inline TP assembly was in the German V-2 rocket engine (1938) with a six pin/sleeve type of flexible coupling. The Soviet Union developed a curvic coupling serrated sleeve as a coupling and it was smaller and lighter. References 10–1 and 10–4 show a section view of these two TPs. The United States did not produce a TP with two inline coupled shafts. When compared to a larger single shaft, the smaller spans between bearings on each of the two shafts results in substantially smaller shaft diameters, which in turn can reduce the mass of the shafts, the diameter and mass of pumps and pump housings, and the inertia of the rotary assembly and can allow some increases of the shaft speed.

Figures 10–4d and 10–4f show TPs with a *gear case* to transmit the power from the turbine to the pumps (Ref. 10–11). The purpose is to allow the turbine to run at high speed and the pumps to rotate at lower speeds, where the efficiencies are relatively high, thus minimizing the amount of gas generator propellant needed to drive the TP. Gear cases for TPs were common in the United States beginning in the early 1950s and one is still in use. In Fig. 10–4e the turbine runs at a higher speed and the two pumps run at lower, but somewhat different speeds. In Fig. 10–4f the fuel is liquid hydrogen; the fuel pump and the turbine run at a higher speed on the same shaft and the oxygen pump is geared down to a lower speed.

Figures 10–4c and 10–4h represent two arrangements for using *booster TPs* in addition to the two main TPs. See Ref. 10–12. The purpose is to reduce the vehicle's tank pressure and inert mass further, thus improving the vehicle performance. A typical booster TP provides about 10% of the propellant pressure rise and the respective main pump about 90%. Booster pumps typically use axial-flow impellers, and a few can operate with considerable cavitation in the leading edges of the booster impellers. With a booster pump the pressure at the inlet to the main pump is raised enough so cavitation does not occur in these higher pressure impellers. The low rotating speed causes the booster pumps to have a relatively large diameter. In some liquid propellant rocket engines they are larger than the main pump. Since pressures in booster pumps are low, the walls are thin, and the booster pump inert mass can be low. Most of the turbines of booster TPs are driven by gas expansion, but some are powered by high-pressure liquid propellant taken from the discharge of the main pump. The total number worldwide of rocket engines with booster pumps is small, perhaps a dozen. Booster pumps provide low suction pressure and good cavitation resistance to the main pumps of the engines, but the engines are more complex and more costly.

Bearings and seals will be overloaded or fail if the shaft deflects (even by a small amount like 0.001 in. in some TPs). See Refs. 10–13 and 10–14. In order to

minimize *deflection of the shaft*, the shaft has to be stiff (less deflection for a given side load) and that means large in diameter and heavy. The rotating assembly (turbine, pumps, seals, bearings) has to be carefully balanced. An unbalance causes a side load (which can be substantial at high rotational speed) and a deflection of the shaft. Both accurate static and dynamic balances are usually required during assembly. The operating speed of the rotating assembly is never chosen to be the same as the *resonant or critical shaft speed*, where deflections can become very high and the bearings, seals, or even the shaft can fail. The *synchronous or critical speed* is usually well above the operating speed. A stiffer shaft (larger diameter, heavier, a shorter distance between bearings, and less overhang beyond the bearing) gives a higher critical speed and allows the pumps to run at higher speed, which allows a lighter TP assembly. There are some TP where the operating speed is actually above the critical speed. Here the shaft momentarily goes through the critical speed during startup and shutdown.

There are usually several *secondary flow passages* in a TP. A bearing, rotating shaft seal, or impeller wear ring are all usually cooled and/or lubricated with a very small flow of propellant, which is heated in the process and can then be fed back to the suction side of a pump or dumped overboard. It requires a set of small external tubes or internal passages in the TP assembly to route several small flows for achieving this cooling and lubrication of rubbing surfaces. There is a good number of seals and bearings that need a small propellant supply and the distribution system for this propellant can be complex; some routes have to be throttled to the desired small flow, and a mixing of unlike propellants has to be avoided. The analysis of these secondary flow passages can be tedious. If a bearing or seal is close to a turbine, they will get warm (needs more coolant) and if they are pumping a cryogenic propellant, the adjacent hardware will become very cold. The clearances of these bearings or seals have to be so designed that the intended clearance is correct at the operating conditions.

Bubbles in the flow of propellant are indeed unwanted. They can be introduced into the propellant feed pipes by extensive *cavitation* in the pumps, (see Refs. 10–4 and 10–9) by leaks in low-pressure suction piping, or by improper priming or filling of the propellant lines before or during start. Bubbles reduce the effective density of the propellant, which in turn reduces the mass flow and the mixture ratio and usually reduces the thrust level somewhat below the nominal value. If the intended operating mixture ratio was fuel rich and bubbles were to reduce the fuel flow, this mixture ratio will approach a stoichiometric value; this creates a very hot gas and would most likely cause a failure of the cooling jacket in less than a second. A major concern with bubbles is that they can readily trigger combustion instability (see Chapter 9), which often leads to thrust chamber failure. The key design objectives are to select a high enough shaft speed (which gives the smallest and lightest TP, but is still not prone to cavitation), a low enough pump suction pressure (which gives the lightest vehicle tank mass, but this promotes pump cavitation), and an impeller configuration, which will be strong and efficient and prevent dangerous cavitation under all operating conditions.

A *balance of axial fluid pressure forces* within the TP rotating assembly and its housings is necessary to prevent excessive axial hydraulic pressure forces

(on surfaces normal to the shaft) from overloading certain parts of the assembly (Refs. 10–1 and 10–15). Unbalance would cause a small axial movement of the rotating assembly (typically just a few thousands of an inch) and often intense rubbing of stationary and rotating parts. These pressure forces are created by the fluids flowing through the pump paths (increasing pressures) and the turbine gases flowing through moving and stationary sets of turbine blades (decreasing pressures), and by the radial placement of wear rings or seals. Some turbopumps have balancing pistons and some use the fluid pressures on the back side of an impeller or turbine disk to make an effective balance piston. Pressure on the piston is controlled by a slight axial movement, which changes clearances at the edge of the piston. During the transient operations (start, stop, change thrust), there typically are brief periods of unbalance caused by changes in the pressure distributions of the internal flows, but they are of short duration. Nevertheless there can be some rubbing or axial contact of a rotating and a stationery surface normal to the shaft during the brief periods of unbalance. If the axial rubbing contact persists, there will be some damage to the TP.

10.4. FLOW, SHAFT SPEEDS, POWER, AND PRESSURE BALANCES

The design of a TP requires the careful balancing of the propellant flows, the shaft speeds, and the power between the key pumps and turbines and the pressure distribution of the propellant along its flow paths. For a TP with two pumps and a gear transmission, the shaft speeds can be written as in Eq. 10–1. The relationship between shaft speeds, torques, and power can readily be seen by reviewing a flow diagram of a TP such as Fig. 1–4. With a gear case the relation between shaft speeds can be written as

$$N_t = a_o N_o = a_f N_f \quad (10-1)$$

Here N is the shaft speed, the subscripts t, f , and o stand for turbine, fuel pump, and oxidizer pump, respectively. The a_o and a_f are the gear ratios for the oxidizer and fuel pumps. When there are no gears, then a_o and a_f become 1.0. For a TP similar to Fig. 10–4a and 10–4b:

$$N_t = N_f = N_o \quad \text{and} \quad L_t = L_o + L_f + L_b \quad (10-2)$$

Here L_b is the torque to overcome friction in bearings, seals, or auxiliaries. For a TP as in Figs. 10–4a and 10–4b, the power of the turbine P_t has to equal the sum of the powers of the pumps plus some losses. This power balance can also be expressed as the product of the torque L and the speed N :

$$P_t = \sum P_p + P_b \quad (10-3)$$

$$P_t = L_t N_t = L_f N_f + L_o N_o + P_b \quad (10-4)$$

Here P_b is the power for overcoming the friction in all the bearings and seals, and in some TP configurations also the power loss in gears, and auxiliaries (such as an oil pump for lubricating gears). The power P_b used in bearing, seals, and auxiliaries is usually small.

For the two separated TP scheme in Fig. 10–4e each of the TPs has its own internal losses. It is obvious that the speeds N and the power P and even the torques L must balance in this configuration:

$$(N_t)_o = (N_p)_o \quad \text{and} \quad (N_t)_f = (N_p)_f \quad (10-5)$$

$$(P_t)_o = (P_p)_o + (P_b)_o \quad \text{and} \quad (P_t)_f = (P_p)_f + (P_b)_f \quad (10-6)$$

The subscripts t and p stand for turbine and pump. The pressure balance equation for the fuel line (the oxidizer line is the same) at a point just past the fuel pump discharge flange can be written as

$$\begin{aligned} (p_f)_d &= (p_f)_s + (\Delta p_f)_{\text{pump}} & (10-7) \\ &= (\Delta p)_{\text{main fuel system}} + p_1 \\ &= (\Delta p)_{\text{gas generator fuel system}} + p_{gg} \end{aligned}$$

Here the fuel pump discharge pressure $(p_f)_d$ equals the fuel pump suction pressure $(\Delta p_p)_s$ plus the pressure rise across the pump $(\Delta p)_{\text{pump}}$. This discharge pressure in turn has to equal the chamber pressure p_1 plus all the pressure drops in the high-pressure main fuel flow system downstream of the pump and upstream of the chamber. This usually includes the pressure losses in the cooling jacket, the injector, the piping, and the open fuel valve. This pump discharge pressure furthermore has to equal the gas generator combustion pressure p_{gg} and all the pressure losses between the fuel pump discharge and the gas generator combustion chamber. A similar pressure balance is needed for the oxidizer systems.

The fourth type of balance is different from the other three (flow, pressure, and power balance); it is aimed at preventing certain high-pressure *axial hydraulic loads* and/or *axial gas pressure loads* from causing damage inside the TP assembly. See Refs. 10–1, 10–4, and 10–15. These axial internal loads (side forces on impellers or turbine disks) can be very high, particularly in large sized TPs. Certain ball bearings are capable of withstanding considerable axial loads, in addition to the usual radial loads. The axial movement of the rotating assembly is limited by design and is very small. This method of controlling axial forces with a ball bearing is used in many TPs, but usually the maximum axial load of ball bearings is limited; therefore it is used mostly with small-diameter TPs or low-pressure TPs. A balance of axial fluid pressure forces within a large TP rotating assembly and its large stationary housing assembly can be accomplished by balance pistons. Some TPs have balancing pistons and some use the fluid pressures on the back side of an impeller or turbine disk to make an effective balance piston. Otherwise it would cause undesirable rubbing of certain parts of the rotating TP assembly with parts of the stationary TP housing assembly.

Unbalanced large high-pressure loads cause a very small axial movement of the rotating assembly (typically just 0.001 to 0.003 inch) and the balancing mechanism can be usually designed to prevent further axial movement and intense rubbing of stationary and rotating parts. Pressure on the balance piston is controlled by a slight axial movement, which changes the circular clearances at the edge of the piston, and the rotating assembly is kept from moving more than a couple of thousands of an inch. During the transient operations (start, stop, change thrust) there typically are brief periods of unbalance caused by changes in the pressure distributions on the internal surfaces normal to the shaft, but they are of short duration. Nevertheless there can be some rubbing or axial contact of a rotating and a stationery surface normal to the shaft during the brief periods of unbalance. If the axial rubbing contact persists, there will usually be some damage to the TP.

A phenomena characteristic of rotating machinery is the relative displacement and very small movement of the center of the rotating shaft within the confinement of small clearances of a fixed sleeve bearing; this is known as whirl. Reference 10–16 describes a condition where the relative small movement of the shaft's center is synchronous or the same as the rotation movement of the shaft itself (revolutions per unit time).

The above equations relate to the steady-state operating condition. The *transient and dynamic conditions* are important and many have been analyzed using iterative procedures and digital computers. Many have been tested, as shown in Ref. 10–17. They are the start, stop, and thrust change. For example, the transient starting condition includes the tank pressurization, the filling of pipes, pumps, or manifolds with liquid propellants, the filling of turbines and their manifolds with heated gas, ignition of gas generators, or thrust buildup. However, no detailed discussion of these transient conditions will be given in this book. These dynamic conditions can be complex, are related to the combustion behavior, and are sometimes difficult to analyze. Each major rocket propulsion organization has developed some method for analyzing these transients and they are often specific to specific engines or specific organizations. A similar yet simpler and different transient analysis of flows and pressure drops is usually performed for engines with a pressurized gas feed system.

10.5. PUMPS

Classification and Description

The *centrifugal pump* is generally considered the most suitable for pumping propellant in medium-sized and large rocket units. For the large flows and high pressures involved, they are efficient as well as economical in terms of mass and space requirement.

Figure 10–5 is a simplified schematic drawing of a centrifugal pump. Fluid entering the *impeller*, which is essentially a wheel with spiral curved vanes rotating within a *casing*, is accelerated within the impeller channels and leaves the

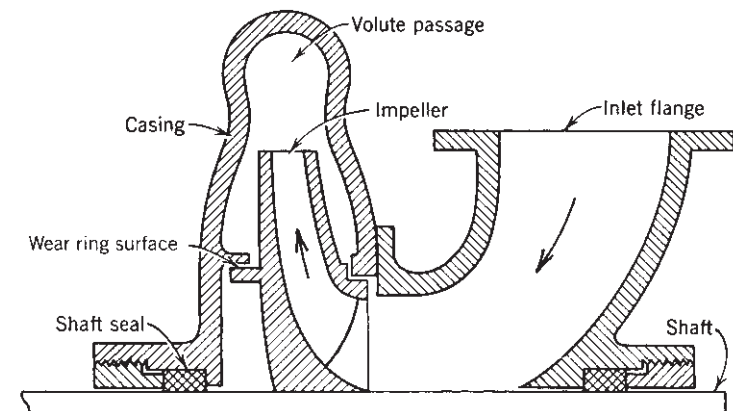


FIGURE 10–5. Simplified schematic half cross section of a typical centrifugal pump.

impeller periphery with a high velocity to enter the *volute*, or collector, and thereafter the *diffuser*, where conversion from kinetic energy (velocity) to potential energy (pressure) takes place. In some pumps the curved diffuser vanes are upstream of the collector. The three-dimensional hydraulic design of impeller vanes, diffuser vanes, and volute passages can be accomplished by computer programs to give high efficiency and adequate strength. Internal leakage, or circulation between the high-pressure (discharge) side and the low-pressure (suction) side of an impeller, is held to a minimum by maintaining close clearances between the rotating and stationary parts at the *seals* or *wear ring surfaces*. External leakage along the shaft is minimized or prevented by the use of a *shaft seal*. Single-stage pumps (one impeller only) are stress limited in the pressure rise they can impart to the liquid, and multiple-stage pumps are therefore needed for high pump head,* such as with liquid hydrogen. References 10–2, 10–5, 10–8, 10–9, and 10–17 give information on different pumps. There is a free passage of flow through the pump at all times, and no positive means for shutoff are provided. The pump characteristics, that is, the pressure rise, flow, and efficiency, are functions of the pump speed, the impeller, the vane shape, and the casing configuration. Figure 10–6 shows a typical set of curves for centrifugal pumps. The negative slope on the head versus flow curve indicates a stable pump behavior. Reference 10–7 describes the development of a smaller turbopump and the testing of a spiral high-speed first-stage impeller, called an inducer.

A *shrouded impeller* has a shroud or cover (in the shape of a surface of revolution) on top of the vanes as shown in Figs. 10–1, 10–3, and 10–5. This type usually has higher stresses and lower leakage around the impeller. In an

**Pump head* means the difference between pump discharge and pump suction head. Its units are meters or feet. The head is the height of a column of liquid with equivalent pressure at its bottom. The conversion from pounds per square inch into feet of head is: $(X) \text{ psi} = 144 (X)/\text{density} (\text{lb}/\text{ft}^3)$. To convert Pascals (N/m^2) of pressure into column height (m), divide by the density (kg/m^3) and g_0 (9.806 m/sec^2).

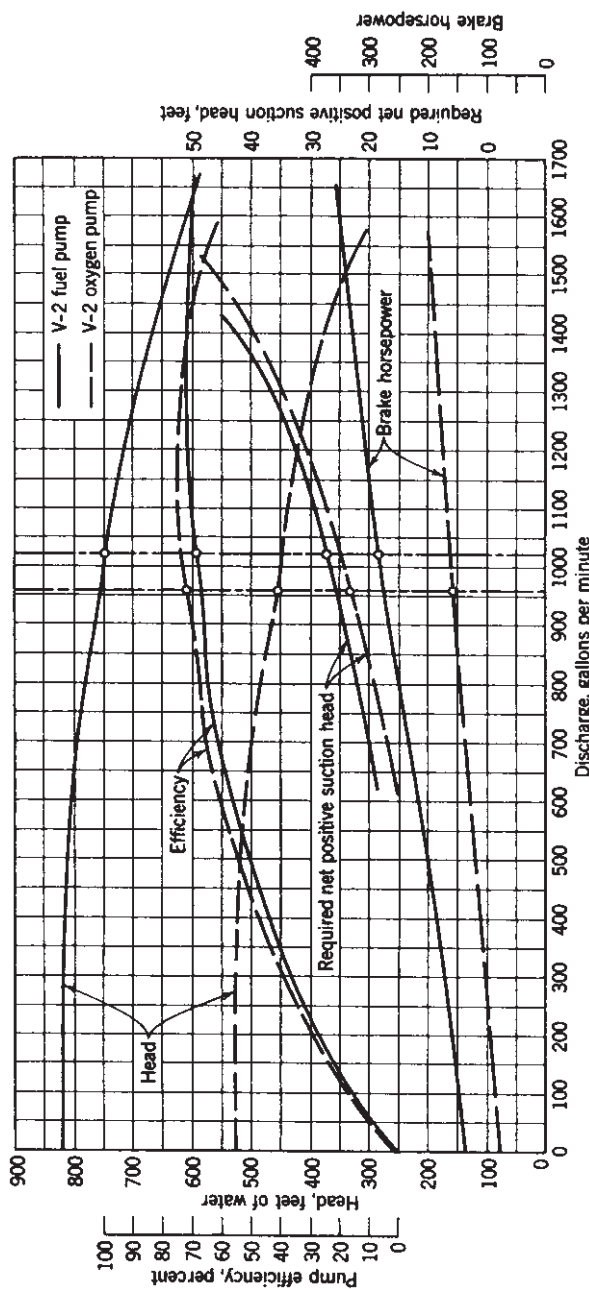


FIGURE 10-6. Water test performance curves of the centrifugal pumps of the German V-2 rocket engine. The propellants are 75% ethyl alcohol and liquid oxygen.

unshrouded impeller or turbine the vanes are not covered as seen in the turbine vanes in Fig. 10–2.

Pump Parameters

This section outlines some of the important parameters and features that have to be considered in the design of rocket propellant centrifugal pumps under steady-flow conditions.

The *required pump flow* is established by the rocket engine design for a given thrust, effective exhaust velocity, propellant densities, and mixture ratio. In addition to the flow required by the thrust chamber, the propellant consumption of the gas generator, and in some designs also a bypass around the turbine and auxiliaries have to be considered in determining the pump flows. The required *pump discharge pressure* is determined from the chamber pressure and the hydraulic losses in valves, lines, cooling jacket, and injectors (see Eq. 10–7). To obtain the rated flow at the rated pressure, an additional adjustable pressure drop for a control valve or orifice is usually included which permits a calibration adjustment or change in the required feed pressure. A regulation of the pump speed can also change the required adjustable pressure drop. As described in Section 11.5, this adjustment of head and flow is necessary to allow for hydraulic and performance tolerances on pumps, valves, injectors, propellant density, and so on.

It is possible to predict the *pump performance at various speeds* if the performance is known at any given speed. Because the fluid velocity in a given pump is proportional to the pump speed N , the flow quantity or discharge Q is also proportional to the speed and the head H is proportional to the square of the speed. This gives the following relations:

$$\begin{aligned} Q(\text{flow}) &\sim N \text{ (rpm or rad/sec)} \\ H(\text{pump head}) &\sim N^2 \\ P(\text{pump power}) &\sim N^3 \end{aligned} \quad (10-8)$$

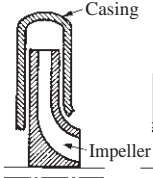
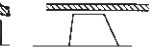
From these relations it is possible to derive a parameter called the *specific speed* N_s . It is a dimensionless number derived from a dimensional analysis of pump parameters as shown in Ref. 10–8.

$$N_s = N \sqrt{Q_e} / (g_0 \Delta H_e)^{3/4} \quad (10-9)$$

Any set of consistent units will satisfy the equation: for example, N in radians per second, Q in m^3/sec , g_0 as 9.8m/sec^2 , and H in meters. The subscript e refers to the *maximum efficiency condition*. In U.S. pump practice it has become the custom to delete g_0 , express N in rpm, and Q in gallons per minute or ft^3/sec . Much of the existing U.S. pump data is in these units. This leads to a modified form of Eq. 10–2, where N_s is not dimensionless, namely

$$N_s = 21.2N \sqrt{Q_e} / (\Delta H_e)^{3/4} \quad (10-10)$$

TABLE 10-2. Pump Types

| | Impeller type | | | | |
|-------------------------------|---|---|---|---|---|
| | Radial | Francis | Mixed Flow | Near Axial | Axial |
| Basic shape (half section) |  |  |  |  |  |
| Specific speed N_s | | | | | |
| U.S. nomenclature | 500–1000 | 1000–2000 | 2000–3000 | 3000–6000 | Above 8000 |
| SI consistent units | 0.2–0.3 | 0.4 | 0.6–0.8 | 1.0–2.0 | Above 2.5 |
| Efficiency % | 50–80 | 60–90 | 70–92 | 76–88 | 75–82 |

Adapted from Ref. 10-8.

The factor 21.2 applies when N is in rpm, Q is in ft^3/sec , and H is in feet. For each range of specific speed, a certain shape and impeller geometry has proved most efficient, as shown in Table 10-2. Because of the low density, hydrogen can be pumped effectively by axial-flow devices.

The *impeller tip speed* in centrifugal pumps is limited by design and material strength considerations to about 200 to 450 m/sec or roughly 655 to 1475 ft/sec. With titanium (lower density than steel) and machined unshrouded impellers a tip speed of over 2150 ft/sec is now possible and used on the pump shown in Fig. 10-2. For cast impellers this limiting value is lower than for machined impellers. This maximum impeller tip speed determines the maximum head that can be obtained from a single stage. The impeller vane tip speed u is the product of the shaft speed, expressed in radians per second, and the impeller radius and is related to the pump head ΔH by

$$u = \psi \sqrt{2g_0 \Delta H} \quad (10-11)$$

where the velocity factor ψ has values between 0.90 and 1.10 for different designs. For many pumps, $\psi = 1.0$.

The volume flow Q defines the impeller inlet and outlet areas according to the equation of continuity. The diameters obtained from this equation should be in the proportion indicated by the diagrams for a given specific speed in Table 10-2. The continuity equation for an incompressible liquid is

$$Q = A_1 v_1 = A_2 v_2 \quad (10-12)$$

where the subscripts refer to the impeller inlet and outlet sections, all areas A being measured normal to their respective flow velocity v . The inlet velocity v_1 ranges usually between 2 and 6 m/sec or 6.5 to 20 ft/sec and the outlet velocity

v_2 between 3 and 15 m/sec or 10 to 47 ft/sec. For a compressible liquid, such as liquid hydrogen, the density ρ will change with pressure. The continuity equation then is in terms of mass flow in

$$\dot{m} = A_1 v_1 \rho_1 = A_2 v_2 \rho_2 \quad (10-13)$$

The head developed by the pump will then also depend on the change in density.

The pump performance is limited by *cavitation*, a phenomenon that occurs when the static pressure at any point in a fluid flow passage becomes less than the fluid's vapor pressure. Cavitation is discussed in Refs. 10-1 to 10-5, 10-8, 10-9, and 10-17. The formation of vapor bubbles in the low-pressure regions causes cavitation. These bubbles collapse when they reach a region of higher pressure, that is, when the static pressure in the fluid is above the vapor pressure. In centrifugal pumps cavitation is most likely to occur behind the leading edge of the pump impeller vane at the inlet because this is the point at which the lowest absolute pressure is encountered. The excessive formation of vapor causes the pump discharge mass flow to diminish and fluctuate and can reduce the thrust and make the combustion erratic and dangerous.

When the bubbles travel along the pump impeller surface from the low-pressure region (where they are formed) to the downstream higher-pressure region, the bubbles collapse. The sudden collapses create local high-pressure pulses that have caused excessive stresses in the metal at the impeller surface. In most rocket applications this cavitation erosion is not as serious as in water or chemical pumps because the cumulative duration is relatively short and the erosion of metal on the impeller is not usually extensive. However, it has been a concern with some test facility transfer pumps.

The *required suction head* $(H_s)_R$ is the limit value of the head at the pump inlet (above the local vapor pressure); below this value cavitation in the impeller may occur. It is a function of the pump and impeller design and its value increases with flow as can be seen in Fig. 10-6. To avoid cavitation the *suction head* above the vapor pressure *required* by the pump $(H_s)_R$ must always be *less* than the *available* or *net positive suction head* furnished by the line up to the pump $(H_s)_A$, that is, $(H_s)_R \leq (H_s)_A$. The required suction head above vapor pressure can be determined from the suction specific speed S :

$$S = 21.2N\sqrt{Q_e}/(H_s)_R^{3/4} \quad (10-14)$$

The suction specific speed S depends on the quality of design and the specific speed N_s , as shown in Table 10-2. The suction specific speed S has a value between 5000 and 60,000 when using ft-lbf units. For pumps with poor suction characteristics it has values near 5000, for the best pump designs without cavitation it has values near 10,000 and 25,000, and for pumps with limited and controllable local cavitation it has values above 40,000. In Eq. 10-14 the required suction head $(H_s)_R$ is usually defined as the critical suction head at which the developed pump discharge head has been diminished arbitrarily by

2% in a pump test with increasing throttling in the suction side. Turbopump development has, over the last several decades, led to impeller designs which can operate successfully with considerably more cavitation than the arbitrary and commonly accepted 2% head loss limit. Inducers are now designed to run stably with extensive vapor bubbles near the leading edge of their vanes, but these bubbles collapse at the trailing end of these vanes. Inducers now can have S values above 80,000. A discussion of one method for the design of impeller blades can be found in Ref. 10-8.

The head that is available at the pump suction flange is called the *net positive suction head* or *available suction head above vapor pressure* ($H_s)_A$. It is an absolute head value determined from the tank pressure (the absolute gas pressure in the tank above the liquid level), the elevation of the propellant level above the pump inlet, diminished by the friction losses in the line between tank and pump, and the vapor pressure of the fluid. When the flying vehicle is undergoing accelerations, the head due to elevation must be corrected accordingly. These various heads are defined in Fig. 10-7. The net positive suction head ($H_s)_A$ is often abbreviated as NPSH and is the maximum head available for suppressing cavitation at the inlet to the pumps:

$$(H_s)_A = H_{\text{tank}} + H_{\text{elevation}} - H_{\text{friction}} - H_{\text{vapor}} \quad (10-15)$$

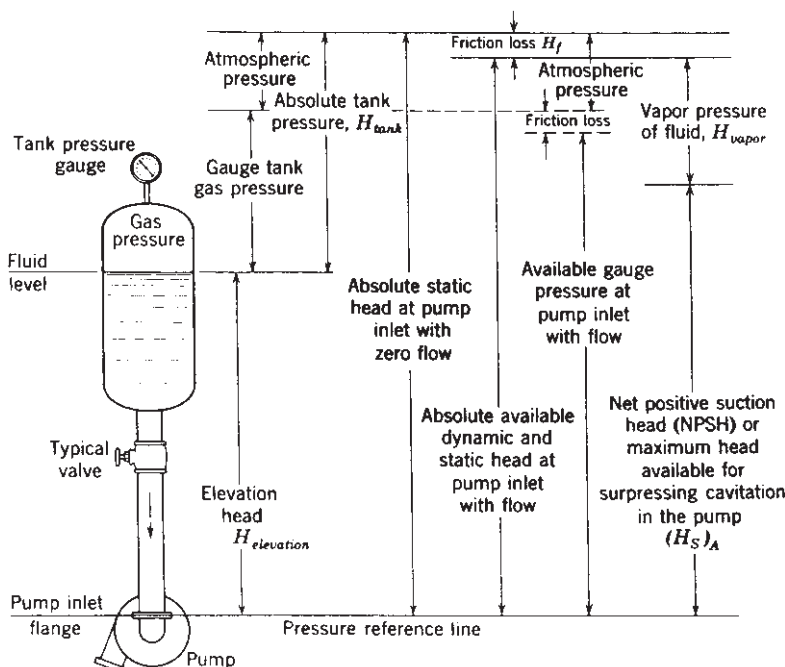


FIGURE 10-7. Definition of pump suction head.

To avoid pump cavitation, $(H_s)_A$ has to be higher than $(H_s)_R$. If additional head is required by the pump, the propellant may have to be pressurized by external means, such as by the addition of another pump in series (called a booster pump) or by gas pressurization of the propellant tanks. This latter method requires thicker tank walls and, therefore, heavier tanks, and a bigger gas-pressurizing system. For example, the oxygen tank of the German V-2 was pressurized to 2.3 atm, partly to avoid pump cavitation. For a given value of $(H_s)_A$, propellants with high vapor pressure require correspondingly higher tank pressures and heavier inert tank masses. For a given available suction head $(H_s)_A$, a pump with a low required suction pressure usually permits designs with high shaft speeds, small diameter, and low pump inert mass. A small value of $(H_s)_R$ is desirable because it may permit a reduction of the requirements for tank pressurization and, therefore, a lower inert tank mass. The value of $(H_s)_R$ will be small if the impeller and fluid passages are well designed and if the shaft speed N is low. A very low shaft speed, however, requires a large-diameter pump, which will be excessively heavy. The trend in selecting centrifugal pumps for rocket application has been to select the highest shaft speed that gives a pump with a low value of $(H_s)_R$, does not require excessive tank pressurization or other design complications, and thereby permits relatively lightweight pump design. This places a premium on pumps with good suction characteristics.

There have been some low-thrust, low-flow, experimental engines that have used positive displacement pumps, such as diaphragm pumps, piston pumps, or rotary displacement pumps (gear and vane pumps). For low values of specific speed N_S these pumps have much better efficiencies, but their discharge pressures fluctuate with each stroke and they are noisy.

One method to provide a lightweight turbopump with low vehicle tank pressure is to use an *inducer*, which is a special pump impeller usually on the same shaft and rotating at the same speed as the main impeller. It has a low head rise and therefore a relatively high specific speed. Inducer impellers are immediately upstream of the main impeller. They are basically axial-flow pumps with a spiral impeller, and many will operate under slightly cavitating conditions. The inducer stage's head rise (typically, 2 to 10% of the total pump head) has to be just large enough to suppress cavitation in the main pump impeller; this allows a smaller, lighter, higher-speed main pump. Figures 10–2 and 10–8 and Reference 10–18 show inducers. Reference 10–19 describes the testing of a pump with an inducer. Most TPs today have inducers.

Influence of Propellants

For the same power and mass flow, the pump head is inversely proportional to the propellant density. Since pumps are basically constant-volume flow machines, the propellant with the highest density requires less head, less power, and thus allows a smaller pump assembly.

Because many of the propellants are dangerous to handle, special provisions have to be made to prevent any leakage through the shaft seals. With

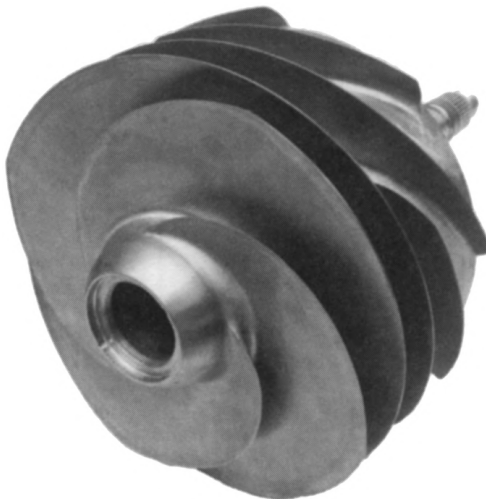


FIGURE 10–8. Fuel pump inducer impeller of the Space Shuttle main engine low-pressure fuel turbopump. It has a diameter about 10 in., a nominal hydrogen flow of 148.6 lbm/sec, a suction pressure of 30 psi, a discharge pressure of 280 psi at 15,765 rpm, an efficiency of 77%, and a suction specific speed of 39,000 when tested with water. (Courtesy of Pratt & Whitney Rocketdyne.)

spontaneously ignitable propellants the leakages can lead to fires in the pump compartment and may cause explosions. Multiple seals are often used with a drainage provision that safely removes or disposes of any propellants that flow past the first seal. Inert-gas purges of seals have also been used to remove hazardous propellant vapors. The sealing of corrosive propellants puts very severe requirements on the sealing materials and design. With cryogenic propellants the pump bearings are usually lubricated by the propellant, since lubricating oil would freeze at the low pump hardware temperature.

Centrifugal pumps should operate at the highest possible *pump efficiency*. This efficiency increases with the volume flow rate and reaches a maximum value of about 90% for very large flows (above $0.05 \text{ m}^3/\text{sec}$) and specific speeds above about 2500 (see Refs. 10–1 and 10–8). Most propellant pump efficiencies are between 30 and 70%. The pump efficiency is reduced by surface roughness of casing and impellers, the power consumed by seals, bearings, and stuffing boxes, and by excessive wear ring leakage and poor hydraulic design. The pump efficiency η_P is defined as the fluid power divided by the pump shaft power P_P :

$$\eta_P = \rho Q \Delta H / P_P \quad (10-16)$$

A correction factor of 550 ft-lbf/hp has to be added if P_P is given in horsepower, the head H in feet, and the volume flow Q in ft^3/sec . When using propellants, the pump power has to be multiplied by the density ratio if the required power for water tests is to be determined.

Example 10–1. Determine the shaft speed and the overall impeller dimensions for a liquid oxygen pump which delivers 500 lbm/sec of propellant at a discharge pressure of 1000 psia and a suction pressure of 14.7 psia. The oxygen tank is pressurized to 35 psia. Neglect the friction in the suction pipe and the suction head changes due to acceleration and propellant consumption. The initial tank level is 15 ft above the pump suction inlet.

SOLUTION. The density of liquid oxygen is 71.2 lbm/ft³ at its boiling point (from Chapter 7). The volume flow will be $500/71.2 = 7.022 \text{ ft}^3/\text{sec}$. The vapor pressure of the oxygen is 1 atm = 14.7 psi = 29.8 ft. The suction head is $35 \times 144/71.2 = 70.8 \text{ ft}$. From Eq. 10–12 the available suction head is $70.8 + 29.8 = 100.6 \text{ ft}$. The available suction head above vapor pressure is $(H_s)_A = 70.8 + 15.0 - 0 - 29.8 = 56.0 \text{ ft}$. The discharge head is $1000 \times 144/71.2 = 2022 \text{ ft}$. The head delivered by the pump is then $2022 - 100.6 = 1921 \text{ ft}$.

The required suction head will be taken as 80% of the available suction head in order to provide a margin of safety for cavitation $(H_s)_R = 0.80 \times 100.6 = 80.48 \text{ ft}$. Assume a suction specific speed of 15,000, a reasonable value if no test data are available. From Eq. 10–14 solve for the shaft speed N :

$$S = 21.2N\sqrt{Q}/(H_s)_R^{3/4} = 21.2N\sqrt{7.022}/80.48^{0.75} = 15,000$$

Solve for $N = 7174 \text{ rpm}$ or 751.3 rad/sec .

The specific speed, from Eq. 10–9, is

$$N_s = 21.2N\sqrt{Q}/H^{3/4} = 21.2 \times 7174\sqrt{7.022}/1921^{0.75} = 1388$$

According to Table 10–2, the impeller shape for this value of N_s will be a Francis type. The impeller discharge diameter D_2 can be evaluated from the tip speed by Eq. 10–11:

$$u = \psi\sqrt{2g_0 \Delta H} = 1.0\sqrt{2 \times 32.2 \times 1921} = 352 \text{ ft/sec}$$

$$D_2 = 353 \times 2/664.7 = 1.062 \text{ ft} = 12.75 \text{ in.}$$

The impeller inlet diameter D_1 can be found from Eq. 10–5 by assuming a typical inlet velocity of 15 ft/sec and a shaft cross section 5.10 in.² (2.549 in. diameter).

$$A = Q/v_1 = 7.022/15 = 0.468 \text{ ft}^2 = 67.41 \text{ in.}^2$$

$$A = \frac{1}{4}\pi D_1^2 = 67.41 + 5.10 = 72.51 \text{ in.}^2$$

$$D_1 = 9.61 \text{ in. (internal flow passage diameter)}$$

This is enough data to draw a preliminary sketch of the impeller.

10.6. TURBINES

The turbine must provide adequate shaft power for driving the propellant pumps (and sometimes also auxiliaries) at the desired shaft speed and torque. The turbine derives its energy from the expansion of a gaseous working fluid through fixed

nozzles and rotating blades. The blades are mounted on disks to the shaft. The gas is expanded to a high, nearly tangential, velocity and through inclined nozzles and then flows through specially shaped *blades*, where the gas energy is converted into tangential forces on each blade. These forces cause the turbine wheel to rotate (see Refs. 10–1 to 10–5, 10–20 and 10–21).

Classification and Description

The majority of turbines have blades at the periphery of a turbine disk and the gas flow is axial, similarly in concept to the axial-flow pattern shown for pumps in Table 10–2 and the single-stage turbine of Fig. 10–1. However, there are a few turbines with radial flow (particularly at high shaft speeds), such as the one shown in Fig. 10–2. Ideally there are two types of axial-flow turbines of interest to rocket pump drives: impulse turbines and reaction turbines, as sketched in Fig. 10–9. In an *impulse turbine* the enthalpy of the working fluid is converted into kinetic energy within the first set of stationary turbine nozzles and not in the rotating blade elements. High-velocity gases are delivered (at a small angle to a tangential direction) to the rotating blades, and blade rotation takes place as a result of the impulse imparted by the momentum of the fluid stream of high kinetic energy to the rotating blades which are mounted on the turbine disk. The *velocity-staged impulse turbine* has a stationary set of blades which changes the flow direction after the gas leaves the first set of rototating blades and directs the gas to enter a second set of rotating blades in which the working fluid gives up further energy to the turbine wheel. In a *pressure-staged impulse turbine*, the expansion of the gas takes place in all the stationary rows of blades. In a *reaction turbine* the expansion of the gas is roughly evenly split between the rotating and stationary blade elements. The high-pressure drop available for the expansion of the turbine working fluid in a gas generator cycles favors simple, lightweight one- or two-stage impulse turbines for high thrust engines. Many rocket turbines are neither pure impulse nor reaction turbines, but often are fairly close to an impulse turbine with a small reaction in the rotating vanes.

With some gas generator engine cycles the turbine exhaust gases pass through a *De Laval Supersonic nozzle* at the exit of the exhaust pipe (see Fig. 1–4). The high turbine outlet pressure gives critical flow conditions at the venturi throat (particularly at high altitudes) and thereby assures a constant turbine outlet pressure and a constant turbine power which will not vary with altitude. Furthermore, it provides a small additional thrust to the engine.

Turbine Performance and Design Considerations

The power supplied by the turbine is given by a combined version of Eqs. 3–1 and 3–7:

$$P_t = \eta_T \dot{m}_t \Delta h \quad (10-17)$$

$$P_t = \eta_t \dot{m}_T c_p T_1 [1 - (p_2/p_1)^{(k-1)/k}] \quad (10-18)$$

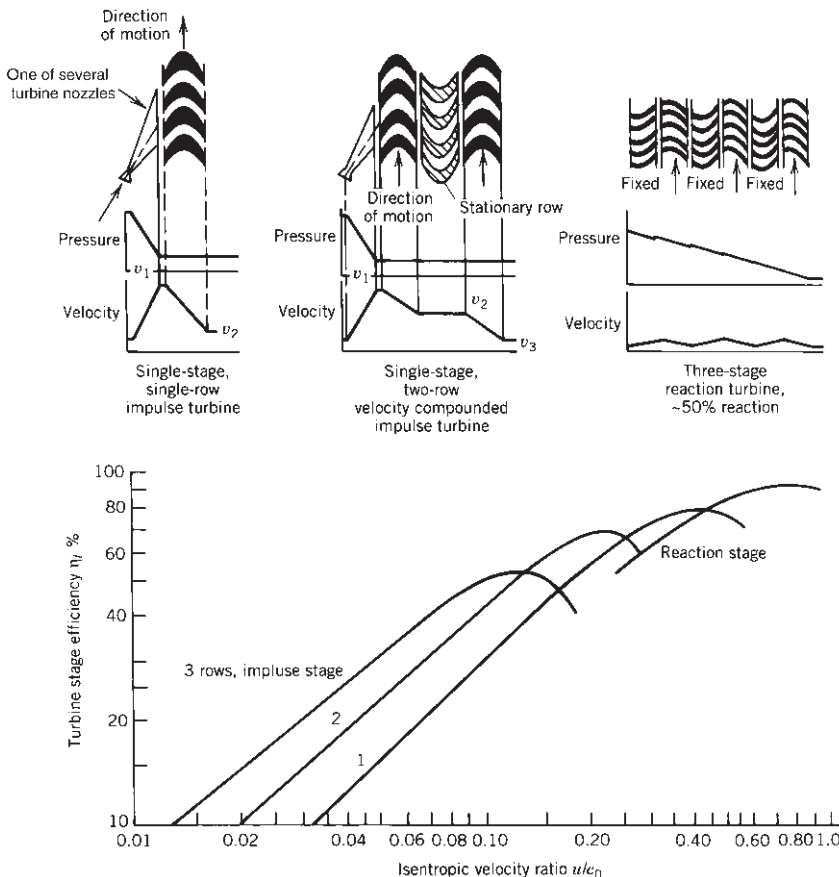


FIGURE 10–9. Top view diagram, pressure and velocity profiles, and efficiency curves for impulse and reaction type turbines. The velocity ratio is the pitch line velocity of the rotating blades u divided by the theoretical gas spouting velocity c_0 derived from the enthalpy drop. (Adapted with permission from Refs. 10–3 and 10–19.)

The power delivered by the turbine P_t is proportional to the turbine efficiency η_t , the mass flow through the turbine \dot{m}_t , and the available enthalpy drop per unit of flow Δh . The units in this equation have to be consistent (1 Btu = 778 ft-lbf = 1055 J). This enthalpy is a function of the specific heat c_p , the nozzle inlet temperature T_1 , the pressure ratio across the turbine, and the ratio of the specific heats k of the turbine gases. For gas generator cycles the pressure drop between the turbine inlet and outlet is relatively high, but the turbine flow is small (typically 2 to 5% of full propellant flow). For staged combustion cycles this pressure drop is very much lower, but the turbine flow is much larger.

For very large liquid propellant engines with high chamber pressure the turbine power can reach over 250,000 hp, and for small engines this could be perhaps around 35 kW or 50 hp.

According to Eq. 6–12, the power delivered by the turbine P_t has to be equal to the power required by the propellant pumps, the auxiliaries mounted on the turbopump (such as hydraulic pumps, electric generators, tachometers, etc.), and power losses in hydraulic friction, bearings, gears, seals, and wear rings. Usually these losses are small and can often be neglected. The effect of the turbine gas flow on the specific impulse of the rocket engine system is discussed in Section 6.6. For gas generator engine cycles, the rocket designer is interested in obtaining a high turbine efficiency and a high turbine inlet temperature T_1 in order to reduce the flow of turbine working fluid, and for gas generator cycles also to raise the overall effective specific impulse, and, therefore, reduce the propellant mass required for driving the turbine. Three-dimensional computer analyses of the gas flow behavior and turbine blade geometry have resulted in efficient blade designs.

Better turbine blade materials (such as single crystals which have been unidirectionally solidified) and specialty alloys can allow turbine inlet temperatures between 1400 K (or about 2050°F) and perhaps 1600 K (or 2420°F); these higher temperatures or higher gas enthalpies reduce the required turbine flow. Reliability, gas temperature variations or nonuniformity, and cost considerations have kept actual turbine inlet temperatures at conservative values, such as 1150 to 1250°F or about 900 to 950 K, using special steel alloys as the blade and disk materials. The *efficiency* of turbines for rocket turbopumps is shown in Fig. 10–9. Maximum *blade speeds* with good design and strong high-temperature materials are typically 400 to 700 m/sec or about 1300 to 2300 ft/sec. Higher blade speeds generally allow an improvement in efficiency. For the efficiency to be high the turbine blade and nozzle profiles have to have smooth surfaces. Small clearances at the turbine blade tips are also needed to minimize leakage around the blades.

Different organizations define *turbine efficiency* in different ways. One way to define the turbine efficiency η_t is the turbine power output LN divided by the turbine input from an ideal uniform heated gas flowing through an ideal turbine. The gas flow can be considered the ideal isentropic enthalpy drop. The actual pressure drop and the actual Δh or usually higher than the ideal:

$$\eta_t = L_t N_t / \dot{m} \Delta h \quad (10-19)$$

Here Δh is the enthalpy drop with isentropic gas expansion across the turbine nozzles and the turbine buckets or blades (moving and stationary) per unit gas mass flow. It is typically based on a uniform gas flow across a flow section, uniform gas properties across a flow section, perfect gases, no leakage or alternatively a nominal leakage around the blades, and perfect blade contours. Even a small clearance at the tip of turbine blades causes substantial losses, particularly at small turbine diameter and small blade heights. Some organizations include a few unavoidable basic losses in defining the ideal power.

The advantage of increased turbine efficiency (less gas generator propellant requirement) can be realized only if the turbopump design has efficient turbine blade contours and allows high blade speeds. This speed can be achieved in

rockets of medium and low thrust by gearing the turbine to the pump shaft or by using pumps that permit high shaft speeds; in rockets of very high thrust the pumps have diameters and shaft speeds close to those of the turbines and can be mounted on the same shaft as the turbine. The power input to the turbine can be regulated by controlling the gas flow and gas temperatures to the turbine inlet through valves or orifices.

Usually, the preliminary analysis for the pump is done first. Avoiding excessive cavitation sets a key pump parameter, namely the maximum pump shaft speed. This is the highest possible shaft speed, which in turn allows the lightest turbopump mass, without excessive cavitation in the pump. If excessive cavitation occurs at the leading edge of the main impeller, then the flow will become unsteady and variable, leading to lower thrust and possible combustion instability. The amount of pressure in the vehicle (gas pressure in propellant tank plus the static elevation pressure) that can be made available to the engine (at the pump inlet) for suppressing cavitation has to be larger than the impeller vanes' own pressure limit to cavitate. This allows us then to determine the shaft speed, which in turn can establish the approximate pump efficiencies, impeller tip speed (usually also limited by the material strength of the impeller), number of pump stages, key dimensions of the impeller.

10.7. APPROACH TO TURBOPUMP PRELIMINARY DESIGN

With all major rocket engine components the principal criteria (high performance or efficiency, minimum mass, high reliability, and low cost) have to be weighted and prioritized for each vehicle mission. For example, high efficiency and low mass usually mean low design margins, and thus lower reliability. A higher shaft speed will allow a lower mass turbopump, but it cavitates more readily and requires a higher tank pressure and heavier vehicle tanks (which usually outweighs the mass savings in the turbopump).

The engine requirements give the initial basic design goals for the preliminary design of the turbopump, namely propellant flow, the pump outlet or discharge pressure (which has to be equal to the chamber pressure plus the pressure drops in the piping, valves, cooling jacket, and injector), the best engine cycle (as shown in Fig. 6–9), the start delay, and the need for restart or throttling, if any. Also, the propellant properties (density, vapor pressure, viscosity, or boiling point) must be known. Some of the design criteria are explained in Refs. 10–2 and 10–3, and basic texts on turbines and pumps are listed as Refs. 10–4 to 10–8.

There are several design variations or geometrical arrangements for transmitting turbine power to one or more propellant pumps; some are shown schematically in Fig. 10–4 and an initial selection has to be made. If there is a mismatch between the optimum pump speed and the optimum turbine speed (which is usually higher), it may save inert mass and turbine drive gas mass to interpose a gear reduction between their shafts. See Fig. 6–11 and Figs. 10–4d and 10–4f. For the last two decades designers have preferred to use direct drive, which avoids

the complication of a gear case but at a penalty in efficiency and the amount of turbine drive propellant gas required. See Figs. 6-12, 10-1, 10-2, and 10-4e.

The key turbine parameter can be estimated because the power output of the turbine essentially has to equal the power demand of the pumps. If the pump is driven directly, that is, without a gear case, then the pump speed and the turbine speed are equal. From the properties of the turbine drive gas (temperature, specific heat, etc.), the strength limits of the turbine materials, and the likely pressure drop, it is possible to determine the basic dimensions of the blades [pitch line velocity, turbine nozzle outlet velocity, number of rows (stages) of blades, turbine type, or turbine efficiency]. The particular arrangement or geometry of the major turbopump components is related to their selection process. Most propellant pumps have a single-stage main impeller. For liquid hydrogen with its low density, a two- or three-stage pump is normally needed. Usually some design limit is reached which requires one or more iterations, each with a new changed approach or parameter. The arrangement of the major turbopump components (Fig. 10-4) is also influenced by the position of the bearings on the shaft. For example, we do not want to place a bearing in front of an impeller inlet because it will cause turbulence, distort the flow distribution, raise the suction pressure requirement, and make cavitation more likely to occur. Also, bearings positioned close to a turbine will experience high temperatures, which influences the lubrication by propellant and may demand more cooling of the bearings.

The use of *booster pumps* allows lower tank pressure, and thus lower inert vehicle mass, and provides adequate suction pressures to the main pump inlet. See Ref. 10-12. Booster pumps are used in the Space Shuttle main engine and the Russian RD-170, as seen in Figs. 6-12 and 11-2. Some booster pumps have been driven by a liquid booster turbine using a small flow of high-pressure liquid propellant that has been tapped off the discharge side of the main pump. The discharged turbine liquid then mixes with the main propellant flow at the discharge of the booster pump.

Mass is at a premium in all flying vehicle installations, and the feed system is selected to have a minimum combined mass of turbines, pumps, gas generator, valves, tanks, and gas generator propellants. Some of the considerations in the design of turbopumps are the thermal stresses, warpage due to thermal expansion or contraction, axial loads, adequate clearances to prevent rubbing yet minimize leakage, alignment of bearings, provisions for dynamic balancing of rotating parts, mounting on an elastic vehicle frame without inducing external forces, and avoiding undue pressure loads in the liquid and gas pipes.

Vibrations of turbopumps have caused problems during development. The analyses of the various vibrations of components (shaft, turbine blades, liquid oscillations, gas flow oscillations, or bearing vibrations) are not given here. At the *critical speed* the natural structural resonance frequency of the rotating assembly (shaft, impellers, turbine disk, etc.) coincides with the rotation operating speed, a condition that must be minimized. A slight unbalance can then be amplified to cause significant shaft deflections, bearing failure, and other damage. The operating speed therefore is usually lower, but occasionally higher than the critical

speed. A large diameter stiff shaft, rigid bearings, and stiff bearing supports will increase this critical speed, and damping (such as the liquid lubricant film in the bearing) will reduce the vibration amplitude. The solving of various internal vibration problems, such as whirl in bearings and blade vibrations, is reported in Ref. 10–16 and the dynamics of the propellant flow in pumps in Ref. 10–15. Vibrations of adjacent components can be excited by a TP and the natural frequency of these components can be analyzed. If the operating frequency or the shaft speed of the rotating assembly coincides with the natural frequency, another engine part, such as injector domes or certain piping assemblies, then an undesirable resonance with excessive stresses can occur. As a result the natural frequencies of affected component or of the TP can be changed by design. For example, whenever the tip of a pump blade goes by the tongue of the pump volute, a pressure wave is generated in the liquid. The frequency is the product of the number of pump vanes and the speed of the vane tip. Vibrations external to the TP, such as those generated by a thrust chamber (see Chapter 9) should not influence the operation of a TP. This interaction, if it occurs, can be determined by hot fire tests of a complete engine with appropriate instruments measuring TP behavior.

The *bearings* in most existing TPs are high precision, special metal alloy ball bearings (Ref. 10–13). A few are roller bearings, which have a higher radial load capacity. Some ball bearings can take both radial and axial loads. Early ball and roller bearings were limited in the loads and speeds at which they could operate reliably. New bearings were developed by the bearing industry. In some TP designs the limits of the bearing loads and speeds determined the shaft speed and thus the minimum size of the turbopump, rather than the cavitation limit of the pump. Various types of bearings, and many types of seals have been explored, tested in laboratory fixtures or experimental TPs. This included hydrostatic (precision sleeve type) bearings, foil bearings, and magnetic bearings (Ref. 10–13). As far as the authors know, none of these have as yet found their way into a production TP. The variety of static and dynamic seals is relatively large, and the selection is strongly influenced by the preferences of the design organization (Ref. 10–14). One type of bearing oscillation problem is discussed in Ref 10–16.

If the turbopump is part of a reusable rocket engine, it becomes more complex. For example, it can include provision to allow for inspection and automatic condition evaluation after each mission or flight. This can include an inspection of bearings through access holes for boroscope instruments, checking for cracks in highly stressed parts (turbine blade roots or hot-gas high-pressure manifolds), or the measurement of shaft torques (to detect possible binding or warpage).

The number of different *materials of construction* of TP appears to have increased. For example, for high-speed, high-load, ball bearings a new ball material (silicon nitride) has been successfully introduced. Relatively common materials, such as stainless steels, have in part been replaced by superalloys, such as Inconel. Powder metallurgy has found its way into impellers and turbine parts. Although the strength is not really better than a forged or cast material,

they have a smooth surface (low friction), uniform physical properties, and can be fabricated in complex shapes (Ref. 10–22).

There is *no warm-up time* available in rocket turbines. The sudden admission of hot gas at full flow causes severe thermal shock and thermal distortion and increases the chances for rubbing between moving metal parts. The most severe stresses of a turbine blade often are thermal stresses; they come during the engine start when the leading edge is very hot but other parts of the blade are still cold.

For low-thrust engines the shaft speeds can become very high, such as over 100,000 rpm. Also, the turbine blade height becomes very short and friction losses can become prohibitive. In order to obtain a reasonable blade height we go to partial admission turbine designs. Here a portion of the turbine nozzles are effectively plugged or eliminated.

10.8. GAS GENERATORS AND PREBURNERS

The purpose of a gas generator or a preburner is to create the “warm” gas (usually between 600 and 2000°F or 315 to 1200°C) to drive the turbine of a TP. See Refs. 10–1 to 10–5. The selected gas temperature depends on nearly uniform gas composition, the engine design, the turbine blade materials, using uncooled hardware, and the acceptable risk of failure. In order to achieve these warm gas temperatures with a bipropellant, most operate at a fuel-rich mixture ratio, but some of the preburners in the Soviet Union (today Russia) operate at an oxidizer-rich mixture usually with engines using staged combustion engine cycles. Each of these combustion devices consists of a combustion chamber, an injector, and a pipe or duct leading to the turbine. They all have separate dedicated propellant control valves, sometimes with some calibrated orifices, for control of the flows. They resemble a thrust chamber, but they do not have a single bow-tie-shaped supersonic nozzle. Instead the warm gas flows subsonically from the gas generator or the preburner through pipes or manifolds into the nozzles of the turbine (here they reach high velocities) and then they flow supersonically through the row(s) of turbine blades, which extract the energy for driving the propellant pumps. Requirements for gas generators or preburners include the delivery of warm gas at the intended mass flows, pressure, and design temperature, an essentially uniform gas temperature across the flow path to the turbine and no high gas temperature spikes. Combustion instability problems are extremely rare.

Gas generators are used exclusively with liquid propellant rocket engines, which operate on a *gas generator engine cycle*, and *preburners* are used exclusively with rocket engines, which operate on a *staged combustion cycle* and they usually operate at a higher pressure. Table 10–3 explains some of the differences between these two and Table 6–6 and Fig. 6–9 describe the engine cycles.

Gas generators are shown as a component of an engine in Fig. 1–4 and Ref. 10–4 and preburners in Figs. 6–1, 6–12, and 11–2. Propellants supplied to the gas generator or the preburner usually are tapped off from discharges of the engines main pumps. When starting an engine, the turbomachinery needs to

TABLE 10–3. Comparison of Key Characteristics of Gas Generators and Preburners

| Parameter | Gas Generator | Preburner |
|---|---|--|
| Engine cycle | Gas generator cycle | Staged combustion cycle |
| Chamber pressure | Usually equal or lower than thrust chamber pressure | 30–60% higher than its thrust chamber pressure |
| Mass flow as % of total propellant flow | 1–7 | 40–85 |
| Cooling | Usually uncooled | Usually uncooled, but may be partially cooled |
| Inert mass | Relatively light | Heavy |
| Size | Relatively small | Can be large |

be brought up to speed before propellant can be supplied at pressure. This gas generator start has also been done with a solid propellant starting cartridge (runs only a few seconds), an auxiliary set of small propellant tanks pressurized by cold gas (also runs only for short duration), or by letting the engine “bootstrap” itself into a start using the modest tank pressure augmented by the liquid column head existing in the vehicle tanks and feed system pipe lines—usually called “tank head” start (requires more time to start). A discussion of engine starts and tank pressurization can be found in Section 6.5 and thrust chamber starts in Section 8.6.

In the past monopropellant gas generators were common and both 80 or 90% hydrogen peroxide or pure hydrazine provided warm gas usually through catalytic decomposition in a bed of solid catalysts. This type has a simpler gas generator system (only one tank and one set of valves, instead of two), has no mixture ratio adjustment, and a predictable, fully reproducible uniform warm gas temperature without potential temperature spikes. The key disadvantages were the complications of providing a third propellant, the potential propellant hazards, the lower performance, or the higher mass of propellant for making enough warm gas for providing the required power.

PROBLEMS

1. A rocket engine with two TPs delivers the fuel, namely UDMH, at a pump discharge pressure of 555 psia, a flow of 10.2 lb/sec, at 3860 rpm, and a fuel temperature of 68°F. Determine the following:
 - (a) The fuel pump power for these nominal conditions.
 - (b) When the fuel flow is reduced to 70% of nominal, what will be the approximate power level, discharge pressure, and shaft speed? Assume that the oxidizer pump is also reduced by 70% and so is the gas flow to the turbines, but the gas temperature is unchanged.

- (c) If the allowed temperature variation of the propellants is at -40°F and on another day $+120^{\circ}\text{F}$, how will this affect the power level, shaft speed, and the discharge pressure of the fuel pump?
2. What are the specific speeds of the four SSME pumps? (See the data given in Table 10-1.)
3. Compute the turbine power output for a gas consisting of 64% by weight of H_2O and 36% by weight of O_2 , if the turbine inlet is at 30 atm and 658 K with the outlet at 1.4 atm and with 1.23 kg flowing each second. The turbine efficiency is 37%.
4. Compare the pump discharge gauge pressures and the required pump powers for five different pumps using water, gasoline, alcohol, liquid oxygen, and diluted nitric acid. The respective specific gravities are 1.00, 0.720, 0.810, 1.14, and 1.37. Each pump delivers 100 gal/min, a head of 1000 ft, and arbitrarily has a pump efficiency of 84%. *Answers:* 433, 312, 350, 494, and 594 psi; 30.0, 21.6, 24.3, 34.2, and 41.1 hp.
5. The following data are given on a liquid propellant rocket engine:

| | |
|--|---------------------------------------|
| Thrust | 40,200 lbf |
| Thrust chamber specific impulse | 210.2 sec |
| Fuel | Gasoline (specific gravity 0.74) |
| Oxidizer | Red fuming nitric acid (sp. gr. 1.57) |
| Thrust chamber mixture ratio | 3.25 |
| Turbine efficiency | 58% |
| Required pump power | 580 hp |
| Power to auxiliaries mounted on turbopump gear case | 50 hp |
| Gas generator mixture ratio | 0.39 |
| Turbine exhaust pressure | 37 psia |
| Turbine exhaust nozzle area ratio | 1.4 |
| Enthalpy available for conversion in turbine per unit of gas | 180 Btu/lb |
| Specific heat ratio of turbine exhaust gas | 1.3 |

6. Determine the engine system mixture ratio and the system specific impulse. *Answers:* 3.07 and 208 sec.

SYMBOLS

| | |
|-----------|--|
| a | gear ratio |
| A | area, $\text{m}^2(\text{ft}^2)$ |
| c_p | specific heat at constant pressure, J/kg K ($\text{Btu/lb}^{\circ}\text{R}$) |
| D | diameter, m (ft) |
| g_0 | sea-level acceleration of gravity, 9.806 m/sec^2 (32.17 ft/sec^2) |
| H | head, m (ft) |
| $(H_s)_A$ | available pump suction head above vapor pressure, often called net positive suction head, m (ft) |
| $(H_s)_R$ | required pump suction head above vapor pressure, m (ft) |

| | |
|-------|--|
| L | torque, Nm (ft-lbf) |
| m | mass flow rate, kg/sec (lbm/sec) |
| N | shaft speed, rpm (rad/sec) |
| N_s | specific speed of pump |
| P | pressure, N/m ² (lbf/in. ²) |
| P | power, W (hp) |
| P_b | power of auxiliaries, bearings, rubbing seals, friction |
| Q | volume flow rate, m ³ /sec (ft ³ /sec) |
| S | suction specific speed of pump |
| T | absolute temperature, K (°R) |
| u | impeller tip speed or mean blade speed, m/sec (ft/sec) |
| v | liquid flow velocity, m/sec (ft/sec) |

Greek Letters

| | |
|----------|--|
| Δ | finite differential |
| η | efficiency |
| ρ | density, kg/m ³ (lb/ft ³) |
| ψ | velocity correction factor |

Subscripts

| | |
|-----|------------------------------|
| e | maximum efficiency condition |
| f | fuel |
| o | oxidizer |
| p | pump |
| t | turbine |
| 0 | initial condition |
| 1 | inlet |
| 2 | outlet |

REFERENCES

- 10–1. G. P. Sutton, “Turbopumps, a Historical Perspective,” AIAA Paper 2006–7531, July 2006.
- 10–2. D. K. Huzel and D. H. Huang, “Design of Turbopump Feed Systems,” Chapter 6 in *Design of Liquid Propellant Rocket Engines*, rev. ed., Vol. 147, *Progress in Astronautics and Aeronautics*, AIAA, Reston, VA, 1992.
- 10–3. M. L. Strangeland, “Turbopumps for Liquid Rocket Engines,” *Threshold, an Engineering Journal for Power Technology*, No. 3, Rocketdyne Propulsion and Power, Summer 1988, pp 34–42.
- 10–4. G. P. Sutton, “Turbopumps,” Chapter 4.4 and “Gas Generators, Preburners and Tank Pressurization,” Chapter 4.5 in *History of Liquid Propellant Rocket Engines*, AIAA, Reston, VA, 2006.

- 10–5. *Turbopump Systems for Liquid Rocket Engines*, NASA Space Vehicle Design Monograph, NASA SP-8107, August 1974.
- 10–6. Personal communications with personnel from Pratt & Whitney Rocketdyne, Northrop Grumman, and The Aerospace Corporation, 2006 to 2008.
- 10–7. A. Minick and S. Peery, “Design and Development of an Advanced Liquid Hydrogen Turbopump,” AIAA paper 98-3681, July 1998, and G. Crease, R. Lyda, J. Park, and A. Minick, “Design and Test Results of an Advanced Liquid Hydrogen Pump,” AIAA paper 99-2190, 1999.
- 10–8. I. Kassarik, W. C. Krutzsch, W. H. Frazer, and J. P. Messina (Eds.), *Pump Handbook*, McGraw-Hill Book Company, New York, 1976 (water hammer and pumps).
- 10–9. C. E. Brennan, *Hydrodynamics of Pumps*, Concepts ETI, Inc. and Oxford University Press, 1994.
- 10–10. *Liquid Rocket Engines Turbopump Shafts and Couplings*, NASA Space Vehicle Design Monograph, NASA SP-8101, Sept. 1972.
- 10–11. *Liquid Rocket Engines Turbopumps Gears*, NASA Space Vehicle Design Monograph, NASA SP-8100, March 1974.
- 10–12. Y. V. Demyanenko, A. I. Dimitrenko, and I. I. Kalatin, “Experience of Developing Propulsion Rocket Engine Feed Systems Using Boost Turbopump Units,” AIAA Paper 2003-5072, 2003.
- 10–13. *Liquid Rocket Engine Turbopump Bearings*, NASA Space Vehicle Design Monograph, NASA SP-8048, March 1971.
- 10–14. *Liquid Rocket Engine Turbopump Rotating Shaft Seals*. NASA SP-8121, February 1978.
- 10–15. J. Kurokawa, K. Kamijo, and T. Shimura, “Axial Thrust Analysis on LOX-Pump,” AIAA Paper 91-2410, June 1991.
- 10–16. M. C. Ek, “Solving Synchronous Whirl in High Pressure Turbine Machinery of the Space Shuttle Main Engine,” *Journal of Spacecraft and Rockets*, Vol. 17, No. 3, May–June 1980, pp. 208–218.
- 10–17. R. S. Ruggeri and R. D. Moore, *Method for Prediction of Pump Cavitation Performance for Various Liquids, Liquid Temperatures, and Rotating Speeds*, NASA TN D5292, June 1969.
- 10–18. *Liquid Rocket Engine Turbopump Inducers*, NASA Space Vehicle Design Monograph, NASA SP-8052, May 1971.
- 10–19. T. Shimura and K. Kamijo, “Dynamic Response of the LE-5 Rocket Engine Oxygen Pump,” *Journal of Spacecraft and Rockets*, Vol. 22, No. 2, March–April 1985.
- 10–20. *Liquid Rocket Engine Turbines*, NASA Space Vehicle Design Criteria Monograph, NASA SP-8110, January 1974.
- 10–21. S. Andersson and S. Trollheden, “Aerodynamic Design and Development of a Two-Stage Supersonic Turbine for Rocket Engines,” AIAA Paper 99-2192, 1999.
- 10–22. D. Guichard and A. DuTetre, “Powder Metallurgy Applied to Impellers of Vinci Turbopump,” International Symposium for Space Transportation of the XXI Century, in CD ROM of the symposium, May 2003.

CHAPTER 11

ENGINE SYSTEMS, CONTROLS, AND INTEGRATION

This chapter discusses the propellant budget, performance of complete or multiple rocket propulsion systems, the design of liquid propellant rocket engines with pressurized or turbopump feed systems, engine controls, engine calibration, system integration, and system optimization. Some of the content also applies to solid propellant motors or hybrid propulsion systems.

11.1. PROPELLANT BUDGET

In all liquid propellant rocket engines the amount of propellant put into the vehicle tanks is always a little greater than the nominal amount of propellant needed to accomplish the intended mission. The extra propellant is needed for uses other than providing thrust (e.g., residual propellant or valve actuation), to compensate for changes from engine to engine, such as dimensional tolerances causing slight changes in flow, for uncertainties of the construction of the engine and minor changes in the flight plan. A propellant budget is the sum of all the propellant utilization categories and losses in an engine; 11 are listed below. See Ref. 11–1. The budget helps to determine how much propellant has to be loaded. It is the aim to minimize this amount of propellant.

1. Enough propellant has to be available for achieving the *required vehicle velocity increase* and/or the *nominal attitude control maneuvers* of the particular application and the particular flight vehicle or stage. The nominal velocity increment is usually defined by systems analysis and mission optimization using an iterative calculation based on Eq. 4–19 or 4–35. If there are alternative flight paths or missions for the same vehicle, the mission

with an unfavorable flight path, such as higher drag or different orbit, and the highest total impulse should be selected. This mission-required propellant is usually the largest portion of the total propellants loaded into the vehicle tanks.

2. In a turbopump system using a *gas generator cycle*, a small portion of the overall propellant is burned in a separate *gas generator*. It has a lower flame temperature than the thrust chamber gas and operates at a different mixture ratio; this causes a slight change in the overall mixture ratio of propellants flowing from the tanks, as shown by Eqs. 11–3 and 11–5.
3. In a rocket propulsion system with a *thrust vector control* (TVC) system, such as a swiveling thrust chamber or nozzle, the thrust vector will be rotated by a few degrees. Thrust vector control systems are described in Chapter 18. There is a slight decrease in the axial thrust and that reduces the vehicle velocity increment in item 1. The extra propellant needed to compensate for the small velocity reduction can be determined from the mission requirements and TVC duty cycle. It could be between 0.1 and 4% of the total propellant depending on the average angle position of this thrust chamber.
4. In some engines a small portion of cryogenic propellants is heated, vaporized, and the gas used to *pressurize cryogenic propellant tanks*. A heat exchanger is used to heat liquid oxygen from the pump discharge and pressurize the oxygen tank, as shown schematically in Fig. 1–4. This method is used in the hydrogen and oxygen tanks of the Space Shuttle external tank (see Ref. 6–9).
5. Auxiliary rocket engines that provide for *trajectory corrections, station keeping, maneuvers, or attitude control* usually have a series of small restartable thrusters (see Chapter 4). The propellants for these auxiliary thrusters have to be included in the propellant budget if they are supplied from the same feed system and tanks as the larger rocket engine. Depending on the mission, the duty cycle, and the propulsion system concept, this auxiliary propulsion system can consume a significant portion of the available propellants.
6. The *residual propellant* that clings to tank walls or remains trapped in valves, pipes, injector passages, or cooling passages is unavailable for producing thrust. It is typically 0.5 to 2% of the total propellant load. All unused residual propellant increases the final vehicle mass at thrust termination and reduces the final vehicle velocity slightly.
7. A *loading uncertainty* exists due to variations in tank volume or changes in propellant density or liquid level in the tank. This is typically 0.25 to 0.75% of the total propellant. It depends, in part, on the accuracy of the method of measuring the propellant mass during loading (weighing the vehicle, flow meters, level gauges, etc.).
8. The *off-nominal rocket performance* is due to variations in the manufacture of hardware from one engine to another (such as slightly different pressure

losses in a cooling jacket, in injectors and valves, or somewhat different pump characteristics); these cause slight changes in combustion behavior, mixture ratio, or specific impulse. If there are slight variations in *mixture ratio*, one of the two liquid propellants will be consumed fully and an unusable residue will remain in the other propellant's tank. If a minimum total impulse requirement has to be met, extra propellant has to be tanked to allow for these mixture ratio variations. This can amount to up to perhaps 2.0% for each of the propellants.

9. *Operational factors* can result in additional propellant requirements, such as filling more propellant than needed into a tank or incorrectly adjusting regulators or control valves. It can also include the effect of changes in flight acceleration from the nominal value. For an engine that has been carefully calibrated and tested, this factor can be small, usually between 0.1 and 1.0%.
10. When using cryogenic propellants, an *allowance for evaporation and cooling down* has to be included. It is the mass of extra propellant that is allowed to evaporate (and be vented overboard while the vehicle is waiting to be launched) or that is fed through the engine to cool it down, before the remaining propellant in the tank becomes less than the minimum needed for the flight mission. Its quantity depends on the amount of time between topping off (partial refilling) of the tank and the engine start.
11. Finally, an *overall contingency* or ignorance factor is needed to allow for unforeseen propellant needs or inadequate or uncertain estimates of any of the items above. This can also include allowances for vehicle drag uncertainties, variations in the guidance and control system, wind, or leaks.

Only some of the items above provide axial thrust (items 1, 2, and sometimes also 3 and 5), but all the items need to be considered in determining the total propellant mass and tank volume.

The example shown in Table 11–1 is for a spacecraft pressure-fed engine system, where the majority of the propellant is consumed in a larger axial thrust chamber, and the second largest amount of propellant is fed to a set of several small thrusters used for extensive attitude control maneuvers. There will be flights where the mission may be more demanding or the engine performance may be slightly lower, and extra propellant will be needed to accomplish the mission. Conversely if the engine performance is actually slightly better than nominal or where the mission can be accomplished with less total impulse (operate with fewer or lower orbits), then the engine will consume less than the nominal amount of propellant.

11.2. PERFORMANCE OF COMPLETE OR MULTIPLE ROCKET PROPULSION SYSTEMS

The simplified relations that follow give the basic method for determining the overall specific impulse, the total propellant flow, and the overall mixture ratio

TABLE 11–1. Example of a Propellant Budget for a Spacecraft Propulsion System with a Pressurized Monopropellant Feed System

| Budget Element | Typical Value |
|--|--|
| 1. Main thrust chamber (increasing the velocity of stage or vehicle) | 85–95% (determined from mission analysis and system engineering) |
| 2. Flight control function (for reaction control thrusters and flight stability) | 5–10% (determined by control requirements) |
| 3. Residual propellant (trapped in valves, lines, tanks, etc.) | 0.5–2% of total load |
| 4. Loading uncertainty | 0.5% of total load |
| 5. Allowance for off-nominal performance | 0.5–1.0% of total load |
| 6. Allowance for off-nominal operations | 0.25–1.0% of total load |
| 7. Mission margin (reserve for first two items above) | 3–5% of items 1 and 2 |
| 8. Contingency | 1–5% of total load |

Source: Adapted from data supplied by predecessor of Propulsion Products Center, Northrop Grumman Corporation

as a function of the corresponding component performance terms for complete rocket engine systems. This applies to engine systems consisting of one or more thrust chambers, auxiliaries, gas generators, turbines, and evaporative propellant pressurization systems all operating at the same time.

Refer to Eqs. 2–5 and 6–1 for the specific impulse I_s , propellant flow rate \dot{w} or \dot{m} and mixture ratio r . The overall thrust F_{oa} is the sum of all the thrusts from thrust chambers and turbine exhausts and the overall flow \dot{m} is the sum of their flows as shown in Eqs. 2–24 and 2–25. The subscripts oa, o, and f designate the overall engine system, the oxidizer, and the fuel, respectively. Then repeating these equations

$$(I_s)_{oa} = \frac{\sum F}{\sum \dot{w}} = \frac{\sum F}{g_0 \sum \dot{m}} \quad (11-1)$$

$$\dot{w}_{oa} = \sum \dot{w} \quad \text{or} \quad \dot{m}_{oa} = \sum \dot{m} \quad (11-2)$$

$$r_{oa} \approx \frac{\sum \dot{w}_o}{\sum \dot{w}_f} = \frac{\sum \dot{m}_o}{\sum \dot{m}_f} \quad (11-3)$$

These same equations should be used for determining the overall performance when more than one rocket engine is contained in a vehicle propulsion system and they are operating simultaneously. They also apply to multiple solid propellant rocket motors and combinations of liquid propellant rocket engines and solid propellant rocket booster motors, as in the Space Shuttle (see Fig. 1–14). All the nozzles point in the same direction in Eqs. 2–24, 11–1, and 11–4.

Example 11–1. For an engine system (LOX/kerosene) with a gas generator similar to the one shown in Fig. 1–4, determine a set of equations that will express (1) the overall

engine performance and (2) the overall mixture ratio of the propellant flows from the tanks. Let the following subscripts be used: c , thrust chamber; gg , gas generator; and tp , tank pressurization. For a nominal burning time t , a 1% residual propellant, and a 6% overall reserve factor, give a formula for the amount of fuel and oxidizer propellant required with constant propellant flow. Ignore stop and start transients, thrust vector control, and evaporation losses.

SOLUTION. Only the oxidizer tank is pressurized by vaporized propellant. Although this pressurizing propellant must be considered in determining the overall mixture ratio, it should not be considered in determining the overall specific impulse since it stays with the vehicle and is not exhausted overboard.

$$(I_s)_{oa} \approx \frac{F_c + F_{gg}}{(\dot{m}_c + \dot{m}_{gg})g_0} \quad (11-4)$$

$$r_{oa} \approx \frac{(\dot{m}_o)_c + (\dot{m}_o)_{gg} + (\dot{m}_o)_{tp}}{(\dot{m}_f)_c + (\dot{m}_f)_{gg}} \quad (11-5)$$

$$m_f = [(\dot{m}_f)_c + (\dot{m}_f)_{gg}]t(1.00 + 0.01 + 0.06)$$

$$m_o = [(\dot{m}_o)_c + (\dot{m}_o)_{gg} + (\dot{m}_o)_{tp}]t(1.00 + 0.01 + 0.06)$$

For this gas generator cycle the engine mixture ratio or r_{oa} is different from the thrust chamber mixture ratio $r_c = (m_o)_c / (m_f)_c$. Similarly, the overall engine specific impulse is slightly lower than the thrust chamber specific impulse $I_c = F_c / m_c$. However, for an expander cycle or a staged combustion cycle these two mixture ratios and two specific impulses are the same, provided that there are no gasified propellant used for tank pressurization. Engine cycles are explained in Section 6.6.

The overall engine specific impulse is influenced by the propellants, the nozzle area ratio, and the chamber pressure, and to a lesser extent by the engine cycle, and the mixture ratio. Table 11–2 describes 10 different rocket engines using liquid oxygen and liquid hydrogen propellants designed by different companies in different countries, and shows the sensitivity of the specific impulse to these parameters. References 11–2 to 11–4 give additional data on several of these engines.

11.3. ENGINE DESIGN

The approach, methods, and resources used for rocket engine preliminary design and final design are usually different for each design organization and for each major type of engine. They also differ by the degree of novelty.

1. A *totally new engine with new major components* and some *novel design concepts* will result in an optimum engine design for a given application, but it is usually the most expensive and longest development approach. One of the major development costs is usually in sufficient testing of

TABLE 11-2. Comparison of Rocket Engines Using Liquid Oxygen and Liquid Hydrogen Propellants^a

| Engine Designation, Engine Cycle, Manuf. or Country (Year Qualified) | Vehicle | Thrust in Vacuum, kN (lbf) | Specific Impulse in Vacuum (sec) | Chamber Pressure, bar (psia) | Mixture Ratio | Nozzle Area Ratio | Engine Mass (dry), kg |
|--|--|----------------------------|----------------------------------|------------------------------|---------------|-------------------|-----------------------|
| SSME, staged combustion, Pratt & Whitney Rocketdyne (1998) | Space Shuttle | 2183 (490,850) | 452.5 | 196 (2747) | 6.0 | 68.8 | 3400 |
| RS-68, gas generator, Pratt & Whitney Rocketdyne (2000) | Delta | 3313 (745,000) | 410 | 97.2 (1410) | 6.0 | 21.5 | 6800 |
| LE-5A, Expander bleed, MHI, Japan, (1991) | HII | 121.5 (27,320) | 452 | 37.2 (540) | 5.0 | 130 | 255 |
| LE-7, staged combustion, MHI, Japan (1992) | HII | 1080 (242,800) | 445.6 | 122 (1769) | 6.0 | 52 | 1720 |
| Vulcain, gas generator, SEP (circa 1996) | Ariane 5 2 nd stage | 1120 (251,840) | 433 | 112 (1624) | 5.35 | 45 | 1585 |
| HM-7, gas generator, SEP, France (1986) | Ariane 1,2,3,4 3 rd stage | 62.7 (14,100) | 444.2 | 36.2 (525) | 5.1 | 45 | 155 |
| RL 10-A3, expander, Pratt & Whitney Rocketdyne (1965) | Various upper stages | 73.4 (16,500) | 444.4 | 32.75 (475) | 5.0 | 61 | 132 |
| RL 10-B2, same as above (1998) | same as above | 110 (24,750) | 466.5 | 44.12 (640) | 6.0 | 375 | 275 |
| YF 73, China (circa 1981) | Long March 3 rd stage | 44,147 (10,000) | 420 | 26.28 (381) | 5.0 | 40 | 236 |
| YF 75 (2 required), China (circa 1991) | same | 78.45 (17,600) | 440 | 36.7 (532) | 5.0 | 80 | 550 |

^aAdditional information on most of these engines is in this book. Use the index to find it.

components and several engines (under various environmental and performance limit conditions), in order to establish credible reliability data with enough confidence to allow the initial flights and initial production. Since the state of the art is relatively mature today, the design and development of a truly novel engine does not happen very often.

2. *New engine using some major components or somewhat modified key components from proven existing engines.* This is a common approach today. The design of such an engine requires working within the capability and limits of existing or slightly modified components. It requires less testing for proving reliability.
3. *Upgraded or improved version of an existing, proven engine.* This approach is quite similar to the second. It is needed when an installed engine for a given mission requires more payload (which really means higher thrust) and/or longer burning duration (more total impulse). Uprating often means more propellant (larger tanks), higher propellant flows and higher chamber and feed pressures, and more feed system power. The engine usually has an increased inert engine mass (thicker walls).

In a simplified way, we describe here a typical process for designing an engine. Chapter 19 and Refs. 11–5 and 11–6 describe this process and the selection of the propulsion system from a different point of view. At first the basic function and requirements of the new engine must be established. These engine requirements are derived from the vehicle mission and vehicle requirements, usually determined by the customer and/or the vehicle designers, often in cooperation with one or more engine designers. The engine requirements can include key parameters such as thrust level, the desired thrust–time variation, restart or pulsing, altitude flight profile, duty cycle, maximum accelerations, engine locations within the vehicle, and limitations or restraints on cost, engine envelope, test location, or schedule. It also includes some of the factors listed later in Table 19–5. If an existing proven engine can be adapted to these requirements, the subsequent design process will be simpler and quite different than the design of a truly new engine.

Usually some early tentative decisions about the engine are made, such as the selection of the propellants, their mixture ratio, or the cooling approach for the hot components. They are based on mission requirements, customer preferences, past experiences, some analysis, and the judgment of the key decision makers. After some studies additional selection decisions can also be made, such as having one, two, or more thrust chambers fed from the same feed system, redundancy of auxiliary thrusters, or type of ignition system.

A systematic approach, a good set of analyses, the use of system engineering, good coordination with the customers, key vendors, and vehicle designers—all are needed for a good preliminary and final design. Before a meaningful proposal for an engine can be prepared, a preliminary design has to be completed. See Refs. 11–5 to 11–7. One of the early design decisions is the choice of feed system: pressurized gas feed or pump feed. The next two paragraphs give some guidelines.

A *pressurized feed system* (see Fig. 1–3) usually gives better vehicle performance for low values of total impulse (thrust less than about 4.5 kN or 1000 lbf with up to perhaps 2 min duration). A pump feed system gives better vehicle performance for high thrust (say above 50,000 lbf or approximately 222 kN) and a long cumulative duration—more than a couple of minutes. For intermediate values of total impulse the choice can go either way, and it is not easy to make the decision only on the basis of total impulse. If the chamber pressure of a pressurized feed system is relatively high (say about 2.4 to 3.5 MPa or about 350 to 500 psia and occasionally more), then the inert weight of the thrust chamber will be high, but the thrust chamber will be small and can usually fit into an engine compartment. The vehicle propellant tanks and pressurizing gas tank will be at relatively high pressure and will be heavy. For a relatively low chamber pressure (0.689 to 1.379 MPa or 100 to 200 psia) the vehicle tank pressure will be lower and the tank walls thinner, but the thrust chamber will be very large in size and often will exceed the limits of the engine compartment, unless it has a low nozzle area ratio, which implies lower performance. Even in some cases of low chamber pressure, a pressurized feed system can be heavier than a comparable engine with a pump feed system. Pressurized feed systems have been relatively simple, very reliable, and they allow fast starts and fast restarts. With restarts the cooling of the thrust chamber can become a problem. Because of the proven reliability of pressure feed system, NASA has at times conservatively selected pressurized feed systems for certain space applications, such as the Apollo service module engine (21,900 lbf thrust), even though there is a major weight penalty and a somewhat inferior vehicle performance compared to a pump-fed system of equal total impulse. Also a decision has to be made on using either a pressurized system with a gas pressure regulator or alternatively a blow-down system. See Table 6–3 and Section 6.4.

For a *turbopump-fed liquid propellant rocket engine* (see Fig. 1–4) the overall inert weight of propellant tanks and engine will be considerably lighter and usually the vehicle performance will be somewhat better. It usually operates at high chamber pressures (3.5 to 24.1 MPa or about 500 to 3500 psia), the thrust chamber is not normally protruding from the vehicle. The smaller and shorter thrust chamber often allows a shortening of the vehicle with a savings in vehicle structure. This further improves the vehicle's performance modestly and the higher specific impulse will slightly reduce the amount of propellant needed for the mission. Compared to an engine with a pressurized feed system, the savings in inert mass (thin vehicle tank walls) and less propellant will allow a smaller, lighter, and probably lower cost vehicle with a somewhat superior performance. The engine with a TP is more complex with more parts and the engine will generally be heavier; however, the vehicles propellant and gas tanks will be much lighter and they will more than compensate for the heavier engine. It will take more tests and more effort to prove high reliability in an engine with a pump feed system. At the higher chamber pressures the heat transfer will be higher and cooling can become a problem, but heat transfer has been solved in other earlier high-pressure rocket engines. Also restart will be more complex. One

of several engine cycles has to be selected. High reliability has been achieved in many turbopump-fed large rocket engines.

Trade-off studies between several options are appropriate at this time. With a modified existing engine these parameters are well established and require fewer trade-off studies or analyses. Initial analyses of the pressure balances, power distribution between pumps and turbines, gas generator flow, propellant flows and reserves, or the maximum cooling capacity are appropriate. Sketches and preliminary estimates of inert mass of key components need to be made, such as tanks, thrust chambers, turbopumps, feed and pressurization systems, thrust vector control, or support structure. Alternate arrangements of components (layouts) are usually examined, often to get the most compact configuration or control of the travel of the center of gravity. An initial evaluation of combustion stability, stress analysis of critical components, water hammer, engine performance at some off-design conditions, safety features, testing requirements, cost, and schedule are often performed at this time. Participation of appropriate experts from the field of manufacturing, field service, materials, stress analysis, or safety can be critical for selecting the proper engine and the key design features. A design review is usually conducted on the selected engine design and the rationale for new or key features.

Test results of subscale or full-scale components, or related or experimental engines, will have a strong influence on this design process. The key engine selection decisions need to be validated later in the development process by testing new components and new engines.

The *inert mass of the engine and other mass properties (center of gravity or moment of inertia)* are key parameters of interest to the vehicle designer or customer. They are needed during preliminary design and again, in more detail, in the final design. The engine mass is usually determined by summing up the component or subsystem masses, each of which is either weighed or estimated by calculating their volumes and knowing their densities. Sometimes early estimates are based on known similar parts or subassemblies.

Preliminary engine performance estimates are often based on data from prior similar engines. If these are not available, then theoretical performance values can be calculated (see Chapters 2, 3, and 5) for F , I_s , k , or \dot{M} , using appropriate established correction factors. Measured static test data are, of course, better than estimates. The final performance values are obtained from flight tests or simulated altitude tests, where airflow and altitude effects can interact with the vehicle or the plume.

If the preliminary design does not meet the engine requirements, then changes need to be made to the initial engine decisions and, if that is not sufficient, sometimes also to the mission requirements themselves. Components, pressure balances, and so forth will be reanalyzed, and the results will be a modified version of the engine configuration, its inert mass, and performance. This process is iterated until the requirements are met and a suitable engine has been found. The initial design effort culminates in preliminary layouts of the engine, a preliminary inert mass estimate, an estimated engine performance, a cost estimate, and a tentative schedule. These preliminary design data form the basis for a written

proposal to the customer for undertaking the final or detail design, development, testing, and for delivering engines.

Optimization studies are made to select the best engine parameters for meeting the requirements; some of them are done before a suitable engine has been identified, some afterwards. They are described further in Section 11.6. We optimize parameters such as chamber pressure, nozzle area ratio, thrust, mixture ratio, or number of large thrust chambers supplied by the same turbopump. The results of optimization studies indicate the best parameter, which will give a further, usually small, improvement in vehicle performance, propellant fraction, engine volume, or cost.

Once the engine proposal has been favorably evaluated by the vehicle designers, and after the customer has provided authorization and funding to proceed, then the final design can begin. Some of the analyses, layouts, and estimates will be repeated, but in more detail, specifications and manufacturing documents will be written, vendors will be selected, and tooling will be built. The selection of some of the key parameters (particularly those associated with some technical risk) will need to be validated. After another design review, key components and prototype engines are built and ground tested as part of a planned development effort. If proven reliable, one or two sets of engines will be installed in a vehicle and operated during flight. In those programs where a fair number of vehicles are to be built, the engine will then be produced in the required quantity.

Table 11–3 shows some of the characteristics of three different Russian combustion cycle engine designs, each at a different thrust and with different propellants (from Ref. 11–8). It shows primary engine parameters (chamber pressure, thrust, specific impulse, weight, propellant combination, nozzle area ratio, dimensions, etc.) which influence the vehicle performance and configuration. It also shows secondary parameters, which are internal to the engine but important in component design and engine optimization. The Space Shuttle main engine (see Figs. 6–1 and 6–12) has two fuel-rich preburners, but the Russian staged combustion engines use oxidizer-rich preburners. Figure 11–1 shows the RD-170 engine with four thrust chambers (and their thrust vector actuators) supplied by a centrally located single large turbopump (257,000 hp; not visible in the photo) and one of the two oxidizer-rich preburners. Figures 11–1 and 11–2 show this turbopump and the two booster turbopumps; one is driven by a turbine using a bleed of oxygen-rich gas from the turbine exhaust (the gas is condensed when it mixes with the liquid oxygen flow) and the other by a liquid turbine using high-pressure liquid fuel. A version of this RD-170 rocket engine is used in the first stage of the U.S. Atlas V space launch vehicle.

Much of today's engine design, preliminary design, and design optimization can be performed with computer programs. These include finite element analyses, codes for stress and heat transfer, weight and mass properties, stress and strain analysis of a variety of structures, water hammer, engine performance analyses, feed system analyses (for balance of flow, pressures, and power), gas pressurization, combustion vibrations, and various exhaust plume effects (Refs. 11–4 and 11–5 are examples of performance analyses). Some customers

TABLE 11–3. Data on Three Russian Large Liquid Propellant Rocket Engines Using a Staged Combustion Cycle

| Engine Designation | RD-120 | RD-170 | RD-253 |
|---|---|--|-------------------------------|
| Application (number of engines) | Zenit second stage (1) | Energia launch vehicle booster (4), Zenit first stage (1), and Atlas V (1) | Proton vehicle booster (1) |
| Oxidizer | Liquid oxygen | Liquid oxygen | N ₂ O ₄ |
| Fuel | Kerosene | Kerosene | UDMH |
| Number and types of turbopumps (TP) | One main TP and two boost TPs | One main TP and two boost TPs | Single TP |
| Thrust control, % | Yes | Yes | ±5 |
| Mixture ratio control, % | ±10 | ±7 | ±12 |
| Throttling (full flow is 100%), % | 85 | 40 | None |
| Engine thrust (vacuum), kg | 85,000 | 806,000 | 167,000 |
| Engine thrust (SL), kg | — | 740,000 | 150,000 |
| Specific impulse (vacuum), sec | 350 | 337 | 316 |
| Specific impulse (SL), sec | — | 309 | 285 |
| Propellant flow, kg/sec | 242.9 | 2393 | 528 |
| Mixture ratio, O/F | 2.6 | 2.63 | 2.67 |
| Length, mm | 3872 | 4000 | 2720 |
| Diameter, mm | 1954 | 3780 | 1500 |
| Dry engine mass, kg | 1125 | 9500 | 1080 |
| Wet engine mass, kg | 1285 | 10500 | 1260 |
| <i>Thrust Chamber Characteristics</i> | | | |
| Chamber diameter, mm | 320 | 380 | 430 |
| Characteristic chamber length, mm | 1274 | 1079.6 | 999.7 |
| Chamber area contraction ratio | 1.74 | 1.61 | 1.54 |
| Nozzle throat diameter, mm | 183.5 | 235.5 | 279.7 |
| Nozzle exit diameter, mm | 1895 | 1430 | 1431 |
| Nozzle area ratio, | 106.7 | 36.9 | 26.2 |
| Thrust chamber length, mm | 2992 | 2261 | 2235 |
| Nominal combustion temperature, K | 3670 | 3676 | 3010 |
| Rated chamber pressure, kg/cm ² | 166 | 250 | 150 |
| Nozzle exit pressure, kg/cm ² | 0.13 | 0.73 | 0.7 |
| Thrust coefficient, vacuum | 1.95 | 1.86 | 1.83 |
| Thrust coefficient, SL | — | 1.71 | 1.65 |
| Gimbal angle, degree | Fixed | 8 | Fixed |
| Injector type | Hot, oxidizer-rich precombustor gas plus fuel | | |
| With a staged combustion cycle the thrust, propellant flow, and mixture ratio for the thrust chamber have the same values as for the entire engine. | | | |

(Continued)

TABLE 11–3. (*Continued*)

| Engine Designation | RD-120 | | RD-170 | | RD-253 | |
|--|-----------------|-------------|-----------------|--------------------|-----------------|--------------------|
| <i>Turbopump Characteristics</i> | | | | | | |
| Pumped liquid | <i>Oxidizer</i> | <i>Fuel</i> | <i>Oxidizer</i> | <i>Fuel</i> | <i>Oxidizer</i> | <i>Fuel</i> |
| Pump discharge pressure, kg/cm ² | 347 | 358 | 614 | 516 | 282 | 251 |
| Flow rate, kg/sec | 173 | 73 | 1792 | 732 | 384 | 144 |
| Impeller diameter, mm | 216 | 235 | 409 | 405 | 229 | 288 |
| Number of stages | 1 | 1 | 1 | 1 + 1 ^a | 1 | 1 + 1 ^a |
| Pump efficiency, % | 66 | 65 | 74 | 74 | 68 | 69 |
| Pump shaft power, hp | 11,210 | 6145 | 175,600 | 77,760 | 16,150 | 8850 |
| Required pump NPSH, m | 37 | 23 | 260 | 118 | 45 | 38 |
| Shaft speed, rpm | 19,230 | | 13,850 | | 13,855 | |
| Pump impeller type | Radial flow | | Radial flow | | Radial flow | |
| Turbine power, hp | 17,588 | | 257,360 | | 25,490 | |
| Turbine inlet pressure, main turbine, kg/cm ² | 324 | | 519 | | 239 | |
| Pressure ratio | 1.76 | | 1.94 | | 1.42 | |
| Turbine inlet temperature, K | 735 | | 772 | | 783 | |
| Turbine efficiency, % | 72 | | 79 | | 74 | |
| Number of turbine stages | 1 | | 1 | | 1 | |
| <i>Preburner Characteristics</i> | | | | | | |
| Flow rate, kg/sec | 177 | | 836 | | 403.5 | |
| Mixture ratio, O/F | 53.8 | | 54.3 | | 21.5 | |
| Chamber pressure, kg/cm ² | 325 | | 546 | | 243 | |
| Number of preburners | 1 | | 2 | | 1 | |

^aFuel flow to precombustor goes through a small second-stage pump. (Courtesy of NPO Energomash, Moscow Region, Russia.)

require that certain analyses (e.g., safety, static test performance) be delivered to them prior to engine deliveries.

Many computer programs are specific to a particular design organization, a certain category of applications (e.g., interplanetary flight, air-to-air combat, long-range ballistic missile, or ascent to earth orbit), and many are specific to a particular engine cycle. One is called *engine balance program*, and it balances the pressure drops in the fuel, oxidizer, and pressurizing gas flow systems; similar programs balance the pump and turbine power, speeds, and torques (see Section 10.4), compare different turbopump configurations (see Section 10.3); some balance programs also calculate approximate masses for engine, tanks, turbine drive fluids. The program allows iterations of various pressures and pressure drops, mixture ratios, thrust levels, number of thrust chambers, distribution of

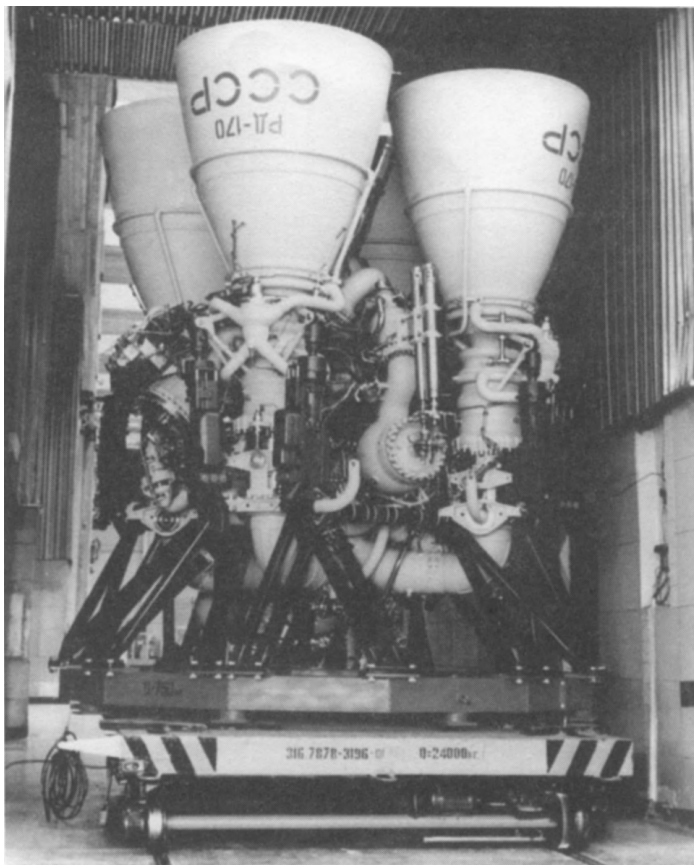


FIGURE 11–1. The RD-170 rocket engine, shown here on a transfer cart, can be used as an expendable or reusable engine (up to 10 flights). It has been used on the Zenith, Soyuz booster, Atlas V and Energiya launch vehicles. The tubular structure supports the four hinged thrust chambers and its control actuators. It is the highest thrust liquid rocket engine in use today. (Courtesy of NPO Energomash, Moscow Region, Ref. 11–8.)

total velocity increment between different vehicle stages, trades between constant thrust (or propellant flow) and decreasing thrust (throttling) or pulsed (intermittent) thrust.

11.4. ENGINE CONTROLS

All liquid propellant rocket engines have controls to accomplish some or all of these tasks:

1. Start rocket operation.
2. Shut down rocket operation.

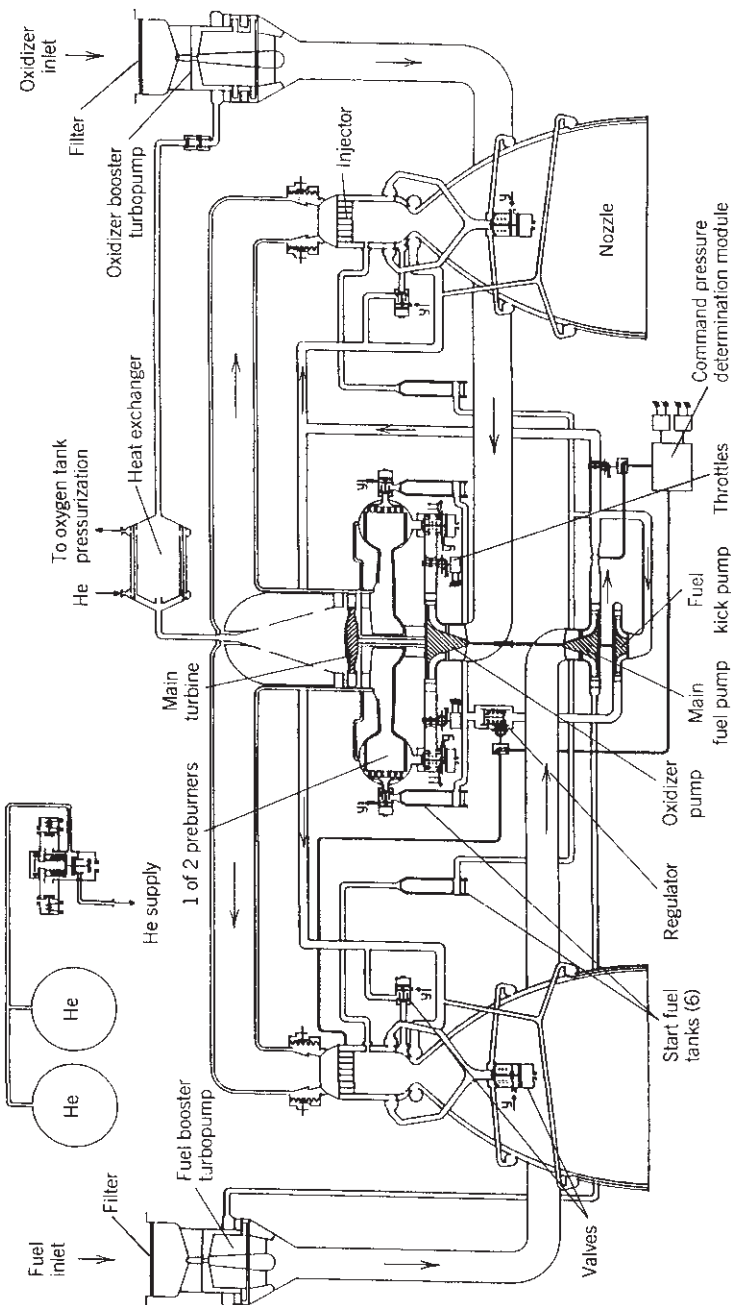


FIGURE 11-2. Simplified flow diagram of the RD-170 high-pressure rocket engine. The single-shaft large turbopump has a single-stage reaction turbine, two fuel pumps, and a single-stage oxygen pump with an inducer impeller. All of the oxygen and a small portion of the fuel flow supply two oxidizer-rich preburners. Only two of the four thrust chambers are shown in this diagram. The two booster pumps prevent cavitation in the main pumps. The pressurized helium subsystem (only shown partially) supplies various actuators and control valves; it is indicated by the symbol y. Ignition is accomplished by injecting a hypergolic fuel into the two preburners and the four thrust chambers. (Courtesy of NPO Energomash, Moscow Region, from Ref. 11-8.)

3. Restart, if desired. With small thrusters there have been thousands of restarts.
4. Maintain programmed operation (e.g., predetermined thrust profile, preset propellant mixture ratio and flow). A constant flow of propellants has been achieved with *sonic flow venturis* in the feed lines. It is briefly discussed in the last paragraph of Section 6.9.
5. Using an engine health monitoring system to prevent certain engine failures or performance losses. This is explained later in this chapter.
6. Fill with propellants.
7. Drain excess propellant after operation of a reusable or a test engine.
8. With cryogenic propellants the pipes, pumps, cooling jackets, injectors, and valves have to be cooled to the cryogenic fluid temperature prior to start, by bleeding cold propellant through them; this cooling propellant is not used to produce thrust. Its periodic flow has to be controlled.
9. Check out proper functioning of critical components or a group of components without actual hot operation before and/or after flight.
10. For recoverable or reusable rocket engines, and for engines use in ground development tests also provide features to perform checks and recycle the engine to a ready condition.

The *complexity* of these control elements and the complexity of the engine systems depend very much on the mission of the vehicle. In general, rockets that are used only once (single-shot devices), that are filled with propellants at the factory, that operate at nearly constant propellant flow, and that have to operate over a narrow range of environmental conditions tend to be simpler than rocket systems intended for repeated use, for applications where satisfactory operation must be demonstrated prior to use, and for manned vehicles. Because of the nature of the liquid propellants, most of the control actuation functions are achieved by valves, regulators, pressure switches, valve position indicators, calibrated orifices, or flow controls. The use of special computers for automatic control in large engines is now common. The flow control devices, namely the valves, were discussed in Section 6.9 and the controls are discussed in this section.

Safety controls are intended to protect personnel and equipment in case of malfunction. This applies mostly to development engines during ground tests, but it can also be applied to certain flight test engines and to certain operating engines. For example, the control system is usually so designed that a failure of the electrical power supply to the rocket causes a nonhazardous shutdown (all electrical valves automatically returning to their normal position) and no mixing or explosion of unreacted propellant can occur. Another example is an electrical interlock device which prevents the opening of the main propellant valves until the igniter has functioned properly.

Check-out controls permit a simulation of the operation of critical control components without actual hot operation of the rocket unit. For example, many

rockets have provisions for permitting actuation of the principal valves without having propellant or pressure in the system.

Control of Engine Starting and Thrust Buildup

In the *starting* and *stopping* process of a rocket engine, it is possible for the mixture ratio to vary considerably from the rated design mixture ratio because of a lead of one of the propellants and because the hydraulic resistances to propellant flow are usually not the same for the fuel and the oxidizer passages. During this transition period, it is possible for the rocket engine to pass through regions of chamber pressure and mixture ratio which can permit combustion instability. The starting and stopping of a rocket engine can be very critical in timing, valve sequencing, and transient characteristics. A good control system must be designed to avoid undesirable transient operation. Close *control* of the *flow* of propellant, of the *pressure*, and of the *mixture ratio* is necessary to obtain reliable and repeatable safe rocket performance. The starting and ignition of thrust chambers has been discussed in Section 8.6.

Fortunately, most rocket units operate with a nearly constant propellant consumption and a constant mixture ratio, which simplifies the operating control problem. Stable operation of liquid propellant flows can be accomplished without automatic control devices because the liquid flow system in general tends to be inherently stable. This means that the hydraulic system reacts to any disturbance in the flow of propellant (a sudden flow increase or decrease) in such a manner as to reduce the effect of the disturbance. The system, therefore, usually has a natural tendency to control itself. However, in some cases the natural resonances of the system and its components can have frequency values that tend to destabilize the system.

The *start delay time* for a pressure feed system is usually small. Prior to start, the pressurization system has to be activated and the ullage volume has to be pressurized. This start delay is the time to purge the system if needed, open valves, initiate combustion, and raise the flow and chamber pressure to rated values. A turbopump system usually requires more time to start. In addition to the foregoing starting steps for a pressurized system, it has to allow a time period for starting a gas generator or preburner and for bringing the turbopumps up to a speed at which combustion can be sustained and thereafter up to full flow. If the propellant is nonhypergolic, additional time has to be allowed for the igniter to function and for feedback to confirm that it is working properly. All these events need to be controlled. Table 11–4 describes many of these typical steps, but not all of them are in every engine.

Starting of small thrusters with a pressurized feed system can be very fast, as short as 3 to 15 msec, enough time for a small valve to open, the propellant to flow to the chamber and to ignite, and the small chamber volume to be filled with high-pressure combustion gas. In an engine with a pressurized feed system the initial flow of each propellant is often considerably higher than the rated flow at full thrust, because the pressure differential ($p_{\text{tank}} - p_1$) is so much higher with

TABLE 11–4. Major Steps in the Starting and Stopping of a Typical Large Liquid Bipropellant Rocket Engine with a Turbopump Feed System

1. Prior to Start

Check out functioning of certain components (without propellant flow), such as the thrust vector control or some valve actuators (optional).

Fill tanks with propellants.

Bleed liquid propellants to eliminate pockets of air or gas in all pipes up to the propellant valves.

When using propellants that can react with air (e.g., hydrogen can freeze air, small solid air crystals can plug injection holes, and solid air crystals with liquid hydrogen can form an explosive mixture), it is necessary to purge the piping system (including injector, valves and cooling jacket) with an inert, dry gas (e.g., helium) to remove air and moisture. In many cases several successive purges are undertaken.

With cryogenic propellants the piping system needs to be cooled to cryogenic temperatures to prevent vapor pockets. This is done by repeated bleeding of cold propellant through the engine system (valves, pumps, pipes, injectors, etc.) just prior to start. The vented cold gas condenses moisture droplets in the air and this looks like heavy billowing clouds escaping from the engine.

Refill or “top off” tank to replace cryogenic propellant that has evaporated or been used for cooling the engine.

Pressurize vehicle’s propellant tanks just before start.

2. Start: Preliminary Operation

Provide start electric signal, usually from vehicle control unit or test operator.

With nonhypergolic propellants, start the ignition systems in gas generator or preburner and main chambers; for nonhypergolic propellants a signal has to be received that the igniter is burning before propellants are allowed to flow into the chambers.

Initial operation: opening of valves (in some cases only partial opening or a bypass) to admit fuel and oxidizer at low initial flows to the high-pressure piping, cooling jacket, injector manifold, and combustion chamber(s). Valve opening rate and sequencing may be critical to achieve proper propellant lead. Propellants start to burn and turbine shaft begins to rotate.

Using an automated engine control, make checks (e.g., shaft speed, igniter function, feed pressures) to assure proper operation before initiating next step.

In systems with gearboxes the gear lubricant and coolant fluid start to flow.

For safety reasons, one of the propellants must reach the chamber first.

3. Start: Transition to Full Flow/Full Thrust

Turbopump power and shaft speed increase.

Propellant flows and thrust levels increase until they reach full-rated values. May use controls to prevent exceeding limits of mixture ratio or rates of increase during transient.

Principal valves are fully opened. Attain full chamber pressure and thrust.

In systems where vaporized propellant is fed into the propellant tanks for tank pressurization, the flow of this heated propellant is initiated.

Systems for controlling thrust or mixture ratio or other parameter are activated.

4. Stop

Signal to stop deactivates the critical valve(s).

Key valves close in a predetermined sequence. For example, the valve controlling the gas generator or preburner will be closed first. Pressurization of propellant tanks is stopped.

As soon as turbine drive gas supply diminishes the pumps will slow down. Pressure and flow of each propellant will diminish quickly until it stops. The main valves are closed, often by spring forces, as the fluid pressures diminish. Tank pressurization may also be stopped. In some engines the propellant trapped in the lines or cooling jacket may be blown out by vaporization or gas purge.

the chamber pressure initially being very low or zero. These higher propellant flows can lead to accumulating propellant in the chamber and can lead what has been called a “hard start” with an initial surge of chamber pressure. In some cases this surge has damaged chambers. One solution has been to open the main propellant valves slowly or build a throttling mechanism into the valves.

For turbopump-fed systems and larger thrust engines, the time from start signal to full chamber pressure is longer, about 1 to 5 sec, because the pump rotors have inertia, the igniter flame has to heat a relatively large mass of initial propellants, the propellant line volumes to be filled are large, and the number of events or steps that need to take place is larger.

Large turbopump-fed rocket engines have been started in at least four ways:

1. A *solid propellant start grain* or start cartridge is used to pressurize the gas generator or preburner, and this starts turbine operations. This method was used on Titan III hypergolic propellant rocket engines (first and second stages) and on the H-1 (nonhypergolic), where the start grain flame also ignites the liquid propellants in the gas generator. This is usually the fastest start method, but it does not normally provide for a restart.
2. This method, known as *tank head start*, is used on the SSME, is slower, does not require a start cartridge, and permits engine restart. The head of liquid from the vehicle tanks (usually in vertically launched large vehicles) plus the tank pressure cause a small initial flow of propellants; then slowly more pressure is built up as the turbine begins to operate and in a couple of seconds the engine “bootstraps” its flows and the pressures then rise to their rated values.
3. A small *auxiliary pressurized propellant feed system* with its own propellant tanks is used to feed the initial quantity of fuel and oxidizer (at essentially full pressure) to the thrust chamber and gas generator. This method was used on one version of the RS-27 engine in the first stage of a Delta II space launch vehicle.
4. The *spinner start* method uses clean high-pressure gas from a separate tank to spin the turbine (usually at less than full speed) until the engine provides enough hot gas to drive the turbine. The high-pressure tank is heavy, the connections add complexity, and it is used on the RS-68. In booster engines, the tank can be part of the ground equipment.

SSME Start and Stop Sequences. This is an example of the transient start and stop behavior of the SSME a complex staged combustion cycle engine with a tank head start. It illustrates the rapid functions of an electronic controller. The SSME flow sheet in Fig. 6–12 identifies the location of the key components mentioned below, and Fig. 11–3 shows the sequence and events of these transients. This section is based on information provided by Pratt & Whitney Rockerdyne.

For a tank head start, initial energy to start the turbines spinning is all derived from initial propellant tank pressures (fuel and oxidizer) and gravity (head of liquid column). Combining the tank head start with a staged combustion cycle

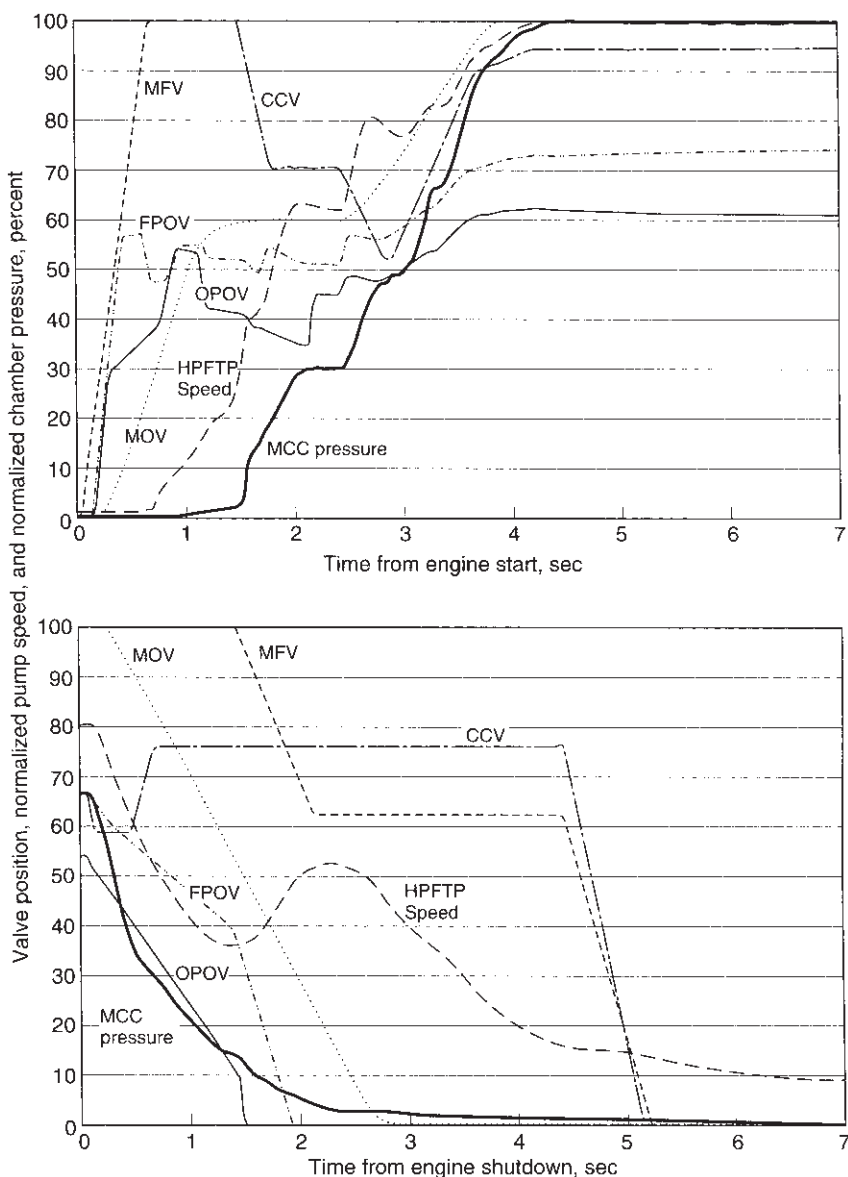


FIGURE 11–3. The sequence and events for starting and shutdown of the SSME (Space Shuttle Main Engine). This particular start sequence leads to a chamber pressure of 2760 psia (normalized here to 100%), a high-pressure fuel turbopump speed of 33,160 rpm (100%), at a sea-level thrust of 380,000 lbf (shown as 100%). This shutdown occurs at altitude when the engine has been throttled to 67% of its power level or a vacuum thrust of 312,559 lbf, which is shown as 67% of the MCC chamber pressure. (Courtesy of Pratt & Whitney Rocketdyne.)

consisting of four pumps, two preburners, and a main combustion chamber (MCC) results in a complicated and sophisticated start sequence, which is very robust and reliable. Prior to the start, the SSME turbopumps and ducting (down to the main propellant valves) are chilled with liquid hydrogen and liquid oxygen (LOX) to cryogenic temperature to ensure liquid propellants for proper pump operation. At engine start command, the main fuel valve (MFV) is opened first to provide chilling below the MFV and a fuel lead to the engine. The three oxidizer valves sequence the main events during the crucial first 2 sec of start. The fuel preburner oxidizer valve (FPOV) is ramped to 56% to provide LOX for ignition in the fuel preburner (FPB) in order to provide initial turbine torque of the high-pressure fuel turbopump (HPFTP). Fuel system oscillations (FSO), which occur due to heat transfer downstream of the initially chilled system, can result in flow rate dips. These fuel flow dips can lead to damaging temperature spikes in the FPB as well as the oxidizer preburner (OPB) at ignition and 2 Hz cycles thereafter until the hydrogen is above critical pressure. The oxidizer preburner oxidizer valve (OPOV) and main oxidizer valve (MOV) are ramped open next to provide LOX for OPB and MCC ignition.

The next key event is FPB prime. Priming is filling of the LOX system upstream of the injectors with liquid propellant. This results in increased combustion and higher power. This event occurs around 1.4 sec into start. The HPFTP speed is automatically checked at 1.24 sec into start to ensure it will be at a high enough level before the next key event, MCC prime, which is controlled by the MOV. Priming and valve timing are critical. We explain some of the events that could go wrong. At MCC prime, an abrupt rise in backpressure on the fuel pump/turbine occurs. If flow rate through the fuel pump at this time is not high enough (high speed), then the heat imparted to the fluid as it is being pumped can vaporize it, leading to unsatisfactory flow in the engine, and subsequent high mixture ratio with high gas temperature and possible burnout in the hot gas system. This occurs if the MCC primes too early or HPFTP speed is abnormally low. If the MCC primes too late, the HPFTP may accelerate too fast due to low backpressure after FPB prime and exceed its safe speed. The MCC prime normally occurs at 1.5 sec. The OPB is primed last since it controls LOX flow and a strong fuel lead and healthy fuel pump flow are desirable to prevent engine burnout due to a high mixture ratio. The OPOV provides minimal flow rate during the early part of the start to force the oxidizer to prime last at 1.6 sec into start. Again, the FSO influences temperature spikes in the OPB and must be sequenced around, prior to the MCC prime which raises the fuel pressure above critical in the fuel system. At 2 sec into start, the propellant valves are sequenced to provide 25% of rated power level (RPL). During the first 2.4 sec of start, the engine is in an open-loop mode, but proportional control of the OPOV is used, based on MCC pressure. At this point, additional checks are carried out to ensure engine health, and a subsequent ramp to mainstage at 2.4 sec is done using closed-loop MCC-chamber-pressure/OPOV control. At 3.6 sec, closed-loop mixture ratio/FPOV control is activated.

The chamber cooling valve (CCV) is open at engine start and sequenced to provide optimum coolant fuel flow to the nozzle cooling jacket and the chamber and preburners during the ignition and main stage operation. It diverts flow to the cooling passages in the nozzle after MCC prime causes the heat load to increase. The description above is simplified and does not mention several other automatic checks, such as verifying ignition in the MCC or FPB or the fuel or chamber pressure buildup, which are sensed and acted upon at various times during the start sequence. The spark-activated igniters are built into the three injectors (MCC, FPB, OPB) using the same propellants. They are not mentioned above or shown in the flow sheet, but one of them can be seen in Fig. 9–6.

The shutdown sequence is initiated by closing the OPOV, which powers down the engine (reduces oxygen flow, chamber pressure, and thrust); this is followed quickly by closing the FPOV, so the burning will shut down fuel rich. Shortly thereafter the MOV is closed. The MFV stays open for a brief time and then is moved into an intermediate level to balance with the oxygen flow (from trapped oxygen downstream of the valves). The MPV and the CCV are closed after the main oxygen mass has been evaporated or expelled.

Automatic Controls

Automatically monitored controls are frequently used in liquid propellant rockets to accomplish thrust control or mixture ratio control. The automatic control of the thrust vector is discussed in Chapter 18.

Before electronic controls became common for large engines, pneumatic controls were used with helium gas. We still use helium to actuate large valves, but no longer for logic control. A pressure ladder sequence control was used, where pressures (and a few other quantities) were sensed and, if satisfactory, the next step of the start sequence was pneumatically initiated. This was used on the H-1 engine and the Russian RD-170 engine, shown in Figs. 11–1 and 11–2.

Most automatic controls use a servomechanism. They generally consist of three basic elements: a *sensing mechanism*, which measures or senses the variable quantity to be controlled; a *computing or controlling mechanism*, which compares the output of the sensing mechanism with a reference value and gives a control signal to the third component, the *actuating device*, which manipulates the variable to be controlled. Additional discussion of computer control with automatic data recording and analysis is given in Chapter 21.

Figure 11–4 shows a typical simple thrust control system for a gas generator cycle aimed at regulating the chamber pressure (and therefore also the thrust) during the flight to a predetermined value. A pressure-measuring device with an electric output is used for the sensing element, and an automatic control device compares this gauge output signal with a signal from the reference gauge or a computer voltage and thus computes an error signal. This error signal is amplified, modulated, and fed to the actuator of the throttle valve. By controlling the propellant flow to the gas generator, the generator pressure is regulated and, therefore, also the pump speed and the main propellant flow; indirectly, the

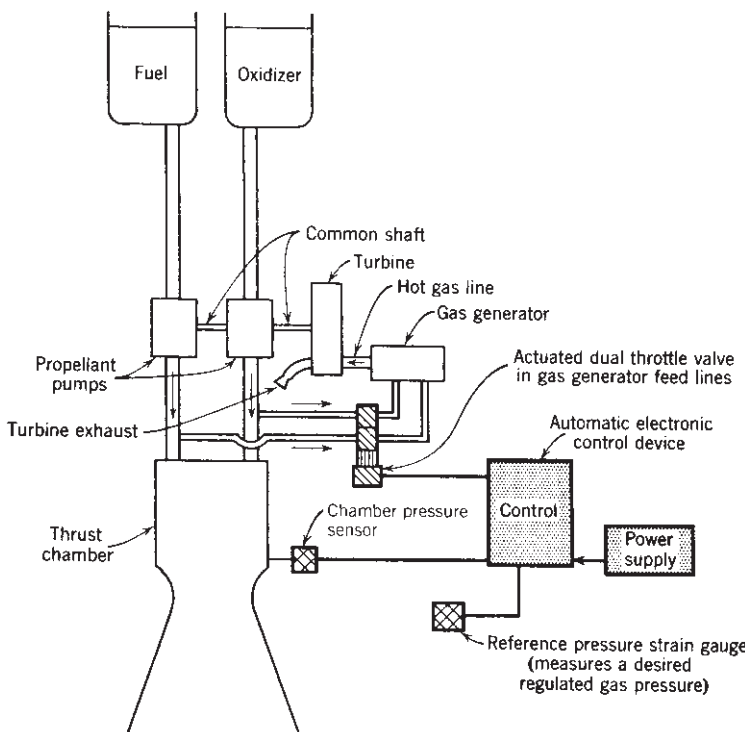


FIGURE 11-4. Simplified schematic diagram of an automatic servomechanism-type chamber pressure control of a liquid propellant rocket engine with a turbopump feed system, a gas generator, and a tank head, boot strap (self-pumping) starting system.

chamber pressure in the thrust chamber is regulated and, therefore, also the thrust. These quantities are varied until such time as the error signal approaches zero. This system is vastly simplified here, for the sake of illustration; in actual practice the system may have to be integrated with other automatic controls. In this diagram the mixture of the gas generator is controlled by the pintle shapes of the fuel and oxidizer valves of the gas generator and by yoking these two valves together and having them moved in unison by a single actuator.

In the expander cycle shown schematically in Fig. 6-11, the thrust is regulated by maintaining a desired chamber pressure and controlling the amount of hydrogen gas flowing to the turbine by means of a variable bypass. The flow through this bypass is small (typically 5% of gas flow) and is controlled by the movement of a control valve.

In a *propellant utilization* system the mixture ratio is varied to ensure that the fuel and oxidizer propellant tanks are both simultaneously and completely emptied; no undue propellant residue should remain to increase the empty mass of the vehicle, which in turn would detrimentally decrease the vehicle mass ratio and the vehicle's flight performance (see Chapter 4). For example, the

oxidizer flow rate may be somewhat larger than normal due to its being slightly denser than normal or due to a lower than normal injector pressure drop; if uncontrolled, a fuel residue would remain at the time of oxidizer exhaustion; however, the control system would cause the engine to operate for a period at a propellant mixture ratio slightly more fuel-rich than normal, to compensate and assure almost simultaneous emptying of both propellant tanks. Such a control system requires accurate measurement of the amount of propellant remaining in the two propellant tanks during the flight.

Any of the three principal components of an automatic control system can have several different forms. Typical sensing devices include those that measure chamber pressure, propellant pressures, pump rotational speeds, tank level, or propellant flow. The actuating device can throttle propellant flow or control a bypass device or the gas generator discharge. There are many operating mechanisms for the controller, such as direct electrical devices, electronic analog or digital computers, hydraulic or pneumatic devices, and mechanical devices. The actuators can be driven by electrical motors or hydraulic, pneumatic, or mechanical power. The hydraulic actuators can provide very high forces and quick response. The exact type of component, the nature of the power supply, the control logic, the system type, and the operating mechanisms for the specific control depend on the details of the application and the requirements. Controls are discussed further in Refs. 11–5 and 11–9.

In applications where the final vehicle velocity must be accurately determined, the amount of impulse that is imparted to the vehicle during the cutoff transient may be sufficiently variable to exceed the desired velocity tolerance. Therefore, in these applications close control over the thrust decay curve is necessary, and this can be accomplished by automatic control over the sequencing and closing rates of the main propellant valves and the location of the valves in relation to the injector.

Control by Computer

Early rocket engines used simple timers and, later, a pressure ladder sequence to send commands to the engine for actuating valves and other steps in the operation. Pneumatic controllers were also used in some engines for starting and stopping. For the last 30 years we have used *digital computers* in large liquid propellant rocket engines for controlling their operation. In addition to controlling the start and stop of engines, they can do a lot more and can contribute to making the engine more reliable. Table 11–5 gives a list of typical functions that a modern engine control computer has undertaken in one or more engines. This list covers primarily large turbopump-fed engines and does not include consideration of multiple small thruster attitude control rocket engines.

The design of control computers is beyond this text. In general it has to consider carefully all the possible engine requirements, all the functions that have to be monitored, all the likely potential failure modes and their compensating or ameliorating steps, all the sensed parameters and their scales, the method of

TABLE 11–5. Typical Functions to be Performed by Digital Computers in Monitoring and Controlling the Operation of a Liquid Propellant Rocket Engine

1. *Sample the signals from significant sensors* (e.g., chamber pressure, gas and hardware temperatures, tank pressure, valve position, etc.) at frequent intervals, say once, 10, 100, or 1000 times per second. For parameters that change slowly, e.g., the temperature of the control box, sampling every second or every 5 sec may be adequate, but chamber pressure would be sampled at a high frequency.
2. *Keep a record of all the significant signals* received and all the signals generated by the computer and sent out as commands or information. Old records have at times been very important.
3. *Control and verify the steps and sequence of the engine start.* Figure 11–3, and Table 11–4 list typical steps that have to be taken, but do not list the measured parameters that will confirm that the commanded step was implemented. For example, if the igniter is activated, a signal change from a properly located temperature sensor or a radiation sensor could verify that the ignition had indeed happened.
4. *Control the shutdown of the engine.* For each of the steps listed at the bottom of Table 11–4 or in Fig. 11–3 there often has to be a sensing of a pressure change or other parameter change to verify that the commanded shutdown step was taken. An *emergency shutdown* may be commanded by the controller, when it senses certain kinds of malfunctions, that allow the engine to be shut down safely before a dramatic failure occurs. This emergency shutdown procedure must be done quickly and safely and may be different from a normal shutdown, and must avoid creating a new hazardous condition.
5. *Limit the duration of full thrust operation.* For example, cutoff is to be initiated just before the vehicle attains the desired mission flight velocity.
6. *Safety monitoring and control.* Detect combustion instability, overtemperatures in precombustors, gas generators, or turbopump bearings, violent turbopump vibration, turbopump overspeed, or other parameter known to cause rapid and drastic component malfunction, that can quickly lead to engine failure. Usually, more than one sensor signal will show such a malfunction. If detected by several sensors, the computer may identify it as a possible failure whose in-flight remedy is well known (and preprogrammed into the computer); then a corrective action or a safe shutdown may be automatically commanded by the control computer. This applies mostly to development engines during ground tests.
7. *Analyze key sensor signals for deviation from nominal performance* before, during, and after engine operation. Determine whether sensed quantities are outside of predicted limits. If appropriate and feasible, if more than one sensor indicates a possible out-of-limit value, and if the cause and remedy can be predicted (preprogrammed), then the computer can automatically initiate a compensating action. Parts of or combinations of items 6 and 7 have been called *engine health monitoring systems*. They are discussed in Section 11.5.
8. *Control propellant tank pressurization.* The tank pressure value has to be within an allowable range during engine operation and also during a coasting flight period prior to a restart. Sensing the activation of relief valves on the tank confirms overpressure. Automatically, the computer can then command stopping or reducing the flow of pressurant.
9. *Perform automatic closed-loop control of thrust and propellant utilization* (described before).
10. *Transmit signals to a flying vehicle's telemetering system*, which in turn can send them to a ground station, thus providing information on the engine status, particularly during experimental or initial flights.
11. *Self-test the computer and software.*

control, such as open, closed, or multiple loops, adaptive or self-learning (expert system), the system architecture, the software approach, the interrelation and division of tasks with other computers on board the vehicle or on the ground, and the method of validating the events and operations. It is also convenient to have software that will allow some changes (which may become necessary because of engine developments or failures) and allow the control of several parameters simultaneously. While the number of functions performed by the control computer seems to have increased in the last 30 years, the size and mass of the control computer has actually decreased.

The control computer is usually packaged in a waterproof, shockproof black box, which is mounted on the engine. Fire-resistant and waterproof cable harnesses lead from this box to all the instrument sensors, valve position indicators, tachometers, accelerometers, actuators, and other engine components, to the power supply, the vehicle's controller, and an umbilical, severable multiwire harness leads to the ground support equipment. Reference 11–10 describes the controller for the Space Shuttle Main Engine.

11.5. ENGINE SYSTEM CALIBRATION

Although an engine has been designed to deliver a specific performance (F , I_s , \dot{m} , r), a newly manufactured engine will not usually perform precisely at these nominal parameters. The calibration process provides the corrections to the engine system, so it will perform of the rated intended operating conditions. If the deviation from the nominal performance values is more than a few percent, the vehicle will probably not complete its intended flight course. There are several reasons for these deviations. Because of unavoidable dimensional tolerances on the hardware, the flow–pressure time profile or the injector impingement (combustion efficiency) will deviate slightly from the nominal design value. Even a small change in mixture ratio will cause a significant increase of residual, unused propellant. Also, minor changes in propellant composition or storage temperature (which affects density and viscosity) can cause deviations. Regulator setting tolerances or changes in flight acceleration (which affects static head) are other factors. An engine calibration is the process of adjusting some of its internal parameters so that it will deliver the intended performance within the allowed tolerance bands. See Refs. 11–5 and 11–6.

Hydraulic and pneumatic components (valves, pipes, expansion joints) can readily be water flow tested on flow benches and corrected for pressure drops and density (and sometimes also viscosity) to determine their pressure drop at rated flow. Components that operate at elevated temperatures (thrust chambers, turbines, preburners, etc.) have to be hot fired and cryogenic components (pumps, some valves) often have to be tested at the cryogenic propellant temperature. The engine characteristics can be estimated by adding together the corrected values of pressure drops at the desired mass flow. Furthermore, the ratio of the rated flows \dot{m}_o/\dot{m}_f has to equal the desired mixture ratio r . This is shown in the example

below. The adjustments include adding pressure drops with judiciously placed orifices or changing valve positions or regulator setting.

In most pressurized feed systems the pressurizing gas is supplied from its high-pressure tank through a regulator to pressurize both the fuel and the oxidizer in their respective tanks. The pressure drop equations for the oxidizer and the fuel (subscripts o and f) are given below for a pressurized feed system at nominal flows:

$$p_{\text{gas}} - (\Delta p_{\text{gas}})_f = p_1 + \Delta p_f + (\Delta p_{\text{inj}})_f + (\Delta p_j)_f + \frac{1}{2} \rho_f v_f^2 - La\rho_f \quad (11-6)$$

$$p_{\text{gas}} - (\Delta p_{\text{gas}})_o = p_1 + \Delta p_o + (\Delta p_{\text{inj}})_o + \frac{1}{2} \rho_o v_o^2 - La\rho_o \quad (11-7)$$

The gas pressure in the propellant tank is the regulated pressure p_{gas} , diminished by the pressure losses in the gasline Δp_{gas} . If includes the pressure drop across a pressure regulator. The static head of the liquid $La\rho$ (L is the distance of the liquid level above the thrust chamber, a is the flight acceleration, and ρ is the propellant density) augments the gas pressure. It has to equal the chamber pressure p_1 plus all the pressure drops in the liquid piping or valves Δp_f , or Δp_o the injector Δp_{inj} , and the cooling jacket Δp_f , or Δp_o and the dynamic flow head $\frac{1}{2} \rho v^2$. If the required liquid pressures (right-hand side of Eq. 11-6 and 11-7.) do not equal the gas pressure in the propellant tank at the nominal propellant flow (left hand side of equations), then an additional pressure drop (calibration orifice) has to be inserted. A good design provides an extra pressure drop margin for this purpose.

Two methods are available for precise control of the engine performance parameters. One uses an automatic system with feedback and a digital computer to control the deviations in real time. The other relies on an initial static calibration of the engine system. The latter approach is simpler and is sometimes preferred, and is still quite accurate.

The *pressure balance* is the process of balancing the available pressure supplied to the engine (by pumps, the static head, and/or pressurized tanks) against the liquid pressure drops plus the chamber pressure. It is necessary to do this balancing in order to calibrate the engine, so it will operate at the desired flows and mixture ratio. Figure 11-5 shows the pressure balance for one of the two branches of the propellant systems in a bipropellant engine with a pressurized feed system. It plots the pressure drops (for injector, cooling jacket passages, pressurizing gas passages, valves, propellant feed lines, etc.) and the chamber pressure against the propellant flow, using actual component pressure drop measurements (or estimated data) and correcting them for different flows. The curves are generally plotted in terms of head loss and volumetric flow to eliminate the fluid density as an explicit variable for a particular regulated pressure. The regulated pressure is usually the same for the fuel and oxidizer pressure balance and it also can be adjusted. This balance of head (the term *head* is defined in Section 10.5) and flow must be made for both the fuel and oxidizer systems because the ratio of their flows establishes the actual mixture ratio and the sum of their flows establishes the thrust. The pressure balance between available and required tank

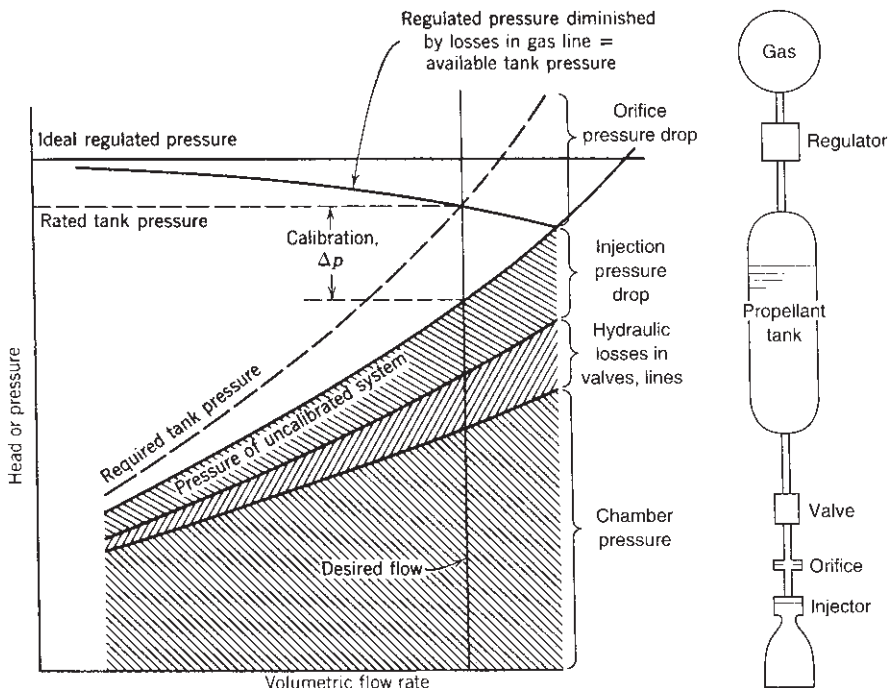


FIGURE 11–5. Simplified flow diagram and balance curves for the fuel or the oxidizer of a typical gas-purified bipropellant feed system. This diagram is also the same for a monopropellant feed system, except that it has no calibration orifice; it is calibrated by setting the proper regulated pressure.

pressure, both at the desired flow, is achieved by adding a calibration orifice into one of the lines, as can be seen in Fig. 11–5. Not shown in the figure is the static head provided by the elevation of the liquid level, since it is small for many space launch systems. However, with high acceleration and dense propellants, it can be a significant addition to the available head.

For a pumped feed system of a bipropellant engine, Fig. 11–6 shows a balance diagram for one branch of the two propellant systems. The pump speed is an additional variable. The calibration procedure is usually more complex for a turbopump system because the pump calibration curves (flow-head-power relation) cannot readily be estimated without good test data and cannot easily be approximated by simple analytical relations. The flow of the propellants to a gas generator or preburner also needs to be calibrated. In this case the turbine shaft torque has to equal the torque required by the pumps and the losses in bearings, seals, or windage. Thus a power balance must be achieved in addition to the matching of pressures and the individual propellant flows. Since these parameters are interdependent, the determination of the calibration adjustments may not always be simple. Many rocket organizations have developed computer programs to carry out this balancing.

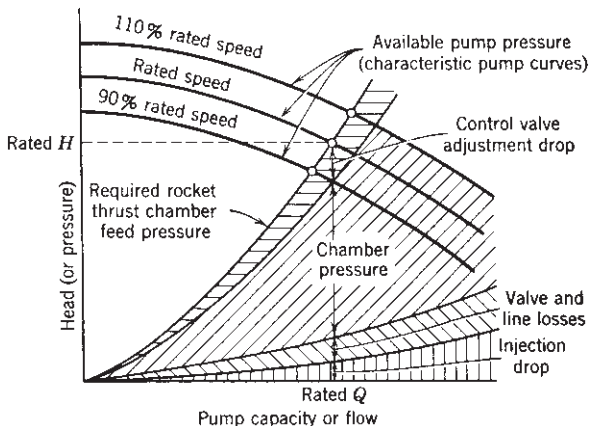


FIGURE 11–6. Simplified diagram of the balance of available and required feed pressures versus flow for one of the propellants in a rocket engine with a turbopump feed system. Chamber pressure is increased by liquid column.

Example 11–2. This example shows one way for converting component test data into nominal engine data. The following component data and design requirements are given for a pressurized liquid propellant rocket system similar to that in Figs. 1–3 and 11–5: fuel, 75% ethyl alcohol; oxidizer, liquid oxygen; desired mixture ratio, 1.30; desired thrust, 500 lbf at sea level. For this propellant combustion gas $k = 1.22$. The propellant temperatures are 70°F for the alcohol fuel and the boiling point (90°K or 162°R) for the liquid oxygen. Assume they do not vary during operation or from run to run. The nozzle throat to exit area ratio is 4.0. Assume a nominal chamber pressure of 300 psia, but correct it later.

Component test data: Pressure losses in gas systems including the pressure regulator were found to be 8.0 psi average for the operating duration at rated propellant flow. Fuel valve and fuel line losses were 9.15 psi at a flow of 0.963 lbm/sec of water. Oxidizer valve and line losses were 14.2 psi at a flow of 1.28 lbm/sec of liquid oxygen. Fuel cooling jacket pressure loss was 35.0 psi at a flow of 0.961 lbm/sec of water. Oxidizer injector pressure drop was 35.0 psi at 1.40 lb/sec of oxygen flow under thrust chamber operating conditions but without fuel or combustion. Fuel injector pressure drop was 40.0 psi at 1.02 lb/sec of fuel flow under thrust chamber operating conditions, but without combustion. Average measured results of several sea-level actual hot thrust chamber tests were: thrust = 541 lbf; mixture ratio = 1.29; specific impulse = 222 sec; and chamber pressure = 328 psia. Determine sea level regulator setting and size and location of calibration orifices.

SOLUTION. First, the corrections necessary to obtain the desired thrust chamber conditions have to be determined. The experimental thrust chamber data must be adjusted for deviations in mixture ratio, thrust, and specific impulse. The variation of specific impulse with *mixture ratio* is determined from experimental data or (on a relative basis) from theoretical calculations similar to those that are the basis of Fig. 5–1. Because the value of I_s at the desired mixture ratio of 1.30 is within 0.08% of the value of I_s under the actual test conditions ($r = 1.29$), any mixture ratio correction of I_s is very small and neglected here.

One has to add the *head of the liquid column* (between the liquid level in the propellant tank and the inlet of the thrust chamber). It is a maximum at the beginning of the flight and decreases as propellant is consumed. For small engine this head can often be small, if

the propellant tanks are close to the thrust chamber. We assume an average head of about 2.5 ft or 0.92 psi of fuel and about 4.0 ft or approximately 2.0 psi of liquid oxygen.

The correction of the *specific impulse* for chamber pressure is made next. The specific impulse is essentially proportional to the thrust coefficients as determined from Eq. 3–30. For $k = 1.22$, the actual measured pressure ratios $p_1/p_3 = 328/14.7 = 22.2$, and the nominal value $300/14.7 = 20.4$, the values of C_F can be calculated as 1.420 and 1.405, respectively. In this calculation p_2 has to be determined for isentropic conditions, such as those in Fig. 3–7 or 3–8 for the given nozzle area ratio. The sea-level specific impulse is therefore corrected to $I_s = 222(1.425/1.420) = 223$ sec. The *chamber pressure* has to be reduced from 328 psi to a lower value in order to bring the thrust from its test value of 541.0 lbf to the design value of 500 lbf. In accordance with Eq. 3–31, $F = C_F A_t p_1$. The throat area A_t is the same for the experimental and flight thrust chambers. The chamber pressure is inversely proportional to the thrust coefficient C_F and proportional to the thrust, and therefore

$$p_1/p'_1 = (F_1/F'_1)(C'_F/C_F) \quad (11-8)$$

The primes refer to the component test condition. The desired value of p_1 is

$$p_1 = 328(500/541)(1.420/1.425) = 304 \text{ psi}$$

It is 1.3% off the value assumed originally (300 psi), and this is close enough for preliminary design. The desired total *propellant flow* is, from Eq. 2–5,

$$\dot{w} = F/I_s = 500/220 = 2.27 \text{ lbf/sec}$$

For a mixture ratio of 1.30, the desired *fuel and oxidizer flows* are obtained from Eqs. 6–3 and 6–4 as $\dot{w}_f = 0.975 \text{ lbf/sec}$ and $\dot{w}_o = 1.267 \text{ lbf/sec}$. Next, the various measured component pressure drops are corrected to the desired flow values and to the corrected propellant densities in accordance with Eq. 8–2, which applies to all hydraulic devices. By neglecting variations in discharge coefficients, which are believed to be very small, this equation can be rewritten into a convenient form:

$$\dot{w}/\dot{w}' = \sqrt{\rho/\rho'} \sqrt{\Delta p/\Delta p'} \quad (11-9)$$

Solve for the estimated pressure drop during operating conditions. Again the prime is for the actual experimental data from component and engine tests.

$$\Delta p = \Delta p' \left(\frac{\dot{w}}{\dot{w}'} \right)^2 \left(\frac{\rho'}{\rho} \right)$$

and for the fuel injector

$$(\Delta p_f)_{\text{inj}} = 40.0 \text{ psi} \left(\frac{0.975}{1.02} \right)^2 \left(\frac{1.00}{0.85} \right) = 42.5 \text{ psi}$$

With this equation and the known specific gravity values (from Fig. 7–1) of 1.14 for cryogenic oxygen, 0.85 for diluted ethyl alcohol, and 1.0 for water, the new pressure drops for the corrected flow conditions can be found, and these are tabulated below with flow values given in pounds per second and pressure values in pounds per square inch.

| Component | Component Test Data | | | Design Conditions | | |
|-------------------------|---------------------|-----------|------------|-------------------|-----------|------------|
| | Fluid | \dot{m} | Δp | Fluid | \dot{m} | Δp |
| Fuel injector | Water | 1.02 | 40.3 | Fuel | 0.975 | 42.9 |
| Oxidizer injector | Oxygen | 1.30 | 35.0 | Oxygen | 1.267 | 30.9 |
| Fuel cooling jacket | Water | 0.961 | 35.0 | Fuel | 0.975 | 42.4 |
| Fuel valve and line | Water | 0.963 | 9.15 | Fuel | 0.975 | 11.0 |
| Oxidizer valve and line | Oxygen | 1.28 | 14.2 | Oxygen | 1.267 | 13.7 |

Adding the liquid line pressure drop, the chamber pressure and the tank column pressures required, one obtains for the tank pressures

$$(p_o)_{\text{tank}} = 30.9 + 304 - 2 + 13.7 = 346.6 \text{ psi}$$

$$(p_f)_{\text{tank}} = 42.8 + 304 - 0.92 + 11 + 42.4 = 399.9 \text{ psi}$$

To equalize the tank pressures so that a single gas pressure regulator can be used and so that the flow system will be in balance, an *additional pressure loss must be introduced into the oxygen system*. The correction to this simple pressurized liquid propellant system is accomplished by means of an orifice, which must be placed in the propellant piping between the oxidizer tank and the thrust chamber. Allowing 10 psi for regulator functioning, the pressure drop available for in a calibration orifice will be $\Delta p = 399.9 - 346.6 = 52.7$ psi. The *regulator setting* should be adjusted to give a regulated pressure downstream of the regulator of 399.9 psi under flow conditions. The orifice area (assume a discharge coefficient $C_d = 0.60$ for a sharp-edged orifice) can be obtained from Eq. 8–2, but corrected with a g_0 for English units:

$$\begin{aligned} A &= \frac{\dot{m}}{C_d \sqrt{2g_0 \rho \Delta p}} = \frac{1.274}{0.60 \sqrt{2 \times 32.2 \times 71.1 \times 59.8}} \\ &= 0.00432 \text{ in.}^2 \text{ (or } 0.074 \text{ in. diameter)} \end{aligned}$$

A set of balancing equations can be assembled into a computer program to assist in the calibration of engines. It can also include some of the system's dynamic analogies that enable proper calibration and adjustment of transient performance of the engine as during start. There is a trend to require tighter tolerances on rocket engine parameters (such as thrust, mixture ratio, or specific impulse), and therefore the measurements, calibrations, and adjustments are also being performed to much tighter tolerances than was customary 40 years ago.

Engine Health Monitoring System

Health monitoring systems (HMS) for rocket engines also called *condition monitoring systems* are sophisticated engine control systems. The HMS evolved from conventional sets of measuring instruments about 20 years ago, when the first rudimentary forms of HMS were used. Today there are several variations or types of HMSs. References 11–5, 11–11, and 11–12 show different aspects of an HMS.

HMSs are used to monitor the performance and behavior of an operating liquid propellant engine by measuring and recording in real time key parameters of an engine such as chamber pressure, pump speed, or turbine gas inlet temperature. It can also be used to calibrate an engine. A computer would compare the actually measured but corrected data with the intended or desired nominal data of an engine operating at the intended design condition (which was obtained by analysis or prior data from earlier engines, which had performed satisfactorily). The computer would analyze the results and provide output indicating a need for action, such as changing calibration orifices, trimming an impeller, or valve timing adjustments. This remedial action would not be actually initiated by the HMS, but the corrective work would be done by test technicians or the factory. This improved calibration can be done on ground tests of R&D engines or production engines.

HMSs are also used extensively during ground development testing where similar parameters are monitored and measured, but many impending potential or incipient failures can also be detected, and the HMS computer can quickly take remedial action before an actual failure occurs. This has saved much R&D hardware. A more detailed description of this second HMS application can be found in Section 21.3. Also this first function and the test stand failure remedy function can be combined.

In the third application the HMS is used during lift-off of a launch vehicle and it is discussed below. The HMS monitors the booster engines during their start period (by checking key engine parameters in real time against their intended design values) and determines if the engine is healthy or is likely to experience an impending failure after the engine has been fully started on the launch stand, but just before the vehicle is released and allowed to fly. It provides a safety feature not only for the booster engine(s), but also for the launch vehicle. The measurements are performed for a few seconds only during the start period and can include readings from instruments for various valve positions, turbopump shaft speed, pump suction pressure, gas temperature of the gas generator or preburner, or chamber pressure. If the HMS determines that the liquid propellant rocket engine(s) are healthy, it gives a signal to the vehicle computer and/or the launch facility computer and the vehicle will be released, allowing the launch to proceed. If the HMS detects a major potential or impending failure in one of the booster engines (and this may often be sensed in many engines before the full thrust is attained), it sends a signal to the vehicle not to launch. It also initiates the safe shutdown of all the booster engines installed in the vehicle held on the launch stand, before the impending failure and major damage can take place. The SSME start sequence in Fig. 11–3 shows that starting requires about 4.4 sec to reach full thrust and about 3 sec to reach 50% of full thrust, so there is sample time for an HMS application.

The nominal intended value of each measured parameter is usually based on a theoretical analysis of the transient behavior of the engine during the start and it usually has been validated and modified by actual data from measurements of prior rocket engines. With each nominal intended value there is an upper and a

lower limit line, known as red lines. If the actual measured value fall between the two limit lines, then the measured parameter is satisfactory. If it goes over one of the limit lines, then it is an indication of improper engine behavior. By itself a single off-limit measurement is not necessarily an indication of failure. If there should be a potential impending failure, the HMS has to have a verification of this fact; it should not rely on just this single malfunction indication because the measuring instrument or its signal processing may be flawed. Usually when there is a real likely future failure, more than one instrument will have measurements which exceed a red line. For example, if the fuel pump discharge line is well below its intended value of pressure or flow at a particular time during the start sequence, it may indicate an insufficient supply of fuel to the pump, fuel that may be warmer than it should be, a low pump speed, or a possible leak of this propellant. It would be validated by measurements of the suction pressure to the pump, temperature measurements at the pump, shaft rpm, or a sensor for fuel in the engine compartment. With three such out of tolerance readings, and with an assessment of the severity of the potential failure, the HMS automatically registers it as a real impending failure. The HMS will immediately send a signal to the vehicle computer and the ground control computer of an impending engine failure (stopping the vehicle release or the launch). This same signal will initiate a safe shutdown of all booster engines.

Once the vehicle is launched the HMS continues to check and record the performance and various engine parameters, but is not usually programmed to implement remedies during flight, such as changing gas temperature or changing thrust level. However, with multiple engines, one of the engines can be shut down and the mission can then be completed by firing the other engines for a longer duration, but providing the same total impulse. The mission can then be completed by firing the remaining functioning engines (at a reduced total thrust, but a longer duration) using essentially all the propellants. The flight controller in the vehicle has to be programmed to allow a lower thrust of longer duration, and the flight path will be different, but the mission can be completed. This shutdown of one of the engines during flight has actually happened in a five-engine cluster configuration and the flight mission was satisfactorily completed on four engines.

11.6. SYSTEM INTEGRATION AND ENGINE OPTIMIZATION

Rocket engines are part of a vehicle and must interact and be integrated with other vehicle subsystems. There are *interfaces* (connections, wires, or pipelines) between the engine and the vehicle's structure, electric power system, flight control system (commands for start or thrust vector control), and ground support system (for check-out or propellant supply). The engine also imposes limitations on vehicle components by its heat emissions, noise, and vibrations.

Integration means that the engine and the vehicle are compatible with each other, interfaces are properly designed, and there is no interference or unnecessary

duplication of functions with other subsystems. The engine works with other subsystems to enhance the vehicle's performance and reliability, and reduce the cost. Some organizations use "system engineering" techniques to achieve this integration. See Ref. 11–7. In Chapter 19 we describe the process of selecting rocket propulsion systems and it includes a discussion of interfaces and vehicle integration. This discussion in Chapter 19 is supplementary and applies to several different rocket propulsion systems. This section concerns liquid propellant rocket engines.

Since the propulsion system is usually the major mass of the vehicle, its structure (which usually includes the tanks) often becomes a key structural element of the vehicle and has to withstand not only the thrust force but also various vehicle loads, such as aerodynamic forces or vibrations. Several alternate tank geometries and locations (fuel, oxidizer, and pressurizing gas tanks), different tank pressures, and different structural connections have to be evaluated to determine the best arrangement.

The thermal behavior of the vehicle is strongly affected by the heat generation (hot plume, hot engine components, or aerodynamic heating) and the heat absorption (the liquid propellants are usually heat sinks) and by heat rejection to its surroundings. Many vehicle components must operate within narrow temperature limits, and their thermal designs can be critical when evaluated in terms of the heat balance during, after, and before the rocket engine operation.

Optimization studies are conducted to select the best values or to optimize various vehicle parameters such as vehicle performance (see below), thrust, number of restarts, or engine compartment geometry. These studies are usually performed by the vehicle designers with help from the propulsion system designers. The rocket engine designers conduct optimization studies (with help from the vehicle designers) on engine parameters such as chamber pressure (or thrust), mixture ratio (which affects average propellant density and specific impulse), number of thrust chambers, nozzle area ratio, or engine volume. By changing one or more of these parameters, it is usually possible to make some improvement to the vehicle performance (0.1 to 5.0%), its reliability, or to reduce costs. Depending on the mission or application, the studies are aimed at maximizing one or more vehicle parameter such as range, vehicle velocity increment, payload, circular orbit altitude, propellant mass fraction, or minimizing costs. For example, the mixture ratio of hydrogen–oxygen engines for maximum specific impulse is about 3.6, but most engines operate at mixture ratios between 5 and 6 because the total propellant volume is less, and this allows a reduced mass for the propellant tanks and the turbopump (resulting in a higher vehicle velocity increment) and a reduced vehicle drag (more net thrust). The selection of the best nozzle area ratio was mentioned in Chapter 3; it depends on the flight path's altitude–time history; the increase in specific impulse is offset by the extra nozzle weight and length. The best thrust–time profile can also usually be optimized, for a given application, by using trajectory analyses.

PROBLEMS

- Estimate the mass and volume of nitrogen required to pressurize an N_2O_4 –MMH feed system for a 4500 N thrust chamber of 25 sec duration ($\zeta_v = 0.92$, the ideal, $I_s = 285$ sec at 1000 psi or 6894 N/m^2 and expansion to 1 atm). The chamber pressure is 20 atm (abs.) and the mixture ratio is 1.65. The propellant tank pressure is 30 atm, and the initial gas tank pressure is 150 atm. Allow for 3% excess propellant and 50% excess gas to allow some nitrogen to dissolve in the propellant. The nitrogen regulator requires that the gas tank pressure does not fall below 29 atm.
- A rocket engine operating on a gas generator engine cycle has the following data as obtained from tests:

| | |
|---|--------------------------------|
| Engine thrust | 100,100 N |
| Engine specific impulse | 250.0 sec |
| Gas generator flow | 3.00% of total propellant flow |
| Specific impulse of turbine exhaust flowing through a low area ratio nozzle | 100.2 sec |

Determine the specific impulse and thrust of the single thrust chamber.

Answers: 254.6 sec and 98,899 N.

- This problem concerns the various potential propellant loss/utilization categories. The first section of this chapter identifies most of them. This engine has a turbopump feed system with a single TP, a single fixed-thrust chamber (no thrust vector control), no auxiliary small thrusters, storable propellants, good priming of the pumps prior to start, and a gas generator engine cycle. Prepare a list of propellant utilization/loss categories for which propellant has to be provided. Which of these categories will have a little more propellant or a little less propellant, if the engine is operated with either warm propellant (perhaps 30 to 35°C) and alternatively in a cold space environment with propellants at -25°C ? Give brief reasons, such as “higher vapor pressure will be more likely to cause pump cavitation.”
- What happens to the thrust and the total propellant flow if an engine (calibrated at 20°C) is supplied with propellants at high or at low storage temperature?

SYMBOLS

| | |
|-------|--|
| a | acceleration, $\text{m/sec}^2(\text{ft/sec}^2)$ |
| A | area, $\text{m}^2(\text{ft}^2)$ |
| C_F | thrust coefficient (see Eq. 3–30) |
| F | thrust, N (lbf) |
| g_0 | sea-level acceleration of gravity, $9.806 \text{ m/sec}^2(32.17 \text{ ft/sec}^2)$ |
| H | head, m (ft) |
| I_s | specific impulse, sec (lbf-sec/lbm) |
| k | specific heat ratio |
| L | length, m (ft) |

| | |
|-------------|--|
| \dot{m}_o | mass flow rate, kg/sec (lb/sec) |
| p | pressure, N/m ² (lbf/in. ²) |
| Q | volume flow rate, m ³ /sec (ft ³ /sec) |
| r | flow mixture ratio (oxidizer to fuel flow) |
| t | time, sec |
| T | absolute temperature, K (°R) |
| v | fluid or liquid velocity, m/sec ³ (ft/sec) |
| \dot{w} | weight flow rate kg-m/sec ³ (lb-ft/sec ³) |

Greek Letters

| | |
|-----------|--|
| Δ | finite difference |
| ζ_d | discharge correction factor |
| ζ_v | velocity correction factor |
| ρ | density, kg/m ³ (lb/ft ³) |

Subscripts

| | |
|-------|---------------------------------|
| c | chamber |
| f | fuel |
| gg | gas generator |
| o | oxidizer |
| oa | overall engine system |
| P | pump |
| T | turbine |
| t_p | tank pressurization |
| 0 | initial condition |
| 1 | inlet or chamber condition |
| 2 | outlet or nozzle exit condition |

REFERENCES

- 11–1. Personal communication from Robert Sackheim, circa 1990.
- 11–2. P. Brossel, S. Eury, P. Signol, H. Laporte, and J. B. Micewicz, “Development Status of the Vulcain Engine,” AIAA Paper 95-2539, 1995.
- 11–3. R. Iffly, “Performance Model of the Vulcain Ariane 5 Main Engine,” AIAA Paper 1996–2609, 1996.
- 11–4. G. Mingchu and L. Guoqui, “The Oxygen/Hydrogen Engine for Long March Vehicle,” AIAA Paper 95–2838, 1995.
- 11–5. D. K. Huzel, and D. H. Huang, “Design of Rocket Engine Controls and Condition Monitoring Systems,” Chapter 7, and “Engine System Design Integration,” Chapter 9 of *Modern Engineering Design of Liquid Propellant Rocket Engines*, rev. ed., Vol. 147 of *Progress in Astronautics and Aeronautics* (Series), AIAA, Reston, VA, 1992.

- 11–6. R. W. Humble, G. N. Henry, and W. J. Larson, “Liquid Rocket Propulsion Systems,” Chapter 5 in *Space Propulsion Analysis and Design*, McGraw-Hill, New York, 1995.
- 11–7. P. Fortescue, J. Stark, and G. Swinerd, *Spacecraft System Engineering*, 3rd ed., John Wiley and Sons, Chichester, England, 2003, reprinted 2005.
- 11–8. Communication with Energomash, Khimki, Moscow Region, Russia, circa 1998. and data from James Morehart, of The Aerospace Corp. 2003–2008.
- 11–9. A. D’Souza, *Design of Control Systems*, Prentice Hall, New York, 1988.
- 11–10. R. M. Mattox and J. B. White, “Space Shuttle Main Engine Controller,” NASA Technical Paper 1932, 1981.
- 11–11. H. Zhang, J. Wu, M. Huang, H. Zhu, and Q. Chen, “Liquid Rocket Engine Health Monitoring Techniques,” *Journal of Propulsion and Power*, Vol. 14, No. 5, September–October 1988, pp. 657–663.
- 11–12. A. Ray, X. Dai, M-K., Wu, M. Carpino, and C. F. Lorenzo, “Damage-Mitigating Control of a Reusable Rocket Engine,” *Journal of Propulsion and Power*, Vol. 10, No. 2, March–April 1994, pp. 225–234.

CHAPTER 12

SOLID PROPELLANT ROCKET FUNDAMENTALS

This is the first of four chapters on solid propellant rockets. It discusses the burning rates, motor performance, grain configurations, and structural analysis. In solid propellant rocket motors—and the word “motor” is as common to solid rockets as the word “engine” is to liquid rockets—the propellant is contained and stored directly in the combustion chamber, sometimes hermetically sealed in the chamber for long-time storage (5 to 20 years). Motors come in many different types and sizes, varying in thrust from about 2 N to over 12 million N (0.4 to over 3 million lbf). Historically, solid propellant rocket motors have been credited with having no moving parts. This is still true of many, but some motor designs include movable nozzles and actuators for vectoring the line of thrust relative to the motor axis. In comparison to liquid rockets, solid rockets are usually relatively simple, are easy to apply (they often constitute most of the vehicle structure), and require little servicing; they cannot be fully checked out prior to use, and thrust cannot usually be randomly varied in flight.

Figures 1–5 and 12–1 show the principal components and features of relatively simple solid propellant rocket motors. The *grain* is the solid body of the hardened *propellant* and typically accounts for 82 to 94% of the total motor mass. Designs and stresses of grains are described later in this chapter. Propellants and their properties are described in the next chapter. The *igniter* (electrically activated) provides the energy to start combustion. The grain starts to burn on its exposed inner surfaces. The combustion and ignition of solid propellants are discussed in Chapter 14. In Fig. 12–1 the grain configuration has a central cylindrical cavity with eight tapered slots, forming an eight-pointed star. Many grains have slots, grooves, holes, or other geometric features which alter the initial burning surface and determine the initial mass flow and the initial thrust. The hot reaction gases flow along the *perforation* or *port cavity*.

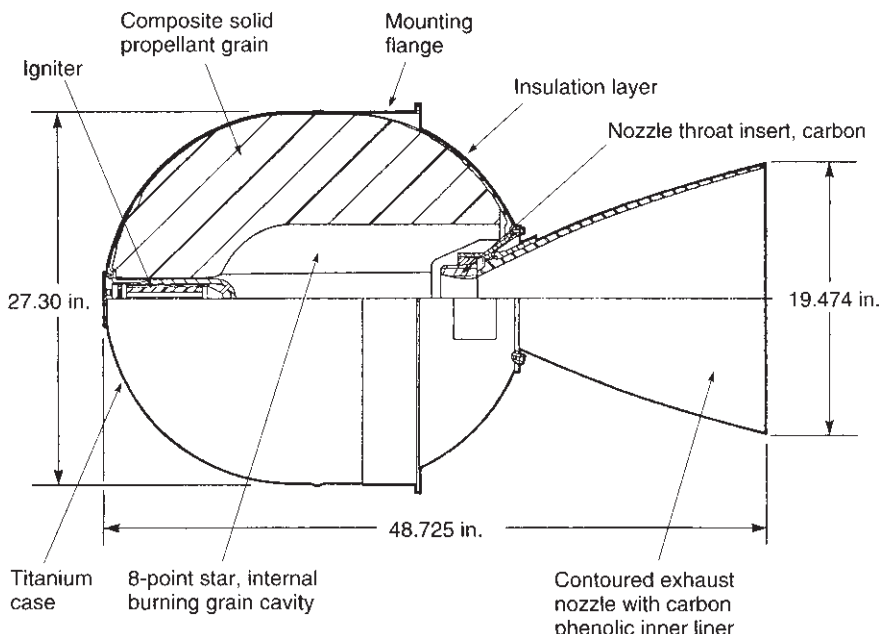


FIGURE 12–1. Cross section of the STAR™ 27 rocket motor, which has been used for orbit and satellite maneuvers. It has an altitude thrust of 6000 lbf, nominally burns for 34.4 sec and has an initial mass of 796 lbm. For more data see Table 12–3. (Courtesy of ATK Launch systems.)

toward the nozzle. The inner surfaces of the *case* (really a pressure vessel), which are exposed directly to hot gas, have a thermal protection or *insulation layer* to keep the case from becoming too hot, in which case it could no longer carry its pressure and other loads. The case is either made of metal (such as steel, aluminum or titanium) or a composite fiber-reinforced plastic material.

The *nozzle* accelerates the hot gas; it is made of high-temperature materials (usually a graphite and/or an ablative material to absorb the heat) to withstand the high temperatures and the erosion. The majority of all solid rockets have a simple fixed nozzle, as shown in these figures, but some nozzles have provisions to rotate it slightly so as to control the direction of the thrust to allow vehicle steering. Chapter 15 describes nozzles, cases, insulators, liners, and the design of solid propellant rocket motors.

Each motor is fastened to its vehicle by a thrust-carrying *structure*. In Fig. 12–1 there is a skirt (with a flange) integral with the case; it is fastened to the vehicle. As indicated above, there is no active cooling and the motor must be designed to withstand the transient heat loads without failure.

The subject of thrust vector control, exhaust plumes, and testing are omitted from these four chapters but are treated for both liquid and solid propellant units in Chapters 18, 20, and 21, respectively. Chapter 19 provides a comparison of

the advantages and disadvantages of solid and liquid propellant rocket units. Chapters 3 to 5 are needed as background for these four chapters.

Applications for solid propellant rockets are shown in Tables 1–3, 1–4, and 12–1; each has its own mission requirements and thus propulsion requirements. Figures 12–2 to 12–4 illustrate representative designs for some of the major categories of rocket motors listed in Table 12–1: namely, a large booster or second stage, a motor for space flight, and a tactical missile motor. Reference 12–1 is useful for component and design information. The Atlas V solid rocket booster (SRB) shown in Fig. 12–2 is representative of a modern, large solid booster designed by Aerojet General Corp. Depending on the payload, there can be up to five boosters mounted in the manner shown in the sketch of Fig. 4–14 labeled *parallel staging*. Several SRBs can be seen in Fig. 1–13 boosting the Atlas V. The motor grain is a tubular design with slots at the aft end; this style of grain corresponds to the third sketch from the top on Fig. 12–16. The propellant consists of aluminized hydroxyl-terminated polybutadiene (HTPB)/ammonium perchlorate (AP) (see Chapter 13). The case structure is a large, lightweight graphite–fiber–composite unit that unlike the Shuttle’s SRMs (see Fig. 15–2) has no segments or joints. This motor has been designed with a mechanical release device, which separates the motor after SRB burnout. A new erosion-resistant internal insulation based on EPDM (ethylene propylene diene monomer, see Section 13.6.) has been introduced; EPDM is a low-density rubber-like material. In common with other SRMs, some nonpropellant material such as insulation and nozzle liner and throat insert is burned, decomposed, eroded, charred, and ejected during propellant burning, which amounts to about 1% of the propellant mass. The *propellant mass fraction* is estimated to be about 0.90 for the bare motor.

There are several ways for classifying solid propellant rockets. Some are listed in Table 12–2 together with some definitions. Table 12–3 gives characteristics for three specific rocket motors, and from these data one can obtain a feeling for the magnitudes of the key parameters. These motors are shown in Figs. 18–5 and 18–9.

Almost all rocket motors are used only once. The hardware that remains after all the propellant has been burned and the mission completed—namely, the nozzle, case, or thrust vector control device—is not reusable. In very rare applications, such as NASA’s Space Shuttle solid booster, is the hardware recovered, cleaned, refurbished, and reloaded; reusability makes the design more complex, but if the hardware is reused often enough a major cost saving will result. Unlike some liquid propellant rocket engines, a solid propellant rocket motor and its key components cannot be operationally pretested. As a result, individual motor reliability must be inferred by assuring the structural integrity and verifying manufacturing quality on the entire population of motors.

12.1. BASIC RELATIONS AND PROPELLANT BURNING RATE

The rocket motor’s operation and design depend on the combustion characteristics of the propellant, its burning rate, burning surface, and grain geometry.

TABLE 12-1. Major Application Categories for Solid Propellant Rocket Motors

| Category | Application | Typical Characteristics |
|---------------------------------------|--|--|
| Large booster and second-stage motors | Space launch vehicles; lower stages of long-range ballistic missiles (see Figs. 12-2 and 15-2) | Large diameter (above 48 in.); L/D of case = 2–7; burn time t = 60–120 sec; low-altitude operations with low nozzle area ratios (6–16) |
| High-altitude motors | Upper stages of multistage ballistic missiles, space launch vehicles; space maneuvers | High-performance propellant; large nozzle area ratio (20–200); L/D of case = 1–2; burn time t = 40–120 sec (see Fig. 12-3) |
| Tactical missiles | <p>1. High acceleration: short-range bombardment, antitank missile</p> <p>2. Modest acceleration, guided or unguided: air-to-surface, surface-to-air, short-range guided surface-to-surface, and air-to-air missiles. Infantry support weapons, shoulder fired antitank on anti-aircraft missiles, mortars</p> | <p>Tube launched, L/D = 4–13; very short burn time (0.25–1 sec); small diameter (2.75–18 in.); some are spin stabilized</p> <p>Small diameter (2.5–18 in.); L/D of case = 5–10; usually has fins and/or wings; thrust is high at launch and then is reduced (boost-sustain); many have blast tubes (see Fig. 12-4); wide ambient temperature limits: sometimes minimum temperature -65°F or -53°C, maximum temperature $+160^{\circ}\text{F}$ or $+71^{\circ}\text{C}$; usually high acceleration; often low-smoke or smokeless propellant</p> |
| Ballistic missile defense | Defense against long- and medium-range ballistic missiles | Booster rocket and a small upper maneuverable stage with multiple attitude control nozzles and one or more larger side or divert nozzles |
| Gas generator | Pilot emergency escape; push missiles from submarine launch tubes or land mobile cannisters; actuators and valves; short-term power supply; jet engine starter; munition dispersion; rocket turbine drive starter; automotive air bags | Usually low gas temperature ($<1300^{\circ}\text{C}$); many different configurations, designs, and propellants; purpose is to create high-pressure, energetic gas rather than thrust |

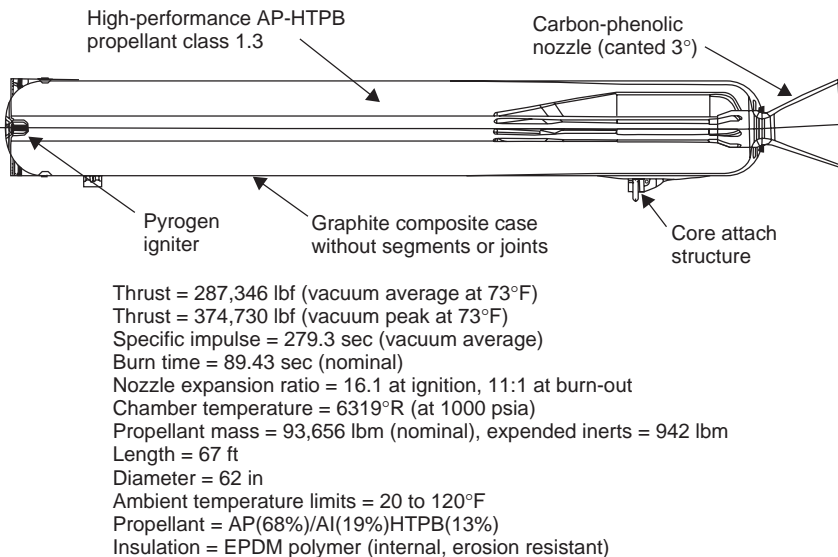


FIGURE 12–2. Atlas V solid rocket booster (SRB) cross-sectional view. This motor has a large monolithic carbon–composite case and other novel features representative of modern solid boosters. (Courtesy of Aerojet General Corp.)

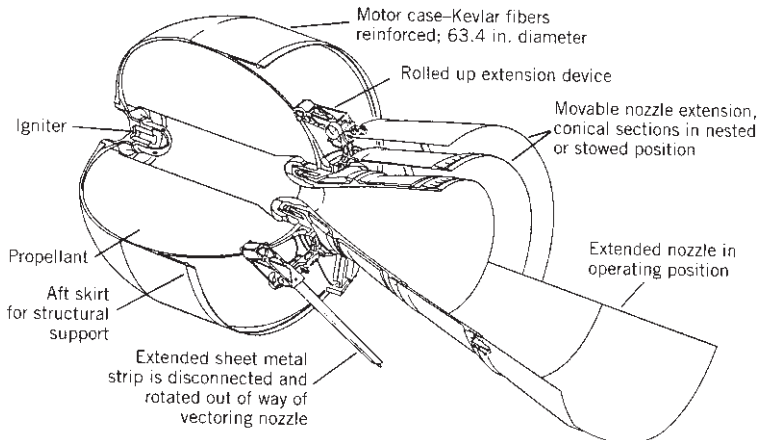


FIGURE 12–3. Inertial upper-stage (IUS) rocket motor with an extendible exit cone (EEC). This motor is used for propelling upper launch vehicle stages or spacecraft. The grain is simple (internal tube perforation). With the EEC and a thrust vector control, the motor has a propellant mass fraction of 0.916. When launched, and while the two lower vehicle stages are operating, the two conical movable nozzle segments are stowed around the smaller inner nozzle segment. Each of the movable segments is deployed in space and moved into its operating position by three identical light-weight, electrically driven actuators. The nozzle area ratio is increased from 49.3 to 181; this improves the specific impulse by about 14 sec. This motor (without the EEC) is described in Table 12–3 and a similar motor is shown in Fig. 18–5. (Courtesy of United Technologies Corp.)

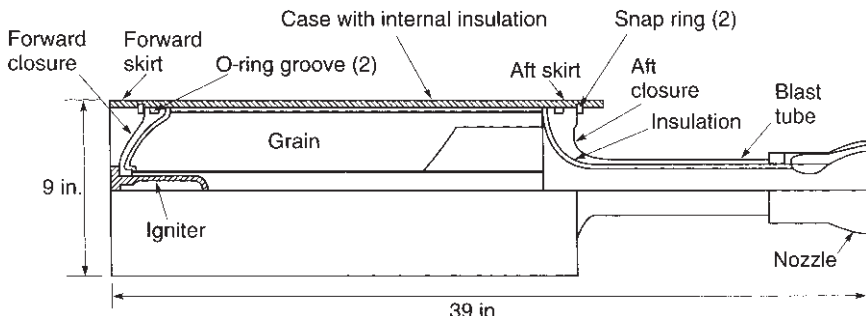


FIGURE 12-4. Simplified cross section through a typical tactical motor. The blast tube allows the grain to be close to the center of gravity of the vehicle; there is very little movement of the center of gravity. The nozzle is at the missile's aft end. The annular space around the blast tube is usually filled with guidance, control, and other nonpropulsive equipment. A freestanding grain is loaded before the aft closure is assembled.

The branch of applied science describing these is known as *internal ballistics*; the effect of grain geometry is treated in Section 12.3.

The burning surface of a propellant grain recedes in a direction essentially perpendicular to the surface. The rate of regression, usually expressed in cm/sec, mm/sec, or in./sec, is the *burning rate* r . In Fig. 12-5 we can visualize the change of the grain geometry by drawing successive burning surfaces with a constant time interval between adjacent surface contours. Figure 12-5 shows this for a two-dimensional grain with a central cylindrical cavity with five slots. Success in rocket motor design and development depends significantly on knowledge of burning rate behavior of the selected propellant under all motor operating conditions and design limit conditions. Burning rate is a function of the propellant composition. For composite propellants it can be increased by changing the propellant characteristics:

1. Add a burning rate *catalyst*, often called burning rate *modifier* (0.1 to 3.0% of propellant) or increase percentage of existing catalyst.
2. *Decrease the oxidizer particle size.*
3. *Increase oxidizer percentage.*
4. Increase the *heat of combustion* of the binder and/or the plasticizer.
5. Imbed *wires* or *metal staples* in the propellant.

Aside from the propellant formulation and propellant manufacturing process, burning rate in a full-scale motor can be increased by the following:

1. Combustion chamber pressure
2. Initial temperature of the solid propellant prior to start
3. Combustion gas temperature

TABLE 12–2. Classification of Solid Rocket Motors

| Basis of Classification | Examples of Classification |
|-------------------------|--|
| Application | See Table 12–1. |
| Diameter/length | 0.005–6.6 m or 0.2–260 in.; 0.025–45 m or 1–1800 in. |
| Propellant | <i>Composite</i> : Heterogeneous (physical) mixture of powdered metal (fuel), crystalline oxidizer and polymer binder <i>Double-base</i> : Homogeneous mixture (colloidal) of two explosives (usually nitroglycerin in nitrocellulose) <i>Composite-modified double-base</i> : Combines composite and double-base ingredients |
| Case design | <i>Gas generator and others</i> : See Chapter 13 <i>Steel monolithic</i> : One-piece steel case <i>Fiber monolithic</i> : Filament wound (high-strength fibers) with a plastic matrix <i>Segmented</i> : Case (usually steel) and grain are in segments which are transported separately and fastened together at launch site |
| Grain configuration | <i>Cylindrical</i> : Cylindrically shaped, usually hollow <i>End-burning</i> : Solid cylinder propellant grain <i>Other configurations</i> : See Figs. 12–16 and 12–17 |
| Grain installation | <i>Case-bonded</i> : Adhesion exists between grain and case or between grain and insulation and case; propellant is usually cast into the case <i>Cartridge-loaded</i> : Grain is formed separately from the motor case and then assembled into case |
| Explosive hazard | <i>Class 1.3</i> : Catastrophic failure shows evidence of burning and explosion, not detonation <i>Class 1.1</i> : Catastrophic failure shows evidence of detonation |
| Thrust action | <i>Neutral grain</i> : Thrust remains essentially constant during the burn period <i>Progressive grain</i> : Thrust increases with time <i>Regressive grain</i> : Thrust decreases with time <i>Pulse rocket</i> : Two or more independent thrust pulses or burning periods <i>Step-thrust rocket</i> : Usually, two distinct levels of thrust |
| Toxicity | Toxic and nontoxic exhaust gases |

4. Velocity of the gas flow parallel to the burning surface
5. Motor motion (acceleration and spin-induced grain stress)

These influencing factors are discussed separately in this chapter. The explanation of the behavior of the burning rate with various parameters is largely found in the combustion mechanism of the solid propellant, which is described in Chapter 14. Analytical models of the burning rate and the combustion process exist and are useful for preliminary designs and for extending actual test

TABLE 12-3. Characteristics of Missile Motor and Space Motor

| Characteristic | First-Stage Minuteman Missile Motor ^a | Orbus-6 Inertial Upper-Stage Motor ^b | STAR™ 27 Apogee Motor ^a |
|--|--|---|--|
| <i>Motor Performance (70°F, sea level)</i> | | | |
| Maximum thrust (lbf) | 201,500 | 23,800 | 6,404 (vacuum) |
| Burn time average thrust (lbf) | 194,600 | 17,175 | 6,010 (vacuum) |
| Action time average thrust (lbf) ^c | 176,600 | 17,180 | 5,177 (vacuum) |
| Maximum chamber pressure (psia) | 850 | 839 | 569 |
| Burn time average chamber pressure (psia) ^c | 780 | 611 | 552 |
| Action time average chamber pressure (psia) ^c | 720 | 604 | 502 |
| Burn time/action time (sec) ^c | 52.6/61.3 | 101.0/103.5 | 34.35/36.93 |
| Ignition delay time (sec) | 0.130 | | 0.076 |
| Total impulse (lbf-sec) | 10,830,000 | 1,738,000 | 213,894 |
| Burn time impulse (lbf-sec) | 10,240,000 | 1,737,000 | |
| Altitude specific impulse (sec) | 254 | 289.6 (vacuum) | 290.8 (vacuum) |
| Temperature limits (°F) | 60–80 | 45–82 | 20–100 |
| <i>Propellant</i> | | | |
| Composition: | | | |
| NH ₄ ClO ₄ (%) | 70 | 68 | 72 |
| Aluminum (%) | 16 | 18 | 16 |
| Binder and additives (%) | 14 | 14 | 12 |
| Density (lbm/in. ³) | 0.0636 | 0.0635 | 0.0641 |
| Burning rate at 1000 psia (in./sec) | 0.349 | 0.276 | 0.280 |
| Burning rate exponent | 0.21 | 0.3–0.45 | 0.28 |
| Temperature coefficient of pressure (% °F) | 0.102 | 0.09 | 0.10 |
| Adiabatic flame temperature (°F) | 5790 | 6150 | 5,909 |
| Characteristic velocity (ft/sec) | 5180 | 5200 | 5,180 |
| <i>Propellant Grain</i> | | | |
| Type | Six-point star | Central perforation | Eight-point star |
| Propellant volume (in. ³) | 709,400 | 94,490 | 11,480 |
| Web (in.) | 17.36 | 24.2 | 8.17 |
| Web fraction (%) | 53.3 | 77.7 | 60 |
| Sliver fraction (%) | 5.9 | 0 | 2.6 |
| Average burning area (in. ²) | 38,500 | 3905 | 1,378 |
| Volumetric loading (%) | 88.7 | 92.4 | 92.6 |
| <i>Igniter</i> | | | |
| Type | Pyrogen | Pyrogen | Pyrogen |
| Number of squibs | 2 | 2 through-the-bulkhead initiators | 2 |
| Minimum firing current (A) | 4.9 | NA | 5.0 |
| <i>Weights (lbf)</i> | | | |
| Total | 50,550 | 6515 | 796.3 |
| Total inert | 4719 | 513 | 60.6 |

TABLE 12–3. (*Continued*)

| Characteristic | First-Stage Minuteman Missile Motor ^a | Orbus-6 Inertial Upper-Stage Motor ^b | STAR TM 27 Apogee Motor ^a |
|----------------------------------|--|---|---|
| Burnout | 4264 | 478 | 53.4 |
| Propellant | 45,831 | 6000 | 735.7 |
| Internal insulation | 634 | 141 | 12.6 |
| External insulation | 309 | 0 | 0 |
| Liner | 150 | Incl. with insulation | 0.4 |
| Igniter | 26 | 21 | 2.9 (empty) |
| Nozzle | 887 | 143 | 20.4 |
| Thrust vector control device | Incl. with nozzle | 49.4 | 0 |
| Case | 2557 | 200 | 23.6 |
| Miscellaneous | 156 | 4 | 0.7 |
| Propellant mass fraction | 0.912 | 0.921 | 0.924 |
| <i>Dimensions</i> | | | |
| Overall length (in.) | 294.87 | 72.4 | 48.725 |
| Outside diameter (in.) | 65.69 | 63.3 | 27.30 |
| <i>Case</i> | | | |
| Material | Ladish D6AC steel | Kevlar fibers/epoxy | 6 A1-4V titanium |
| Nominal thickness (in.) | 0.148 | 0.35 | 0.035 |
| Minimum ultimate strength (psi) | 225,000 | — | 165,000 |
| Minimum yield strength (psi) | 195,000 | — | 155,000 |
| Hydrostatic test pressure (psi) | 940 | ~ 1030 | 725 |
| Hydrostatic yield pressure (psi) | 985 | NA | 767 |
| Minimum burst pressure (psi) | — | 1225 | 76.7 |
| Typical burst pressure (psi) | — | > 1350 | — |
| <i>Liner</i> | | | |
| Material | Polymeric | HTPB system | TL-H-304 |
| <i>Insulation</i> | | | |
| Type | Hydrocarbon– asbestos | Silica-filled EPDM | Polyisoprene |
| Density (lbm/in. ³) | 0.0394 | 0.044 | 0.044 |
| <i>Nozzle</i> | | | |
| Number and type | 4, movable | Single, flexible | Fixed, contoured |
| Expansion area ratio | 10:1 | 47.3 | 48.8/45.94 |
| Throat area (in. ²) | 164.2 | 4.207 | 5.900 |
| Expansion cone half angle (deg) | 11.4 | Initial 27.4, Final 17.2 | Initial 18.9, Exit 15.5 |
| Throat insert material | Forged tungsten | Three-dimensional carbon–carbon | 3D carbon–carbon |
| Shell body material | AISI 4130 steel | NA | NA |
| Exit cone material | NA | Two-dimensional carbon–carbon | Carbon phenolic carbon–carbon |

^aCourtesy of ATK Launch Systems.^bCourtesy United Technologies Corp., there is also a version Orbus-6 E (see Fig. 12–3) with an extendible, sliding nozzle; it has a specific impulse of 303.8 sec, a total weight of 6604 lb and a burnout weight of 567 lb.^cBurn time and action time are defined in Fig. 12–13.

NA: not applicable or not available.

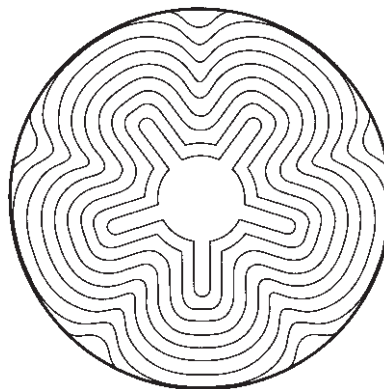


FIGURE 12–5. Diagram of successive burning surface contours, each a fixed small time apart. It shows the growth of the internal cavity. The lengths of these contour lines are roughly the same (within $\pm 15\%$), which means that the burning area is roughly constant.

data; for detail designs and for evaluation of new or modified propellants, engineers need some actual test data. *Burning rate data* are usually obtained in three ways—namely, from testing by:

1. Standard *strand burners*, often called *Crawford burners*
2. Small-scale *ballistic evaluation motors*
3. *Full-scale motors* with good instrumentation

A strand burner is a small pressure vessel (usually with windows) in which a thin strand or bar of propellant is ignited at one end and burned to the other end. The strand can be inhibited with an external coating so that it will burn only on the exposed cross-sectional surface; chamber pressure is simulated by pressurizing the container with inert gas. The burning rate can be measured by electric signals from embedded wires, by ultrasonic waves, or by optical means (Ref. 12–2). The burning rate measured on strand burners is usually lower than that obtained from motor firing (by 4 to 12%) because it does not truly simulate the hot chamber environment. Also small ballistic evaluation motors usually have a slightly lower burning rate than full-scale larger motors because of scaling factors. The relationship between the three measured burning rates is determined empirically for each propellant category and grain configuration. Strand burner data are useful in screening propellant formulations and in quality control operations. Data from full-scale motors tested under a variety of conditions constitute the final proof of burning rate behavior. Obviously, the strand burner and other substitutes for the full-scale motor must be exploited to explore as many variables as practicable.

During development of a new or modified solid propellant, it is tested extensively or *characterized*. This includes the testing of the burn rate (in several different ways) under different temperatures, pressures, impurities, and conditions. Characterization also requires measurements of physical, chemical, and

manufacturing properties, ignitability, aging, sensitivity to various energy inputs or stimuli (e.g., shock, friction, fires), moisture absorption, and compatibility with other materials (liners, insulators, cases). It is a lengthy, expensive, often hazardous program with many tests, samples, and analyses.

The burning rate of propellant in a motor is a function of many parameters, and at any instant governs the mass flow rate \dot{m} of hot gas generated and flowing from the motor (steady combustion):

$$\dot{m} = A_b r \rho_b \quad (12-1)$$

Here A_b is the burning area of the propellant grain, r the burning rate, and ρ_b the solid propellant density prior to motor start. The total mass m of effective propellant burned can be determined by integrating Eq. 12-1:

$$m = \int \dot{m} dt = \rho_b \int A_b r dt \quad (12-2)$$

where A_b and r vary with time and pressure.

Mass Flow Relations

The first basic performance relation is derived from the principle of conservation of matter. The gaseous propellant mass evolving from the burning surface per unit time must equal the sum of the change in mass storage per unit time in the combustion chamber (due to increases in volume of the grain cavity) and the mass flowing out through the exhaust nozzle per unit time,

$$A_b r \rho_b = d(\rho_1 V_1)/dt + A_t p_1 / c^* \quad (12-3)$$

The term on the left side of the equation represents the rate of gas generation from Eq. 12-1. The first term on the right represents the storage rate of the hot gas in the combustion chamber volume, and the last term represents the propellant flow rate through the nozzle according to Eqs. 3-24 and 3-32. The propellant burning rate is r and A_b is the propellant burning area; ρ_b is the solid propellant density and ρ_1 is the chamber hot-gas density; V_1 represents the chamber gas cavity volume which becomes larger as the propellant is burnt and expended; A_t is the throat area; p_1 the chamber pressure; c^* is the characteristic velocity which is proportional to T_1 , the absolute chamber temperature (which is known from the thermochemistry for a given propellant); and k is the specific heat ratio of the combustion gases (see Eq. 3-32). Equation 12-3 is useful in numerical solutions of transient conditions, such as during startup or shutdown, but the version without the storage rate term is the one most often used. During startup the rate of change of hot gas in the grain cavity is always an important factor.

The value of the burning surface A_b may or may not change with time and is a function of the grain design as described in Section 12.3. For preliminary performance calculations, the throat area A_t is usually assumed to be constant

for the entire burning duration but, for accurate performance predictions, it is necessary to include erosion in the nozzle material which causes an increase in nozzle throat area as the propellant burns; this nozzle enlargement is usually small as described in Chapter 15. An enlarging throat area A_t with time causes a decrease of chamber pressure, burning rate, and thrust.

The chamber gas volume V_1 will increase measurably with burn time. But to fill this void requires relatively small amounts of gaseous propellant mass compared to what flows through the nozzle (the volume change of a unit of mass is about 1000 to 1 as the propellant gasifies during the combustion). As a result, the term $d(\rho_1 V_1)/dt$ can usually be neglected. This then yields the commonly used relation for the pressure in steady burning:

$$p_1 = K \rho_b r c^* \quad (12-4)$$

where

$$K \equiv A_b/A_t$$

Here K represents a new and important dimensionless motor parameter, the ratio of burning area to nozzle throat area, which has typical values much larger than one. For steady flow and steady burning the value of A_b (or K) must remain essentially constant. We will return to Eq. 12-4 in Eq. 12-6 after introducing an empirical relation for the burning rate.

Burning Rate Relation with Pressure

Classical equations relating to the burning rate are helpful in preliminary design, data extrapolation, and in understanding the phenomena involved; however, analytical modeling and the supportive research have yet to adequately predict the burning rate of a new propellant in a new motor. Ordinary laws and equations on burning rate only deal with the influence of some of the important parameters individually. Unless otherwise stated, the burning rate specified is based on an ambient temperature of 70°F or 294 K for the propellant (prior to ignition) and a reference chamber operating pressure of 1000 psia or 6.895 MPa.

With many propellants it is possible to approximate the *burning rate* as a function of *chamber pressure*, at least over a limited range of chamber pressures. A log-log set of plots is shown in Fig. 12-6. For a majority of production-type propellants the most commonly used empirical equation is

$$r = ap_1^n \quad (12-5)$$

where r , the burning rate, is usually in mm/sec or in./sec and the chamber operating pressure p_1 is in MPa or psia. Known as the *temperature coefficient*, a is an empirical constant influenced by the ambient grain temperature (T_b) whose dimensions are defined by the other terms in Eq. 12-5. The *burning rate exponent* n , sometimes also called the *pressure exponent* or the *combustion index*, is

considered to be independent of the propellant initial temperature but influences the chamber operating pressure and the burning rate. For combustion stability, $n < 1.0$ (see Ref. 12-3), otherwise any pressure disturbances present will be amplified in the chamber. Equation 12-5 applies to all the commonly used double-base, composite, or composite double-based propellants, several of which are described in the next chapter. Changes in ambient temperature (T_b) do not alter the propellant's chemical energy available for release during combustion; they do change the rate of reaction at which the energy is released and have a slight effect on c^* through changes in T_1 .

The curves shown in Fig. 12-6 are calculated over limited pressure ranges of interest and become straight lines on a log-log plot; however, many actual burning rates deviate somewhat from linearity and the actual data have some slight bends in parts of the curve as the pressure range increases, as seen in Fig. 12-7. For any particular propellant and for wide temperature and pressure limits, the burning rate can vary by factors of 3 or 4. For all propellants this translates to a range from about 0.05 to 75 mm/sec or 0.02 to 3 in./sec; the higher values are presently difficult to achieve, even with considerable burning rate catalyst additives, embedded metal wires or high pressures (above 14 MPa or 2000 psia). A technology that would give a burning rate of more than 250 mm/sec at a chamber pressure of 1000 psia is desired by motor designers for some applications.

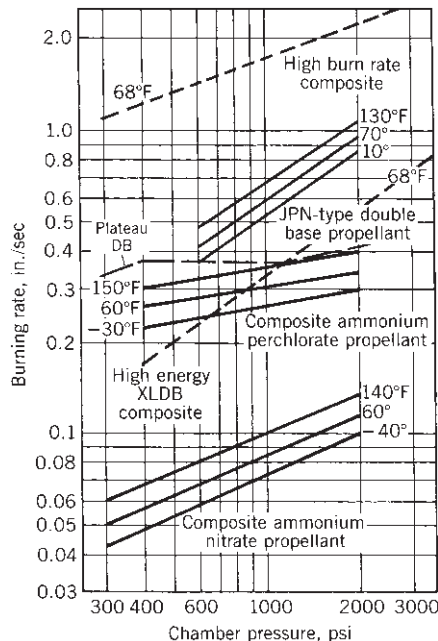


FIGURE 12-6. Plot of the calculated burning rate versus chamber pressure for several typical solid rocket propellants, some at three different temperatures. A particular *double-base* plateau propellant shows a constant burning rate over a fairly wide pressure range.

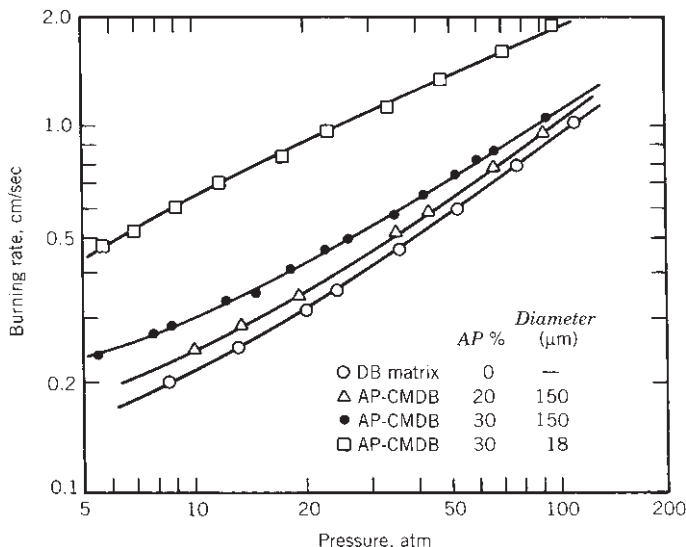


FIGURE 12-7. Measured burning rate characteristics of a double-base (DB) propellant and three composite-modified double-base (CMDB) propellants which contain an increasing percentage of small-diameter (159-μm) particles of ammonium perchlorate (AP). When the size of the AP particles is reduced or the percentage of AP is increased, an increase in burning rate is observed. None of these data form straight lines. (Reproduced with permission of the AIAA from Chapter 1 of Ref. 12-3.)

Inserting Eq. 12-5 we now rewrite Eqs. 12-4 and the generated mass flow rate, Eq. 12-1:

$$K = p_1^{(1-n)} / (\rho_b a c^*) \quad (12-6)$$

$$\dot{m} = A_b \rho_b a p_1^n \quad (12-7)$$

Example 12-1. As a function of n , explore what happens to the mass flow rate when p_1 fluctuates by ±0.1 MPa from its nominal steady-state value as given by Eq. 12-3 (neglecting the storage term) together with Eq. 12-5. Take one propellant at $n = 0.5$ and a hypothetical one at $n = 1.5$ and a nominal pressure $p_1 = 7.00$ MPa. Assume that only the pressure changes significantly (note that $n = 1.5$ is unrealistic for steady flows).

SOLUTION. Propellant flow through the nozzle is proportional to p_1 (see Eq. 3-32), whereas the hot gas mass generation is proportional to p_1^n so their ratio is proportional to p_1^{1-n} . Define Δ as the difference between the mass flowing through the nozzle and the mass generated by the propellant combustion, that is,

$$\Delta \equiv p_1 A_t / c^* - A_b \rho_b a p_1^n = (A_t / c^*) (p_1 - K c^* \rho_b a p_1^n)$$

or

$$(c^* / A_t) \Delta = (p_1 - \kappa_1 P_1^n)$$

The new constant κ_1 is found from the nominal pressure since the change $\Delta = 0$ at that pressure. In this problem at 7.0 MPa $\kappa_1 = 2.646$ for $n = 0.5$ and $\kappa_1 = 0.378$ for $n = 1.5$. The table below shows values of pressures together with values of $(c^*/A_t)\Delta$ for the two propellants. The units are not shown but are consistent:

| Pressure p_1 (MPa) | $(c^*/A_t)\Delta$ | |
|----------------------|-------------------|-----------|
| | $n = 0.5$ | $n = 1.5$ |
| 6.90 | -0.05 | +0.05 |
| 7.00 (nominal) | 0.00 | 0.00 |
| 7.10 | +0.05 | -0.05 |

These results indicate that with $n < 1.0$ the Δ values are negative when the pressure drops below nominal—a situation which will drive the pressure up; when the pressure rises above nominal Δ values are positive and this will drive the pressure down because more flow can pass through the nozzle than is generated. The precise opposite is true with $n > 1.0$. In other words, as the pressure decreases, the nozzle can accommodate less flow than is being generated for $n < 1$ but more for $n > 1$. From stability considerations, in the former case the flow can physically adjust and remain quasi-steady while in the latter it cannot. Hence, n must be less than one for all solid propellants (with constant throat area systems). It will be seen that $n = 1.0$ is problematic from other considerations. [Note that, strictly speaking, any flow equality at the nominal pressure is invalid as the chamber pressure fluctuates, meaning that a steady state is no longer valid but for small changes the arguments presented are valid.]

From inspection of the above results and also from Eq. 12–7, it can be seen that the hot gas flow rate is quite sensitive to the exponent n . High values on n give rapid changes of burning rate with pressure. This implies that even a small natural variation in chamber pressure induces substantial changes in the amount of hot gas produced. Most commercially available propellants have a pressure exponent n ranging between 0.2 and 0.6. As n approaches 1.0, the burning rate and chamber pressure become very sensitive to one another and a disastrous rise in chamber pressure can occur in a few milliseconds. On the other hand, a propellant having a pressure exponent of zero displays essentially zero change in burning rate over a wide pressure range. *Plateau propellants* is the name given to those that exhibit nearly constant burning rate over a limited pressure range, and they are desirable for minimizing the effects of changes in initial temperature on motor operation as described in the next section. One plateau propellant is shown as a dash line in Fig. 12–6. These propellants are only insensitive to major changes in chamber pressure over a limited range. Several double-based propellants and a few composite propellants have this desirable plateau characteristic. Table 13–1 lists the nominal burning rate r and the pressure exponent for several operational (production) propellants.

Burning Rate Relation with Ambient Temperature

Temperature influences chemical reaction rates, and the initial (i.e., prior to combustion) or *ambient temperature* of a propellant (T_b) noticeably changes the

burning rate as shown in Figs. 12–6 and 12–8. Common practice in developing and testing larger rocket motors is to “condition” the motor for many hours at a particular temperature before firing to ensure that the propellant grain is uniformly at the desired temperature since motor performance characteristics must stay within specified acceptable limits. For air-launched missile motors the extremes are usually 219 K (-65°F) and 344 K (160°F). Motors using typical composite propellant mixtures experience a 20 to 35% variation in chamber pressure and a 20 to 30% variation in operating time over such a range of propellant temperatures (see Fig. 12–8). In large rocket motors an uneven heating of the grain (e.g., by the sun heating on one side) can cause a sufficiently large difference in burning rate so that noticeable thrust misalignments can result (see Ref. 12–4). Thus the effects of ambient temperature on motor performance are of some importance and discussion of this topic is necessary to understand solid propellant behavior.

The sensitivity of burning rate to propellant temperature can be expressed in the form of temperature coefficients, the two most common being

$$\sigma_p = \left(\frac{\partial \ln r}{\partial T_b} \right)_{p_1} = \frac{1}{r} \left(\frac{\partial r}{\partial T_b} \right)_{p_1} \quad (12-8)$$

$$\pi_K = \left(\frac{\partial \ln p_1}{\partial T_b} \right)_K = \frac{1}{p_1} \left(\frac{\partial p_1}{\partial T_b} \right)_K \quad (12-9)$$

with σ_p known as the *temperature sensitivity of burning rate*, expressed as the change of burning rate per degree change in propellant ambient temperature at a fixed value of chamber pressure, and π_K known as the *temperature sensitivity*

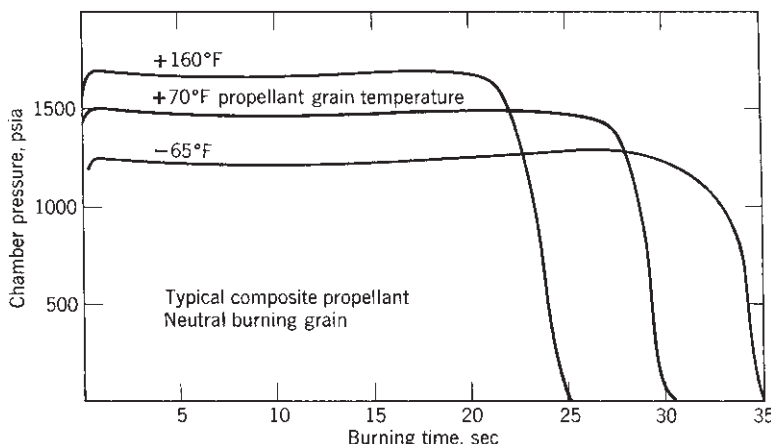


FIGURE 12–8. Effect of propellant temperature on burning time and chamber pressure for a particular motor. The integrated areas under the curves are proportional to the total impulse, which is the same for the three curves.

of pressure expressed as the change of chamber pressure per degree change of propellant ambient temperature at a particular value of K . Here K is the geometric factor introduced earlier, namely, the ratio of the burning surface A_b to the nozzle throat area A_t .

The coefficient σ_p for a new propellant is usually found from strand burner test data, and π_K is usually found from small-scale or full-scale motors. Values of σ_p typically range between 0.001 and 0.009 per $^{\circ}\text{C}$, or 0.002 and 0.04 per $^{\circ}\text{F}$, and for π_K they range between 0.00067 and 0.0027 per $^{\circ}\text{C}$, or 0.0012 and 0.005 per $^{\circ}\text{F}$. Since the sensitivity coefficients are small numbers, Eqs. 12–8 and 12–9 are sometimes written in terms of differences for more convenient manipulation. Furthermore, when π_K remains sufficiently constant over the interval of interest, we may integrate Eq. 12–9 at constant K for the pressure and obtain a useful equation for predicting chamber pressure excursions with ambient temperature changes from a given or defined reference condition, subscripted as 0 (i.e., p_{01} and T_{0b}):

$$\ln p_1 = \ln p_{01} + \pi_K (T_b - T_{0b}) \quad (12-10)$$

Values of σ_p and π_K depend primarily on the nature of the propellant burning rate, the composition, and the combustion mechanism of the propellant. It is not simple to predict motor performance because of variations in manufacturing tolerances which act in addition to changes of ambient temperature. Reference 12–4 reports on analyses of the prediction of burning time.

In order to arrive at a relationship between the two sensitivity coefficients introduced above, Eq. 12–5 is rewritten in log form and then derivatives are taken under the assumption that the coefficient a depends only on T_b and that n is a constant:

$$\ln r = \ln a + n \ln p_1 \quad (12-11)$$

$$(\partial \ln r / \partial T_b)_{p_1} = d(\ln a) / dT_b$$

hence

$$\sigma_p = d(\ln a) / dT_b \quad (12-12)$$

Next Eq. 12–6 is solved for p_1 and written in log form. Its ambient temperature derivative is then taken, keeping the second term in the right-hand-side brackets as constant:

$$\ln p_1 = \frac{1}{1-n} [\ln a + \ln(K \rho_b c^*)] \quad (12-13)$$

hence

$$\pi_K = \frac{1}{1-n} \frac{d \ln a}{dT_b} = \frac{\sigma_p}{1-n} \quad (12-14)$$

Note that this results from taking the entire product $K \rho_b c^*$ as constant in T_b which involves more than the geometry factor K (i.e., chamber temperature, propellant

density, and composition do not change); according to Eq. 12–4, a good indicator for the constancy of $K \rho_b c^*$ in any data is how constant the ratio p_1/r remains in the measurements. Since σ_p is an often tabulated material/propellant property, Eq. 12–14 shows how π_K may be obtained from σ_p and highlights a strong dependence of π_K on the burning rate exponent n . Both these conclusions hinge on the assumption that the two sensitivities may be considered unchanged over limited temperature and pressure ranges.

Example 12–2. For a given propellant with a neutrally burning grain the value of the temperature sensitivity at constant burning area is $\pi_K = 0.005/^\circ\text{F}$ and the value of the pressure exponent n is 0.6. The burning rate r is 0.32 in./sec at 70°F at a chamber pressure of $p_1 = 1500$ psia with an effective nominal burning time (t_b) of 55 sec. Determine the variation in p_1 and in t_b for a change of $\pm 40^\circ\text{F}$ (from $+30^\circ$ to $+110^\circ\text{F}$) assuming that the variation is linear.

SOLUTION. We may use Eq. 12–10, taking exponents on both sides, to calculate the pressure excursions:

$$(p_1)_1 = 1500 e^{[0.005 \times (-40)]} = 1230 \text{ psia}$$

$$(p_1)_2 = 1500 e^{[0.005 \times (+40)]} = 1830 \text{ psia}$$

This translates into a total excursion of 600 psi or 40% of the nominal chamber pressure. This large change in p_1 is typical of many solid rocket motors.

It has been assumed that the total impulse or the chemical energy released remains constant as the grain ambient temperature is changed; only the rate at which the energy is released changes. When pressure thrust is negligible, the thrust is mostly proportional to the chamber pressure and will change accordingly (when A_t and C_F may be taken as constant in the equation $F = C_F p_1 A_t$). For a constant total impulse, then

$$F t_b = \text{constant} \quad \text{or} \quad (p_1)_1 t_{b1} = (p_1)_2 t_{b2} = (1500) \times (55) = 82,500 \text{ psia-sec}$$

Thus

$$t_{b1} = 67.1 \text{ sec} \quad \text{and} \quad t_{b2} = 45.1 \text{ sec}$$

A change of 22 sec between these two values of t_b is 40% of the nominal burning time. These results would be somewhat similar to what is shown in Fig. 12–8. The inclusion of C_F changes would affect these results by only a few percent.

In the example above the variation of chamber pressure affects the thrust and burning time of the rocket motor. When operating with warm or cold grains, the thrust can easily vary by a factor of 2, and this may cause significant changes of flight performance during atmospheric flight (because of different drag in the vehicle's flight path). Thrust and chamber pressure increases become more dramatic at the higher ranges of n . The least variations in thrust or chamber pressures occur when n is small (0.2 or less) and when the temperature sensitivity is relatively low.

Variable Burning Rate Exponent n

A closer look at burning rate data (e.g., Fig. 12–7) indicates that n in Eq. 12–5 may not be really constant but a function of p_1 (and perhaps even T_b). Here, it may no longer be possible to predict the pressure excursions with ambient temperature changes using Eq. 12–10; this can be seen from Eq. 12–14 by noting that in the constant- n case π_K depends only on a material/propellant property (σ_p) and on n . An upward concavity in the propellant burning rate data may result in larger excursions of chamber pressure than constant- n cases would predict. The opposite would hold true for a downward concavity. Such variations may be accommodated by piecewise curve fitting the data with constant n values in preselected ranges of interest (see Ref. 12–4), provided the pressure increments in these curve fits are small enough.

When the piecewise constant-burning-rate-exponent n approach is not satisfactory, a useful approach would be to assume that n depends only on p_1 , keeping all previous dependences intact (retaining a in Eq. 12–5 as the only function of T_b). This then can be shown to imply that π_K (a rocket motor parameter) becomes now a function of p_1 and that the differential relation shown below needs to be solved:

$$\ln p_1 \frac{dn}{d \ln p_1} = (1 - n) - \frac{\sigma_p}{\pi_K} \quad (12-15)$$

The above reverts to the form of Eq. 12–14 when n is constant. Results from Eq. 12–15 depend on having suitable (empirical) information on n as a function of p_1 . In order to obtain an explicit relation for p_1 which reflects ambient temperature changes with the variable n influence, we introduce Eq. 12–9 and solve (for constant K and c^*):

$$(1 - n) \ln p_1 - (1 - n_0) \ln p_{01} = \sigma_p \int \frac{d \ln p_1}{\pi_k} = \sigma_p (T_b - T_{0b})$$

or

$$\left(\frac{1 - n}{1 - n_0} \right) \ln p_1 = \ln p_{01} + \frac{\sigma_p}{1 - n_0} (T_b - T_{0b}) \quad (12-16)$$

which appropriately reverts back to the form of Eq. 12–10 when n is unchanging. Note that because n has been assumed only a function of p_1 , values of n may be obtained at any T_b from available burning rate data as a function of chamber pressure for the propellant in question (provided that the variation of n with p_1 is monotonic over the interval). The nonexplicit nature of Eq. 12–16 is such that it will require several trials to solve it, for example, first, let $n = n_0$ and find p_1 (which is equivalent to just getting the constant- n constant- K solution), then update n at this new pressure from the relevant empirical information and repeat solving Eq. 12–16 until the solution converges for the new ambient temperature; Problem 11 provides an application for this procedure; another approach would

be to introduce a polynomial fit for n as a function of p_1 into Eq. 12–16. As to results, with $\Delta T_b > 0$ and for given values of σ_p and p_{01} , when $n > n_0$ the final chamber pressure will be greater than that resulting from Eq. 12–10 and when $n < n_0$ the final chamber pressure will be less. While these trends are consistent with intuition, any quantitative inferences must be tempered by the nature of the assumptions. As stated earlier, Eq. 12–5 is only approximately met for many solid propellants.

Burning Enhancement by Erosion

Erosive burning refers to the increase in the propellant burning rate caused by the high-velocity flow of combustion gases over the burning propellant surface. It can seriously affect the performance of solid propellant rocket motors. It occurs primarily in the port passages or perforations of the grain as the combustion gases flow toward the nozzle; it is more likely to occur when the port passage cross-sectional area A is small relative to the throat area A_t with a port-to-throat area ratio of 4 or less. An analysis of erosive burning is given in Ref. 12–5. The high velocity near the burning surface and the turbulent mixing in the boundary layers increase the heat transfer to the solid propellant and thus increase the burning rate. Chapter 10 of Ref. 12–6 surveys about 29 different theoretical analytical treatments and a variety of experimental techniques aimed at a better understanding of erosive burning.

Erosive burning increases the mass flow and thus also the chamber pressure and thrust during the early portion of the burning, as shown in Fig. 12–9 for a particular motor. As soon as the burning enlarges the flow passage (without a major increase in burning area), the port area flow velocity is reduced and erosive burning diminishes until normal burning will again occur. Since propellant is

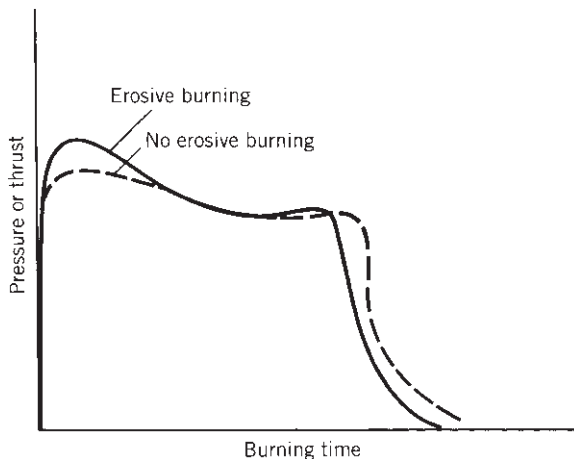


FIGURE 12–9. Typical pressure–time curve with and without erosive burning.

consumed more rapidly during the early erosive burning, there usually is also a reduction of flow and thrust at the end of burning. Erosive burning also causes early burnout of the web, usually at the nozzle end, and exposes the insulation and aft closure to hot combustion gas for a longer period of time; this usually requires more insulation layer thickness (and more inert mass) to prevent local thermal failure. In designing motors, erosive burning is either avoided or controlled to be reproducible from one motor to the next.

A relatively simple model for erosive burning, based on heat transfer, was first developed in 1956 by Lenoir and Robillard (Ref. 12-5) and has since been improved and used widely in motor performance calculations. It is based on adding together two burn rates: r_0 , which is primarily a function of pressure and ambient grain temperature (basically Eq. 12-5) without erosion, and r_e , the increase in burn rate due to gas velocity or erosion effects:

$$\begin{aligned} r &= r_0 + r_e \\ &= ap_1^n + \alpha G^{0.8} D^{-0.2} \exp(-\beta r \rho_b / G) \end{aligned} \quad (12-17)$$

Here G is the mass flow velocity per unit area in kg/m²-sec, D is a characteristic dimension of the port passage (usually, $D = 4A_p/S$, where A_p is the port area and S is its perimeter), ρ_b is the density of the unburned propellant (kg/m³), and α and β are empirically constants. Apparently, β is independent of propellant formulation and has a value of about 53 when r is in m/sec, p_1 is in pascals, and G is in kg/m²-sec. The expression of α was determined from heat transfer considerations to be

$$\alpha = \frac{0.0288 c_p \mu^{0.2} \text{Pr}^{-2/3}}{\rho_b c_s} \frac{T_1 - T_s}{T_2 - T_b} \quad (12-18)$$

Here c_p is the average specific heat of the combustion gases in kcal/kg-K, μ the gas viscosity in kg/m-sec, Pr the dimensionless Prandtl number ($\mu c_p/\kappa$) based on the molecular properties of the gases, κ the thermal conductivity of the gas, c_s the heat capacity of the solid propellant in kcal/kg-K, T_1 the combustion gas reaction absolute temperature, T_s the solid propellant surface temperature, and T_b the initial ambient temperature within the solid propellant grain.

Figure 12-10 shows the augmentation ratio r/r_0 , or the ratio of the burning rate with and without erosive burning, as a function of gas velocity for two similar propellants, one of which has an iron oxide burn rate catalyst. Augmentation ratios up to 3 can be found in some motor designs. There is a pressure drop from the forward end to the aft end of the port passage, because static pressure energy is converted into kinetic gas energy as the flow is accelerated. This pressure differential during erosive burning causes an extra axial load and deformation on the grain, which must be considered in the stress analysis. The erosion or burn rate augmentation is not the same throughout the length of the port passage. The erosion is increased locally by turbulence if there are discontinuities such as protrusions, edges of inhibitors, structural supports, or gaps between segmented grains.

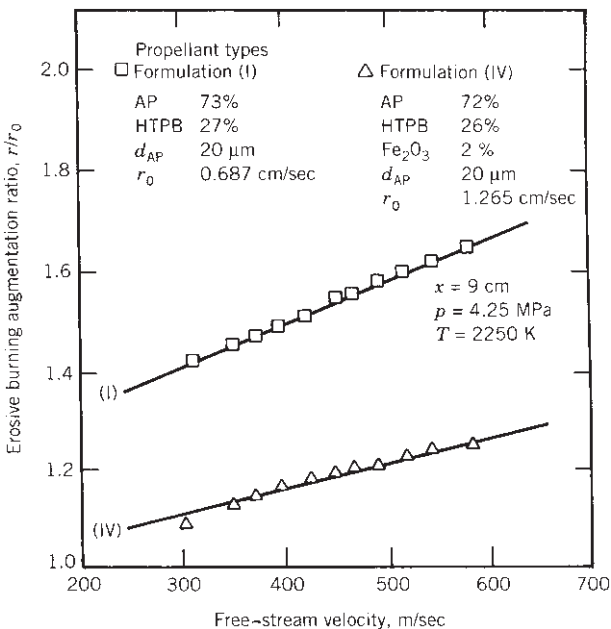


FIGURE 12–10. Effect of gas velocity in the perforation or grain cavity on the erosive burning augmentation factor, which is the burning rate with erosion r divided by the burning rate without erosion r_0 . (Reproduced with permission of the AIAA from Chapter 10 of Ref. 12–6.)

Other Burning Rate Enhancements

Enhancement of burning rate can be expected in vehicles that *spin* the rocket motor about its longitudinal axis (necessary for spin-stabilized flight) or that have high *lateral* or *longitudinal acceleration*, as occurs typically in antimissile rockets. This phenomenon has been experienced with a variety of propellants, with and without aluminum fuel, and the propellant formulation is one of the controlling variables (see Fig. 12–11). Whether the acceleration is from spin or longitudinal force, burning surfaces that form an angle of 60 to 90° with the acceleration vector are most prone to burning rate enhancement. For example, spinning cylindrical interal burning grains are heavily affected. The effect of spin on a motor with an operational composite propellant internal burning grain is shown in Fig. 12–12. The accelerated burning behavior of candidate propellants for a new motor design is often determined in small-scale motors, or in a test apparatus which subjects burning propellant to acceleration (Refs. 12–8 and 12–9). The stresses induced by rapid acceleration or rapid chamber pressure rise can cause crack formation (see Ref. 12–10), which exposes additional burning surface.

The burning rate of the propellant in an end-burning grain at a location immediately adjacent to or near the propellant-to-insulation bondline along the case

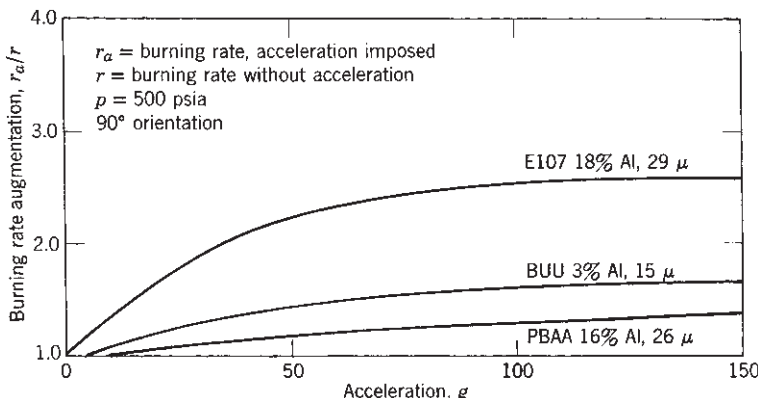


FIGURE 12-11. Acceleration effect on burning rate for three different propellants. (Adapted with permission from Ref. 12-7.)

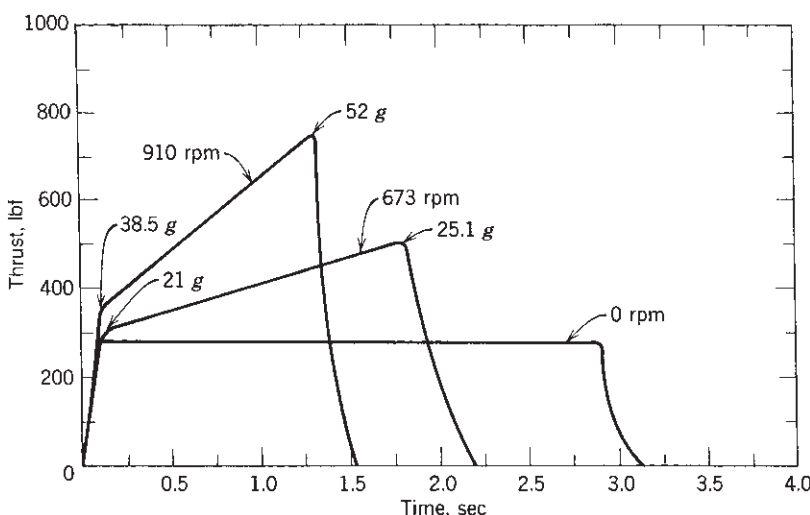


FIGURE 12-12. Effect of axial spin on the thrust-time behavior of a rocket motor with composite propellant using aluminum and PBAN (polybutadiene acrylonitrile) as fuels. (Adapted with permission from Ref. 12-7.)

wall, can, depending on the propellant formulation and manufacturing process, be higher than that of the propellant elsewhere in the grain.

The *embedding of wires* or other shapes of good metal heat conductors in the propellant grain increases the burning rate. One technique has several silver wires arranged longitudinally in an end-burning grain (see Ref. 12-11). Depending on wire size and the number of wires per grain cross-sectional area, the burning rate can easily be doubled. Aluminum wires are about half as effective as silver

wires. Other forms of heat conductors have been wire staples (short bent wires) mixed with the propellant prior to the casting operation.

Intense *radiation emissions* from the hot gases in the grain cavity transfer heat to the burning propellant surfaces. More energetic radiation causes an increase in burning rate. Radiation of the exhaust plume (outside of the nozzle) and the effect of particles in the gas are discussed in Chapter 20.

Combustion instability, also called oscillatory combustion, can affect the burning rate of the propellant because of increased heat transfer rate, gas velocity, and high pressure. This is discussed in Chapter 14.

12.2. OTHER PERFORMANCE ISSUES

Those parameters that govern the burning rate and mass discharge rate of motors are called *internal ballistic properties*; they include r , K , σ_p , π_K , and the influences caused by pressure, propellant ingredients, gas velocity, or acceleration. The subsequent solid propellant rocket parameters are *performance parameters*; they include thrust, ideal exhaust velocity, specific impulse, propellant mass fraction, flame temperature, temperature limits, and duration.

The *ideal nozzle exhaust velocity* of a solid propellant rocket is dependent on the thermodynamic theory as given by Eq. 3–15 or 3–16. As explained in Chapter 5, this equation holds only for frozen equilibrium conditions; for shifting equilibrium the exhaust velocity is best defined in terms of the enthalpy drop ($h_1 - h_2$), which can be computed from $v_2 = \sqrt{2(h_1 - h_2)}$. In deriving the exhaust velocity equation, it was assumed that the approach velocity of gases upstream of the nozzle is small and can be neglected. This is true if the port area A_p (the flow area of gases between and around the propellant grains) is relatively large compared to the nozzle throat area A_t . When the port-to-throat-area ratio A_p/A_t is less than about 4, a pressure drop correction must be made to the effective exhaust velocity.

The thrust for solid propellant rockets is given by the identical definitions developed in Chapters 2 and 3, namely, Eqs. 2–14 and 3–29. The *flame* or *combustion temperature* is a thermochemical property of the propellant formulation and the chamber pressure. It not only affects the exhaust velocity, but also the hardware design, flame radiation emission, materials selection, and the heat transfer to the grain and hardware. In Chapter 5 methods for its calculation are explained. The determination of the nozzle throat area, nozzle expansion area ratio, and nozzle dimensions is discussed in Chapter 3.

The *effective exhaust velocity* c and the *specific impulse* I_s are defined by Eqs. 2–3, 2–4, and 2–6. It is experimentally difficult to measure the instantaneous propellant flow rate or the effective exhaust velocity. However, total impulse and total propellant mass consumed during the test can be measured. The approximate propellant mass is determined by weighing the rocket before and after a test. The effective propellant mass is often slightly less than the total propellant mass, because some grain designs permit small portions of the propellant to remain unburned during combustion, as is explained in a later chapter.

Also, a portion of the nozzle and insulation materials erodes and vaporizes during the rocket motor burning, and this reduces the final inert mass of the motor and also slightly increases the nozzle mass flow. This explains the difference between the total inert mass and the burnout mass in Table 12–3. It has been found that the *total impulse* can be accurately determined in testing by integrating the area under a thrust time curve. For this reason the average specific impulse is usually calculated from total measured impulse and effective propellant mass. The total impulse I_t is defined by Eq. 2–1 as the integration of thrust F over the operating duration t_b :

$$I_t = \int_0^{t_b} F \, dt = \bar{F} t_b \quad (12-19)$$

where \bar{F} is an average value of thrust over the burning duration t_b .

The *burning time, action time*, and *pressure rise time* at ignition are defined in Fig. 12–13. Time zero is actually when the firing voltage is applied to the ignition squib or prime charge. Visible exhaust gas will actually come out of the rocket nozzle for a period longer than the action time, but the effluent mass flow ahead and behind the action time is actually very small. These definitions are somewhat arbitrary but are commonly in use and documented by standards such as Ref. 2–2.

For flight tests it is possible to derive the instantaneous thrust from the measured flight path acceleration (reduced by an estimated drag) and the estimated

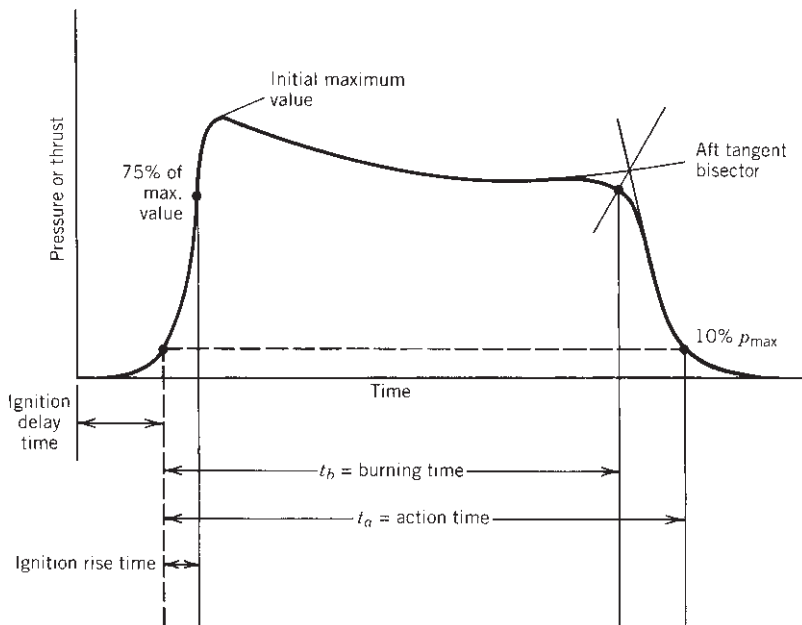


FIGURE 12–13. Definitions of burning time and action time.

instantaneous mass from the chamber pressure measurements, which is essentially proportional to the rocket nozzle mass flow; this gives another way to calculate specific impulse and total impulse.

As explained in Section 3.5, there are at least four values of *specific impulse*: (1) *theoretical specific impulse*, (2) *delivered* or *actual* values as measured from flight tests, static tests, or demonstrations (see Ref. 12–12), (3) delivered specific impulse *at standard or reference conditions*, and (4) the *minimum guaranteed value*. Merely quoting a number for specific impulse without further explanation leaves many questions unanswered. This is similar to the four performance values for liquid propellant engines listed in Section 3.5. Specific impulse as diminished by several losses can be predicted as shown in Ref. 12–13.

Losses include the nozzle inefficiencies due to viscous boundary layer friction and nonaxial flow as described in Chapter 3, thrust vector deflection as described in Chapter 18, residual unburned propellants, heat losses to the walls or insulators, incomplete combustion, or the presence of solid particles in the gas which need to be accelerated. There are also some performance *gains*; the gases (created by ablation of the ablative nozzle and insulators or the igniter propellants) contribute to an increased mass flow, in many cases also to a somewhat lower average molecular weight of the gas and to a slight reduction of the final inert mass after rocket motor operation.

The *two-phase flow* equations for calculating specific impulse can be solved if the size distribution, shape, and percentage of solid particles in the exhaust gas are known. The assumption of a uniform average spherical particle diameter simplifies the analysis (Ref. 12–13), and this diameter can be estimated from specific impulse measurements on rocket motor tests (Ref. 12–14). Section 3.5 gives a simple theory for two-phase flow of solid particles in a gas flow. Sometimes *density-specific impulse*, the specific gravity of the propellant grain multiplied by specific impulse, is stated as a performance parameter, particularly in rocket motor applications where a compact design is desirable (see Eq. 7–3).

Propellants burn to varying degrees of completeness depending on the fuel, the oxidizer, their ratios, the energy losses, and the environment within the motor. Propellants with nonmetal fuels usually burn with a velocity correction factor of 97 or 98%, as contrasted to 90 to 96% for propellants with aluminum powder as the fuel. The solid particles in the exhaust do not contribute to the gas expansion, require energy to be accelerated, and two-phase flow is less efficient. However, the addition of the aluminum increases the heat of combustion, the chamber gas temperature, and thus the exhaust velocity or specific impulse. This increase usually outweighs the loss for having to accelerate the small solid aluminum oxide particles.

The *propellant mass fraction* ζ was defined in Eq. 2–8 as $\zeta = m_p/m_0$, and it is directly related to the *motor mass ratio* and therefore also to the flight performance of the vehicle. The initial motor mass m_0 is the sum of the useful solid propellant mass m_p and the nonburning, inert hardware mass of the motor.

For a vehicle's propellant mass fraction, the payload mass and the nonpropulsion inert mass (vehicle structure, guidance and control, communications equipment, and power supply) have to be added. A high value of ζ indicates a low inert motor mass, an efficient design of the hardware, and high stresses. This parameter has been used to make approximate preliminary design estimates. It is a function of motor size or mass, thrust level, the nozzle area ratio, and the material used for the case. For very small motors (less than 100 lbm) the value of the propellant fraction is between 0.3 and 0.75. Medium-sized motors ($100 < m_0 < 1000$ lbm) have ζ values between 0.8 and 0.91. For larger motors ($1000 < m_0 < 50,000$ lbm) ζ is between 0.88 and 0.945. A range of values is given for each category because of the influence of the following other variables. Medium- and large-sized motors with steel cases generally have lower ζ values than those with titanium cases, and their values are lower than for cases made of Kevlar fibers in an epoxy matrix. The highest values are for cases made of graphite or carbon fibers in an epoxy matrix. The ζ values are lower for larger area ratio nozzles and motors with thrust vector control. The STARTM 27 rocket motor, shown in Fig. 12–1 and described in Table 12–3, has a propellant mass fraction of 0.924. This is high for a medium-sized motor with a titanium metal case and a relatively large nozzle exit section.

A number of performance parameters are used to evaluate solid propellant rockets and to compare the quality of design of one rocket with another. The first is the *total-impulse-to-loaded-weight ratio* (I_t/w_G). The loaded weight w_G is the sea-level initial gross weight of propellant and rocket propulsion system hardware. Typical values for I_t/w_G are between 100 and 230 sec, with the higher values representative of high-performance rocket propellants and highly stressed hardware, which means a low inert mass. The total-impulse-to-loaded-weight ratio ideally approaches the value of the specific impulse. When the weight of hardware, metal parts, inhibitors, and so on becomes very small in relation to the propellant weight w_p , then the ratio I_t/w_G approaches I_t/w , which is the definition of the average specific impulse (Eqs. 2–3 and 2–4). The higher the value of I_t/w_G , the better the design of a rocket unit. Another parameter used for comparing propellants is the *volume impulse*; it is defined as the total impulse per unit volume of propellant grain, or I_t/V_b .

The *thrust-to-weight ratio* F/w_G is a dimensionless parameter that is identical to the acceleration of the rocket propulsion system (expressed in multiples of g_0) if it could fly by itself in a gravity-free vacuum; it excludes other vehicle component weights. It is peculiar to the application and can vary from very low values of less than one g_0 to over 1000 g_0 for high acceleration applications of solid propellant rocket motors. Some rocket-assisted gun munitions have accelerations of 20,000 g_0 .

The *temperature limits* refer to the maximum and minimum storage temperatures to which a motor can be exposed without risk of damage to the propellant grain. They are discussed further in Section 11.4.

Example 12–3. The following requirements are given for a solid propellant rocket motor:

| | |
|---------------------|------------------------------|
| Sea-level thrust | 2000 lbf average |
| Thrust duration | 10 sec |
| Chamber pressure | 1000 psia |
| Ambient temperature | 70°F |
| Propellant | Ammonium nitrate-hydrocarbon |

The properties of this propellant are: $k = 1.26$; $T_1 = 2790^\circ\text{R}$; $r = 0.10 \text{ in./sec}$ at 1000 psia and 70°F; $\rho_b = 0.0546 \text{ lbm/in}^3$; $R = 76.82 \text{ ft-lbf/lbm}^\circ\text{R}$. Given that the actual value of $c^* = 3967 \text{ ft/sec}$ implies a correction factor $\zeta_{c^*} = 0.997$. Assume moreover a thrust-coefficient correction factor of $\zeta_{C_F} = 0.98$ and optimum operation at sea level. [This propellant can be smokeless.]

Determine the specific impulse, the throat and exit areas, the propellant flow rate, the total propellant weight at sea level, the total impulse, the burning area, and an estimated sea-level mass assuming that the total impulse-to-weight ratio, I_t/w_G , is 143 sec (a moderately efficient design).

SOLUTION. From Figs. 3–4 and 3–6, $C_F = 1.57$ and $\epsilon = 7.8$ (using a pressure ratio of $1000/14.7 = 68.03$ and $k = 1.26$ and optimum nozzle expansion). The actual thrust coefficient is $C_F = 1.57 \times 0.98 = 1.54$. The *specific impulse* is (Eq 3–32)

$$I_s = c^* C_F / g_0 = (3967 \times 1.54) / 32.2 = 190 \text{ sec}$$

The require *throat area* is obtained from Eq. 3–31:

$$A_t = F / (p_1 C_F) = 2000 / (1000 \times 1.54) = 1.30 \text{ in.}^2$$

The *exit area* is $7.8 \times 1.30 = 10.1 \text{ in.}^2$. The average propellant *weight flow rate* at sea level is obtained from Eq. 2–5, namely, $\dot{w} = F/I_s = 2000/190 = 10.5 \text{ lbf/sec}$. The effective *propellant weight* for a duration of 10 sec is about 105 lbf. Allowing for residual propellant and for inefficiencies in combustion and lower pressure during thrust buildup, the *total loaded propellant weight* may be assumed 2% larger or 107 lbf.

The *total impulse* is from Eq. 2–2: $I_t = 2000 \times 10 = 20,000 \text{ lbf-sec}$. The propellant burning surface is found by using Eq. 12–4, $p_1 = K \rho_b r c^*$ together with the definition of K :

$$A_b = A_t p_1 / \rho_b r c^* = [1.30 \times 1000 / (0.0546 \times 0.10 \times 3967)] \times 32.2 = 1933 \text{ in.}^2$$

The factor of 32.2 is needed to convert the units of the density. Now, the loaded gross weight of the rocket motor only can be estimated. Using the value

$$I_t/w_G = 143 \text{ sec}$$

$$w_G = I_t / (I_t/w_G) = 20,000 / 143 = 140 \text{ lbf}$$

Because the propellant itself accounts for 107 lbf, the estimate for the hardware parts then becomes 33 lbf.

12.3. PROPELLANT GRAIN AND GRAIN CONFIGURATION

The grain is the shaped mass of processed solid propellant inside the rocket motor. The propellant material and geometrical configuration of the grain determine the motor performance characteristics. The propellant grain is a cast, molded, or extruded body, and its appearance and feel is similar to that of hard rubber or plastic. Once ignited, it will burn on all its exposed surfaces to form hot gases that are then exhausted through a nozzle. A few rocket motors have more than one grain inside a single case or chamber, and very few grains have segments made of different propellant composition (e.g., to allow different burning rates). However, most rockets have a single grain.

There are two methods of holding the grain in the case, as seen in Fig. 12–14. *Cartridge-loaded or freestanding grains* are manufactured separately from the case (by extrusion or by casting into a cylindrical mold or cartridge) and then loaded into or assembled into the case. In *case-bonded grains* the case is used as a mold and the propellant is cast directly into the case and is bonded to the case or case insulation. Freestanding grains can more easily be replaced if the propellant grain has aged excessively. Aging is discussed in the next chapter. Cartridge-loaded grains are used in some small tactical missiles and a few medium-sized motors. They often have a lower cost and are easier to inspect. The case-bonded grains give a somewhat better performance, a little less inert mass (no holding device, support pads, and less insulation), a better volumetric loading fraction, are more highly stressed, and often somewhat more difficult and expensive to manufacture. Today almost all larger motors and many tactical missile motors use case bonding. Stresses in these two types of grains are briefly discussed under structural design in the next section.

Definitions and terminology important to grains include:

Configuration: The shape or geometry of the initial burning surfaces of a grain as it is intended to operate in a motor.

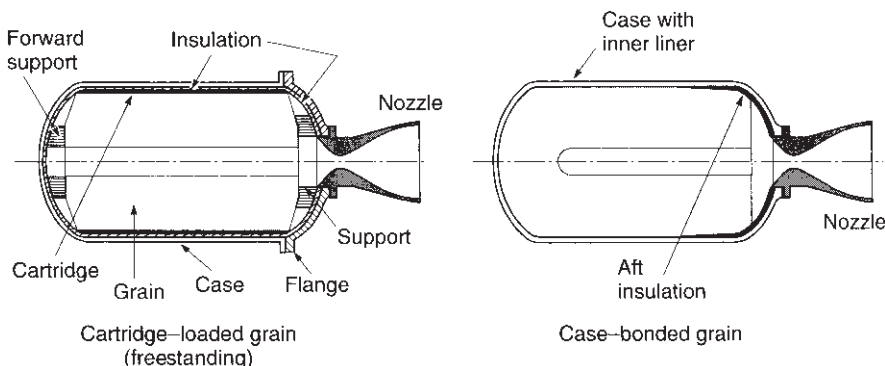


FIGURE 12–14. Simplified schematic diagrams of a freestanding (or cartridge-loaded) and a case-bonded grain.

Cylindrical Grain: A grain in which the internal cross section is constant along the axis regardless of perforation shape (see Fig. 12–3).

Neutral Burning: Motor burn time during which thrust, pressure, and burning surface area remain approximately constant (see Fig. 12–15), typically within about $\pm 15\%$. Many grains are neutral burning.

Perforation: The central cavity port or flow passage of a propellant grain; its cross section may be a cylinder, a star shape, and the like (see Fig. 12–16).

Progressive Burning: Burn time during which thrust, pressure, and burning surface area increase (see Fig. 12–15).

Regressive Burning: Burn time during which thrust, pressure, and burning surface area decrease (see Fig. 12–15).

Sliver: Unburned propellant remaining (or lost—i.e., expelled through the nozzle) at the time of web burnout (see sketch in Problem 6).

Burning Time, or Effective Burning Time, t_b : Usually, the interval from 10% maximum initial pressure (or thrust) to web burnout, with web burnout usually taken as the aft tangent-bisector point on the pressure–time trace (see Fig. 12–13).

Action Time, t_a : The burning time plus most of the time to burn slivers; typically, the interval between the initial and final 10% pressure (or thrust) points on the pressure–time trace (see Fig. 12–13).

Deflagration Limit: The minimum pressure at which combustion can still be barely self-sustained and maintained without adding energy. Below this pressure the combustion ceases altogether or may be erratic and unsteady with the plume appearing and disappearing periodically.

Inhibitor: A layer or coating of slow- or nonburning material (usually, a polymeric rubber type with filler materials) applied (glued, painted, dipped, or sprayed) to a part of the grain's propellant surface to prevent burning on

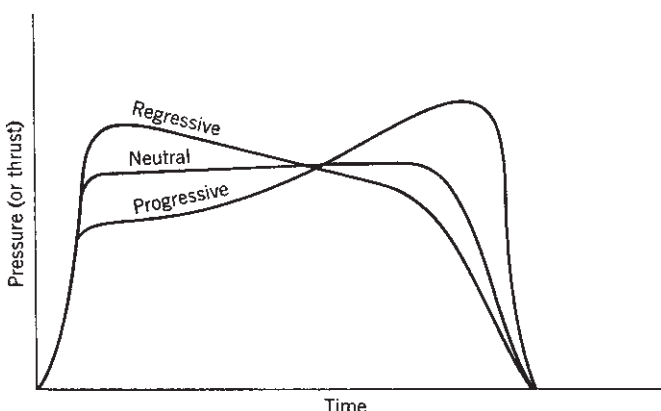


FIGURE 12–15. Classification of grains according to their pressure–time characteristics.

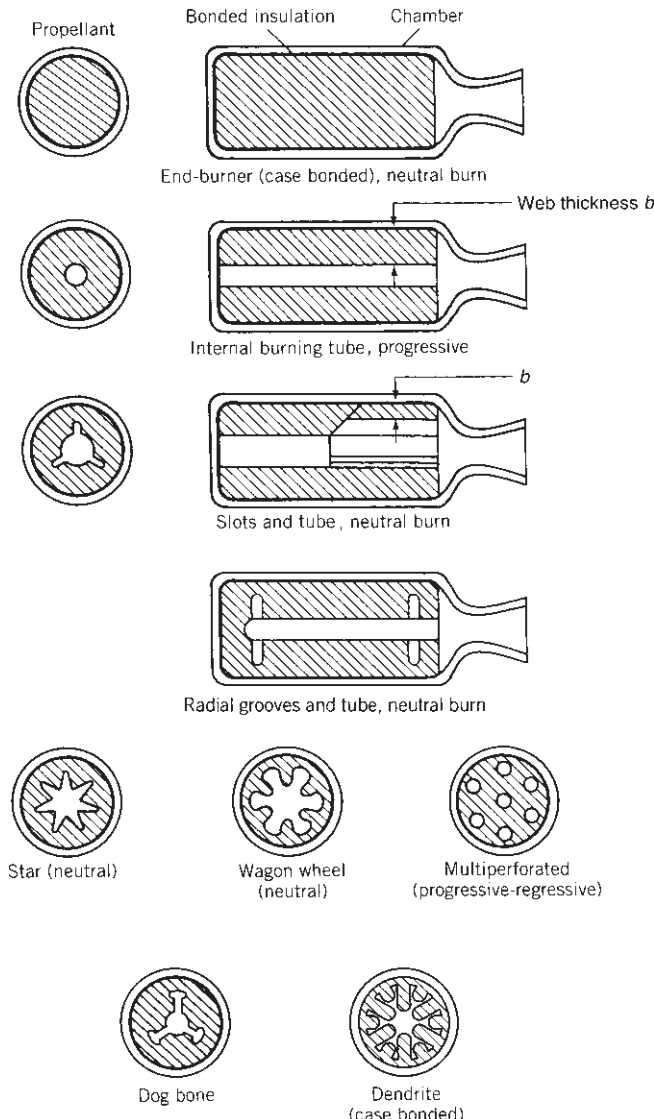


FIGURE 12–16. Simplified diagrams of several grain configurations.

that surface. By preventing burning on inhibited surfaces the initial burning area can be controlled and reduced. Also called *restrictor*.

Liner: A sticky non-self-burning thin layer of polymeric-type material that is applied to the cases prior to casting the propellant in order to promote good bonding between the propellant and the case or the insulator. It also allows some axial motion between the grain periphery and the case.

Internal Insulator: An internal layer between the case and the propellant grain made of an adhesive, thermally insulating material that will not burn readily. Its purpose is to limit the heat transfer to and the temperature rise of the case during rocket operation. Liners and insulators can be seen in Figs. 12–1, 12–4, and 12–14, and are described in Chapter 13.

Web Thickness, b : The minimum thickness of the grain from the initial burning surface to the insulated case wall or to the intersection of another burning surface; for an end-burning grain, b equals the length of the grain (see Fig. 12–16).

Web Fraction, b_f : For a case-bonded internal burning grain, the ratio of the web thickness b to the outer radius of the grain:

$$b_f = b/\text{radius} = 2b/\text{diameter} \quad (12-20)$$

Volumetric Loading Fraction, V_f : The ratio of propellant volume V_b to the chamber volume V_c (excluding nozzle) available for propellant, insulation, and restrictors. Using Eq. 2–4 and $V_b = m/\rho$:

$$V_f = V_b/V_c = I_t/(I_s \rho_b g_0 V_c) \quad (12-21)$$

where I_t is the total impulse, I_s the specific impulse, and ρ_b the propellant density. A grain has to satisfy several *interrelated requirements*:

1. From the *flight mission* one can determine the *rocket motor requirements*. They have to be defined and known before the grain can be designed. They are usually established by the vehicle designers. This can include total impulse, a desired thrust–time curve and a tolerance thereon, motor mass, ambient temperature limits during storage and operation, available vehicle volume or envelope, and vehicle accelerations caused by vehicle forces (vibration, bending, aerodynamic loads, etc.).
2. The *grain geometry* is selected to fit these requirements; it should be compact and use the available volume efficiently, have an appropriate burn surface versus time profile to match the desired thrust–time curve, and avoid or predictably control possible erosive burning. The remaining unburned propellant slivers, and often also the shift of the center of gravity during burning, should be minimized. This selection of the geometry can be complex, and it is discussed in Refs. 12–1 and 12–7 and also below in this section.
3. The *propellant* is usually selected on the basis of its performance capability (e.g., characteristic velocity), mechanical properties (e.g., strength), ballistic properties (e.g., burning rate), manufacturing characteristics, exhaust plume characteristics, and aging properties. If necessary, the propellant formulation may be slightly altered or “tailored” to fit exactly the required burning time or grain geometry. Propellant selection is discussed in Chapter 13 and in Ref. 12–7.

4. The *structural integrity* of the grain, including its liner and/or insulator, must be analyzed to assure that the grain will not fail in stress or strain under all conditions of loading, acceleration, or thermal stress. The grain geometry can be changed to reduce excessive stresses. This is discussed in the next section of this chapter.
5. The complex *internal cavity volume* of perforations, slots, ports, and fins increases with burning time. These cavities need to be checked for resonance, damping, and *combustion stability*. This is discussed in Chapter 14.
6. The *processing* of the grain and the *fabrication* of the propellant should be repeatable, simple, low cost (see Chapter 13), and cause acceptable thermal stresses.

The grain configuration is designed to satisfy most requirements, but sometimes some of these six categories are satisfied only partially. The geometry is crucial in grain design. For a neutral burning grain (approximately constant thrust), for example, the burning surface A_b has to stay approximately constant, and for a regressive burning grain the burning area will diminish during the burning time. From Eqs. 12–5 and 12–6 the trade-off between burning rate and the burning surface area is evident, and the change of burning surface with time has a strong influence on chamber pressure and thrust. Since the density of most modern propellants falls within a narrow range (about 0.066 lbm/in.³ or 1830 kg/m³+2 to –15%), it has little influence on the grain design.

As a result of motor developments of the past four decades, many *grain configurations* are available to motor designers. As methods evolved for increasing the propellant burning rate, the number of configurations needed decreased. Current designs concentrate on relatively few configurations, since the needs of a wide variety of solid rocket applications can be fulfilled by combining known configurations or by slightly altering a classical configuration. The trend has been to discontinue configurations that give weak grains which can form cracks, produce high sliver losses, have a low volumetric loading fraction, or are expensive to manufacture.

The effect of propellant burning on surface area is readily apparent for simple geometric shapes such as rods, tubes, wedges, and slots, as shown in the top four configurations of Fig. 12–16. Certain other basic surface shapes burn as follows: external burning rod—regressive; external burning wedge—regressive. Most propellant grains combine two or more of these basic surfaces to obtain the desired burning characteristic. The star perforation, for example, combines the wedge and the internal burning tube. Figure 12–17 indicates typical single grains with combinations of two basic shapes. The term *conocyl* is a contraction of the words *cone* and *cylinder*.

Configurations that combine both radial and longitudinal burning, as does the internal–external burning tube without restricted ends, are frequently referred to as “three-dimensional grains” even though all grains are geometrically three-dimensional. Correspondingly, grains that burn only longitudinally or only radially are “two-dimensional grains.” Grain configurations can be classified

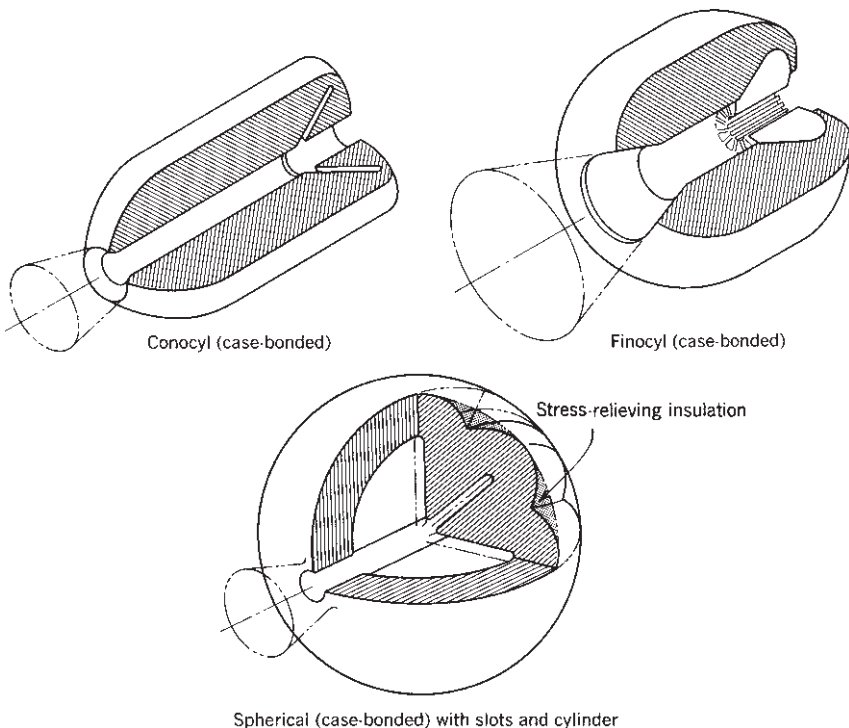


FIGURE 12–17. Typical common grain configurations using combinations of two basic shapes for the grain cavity.

according to their web fraction b_f , their length-to-diameter ratio L/D , and their volumetric loading fraction V_f . These three dependent variables are often used in selecting a grain configuration in the preliminary design of a motor for a specific application. Obvious overlap of characteristics exists with some of the configurations, as given in Table 12–4 and shown by simple sketches in Fig. 12–16. The configurations listed above the line in the table are common in recent designs. The bottom three were used in earlier designs and usually are more difficult to manufacture or to support in a case. The end burner has the highest volumetric loading fraction, the lowest grain cavity volume for a given total impulse, and a relatively low burning area or thrust with a long duration. The internal burning tube is relatively easy to manufacture and is neutral burning with unrestricted ends of $L/D \approx 2$. By adding fins or cones (see Fig. 12–17) this configuration works for $2 < L/D < 4$. The star configuration is ideal for web fractions of 0.3 to 0.4; it is progressive above 0.4 but can be neutralized with fins or slots. The wagon wheel is structurally superior to the star shape around 0.3 and is necessary at a web fraction of 0.2 (high thrust and short burn time). Dendrites are used in the lowest web fraction when a relatively large burning area is needed (high thrust and short duration), but stresses may be high. Although the limited number of configurations given in this table may not encompass all

TABLE 12–4. Characteristics of Several Grain Configurations

| Configuration | Web Fraction | L/D Ratio | Volumetric Fraction | Pressure–Time Burning Characteristics | CG Shift |
|--|--------------|-----------|---------------------|---------------------------------------|-------------------|
| End burner | >1.0 | NA | 0.90–0.98 | Neutral | Large |
| Internal burning tube (including slotted tube, trumpet, conocyl, finocyl) | 0.5–0.9 | 1–4 | 0.80–0.95 | Neutral ^a | Small to moderate |
| Segmented tube (large grains) | 0.5–0.9 | >2 | 0.80–0.95 | Neutral | Small |
| Internal star ^b | 0.3–0.6 | NA | 0.75–0.85 | Neutral | Small |
| Wagon Wheel ^b | 0.2–0.3 | NA | 0.55–0.70 | Neutral | Small |
| Dendrite ^b | 0.1–0.2 | 1–2 | 0.55–0.70 | Neutral | Small |
| Internal–external burning tube | 0.3–0.5 | NA | 0.75–0.85 | Neutral | Small |
| Rod and tube | 0.3–0.5 | NA | 0.60–0.85 | Neutral | Small |
| Dog bone ^b | 0.2–0.3 | NA | 0.70–0.80 | Neutral | Small |

^aNeutral if ends are unrestricted, otherwise progressive.

^bHas up to 4 or sometimes 8% sliver mass and thus a gradual thrust termination.

NA: not applicable or not available.

the practical possibilities for fulfilling a nearly constant thrust–time performance requirement, combinations of these features should be considered to achieve a neutral pressure–time trace and high volumetric loading before a relatively unproven configuration is accepted. The capabilities of basic configurations listed in these tables can be extended by alterations. The movement of the center of gravity (CG) influences the flight stability of the vehicle. Relative values of this CG shift are also shown in Table 12–4. Most solid propellant manufacturers have specific approaches and sophisticated computer programs for analyzing and optimizing grain geometry alternatives and permitting burn surface and cavity volume analysis. See Refs. 12–15 and 12–16 and Chapters 8 and 9 of Ref. 12–1.

The *end burning grain* (burning like a cigarette) is unique; it burns solely in the axial direction and maximizes the amount of propellant that can be placed in a given cylindrical motor case. In larger motors (over 0.6 m diameter) these end burners show a progressive thrust curve. Figure 12–18 shows that the burning surface soon forms a conical shape, causing a rise in pressure and thrust. Although the phenomenon is not fully understood, two factors contribute to higher burning rate near the bondline: chemical migration of the burning rate catalyst into and toward the bondline, and local high propellant stresses and strains at the bond surface, creating local cracks (Ref. 12–17).

Rockets used in air-launched or certain surface-launched missile applications, weather rockets, certain anti-aircraft or antimissile rockets, and other tactical applications actually benefit by reducing the thrust with burn time. A high thrust is desired to apply initial acceleration, but, as propellant is consumed and the

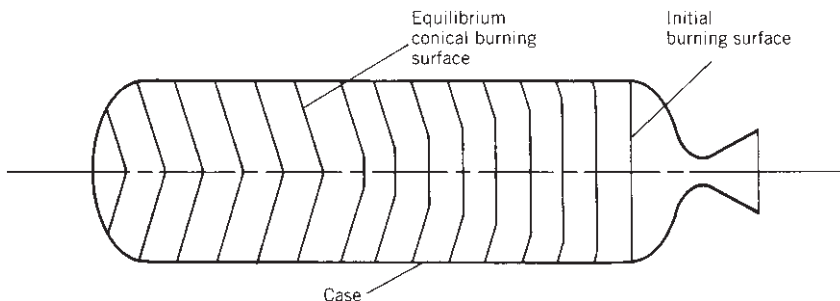


FIGURE 12–18. Schematic diagram of end-burning grain coning effect. In larger sizes (above approximately 0.5 m diameter) the burning surface does not remain flat and perpendicular to the motor axis, but gradually assumes a conical shape. The lines in the grain indicate successively larger-area burning surface contours.

vehicle mass is reduced, a decrease in thrust is desirable; this limits the maximum acceleration on the rocket-propelled vehicle or its sensitive payload, often reduces the drag losses, and usually permits a more effective flight path. Therefore, there is a benefit to vehicle mass, flight performance, and cost in having a higher initial thrust during the *boost phase* of the flight, followed by a lower thrust (often 10 to 30% of boost thrust) during the *sustaining phase* of the powered flight. Figure 12–19 shows grains which give two or more discrete thrust periods in a single burn operation. The configurations are actually combinations of the configurations listed in Table 12–4.

In a single-propellant dual-thrust level solid rocket motor, factors relating to the sustain portion usually dominate in the selection of the propellant type and grain configuration if most of the propellant volume is used during the longer sustain portion.

A *restartable rocket motor* has advantages in a number of tactical rocket propulsion systems used for aircraft and missile defense applications. Here two (or sometimes three) grains are contained inside the same case, each with its own igniter. The grains are physically separated typically by a structural bulkhead or by an insulation layer. One method for accomplishing this is shown in Fig. 12–20. The timing between thrust periods (sometimes called *thrust pulses*) can be controlled and commanded by the missile guidance system, so as to change the trajectory in a nearly optimum fashion and minimize the flight time to target. The separation mechanism has to prevent the burning-hot pressurized gas of the first grain from reaching the other grain and causing its inadvertent ignition. When the second grain is ignited, the separation devices are automatically removed, fractured, or burned, but in such a manner that the fragments of hardware pieces will not plug the nozzle or damage the insulation (see Refs. 12–18 and 12–19).

Slivers

Any remaining unburnt propellant is known as *slivers*. Figure 12–5 and the figure in Problem 6 show small slivers or pieces of unburnt propellant remaining

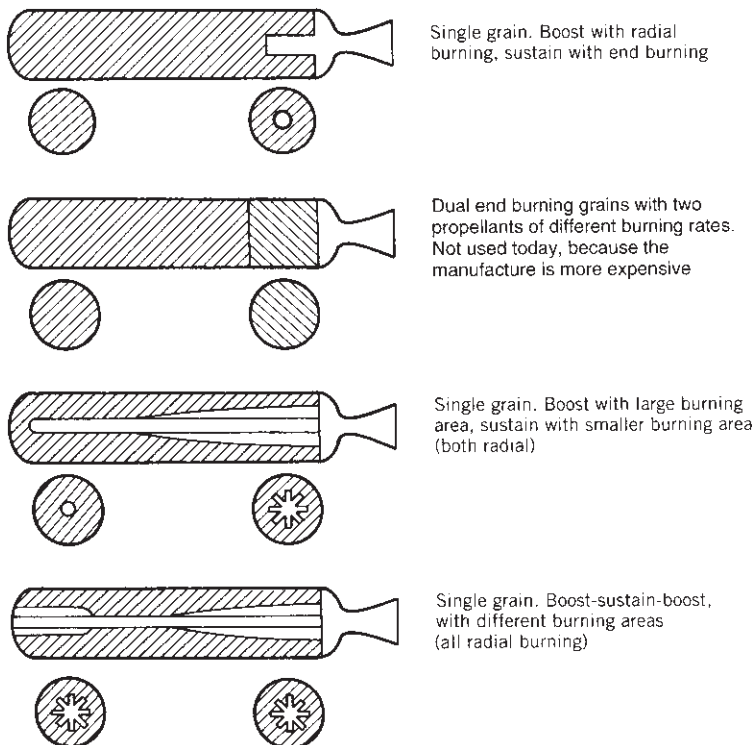


FIGURE 12-19. Several simplified schematic diagrams of grain configurations for an initial period of high thrust followed by a lower-thrust period.

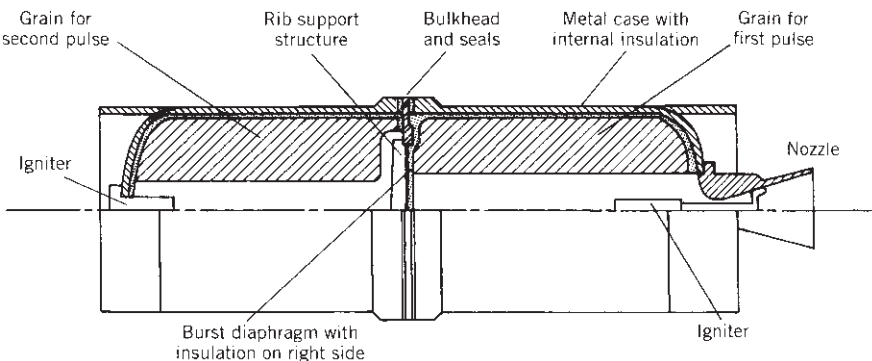


FIGURE 12-20. Simplified diagram of one concept of a two-pulse experimental rocket motor with two grains separated by a bulkhead. During the first pulse operation the metal diaphragm is supported by a spider-web-like structure made of high-temperature material. Upon ignition of the second stage, the scored diaphragm is loaded in the other direction; it breaks and its leaves peel back. The bulkhead opening has a much larger area than the nozzle throat.

at the periphery of the grain, because the pressure went below the deflagration limit (see Ref. 12–20). About 35 years ago grain designs had 2 to 7% propellant slivers; this useless material caused a reduction in propellant mass fraction and vehicle mass ratio. The technology of grain design has advanced so that there are almost no slivers (usually less than 1%). If slivers were to occur in a new unusual grain design, the designer would try to replace the sliver volume with a lower-density insulator, which gives less of a mass ratio penalty than the higher-density propellant residue. This is shown in Fig. 12–17.

12.4. PROPELLANT GRAIN STRESS AND STRAIN

The objective of stress analysis of rocket motors is to design the configuration of the grain, the liners, or the grain support in such a way that excessive stresses or excessive strains will not occur and so that there will be no failure. Static and dynamic loads and stresses are imposed on the propellant grains during manufacture, transportation, storage, and operation. Structurally, a rocket motor is a thin shell of revolution (motor case) almost completely filled with a viscoelastic material, the propellant, which usually accounts for 80 to 94% of the motor mass. Propellants have some mechanical properties that are not found in ordinary structural materials and these have received relatively little study. The viscoelastic nature of solid propellant is time–history dependent and the material accumulates damage from repeated stresses; this is known as the *cumulative-damage phenomenon*.

The most common *failure modes* are:

1. Surface cracks are formed when the surface strain is excessive. They open up new additional burning surfaces, and this in turn causes the chamber pressure as well as the thrust to be increased. The higher, shorter duration thrust will cause the vehicle to fly a different trajectory, and this may cause the mission objective to be missed. With many cracks or deep cracks, the case becomes overpressurized and will fail. The limiting strain depends on the stress level, grain geometry, temperature, propellant age, load history, and the sizes of flaws or voids. At a high strain rate, deeper, more highly branched cracks are more readily formed than at a lower strain rate (see Ref. 12–10).
2. The bond at the grain periphery is broken and an unbonded area or gap can form next to the liner, insulator, or case. As the grain surface regresses, a part of the unbonded area will become exposed to the hot, high-pressure combustion gases, and then suddenly the burning area is increased by the unbonded area.

Other failure modes, such as an excessively high ambient grain temperature causing a large reduction in the physical strength properties, ultimately result in grain cracks and/or debonding. Air bubbles, porosity, or uneven density can

locally reduce the propellant strength sufficiently to cause failure, again by cracks or debonds. Other failure modes are excessive deformations of the grain (e.g., slump of large grains can restrict the port area) and involuntary ignition due to the heat absorbed by the viscoelastic propellant from excessive mechanical vibration (e.g., prolonged bouncing during transport).

If the grain has a large number of small cracks or a few deep cracks or large areas of unbonding prior to firing, the burning area will increase, often progressively and unpredictably, and the resulting higher pressure will almost always cause the case to burst. A few small cracks or minor unbonded areas will usually not impede satisfactory motor operation.

Material Characterization

Before a structural analysis can be performed it is necessary to understand the materials and obtain data on their properties. The grain materials (propellant, insulator, and liner) are rubber-like materials that are nearly incompressible. They all have a *bulk modulus in compression* of at least 1400 MPa or about 200,000 psi in their original state (undamaged). Since there are very few voids in a properly made propellant (much less than 1%), its compression strain is low. However, the propellant is easily damaged by applied tension and shear loads. If the strength of propellant in tension and shear (typically between 50 and 1000 psi) is exceeded, the grain will be damaged or fail locally. Since grains are three-dimensional, all stresses are combined stresses and not pure compression stresses, and grains are thus easily damaged. This *damage* is due to a “dewetting” of the adhesion between individual solid particles and the binder in the propellant and appears initially as many small voids or porosity. Those very small holes or debonded areas next to or around the solid particles may initially be under vacuum, but they become larger with strain growth.

The propellant, liner, and insulator with a solid filler are viscoelastic materials. They show a nonlinear viscoelastic behavior, not a linear elastic behavior. This means that the maximum stress and maximum elongation or strain diminish each time a significant load is applied. The material becomes weaker and suffers some damage with each loading cycle or thermal stress application. The physical properties also change with the time rate of applying loads; for example, very fast pressurization actually gives a stronger material. Certain binders, such as HTPB, give good elongation and a stronger propellant than other polymers used with the same percentage of binder. Therefore HTPB is a preferred binder today. The physical properties are also affected by the manufacturing process. For example, tensile specimens cut from the same conventionally cast grain of composite propellant can show 20 to 40% variation in the strength properties between samples of different orientations relative to the local casting slurry flow direction. Viscoelastic material properties change as a function of prior loading and damage history. They have the capability to reheat and recover partially following damage. Chemical deterioration will in time degrade the properties of many propellants. These phenomena make it difficult to characterize these materials and predict their behavior or physical properties in engineering terms.

Several kinds of laboratory tests on small samples are routinely performed today to determine the physical properties of these materials. (see Refs. 12–21 and 12–22). Simple tests, however, do not properly describe the complex nonlinear behavior. These laboratory tests are conducted under ideal conditions—mostly uniaxial stresses instead of complex three-dimensional stresses—with a uniform temperature instead of a thermal gradient and usually with no prior damage to the material. The application of laboratory test results to real structural analysis therefore involves several assumptions and empirical correction factors. The test data are transformed into derived parameters for determining safety margins and useful life, as described in Chapter 9 of Ref. 12–1. There is no complete agreement on how best to characterize these materials. Nevertheless, laboratory tests provide useful information and several are described below.

The most common test is a simple *uniaxial tensile test* at constant strain rate. One set of results is shown in Fig. 12–21. The test is commonly used for manufacturing quality control, propellant development, and determining failure criteria. Once the sample has been loaded, unloaded, and restressed several times,

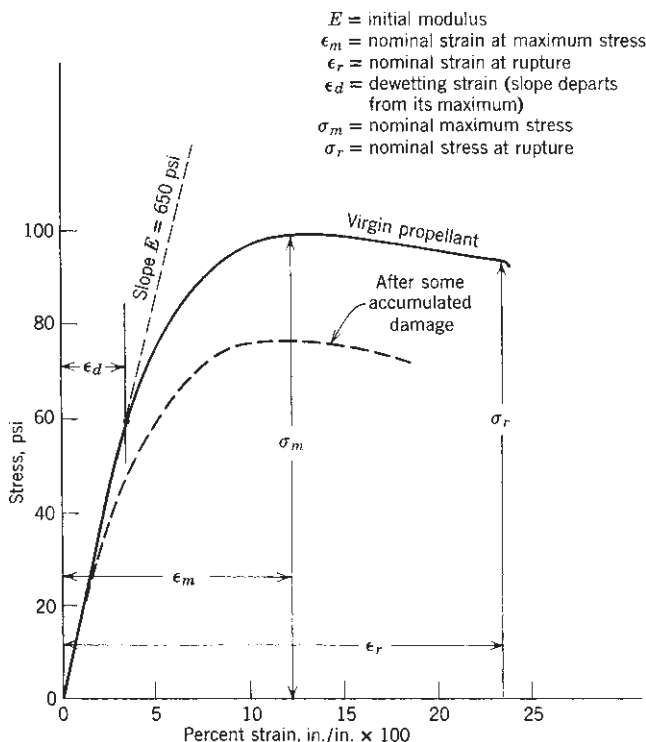


FIGURE 12–21. Stress–strain curves for a typical composite-type solid propellant showing the effect of cumulative damage. The maximum stress σ_m is higher than the rupture stress σ_r , of the tensile test sample.

the damage to the material changes its response and properties as shown by the dashed curve in Fig. 12–21.

The dewetting strain is, by definition, the strain (and corresponding maximum stress) where incipient failure of the interface bonds between small solid oxidizer crystals and the rubbery binder occurs. The dewetting stress is analogous to the yield point in elastic materials, because this is when internal material damage begins to happen. The slope E , the modulus at low strain, is not ordinarily used in design, but is often used as a quality control parameter. Data from several such uniaxial tests at different temperatures can then be manipulated to arrive at allowable stresses, permissible safe strains, and a derived artificial modulus, as described later. Once a case-bonded grain has been cooled down from its casting temperature, it will have shrunk and be under multidirectional strain. Samples cut from different parts of a temperature-cycled grain will usually give different tensile test results.

Biaxial strength tests are also performed frequently in the laboratory. One type is described in Ref. 12–21. Meaningful three-dimensional stress tests are difficult to perform in the laboratory and are usually not done. There are other sample tests that give information about propellant behavior, such as strain endurance tests to obtain the levels of strain at which the propellant has long endurance and does not suffer significant damage, tests at constant stress levels, fracture tests of samples with known cracks or defects, tensile tests under simulated chamber pressure, or tests to measure the thermal coefficient of expansion. Peel tests of the adhesive bonds of propellants to liners or insulators are very common and their failures are discussed in Ref 12–22. The application and interpretation of all these tests depend on the stress conditions in the grain and company preferences. In addition, strain or stress measurements are made occasionally on full-scale, experimental, flight-weight motors using special embedded sensors. Care must be taken that the implanting of these sensors into the grain will not disturb the local stress–strain distribution, which would lead to erroneous measurements.

The maximum failure stresses of most propellants are relatively low compared to those of plastic materials. Typical values range from about 0.25 to 8 MPa or about 40 to about 1200 psi, with average values between 50 and 300 psi, and elongations range from 4 to 250%, depending on the specific propellant, its temperature, and its stress history. Table 12–5 shows properties for a relatively strong propellant. Some double-base propellants and binder-rich composite propellants can withstand higher stresses (up to about 32 MPa or 4600 psi). The pressure and the strain rate have a major influence on the physical properties. Tensile tests performed at chamber pressure give higher strength than those done at atmospheric pressure, in some cases by a factor of 2 or more. High strain rates (sudden-start pressurization) can also improve the propellant properties temporarily.

The strength properties of the grain material are commonly determined over a range of propellant temperatures. For air-launched missiles these limits are wide, with -65 and $+160^{\circ}\text{F}$ or 219 and 344 K often being the lower and upper extremes expected during motor exposure. Propellant grains must be strong enough and have elongation capability sufficient to meet the high stress concentrations present

TABLE 12-5. Range of Tensile Properties of Reduced Smoke Composite Propellant for a Tactical Missile^a

| | Temperature (°F) | | |
|---|------------------|-------------|-------------|
| | 158 | 77 | -40 |
| Maximum stress (psi) | 137–152 | 198–224 | 555–633 |
| Modulus (psi) | 262–320 | 420–483 | 5120–6170 |
| Strain at maximum stress–strain and at ultimate stress (%) | 54/55–65/66 | 56/57–64/66 | 46/55–59/63 |

^aPolybutadiene binder with reduced aluminum and ammonium perchlorate; data are from four different 5-gallon mixes.

Source: Data taken with permission of the AIAA from Ref. 12–23.

during shrinkage at low temperature and also under the dynamic load conditions of ignition and motor operation. The mechanical properties (strength, elongation) can be increased by increasing the percent of binder material in the propellant, but at a reduction in performance.

Structural Design

The structural analysis of a typical case-bonded grain has to consider not only the grain itself but also the liner, insulator, and case, which interact structurally with the propellant grain under various loading conditions (see Chapter 9 of Ref. 12–1). The need to obtain strong bonds between the propellant and the liner, the liner and the insulator, or the insulator and the case is usually satisfied by using properly selected materials and manufacturing procedures to assure a good set of bonds. Liners are usually flexible and can accept large strains without failure, and the vehicle loads can be transmitted from the case (which is usually part of the vehicle structure) into the propellant.

When the propellant is cured (heated in an oven), it is assumed to have uniform internal temperature and to be free of thermal stresses. As the grain cools and shrinks after cure and reaches an equilibrium uniform ambient temperature (say, from -40 to +75°F), the propellant experiences internal stresses and strains which can be relatively large at low temperature. The stresses are increased because the case material usually has a thermal coefficient of expansion that is smaller than that of the propellant by an order of magnitude. The stress-free temperature range of a propellant can be changed by curing the motor under pressure. Since this usually reduces the stresses at ambient temperature extremes, this pressure cure is now being used more commonly.

The structural analysis begins when all loads can be identified and quantified. Table 12–6 lists typical loads that are experienced by a solid propellant motor during its life cycle and some of the failures they can induce. Some of these loads are unique to specific applications. The loads and the timing of these loads during the life cycle of a solid propellant rocket motor have to be analyzed for each application and each motor. They depend on the motor design and use. Although

TABLE 12–6. Summary of Loads and Likely Failure Modes in Case-Bonded Rocket Motors

| Load Source | Description of Load and Critical Stress Area |
|--|--|
| 1. Cool-down during manufacture after hot cure | Temperature differential across case and grain; tension and compression stresses on grain surfaces; hot grain, cool case |
| 2. Thermal cycling during storage or transport | Alternative hot and cold environment; critical condition is with cold grain, hot case; two critical areas: bond-line tensile stress (tearing), inner-bore surface cracking |
| 3. Improper handling and transport vibrations | Shock and vibration, $5\text{--}30g_0$ forces during road transport at 5–300 Hz (5–2500 Hz for external aircraft carry) for hours or days; critical failure: grain fracture or grain debonding |
| 4. Ignition shock/initial pressure loading | Case expands and grain compresses; axial pressure differential is severe with end-burning grains; critical areas; fracture and debonding at grain periphery |
| 5. Friction of internal gas flow in cavity | Axially rearward force on grain |
| 6. Launch and axial flight acceleration | Inertial load mostly axial; shear stress at bond line; slump deformation in large motors can reduce port diameter |
| 7. Flight maneuvers (e.g., antimissile rocket) | High side accelerations cause unsymmetrical stress distribution; can result in debonding or cracks |
| 8. Centrifugal forces in spin-stabilized projectiles/missiles | High strain at inner burning surfaces; cracks can form |
| 9. Gravity slump during storage; only in large motors | Stresses and deformation in perforation can be minimized by rotating the motor periodically; port area can be reduced by slump |
| 10. External air friction when case is also the vehicle's skin | Heating of propellant, liner and insulators will lower their strengths causing premature failure. Induces thermal stresses |

ignition and high accelerations (e.g., impact on a motor that falls off a truck) usually cause high stresses and strains, they may not always be the critical loads. The stresses induced by ambient environmental temperature cycling or gravity slumps are often relatively small; however, they are additive to stresses caused by other loads and thus can be critical. A space motor that is to be fired within a few months after manufacture presents a different problem than a tactical motor that is to be transported, temperature cycled, and vibrated for a long time, and this is different yet from a large-diameter ballistic missile motor that sits in a temperature-conditioned silo for more than 10 years.

Furthermore, the structural analysis requires a knowledge of the material characteristics and *failure criteria*: namely, the maximum stress and strains that can

safely be accepted by the propellant under various conditions. The failure criteria are derived from cumulative damage tests, classical failure theories, actual motor failures, and fracture mechanics. This analysis may be an iterative analysis, because the materials and geometry need to be changed if analysis shows that the desired margins of safety are exceeded.

Ideally, the analysis would be based on a nonlinear viscoelastic stress theory; however, such an approach is not yet reliable (see Ref. 12–1). An analysis based on a viscoelastic material behavior is feasible, relatively complex, and requires material property data that are difficult to obtain and uncertain in value. Most structural analyses have been based on an elastic material model; it is relatively simple and many two- and three-dimensional finite element analysis computer programs of this approach are available at rocket motor manufacturing companies. Admittedly, this theory does not fit all the facts, but with some empirical corrections it has given approximate answers to many structural grain design problems. An example of a two-dimensional finite element grid from a computer output is shown in Fig. 12–22 for a segment of a grain using an elastic model (see Refs. 12–24 and 12–25).

With elastic materials the stress is essentially proportional to strain and independent of time; when the load is removed, the material returns to its original condition. Neither of these propositions is valid for grains or their propellant materials. In viscoelastic material a time-related dependency exists between stresses and strains; the relationship is not linear and is influenced by the rate of strain. The stresses are not one-dimensional as many laboratory tests are, but three-dimensional, which are more difficult to visualize. When the load is removed, the grain does not return to its exact original position. References 12–26 and 12–27 and Chapters 9 and 10 of Ref. 12–1 discuss three-dimensional

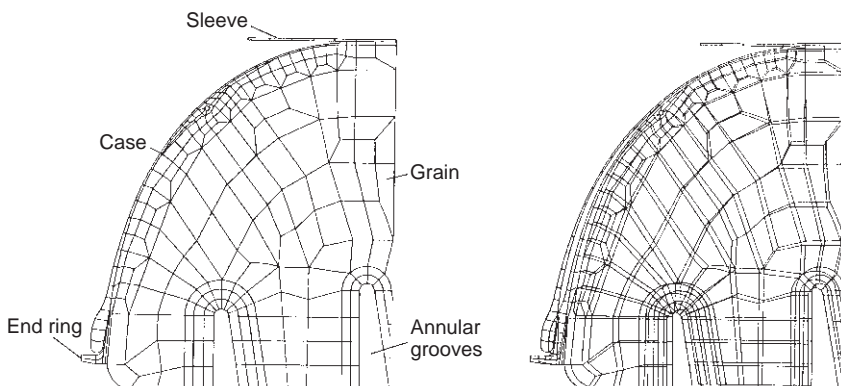


FIGURE 12–22. Finite element analysis grid of the forward end of a cast grain in a filament-wound plastic case. The grain has an internal tube and annular grooves. The top diagram shows the model grid elements and the bottom shows one calculated strain or deformation condition. (Reprinted with permission from A. Turchot, Chapter 10 of Ref. 12–1.)

analysis techniques and viscoelastic design. A satisfactory analysis technique has yet to be developed to predict the influence of cumulative damage.

Various techniques have been used to compensate for the nonelastic behavior by using allowable stresses that have been degraded for nonlinear effects and/or an effective modulus that uses a complex approximation based on laboratory strain test data. Many use a modified modulus (maximum stress-strain at maximum stress or σ_m/ϵ_m in Fig. 12-21) called the *stress relaxation modulus* E_R in a master curve against temperature-compensated time to failure, as shown in Fig. 12-23. It is constructed from data collected from a series of uniaxial tests at constant strain rate (typically, 3 to 5%) performed at different temperatures (typically -55 to $+43^\circ\text{C}$). The shifted temperature T_s/T is shown in the inset on the upper right for 3% strain rate and sample tests taken at different temperatures. The factor λ in the ordinate corrects for the necking down of the tension sample during test. The small inset in this figure explains the correction for temperature that is applied to the reduced time to failure. The empirical time-temperature shift factor α_T is set to zero at ambient temperatures (25°C or 77°F) and graphically shifted for higher and lower temperatures. The master curve then provides time-dependent stress-strain data to calculate the response of the propellant for structural analysis (see Ref. 12-21 and Chapter 9 of Ref. 12-1).

Usually, several different grain loading and operating conditions need to be analyzed. Such a structural analysis is useful for identifying locations of maximum stress or strain and to any structural members or grain sectors that are too weak or too heavy, but these analyses have not always been successful. The choice of the best analysis tool and the best pseudo-viscoelastic compensation factors will depend on the experience of the stress analyst, the specific motor design

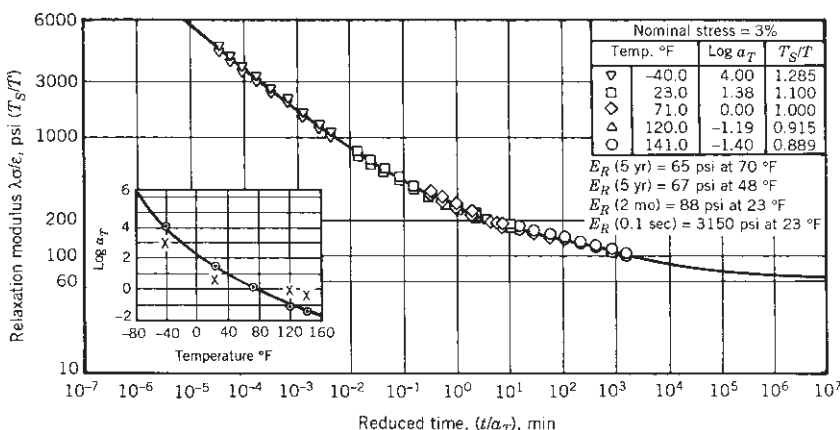


FIGURE 12-23. This stress-relaxation modulus master curve for a particular composite solid propellant is constructed from manipulated data taken from a number of uniaxial tensile tests at constant strain rate but different temperatures. (Reproduced with permission of United Technologies Corp., from Ref. 12-27.)

conditions, the complexity of the motor, the geometry, and suitable, available, valid propellant property data.

In a case-bonded motor, special provision is required to reduce the stress concentrations at the grain ends where the case and grain interface, especially for motors expected to operate satisfactorily over a wide range of temperatures. Basically, the high stresses arise from two primary sources. First, the physical properties, including the coefficient of thermal expansion of the case material and the propellant, are grossly dissimilar. The coefficient of expansion of a typical solid propellant is 1.0×10^{-4} m/m-K, which is five times as great as that of a steel motor case. Secondly, the aft-end and head-end geometries at the grain-case juncture often present a discontinuity, with the grain stress theoretically approaching infinity. Actually, finite stresses exist because viscoplastic deformations do occur in the propellant, the liner, and the case insulation. Calculating the stress in a given case-grain termination arrangement is usually impractical, and designers rely on approximations supported by empirical data.

For simple cylindrical grains the highest stresses usually occur at the outer and inner surfaces, at discontinuities such as the bond surface termination point, or at stress concentration locations, such as sharp radii at the roots or tips of star or wagonwheel perforations, as shown in Fig. 12-16. Figure 12-24 shows a *stress relief flap*, sometimes called a *boot*, a device to reduce local stresses. It is usually an area on the outside of the grain near its aft end (and sometimes also its forward end), where the liner material is not sticky but has a nonadhesive coating

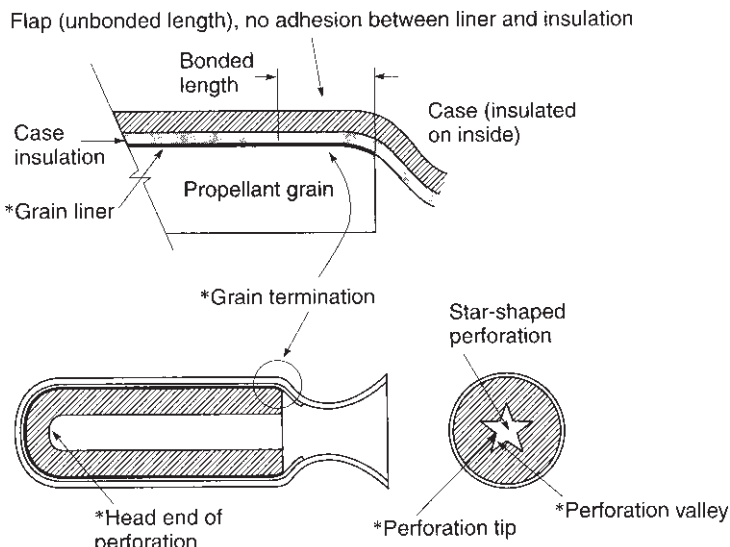


FIGURE 12-24. Stress relief system. The asterisks in the bottom simplified diagram denote potentially critical failure areas. The top sketch is an enlargement of the aft termination region of the grain and shows a boot or stress relief flap.

that permits the grain to shrink away from the wall. It allows for a reduction of the grain at the bond termination point. It moves the location of highest stress into the liner or the insulation at the flap termination or hinge. Normally, the liner and insulation are much stronger and tougher than the propellant.

Parametric studies of propellant and case-bond stresses of a typical grain-case termination design (Fig. 12-24) reveal the following:

1. Flap length is less significant than the thickness of the insulation or the separate flap boot, if one is used, in controlling the local level of stresses at the grain-case termination.
2. The distribution of stresses at the grain-case termination is sensitive to the local geometry; the level of stress at the case bond increases with web fraction and length-to-diameter ratio under loading by internal pressure and thermal shrinkage.
3. As the L/D and web fraction increase, the inner-bore hoop stress and the radial stress at the grain-case bond increase more rapidly than does the grain-case termination stress under internal pressure and thermal shrinkage loads.
4. The radial case-bond stress level at the grain-case termination is much larger than the case-bond shear stress under axial acceleration loading as well as under internal pressure and thermal shrinkage loading.

Aging of propellants in rocket motors refers to their deterioration in the physical properties with time. It is caused by the *cumulative damage* done to the grain (such as by thermal cycling, and load applications) during storage, handling, or transport. It can also be caused by chemical changes with time, such as the gradual depletion (evaporation) of certain liquid plasticizers or moisture absorption. The ability to carry stress or to allow elongation in propellants diminishes with cumulative damage. The *aging limit* is the estimated time when the motor is no longer able to perform its operation reliably or safely (see Refs. 12-28 and 12-29). Depending on the propellant and the grain design, this age limit or motor life can be between 8 and 25 years. Before this limit is reached, the motor should be deactivated and have its propellant removed and replaced. This refurbishing of propellant is routinely done on larger and more expensive rocket motors in the military inventory.

With small tactical rocket motors the aging limit is usually determined by full-scale motor-firing tests at various time periods after manufacture, say 2 or 3 years and with an extrapolation to longer time periods. Accelerated temperature aging (more severe thermal cycles) and accelerated mechanical pulse loads and overstressing are often used to reduce the time needed for these tests. For large rocket motors, which are more expensive, the number of full-scale tests has to be relatively small, and aging criteria are then developed from structural analysis, laboratory tests, and subscale motor tests.

Many of the early grains were *cartridge loaded* and kept the grain isolated from the motor case to minimize the interrelation of the case and the grain stresses and strains resulting from thermal expansion. Also, upon pressurization the case would expand, but the grain would shrink. The case-bonded grain presents a far more complex problem in stress analysis. With the propellant grain bonded firmly to the case, being a semirubber-like and relatively weak material, it is forced to respond to case strains. As a result, several critically stressed areas exist in every case-bonded motor design; some are shown with an asterisk in Fig. 12-24.

The varying nature of the stress analysis problem is brought about by the physical character of propellant; in general terms, solid propellant is relatively weak in tension and shear, is semielastic, grows softer and weaker at elevated temperatures, becomes hard and brittle at low temperatures, readily absorbs and stores energy upon being vibrated, degrades physically during long-term storage because of decomposition and chemical or crystalline changes, and accumulates structural damage under load, including cyclic load. This last phenomenon is shown graphically in Fig. 12-25 and is particularly important in the analysis of motors that are to have a long shelf-life (more than 10 years).

No a priori reason is known for materials to exhibit *cumulative damage*, but propellants and their bond to case material exhibit this trait even under constant load, as shown in Fig. 12-26. Valid theories and analytical methods applicable to cumulative damage include a consideration of both the stress-strain history and the loading path (the material effected). The most important environmental

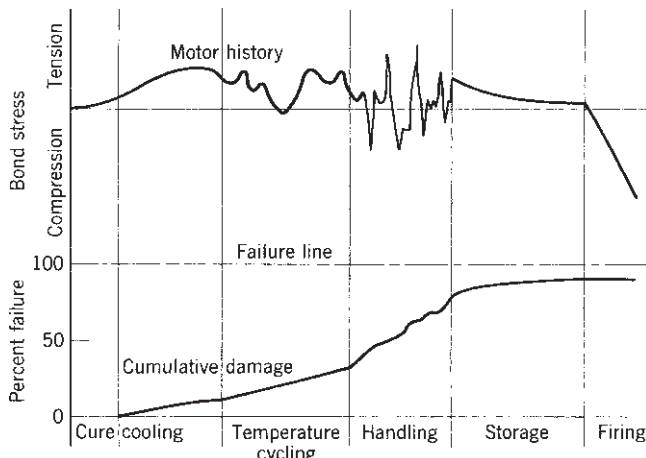


FIGURE 12-25. Representation of the progress in cumulative damage to the bond between the grain and the case in a case-bonded rocket motor experiencing a hypothetical stress history. (Adapted from Ref. 12-30.)

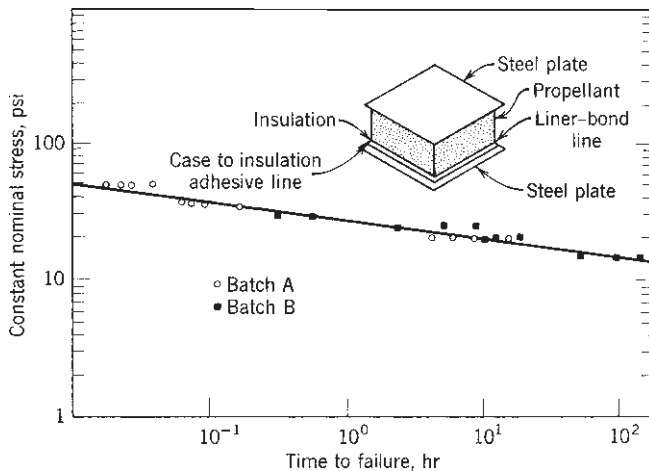


FIGURE 12-26. Time-dependent reduction of the propellant–liner–insulator bond strength when subjected to constant load at 77°F. (From Ref. 12-31.)

variables affecting the shelf life of a motor are time, temperature cycles, propellant mass, stress (gravity forces for large motors), and shock and vibration. Failure due to cumulative damage usually appears as cracks in the face of the perforation or as local “unbonds” in case-bonded motors.

The strength of most propellants is sensitive to the rate of strain; in effect they appear to become more brittle at a given temperature as the strain rate is increased, a physical trait that is important during the ignition process.

12.5. ATTITUDE CONTROL AND SIDE MANEUVERS WITH SOLID PROPELLANT ROCKET MOTORS

A clever attitude control (also called reaction control) system with solid propellants is used on some ballistic missiles. Its hot reaction gas has a low enough temperature so that uncooled hardware can be used for long durations. Ammonium nitrate composite propellant (mentioned as gas generator propellants in Tables 13-1 and 13-2) or a propellant consisting of a nitramine (RDX or HMX, described in Chapter 13) with a polymer binding are suitable. The version shown schematically in Fig. 12-27 provides pitch and yaw control see Chapter 18; hot gas flows continuously through insulated manifolds, open hot gas valves, and all four nozzles. When one of these valves is closed, it causes an unbalance of gas flow and produces a side force. The chamber pressure rises when the valve is closed. To keep things simple, the four roll-control thrusters have been deleted from this figure.

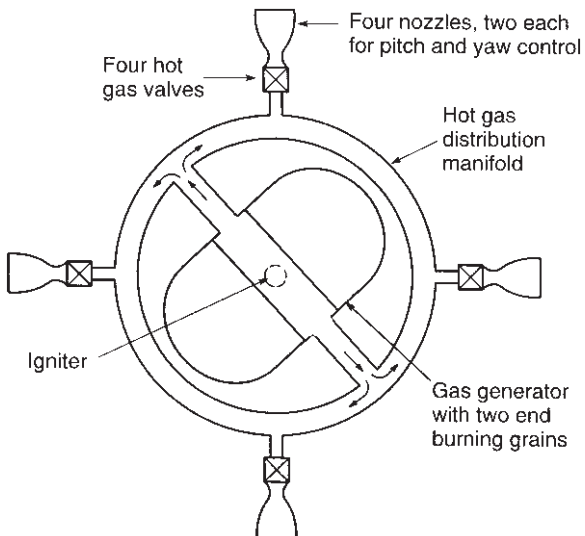


FIGURE 12–27. Simplified diagram of a rocket attitude control system using solid propellant. All four valves are normally open and gas flows equally through all nozzles.

With this type of attitude control system it is possible to achieve variable duration thrust pulsing operations and random pitch, yaw, and roll maneuvers. It is competitive with multithruster liquid propellant attitude control systems. The solid propellant versions are usually heavier because they have heavy insulated hardware and require more propellant (for continuous gas flow), whereas the liquid version is operated only when attitude control motions are required.

A similar approach with hot gas valves applies to upper stages of interceptor vehicles used for missile defense; there is little time available for maneuvers of the upper stage to reach the incoming missile or aircraft and therefore the burning durations are usually short. The solid propellant gas temperatures are higher than with gas generators (typically 1260°C or 2300°F), but lower than with typical composite propellants (3050 K or 5500°F), and this allows the valves and manifolds to be made of high-temperature material (such as rhenium or carbon). In addition to attitude control, the system provides a substantial side force or divert thrust. It displaces the flight path laterally. Figure 12–28 shows such a system. Since all hot gas valves are normally open, a valve has to be closed to obtain a thrust force as explained in the previous figure. The attitude control system provides pitch, yaw, and roll control to stabilize the vehicle during its flight, to orient the divert nozzle into the desired direction, and sometimes to orient the seeker (at the front of the vehicle) toward the target. Thrust vector control is treated in Chapter 18.

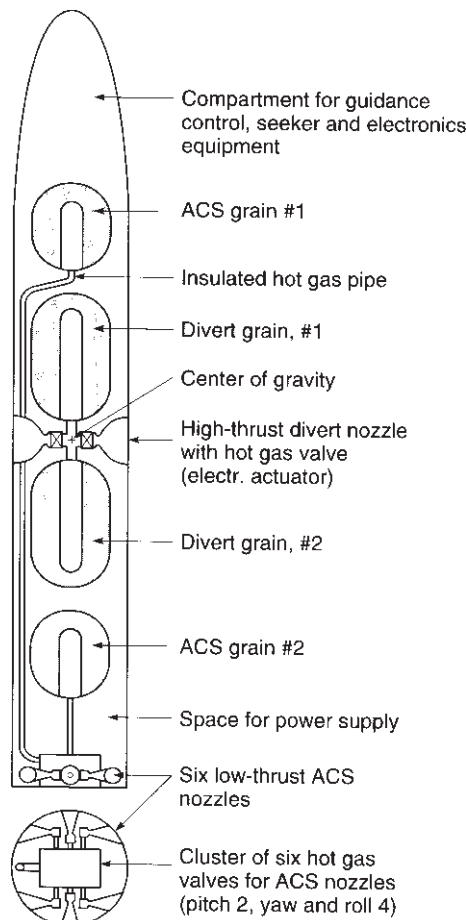


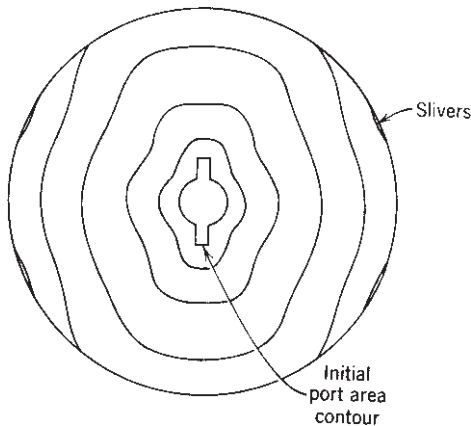
FIGURE 12–28. Simplified schematic diagram of two propulsion systems for one type of maneuverable upper stage of an interceptor missile. The side or divert forces are relatively large and go essentially through the center of gravity (CG) of the upper-stage vehicle. To minimize the CG travel two grains are above and two grains are below the CG. Each nozzle has its own hot gas valve, which is normally open and can be pulsed. The attitude control system (ACS) is fed from the reaction gas of two grains and has six small nozzles.

PROBLEMS

1. What is the ratio of the burning area to the nozzle throat area for a solid propellant motor with these characteristics? Also, calculate the temperature coefficient (α) and the temperature sensitivity of pressure (π_K).

| | |
|------------------------------------|--------------------------|
| Propellant specific gravity | 1.71 |
| Chamber pressure | 14 MPa |
| Burning rate | 38 mm/sec |
| Temperature sensitivity σ_p | 0.007 (K)^{-1} |
| Specific heat ratio | 1.27 |
| Chamber gas temperature | 2220 K |
| Molecular mass | 23 kg/kg-mol |
| Burning rate exponent n | 0.3 |

- Plot the burning rate against chamber pressure for the motor in Problem 1 using Eq. 12-5 between chamber pressures of 11 and 20 MPa.
- What would the area ratio A_b/A_t in Problem 1 be if the pressure were increased by 10%? (Use curve from Problem 2.)
- Design a simple rocket motor for the conditions given in Problems 1 and 2 for a thrust of 5000 N and a duration of 15 sec. Determine principal dimensions and approximate weight.
- For the Orbus-6 rocket motor described in Table 12-3 determine the total impulse-to-weight ratio, the thrust-to-weight ratio, and the acceleration at start and burnout if the vehicle inert mass and the payload come to about 6000 lbm. Use burn time from Table 12-3 and assume $g \approx 32.2 \text{ ft/sec}^2$.
- For a cylindrical two-dimensional grain with two slots the burning progresses in finite time intervals approximately as shown by the successive burn surface contours in the following drawing. Draw a similar set of progressive burning surfaces for any one configuration shown in Figure 12-16 and one shown in Figure 12-17, and draw an approximate thrust-time curve from these plots, indicating the locations where slivers will remain. Assume the propellant has a low value of n and thus the motor experiences little change in burning rate with chamber pressure.



7. Explain the significance of the web fraction, the volumetric loading ratio, and the L/D ratio in terms of vehicle performance and design influence.
8. Equations 12–8 and 12–9 express the influence of temperature on the burning of a solid propellant. Explain how a set of tests should be set up and what should be measured in order to determine these coefficients over a range of operating conditions.
9. What would be the likely change in r , I_s , p_1 , F , t_b , and I_t if the three rocket motors described in Table 12–3 were fired with the grain 100°F cooler than the data shown in the table? Assume typical average temperature effects.
10. A newly designed case-bonded rocket motor with a simple end-burning grain failed and exploded on its first test. The motor worked well for about 20% of its burn time, when the record showed a rapid rise in chamber pressure. It was well conditioned at room temperature before firing, and the inspection records did not show any flaws or voids in the grain. Make a list of possible causes for this failure and suggestions on what to do in each case to avoid a repetition of the failure.
11. For the AP-CMDB (30%, 150 μm) propellant shown in Fig. 12–7 as the solid dots, find the chamber pressure that would result from an increase of $\sigma_p \Delta T_b = 0.3$ (this would correspond to a 30°F change with $\sigma_p = 0.01/\text{°F}$). Take the reference values as 28 atm and 70°F. Values of $n(p_1)$ at various pressure ranges from Fig. 12–7 may be taken as:

$$n(5\text{--}10 \text{ atm}) = 0.38, \quad n(10\text{--}30 \text{ atm}) = 0.54, \quad n(30\text{--}100 \text{ atm}) = 0.58$$

Answer: $p_1 = 78.6 \text{ atm}$.

12. What will be the percent change in nominal values of A_t , r , I_s , T_0 , t_b , A_b/A_t and the nozzle throat heat transfer rate, if the Orbus-6 rocket motor listed in Table 12–3 is to be downgraded in thrust for a particular flight by 15% by substituting a new nozzle with a larger nozzle throat area but the same nozzle exit area? The propellants, grain, insulation, and igniter will be the same.
13. What would be the new values of I_t , I_s , p_1 , F , t_b , and r for the first stage of the Minuteman rocket motor described in Table 12–3, if the motor were fired at sea level with the grain temperature 20°F hotter than the data shown. Use only data from this table.

Answers:

$$\begin{aligned} I_t &= 10,240,000 \text{ lbf-sec}, \quad I_s = 254 \text{ sec}, \quad p_1 = 799 \text{ psia}, \quad F = 1.99 \times 10^5 \text{ lbf}, \\ t_b &= 51.4 \text{ sec}, \quad r = 0.339 \text{ in./sec}. \end{aligned}$$

14. Calculate K -ratio of the burning area to the nozzle throat area in two separate ways for the STAR™ 27 motor using *only* the data found in Table 12–3. Refer to Figure 12–13 for several of the definitions. Compare the two values of K and comment.

SYMBOLS

| | |
|-----------|---|
| a | burning rate constant, also called temperature coefficient |
| A_b | solid propellant burning area, m ² (ft ²) |
| A_p | port area (flow area of gases inside grain cavity or between and around propellant grains), m ² (ft ²) |
| A_t | nozzle throat cross-sectional area, m ² (ft ²) |
| b | web thickness, m (in.) |
| b_f | web fraction, or web thickness-to-radius ratio |
| c | effective exhaust velocity, m/sec (ft/sec) |
| c^* | characteristic exhaust velocity, m/sec (ft/sec) |
| c_p | specific heat of gas, kcal/kg-K |
| c_s | specific heat of solid, kcal/kg-K |
| C_F | thrust coefficient |
| D | diameter or a certain dimension, m (ft) |
| E_R | relaxation modulus, MPa (psi) |
| F | thrust, N (lbf) |
| \bar{F} | average thrust, N (lbf) |
| g_0 | acceleration due to gravity at sea level, 9.8066m/sec ² (32.2 ft/sec ²) |
| G | mass flow velocity per unit area kg/m ² sec |
| h | enthalpy per unit mass, J/kg (Btu/lbm) |
| I_s | specific impulse, sec |
| I_t | total impulse, N-sec (lbf-sec) |
| k | specific heat ratio |
| K | ratio of burning surface to throat area, A_b/A_t |
| L | length, m (ft) |
| m | mass, kg (lbm) |
| \dot{m} | mass flow rate, kg/sec |
| n | burning rate exponent |
| p | pressure, MPa (lbf/in. ²) |
| p_1 | chamber pressure, MPa (lbf/in. ²) |
| \Pr | Prandtl number, $\mu c_p/\kappa$ |
| r | propellant burning rate (velocity of consumption), m/sec or mm/sec or in./sec |
| R | gas constant, J/kg-K (Btu/lbm-°R) |
| S | perimeter, m |
| t | time, sec |
| t_a | action time, sec |
| t_b | burn time, sec |
| T | absolute temperature, K (°R) |
| T_1 | chamber temperature, K (°R) |
| T_b | propellant ambient temperature, °F(°C) |
| v_2 | theoretical exhaust velocity, m/sec (ft/sec) |
| V_b | propellant volume, m ³ (ft ³) |

| | |
|-----------|--|
| V_c | chamber volume, m ³ (ft ³) |
| V_f | volumetric loading fraction, % |
| w | total effective propellant weight, N (lbf) |
| w_G | total loaded rocket weight, or gross weight, N (lbf) |
| \dot{w} | weight rate of flow, N/sec (lbf/sec) |

Greek Letters

| | |
|------------|--|
| α | heat transfer factor |
| β | constant |
| δ | partial derivative |
| ϵ | elongation or strain |
| κ | conductivity |
| μ | viscosity |
| π_K | temperature sensitivity coefficient of pressure, K ⁻¹ (°R ⁻¹) |
| ρ | density, kg/m ³ (lbm/ft ³) |
| σ | stress, N/cm ² (psi) |
| σ_p | temperature sensitivity coefficient of burning rate, K ⁻¹ (°R ⁻¹) |
| ζ | propellant mass fraction |

Subscripts

| | |
|-----|---------------------------------------|
| a | action time |
| b | solid propellant burning conditions |
| p | pressure or propellant or port cavity |
| t | throat conditions |
| 0 | initial or reference condition |
| 1 | chamber condition |
| 2 | nozzle exit condition |

REFERENCES

- 12–1. P. R. Evans, “Composite Motor Case Design,” Chapter 4A; H. Badham and G. P. Thorp, “Considerations for Designers of Cases for Small Solid Propellant Rocket Motors,” Chapter 6; B. Zeller, “Solid Propellant Grain Design,” Chapter 8; D. I. Thrasher, “State of the Art of Solid Propellant Rocket Motor Grain Design in the United States,” Chapter 9; and A. Truchot, “Design and Analysis of Rocket Motor Internal Insulation,” Chapter 10; all in *Design Methods in Solid Propellant Rocket Motors*, AGARD Lecture Series 150, Revised Version, NATO, Brussels, 1988.
- 12–2. N. Eisenreich, H. P. Kugler, and F. Sinn, “An Optical System for Measuring Burning Rates of Solid Propellants,” *Propellants, Explosives, Pyrotechnics*, Vol. 12, 1987, pp. 78–80.

- 12–3. N. Kubota, “Survey of Rocket Propellants and Their Combustion Characteristics,” Chapter 1 in *Fundamentals of Solid Propellant Combustion*; K. K. Kuo and M. Summerfield (Eds.), *Progress in Astronautics and Aeronautics*, Vol. 90, AIAA, New York, 1984. See also A. Davenas, “Development of Modern Solid Propellants,” *Journal of Propulsion and Power*, Vol. 19, No. 6, May–June 2003, pp. 1108–1128; V. Yang, T. B. Brill, and W.-Z. Ren (Eds.), *Solid Propellant Chemistry, Combustion, and Motor Interior Ballistics, Progress in Aeronautics and Astronautics*, Vol. 185, AIAA, Reston, VA, 2000.
- 12–4. S. D. Heister and J. Davis, “Predicting Burning Time-Variations in Solid Rocket Motors,” *Journal of Propulsion and Power*, Vol. 8, No. 3, May–June 1992; J. R. Osborn and S. D. Heister, “Solid Rocket Motor Temperature Sensitivity,” *Journal of Propulsion and Power*, Vol. 10, No. 6, November–December 1994, pp. 908–910.
- 12–5. J. M. Lenoir and G. Robillard, “A Mathematical Method to Predict the Effects of Erosive Burning in Solid-propellant Rocket,” *Sixth Symposium (International) on Combustion*, Reinhold, New York, 1957, pp. 663–667.
- 12–6. M. K. Razdan and K. Kuo, “Erosive Burning of Solid Propellants,” Chapter 10 in *Fundamentals of Solid Propellant Combustion*, K. K. Kuo and M. Summerfield (Eds.), *Progress in Astronautics and Aeronautics*, Vol. 90, AIAA, New York, 1984.
- 12–7. “Solid Propellant Selection and Characterization,” *NASA SP-8064*, June 1971 (N72-13737).
- 12–8. M. S. Fuchs, A. Peretz, and Y. M. Timnat, “Parametric Study of Acceleration Effects on Burning Rates of Metallized Solid Propellants,” *Journal of Spacecraft and Rockets*, Vol. 19, No. 6, November–December 1982, pp. 539–544.
- 12–9. P. Yang, Z. Huo, and Z. Tang, “Combustion Characteristics of Aluminized HTPB/AP Propellants in Acceleration Fields,” Chapter 3 in V. Yang, T. B. Brill and W.-Z. Ren (Eds.), *Solid Propellant Chemistry, Combustion, and Motor Interior Ballistics, Progress in Aeronautics and Astronautics*, Vol. 185, AIAA, Reston VA, 2000.
- 12–10. K. K. Kuo, J. Moreci, and J. Mantzaras, “Modes of Crack Formation in Burning Solid Propellant,” *Journal of Propulsion and Power*, Vol. 3, No. 1, January–February 1987, pp. 19–25.
- 12–11. M. K. King, “Analytical Modeling of Effects of Wires on Solid Motor Ballistics,” *Journal of Propulsion and Power*, Vol. 7, No. 3, May–June 1991, pp. 312–320.
- 12–12. “Solid Rocket Motor Performance Analysis and Prediction,” *NASA SP-8039*, May 1971 (N72-18785).
- 12–13. E. M. Landsbaum, M. P. Salinas, and J. P. Leavy, “Specific Impulse Predictions of Solid Propellant Motors,” *Journal of Spacecraft and Rockets*, Vol. 17, 1980, pp. 400–406.
- 12–14. R. Akiba and M. Kohno, “Experiments with Solid Rocket Technology in the Development of M-3SII,” *Acta Astronautica*, Vol. 13, No. 6–7, 1986, pp. 349–361.
- 12–15. “SPP’04TM,” Computer Program from Software & Engineering Associates, Inc., <http://www.seainc.com>.
- 12–16. R. J. Hejl and S. D. Heister, “Solid Rocket Motor Grain Burnback Analysis Using Adaptive Grids,” *Journal of Propulsion and Power*, Vol. 11, No. 5, September–October 1995.

- 12–17. W. H. Jolley, J. F. Hooper, P. R. Holton, and W. A. Bradfield, “Studies on Coning in End-Burning Rocket Motors,” *Journal of Propulsion and Power*, Vol. 2, No. 2, May–June 1986, pp. 223–227.
- 12–18. S. Nishi, K. Fukuda, and N. Kubota, “Combustion Tests of Two-Stage Pulse Rocket Motors,” AIAA Paper 89-2426, July 1989.
- 12–19. L. C. Carrier, T. Constantinou, P. G. Harris, and D. L. Smith, “Dual Interrupted Thrust Pulse Motor,” *Journal of Propulsion and Power*, Vol. 3, No. 4, July–August 1987, pp. 308–312.
- 12–20. C. Bruno et al., “Experimental and Theoretical Burning of Rocket Propellant near the Pressure Deflagration Limit,” *Acta Astronautica*, Vol. 12, No. 5, 1985, pp. 351–360.
- 12–21. F. N. Kelley, “Solid Propellant Mechanical Property Testing, Failure Criteria and Aging,” Chapter 8 in C. Boyars and K. Klager (Eds.), *Propellant Manufacture Hazards and Testing*, Advances in Chemistry Series 88, American Chemical Society, Washington, DC, 1969.
- 12–22. T. L. Kuhlmann, R. L. Peeters, K. W. Bills, and D. D. Scheer, “Modified Maximum Principal Stress Criterion for Propellant Liner Bond Failures,” *Journal of Propulsion and Power*, Vol. 3, No. 3, May–June 1987.
- 12–23. R. W. Magness and J. W. Gassaway, “Development of a High Performance Rocket Motor for the Tactical VT-1 Missile,” AIAA Paper 88-3325, July 1988.
- 12–24. I-Shih Chang and M. J. Adams, “Three-Dimensional, Adaptive, Unstructured, Mesh Generation for Solid-Propellant Stress Analysis,” AIAA Paper 96-3256, July 1996.
- 12–25. W. A. Cook, “Three-Dimensional Grain Stress Analysis Using the Finite Element Method,” AFRPL Report TT-71-51, Thiokol Corp., April 1971 (AD725043).
- 12–26. G. Meili, G. Dubroca, M. Pasquier, and J. Thenpenier, “Nonlinear Viscoelastic Design of Case-Bonded Composite Modified Double Base Grains,” AIAA Paper 80-1177R, July 1980; and S. Y. Ho and G. Care, “Modified Fracture Mechanics Approach in Structural Analysis of Solid-Rocket Motors,” *Journal of Propulsion and Power*, Vol. 14, No. 4, July–August 1998.
- 12–27. P. G. Butts and R. N. Hammond, “IUS Propellant Development and Qualification,” Paper presented at the 1983 JANNAF Propulsion Meeting, Monterey, February 1983.
- 12–28. A. G. Christianson et al., “HTPB Propellant Aging,” *Journal of Spacecraft and Rockets*, Vol. 18, No. 3, May–June 1983.
- 12–29. D. I. Thrasher and J. H. Hildreth, “Structural Service Life Estimates for a Reduced Smoke Rocket Motor,” *Journal of Spacecraft and Rockets*, Vol. 19, No. 6, November 1982, pp. 564–570.
- 12–30. S. W. Tsa, Ed., *Introduction to Viscoelasticity*, Technomic Publishing, Stamford, CT, 1968.
- 12–31. J. D. Ferry, *Viscoelastic Properties of Polymers*, John Wiley & Sons, New York, 1970.

CHAPTER 13

SOLID PROPELLANTS

This is the second of four chapters dealing with solid propellant rocket motors. In this chapter we describe several common solid rocket propellants, their principal categories, ingredients, hazards, manufacturing processes, and quality control. We also discuss liners and insulators, propellants for igniters, tailoring of propellants, and propellants for gas generators.

Thermochemical analyses are needed to characterize the performance of a given propellant. The analysis methods are described in Chapter 5. Such analyses provide theoretical values of average molecular mass, combustion temperature, average specific heat ratio, and the characteristic velocity; they are functions of the propellant composition and chamber pressure. Specific impulse can also be computed for a particular nozzle configuration.

The term *solid propellant* has several connotations, including: (1) the rubbery or plastic-like mixture of oxidizer, fuel, and other ingredients that have been processed and constitute the finished grain; (2) the processed but uncured product; (3) a single ingredient, such as the fuel or the oxidizer. Acronyms and chemical symbols are used indiscriminately as abbreviations for propellant and ingredient names; only some of these will be used here.

13.1. CLASSIFICATION

Processed modern propellants can be classified in several ways, as described below. This classification is not rigorous or complete. Sometimes the same propellant will fit into two or more of the classifications.

1. Propellants are often tailored to and classified by *specific applications*, such as space launch booster propellants or tactical missile propellants; each has somewhat specific chemical ingredients, different burning rates, different physical properties, and different performance. Table 12–1 shows four kinds of *rocket motor applications* (each has somewhat different propellants) and several *gas generator applications*. Propellants for rocket motors have hot (over 2400 K) gases and are used to produce thrust, but gas generator propellants have lower-temperature combustion gases (800 to 1200 K) and they are used to produce power, not thrust.
Historically, the early rocket motor propellants used to be grouped into two classes: *double-base* (DB)* propellants were used as the first production propellants, and then the development of polymers as binders made the *composite* propellants feasible.
2. *Double-base* (DB) propellants form a *homogeneous* propellant grain, usually a nitrocellulose (NC)*, a solid ingredient which absorbs liquid nitroglycerine (NG) plus minor percentages of additives. Both the major ingredients are explosives and function as a combined fuel and oxidizer. Both *extruded double-base* (EDB) and *cast double-base* (CDB) propellant have found extensive applications, mostly in small tactical missiles of older design. By adding crystalline nitramines (HMX or RDX)* the performance and density can be improved; this is sometimes called *cast-modified double-base* propellant. A further improvement is to add an elastomeric binder (rubber-like, such as crosslinked polybutadiene), which improves the physical properties and allows more nitramine and thus improves the performance slightly. The resulting propellant is called *elastomeric-modified cast double-base* (EMCDB). These four classes of double base have nearly smokeless exhausts. Adding some solid ammonium perchlorate (AP) and aluminum (Al) increases the density and the specific impulse slightly, but the exhaust gas is smoky. The propellant is called *composite-modified double-base propellant* or CMDB.
3. *Composite propellants* form a *heterogeneous* propellant grain with the oxidizer crystals and a powdered fuel (usually aluminum) held together in a matrix of synthetic rubber (or plastic) binder, such as polybutadiene (HTPB)*. Composite propellants are cast from a mix of solid (AP crystals, Al powder)* and liquid (HTPB, PPG)* ingredients. The propellant is hardened by crosslinking or curing the liquid binder polymer with a small amount of curing agent, and curing it in an oven, where it becomes hard and solid. In the past three decades the composite propellants have been the most commonly used class. They can be further subdivided:
 - (a) Conventional *composite propellants* usually contain between 60 and 72% AP as crystalline oxidizer, up to 22% Al powder as a metal fuel,

*Acronyms, symbols, abbreviations, and chemical names of propellant ingredients are explained in Tables 13–6 and 13–7 in Section 13.4.

- and 8 to 16% of elastomeric binder (organic polymer) including its plasticizer.
- (b) Modified composite propellant where an *energetic nitramine* (HMX or RDX) is added for obtaining a little more performance and also a somewhat higher density.
 - (c) Modified composite propellant where an *energetic plasticizer* such as nitroglycerine (used in double-base propellant) is added to give a little more performance. Sometimes HMX is also added.
 - (d) A *high-energy composite solid propellant* (with some aluminum), where the organic elastomeric binder and plasticizer are largely replaced by energetic materials (such as certain explosives) and where some of the AP is replaced by HMX. Some of these are called elastomer-modified cast double-base propellants (EMCDB). Most are experimental propellants. The theoretical specific impulse can be between 270 and 275 sec at standard conditions.
 - (e) A *lower-energy composite propellant*, where ammonium nitrate (AN) is the crystalline oxidizer (no AP). It is used for gas generator propellant. If a large amount of HMX is added, it can become a minimum smoke propellant with fair performance.

Figures 13–1 and 13–2 show the general regions for the specific impulse, burning rate, and density for the more common classes of propellants. Composite propellants give higher densities, specific impulse, and a wider range of burning rates. The ordinate in these figures is an actual or estimated specific impulse at standard conditions (1000 psi and expansion to sea-level atmosphere). It does not include any pressure drops in the chamber, any nozzle erosion, or an assumption about combustion losses and scaling. The composite propellants are shown to have a wide range of burning rates and densities; most of them have specific gravities between 1.75 and 1.81 and burning rates between 7 and 20 mm/sec. Table 13–1 lists performance characteristics for several propellants. The DB propellants and the AN propellants have lower performance and density. Most composite propellants have almost the same performance and density but a wide range of burning rates. The highest performance is for a CMDB propellant whose ingredients are identified as DB/AP-HMX/Al, but it is only 4% higher. Several of the classifications can be confusing. The term composite-modified double-base propellant (CMDB) has been used for (1) a DB propellant, where some AP, Al, and binder are added; (2) alternatively, the same propellant could be classified as a composite propellant to which some double-base ingredients have been added.

4. Propellants can be classified by the density of the smoke in the exhaust plume as *smoky*, *reduced smoke*, or *minimum smoke* (essentially smokeless). Aluminum powder, a desirable fuel ingredient, is oxidized to aluminum oxide, which forms visible small solid smoke particles in the exhaust gas. Most composite propellants are smoky. By reducing the aluminum content

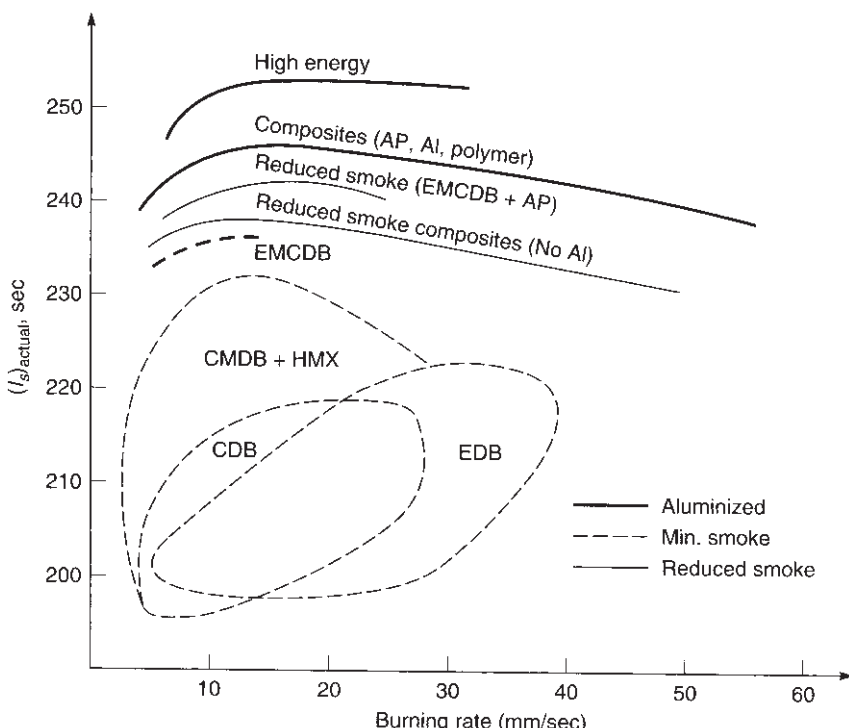


FIGURE 13-1. Typical delivered specific impulse and burning rate for several solid propellant categories. (Adapted and reproduced from Ref. 13-1 with permission of the AIAA.)

in composite propellant, the amount of smoke is also reduced. Carbon (soot) particles and metal oxides, such as zirconium oxide or iron oxide, can also be visible if in high enough concentration. This is further discussed in Chapter 20.

5. The *safety rating* for detonation can distinguish propellants as a potentially *detonable* material (class 1.1) or as a *nondetonable* material (class 1.3), as described in Section 13.3. Examples of class 1.1 propellant are a number of double-base propellants and composite propellants containing a significant portion of solid explosive (e.g., HMX or RDX), together with certain other ingredients.
6. Propellants can be classified by some of the principal manufacturing processes that are used. *Cast propellant* is made by mechanical mixing of solid and liquid ingredients, followed by casting and curing; it is the most common process for composite propellants. *Curing* of many cast propellants is by chemical reaction between binder and curing agent at elevated temperature (45 to 150°C); however, there are some that can be cured at ambient temperatures (20 to 25°C) or hardened by a nonchemical process such as

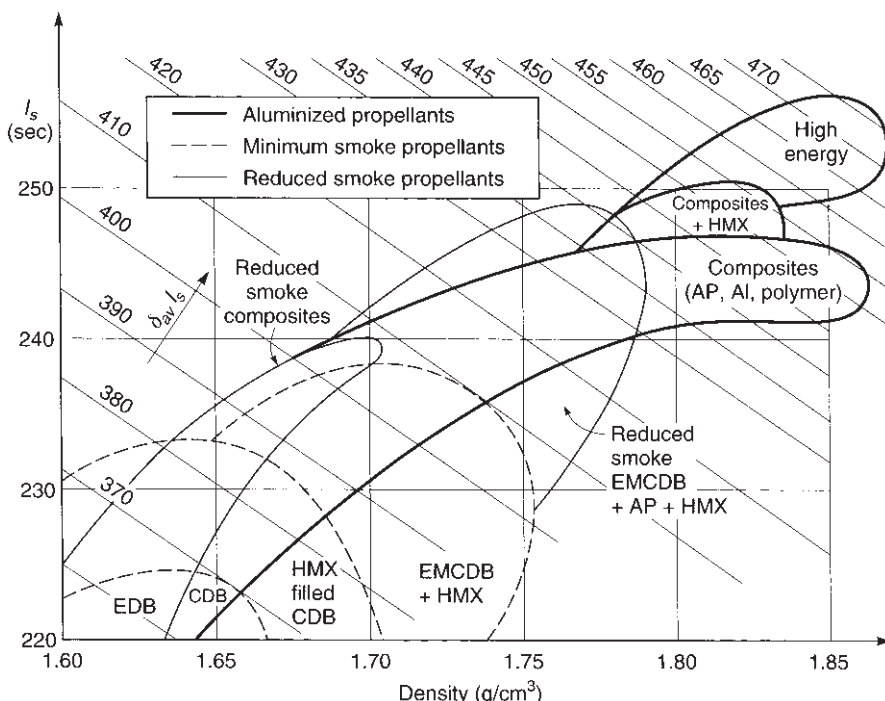


FIGURE 13–2. Typical delivered specific impulse and density-specific impulse for several solid propellant categories with an expansion of 7 to 0.1 MPa. (Adapted and reproduced from Ref. 13–1 with permission of the AIAA.)

crystallization. Propellant can also be made by a *solvation* process (dissolving a plasticizer in a solid pelletized matrix, whose volume is expanded). *Extruded propellant* is made by mechanical mixing (rolling into sheets) followed by extrusion (pushing through a die at high pressure). Solvation and extrusion processes apply primarily to double-base propellants.

7. Propellants have also been classified by their *principal ingredient*, such as the *principal oxidizer* (*ammonium perchlorate propellants*, *ammonium nitrate propellants*, or *azide-type propellants*) or their *principal binder* or *fuel ingredient*, such as *polybutadiene propellants* or *aluminized propellants*. This classification of propellants by ingredients is described in Section 13.4 and Table 13–8.
8. Propellants with *toxic* and *nontoxic* exhaust gases. This is discussed in more detail in Section 13.3.
9. *Experimental* or *production* propellants. The culmination of good R&D is to have a propellant selected for production in a flight vehicle application. Such propellant is selected after extensive testing (preflight test, qualification tests) and demonstrated safety, life, and other unique properties.

TABLE 13-1. Characteristics of Some Operational Solid Propellants

| Propellant Type ^a | I_s Range (sec) ^b | Flame Temperature ^c (°F) | Density or Spec. Gravity ^c (lbm/in. ³) | Metal Content (mass %) | Burning Rate ^{c,e} (in./sec) | Pressure Exponent ^e n | Hazard Classification | Stress (psi)/Strain(%) | | Processing Method |
|------------------------------|--------------------------------|-------------------------------------|---|------------------------|---------------------------------------|----------------------------------|-----------------------|------------------------|--------|----------------------|
| | | | | | | | | -60°F | +150°F | |
| DB | 220–230 | 4100 | 2550 | 0.058 | 1.61 | 0 | 0.05–1.2 | 0.30 | 1.1 | 4600/2 |
| DB/AP/AI | 260–265 | 6500 | 3880 | 0.065 | 1.80 | 20–21 | 0.2–1.0 | 0.40 | 1.3 | 2750/5 |
| DB/AP ₋ | 265–270 | 6700 | 4000 | 0.065 | 1.80 | 20 | 0.2–1.2 | 0.49 | 1.1 | 2375/3 |
| HMX/AI | | | | | | | | | | Solvent cast |
| PVC/AP/AI | 260–265 | 5600 | 3380 | 0.064 | 1.78 | 21 | 0.3–0.9 | 0.35 | 1.3 | 369/150 |
| PU/AP/AI | 260–265 | 5700 | 3440 | 0.064 | 1.78 | 16–20 | 0.2–0.9 | 0.15 | 1.3 | 1170/6 |
| PBAN/AP/AI | 260–263 | 5800 | 3500 | 0.064 | 1.78 | 16 | 0.25–1.0 | 0.33 | 1.3 | 520/16 (at -10°F) |
| CTPB/AP/AI | 260–265 | 5700 | 3440 | 0.064 | 1.78 | 15–17 | 0.25–2.0 | 0.40 | 1.3 | 325/26 |
| HTPB/AP/AI | 260–265 | 5700 | 3440 | 0.067 | 1.86 | 4–17 | 0.25–3.0 | 0.40 | 1.3 | 910/50 |
| HTPE ^f /AP/AI | 248–269 | 5909 | 3538 | 0.07 | 1.70 | | 0.4–0.7 | 0.50 | 1.3 | 174/44 (77°F) |
| PBAA/AP/AI | 260–265 | 5700 | 3440 | 0.064 | 1.78 | 14 | 0.25–1.3 | 0.35 | 1.3 | 500/13 |
| AN/Polymer | 180–190 | 2300 | 1.550 | 0.053 | 1.47 | 0 | 0.06–0.5 | 0.60 | 1.3 | 200/5 |
| | | | | | | | | | NA | Cast |

^aAl, aluminum; AN, ammonium nitrate; AP, ammonium perchlorate; CTPB, carboxy-terminated polybutadiene; DB, double-base; HMX, cyclotetramethylene tetrinitramine; HTPB, hydroxyl-terminated polybutadiene; PBA, polybutadiene-acrylic acid polymer; PBAN, polybutadiene-acrylic acid-acrylonitrile terpolymer; PU, polyurethane; PVC, polyvinyl chloride.

^bAt 1000 psia expanding to 14.7 psia, ideal or theoretical value at reference conditions.

^cAt 1000 psia.

^dSee hazard classification section.

^e I_s flame temperature, density, burn rate, and pressure exponent will vary slightly with specific composition.

^fData from Ref. 13–8 and CPIAC, and ATK Launch systems.

A large variety of different *chemical ingredients* and propellant formulations have been synthesized, analyzed, and tested in experimental motors. Later we list many of them. Perhaps only 12 basic types of propellant are in common use today. Other types are still being investigated. Table 13-2 evaluates some of the advantages and disadvantages of several selected propellant classes. A typical propellant has between 4 and 12 different ingredients. Representative formulations for three types of propellant are given in Table 13-3. In actual practice, each manufacturer of a propellant has his own precise formulation and processing procedure. The exact percentages of ingredients, even for a given propellant such as PBAN, not only vary among manufacturers but often vary from motor application to motor application. The practice of adjusting the mass percentage and even adding or deleting one or more of the minor ingredients (additives) is known as *propellant tailoring*. Tailoring is the practice of taking a well-known propellant and changing it slightly to fit a new application, different processing equipment, altered motor ballistics, storage life, temperature limits, or even a change in ingredient source.

New propellant formulations are normally developed using laboratory-size mixers, curing ovens, and related apparatus with the propellant mixers (1 to 5 liters) operated by remote control for safety reasons. Process studies usually accompany the development of the formulation to evaluate the "processibility" of a new propellant and to guide the design of any special production equipment needed in preparing ingredients, mixing, casting, or curing the propellant.

Historically, black powder (a pressed mixture of potassium nitrate, sulfur, and an organic fuel such as ground peach stones) was the first to be used. Other types of ingredients and propellants have been used in experimental motors, including fluorine compounds, propellants containing powdered beryllium, boron, hydrides of boron, lithium, or beryllium, or new synthetic organic plasticizer and binder materials with azide or nitrate groups. Most have not yet been considered satisfactory or practical for production in rocket motors.

13.2. PROPELLANT CHARACTERISTICS

The propellant selection is critical to rocket motor design. The *desirable propellant characteristics* are listed below and are discussed again in other parts of this book. The requirements for any particular motor will influence the priorities of these characteristics:

1. High performance or *high specific impulse*; this really means high gas temperature and/or low gas molecular mass.
2. Predictable, reproducible, and initially adjustable *burning rate* to fit the need of the grain design and the thrust-time requirement.
3. For minimum variation in thrust or chamber pressure, the *pressure or burning rate exponent* and the *temperature coefficient* should be small.

TABLE 13–2. Characteristics of Selected Propellants

| Propellant Type | Advantages | Disadvantages |
|---|--|---|
| Double base (extruded) | Modest cost; nontoxic clean exhaust, smokeless; good burn rate control; wide range of burn rates; simple well-known process; good mechanical properties; low-temperature coefficient; very low pressure exponent; plateau burning is possible | Freestanding grain requires structural support; low performance, low density; high to intermediate hazard in manufacture; can have storage problems with NG bleeding out; diameter limited by available extrusion presses; class 1.1 ^a |
| Double base (castable) | Wide range of burn rates; nontoxic smokeless exhaust; relatively safe to handle; simple, well-known process; modest cost; good mechanical properties; good burn rate control; low-temperature coefficient; plateau burning can be achieved | NG may bleed out or migrate; high to intermediate manufacture hazard; low performance; low density; higher cost than extruded DB; class 1.1 ^a |
| Composite modified double base or CMDB with some AP and Al | Higher performance; good mechanical properties; high density (SG 1.83–1.86); less likely to have combustion stability problems; intermediate cost; good background experience | Storage stability can be marginal; complex facilities; some smoke in exhaust; high flame temperature; moisture sensitive; moderately toxic exhaust; hazards in manufacture; modest ambient temperature range; the value of n is high (0.8–0.9); moderately high temperature coefficient |
| Composite AP, Al, and PBAN or PU or CTPB binder | Reliable; high density; long experience background; modest cost; good aging; long cure time; good performance; usually stable combustion; low to medium cost; wide temperature range; high density; low to moderate temperature sensitivity; good burn rate control; usually good physical properties; class 1.3 | Modest ambient temperature range; high viscosity limits at maximum solid loading; high flame temperature; toxic, smoky exhaust; some are moisture sensitive; some burn-rate modifiers (e.g., aziridines) are carcinogens |
| Composite AP, Al, and HTPB binder; most common composite propellant | Slightly better solids loading % and performance than PBAN or CTPB; widest ambient temperature limits; good burn-rate control; usually stable combustion; medium cost; good storage stability; widest range of burn rates; good physical properties; good experience; class 1.3 | Complex facilities; moisture sensitive; fairly high flame temperature; toxic, smoky exhaust |

(Continued)

TABLE 13–2. (*Continued*)

| Propellant Type | Advantages | Disadvantages |
|---|--|---|
| Modified composite AP, Al, PB binder plus some HMX or RDX | Higher performance; good burn-rate control; usually stable combustion; high density; moderate temperature sensitivity; can have good mechanical properties | Expensive, complex facilities; hazardous processing; harder-to-control burn rate; high flame temperature; toxic, smoky exhaust; can be impact sensitive; can be class 1.1 ^a , high cost; pressure exponent 0.5–0.7 |
| Composite with energetic binder and plasticizer such as NG, AP, HMX | Highest performance; high density (SG 1.8–1.86); narrow range of burn rates | Expensive; limited experience; impact sensitive; high-pressure exponent |
| Modified double-base with HMX | Higher performance; high density (SG 1.78–1.88); stable combustion; narrow range of burn rates | Same as CMDB above; limited experience; most are class 1.1 ^a ; high cost |
| Modified AN propellant with HMX or RDX added | Fair performance; relatively clean; smokeless; nontoxic exhaust | Relatively little experience; can be hazardous to manufacture; need to stabilize AN to limit grain growth; low burn rates; impact sensitive; medium density; class 1.1 or 1.3 ^a |
| Ammonium nitrate plus polymer binder (gas generator) | Clean exhaust; little smoke; essentially nontoxic exhaust; low-temperature gas; usually stable combustion; modest cost; low-pressure exponent | Low performance; low density; need to stabilize AN to limit grain growth and avoid phase transformations; moisture sensitive; low burn rates |
| RDX/HMX with polymer | Low smoke; nontoxic exhaust; lower combustion temperature | Low performance; low density; class 1.1 ^a |

^aClass 1.1 and 1.3—see section on Hazard Classification.

4. Adequate *physical properties* (including bond strength) over the intended operating temperature range.
5. High *density* (allows a small-volume motor).
6. Predictable, reproducible ignition qualities (such as reasonable ignition overpressure).
7. Desirable *aging characteristics* and *long life*. Aging and life predictions depend on the propellant's chemical and physical properties, the cumulative damage criteria with load cycling and thermal cycling (see section 12.4), and actual tests on propellant samples and test data from failed motors.
8. Low absorption of *moisture*, which often causes chemical deterioration.
9. Simple, reproducible, safe, low-cost, controllable, and low-hazard *manufacturing*.
10. Guaranteed availability of all *raw materials* and *purchased components* over the production and operating life of the propellant, and acceptable control over undesirable impurities.

TABLE 13–3. Representative Propellant Formulations

| Double Base (JPN Propellant) | Composite (PBAN Propellant) | Composite Double Base (CMDB Propellant) | | | |
|------------------------------------|-----------------------------------|---|--------|----------------------|--------|
| Ingredient | Mass % | Ingredient | Mass % | Ingredient | Mass % |
| Nitrocellulose | 51.5 | Ammonium perchlorate | 70.0 | Ammonium perchlorate | 20.4 |
| Nitroglycerine | 43.0 | Aluminum powder | 16.0 | Aluminum powder | 21.1 |
| Diethyl phthalate | 3.2 | Polybutadiene–acrylic acid–acrylonitrile | 11.78 | Nitrocellulose | 21.9 |
| Ethyl centralite | 1.0 | Epoxy curative | 2.22 | Nitroglycerine | 29.0 |
| Potassium sulfate | 1.2 | | | Triacetin | 5.1 |
| Carbon black | < 1% | | | Stabilizers | 2.5 |
| Candelilla wax | < 1% | | | | |

Source: Courtesy of Air Force Phillips Laboratory, Edwards, California.

11. *Low technical risk*, such as a favorable history of prior applications.
12. Relative *insensitivity* to certain energy stimuli described in the next section.
13. *Nontoxic* and *noncorrosive exhaust gases*, also called *green exhaust*.
14. Not prone to *combustion instability* (see next chapter).
15. Same composition, performance and properties with every new propellant batch.
16. No slow or long-term chemical reaction or migration between propellant ingredients or between propellant and insulator.

Some of these desirable characteristics will apply also to all materials and purchased components used in solid motors, such as the igniter, insulator, case, or safe and arm device. Several of these characteristics are sometimes in conflict with each other. For example, increasing the physical strength (more binder and/or more crosslinker) will reduce the performance and density. So a modification of the propellant for one of these characteristics can often cause changes in several of the others.

Several illustrations will now be given on how the characteristics of a propellant change when the concentration of one of its major ingredients is changed. For composite propellants using a polymer binder [hydroxyl-terminated polybutadiene (HTPB)] and various crystalline oxidizers, Fig. 13–3 shows the calculated variation in combustion or flame temperature, average product gas molecular weight, and specific impulse as a function of oxidizer concentration; this is calculated data taken from Ref. 13–2, based on a thermochemical analysis as explained in Chapter 5. The maximum values of I_s and T_f occur at approximately the same concentration of oxidizer. In practice the optimum percentage for AP (about 90

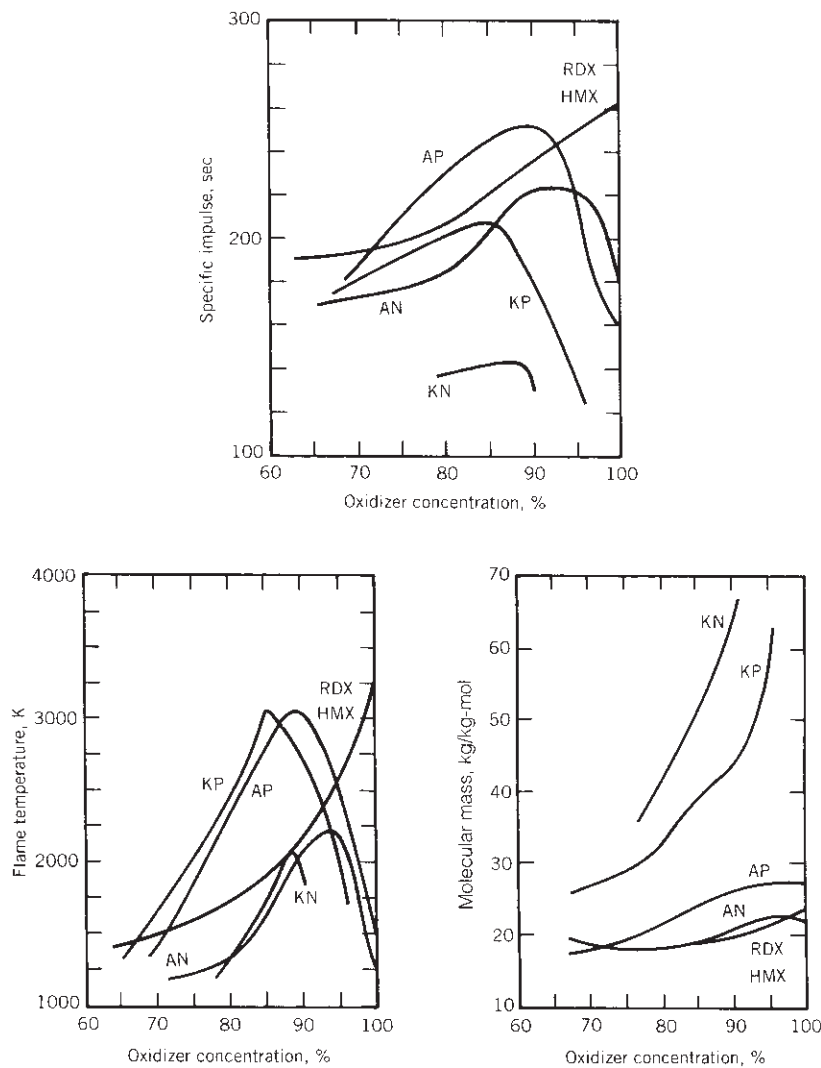


FIGURE 13-3. Variation of combustion temperature, average molecular mass of the combustion gases, and theoretical specific impulse (at frozen equilibrium) as a function of oxidizer concentration for HTPB-based composite propellants. Data are for a chamber pressure of 68 atm and nozzle exit pressure of 1.0 atm. (Reproduced from Ref. 13-2 with permission of the AIAA.)

to 93%) and AN (about 93%) cannot be achieved because concentrations greater than about 90% total solids (including the aluminum and solid catalysts) cannot be processed in a mixer. A castable slurry that will flow into a mold requires 10 to 15% liquid content.

A typical composition diagram for a composite propellant is shown in Fig. 13–4. It shows how the specific impulse varies with changes in the composition of the three principal ingredients: the solid AP, solid Al, and viscoelastic polymer binder.

For DB propellant the variations of I_s and T_1 are shown in Figs. 13–1 and 13–5 as a function of the NG or plasticizer percentage. The theoretical maximum specific impulse occurs at about 80% NG. In practice, nitroglycerine, which is a liquid, is seldom found in concentrations over 60% because the physical properties are poor if NG is high. Other major solid or soluble ingredients are needed to make a usable DB propellant.

For CMDB propellant the addition of either AP or a reactive nitramine such as RDX allows a higher I_s than ordinary DB (where AP or RDX percent is zero), as shown in Fig. 13–6. Both AP and RDX greatly increase the flame temperature and make heat transfer more critical. The maximum values of I_s occur at about 50% AP and at 100% RDX (which is an impractical propellant that cannot be manufactured and will not have reasonable physical properties). At high concentrations of AP or RDX the exhaust gases contain considerable H₂O and O₂ (as shown in Fig. 13–7); these enhance the erosion rate of carbon-containing insulators or nozzle materials. The toxic HCl is present in concentrations between 10 and 20%, but for practical propellants it seldom exceeds 14%.

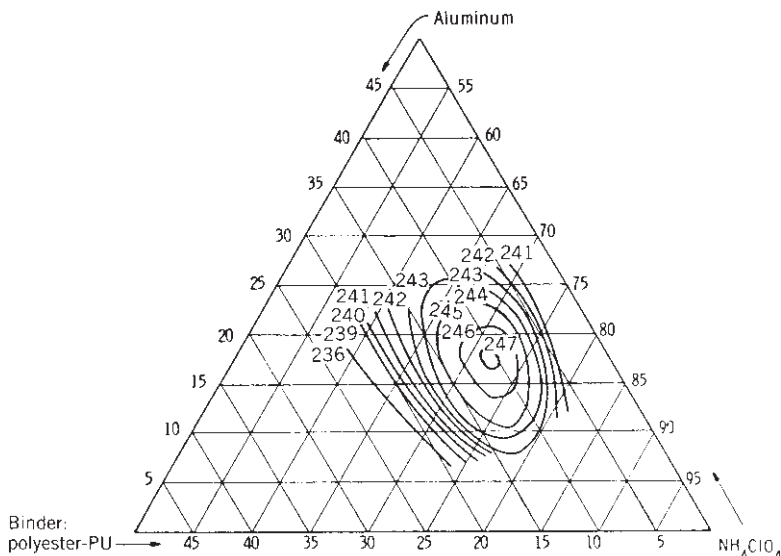


FIGURE 13–4. Composition diagram of calculated specific impulse for an ammonium perchlorate–aluminum–polyurethane propellant (PU is a polyester binder) at standard conditions (1000 psi and expansion to 14.7 psi). The maximum value of specific impulse occurs at about 11% PU, 72% AP, and 17% Al. (Reproduced from Ref. 13–3 with permission of the American Chemical Society.)

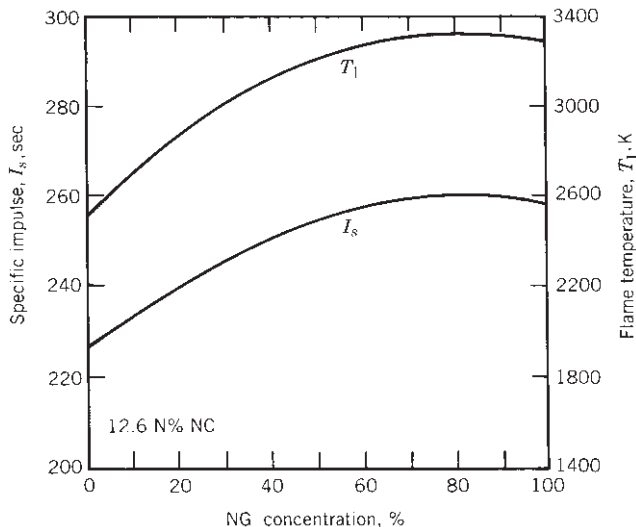


FIGURE 13-5. Specific impulse and flame temperature versus nitroglycerine (NG) concentration of double-base propellants. (Reproduced from Ref. 13-2 with permission of the AIAA.)

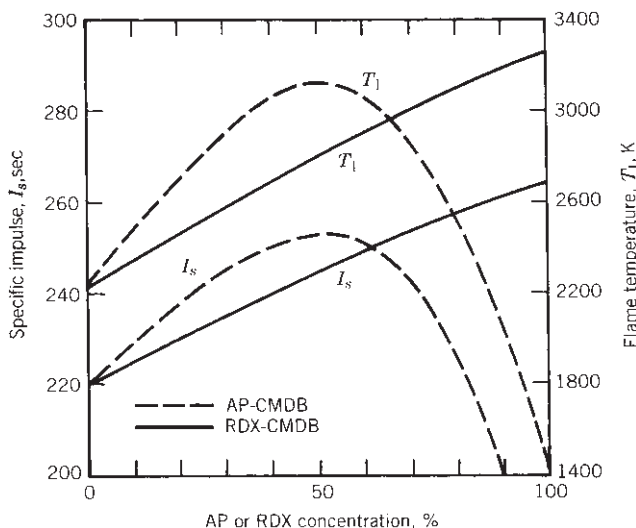


FIGURE 13-6. Specific impulse and flame temperature versus AP or RDX concentration of AP-CMDB propellants. (Reproduced from Ref. 13-2 with permission of the AIAA.)

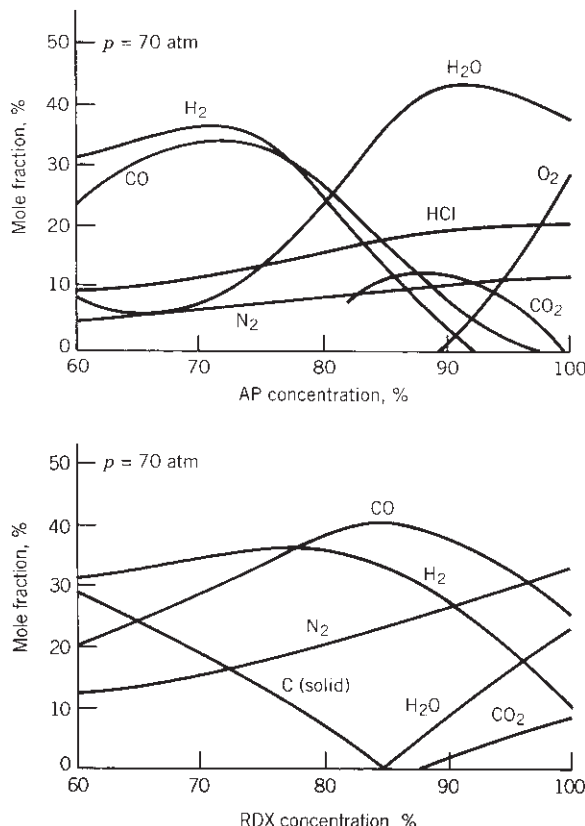


FIGURE 13–7. Calculated combustion products of composite propellant with varying amounts of AP or RDX. (Adapted from Chapter 1 of Ref. 13–2 with permission of the AIAA.)

Nitramines such as RDX or HMX contain relatively few oxidizing radicals, and the binder surrounding the nitramine crystals cannot be fully oxidized. The binder is decomposed at the combustion temperature, forms gases rich in hydrogen and carbon monoxide (which reduces the molecular mass), and cools the gases to a lower combustion temperature. The exhaust gases of AP-based and RDX-based CMDB propellant are shown in Fig. 13–7. The solid carbon particles seem to disappear if the RDX content is high.

13.3. HAZARDS

With proper precautions and equipment, all common propellants can be manufactured, handled, and fired safely. It is necessary to fully understand the hazards and the methods for preventing hazardous situations from arising. Each material

has its own set of hazards; some of the more common ones are described briefly below and also in Refs. 13–4 and 13–5. Not all apply to each propellant.

Inadvertent Ignition

If a rocket motor is ignited and starts combustion when it is not expected to do so, the consequences can include very hot gases, local fires, or ignition of adjacent rocket motors. Unless the motor is constrained or fastened down, its thrust will suddenly accelerate it to unanticipated high velocities or erratic flight paths that can cause damage. Its exhaust cloud can be toxic and corrosive. Inadvertent ignition can be caused by these effects:

Stray or induced currents activate the igniter.

Electrostatic charging causes a spark or arc discharge.

Fires can cause excessive heating of motor exterior, which can raise the propellant temperature above the ignition point.

Impact (bullet penetration or dropping the motor onto a hard surface).

Energy absorption from prolonged mechanical vibration can cause the propellant to overheat.

Radiation from a nuclear explosion.

An electromechanical system is usually provided that prevents stray currents from activating the igniter; it is called *safe and arm system*. It prevents ignition induced by currents in other wires of the vehicle, radar- or radio-frequency-induced currents, electromagnetic surges, or pulses from a nuclear bomb explosion. It prevents electric currents from reaching the igniter circuit during its “unarmed” condition. When put into the “arm” position, it is ready to accept and transmit the start signal to the igniter.

Electrostatic discharges (ESD) can be caused by lightning, friction of insulating materials, or the moving separation of two insulators. The buildup of a high electrostatic potential of thousands of volts can, upon discharge, allow a rapid increase in electric current, which in turn can lead to arcing or exothermic reactions along the current’s path. For this reason all propellants, liners, or insulators should have sufficient electric conductivity to prevent the buildup of an electrostatic charge. The inadvertent ignition of a Pershing ground-to-ground missile is believed to have been caused by an electrostatic discharge while in the transporter-erector vehicle. ESD is a function of the materials, their surface and volume resistivities, dielectric constants, and the breakdown voltages.

Viscoelastic propellants are excellent absorbers of *vibration* energy and can become locally hot when oscillated for extensive periods at particular frequencies. This can happen in designs where a segment of the grain is not well supported and is free to vibrate at natural frequencies. A propellant can also be accidentally ignited by various other energy inputs, such as mechanical friction or bullet impact, or accidentally dropping a motor. Standard tests have been developed to

measure the propellant's resistance to these energy inputs. Considerable effort has been spent in developing new propellants which resist these energy inputs.

Aging and Useful Life

This topic was discussed briefly in the section on Structural Design in the previous chapter. The *aging* of a propellant can be measured with test motors and propellant sample tests if the loading during the life of the motor can be correctly anticipated. It is then possible to estimate and predict the useful *shelf or storage life* of a rocket motor (see Refs. 13–5 and 13–6). When a reduction in physical properties, caused by estimated thermal or mechanical load cycles (cumulative damage), has reduced the safety margin on the stresses and/or strains to a danger point, the motor is no longer considered to be safe to ignite and operate. Once this age limit or its predicted, weakened condition is reached, the motor has a high probability of failure. It needs to be pulled from the ready inventory, and the old aged propellant needs to be removed and replaced.

The *life* of a particular motor depends on the particular propellants, the frequency and magnitude of imposed loads or strains, the design, and other factors. Typical life values range from 5 to 25 years. Shelf life can usually be increased by increasing the physical strength of the propellants (e.g., by increasing the amount of binder), selecting chemically compatible, stable ingredients with minimal long-term degradation, or by minimizing the vibration loads, temperature limits, or number of cycles (controlled storage and transport environment).

Case Overpressure and Failure

The motor case will break or explode if the chamber pressure exceeds the case's burst pressure. The release of high-pressure gas energy can cause an explosion; motor pieces could be thrown out into the adjacent area. The sudden depressurization from chamber pressure to ambient pressure, which is usually below the deflagration limit, would normally cause a class 1.3 propellant to stop burning. Large pieces of unburned propellant can often be found after a violent case burst. This type of motor failure can be caused by one of the following:

1. The grain is overaged, porous, or severely cracked and/or has major unbonded areas due to severe accumulated damage.
2. There has been a significant chemical change in the propellant due to migration or slow, low-order chemical reactions. This can reduce the allowable physical properties, weakening the grain, so that it will crack or cause unfavorable increases in the burning rate. In some cases chemical reactions create gaseous products which create many small voids and raise the pressure in sealed stored motors.
3. The motor has not properly been manufactured. Obviously, careful fabrication and inspection are necessary.

4. The motor has been damaged. For example, a nick or dent in the case caused by improper handling will reduce the case strength. This can be prevented by careful handling and repeated inspections.
5. All obstruction plugs the nozzle (e.g., a loose large piece of insulation) and causes a rapid increase in chamber pressure.
6. Moisture absorption can degrade the strength and strain capabilities by a factor of 3 to 10 in propellants that contain hygroscopic ingredients. Motors are usually sealed to prevent humid air access.

Detonation versus Deflagration. When burning rocket motor propellant is overpressurized, it can either deflagrate (or burn) or detonate (explode violently), as described in Table 13–4. In a detonation the chemical reaction energy of the whole grain can be released in a very short time (microseconds), and in effect it becomes an exploding bomb. This detonation condition can happen with some propellants and some ingredients (e.g., nitroglycerine or HMX), which

TABLE 13–4. Comparison of Burning and Detonation

| Characteristic | Burning | | |
|---|--|---|---|
| | With Air | Within Rocket Motors | Explosive Detonation |
| Typical material | Coal dust and air | Propellant, no air | Rocket propellant or explosives |
| Common means of initiating reaction | Heat | Heat | Shock wave; sudden pressure rise plus heat |
| Linear reaction rate (m/sec) | 10^{-6} (subsonic) | 0.2 to 5×10^{-2} (subsonic) | 2 to 9×10^3 (supersonic) |
| Produces shock waves | No | No | Yes |
| Time for completing reaction (sec) | 10^{-1} | $10^{-2} - 10^{-3}$ | 10^{-6} |
| Maximum pressure [MPa (psi)] | 0.07–0.14 (10–20) | 0.7–100 (100–14,500) | $7000 - 70,000$ ($10^6 - 10^7$) |
| Process limitation | By vaporization and heat transfer at burning surface | | By physical and chemical properties of material, (e.g., density, composition) |
| Increase in burning rate can result in: | Potential furnace failure | Overpressure and sudden failure of pressure container | Detonation and violent rapid explosion of all the propellant |

are described later in this chapter). Detonations can be minimized or totally avoided by proper design, correct manufacture, and safe handling and operating procedures.

The same material may either burn or detonate depending on the chemical formulation, the type and intensity of the initiation, the degree of confinement, the physical propellant properties (such as density or porosity), and the geometric characteristics of the motor. It is possible for certain propellants to change suddenly from an orderly deflagration to a detonation. A simplified explanation of this transition starts with normal burning at rated chamber pressure; the hot gas then penetrates pores or small cracks in the unburned propellant, where the local confinement can cause the pressure to become very high locally, the combustion front speeds up to shock wave speed with a low-pressure differential, and it then accelerates further to a strong, fast, high-pressure shock wave, characteristic of detonations. The degree and rigidity of the geometric confinement and a scale factor (e.g., larger-diameter grain) influence the severity and occurrence of detonations.

Hazard Classification. Propellants that can experience a transition from deflagration to detonation are considered more hazardous and are usually designated as class 1.1-type propellants. Most propellants will burn, the case may burst if chamber pressure becomes too high, but the propellant will not detonate and are class 1.3 propellants. The required tests and rules for determining this hazard category are explained in Ref. 13–7. Propellant samples are subjected to various tests, including impact tests (dropped weight) and card gap tests (which determine the force needed to initiate a propellant detonation when a sample is subjected to a blast from a known booster explosive). If the case should burst violently with a class 1.3 propellant, much of the remaining unburnt propellant would be thrown out, but would then usually stop burning. With a class 1.1 propellant, a powerful detonation can sometimes ensue, which rapidly gasifies all the remaining propellant, and is much more powerful and destructive than the bursting of the case under high pressure. Unfortunately, the term “explosion” has been used to describe both a bursting of a case with its fragmentation of the motor and also the higher rate of energy release of a detonation, which leads to a very rapid and more energetic fragmentation of the motor.

The Department of Defense (DOD) classification of 1.1 or 1.3 determines the method of labeling and the cost of shipping rocket propellants, loaded military missiles, explosives, or ammunition; it also determines the required limits on the amount of that propellant stored or manufactured in any one site and the minimum separation distance of that site to the next building or site. The DOD system (Ref. 13–7) is the same as that used by the United Nations.

Insensitive Munitions

In military operations an accidental ignition and unplanned operation or an explosion of a rocket missile can cause severe damage to equipment and injure or kill

personnel. This has to be avoided or minimized by making the motor designs and propellants insensitive to a variety of energy stimuli. The worst scenario is a detonation of the propellant, releasing the explosive energy of all of the propellant mass, and this scenario is to be avoided. The missiles and its motors must undergo a series of prescribed tests to determine their resistance to inadvertent ignition with the most likely energy inputs during a possible battle situation. Table 13–5 describes a series of tests called out in a military specification, which are detailed in Refs. 13–8 and 13–9. A *threat hazard assessment* must be made prior to the tests, to evaluate the logistic and operational threats during the missile's life cycle. This may result in modifications to the test setups, changes in the passing criteria, or the skipping of some of these tests.

The missiles, together with their motors, are destroyed in these tests. If the motor should detonate (an unacceptable result), the motor has to be redesigned and/or have a change in propellant. There are some newer propellants that are more resistant to these stimuli and are therefore preferred for tactical missile applications, even though there is usually a penalty in propulsion performance. If explosions (not detonations) occur, it may be possible to redesign the motor and mitigate the effects of the explosion (make it less violent). For example, the case can have a provision to vent itself prior to an explosion. Changes to the shipping container can also mitigate some of these effects. If the result is a fire (an acceptable result), it should be confined to the particular grain or motor. Under some circumstances a burst failure of the case is acceptable. A new class of insensitive propellants has been developed with new types of binders in the past decade. Their purpose remains to minimize any drastic consequences (such as detonation) when the motor is exposed to various unexpected energetic stimuli, such as

TABLE 13–5. Testing for Insensitivity of Rockets and Missiles

| Test | Description | Criteria for Passing |
|--------------------------------|---|---|
| Fast cook off | Build a fire (of jet fuel or wood) underneath the missile or its motor | No reaction more severe than burning propellant |
| Slow cook off | Gradual heating ($6^{\circ}\text{F}/\text{hr}$) to failure | Same as above |
| Bullet impact | One to three 50-caliber bullets fired at short intervals | Same as above |
| Fragment impact | Small high-speed steel fragment | Same as above |
| Sympathetic detonation | Detonation from an adjacent similar motor or a nearby specific munition | No detonation of test motor |
| Shaped explosive charge impact | Blast from specified shaped charge in specified location | No detonation |
| Spall impact | Several high-speed spalled fragments from a steel plate which is subjected to a shaped charge | Fire, but no explosion or detonation |

external fires, and impact or pressure waves (see Table 13–5). Recently, these propellants have been selected for production with military missions, reflecting an important milestone in propellant development. The leading example is a new composite propellant with HTPE (hydroxyl-terminated polyether) as the binder developed by ATK Launch Systems, see Ref. 13–10. HTPE has been qualified and applied to the MK 134 rocket motor for the ship-launched Evolved Sea Sparrow Missile (ESSM). This motor is co-manufactured by ATK in the United States and NAMMO Raufoss in Norway for member nations of the NATO Sea Sparrow Consortium. A relatively insensitive propellant has also been developed in France, namely, a nonmigrating ferrocene-grafted HTPB binder called Butacene. It has been qualified for a few systems in the United States and other countries; see Ref. 13–10.

Upper Pressure Limit

If the pressure-rise rate and the absolute pressure become sufficiently high (as in some impact tests or in the high acceleration of a gun barrel), some propellants will detonate. For many propellants these pressures are above approximately 1500 MPa or 225,000 psi, but for others they are lower (as low as 300 MPa or 45,000 psi). These values represent an *upper pressure limit* beyond which a propellant should not operate.

Toxicity

A large share of all rockets do not have a significant toxicity problem. A number of propellant ingredients (e.g., some crosslinking agents and burning rate catalysts) and a few of the plastics used in fiber-reinforced cases can be dermatological or respiratory toxins; a few are carcinogens (cancer-causing agents) or suspected carcinogens. They, and the mixed uncured propellant containing these materials, have to be handled carefully to prevent operator exposure. This means using gloves, face shields, good ventilation, and, with some high-vapor-pressure ingredients, gas masks. The finished or cured grain or motor is usually not toxic.

The exhaust plume gases can be very toxic if they contain beryllium or beryllium oxide particles, chlorine gas, hydrochloric acid gas, hydrofluoric acid gas, or some other fluorine compounds. When an ammonium perchlorate oxidizer is used, the exhaust gas can contain up to about 14% hydrochloric acid which is a toxic gas. For large rocket motors this can be many tons of highly toxic gas. Test and launch facilities for rockets with toxic plumes require special precautions and occasionally decontamination processes, as explained in Chapter 21.

Safety Rules

The most effective way to control hazards and prevent accidents is (1) to train personnel in the hazards of each propellant of concern and to teach them how to avoid hazardous conditions, prevent accidents, and how to recover from an

accident; (2) to design the motors, facilities, and the equipment to be safe; and (3) to institute and enforce rigid safety rules during design, manufacture, and operation. There are many such rules. Examples are no smoking and no matches in areas where there are propellants or loaded motors, wearing spark-proof shoes and using spark-proof tools, shielding all electrical equipment, providing a water-deluge fire extinguishing system in test facilities to cool motors or extinguish burning, or proper grounding of all electrical equipment and items that could build up static electrical charges.

13.4. PROPELLANT INGREDIENTS

A number of relatively common propellant ingredients are listed in Table 13–6 for double-base propellants and in Table 13–7 for composite-type solid propellants. They are categorized by major *function*, such as *oxidizer*, *fuel*, *binder*, *plasticizer*, *curing agent*, and so on, and each category is described in this section. However, several of the ingredients have more than one function. These lists are not complete and at least 200 other ingredients have been tried in experimental rocket motors.

A classification of modern propellants, including some new types that are still in the experimental phase, is given in Table 13–8, according to their binders, plasticizers, and solid ingredients; these solids may be an oxidizer, a solid fuel, or a combination or compound of both.

The ingredient properties and impurities can have a profound effect on the propellant characteristics. A seemingly minor change in one ingredient can cause measurable changes in ballistic properties, physical properties, migration, aging, or ease of manufacture. When the propellant's performance or ballistic characteristics have tight tolerances, the ingredient purity and properties must also conform to tight tolerances and careful handling (e.g., no exposure to moisture). In the remainder of this section a number of the important ingredients, grouped by function, are briefly discussed.

Inorganic Oxidizers

Some of the thermochemical properties of several oxidizers and oxygen radical-containing compounds are listed in Table 13–9. Their values depend on the chemical nature of each ingredient.

Ammonium perchlorate (NH_4ClO_4) is the most widely used crystalline oxidizer in solid propellants. Because of its good characteristics, including compatibility with other propellant materials, good performance, quality, uniformity, and availability, it dominates the solid oxidizer field. Other solid oxidizers, particularly ammonium nitrate and potassium perchlorate, were used and occasionally are still being used in production rockets but to a large extent have been replaced by more modern propellants containing ammonium perchlorate. Many oxidizer compounds were investigated during the 1970s, but none reached production status.

TABLE 13–6. Typical Ingredients of Double-Base (DB) Propellants and Composite-Modified Double-Base (CMDB) Propellants

| Type | Percent | Acronym | Typical Chemicals |
|--|---------|--|--|
| Binder | 30–50 | NC | Nitrocellulose (solid), usually plasticized with 20–50% nitroglycerine |
| Reactive plasticizer (liquid explosive) | 20–50 | { NG DEGDN TEGDN PDN TMETN | Nitroglycerine Diethylene glycol dinitrate Triethylene glycol dinitrate Propanedial-dinitrate Trimethylolethane trinitrate |
| Plasticizer (organic liquid fuel) | 0–10 | { DEP TA DMP EC DBP | Diethyl phthalate Triacetin Dimethyl phthalate Diocetyl phthalate Ethyl centralite Dibutyl phthalate |
| Burn rate modier | Up to 3 | { PbSa PbSt CuSa CuSt | Lead salicylate Lead stearate Copper salicylate Copper stearate |
| Coolant | | OXM | Oxamide |
| Opacier | | C | Carbon black (powder or graphite powder) |
| Stabilizer and/or antioxidant | > 1 | { DED EC DPA | Diethyl diphenyl Ethyl centralite Diphenyl amine |
| Visible flame Suppressant | Up to 2 | { KNO ₃ K ₂ SO ₄ | Potassium nitrate Potassium sulfate |
| Lubricant (for extruded propellant only) | > 0.3 | C | Graphite Wax |
| Metal fuel ^a | 0–15 | Al | Aluminum, fine powder (solid) |
| Crystalline oxidizer ^a | 0–15 | { AP AN | Ammonium perchlorate Ammonium nitrate |
| Solid explosive crystals ^a | 0–20 | { HMX RDX NQ | Cyclotetramethylenetrinitramine Cyclotrimethylenetrinitramine Nitroguaudine |

^aSeveral of these, but not all, are added to CMDB propellant.

The oxidizing potential of the perchlorates is generally high, which makes this material suited to high specific impulse propellants. Both ammonium and potassium perchlorate are only slightly soluble in water, a favorable trait for propellant use. All the perchlorate oxidizers produce hydrogen chloride (HCl) and other toxic and corrosive chlorine compounds in their reaction with fuels. Care is required in firing rockets, particularly the very large rockets, to safeguard

TABLE 13–7. Typical Ingredients of Composite Solid Propellants

| Type | Percent | Acronym | Typical Chemicals |
|---|---------|---|--|
| Oxidizer (crystalline) | 0–70 | { AP AN KP KN ADN | Ammonium perchlorate Ammonium nitrate Potassium perchlorate Potassium nitrate Ammonium dinitramine |
| Metal fuel (also acts as a combustion stabilizer) | 0–30 | { Al Be Zr | Aluminum Beryllium (experimental propellant only) Zirconium (also acts as burn rate modier) |
| Fuel/binder, polybutadiene type | 5–18 | { HTPB CTPB PBAN PBAA | Hydroxyl-terminated polybutadiene Carboxyl-terminated polybutadiene Polybutadiene acrylonitrile acrylic acid Polybutadiene acrylic acid |
| Fuel/binder, polyether and polyester type | 0–15 | { PEG PCP PGA PPG HTPE PU | Polyethylene glycol Polycaprolactone polyol Polyglycol adipate Polypropylene glycol Hydroxyl-terminated polyether Polyurethane polyester or polyether |
| Curing agent or crosslinker, which reacts with polymer binder | 0.2–3.5 | { MAPO IPDI TDI HMDI DDI TMP BITA | Methyl aziridinyl phosphine oxide Isophorone diisocyanate Toluene-2,4-diisocyanate Hexamethylene diisocyanide Dimethyl diisocyanate Trimethylol propane Trimesoyl-1(2-ethyl)-aziridine |
| Burn rate modier | 0.2–3 | { FeO nBF | Ferric oxide <i>n</i> -Butyl ferrocene Oxides of Cu, Pb, Zr, Fe Alkaline earth carbonates Alkaline earth sulfates Metallo-organic compounds |
| Explosive filler (solid) | 0–40 | { HMX RDX NQ | Cyclotetramethylenetrinitramine Cyclotrimethylenetrinitramine Nitroguaudine |
| Plasticizer/pot life control (organic liquid) | 0–7 | { DOP DOA DOS DMP IDP | Diethyl phthalate Diethyl adipate Diethyl sebacate Dimethyl phthalate Isodecyl pelargonate |
| Energetic plasticizer (liquid) | 0–14 | { GAP NG DEGDN BTTN TEGDN TMETN PCP | Glycidyl azide polymer Nitroglycerine Diethylene glycol dinitrate Butanetriol trinitrate Triethylene glycol dinitrate Trimethylolethane trinitrate Polycaprolactone polymer |

TABLE 13–7. (Continued)

| Type | Percent | Acronym | Typical Chemicals |
|---|---------|--|--|
| Energetic fuel/binder | 0–15 | GAP PGN BAMO/ AMMO BAMO/ NMMO | Glycidyl azide polymer Propylglycidyl nitrate Bis-azidomethyloxetane/Azidomethyl-methyloxetane copolymer Bis-azidomethyloxetane/Nitramethyl-methyloxetane copolymer |
| Bonding agent (improves bond to solid particles) | > 0.1 | MT-4 HX-752 | MAPO–tartaric acid–adipic acid condensate Bis-isophthal-methyl-aziridine |
| Stabilizer (reduces chemical deterioration) | > 0.5 | DPA — NMA — | Diphenylamine Phenylnaphthylamine <i>N</i> -methyl- <i>p</i> -nitroaniline Dinitrodiphenylanine |
| Processing aid | > 0.5 | — — | Lecithin Sodium lauryl sulfate |

operating personnel or communities in the path of exhaust gas clouds. Ammonium perchlorate (AP) is supplied in the form of small white crystals. Particle size and shape influences the manufacturing process and the propellant burning rate. Therefore, close control of the crystal sizes and the size distribution present in a given quantity or batch is required. AP crystals are rounded (nearly ball shaped) to allow easier mixing than sharp, fractured crystals. They come in sizes ranging from about 600 µm ($1\text{ }\mu\text{m} = 10^{-6}\text{ m}$) diameter to about 80 µm from the factory. Sizes below about 40 µm diameter are considered hazardous (can easily be ignited and sometimes detonated) and are not shipped; instead, the propellant manufacturer takes larger crystals and grinds them (at the motor factory) to the smaller sizes (down to 2 µm) just before they are incorporated into a propellant.

The *inorganic nitrates* are relatively low-performance oxidizers compared with perchlorates. However, *ammonium nitrate* is used in some applications because of its very low cost and smokeless and relatively nontoxic exhaust. Its principal use is with low-burning-rate, low-performance rocket and gas generator applications. Ammonium nitrate (AN) changes its crystal structure at several phase transformation temperatures. These changes cause slight changes in volume. One phase transformation at 32°C causes about a 3.4% change in volume. Repeated temperature cycling through this transition temperature creates tiny voids in the propellant, and causes growth in the grain and a change in physical or ballistic properties. The addition of a small amount of stabilizer such as nickel oxide (NiO) or potassium nitrate (KNO₃) seems to change the transition temperature to above 60°C, a high enough value so that normal ambient temperature cycling will no longer cause recrystallization (Refs. 13–11 and 13–12). AN with such an additive is known as *phase-stabilized ammonium nitrate* (PSAN). AN is hygroscopic, and the absorption of moisture will degrade propellant made with AN.

TABLE 13–8. Classification of Solid Rocket Propellants Used in Flying Vehicles According to Their Binders, Plasticizers, and Solid Ingredients

| Designation | Binder | Plasticizer | Solid Oxidizer and/or Fuel | Propellant Application |
|--------------------------------------|---|---|--|--|
| Double base, DB CMDB ^a | Plasticized NC | NG, TA, etc. | None | Minimum signature and smoke |
| | Plasticized NC | NG, TMETN, TA, BTTN, etc. | Al, AP, KP | Booster, sustainer, and spacecraft |
| EMCDB ^a | Same | Same | HMX, RDX, AP | Reduced smoke |
| | Same | Same | HMX, RDX, azides | Minimum signature, gas generator |
| Polybutadiene | Plasticized NC + elastomeric polymer | Same | Like CMDB above, but generally superior mechanical properties with elastomer added as binder | |
| | HTPB | DOA, IDP, DOP, DOA, etc. | Al, AP, KP, sometimes also HMX, RDX | Booster, sustainer, or spacecraft; used extensively in many applications |
| TPE ^a | HTPB | DOA, IDP, DOP, DOA, etc. | AN, HMX, RDX, some AP | Reduced smoke, gas generator |
| | CTPB, PBAN, PBAA | All like HTPB above, but somewhat lower performance due to higher processing viscosity and consequent lower solids content. Still used in applications with older designs. | | |
| Polyether and polyesters | Thermoplastic elastomer PEG, PPG, PCP, PGA, HTPE, ^b and mixtures | Similar to HTPB, but without chemical curing process. TPEs cure (crosslink) via selective crystallization of certain parts of the binder. Still are experimental propellants. | | |
| | GAP, PGN, BAMO/ NMMO, BAMO/AMMO | DOA, IDP, TMETN, DEGDN, etc. Al, AP, KP, HMX, BiO ₃ | TMETN, BTTN, etc. GAP-azide, GAP-nitrate, NG | Booster, sustainer, or spacecraft |
| Energetic binder (other than NC) | | | Like polyether/polyester propellants above, but with slightly higher performance. Experimental propellant. | |

^aCMDB, composite-modified double-base; EMCDB, elastomer-modified cast double-base; TPE, thermoplastic elastomer. For definition of acronyms and abbreviations of propellant ingredients see Tables 13–6 and 13–7.

^bHTPE, hydroxyl-terminated polyether, binder for propellant developed for Inertial Munitions by ATK Launch Systems.

TABLE 13–9. Comparison of Crystalline Oxidizers

| Oxidizer | Chemical Symbol | Molecular Mass (kg/kg-mol) | Density (kg/m ³) | Oxygen Content (mass%) | Remarks |
|-----------------------|----------------------------------|----------------------------|------------------------------|------------------------|--|
| Ammonium perchlorate | NH ₄ ClO ₄ | 117.49 | 1949 | 54.5 | Low <i>n</i> , low cost, readily available, high performance |
| Potassium perchlorate | KClO ₄ | 138.55 | 2519 | 46.2 | Low burning rate, medium performance |
| Sodium perchlorate | NaClO ₄ | 122.44 | 2018 | 52.3 | Hygroscopic, high performance, bright flame |
| Ammonium nitrate | NH ₄ NO ₃ | 80.0 | 1730 | 60.0 | Smokeless, medium performance, low cost |

Fuels

This section discusses solid fuels of which *powdered spherical aluminum* is the most common. It consists of small spherical particles (5 to 60 µm diameter) and is used in a wide variety of composite and composite-modified double-base propellant formulations, usually constituting 14 to 20% of the propellant by weight. Small aluminum particles can burn in air and this powder is mildly toxic if inhaled. During rocket combustion this fuel is oxidized into aluminum oxide. These oxide particles tend to agglomerate and form larger particles. Aluminum increases the heat of combustion, the propellant density, the combustion temperature, and thus the specific impulse. The oxide is in liquid droplet form during combustion and solidifies in the nozzle as the gas temperature drops. When in the liquid state the oxide can form a molten slag which can accumulate in pockets (e.g., around an improperly designed submerged nozzle), thus adversely affecting the vehicle's mass ratio. It also can deposit on walls inside the combustion chamber, as described in Refs. 13–13 and 13–14.

Boron is a high-energy fuel that is lighter than aluminum and has a high melting point (2304°C). It is difficult to burn with high efficiency in combustion chambers of reasonable length. However, it can be oxidized at reasonable efficiency if the boron particle size is very small. Boron is used advantageously as a propellant in combination rocket-air-burning engines, where there is adequate combustion volume and oxygen from the air.

Beryllium burns much more easily than boron and improves the specific impulse of a solid propellant motor, by about 15 sec, but it and its oxide are highly toxic powders absorbed by animals and humans when inhaled. The technology with composite propellants using powdered beryllium fuel has been experimentally proven, but its severe toxicity makes any application unlikely.

Theoretically, both aluminum hydride (AlH_3) and beryllium hydride (BeH_2) are attractive fuels because of their high heat release and gas-volume contribution. Specific impulse gains are 10 to 15 sec for Al_2H_3 and 25 to 30 sec for BeH_2 . Both are difficult to manufacture and both deteriorate chemically during storage, with loss of hydrogen. These compounds are not used today in practical fuels.

Binders

The binder provides the structural glue or matrix in which solid granular ingredients are held together in a composite propellant. The raw materials are liquid prepolymers or monomers. Polyethers, polyesters, and poly-butadienes have been used (see Tables 13–6 and 13–7). After they are mixed with the solid ingredients, cast and cured, they form a hard rubber-like material that constitutes the grain. Polyvinylchloride (PVC) and polyurethane (PU) (Table 13–1) were used 50 years ago and are still used in a few motors, mostly of old design. Binder materials are also really fuels for solid propellant rockets and are oxidized in the combustion process. The binding ingredient, usually a polymer of one type or another, has a primary effect on motor reliability, mechanical properties, propellant processing complexity, storability, aging, and costs. Some polymers undergo complex chemical reactions, crosslinking, and branch chaining during curing of the propellant. HTPB has been the favorite binder in recent years, because it allows a somewhat higher solids fraction (88 to 90% of AP and Al) and relatively good physical properties at the temperature limits. Several common binders are listed in Tables 13–1, 13–6, and 13–7. Elastomeric binders have been added to plasticized double-base-type nitrocellulose to improve physical properties. Polymerization occurs when the binder monomer and its crosslinking agent react (beginning in the mixing process) to form long-chain and complex three-dimensional polymers. Other types of binders, such as PVC, cure or plasticize without a molecular reaction (see Refs. 13–2, 13–3, and 13–14). Often called plastisol-type binders, they form a very viscous dispersion of a powdered polymerized resin in nonvolatile liquid; they polymerize slowly.

Burning-Rate Modifiers

A burning-rate *catalyst* or burning-rate *modifier* helps to accelerate or decelerate the combustion at the burning surface and increases or decreases the propellant burning rate. It permits the tailoring of the burning rate to fit a specific grain design and thrust-time curve. Several are listed in Tables 13–6 and 13–7. Some, like iron oxide or lead stearate, increase the burning rate; however, others, like lithium fluoride, will reduce the burning rate of some composite propellants. The inorganic catalysts do not contribute to the combustion energy, but consume energy when they are heated to the combustion temperature. These modifiers are effective because they change the combustion mechanism, which is described in Chapter 14 (Chapter 2 of Ref. 13–2 gives examples of modifiers that change the burning rate of composite propellants).

Plasticizers

A plasticizer is usually a relatively low-viscosity liquid organic ingredient which is also a fuel. It is added to improve the elongation of the propellant at low temperatures and to improve processing properties, such as lower viscosity for casting or longer pot life of the mixed but uncured propellants. The plasticizers listed in Tables 13–6, 13–7, and 13–8 show several examples.

Curing Agents or Crosslinkers

A curing agent or crosslinker causes the prepolymers to form longer chains of larger molecular mass and interlocks between chains. Even though these materials are present in small amounts (0.2 to 3%), a minor change in the percentage will have a major effect on the propellant physical properties, manufacturability, and aging. They are used only with composite propellants and are the ingredient that causes the binder to solidify and become hard. Several curing agents are listed in Table 13–7.

Energetic Binders and Plasticizers

Energetic binders and/or plasticizers are used in lieu of the conventional organic materials. They contain oxidizing species (such as azides or organic nitrates) as well as organic species. They add some additional energy to the propellant causing a modest increase in performance. They serve also as a binder to hold other ingredients, or as an energetic plasticizer liquid. They can self-react exothermally and burn without a separate oxidizer. Glycidyl azide polymer (GAP) is an example of an energetic, thermally stable, hydroxyl-terminated prepolymer that can be polymerized. It has been used in experimental propellants. Other energetic binder or plasticizer materials are listed in Tables 13–6, 13–7, and 13–8.

Organic Oxidizers or Explosives

Organic oxidizers are explosive organic compounds with $-\text{NO}_2$ radical or other oxidizing fractions incorporated into the molecular structure. References 13–2 and 13–14 describe their properties, manufacture, and application. These are used with high-energy propellants or smokeless propellants. They can be crystalline solids, such as the *nitramines* HMX or RDX, fibrous solids such as NC, or energetic plasticizer liquids such as DEGN or NG. These materials can react or burn by themselves when initiated with enough activating energy, but all of them can be detonated under certain conditions. Both HMX and RDX are stoichiometrically balanced materials and the addition of either fuel or oxidizer only will reduce the T_1 and I_s values. Therefore, when binder fuels are added to hold the HMX or RDX crystals in a viscoelastic matrix, it is also necessary to add an oxidizer such as AP or AN.

RDX and HMX are quite similar in structure and properties. Both are white crystalline solids that can be made in different sizes. For safety, they are shipped

in a desensitizing liquid, which has to be removed prior to propellant processing. HMX has a higher density, a higher detonation rate, yields more energy per unit volume, and has a higher melting point. NG, NC, HMX, and RDX are also used extensively in military and commercial explosives. HMX or RDX can be included in DB, CMDB, or composite propellants to achieve higher performance or other characteristics. The percentage added can range up to 60% of the propellant. Processing propellant with these or similar ingredients can be hazardous, and the extra safety precautions make the processing more expensive.

Liquid *nitroglycerine* (NG) by itself is very sensitive to shock, impact, or friction. It is an excellent plasticizer for propellants when desensitized by the addition of other liquids (like triacetin or dibutyl phthalate) or by compounding with nitrocellulose. It readily dissolves in many organic solvents, and in turn it acts as a solvent for NC and other solid ingredients (Ref. 13–14).

Nitrocellulose (NC) is a key ingredient in DB and CMDB propellant. It is made by the acid nitration of natural cellulose fibers from wood or cotton and is a mixture of several organic nitrates. Although crystalline, it retains the fiber structure of the original cellulose (see Ref. 13–14). The nitrogen content is important in defining the significant properties of nitrocellulose and can range from 8 to 14%, but the grades used for propellant are usually between 12.2 and 13.1%. Since it is impossible to make NC from natural products with an exact nitrogen content, the required properties are achieved by careful blending. Since the solid fiber-like NC material is difficult to make into a grain, it is usually mixed with NG, DEGN, or other plasticizer to gelatinize or solvate it when used with DB and CMDB propellant.

Additives

Small amounts of *additives* are used for many purposes, including accelerating or lengthening the *curing time*, improving the *rheological properties* (easier casting of viscous raw mixed propellant), improving the *physical properties*, adding *opaqueness* to a transparent propellant to prevent radiation heating at places other than the burning surface, limiting *migration of chemical species* from the propellant to the binder or vice versa, minimizing the slow oxidation or *chemical deterioration* during storage, and improving the *aging* characteristics or the moisture resistance. *Bonding agents* are additives to enhance adhesion between the solid ingredients (AP or Al) and the binder. *Stabilizers* are intended to minimize the slow chemical or physical reactions that can occur in propellants. *Catalysts* are sometimes added to the crosslinker or curing agent to slow down the curing rate. Lubricants aid the extrusion process. Desensitizing agents help to make a propellant more resistant to inadvertent energy stimulus. These are usually added in very small quantities.

Particle-Size Parameters

The size, shape, and size distribution of the solid particles of AP, Al, or HMX in the propellant can have a major influence on the composite propellant characteristics. The particles are spherical in shape because this allows easier mixing

and a higher percentage of solids in the propellant than shapes of sharp-edged natural crystals. Normally, the ground AP oxidizer crystals are graded according to particle size ranges as follows:

| | |
|-----------|--|
| Coarse | 400 to 600 μm ($1 \mu\text{m} = 10^{-6} \text{ m}$) |
| Medium | 50 to 200 μm |
| Fine | 5 to 15 μm |
| Ultrafine | submicrometer to 5 μm |

Coarse and medium-grade AP crystals are handled as class 1.3 materials, whereas the fine and ultrafine grades are considered as class 1.1 high explosives and are usually manufactured on-site from the medium or coarse grades. (See Section 13.3 for a definition of these explosive hazard classifications.) Most propellants use a blend of oxidizer particle sizes, if only to maximize the weight of oxidizer per unit volume of propellant, with the small particles filling part of the voids between the larger particles.

Figure 13–8 shows the influence of varying the ratio of coarse to fine oxidizer particle sizes on propellant burning rate and also the influence of a burning rate additive. Figure 13–9 shows that the influence of particle size of the aluminum fuel on propellant burning rate is much less pronounced than that of oxidizer particle size. Figure 13–8 also shows the effect of particle size. Particle size range and particle shape of both the oxidizer [usually ammonium perchlorate (AP)] and solid fuel (usually aluminum) have a significant effect on the solid packing fraction and the rheological properties (associated with the flowing or pouring of viscous liquids) of uncured composite propellant. By definition, the *packing fraction* is the volume fraction of all solids when packed to minimum volume (a theoretical condition). High packing fraction makes mixing, casting, and handling during propellant fabrication more difficult. Figure 13–10 shows the distribution of AP particle size using a blend of sizes; the shape of this curve can be altered drastically by controlling the size ranges and ratios. Also, the size range and shape of the solid particles affect the *solids loading ratio*, which is the mass ratio of solid to total ingredients in the uncured propellants. Computer-optimized methods exist for adjusting particle-size distributions for improvement of the solids loading. The solids loading can be as high as 90% in some composite propellants. High solids loading, desired for high performance, introduces complexity and higher costs into the processing of propellant. Trade-off among ballistic (performance) requirements, processibility, mechanical strength, rejection rates, and facility costs is a continuing problem with many high-specific-impulse composite propellants. References 13–2 and 13–14 report on the influence of particle size on motor performance.

A *monomodal* propellant has one size of solid oxidizer particles, a *bimodal* has two sizes (say, 20 and 200 μm), and a *trimodal* propellant has three sizes, because this allows a larger mass of solids to be placed into the propellant. Problem 1 has a sketch that explains how the voids between the large particles are filled with smaller particles.

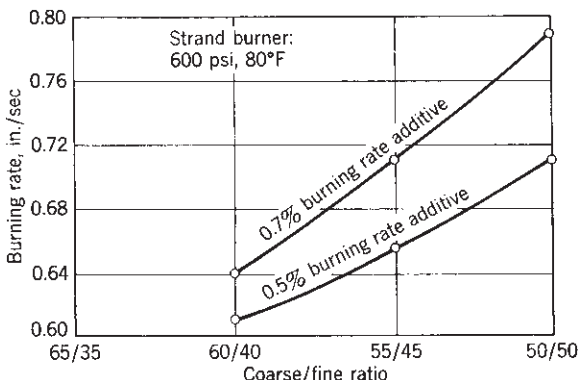


FIGURE 13–8. Typical effect of oxidizer (ammonium perchlorate) particle size mixture and burning rate additive on the burning rate of a composite propellant. (From NASA report SP-72262, Motor Propellant Development, July 1, 1967.)

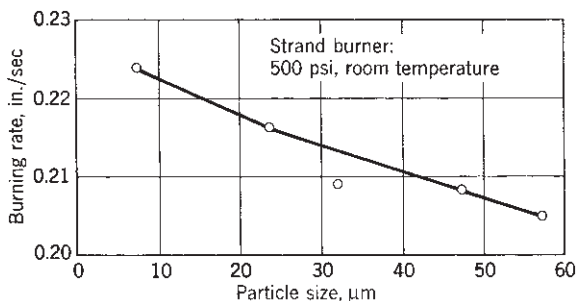


FIGURE 13–9. Typical effect of aluminum particle size on propellant burning rate for a composite propellant. (From NASA Report 8075, Solid Propellant Processing Factors in Rocket Motor Design, October 1971.)

13.5. OTHER PROPELLANT CATEGORIES

Gas Generator Propellants

Gas generator propellants produce hot gas but not thrust. They usually have a low combustion temperature (800 to 1600 K), and most do not require internal insulators when used in metal cases. Typical applications of gas generators were listed in Table 12–1. A large variety of propellants have been used to create hot gas for gas generators, but only a few will be mentioned.

Stabilized *AN-based propellants* have been used for many years with various ingredients or binders. They give a clean, essentially smokeless exhaust and a low combustion temperature. Because of their low burning rate they are useful for long-duration gas generator applications, say 30 to 300 sec. Typical compositions

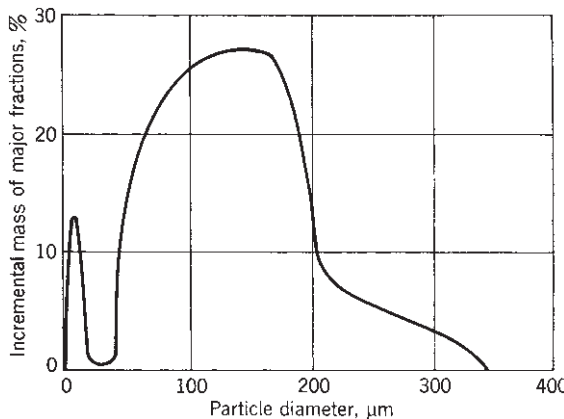


FIGURE 13–10. The oxidizer (AP) particle size distribution is a blend of two or more different particle sizes; this particular composite propellant consists of a narrow cut at about 10 μm and a broad region from 50 to 200 μm .

are shown in Ref. 13–12, and a propellant representative of early gas generators is described in Table 13–10.

One method of reducing flame temperature is to burn conventional hot AP propellant and then add water to it to cool the gases to a temperature where uncooled metals can contain them. This is used on the MX missile launcher tube gas generator (Ref. 13–15). Another formulation uses HMX or RDX with an excess of polyether- or polyester-type polyurethane.

For the inflation of automobile collision safety bags the exhaust gas must be nontoxic, smoke free, have a low temperature (will not burn people), be quickly initiated, and be reliably available. One solution is to use alkali azides (e.g., NaN_3 or KN_3) with an oxide and an oxidizer. The resulting nitrates or oxides are solid materials that are removed by filtering and the gas is clean and is largely moderately hot nitrogen. In one model, air can be aspirated into the air bag by the hot, high-pressure gas (see Ref. 13–16). One particular composition uses 65 to 75% NaN_3 , 10 to 28% Fe_2O_3 , 5 to 16% NaNO_3 as an oxidizer, a burn rate modifier, and a small amount of SiO_2 for moisture absorption. The resultant solid nitride slag is caught in a filter.

The ideal power P delivered by a gas generator can be expressed as (see Chapters 3 and 5)

$$P = \dot{m}(h_1 - h_2) = [\dot{m}T_1Rk/(k-1)][1 - (p_2/p_1)^{(k-1)/k}] \quad (13-1)$$

where \dot{m} is the mass flow rate, h_1 and h_2 the enthalpies per unit mass, respectively, at the gas generator chamber and exhaust pressure conditions, T_1 is the flame temperature in the gas generator chamber, R the gas constant, p_2/p_1 is the reciprocal of the pressure ratio through which these gases are expanded, and k

TABLE 13–10. Typical Gas Generator Propellant Using Ammonium Nitrate Oxidizer

| <i>Ballistic Properties</i> | |
|---|-------|
| Calculated flame temperature (K) | 1370 |
| Burning rate at 6.89 MPa and 20°C (mm/sec) | 2.1 |
| Pressure exponent n (dimensionless) | 0.37 |
| Temperature sensitivity σ_p (%/K) | 0.22 |
| Theoretical characteristic velocity, c^* (m/sec) | 1205 |
| Ratio of specific heats | 1.28 |
| Molecular mass of exhaust gas | 19 |
| <i>Composition (Mass Fraction)</i> | |
| Ammonium nitrate (%) | 78 |
| Polymer binder plus curing agent (%) | 17 |
| Additives (processing aid, stabilizer, antioxidant) (%) | 5 |
| Oxidizer particle size, (μm) | 150 |
| <i>Exhaust Gas Composition (Molar %)</i> | |
| Water | 26 |
| Carbon monoxide | 19 |
| Carbon dioxide | 7 |
| Nitrogen | 21 |
| Hydrogen | 27 |
| Methane | Trace |
| <i>Physical Properties at 25°C or 298 K</i> | |
| Tensile strength (MPa) | 1.24 |
| Elongation (%) | 5.4 |
| Modulus of elasticity in tension (N/m ²) | 34.5 |
| Specific gravity | 1.48 |

the specific heat ratio. Because the flame temperature is relatively low, there is no appreciable dissociation, and frozen equilibrium calculations are usually adequate.

Smokeless or Low-Smoke Propellant

Certain types of DB propellant, DB modified with HMX, and AN composites can be nearly smokeless. There is no or very little particulate matter in the exhaust gas. These minimum-smoke propellants are not a special class with a peculiar formulation but a variety of one of the classes mentioned previously. Propellants containing Al, Zr, Fe₂O₃ (burn rate modifier), or other metallic species will form visible clouds of small solid metal or metal oxide particles in the exhaust.

For certain military applications a smokeless propellant is needed and the reasons are stated in Chapter 20 (Exhaust Plumes). It is very difficult to make a propellant which has a truly smokeless exhaust gas. We therefore distinguish between *low-smoke* also called *minimum-smoke* (almost smokeless), and *reduced-smoke propellants*, which have a faintly visible plume. A visible smoke trail comes from solid particles in the plume, such as aluminum oxide. With enough of

these particles, the exhaust plume will scatter or absorb light and become visible as *primary smoke*. The particles can act as focal points for moisture condensation, which can occur in saturated air or under high-humidity, low-temperature conditions. Also, vaporized plume molecules, such as water or hydrochloric acid, can condense in cold air and form droplets and thus a cloud trail. These processes create a *vapor trail* or *secondary smoke*.

Several types of DB propellant, DB modified with HMX, nitramine (HMX or RDX) based composites, AN composites, or combinations of these, give very few or no solid particles in their exhaust gas. They do not contain aluminum or AP, generally have lower specific impulse than comparable propellants with AP, and have very little primary smoke, but can have secondary smoke in unfavorable weather. Several of these propellants have been used in tactical missiles.

Reduced-smoke propellants are usually composite propellants with low concentrations of aluminum (1 to 6%); they have a low percentage of aluminum oxide in the exhaust plume, are faintly visible as primary smoke, but can precipitate heavy secondary smoke in unfavorable weather. Their performance is much better than that of minimum-smoke propellants, as seen in Fig. 13-1.

Igniter Propellants

The process of propellant ignition is discussed in Section 14.2, and several types of igniter hardware are discussed in Section 15.3. Propellants for igniters, a specialized field of propellant technology, is described here briefly. The requirements for an igniter propellant will include the following:

Fast high heat release and high gas evolution per unit igniter propellant mass to allow rapid filling of grain cavity with hot gas and partial pressurization of the chamber.

Stable initiation and operation over a wide range of pressures (subatmospheric to chamber pressure) and smooth burning at low pressure with no ignition overpressure surge.

Rapid initiation of igniter propellant burning and low ignition delays.

Low sensitivity of burn rate to ambient temperature changes and low burning rate pressure exponent.

Operation over the required ambient temperature range.

Safe and easy to manufacture, safe to ship and handle.

Good aging characteristics and long life.

Minimal moisture absorption or degradation with time.

Low cost of ingredients and fabrication.

Some igniters not only generate hot combustion gas, but also hot solid particles or hot liquid droplets, which radiate heat and impinge on the propellant surface, embed themselves into this surface, and assist in achieving propellant burning on the exposed grain surface.

There have been a large variety of different igniter propellants and their development has been largely empirical. Black powder, which was used in early motors, is no longer favored because it is difficult to duplicate its properties. Extruded double-base propellants are used frequently, usually as a large number of small cylindrical pellets. In some cases rocket propellants that are used in the main grain are also used for the igniter grain; sometimes they are slightly modified. They are used in the form of a small rocket motor within a large motor that is to be ignited. A common igniter formulation uses 20 to 35% boron and 65 to 80% potassium nitrate with 1 to 5% binder. Binders typically include epoxy resins, graphite, nitrocellulose, vegetable oil, polyisobutylene, and other binders listed in Table 13-7. Another formulation uses magnesium with a fluorocarbon (Teflon); it gives hot particles and hot gas (Refs. 13-17 and 13-18). Other igniter propellants are listed in Ref. 13-10.

13.6. LINERS, INSULATORS, AND INHIBITORS

These three layers at the interface of a grain were defined in Section 12.3. Their materials do not contain any oxidizing ingredients; they will ablate, cook, char, vaporize, or disintegrate in the presence of hot gases. Many will burn if the hot combustion gas contains even a small amount of oxidizing species, but they will not usually burn by themselves. The liner, internal insulator, or inhibitor must be *chemically compatible* with the propellant and each other to avoid migration (described below) or changes in material composition; they must have *good adhesive strength*, so that they stay bonded to the propellant, or to each other. The *temperature* at which they suffer damage or experience a large *surface regression* should be high. They should all have a low density, thus reducing inert mass. Typical materials are neoprene (specific gravity 1.23), butyl rubber (0.93), a synthetic rubber called ethylenepropylene diene or EPDM (0.86), or the binder used in the propellant, such as polybutadiene (0.9 to 1.0); these values are low compared with a propellant specific gravity of 1.6 to 1.8. For low-smoke propellant these three rubber-like materials should give off some gas, but few, if any, solid particles (see Ref. 13-19).

In addition to the desired characteristics listed in the previous paragraph, the *liner* should be a soft stretchable rubber-type thin material (typically 0.02 to 0.04 in. thick with 200 to 450% elongation) to allow relative movement along the bond line between the grain and the case. This differential expansion occurs because the thermal coefficient of expansion of the grain is typically an order of magnitude higher than that of the case. A liner will also seal fiber-wound cases (particularly thin cases), which are often porous, so that high-pressure hot gas cannot escape. A typical liner for a tactical guided missile has been made from polypropylene glycol (about 57%), a titanium oxide filler (about 20%), a di-isocyanate crosslinker (about 20%), and minor ingredients such as an antioxidant. The motor

case had to be preheated to about 82°C prior to application. Ethylenepropylene diene monomer (EPDM) is linked into ethylenepropylene diene terpolymer to form a synthetic rubber which is often used as polymer for liners; it adheres and elongates nicely.

In some motors today the *internal insulator* not only provides for the thermal protection of the case from the hot combustion gases, but also often serves the function of the *liner* for good bonding between propellant and insulator or insulator and case. Most motors still have a separate liner and an insulating layer. Internal thermal insulation should fulfill these additional requirements:

1. It must be erosion resistant, particularly in the insulation of the motor aft end or blast tube. This is achieved in part by using tough elastomeric materials, such as neoprene or butyl rubber, that are chemically resistant to the hot gas and the impact of particulates. This surface integrity is also achieved by forming a porous black carbon layer on its heated surface called a porous char layer, which remains after some of the interstitial materials have been decomposed and vaporized.
2. It must provide good thermal resistance and low thermal conductivity to limit heat transfer to the case and thus keep the case below its maximum allowable temperature, which is usually between 160 and 350°C for the plastic in composite material cases and about 550 and 950°C for most steel cases. This is accomplished by filling the insulator with silicon oxide, graphite, Kevlar, or ceramic particles. Asbestos is an excellent filler material but is no longer used because of its health hazard.
3. It should allow a large-deformation or strain to accommodate grain deflections upon pressurization or temperature cycling, and transfer loads between the grain and the case.
4. The surface regression should be minimal so as to retain much of its original geometric surface contour and allow a thin insulator.

A simple relationship for the thickness d at any location in the motor depends on the exposure time t_e , the erosion rate r_e (obtained from erosion tests at the likely gas velocity and temperature), and the safety factor f which can range from 1.2 to 2.0:

$$d = t_e r_e f \quad (13-2)$$

Some designers use the rule that the insulation depth is twice the charred depth.

The thickness of the insulation is not usually uniform; it can vary by a factor of up to 20. It is thicker at locations such as the dome where it is exposed for longer intervals and at higher scrubbing velocities than the insulator layers protected by bonded propellant. Before making a material selection, it is necessary to evaluate the flow field and the thermal environment (combustion temperature,

gas composition, pressure, exposure duration, internal ballistics) in order to carry out a thermal analysis (erosion prediction and estimated thickness of insulator). An analysis of loads and the deflections under loads at different locations of the motor are needed to estimate shear and compression stresses. If it involves high stresses or a relief flap, a structural analysis is also needed. Various computer programs, such as the one mentioned in Refs. 13–20 and 13–21, are used for these analyses.

An *inhibitor* is usually made of the same kinds of materials as internal insulators. They are applied (bonded, molded, glued, or sprayed) to grain surfaces that should not burn. In a segmented motor, for example (see Fig. 15–2), where burning is allowed only on the internal port area, the faces of the cylindrical grain sections are inhibited.

Migration is the transfer of mobile (liquid) chemical species from the solid propellant to the liner, insulator, or inhibitor, or vice versa. Liquid plasticizers such as NG or DEGN or unreacted monomers or liquid catalysts are known to migrate. This migratory transfer occurs very slowly; it can cause dramatic changes in physical properties (e.g., the propellant next to the liner becomes brittle or weak), and there are several instances where nitroglycerine migrated into an insulator and made it flammable. Migration can be prevented or inhibited by using (1) propellants without plasticizers, (2) insulators or binders with plasticizers identical to those used in propellants, (3) a thin layer of an impervious material or a migration barrier (such as PU or a thin metal film), and (4) an insulator material that will not allow migration (e.g., PU) (see Ref. 13–22).

The graphite–epoxy motors used to boost the Delta launch vehicle use a three-layer *liner*: EPDM (ethylene-propylene diene terpolymer) as a thin primer to enhance bond strength, a polyurethane barrier to prevent migration of the plasticizer into the EPDM liner, and a plasticized HTPB-rich liner to prevent burning next to the case–bond interface. The composite AP–Al propellant also uses the same HTPB binder.

Liners, insulators, or inhibitors can be applied to the grain in several ways: by painting, coating, dipping, spraying, or by gluing a sheet or strip to the case or the grain. Often an automated, robotic machine is used to achieve uniform thickness and high quality. Reference 13–21 describes the manufacture of particular insulators.

An *external insulation* is often applied to the outside of the motor case, particularly in tactical missiles or high-acceleration launch boosters. This insulation reduces the heat flow from the boundary layer outside the vehicle surface (which is aerodynamically heated) to the case and then to the propellant. It thus prevents fiber-reinforced plastic cases from becoming weak or the propellant from becoming soft or, in extreme situations, from being ignited. This insulator must withstand the oxidation caused by heated air, have good adhesion, have structural integrity to loads imposed by the flight or launch, and must have a reasonable cure temperature. Materials ordinarily used as internal insulators are unsatisfactory, because they burn in the atmosphere and generate heat. The best is a non-pyrolyzing, low-thermal-conductivity refractory material (Ref. 13–23) such as

high-temperature paint. The internal and external insulation also helps to reduce the grain temperature fluctuations and thus thermal stresses imposed by thermal cycling, such as day–night variations or high- and low-altitude temperature variations for airborne missiles.

13.7. PROPELLANT PROCESSING AND MANUFACTURE

The manufacture of solid propellant involves complex physical and chemical processes. In the past, propellant has been produced by several different processes, including the compaction or pressing of powder charges, extrusion of propellant through dies under pressure using heavy presses, and mixing with a solvent which is later evaporated. Even for the same type of propellant (e.g., double-base, composite, or composite double-base) the fabrication processes are usually not identical for different manufacturers, motor types, sizes, or propellant formulation, and no single simple generalized process flowsheet or fabrication technique is prevalent. Most of the rocket motors in production today use composite-type propellants and therefore some emphasis on this process is given here.

Figure 13–11 shows a representative flowsheet for the manufacture of a complete solid rocket motor with a composite propellant made by batch processes. Processes marked with an asterisk are potentially hazardous, are usually operated or controlled remotely, and are usually performed in buildings designed to withstand potential fires or explosions. The mixing and casting processes are the most complex and are more critical than other processes in determining the quality, performance, burn rate, and physical properties of the resulting propellant.

The rheological properties of the uncured propellant, meaning its flow properties in terms of shear rate, stress, and time, are all-important to the processibility of the propellant, and these properties usually change substantially throughout the length of the processing line. Batch-type processing of propellant, including the casting (pouring) of propellant into motors that serve as their own molds, is the most common method. For very large motors several days are needed for casting perhaps 40 batches into a single case, forming a single grain. Vacuum is almost always imposed on the propellant during the mixing and casting operations to remove air and other dispersed gases and to avoid air bubbles in the grain. Viscosity measurements of the mixed propellant (10,000 to 20,000 poise) are made for quality control. Vacuum, temperature, vibration, energy input of the mixer, and time are some of the factors affecting the viscosity of the uncured propellant. Time is important in terms of *pot life*, that period of time the uncured propellant remains reasonably fluid after mixing before it cures and hardens. Short pot life (a few hours) requires fast operations in emptying mixers, measuring for quality control, transporting, and casting into motors. Some binder systems, such as those using PVC, give a very long pot life and avoid the urgency or haste in the processing line. References 13–3, 13–10, and 13–24 give details on propellant processing techniques and equipment.

Double-base propellants and modified double-base propellants are manufactured by a different set of processes. The key is the diffusion of the liquid

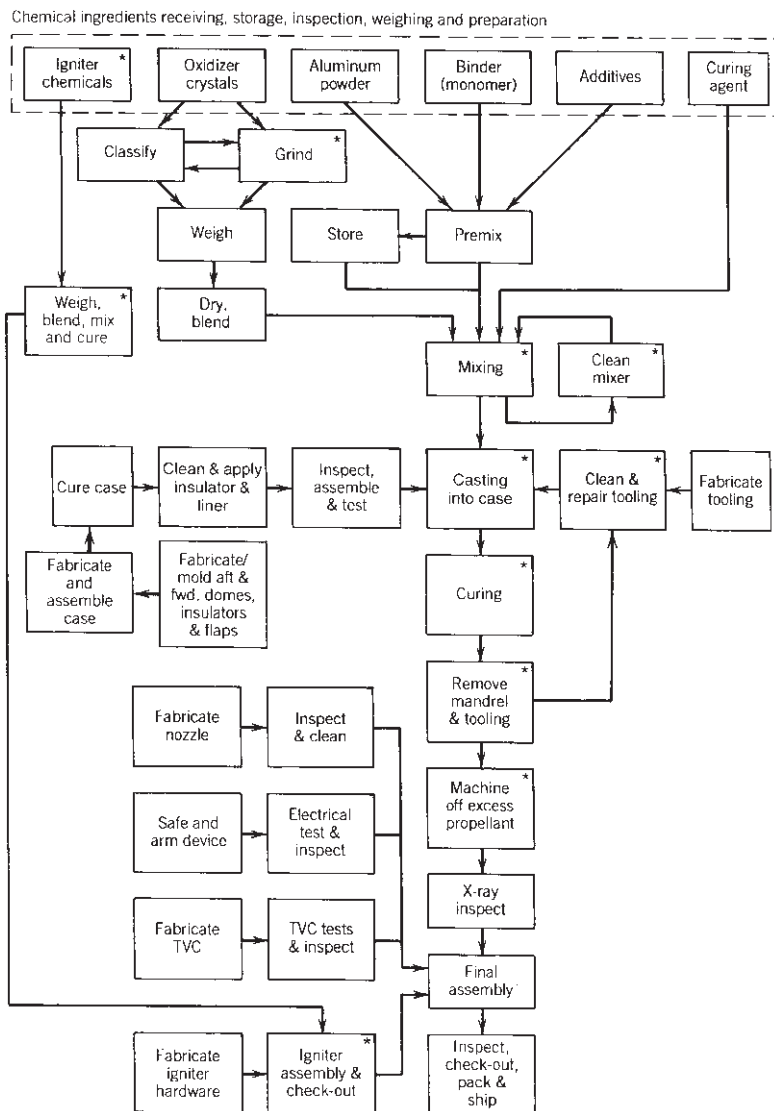


FIGURE 13–11. Simplified manufacturing process flow diagram for a rocket motor and its composite solid propellant. An asterisk * means it is a potentially hazardous operation.

nitroglycerine into the fibrous solid matrix of nitrocellulose, thus forming, by means of solvation, a fairly homogeneous, well-dispersed, relatively strong solid material. Several processes for making double-base rocket propellant are in use today, including extrusion and slurry casting. In the slurry casting process the case (or the mold) is filled with solid casting powder (a series of small solid pellets of nitroglycerine) and the case is then flooded

with liquid nitroglycerine, which then solvates the pellets. Figure 13–12 shows a simplified diagram of a typical setup for a slurry cast process. Double-base propellant manufacturing details are shown in Refs. 13–3 and 13–14.

Mandrels are used during casting and curing to assure a good internal cavity or perforation. They are made of metal in the shape of the internal bore (e.g., star or dogbone) and are often slightly tapered and coated with a nonbonding material, such as Teflon, to facilitate the withdrawal of the mandrel after curing without tearing the grain. For complicated internal passages, such as a conocyl, a complex built-up mandrel is necessary, which can be withdrawn through the nozzle flange opening in smaller pieces or which can be collapsed. Some manufacturers have had success in making permanent mandrels (which are not withdrawn but stay

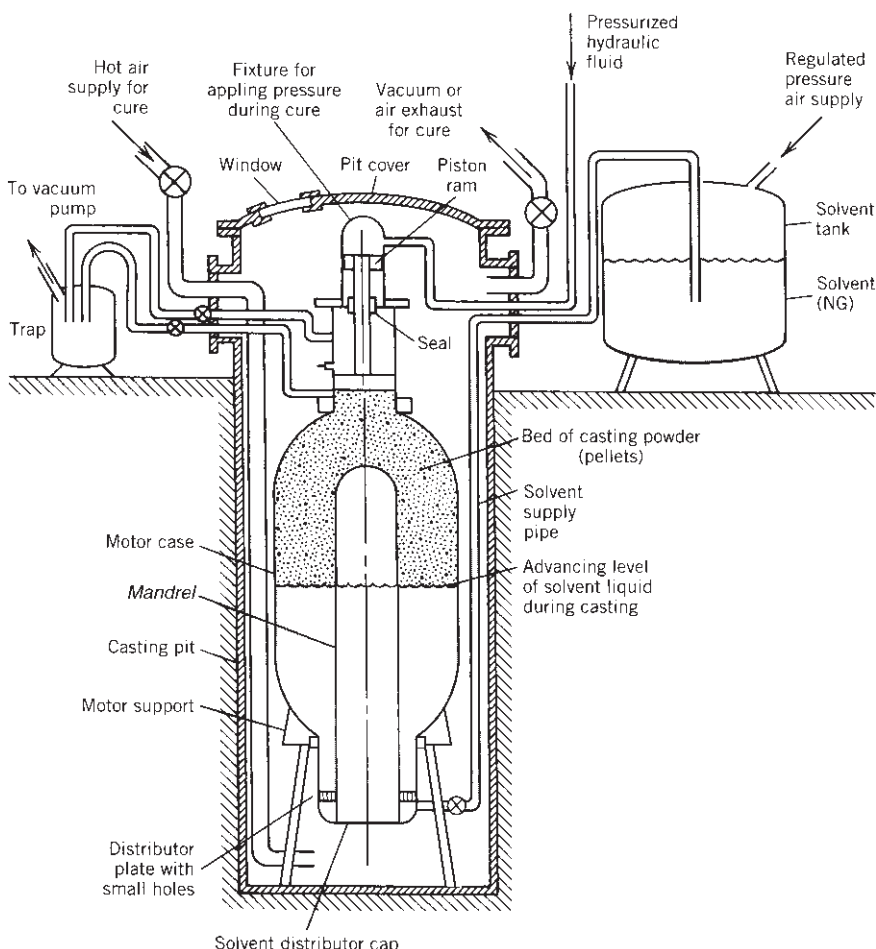


FIGURE 13–12. Simplified diagram of one system for slurry casting and initial curing of a double-base solid propellant.

with the motor) out of lightweight foamed propellant, which burns very quickly once it is ignited.

An important objective in processing is to produce a propellant grain free of cracks, low-density areas, voids, or other flaws. In general, voids and other flaws degrade the ballistic and mechanical properties of the propellant grain. Finely dispersed gas in a propellant grain may result in an abnormally high burning rate, one so high as to cause catastrophic motor failure.

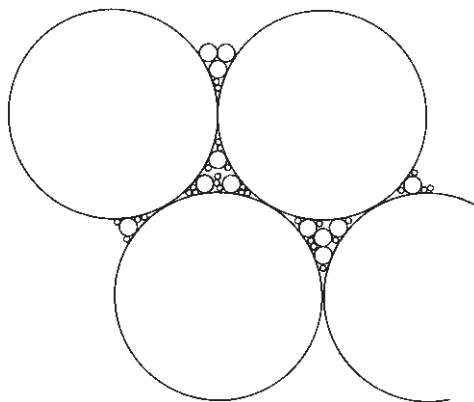
The finished grain (or motor) is usually inspected for defects (cracks, voids, and debonds) using X-ray, ultrasonic, heat conductivity, or other nondestructive inspection techniques. Samples of propellant are taken from each batch, tested for rheological properties, and cast into physical property specimens and/or small motors which are cured and subsequently tested. A determination of the sensitivity of motor performance, including possible failure, to propellant voids and other flaws often requires the test firing of motors with known defects. Data from the tests are important in establishing inspection criteria for accepting and rejecting production motors.

Special process equipment is needed in the manufacture of propellant. For composite propellants this includes mechanical mixers (usually with two or three blades rotating on vertical shafts agitating propellant ingredients in a mixer bowl under vacuum), casting equipment, curing ovens, or machines for automatically applying the liner or insulation to the case. Double-base processing requires equipment for mechanically working the propellant (rollers, presses) or special tooling for allowing a slurry cast process. Computer-aided filament winding machines are used for laying the fibers of fiber-reinforced plastic cases and nozzles.

PROBLEMS

1. Ideally the solid oxidizer particles in a propellant can be considered spheres of uniform size. Three sizes of particles are available: coarse at $500 \mu\text{m}$, medium at $50 \mu\text{m}$, and fine at $5 \mu\text{m}$, all at a specific gravity of 1.95, and a viscoelastic fuel binder at a specific gravity of 1.01. Assume that these materials can be mixed and vibrated so that the solid particles will touch each other, there are no voids in the binder, and the particles occupy a minimum of space similar to the sketch of the cross section shown here. It is desired to put 94 wt % of oxidizer into the propellant mix, for this will give maximum performance. (a) Determine the maximum weight percentage of oxidizer if only coarse crystals are used or if only medium-sized crystals are used. (b) Determine the maximum weight of oxidizer if both coarse and fine crystals are used, with the fine crystals filling the voids between the coarse particles. What is the optimum relative proportion of coarse and fine particles to give a maximum of oxidizer? (c) Same as part (b), but use coarse and medium crystals only. Is this better and, if so, why? (d) Using all three sizes, what is the ideal weight mixture ratio and what is the maximum oxidizer content possible and the theoretical maximum specific gravity of the propellant? (*Hint:*

The centers of four adjacent coarse crystals form a tetrahedron whose side length is equal to the diameter.)



2. Suggest one or two specific applications (intercontinental missile, anti-aircraft, space launch vehicle upper stage, etc.) for each of the propellant categories listed in Table 13-2 and explain why it was selected when compared to other propellants.
3. Prepare a detailed outline of a procedure to be followed by a crew operating a propellant mixer. This 1-m³ vertical solid propellant mixer has two rotating blades, a mixing bowl, a vacuum pump system to allow mix operations under vacuum, feed chutes or pipes with valves to supply the ingredients, and variable-speed electric motor drive, a provision for removing some propellant for laboratory samples, and a double-wall jacket around the mixing bowl to allow heating or cooling. It is known that the composite propellant properties are affected by mix time, small deviations from the exact composition, the temperature of the mix, the mechanical energy added by the blades, the blade speed, and the sequence in which the ingredients are added. It is also known that bad propellant would be produced if there are leaks that destroy the vacuum, if the bowl, mixing blades, feed chutes, and so on, are not clean but contain deposits of old propellant on their walls, if they are not mixed at 80°C, or if the viscosity of the mix becomes excessive. The sequence of loading ingredients shall be: (1) prepolymer binder, (2) plasticizer, (3) minor liquid additives, (4) solid consisting of first powdered aluminum and thereafter mixed bimodal AP crystals, and (5) finally the polymerizing agent or crosslinker. Refer to Fig. 13-11. Samples of the final liquid mix are taken to check viscosity and density. Please list all the sequential steps that the crew should undertake before, during, and after the mixing operation. If it is desired to control to a specific parameter (weight, duration, etc.), that fact should be stated; however, the specific data of ingredient mass, time, power, temperature, and so on, can be left blank. Mention all instruments (e.g., thermometers, wattmeter, etc.) that the crew should have and identify those that they must monitor closely. Assume that all ingredients were found to be of the desired composition, purity, and quality.
4. Determine the longitudinal growth of a 24-in.-long freestanding grain with a linear thermal coefficient of expansion of $7.5 \times 10^{-5}/^{\circ}\text{F}$ for temperature limits of -40 to 140°F

Answer: 0.32 in.

5. The following data are given for an internally burning solid propellant grain with inhibited end faces and a small initial port area:

| | |
|---|----------------------------|
| Length | 40 in. |
| Port area | 27 in. ² |
| Propellant weight | 240 lbf |
| Initial pressure at front end of chamber | 1608 psi |
| Initial pressure at nozzle end of chamber | 1412 psi |
| Propellant density | 0.060 lbm/in. ³ |
| Vehicle acceleration | 21.2g ₀ |

Determine the initial forces on the propellant supports produced by pressure differential and vehicle acceleration.

Answers: 19,600 lbf, 5090 lbf.

6. A solid propellant unit with an end-burning grain has a thrust of 4700 N and a duration of 14 sec. Four different burning rate propellants are available, all with approximately the same performance and the same specific gravity, but different AP mix and sizes and different burning rate enhancements. They are 5.0, 7.0, 10, and 13 mm/sec. The preferred L/D is 2.60, but values of 2.2 to 3.5 are acceptable. The impulse-to-initial-weight ratio is 96 at an L/D of 2.5. Assume optimum nozzle expansion at sea level. Chamber pressure is 6.894 MPa or 1000 psia and the operating temperature is 20°C or 68°F. Determine grain geometry, propellant mass, hardware mass, and initial mass.
7. For the rocket in Problem 6 determine the approximate chamber pressure, thrust, and duration at 245 and 328 K. Assume the temperature sensitivity (at a constant value of A_b/A_t) of 0.01%/K does not change with temperature.
8. A fuel-rich solid propellant for a gas generator drives a turbine of a liquid propellant turbopump. Determine its mass flow rate. The following data are given:

| | |
|--|-----------------------|
| Chamber pressure | $p_1 = 5\text{ MPa}$ |
| Combustion temperature | $T_1 = 1500\text{ K}$ |
| Specific heat ratio | $k = 1.25$ |
| Required pump input power | 970 KW |
| Turbine outlet pressure | 0 psia |
| Turbine efficiency | 65% |
| Molecular mass of gas | 22 kg/kg-mol |
| Pressure drop between gas generator and turbine nozzle inlet | 0.10 MPa |

Windage and bearing friction is 10 kW. Neglect start transients.

Answer: $\dot{m} = 0.257 \text{ kg/sec}$.

9. The propellant for this gas generator has these characteristics:

| | |
|----------------------------------|------------|
| Burn rate at standard conditions | 4.0 mm/sec |
| Burn time | 110 sec |
| Chamber pressure | 5.1 MPa |
| Pressure exponent n | 0.55 |
| Propellant specific gravity | 1.47 |

Determine the size of an end-burning cylindrical grain.

Answer: Single end-burning grain 27.2 cm in diameter and 31.9 cm long, or two end-burning opposed grains (each 19.6 cm diameter \times 31.9 cm long) in a single chamber with ignition of both grains in the middle of the case.

REFERENCES

- 13–1. A Davenas, “Solid Rocket Motor Design,” Chapter 4 of G. E. Jensen and D. W. Netzer (Eds.), *Tactical Missile Propulsion*, Vol. 170, *Progress in Astronautics and Aeronautics*, AIAA, Reston, VA, 1996.
- 13–2. N. Kubota, “Survey of Rocket Propellants and Their Combustion Characteristics,” Chapter 1 in K. K. Kuo and M. Summerfield (Eds.), *Fundamentals of Solid-Propellant Combustion, Progress in Astronautics and Aeronautics*, Vol. 90, American Institute of Aeronautics and Astronautics, New York, 1984; see also Chapters 1.1 to 1.8 in V. Yang, T. B. Brill, and W.-Z. Ren (Eds.), *Solid Propellant Chemistry, Combustion, and Motor Interior Ballistics, Progress in Astronautics and Aeronautics*, Vol. 185, AIAA, Reston VA, 2000.
- 13–3. C. Boyars and K. Klager, *Propellants: Manufacture, Hazards and Testing*, Advances in Chemistry Series 88, American Chemical Society, Washington, DC, 1969.
- 13–4. Chemical Propulsion Information Agency, *Hazards of Chemical Rockets and Propellants*. Vol. II, *Solid Rocket Propellant Processing, Handling, Storage and Transportation*, NTIS AD-870258, May 1972.
- 13–5. H. S. Sibdeh and R. A. Heller, “Rocket Motor Service Life Calculations Based on First Passage Method,” *Journal of Spacecraft and Rockets*, Vol. 26, No. 4, July–August 1989, pp. 279–284.
- 13–6. D. I. Thrasher, “State of the Art of Solid Propellant Rocket Motor Grain Design in the United States,” Chapter 9 in *Design Methods in Solid Rocket Motors*, Lecture Series LS 150, AGARD/NATO, April 1988.
- 13–7. “Explosive Hazard Classification Procedures,” DOD, U.S. Army Technical Bulletin TB 700-2, updated 1989; T. L. Boggs et al., “Hazards Associated with Solid Propellants,” Chapter 1.9 in V. Yang, T. B. Brill, and W.-Z. Ren (Eds.), *Solid Propellant Chemistry, Combustion, and Motor Interior Ballistics, Progress in Astronautics and Aeronautics*, Vol. 185, AIAA, Reston VA, 2000.
- 13–8. “Hazards Assessment Tests for Non-Nuclear Ordnance,” Military Standard MIL-STD-2105B (government-issued specification), 1994; M. L. Chan et al., “Advances in Solid Propellant Formulations,” Chapter 1.7 in V. Yang, T. B. Brill, and W.-Z. Ren (Eds.), *Solid Propellant Chemistry, Combustion, and Motor Interior Ballistics, Progress in Astronautics and Aeronautics*, Vol. 185, AIAA, Reston VA, 2000, pp 185–206.
- 13–9. “Department of Defense—Ammunition and Explosive Safety Standard,” U.S. Department of Defense, U.S. Army TB 700-2, U.S. Navy NAVSEAINST 8020.8, U.S. Air Force TO 11A-1-47, Defense Logistics Agency DLAR 8220.1, 1994 rev.
- 13–10. A. Davenas, *Solid Rocket Propulsion Technology*, Elsevier Science, New York, 1992 (originally published in French); see also A. Davenas, “Development of Modern Solid Propellants,” *Journal of Propulsion and Power*, Vol. 19, No. 6, November–December 2003, pp. 1108–1128.

- 13–11. G. M. Clark and C. A. Zimmerman, “Phase Stabilized Ammonium Nitrate Selection and Development,” *JANNAF Publication 435*, October 1985, pp. 65–75.
- 13–12. J. Li and Y. Xu, “Some Recent Investigations in Solid Propellant Technology for Gas Generators,” AIAA Paper 90-2335, July 1990.
- 13–13. S. Boraas, “Modeling Slag Deposition in the Space Shuttle Solid Motor,” *Journal of Spacecraft and Rockets*, Vol. 21, No. 1, January–February 1984, pp. 47–54.
- 13–14. V. Lindner, “Explosives and Propellants,” Kirk-Othmer, *Encyclopedia of Chemical Technology*, Vol. 9, pp. 561–671, John Wiley & Sons, New York, 1980.
- 13–15. J. A. McKinnis and A. R. O’Connell, “MX Launch Gas Generator Development,” *Journal of Spacecraft and Rockets*, Vol. 20, No. 3, May–June 1983.
- 13–16. T. H. Vos and G. W. Goetz, “Inflatable Restraint Systems, Helping to Save Lives on the Road,” *Quest*, TRW, Inc., Redondo Beach, CA, Vol. 12, No. 2, Winter 1989–1990, pp. 2–27.
- 13–17. A. Peretz, “Investigation of Pyrotechnic MTV Compositions for Rocket Motor Igniters,” *Journal of Spacecraft and Rockets*, Vol. 21, No. 2, March–April 1984, pp. 222–224.
- 13–18. I. Blog, “Laser Diode Ignition of B/KNO₃ Pyrotechnic Mixture,” *Combustion Science and Technology*, Vol. 179, No. 8, Aug. 2007, pp. 1667–1699; G. Grut, “Mistral Missile Propulsion System,” AIAA Paper 89–2428, July 1989.
- 13–19. J. L. Laird and R. J. Baker, “A Novel Smokeless Non-flaking Solid Propellant Inhibitor,” *Journal of Propulsion and Power*, Vol. 2, No. 4, July–August 1986, pp. 378–379.
- 13–20. M. Q. Brewster, “Radiation–Stagnation Flow Model of Aluminized Solid Rocket Motor Insulation Heat Transfer,” *Journal of Thermophysics*, Vol. 3, No. 2, April 1989, pp. 132–139.
- 13–21. A. Truchot, “Design of Solid Rocket Motor Internal Insulation,” Chapter 10 in *Design Methods in Solid Rocket Motors*, Lecture Series LS 150, AGARD/NATO, Brussels, April 1988.
- 13–22. M. Probster and R. H. Schmucker, “Ballistic Anomalies in Solid Propellant Motors Due to Migration Effects,” *Acta Astronautica*, Vol. 13, No. 10, 1986, pp. 599–605.
- 13–23. L. Chow and P. S. Shadlesky, “External Insulation for Tactical Missile Motor Propulsion Systems,” AIAA Paper 89–2425, July 1989.
- 13–24. W. W. Sobol, “Low Cost Manufacture of Tactical Rocket Motors,” *Proceedings of 1984 JANNAF Propulsion Meeting*, Vol. II, Chemical Propulsion Information Agency, Johns Hopkins University, Columbia, MD, 1984, pp. 219–226.

CHAPTER 14

SOLID PROPELLANT COMBUSTION AND ITS STABILITY

In this the third of four chapters on solid propellant motors, we discuss the combustion of solid propellants, the physical and chemical processes of burning, the ignition or startup process, the extinction of burning, and combustion instability.

The combustion process in rocket propulsion systems is very efficient, when compared to other power plants, because the combustion temperatures are relatively very high; this accelerates the rate of chemical reaction, helping to achieve nearly complete combustion. As was mentioned in Chapter 2, the energy released in the combustion is between 95 and 99.5% of the possible maximum. This is difficult to improve. The rocket motor designers have been concerned not so much with the burning process as with controlling the combustion (start, stop, heat effects) and with preventing the occurrence of combustion instability.

14.1. PHYSICAL AND CHEMICAL PROCESSES

Combustion in a solid propellant motor involves exceedingly complex reactions taking place in the solid, liquid, and gas phases of a heterogeneous mixture. Not only are the physical and chemical processes occurring during solid propellant combustion not fully understood, but analytical combustion models remain oversimplified and unreliable. Experimental observations of burning propellants show complicated three-dimensional microstructures, a three-dimensional flame structure, intermediate products in the liquid and gaseous phase, spatially and temporally variant processes, aluminum agglomeration, nonlinear response behavior, formation of carbon particles, and other complexities yet to be adequately reflected in mathematical models.

Some insight into this combustion process can be gained by understanding the behavior of the major ingredients, such as ammonium perchlorate, which is fairly well explored. This oxidizer is capable of self-deflagration with a low-pressure combustion limit at approximately 2 MPa and at least four distinct "froth" zones of combustion between 2 and 70 MPa, the existence of a liquid froth on the surface of the crystal during deflagration between 2 and 6 MPa, and a change in the energy transfer mechanism (particularly at about 14 MPa). Its influence on combustion is critically dependent on oxidizer purity. The surface regression rate ranges from 3 mm/sec at 299 K and 2 MPa to 10 mm/sec at 423 K and 1.4 MPa.

The various polymeric binders used in composite propellants are less well characterized, and their combustion properties vary, depending on the binder type, heating rate, and combustion chamber pressure.

The addition of powdered aluminum (2 to 40 μm) is known to favorably influence specific impulse and combustion stability. Photographs of the burning aluminum particles show that the particles usually collect into relatively large accumulates (100 or more particles) during the combustion process. The combustion behavior of this ingredient depends on many variables, including particle size and shape, surface oxides, the binder, and the combustion wave environment. Reference 14-1 describes solid propellant combustion.

Visual observations and measurements of flames in simple experiments, such as strand burner tests, give an insight into the combustion process. For double-base propellants the combustion flame structure appears to be homogeneous and one-dimensional along the burning direction, as shown in Fig. 14-1. When heat from the combustion melts, decomposes, and vaporizes the solid propellant at the burning surface, the resulting gases seem to be already premixed. One can see a brilliantly radiating bright flame zone where most of the chemical reaction is believed to occur and a dark zone between the bright flame and the burning surface. The brightly radiating hot reaction zone appears to be detached from the combustion surface. The combustion that occurs inside the dark zone does not emit strongly in the visible spectrum but does emit in the infrared spectral region. The dark zone thickness decreases with increasing chamber pressure, and higher heat transfer to the burning surface causes the burning rate to increase. Experiments on strand burners in an inert nitrogen atmosphere, reported in Chapter 1 of Ref. 14-1, show this dramatically: for pressures of 10, 20, and 30 atm the dark zone thickness is 12, 3.3, and 1.4 mm, respectively, and the corresponding burning rates are 2.2, 3.1, and 4.0 mm/sec. The overall length of the visible flame becomes shorter as the chamber pressure increases and the heat release per unit volume near the surface also increases. In the bright, thin fizz zone or combustion zone directly over the burning surface of a DB propellant, some burning and heat release occurs. Beneath is a zone of liquefied bubbling propellant which is thought to be very thin (less than 1 μm) and which has been called the foam or degradation zone. Here the temperature becomes high enough for the propellant molecules to vaporize and break up or degrade into smaller molecules, such as NO_2 , aldehydes, or NO, which leave the foaming surface. Underneath is the solid

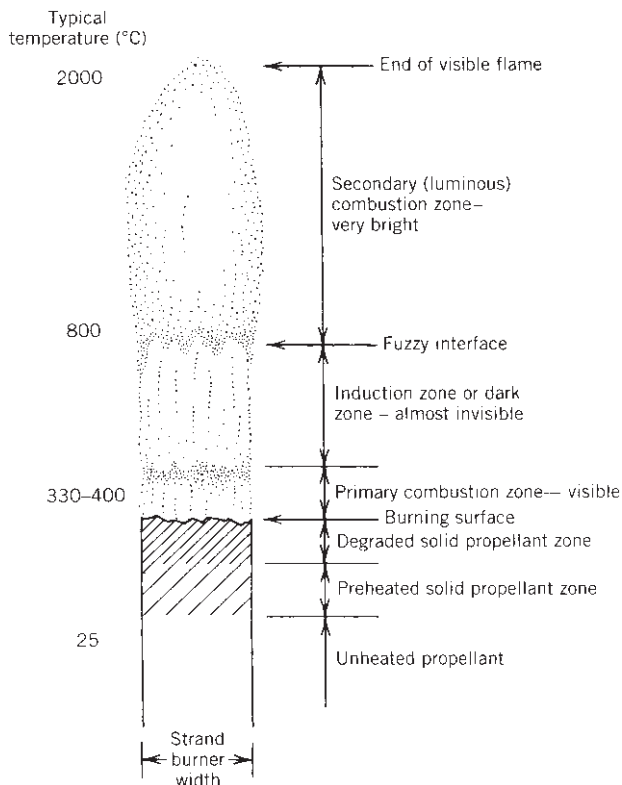


FIGURE 14–1. Schematic diagram of the combustion flame structure of a *double-base propellant* as seen with a strand burner in an inert atmosphere. (Adapted from Chapter 1 of Ref. 14–1 with permission of the AIAA.)

propellant, but the layer next to the surface has been heated by conduction within the solid propellant material.

Burn rate catalysts seem to affect the primary combustion zone rather than the processes in the condensed phase. They catalyze the reaction at or near the surface, increase or decrease the heat input into the surface, and change the amount of propellant that is burned.

A typical flame for an AP/Al/HTPB* propellant looks very different, as seen in Fig. 14–2. Here the luminous flame seems to be attached to the burning surface, even at low pressures. There is no dark zone. The oxidizer-rich decomposed gases from the AP diffuse into the fuel-rich decomposed gases from the fuel ingredients, and vice versa. Some solid particles (aluminum, AP crystals, small pieces of binder, or combinations of these) break loose from the surface and the particles continue to react and degrade while in the gas flow. The burning gas contains liquid particles of hot aluminum oxides, which radiate intensively.

*Acronyms are explained in Tables 13–6 and 13–7.

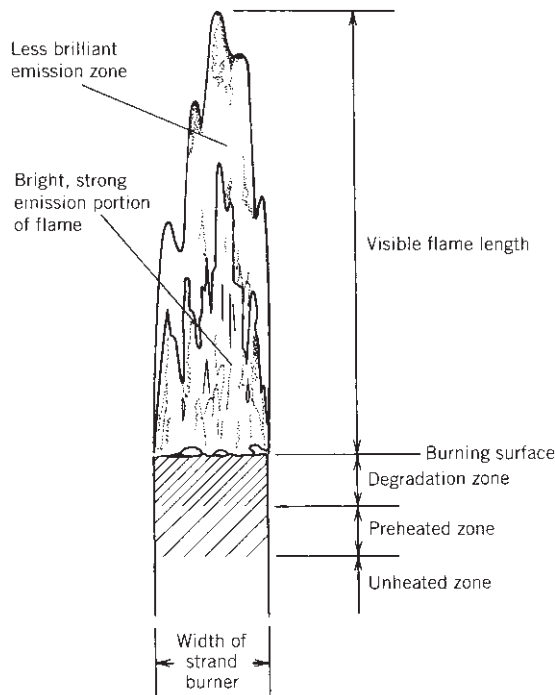


FIGURE 14–2. Diagram of the flickering, irregular combustion flame of a *composite propellant* (69% AP, 19% Al, plus binder and additives) in a strand burner with a neutral atmosphere. (Adapted from Chapter 1 of Ref. 14–1 with permission of AIAA.)

The propellant material and the burning surface are not homogeneous. The flame structure is unsteady (flicker), three dimensional, and not truly axisymmetrical. The flame structure and the burning rates of composite-modified cast double-base (CMDB) propellant with AP and Al seem to approach those of composite propellant, particularly when the AP content is high. Again there is no dark zone and the flame structure is unsteady and not axisymmetrical. It also has a complex three-dimensional flame structure.

According to Ref. 14–1, the flame structure for double-base propellant with a nitramine addition shows a thin dark zone and a slightly luminous degradation zone on the burning surface. The dark zone decreases in length with increased pressure. The decomposed gases of RDX or HMX are essentially neutral (not oxidizing) when decomposed as pure ingredients. In this CMDB/RDX propellant the degradation products of RDX solid crystals interdiffuse with the gas from the DB matrix just above the burning surface, before the RDX particles can produce monopropellant flamelets. Thus an essentially homogeneous premixed gas flame is formed, even though the solid propellant itself is heterogeneous. The flame structure appears to be one-dimensional. The burning rate of this propellant decreases when the RDX percentage is increased and seems to be

almost unaffected by changes in RDX particle size. Much work has been done to characterize the burning behavior of different propellants. See Chapters 2, 3, and 4 by Kishore and Gayathri, Boggs, and Fifer, respectively, in Ref. 14–1, and Refs. 14–2 to 14–8.

The burning rate of all propellants is influenced by pressure (see Section 12.1 and Eq. 12–5), the initial ambient solid propellant temperature, the burn rate catalyst, the aluminum particle sizes and their size distribution, and to a lesser extent by other ingredients and manufacturing process variables. Erosive burning was discussed in Chapter 12. Analysis of combustion is treated later in this chapter.

14.2. IGNITION PROCESS

This section is concerned with the mechanism or the process for initiating the combustion of a solid propellant grain. Specific propellants that have been successfully used for igniters have been mentioned in Section 13.5. The hardware, types, design, and integration of igniters into the motor are described in Section 15.4. Chapters 2, 5, and 6 of Ref. 14–1 review the state of the art of ignition, data from experiments, and analytical models.

Solid propellant ignition consists of a series of complex rapid events, which start on receipt of a signal (usually electric) and include heat generation, transfer of the heat from the igniter to the motor grain surface, spreading the flame over the entire burning surface area, filling the chamber free volume (cavity) with gas, and elevating the chamber pressure without serious abnormalities such as overpressures, combustion oscillations, damaging shock waves, hangfires (delayed ignition), extinguishment, and chuffing. The *igniter* in a solid rocket motor generates the heat and gas required for motor ignition.

Motor ignition must usually be complete in a fraction of a second for all but the very large motors (see Ref. 14–9). The motor pressure rises to an equilibrium state in a very short time, as shown in Fig. 14–3. Conventionally, the ignition process is divided into three phases for analytical purposes:

Phase I, *Ignition time lag*: the period from the moment the igniter receives a signal until the first surface grain burns.

Phase II, *Flame-spreading interval*: the time from first ignition of the grain surface until the complete grain burning area has been ignited.

Phase III, *Chamber-filling interval*: the time for completing the chamber-filling process and for reaching equilibrium chamber pressure and flow.

The ignition will be successful once enough grain surface is ignited and burning, so that the motor will continue to raise its own pressure to the operating chamber pressure. The critical process seems to be a gas-phase reaction above the burning surface, when propellant vapors or decomposition products interact with each other and with the igniter gas products. If the igniter is not powerful

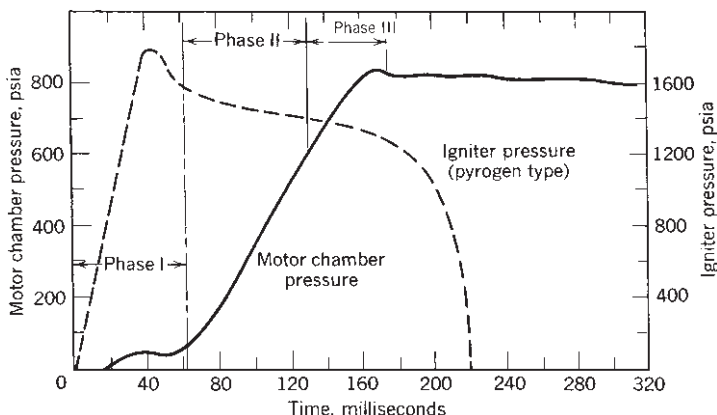


FIGURE 14-3. Typical ignition pressure as a function of time. It shows the time trace of the igniter propellant together with the propellant of the main grain. An electric signal is received a few milliseconds before time zero.

enough, some grain surfaces may burn for a short time, but the flame will be extinguished.

Satisfactory attainment of equilibrium chamber pressure with full gas flow is dependent on (1) characteristics of the igniter and the gas temperature, composition and flow issuing from the igniter, (2) motor propellant composition and grain surface ignitability, (3) heat transfer characteristics by radiation and convection between the igniter gas and grain surface, (4) grain flame spreading rate, and (5) the dynamics of filling the motor free volume with hot gas (see Ref. 14-10). The quantity and type of caloric energy needed to ignite a particular motor grain in the prevailing environment has a direct bearing on most of the igniters' design parameters—particularly those affecting the required heat output. The ignitability of a propellant at a given pressure and temperature is normally shown as a plot of ignition time versus heat flux received by the propellant surface, as shown in Fig. 14-4; these data are obtained from laboratory tests. Ignitability of a propellant is affected by many factors, including (1) the propellant formulation, (2) the initial temperature of the propellant grain surface, (3) the surrounding pressure, (4) the mode of heat transfer, (5) grain surface roughness, (6) age of the propellant, (7) the composition and hot solid particle content of the igniter gases, (8) the igniter propellant and its initial temperature, (9) the velocity of the hot igniter gases relative to the grain surface, and (10) the cavity volume and configuration. Figure 14-4 and data in Chapter 15 show that the ignition time becomes shorter with increases in both heat flux and chamber pressure. If a short ignition delay is required, then a more powerful igniter will be needed. The radiation effects can be significant in the ignition transient as described in Ref. 14-11. In Section 15.3 we describe an analysis and design for igniters.

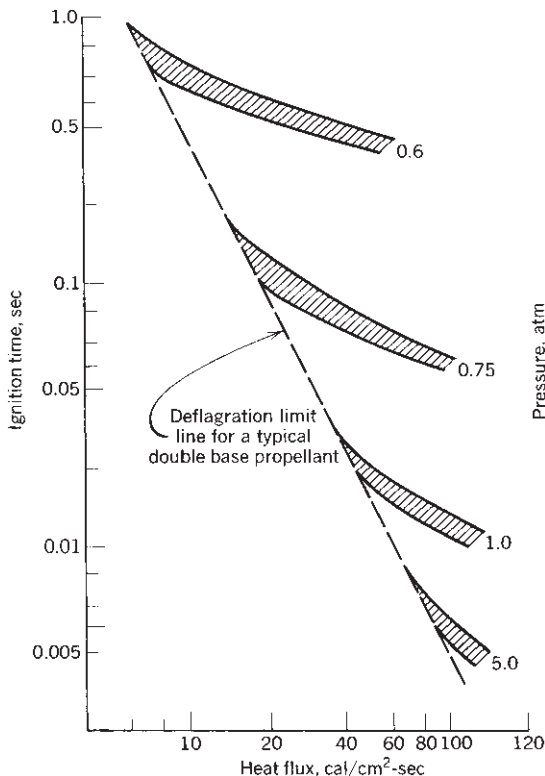


FIGURE 14-4. Propellant ignitability curves: effect of heat flux on ignition time for a specific motor.

14.3. EXTINCTION OR THRUST TERMINATION

Sometimes it is necessary to stop or extinguish the burning of a solid propellant motor before all the propellant has been consumed:

1. When a flight vehicle has reached the desired flight velocity (for a ballistic missile to attain a predetermined velocity or for a satellite to achieve an accurate orbit), or a precise total impulse cutoff is needed
2. As a safety measure, when it appears that a flight test vehicle will unexpectedly fly out of the safe boundaries of a flight test range facility
3. To avoid collisions of stages during a stage separation maneuver (requiring a thrust reversal) for multistage flight vehicles
4. During research and development testing, when one wants to examine a partially burned motor

The common mechanisms for achieving extinction are listed below and described in Chapters 2, 5, and 6 of Ref. 14–1.

1. *Very rapid depressurization*, usually by a sudden, large increase of the nozzle throat area or by fast opening of additional gas escape areas or ports. The most common technique neutralizes the thrust or reverses the net thrust direction by suddenly opening exhaust ports in the forward end of the motor case. Such a thrust reversal using ports located on the forward bulkhead of the case is achieved in the upper stages of Minuteman and Poseidon missiles. This is done by highly predictable and reproducible explosive devices which suddenly open additional gas escape areas (thus causing pressure reduction) and neutralize the thrust by exhausting gases in a direction opposite to that of the motor nozzle. To balance side forces, the thrust termination blow-out devices and their ducts are always designed in symmetrically opposed sets (two or more). In Fig. 1–5 there are four symmetrically placed openings that are blown into the forward dome of the case by circular explosive cords. Two of the sheathed circular cord assemblies are sketched on the outside of the forward dome wall. The ducts that lead the hot gas from these openings to the outside of the vehicle are not shown in this figure. The forward flow of gas occurs only for a very brief period of time, during which the thrust is actually reversed. The rapid depressurization causes a sudden stopping of the combustion at the propellant burning surface. With proper design the explosive cords do not cause a detonation or explosion of the remaining unburned propellant.
2. During some motor development projects it can be helpful to see a partially consumed grain. The motor operation is stopped when the flames are quenched by an inhibiting liquid such as water. Reference 14–12 shows that adding a detergent to the water allows better contact with the burning surface and reduces the amount of water needed for quenching.
3. *Lowering the combustion pressure* below the pressure deflagration limit. Compared to item 1, this depressurization occurs quite slowly. Many solid propellants have a low-pressure combustion limit of 0.05 to 0.15 MPa. This means that some propellants will not extinguish when vented during a static sea-level test at 1 atm (0.1 MPa) but will stop burning if vented at high altitude.

A sudden depressurization is effective because the primary combustion zone at the propellant surface has a time lag compared to the gaseous combustion zone which, at the lower pressure, quickly adjusts to a lower reaction rate and moves farther away from the burning surface. The gases created by the vaporization and pyrolysis of the hot solid propellant cannot all be consumed in a gas reaction close to the surface, and some will not burn completely. As a result, the heat transfer to the propellant surface will be quickly reduced by several orders of magnitude, and the reaction at the propellant surface will diminish and

stop. Experimental results (Chapter 12 of Ref. 14–1) show that a higher initial combustion pressure requires a faster depressurization rate (dp/dt) to achieve extinction.

14.4. COMBUSTION INSTABILITY

There are two types of combustion instability: a set of acoustic resonances or pressure oscillations, which can occur with any rocket motor, and vortex shedding phenomena, which occur only with relatively large segmented grains or in grains with circular slots.

Acoustic Instabilities

When a solid propellant rocket motor experiences unstable combustion, the pressure in the interior gaseous cavities (made up by the volume of the port or perforations, fins, slots, conical or radial grooves) oscillates by at least 5% and often by more than 30% of the chamber pressure. When instability occurs, the heat transfer to the burning surfaces, the nozzle, and the insulated case walls is greatly increased; the burning rate, chamber pressure, and thrust usually increase; but the burning duration is thereby decreased. The change in the thrust–time profile causes significant changes in the flight path, and at times this can lead to failure of the mission. If prolonged and if the vibration energy level is high, the instability can cause damage to the hardware, such as overheating the case and causing a nozzle or case failure. Instability is a condition that should be avoided and must be carefully investigated and remedied if it occurs during a motor development program. Final designs of motors must be free of such instability.

There are fundamental differences with liquid propellant combustion behavior. In liquid propellants there is a fixed chamber geometry with a rigid wall; liquids in feed systems and in injectors that are not part of the oscillating gas in the combustion chamber, can interact strongly with the pressure fluctuations. In solid propellant motors the geometry of the oscillating cavity increases in size as burning proceeds and there are stronger damping factors, such as solid particles and energy-absorbing viscoelastic materials. In general, combustion instability problems do not occur frequently or in every motor development, and, when they do occur, it is rarely the cause for a drastic sudden motor failure or disintegration. Nevertheless, drastic failures have occurred.

Undesirable oscillations in the combustion cavity propellant rocket motors is a continuing problem in the design, development, production, and even long-term (10 yr) retention of solid rocket missiles. While acoustically “softer” than a liquid rocket combustion chamber, the combustion cavity of a solid propellant rocket is still a low-loss acoustical cavity containing a very large acoustical energy source, the combustion process itself. A small fraction of the energy released by combustion is more than sufficient to drive pressure vibrations to an unacceptable level.

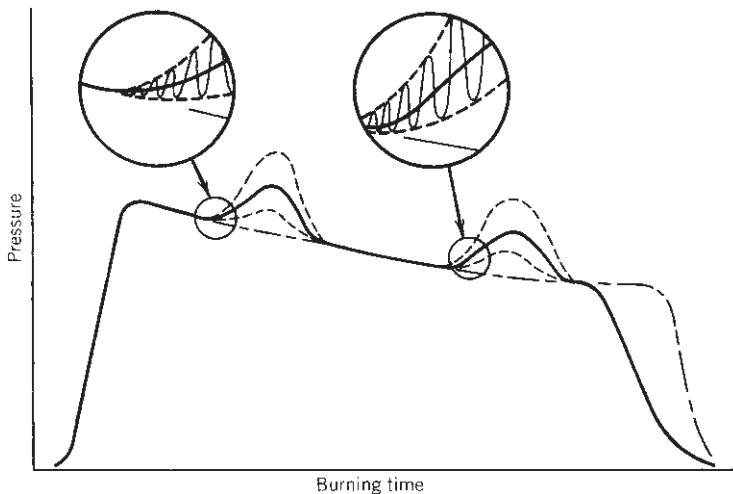


FIGURE 14-5. Simplified diagram showing two periods of combustion instability in the pressure-time history, with enlargements of two sections of this curve. The dashed lines show the upper and lower boundaries of the high-frequency pressure oscillations, and the dot-dash curve is the behavior without instability after a slight change in propellant formulation. The vibration period shows a rise in the mean pressure. With vibration, the effective burning time is reduced and the average thrust is higher. The total impulse is essentially unchanged.

Combustion instability can occur spontaneously, often at some particular time during the motor burn period, and the phenomenon is usually repeatable in identical motors. Both longitudinal and transverse waves (radial and tangential) can occur. Figure 14-5 shows a pressure-time profile with typical instability. The pressure oscillations increase in magnitude, and the thrust and burning rate also increase. The frequency seems to be a function of the cavity geometry, propellant composition, pressure, and internal flame field. As the internal grain cavity is enlarged and local velocities change, the oscillation often abates and disappears. The time and severity of the combustion vibration tend to change with the ambient grain temperature prior to motor operation.

For a simple grain with a cylindrical port area, the resonant transverse mode oscillations (tangential and radial) correspond roughly to those shown in Fig. 9-4 for liquid propellant thrust chambers. The longitudinal or axial modes, usually at a lower frequency, are an acoustic wave traveling parallel to the motor axis between the forward end of the perforation and the convergent nozzle section. Harmonic frequencies of these basic vibration modes can also be excited. The internal cavities can become very complex and can include igniter cases, movable as well as submerged nozzles, fins, cones, slots, star-shaped perforations, or other shapes, as described in the section on grain geometry in Chapter 12; determination of the resonant frequencies of complex cavities is not always easy. Furthermore, the geometry of the internal resonating cavity changes continually as the burning

propellant surfaces recede; as the cavity volume becomes larger, the transverse oscillation frequencies are reduced.

As the internal grain cavity grows, the resonant frequency changes and the instability abates and then disappears. Figure 14–5 shows two instances where a combustion instability was triggered and its amplitude increased for a brief period and then diminished, the frequency decreased (due to cavity volume increase) and then the instability disappeared. Nevertheless, the resulting thrust–time curve is different and the flight path will be changed, often preventing the reaching of a mission target.

The *bulk mode*, also known as the Helmholtz mode, L^* mode, or chuffing mode, is not a wave mode as described above. It occurs at relatively low frequencies (typically below 150 Hz and sometimes below 1 Hz), and the pressure is essentially uniform throughout the volume. The unsteady velocity is close to zero, but the pressure rises and falls. It is the gas motion (in and out of the nozzle) that corresponds to the classical Helmholtz resonator mode, similar to exciting a tone when blowing across the open mouth of a bottle (see Fig. 9–7). It occurs at low values of L^* (see Eq. 8–9), sometimes during the ignition period, and disappears when the motor internal volume becomes larger or the chamber pressure becomes higher. *Chuffing* is the periodic low-frequency discharge of a bushy, unsteady flame of short duration (typically less than 1 sec) followed by periods of no visible flame, during which slow out-gassing and vaporization of the solid propellant accumulates hot gas in the chamber. The motor experiences spurts of combustion and consequent pressure buildup followed by periods of nearly ambient pressure. This dormant period can extend for a fraction of a second to a few seconds (Ref. 14–13 and Chapter 13 by Price in Ref. 14–1).

A useful method of visualizing unstable pressure waves is shown in Figs. 9–5 and 14–6 and Ref. 14–14. It consists of a series of Fourier analyses of the measured pressure vibration spectrum, each taken at a different time in the burning duration and displayed at successive vertical positions on a time scale, providing a map of amplitude versus frequency versus burning time. This figure shows a low-frequency axial mode and two tangential modes, whose frequency is reduced in time by the enlargement of the cavity; it also shows the timing of different vibrations, and their onset and demise.

The initiation or triggering of a particular vibration mode is still not well understood but has to do with energetic combustion at the propellant surface. A sudden change in pressure is known to be a trigger, such as when a piece of broken-off insulation or unburned propellant flows through the nozzle and temporarily blocks all or a part of the nozzle area (causing a momentary pressure rise).

The shifting balance between amplifying and damping factors changes during the burning operation and this causes the growth and also the abatement of specific modes of vibration. The *response* of a solid propellant describes the change in the gas mass production or energy release at the burning surface when it is stimulated by pressure perturbations. When a momentary high-pressure peak occurs on the surface, it increases the instantaneous heat transfer and thus the burning rate, causing the mass flow from that surface to also increase. Velocity

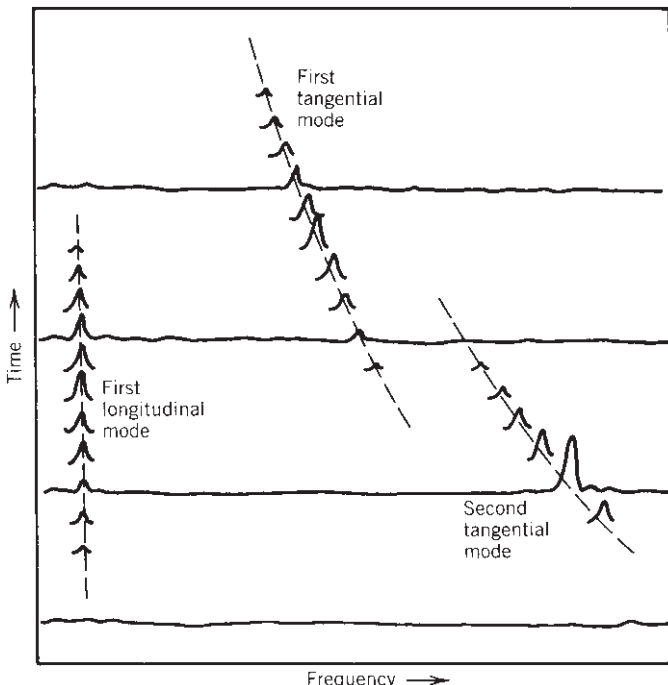


FIGURE 14-6. Example of mode frequency display; also called a “waterfall” diagram of a motor firing. Only four complete time–frequency curves are shown; for easy visualization the other time lines are partly omitted except near the resonating frequencies. The height of the wave is proportional to pressure. As the cavity volume increases, the frequencies of the transverse modes decrease. (Adapted from E. W. Price, Chapter 13 of Ref. 14-1, with permission of AIAA.)

perturbations along the burning surface are also believed to cause changes in mass flow. Phenomena that contribute to amplifying the vibrations, or to gains in the acoustic energy (see Ref. 14-1, Chapter 13 by Price), are:

1. The dynamic response of the combustion process to a flow disturbance or the oscillations in the burning rate. This combustion response can be determined from tests of T-burners as described on the following pages. The response function depends on the frequency of these perturbations and the propellant formulation. The combustion response may not be in a phase with the disturbance. The effects of boundary layers on velocity perturbations have been investigated in Ref. 14-15.
2. Interactions of flow oscillations with the main flow, similar to the basis for the operation of musical wind instruments or sirens (see Ref. 14-16).
3. The fluid dynamic influence of vortices.

Phenomena that contribute to a diminishing of vibration or to damping are energy-absorbing processes; they include the following:

1. Viscous damping in the boundary layers at the walls or propellant surfaces.
2. Damping by particles or droplets flowing in an oscillating gas/vapor flow is often substantial. The particles accelerate and decelerate by being “dragged” along by the motion of the gas, a viscous flow process that absorbs energy. The attenuation for each particular vibration frequency is an optimum at a particular size of particles; high damping for low-frequency oscillation (large motors) occurs with relatively large solid particles (8 to 20 μm); for small motors or high-frequency waves the best damping occurs with small particles (2 to 6 μm). The attenuation drops off sharply if the particle size distribution in the combustion gas is not concentrated near the optimum for damping.
3. Energy from longitudinal and mixed transverse/longitudinal waves is lost out through the exhaust nozzle. Energy from purely transverse waves does not seem to be damped by this mechanism.
4. Acoustic energy is absorbed by the viscoelastic solid propellant, insulator, and the motor case; its magnitude is difficult to estimate.

The *propellant characteristics* have a strong effect on the susceptibility to instability. Changes in the binder, particle-size distribution, ratio of oxidizer to fuel, and burn-rate catalysts can all affect stability, often in ways that are not predictable. All solid propellants can experience instability. As a part of characterizing a new or modified propellant (e.g., determining its ballistic, mechanical, aging, and performance characteristics), many companies now also evaluate it for its stability behavior, as described below.

Analytical Models and Simulation of Combustion Stability

Many investigations have been aimed at mathematical models that will simulate the combustion behavior of solid propellants. This was reviewed by T'ien in Chapter 14 of Ref 14–1. Several aspects of *combustion stability* are treated in some depth in Refs. 14–17 and 14–18.

Using computers it has been possible to successfully simulate the combustion for some limited cases, such as for validating or extrapolating experimental results or making limited predictions of the stability of motor designs. This applies to well-characterized propellants, where empirical constants (such as propellant response or particle-size distribution) have been determined and where the range of operating parameters, internal geometries, or sizes has been narrow. It is unlikely that a reliable simple analysis will be found for predicting the occurrence, severity, nature, and location of instability for a given propellant and motor design. The physical and chemical phenomena are complex, multidimensional, unsteady, nonlinear, influenced by many variables, and difficult to emulate mathematically without a good number of simplifying assumptions. However,

theoretical analysis gives insight into the physical phenomena, can be a valuable contributor to solving instability problems, and has been used for preliminary design evaluation of grain cavities.

Combustion Stability Assessment, Remedy, and Design

In contrast with liquid rocket technology, an accepted combustion stability rating procedure does not now exist for full-scale solid rockets. Undertaking stability tests on large full-scale flight-hardware rocket motors is expensive, and therefore lower-cost methods, such as subscale motors, T-burners, and other test equipment, have been used to assess motor stability.

The best known and most widely used method of gaining combustion stability-related data is the use of a *T-burner*, an indirect, limited method that does not use a full-scale motor. Figure 14–7 is a sketch of a standard T-burner; it has a 1.5-in. internal diameter double-ended cylindrical burner vented at its midpoint

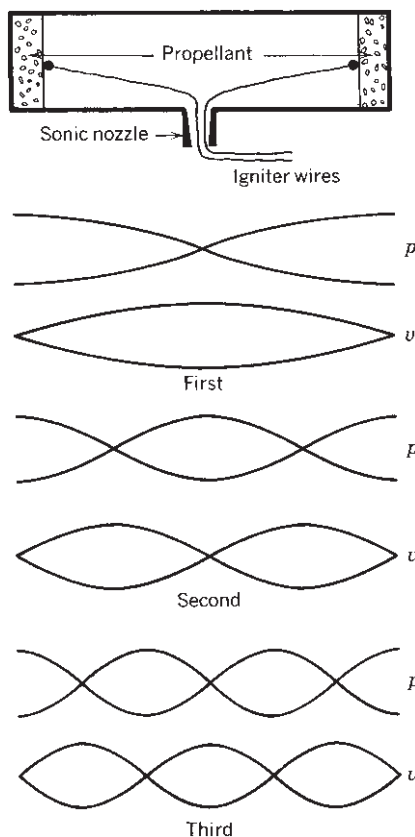


FIGURE 14–7. Standard T-burner and its three longitudinal mode standing waves (pressure and velocity).

(see Ref. 14–19). Venting can be through a sonic nozzle to the atmosphere or by a pipe connected to a surge tank which maintains a constant level of pressure in the burner cavity. T-burner design and usage usually concentrate on the portion of the frequency spectrum dealing with the transverse oscillations expected in a full-scale motor. The desired acoustical frequency, to be imposed on the propellant charge as it burns, determines the burner length (distance between closed ends).

The nozzle location, midway between the ends of the T-burner, minimizes attenuation of fundamental longitudinal mode oscillations (in the propellant grain cavity). Theoretically, an acoustic pressure node exists at the center and antinodes occur at the ends of the cavity. Acoustic velocity nodes are out of phase with pressure waves and occur at the ends of the burner. Propellant charges are often in the shape of disks or cups cemented to the end faces of the burner. The gas velocity in the burner cavity is kept intentionally low (Mach 0.2 or less) compared with the velocity in a full-scale motor. This practice minimizes the influence of velocity-coupled energy waves and allows the influence of pressure-coupled waves to be more clearly recognized.

Use of the T-burner for assessing the stability of a full-scale solid rocket presupposes valid theoretical models of the phenomena occurring in both the T-burner and the actual rocket motor; these theories are still not fully validated. In addition to assessing solid rocket motor combustion stability, the T-burner also is used to evaluate new propellant formulations and the importance of seemingly small changes in ingredients, such as a change in aluminum powder particle size and oxidizer grind method.

Once an instability has been observed or predicted in a given motor, the designer has to fix the problem. There is no sure method for selecting the remedy, and none of the cures suggested below may work. The usual alternatives are:

1. Changing the grain geometry to shift the frequencies away from the undesirable values. Sometimes, changing fin locations, port cross-section profile, or number of slots has been successful.
2. Changing the propellant composition. Using aluminum as an additive has been most effective in curing transverse instabilities, provided that the particle-size distribution of the aluminum oxide is favorable to optimum damping at the distributed frequency. Changing size distribution and using other particulates (Zr , Al_2O_3 , or carbon particles) has been effective in some cases. Sometimes changes in the binder have worked.
3. Adding a mechanical device for attenuating the unsteady gas motions or changing the natural frequency of cavities. Various inert resonance rods, baffles, or paddles have been added, mostly as a fix to an existing motor with observed instability. They can change the resonance frequencies of cavities, but introduce additional viscous surface losses, and cause extra inert mass and potential problems with heat transfer or erosion.

Combustion instability has to be addressed during the design process, usually through a combination of some mathematical simulation, understanding similar problems in other motors, studies of possible changes, and supporting experimental work (e.g., T-burners, measuring particle-size distribution). Most solid propellant rocket companies have in-house two- and three-dimensional computer programs to calculate the likely acoustic modes (axial, tangential, radial, and combinations of these) for a given grain/motor, the initial and intermediate cavity geometries, and the combustion gas properties calculated from thermochemical analysis. Data on combustion response (dynamic burn rate behavior) and damping can be obtained from T-burner tests. Data on particle sizes can be estimated from prior experience, observation through windows or plume measurements (Ref. 14–20). Estimates of nozzle losses, friction, or other damping need to be included. Depending on the balance between gain and damping, it may be possible to arrive at conclusions on the grain's propensity to instability for each specific instability mode that is analyzed. If unfavorable, either the grain geometry or the propellant usually have to be modified. If favorable, full-scale motors have to be built and tested to validate the predicted stable burning characteristics. There is always a trade-off between the amount of work spent on extensive analysis, subscale experiments, and computer programs (which will not always guarantee a stable motor) and taking a chance that a retrofit will be needed after full-scale motors have been tested. If the instability is not discovered until after the motor is in production, it is usually more difficult, time consuming, and expensive to fix the problem.

Vortex-Shedding Instability

This instability is associated with burning on the inner surfaces of slots in the grain. Large segmented rocket motors have slots between segments, and some grain configurations have slots that intersect the centerline of the grain. Figure 14–8 shows that hot gases from the burning slot surfaces enter the main flow in the perforation or central cavity of the grain. The hot gas from the slot is turned into a direction toward the nozzle. The flow from the side stream restricts the flow emanating from the upstream side of the perforation and, in effect, reduces the port area. This restriction causes the upstream port pressure to rise; sometimes there is a substantial pressure rise. The interaction of the two subsonic gas flows causes turbulence. Vortices form and are periodically shed or allowed to flow downstream, thereby causing an unstable flow pattern. The vortex shedding patterns can interact with the acoustic instabilities. Reference 14–21 gives a description and Ref. 14–22 a method for analyzing these vortex-shedding phenomena. The remedy usually is to apply inhibitors to some burning surfaces or to change the grain geometry; for example, by increasing the width of the slot, the local velocities are reduced and the vortices become less pronounced.

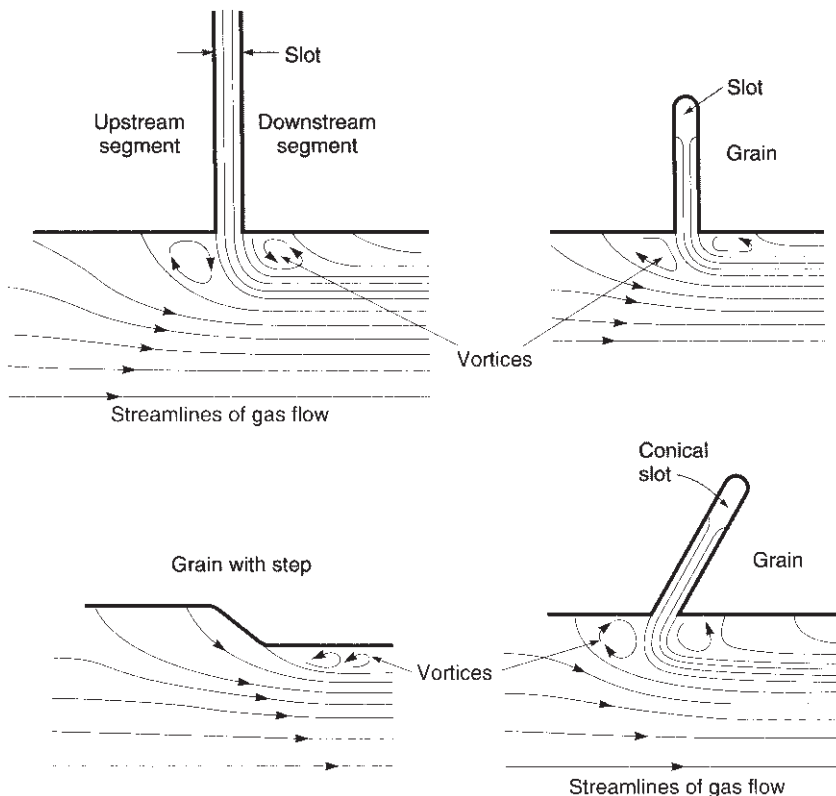


FIGURE 14-8. Simple sketches of four partial grain sections each with a slot or a step. Heavy lines identify the burning surfaces. The flow patterns cause the formation of vortices. The shedding of these vortices can induce flow oscillations and pressure instabilities.

PROBLEMS

1. (a) Calculate the length of a T-burner to give a first natural oscillation of 2000 Hz using a propellant that has a combustion temperature of 2410 K, a specific heat ratio of 1.25, a molecular mass of 25 kg/kg-mol, and a burning rate of 10.0 mm/sec at a pressure of 68 atm. The T-burner is connected to a large surge tank and prepressurized with nitrogen gas to 68 atm. The propellant disks are 20 mm thick. Make a sketch to indicate the T-burner dimensions, including the disks.
- (b) If the target frequencies are reached when the propellant is 50% burned, what will be the frequency at propellant burnout?

Answers: (a) Length before applying propellant = 0.270 m (b) frequency at burnout = 1854 Hz

2. An igniter is needed for a rocket motor similar to one shown in Fig. 12–1. Igniters have been designed by various oversimplified design rules such as Fig. 14–3. The motor has an initial internal grain cavity volume of 0.055 m^3 and an initial burning surface of 0.72 m^2 . The proposed igniter propellant has these characteristics: combustion temperature 2500 K and an energy release of about 40 J/kg-sec . Calculate the minimum required igniter propellant mass **(a)** if the cavity has to be pressurized to about 2 atm (ignore heat losses); **(b)** if only 6% of the igniter gas energy is absorbed at the burning surface, and it requires about $20 \text{ cal/cm}^2\text{-sec}$ to ignite in about 0.13 sec .
3. Using the data from Fig. 14–4, plot the total heat flux absorbed per unit area versus pressure to achieve ignition with the energy needed to ignite being just above the deflagration limit. Then, for 0.75 atm , plot the total energy needed versus ignition time. Give an interpretation of the results and trend for each of the two curves.

REFERENCES

- 14–1. N. Kubota, “Survey of Rocket Propellants and Their Combustion Characteristics,” Chapter 1; K. Kishore and V. Gayathri, “Chemistry of Ignition and Combustion of Ammonium-Perchlorate-Based Propellants,” Chapter 2; T. L. Boggs, “The Thermal Behavior of Cyclotrimethylene Trinitrate (RDX) and Cyclotetramethylene Tetranitrate (HMX),” Chapter 3; R. A. Fifer, “Chemistry of Nitrate Ester and Nitramine Propellants,” Chapter 4; C. E. Hermance, “Solid Propellant Ignition Theories and Experiments,” Chapter 5; M. Kumar and K. K. Kuo, “Flame Spreading and Overall Ignition Transient,” Chapter 6; E. W. Price, “Experimental Observations of Combustion Instability,” Chapter 13; J. S. T’ien, “Theoretical Analysis of Combustion Instability,” Chapter 14; all in K. K. Kuo and M. Summerfield (Eds.), *Fundamentals of Solid-Propellant Combustion*, Vol. 90, *Progress in Astronautics and Aeronautics*, American Institute of Aeronautics and Astronautics, New York, 1984.
- 14–2. G. Lengelle, J. Duterque, and J. F. Trubert, “Physico-Chemical Mechanisms of Solid Propellant Combustion,” Chapter 2.2 in V. Yang, T. B. Brill, and W.-Z. Ren (Eds.), *Solid Propellant Chemistry, Combustion, and Motor Interior Ballistics*, Vol. 185, *Progress in Astronautics and Aeronautics*, AIAA, Reston VA, 2000.
- 14–3. C. Youfang, “Combustion Mechanism of Double-Base Propellants with Lead Burning Rate Catalyst,” *Propellants, Explosives, Pyrotechnics*, Vol. 12, 1987, pp. 209–214.
- 14–4. N. Kubota et al., “Combustion Wave Structures of Ammonium Perchlorate Composite Propellants,” *Journal of Propulsion and Power*, Vol. 2, No. 4, July–August 1986, pp. 296–300.
- 14–5. T. Boggs, D. E. Zurn, H. F. Cordes, and J. Covino, “Combustion of Ammonium Perchlorate and Various Inorganic Additives,” *Journal of Propulsion and Power*, Vol. 4, No. 1, January–February 1988, pp. 27–39.
- 14–6. T. Kuwahara and N. Kubota, “Combustion of RDX/AP Composite Propellants at Low Pressure,” *Journal of Spacecraft and Rockets*, Vol. 21, No. 5, September–October 1984, pp. 502–507.
- 14–7. P. A. O. G. Korting, F. W. M. Zee, and J. J. Meulenbrugge, “Combustion Characteristics of Low Flame Temperature, Chlorine-Free Composite Propellants,” *Journal of Propulsion and Power*, Vol. 6, No. 3, May–June 1990, pp. 250–255.

- 14–8. N. Kubota and S. Sakamoto, “Combustion Mechanism of HMX,” *Propellants, Explosives, Pyrotechnics*, Vol. 14, 1989, pp. 6–11.
- 14–9. L. H. Caveny, K. K. Kuo, and B. J. Shackleford, “Thrust and Ignition Transients of the Space Shuttle Solid Rocket Booster Motor,” *Journal of Spacecraft and Rockets*, Vol. 17, No. 6, November–December 1980, pp. 489–494.
- 14–10. “Solid Rocket Motor Igniters,” NASA SP-8051, March 1971 (N71-30346).
- 14–11. I. H. Cho and S. W. Baek, “Numerical Simulation of Axisymmetric Solid Rocket Motor Ignition with Radiation Effect,” *Journal of Propulsion and Power*, Vol. 16, No. 4, July–August 2000, pp. 725–728.
- 14–12. J. Yin and B. Zhang, “Experimental Study of Liquid Quenching of Solid Rocket Motors,” AIAA Paper 90–2091.
- 14–13. B. N. Raghunandam and P. Bhaskariah, “Some New Results of Chuffing in Composite Solid Propellant Rockets,” *Journal of Spacecraft and Rockets*, Vol. 22, No. 2, March–April 1985, pp. 218–220.
- 14–14. P. M. J. Hughes and E. Cerny, “Measurement and Analysis of High Frequency Pressure Oscillations in Solid Rocket Motors,” *Journal of Spacecraft and Rockets*, Vol. 21, No. 3, May–June 1984, pp. 261–265.
- 14–15. R. A. Beddini and T. A. Roberts, “Response of Propellant Combustion to a Turbulent Acoustic Boundary Layer,” *Journal of Propulsion and Power*, Vol. 8, No. 2, March–April 1992, pp. 290–296.
- 14–16. F. Vuillot and G. Avalon, “Acoustic Boundary Layers in Solid Propellant Rocket Motors Using Navier-Stokes Equations,” *Journal of Propulsion and Power*, Vol. 7, No. 2, March–April 1991, pp. 231–239.
- 14–17. L. De Luca, E. W. Price, and M. Summerfield (Eds.), *Nonsteady Burning and Combustion Stability of Solid Propellants*, Vol. 143, *Progress in Astronautics and Aeronautics*, AIAA, Washington DC, 1992.
- 14–18. V. Yang, T. B. Brill, and W.-Z. Ren (Eds.), *Solid Propellant Chemistry, Combustion, and Motor Interior Ballistics*, Vol. 185, *Progress in Astronautics and Aeronautics*, AIAA, Reston VA, 2000.
- 14–19. R. L. Coates, “Application of the T-Burner to Ballistic Evaluation of New Propellants,” *Journal of Spacecraft and Rockets*, Vol. 3, No. 12, December 1966, pp. 1793–1796; M. Barrere, “Introduction to Nonsteady Burning and Combustion Stability,” Chapter 2, pp. 17–58, and L. D. Strand and R. S. Brown, “Laboratory Test Methods for Combustion Stability Properties of Solid Propellants,” Chapter 17, pp. 689–718, in L. De Luca, E. W. Price, and M. Summerfield (Eds.), *Nonsteady Burning and Combustion Stability of Solid Propellants*, Vol. 143, *Progress in Astronautics and Aeronautics*, AIAA, Washington DC, 1992.
- 14–20. E. D. Youngborg, J. E. Pruitt, M. J. Smith, and D. W. Netzer, “Light-Diffraction Particle Size Measurements in Small Solid Propellant Rockets,” *Journal of Propulsion and Power*, Vol. 6, No. 3, May–June 1990, pp. 243–249.
- 14–21. F. Vuillot, “Vortex Shedding Phenomena in Solid Rocket Motors,” *Journal of Propulsion and Power*, Vol. 11, No. 4, 1995.
- 14–22. A. Kourta, “Computation of Vortex Shedding in Solid Rocket Motors using a Time-Dependent Turbulence Model,” *Journal of Propulsion and Power*, Vol. 15, No. 3, May–June 1999.

CHAPTER 15

SOLID ROCKET COMPONENTS AND MOTOR DESIGN

In this last chapter on solid propellant rockets, we describe the key inert components of solid propellant rocket motors, namely the motor case, nozzle, and igniter case, and then discuss the design of motors. Although the thrust vector control mechanism is also a component of many rocket motors, it is described separately in Chapter 18. The key to the success of many of these components is new materials which have been developed in recent years. Motor case technology and pyrogen igniters are discussed.

15.1. MOTOR CASE

The solid propellant motor case not only contains the propellant grain, but also serves as a highly loaded pressure vessel. Case design and fabrication technology has progressed to where efficient and reliable motor cases can be produced consistently for any solid rocket application. Most problems arise when established technology is used improperly or from improper design analysis, understating the requirements, or improper material and process control, including the omission of nondestructive tests at critical points in the fabrication process. Case design is usually governed by a combination of motor and vehicle requirements. Besides constituting the structural body of the rocket motor with its nozzle, propellant grain, and so on, the case frequently serves also as the primary structure of the missile or launch vehicle. Thus the optimization of a case design frequently entails trade-offs between case design parameters and vehicle design parameters. Often, case design is influenced by assembly and fabrication requirements.

Table 15–1 lists many of the types of loads and their sources; they must be considered at the beginning of a case design. Only some of them apply to any

TABLE 15–1. Rocket Motor Case Loads

| Origin of Load | Type of Load/Stress |
|---|---|
| Internal pressure | Tension biaxial, vibration |
| Axial thrust | Axial, vibration |
| Motor nozzle | Axial, bending, shear |
| Thrust vector control actuators | Axial, bending, shear |
| Thrust termination equipment | Biaxial, bending |
| Aerodynamic control surfaces or wings mounted to case | Tension, compression, bending, shear, torsion |
| Staging | Bending, shear |
| Flight maneuvering | Axial, bending, shear, torsion |
| Vehicle mass and wind forces on launch pad | Axial, bending, shear |
| Dynamic loads from vehicle oscillations | Axial, bending, shear |
| Start pressure surge | Biaxial tension |
| Ground handling, including lifting | Tension, compression, bending, shear, torsion |
| Ground transport | Tension, compression, shear, vibration |
| Earthquakes (large motors) | Axial, bending, shear |

one rocket motor application. In addition, the environmental conditions peculiar to a specific motor and its usage must be carefully considered. Typically, these conditions include the following: (1) temperature (internal heating, aerodynamic heating, ambient temperature cycling during storage, or thermal stresses and strains); (2) corrosion (moisture/chemical, galvanic, stress corrosion, or hydrogen embrittlement); (3) space conditions: vacuum or radiation.

Three classes of materials have been used: high-strength metals (such as steel, aluminum, or titanium alloys), wound-filament reinforced plastics, and a combination of these in which a metal case has externally wound filaments for extra strength. Table 15–2 gives a comparison of several typical materials. For filament-reinforced materials it gives the data not only for the composite material, but also for several strong filaments and a typical binder. The strength-to-density ratio is higher for composite materials, which means that they have less inert mass. Even though there are some important disadvantages, the filament-wound cases with a plastic binder are usually superior on a vehicle performance basis. Metal cases combined with an external filament-wound reinforcement and spiral-wound metal ribbons glued together with plastic have also been successful.

The shape of the case is usually determined from the grain configuration or from geometric vehicle constraints on length or diameter. The case configurations range from long and thin cylinders (L/D of 10) to spherical or near-spherical geometries (see Figs. 1–5, 12–1 to 12–4, and 12–17). The spherical shape gives the lowest case mass per unit of enclosed volume. The case is often a key structural element of the vehicle, and it sometimes has to provide for mounting of other components, such as fins, skirts, electric conduits, or thrust vector control actuators. The propellant mass fractions of the motor are usually strongly

TABLE 15–2. Physical Properties of Selected Solid Propellant Motor Case Materials at 20°C

| Material | Tensile Strength, N/mm ² (10 ³ psi) | Modulus of Elasticity, N/mm ² (10 ⁶ psi) | Density, g/cm ³ (lbm/in. ³) | Strength to Density Ratio (1000) |
|---|--|---|--|-------------------------------------|
| <i>Filaments</i> | | | | |
| E-glass | 1930–3100 (280–450) | 72,000 (10.4) | 2.5 (0.090) | 1040 |
| Aramid (Kevlar 49) | 3050–3760 (370–540) | 124,000 (18.0) | 1.44 (0.052) | 2300 |
| Carbon fiber or graphite fibers | 3500–6900 (500–1000) | 230,000–300,000 (33–43) | 1.53–1.80 (0.055–0.065) | 2800 |
| <i>Binder (by itself)</i> | | | | |
| Epoxy | 83 (12) | 2800 (0.4) | 1.19 (0.043) | 70 |
| <i>Filament-Reinforced Composite Material</i> | | | | |
| E-glass | 1030 (150–170) | 35,000 (4.6–5.0) | 1.94 (0.070) | 500 |
| Kevlar 49 | 1310 (190) | 58,000 (8.4) | 1.38 (0.050) | 950 |
| Graphite IM | 2300 (250–340) | 102,000 (14.8) | 1.55 (0.056) | 1400 |
| <i>Metals</i> | | | | |
| Titanium alloy | 1240 (155–160) | 110,000 (16) | 4.60 (0.166) | 270 |
| Alloy steel (heat treated) | 1400–2000 (200–280) | 207,000 (30) | 7.84 (0.289) | 205 |
| Aluminum alloy 2024 (heat treated) | 455 (66) | 72,000 (10.4) | 2.79 (0.101) | 165 |

Source: Data adapted in part from Chapter 4A by Evans and Chapter 7 by Scippa of Ref. 12–1.

influenced by the case mass and typically range from 0.70 to 0.94. The higher values apply to upper-stage motors. For small-diameter motors the mass fraction is lower, because of practical wall thicknesses and the fact that the ratio of the wall surface area (which varies roughly as the square of the diameter) to chamber volume (which varies roughly as the cube of diameter) is less favorable in small sizes. The minimum thickness is higher than would be determined from simple stress analysis; for a fiber composite case it is two layers of filament strands, and the minimum metal thickness is dictated by manufacturing and handling considerations.

Simple membrane theory can be used to predict the approximate stress in solid propellant rocket chamber cases; this assumes no bending in the case walls and that all the loads are taken in tension. For a simple cylinder of average radius R and thickness d , with a chamber pressure p , the longitudinal stress σ_l is one-half

of the tangential or hoop stress σ_θ :

$$\sigma_\theta = 2\sigma_l = pR/d \quad (15-1)$$

For a cylindrical case with hemispherical ends, the cylinder wall has to be twice as thick as the walls of the end closures.

The combined stress should not exceed the working stress of the wall material. As the rocket motor begins to operate, the internal pressure p causes a growth of the chamber in the longitudinal as well as in the circumferential direction, and these deformations must be considered in designing the support of the motor or propellant grain. Let E be Young's modulus of elasticity, ν be Poisson's ratio (0.3 for steel), and d be the wall thickness; then the growth in length L and in diameter D due to pressure can be expressed as

$$\Delta L = \frac{pLD}{4Ed} (1 - 2\nu) = \frac{\sigma_l L}{E} (1 - 2\nu) \quad (15-2)$$

$$\Delta D = \frac{pD^2}{4Ed} \left(1 - \frac{\nu}{2}\right) = \frac{\sigma_\theta D}{2E} \left(1 - \frac{\nu}{2}\right) \quad (15-3)$$

Details can be found in a text on thin shells or membranes. For a hemispherical chamber end, the stress in each of two directions at right angles to each other is equal to the longitudinal stress of a cylinder of identical radius. For ellipsoidal end-chamber closures, the local stress varies with the position along the surface, and the maximum stress is larger than that of a hemisphere. The radial displacement of a cylinder end is not the same as that of a hemispherical or ellipsoidal closure if computed by thin-shell theory. Thus a discontinuity exists which causes some shearing and bending stresses. Similarly, a boss for the attachment of an igniter, a pressure gauge, or a nozzle can make it necessary for bending and shear stresses to be superimposed on the simple tension stresses of the case. In these locations it is necessary to reinforce or thicken the chamber wall locally.

Finite element computerized stress analysis programs are used in motor design companies today to determine the case design configuration with reasonable stress values. This analysis must be done simultaneously with the stress analysis on the grain (since it imposes loads on the case), and with a finite element thermal analysis to determine thermal stresses and deformations, since these analyses are interdependent on each other.

The fast heating of the inner wall surface produces a large temperature gradient and therefore thermal stresses across the wall. The theory of transient heat transfer has been treated by a number of authors, and, by means of a relaxation method, a reasonable approximation of the temperature-time history at any location may be obtained. The inner wall of the case, which is exposed to hot gas, is usually protected by thermal insulation, as described in Section 13.6. Therefore the heat transfer to the case is very low. In fact, for a single operation (not two thrust periods) it is the designer's aim to keep the case temperatures near ambient or at the most 100°C above ambient.

The case design has to provide means for attaching a nozzle (rarely more than one nozzle), for attaching it to the vehicle, igniters, and provisions for loading the grain. Sometimes there are also attached aerodynamic surfaces (fins), sensing instruments, a raceway (external conduit for electrical wires), handling hooks, and thrust vector control actuators with their power supply. For upper stages of ballistic missiles the case can also include blow-out ports or thrust termination devices, as described in Chapter 14. Typical methods for attaching these items include tapered or straight multiple pins, snap rings, or bolts. Gaskets and/or O-ring seals prevent gas leaks.

Metal Cases

Metal cases have several advantages compared to filament-reinforced plastic cases: they are rugged and will take considerable rough handling (required in many tactical missile applications), are usually reasonably ductile and can yield before failure, can be heated to a relatively high temperature (700 to 1000°C or 1292 to 1832°F and higher with some special materials), and thus require less insulation. They will not deteriorate significantly with time or weather exposure and are easily adapted to take concentrated loads, if made thicker at a flange or boss. Since the metal case has much higher density and less insulation, it occupies less volume than does a fiber-reinforced plastic case; therefore, for the same external envelope it can contain somewhat more propellant.

Figure 15–1 shows the various sections of a typical large solid rocket case made of welded steel. The shape of the case, particularly the length-to-diameter

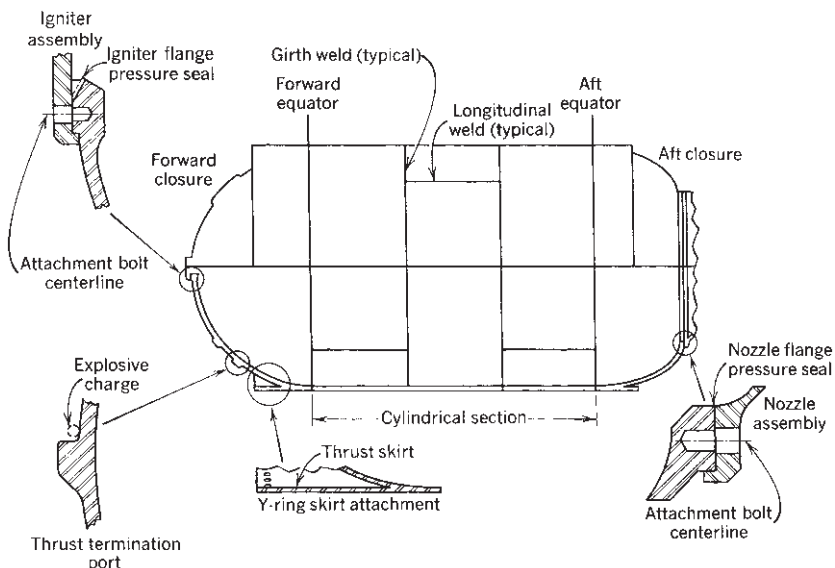


FIGURE 15–1. Typical large solid rocket motor case made of welded alloy steel.

ratio for cylindrical cases, influences not only the stresses to be withstood by the case but the amount of case material required to encase a given amount of propellant. For very large and long motors both the propellant grain and the motor case are made in sections; the *case segments* are mechanically attached and sealed to each other at the launch site. The segmented solid rocket booster for the Space Shuttle is shown in Fig. 15–2 and discussed in Ref. 15–1. For the critical seal between the segments a multiple-O-ring joint is often used, as shown in Fig. 15–3 and discussed in Ref. 15–2. Segments are used when an unsegmented motor would be too large and too heavy to be transported over ordinary roads (cannot make turns) or railways (will not go through some tunnels or under some bridges) and are often too difficult to fabricate.

Small metal *cases for tactical missile motors* can be extruded or forged (and subsequently machined), or made in three pieces as shown in Fig. 12–4. This case is designed for loading a freestanding grain and the case, nozzle, and blast tube are sealed by O-rings (see Chapter 6 of Ref. 15–3 and Chapter 7 of Ref. 15–4). Since the mission velocities for most tactical missiles are relatively low (100 to 1500 m/sec), their propellant mass fractions are also relatively low (0.5 to 0.8) and the percentage of inert motor mass is high. Safety factors for tactical missile cases are often higher to allow for rough handling and cumulative damage. The emphasis in selecting motor cases (and other hardware components) for tactical missiles is therefore not on highest performance (lowest inert motor mass), but on reliability, long life, low cost, safety, ruggedness, or survivability.

High-strength alloy steels have been the most common case metals, but others, like aluminum, titanium, and nickel alloys, have also been used. Table 15–2 gives

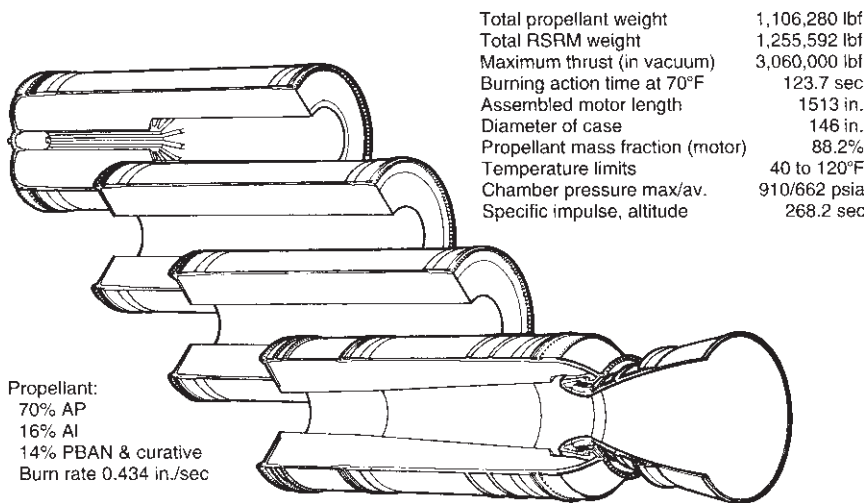


FIGURE 15–2. Simplified diagram of the four segments of the Space Shuttle solid rocket motor. Details of the thrust vector actuating mechanism or the ignition system are not shown. (Courtesy of NASA and ATK launch systems.)

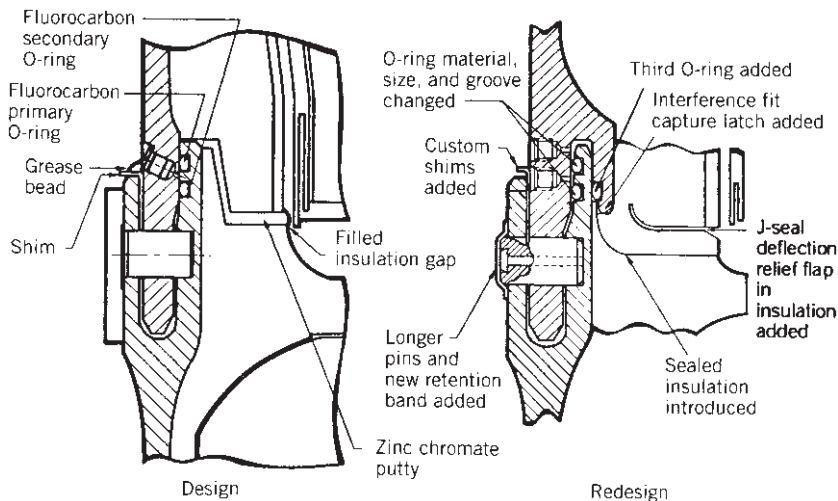


FIGURE 15–3. The joints between segments of the Shuttle solid rocket booster (SRB) were redesigned after a dramatic failure. The improvements were not only in a third O-ring, the mechanical joint, and its locking mechanism, but also featured a redesign of the insulation between propellant segments. (Courtesy of NASA.)

a comparison of motor case material properties. Extensive knowledge exists for designing and fabricating motor cases with low-alloy steels with strength levels to 240,000 psi.

The *maraging steels* have strengths up to approximately 300,000 psi in combination with high fracture toughness. The term *maraging* is derived from the fact that these alloys exist as relative soft low-carbon martensites in the annealed condition and gain high strength from aging at relatively low temperatures.

Stress-corrosion cracking of certain metals presents a unique problem which can result in spontaneous failure without any visual evidence of impending catastrophe. Emphasis given to lightweight thin metal cases aggravates stress corrosion and crack propagation, often starting from a flaw in the metal, with failure occurring at a stress level below the yield strength of the metal.

Wound-Filament-Reinforced Plastic Cases

Filament-reinforced cases use continuous filaments of strong fibers wound in precise patterns and bonded together with a plastic, usually an epoxy resin. Their principal advantage is their lower weight. Most plastics soften when they are heated above about 180°C or 355°F; they need inserts or reinforcements to allow fastening or assembly of other components and to accept concentrated loads. The thermal expansion of reinforced plastics is often higher than that of metal and the thermal conductivity is much lower, causing a higher temperature gradient. References 15–3 and 15–4 explain the design and winding of these composite cases, and Ref. 15–5 discusses their damage tolerance.

Typical fiber materials are, in the order of increasing strength, glass, aramids (Kevlar), and carbon, as listed in Table 15–2. Typically, the inert mass of a case made of carbon fiber is about 50% of a case made with glass fibers and around 67% of a case mass made with Kevlar fibers.

Individual fibers are very strong in tension (2400 to 6800 MPa or 350,000 to 1,000,000 psi). The fibers are held in place by a plastic binder of relatively low density; it prevents fibers slipping and thus weakening in shear or bending. In a filament-wound composite (with tension, hoop, and bending stresses) the filaments are not always oriented along the direction of maximum stress and the material includes a low-strength plastic; therefore, the composite strength is reduced by a factor of 3 to 5 compared to the strength of the filament itself. The plastic binder is usually a thermosetting epoxy material, which limits the maximum temperature to between 100 and 180°C or about 212 and 355°F. Although resins with higher temperature limits are available (295°C or 563°F), their adhesion to the fibers has not been as strong. The safety factors used (in deterministic structural analysis) are typically for failure to occur at 1.4 to 1.6 times the maximum operating stress, and proof testing is done to 1.15 to 1.25 times the operating pressure.

A typical case design is shown schematically in Fig. 15–4. The forward end, aft end, and cylindrical portion are wound on a preform or mold which already contains the forward and aft rings. The direction in which the bands are laid onto the mold and the tension that is applied to the bands is critical in obtaining a good case. The curing is done in an oven and may be done under pressure to assure high density and minimum voids of the composite material. The preform is then

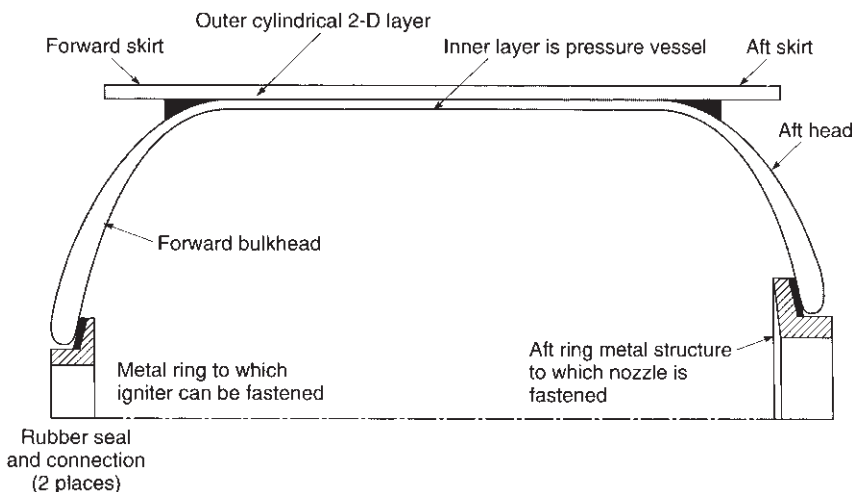


FIGURE 15–4. Simplified half-section of a typical design of a filament-wound composite material case. Elastomeric adhesives are shown in black. The outer layer reinforces the cylinder portion and provides attachment skirts. The thickness of the inner case increases at smaller diameter.

removed. One way is to use sand with a water-soluble binder for the preform; after curing the case, the preform is washed out with water. Since filament-wound case walls can be porous, they must be sealed. The liner between the case and the grain can be the seal that prevents hot gases from seeping through the case walls. Scratches, dents, and moisture absorption can degrade the strength of the case.

In some designs the insulator is placed on the preform before winding and the case is cured simultaneously with the insulator, as seen in Ref. 15–6. In another design the propellant grain with its forward and aft closures is used as the preform. A liner is applied to this grain, then an insulator, and the high-strength fibers of the case are wound in layers directly over the insulated live propellant. Curing has to be done at a relatively low temperature so that the propellant will not be adversely affected. This process works well with extruded cylindrical grains. There are also cylindrical cases made of steel with an overwrap layer of filament-wound composite material, as described in Ref. 15–7.

The allowable stresses are usually determined from tensile tests of a roving or band and rupture tests on subscale composite cases made by an essentially identical filament winding process. Some companies reduce the allowable strength to account for the degradation due to moisture, manufacturing imperfections, or nonuniform density.

In a motor case the filaments must be oriented in the direction of principal stress and must be proportioned in number to the magnitude of stress. Compromise occurs around parts needed for nozzles, igniters, and so on, and then orientation is kept as close to the ideal as is practicable. Filaments are customarily clustered in *yarns*, *rovings*, or *bands*, as defined in Fig. 15–5. By using two or more winding angles (i.e., helicals and circumferentials) and calculating the proportion of filaments in each direction, a balanced stress structure is achieved. The ideal in balance is for each fiber in each direction to carry an equal load (tension only). Realistically, the filaments supported by the epoxy resin must absorb stress compression, bending loads, cross-laminar shear, and interlaminar shear. Even though the latter stresses are small compared to the tensile stress, each must be examined by analysis since each can lead to case failure before a filament fails in tension. In a proper design, failure occurs when the filaments reach their ultimate tensile strength, rather than because of stresses in other directions. Figure 18–5 shows a cross section of a Kevlar filament motor case and flexible nozzle made of ablative materials.

15.2. NOZZLES*

The supersonic nozzle provides for the expansion of the hot gases and has to withstand the severe environment of high heat transfer and erosion. Advances in material technology have allowed substantial mass reductions and performance

*In the 7th edition of this book this nozzle section was revised and partly rewritten by Terry A. Boardman of the predecessor organization to ATK launch systems.

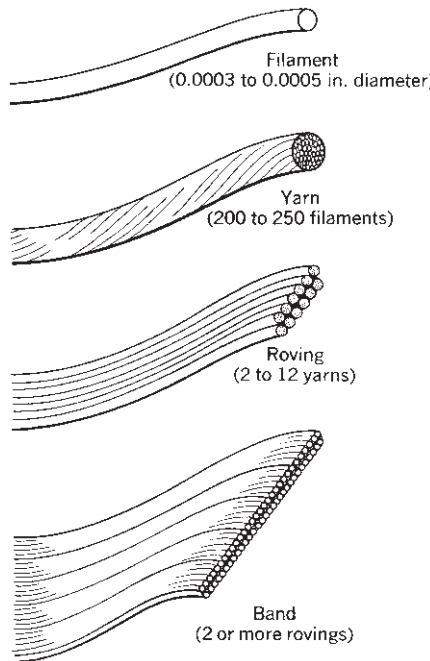


FIGURE 15–5. Filament winding terminology (each sketch is drawn to a different scale).

improvements. Nozzles range in size from 0.05 in. throat diameter to about 54 in., with operating durations of a fraction of a second to several minutes (see Chapters 2 and 3 of Ref. 15–3 and Chapter 6 in Ref. 15–4).

Classification

Nozzles for solid propellant rocket motors can be classified into five categories as listed below and shown in Fig. 15–6.

1. *Fixed Nozzle.* Simple and used frequently in tactical weapon propulsion systems for short-range air-, ground-, and sea-launched missiles, also as strap-on propulsion for space launch vehicles such as Atlas and Delta, and in spacecraft motors for orbital transfer. Typical throat diameters are between 0.25 and 5 in. for tactical missile nozzles and approximately 10 in. for some strap-on motors. Fixed nozzles are generally not submerged (see below) and do not provide thrust vector control (although there are exceptions). See Fig. 15–7.
2. *Movable Nozzle.* Provides thrust vector control for the flight vehicle. As explained in Chapter 18, one movable nozzle can provide pitch and yaw control and two are needed for roll control. Movable nozzles are typically submerged and use a flexible sealed joint or bearing with two actuators

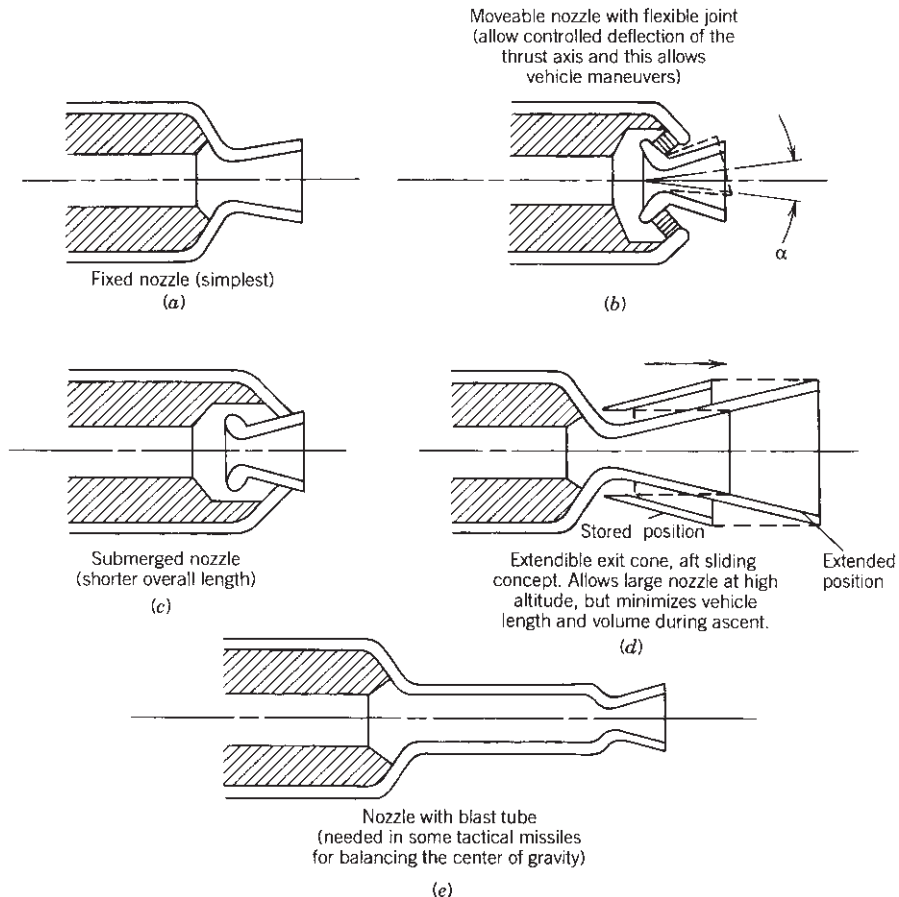


FIGURE 15–6. Simplified diagrams of five common nozzle configurations.

90 degrees apart to achieve omniaxial motion. Movable nozzles are primarily used in long-range strategic propulsion ground- and sea-launched systems (typical throat diameters are 7 to 15 in. for the first stage and 4 to 5 in. for the third stage) and in large space launch boosters such as the Space Shuttle reusable solid rocket motor, Titan boost rocket motor, and Ariane V solid rocket booster, with throat diameters in the 30- to 50-in. range.

3. *Submerged Nozzles.* A significant portion of the nozzle structure is submerged within the combustion chamber or case, as shown in Figs. 15–2 and 15–6b,c. Submerging the nozzle reduces the overall motor length somewhat, which in turn reduces the vehicle length and its inert mass. It is important for length-limited applications such as silo- and submarine-launched strategic missiles as well as their upper stages, and space motor propulsion systems. It also reduces the mass of propellant inside the case. Reference 15–8 describes the sloshing of trapped molten aluminum oxide

that can accumulate in the groove around a submerged nozzle. This accumulation is undesirable, but can be minimized by good design.

4. *Extendible Nozzle*. Commonly referred to as an extendible exit cone, (EEC), although it is not always exactly conical. It is used on strategic missile propulsion upper-stage systems and upper stages for space launch vehicles to maximize motor-delivered specific impulse. As shown in Fig. 12–3, it has a fixed low-area-ratio nozzle section which is enlarged to a higher area ratio by adding a nozzle cone extension piece. The extended nozzle improves specific impulse by doubling or tripling the initial expansion ratio, thereby significantly increasing the nozzle thrust coefficient. This system thus allows a very high expansion ratio nozzle to be packaged in a relatively short length, thereby reducing vehicle inert mass. The nozzle cone extension is in its retracted position during the boost phase of the flight and is moved into place before the motor is started but after separation from the lower stage. Typically, electromechanical ball screw actuators deploy the exit cone extension.
5. *Blast-Tube-Mounted Nozzle*. Used with tactical air- and ground-launched missiles, with diameter constraints to allow space for aerodynamic fin actuation or TVC power supply systems. The blast tube also allows the rocket motor's center of gravity (CG) to be close to or ahead of the vehicle CG. This limits the CG travel during motor burn and makes flight stabilization much easier.

Each motor usually has a single nozzle. A few larger motors have had four movable nozzles, which are used for thrust vector control (see Chapter 18).

Design and Construction

Almost all solid rocket nozzles are ablatively cooled. The general construction of a solid rocket nozzle features steel or aluminum shells (housings) designed to carry structural loads (motor operating pressure and nozzle TVC actuator load are usually the biggest), and composite ablative liners which are bonded to the housings. The ablative liners are designed to insulate the steel or aluminum housings, provide the internal aerodynamic contour necessary to efficiently expand combustion gases to generate thrust, and to ablate and char in a controlled and predictable manner to prevent the buildup of heat which could substantially weaken the structural housings or the bonding materials. Solid rocket nozzles are designed to ensure that the thickness of ablative liners is sufficient to maintain the liner-to-housing adhesive bond line below the temperature that would degrade the adhesive structural properties during motor operation. Nozzle designs are shown in Figs. 1–5, 12–1 to 12–4, and 15–7.

The construction of nozzles ranges from simple single-piece nonmovable graphite nozzles to complex multipiece nozzles capable of moving to control the direction of the thrust vector. The simpler, smaller nozzles are typically for applications with low chamber pressure, short durations (perhaps less than

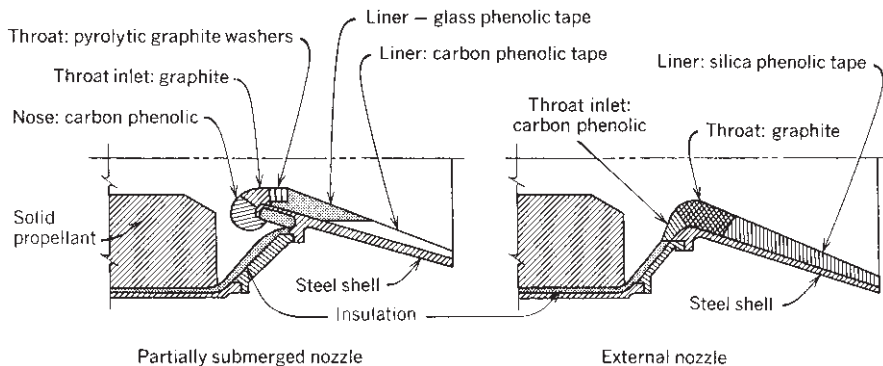


FIGURE 15–7. Nozzle designs for small solid propellant motors employ ablative heat sink wall pieces and graphite throat inserts resistant to high temperatures, erosion, and oxidation. The pyrolytic washers or disks are so oriented that their high conductivity direction is perpendicular to the nozzle axis.

10 sec), low area ratios, and/or low thrust. Typical small, simple built-up nozzles are shown in Fig. 15–7. Complex nozzles are usually necessary to meet more difficult design requirements such as providing thrust vector control, operating at high chamber pressures (and thus at higher heat transfer rates) and/or higher altitudes (large nozzle expansion ratios), producing very high thrust levels, and surviving longer motor burn durations (above 30 sec).

Figures 15–8 and 15–9 illustrate the design features of the largest and one of the most complex solid rocket nozzles currently in production. This nozzle is

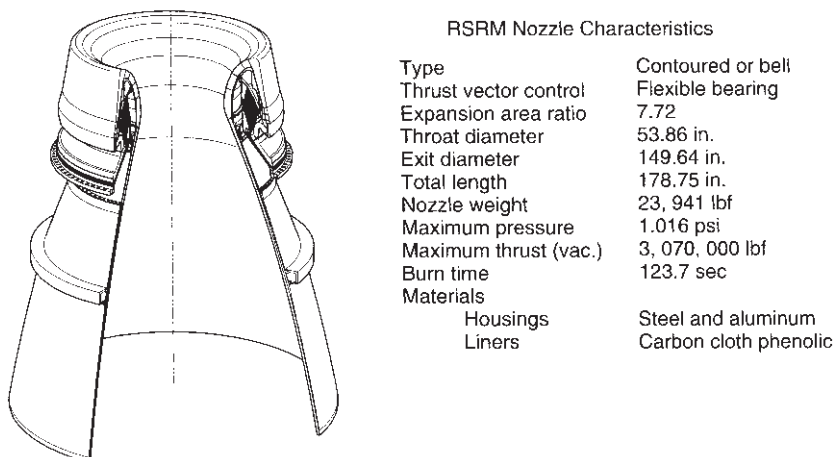


FIGURE 15–8. External quarter section view of nozzle configuration of the Space Shuttle reusable solid rocket motor (RSRM). (Courtesy of ATK Launch Systems.)

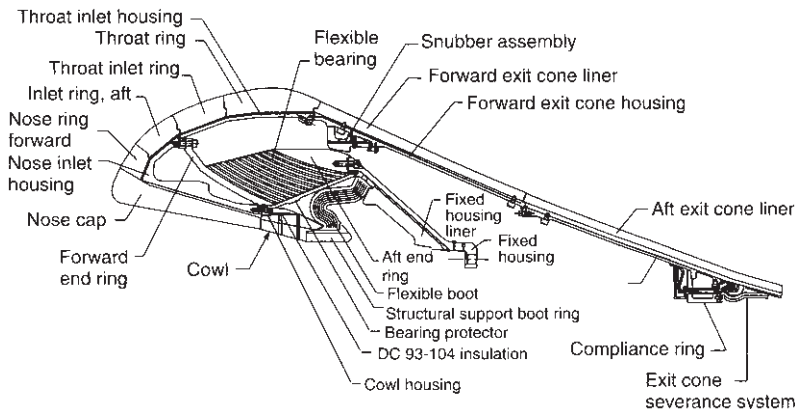


FIGURE 15–9. Section through movable nozzle shown in Fig. 15–8 with component identification. (Courtesy of ATK Launch Systems.)

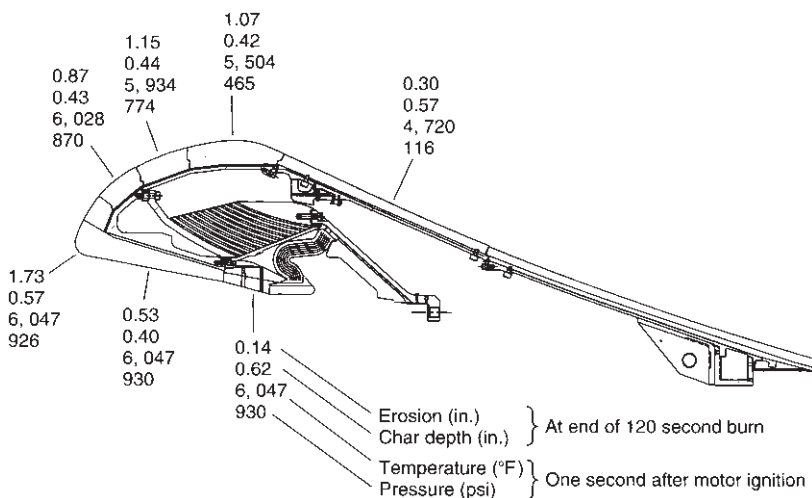
used on the reusable solid rocket booster (RSRM) to provide 71.4% of the lift-off thrust of the Space Shuttle launch vehicle shown in Figs. 1–14 and 15–2. The nozzle is designed to provide large structural and thermal safety margins during the shuttle booster's 2-min burn time and consists of nine carbon cloth phenolic ablative liners bonded to six steel and aluminum housings. The housings are bolted together to form the structural foundation for the nozzle. A flexible bearing (described further in Chapter 18), made of thin rubber sheets vulcanized to steel shims, enables the nozzle to vector omnirotationally up to 8 degrees from centerline to provide thrust vector control. Since the metal housings are recovered and reused after flight, an exit cone severance system (a circumferential linear shaped charge) is used to cut off a major section of the aft exit cone just below the aft exit cone aluminum housing to minimize splashdown loading on the remaining components. NASA's new Ares I first-stage booster (a five-segment solid propellant rocket) is being patterned after the Space Shuttle's SRM nozzle design.

From a performance perspective, the nozzle should efficiently expand the gas flow from the motor combustion chamber to produce thrust. Simple nozzles with noncontoured conical exit cones can be designed using the basic thermodynamic relationships presented in Chapter 3 to determine throat area, nozzle half angle, and expansion ratio. A more complex contoured (bell-shaped) nozzle is used to reduce the divergence loss, improve the specific impulse slightly, and reduce nozzle length and mass. Section 3.4 gives data on designing bell-shaped nozzles with optimum wall contour (to avoid shock waves) and minimum impact of particulates in the exhaust gas.

Two-dimensional, two-phase, reacting gas method-of-characteristics flow codes are used to analyze the gas-particle flow in the nozzle and determine the optimal nozzle contour which maximizes specific impulse while yielding acceptable erosion characteristics. Such codes provide analytical solutions to

TABLE 15–3. Calculated Losses in the Space Shuttle Booster RSRM Nozzle

| | |
|---|-----------------|
| Theoretical specific impulse (vacuum conditions) | 278.1 sec |
| Delivered specific impulse (vacuum conditions) | 268.2 sec |
| <i>Losses (calculated):</i> | (9.9 sec total) |
| Two-dimensional two-phase flow (includes divergence loss) | 7.4 sec |
| Throat erosion (reduces nozzle area ratio) | 0.9 sec |
| Boundary layer (wall friction) | 0.7 sec |
| Submergence (flow turning) | 0.7 sec |
| Finite rate chemistry (chemical equilibrium) | 0.2 sec |
| Impingement (of Al_2O_3 particles on nozzle wall) | 0.0 sec |
| Shock (if turnback angle is too high or nozzle length too low) | 0.0 sec |
| Combustion efficiency (incomplete burning) | 0.0 sec |

**FIGURE 15–10.** Erosion measurements and char depth data of the carbon fiber phenolic material of the nozzle of the Space Shuttle reusable solid rocket motor. (Courtesy of ATK Launch Systems.)

all identified specific impulse loss mechanisms which result in less than ideal performance. An example is given in Table 15–3.

Figure 15–10 illustrates the amount of carbon cloth phenolic liner removed by chemical erosion and particle impingement, the liner char depth, and gas temperature and pressure at selected locations in the RSRM nozzle. Erosion on the nose cap (1.73 in.) is high primarily as a result of impingement by Al_2O_3 particles traveling down the motor bore. The impact of the particles mechanically removes the charred liner material. In contrast, the radial throat erosion of 1.07 in. results primarily from the carbon liner material reacting chemically with oxidizing species in the combustion gas flow at the region of greatest heat transfer. At the

throat location, impingement erosion is essentially zero because Al_2O_3 particles are traveling parallel to the nozzle surface.

The acronym ITE is often used; it means *integral throat/entrance* and refers to a single-piece nozzle throat insert that also includes a part of the converging entry section. ITE nozzle inserts can be seen in Figs. 1–5, 12–1, 12–3, and 12–4.

Nozzle throat erosion causes the throat diameter to enlarge during operation and is one of the problems encountered in nozzle design. Usually, a throat area increase larger than 5% is considered unacceptable for most solid rocket applications, since it causes a significant reduction in thrust and chamber pressure. Erosion occurs not only at the throat region (typically, at 0.01 to 0.25 mm/sec or 0.004 to 0.010 in./sec), but also at the sections immediately upstream and downstream of the throat region, as shown in Fig. 15–10. Nozzle assemblies typically lose 3 to 12% of their initial inert mass during operation. Erosion is caused by the complex interaction between the high-temperature, high-velocity gas flow, the chemically aggressive species in the gas, and the mechanical abrasion by particles. The carbon in the nozzle material reacts with species like O_2 , O , OH , or H_2O and is oxidized; the cumulative concentration of these species is an indication of the likely erosion. Tables 5–6 and 5–7 give chemical concentrations for the exhaust species from aluminized propellant. Fuel-rich propellants (which contain little free O_2 or O) and propellants where some of the gaseous oxygen is removed by aluminum oxidation show less tendency to cause erosion. Uneven erosion of a nozzle causes thrust misalignment.

Finding the optimum nozzle wall contour requires an analysis (computer codes for bell-shaped nozzles using the method of characteristics are mentioned in Section 3.4) to determine the wall contour which most rapidly turns the gas to near axial flow without introducing shock waves or impinging excessive aluminum oxide (Al_2O_3) particles on the nozzle wall. Figure 3–14 illustrates the key parameters which govern design of the nozzle contour; the initial angle θ_i (angle through which supersonic flow is turned immediately downstream of the nozzle throat), the throat to exit plane length L , the exit plane exit angle θ_e , and the turnback angle $\theta_i - \theta_e$. With solid or liquid particles in the exhaust the impingement can be minimized with an initial angle typically between 20 and 26° and a turnback angle of typically 10 to 15°. The length reduction of a bell-shaped nozzle (with solid particles in the gas) is typically 80 to 90% of the length of an equivalent conical nozzle with 15° half angle. The nozzle throat inlet contour is generally based on a hyperbolic spiral that uniformly accelerates the combustion gas flow to supersonic velocity at the throat plane.

Heat Absorption and Nozzle Materials

Rocket motors never reach thermal equilibrium during their firing. The temperatures of all components exposed to the heat flow increase continuously during operation. In a good thermal design the critical locations reach a maximum allowable temperature a short time after the motor stops running. The nozzle

components rely on their heat-absorbing capacity (high specific heat and high energy demand for material decomposition) and slow heat transfer (good insulation with low thermal conductivity) to withstand the stresses and strains imposed by the thermal gradients and loads. The maximum allowable temperature for any of the motor materials is just below the temperature at which excessive degradation occurs (the material loses strength, melts, becomes too soft, cracks, pyrolyses, unglues, oxidizes too rapidly). The operating duration is limited by the design and amount of heat-absorbing and insulating material pieces. Stated in a different way, the objective is to design a nozzle with just sufficient heat-absorbing material mass and insulation mass at the various locations within the nozzle, so that its structures and joints will do the job for the duration of the application under all likely operating conditions.

The selection and application of the proper material is the key to the successful design of a solid rocket nozzle. Table 15-4 groups various typical nozzle materials according to their usage. The high-temperature exhaust of solid rockets presents an unusually severe environment for the nozzle materials, especially when metalized propellants are employed.

About 70 years ago nozzles were made out of a single piece of *molded polycrystalline graphite* and some were supported by metal housing structures. They eroded easily, but were low in cost. We still use them today for short duration, low chamber pressure, low altitude flight applications of low thrust, such as in certain tactical missiles. For more severe conditions a throat insert or ITE (integrated throat entrance) was placed into the graphite piece; this insert was a denser, better grade of graphite; later pyrolytic graphite washers and fiber-reinforced carbon materials came into use. For a period of time tungsten inserts were used; they had very good erosion resistance, but were heavy and often cracked. *Pyrolytic graphite* was introduced and is still being used as washers for the throat insert of small nozzles, as shown in Fig. 15-7. The high-strength carbon fiber and the carbon matrix were major advances in high-temperature materials. For small and medium-sized nozzles, ITE pieces were then made of *carbon–carbon*, which is an abbreviation for carbon fibers in a carbon matrix (see Ref. 15-9). The orientation of the fibers can be two-dimensional (2D) or three-dimensional (3D), as described below. Some properties of all these materials are listed in Tables 15-4 and 15-5. For large nozzles the then existing technology did not allow the fabrication of large 3D carbon–carbon ITE pieces, so layups of carbon fiber (or silicon fiber) cloth in a phenolic matrix were used.

The regions immediately upstream and downstream of the throat have less heat transfer, less erosion, and lower temperatures than the throat region, and less expensive materials are usually satisfactory. This includes various grades of graphite, or ablative materials, strong high-temperature fibers (carbon or silica) in a matrix of phenolic or epoxy resins, which are described later in this section. Figure 18-5 shows a movable nozzle with multilayer *insulators* behind the graphite nozzle pieces directly exposed to heat. These insulators (between the very hot throat piece and housing) limit the heat transfer and prevent excessive housing temperatures.

TABLE 15–4. Typical Motor Nozzle Materials and Their Functions

| Function | Material | Remarks |
|---|---|--|
| Structure and pressure container (housing) | Aluminum Low-carbon steel, high-strength steels, and special alloys | Limited to 515°C (959°F) Good between 625 and 1200°C (1100 and 2200°F), depending on material; rigid and strong |
| Heat sink and heat-resistant material at inlet and throat section; severe thermal environment and high-velocity gas, with erosion | Molded graphite Pyrolytic graphite Tungsten, molybdenum, or other heavy metal Carbon or Kevlar fiber cloth with phenolic or plastic resins Carbon–carbon | For low chamber temperatures and low pressures only; low cost Has anisotropic conductivity Heavy, expensive, subject to cracking; resists erosion Sensitive to fiber orientation. Ablative materials Used with large throats Three- or four-dimensional interwoven filaments, strong, expensive, limited to 3300°C (6000°F) |
| Insulator (behind heat sink or flame barrier); not exposed to flowing gas | Ablative plastics, with fillers of silica or Kevlar, phenolic resins | Want low conductivity, good adhesion, ruggedness, erosion resistance; can be filament wound or impregnated cloth layup with subsequent machining |
| Flame barrier (exposed to hot low-velocity gas) | Ablative plastics (same as insulators but with less filler and tough rubber matrix) Carbon, Kevlar, or silica fibers with phenolic or epoxy resin Carbon–carbon | Lower cost than carbon–carbon; better erosion resistance than many insulators Cloth or ribbon layups; woven and compressed, glued to housing |
| Nozzle exit cone | Ablative plastic with metal housing structure Refractory metal (tantalum, molybdenum) Carbon–carbon, may need gas seal Niobium | Higher temperature than others, three-dimensional weave or layup Heavy, limited duration; cloth or woven ribbon layups, glued to housing Radiation cooled, strong, needs coating for oxidation resistance; can be thin, limited to 1650°C (3000°F), unlimited duration, heavy Radiation cooled, higher allowable temperature than metals; two- or three-dimensional weave, strong, often porous Section near nozzle exit, radiation cooled |

TABLE 15-5. Comparison of Properties of Molded and Pyrolytic Graphite, Carbon-Carbon, Carbon Cloth, and Silica Cloth Phenolic

| | ATJ Modern Graphite | Pyrolytic Graphite | Three-Dimensional Carbon Fibers in a Carbon Matrix | Carbon Cloth | Silica Cloth | Phenolic |
|--|---|---|--|--|--|---|
| Density (lbm/in. ³) | 0.05556 | 0.079 | 0.062–0.072 | 0.053 | 0.062 | |
| Thermal expansion (in./in./°F.) | 0.005–0.007 | 0.00144 (warp) | 1–9 × 10 ⁻⁶ | 8.02 × 10 ⁻⁶ | 7.6 × 10 ⁻⁶ | |
| Thermal conductivity (Btu/in.-sec/°F.) at room temperature | | 0.0432 (fill) | 4.9 × 10 ⁻⁵ (warp) ^a | 2 to 21 × 10 ⁻⁵ (warp) ^a | 2.2 × 10 ⁻³ (warp) ^a | 1.11 × 10 ⁻³ (warp) ^a |
| Modulus of elasticity (psi) at room temperature | 1.5 × 10 ⁶ (warp) ^a | 4.5 × 10 ⁶ (warp) ^a | 4.2 × 10 ⁻⁵ (fill) ^a | 8 to 50 × 10 ⁻⁵ (fill) ^a | 35 to 80 × 10 ⁶ | 2.86 × 10 ⁻⁶ (warp) ^a |
| Shear modulus (psi) | 1.2 × 10 ⁶ (fill) ^a | — | 1.5 × 10 ⁶ (fill) ^a | — | 0.81 × 10 ⁶ | 3.17 × 10 ⁻⁶ (warp) ^a |
| Erosion rate (typical) (in./sec) | 0.004–0.006 | 0.001 to 0.002 | 2.7 × 10 ⁶ (fill) ^a | 0.0005–0.001 | 0.005–0.010 | 0.010–0.020 |

^aWarp is in direction of principal fibers. Fill is at right angles to warp.

In the *diverging exit section* the heat transfer and temperatures are even lower and similar, but less capable and less expensive materials can be used here. This exit segment can be built integral with the nozzle throat segment (as it is in most small nozzles), or it can be a separate one- or two-piece subassembly which is then fastened to the smaller diameter throat segment. Ablative materials without oriented fibers as in cloth or ribbons, but with short fibers or insulating ceramic particles, can be used here. For large area ratios (upper stages and space transfer), the nozzle will often protrude beyond the vehicle's boat tail surface. This allows radiation cooling, since the exposed exit cone can reject heat by radiation to space. Lightweight thin high-temperature metals (niobium, titanium, stainless steel, or a thin carbon–carbon shell) with radiation cooling have been used in a few upper-stage or spacecraft exit cone applications. Since radiation-cooled nozzle exit sections can reach thermal equilibrium, their duration is unlimited.

The *housing* or *structural support of the nozzle* uses the same material as the metal case, such as steel or aluminum. Housings are never allowed to become very hot. Some of the simpler, smaller nozzles (with one, two, or three pieces, mostly graphite) do not have a separate housing structure, but use the ITE for the structure.

Estimates of nozzle internal temperatures and temperature distributions with time can be made using two-dimensional finite element difference methods for *transient heat transfer analyses*. These are similar in principle to the transient heat transfer method described in Section 8.5 and shown in Fig. 8–20. After firing, the nozzle temperatures reach an equilibrium value by conducting heat from the hotter inner parts, which were exposed to the hot gas, to the cooler outer pieces. Sometimes the outer pieces will exceed their limit temperatures and suffer damage after firing. The *structural analysis* (stresses and strains) of the key nozzle components is dependent on the heat transfer analysis, which determines the component temperatures. This allows use of the proper material physical properties, which are temperature dependent. The design must also allow for the thermal growth and the differential expansion of adjacent parts.

Typical materials used for the ITE or nozzle throat insert are listed in Table 15–5. They are exposed to the most severe conditions of heat transfer, thermal stresses, and high temperatures. Their physical properties are often anisotropic; that is, their properties vary with the orientation or direction of the crystal structure or the direction of reinforcing fibers. *Polycrystalline graphites* are extruded or molded. Different grades with different densities and capabilities are available. As already mentioned, they are used extensively for simple nozzles and for ITE parts. *Pyrolytic graphite* is strongly anisotropic and has excellent conductivity in a preferred direction. A nozzle using it is shown in Fig. 15–7. It is fabricated by depositing graphite crystals on a substratum in a furnace containing methane gas. Its use is declining, but it is still installed in current rocket motors of older design.

The *carbon–carbon* material is made from carefully oriented sets of *carbon fibers* (woven, knitted, threaded, or laid up in patterns) in a *carbon matrix*. Two-dimensional (2D) material has fibers in two directions, 3D has fibers oriented in

three directions (usually at right angle to each other), and 4D has an extra set of fibers at about a 45° angle to one or two of the other three directions. An organic liquid resin is injected into the spaces between the fibers. The assembly is pressurized, the filler is transformed into a carbon char by heating and is compacted by further injection and densification processes. The graphitization is then performed at temperatures higher than 2000°C . This material is expensive but suited to nozzle applications. Highly densified material is superior in high heat transfer regions, such as the throat. The multidirectional fiber reinforcements allow them to better withstand the high thermal stresses introduced by the steep temperature gradients within the component.

Ablative Materials. These are not only commonly used in the nozzles of rocket motors but also in some insulation materials. They are usually a composite material of high-temperature organic or inorganic high-strength fibers, namely high silica glass, aramids (Kevlar), or carbon fibers, impregnated with organic plastic materials such as phenolic or epoxy resin. The fibers may be individual strands or bands (applied in a geometric pattern on a winding machine), or come as a woven cloth or ribbon, all impregnated with resin.

The ablation process is a combination of surface melting, sublimation, charring, evaporation, decomposition in depth, and film cooling. As shown in Fig. 15–11, progressive layers of the ablative material undergo an endothermic degradation, that is, physical and chemical changes that absorb heat. While some of the ablative material evaporates (and some types also have a viscous liquid phase), enough charred and porous solid material remains on and below the surface to preserve the basic geometry and surface integrity. Upon rocket start the ablative material acts like any thermal heat sink, but the poor conductivity causes the surface temperature to rise rapidly. At 650 to 800 K some of the resins start to decompose endothermically into a porous carbonaceous char and pyrolysis gases. As the char depth increases, these gases undergo an endothermic cracking process as they percolate through the char in a counterflow direction to the heat flux. These gases then form an artificial fuel-rich, protective, relatively cool, but flimsy boundary layer over the char.

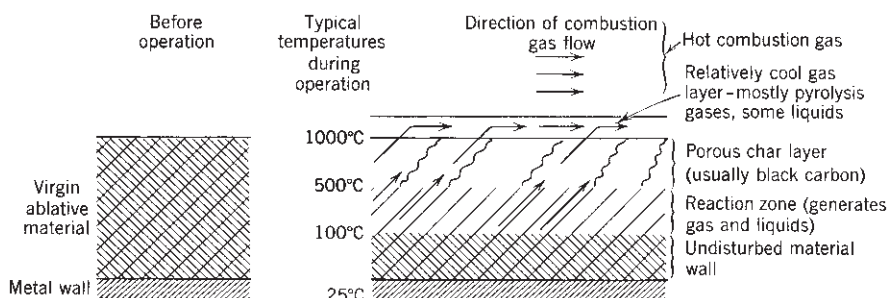


FIGURE 15–11. Zones in an ablative material during rocket operation with fibers at 45° to the flow.

Since char is almost all carbon and can withstand 3500 K or 6000 R, the porous char layer allows the original surface to be maintained (but with a rough surface texture) and provides geometric integrity, alternatively the char's carbon can be oxidized by certain species in the combustion gas; in this case there is a slow regression of the charred surface. Char is a weak material and can be damaged or abraded by direct impingement of solid particles in the gas. Ablative material construction is used for part or all of the chambers and/or nozzles shown in Figs. 1–5, 6–10, 12–1 to 12–4, and 15–10.

Ablative parts are formed either by high-pressure molding (\sim 55 to 69 MPa or 8000 to 10,000 psi at 149°C or 300°F) or by tapewrapping on a shaped mandrel followed by an autoclave curing process at 1000 to 2000 psi pressure and 300°F temperature. *Tapewrapping* is a common method of forming very large nozzles. The wrapping procedure normally includes heating the shaped mandrel (\sim 54°C or 130°F), heating the tape and resin (66 to 121°C or 150 to 250°F), pressure rolling the tape of fiber material and the injected resin in place while rolling (\sim 35,000 N/m or 200 lbf/in. width), and maintaining the proper rolling speed, tape tension, wrap orientation, and resin flow rate. Experience has proven that as-wrapped density is an important indicator of procedural acceptability, with the desired criterion being near 90% of the autoclaved density. Resin content usually ranges between 25 and 35%, depending on the fabric-reinforcing material and the particular resin and its filler material. Normally, the mechanical properties of the cured ablative material, and also the durability of the material during rocket operation, correlate closely with the cured material density. Within an optimal density range, low density usually means poor bonding of the reinforcing layers, high porosity, low strength, and high erosion rate.

In liquid propellant rockets, ablatives have been effective in very small thrust chambers (where there is insufficient regenerative cooling capacity), in pulsing, restartable spacecraft control rocket engines, in the exit region of large nozzle and in variable-thrust (throttled) rocket engines. Figure 6–10 shows an ablative nozzle extension for a large liquid propellant rocket engine.

The heat transfer properties of the many available ablative and other fiber-based materials will depend on their design, composition, and construction. Figure 15–12 shows several common fiber orientation and approaches. The *orientation of fibrous reinforcements*, whether in the form of tape, cloth, filaments, or random short fibers, has a marked impact on the erosion resistance of composite

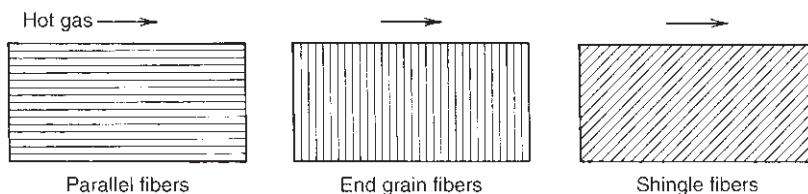


FIGURE 15–12. Simplified sketches of three different types of fiber-reinforced ablative materials.

nozzles (for erosion data see Fig. 15–10). When perpendicular to the gas flow, the heat transfer to the wall interior is high because of the short conducting path. Good results have been obtained when the fibers are at 40 to 60° relative to the gas flow over the surface. Fabrication variables present wide variations in nozzle life for a given design; the variables include the method of wrapping, molding, and curing, resin batch processes, and resin sources.

15.3. IGNITER HARDWARE

In Section 14.2 the process of ignition was described, and in Section 13.5 some of the propellants used in igniters were mentioned briefly. In this section we discuss specific igniter types, locations, and their hardware (see Ref. 15–10).

Since the igniter propellant mass is small (often less than 1% of the motor propellant) and burns mostly at low chamber pressure (low I_s), it contributes very little to the motor overall total impulse. It is the designer's aim to reduce the igniter propellant mass and the igniter inert hardware mass to a minimum, just big enough to assure ignition of the grain under all operating conditions.

Figure 15–13 shows several alternative locations for the igniter. When mounted on the forward end, the gas flow over the propellant surface helps to achieve ignition. With aft mounting there is little gas motion, particularly near the forward end; here ignition must rely on the temperature, pressure, and heat transfer from the igniter gas. If mounted internally through the nozzle, the igniter hardware and its support are discarded shortly after the igniter has used all its propellants and there is no inert mass penalty for the igniter case. There are two basic types: *pyrotechnic igniters* and *pyrogen igniters*; both are discussed below.

Pyrotechnic Igniters

In industrial practice, pyrotechnic igniters are defined as igniters (other than pyrogen-type igniters) using solid explosives or energetic propellant-like chemical

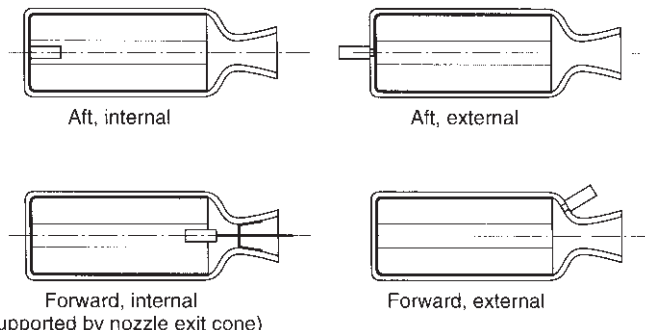


FIGURE 15–13. Simple diagrams of mounting options for igniters. Grain configurations are not shown.

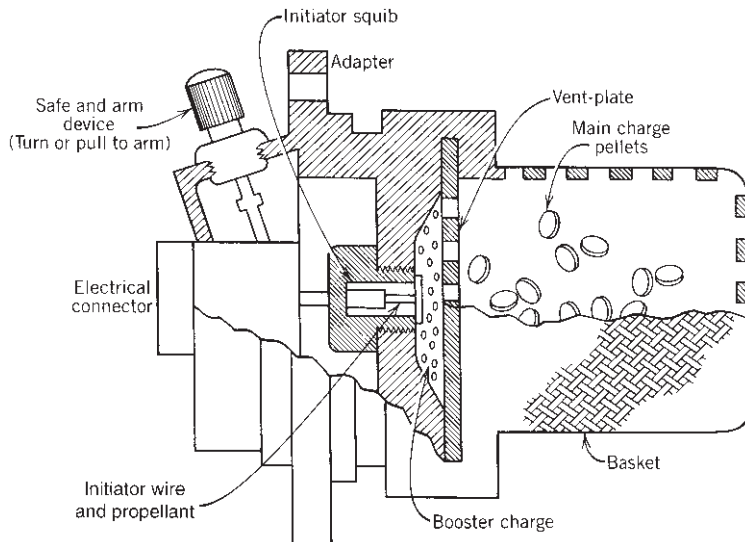


FIGURE 15–14. Typical pyrotechnic igniter with three different propellant charges that ignite in sequence.

formulations (usually small pellets of propellant which give a large burning surface and a short burning time) as the heat-producing material. This definition fits a wide variety of designs, known as bag and carbon igniters, powder can, plastic case, pellet basket, perforated tube, combustible case, jellyroll, string, or sheet igniters. The common pellet-basket design shown in Fig. 15–14 is typical of the pyrotechnic igniters. Ignition of the main charge, in this case pellets consisting of 24% boron–71% potassium perchlorate–5% binder, is accomplished by stages; first, on receipt of an electrical signal the initiator releases the energy of a small amount of sensitive powdered pyrotechnic housed within the initiator, commonly called the squib or the primer charge; next, the booster charge is ignited by heat released from the squib; and finally, the main ignition charge propellants are ignited.

A special form of pyrotechnic igniter is the *surface-bonded* or *grain-mounted igniter*. Such an igniter has its initiator included within a sandwich of flat sheets; the layer touching the grain is the main charge of pyrotechnic. This form of igniter is used with multipulse motors with two or more end-burning grains. The ignition of the second and successive pulses of these motors presents unusual requirements for available space, compatibility with the grain materials, life, and the pressure and temperature resulting from the booster grain operation. Advantages of the sheet igniter include light weight, low volume, and high heat flux at the grain surface. Any inert material employed (such as wires and electric ceramic insulators) is usually blown out of the motor nozzle during ignition and their impacts have caused damage to the nozzle or plugged it, particularly if they are not intentionally broken up into small pieces.

Pyrogen Igniters

A pyrogen igniter is basically a small rocket motor that is used to ignite a larger rocket motor. The pyrogen is not designed to produce thrust. All use one or more nozzle orifices, both sonic and supersonic types, and most use conventional rocket motor grain formulations and design technology. Heat transfer from the pyrogen to the motor grain is largely convective, with the hot gases contacting the grain surface as contrasted to a highly radiative energy emitted by pyrotechnic igniters. Figures 12–1, 12–2, and 12–20 illustrate rocket motors with a typical pyrogen igniter. The igniter in Fig. 18–5 has three nozzles and a cylindrical grain with high-burn-rate propellant. For pyrogen igniters the initiator and the booster charge are very similar to the designs used in pyrotechnic igniters. Reaction products from the main charge impinge on the surface of the rocket motor grain, producing motor ignition. Common practice on the very large motors is to mount externally, with the pyrogen igniter pointing its jet up through the large motor nozzle. In this case, the igniter becomes a piece of ground-support equipment.

Two approaches are commonly used to safeguard against motor misfires, or inadvertent motor ignition; one is the use of the classical *safe and arm device* and the second is the *design of safeguards* into the initiator. Energy for unintentional ignition—usually a disaster when it happens—can be (1) static electricity, (2) induced current from electromagnetic radiation, such as radar, (3) induced electrical currents from ground test equipment, communication apparatus, or nearby electrical circuits in the flight vehicle, and (4) heat, vibration, or shock from handling and operations. Functionally, the safe and arm device serves as an electrical switch to keep the igniter circuit grounded and interrupted when not operating; in some designs it also mechanically misaligns or blocks the ignition train of events so that unwanted ignition is precluded even though the initiator fires. When the device is transposed into the *arm* position, the ignition circuit is no longer blocked and the ignition flame can be reliably propagated to the igniter's booster and main charges.

Electric initiators in motor igniters are also called squibs, glow plugs, primers, and headers; they always constitute the initial element in the ignition train and, if properly designed, can be a safeguard against unintended ignition. Three typical designs of initiators are shown in Fig. 15–15. Both (a) and (b) structurally form a part of the rocket motor case and generically are headers. In the integral diaphragm type (a) the initial ignition energy is passed in the form of a shock wave through the diaphragm activating the acceptor charge, with the diaphragm remaining integral. This same principle is also used to transmit a shock wave through a metal case wall or a metal insert in a filament-wound case; the case would not need to be penetrated and sealed. The header type (b) resembles a simple glow plug with two high-resistance bridgewires buried in the initiator charge. The exploding bridgewire design (c) employs a small bridgewire (0.02 to 0.10 mm) of low-resistance material, usually platinum or gold, that is exploded by application of a high-voltage discharge.

The safeguard aspect of the initiator appears as a basic design feature in the form of (1) minimum threshold electrical energy required for activation, (2)

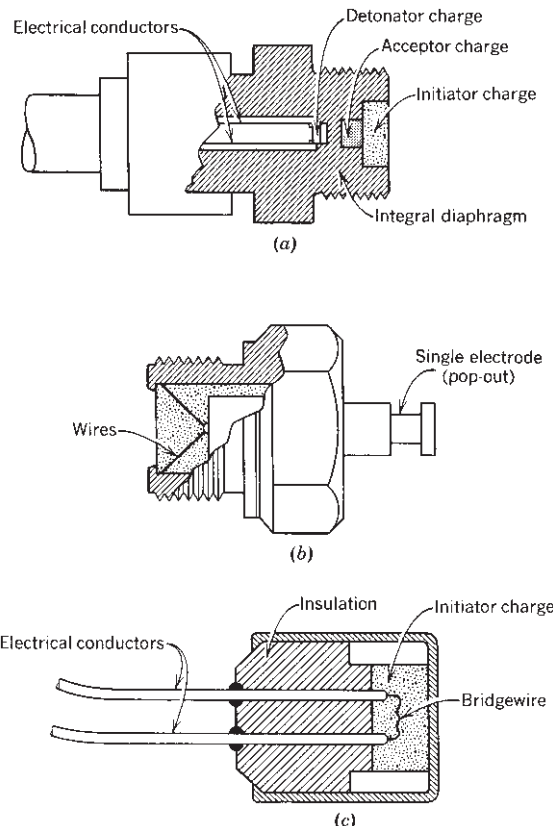


FIGURE 15–15. Typical electric initiators; (a) integral diaphragm type; (b) header type with double bridgewire; (c) exploding bridgewire type.

voltage blockage provisions (usually, air gaps or semiconductors in the electrical circuit), or (3) responsiveness only to a specific energy pulse or frequency band. Invariably, such safeguards compromise to some degree the safety provided by the classical safe and arm device.

Another method of initiating the action of an igniter is to use laser energy to start the combustion of an initiator charge. Here there are no problems with induced currents and other inadvertent electrical initiation. The energy from a small neodymium/YAG laser, external to the motor, travels in fiber-optical glass cables to the pyrotechnic initiator charge (Ref. 15–11). Sometimes an optical window in the case or closure wall allows the initiator charge to be inside the case.

Igniter Analysis and Design

The basic theories of initiating ignition, heat transfer, propellant decomposition, deflagration, flame spreading, and chamber filling are common to the design and

application of all pyrotechnic and pyrogen igniters. In general, the analytical models of the physical and chemical processes that must be considered in the design of igniters are far from complete and accurate. See Chapter 5 by Hermance and Chapter 6 by Kumar and Kuo in Ref. 14–1, and Ref. 15–10.

Analysis and design of igniters, regardless of the type, depend heavily on experimental results, including past successes and failures with full-scale motors. The effect of some of the important parameters has become quite predictable, using data from developed motors. For example, Fig. 15–16 is of benefit in estimating the mass of igniter main charge for motors of various sizes (motor free volume). From these data,

$$m = 0.12(V_F)^{0.7} \quad (15-4)$$

where m is the igniter charge in grams and V_F is the motor free volume in cubic inches (the void in the case not occupied by propellant). A larger igniter mass flow means a shorter ignition delay. Ignition time events are shown in Fig. 14–3.

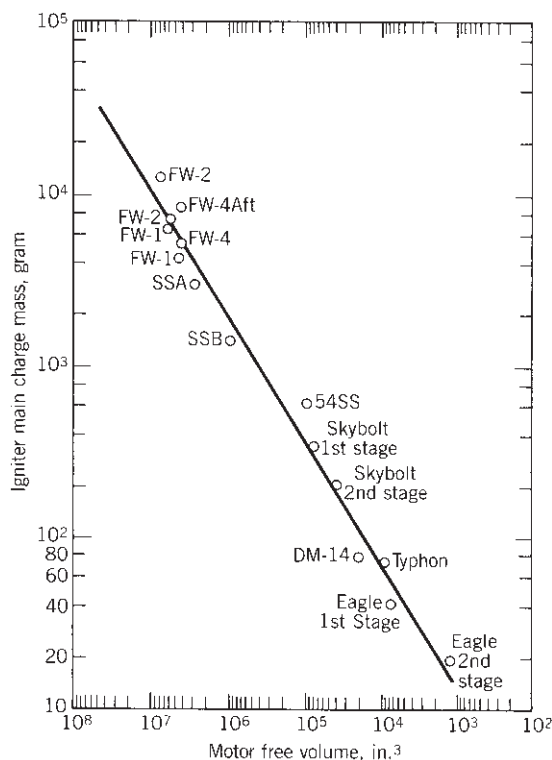


FIGURE 15–16. Igniter charge mass versus motor free volume, based on experience with various-sized rocket motors using AP/Al composite propellant. (Data with permission from Ref. 15–12.)

15.4. ROCKET MOTOR DESIGN APPROACH

Although there are some common elements in the design of all solid propellant rocket motors, there is no universal, well-defined procedure or design method. Each class of application has some different requirements. Individual designers and their organizations have different approaches, background experiences, sequences of steps, or emphasis. The approach also varies with the amount of available data on design issues, propellants, grains, hardware, or materials, with the degree of novelty (many “new” motors are actually modifications of proven existing motors), or the available computer programs.

Usually the following items are part of the preliminary design process. We start with the requirements for the flight vehicle and the motor, such as those listed in Table 15–6. If the motor to be designed has some similarities to proven existing motors, their parameters and flight experience will be helpful in reducing the design effort and enhancing the confidence in the design. The selection of the propellant and the grain configuration are usually made early in the preliminary design; propellant selection was discussed in Chapter 13 and grains in Chapter 12.

TABLE 15–6. Typical Requirements and Constraints for Solid Rocket Motors

| Requirement Category | Examples |
|---|---|
| Application | Definition of mission, vehicle and propulsion requirements, flight paths, maneuvers, environment |
| Functional | Total impulse, thrust–time curve, ignition delay, initial motor mass, specific impulse, TVC angles and angular accelerations, propellant fraction, class 1.1 or 1.3, burn time, and tolerances on all of these parameters |
| Interfaces | Attachments to vehicle, fins, TVC system, power supply, instruments, lifting and transport features, grain inspection, control signals, shipping container |
| Operation | Storage, launch, flight environment, temperature limits, transport loads or vibrations, plume characteristics (smoke, toxic gas, radiation), life, reliability, safe and arm device functions, field inspections |
| Structure | Loads and accelerations imposed by thrusting and by vehicle (flight maneuvers), stiffness to resist vehicle oscillations, safety factors |
| Insensitive munitions (military application) | Response to slow and fast cook-off, bullet impact, sympathetic detonation, shock tests |
| Cost and schedule | Stay within the allocated time and money |
| Deactivation | Method of removing/recycling of propellants, safe disposal of overage motors |
| Constraints | Limits on volume, length, or diameter; minimum acceptable performance, maximum cost |
| Schedule | Design completion test articles completion, qualification, delivery |

It is not always easy for any one propellant to satisfy the three key requirements, namely the performance (I_s), burning rate to suit the thrust–time curve, and strength (maximum stress and strain). A well-characterized propellant, a proven grain configuration, or a well-tested piece of hardware will usually be preferred and is often modified somewhat to fit the new application.

An analysis of the structural integrity should be undertaken, at least in a few of the likely places, where stresses or strains might exceed those that can be tolerated by the grain or the other key components at the limits of loading or environmental conditions. An analysis of the nozzle should be done, particularly if the nozzle is complex or includes thrust vector control. Such a nozzle analysis was described briefly in an earlier section of this chapter. If gas flow analysis shows that erosive burning is likely to happen during a portion of the burning duration, it must be decided whether it can be tolerated, or whether it is excessive and a modification of the propellant, the nozzle material, or the grain geometry needs to be made. Usually a preliminary evaluation is also done of the resonances of the grain cavity with the aim of identifying possible combustion instability modes (see Chapter 14). Motor performance analysis, heat transfer, and stress analyses in critical locations will usually be done.

There is considerable interdependence and feedback between the propellant formulation, grain geometry/design, stress analysis, thermal analysis, major hardware component designs, and their manufacturing processes. It is difficult to finalize one of these without considering all the others, and there may be several iterations of each. Data from tests of laboratory samples, subscale motors, and full-scale motors have a strong influence on these steps.

Preliminary layout drawings or CAD (computer-aided design) images of the motor with its key components will be made in sufficient detail to provide sizes and reasonably accurate dimensions. For example, a preliminary design of the thermal insulation (often with a heat transfer analysis) will provide preliminary dimensions for that insulator. The layout is used to estimate volumes, inert masses, or propellant masses, and thus the propellant mass fraction.

If any of these analyses or layouts show a potential problem or a possible failure to meet the initial requirements or constraints, then a modification of the design, possibly of the propellant, or of the grain configuration may need to be made. The design process needs to be repeated with the changed motor design. If the proposed changes are too complex or not effective, then a change in the motor requirements may be the cure to a particular problem of noncompliance with the requirements. It is common to have several iterations between the preliminary design and the final design. Any major new feature can result in additional development and testing to prove its performance, reliability, operation, or cost; this means a longer program and extra resources.

A simplified diagram of one particular approach to motor preliminary design and development activities for a rocket motor is shown in Fig. 15–17. Not shown in this diagram are many other steps, such as igniter design and tests, liner/insulating selection, thrust vector control design and test, reliability analysis, evaluation of alternative designs, material specifications, inspection/quality

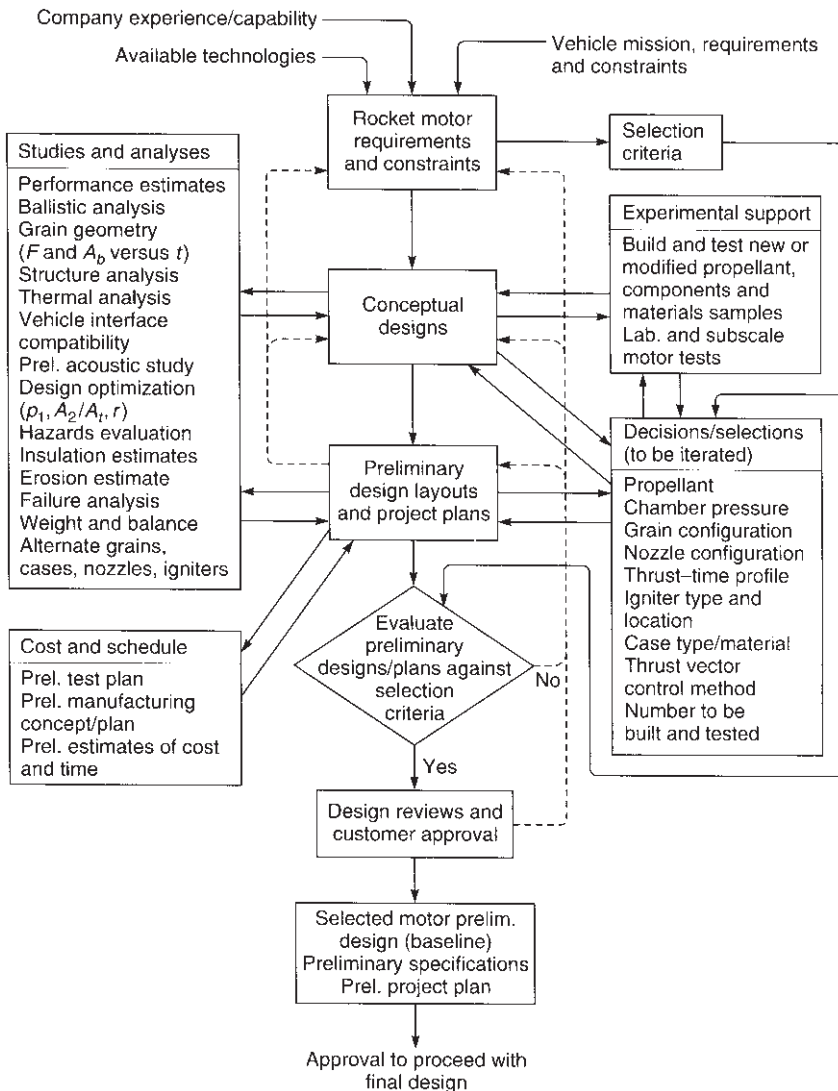


FIGURE 15–17. Diagram of one approach to the preliminary design activity sequences and interrelations. Dashed lines indicate feedback paths. Some specific items listed here apply only to certain types of rocket motors.

control steps, safety provision, special test equipment, special test instrumentation, and so on.

If the performance requirements are narrow and ambitious, it will be necessary to study the cumulative tolerances of the performance or of various other parameters. For example, practical tolerances may be assigned to the propellant density, nozzle throat diameter (erosion), burn rate scale factor, initial burning

surface area, propellant mass, or pressure exponent. These, in turn, reflect themselves into tolerances in process specifications, specific inspections, dimensional tolerances, or accuracy of propellant ingredient weighing. Cost is always a major factor and a portion of the design effort will be spent looking for lower-cost materials, simpler manufacturing processes, fewer assembly steps, or lower-cost component designs. For example, tooling for casting, mandrels for case winding, and tooling for insulator molding can be expensive. The time needed for completing a design can be shortened when there is good communication and a cooperative spirit between designers, propellant specialists, analysts, customer representatives, manufacturing people, test personnel, or vendors concerned with this effort. Reference 15–13 deals with some of the uncertainties of a particular booster motor design, and Ref. 15–14 discusses design optimization.

A *preliminary project plan* is usually formulated simultaneously with the preliminary design work. A decade or more ago the project plan was made after the preliminary design was completed. With today's strong emphasis on low cost, the people working on the preliminary designs have also to work on reducing costs on all components and processes. The project plan reflects decisions and defines the number of motors and key components to be built, the availability and lead time of critical materials or components, the type and number of tests (including aging or qualification tests); it identifies the manufacturing, inspection, and test facilities to be used, the number and kind of personnel (and when they will be needed), or any special tooling or fixtures. These decisions and data are needed to make a realistic *estimate of cost* and a *preliminary schedule*. If these exceed the allowable cost or the desired delivery schedule, then some changes have to be made. For example, this may include changes in the number of units to be built, the number and types of tests, or a redesign for easier, less costly assembly. However, such changes must not compromise reliability or performance. It is difficult to make a good plan, and good cost or time estimates, when the rocket motor has not been well defined or designed in sufficient detail. These plans and estimates are therefore largely based on experience with prior successful similar rocket motors.

The final result of a preliminary design will be layout drawings or CAD images of the selected configuration, a prediction of performance, an estimate of motor mass (and, if needed, also the travel of the center of gravity), an identification of the propellant, grain, geometry, insulation, and several of the key materials of the hardware components. An estimate of predicted reliability and motor life would be accompanied by supporting data. All this information would be presented for review of the selected preliminary design. The review would be undertaken by a diverse group of motor experts, the vehicle designer, safety engineers, specialists in manufacturing, assembly, or inspection, customer representatives, analysts, and others. Here the preliminary design team explains why they selected their particular design and how it meets the requirements. With competent reviewers there usually will be suggestions for changes or further improvements. The project plan, preliminary cost estimates, and preliminary schedule are sometimes included with the design review, but more often these are presented to a different group of experts, or just to the customer's experts.

After the design review and the approval of the selected preliminary design, the detail or *final design* of all parts and components and the writing of certain specifications can begin. During manufacture and development testing some design changes may become necessary to improve the manufacture, reduce cost, or remedy a technical problem that became evident. In many organizations the final, detailed design is again submitted to a design review before manufacturing can begin. The new motor will then start its development testing. In some larger, expensive motors, that have a lot of heritage from prior proven motors, the development may consist of a single motor firing. For motors which are built in large quantities and for motors with major new features, the development and qualification may involve the testing of 10 to 30 motors. The final design ends when all detail drawings or CAD images and a final parts list are completed, and specifications for motor testing, certain manufacturing operations, or materials/component acceptance have been prepared. The detail design is considered to be completed when the motor successfully passes its development and qualification tests and begins production.

Example 15–1. This example shows one method for making a preliminary determination of the design parameters of a solid rocket using a composite propellant. The rocket is launched at altitude and flies at constant altitude. The following data are given:

| | |
|---------------------------|---|
| Specific impulse (actual) | $I_s = 240$ sec at altitude and 1000 psia |
| Burning rate | $r = 0.8$ in./sec at 1000 psia and 60°F grain temperature |
| Propellant density | $\rho_b = 0.066$ lbm/in. ³ |
| Specific heat ratio | $k = 1.25$ |
| Chamber pressure, nominal | $p_1 = 1000$ psi |
| Desired average thrust | $F = 20,000$ lbf |
| Maximum vehicle diameter | $D = 16$ in. |
| Desired burn duration | $t_b = 5.0$ sec |
| Ambient pressure | 3.0 psi (at altitude) |
| Vehicle payload | 5010 lbm (includes structure) |

Approximately neutral burning is desired. Assume no erosion of nozzle material and no loss of insulation during burning.

SOLUTION

- Basic Design.** The total impulse I_t and propellant weight at sea level w_b are obtained from Eqs. 2–2 and 2–5. $I_t = Ft_b = I_s w_b = 20,000 \times 5.0 = 100,000$ lbf-sec. The propellant weight is $100,000/240 = 417$ lbf. Allowing for a loss of 2% for manufacturing tolerances and slivers, the total propellant weight is $1.02 \times 417 = 425$ lbf. The volume required for this propellant V_b is given by $V_b = w_b/\rho_b = 425/0.066 = 6439$ in.³. The web thickness $b = rt_b = 0.80 \times 5 = 4.0$ in.
- Case Dimensions.** The outside diameter is fixed at 16.0 in. Heat-treated steel with an ultimate tensile strength of 220,000 psi is to be used. The wall thickness t can be determined from Eq. 15–1 for simple circumferential stress as $t = (p_1 D)/(2\sigma)$. The value of p_1 depends on the safety factor selected, which in turn depends on the heating of the wall, the prior experience with the material, and so on; a safety factor of 2.0 is suggested to allow for surface scratches, combined stresses and welds, and

rough field handling. The value of D is the average diameter to the center of the wall. The wall thickness d is

$$d = 2.0 \times 1000 \times 15.83 / (2 \times 220,000) = 0.072 \text{ in.}$$

A spherical head end and a spherical segment at the nozzle end similar to Fig. 12-1 is assumed.

c. *Grain Configuration.* The grain will be cast into the case but will be thermally isolated from the case with an elastomeric insulator with an average thickness of 0.100 in. inside the case; the actual thickness will be less than 0.10 in. in the cylindrical and forward closure regions, but thicker in the nozzle entry area. The outside diameter D_o for the grain is determined from the case thickness and liner to be $16.0 - 2 \times 0.072 - 2 \times 0.10 = 15.66$ in. The inside diameter D_i of a simple hollow cylinder grain would be the outside diameter D_o minus twice the web thickness or $D_i = 15.66 - 2 \times 4.0 = 7.66$ in. For a simple cylindrical grain, the volume determines the effective length, which can be determined from the equation

$$V_b = \frac{\pi}{4} L(D_o^2 - D_i^2)$$

$$L = \frac{6439 \times 4}{\pi(15.66^2 - 7.66^2)} = 43.95 \text{ in.}$$

The web fraction would be $2b/D_o = 8/15.66 = 0.511$. The L/D_o of the grain is (approximately) $43.95/15.66 = 2.81$.

For grains with this web fraction and this L/D_o ratio, Table 12-4 suggests the use of an internal burning tube with some fins for a cone. A conocyl configuration is selected, although a slotted tube or fins would also be satisfactory. These grain shapes are shown in Figs. 12-1 and 12-17. The initial or average burning area will be found from Eqs. 12-1 and 2-5: namely $F = \dot{w}I_s = \rho_b A_b r I_s$

$$A_b = \frac{F}{\rho_b r I_s} = \frac{20,000}{0.066 \times 0.8 \times 240} = 1578.3 \text{ in.}^2$$

The actual grain now has to be designed into the case with spherical ends, so it will not be a simple cylindrical grain. The approximate volume occupied by the grain is found by subtracting the perforation volume from the chamber volume. There is a full hemisphere at the head end and a partial hemisphere of propellant at the nozzle end (0.6 volume of a full hemisphere):

$$V_b = \frac{1}{2}(\pi/6)D_o^3(1 + 0.6) + (\pi/4)D_o^2L$$

$$- (\pi/4)D_i^2(L + D_i/2 + 0.3D_i/2) = 6439 \text{ in.}^3$$

This is solved for L , with $D = 15.62$ in. and the inside diameter $D_i = 7.66$ in. The answer is $L = 38.24$ in. The initial internal hollow-tube burn area is about

$$\pi D_i(L + D_i/2 + 0.3D_i/2) = 1040 \text{ in.}^2$$

The desired burn area of 1578 in.² is larger than 1040 in.², by about 538 in.². Therefore, an additional burn surface area of 538 in.² will have to be designed into

the cones of a conocyl configuration or as slots in a slotted tube design. Actually, a detailed geometrical study should be made analyzing the instantaneous burn surface after arbitrary short time intervals and selecting a detailed grain configuration where A_b stays approximately constant. This example does not go through a preliminary stress and elongation analysis, but it should be done.

- d. *Nozzle Design.* From Chapter 3 the nozzle parameters can be determined. The thrust coefficient C_F can be found from curves of Figs. 3–6, 3–7, and 3–8 or Eq. 3–30 for $k = 1.25$ and a pressure ratio of $p_1/p_2 = 1000/3 = 333$. Then $C_F = 1.73$. The throat area is from Eq. 3–31:

$$A_t = F/p_1 C_F = 20,000/(1000 \times 1.73) = 11.56 \text{ in.}^2$$

The throat diameter is $D_t = 3.836$ in. The nozzle area ratio for optimum expansion (Fig. 3–6) A_2/A_t is about 27. The exit area and diameter are therefore about $A_e = 312 \text{ in.}^2$ and $D_e = 19.93$ in. However, this is larger than the maximum vehicle diameter of 16.0 in. ($A_2 = 201 \text{ in.}^2$), which is the maximum for the outside of the nozzle exit. Allowing for an exit cone thickness of 0.10 in., the internal nozzle exit diameter D_2 is 15.80 in. and A_2 is 196 in.^2 . This would allow only a maximum area ratio of $196/11.56$ or 16.95. Since the C_F values are not changed appreciably for this new area ratio, it can be assumed that the nozzle throat area is unchanged.

This nozzle can have a thin wall in the exit cone, but requires heavy ablative materials, probably in several layers near the throat and convergent nozzle regions. The thermal and structural analysis of the nozzle is not shown here.

- e. *Weight Estimate.* The steel case weight (assume a cylinder with two spherical ends and that steel weight density is 0.3 lbf/in.^3) is

$$\begin{aligned} d\pi DL\rho + (\pi/4)dD^2\rho &= 0.072\pi \times 15.83 \times 38.24 \times 0.3 \\ &\quad + 0.785 \times 0.072 \times 15.83^2 \times 0.3 \\ &= 45.3 \text{ lbf} \end{aligned}$$

With attachments, flanges, igniter, and pressure tap bosses, this is increased to 51 lbf. The nozzle weight is composed of the weights of the individual parts, estimated for their densities and geometries. This example does not go through the detailed calculations, but merely gives the result of 30.2 lbf. Assume an expended igniter propellant weight of 2.0 lbf and a full igniter weight of 5.0 lbf. The total weight then is

| | |
|-------------------------------|-----------|
| Case weight at sea level | 51.0 lbf |
| Liner/insulator | 14.2 lbf |
| Nozzle, including fasteners | 30.2 lbf |
| Igniter case and wires | 2.0 lbf |
| | |
| Total inert hardware weight | 97.4 lbf |
| Igniter powder | 3 lbf |
| Propellant (effective) | 417 lbf |
| Unuseable propellant (2%) | 8 lbf |
| | |
| Total weight | 525.4 lbf |
| Propellant and igniter powder | 428.0 lbf |

- f. *Performance.* Since the total impulse is $I_t = F\Delta t = 20,000 \times 5 = 100,000$ lbf-sec, the total impulse-to-weight ratio is $100,000/525.4 = 190.3$. Comparison with I_s shows this to be an acceptable value, indicating a good performance. The total launch weight is $5010 + 525.4 = 5535$ lbf, and the weight at burnout or thrust termination is $5535 - 428 = 5107$ lbf. The initial and final thrust-to-weight ratios and accelerations are

$$F_i/w = 20,000/5535 = 3.61$$

$$F_f/w = 20,000/5107 = 3.92$$

The acceleration in the direction of thrust is 3.61 times the gravitational acceleration at start and 3.92 at burnout.

- g. *Erosive Burning.* The ratio of the port area to the nozzle throat area at start is $(7.66/3.836)^2 = 3.97$. This is close to the limit of 4.0, and erosive burning is not likely to be significant. A simple analysis of erosive burning in the conical cavity should also be made, but it is not shown here.

With partial loss of nozzle material and insulation, the thrust and nozzle area will increase, the chamber pressure will decrease, and the specific impulse will be lower due to the additional mass flow from the nozzle and insulation.

PROBLEMS

- In Figs. 14–4 and 14–16 it can be seen that higher pressures and higher heat transfer rates promote faster ignition. One way to promote more rapid ignition is for the nozzle to remain plugged until a certain minimum pressure has been reached, at which time the nozzle plug will be ejected. Analyze the time saving achieved by such a device, assuming that the igniter gas evolution follows Eqs. 12–5 and 12–3. Under what circumstances is this an effective method? Make assumptions about cavity volume, propellant density, and so on.
- Compare a simple cylindrical case with hemispheric ends (ignore nozzle entry or igniter flanges) for an alloy steel metal and two reinforced fiber (glass and carbon)-wound filament case. Use the properties in Table 15–2 and thin shell structure theory. Given:

| | |
|--|---------|
| Length of cylindrical portion | 370 mm |
| Outside cylinder diameter | 200 mm |
| Internal pressure | 6 MPa |
| Web fraction | 0.52 |
| Insulator thickness (average) | |
| for metal case | 1.2 mm |
| for reinforced plastic case | 3.0 mm |
| Volumetric propellant loading | 88% |
| Propellant specific gravity | 1.80 |
| Specific impulse (actual) | 248 sec |
| Nozzle igniter and mounting provisions | 0.20 kg |

Calculate and compare the theoretical propulsion system flight velocity (without payload) in a gravity-free vacuum for these three cases.

3. The following data are given for a case that can be made of either alloy steel or fiber-reinforced plastic.

| Type | Metal | Reinforced Plastic |
|--|-------|-------------------------------------|
| Material | D6aC | Organic filament composite (Kevlar) |
| Physical properties | | See Table 15-2 |
| Poisson ratio | 0.27 | 0.38 |
| Coefficient of thermal expansions, m/m-K $\times 10^{-6}$ | 8 | 45 |
| Outside diameter (m) | 0.30 | 0.30 |
| Length of cylindrical section (m) | 0.48 | 0.48 |
| Hemispherical ends | | |
| Nozzle flange diameter (m) | 0.16 | 0.16 |
| Average temperature rise of case material during operation ($^{\circ}\text{F}$) | 55 | 45 |

Determine the growth in diameter and length of the case due to pressurization, heating, and the combined growth and interpret the results.

4. A high-pressure helium gas tank at 8000 psi maximum storage pressure and 1.5 ft internal diameter is proposed. Use a safety factor of 1.5 on the ultimate strength. The following candidate materials are to be considered:

Kevlar fibers in an epoxy matrix (see Table 15-2)

Carbon fibers in an epoxy matrix

Heat-treated welded titanium alloy with an ultimate strength of 150,000 psi and a weight density of 0.165 lb/in.³

Determine the dimensions and sea-level weight of these three tanks and discuss their relative merits. To contain the high-pressure gas in a composite material that is porous, it is also necessary to include a thin metal inner liner (such as 0.016-in.-thick aluminum) to prevent loss of gas; this liner will not really carry structural loads, but its weight and volume need to be considered.

5. Make a simple sketch and determine the mass or sea-level weight of a rocket motor case that is made of alloy steel and is cylindrical with hemispherical ends. State any assumptions you make about the method of attachment of the nozzle assembly and the igniter at the forward end.

| | |
|-------------------------------------|-------------|
| Outer case and vehicle diameters | 20.0 in. |
| Length of cylinder portion of case | 19.30 in. |
| Ultimate tensile strength | 172,000 psi |
| Yield strength | 151,300 psi |
| Safety factor on ultimate strength | 1.65 |
| Safety factor on yield strength | 1.40 |
| Nozzle bolt circle diameter | 12.0 in. |
| Igniter case diameter (forward end) | 3.00 in. |
| Chamber pressure, maximum | 1520 psi |

6. Design a solid propellant rocket motor with insulation and liner. Use the AP/Al-HTPB propellant from Table 12-3 for Orbus 6. The average thrust is 3600 lbf and the average burn time is 25.0 sec. State all the assumptions and rules used in your solution and give your reasons for them. Make simple sketches of a cross section and a half section with overall dimensions (length and diameter), and determine the approximate loaded propellant mass.
7. The STAR 27 rocket motor (Fig. 12-1 and Table 12-3) has an average erosion rate of 0.0011 in./sec. **(a)** Determine the change in nozzle area, thrust, chamber pressure, burn time, and mass flow at cutoff. **(b)** Also determine those same parameters for a condition when, somehow, a poor grade of ITE material was used that had three times the usual erosion rate. Comment on the difference and acceptability.
Answer: Nozzle area increases by about **(a)** 5.3% and **(b)** 14.7% and chamber pressure at cutoff decreases by approximately the same percentage.

REFERENCES

- 15-1. NASA, *National Space Transportation System*, Vols. 1 and 2, U.S. Government Printing Office, Washington, DC, June 1988.
- 15-2. M. Salita, "Simple Finite Element Analysis Model of O-Ring Deformation and Activation during Squeeze and Pressurization," *Journal of Propulsion and Power*, Vol. 4, No. 6, November–December 1988.
- 15-3. J. H. Hildreth, "Advances in Solid Rocket Motor Nozzle Design and Analysis Technology since 1970," Chapter 2; A. Truchot, "Design and Analysis of Solid Rocket Motor Nozzle," Chapter 3; P. R. Evans, "Composite Motor Case Design," Chapter 4; A. J. P. Denost, "Design of Filament Wound Rocket Cases," Chapter 5; H. Baham and G. P. Thorp, "Consideration for Designers of Cases for Small Solid Propellant Rocket Motors," Chapter 6; all in *Design Methods in Solid Rocket Motors*, AGARD Lecture Series LS 150, Advisory Group for Aerospace Research and Development, NATO, revised 1988.
- 15-4. B. H. Prescott and M. Macocha, "Nozzle Design," Chapter 6; M. Chase and G. P. Thorp, "Solid Rocket Motor Case Design," Chapter 7; in G. E. Jensen and D. W. Netzer (Eds.), Vol. 170, *Progress in Astronautics and Aeronautics*, American Institute of Aeronautics and Astronautics, 1996.
- 15-5. A. de Rouvray, E. Haug, and C. Stavrindis, "Analytical Computations for Damage Tolerance Evaluations of Composite Laminate Structures," *Acta Astronautica*, Vol. 15, No. 11, 1987, pp. 921–930.
- 15-6. D. Beziers and J. P. Denost, "Composite Curing: A New Process," AIAA Paper 89-2868, July 1989.
- 15-7. A. Groves, J. Margetson, and P. Stanley, "Design Nomograms for Metallic Rocket Cases Reinforced with a Visco-elastic Fiber Over-wind," *Journal of Spacecraft and Rockets*, Vol. 24, No. 5, September–October 1987, pp. 411–415.
- 15-8. S. Boraas, "Modeling Slag Deposition in Space Shuttle Solid Rocket Motor," *Journal of Spacecraft and Rockets*, Vol. 21, No. 1, January–February 1984.
- 15-9. B. H. Broguere, "Carbon/Carbon Nozzle Exit Cones: SEP's Experience and New Developments," AIAA Paper 97-2674, July 1997.
- 15-10. "Solid Rocket Motor Igniters," NASA SP-8051, March 1971 (N71-30346).

- 15–11. R. Bauchalk, “High Mass Fraction Booster Demonstration,” AIAA Paper 90–2326, July 1990.
- 15–12. L. LoFiego, *Practical Aspects of Igniter Design*, Combustion Institute, Western States Section, Menlo Park, CA, 1968 (AD 69–18361).
- 15–13. R. Fabrizi and A. Annovazzi, “Ariane 5 P230 Booster Grain Design and Performance Study,” AIAA Paper 89–2420, July 1989.
- 15–14. A. Truchot, “Overall Optimization of Solid Rocket Motors,” Chapter 11 in *Design Methods in Solid Rocket Motors*, AGARD Lecture Series LS 150, Advisory Group for Aerospace Research and Development, NATO, revised 1988.

CHAPTER 16

HYBRID PROPELLANT ROCKETS*

Rocket propulsion concepts in which one propellant component is stored in the liquid phase while the other is stored in the solid phase are called *hybrid propulsion systems*. Hybrid propulsion has been of considerable interest in the commercial rocket business and in space applications. The main advantages of these propulsion systems are: (1) enhanced safety from explosion or detonation during fabrication, storage, and operation; (2) start–stop–restart capabilities; (3) relative simplicity which may translate into low overall system cost compared to liquids; (4) higher specific impulse than solid rocket motors and higher density-specific impulse than liquid bipropellant engines; and (5) the ability to smoothly change thrust over a wide range on demand. Although hybrids have many unique features of their own, they do benefit from the developments in liquid and solid rockets. Early hybrid motors were produced for target drones and some tactical missiles. Experimental hybrid motors in sizes between 2 and 250,000 lbf thrust have been developed and ground tested. A few of the large and small hybrid motors have flown in experimental vehicles. However, to date none of the larger systems have been selected for production applications.

Among the disadvantages of hybrid systems are: (1) mixture ratio and hence specific impulse may vary during steady-state operation (as well as during throttling); (2) relatively complicated fuel geometries with significant unavoidable fuel residues (slivers) at end of burn, which somewhat reduces the mass fraction and can vary if there is random throttling; (3) prone to large-amplitude, low-frequency pressure fluctuations (termed chugging); and (4) relatively complicated internal motor ballistics resulting in incomplete descriptions, both of regression rates of

*This chapter was contributed originally for the 6th edition by Terry A. Boardman and a modified version appeared in the 7th edition. That version has been further revised for this edition.

the fuel and of motor-scaling effects, affecting the design of large hybrid systems. While cracks in the solid component may not be as catastrophic as those in solid motors, the total surface area does influence the fuel release, and this area may change in unpredictable ways during rocket operation in some of the more complicated designs.

There are presently three distinct configurations of hybrid propulsion systems (Ref. 16–1). By far the most common arrangement, termed the *classical* or *typical configuration*, is for the fuel to be in the solid phase and for the oxidizer to be stored as a liquid, and many such combinations have been experimentally evaluated. The *inverse* or *reverse configuration* has the oxidizer as a solid and the fuel is in liquid form. The third one, called the *mixed hybrid configuration*, has a small amount of solid oxidizer imbedded in the solid fuel, and the fuel-rich mixture is then burned with additional oxidizer injected in an afterburner chamber, or simultaneously at the head and at the end of the grain cavity. This last configuration results from attempts to enhance the regression rates and thus decrease the chamber volume (Ref. 16–2). Increased regression rates can also be obtained in the classical configuration with metallized fuel added to the grain. Designs with special chambers upstream and downstream of the solid component region are common to most configurations. Figure 16–1 shows a proposed classical configuration design consisting of liquid oxygen–hydroxyl-terminated polybutadiene (HTPB) solid fuel combination intended for Space Shuttle type of

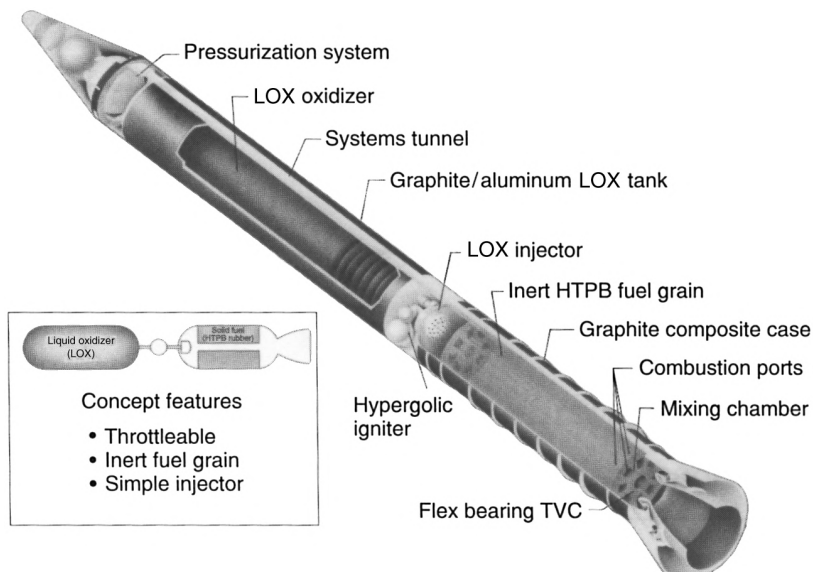


FIGURE 16–1. Large hybrid rocket booster concept capable of boosting the Space Shuttle. It has an inert solid fuel grain, a pressurized liquid oxygen feed system, and can be throttled. Multiple ports are required to achieve the large fuel surface necessary for high fuel flow rates.

applications. The oxidizer is shown in Fig. 16–1 as a pressure-fed system but a turbopump system could also be used. The oxidizer can be either a noncryogenic (storable) liquid or a cryogenic liquid depending on the application and the required specific impulse. In this hybrid propulsion system concept, the oxidizer is injected into a precombustion or vaporization chamber upstream of the primary fuel region. The fuel grain cavity contains numerous axial combustion ports that generate fuel vapor to react with the injected oxidizer. An aftermixing chamber is provided to ensure that all fuel and oxidizer are essentially completely burned before entering the nozzle.

16.1. APPLICATIONS AND PROPELLANTS

Hybrid propulsion is well suited to applications or missions requiring throttling, command shutdown and restart, long-duration missions requiring storable nontoxic propellants, or infrastructure operations (manufacturing and launch) that would benefit from a non-self-deflagrating propulsion system. Such applications would include primary boost propulsion for space launch vehicles, upper stages, and satellite maneuvering systems. Hybrids have been used to boost a winged manned space ship.

Many early hybrid rocket motor developments were aimed at target missiles and low-cost tactical missile applications (Ref. 16–3). Other development efforts focused on high-energy upper-stage motors. In recent years development efforts have concentrated on booster prototypes for space launch applications. In another program (Ref. 16–3), a hybrid motor was developed for high-performance upper-stage applications with design requirements that included a nominal thrust level of 22,240 N and an 8:1 throttling range. Oxygen difluoride was selected as the oxidizer for use with a lithium hydride/polybutadiene fuel grain. Analytical and experimental investigations have been made using other high-performance propellants. High-energy oxidizers include chlorine/fluorine compounds such as ClF_3 and ClF_5 . Complementary high-energy fuels are typically hydrides of light metals, such as beryllium, lithium, and aluminum, mixed with a suitable polymeric binder (Ref. 16–4). Delivered vacuum-specific impulse levels for these high-energy hybrid propellants are in the 350- to 380-sec range, depending on nozzle expansion ratio. Combustion efficiencies of 95% of theoretical values have been achieved in tests with these propellants; however, none of these exotic formulation systems have seen use on flight vehicles.

A more practical, although lower energy, upper-stage hybrid propellant system is 90 to 95% hydrogen peroxide oxidizer combined with HTPB fuel. Hydrogen peroxide (Ref. 16–5) is considered storable for time periods typical of upper-stage mission cycles (oxidizer tanking to mission completion on the order of several months) and is relatively inexpensive. In solid rocket motors, HTPB is used as the binder to consolidate the aluminum fuel and ammonium perchlorate oxidizer matrix. In a hybrid, HTPB becomes the entire fuel constituent. HTPB is low cost, processes easily, and will not self-deflagrate under any conditions.

A common propellant system for large hybrid booster applications is liquid oxygen (LOX) oxidizer and HTPB fuel. Liquid oxygen is a widely used oxidizer in the space launch industry, is relatively safe, and delivers high performance at low cost. This hybrid propellant combination produces a nontoxic, relatively smoke-free exhaust. The LOX/HTPB propellant combination favored for booster applications is chemically and performance-wise equivalent to a LOX–kerosene bipropellant system. In general, metallized solid fuels are expected to increase performance, but beryllium is very toxic, boron is hard to ignite, lithium has a low heat of combustion, and aluminum oxides increase the molecular mass of the combustion products beyond the temperature gain. Hence the search for hydrides and slurries containing these metals to offset their intrinsic disadvantages but this field is still in the research stages. As far as recently considered liquid oxidizers, hydrogen peroxide (H_2O_2), nitrous oxide (N_2O), and HAN (hydroxyl ammonium nitrate) have been considered because of their desirable thermochemical properties and density-specific impulse. Their regression rates and combustion efficiencies are comparable to those obtained using LOX, but they have storage advantages and comparable degrees of “greenness.”

Where a smoky exhaust is not a detriment, hybrid propellants for certain applications may benefit from the addition of powdered aluminum to the fuel. This increases the combustion temperature, reduces the stoichiometric mixture ratio, and increases fuel density as well as overall density-specific impulse. Although density-specific impulse ($\rho_f I_s$) is increased, addition of aluminum to the fuel actually reduces specific impulse. Figure 16–2 illustrates theoretical vacuum-specific impulse levels (calculated at 1000 psia chamber pressure and a 10:1 nozzle expansion ratio) for a variety of cryogenic and storable oxidizers used in conjunction with HTPB fuel. Table 16–1 tabulates the heat of formation for HTPB reacted with various oxidizers.

A suborbital sounding rocket was successfully launched in 2002 by Lockheed Martin using a large-scale hybrid rocket motor. The American Rocket Company (AMROC) before its demise tested many hybrid motors from 100 to 250,000 lbf of thrust. In 1998, SpaceDev (Ref. 16–6) obtained the technical rights, proprietary data, and patents produced by AMROC. A smaller commercial version of the Space Shuttle has been made by Scaled Composites with a hybrid propulsion system (developed by SpaceDev) which, in a well-publicized accomplishment, won the Ansari X-Prize when it's SpaceShipOne (see Fig. 16–3) reached space in 2004 with two suborbital manned flights. In 1999, a consortium of aerospace companies also tested several 250,000-lbf thrust LOX/HTPB hybrid prototypes as a candidate strap-on booster for space launch vehicles (see Ref. 16–7). In these motors, polycyclopentadiene (PCPD) is added to the HTPB fuel to increase fuel density by about 10% over HTPB alone. The motors were designed to operate for 80 sec at a LOX flow rate of 600 lbm/sec with a maximum chamber pressure of 900 psi. Figure 16–4 illustrates a cross section of one motor configuration. Test results indicated additional work is necessary to develop large hybrid motor configurations that exhibit stable combustion throughout the motor burn, and in understanding fuel regression-rate scale-up factors.

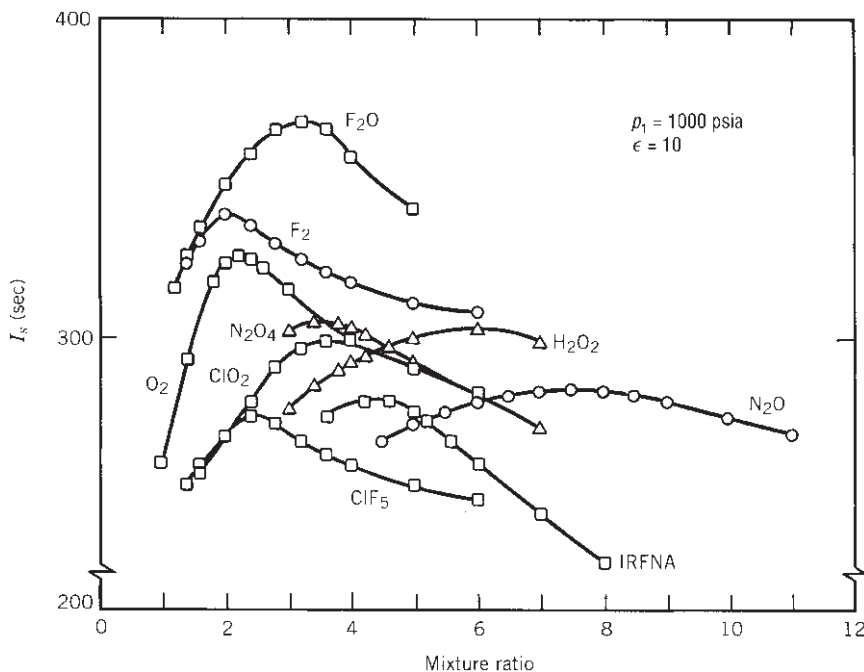


FIGURE 16–2. Theoretical vacuum-specific impulse of selected oxidizers reacted with hydroxyl-terminated polybutadiene fuel. The I_s of the O_2 /HTPB propellant is comparable to that of a LOX/kerosene bipropellant engine.

TABLE 16–1. Thermochemical Properties of Selected Oxidizers Reacted with HTPB Fuel

| Oxidizer | Type | Boiling Point (°C) | Density (g/cm ³) | $\Delta_f H^a$ (kcal/mol) |
|--------------------|-----------|-----------------------|---------------------------------|---------------------------|
| O_2 | Cryogenic | -183 | 1.149 | -3.1 |
| F_2^c | Cryogenic | -188 | 1.696 | -3.0 |
| O_3 | Cryogenic | -112 | 1.614 | +30.9 |
| F_2O^c | Cryogenic | -145 | 1.650 | +2.5 |
| $F_2O_2^c$ | Cryogenic | -57 | 1.450 | +4.7 |
| N_2O | Cryogenic | -88 | 1.226 | +15.5 |
| N_2O_4 | Storable | +21 | 1.449 | +2.3 |
| IRFNA ^b | Storable | +80 – +120 | 1.583 | -41.0 |
| H_2O_2 | Storable | +150 | 1.463 | -44.8 |
| ClO_2^c | Storable | +11 | 1.640 | +24.7 |
| CIF_5^c | Storable | +11 | 1.810 | -44.4 |

^a $\Delta_f H$ is the heat of formation at standard conditions as defined in Chapter 5.

^bInhibited red fuming nitric acid.

^cHighly toxic, explored but not pursued.

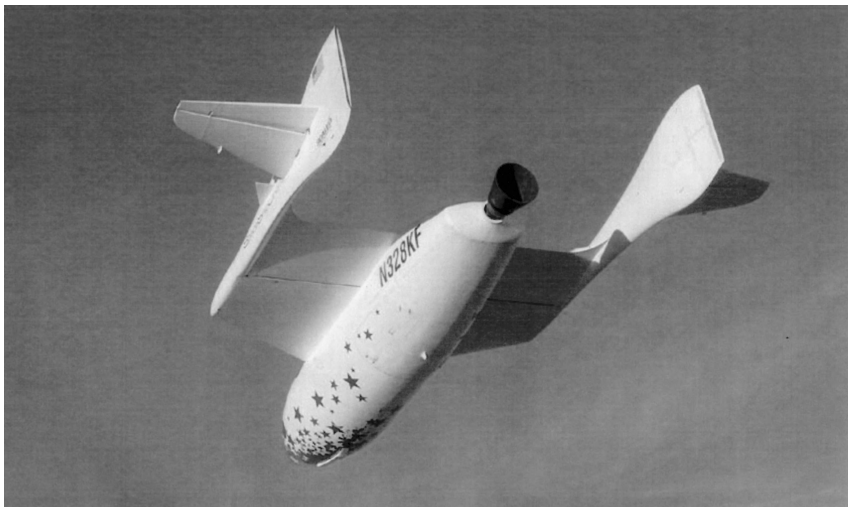
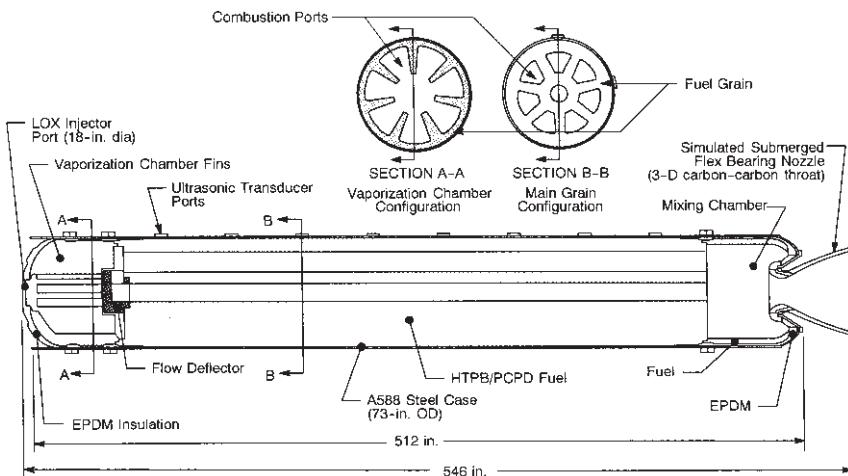


FIGURE 16–3. SpaceShipOne gliding down for landing. This air ship uses a hybrid propulsion system to produce its main thrust. The propellant is N₂O-HTPB. (Photo by scaled composites. SpaceShipOne is a Paul G. Allen Project © Mojave Aerospace Ventures, LLC.)



| | |
|---------------------------------|-----------------------------|
| Maximum operating pressure | 900 psia |
| Maximum vacuum thrust | 250,000 lbf |
| Throat diameter, initial | 14.60 in. |
| Nozzle expansion ratio, initial | 12 |
| Liquid oxygen flow rate | 420–600 lbm/sec (throttles) |
| Fuel weight | 45,700 lbf |
| Burn time | 80 sec |

FIGURE 16–4. 250,000 lbf thrust hybrid booster design parameters and section of fuel grain and nozzle. The vaporization chamber fins and flow deflector are designed to promote flame holding in combustion ports.

A hybrid fuel grain is ignited by providing a source of heat, which initiates gasification of the solid fuel grain at the head end of the motor. Subsequent initiation of oxidizer flow provides the required flame spreading to fully ignite the motor. Ignition is typically accomplished by injection of a hypergolic fluid into the motor combustion chamber. Using the motor described in Fig. 16-4 as an example, a mixture of triethyl aluminum (TEA) and triethyl borane (TEB) is injected into the vaporization chamber. The TEA-TEB mixture ignites spontaneously on contact with air in the combustion chamber, vaporizing fuel in the dome region. Subsequent injection of liquid oxygen completes ignition of the motor. TEA-TEB mixtures are currently used for motor ignition in the Atlas and Delta commercial launch vehicles. Experimenters (Refs. 16-8 and 16-9) describe solid fuels that will ignite spontaneously at ambient temperature and pressure when sprayed with specific oxidizers other than LOX. Small hybrid motors, such as those used in a laboratory environment with gaseous oxygen oxidizer, are often electrically ignited by passing current through a resistor such as steel wool located in the combustion port, or by use of a propane or hydrogen ignition system.

16.2. INTERIOR HYBRID MOTOR BALLISTICS

As the fuel grain in the classical hybrid configuration contains no oxidizer, combustion processes occur in the gaseous phase and hence fuel surface regression is markedly different from that of a solid rocket motor. Because the solid fuel must vaporize before combustion occurs, fuel surface regression is intrinsically related to the coupling of combustion port fluid dynamics and the heat transferred to the fuel grain surface. The primary combustion region has been shown to be contained within a relatively narrow flame zone located within a boundary layer region that develops and grows over the fuel grain surface (Ref. 16-10). Among the mechanisms of heat transfer to the fuel grain surface are convection and radiation. Because the hybrid's field is largely empirical, it should be understood that any motor characteristics will strongly depend on the propellant system and on the scale and configuration of the combustor chamber being described.

Figure 16-5 depicts a simplified model of the hybrid combustion process for a nonmetallized (or nonradiating) fuel system. Fuel is vaporized as a result of heat being transferred from the flame zone to the fuel mass. Vaporized fuel is convected away from the heated surface toward the flame zone while the oxidizer from the free stream (core flow) is transported to the flame zone by turbulent diffusion. The flame becomes established at a location within the boundary layer determined by the stoichiometric conditions under which combustion can occur. The thickness of the flame zone is governed primarily by the rate at which the oxidation reaction occurs. This rate is largely dependent on the pressure and typically follows an exponential dependence on temperature.

Factors affecting the development of the fuel grain boundary layer and, hence, fuel regression characteristics include pressure and gas temperature, grain composition, combustion port oxidizer mass flow rate, and combustion port length

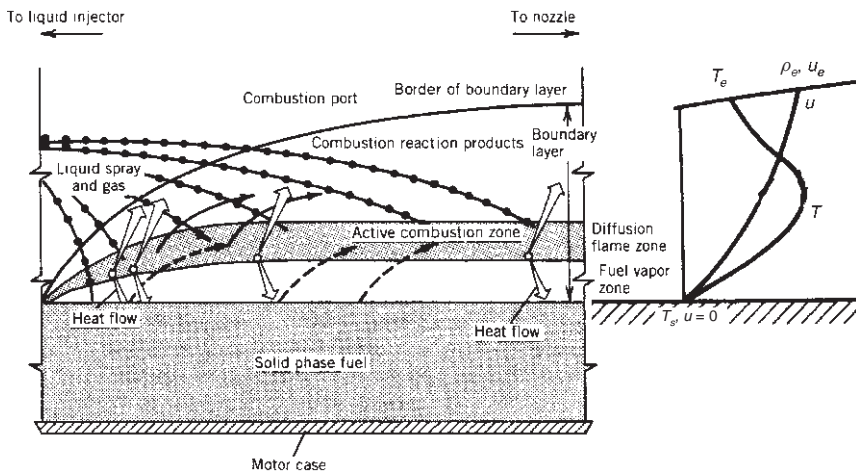


FIGURE 16–5. Simplified model of the diffusion-controlled hybrid combustion process, illustrating the flame zone embedded within the fuel boundary layer.

and diameter. This boundary layer is more complex and more robust than that introduced in Chapter 3 for the supersonic nozzle. Heat transfer relationships between the gas and the solid phase depend on whether the boundary layer is laminar or turbulent. In a typical hybrid using oxygen, the Reynolds number per unit axial length is on the order of 1 to 2×10^5 per inch of grain length for flux levels between 0.3 and 0.67 lbm/sec/in.². Thus the properties of turbulent boundary layers govern the convective heat transfer (to nonmetallized fuel grains) and empirical equations are often utilized. Figure 16–6 summarizes the overall behavior of many oxidizer/solid-fuel combinations. As shown in this figure, there are three distinct regimes as a function of increasing mass-flow–velocity in the free stream ($G = \rho v$, total or oxidizer mass flow rate). At the low mass flux regime, radiative heat transfer phenomena are manifest in the form of pressure and diameter effects on the optical transmissivity of the propellant gas (Ref. 16–12), effects which may also arise from any metal loading present (at the “melting limit” the fuel grain may melt, char, or undergo subsurface decomposition; Ref. 16–11); the intermediate range represents fully turbulent heat and mass transfer, and the regression rate dependence on G is consistent with the traditional convective diffusion results; at the high end results from gas-phase kinetics on chemical reactions are apparent, and a different type of pressure dependence appears (the “flooding limit” results when the flame is extinguished by the high oxidizer flow rates and depends on the pressure and the chemical reactivity of the propellants). Since solid fuel regression rates are a function of many parameters, the reader is encouraged to consult the relevant literature before using any of the correlations included in this chapter. A thorough summary of classical hybrid regression rate equations is given in Ref. 16–11, which clearly exemplifies the complexity of this subject.

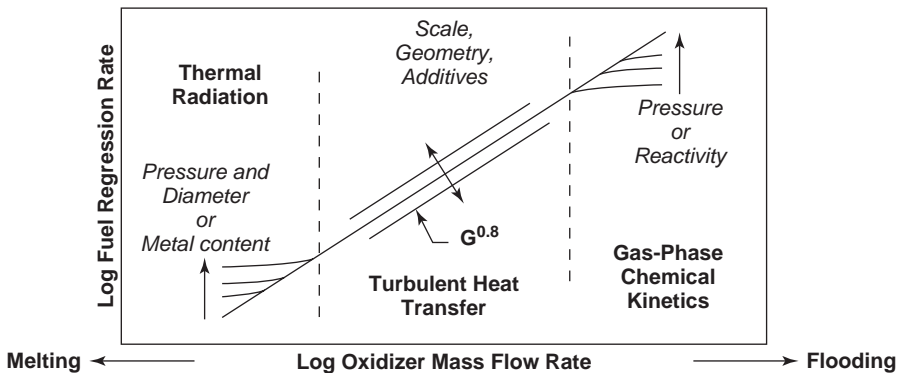


FIGURE 16–6. Hybrid regimes of regression rate dependencies. (Adapted from Ref. 16–11.)

In a nonmetallized fuel grain, at the pressures and flux levels of interest for propulsion applications, heat transfer by convection is thought to be much larger than that transferred by gas-phase radiation or radiation from soot particles in the flow. As a result the basic characteristics of fuel grain regression may be explored via an analysis of convective heat transfer in a turbulent boundary layer. Thus, for the intermediate regime of Fig. 16–6, the following equation may be used for the fuel regression rate, \dot{r} :

$$\dot{r} = 0.036 \frac{G^{0.8}}{\rho_f} \left(\frac{\mu}{x} \right)^{0.2} \beta^{0.23} \quad (16-1)$$

where G is the free-stream propellant mass velocity (total oxidizer and fuel flow per unit area) in a combustion port at any given axial location x , ρ_f is the solid-phase fuel density, μ is the combustion gas viscosity, and β is a nondimensional fuel mass flux reflecting the fuel vaporization and evaluated at the fuel surface. All dimensions in Eq. 16–1 need to be in the English engineering system of units to match the numerical constant. The parameter β is frequently called the *blowing coefficient* and can be shown to also represent a nondimensional enthalpy difference between the fuel surface and flame zone (i.e., $\Delta h/h_v$ where h_v is the heat of gasification). Equation 16–1 indicates that, for nonradiative systems, hybrid fuel regression rates in this regime are strongly dependent on G and rather weakly dependent on axial location (x) and fuel blowing characteristics (β). It should also be noted that these regression rates are not explicitly dependent on chamber pressure. This is not the case for the other regimes shown in Fig. 16–6 because metallized hybrid fuel systems may exhibit a pronounced pressure dependence (see Ref. 16–13).

As the combustion port length increases, fuel added to the port increases the total port mass flux. In locations operating at low mixture ratios, the fuel mass increase may be of the same order as the oxidizer mass flow initially entering

the port. Given the weak dependence of regression rate on x in Eq. 16–1, it would be expected that fuel regression would increase along the flow direction with increases of G . While this generally turns out to be the case, fuel regression has been observed to both increase and decrease with increasing x , depending on the specifics of the motor configuration. In practice, axial fuel regression characteristics are strongly influenced by the oxidizer injection method and by precombustion/vaporization chamber design characteristics. General trends that have been observed with increasing x are: total mass flux increases, boundary layer thickness growths, flame-standoff distance increases from the surface, combustion port average gas density increases, and oxidizer concentration decreases.

Since the blowing coefficient β is not only an aerodynamic parameter but also a thermochemical parameter, and since its x dependence is of the same order, Eq. 16–1 is often simplified for purposes of preliminary engineering design by lumping the effects of x , β , fuel density, and gas viscosity into one parameter, usually called a . Moreover, in practice, deviations from the theoretical 0.8 power of the mass velocity exponent are often noted. The resulting simplified form of Eq. 16–1 is therefore written as

$$\dot{r} = a(G_o)^n \quad (16-2)$$

here G_o is the oxidizer mass velocity (i.e., the oxidizer mass flow rate divided by the combustion port area). The parameters a and n are empirically fitted constants. In the central range of Fig. 16–6, \dot{r} has been observed to have values between 0.05 and 0.2 in./sec and n has been observed to range between 0.4 and 0.7.

In the low mass flux end of Fig. 16–6 or when metallized fuels are utilized, radiation heat transfer cannot be neglected. Recent studies of this region have yielded accurate but elaborate empirical fits which are reported in Ref. 16–11. In essence, a radiation heat flux term must be added to the convective heat flux arriving at the fuel surface, and this results in modifications to the turbulent diffusion relations applicable here. A simpler empirical correlation that somewhat represents modifications in this end range behavior (Ref. 16–14) may be written as follows:

$$\dot{r} \approx 2.50\dot{r}_{\text{ref}}(1 - e^{-p_1/p_{\text{ref}}})(1 - e^{-D/D_{\text{ref}}}) \quad (16-3)$$

where p_{ref} and D_{ref} are empirically selected reference pressures and diameters, and the form of \dot{r}_{ref} is given by Eq. 16–2 (multiplied by 2.50 to normalize it).

In the high mass flux end, chemical kinetic effects dominate, and here a strong pressure dependence of the form $(p_1)^{0.5}$ is both predicted and observed. A useful empirical fit in the region where heterogenous reaction kinetics plays a role is of the form

$$\dot{r} = (\text{constant})(p_1)^{0.5}G^n x^{-m} \quad (16-4)$$

where the exponent n varies between 0.3 and 0.4 (lower values than 0.8 from the middle domain), and the exponent m varies between 0.1 and 0.2 which reflects a consistently weak dependence on the axial location (see Ref. 16–11 for details).

Whenever there is heavy reliance on empirical information, as in this field, special needs arise for further guidelines in using any given formulation; otherwise, applying these equations must be restricted only to their range of experimental observation. *Dimensional analysis and similarity theories* are designed to generalize experimental results by casting the variables in suitable dimensionless forms (e.g., see Eqs. 8–20, 8–21, and Problem 16–2) but the most satisfactory approach is the one where theory and experiment go hand in hand. The interested reader should consult Refs. 16–12 and 16–15.

16.3. PERFORMANCE ANALYSIS AND GRAIN CONFIGURATION

A characteristic operating feature of hybrids is that the fuel regression rate is typically less than one-third that of composite solid rocket propellants. It is very difficult to obtain fuel regression rates comparable to propellant burn rates in solid rocket motors. Consequently, practical high-thrust hybrid motor designs must have multiple perforations (combustion ports) in the fuel grain to produce the required fuel surface area. The performance of a hybrid motor (defined in terms of delivered specific impulse) depends critically on the degree of flow mixing attained in the combustion chamber. High performance stems from high combustion efficiency that is a direct function of the thoroughness with which unburned oxidizer exhausting from the combustion port is mixed with unburned fuel from within sublayers of the boundary layer. Multiple combustion ports serve to promote high combustion efficiency as a result of the turbulent mixing environment for unreacted fuel and oxidizer in the mixing chamber region downstream of the fuel grain.

A cross section of a typical high-thrust hybrid fuel grain is shown in Fig. 16–4. The number of combustion ports required is a motor optimization problem that must account for the desired thrust level, acceptable shifts in mixture ratio during burn, motor length and diameter constraints, and desired oxidizer mass velocity. Hybrid rocket motor design typically begins by specifying a desired thrust level and a propellant system. Subsequently, selection of the desired operating oxidizer-to-fuel mixture ratio (O/F ratio) determines the propellant characteristic velocity. Once the characteristic velocity and mixture ratio are specified, the total propellant flow rate and the subsequent split between oxidizer and fuel flow rates necessary to produce the required thrust level can be computed. The necessary fuel flow rate in a hybrid is determined by the total fuel surface area (perimeter and length of the combustion ports) and the fuel regression rate. As will be shown in subsequent sections, the fuel regression rate is primarily determined by the oxidizer mass velocity, also called oxidizer flux. The oxidizer flux is equal to the mass flow rate of oxidizer in a combustion port divided by the port cross-sectional area. Thus the fuel flow rate is intrinsically linked to the oxidizer flow rate and cannot be independently specified, as in a liquid rocket engine.

Much of the technology from liquid and solid propellant rockets is directly applicable to hybrid rockets; the main differences lie in the driving mechanisms for solid propellant burning and hybrid fuel regression. In a solid system, the oxidizer and fuel ingredients are well mixed during the propellant manufacturing process. Combustion occurs as a result of heterogeneous chemical reactions on or very near the surface of the solid propellant. The solid propellant burning rate is controlled by chamber pressure and follows the well-established law of Eq. 12–5, with empirical coefficients derived experimentally for specific propellant formulations. Since the rate of propellant gasification per unit area in a solid rocket motor, at a given propellant bulk temperature and in the absence of erosive burning, is determined only by chamber pressure, motor thrust is predetermined by the initial propellant grain surface area and grain geometrical characteristics.

In hybrids with metallized fuel grains, radiation from the metal oxide particle cloud in the combustion port contributes a major portion of the total heat flux to the fuel grain. The local regression rate of the fuel is also quite sensitive to the general turbulence level of the combustion port gas flow (Refs. 16–16 and 16–17). Localized combustion gas eddies or recirculation zones adjacent to the fuel surface act to significantly enhance the regression rate in these areas. Hybrid fuel regression rate is thought to be insensitive to fuel grain bulk temperatures over the range in which solid rocket motors may operate (-65 to 165°F). This is due to the absence of heterogeneous fuel/oxidizer reactions at the fuel surface (in which the reaction rates are temperature dependent) and because, over the above temperature range, the change in heat content of the solid fuel is small compared to the heat necessary to initiate vaporization of the fuel surface.

Selection of fuel ingredients can also have a significant impact on the grain regression rate, which is largely a function of the energy required to convert the fuel from solid to vapor phase (h_v). This energy is called the heat of gasification and, for polymeric fuels, includes the energy required to break polymer chains (heat of depolymerization) and the heat required to convert polymer fragments to gaseous phase (heat of vaporization). The term “heat of vaporization” is often used as a catchall phrase to include all decomposition mechanisms in hybrid fuels. In nonmetallized fuels, low heats of gasification tend to produce higher regression rates. In metallized fuels, the addition of ultra-fine aluminum (UFAI) powder (particle sizes on the order of 0.05 to 0.1 μm) to HTPB has been noted to significantly increase the fuel regression rate relative to a pure HTPB baseline (see Ref. 16–18 and Fig. 16–7). Hybrid propellants containing aluminum particles with diameters typical of those used in solid rocket propellants (40 to 400 μm) do not exhibit this effect.

An alternative form of Eq. 16–2, to account for an observed pressure and/or port diameter dependency, is given as

$$\dot{r} = aG_o^n p_1^m D_p^l \quad (16-5)$$

where m and l have been observed to vary between zero and 0.25 and zero and 0.7, respectively.

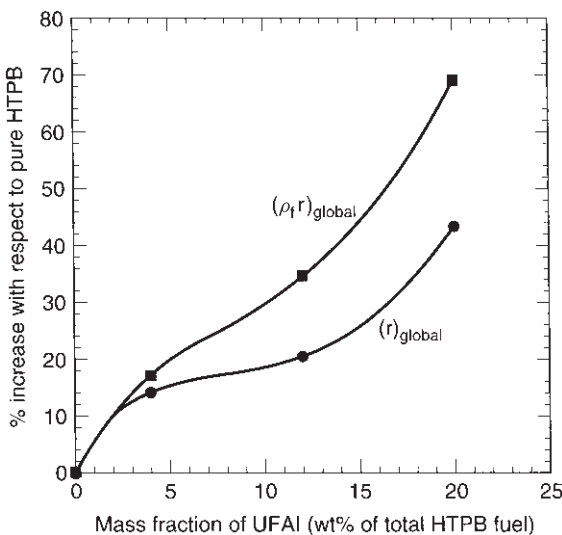


FIGURE 16-7. Ultra-fine aluminum (UFAI) powder mixed with HTPB significantly increases the fuel regression rate.

Figure 16-8 illustrates surface regression rate data obtained for the combustion of HTPB fuel grains and gaseous oxygen in rocket motor tests at two different scales. The first data set were obtained by testing fuel grains in a small laboratory-scale (2-in. motor diameter with a 0.43-in. combustion port diameter) rocket at varying gaseous oxygen flux levels. A least-squares regression analysis, performed to determine the constants in Eq. 16-2, indicates that, at this scale, the following relationship best describes the regression rate characteristics of HTPB as a function of oxygen mass flux:

$$\dot{r}_{\text{HTPB}} = 0.104 G_o^{0.681} \quad (16-6)$$

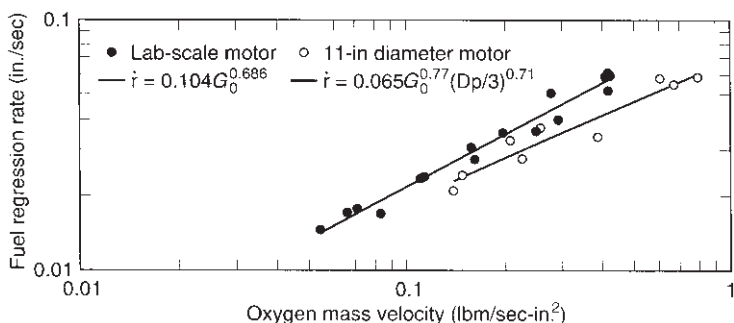


FIGURE 16-8. Hybrid regression rate has been observed to decrease as motor scale (combustion port diameter) increases.

Data obtained with the same propellant system in a larger 11-in.-diameter hybrid motor with combustion port diameters ranging between 3 and 6 in. exhibited a relatively strong dependence on combustion port diameter. Data from this testing was best matched with an expression in the form of Eq. 16–5:

$$\dot{r}_{\text{HTPB}} = 0.065G_o^{0.77}(D_p/3)^{0.71} \quad (16-7)$$

The difference in fuel regression characteristics between the two motor scales illustrates one of the central difficulties of hybrid motor design, that is, that of scaling ballistic performance. Scaling issues in hybrid motors are currently not well understood (in part because of the lack of sufficient valid data for different motor sizes) and the literature abounds with empirical regression rate scaling relationships. Computational fluid dynamic approaches to resolving the hybrid flow field and calculating fuel surface heating appear to offer the best hope of analytically evaluating scale effects (Ref. 16–19).

Dynamic Behavior

Dynamic behavior in hybrid propulsion systems is important because, as stated earlier, the mixture ratio varies even during steady-state flow of the oxidizer. When mass storage term changes (i.e., the propellant gas that remains to fill the increasing chamber volume as in solid motors, Section 12.1) may be neglected in the combustor cavity, then Eqs. 6–2 and 3–24 apply, namely,

$$\dot{m} = \dot{m}_o + \dot{m}_f = \frac{p_1 A_t}{c^*} \quad (16-8)$$

The steady thrust of a hybrid rocket motor can then be expressed as

$$F = \dot{m} I_s g_0 = (\dot{m}_o + \dot{m}_f) I_s g_0 \quad (16-9)$$

Changing the thrust or throttling of a hybrid is achieved by changing the oxidizer flow rate, usually by means of a throttling valve in the oxidizer feed line. The fuel flow is a function of the oxidizer flow but not necessarily a linear function. For circular port geometries with radius R , Eq. 16–2 may be recast as

$$\dot{r} = a \left(\frac{\dot{m}_o}{\pi R^2} \right)^n \quad (16-10)$$

The mass production rate of fuel is given by

$$\dot{m}_f = \rho_f A_b \dot{r} = 2\pi \rho_f R L \dot{r} \quad (16-11)$$

where A_b is the combustion port surface area and L is the port length. Combining Eqs. 16–10 and 16–11, one obtains the fuel production rate in terms of port radius and oxidizer mass flow rate:

$$\dot{m}_f = 2\pi^{1-n} \rho_f La \dot{m}_o^n R^{1-2n} \quad (16-12)$$

From this expression one will note that, for the particular value of $n = \frac{1}{2}$, the fuel mass flow rate is independent of combustion port radius and varies as the square root of oxidizer mass flow rate. For such a situation, if the oxidizer flow is reduced to one-half of its rated value, then the fuel flow will be reduced by a factor of 0.707 and the motor thrust, which depends on the total propellant flow ($\dot{m}_f + \dot{m}_o$), will not vary linearly with the change in oxidizer flow. Usually, as the thrust is decreased by reducing the oxidizer flow, the mixture ratio (\dot{m}_o/\dot{m}_f) is reduced, becoming increasingly fuel rich. In some hybrid motor concepts, a portion of the oxidizer is injected in a mixing chamber downstream of the fuel grain in order to maintain a more constant mixture ratio. However, for most applications, the system design can be optimized over the range of mixture ratios encountered with very little degradation of average specific impulse due to throttling.

Equation 16–12 also indicates that, for constant oxidizer flow, fuel production will increase with increasing port radius if $n < \frac{1}{2}$. For $n > \frac{1}{2}$, fuel production will decrease with increasing port radius.

For a fuel grain incorporating N circular combustion ports, Eq. 16–10 can be simply integrated to give combustion port radius, instantaneous fuel flow rate, instantaneous mixture ratio, and total fuel consumed as functions of burn time:

Combustion port radius R as a function of time and oxidizer flow rate:

$$R(t) = \left\{ a(2n+1) \left(\frac{\dot{m}_o}{\pi N} \right)^n t + R_i^{2n+1} \right\}^{1/(2n+1)} \quad (16-13)$$

Instantaneous fuel flow rate:

$$\dot{m}_f(t) = 2\pi N \rho_f La \left(\frac{\dot{m}_o}{\pi N} \right)^n \left\{ a(2n+1) \left(\frac{\dot{m}_o}{\pi N} \right)^n t + R_i^{2n+1} \right\}^{(1-2n)/(1+2n)} \quad (16-14)$$

Instantaneous mixture ratio:

$$\frac{\dot{m}_o}{\dot{m}_f}(t) = \frac{1}{2\rho_f La} \left(\frac{\dot{m}_o}{\pi N} \right)^{1-n} \left\{ a(2n+1) \left(\frac{\dot{m}_o}{\pi N} \right)^n t + R_i^{2n+1} \right\}^{(2n-1)/(2n+1)} \quad (16-15)$$

Total fuel consumed:

$$m_f(t) = \pi N \rho_f L \left[\left\{ a(2n+1) \left(\frac{\dot{m}_o}{\pi N} \right)^n t + R_i^{2n+1} \right\}^{2/(2n+1)} - R_i^2 \right] \quad (16-16)$$

where L is the fuel grain length, R_i is the initial port radius, N is the number of combustion ports of radius R_i in the fuel grain, and \dot{m}_o and \dot{m}_f are the total oxidizer and fuel flow rates, respectively. Although the above equations are strictly valid only for circular combustion ports, they may be used to give a qualitative understanding of hybrid motor behavior which is applicable to the burnout of noncircular ports as well.

16.4. DESIGN EXAMPLE

The preliminary design problem typically posed is to determine the approximate size of a hybrid booster, given numerous system requirements and design assumptions.

Example 16–1. Suppose that the operating characteristics of a Space Shuttle–class hybrid rocket booster are to be determined, given the following initial design requirements:

| | |
|--|-----------------------|
| Fuel | HTPB |
| Oxidizer | Liquid oxygen |
| Required booster initial thrust (vacuum) | 3.1×10^6 lbf |
| Burn time | 120 sec |
| Fuel grain outside diameter | 150 in. |
| Initial chamber pressure | 700 psia |
| Initial mixture ratio | 2.0 |
| Initial expansion ratio | 7.72 |

SOLUTION. Using the ratio of specific heats from Table 16–2 and the given initial nozzle expansion ratio, the vacuum thrust coefficient is determined from tables or direct calculation to be 1.735. Initial nozzle throat area and throat diameter are determined from

$$A_t = \frac{F_v}{C_{F_v} p_1} = \frac{3.1 \times 10^6 \text{ lbf}}{(1.735)(700 \text{ lbf/in.}^2)} = 2552.5 \text{ in.}^2$$

then $D_t = 57.01$ in. From the data of Table 16–2 for c^* versus mixture ratio, c^* corresponding to an initial mixture ratio of 2.0 is 5912 ft/sec. Theoretical c^* values are typically degraded to account for combustion inefficiency due to incomplete oxidizer/fuel mixing. Using a factor of 95%, the delivered c^* is 5616 ft/sec. Total initial propellant flow rate can now be determined as

$$\dot{m} = \frac{g_0 p_1 A_t}{c^*} = \frac{\left(32.174 \frac{\text{lbf}\cdot\text{ft}}{\text{lbf}\cdot\text{sec}^2}\right) (700 \text{ lbf/in.}^2) (2552.5 \text{ in.}^2)}{(0.95)(5912 \text{ ft/sec}^2)} = 10,236 \text{ lbm/sec}$$

Noting that *mixture ratio* is defined as in Chapter 6, Eq. 6–1,

$$r = \dot{m}_o / \dot{m}_f$$

TABLE 16-2. Theoretical Characteristic Velocity c^* and Ratio of Specific Heats k for Reaction Gases of Liquid Oxygen–HTPB Fuel

| Mass Mixture Ratio | c^* (ft/sec) | k |
|--------------------|----------------|-------|
| 1.0 | 4825 | 1.308 |
| 1.2 | 5180 | 1.282 |
| 1.4 | 5543 | 1.239 |
| 1.6 | 5767 | 1.201 |
| 1.8 | 5882 | 1.171 |
| 2.0 | 5912 | 1.152 |
| 2.2 | 5885 | 1.143 |
| 2.4 | 5831 | 1.138 |
| 2.6 | 5768 | 1.135 |
| 2.8 | 5703 | 1.133 |
| 3.0 | 5639 | 1.132 |

initial fuel and oxidizer flow rates follow at the initial mixture ratio of 2.0:

$$\begin{aligned}\dot{m} &= \dot{m}_o + \dot{m}_f = \dot{m}_f(r + 1) \\ \dot{m}_f &= \frac{10,236 \text{ lbm/sec}}{3} = 3412 \text{ lbm/sec} \\ \dot{m}_o &= 10,236 - 3412 = 6824 \text{ lbm/sec}\end{aligned}$$

Figure 16–9a illustrates a candidate seven-circular-port symmetric fuel grain configuration. The dashed lines represent the diameters to which the combustion ports burn at the end of 120 sec. The problem is to determine the initial port diameter such that, at the end of the specified 120-sec burn time, the grain diameter constraint of 150 in. is satisfied. The unknown quantity in this problem is the initial combustion port radius, R_i , and the fuel burn distance, d_b . In terms of initial port radius, the burn distance can be expressed via Eq. 16–13 as

$$d_b = R(t, R_i)|_{t=120} - R_i$$

The fuel grain diameter requirement of 150 in. is satisfied by the following relation:

$$150 \text{ in.} = 6R_i + 6d_b$$

Subscale motor test data indicate that one expression for the fuel surface regression rate can be described by Eq. 16–6. Assuming that these data are valid for the flux levels and port diameters under consideration (ignoring potential regression rate scaling issues), the above two relations can be combined to solve for the initial port radius and distance burned, yielding

$$R_i = 14.32 \text{ in.} \quad d_b = 10.68 \text{ in.}$$

Knowing the initial port radius, the oxidizer mass velocity can be determined:

$$G_o = \frac{\dot{m}_o}{NA_p} = \frac{6824 \text{ lbm/sec}}{7\pi(14.32 \text{ in.})^2} = 1.51 \text{ lbm/in.}^2\text{-sec}$$

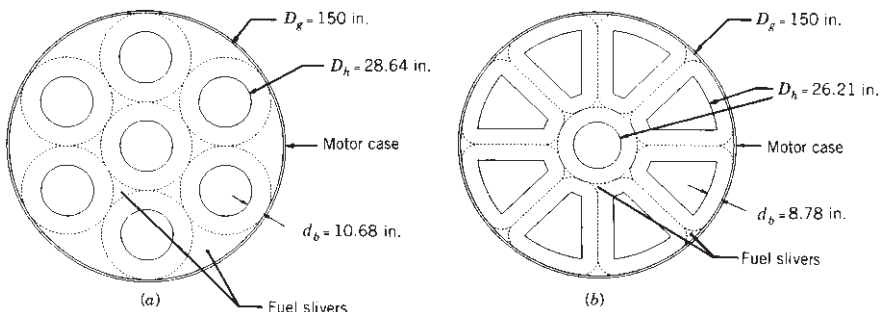


FIGURE 16-9. (a) Circular fuel grain combustion ports are volumetrically inefficient and leave large slivers at burnout. (b) Quadrilateral port hybrid grain configuration minimizes residual fuel sliver at burnout.

The initial fuel regression rate may be explicitly determined from Eq. 16-6:

$$\dot{r}_i = 0.104G_{oi}^{0.681} = 0.104(1.51 \text{ lbm}/\text{ft}^2\text{-sec})^{0.681} = 0.138 \text{ in./sec}$$

From the initial fuel mass flow rate, determined to be 3412 lbm/sec, the fuel grain length required for a seven-circular-port design may be found from Eq. 16-11:

$$L = \frac{\dot{m}_f/N}{2\pi R_i \rho_f \dot{r}_i} = \frac{(3412 \text{ lbm/sec})/7}{\pi(28.65 \text{ in.})(0.033 \text{ lbm/in.}^3)(0.138 \text{ in./sec})} = 1189.6 \text{ in.}$$

Using Eqs. 16-8, 16-9, 16-14, 16-15, and 16-16, while neglecting effects of throat erosion, the general operating characteristics of the booster may be computed with respect to time. The total fuel and oxidizer required for a 120-sec burn time are determined to be 362,577 and 818,880 lbm, respectively. The total propellant mass required is therefore 1,181,457 lbm.

Selection of circular fuel ports is not an efficient way of designing a hybrid grain since large fuel slivers will remain at the end of burn. In the preceding example, a sliver fraction (1 minus fuel consumed divided by fuel loaded) of 29.8% can be calculated. Recognizing that uniform burn distances around each port, as well as between combustion ports and the case wall, will minimize residual fuel sliver, the outer ring of circular ports may be replaced with quadrilateral-shaped ports. Such a grain is illustrated in Fig. 16-9b. If, as before, the grain diameter is constrained to be 150 in., the grain geometry is uniquely determined by specification of the initial fuel and oxidizer flow rates, number of ports, burn time, and the requirement that the burn distance around each port be equal. Additionally, the hydraulic diameter D_h (four times port area divided by port perimeter) of all ports should be equal to assure that all ports have the same mass flow rate.

For this example, the nine-port grain configuration results in a theoretical fuel sliver fraction of 4.3%. In reality, the sliver fraction for both designs will be somewhat greater than theoretical values since some web must be designed to remain between ports at the end of the burn duration to prevent slivers from being expelled out of the nozzle. Table 16-3 compares key features of the circular port grain design (Fig. 16-9a) and the quadrilateral grain design (Fig. 16-9b).

TABLE 16–3. Comparison of Circular Port and Quadrilateral Port Grain Designs

| Design Parameter | Circular Port | Quadrilateral Port |
|---|---------------|--------------------|
| Oxidizer flow rate (lbm/sec) | 6824 | 6824 |
| Initial fuel flow rate (lbm/sec) | 3412 | 3412 |
| Burn time (sec) | 120 | 120 |
| Grain diameter (in.) | 150 | 150 |
| Number of combustion ports | 7 | 9 |
| Oxidizer flux (lbm/sec/in. ²) | 1.51 | 1.07 |
| Fuel regression rate (in./sec) | 0.138 | 0.109 |
| Distance burned (in.) | 10.68 | 8.78 |
| Grain length (in.) | 1,189.6 | 976.1 |
| Combustion port <i>L/D</i> | 41.5 | 37.2 |
| Loaded fuel mass (lbm) | 516,664 | 364,170 |
| Fuel consumed (lbm) | 362,577 | 348,584 |
| Theoretical sliver fraction (%) | 29.8 | 4.28 |

In this example, the fuel consumed by the quadrilateral port design is less than that consumed by the circular port design. Therefore, the total impulse of the two designs will be different. If fuel consumed were constrained to be the same in each design, one would find that, as the number of quadrilateral fuel ports would be increased, the grain length would decrease and grain diameter would increase. In practice, the hybrid motor designer must carefully balance launch vehicle system requirements, such as total impulse and envelope constraints, with available grain design options to arrive at an optimum motor configuration. Total propellant and propellant contingency necessary to accomplish a specific mission will depend upon such factors as residual fuel and oxidizer allowances at motor cutoff, ascent trajectory throttling requirements, which impact overall mixture ratio and oxidizer utilization, and additional propellant if a Δu (vehicle velocity necessary to achieve mission objectives) contingency reserve is required.

Using Table 16–2 to obtain c^* , the initial vacuum-delivered specific impulse for the circular port booster design may be calculated as

$$I_{sv} = \frac{(C_F)_v c^*}{g_0} = \frac{(1.735)(0.95)(5912 \text{ ft/sec})}{32.174 \frac{\text{lbm-ft}}{\text{lbf-sec}^2}} = 302.87 \text{ sec}$$

At the end of burn, the mixture ratio is determined from Eq. 16–15 to be 2.45. The theoretical characteristic velocity corresponding to the mixture ratio is 5815 ft/sec. Assuming the same combustion efficiency factor of 95%, the chamber pressure, neglecting throat erosion, is determined to be

$$p_1 = \frac{\dot{m} c^*}{g_0 A_t} = \frac{(9611 \text{ lbm/sec})(0.95)(5815 \text{ ft/sec})}{\left(32.174 \frac{\text{lbm-ft}}{\text{lbf-sec}^2}\right) (2552.5 \text{ in.}^2)} = 646.5 \text{ lbf/in.}^2$$

Using the end-of-burn chamber pressure of 646.5 psia, the end-of-burn specific impulse is calculated to be 299.3 sec.

The throat material erosion rate in a hybrid is generally significantly greater than that of a solid propellant system and is a strong function of chamber pressure and mixture ratio. Erosion of carbonaceous throat materials (carbon cloth phenolic, graphite, etc.) is primarily governed by heterogeneous surface chemical reactions involving the reaction of carbon with oxidizing species present in the flow of combustion gases such as O₂, O, H₂O, OH, and CO₂ to form CO. Hybrid motor operation at oxygen-rich mixture ratios and high pressure will result in very high throat erosion rates. Operation at fuel-rich mixture ratios and pressures below 400 psi will result in very low throat erosion rates.

In general, the effect of throat erosion in ablative nozzles on overall motor performance depends on initial throat diameter. For the booster design under consideration, a 0.010-in./sec erosion rate acting only at the throat will reduce the expansion ratio from 7.72 to 7.11 over the 120-sec burn time. Using the end-of-burn mixture ratio of 2.45 corresponding to a ratio of specific heats of 1.137 (Table 16-2), an end-of-burn chamber pressure and vacuum thrust coefficient of 595.3 psia and 1.730, respectively, may be calculated. Therefore, if throat erosion is accounted for, delivered specific impulse at the end of burn is 297.0 sec, a reduction of only 0.77% compared with the noneroding throat assumption. As initial throat diameter is reduced, the reduction in expansion ratio due to throat erosion becomes greater, thereby resulting in greater performance losses.

Current practice for preliminary design of hybrid booster concepts is to couple a fuel regression rate model, a grain design model, and booster component design models in an automated preliminary design procedure. Using numerical optimization algorithms, such a computer model can pick the optimum booster design that maximizes selected optimization variables, such as booster ideal velocity or total impulse, while minimizing booster propellant and inert weight.

16.5. COMBUSTION INSTABILITY

The hybrid combustion process tends to produce rough pressure versus time characteristics. However, a well-designed hybrid can typically limit combustion roughness to approximately 2 to 3% of mean chamber pressure. In any combustion device, pressure fluctuations will tend to organize themselves around the natural acoustic frequencies of the combustion chamber or oxidizer feed system. While significant combustion pressure oscillations at chamber natural-mode acoustic frequencies have been observed in numerous hybrid motor tests, such oscillations have not proved to be an insurmountable design problem. When pressure oscillations have occurred in hybrid motors, they have been observed to grow to a limiting amplitude which is dependent on such factors as oxidizer feed system and injector characteristics, fuel grain geometric characteristics, mean chamber pressure level, and oxidizer mass velocity. Unbounded growth of pressure oscillations, such as may occur in solid and liquid rocket motors, has not been observed in hybrid motors.

Hybrid motors have exhibited two basic types of instabilities in static test environments: oxidizer feed system-induced instability (nonacoustic), and flame holding instability (acoustic). Oxidizer feed system instability is essentially a

chugging type as described in Chapter 9 and arises when the feed system is sufficiently “soft.” In cryogenic systems, this implies a high level of compressibility from sources such as vapor cavities or two-phase flow in feed lines combined with insufficient isolation from motor combustion processes. Figure 16–10a illustrates feed system induced instability in a 24-in.-diameter hybrid motor operated at a LOX flow rate of 20 lbm/sec with HTPB fuel. The instability is manifested by high-amplitude, periodic oscillations well below the first longitudinal (1-L) acoustic mode of the combustor. In this example the oscillation frequency is 7.5 Hz whereas the 1-L mode frequency is approximately 60 Hz. Stiffening the feed/injection system can eliminate the oscillation. This is accomplished by increasing the injector pressure drop (thus making propagation of motor pressure disturbances upstream through the feed system more difficult) and eliminating sources of compressibility in the feed system. Chugging-type instabilities in hybrid motors have proven amenable to analysis in terms of prediction and prevention (Ref. 16–20). For purposes of comparison, Fig. 16–10b shows a pressure–time trace from the same 24-in.-diameter hybrid motor exhibiting stable combustion while being operated at a LOX flow rate of 40 lbm/sec at a maximum chamber pressure of 900 psi.

Flame-holding instability relevant to hybrid motors was first observed during the development of solid fuel ramjets (Ref. 16–21). A solid fuel ramjet is essentially a hybrid motor operating on the oxygen available in ram air. Flame-holding instabilities in hybrids are typically manifested at acoustic frequencies and appear in longitudinal modes. No acoustic instabilities in hybrid motors have been observed in higher frequency tangential or radial modes such as in solid rocket motors or liquid engines. Flame-holding instabilities arise due to inadequate flame stabilization in the boundary layer (Ref. 16–22) and are not associated with feed system flow perturbations. For example, flame-holding instability in an 11-in.-diameter hybrid motor operated with gaseous oxygen (GOX) oxidizer and HTPB fuel, using an injector producing a conical flow field. In this test, oxygen flow was initiated through the motor at a pressure of 90 psi for 2 sec prior to motor ignition. The motor was ignited using a hydrogen torch that continued to operate for approximately 1 sec following motor ignition. During the first second of motor operation, the hydrogen igniter flame stabilizes the motor. When the igniter flame is extinguished, the motor becomes unstable. In this case stable combustion was achieved by changing the flow field within the motor, using an injector producing an axial flow field. Figure 16–11 shows the result of decomposing the pressure versus time signal for this unstable example into its frequency components via fast Fourier transform techniques. The 1-L acoustic oscillation mode is clearly visible at approximately 150 Hz.

It is apparent that flame-holding instability can be eliminated by several means, all of which act to stabilize combustion in the boundary layer. The first method is to use a pilot flame derived from injection of a combustible fluid such as hydrogen or propane to provide sufficient oxidizer preheating in the leading edge region of the boundary layer flame zone. With this technique, motor stability

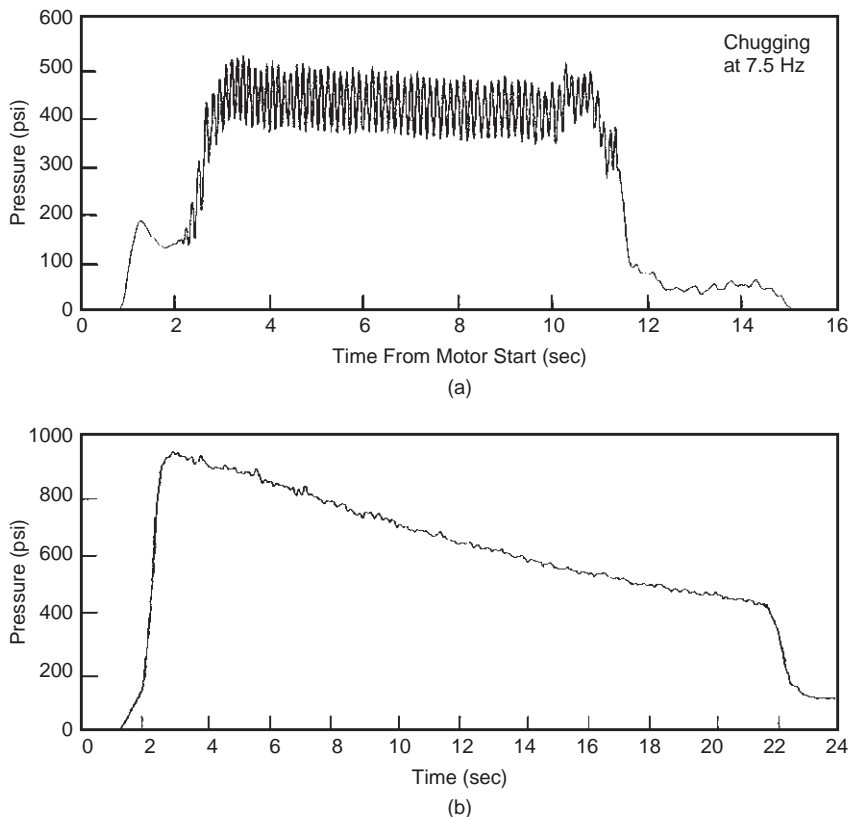


FIGURE 16–10. (a) Periodic, large-amplitude, low-frequency combustion pressure oscillations are an example of oxidizer feed system induced “chug”-type combustion instability in a 24-in.-diameter LOX/HTPB motor. (b) An example of stable combustion in a 24-in.-diameter LOX/HTPB motor, exhibiting an overall combustion roughness level of 1.3%.

characteristics are relatively insensitive to the nature of the injector flow field. In the previous example, the hydrogen torch igniter acted as a pilot during its period of operation. A second method involves changing the injector flow field to ensure that a sufficiently large hot gas recirculation zone is present at the head end of the fuel grain. Such a zone can be created by forcing the upstream flow over a rearward-facing step or by strong axial injection of oxidizer (see Fig. 16–12). Axial injection in the correct configuration produces a strong counter-flowing hot gas recirculation zone, similar to that of a rearward-facing step, at the head end of the diffusion flame (conical injection produces a much smaller and usually ineffective recirculation zone). These techniques produce a flow field result very similar to that produced by bluff body flame stabilizers used in jet engine afterburners and solid fuel ramjets to prevent flame blowoff. The recirculation zone

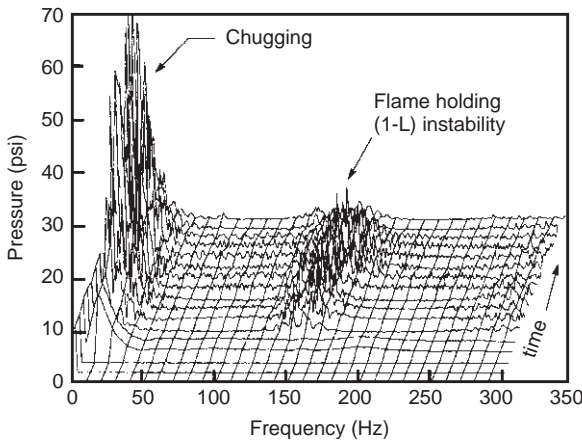


FIGURE 16-11. A frequency-versus-amplitude plot at successive time intervals for an 11-in.-diameter GOX/HTPB motor test shows pressure oscillations in the motor first longitudinal (1-L) acoustic mode at 150 Hz due to flame-holding instability.

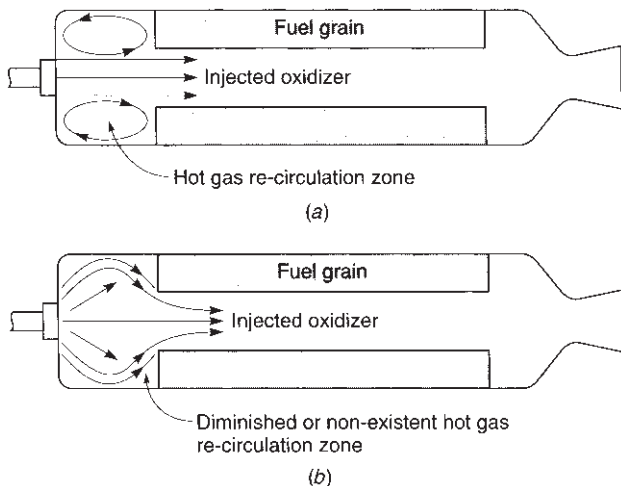


FIGURE 16-12. (a) Axial injection of oxidizer results in a strong hot gas flow recirculation zone at the fuel grain leading edge, producing stable combustion. (b) Conical injection of oxidizer can produce a weak or nonexistent hot gas flow recirculation zone at the fuel grain leading edge, resulting in unstable combustion.

acts to entrain hot gas from the core flow, which provides sufficient oxidizer preheating for the leading edge of the boundary layer diffusion flame to stabilize combustion.

Comparison of the average pressure levels in the above-mentioned instability illustrates an interesting phenomenon. For the same motor operating conditions

(oxidizer flow rate, grain geometry and composition, and throat diameter) the average pressure in the unstable motor is significantly greater than that in the stable motor. This same phenomenon has been noted in solid propellant motors and the results from intensification of heat transfer to the fuel surface due to the gas velocity at the fuel surface oscillating at high frequency. The high heating rate results in the vaporization of more fuel than would otherwise occur in equilibrium conditions, thus producing a higher average chamber pressure.

Despite recent advances in understanding causes of and solutions for combustion instability in hybrid motors, development of a comprehensive, predictive theory of combustion stability remains one of the major challenges in hybrid technology development (see Ref. 16–23).

PROBLEMS

- 1.** Consider a classical hybrid motor with a single solid fuel grain stored in a single cylindrical enclosure. The combustion port radius is R and the length L . For a fuel burning rate given by Eq. 16–2, $\dot{r} = a(G_o)^n$, with $n = 0.7$:

(a) What happens to the thrust with time for a constant oxidizer mass flow rate during the burn?

(b) What happens to the mixture ratio if the oxidizer rate is decreased?

Answer: (a) and (b) decrease.

- 2. (a)** Write Eq. 16–1 in terms of a *Reynolds number* based on the free-stream gas flow and the axial location x . What does this say about the Reynolds number dependence of surface regression rate?

(b) It is known that the blowing coefficient is itself roughly proportional to $x^{0.2}$. What additional assumptions might be necessary to transform Eq. 16–1 into 16–2?

- 3.** Calculate the ideal density-specific impulse (in units of kg-sec/m³) for the propellant combination LOX/HTPB at an oxidizer-to-fuel ratio of 2.3 at a pressure ratio across the nozzle of 1000/14.7 and an optimum expansion. Use the information in Table 16–2 and a fuel density of 920 kg/m³. Compare your result with the value of LOX/RP-1 bipropellant listed in Table 5–5.

Answer: 3×10^5 kg-sec/m³

- 4.** Plot the instantaneous mixture ratio given by Eq. 16–15 as a function of the index n and time. Use values of n greater and less than $\frac{1}{2}$ (at $n = \frac{1}{2}$ the time dependence vanishes). In order to only focus on the effects of n , work with the modified variables ψ (related to mixture ratio) and τ (related to time) as follows:

$$\psi = [(2n + 1)\tau + 1]^{(2n - 1)/(2n + 1)}$$

$$\psi \equiv \frac{\dot{m}_o}{\dot{m}_f} \frac{2\rho_f La}{R_i \left(\frac{\dot{m}_o}{\pi N R_i} \right)^{1-n}} \quad \text{and} \quad \tau \equiv a \left(\frac{\dot{m}_o}{\pi N R_i^2} \right)^n \frac{t}{R_i}$$

5. A classical hybrid propulsion system has the following characteristics:

| | |
|--------------------------------|-----------------------------|
| Propellants | LOX/HTPB |
| Nominal burn time | 20 sec |
| Initial chamber pressure | 600 psi |
| Initial mixture ratio | 2.0 |
| Initial nozzle exit area ratio | 10.0 |
| Fuel grain outside diameter | 12 in |
| Grain geometry | Single cylinder case bonded |
| Initial HTPB temperature | 65°F |

Determine initial and final thrust, specific impulse, propellant masses, and useful propellant.

SYMBOLS

| | | |
|------------|--|---|
| <i>a</i> | burning or regression rate coefficient (units of <i>a</i> depend on value of oxidizer flux exponent) | variable |
| A_p | combustion port area | $\text{m}^2(\text{in.}^2)$ |
| A_s | fuel grain surface area | $\text{m}^2(\text{in.}^2)$ |
| A_t | nozzle throat area | $\text{m}^2(\text{ft}^2)$ |
| c^* | characteristic velocity | m/sec (ft/sec) |
| C_{F_v} | vacuum thrust coefficient | dimensionless |
| c_p | heat capacity | $\text{J/kg-K (Btu/lbm-}^\circ\text{R)}$ |
| d_b | fuel grain burn distance | m (in.) |
| D_h | hydraulic diameter ($4A_p/P$) | m (in.) |
| D_p | combustion port diameter | m (in.) |
| D_t | nozzle throat diameter | m (in.) |
| F_v | vacuum thrust | N (lbf) |
| G | mass velocity | $\text{kg/m}^2\text{-sec (lbm/ft}^2\text{-sec)}$ |
| G_o | oxidizer mass velocity | $\text{kg/m}^2\text{-sec (lbm/ft}^2\text{-sec)}$ |
| g_0 | conversion factor—acceleration of gravity | $\text{m/sec}^2 \text{ (lbm-ft/lbf/sec}^2)$ |
| h | convective heat transfer coefficient | $\text{J/m}^2\text{-sec/K (Btu/ft}^2\text{-sec}^\circ\text{R)}$ |
| h_v | heat of gasification | J/kg (Btu/lbm) |
| Δh | flame zone-fuel surface enthalpy difference | J/kg (Btu/lbm) |
| H_f | heat of formation | $\text{J/kg-mol (kcal/mol)}$ |
| I_s | specific impulse | sec |

| | | |
|-------------|--|-----------------------------|
| k | specific heat ratio | dimensionless |
| L | combustion port length | m (in.) |
| \dot{m} | propellant flow rate | kg/sec (lbm/sec) |
| \dot{m}_f | fuel flow rate | kg/sec (lbm/sec) |
| \dot{m}_o | oxidizer flow rate | kg/sec (lbm/sec) |
| n, m, l | burning or regression rate pressure exponent | dimensionless |
| P | combustion port perimeter | m (in.) |
| p_1 | chamber pressure | MPa (lbf/in. ²) |
| R | combustion port radius | m (in.) |
| R_i | initial combustion port radius | m (in.) |
| Re | Reynolds number | dimensionless |
| \dot{r} | fuel regression rate | mm/sec (in./sec) |
| r | oxidizer to fuel mixture ratio | dimensionless |
| T | temperature | K (F) |
| u_e | gas free-stream velocity in axial direction | m/sec (ft/sec) |
| v | gas velocity normal to fuel surface | m/sec (ft/sec) |
| x | axial distance from leading edge of fuel grain | m (in.) |
| y | length coordinate normal to fuel surface | m (in.) |

Greek Letters

| | | |
|----------|------------------------------------|---|
| α | fuel surface absorptivity | dimensionless |
| β | boundary layer blowing coefficient | dimensionless |
| μ | gas viscosity | N-sec/m ² (lbf-sec/ft ²) |
| ρ_1 | combustion chamber gas density | kg/m ³ (lbm/in. ³) |
| ρ_e | free stream gas density | kg/m ³ (lbm/in. ³) |
| ρ_f | fuel density | kg/m ³ (lbm/in. ³) |

Subscripts

| | | |
|-----|--|---------|
| e | boundary layer edge conditions | |
| f | fuel | |
| i | initial conditions | |
| o | oxidizer | |
| s | surface conditions | |
| x | axial distance from leading edge of fuel grain | m (in.) |
| ref | reference conditions | |

REFERENCES

- 16–1. K. K. Kuo, “Challenges of Hybrid Rocket Propulsion in the 21st Century,” in M. A. Chiaverini and K. K. Kuo (Eds.), *Fundamentals of Hybrid Rocket Combustion and Propulsion*, Vol. 218, *Progress in Astronautics and Aeronautics*, AIAA, Reston, VA, 2007, Chapter 15.
- 16–2. R. A. Frederick Jr., J. J. Whitehead, L. R. Knox, and M. D. Moser, “Regression Rates of Mixed Hybrid Propellants,” *Journal of Propulsion and Power*, Vol. 23, No. 1, January–February 2007.
- 16–3. D. Altman and A. Holzman, “Overview and History of Hybrid Rocket Propulsion,” in M. A. Chiaverini and K. K. Kuo (Eds.), *Fundamentals of Hybrid Rocket Combustion and Propulsion*, Vol. 218, *Progress in Astronautics and Aeronautics*, AIAA, Reston, VA, 2007, Chapter 1.
- 16–4. H. R. Lips, “Experimental Investigation of Hybrid Rocket Engines Using Highly Aluminized Fuels,” *Journal of Spacecraft and Rockets*, Vol. 14, No. 9, September 1977, pp. 539–545.
- 16–5. S. Heister and E. Wernimont, “Hydrogen Peroxide, Hydroxil Ammonium Nitrate, and Other Storable Oxidizers,” in M. A. Chiaverini and K. K. Kuo (Eds.), *Fundamentals of Hybrid Rocket Combustion and Propulsion*, Vol. 218, *Progress in Astronautics and Aeronautics*, AIAA, Reston, VA, 2007, Chapter 11.
- 16–6. SpaceDev website: <http://www.spacedev.com>.
- 16–7. T. A. Boardman, T. M. Abel, S. E. Chaflin, and C. W. Shaeffer, “Design and Test Planning for a 250-klbf-Thrust Hybrid Rocket Motor under the Hybrid Demonstration Program,” AIAA Paper 97-2804, July 1997.
- 16–8. S. R. Jain and G. Rajencran, “Performance Parameters of Some New Hybrid Hypergols,” *Journal of Propulsion and Power*, Vol. 1, No. 6, November–December 1985, pp. 500–501.
- 16–9. U. C. Durgapal and A. K. Chakrabarti, “Regression Rate Studies of Aniline-Formaldehyde-Red Fuming Nitric Acid Hybrid System,” *Journal of Spacecraft and Rockets*, Vol. 2, No. 6, 1974, pp. 447–448.
- 16–10. G. A. Marxman, “Combustion in the Turbulent Boundary Layer on a Vaporizing Surface,” Tenth Symposium on Combustion, The Combustion Institute, 1965, pp. 1337–1349.
- 16–11. M. A. Chiaverini, “Review of Solid-Fuel Regression Rate Behavior in Classical and Nonclassical Hybrid Rocket Motors,” in M. A. Chiaverini and K. K. Kuo (Eds.), *Fundamentals of Hybrid Rocket Combustion and Propulsion*, Vol. 218, *Progress in Astronautics and Aeronautics*, AIAA, Reston, VA, 2007, Chapter 2.
- 16–12. F. P. Incropera and D. P. DeWitt, *Fundamentals of Heat and Mass Transfer*, 5th ed., John Wiley & Sons, Hoboken NJ, 2002.
- 16–13. L. D. Smooth and J. C. Price, “Regression Rates of Metallized Hybrid Fuel Systems,” *AIAA Journal*, Vol. 4, No. 5, September 1965, pp. 910–915.
- 16–14. D. Altman and R. Humble, “Hybrid Rocket Propulsion Systems,” in R. W. Humble, G. N. Henry, and W. J. Larson, *Space Propulsion Analysis and Design*, McGraw-Hill, New York 1995, Chapter 7.

- 16–15. A. Gany, “Similarity and Scaling Effects in Hybrid Rocket Motors,” in M. A. Chiaverini and K. K. Kuo (Eds.), *Fundamentals of Hybrid Rocket Combustion and Propulsion*, Vol. 218, *Progress in Astronautics and Aeronautics*, AIAA, Reston, VA, 2007, Chapter 12.
- 16–16. P. A. O. G. Korting, H. F. R. Schoyer, and Y. M. Timnat, “Advanced Hybrid Rocket Motor Experiments,” *Acta Astronautica*, Vol. 15, No. 2, 1987, pp. 97–104.
- 16–17. W. Waidmann, “Thrust Modulation in Hybrid Rocket Engines,” *Journal of Propulsion and Power*, Vol. 4, No. 5, September–October 1988, pp. 421–427.
- 16–18. M. A. Chiaverini, K. K. Kuo, A. Peretz, and G. C. Harting, “Regression-Rate and Heat-Transfer Correlations for Hybrid Rocket Combustion,” *Journal of Propulsion and Power*, Vol. 17, No. 1, January–February 2001, pp. 99–110.
- 16–19. V. Sankaran, “Computational Fluid Dynamics Modeling of Hybrid Rocket Flow-fields,” in M. A. Chiaverini and K. K. Kuo (Eds.), *Fundamentals of Hybrid Rocket Combustion and Propulsion*, Vol. 218, *Progress in Astronautics and Aeronautics*, AIAA, Reston, VA, 2007, Chapter 8.
- 16–20. T. A. Boardman, K. K. Hawkins, R. S. Wasson, and S. E. Claflin, “Non-Acoustic Feed System Coupled Combustion Instability in Hybrid Rocket Motors,” AIAA Hybrid Rocket Technical Committee Combustion Stability Workshop, 31st Joint Propulsion Conference, 1995.
- 16–21. B. L. Iwanciow, A. L. Holzman, and R. Dunlap, “Combustion Stabilization in a Solid Fuel Ramjet,” 10th JANNAF Combustion Meeting, 1973.
- 16–22. T. A. Boardman, D. H. Brinton, R. L. Carpenter, and T. F. Zoladz, “An Experimental Investigation of Pressure Oscillations and Their Suppression in Subscale Hybrid Rocket Motors,” AIAA Paper 95-2689, July 1995.
- 16–23. A. Karabeyoglu, “Combustion Instability and Transient Behavior in Hybrid Motors,” in M. A. Chiaverini and K. K. Kuo (Eds.), *Fundamentals of Hybrid Rocket Combustion and Propulsion*, Vol. 218, *Progress in Astronautics and Aeronautics*, AIAA, Reston, VA, 2007, Chapter 9.

CHAPTER 17

ELECTRIC PROPULSION

Chapters 1 and 2 include information on electric rocket propulsion devices that use electrical energy for heating and/or directly ejecting propellant, utilizing an energy source that is independent of the propellant itself. The purpose of this chapter is to provide an introduction to this field. Vector notation is used in several of the background equations presented.

The basic subsystems of a typical electric propulsion thruster are: (1) a raw *energy source* such as solar or nuclear energy with its auxiliaries such as concentrators, heat conductors, pumps, panels, radiators, and/or controls; (2) *conversion devices* to transform this energy into electrical form at the proper voltage, frequency, pulse rate, and current suitable for the electrical propulsion system; (3) a *propellant system* for storing, metering, and delivering the propellant; and (4) one or more *thrusters* to convert the electric energy into kinetic energy of the exhaust. The term *thruster* is commonly used here, as thrust chamber is in liquid propellant rockets.

Electric propulsion is unique in that it includes both thermal and nonthermal systems as classified in Chapter 1. Also, since the energy source is divorced from the propellant, the choice of propellant is guided by factors much different to those in chemical propulsion. In Chapter 3, ideal relations that apply to all thermal thrusters are developed which are also relevant to thermal-electric (or electrothermal) systems. Concepts and equations for nonthermal electric systems are defined in this chapter. From among the many ideas and designs of electric propulsion devices reported to date, one can distinguish the following three fundamental types:

1. *Electrothermal*. Propellant is heated electrically and expanded thermodynamically; that is, the gas is accelerated to supersonic speeds through a nozzle, as in the chemical rocket.

2. *Electrostatic.* Acceleration is achieved by the interaction of electrostatic fields on non-neutral or charged propellant particles such as atomic ions, droplets, or colloids.
3. *Electromagnetic.* Acceleration is achieved by the interaction of electric and magnetic fields within a plasma. Moderately dense plasmas are high-temperature or nonequilibrium gases, electrically neutral, and reasonably good conductors of electricity.

A general description of these three types was given in Chapter 1, Figs. 1–8 to 1–10. Figure 17–1 and Tables 2–1 and 17–1 show approximate power and performance values for several types of electric propulsion units. Note that the thrust levels are small relative to those of chemical and nuclear rockets, but that values of specific impulse can be substantially higher; this may translate into a longer operational life for satellites whose life is presently propellant limited. Inherently, electric thrusters give accelerations too low for overcoming the high-gravity field of earth launches. They function best in space, which also matches the near-vacuum exhaust pressures required of electrostatic and electromagnetic systems. All flights envisioned with electric propulsion operate in a reduced gravity or gravity-free space and, therefore, must be launched from earth by chemical rocket systems. Launching from low-gravity bodies such as asteroids, however, is feasible without any chemical assist.

Recent interest in very small spacecraft has given rise to the specialized field of *micropropulsion*. Here power levels below 500 W and thrusts below 1 mN are needed for these spacecraft because the total mass vehicle (m_0) is less than 100 kg. According to Fig. 17–1 only the pulsed-plasma thruster (PPT) would fit in this category, but new miniaturized electrothermal and electrostatic thrusters are under development (together with some which are purely chemical), based on advances in micromanufacturing such as MEMS (micro-electro-mechanical systems) and nanotechnologies. But not all the present thruster concepts can be effectively scaled down to meet micropropulsion needs. Conventional gas dynamic micronozzles have a much reduced performance because viscous losses are inherent in increased surface-to-volume ratios. Magnetic fields are also difficult to scale down. For all systems, except those with propellant self-feeding features, a significant scaling problem is propellant leakage associated with valve miniaturization. Also, machining traditional metals to the microscale remains challenging, and nanotechnology fabricated pieces that use glasses or silicon are quite porous to gaseous propellants often exceeding acceptable leakage rates, (Ref. 17–1).

The many advantages of electric propulsion had been offset by their required use of substantial quantities of electricity which, at certain power levels, had been an expensive commodity in space until recently. All types of electric propulsion presently depend on a vehicle-borne power source—based on solar, chemical, or nuclear energy—and power conversion and conditioning equipment. The mass of the electric generating equipment, even when solar energy is employed, can become much larger than that of the thrusters, particularly when thruster efficiency is low. This causes appreciable increases in inert-vehicle mass (or dry

TABLE 17-1. Typical Performance Parameters of Various Types of Electrical Propulsion Systems

| Type | Thrust Range (mN) | Specific Impulse (sec) | Thruster Efficiency ^a (%) | Thrust Duration | Typical Propellants | Kinetic Power per Unit Thrust (w/mN) |
|------------------------------------|-------------------|------------------------|--------------------------------------|------------------|---|--------------------------------------|
| Resistojet (thermal) | 200–300 | 200–350 | 65–90 | Months | NH ₃ , N ₂ H ₄ , H ₂ | 0.5–6 |
| Arcjet (thermal) | 200–1000 | 400–1000 | 30–50 | Months | H ₂ , N ₂ , N ₂ H ₄ , NH ₃ | 2–3 |
| Ion thruster | 0.01–500 | 1500–8000 | 60–80 | Years | Xe,Kr,Ar,Bi | 10–70 |
| Solid pulsed plasma (PPT) | 0.05–10 | 600–2000 | 10 | Years | Teflon | 10–50 |
| Magnetoplasma dynamic (MPD) | 0.001–2000 | 2000–5000 | 30–50 | Weeks | Ar,Xe,H ₂ ,Li | 100 |
| Hall thruster | 0.01–2000 | 1500–2000 | 30–50 | Months | Xe,Ar | 100 |
| Monopropellant rocket ^b | 30–100,000 | 200–250 | 87–97 | Hours or minutes | N ₂ H ₄ | |

^aSee Eq. 17–2.^bListed for comparison only.

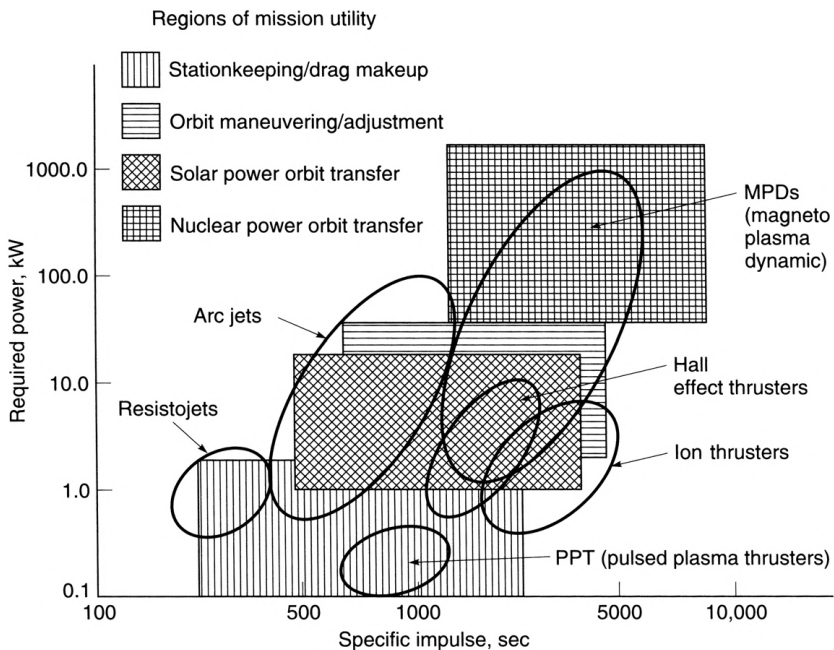


FIGURE 17–1. Overview of the approximate regions of application of different electrical propulsion systems in terms of power and specific impulse.

mass). Modern satellites and other spacecraft have substantial communications requirements. Typically these satellites can share their electrical power sources, thus avoiding the penalty to the propulsion system. What remains to be tagged to the propulsion system is the power-conditioning equipment, except in instances where it is also shared with other spacecraft components.

Electric propulsion has been considered for space applications since the inception of the space program in the 1950s but has only begun to make widespread impact since the mid-1990s. This is a result of the availability of sufficiently large amounts of electrical power in spacecraft. References 17–2 to 17–4 are devoted to electric propulsion. Basic principles on electric propulsion devices are given in these references, along with applications, although the information relates to older versions of such devices. Table 17–2 gives a comparison of advantages and disadvantages of several types of electric propulsion. Pulsed devices differ from continuous or steady state in that startup and shutdown transients may degrade their effective performance. Pulsed devices, however, are of practical importance, as is detailed later in this chapter.

The *applications* for electric propulsion fall into several broad mission categories (these have already been introduced in Chapter 4):

1. *Overcoming translational and rotational perturbations* in satellite orbits, such as north–south station keeping (NSSK) of satellites in geosynchronous

TABLE 17–2. Comparison of Electrical Propulsion Systems

| Type | Advantages | Disadvantages | Comments |
|--|--|---|--|
| Resistojet (electrothermal) | Simple device; easy to control; simple power conditioning; low cost; relatively high thrust and efficiency; can use many propellants, including hydrazine augmentation | Lowest I_s ; heat loss; gas dissociation; indirect heating of gas; nozzle erosion | Operational |
| Arcjet (electrothermal & electromagnetic) | Direct heating of gas; low voltage; relatively simple device; relatively high thrust; can use catalytic hydrazine augmentation; inert propellant | Low efficiency; erosion at high power; low I_s ; high current; heavy wiring; heat loss; more complex power conditioning | High-thrust units need P_e of 100 kW or more. Operational |
| Ion propulsion (electrostatic) | High specific impulse; high efficiency; inert propellant (Xenon) | Complex power conditioning; high voltages; low thrust per unit area; heavy power supply | Operational in GEO satellites, space probes (DS1/DAWN, RITA, HAYABUSA) |
| Pulsed plasma (PPT) (electromagnetic) | Simple device; low power; solid propellant; no gas or liquid feed system; no zero-g effects on propellant | Low thrust; Teflon reaction products are toxic, may be corrosive or condensable; inefficient | Operational |
| MPD steady-state plasma (electromagnetic) | Can be relatively simple; high I_s ; high thrust per unit area | Difficult to simulate analytically; high specific power; heavy power supply; lifetime issues. | Several have flown |
| Hall thruster (electromagnetic) | Desirable I_s range; compact, relatively simple power conditioning; inert propellant (Xenon) | Single propellant; high beam divergence; erosion | Operational (SMART-1) |

orbits (GEO) or aligning telescopes or antennas or drag compensation of satellites in low (LEO) and medium earth orbits (MEO). For a typical north-south station-keeping task in a 350-km orbit, a velocity increment of about 50 m/sec every year or 500 m/sec for 10 years might be needed. Several different electric propulsion systems have actually flown in this type of mission.

2. Increasing satellite speed while overcoming the relatively weak gravitational field some distance away from the earth, such as *orbit raising* from an LEO to a higher orbit or even to a GEO. Circularizing an elliptical orbit may require a vehicle velocity increase of 2000 m/sec and going from LEO to GEO typically might require up to 6000 m/sec. Several electric propulsion units are being developed for these types of mission.
3. Potential missions such as *interplanetary travel* and *deep space probes* are also candidates for electric propulsion. A return to the moon, missions to Mars and Jupiter, and missions to comets and asteroids are of present interest. A few electric thruster missions are underway.
4. A number of new missions look at electric propulsion for either precision attitude/position control or formation-flying relative position control.

As an illustration of the benefit in applying electric propulsion, consider a typical geosynchronous communications satellite with a 15-year lifetime and with a mass of 2600 kg. For NSSK the satellite might need an annual velocity increase of some 50 m/sec; this requires about 750 kg of chemical propellant for the entire period, which is more than one-quarter of the satellite mass. Using an electric propulsion system can increase the specific impulse to 2800 sec (about nines times higher than a chemical rocket), and the propellant mass can be reduced to perhaps less than 100 kg. A power supply and electric thrusters would have to be added, but the inert mass of the chemical system can be deleted. Such an electric system would save perhaps 450 kg or about 18% of the satellite mass. At launch costs of \$10,000 per kilogram delivered to GEO, this is a potential saving of some \$4,500,000 per satellite. Alternatively, more propellant could be stored in the satellite, thus extending its useful life. Additional savings could materialize if electric propulsion were also used for orbit raising.

The propulsive output or *kinetic power of the jet* P_j results from the energy rate supplied by the available power source, principally diminished by (1) losses in the power conversion, such as from solar or nuclear into electrical energy; (2) conversions into forms of electric energy (voltage, frequency, etc.) suitable for the thrusters; and (3) losses of the conversion of the electric energy delivered to the thruster into propulsive jet energy (η_t). The kinetic power (P_j) per unit thrust (F) may be expressed by the following relation (assuming no significant pressure thrust or exit flow divergence):

$$\frac{P_j}{F} = \frac{\frac{1}{2}\dot{m}v^2}{\dot{m}v} = \frac{1}{2}v = \frac{1}{2}g_0 I_s \quad (17-1)$$

where \dot{m} is the mass flow rate, v the mass-average jet discharge velocity (v_2 or c in Chapters 2 and 3), and I_s the specific impulse. This power-to-thrust ratio of the jet is therefore proportional to the effective exhaust velocity or its equivalent the specific impulse. It is usually concluded here that thrusters with substantially high values of I_s will require more power and therefore bigger power supplies, but this is not necessarily so. It is shown in this chapter that systems with high specific impulse optimize at much longer *propulsive times* (t_p) and thus at smaller thrust levels so that the power requirements may actually decrease.

Thruster efficiency η_t is defined as the ratio of the thrust producing (axial component) kinetic power of the exhaust beam to the total electrical power applied to the thruster, including any used in evaporating and/or ionizing the propellant:

$$\eta_t = \frac{\text{power of the jet}}{\text{electrical power input}} = \frac{\frac{1}{2}\dot{m}v^2}{\sum(IV)} \quad (17-2)$$

Then, from the fundamentals in Chapter 2 (Eqs. 2–19 and 2–22)

$$\frac{F}{P_e} = \frac{2\eta_t}{g_0 I_s} \quad (17-3)$$

with P_e representing the electric power input to the thruster in watts and given by the product of the electrical current and all associated voltages (hence the summation, \sum , sign). The power needed from the source is found through the inclusion of the first two additional conversion efficiencies outlined above Eq. 17–1.

Thruster efficiency accounts for all the energy losses that do not result in kinetic energy, including (1) the wasted electrical power (stray currents, ohmic resistance, etc.); (2) unaffected or improperly activated propellant particles (propellant utilization); (3) loss of thrust resulting from dispersion of the exhaust (direction and magnitude); and (4) heat losses. It is a measure of how effectively electric power and propellant are used in the production of thrust.

When electrical energy is not the only input energy, Eq. 17–2 has to be modified; for example, the propellant may release energy (chemical monopropellant), as in hydrazine decomposition with a resistojet.

17.1. IDEAL FLIGHT PERFORMANCE

For the low thrust of electric propulsion with its relatively massive power generating systems, the flight regimes of space vehicles propelled by electric rockets are quite different from those using chemical rockets. Accelerations tend to be very low (10^{-4} to $10^{-6} g_0$), thrusting times are typically long (several months), and spiral trajectories were originally suggested for spacecraft accelerated by these low thrusts. Figure 17–2 shows schemes for going from LEO to GEO including a spiral, a Hohman ellipse (see Section 4.5 on the *Hohman orbit*, which is optimum for chemical propulsion) as well as a “supersynchronous” orbit transfer (Ref. 17–5). Because of the long transfer orbit durations, trajectories other than

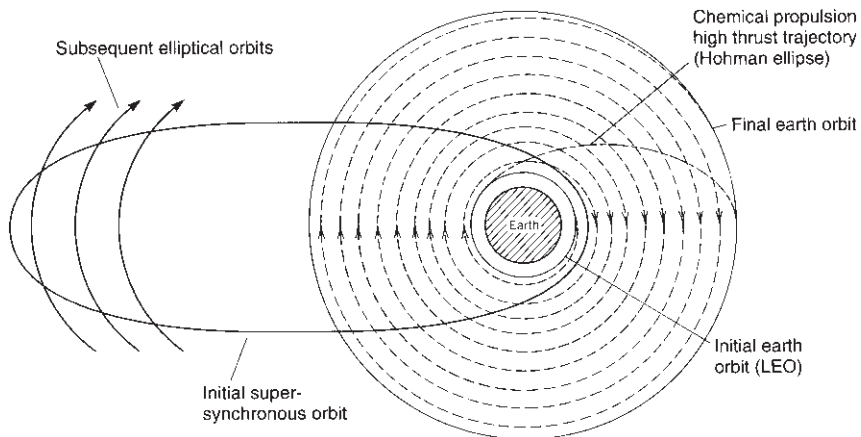


FIGURE 17–2. Simplified diagram of trajectories going from a low earth orbit (LEO) to a high earth orbit using chemical propulsion (short duration), electric propulsion with a multiple spiral trajectory (long duration), and a supersynchronous chemical orbit approach as an alternate to LEO (intermediate duration). From the supersynchronous orbit continuous thrusting with electric propulsion at a fixed inertial attitude lowers the apogee and raises the perigee in each orbit until it reaches the final high circular orbit. See Ref. 17–5.

spiral are presently being considered where one utilizes chemical propulsion to arrive at a very eccentric, supersynchronous elliptical orbit; from there electric propulsion can continuously and effectively be fired to attain a GEO orbit.

The performance of an electrical rocket can be conveniently analyzed in terms of the power and the relevant masses (Ref. 17–6). Let m_0 be the total initial mass of the vehicle stage, m_p the total mass of the propellant to be expelled, m_{pl} the payload mass to be carried by the particular stage under consideration, and m_{pp} the mass of the power plant consisting of the empty propulsion system including the thruster, propellant storage and feed system, the energy source with its conversion system and auxiliaries, and the associated structure. Then

$$m_0 = m_p + m_{pl} + m_{pp} \quad (17-4)$$

The energy source input to the power supply (i.e., solar or nuclear) has to be larger than its electrical power output; they are related by the power conversion efficiency (about 10 to 15% for photovoltaic and up to 30% for rotating machinery) for converting the raw energy into electrical power at the desired voltages, frequencies, and power levels. The converted electrical output P_e is then supplied to the propulsion system. The ratio of the electrical power P_e to the mass of the power plant m_{pp} is defined as α , which is often referred to as the *specific power* (or its inverse the *specific mass*) of the power plant or of the entire propulsion system. This specific power must be defined for each design, because even for the same type of engine, α is somewhat dependent on the engine–module configuration (this includes the number of engines that share the same power

conditioner, redundancies, valving, etc.):

$$\alpha = P_e / m_{pp} \quad (17-5)$$

The specific power is considered to be proportional to engine power and reasonably independent of m_p . Its value hinges on technological advances and the electric-propulsion engine module configuration. Presently, typical values of α range between 100 and 200 W/kg. In the future it is hoped that α will attain values of 500 to 2000 W/kg pending some breakthrough in power conditioning equipment. Electrical power is converted by the thruster into kinetic energy of the exhaust. Allowing for losses by using the thruster efficiency η_t , defined in Eqs. 17-2, the mass of the power plant becomes

$$m_{pp} = m_p v^2 / (2\alpha t_p \eta_t) \quad (17-6)$$

where m_p is the propellant mass, v the effective exhaust velocity, and t_p the time of operation or propulsive time when the propellant is being ejected at a uniform rate.

Using Eqs. 17-4, 17-5, and 17-6 together with 4-7, one can obtain a relation for the reciprocal payload mass fraction:

$$\frac{m_0}{m_{pl}} = \frac{e^{\Delta u/v}}{1 - (e^{\Delta u/v} - 1)v^2 / (2\alpha t_p \eta_t)} \quad (17-7)$$

This assumes a gravity-free and drag-free flight. The change of vehicle velocity Δu which results from the propellant being exhausted at a speed v is plotted in Fig. 17-3 as a function of propellant mass fraction. The specific power α and the thruster efficiency η_t as well as the propulsive time t_p may be combined into a *characteristic speed* v_c (Ref. 17-6):

$$v_c = \sqrt{2\alpha t_p \eta_t} \quad (17-8)$$

This characteristic speed is not a physical speed but rather a defined grouping of parameters that has units of speed; it can be visualized as the speed the power plant would have if its full power output were converted into the form of kinetic energy of its own inert mass m_{pp} . Equation 17-8 includes the propulsive time t_p which is the actual mission time (certainly, mission time cannot be smaller than the thrusting time). From Fig. 17-3 it can be seen that, for a given payload fraction (m_{pl}/m_0) and characteristic speed (v_c), there is an optimum value of v corresponding to the peak vehicle velocity increment; this is later shown to signify that there exists a particular set of most desirable flight operating conditions.

The peak for the curves in Fig. 17-3 exists because the inert mass of the power plant m_{pp} increases with the specific impulse while the propellant mass decreases with specific impulse. For a constant flow rate, other components are fixed in mass so that they only displace the curves by a constant amount. As indicated in

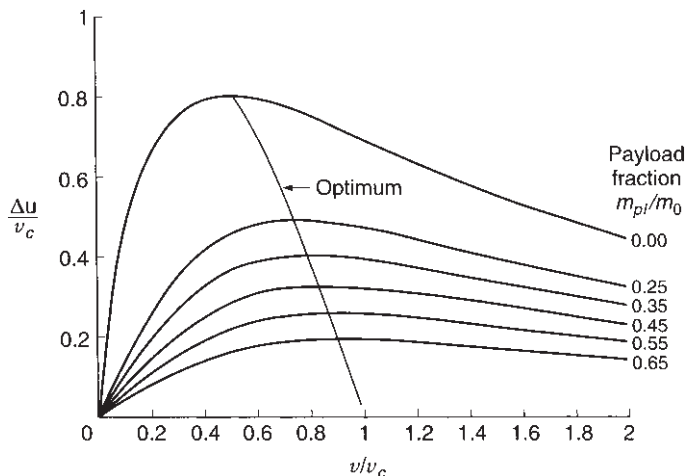


FIGURE 17–3. Normalized vehicle velocity increment as a function of normalized exhaust velocity for various payload fractions with zero inert mass of the propellant tank (Ref. 17–6). The optima of each curve are connected by a line that represents Eq. 17–9.

Chapter 19 and elsewhere, this trend is generally true for all propulsion systems and leads to the statement that, *for a given mission, there is theoretically an optimum range of specific impulse and thus an optimum propulsion system design*. The peak of each curve in Fig. 17–3 is nicely bracketed by the ranges $\Delta u/v_c \leq 0.805$ and $0.505 \leq v/v_c \leq 1.0$. This means that for any given electric propulsion system an *optimum operating time* t_p^* will be proportional to the square of the total required change in vehicle velocity and thus large Δu 's would correspond to very long mission times. Similarly, an *optimum specific impulse* I_s^* will be (nearly) proportional to the change in vehicle velocity and large changes here would necessitate correspondingly high specific impulses. These conclusions will be refined in Section 17.4.

The peak of the curves in Fig. 17–3 can be found by differentiating Eq. 17–7

$$\left(\frac{v}{\Delta u}\right)\left(e^{\Delta u/v} - 1\right) - \frac{1}{2}\left(\frac{v_c}{v}\right)^2 - \frac{1}{2} = 0 \quad (17-9)$$

This relates Δu , v , and v_c for maximum payload fraction (see Ref. 17–2).

All the equations quoted so far apply to all three fundamental types of electric rocket systems. No engine parameters are necessary except for the overall efficiency, which ranges from 0.4 to 0.8 in well-designed electric propulsion units, and α , which varies more broadly.

The problem with the above formulation is that the equations are underconstrained in that, given a velocity increment, mission time and specific impulse can be independently assigned. We will return to this topic in Section 17.4.

Example 17–1. Determine the flight characteristics of an electrical propulsion rocket for raising a low satellite orbit. The following are given:

$$I_s = 2000 \text{ sec}$$

$$F = 0.20 \text{ N}$$

$$\text{Duration} = 4 \text{ weeks} = 2.42 \times 10^6 \text{ sec}$$

$$\text{Payload mass} = 100 \text{ kg}$$

$$\alpha = 100 \text{ W/kg}$$

$$\eta_t = 0.5$$

SOLUTION. The propellant flow is, from Eq. 2–13,

$$\dot{m} = F/(I_s g_0) = 0.2/(2000 \times 9.81) = 1.02 \times 10^{-5} \text{ kg/sec}$$

The total required propellant is

$$m_p = \dot{m} t_p = 1.02 \times 10^{-5} \times 2.42 \times 10^6 = 24.69 \text{ kg}$$

The required electrical power is

$$P_e = \frac{1}{2} \dot{m} v^2 / \eta_t = \frac{1}{2} (1.02 \times 10^{-5} \times 2000^2 \times 9.81^2) / 0.5 = 3.92 \text{ kW}$$

The mass of the energy supply system is, from Eq. 17–5,

$$m_{pp} = P_e / \alpha = 3.92 / 0.1 = 39.2 \text{ kg}$$

The mass before and after engine operation (see Eq. 17–4) is

$$m_1 = 100 + 24.7 + 39.2 = 163.9 \text{ kg}$$

$$m_2 = 139.2 \text{ kg}$$

The velocity increase of the stage under ideal vacuum and zero-g conditions (Eq. 4–6) is

$$\begin{aligned} \Delta u &= v \ln[m_0 / (m_0 - m_p)] \\ &= 2000 \times 9.81 \ln(163.9 / 139.2) = 3200 \text{ m/sec} \end{aligned}$$

The acceleration of the vehicle is

$$\begin{aligned} a &= \Delta u / t = 3200 / 2.42 \times 10^6 = 1.32 \times 10^{-3} \text{ m/sec}^2 \\ &= 1.35 \times 10^{-4} g_0 \end{aligned}$$

The flight's energy increase after 4 weeks of continuous thrust-producing operation is not enough to get from LEO to GEO (which would have required a change of vehicle

velocity of about 4700 m/sec with continuous low thrust). During its travel the satellite will have made about 158 revolutions around the earth and raised the orbit by about 13,000 km. Moreover, this does not represent an optimum. In order to satisfy Eq. 17-9 it would be necessary to increase the burn duration (operating time) or change the thrust, or both. The above approach may be compared to the Hohmann method in Example 4-2.

17.2. ELECTROTHERMAL THRUSTERS

In this category, electric energy is used to heat the propellant, which is then thermodynamically expanded through a nozzle. There are two basic types in use today:

1. The *resistojet*, in which components with high electrical resistance dissipate power and in turn heat the propellant, largely by convection.
2. The *arcjet*, in which current flows through the bulk of the propellant gas which has been ionized in an electrical discharge. Being relatively devoid of material limitations, this method introduces more heat directly into the gas (it can reach local temperatures of 20,000 K or more). The electrothermal arcjet is a unit where magnetic fields (either external or self-induced by the current) are not as essential for producing thrust as is the nozzle. As shown in Section 17.3 (and Fig. 17-9), arcjets can also operate as electromagnetic thrusters, but here the magnetic fields are essential for acceleration and propellant densities are much lower. Thus, there are some arc-thruster configurations that could be classified as both electrothermal and electromagnetic.

Resistojets

These devices are the simplest type of electrical thruster because the technology is based on conventional conduction, convection, and radiation heat exchange. The propellant is heated by flowing over an ohmically heated refractory-metal surface, such as (1) coils of heated wire, (2) through heated hollow tubes, (3) over heated knife blades, and (4) over heated cyclinders. Power requirements range between 1 W and several kilowatts; a broad range of terminal voltages, AC or DC, can be designed for, and there are no special requirements for power conditioning. Thrust can be steady or intermittent as programmed in the propellant flow.

Material limitations presently cap the operating temperatures to under 2700 K, yielding maximum specific impulses of about 300 sec. The highest specific impulse has been achieved with hydrogen (because of its lowest molecular mass), but its low density causes propellant storage to be bulky (cryogenic storage being unrealistic for space missions). Since virtually any propellant is appropriate, a large variety of different gases has been used, such as O₂, H₂O, CO₂, NH₃, CH₄, and N₂. Also, hot gases resulting from the catalytic decomposition of hydrazine (which produces approximately 1 volume of NH₃ and 2 volumes of H₂ [see Chapter 7]) have been successfully operated. The system using liquid hydrazine

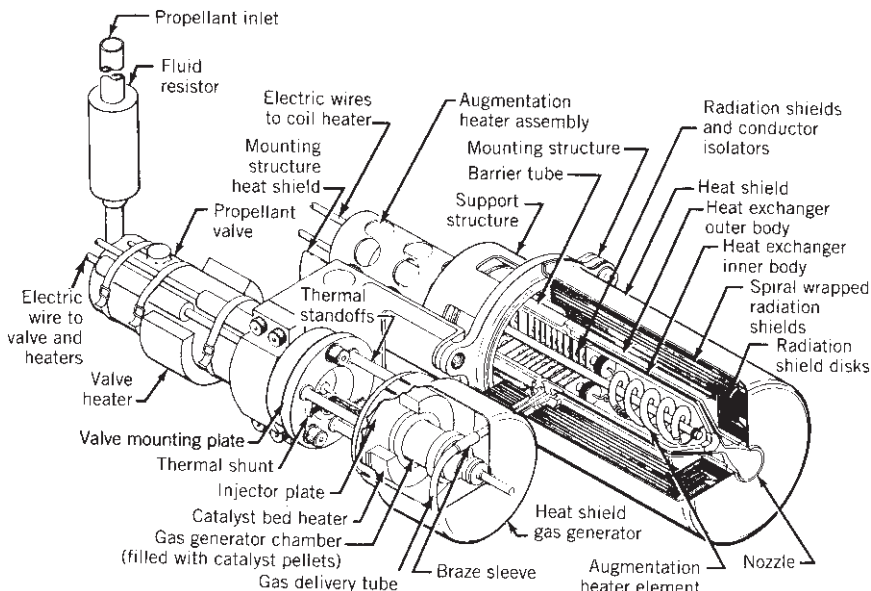


FIGURE 17-4. Resistojet augmented by hot gas from catalytically decomposed hydrazine; two main assemblies are present: (1) a small catalyst bed with its electro-magnetically operated propellant valve and heaters to prevent hydrazine from freezing, and (2) an electrical resistance spiral-shaped heater surrounded by thin radiation shields, a refractory metal exhaust nozzle, and high-temperature electrical insulation supporting the power leads. (Courtesy of Aerojet General.)

(Ref. 17-7) has the advantage of being compact and the catalytic decomposition preheats the mixed gases to about 700°C (1400°F) prior to their being heated electrically to an even higher temperature; this reduces the required electric power while taking advantage of a well-proven space chemical propulsion concept. Figure 17-4 shows details of such a hybrid resistojet which is fed downstream from a catalyst bed where hydrazine is decomposed into hot gases. Table 17-3 shows its performance values.

Resistojets have been proposed for manned long-duration deep space missions, where the spacecraft's waste products (e.g., H_2O or CO_2) could then be used as propellants. Unlike the ion engine and the Hall thruster, the same resistojet design can be used with different propellants.

In common with nearly all electric propulsion systems, resistojets have a propellant feed system that has to supply either gas from high-pressure storage tank or liquid under zero gravity conditions. Liquids require positive tank expulsion mechanisms, which are discussed in Chapter 6, and pure hydrazine needs heaters to keep it from freezing.

Engineering considerations in the development of these rockets include intermittent heat transfer from the heating element to the propellant, conduction and radiation losses from the chamber, the capability of materials to withstand the

TABLE 17–3. Selected Performance Values of a Typical Resistojet with Augmentation

| | |
|-----------------------------------|---|
| Propellant for resistojet | Hydrazine liquid, decomposed by catalysis |
| Inlet pressure (MPa) | 0.689–2.41 |
| Catalyst outlet temperature (K) | 1144 |
| Resistojet outlet temperature (K) | 1922 |
| Thrust (N) | 0.18–0.33 |
| Flow rate (kg/sec) | $5.9 \times 10^{-5} – 1.3 \times 10^{-4}$ |
| Specific impulse in vacuum (sec) | 280–304 |
| Power for heater (W) | 350–510 |
| Power for valve (max.) (W) | 9 |
| Thruster mass (kg) | 0.816 |
| Total impulse (N-sec) | 311,000 |
| Number of pulses | 500,000 |
| Status | Operational |

Source: Data sheet for model MR-501, Aerojet General.

hot environment, and the heat capacity of the propellant. Procedures have been developed to account for specific heat, thermal conductivity, dissociation, and gas density variations with temperature. The gas flow in the heating chamber is typically considered to be either laminar or vortex flow, and the heat transfer to the stream is by convection.

Available materials limit the maximum gas temperature of a resistojet. High-temperature materials used for the resistance element include rhenium and refractory metals and their alloys (e.g., tungsten, tantalum, molybdenum), platinum (stabilized with yttrium and zirconia), as well as cermets. For high-temperature electrical (but not thermal) insulation, boron nitride has been used effectively.

A design objective is to keep heat losses in the chamber at a low level relative to the power consumed. This can be done by (1) the use of external insulation, (2) internally located radiation shields, and (3) entrant flow layers or cascades. Within reason, the mass of insulation and radiation shields should be small compared to that of the thruster and of the total propulsion system.

The choice of chamber pressure is influenced by several factors. High pressures reduce molecular gas dissociation losses in the chamber, increase the rate of recombination in the exhaust nozzle, improve the heat exchanger performance, and reduce the size of both the chamber and the nozzle for a given mass flow rate. However, high pressures cause higher heat transfer losses, higher stresses on the chamber walls, and can accelerate the rate of nozzle throat erosion. The lifetime of a resistojet is often dictated by the nozzle throat life. Good design practice, admittedly a compromise, sets the chamber pressure in the range of 15 to 200 psia.

Thruster efficiencies of resistojets range between 65 and 85%, depending on the propellant and the exhaust gas temperature, among other things. The specific impulse delivered by any given electrothermal design depends primarily on (1) the molecular mass of the propellant and (2) the maximum temperature that the chamber and the nozzle surfaces can tolerate.

Table 17-3 gives typical performance values for a resistojet augmented by chemical energy release. The specific impulse and thrust increase as the electric power of the heater is increased. An increase in flow rate (at constant specific power) results in an actual decrease in performance. The highest specific power (power over mass flow rate) is achieved at relatively low flow rates, low thrusts, and modest heater augmentation. At the higher temperatures the dissociation of molecular gases noticeably reduces the energy that is available for thermodynamic expansion.

Even with its comparatively lower value of specific impulse, the resistojet's superior efficiency contributes to far higher values of thrust/power than any of its (see Eq. 17-3) competitors. Additionally, these engines possess the lowest overall system empty mass since they do not require a power processor and their plumes are uncharged (thus avoiding the additional equipment that ion engines require). Resistojets have been employed in Intelsat V, Satcom 1-R, GOMS, Meteor 3-1, Gstar-3, and Iridium spacecraft. They are most attractive for low to modest levels of mission velocity increments, where power limits, thrusting times, and plume effects are mission drivers.

Arcjets

The basic elements of an arcjet thruster are shown in Fig. 1-8 where the relative simplicity of the physical design masks its rather complicated phenomenology. The arcjet overcomes the gas temperature limitations of the resistojet by the use of an electric arc for direct heating of the propellant stream to temperatures much higher than the wall temperatures. The arc stretches between the tip of a central cathode and an anode, which is part of the coaxial nozzle that accelerates the heated propellant. These electrodes must be electrically insulated from each other and be able to withstand high temperatures. At the nozzle it is desirable for the arc to attach itself as an annulus in the divergent portion just downstream of the throat (see Figs. 1-8 and 17-5 for location). The region of attachment is known to move around depending on the magnitude of the arc voltage and on the mass flow rate. In reality, arcs are highly filamentary and tend to heat only a small portion of the flowing gas unless the throat dimension is sufficiently small; bulk heating is done by mixing, often with the aid of vortex flow and turbulence.

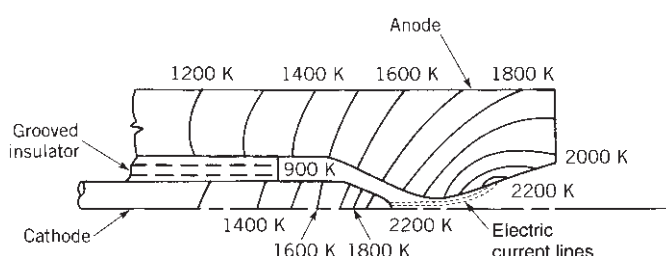


FIGURE 17-5. Typical estimated temperature distribution in the electrodes of an arcjet.

Arcs are inherently unstable, often forming pinches and wiggles; they can be somewhat stabilized by an external electric field or by swirling vortex motion in the outer layers of the gas flow. The flow structure at the nozzle throat is quite nonuniform and arc instabilities and erosion at the throat are life limiting. The mixing of cooler outer gas with the arc-heated inner gas tends to stabilize the arc while lowering its conductivity, which in turn requires higher voltages of operation. In some designs the arc is made longer by lengthening the throat.

The analysis of arcjets is based on plasma physics, as it applies to a moving ionized fluid. The conduction of electricity through a gas requires that a certain level of ionization be present. This ionization must be obtained from an electrical discharge, that is, the breakdown of the cold propellant resembling a lightning discharge in the atmosphere (but, unlike lightning, a power supply may feed the current in a continuous or pulsed fashion). Gaseous conductors of electricity follow a modified version of *Ohm's law*. In an ordinary *uniform medium* where an electrical current I is flowing across an area A through a distance d by virtue of a voltage drop V , we can write Ohm's law as

$$V = IR = (I/A)(AR/d)(d) \quad (17-10)$$

As given, the medium is uniform and thus we may define the electric field as $E = V/d$, the current density as $j = I/A$, and we introduce the *electrical conductivity* as $\sigma = d/AR$. We can now rewrite the basic Ohm's law as simply $j = \sigma E$. The scalar electrical conductivity is directly proportional to the density of unattached or *free electrons* that, under equilibrium, may be found from Saha's equation (Ref. 17-8). Strictly speaking, Saha's equation applies to thermal ionization only (and not necessarily to electrical discharges). For most gases, either high temperatures or low ionization energies or both are required for plentiful ionization. However, since only about one in a million electrons is sufficient for good conductivity, an inert gas can be seeded with alkali-metal vapors, as is amply demonstrated in plasmas for power generation. The value of plasma electrical conductivity σ may be calculated from

$$\sigma = e^2 n_e \tau / \mu_e \quad (17-11)$$

Here e is the electron charge, n_e the electron number density, τ the mean time between collisions, and μ_e the electron mass.

Actually, arc currents are nearly always influenced by magnetic fields, external or self-induced, and a *generalized Ohm's law* (Ref. 17-9) in a moving gas is needed such as the following vector form (this equation is given in scalar forms in the section on electromagnetic devices):

$$\mathbf{j} = \sigma [\mathbf{E} + \mathbf{v} \times \mathbf{B} - (\beta/\sigma B)(\mathbf{j} \times \mathbf{B})] \quad (17-12)$$

The motion of the gas containing charged particles is represented by the velocity \mathbf{v} ; the magnetic induction field is given as \mathbf{B} (a scalar B in the above equation

is required in the last term) and the electric field as \mathbf{E} . In Eq. 17–12, both the current density \mathbf{j} and the conductivity are understood to relate to the free electrons as does β , the Hall parameter. This Hall parameter is made up from the electron cyclotron frequency (ω) multiplied by the mean time it takes an electron to lose its momentum by collisions with the heavier particles (τ). The second term in Eq. 17–12 is the induced electric field due to the motion of the plasma normal to the magnetic field, and the last term represents the Hall electric field which is perpendicular to both the current vector and the applied magnetic field vector as the cross product (i.e., the “ \times ”) implies (ionslip and the electron pressure gradient have been omitted above, for simplicity). Magnetic fields are responsible for most of the peculiarities observed in arc behavior, such as pinching (a constriction arising from the current interacting with its own magnetic field), and play a central role in nonthermal electromagnetic forms of thrusting, as discussed in a following section.

Analytical descriptions of arcjets, based on the configuration shown in Figs. 1–8 and 17–5, may include the following:

1. The energy input occurs largely in the small-diameter laminar flow arc region within the throat of the nozzle. As a first approximation, the power can be computed from Joule heating [$\mathbf{j} \cdot \mathbf{E}$]; here the current density and the voltage gradient across the arc have to be determined.
2. The cathode tip needs to be hot for thermionic emission of the arc electrons. It is heated by the arc and cooled by the propellant flow. The cathode, typically a coaxial pointed rod, is located in the plenum region.
3. The nozzle inner walls are heated by the arc, which may be at a temperature of 10,000 to 20,000 K. Typically the nozzle is cooled only by conduction and the heat transfer is reduced by the boundary layers.
4. The hot gas in the arc proper must mix quickly with the rest of the propellant; this is done by vortexing and turbulence.
5. Portions of the anode are heated to extreme temperatures in a section of the divergent nozzle at the arc footpoint (the arc attachment region of the electrode). The heating of the propellant is not all contained in the plenum chamber, and heating of a supersonic flow is a source of losses.

To start an arcjet, a much higher voltage than necessary for operation has to be applied momentarily in order to break down the cold gas. Some arcjets require an extended initial burn-in period before stable consistent running ensues. Because the conduction of electricity through a gas is inherently unstable, arcs require an external ballast resistance to allow steady-state operation. The cathode must run hot and is usually made of tungsten with 1 or 2% thorium (suitable up to about 3000 K). Boron nitride, an easily shaped high-temperature electrical insulator, is commonly used.

Presently, most arcjets are rather inefficient since less than half of the electrical energy goes into kinetic energy of the jet; the nonkinetic part of the exhaust plume (residual internal energy and ionization) is the largest loss. About 10 to

20% of the electric power input is usually dissipated and radiated as heat to space or transferred by conduction from the hot nozzle to other parts of the system. Arcjets, however, are potentially more scalable to large thrust levels than other electric propulsion systems. Generally, arcjets exhibit about six times the thrust-to-power ratio of a resistojet because of their increased specific impulse coupled with relatively low values of efficiency. Arcjets have another disadvantage in that the required power processing units are somewhat more complex than those for resistojets, due to the complexity of arc phenomena.

The life of an arcjet can be severely limited by local electrode erosion and vaporization, which is specifically due to action of the arc attachment point and of the high operating temperatures in general. The rate of erosion is influenced by the particular propellant in combination with the electrode materials (argon and nitrogen give higher erosion rates than hydrogen), and by pressure gradients, which are usually higher during start or pulsing transients (sometimes by a factor of 100) than during steady-state operation. A variety of propellants has been used in arcjet devices, but the industry has settled on the catalytic decomposition products of N_2H_4 ; see Section 7.4.

An arcjet downstream of a catalytic hydrazine decomposition chamber looks similar to the resistojet of Fig. 17–4, except that the resistor is replaced by a smaller diameter arc heater. Also, larger cables are needed to supply the relatively much larger currents. Decomposed hydrazine would enter the arc at a temperature of about 760°C . Liquid hydrazine is easier to store and provides a low-volume, lighter-weight propellant supply system when compared to gaseous propellants. Table 17–4 shows on-orbit performance of a system of 2-kW hydrazine arcjets. Specific impulses from 400 to nearly 600 sec are typical for hydrazine arcjets (Ref. 17–10). A 26-kW ammonia arcjet program (ESEX) flew in 1999 (Ref. 17–11) with 786 sec specific impulse and 2 N thrust.

TABLE 17–4. On-Orbit 2-kW Hydrazine Arcjet System

| | |
|--------------------------------|--|
| Propellant | Hydrazine |
| Steady thrust | 222–258 mN |
| Mass flow rate | 36–47 mg/sec |
| Feed pressure | 185–330 psia |
| Power control unit (PCU) input | 4.4 kW (two thrusters) |
| System input voltage | 68–71 V DC |
| PCU efficiency | 93% |
| Specific impulse | 570–600 sec |
| Dimensions | |
| Arcjet | $237 \times 125 \times 91 \text{ mm}^3$ |
| PCU | $632 \times 361 \times 109 \text{ mm}^3$ |
| Mass | |
| Arcjet (4) and cable | 6.3 kg |
| PCU | 15.8 kg |
| Total impulse | 1,450,000 N-sec |

Source: From Ref 17–10.

17.3. NONTHERMAL ELECTRICAL THRUSTERS

The acceleration of a hot propellant through the use of a supersonic nozzle is the most conspicuous feature of thermal thrusting. Now we turn our study to acceleration of a propellant by electrical forces where no area changes are essential for direct gas acceleration. The electrostatic (or Coulomb) force and the electromagnetic (or Lorentz) force can be used to accelerate a suitable propellant to speeds ultimately limited by the speed of light (note that thermal thrusting is essentially limited by the speed of sound in the plenum chamber). The microscopic vector force \mathbf{f}_e on a *singly charged particle* can be written as

$$\mathbf{f}_e = e\mathbf{E} + ev_e \times \mathbf{B} \quad (17-13)$$

where e is the electron charge magnitude, \mathbf{E} the electric field vector, v_e the velocity of the charged particle, and \mathbf{B} the magnetic field vector. The sum of the electromagnetic forces on all the charges gives the total force per unit volume vector $\tilde{\mathbf{F}}_e$ (scalar forms of this equation follow):

$$\tilde{\mathbf{F}}_e = \rho_e \mathbf{E} + \mathbf{j} \times \mathbf{B} \quad (17-14)$$

Here ρ_e is the *net charge density* and \mathbf{j} the electric current vector density. With plasmas, which by definition have an equal mixture of positively and negatively charged particles within a volume of interest, this net charge density vanishes. On the other hand, the current due to an electric field does not vanish because positive ions move opposite to electrons, thus adding to the current (but in plasmas with free electrons this ion current can be very small). From Eq. 17-14, we see that an electrostatic accelerator must have a nonzero net charge density that is commonly referred to as a *space-charge density*. An example of an electrostatic accelerator is the ion engine, which operates with positive ions; here magnetic fields are unimportant in the accelerator region. Electromagnetic accelerators operate only with plasmas and rely solely on the Lorentz force to accelerate the propellant. The Hall accelerator may be thought of as a crosslink between an ion engine and an electromagnetic engine. These three types of accelerator are discussed next. Research and development efforts in the field of nonthermal thrusters have been extensive and truly international.

Electrostatic and electromagnetic devices require an understanding of the basic laws of electricity and magnetism which are most elegantly summarized in Maxwell's equations complemented by the force relation and Ohm's law, both previously introduced. Moreover, various processes in ionization and gaseous conduction need to be considered. This subject forms the basis of the discipline of magnetohydrodynamics or MHD; however, a proper treatment of this subject is beyond the scope of this book.

Electrostatic Devices

Electrostatic thrusters rely on Coulomb forces to accelerate a propellant composed of nonneutral charged particles. They can operate only in a near vacuum. The electric force depends only on the charge, and all charged particles must be of the same “sign” if they are to move in the same direction. Electrons are easy to produce and are readily accelerated, but they are so extremely light in mass as to be impractical for electric propulsion. From thermal propulsion fundamentals one might deduce that “the lighter the exhaust particle the better.” However, the momentum carried by electrons is relatively negligible even at velocities near the speed of light. Thus, the thrust per unit area that can be imparted to such an electron flow remains negligible even when the effective exhaust velocity or specific impulse gets to be very high. Accordingly, electrostatic thrusters use charged heavy-molecular-mass atoms as *positive ions* (a proton is 1840 times heavier than the electron and a typical ion of interest contains hundreds of protons). There has been some research work with small liquid droplets or *charged colloid* which can in turn be some 10,000 times heavier than atomic particles. In terms of power sources and transmission equipment, the use of the heavier particles contributes to more desirable characteristics for electrostatic thrusters—for example, high voltages and low currents in contrast to low voltages and high currents with their associated massive wiring and switching.

Electrostatic thrusters can be further categorized by the source of charged particles. Exit beam neutralization is required for all these schemes.

1. *Electron bombardment thrusters*. Positive ions in a gas are produced by bombarding a gas or vapor, such as xenon or mercury, with electrons usually emitted from a heated cathode. Ionization can be either DC or RF. In these ion engines, acceleration is accomplished with a separate electrical source applied through a series of suitably manufactured and positioned electrically conducting grids (see Fig. 1–9). This is presently the most common method.
2. *Field emission thrusters*. In the field emission electric propulsion (FEEP) concept, positive ions are obtained from a liquid metal source flowing through a capillary tube and several geometrical arrangements are possible (Ref. 17–12). Liquid metals such as indium (Ref. 17–13) or cesium when subjected to a high electric field ($> 10^6$ V/cm) may produce molecular ions flowing into the accelerating region. The injector, ionizer, and accelerator are part of the same voltage circuit which operates typically at values over 10 kV. This is a robust concept that is being considered for micropropulsion space applications with I_s values of around 8000 to 9000 sec. The FEEP has been space qualified.

Examples of space flights with electrostatic units that have successfully flown are the XIPS (xenon ion propulsion system, Ref. 17–14) used in NASA’s DS1 and DAWN missions, and RITA (radio frequency ion thrusters, Ref. 17–15) flown in several European missions. Japan’s Hayabusa spacecraft with four microwave ion engines is another notable mission which includes landing and taking-off from an asteroid. The following general design criteria are desirable regardless of the type of thruster:

1. Minimum energy expenditure per charged particle produced. The propellant ionization potential is only part of this loss, which also includes ionizer losses and heating for cathodes or heating to maintain metal propellants in liquid form.
2. Minimum ion impingement damage to the cathode and to the accelerating electrode(s), or *sputtering*, and minimum deterioration of component characteristics over thrust lifetime (capillaries tend to plug).
3. Maximum supply of ionized particles for acceleration, or high *propellant utilization factor* (hollow cathode neutralizers use propellant which is not accelerated).
4. Stabilized uniform operation near the space–charge limitations of the thruster at maximum saturation current (as defined in Eq. 17–21) within the accelerator electrodes, see Ref. 17–2).
5. Production of particles of uniform mass and charge for effective electric field acceleration (electrical spraying may produce charged droplets at the higher currents).
6. No reaction of exhaust plume with spacecraft materials and no condensations on spacecraft optical components—windows, lenses, mirrors, photovoltaic surfaces, or heat rejection surfaces. (Liquid metals of interest for FEEP can react with and condense on spacecraft materials.)
7. Propellants with desirable storage properties in space (i.e., high-density storage, noncorrosive, with desirable freezing/boiling points, and stable over time) and low *tankage fraction* (mass related to propellant containment). This may include the valves and pressure vessels.
8. Specific impulse near optimum for the given mission (with electron bombardment thrusters the specific impulse may be throttled by the accelerating voltage with little loss in performance, or changed through the use different molecular mass propellants).

Basic Relationships for Electrostatic Thrusters

An electrostatic thruster, regardless of type, consists of the same series of basic ingredients, namely, a propellant source, several forms of electric power, an ionizing chamber, an accelerator region, and a means of neutralizing the exhaust. While Coulomb accelerators require a net charge density of one polarity, the

exhaust beam must be neutralized to avoid a space-charge buildup outside of the craft which could easily nullify the operation of the thruster. Neutralization is achieved by the injection of electrons downstream (see the device descriptions that follow). The exhaust velocity is a function of the voltage V_{acc} imposed across the accelerating chamber or grids, the mass of the charged particle μ , and its electrical charge e . In the conservation of energy equation the kinetic energy of a charged particle must equal the electrical energy gained in the field, provided that there are no collisional losses. In its simplest form,

$$\frac{1}{2}\mu v^2 = eV_{\text{acc}} \quad (17-15)$$

Now, solving for the speed gained in the accelerator,

$$v = \sqrt{2eV_{\text{acc}}/\mu} \quad (17-16)$$

When e is in coulombs, μ in kilograms, and V_{acc} is in volts, then v is in meters per second. Using \mathfrak{M} to represent the molecular mass of the ion ($\mathfrak{M} = 1$ for a proton), then, for singly charged ions, the equation above becomes $v(\text{m/sec}) = 13,800\sqrt{V_{\text{acc}}/\mathfrak{M}}$. References 17-3 and 17-4 contain a detailed treatment of the applicable theory.

In an ideal ion thruster, the current I across the accelerator represents the sum of all the propellant mass (fully but singly ionized) carried per second by the particles accelerated:

$$I = \dot{m}(e/\mu) \quad (17-17)$$

The total ideal thrust from the accelerated particles is given by Eq. 2-14 (without the pressure thrust term, as pressures are extremely low):

$$F = \dot{m}v = I\sqrt{2\mu V_{\text{acc}}/e} \quad (17-18)$$

As can be seen, for a given current and accelerator voltage the thrust is proportional to the mass-to-charge ratio of the charged particles and high molecular mass ions are favored for high thrust density. The thrust and power absorbed by the neutralizing electrons are both small (about 1%) and can easily be neglected.

The current density j that can be obtained with a charged particle beam has a *saturation value* depending on the geometry and the electrical field (see Ref. 17-16). This fundamental limit is caused by the internal electric field associated with the ion cloud opposing the electric field from the accelerator when too many charges of the same sign try to pass simultaneously through the accelerator. The saturation current can be derived for a plane-geometry electrode configuration from basic principles. A definition of the current density in terms of the space-charge density follows:

$$j = \rho_e v \quad (17-19)$$

The voltage in a one-dimensional space-charge region is found from Poisson's equation, where x represents distance and ϵ_0 is the *permittivity of free space* which, in SI units, has the value of 8.854×10^{-12} farads per meter:

$$d^2V/dx^2 = \rho_e/\epsilon_0 \quad (17-20)$$

By solving Eqs. 17-16, 17-19, and 17-20 simultaneously and applying the proper boundary conditions, we obtain the following relation known as the *Child-Langmuir law*:

$$j = \frac{4\epsilon_0}{9} \sqrt{\frac{2e}{\mu}} \frac{(V_{\text{acc}})^{3/2}}{d^2} \quad (17-21)$$

In this equation, d is the accelerator interelectrode distance. In SI units the equation for the saturation current density can be expressed (for atomic or molecular ions) as

$$j = 5.44 \times 10^{-8} V_{\text{acc}}^{3/2} / (\mathfrak{M}^{1/2} d^2) \quad (17-22)$$

Here the current density is in A/m², the voltage is in volts, and the distance in meters. For xenon with electron bombardment schemes, values of j vary from 2 to about 10 mA/cm². The current density and the area are very sensitive to the accelerator voltage as well as to the electrode configuration and spacing.

Using Eqs. 17-18 and 17-22 and letting the cross section be circular so that the current $I = (\pi D^2/4)j$, the thrust can be rewritten as

$$F = (2/9)\pi\epsilon_0 D^2 V_{\text{acc}}^2 / d^2 \quad (17-23)$$

In SI units, this becomes

$$F = 6.18 \times 10^{-12} V_{\text{acc}}^2 (D/d)^2 \quad (17-24)$$

The ratio of the exhaust beam emitter diameter D to the accelerator-electrode grid spacing d can be regarded as an *aspect ratio* of the ion accelerator region. For multiple grids with many holes (see Figs. 17-6 and 17-7) the diameter D is that of the individual perforation hole and the distance d is the mean spacing between grids. Because of space-charge limitations, D/d can have values no higher than about one for simple, single-ion beams. This implies a rather stubby engine design with many perforations and the need for multiple parallel ion engines for larger thrust values.

Using Eqs. 17-1, 17-2, and 17-17, and assuming η_t conversion of potential energy to kinetic energy, the power of the electrostatic accelerator region is

$$P_e = \frac{IV_{\text{acc}}}{\eta_t} = (\frac{1}{2})\dot{m}v^2/\eta_t \quad (17-25)$$

The overall efficiency of an electrostatic thruster will be a function of the thruster efficiency η_t , as well as of other loss factors. One loss of energy which is intrinsic to the thruster is the energy expended in charging the propellant, which is related to the ionization energy; it is similar to the dissociation energy in electrothermal devices. Ionization represents an input necessary to make the propellant respond to the electrostatic force and is nonrecoverable. The ionization energy is found from the ionization potential (ϵ_I) of the atom or molecule times the current flow, as the example below shows. Table 17-5 shows the molecular mass and ionization potential for different propellants. In actual practice, considerably higher voltages than the ionization potential are required to operate the ionization chamber.

Example 17-2. For an electron-bombardment ion thruster using xenon the following data are given:

| | |
|-----------------------------------|-----------------------------------|
| Working fluid | xenon (131.3 kg/kg-mol, 12.08 eV) |
| Net accelerator voltage | 750 V |
| Distance d between grids | 2.5 mm |
| Diameter D of each grid opening | 2.0 mm |
| Number of holes in the grid | 25,000 |

Determine the thrust, exhaust velocity, specific impulse, mass flow rate, propellant needed for 91 days' operation, the power of the exhaust jets, and the thruster efficiency including ionization losses.

SOLUTION. The ideal thrust is obtained from Eq. 17-24:

$$F = 6.18 \times 10^{-12} \times (750)^2 \times (2/2.5)^2 = 2.23 \times 10^{-6} \text{ N per grid opening}$$

The total ideal thrust is then obtained by multiplying by the number of holes:

$$F = 25,000 \times 2.23 \times 10^{-6} = 55.67 \text{ mN}$$

The exhaust velocity and specific impulse are obtained from Eq. 17-16:

$$v = 13,800\sqrt{750/131.3} = 32,982/\text{sec}$$

$$I_s = 32,982/9.81 = 3362 \text{ sec}$$

The mass flow rate, obtained from Eq. 2-6, is

$$\dot{m} = F/v = 55.67 \times 10^{-3}/32,982 = 1.68 \times 10^{-6} \text{ kg/sec}$$

For a cumulative period of 91 days of operation, the amount of xenon propellant needed (assuming no losses) is

$$m = \dot{m} t_p = 1.68 \times 10^{-6} \times 91 \times 24 \times 3600 = 13.27 \text{ kg}$$

TABLE 17–5. Ionization Potentials for Various Gases

| Gas | Ionization Potential (eV) | Molecular/Atomic Mass (kg/kg-mol) |
|---------------------|---------------------------|-----------------------------------|
| Cesium vapor | 3.9 | 132.9 |
| Bismuth | 7.3 | 209 |
| Mercury vapor | 10.4 | 200.59 |
| Xenon | 12.08 | 131.30 |
| Krypton | 14.0 | 83.80 |
| Hydrogen, molecular | 15.4 | 2.014 |
| Argon | 15.8 | 39.948 |

The kinetic energy rate in the jet is

$$\frac{1}{2}\dot{m}v^2 = 0.5 \times 1.68 \times 10^{-6} \times (32,982)^2 = 914 \text{ W}$$

The ionization losses (I_I) represent the nonrecoverable ionization energy which is related to the ionization potential of the atom (ϵ_I) times the number of coulombs produced per second (see Table 17–5 and Eq. 17–17):

$$I_I = (12.08) \times (1.68 \times 10^{-6} \times 1.602 \times 10^{-19}) / (1.66 \times 10^{-27} \times 131.3) = 14.9 \text{ W}$$

As can be seen, the ionization energy in this ideal case is about 2% of the accelerator energy rate. An equivalent way of calculating the ionization energy is to multiply the ionization potential by the total ion current. The current is found from Eq. 17–17 to be just under 10 mA. Discharge losses detract from the high ideal efficiency of this device, which is 98.3%, in fact, the energy needed per ion in the XIPS is reported to be more than 200 eV which brings the efficiency down to 60%; see Ref. 17–3.

Ionization Schemes. Even though all ion acceleration schemes are the same, there are several ionization schemes for electrostatic engines. Most devices are DC but some are RF. To a great extent, the ionization chamber is responsible for most of the size, mass, and perhaps efficiency of these devices. We discuss some of these next.

Ionization of a gas by electron bombardment is a well-established technology (Ref. 17–16). Electrons are emitted from a thermionic (hot) cathode or the more efficient hollow cathode and are forced to interact with the gaseous propellant flow in a suitable ionization chamber. The chamber pressures are low, about 10^{-3} torr or 0.134 Pa. Figure 17–6 depicts a typical electron-bombardment ionizer which contains neutral atoms, positive ions, and electrons. Emitted electrons are attracted toward the cylindrical anode but are forced by the axial magnetic field to spiral in the chamber, causing numerous collisions with propellant atoms which lead to ionization. The radial electric field removes the electrons from the chamber and an axial electric field moves the ions toward the accelerator grids. These grids act as porous electrodes, which electrostatically accelerate the positive ions. Loss of electrons is prevented by maintaining the cathode potential negatively biased

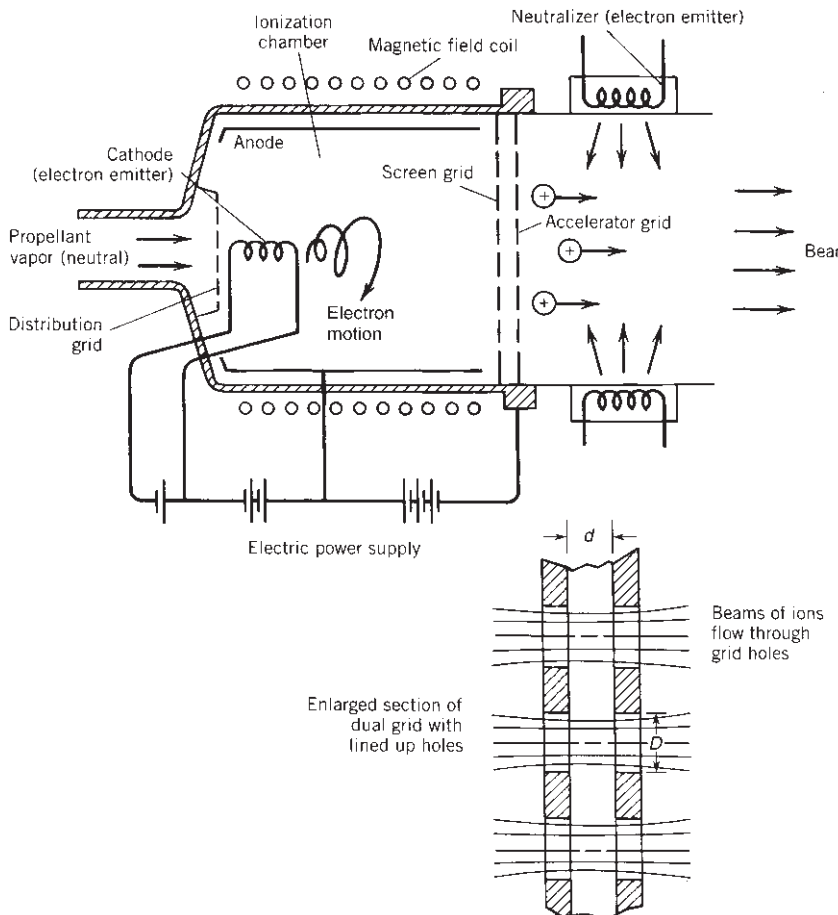


FIGURE 17–6. Simplified schematic diagram of an electron bombardment ion thruster, showing an enlarged section of the double grid.

on both the inner grid electrode and the opposite wall of the chamber. Electrons are routed from the cylindrical anode through an external circuit to another hot cathode at the exhaust beam in order to neutralize the exit beam.

Figure 17–7 shows a cross section of an ion propulsion thruster using xenon as a propellant. It has three perforated electrically charged grids: the inner one keeps the electrons in the ionizer, the middle one has a high voltage (1000 V or more) and accelerates the ions, and the outer one keeps the neutralizing electrons from entering the accelerator region. Each grid hole is lined up with a similar opening in the other grids and the ion beam flows through these holes. If the grids are properly designed, only a few ions are lost by collision with the surface; however, these collisions cause sputtering and greatly diminish the life of the grids. Heavy metals such as molybdenum have been used, with graphite composites being

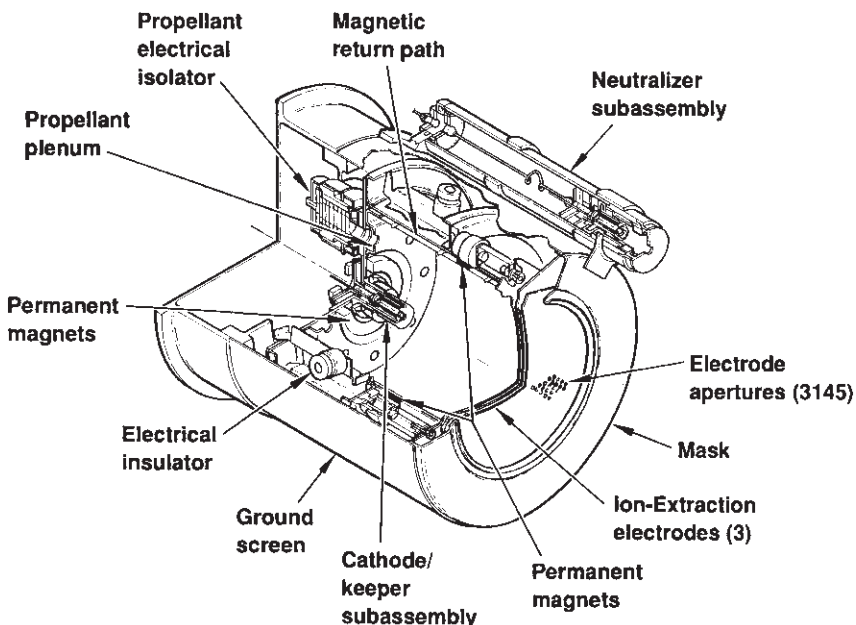


FIGURE 17–7. External view and section of a 500-watt ion propulsion system (XIPS), rated at 18 mN and 2800 sec. Permanent magnets are used on the outside of the ionization chamber; also shown are cathodes for ionization and for beam neutralization. Xenon gas is delivered to the ionizer, then accelerated through the three-sheet electrodes, and then the ion beam is neutralized. (Drawing courtesy of L-3 Communications Electron Technologies, Inc., and the American Physical Society.)

recently introduced. The neutralizer electron source is positioned outside the beam.

Other key components are (1) the heaters for the ionizer and neutralizer cathode, (2) propellant feed and electrical isolator, (3) electrical insulators, and (4) permanent magnets. Reference 17–14 describes a 500-W xenon thruster. Hollow cathodes represent an advancement in the state-of-the-art in electron emission; this cathode consists of a high-temperature metal tube with a flow-limiting orifice and a porous tungsten cylinder impregnated with a barium–oxygen compound located next to the orifice. At about 1370 K the cathode is a good thermionic emitter and thus the hot cylinder produces enough electrons at a relatively low temperature. Xenon, the stable inert gas with the highest molecular mass, is the propellant of choice. Xenon is a minor component of air, in a concentration of about 9 parts in 100 million, so it is a relatively rare and expensive propellant. Its critical point is 289.7 K and 5.84 MPa (the critical density is 1100 kg/m³). It is easily stored below its critical temperature as a liquid and it does not pose any problems of condensation or toxicity. Pressure regulators for xenon need to be more sophisticated, because no leakages can be tolerated and because flows are very small.

Electromagnetic Thrusters

This third major type of electric propulsion device accelerates propellant gas that has been heated to a plasma state. Plasmas are mixtures of electrons, positive ions, and neutral atoms or molecules that readily conduct electricity at temperatures usually above 5000 K or 9000° R. According to electromagnetic theory, whenever a conductor carries a current perpendicular to a magnetic field, a body force is exerted on the conductor in a direction at right angles to both the current and the magnetic field. Unlike the ion thruster, this acceleration process yields a neutral exhaust beam. Another advantage is the relatively high thrust density, or thrust per unit area, which is normally about 10 to 100 times that of the ion thrusters.

Many conceptual arrangements have undergone laboratory study, some with external and some with self-generated magnetic fields, some suited to continuous thrusting and some limited to pulsed thrusting. Table 17–6 shows ways in which electromagnetic thrusters can be categorized. There is a wide variety of devices with a correspondingly wide array of names. We will use the term Lorentz-force accelerators when referring to the principle of operation. For all of these devices the plasma is part of the current-carrying electrical circuit and most are accelerated without area changes. Motion of the propellant, a moderate-density plasma or in some cases a combination of plasma and cooler gas particles, is due to a complex set of interactions. This is particularly true of short duration (3 to 10 μ sec) pulsed-plasma thrusters where nothing reaches an equilibrium state. Basically, the designer of an electromagnetic thruster tries to (1) create a body of electrically conductive gas, (2) establish a high current by means of an applied electric field, and (3) accelerate the propellant to a high velocity in the thrust vector direction with a significantly intense magnetic field (often self-induced).

Conventional Thrusters – MPD and PPT. The description of *magneto-plasma-dynamic (MPD)* and *pulsed-plasma (PPT)* electromagnetic thrusters is

TABLE 17–6. Characterization of Electromagnetic Thrusters

| | Thrust Mode | |
|-----------------------------------|--|---|
| | Steady State | Pulsed (Transient) |
| Magnetic field source | External coils or permanent magnets | Self-induced |
| Electric current source | Direct-current supply | Capacitor bank and fast switches |
| Working fluid | Pure gas, mixtures, seeded gas, or vaporized liquid | Pure gas or stored as solid |
| Geometry of path of working fluid | Axisymmetric (coaxial) rectangular, cylindrical, constant or variable cross section | Ablating plug, axisymmetric, other |
| Special features | Using Hall current or Faraday current | Simple requirement for propellant storage |

based on the Faraday accelerator (Ref. 17–9). In its simplest form, a plasma conductor carries a current in the direction of an applied electric field but perpendicular to a magnetic field, with both of these vectors in turn normal to the direction of plasma acceleration. Equation 17–12 can be specialized to a Cartesian coordinate system where the plasma's "mass-mean velocity" is in the x direction, the external electric field is in the y direction, and the magnetic field acts in the z direction. A simple manipulation of Eq. 17–12, with negligible Hall parameter β , yields a scalar equation for the current, noting that only j_y, E_y , and B_z are present:

$$j_y = \sigma(E_y - v_x B_z) \quad (17-26)$$

and the Lorentz force becomes

$$\tilde{F}_x = j_y B_z = \sigma(E_y - v_x B_z) B_z = \sigma B_z^2 (E_y/B_z - v_x) \quad (17-27)$$

Here \tilde{F}_x represents the *force "density" within the accelerator* and should not be confused with F the thrust force; \tilde{F}_x has units of force per unit volume (e.g., N/m³). The axial velocity v_x is a mass-mean velocity that increases internally along the accelerator length; the thrust equals the exit value (v_{\max} or v_2) multiplied by the mass flow rate. It is noteworthy that, as long as E_y and B_z (or E/B) remain constant, both the current and the force decrease along the accelerator length due to the *induced field* $v_x B_z$ which subtracts from the impressed value E_y . This increase in plasma velocity translates into a diminishing force along such Faraday accelerators, which limits the final axial velocity. Although not practical it would seem desirable to design for increasing E/B along the channel in order to maintain a substantial accelerating force throughout. But it is not necessarily of interest to design for peak exit velocity because this might translate into unrealistic accelerator lengths (see Problem 8). It can be shown that practical considerations would restrict the exit velocity to below one-tenth of the maximum value of E_y/B_z .

A "gas-dynamic approximation" (essentially an extension of the classical concepts of Chapter 3 to plasmas in an electromagnetic field) by Resler and Sears (Ref. 17–17) indicates that further complications are possible, namely, that a constant area accelerator channel would *choke* if the plasma velocity does not have the very specific value of $[(k - 1)/k](E/B)$ at the sonic location of the accelerator. This *plasma tunnel velocity* would have to be equal to 40% of the value of E/B for inert gases, since k (the ratio of specific heats) equals 1.67. Thus constant area, constant E/B accelerators could be severely constrained because Mach 1 corresponds only to about 1000 m/sec in typical inert gas plasmas. Constant-area choking in real systems, where the properties E, B , and σ are actually quite variable, is likely to manifest itself as one or more instabilities. Another problem is that values of the conductivity and electric field are usually difficult to determine and a combination of analysis and measurement is required to evaluate, for example, Eq. 17–12. Fortunately, most plasmas are reasonably good conductors when less than 10% of the particles are ionized.

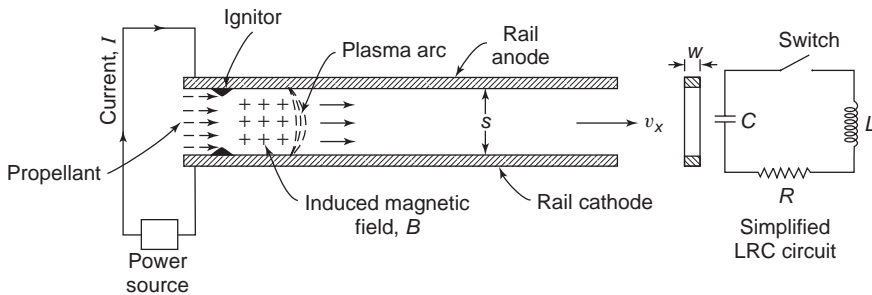


FIGURE 17–8. Simple rail accelerator for self-induced magnetic field acceleration of current-carrying plasma. The concept illustrates the basic physical interactions but suffers from loss of propellant, resulting in low efficiency.

Figure 17–8 shows the simplest plasma accelerator which employs a self-induced magnetic field. This is the *pulsed plasma thruster* (PPT) where an accelerating plasma burst or “bit,” initiated by a spark between the accelerator electrodes, is powered by a capacitor which in turn is charged from the spacecraft power supply. The current flow through the plasma quickly discharges the capacitor and hence the mass flow rate pulse must be synchronized to a “discharge schedule.” The discharge current closes a “current loop,” one which induces a significant magnetic field perpendicular to the plane of the rails. Analogous to a metal conductor in an electric motor, the Lorentz force acts on the movable plasma segment, accelerating it along the rails. Hence no area changes are necessary to accelerate the propellant but some designs do incorporate nozzles.

As indicated in Fig. 17–8, the system (though containing a plasma along with other more ordinary resistances) may be modeled with an equivalent *L-R-C pulsed circuit* where L is the lumped-parameter total circuit inductance, R is the total Ohmic resistance, and C is an effective capacitance. It is undesirable to let the current reverse during the pulsing as this diminishes the overall thrust, and a nonoscillatory pulse may be realized through the $R > 2\sqrt{L/C}$ impedance balancing criterion (when this is not physically possible, a “quenching diode” may be inserted, Ref. 17–18). In some designs, the hot plasma pulse has significant gas-dynamic expansion capabilities that may contribute to the thrust (with a nozzle for thermal expansion). In many typical configurations, the rate of increase of the circuit inductance with the distance the arc travels (x) is the sole propulsive contributor ($F = \frac{1}{2}I^2(dL/dx)$ where I is the current in the loop); since the induced magnetic field is a function of the accelerator’s geometry, the axial thrust realized may be written for a given configuration as

$$\text{Linear : } F = \frac{1}{2}\mu_0 I^2(s/w) \quad (17-28)$$

$$\text{Coaxial : } F = (\frac{1}{4}\pi)\mu_0 I^2 \ln(r_o/r_i + \frac{3}{4}) \quad (17-29)$$

The *linear* rail spacing is s and the rail width is w as shown in Fig. 17–8; for the *coaxial* accelerator the above equation relates to an electrode geometry of

inner radius r_i and constant outer radius r_o . Space qualification of the coaxial micro-PPT has not been reported to date. Because the plasma is nonmagnetic, the value of μ_0 remains the same as free space, namely, $4\pi \times 10^{-7}$ hr/m.

A practical version of the PPT which was first put into operation in 1968 is shown in Chapter 1 as Fig. 4. The propellant is stored in a solid Teflon bar that is pushed against two linear rails by a spring. A pulsed discharge is initiated across the Teflon surface which momentarily ablates a small portion of it. Teflon stores well in space, is easy to handle, and ablates with insignificant charring. There are no tanks, valves, synchronizing controls, or zero gravity feed requirements. A rechargeable capacitor fed from a power processing unit in the spacecraft provides the power input. The thrust is applied only as rapid pulses unlike most other electric propulsion devices; pulsed thrusting is very compatible with precise control and positioning needs where the mean thrust can be varied by changing the pulsing rate or the total number of pulses N . If a “total impulse per pulse” or *impulse bit* (in N-sec or lbf-sec) is denoted by I_{bit} , then the overall vehicle change of velocity Δu would be the sum of N tiny but equal pulses; using Eqs. 2–4 and 4–6 a much simplified result equivalent to Eq. 4–36 may be obtained provided that $NI_{\text{bit}}/m_0c \ll 1$ where m_0c is the product of the initial mass times the effective exhaust velocity, as would be expected for the PPT:

$$\begin{aligned}\Delta u &= c \sum_{n=1}^N \ln \left[\frac{m_0 - (n-1)I_{\text{bit}}/c}{m_0 - nI_{\text{bit}}/c} \right] \approx \sum_{n=1}^N \frac{I_{\text{bit}}/m_0}{1 - nI_{\text{bit}}/m_0c} \\ &\approx \frac{I_{\text{bit}}}{m_0} \left[1 + \frac{N}{2}(N+1) \frac{I_{\text{bit}}}{m_0c} \right]\end{aligned}\quad (17-30)$$

Much electrical energy is lost in PPT circuits and the ionization energy is never recovered; moreover, the bits of pulsed mass being accelerated do not exit well collimated and propellant utilization has been poor in the earlier designs. Besides its very low efficiency, a big disadvantage of the PPT has been the size and mass of the capacitor and power conditioning equipment.

Figure 17–9 shows a hybrid electrothermal–electromagnetic concept. It produces continuous thrust and Russians claim to have flown several versions. Compared to an electrothermal arcjet, these devices operate at relatively lower pressures and much higher electric and magnetic fields. Hydrogen and argon are common propellants for such MPD arcjets. As with other electromagnetic thrusters, exhaust beam neutralization is unnecessary. Problems of electrode erosion, massive electrical components, and low efficiencies (with their associated heat dissipation) have slowed implementation of these devices.

Hall-Effect Thrusters. When plasma densities are low enough and/or magnetic fields are high enough, the Hall-effect electric field becomes quite significant. This is the same phenomenon that is observed in the semiconductor Hall effect where a voltage arises transverse to the applied electric field. The Hall current can be understood to represent the motion of the electron “guiding center” (Ref. 17–8)

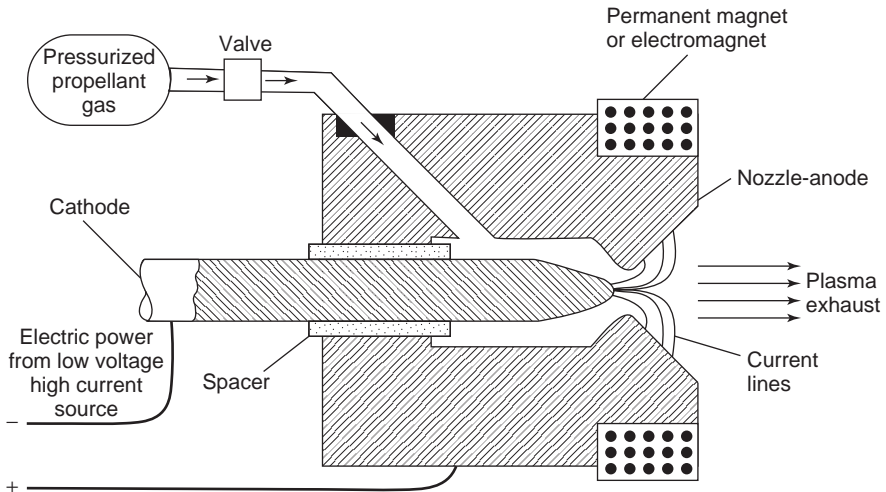


FIGURE 17–9. Simplified diagram of a magnetoplasma dynamic (MPD) arcjet thruster. It is similar in construction to the thermal arcjet shown in Fig. 1–8, but it has a stronger magnetic field to enhance the propellant acceleration.

in a crossed electric and magnetic field arrangement where collisions must be relatively insignificant. The Hall thruster is of interest because it represents a practical operating region for space propulsion, which Russian scientists were the first to successfully exploit in a design originally called the *stationary plasma thruster* or SPT. Hall thrusters are treated in Ref. 17–3.

In order to understand the principle of the Hall thruster, it is necessary to rewrite in scalar form the generalized Ohm's law, Eq. 17–12. Because the *electron Hall parameter* $\beta = \omega\tau$ is no longer negligible, we arrive at two equations, which are (in Cartesian form):

$$j_x = \frac{\sigma}{1 + \beta^2} [E_x - \beta(E_y - v_x B_z)] \quad (17-31)$$

$$j_y = \frac{\sigma}{1 + \beta^2} [(E_y - v_x B_z) + \beta E_x] \quad (17-32)$$

For a typical design, the application of a longitudinal electric field E_x causes a current density j_x to flow in the applied field direction together with a Hall current density j_y which flows in the direction transverse to E_x . The Hall electric field E_y is externally shorted to maximize that current, and the electrodes are “segmented” in order not to short out the axial electric field E_x . Note that $\beta E_x > v_x B_z$. This arrangement results in a reasonably complicated design, one which was deemed impractical. As will be discussed next, for space propulsion, engineers prefer the cylindrical geometry over the rectangular. It yields a simpler, more practical design; here the applied magnetic field (B_r) is radial and the applied electric field is axial (E_x); the thrust-producing Hall current j_θ is

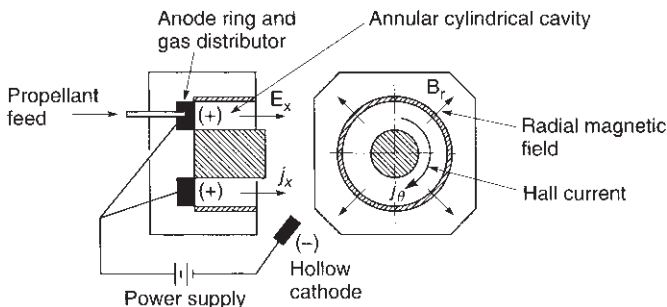


FIGURE 17–10. Cylindrical Hall accelerator configuration showing how an applied axial field results in a transverse current that accelerates the plasma. The presence of any significant axial current density j_x represents an inefficiency in Hall devices.

azimuthal and counterclockwise and, because it closes on itself, it automatically shorts out its associated Hall electric field. The relevant geometry is shown in Fig. 17–10, and the equations now become

$$j_x = \frac{\sigma}{1 + \beta^2} [E_x + \beta v_x B_r] \quad (17-33)$$

$$j_\theta = \frac{\sigma}{1 + \beta^2} [\beta E_x - v_x B_r] \quad (17-34)$$

where, for an accelerator, $\beta E_x > v_x B_r$.

The current density j_x is needed for ionization (by electron bombardment) because here the discharge chamber coincides with a portion of the accelerator region. The Hall current j_θ performs the acceleration through the Lorentz force $j_\theta B_r$. The Hall parameter is calculated from the product of the *electron cyclotron frequency* (Ref. 17–8) $\omega = eB/\mu_e$ and the *collision time* τ of the electrons with the heavier particles, which is part of the electrical conductivity in Eq. 17–11. In order for a Hall generator to be of interest, the electron Hall parameter must be much greater than one (in fact, Ref. 17–19 indicates that it should be at least 100), whereas ion motion must proceed relatively unaffected by magnetic effects. Large electron Hall parameters are obtained most readily with low plasma densities which translate into large times between collisions. Figure 17–11 shows a cutout of an SPT design with a redundant set of hollow cathodes (presently only one is needed) and the solenoid magnetic pair responsible for the magnetic field. In Hall thrusters, the propellant gas, xenon or argon, is fed in the vicinity of the anode; some gas is also provided through the cathode for more efficient cathode operation. While the discharge chamber is not physically separated from the accelerator region, the absence of ions in the first portion of the chamber effectively differentiates the ionization region from the rest of the accelerator. The local charge mass and density of the ions and electrons, together with the magnetic field profiles, need to be tailored such that the ion motion is mostly axial and the electron motion mostly spiral; this makes any given physical design

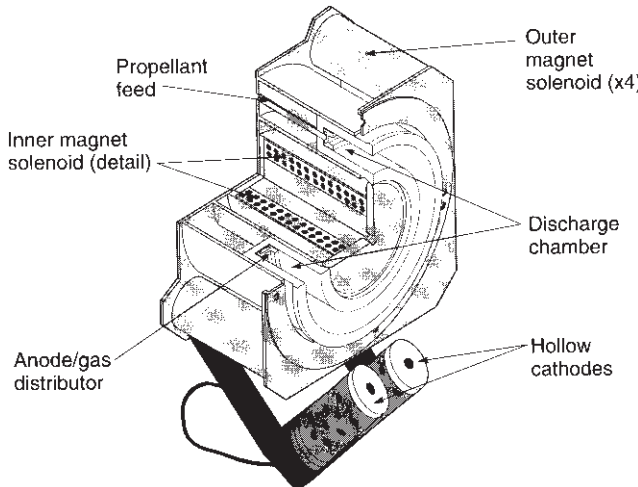


FIGURE 17–11. External view and quarter section of a 1350-watt Hall accelerator (SPT-100). It is rated at a thrust of 83 mN at a specific impulse of 1600 sec. The radial magnetic field is produced by an inner solenoid and four external solenoids. Ionization takes place at the beginning of the insulated annular channel. Modern Hall thrusters have only one hollow cathode positioned like the neutralizer in Fig. 17–7. (Drawing courtesy of Atlantic Research Corporation and FAKEL.)

inflexible to changes of propellant. A variation of the original nonconducting accelerator wall SPT design is a smaller channel with metallic walls; this “thruster with an anode layer” (TAL) has comparable performance with a higher thrust density.

The Hall thruster may be classified as either an electromagnetic device (as above) or an electrostatic device where the space-charge in the ion acceleration region is neutralized by an electron current transverse to the ion flow (Refs. 17–19 and 17–20). If we can mentally separate the process of ionization from that of acceleration, then it is easy to see that electrons swirling within the accelerator neutralize the ionic space-charge as it moves from anode to cathode. This, in effect, decreases the magnitude of the accelerating fields and removes most of the beam-focusing requirements. In reality, there is some small interaction between the azimuthal electron current and the ion current, but it diminishes in proportion to the magnitude of the Hall parameter β .

The Hall thruster yields the best β efficiency (η_H as defined below) when β is very large. The high β limit is found, from Eqs. 17–33 and 17–34 and the definition of the plasma conductivity σ (Eq. 17–11), as

$$j_x \rightarrow \sigma v_x B_r / \beta = \rho_e v_x \quad \text{and} \quad j_\theta \rightarrow \sigma E_x / \beta \quad (17-35)$$

$$\tilde{F} = j_\theta B_r \rightarrow \rho_e E_x \quad (17-36)$$

$$\eta_H = \tilde{F} v_x / j_x E_x \rightarrow 1.0 \quad (17-37)$$

The magnetic flux density B_r is shown in Fig. 17–10. As can be seen, the accelerating force at this high Hall parameter limit is the electrostatic force and, since the exit ionization levels are about 90%, this corresponds in principle to the ion engine without any of its severe space-charge current limitations. Even though electron densities are on the order of 10^{15} to $10^{17}/\text{m}^3$, the effective space-charge densities (ρ_e) are considerably lower because of positive ion neutralization and they approach zero at the exit. Furthermore, the Hall β -efficiency η_H as defined in the equations above reflects strictly the influence of β ; this efficiency is ideal, being an internal parameter that represents the loss that arises from the total current vector not being perfectly normal to the flow direction. The overall efficiency is still given by Eq. 17–2.

Example 17–3. The BPT-4000 Hall thruster is an advanced propulsion system being qualified for GEO satellites (Ref. 17–21). It has an overall efficiency of 59% at a specific impulse of 2000 sec with an input power of 4.5 kW, while delivering a thrust of 280 mN. During > 5800 hr of operation, the system has > 25 kg of xenon throughput which represents the flow rate magnitude. Calculate the mass flow rate for this device and the overall efficiency and compare to the given values.

SOLUTION. The mass flow rate may be calculated from Eq. 2–17 as

$$\dot{m} = \frac{F}{I_s g_0} = \frac{0.28}{(2000)(9.81)} = 14.3 \times 10^{-6} \text{ kg/sec}$$

And the efficiency from Eq. 17–3

$$\eta_t = \frac{FI_s g_0}{2P_e} = \frac{(0.28)(2000)(9.81)}{2(4500)} = 0.61$$

The mass flow rate of the propellant is very low and this is desirable for long duration applications; the calculated mass flow rate is larger than the 12×10^{-6} kg/sec implied in the order-of-magnitude statement above. The calculated efficiency is somewhat greater than the quoted 59% because minor system losses have not been taken into account. The internal or Hall efficiency (Eq. 17–37) should be higher than this value, but it cannot be determined here because additional information is necessary; for very high values of β the Hall efficiency will always approach one.

Hall thrusters have flown in the European Space Agency's (ESA) SMART-1 mission and are being implemented for orbit raising and station keeping on geostationary satellites. Higher specific impulses and enhanced throttling capabilities are desirable.

17.4. OPTIMUM FLIGHT PERFORMANCE

Now that we have discussed the various electric propulsion devices available, we return to the discussion of flight performance. In Section 17.1 the fundamental

background for an optimum propulsion system operating design was introduced. The discussion remained incomplete because the specific power and the efficiency of individual thrusters, among other things, need to be known for further analysis. In a given mission, the payload m_{pl} and velocity increment Δu are specified along with upper limits on electric power available (Ref. 17–22). In the analysis of Section 17.1, for any desired $\Delta u/v_c$, one can find an optimum v/v_c given a payload ratio; however, even when the choice of an electric propulsion system has been made, thrust time t_p is unspecified and thus the total mass also remains unspecified. Thrust time or “burn time” is the smallest for zero payload and continuously increases with increasing payload ratio. Concurrently, the specific impulse changes, making the problem underconstrained.

Given the payload mass and the vehicle velocity increment, a spacecraft design procedure could be followed using the optimum results of Section 17.1, for example:

1. Pick a payload mass fraction—from Fig. 17–3 this yields an optimum $\Delta u/v_c$.
2. From the given Δu , deduce the value of the characteristic speed v_c .
3. From the optimum value of v/v_c in Fig. 17–3 at the given mass fraction, or Eq. 17–9, calculate the corresponding value of v or I_s .
4. Select an engine that can deliver this optimum I_s and from its characteristics (i.e., α and η_t) find the thrusting time t_p from Eq. 17–8.
5. Calculate m_p from Section 17.1, including Eq. 4–7 and the given payload ratio.
6. Check that the available vehicle electrical power (from Eq. 17–6), vehicle volume, and the desirable mission time and total cost are not exceeded.

As may be evident, a unique criterion for the choice of the assumed payload mass fraction is missing above. One possible solution to this problem is to look for a “dual optimum,” namely, to seek the shortest burn time consistent with the highest payload mass fraction of the flight vehicle. A maximum for the product of m_{pl}/m_0 with $\Delta u/v_c$ does exist as a function of v/v_c . In other words, this dual optimum defines a minimum overall mass for a specified payload consistent with minimum transfer time. Table 17–7 gives estimated values of α along with the corresponding range of specific impulse and the efficiency for electric propulsion systems in present engine inventories.

The optimum formulation in Section 17.1, however, needs to be modified to account for the portion of tankage mass which results from propellant loading; with few exceptions, an additional 10% of the propellant mass shows up as tank or container mass (this could be further refined to include reserve propellant). Reference 17–23 includes information on this *tankage fraction* for various thrusters. Fortunately, the analysis presented earlier is little modified and it turns out that the optima are driven toward higher specific impulses and longer times

TABLE 17-7. Summary of Current Technology in Typical Electric Propulsion Systems

| Engine Type | Identification (Reference) | Specific Power, α (W/kg) (estimated) | Thruster Efficiency, η_t | Specific Impulse, I_s (sec) | Power (W) | Thrust (N) | Lifetime (hr) | Status |
|-----------------------|---|---|-------------------------------------|-------------------------------------|--|--------------------------------|-------------------------------------|------------------------|
| <i>Resistojet</i> | N ₂ H ₄ (17-16, 17-24) | 333-500 | 0.8-0.9 | 280-310 | 500-1500 | 0.2-0.8 | >390 | Operational |
| | NH ₃ (17-16) Primex MR-501B (17-24) | 0.8 | 350 303-294 | 350-510 | 500 | 0.369-0.182 | >389 | Operational |
| <i>Arcjet</i> | N ₂ H ₄ (17-24) | 313 | 0.33-0.35 | 450-600 | 300-2000 | 0.2-0.25 | >830 - 1000 | Operational |
| | NH ₃ (17-16) MR-509 (17-24) (c) MR-510 (17-24) (c) | 0.27-0.36 >0.31 115.3 150 | 500-800 >502 (545) >570 - 600 | 500-30 k 1800 2170 | 0.2-0.25 0.213-0.254 0.222-0.258 | >1505 >1575 >2595 | Qualified Qualified Qualified | Operational |
| <i>Ion propulsion</i> | Busek CMNT Colloid | 1.7 | >0.9 | 150-275 | 24 | 5-30 μ N | >2200 | Qualified |
| | Alta FEEP-150 XIPS-13 (17-24) (a) | 588 | 0.46, 0.54 0.65, 0.67 | 5000-8000 2585, 2720 | 20 427, 439 | 1-150 μ N 0.0178, 0.018 | 12,000 12,000 | Qualified Qualified |
| | XIPS-25 (17-24) (a) | 45 | 0.62 | 2800 | 1400 | 0.0635 | >4350 | Qualified |
| | NSTAR/DSI/DAWN (a) | 400 | 0.7 | 3100 | 2300-2500 | 0.093 | >30,000 | Operational |
| | NEXT NASA GRC | | | 1400-4300 | 560-6900 | 0.25-0.235 | >30,000 | R&D |
| | EITS-VI IES (Jap.) (17-24) | | | 3000 | 730 | 0.02 | Operational | Operational |
| | DASA RIT-10 (Ger.) (17-24) (a) | 0.38 | | 3000-3150 | 585 | 0.015 | Operational | Operational |
| | | | | | | | | |
| <i>Hall</i> | Smeerna—PPS 1350 | 283 | 0.55 | 1650 | 1200-1600 | 0.088 | 9500 | Operational |
| | SPT (XE) (17-24) | | 0.48 | 1600 | 150-1500 | 0.04-0.2 | >4000 | Operational |
| | ARC/Fakel SPT-100 (17-16) (b) | 169.8 | 0.48 | 1600 | 1350 | 0.083 | >7424 | Operational |
| | Fakel SPT-70 (17-3) (b) | | 0.46, 0.50 | 1510, 1600 | 640-660 | 0.04 | 9000 | Operational |
| | TAL-D-55 (Russia) (17-24) | | 0.48, 0.50-0.60 | 950-1950 | 600-1500 | 0.082 | >5000 | Operational |
| | BPT-4000 Hall (c) (17-21) | ~ 50.9 | 0.59 | 2000 | 4500 | 0.28 | >8000 | Qualified |
| <i>MPD-steady</i> | Applied Field (17-16) | 0.5 | | 2000-5000 | 1-100 k | | | R&D |
| | Self-field (17-16) | 0.3 | | 2000-5000 | 200-4000 k | | | R&D |
| <i>MPD-pulsed</i> | Teflon PPT (17-16) | 1 | 0.07 | 1000 | 1-200 | 4000 N-sec | >10 ⁷ pulses | Operational |
| | LES 8/9 PPT (17-24) | | 0.0068, 0.009 | 836, 1000 | 25-, 30 | 0.0003 | >10 ⁷ pulses | Operational |
| | NASA/Prime EO-1 (c) | ~ 20 | 0.098 | 1150 | up to 100 | 3000 N-sec | Operational | Operational |
| | PRS-101 (c) | | | 1150 | 1.4 mN, 2 Hz | | | Operational |
| | EPEX arcjet (Jap.) (17-24) | | 0.16 | 600 | 430 | 0.023 | | Operational |

*Manufacturers: (a): L3 Communications, (b): Atlantic Research Corporation, USA Fakel (Russia), (c): Aerojet General.

of operation. For an arbitrary tankage fraction allowance φ ,

$$\frac{\Delta u}{v_c} = \frac{v}{v_c} \ln \left[\frac{(1 + \varphi) + (v/v_c)^2}{(m_{pl}/m_0 + \varphi) + (v/v_c)^2} \right] \quad (17-38)$$

When $\varphi = 0.1$ the actual value for the jointly optimized payload ratio can be shown to be 0.46, with corresponding ratios of vehicle velocity increment as 0.299 and propellant exhaust velocity as 0.892. Further scrutiny indicates that this peak is rather broad and that payload ratios between 0.34 and 0.58 are within 6% of the mathematical optimum. Since engine parameters are rather "inelastic," and since spacecraft designers have to deal with numerous constraints which are not propulsion related, this wider range of optima is deemed a practical necessity.

Given the desirable 0.34 to 0.58 optimum payload-ratio range, we may first select one or more thrusters within the range $0.2268 \leq (I_s^*/\Delta u) \leq 0.4263$, where the optimized specific impulse (I_s^*) is in seconds and the velocity change in m/sec. Since the vehicle's change in velocity is known, this criterion yields the resulting desirable limits in specific impulse. Figure 17-12 shows curves depicting the parameters in Eq. 17-38 for $\varphi = 0.1$ in an expanded dual-optimum neighborhood. The oval insert encloses a region of interest bounded by a contour curve representing values down to 10% below the mathematical peak.

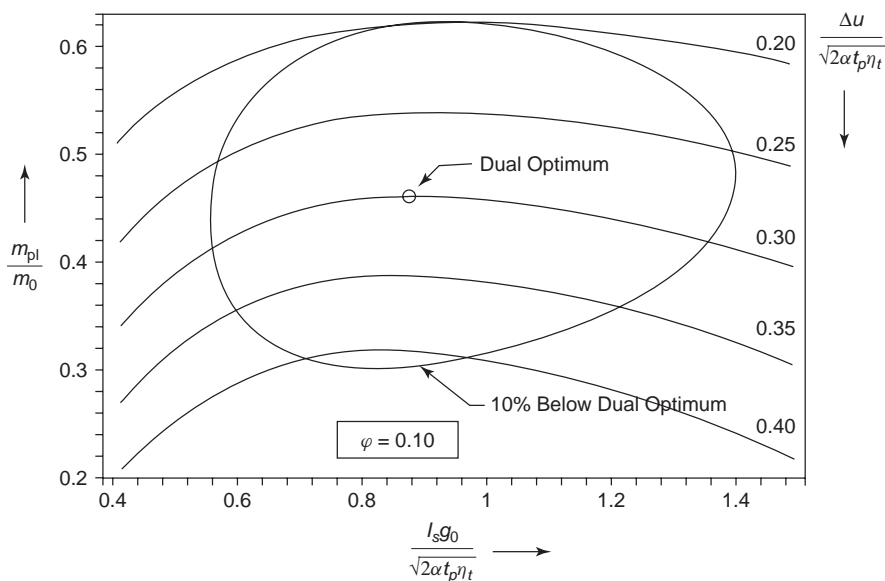


FIGURE 17-12. Payload fraction in the neighborhood of the dual optimum. The oval represents a contour 10% below the dual optimum peak. The parameters v/v_c and $\Delta u/v_c$ in Fig. 17-3 are shown here in their equivalent form.

The success of this approach hinges on the validity of the engine information employed. In particular, the specific power should represent all the inert components of the propulsion system, which can be reasonably assumed to depend on the power level. The payload mass must reflect all mass that is neither proportional to the electrical power nor propellant related. The tankage fraction allowance must reflect the total propellant mass and thus the use of Eq. 17–38 is necessary. It is assumed that there is available a source of electricity (typically from 28 to 300 VDC for solar-powered craft) which is not tagged to the propulsion system. The analysis also assumes that the efficiency is not a function of specific impulse (in contrast to Ref. 17–25); this implies that an average or effective value can be used. Since each individual engine type spans a somewhat limited range of specific impulse, this assumption is not deemed to be too restrictive. For the continuous thrust schedules required by electric propulsion systems, thrust time is equal to mission time.

Example 17–4. For the three electric propulsion systems listed below (from Table 17–7) and for a proposed mission that would carry a 100-kg payload through a change of velocity of 7000 m/sec, find the thrust times that fall within the dual-optimum region shown in Fig. 17–12. Also, for one specific thruster, calculate total mass, thrust, and input power requirements at a preselected propulsive time.

| | Hall Thruster (Demonstrated) | Xenon Ion System (Demonstrated) | MPD (Experimental) |
|-----------------------|---------------------------------|------------------------------------|-----------------------|
| I_s (sec) | 1600 | 2585 | 3500 |
| $\alpha\eta_t$ (W/kg) | 80 | 46 | 30 |

SOLUTION. The thrust duration (t_p) is the only quantity needed to place each electric propulsion system within the identified dual-optimum region in Fig. 17–12 since all other parameters are now fixed. Lower and upper bounds for the thrust time need to be found which by construction include results that are within 10% of the peak performance. Once t_p is found, the payload fraction may be inferred along with its associated thrust and power levels.

From the given data, the ratio $\Delta u/(I_s g_0)$ for each thruster may be calculated which is independent of v_c . Then, from the plotted information on $\Delta u/v_c$ (e.g., using $\Delta u/v_c = 0.2, 0.25 \dots$ until 0.4), discrete values of $I_s g_0/v_c$ may be found and their corresponding v_c 's solved for, which then yields the desired t_p range. The following is a list of the results:

| | Hall Thruster | Xenon Ion System | MPD |
|--------------|---------------|------------------|---------|
| t_p (days) | 22.1–56.6 | 50.1–154 | 105–326 |

For each thruster the lower propulsive time corresponds to a higher thrust and input power levels and, conversely, the higher burn time corresponds to lower values of thrust and power. These correspondences, however, do not follow a linear inverse. As may be

seen from the results above, there is some overlap in resulting propulsive time ranges. Furthermore, unless time limits are imposed (say, as travel time), additional selection criteria such as maximum or available input power levels are needed.

Now, choosing one specific case at $t_p = 68.5$ days with an ion thruster [which results from $\Delta u/(I_s g_0) = 0.276$, or $\Delta u/v_c = 0.3$ and $v/v_c = 1.086$] the propellant masses may be calculated from Eq. 17–6 and the overall masses from the corresponding payload fractions which are found from Eq. 17–38 or Fig. 17–12. The mass flow rates, thrusts, and electrical power requirements follow from other equations in this chapter which are summarized below:

$$m_p = \frac{m_0 - m_{pl}}{1.1 + (v/v_c)^2} \quad m_0 = \frac{m_{pl}}{m_{pl}/m_0}$$

$$F = \frac{m_p}{t_p} I_s g_0 \quad P_e = \frac{F I_s g_0}{2\eta_t}$$

The following is a summary of the given data and the results:

$$\Delta u = 7000 \text{ m/sec} \quad m_{pl} = 100 \text{ kg} \quad I_s = 2585 \text{ sec} \quad \alpha\eta_t = 80 \text{ W/kg} \quad (\eta_t = 0.6)$$

$$t_p = 68.5 \text{ days} \quad m_0 = 222.2 \text{ kg} \quad m_p = 53.6 \text{ kg} \quad F = 230 \text{ mN} \quad P_e = 4.86 \text{ kW}$$

As evident from this example, the higher specific impulses do not necessarily translate into higher electrical-power input requirements as Eq. 17–1 would appear to indicate. This is because for a given mission the values of F do not necessarily scale in proportion with the specific impulse. The longer propulsive times associated with these dual-optimum calculations yield P_e values which actually decrease and which result in the smallest range for the MPD thruster [1.75 kW (236 days) to 5.97 kW (105 days)] when compared to the Hall electrical propulsion system [3.83 kW (56.6 days) to 14.7 kW (22.1 days)], where the t_p values are shown above in parentheses. Resulting amounts for optimal thrust F and total mass m_0 can also be shown to decrease with increasing specific impulse.

17.5. MISSION APPLICATIONS

Three principal application areas have been described in the introduction to this chapter. The selection of a particular electric propulsion system for a given flight application depends not only on the characteristics of the propulsion system (which are described in this chapter) but also on the propulsive requirements of the particular flight mission, the proven performance of the specific candidate propulsion system, along with vehicle interfaces and the power conversion and storage systems. In general, the following criteria can be enumerated:

1. For very precise low-thrust station-keeping and attitude control applications, *pulsed thrusters* are generally best suited. Some systems, however, must have continuous thrust because pulsing generates noise that cannot be tolerated.
2. For deep-space missions where the vehicle velocity increment is appreciably high, systems with *very high specific impulse* will give better

performance. As shown in Section 17.1, the optimum specific impulse is proportional to the square root of the thrust operating time.

3. While very high spacecraft velocity increments optimize at the higher specific impulses, the propulsive times also increase, making the optimum thrust and corresponding power generally lower. This is favorable to electrostatic and electromagnetic units that operate in the specific impulse range above 1000 sec. See Example 17-4.
4. Since most missions of interest require long life, *system reliability* is a key selection criterion. *Extensive testing* under all likely environmental conditions (temperatures, pressures, accelerations, vibration, and radiation conditions) is required for high reliability. Ground testing and qualification of electric engines should be as thorough as that of their chemical counterparts, where large resources have made it possible to develop the present inventory of reliable engines. Simulation of the low pressures in space requires large vacuum test chambers.
5. There is a premium on *high thruster efficiency* and *high power-conversion efficiency*. This will reduce the inert mass of the power supply system and reduce thermal control requirements, all of which usually results in lower total mass and higher vehicle performance. Technology advances in specific power (α) and decreases in tankage fraction (φ) are also desirable toward minimizing inert mass.
6. For every propulsion mission there is a theoretically *optimum range of specific impulse* (see Fig. 17-3) and thus an optimum electrical propulsion system design. While this optimum may be blurred by some conflicting system constraints (e.g., flight time or maximum power or size constraints or cost), the present variety in the electrical propulsion systems inventory can meet most goals.
7. The present *state of the art in electrical power sources* appears to limit the type and size of electric propulsion systems that can be integrated, particularly for missions to the outer planets, unless nuclear energy power generation on board the spacecraft becomes more developed and acceptable.
8. Practical factors, such as the storing and feeding of liquids in zero gravity, the availability of propellant (in the case of xenon), the conditioning of power to the desired voltage, frequency, and pulse duration, as well as the redundancy in key system elements, the survival of sensors or controllers in long flights, and the inclusion of automatic self-checking devices along with cost, will all influence the selection and application of specific types of electric rockets.
9. In addition to tankage considerations, *propellant selection* will also be influenced by certain interface criteria such as plume noninterference with communication signals. Plumes must also be thermally benign and noncondensing on sensitive surfaces of the spacecraft such as optical windows, mirrors, and solar cells.

TABLE 17–8. Space Propulsion Application and Characteristics for Three Thrust Levels of Electric Propulsion Thrusters

| Thrust Class | Application (Life) | Characteristics | Status |
|-----------------------------------|--|--|--|
| Micronewtons (μN) | E–W station keeping Attitude control Momentum wheel unloading (15–20 years) | 10–500 W power Precise impulse bits of $\sim 2 \times 10^{-5}$ N–sec | Operational & in development (micropropulsion) |
| Millinewtons (mN) | N–S station keeping Orbit changes Drag cancellation Vector positioning (20 years) | Kilowatts of power Impulse bits $\sim 2 \times 10^{-3}$ N–sec for N–S, impulse/year of 46,000 N–sec/100 kg spacecraft mass | Operational |
| 0.2–10 N | Orbit raising Interplanetary travel Solar system exploration (1–3 years) | Long duration 10–300 kW of power Intermittent and continuous operation | In development |

Synchronous or geostationary satellites are attractive for communications and earth observation; their long life requires extensive station-keeping propulsion requirements. Until recently, the main limitation to any such life increase had been the propellant requirement. There are also electric propulsion opportunities for orbit raising from LEO to GEO. Earth satellites in inclined orbits with precise time–trajectory position requirements need propulsion units to maintain such orbits, counteracting certain perturbing natural forces described in Chapter 4.

The increasing life trend in earth-orbit satellites from a minimum of 8 years to at least 15 years significantly increases their total impulse and durability requirements of the propulsion system. For example, the north–south station-keeping (NSSK) function of a typical geosynchronous satellite requires about 40,000 to 45,000 N–sec or 9000 to 10,000 lbf–sec of impulse per year. Table 17–8 shows some of the characteristics required of small and large electric thrusters for various propulsion functions in space. A good review of the state of the art upto 1997 is found in Ref. 17–26.

17.6. ELECTRIC SPACE-POWER SUPPLIES AND POWER-CONDITIONING SYSTEMS

The availability of substantial amounts of electrical power in space is considered to be one of the most significant needs in electrical propulsion. Several combinations of energy sources and conversion methods have reached prototype

stages, but only solar cells (photovoltaic), isotope thermoelectric generation units (nuclear), and fuel cells (chemical) have advanced to the point of routine space flight operation. Power output capacity of operational systems has been increasing from the low one-kilowatt range to the medium tens of kilowatts required for some missions. The high end of a hundred or more kilowatts is still pending some technological (and political) breakthroughs.

Space power level requirements have been increasing with the increased capacity of earth-orbit communications satellites and with planned missions, manned and robotic, to the moon and nearby planets. Payload requirements and thrust duration dictate the power level. Commercial communications satellites can temporarily reduce the communications volume during orbit maintenance so that the electric power does not require a dedicated power supply for the propulsion system, but larger power demands require enhanced solar cell capabilities. Some communications satellites actually share part or all of the power-conditioning equipment with their electric thrusters.

Power Generation Units

Electric power generation units are classified as either direct (no moving mechanical parts) or dynamic. When the primary driver is reliability and the total power is small, direct conversion has been preferred but, with the advent of the Space Shuttle and with the manned International Space Station (ISS), dynamic systems are being reconsidered. Many diverse concepts have been evaluated for meeting the electrical power demands of spacecraft, including electric propulsion needs. Direct energy conversion methods considered include photovoltaic, thermoelectric, thermionic, and electrochemical, while indirect methods (with moving parts) include the Brayton, Rankine, and Stirling cycles.

Batteries. Batteries can basically be classified as either primary or secondary. *Primary batteries* consume their active materials and convert chemical energy into electrical. *Secondary batteries* store electricity by utilizing a reversible chemical reaction and are designed to be recharged many times. There are both dry-cell and wet-cell primary batteries. The importance of primary batteries passed with the short-lived satellites of the early 1960s. Secondary batteries with recharging provisions provide electrical power at output levels and lifetimes longer than primary batteries. Batteries must be sealed against the space vacuum or housed inside pressurized compartments. Secondary batteries are a critical component of solar cell systems for power augmentation and emergency backup and the periods when the satellite is in the earth's shadow.

Fuel Cells. *Chemical fuel cells* are conversion devices used to supply space-power needs for 2 to 4 weeks and for power levels up to 40 kW in manned missions. A catalyst controls the reaction to yield electricity directly from the chemical reaction; there is also some heat evolved, which must be removed to maintain a desirable fuel cell temperature. They are too massive for both

robotic and long-duration missions, having also had some reliability problems. Recent improvements in fuel cell technology have considerably advanced their performance.

Solar Cell Arrays. Solar cells rely on the photovoltaic effect to convert the electromagnetic radiation to electricity. In silicon cells, sunlight generates a voltage and a photocurrent across a *p-n junction* running as an inverse photodiode. Present devices have reached a 15 to 20% efficiency range, but single-bandgap (i.e., single-junction) semiconductors suffer from a theoretical upper limit of 31%. Multijunction solar cells can circumvent this efficiency limit because each layer can absorb a separate part of the spectrum as the light passes through the stack; presently arrays with greater than 21% efficiencies are being launched with multijunction semiconductors. Another aspect of typical solar cell arrays is that many had been originally designed for only a 28 VDC output, although the newer designs such as those for the ISS bus operate at 160 VDC and the NSTAR/DAWN missions uses 80 to 160 VDC. Today, there are designs (termed *high-voltage* or *direct drives*, Ref. 17–27) that produce increased output voltages of the solar cell arrays, up to 300 VDC and beyond. These higher output voltages, when operational, will considerably simplify the power-conditioning equipment in many existing electric-propulsion systems resulting in valuable inert mass savings. But care must be taken to avoid electrostatic discharges that occur more easily in some earth orbits. Solar cells supplied electrical power for most of the long-duration space missions. The first solar cell was launched in March 1958 on Vanguard I and successfully energized data transmission for 6 years. Solar arrays exist in sizes up to 10 kW and could potentially grow to 10 MW sizes in earth orbits.

Typically, solar cell arrays are designed for 20% overcapacity to allow for material degradation toward the end of life. Loss in performance is due to radiation and particle impact damage, particularly in the radiation belts around the earth. There has been some improvement in efficiency, reliability, and power per unit mass. For example, standard silicon cells deliver 180 W/m^2 and arrays have 40 W/kg . Newer gallium arsenide cells produce 220 W/m^2 and are more radiation resistant than silicon cells; gallium arsenide cells are presently space qualified and integrated; together with parabolic concentrators, their arrays can reach 100 W/kg (Ref. 17–23).

Factors that affect the specific mass of a solar array, besides conversion efficiency, include the solar constant (which varies inversely as the square of the distance from the sun) and the manufactured thinness of the cell. Orientation to the sun is a more critical factor when solar concentrators are being used. Cell output is a function of cell temperature; performance can suffer as much as 20% for a 100°F increase in operating temperature so that thermal control is critical. Solar cell panels can be (1) fixed and body mounted to the spacecraft, (2) rigid and deployable (protected during launch and positioned in space), (3) flexible panels that are deployed (rolled out or unfolded), and (4) deployed with concentrator assist.

In addition to the solar arrays, their structure, deployment, and orientation equipment, other items including batteries, plus power-conditioning and distribution systems are assigned to the power source. Despite their apparent bulkiness

and battery dependence, solar-cell electrical systems have emerged as the dominant generating power system for unmanned spacecraft.

Nuclear Thermoelectric and Thermionic Systems. Nuclear energy from long-decay radioisotopes and from fission reactors has played a role in the production of electricity in space. Both thermoelectric (based on the Seebeck effect) and thermionic (based on the Edison effect) devices have been investigated. These generators have no moving parts and can be made of materials reasonably resistant to the radioactive environment. But their specific power is relatively low and cost, availability, and efficiency have been marginal.

Throughout the 1950s and 1960s nuclear fission reactors were regarded as the most promising way to meet the high power demands of space missions, particularly trips to the outer planets involving months and perhaps years of travel. Radioisotope thermoelectric power has been embodied in a series of SNAP (Systems for Nuclear Auxiliary Power) electrical generating units which were designed and tested, ranging from 50 W to 300 kW of electrical output. Fission reactors were included in the SPAR (Space Power Advance Reactor) program, later renamed SP-100, which was to feature a nuclear-thermoelectric generator with an electrical output of 100 kW; this program was discontinued in 1994. More recent space nuclear reactor programs include NASA's Project Prometheus and the Russian TOPAZ that has been space tested up to nearly 6 kW. The latter consists of sets of nuclear rods each surrounded by a thermionic generator.

Thermionic converters have a significant mass advantage over thermoelectric ones, based on their higher effective radiator temperatures. Since thermal efficiencies for both thermoelectric and thermionic conversion are below 10% and since all unconverted heat must be radiated, at higher temperatures thermionic radiators are less massive. Moreover, cooling must be present at times when no electricity is generated since the heat source cannot be "turned off." Depending on the location of the waste heat, clever designs are needed, involving heat pipes or recirculating cooling fluids.

Long-Duration High-Output Dynamic Systems. Designs of electric power generation with outputs of 10 to 1000 kW here on earth have been based on Stirling or Rankine heat engine cycles with nuclear, chemical, and even solar power sources. Overall efficiencies can be between 10 and 40%, but the hardware is complex, including bearings, pumps, reactors, control rods, shielding, compressors, turbines, valves, and heat exchangers. Superconducting magnets together with advances in the state-of-the-art of seals, bearings, and flywheel energy storage have made some dynamic units relatively more attractive. There remain development issues about high-temperature materials that will withstand intense nuclear radiation fluxes over several years; there are still some concerns about achieving the required reliability in such complex systems in the space environment. While limited small-scale experiments have been conducted, the development of these systems remains a challenge. An advanced Stirling radioisotope generator is under development to replace radioisotope thermoelectric generators (RTGs) in some NASA missions.

Power-Conditioning Equipment

Power-conditioning equipment is a necessary part of electric propulsion systems because of inevitable mismatches in voltage, frequency, power rate, and other electrical properties between the space-power generating unit and the electric thruster. In some earlier systems, the power-conditioning equipment was more expensive, more massive, and more difficult to qualify than the thruster itself. If the thrust is pulsed, as in the PPT, the power-conditioning unit has to provide pulse-forming networks for momentary high currents, exact timing of different outputs, and control and recharging of condensers. Electrostatic engines typically require from 1000 to 10,000 VDC; the output of solar-cell arrays is 28 to 300 VDC so there is a need for DC-to-DC inverters and stepup transformers to accomplish the task. Often this equipment is housed in a single “black box,” termed the *power conditioner*. Modern conditioning equipment contains all the internal logic required to start, safely operate, and stop the thruster; it is controlled by on-off commands sent by the spacecraft control processor. Besides the above functions that are specific to each engine, power-conditioning equipment may provide circuit protection and propellant flow control as well as necessary redundancies.

As may be apparent from Table 17–7, one of the largest contributors to the specific mass of the system (α) is the power-conditioning equipment. Here, electrothermal units have the simplest and lightest conditioning equipment. Ion engines, on the other hand, have the heaviest equipment, with Hall thrusters somewhere in between (Ref. 17–20). PPTs tend to be massive, but advances in energy storage capacitors can improve this situation. In fact, advances in solid-state electronic pulse circuits together with lighter, more efficient, and higher temperature power-conditioning hardware are areas of great interest in electric propulsion. The efficiency of the equipment tends to be high, about 90% or more, but the heat generated is at a low temperature and must be removed to maintain the required moderately low temperatures of operation. When feasible, the elimination of conditioning equipment is desirable, the so-called direct drive, but a low-pass filter would still be necessary for electromagnetic interference (EMI) control (more information in Ref. 17–25).

PROBLEMS

1. The characteristic velocity $v_c = \sqrt{2t_p\alpha\eta}$ is used to achieve a dimensionless representation of flight performance analysis. Derive Eq. 17–38 without any tankage fraction allowance. Also, plot the payload fraction against v/v_c for several values of $\Delta u/v_c$. Discuss your results with respect to optimum performance.
2. For the special case of zero payload, determine the maximized values of $\Delta u/v_c$, v/v_c , m_p/m_0 , and m_{pp}/m_0 in terms of this characteristic velocity.
Answer: $\Delta u/v_c = 0.805$, $v/v_c = 0.505$, $m_p/m_0 = 0.796$, $m_{pp}/m_0 = 0.204$.
3. For a space mission with an incremental vehicle velocity of 85,000 ft/sec and a specific power of $\alpha = 100$ W/kg, determine the optimum values of I_s and t_p for

two maximum payload fractions, namely 0.35 and 0.55. Take the thruster efficiency as 100% and $\varphi = 0$.

Answer: For 0.35: $I_s = 5.11 \times 10^3$ sec; $t_p = 2.06 \times 10^7$ sec; for 0.55 : $I_s = 8.88 \times 10^3$ sec; $t_p = 5.08 \times 10^7$ sec.

4. Derive Eq. 17-7 using $m_{pp} = m_p[(v/v_c)^2 + (v/v_c)^3]$ instead of Eq. 17-6 (use $\varphi = 0$); this form penalizes the high I_s and/or short t_p missions. Plot and compare to the results shown on Fig. 17-3.

5. An ion thruster uses heavy positively charged particles with a charge-to-mass ratio of 500 coulombs per kilogram, producing a specific impulse of 3000 sec. (a) What acceleration voltage would be required for this specific impulse? (b) If the accelerator spacing is 6 mm, what would be the diameter of an ion beam producing 0.5 N of thrust at this accelerator voltage?

Answer: (a) 8.66×10^5 V; (b) $D = 1.97$ mm.

6. An argon ion thruster has the following characteristics and operating conditions:

$$\text{Voltage across ionizer} = 400 \text{ V} \quad \text{Voltage across accelerator} = 3 \times 10^4 \text{ V}$$

$$\text{Diameter of ion source} = 5 \text{ cm} \quad \text{Accelerator electrode spacing} = 1.2 \text{ cm}$$

Calculate the mass flow rate of the propellant, the thrust, and the thruster overall efficiency (including ionizer and accelerator). Assume singly charged ions.

Answer: $\dot{m} = 2.56 \times 10^{-7}$ kg/sec; $F = 9.65 \times 10^{-2}$ N; $\eta_t = 98.7\%$.

7. For a given power source of 300 kW electrical output, a propellant mass of 6000 lbm, $\alpha = 450$ W/kg, and a payload of 4000 lbm, determine the thrust, ideal velocity increment, and duration of powered flight for the following three cases:

(a) Arcjet: $I_s = 500$ sec $\eta_t = 0.35$

(b) Ion engine: $I_s = 3000$ sec $\eta_t = 0.75$

(c) Hall engine: $I_s = 1500$ sec $\eta_t = 0.50$

Answers:

(a) $t_p = 3.12 \times 10^5$ sec; $\Delta u = 3.63 \times 10^3$ m/sec; $F = 42.8$ N.

(b) $t_p = 5.24 \times 10^6$ sec; $\Delta u = 2.18 \times 10^4$ m/sec; $F = 15.29$ N.

(c) $t_p = 1.69 \times 10^6$ sec; $\Delta u = 1.09 \times 10^4$ m/sec; $F = 20.4$ N.

8. A formulation for the exit velocity that allows for a simple estimate of the accelerator length is shown below; these equations relate the accelerator distance to the velocity implicitly through the acceleration time t . Considering a flow at a constant plasma of density ρ_m (which does not choke), solve Newton's second law first for the speed $v(t)$ and then for the distance $x(t)$ and show that

$$v(t) = (E_y/B_z)[1 - e^{-t/\tau}] + v(0)e^{-t/\tau}$$

$$x(t) = (E_y/B_z)[t + \tau e^{-t/\tau} - \tau] + x(0)$$

where $\tau = \rho_m/\sigma B_z^2$ and has units of seconds. For this simplified plasma model of an MPD accelerator, calculate the distance needed to accelerate the plasma from rest

up to $v = 0.01(E/B)$ and the time involved. Take $\sigma = 100 \text{ mho/m}$, $B_z = 10^{-3} \text{ tesla}$ (Wb/m^2), $\rho_m = 10^{-3} \text{ kg/m}^3$, and $E_y = 1000 \text{ V/m}$.

Answer: 503 m, 0.1005 sec.

9. Assume that a materials breakthrough makes it possible to increase the operating temperature in the plenum chamber of an *electrothermal engine* from 3000 to 4000 K. Nitrogen gas is the propellant which is available from tanks at 250 K. Neglecting dissociation, and taking $\alpha = 200 \text{ W/kg}$ and $\dot{m} = 3 \times 10^{-4} \text{ kg/sec}$, calculate the old and new Δu corresponding to the two temperatures. Operating or thrust time is 10 days, payload mass is 1000 kg, and $k = 1.3$ for the hot diatomic molecule.

Answer: 610 m/sec old, 910 new.

10. An arcjet delivers 0.26 N of thrust. Calculate the vehicle velocity increase under gravitationless, dragless flight for a 28-day thrust duration with a payload mass of 100 kg. Take thruster efficiency as 50%, specific impulse as 2600 sec, and specific power as 200 W/kg. This is not an optimum payload fraction; estimate an I_s which would maximize the payload fraction with all other factors remaining the same.

Answer: $\Delta u = 4.34 \times 10^3 \text{ m/sec}$; $I_s = 2020 \text{ sec}$ (decrease).

11. A patent application describes an electrostatic thruster that accelerates electrons as the propellant. The inventor points out that the space-charge limited thrust is independent of the propellant mass and that electrons are very easy to produce (by cathode surface emission) and much easier to accelerate than atomic ions. Show using the basic relationships for electrostatic thrusters given in this chapter that electron acceleration is impractical for any such thruster. Assume that the required thrust is 10^{-5} N per accelerator hole, that there are several thousand holes of "aspect ratio" $D/d = 1.0$ in the accelerator, and that the neutralizer operates with protons (which have a mass 1822 times that of the electron).

SYMBOLS

| | |
|-------|---|
| a | acceleration, m/sec^2 (ft/sec^2) |
| A | area, cm^2 or m^2 |
| B | magnetic flux density, web/m^2 or tesla |
| B_r | radial magnetic flux density web/m^2 |
| c | effective exhaust velocity, m/sec |
| C | circuit capacitance, farad/m |
| c_p | specific heat, J/kg-K |
| d | accelerator grid spacing, cm (in.) |
| D | hole or beam diameter, cm (in.) |
| e | electronic charge, 1.602×10^{-19} coulomb |
| E | electric field, V/m |
| E_x | longitudinal electric field, V/m |
| E_y | transverse electric field, V/m |
| f | microscopic force on a particle |
| F | thrust force, N or mN (lbf or mlbf) |

| | |
|------------------|---|
| \tilde{F}_x | accelerating force density inside channel, N/m ³ (lbf/ft ³) |
| g_0 | constant converting propellant ejection velocity units to sec, 9.81 m/sec ² or 32.2 ft/sec ² |
| I | total current, A |
| I_{bit} | impulse bit, N-sec or lbf-sec |
| I_s | specific impulse, sec [I_s^* optimum] |
| j | current density, A/m ² |
| j_x, j_y | orthogonal current density components |
| j_θ | Hall current density, A/m ² |
| k | specific heat ratio |
| l_I | ionization loss, W |
| L | circuit inductance, henry |
| m_p | propellant mass, kg (lbm) |
| m_{pp} | power plant mass, kg (lbm) |
| m_{pl} | payload mass, kg (lbm) |
| m_0 | initial total vehicle mass, kg (lbm) |
| \dot{m} | mass flow rate, kg/sec (lbm/sec) |
| \mathfrak{M} | atomic or molecular mass, kg/kg-mol (lbm/lb-mol) |
| n_e | electron number density, m ⁻³ (ft ⁻³) |
| N | number of pulses |
| P | power, W |
| P_e | electrical power, W |
| P_{jet} | kinetic power of jet, W |
| r_i | inner radius, m |
| r_o | outer radius, m |
| R | plasma resistance, Ω |
| S | distance, cm (in.) |
| t | time or duration, sec |
| t_p | propulsive time, sec [t_p^* optimum] |
| T | absolute temperature, K ($^{\circ}$ R) |
| Δu | vehicle velocity change, m/sec (ft/sec) |
| v | propellant or charged particle ejection velocity, m/sec (ft/sec) |
| v_x | plasma velocity along accelerator, m/sec |
| v_c | characteristic speed |
| V | voltage, V |
| V_{acc} | accelerator voltage, V |
| w | rail width, m |
| x | linear dimension, m (ft) |

Greek Letters

| | |
|--------------|--|
| α | specific power, W/kg (W/lbm) |
| β | electron Hall parameter (dimensionless) |
| ϵ_0 | permittivity of free space, 8.85×10^{-12} farad/m |

| | |
|-----------------|--|
| ε_I | ionization energy, eV |
| η_H | Hall thruster β efficiency |
| η_t | thruster efficiency |
| μ | ion mass, kg |
| μ_e | electron mass, 9.11×10^{-31} kg |
| μ_0 | permeability of free space, $4\pi \times 10^{-7}$ hr/m |
| φ | propellant mass tankage allowance |
| ρ_e | space-charge, coulomb/m ³ |
| σ | plasma electrical conductivity, mho/m |
| τ | mean collision time, sec (also characteristic time, sec) |
| ω | electron cyclotron frequency, (sec) ⁻¹ |

REFERENCES

- 17–1. M. M. Micci and A. D. Ketsdever (Eds.), *Micropropulsion for Small Spacecraft*, Progress in Astronautics and Aeronautics, Vol. 187, AIAA, Reston, VA, 2000.
- 17–2. R. G. Jahn, *Physics of Electric Propulsion*, McGraw-Hill Book Company, New York, 1968, pp. 103–110. See also <http://alfven.princeton.edu/papers/Encyclopedia.pdf>
- 17–3. D. M. Goebel and I. Katz, *Fundamentals of Electric propulsion—Ion and Hall Thrusters*, John Wiley and Sons, Hoboken, NJ, 2008.
- 17–4. P. J. Turchi, “Electric Rocket Propulsion Systems,” Chapter 9 in R. W. Humble, G. N. Henry, and W. J. Larson (Eds.), *Space Propulsion Analysis and Design*, McGraw-Hill, New York, 1995, pp. 509–598.
- 17–5. A. Spitzer, “Near Optimal Transfer Orbit Trajectory Using Electric Propulsion,” AAS Paper 95–215, American Astronautical Society Meeting, Albuquerque, NM, 13–16 February 1995.
- 17–6. D. B. Langmuir, “Low-Thrust Flight: Constant Exhaust Velocity in Field-Free Space,” in H. Seifert (Ed.), *Space Technology*, John Wiley & Sons, New York, 1959, Chapter 9.
- 17–7. C. D. Brown, *Spacecraft Propulsion*, AIAA Education Series, Washington, DC, 1996.
- 17–8. F. F. Chen, *Introduction to Plasma Physics*, Plenum Press, New York, 1974.
- 17–9. G. W. Sutton and A. Sherman, *Engineering Magnetohydrodynamics*, McGraw-Hill Book Company, New York, 1965.
- 17–10. D. M. Zube, P. G. Lichon, D. Cohen, D. A. Lichtin, J. A. Bailey, and N. V. Chilelli, “Initial On-Orbit Performance of Hydrazine Arcjets on A2100 Satellites,” AIAA Paper 99–2272, June 1999.
- 17–11. D. R. Bromaghim, et al., “Review of the Electric Propulsion Space Experiment (ESEX) Program,” *Journal of Propulsion and Power*, Vol. 18, No. 4, July–August 2002, pp. 723–730.
- 17–12. J. Mueller, Chapter 3, in Ref. 17–1.

- 17–13. M. Tajmar, A. Genovese, and W. Steiger, “Indium Field Emission Electric Propulsion Microthruster Experimental Characterization,” *Journal of Propulsion and Power*, Vol. 20, No. 2, March–April 2004.
- 17–14. J. R. Beattie, “XIPS Keeps Satellites on Track,” *The Industrial Physicist*, Vol. 4, No. 2, June 1998.
- 17–15. K. J. Groh and H. W. Loeb, “State of the Art of Radio Frequency Ion Thrusters,” *J. Propulsion*, Vol. 7 No. 4, July–August 1991, pp 573–579.
- 17–16. P. G. Hill and C. R. Peterson, *Mechanics and Thermodynamics of Propulsion*, Addison-Wesley Publishing Company, Reading, MA, 1992.
- 17–17. E. L. Resler, Jr., and W. R. Sears, “Prospects of Magneto-Aerodynamics,” *Journal of Aeronautical Sciences*, Vol. 24, No. 4, April 1958, pp. 235–246.
- 17–18. S. S. Bushman and R. L. Burton, “Heating and Plasma Properties in a Coaxial Gasdynamic Pulsed Plasma Thruster,” *Journal of Propulsion and Power*, Vol. 17, No. 5, September–October, 2001, pp. 959–966.
- 17–19. V. Kim, “Main Physical Features and Processes Determining the Performance of Stationary Plasma Thrusters,” *Journal of Propulsion and Power*, Vol. 14, No. 5, September–October 1998, pp. 736–743.
- 17–20. C. H. McLean, J. B. McVey, and D. T. Schappell, “Testing of a U.S.-built HET System for Orbit Transfer Applications,” AIAA Paper 99-2574, June 1999.
- 17–21. B. Welander, et al., “Life and Operating Range Extension of the BPT 4000 Qualification Model Hall Thruster,” AIAA Paper 2006-5263, Sacramento, CA, July 2006.
- 17–22. D. Baker, “Mission Design Case Study,” in R. W. Humble, G. N. Henry, and W. J. Larson (Eds.), *Space Propulsion Analysis and Design*, McGraw-Hill, New York, 1995, Chapter 10
- 17–23. M. Martinez-Sanchez and J. E. Pollard, “Spacecraft Electric Propulsion—An Overview,” *Journal of Propulsion and Power*, Vol. 14, No. 5, September–October 1998, pp. 688–699.
- 17–24. J. D. Filliben, “Electric Propulsion for Spacecraft Applications,” *Chemical Propulsion Information Agency Report CPTR 96-64*, The Johns Hopkins University, December 1996.
- 17–25. M. A. Kurtz, H. L. Kurtz, and H. O. Schrade, “Optimization of Electric Propulsion Systems Considering Specific Power as a Function of Specific Impulse,” *Journal of Propulsion and Power*, Vol. 4, No. 2, 1988, pp. 512–519.
- 17–26. J. D. Filliben, “Electric Thruster Systems,” *Chemical Propulsion Information Agency Report CPTR-97-65*, The Johns Hopkins University, June 1997.
- 17–27. T. W. Kerslake, “Effect of Voltage Level on Power System Design for Solar Electric Propulsion Missions,” *Journal of Solar Energy Engineering*, Vol. 126, No. 3, August 2004, pp. 936–944.

CHAPTER 18

THRUST VECTOR CONTROL

Controlling the flight path and the attitude of a rocket-propelled vehicle makes it possible to reach a precise flight destination. Rocket propulsion systems always provide a “push” toward an intended target, but they also can be made to provide torques to rotate the vehicle in conjunction with the propulsive force. By controlling the direction of the thrust vectors through mechanisms described in this chapter, it is possible to influence a vehicle’s pitch, yaw, and roll rotary motions. Integrated thrust vector control units are only effective while the principal propulsion system is operating and producing an exhaust jet. For periods of free flight, when the main rocket is off, a separate propulsion mechanism is needed for achieving control over attitude or flight path. In space (see Figs. 4–13 and 8–13), many vehicles utilize dedicated attitude-control systems with multiple thrusters in addition to their thrust-producing main propulsion system. Examples of other dedicated attitude control arrangements are shown in Figs. 3–17, 6–13, 12–27, and 12–28. A relevant history of flight trajectory control in liquid propellant rocket engines is given in Ref. 18–1.

All chemical propulsion systems can be provided with one of several types of thrust vector control (TVC) mechanisms. Some of these apply either to solid, hybrid, or to liquid propellant rocket propulsion systems, but most are specific to only one of these propulsion categories. We will describe two types of thrust vector control concept: (1) for an engine or a motor with a single nozzle and (2) for those that have two or more nozzles.

Aerodynamic fins (fixed and movable) continue to be very effective for controlling vehicle flight within the earth’s atmosphere, and almost all weather rockets, anti-aircraft missiles, and air-to-surface missiles use them. Even though aerodynamic control surfaces provide some additional drag, their effectiveness in terms of vehicle weight, turning moment, and actuating power consumption is

difficult to surpass with any other flight control method. Vehicle flight control can also be achieved by a separate attitude control propulsion system as described in Sections 4.5. and 6.7. Here six or more small liquid propellant thrusters (with a separate feed system and a separate control) provide small moments to the vehicle in flight during, before, or after the operation of the main rocket propulsion system.

The reasons for TVC are: (1) to willfully change a flight path or trajectory (e.g., changing the direction of the flight path of a target-seeking missile); (2) to rotate the vehicle or change its attitude during powered flight; (3) to correct for deviation from the intended trajectory or the attitude during powered flight; or (4) to correct for thrust misalignment of a fixed nozzle in the main propulsion system during its operation, when the main thrust vector misses the vehicle's center of mass. In all prior analyses, we have implicitly assumed that the thrust vector passes through the center of mass and is perfectly aligned with the direction of flight (see Fig. 4–5). In TVC, moments are purposely generated about the *center of mass* to control flight trajectories. The location of the side force (or its perpendicular component) along the vehicle's axis determines its moment arm and thus the magnitude of the force needed for a given application; this implies that locations as far away as possible from the center of mass (i.e., with long moment arms) are the most desirable to minimize the force action and thus the propellant usage.

Pitch moments are those that raise or lower the nose of a vehicle; *yaw moments* turn the nose sideways; and *roll moments* are applied about the main axis of the flying vehicle (Fig. 18–1). Usually, the thrust vector of the main rocket nozzle is in the direction of the vehicle axis and goes through the vehicle's center of mass. Thus it is possible to obtain pitch and yaw control moments by the simple deflection of the main rocket thrust vector; however, roll control usually requires the use of two or more rotary vanes or two or more separately hinged propulsion system nozzles. Figure 18–2 explains the pitch moment obtained by a hinged thrust chamber or nozzle. The side force and the pitch moment vary as the *sine* of the effective angle of thrust vector deflection.

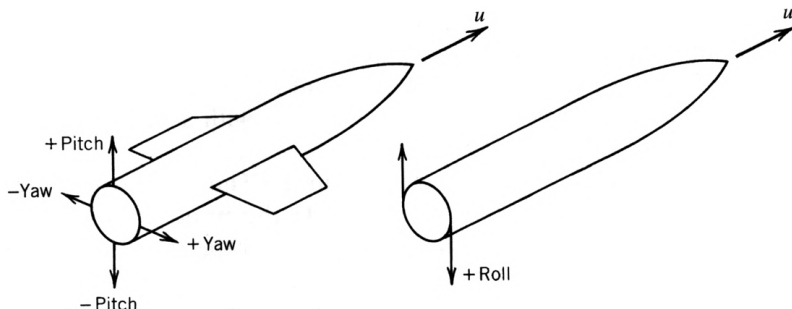


FIGURE 18–1. Moments applied to a flying vehicle.

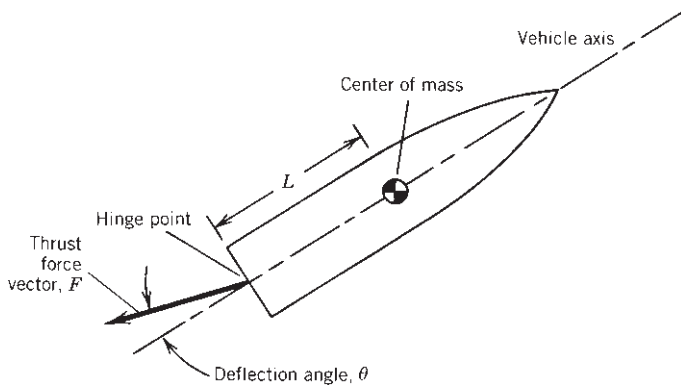


FIGURE 18–2. The pitch moment applied to the vehicle is $FL \sin\theta$.

18.1. TVC MECHANISMS WITH A SINGLE NOZZLE

Many different mechanisms have been used successfully. Several are illustrated in Refs. 18–2 and 18–3. They can be classified into four categories:

1. Mechanical deflection of the nozzle or thrust chamber.
2. Insertion of heat-resistant movable bodies into the exhaust jet; these experience aerodynamic forces and cause a deflection of a part of the exhaust gas flow.
3. Injection of fluid into the side of the diverging nozzle section, causing an asymmetrical distortion of the supersonic exhaust flow.
4. Separate thrust-producing devices that are not part of the main propulsion system providing flow through the nozzle.

Each category is described briefly below and in Table 18–1, where the four categories are separated by horizontal lines. Figure 18–3 illustrates several TVC mechanisms. All of the TVC schemes shown here have been used in production vehicles.

In the *hinge* or *gimbal* scheme (a hinge permits rotation about one axis only, whereas a gimbal is essentially a universal joint), the whole engine is pivoted on a bearing and thus the thrust vector is rotated. For small angles this scheme has negligible losses in specific impulse and is used in many vehicles. It requires a flexible set of propellant piping (bellows) to allow the propellant to flow from the tanks of the vehicle to the movable engine. The Space Shuttle (Fig. 1–14) has two gimballed orbit maneuver engines, and three gimballed main engines. Figures 6–1, 6–7, and 8–17 show gimballed engines. Some Soviet launch vehicles use multiple thrusters and hinges (Fig. 11–1 shows four hinges), while many U.S. vehicles use gimbals.

Jet vanes are pairs of heat-resistant, aerodynamic wing-shaped surfaces submerged in the exhaust jet of a fixed rocket nozzle. They were first used in

TABLE 18–1. Thrust Vector Control Mechanisms

| Type | L/S ^a | Advantages | Disadvantages |
|---|------------------|---|--|
| Gimbal or hinge | L | Simple, proven technology; low torques, low power; up to $\pm 12^\circ$; duration limited only by propellant supply; very small thrust loss | Requires flexible piping; high inertia; large actuators and a power supply for high slew rate |
| Movable nozzle (flexible bearing) | S | Proven technology; no sliding, moving seals; predictable actuation power; up to $\pm 12^\circ$ | High actuation forces; high torque at low temperatures; variable actuation force |
| Movable nozzle (rotary ball with gas seal) | S | Proven technology; no thrust loss if entire nozzle is moved; $\pm 20^\circ$ possible | Sliding, moving hot gas spherical seal; highly variable actuation power; limited duration; needs continuous load to maintain seal |
| Jet vanes | L/S | Proven technology; low actuation power; high slew rate; roll control with single nozzle; $\pm 9^\circ$ | Thrust loss of 0.5–3%; erosion of jet vanes; limited duration; extends missile length |
| Jet tabs | S | Proven technology; high slew rate; low actuation power; compact package | Erosion of tabs; thrust loss, but only when tab is in the jet; limited duration |
| Jetavator | S | Proven on Polaris missile; low actuation power; can be lightweight | Erosion and thrust loss; induces vehicle base hot gas recirculation; limited duration |
| Liquid-side injection | S/L | Proven technology; specific impulse of injectant nearly offsets weight penalty; high slew rate; easy to adapt to various motors; can check out before flight; components are reusable; duration limited by liquid supply; $\pm 6^\circ$ | Toxic liquids are needed for high performance; often difficult packaging for tanks and feed system; sometimes requires excessive maintenance; potential spills and toxic fumes with some propellants; limited to low vector angle applications |
| Hot-gas-side injection | S/L | Lightweight; low actuation power; high slew rate; low volume/compact; low performance loss | Multiple hot sliding contacts and seals in hot gas valve; hot piping expansion; limited duration; requires special hot gas valves; technology is not yet proven |
| Hinged auxiliary thrust chambers for high thrust engine | L | Proven technology; feed from main turbopump; low performance loss; compact; low actuation power; no hot moving surfaces; unlimited duration | Additional components and complexity; moments applied to vehicle are small; not used for 15 years in United States |
| Turbine exhaust gas swivel for large engine | L | Swivel joint is at low pressure, low performance loss; lightweight; proven technology | Limited side forces; moderately hot swivel joint; used mostly for roll control |

^aL, used with liquid propellant engines; S, used with solid propellant motors.

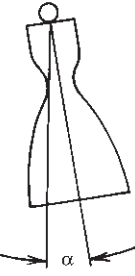
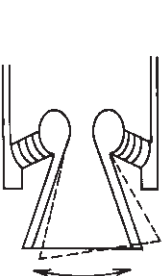
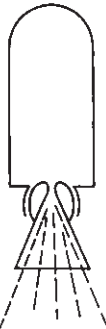
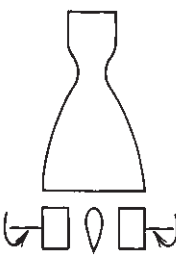
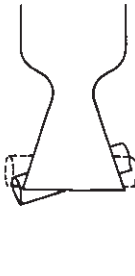
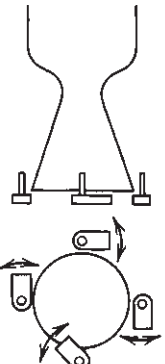
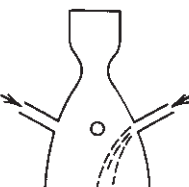
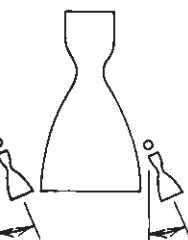
| Gimbal or hinge | Flexible laminated bearing | Flexible nozzle joint | Jet vanes |
|--|---|--|--|
|  |  |  |  |
| Universal joint suspension for thrust chamber | Nozzle is held by ring of alternate layers of molded elastomer and spherically formed sheet metal | Sealed rotary joint | Four rotating heat resistant aerodynamic vanes in jet |
| L | S | S | L/S |
| Jetavator | Jet tabs | Side injection | Small control thrust chambers |
|  |  |  |  |
| Rotating airfoil shaped collar, gimballed near nozzle exit | Four paddles that rotate in and out of the hot gas flow | Secondary fluid injection on one side at a time | Two or more gimballed auxiliary thrust chambers |
| S | S | S/L | L |

FIGURE 18–3. Simple schematic diagrams of eight different TVC mechanisms. Actuators and structural details are not shown. The letter L means it is used with liquid propellant rocket engines and S means it is used with solid propellant motors.

the 1940s. They cause extra drag (2 to 5% less I_s ; drag increases with larger vane deflections) and erosion of the vane material. Graphite jet vanes were used in the German V-2 missile in World War II and in the Scud missiles fired by Iraq in 1991. The advantage of having roll control with a single nozzle often outweighs the performance penalties. A recent application is discussed in Ref. 18-4.

Small auxiliary thrust chambers were used in the Thor and early version of Atlas missiles. They provide roll control while the principal rocket engine operates. They are fed from the same feed system as the main rocket engine. This scheme is still used on some Russian booster rocket vehicles.

The *injection of secondary fluid* through the wall of the nozzle into the main gas stream has the effect of forming oblique shocks in the nozzle diverging section, thus causing an unsymmetrical distribution of the main gas flow, which produces a side force. The secondary fluid can be stored liquid or gas from a separate hot gas generator (the gas would then still be sufficiently cool to be piped), a direct bleed from the chamber, or the injection of a catalyzed monopropellant. When the deflections are small, this is a low-loss scheme, but for large moments (large side forces) the amount of secondary fluid becomes excessive. This scheme has found application in a few large solid propellant rockets, such as Titan IIIC and one version of Minuteman.

Of all the mechanical deflection types, the *movable nozzles* and the *gimballed engine* are the most efficient. They do not significantly reduce the thrust or the specific impulse and are weight-competitive with the other mechanical types. The flexible nozzle, shown in Figs. 18-3 and 18-4, is a common type of TVC used with solid propellant motors. The molded, multilayer bearing pack acts as a seal, a load transfer bearing, and a viscoelastic flexure. It uses the deformation of a stacked set of doubly curved elastomeric (rubbery) layers between spherical metal sheets to carry the loads and allow an angular deflection of the nozzle axis. The flexible seal nozzle has been used in launch vehicles and large strategic missiles, where the environmental temperature extremes are modest. At low temperature the elastomer becomes stiff and the actuation torques increase substantially, requiring a much larger actuation system. Figure 18-5 describes a different type of flexible nozzle. It uses a movable joint with a toroidal hydraulic bag to transfer loads. There are double seals to prevent leaks of hot gas and various insulators to keep the structure below 200°F or 93°C.

Two of the gimbals will now be described in more detail. Figure 18-6 shows the gimbal bearing assembly of the Space Shuttle main engine. It supports the weight of the engine and transmits the thrust force. It is a ball-and-socket universal joint with contact and intermeshing spherical (concave and convex) surfaces. Sliding occurs on these surfaces as the gimbal assembly is rotated. When assembling the engine to the vehicle, some offset bushings are used to align the thrust vector. Some of the design features and performance requirements of this gimbal are listed in Table 18-2. The maximum angular motion is actually larger than the deflection angle during operation so as to allow for various tolerances and alignments. The actual deflections, alignment tolerances, friction coefficients,

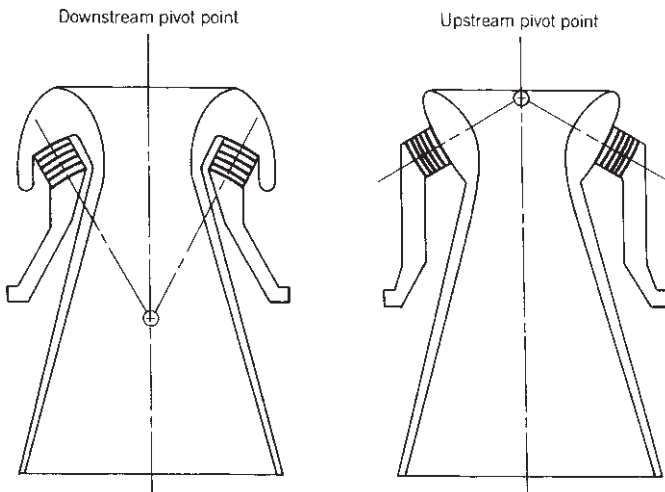


FIGURE 18–4. Two methods of using flexible nozzle bearings with different locations for the center of rotation. The bearing support ring is made of metal or plastic sheet shims formed into rings with spherical contours (white) bonded together by layers of molded elastomer or rubber (black stripes). Although only five elastomeric layers are shown for clarity, many flexible bearings have 10 to 20 layers. (Used with permission from Ref. 18–2.)

angular speeds, and accelerations during operation are usually much smaller than the maximum values listed in the table.

In Table 18–1 a scheme is shown which is suitable only for a liquid propellant rocket engine operating on a gas generator cycle. The exhaust gas from the turbine is fed into one or more nozzles and the maximum torque is limited by the amount of the hot gas. The Russian RD-119 upper-stage engine used six hot gas valves to control the flow of turbine exhaust gas to four pitch and yaw fixed nozzles and four smaller roll control fixed nozzles. Clearly visible in Fig. 6–10, the RS-68 engine shown has only one continuously flowing nozzle for the turbine exhaust, without a valve, which augments the thrust. With a swivel, it is used for roll control only.

Table 18–3 and Ref. 18–5 give the design requirements for the *actuator system* for the TVC for a flexible bearing in the IUS solid rocket motor nozzle. This system is shown in Figs. 12–3 and 18–5 and in Table 12–3. One version of this nozzle can deflect 4° maximum plus 0.5° for margin and another is rated at 7.5° . It has two electrically redundant electromechanical actuators using ball screws, two potentiometers for position indication, and one controller that provides both the power drive and the signal control electronics for each actuator. A variable-frequency, pulse-width-modulated (PWM) electric motor drive is used to allow small size and low weight for the power and forces involved. Also, it has a pair of locking mechanisms that will lock the nozzle in a fixed pitch-and-yaw position as a fail-safe device.

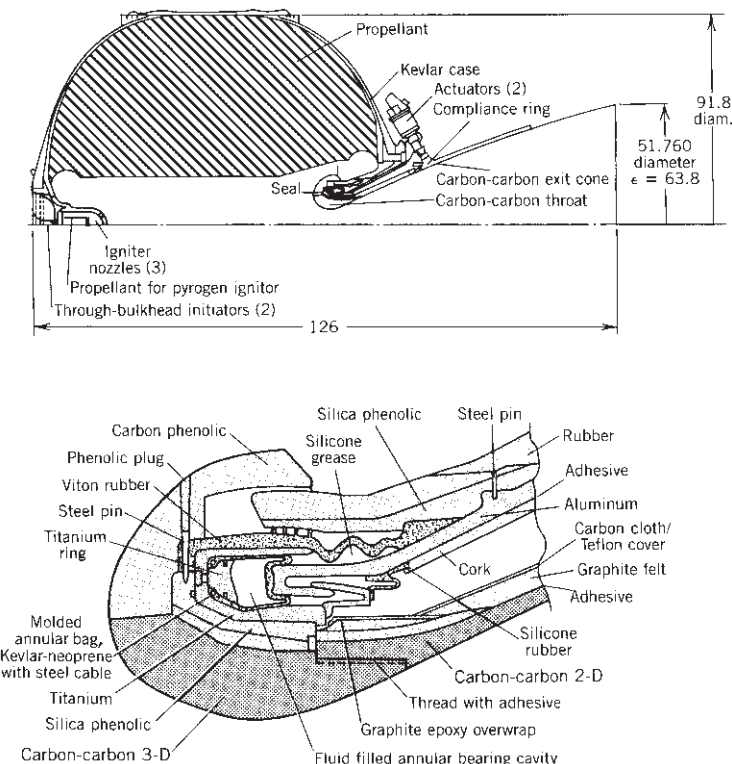


FIGURE 18-5. Simplified cross section of an upper-stage solid propellant rocket motor (IUS) using an insulated carbon-fiber/carbon-matrix nozzle, an insulated Kevlar filament-wound case, a pyrogen igniter, forward and aft stress-relieving boots, a fluid-filled bearing, and an elastomeric seal assembly in the nozzle to allow $4\frac{1}{2}$ ° of thrust vector deflection. This motor has a loaded weight of 22,874 lbf, a propellant with hydroxyl-terminated polybutadiene binder, a weight of 21,400 lbf, a burnout weight of 1360 lbf, a motor mass fraction of 0.941, a nozzle throat diameter of 6.48 in., and a nozzle exit area ratio of 63.8. The motor burns 146 sec at an average pressure of 651 psi (886 psi maximum) and an average thrust of 44,000 lbf (60,200 lbf maximum), with an effective altitude specific impulse of 295 sec. Top drawing is cross section of motor; bottom drawing is enlarged cross section of nozzle package assembly. The motor is an enlarged version of Orbus-6 described in Fig. 12-3. (From C. A. Chase, "IUS Solid Motor Overview," JANNAF Conference, Monterey, California, 1983; courtesy of United Technologies Corp. formerly Chemical Systems Operations.)

The *alignment* of the thrust vector is a necessary activity during assembly. The thrust vector in the neutral position (no deflection or, in many vehicles, the thrust axis coincides with the vehicle axis) should usually go through the center of gravity of the vehicle. The TVC mechanism has to allow for alignment or

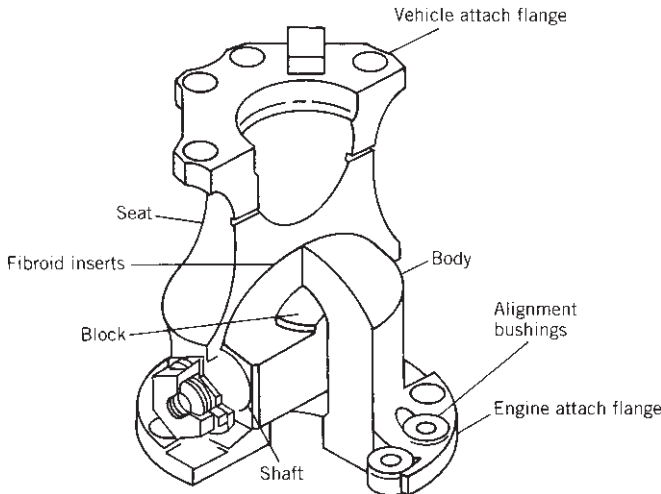


FIGURE 18–6. Gimbal bearing of the Space Shuttle main engine. (Courtesy of Pratt & Whitney Rocketdyne, Inc.)

TABLE 18–2. Characteristics and Performance Requirements of the Gimbal Bearing Assembly of the Space Shuttle Main Engine

| | |
|--|--------------|
| Engine weight to be supported (lbf) | Approx. 7000 |
| Thrust to be transmitted, (lbf) | 512,000 |
| Gimbal assembly weight (lbf) | 105 |
| Material is titanium alloy | 6Al-6V-2Sn |
| Dimensions (approximate) (in.) | 11 dia. × 14 |
| Angular motion (deg) | |
| Operational requirement (max.) | ±10.5 |
| Snubbing allowance in actuators | 0.5 |
| Angular alignment | 0.5 |
| Gimbal attach point tolerance | 0.7 |
| Overtravel vector adjustment | 0.1 |
| Maximum angular capability | ±12.5 |
| Angular acceleration (max.) (rad/sec ²) | 30 |
| Angular velocity (max.) (deg/sec) | 20 |
| Angular velocity (min.) (deg/sec) | 10 |
| Lateral adjustment (in.) | ±0.25 |
| Gimbal duty cycle about each axis | |
| Number of operational cycles to 10.5° | 200 |
| Nonoperational cycles to 10.5° | 1400 |
| Coefficient of friction (over a temperature range of 88–340 K) | 0.01–0.2 |

Source: Courtesy of Pratt & Whitney Rocketdyne, Inc.

TABLE 18–3. Design Requirements for TVC Actuation System of an IUS Solid Rocket Motor

| Item | Requirement |
|-----------------------|---|
| Performance parameter | |
| Input power | 31 A/axis maximum at 24–32 VDC; >900 W (peak) |
| Stroke | 10.2 cm (4.140 in.) minimum |
| Stall force | 1.9 kN (430 lbf) minimum |
| Accuracy | ±1.6mm (± 0.063 in.) maximum |
| Frequency response | >3.2 Hz at 100° phase lag |
| No load speed | 8.13 cm/sec (3.2 in./sec) minimum |
| Stiffness | 28.9 kN/cm (16,600 lbf/in.) minimum |
| Backlash | ±0.18 mm (0.007 in.) maximum |
| Reliability | >0.99988 redundant drive train, >0.999972 single thread element |
| Weight | |
| Controller | 5.9 kg (13 lbf) maximum, each |
| Actuator | 7.04 kg (15.5 lbf) maximum, each |
| Potentiometer | 1.23 kg (2.7 lbf) maximum, each |
| System | 22.44 kg (49.4 lbf) maximum |

Source: Reproduced from Ref. 18–5 with permission of United Technologies Corp./former Chemical Systems Operations.

adjustments in angle as well as position of the TVC center point with the intended vehicle axis. The geometric centerline of the diverging section of the nozzle is generally considered to be the thrust direction. One alignment provision is shown in Fig. 18–6. An alignment accuracy of one-quarter of a degree and an axis offset of 0.020 in. have been achieved with good measuring fixtures for small-sized nozzles.

The *jet tab TVC system* has low torque and is simple for flight vehicles with low-area-ratio nozzles. Its thrust loss is high when tabs are rotated at full angle into the jet, but is zero when the tabs are in their neutral position outside of the jet. On most flights the time-averaged position of the tab is a very small angle and the average thrust loss is small. Jet tabs can form a very compact mechanism and have been used successfully on tactical missiles using solid propellant rocket motors. An example is the jet tab assembly for the booster rocket motor of the Tomahawk cruise missile, shown in Fig. 18–7. Four tabs, independently actuated, are rotated in and out of the motor's exhaust jet during the 15-sec duration of rocket operation. A tab that blocks 16% of the nozzle exit area is equivalent to a thrust vector angle deflection of 9°. The maximum angle is 12° and the slew rate is fast (100°/sec). The vanes are driven by four linear small push–pull hydraulic actuators with two servo valves and an automatic integral controller. The power is supplied by compressed nitrogen stored at 3000 psi. An explosive valve releases the gas to pressurize an oil accumulator in a blowdown mode. The

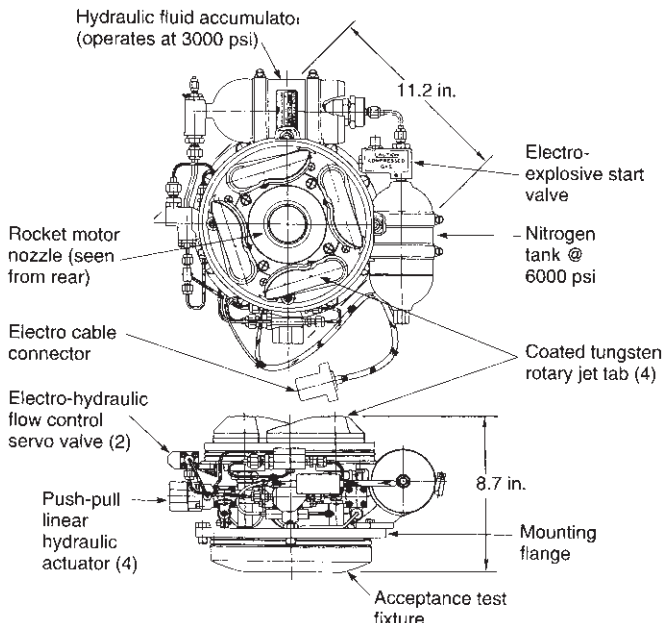


FIGURE 18–7. Two views of the jet tab assembly, packaged in a doughnut shape volume around the nozzle of the Tomahawk cruise missile's solid propellant booster rocket motor. Hydraulic actuators rotate the tabs in and out of the nozzle exhaust jet and are located just beyond the nozzle exit. (Courtesy of Space and Electronics Group, Northrop Grumman.)

vanes are made of tungsten to minimize the erosion from the solid particles in the exhaust gas.

The *jetavator* was used on submarine-launched missiles. The thrust loss is roughly proportional to the vector angle. This mechanism is shown in Fig. 18–3 and mentioned in Table 18–1.

The concept of TVC by *secondary fluid injection* into the exhaust stream dates back to 1949 and can be credited to A. E. Wetherbee, Jr. (U.S. Patent 2,943,821). Application of *liquid injection thrust vector control* (LITVC) to production vehicles began in the early 1960s. Both inert (water) and reactive fluids (such as hydrazine or nitrogen tetroxide) have been used. Although side injection of reactive liquids is still used on some of the older vehicles, it requires a pressurized propellant tank and a feed system. A high-density injection liquid is preferred because its tank will be relatively small and its pressurization will require less mass. Because other schemes have better performance, liquid injection TVC will probably not be selected for new applications.

Hot gas injection (HGITVC) of solid rocket propellant or liquid propellant combustion products is inherently attractive from a performance and packaging viewpoint. In the past there has not been a production application of HGITVC

because of erosion of materials in hot gas valves. However, two factors now make hot-gas-side injection feasible: First, hot gas valves can be made with the newer carbon–carbon structural parts and modern insulators. A hot gas system with a limited duration hot gas carbon valve is described in Ref. 18–6. Also, advances in metallurgy have made possible the development of hot valves made of rhenium alloy, a high-temperature metal suitable for hot gas valve applications. The second factor is the development of solid propellants that are less aggressive (less AP, Al₂O₃, and/or fewer oxidizing gas ingredients) and reduce the erosion in nozzles and valves; this helps the hot gas valves and insulated hot gas plumbing to better survive for limited durations but often at the expense of propulsion system performance. Experimental hot gas systems have had difficulties with thermal distortions and in keeping key components cool enough to prevent failure.

With either liquid or solid propellants, the hot gas can be bled off the main combustion chamber or generated in a separate gas generator. The hot gas valves can be used to (1) control side injection of hot gas into a large nozzle, or (2) control a pulsing flow through a series of small fixed nozzles similar to small attitude control thrusters described in Chapters 4, 6, and 12. In liquid propellant engines it is feasible to tap or withdraw gas from the thrust chamber at a location where there is an intentional fuel-rich mixture ratio; the gas temperature would then be low enough (about 1100°C or 2000°F) so that uncooled metal hardware can be used for HGITVC valves and piping.

The total side force resulting from secondary injection of a fluid into the main stream of the supersonic nozzle can be expressed as two force components: (1) the force associated with the momentum of the injectant and (2) the pressure unbalance acting over areas of the internal nozzle wall. The second term results from the unbalanced wall pressures within the nozzle caused by shock formation, boundary layer separation, difference between injectant and undisturbed nozzle stream pressures, and primary-secondary combustion reactions (for chemically active injectants). The strength of the shock pattern and the pressure unbalance created between opposite walls in the nozzle is dependent on many variables, including the properties of the injectant and whether it is liquid or gas. In the case of injecting a reactive fluid, the combustion occurring downstream of the injection port(s) usually produces a larger pressure unbalance effect than is obtained by liquid vaporization only. However, benefit from combustion is dependent on a chemical reaction rate high enough to keep the reaction zone close to the injection port. The TVC performance that is typical of inert and reactive liquids and hot gas (solid propellant combustion products) is indicated in Fig. 18–8. This plot of force ratios to mass flow ratios is a parametric representation commonly used in performance comparisons.

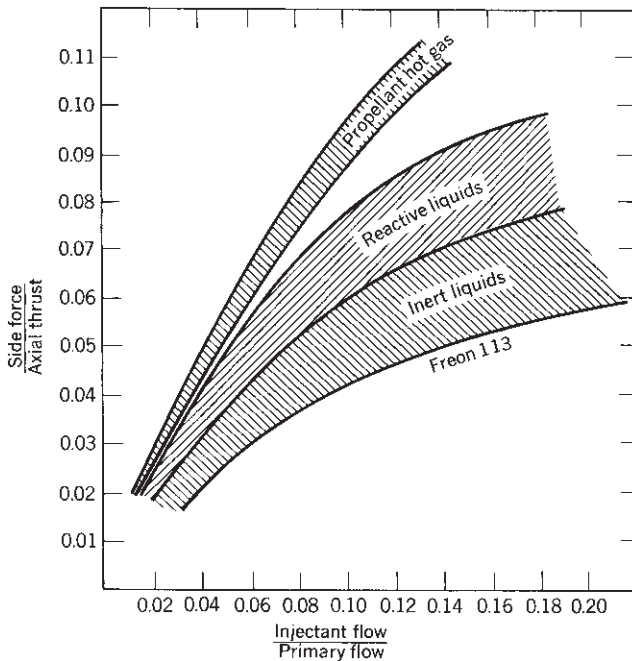


FIGURE 18–8. Typical performance regions of various side injectants in TVC nozzles.

18.2. TVC WITH MULTIPLE THRUST CHAMBERS OR NOZZLES

All the various concepts shown in Fig. 18–3 can provide pitch and yaw moments to a vehicle. Roll control can be obtained only if there are at least two separate vectorable nozzles, four fixed pulsing or throttled flow nozzles, or two jet vanes submerged in the exhaust gas from a single nozzle.

Several concepts have been developed and flown that use two or more rocket engines or a single engine or motor with two or more actuated nozzles. Two fully gimballed thrust chambers or motor nozzles can provide roll control with very slight differential angular deflections. For pitch and yaw control, the deflection would be larger, be of the same angle and direction for both nozzles, and the deflection magnitude would be the same for both nozzles. This can also be achieved with four hinged (see Fig. 11–1) or gimballed nozzles. Figure 18–9 shows the rocket motor of an early version of the Minuteman missile booster (first stage) with four movable nozzles. This motor is described in Table 12–3.

The differential throttling concept shown in Fig. 18–10 has no gimbal and does not use any of the methods used with single nozzles as described in Fig. 18–3. It has four fixed thrust chambers and their axes are almost parallel to and set off from the vehicle's centerline. Two of the four thrust chambers are

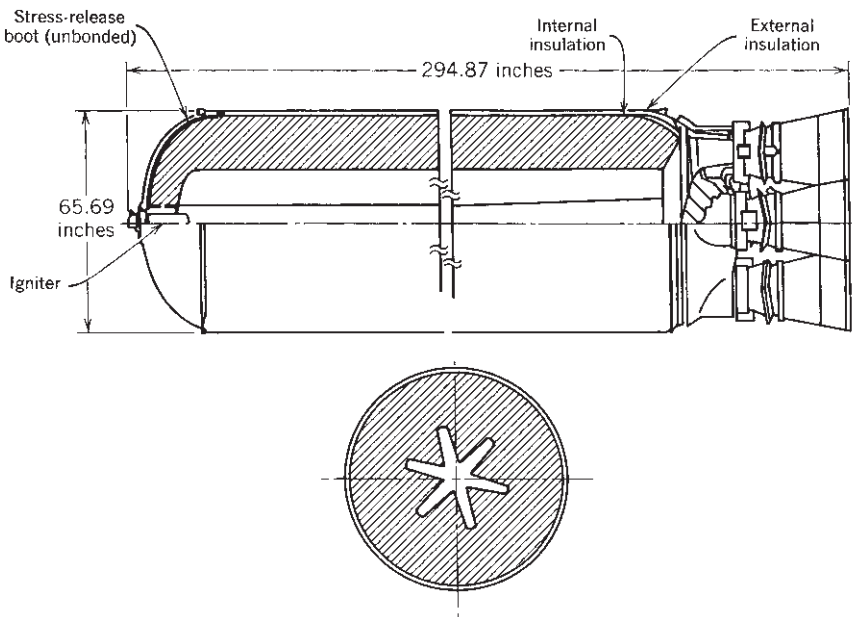


FIGURE 18–9. Simplified view of an early version of the first-stage Minuteman missile motor using composite-type propellant bonded to the motor case. Four movable nozzles provide pitch, yaw, and roll control. (Source: U.S. Air Force.)

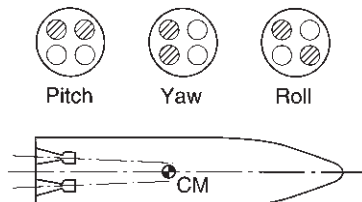


FIGURE 18–10. Differential throttling with four fixed-position thrust chambers can provide flight maneuvers. In this simple diagram the shaded nozzle exits indicate a throttled condition or reduced thrust. The larger forces from the unthrottled engines impose turning moments on the vehicle. For roll control the nozzles are slightly inclined and their individual thrust vectors do not go through the center of mass of the vehicle.

selectively throttled (typically the thrust is reduced by only 2 to 15%). The four nozzles may be supplied from the same feed system or they may belong to four separate but identical rocket engines. This differential throttling system was used on an experimental Aerospike rocket engine described in Chapter 8 and on a Russian launch vehicle.

18.3. TESTING

Testing of thrust vector control systems often includes actuation of the system when assembled on the propulsion system and the vehicle. For example, the Space Shuttle main engine can be put through some gimbal motions (without rocket firing) prior to a flight. A typical acceptance test series of the TVC system (prior to the delivery to an engine manufacturer) may include the determination of input power, accuracy of deflected positions, angular speeds or accelerations, signal response characteristics, or validation of overtravel stops. The ability to operate under extreme thermal environment, operation under various vehicle or propulsion system generated vibrations, temperature cycling, and ignition shock (high momentary acceleration) would probably be a part of the qualification tests.

Side forces and roll torques are usually relatively small compared to the main thrust and the pitch or yaw torques. Their accurate static test measurement can be difficult, particularly at low vector angles. Elaborate, multicomponent test stands employing multiple load cells and isolation flexures are needed to assure valid measurements.

18.4. INTEGRATION WITH VEHICLE

The actuators or movements of the TVC system are directed by the vehicle's guidance and control system (see Ref. 18-7). This system measures the three-dimensional position, velocity vectors, and rotational rates of the vehicle and compares them with the desired position, velocity, and rates. The error signals between these two sets of parameters are transformed by computers in TVC controllers into control commands for actuating the TVC system until the error signals are reduced to zero. The vehicle's computer control system determines the timing of the actuation, the direction, and magnitude of the deflection. With servomechanisms, power supplies, monitoring/failure detection devices, actuators with their controllers, and kinetic compensation, the systems tend to become complex.

The criteria governing the selection and design of a TVC system stem from vehicle needs and include the steering-force moments, force rates of change, flight accelerations, duration, performance losses, dimensional and weight limitations, available vehicle power, reliability, delivery schedules, and cost. For the TVC designer these translate into such factors as duty cycle, deflection angle, angle slew rate, power requirement, kinematic position errors, and many vehicle-TVC and motor-TVC interface details, besides the program aspects of costs and delivery schedules.

Interface details include electrical connections to and from the vehicle flight controller, the power supply, mechanical attachment with fasteners for actuators, and sensors to measure the position of the thrust axis or the actuators. Design features to facilitate the testing of the TVC system, easy access for checkout or repair, or to facilitate resistance to a high-vibration environment

are usually included. The TVC subsystem is usually physically connected to the vehicle and mounted to the rocket's nozzle. The designs of these components must be coordinated and integrated. Nozzle–TVC interfaces are discussed in Refs. 6–1 (TVC of liquid rocket engines and their control architecture) and 18–7.

The actuators can be hydraulic, pneumatic, or electromechanical (lead screw), and usually include a position sensor to allow feedback to the controller. The proven power supplies include high-pressure cold stored gas, batteries, warm gas from a gas generator, hydraulic fluid pressurized by cold gas or a warm gas generator, electric or hydraulic power from the vehicle's power supply, and electric or hydraulic power from a separate turbogenerator (in turn driven by a gas generator). The last type is used for relatively long-duration high-power applications, such as the power package used in the Space Shuttle solid rocket booster TVC, explained in Ref. 18–8. The selection of the actuation scheme and its power supply depends on the minimum weight, minimum performance loss, simple controls, ruggedness, reliability, ease of integration, linearity between actuating force and vehicle moments, cost, and other factors. The required frequency response is higher if the vehicle is small, such as with small tactical missiles. The response listed in Table 18–3 is more typical of larger spacecraft applications. Sometimes the TVC system is integrated with a movable aerodynamic fin system, as shown in Ref. 18–9. The control aspects of electromechanical actuators are discussed in Ref. 18–10.

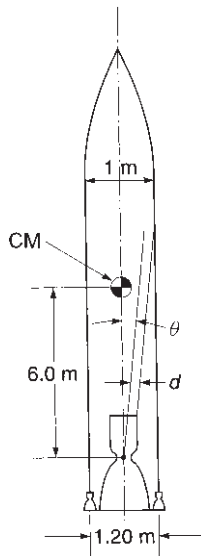
PROBLEMS

When solving problems in thrust vector control, information regarding the *center of mass* of the vehicle and either the *centroidal radius of gyration* or the appropriate *mass moment of inertia* should be deducible from the geometry of the rocket vehicle or should be given explicitly. Many elementary books in dynamics carry useful tables in this regard (see, for example, J. L. Meriam and L. G. Kraige, *Engineering Mechanics: Dynamics*, 6th edition, John Wiley and Sons, Inc., Hoboken, NJ, 2006). Note that in most propulsion systems, the *center of mass* moves during operation along the vehicle axis as the propellant is consumed.

1. A single-stage weather sounding rocket has a takeoff mass of 1020 kg, a sea-level initial acceleration of $2.00 g_0$, carries 799 kg of useful propellant, has an average specific gravity of 1.20, a burn duration of 42 sec, a vehicle body shaped like a cylinder with an L/D ratio of 5.00 with a nose cone having a half angle of 12° . Assume the center of mass does not change during the flight. The vehicle tumbled (rotated in an uncontrolled manner) during the flight and failed to reach its objective. Subsequent evaluation of the

design and assembly processes showed that the maximum possible thrust misalignment of the main thrust chamber was 1.05° with a maximum lateral off-set d of 1.85 mm. Assembly records show it was 0.7° and 1.1 mm for this vehicle. Since the propellant flow rate was essentially constant, the thrust at altitude cutoff was 16.0% larger than at takeoff. Determine the maximum torque applied by the main thrust chamber at start and at cutoff, without operating any auxiliary propulsion system. Then determine the approximate maximum angle through which the vehicle will rotate during powered flight, assuming no drag. Discuss the result.

2. A propulsion system with a thrust of 400,000 N is expected to have a maximum thrust misalignment θ of $\pm 0.50^\circ$ and a horizontal off-set d of the thrust vector of 0.125 in. as shown in the following sketch. One of four small reaction control thrust chambers will be used to counteract the disturbing torque. What should be its maximum thrust level and best orientation? Distance of vernier gimbal to center of mass (CM) is 7 m.



REFERENCES

- 18–1. G. P. Sutton, Section 4.9, “Steering or Flight Trajectory Control,” *History of Liquid Propellant Rocket Engines*, AIAA, 2006, pp. 218–227.
- 18–2. A. Truchot, “Design and Analysis of Solid Rocket Motor Nozzles,” in *Design Methods in Solid Rocket Motors*, AGARD Lecture Series 150, Advisory Group for Aerospace Research and Development, NATO, Revised Version, 1988, Chapter 3.

- 18-3. B. H. Prescott and M. Macocha, "Nozzle Design," in G. E. Jensen and D. W. Netzer (Eds.), *Tactical Missile Propulsion*, Vol. 170, *Progress in Astronautics and Aeronautics*, American Institute of Aeronautics and Astronautics, 1996, pp. 177–186.
- 18-4. A. B. Facciano, et al., "Evolved SeaSparrow Missile Jet Vane Control System Prototype Hardware Development," *Journal of Spacecraft and Rockets*, Vol. 39, No. 4, July–August 2002, pp. 522–531.
- 18-5. G. E. Conner, R. L. Pollock, and M. R. Riola, "IUS Thrust Vector Control Servo System," paper presented at 1983 JANNAF Propulsion Meeting, Monterey, CA, February 1983.
- 18-6. M. Berdoyes, "Thrust Vector Control by Injection of Hot Gas Bleed from the Chamber Hot Gas Valve," AIAA Paper 89–2867, July 1989.
- 18-7. J. H. Blakelock, *Automatic Control of Aircraft and Missiles*, 2nd ed., John Wiley & Sons, New York, 1991.
- 18-8. A. A. McCool, A. J. Verble, Jr., and J. H. Potter, "Space Transportation System's Rocket Booster Thrust Vector Control System," *Journal of Spacecraft and Rockets*, Vol. 17, No. 5, September–October 1980, pp. 407–412.
- 18-9. S. R. Wassom, L. C. Faupel, and T. Perley, "Integrated Aerofin/Thrust Vector Control for Tactical Missiles," *Journal of Propulsion and Power*, Vol. 7, No. 3, May–June 1991, pp. 374–381.
- 18-10. D. E. Schinstock, D. A. Scott, and T. T. Haskew, "Modelling and Estimation for Electromechanical Thrust Vector Control of Rocket Engines," *Journal of Propulsion and Power*, Vol. 14, No. 4, July–August 1998, pp. 440–446.

CHAPTER 19

SELECTION OF ROCKET PROPULSION SYSTEMS

In this chapter we discuss in general terms the process of selecting propulsion systems for a given mission. There are many factors, restraints, and analyses that have to be considered and evaluated before making a good selection. It can be complex because design problems usually have several possible engineering solutions from which to select. Four specific aspects are covered in some detail:

1. comparison of the merits and disadvantages of liquid propellant rocket engines with solid propellant rocket motors.
2. Some key factors used in evaluating particular propulsion systems and selecting from several competing candidate rocket propulsion systems.
3. The interfaces between the propulsion system and the flight vehicle and/or the overall system.
4. Computer integration of computer programs related to the propulsion system.

A propulsion system is really a subsystem of a flight vehicle. The vehicle, in turn, can be part of an overall system. An example of an overall system would be a communications network with ground stations, computers, transmitters, and several satellites; each satellite is a flight vehicle and has an attitude-control propulsion system with specific propulsion requirements. For example, the length of time in orbit is a system parameter that affects the satellite size and the total impulse requirement of its propulsion system.

Subsystems of a vehicle system (such as the structure, power supply, propulsion, guidance, control, communications, ground support, or thermal control) often pose conflicting requirements. *Only through careful analyses and system*

engineering studies is it possible to find compromises that allow all subsystems to operate satisfactorily and be in harmony with each other. The subject of engineering design has advanced considerably in recent times and computer-aided design is now common. System engineering is now used routinely. See Ref. 19–1. Other works address the design of space systems (e.g., Refs. 19–1 to 19–3) and the design of liquid propellant engines (e.g., Ref. 19–4). Section 11.6, “System Integration and Engine Optimization,” and Section 15.4, “Rocket Motor Design Approach,” are preludes to this chapter and have in part some duplicate content.

System engineering is a useful tool in making a rocket engine selection. It can be defined in several ways. One way (adapted from Ref. 19–5) is “a logical process of activities, analyses and engineering designs, that transforms a set of requirements arising from specific mission objectives in an optimum way. It ensures that all the likely aspect of a project or engineering system have been considered and integrated into a consistent whole.” It comprises all the elements of a propulsion system and its ground support, all interfaces with other vehicle subsystems or ground-based equipment, considers safety aspects, risks, costs, system and component analyses, and the orderly selection of the most suitable propulsion system. System engineering can also be useful in other applications (such as ship building, flight vehicles, or test facilities) each with its own set of missions.

There are usually *three levels of requirements* from which propulsion systems can be derived. (Ref. 19–5). At every level there are some activities, studies, or trade-off evaluations.

1. The top level are the requirements defining the mission, such as a space communication system or a missile defense system. The analysis and optimization are usually done by the organization responsible for the mission. They define parameters like trajectories or orbits, payloads, number of vehicles, life, and the like and record them in a document, often called mission requirements specification.
2. From the mission requirements documents the definition and requirement of the flight vehicle are derived. It could include ambient temperature limits, vehicle size, vehicle mass, number and sizes of vehicle stages, type of propulsion, required mass fraction, minimum specific impulse, need for thrust vector control and/or attitude control, allowable accelerations, acceptable propellants, restraints on engine size or inert mass, cost restraints, allowable start delay, desired thrust–time profile, preferred propulsion system type (liquid, solid, electrical), and so forth. The analysis, studies, engineering, and preliminary design and requirements specification are usually done by the organization responsible for the flight vehicle.
3. The propulsion requirements are the basis for the design and development of the propulsion system, and they are derived from the above two sets of requirements. It may include, for example, an optimum thrust–time profile, restart requirements, if any, liquid propellant engine cycle, pulsing requirements, rocket motor case L/D , grain configuration, restraints on travel of

the center of mass, details of the thrust vector control device or attitude control mechanism, reliability, cost or schedule restraints, or expected number of propulsion systems and spare parts to be delivered. This effort is usually done by the selected propulsion organization.

Important in this work are the *interfaces* between the propulsion system and the various subsystems of the flight vehicle and the ground equipment, such as the liquid propellant transfer system for loading propellants, the ground power supply before launch, and the ground-based computers that store, analyze, display, and generate data. See Section 19.3.

Much of the design (three-dimensional model of the propulsion system), most of the analyses (such as stress analysis), the testing, the keeping track of all hardware assemblies and parts, and the inspection records or NC programming are done today by a computer using different available or newly developed computer programs. Connecting and integrating these programs with each other and with other parts of the organization, which deal with some aspects of the propulsion system, has become an objective.

All mission (overall system), vehicle, and propulsion system *requirements* can be related to either performance, cost, or reliability. If cost criteria have the highest priority, then the engine will be different from the one that has performance as its top priority. For a given mission, one of these criteria is usually more important than the other two. There is a strong interdependence between the three levels of requirements and the three categories of criteria mentioned above. Some of the characteristics of the propulsion system (which is usually a second-tier subsystem) can have a strong influence on the vehicle and vice versa. An improvement in the propulsion performance, for example, can have a direct influence on the vehicle size, overall system cost, or life (which can be translated into reliability and cost).

19.1. SELECTION PROCESS

The selection process is a part of the overall design effort for the vehicle system and its rocket propulsion system. The selection is based on a *series of criteria*, which are based on the requirements and which will be used to evaluate and compare alternate propulsion systems. This process for determining the most suitable rocket propulsion system depends on the application, the ability to express many of the characteristics of the propulsion systems quantitatively, the amount of applicable data that are available, the experience of those responsible for making the selection, and the available time and resources to examine the alternate propulsion systems. What is described here is one somewhat idealized selection process as depicted in Fig. 19-1, but there are alternate sequences and other ways to do this job.

Since the total vehicle's performance, flight control, operation, or maintenance are usually critically dependent on the performance, control, operation, or maintenance of the rocket propulsion system (and vice versa), the process will usually

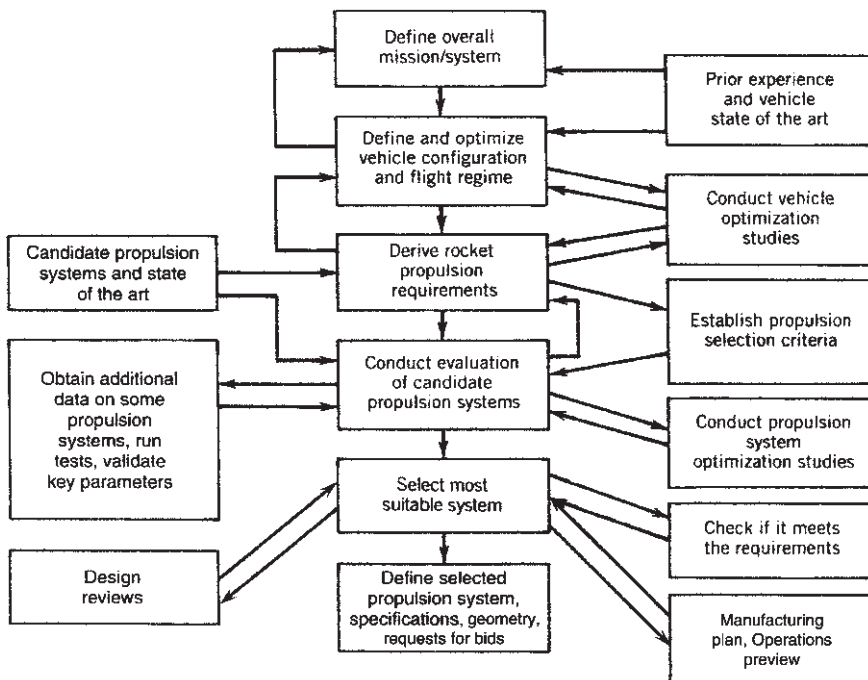


FIGURE 19–1. One idealized process for selecting propulsion systems.

go through several iterations in defining both the vehicle and propulsion requirements, which will satisfy the mission. This iterative process involves both the system organization (or the vehicle/system contractor) and one or more propulsion organizations (or rocket propulsion contractors). Documentation can take many forms; electronic computers have expanded their capability to network, record, and retrieve documents.

A number of competing candidate systems are usually evaluated. They may be proposed by different rocket propulsion organizations, perhaps on the basis of modifications of some existing rocket propulsion system, or may include some novel technology, or may be new types of systems specifically configured to fit the vehicle or mission needs. In making these evaluations it will be necessary to compare several candidate propulsion systems with each other and to rank-order them (in accordance with the selection criteria) on how well they meet each requirement. This requires analysis of each candidate system and also, often, some additional testing. For example, statistical analyses of the functions, failure modes, and safety factors of all key components can lead to quantitative reliability estimates. For some criteria, such as safety or prior related experience, it may not be possible to compare candidate systems quantitatively but only somewhat subjectively.

Various rocket parameters for a particular mission need to be optimized. *Trade-off studies* are used often to optimize certain parameters in accordance with the requirements. Trade-off studies have been performed on the following items and they helped in making the decisions on the best parameters of the propulsion system: number of trust chambers, optimum chamber pressure (considers performance and inert propulsion system mass), selected mixture ratio (performance, tank volume), solid propellant case configuration (L/D), the cost versus propulsion system performance, chamber pressure versus size and/or mass of propulsion system, chamber pressure versus heat transfer or cooling method, alternate grain configurations, minimizing travel of center of mass during operation, thrust magnitude/profile versus powered flight duration, nozzle exit area ratio versus performance, nozzle mass, or nozzle dimensions (L,D), alternate TVC concepts versus mass and power, chamber pressure versus heat transfer (cooling method or insulation) and inert mass. See Ref. 19–5.

Early in the selection process a tentative recommendation is usually made as to whether the propulsion system should be a solid propellant motor, a liquid propellant engine, an electrical propulsion system, or some other type. Each type has its own regime of thrust, specific impulse, thrust-to-weight ratio (acceleration), or likely duration, as shown in Table 2–1 and Fig. 2–1; these factors are listed for several chemical rocket engines and several types of nonchemical engines. Liquid engines and solid motors are covered in Chapters 6 to 15, hybrids in Chapter 16, and electric propulsion in Chapter 17.

If an existing vehicle is to be upgraded or modified, its propulsion system is usually also improved or modified (e.g., higher thrust, more total impulse, or faster thrust vector control). While there might still be some trade-off studies and optimization of the propulsion parameters that can be modified, one normally does not consider an entirely different propulsion system as is often done in an entirely new vehicle or mission. Also, it is rare that an identical rocket propulsion system is selected for two different applications; usually, some design changes, interface modifications, and requalification are usually necessary to adapt an existing rocket propulsion system to another application. Proven existing and qualified propulsion systems, that fit the desired requirements, usually have an advantage in cost and reliability.

Electric propulsion systems have a set of unique applications with low thrusts, low accelerations, trajectories in space, high specific impulse, long operating times, and generally a relatively massive power supply system. They perform well in certain space transfer and orbit maintenance missions. With more electric propulsion systems flying than ever before, the choice of proven electric propulsion thruster types is becoming larger. These systems, together with design approaches, are described in Chapter 17 and Ref. 19–3.

When a chemical rocket is deemed most suitable for a particular application, the selection has to be made between a liquid propellant engine, a solid propellant motor, or a hybrid propulsion system. Some of the major advantages and disadvantages of liquid propellant engines and solid propellant motors are given in Tables 19–1 to 19–4. These lists are general in nature; some items can be

TABLE 19–1. Solid Propellant Rocket Motor Advantages

| |
|---|
| Simple design (few or no moving parts). |
| Easy to operate (little preflight checkout). |
| Ready to operate quickly. |
| Will not leak, spill, or slosh. |
| Sometimes less overall weight for low total impulse application. |
| Can be throttled or stopped and restarted (usually only once) if preprogrammed and predesigned |
| Can provide TVC, but at increased complexity. |
| Can be stored for 10 to 30 years. |
| Usually, higher overall density; allows more compact package, smaller vehicle (less drag). |
| Some propellants have nontoxic, clean exhaust gases, but often at a performance penalty. |
| Thrust termination devices permit control over total impulse. |
| Ablation and gasification of insulator, nozzle, and liner materials contribute to mass flow and thus to total impulse. |
| Can avoid detonation when a tactical motor is subjected to energetic stimulant (e.g., bullet impact or external fire.) by judicious design and special propellant. |
| Some tactical missile motors have been produced in large quantities (over 200,000 per year). |
| Can be designed for recovery, refurbishing, and reuse (Space Shuttle solid rocket motor). |

TABLE 19–2. Liquid Propellant Rocket Engine Advantages

| |
|---|
| The highest specific impulse, can be attained with certain liquid propellants. This increases the vehicle velocity increment and the attainable mission velocity. |
| Can be randomly throttled and randomly stopped and restarted; can be efficiently pulsed (some small thrust sizes over 250,000 times). Thrust–time profile can be randomly controlled; this allows a reproducible flight trajectory. |
| Cutoff impulse can be controllable with thrust termination device (better control of vehicle terminal velocity). |
| Can be largely checked out just prior to operation. Can be tested at full thrust on ground or launch pad prior to flight. |
| Can be designed for reuse after field services and checkout. |
| Thrust chamber (or some part of the vehicle) can be cooled by propellant and made lightweight. |
| Storable liquid propellants have been kept in vehicle for more than 20 years and engine can be ready to operate quickly. |
| With pumped propulsion feed systems and large total impulse, the inert propulsion system mass (including tanks) can be very low (thin tank walls and low tank pressure), allowing a high propellant mass fraction. |
| Most propellants have nontoxic exhaust, which is environmentally acceptable. |
| Same propellant feed system can supply several thrust chambers in different parts of the vehicle. |
| Can provide component redundancy (e.g., dual check valves) to enhance reliability. |
| With multiple engines, can operate with one or more shut off (engine out capability). |
| The geometry of low-pressure tanks can be designed to fit most vehicles' space constraints (i.e., mounted inside wing or nose cone). |
| Can withstand many ambient temperature cycles. |
| The placement of propellant tanks within the vehicle can minimize the travel of the center of gravity during powered flight. This enhances the vehicle's flight stability and reduces flight control forces. |
| Plume radiation and smoke are usually low with many liquid propellants. |

TABLE 19–3. Solid Propellant Rocket Motor Disadvantages

| |
|--|
| Explosion and fire potential is larger; failure can be catastrophic; most cannot accept bullet impact or being dropped onto a hard surface. |
| Many require environmental permit and safety features for transport on public conveyances. |
| Under certain conditions some propellants and grains can detonate. |
| Cumulative grain damage can occur through daily temperature cycling or rough handling (transport); this limits the useful life. |
| If designed for reuse, it requires extensive factory rework and new propellants. |
| Requires an ignition system. |
| Each restart requires a separate ignition system and additional insulation—in practice, one restarts. |
| Random throttling is difficult and is not currently proven. |
| Exhaust gases are usually toxic for composite propellants containing ammonium perchlorate. |
| Some propellants or propellant ingredients can deteriorate (self-decompose) in storage. |
| Most solid propellant plumes cause more radio-frequency attenuation than liquid propellant plumes. |
| Only some motors can be stopped at random, but motor becomes disabled (not reusable). |
| Once ignited, cannot change predetermined thrust or duration. A moving pintle design with a variable throat area will allow random thrust changes, but experience is limited. |
| If combustion gases contain more than a few percent particulate carbon, aluminum, or other metal, the exhaust will be smoky and the plume radiation will be intense. |
| Integrity of grain (cracks, unbonded areas) is difficult to determine in the field. |
| Thrust and operating duration will vary with initial ambient grain temperature and cannot be easily controlled. Thus the flight path, velocity, altitude, and range of a motor will vary with the grain temperature. |
| Large boosters take a few seconds to start. |
| Thermal insulation is required in almost all rocket motors. |
| Cannot be hot fire tested prior to use. |
| Needs a safety provision to prevent inadvertent ignition, which would lead to an unplanned motor firing. Can cause a disaster. |

TABLE 19–4. Liquid Propellant Rocket Engine Disadvantages

| |
|--|
| Relatively complex design, more parts or components, more things to go wrong. |
| Cryogenic propellants cannot be stored for long periods except when tanks are well insulated and escaping vapors are recondensed. Propellant loading occurs at the launch stand or the test facility and requires cryogenic propellant storage facilities. |
| Spills or leaks of several propellants can be hazardous, corrosive, toxic, and cause fires, but this can be minimized with gelled propellants. |
| More overall weight for most short-duration, low-total-impulse applications (low propellant mass fraction). |
| Nonhypergolic propellants require an ignition system. |
| Tanks need to be pressurized by a separate pressurization subsystem. This can require high-pressure inert gas storage (2000–10,000 psi) for long periods of time. |
| More difficult to control combustion instability. |
| Bullet impact will cause leaks, sometimes a fire, but usually no detonations; gelled propellants can minimize or eliminate these hazards. |
| A few propellants (e.g., red fuming nitric acid) give toxic vapors or fumes. |
| Usually requires more volume due to lower average propellant density and the relatively inefficient packaging of engine components. |
| If vehicle breaks up and fuel and oxidizer are intimately mixed, it is possible (but not likely) for an explosive mixture to be created. |
| Sloshing in tank can cause a flight stability problem, but it can be minimized with baffles. |
| If tank outlet is uncovered, aspirated gas can cause combustion interruption or instability. |
| Smoky exhaust (soot) plume can occur with some hydrocarbon fuels. |
| Needs special design provisions for start in zero gravity. |
| With cryogenic liquid propellants there is a start delay caused by the time needed to cool the system flow passage hardware to cryogenic temperatures. |
| Life of cooled large thrust chambers may be limited to perhaps 100 or more starts. |
| High-thrust unit requires several seconds to start. |

controversial, and a number are restricted to particular applications. Most of the items from this list can be transformed into evaluation criteria. For a specific mission, the relevant items on these lists would be rank-ordered in accordance with their relative importance. A quantification of many of the items would be needed. These tables apply to generic rocket propulsion systems; they do not cover systems that use liquid–solid propellant combinations.

A favorite student question has been: Which are better, solid or liquid propellant rockets? A clear statement of strongly favoring one or the other can only be made when referring to a specific set of flight vehicle missions. Today, solid propellant motors seem to be preferred for tactical missiles (air-to-air, air-to-surface, surface-to-air, or short-range surface-to-surface) and ballistic missiles (long- and short-range surface-to-surface) because instant readiness, compactness, and their lack of spills or leaks of hazardous liquids are important criteria for these applications. Liquid propellant engines seem to be preferred for space-launched main propulsion units and upper stages, because of their higher specific impulse, relatively clean exhaust gases, and random throttling capability. They are favored for postboost control systems and attitude control systems, because of their random multiple pulsing capability with precise cutoff impulse, and for pulsed axial and lateral thrust propulsion on hit-to-kill defensive missiles. However, there are always some exceptions to these preferences.

When selecting the rocket propulsion system for a major new multiyear high-cost project, considerable time and effort are spent in evaluation and in developing rational methods for quantitative comparison. In part this is in response to government policy as well as international competition. Multiple studies are done by competing system organizations and competing rocket propulsion organizations; formal reviews are used to assist in considering all the factors, quantitatively comparing important criteria, and arriving at a proper selection.

Computer Integration

Better methods of design, development, manufacturing, and testing have accelerated the selection and fabrication processes. Advances in computing power and better simulation of physical phenomena are multiplying the capabilities of propulsion systems organizations and particularly their design engineers. In some of the larger commercial rocket engine systems organizations the design, development, testing, and production of new liquid rocket engines has been done essentially 100% by several separate computer systems during the last few years. Some of these programs are difficult to integrate or link.

The organization that is truly able to integrate or link the various functions into a single new computer system will have an advantage over its competitors. Table 19–5 really represents a concept for an ideal integration and this has not yet been achieved. If only a few of the programs listed in this table would be

linked or integrated (such as the system description and the supporting analyses), it would have an impact. The figure gives examples of the types of programs, data, and information packages that are candidates and could be put on or linked to an integrated computer system with an accurate geometric three-dimensional model or digital description of the propulsion system at its core, (Ref. 19–6). Some parts of this table, such as management systems or accounting systems may never be properly integrated. This table is not real, not complete and certainly not all of the items listed apply to any one particular rocket engine. Typical benefits of computer integration are the speed of design, and the potential speed-up in other parts of an organization, the larger number of iterations or optimization studies or analyses, and the speed of obtaining and/or analyzing useful manufacturing data or test data, the instant transfer of information from one module to another or from one department to another, all hopefully can be done much more quickly, more accurately, and in more detail. There are no more design drawings, much less paperwork in manufacturing, or vendors receiving computer information instead of papers.

Table 19–5 contains items specifically related to liquid propellant rocket engines. This table does not identify the many interactions between items in the table or between personnel involved in specific functions. The availability of data from prior propulsion systems can help to validate computer simulations of many functions listed in the table, such as combustion analysis, receiving inspection, or alternate start techniques.

19.2. CRITERIA FOR SELECTION

Many criteria used in selecting a particular rocket propulsion system are peculiar to the particular mission or vehicle application. However, some of these selection factors apply to a number of applications, such as those listed in Table 19–6. Again, this list is incomplete and not all the criteria in this table apply to every application. The table can be used as a checklist to see that none of the criteria relevant analyses and design studies listed here are omitted.

Here are some examples of important criteria in a few specific applications. For a spacecraft that contains optical instruments (e.g., telescope, horizon seeker, star tracker, or infrared radiation seeker) the exhaust plume must be free of possible contaminants that may deposit or condense on optical windows, mirrors, lenses, photovoltaic cells, or radiators, and degrade their performance, and be free of particulates that could scatter sunlight into the instrument aperture, which could cause erroneous signals. Conventional composite solid propellants and pulsing storable bipropellants are usually not satisfactory, but cold or heated clean gas jets (H_2 , Ar, N_2 , etc.) and monopropellant hydrazine reaction gases are usually acceptable. Another example is an emphasis on smokeless propellant exhaust

TABLE 19–5. Idealized Concept of a Computer Integration Breakdown for a Liquid Rocket Engine Organization

| <i>I. Design Description</i> | <i>II. Building the Propulsion System</i> | <i>III. Field Operations; IV. Management Information V Customer/Vehicle Developer Interactions; VI. Other</i> |
|--|---|---|
| <i>A. Propulsion System Identification, Plans, and Parameters</i> | <i>A. Purchasing</i> | <i>III. Field Operations</i> |
| Engine requirements | Purchase specifications, orders | Maintenance procedures |
| Customer requirements | Vendor selection/interactions | Check-out procedures |
| Application (vehicle) | Parts, material procurement | Launch preparations |
| Model number, Serial number | Vendor delivery schedule | Field inspections |
| Release schedule, plan | Receiving inspection of hardware, propellants, etc. | Inventory of parts, systems |
| Basic parameters (thrust, ΔF , propellant, spec. impulse, etc) | <i>B. Manufacturing, General</i> | Installation in vehicle |
| Contract requirements | Factory layout, capability | Part changes |
| <i>B. Propulsion System Description</i> | Special manufg. equipment | Field assembly |
| 3-D accurate design model include. | Summary reports on key events | <i>IV. Management Information</i> |
| assembly, subassemblies, components, parts, supplies | Make or buy decisions | Deliveries of systems versus plan |
| Parts lists | Design change implementation | Master schedule, costs and their key deviations, overall budget |
| Specifications (several types) | Manufg. schedule, % implemented | Cost of computer integration |
| Design changes, implementing plan | Delivery schedule, of propulsion systems, spare parts; actual versus plan | Cost/schedule of design releases & development versus plan, % completion |
| System design budget | Actual mfg. cost versus plan | Cost of manufacturing versus mfg. plan, % completion |
| Weight, CG, moment of inertia | <i>C. Manufacturing for Specific Propulsion System</i> | Summary reports on key events, key customer contacts or inquiries |
| <i>C. Analyses Supporting the Design</i> | Manufacturing plan/schedule | Cost of poor quality (scrap, rework, repair) |
| Performance analyses | Parts identifications | <i>V. Customer/Vehicle Developer Interactions</i> |
| Stress analysis | Assembly line and tests | Data to be furnished |
| Heat transfer, temperatures | Subassemblies fabrication | Data to be received |
| Health monitoring analysis | Components or parts making | |

| | | |
|--|--|--|
| Optimization studies (r, F, ϵ, p_1) | Factory routing (sequence of operations) | Approvals of key inspections, deliveries, etc. |
| Turbopump optimization | Fixtures and tooling | Qualification test approvals |
| Pressurizing system studies | NC machine programming | Review meetings |
| Transient performance studies | In-process inspection | Progress reports |
| Pressure and flow balances | Electromechanical checkouts | Static tests in a vehicle |
| Combustion analysis | Inspection of all finished hardware including assemblies | Flight test requirements |
| Plume effects studies | Package and ship all deliverable propulsion systems, spare parts | |
| Lessons learned | Engine hot fire acceptance tests | |
| Power demand/availability | | |
| Start (restart) alternatives | | |
| Alternate layouts | | |
| Alternate TVC | | |
| | | <i>D. Manufacturing and Purchasing Exceptions</i> |
| | Deviations from 3-D model or specification for each deficient part, assembly | |
| | Approval, disapproval, or rework of deviations | |
| | Scrapped (rejected) hardware or propellants | |
| | Data acquisition/recording | Inventory of available spare parts and their locations |
| | Special test equipment | Data storage and retrieval |
| | Test location, installations | |
| | Data analyses/displays | |
| | Instrument check out | |
| | Instrument calibrations | |

^aCG: Center of gravity.

plumes, so as to make visual detection of a smoke or vapor trail very difficult. This applies particularly to tactical missile applications. Only a few solid propellants and several liquid propellants would be nearly smokeless and essentially free of a vapor trail under all weather conditions.

Several selection criteria may be in conflict with each other. For example, some propellants with a very high specific impulse are more likely to experience combustion instabilities. In liquid propellant systems, where the oxidizer tank is pressurized by a solid propellant gas generator and where the fuel-rich hot pressurizing gases are separated only by a thin flexible diaphragm from the oxidizer liquid in the tank, there is a trade-off between a very compact system and no propellant dilution with dissolved gases and the potential for a damaging system failure (fire, possible explosion, and malfunction of system) if the diaphragm leaks or tears. In electric propulsion, high specific impulse and modestly high thrust is usually accompanied by heavy power-generating and conditioning equipment.

Actual selection will depend on the balancing of the various selection factors in accordance with their importance (priority), benefits, or potential impact on the system, and on quantifying as many of these selection factors as possible through analysis, extrapolation of prior experience/data, cost estimates, weights, and/or separate tests. See Ref. 19–5. Layouts, inert mass estimates, center-of-gravity analyses, vendor cost estimates, preliminary stress or thermal analysis, and other preliminary design efforts are usually necessary to put numerical values on some of the selection parameters. A comparative examination of the interfaces of alternate propulsion systems is also a part of the process. Some propulsion requirements are incompatible with each other and a compromise has to be made. For example, the monitoring of extra sensors can prevent the occurrence of certain types of failures and thus enhance the propulsion system reliability, yet the extra sensors and control components contribute to the system complexity and their possible failures will reduce the overall reliability. The selection process may also include feedback when the stated propulsion requirements cannot be met or do not make sense, and this can lead to a revision of the initial mission requirements or definition.

Once the cost, performance, and reliability drivers have been identified and quantified, the selection of the best propulsion system for a specified mission proceeds. The final propulsion requirement may come as a result of several iterations and will usually be documented, for example, in a *propulsion requirement specification*. A substantial number of records is required (such as engine or motor acceptance documents, CAD (computer-aided design) images, parts lists, inspection records, laboratory test data, etc.). There are many specifications associated with design and manufacturing as well as with vendors, models, and so on. There must also be a disciplined procedure for approving and making design and manufacturing changes. This now becomes the starting point for the design and development of the selected propulsion system.

TABLE 19–6. Typical Criteria Used in the Selection or Evaluation of a Particular Rocket Propulsion System*Mission Definition*

Purpose, function, and final objective of the mission of an overall system are well defined and their implications well understood. There is an expressed need for the mission, and the benefits are evident. The mission requirements are well defined. The payload, flight regime, vehicle, launch environment, and operating conditions are established. The risks, as perceived, appear acceptable. The project implementing the mission must have political, economic, and institutional support with assured funding. The propulsion system requirements, which are derived from mission definition and the vehicle definition, must be reasonable and must result in a viable propulsion system.

Affordability (Cost)

Estimated life-cycle costs are acceptable. They are the sum of R&D costs, production costs, facility costs, operating costs, and decommissioning costs, from inception to the retirement of the system (see Ref. 19–7). Benefits of achieving the mission should appear to justify costs. Investment in new facilities should be low. Few, if any, components should require expensive materials. For commercial applications, such as communications satellites, the return on investment must look attractive. Minimize the hiring of new, inexperienced personnel, who need to be trained and are more likely to make expensive errors. Cost comparisons of the selected engine with alternate propulsion systems has been favorable.

System Performance

The propulsion system is designed to optimize vehicle and system performance, using the most appropriate and proven technology. Inert mass is reduced to a practical minimum, using improved materials and better understanding of loads and stresses. Residual (unused) propellant is minimal. Propellants have the highest practical specific impulse without undue hazards, without excessive inert propulsion system mass, and with simple loading, storing, and handling. Thrust–time profiles and number of restarts must be selected to optimize the vehicle mission. Vehicles must operate with adequate performance for all the possible conditions (pulsing, throttling, temperature excursions, etc.). Vehicles should be storable over a specified lifetime. Will meet or exceed operational life. Performance parameters (e.g., chamber pressure, ignition time, or nozzle area ratio) should be near optimum for the selected mission. Vehicle should have adequate TVC. Solid propellant has enough strength and elongation to avoid grain cracks with daily temperature cycling and rough handling. Erosion in electric propulsion (electrodes, acceleration grids, nozzles) or in solid propellant motor nozzle throat are acceptable. TVC and attitude control thrusters conform to their requirements.

Survivability (Safety)

All hazards are well understood and known in detail. If failure occurs, the risk of personnel injury, damage to equipment, facilities, or the environment is minimal. Certain mishaps or failures will result in a change in the operating condition or the safe shutdown of the propulsion system. Applicable safety standards must be obeyed. Inadvertent energy input to the propulsion system (e.g., bullet impact, external fire) should not result in a detonation. The probability for any such drastic failures should be very low. Safety monitoring and inspections must have proven effective in identifying and preventing a significant share of possible incipient failures (see Ref. 19–8). Adequate safety factors must be included in the design. Spilled liquid propellants should cause no undue hazards. All systems and procedures must conform to the applicable safety standards. Launch test range has accepted the system as being safe enough to launch. Specified life of propulsion system has been proven feasible. Provisions are available to prevent solid motors from being stored at temperatures beyond the specified ambient temperature limits.

Reliability

Statistical analyses of test results indicate a satisfactory high-reliability level. Technical risks, manufacturing risks, and failure risks are very low, well understood, and the impact on the

(Continued)

TABLE 19–6. (*Continued*)

overall system is known. There are few complex components. Adequate storage and operating life of components (including propellants) have been demonstrated. If certain likely failures occur, the system must shut down safely. Redundancy of key components should be provided, where effective. High probability that all propulsion functions must be performed within the desired tolerances. Risk of combustion vibration or damaging mechanical vibration should be zero or very close to zero. Long life requirements can be met. See Ref. 19–7.

Controllability

Thrust buildup and decay are within specified limits. Combustion is stable under all operating conditions. The time responses to control or command signals are within acceptable tolerances. Controls need to be foolproof and not inadvertently create a hazardous condition. Thrust vector control response must be satisfactory. Mixture ratio control must assure nearly simultaneous emptying of the fuel and oxidizer tanks. Thrust from and duration of afterburning should be negligible. Accurate thrust termination feature must allow selection of final velocity of flight. Changing to a certain alternate mission profile should be feasible. Liquid propellant sloshing and pipe oscillations need to be adequately controlled. In a zero-gravity environment, a propellant tank should be essentially fully emptied.

Maintainability

Simple servicing, foolproof adjustments, easy parts replacement, and fast, reliable diagnosis of internal failures or problems. Minimal hazard to service personnel. There must be easy access to all components that need to be checked, inspected, or replaced. Trained maintenance personnel are available.

Geometric Constraints

Propulsion system fits into vehicle, into available engine compartment volume, meet specified length, or vehicle diameter. There is usually an advantage for the propulsion system that has the smallest volume or the highest average density. If the travel of the center of gravity has to be controlled, as is necessary in some missions, the propulsion system can do so.

Prior Related Experience

There is a favorable history and valid, available, relevant data of similar propulsion systems or critical components supporting the practicality of the technologies, manufacturability, performance, and reliability. Experience and validated computer simulation programs are available. Experienced, skilled personnel are available. Successful flight history.

Operability

Simple to operate. Validated operating manuals exist. Procedures for loading propellants, arming the power supply, launching, igniter checkout, and so on, must be simple. If applicable, a reliable automatic status monitoring and checkout system should be available. Crew training needs to be minimal. Should be able to ship the loaded vehicle on public roads or railroads without need for environmental permits and without the need for a decontamination unit and crew to accompany the shipment. Supply of spare parts assured.

Producibility

Easy to manufacture, inspect, and assemble. All key manufacturing processes are well proven and understood. All materials are well characterized, critical material properties are well known, and the system can be readily inspected. Proven vendors for key components have been qualified. Uses standard manufacturing machinery and relatively simple tooling. Hardware quality and propellant properties must be repeatable. Scrap should be minimal. Designs must make good use of standard materials, parts, common fasteners, and off-the-shelf components. There should be maximum use of existing manufacturing facilities and equipment. Excellent reproducibility, i.e., minimal operational variation between identical propulsion units or their components. Validated specifications should be available for major manufacturing processes, inspection, critical parts fabrication, and assembly. The make-or-buy decisions will consider the selection criteria.

Existing standards and manufacturing specifications apply. Deliverable assemblies or components will essentially be identical to each other.

TABLE 19–6. (*Continued*)*Schedule*

The overall mission can be accomplished on a time schedule that allows the system benefits to be realized. R&D, qualification, flight testing, and/or initial operating capability are completed on a preplanned schedule. No unforeseen delays. Critical materials and qualified suppliers must be readily available.

Environmental Acceptability

No unacceptable damage to personnel, equipment, or the surrounding countryside. No toxic species in the exhaust plume. Noise in communities close to a test or launch site should remain within tolerable levels. Minimal risk of exposure to cancer-causing chemicals. Hazards must be sufficiently low, so that issues on environmental impact statements are not contentious and approvals by environmental authorities become routine. There should be compliance with applicable laws and regulations. No unfavorable effects from currents generated by an electromagnetic pulse, static electricity, or electromagnetic radiation.

Reusability

Some applications (e.g., shuttle main engine, shuttle solid rocket booster, or aircraft rocket-assisted altitude boost) require a reusable propulsion system. The number of flights, serviceability, and the total cumulative firing time then become key requirements that will need to be demonstrated. Fatigue failure and cumulative thermal stress cycles can be critical in some of the system components. The critical components have been properly identified; methods, instruments, and equipment exist for careful checkout and inspection after a flight or test (e.g., certain leak tests, inspections for cracks, bearing clearances, etc.). Replacement and/or repair of unsatisfactory parts should be readily possible. Number of firings before disassembly should be large, and time interval between overhauls should be long.

Other Criteria

Radio signal attenuation by exhaust plume to be low. A complete propulsion system, loaded with propellants and pressurizing fluids, can be storable for a required number of years without deterioration or subsequent performance decrease. Interface problems are minimal. Provisions for safe packaging and shipment are available. The system includes features that allow decommissioning (such as to deorbit a spent satellite) or disposal (such as the safe removal and disposal of over-age propellant from a refurbishable rocket motor). Ground support equipment is compatible. See Table 19–7. When future engine growth versions can be predicted, then it may be cost effective to design some key components in such a way that they easily can be modified or strengthened with minimal effort and some extra mass. See Ref. 19–8. Heat transfer, particularly radiative heat transfer, from hot components (such as a gas generator) or from the exhaust gas plume to the near-by vehicle components or structure or to test facilities or to the environment, must be low enough not to cause overheating. Disconnect fitting between engine/vehicle and launch stand/ground must not leak; they disengage and close automatically when vehicle lifts off launch stand.

19.3. INTERFACES

In Section 19.2 the interfaces between the propulsion system and the vehicle and/or overall system were identified as some of the criteria and studies to be considered in the selection of a propulsion system. See also Ref. 19–5. A few rocket propulsion systems are easy to integrate and interface with the vehicles. Furthermore, these interfaces are an important aspect of a disciplined design and development effort. Table 19–7 gives a partial listing of typical interfaces that have been considered in the propulsion system selection, design, and development. It too may be a useful checklist. The interfaces assure system functionality

TABLE 19–7. Typical Interfaces between Rocket Propulsion Systems and Flight Vehicle

| Interface Category | Typical Detailed Interfaces |
|--------------------|--|
| Structural | <p>Interface (geometry/location/fastening mechanism) for mounting propulsion system</p> <p>Restraints on masses, moments of inertia, or the location of the center of gravity</p> <p>Type and degree of damping to minimize vibrations</p> <p>Attachment of vehicle components to propulsion system structure, such as wings, electrical components, or TVC.</p> <p>Loads (aerodynamic, acceleration, vibrations, thrust, sloshing, dynamic interactions) from vehicle to propulsion system, and vice versa</p> <p>Dimensional changes due to loads and/or heating and means for allowing expansions or deflections to occur without overstress</p> <p>Interactions from vibration excitation</p> |
| Mechanical | <p>Interfaces for electric connectors; for pneumatic, hydraulic, propellant pipe connections</p> <p>Volume/space for propulsion system is available and no geometric interference with other subsystems</p> <p>Access for assembly, part replacement, inspection, maintenance, repair</p> <p>Disconnect fittings between stages and between engine/vehicle and the launch stand</p> <p>Lifting or handling devices, and lifting attachments</p> <p>Measurement and adjustment of alignment of fixed nozzles</p> <p>Matching of thrust levels when two or more units are fired simultaneously</p> <p>Sealing or other closure devices to minimize air breathing and moisture condensation in vented tanks, motor cases, nozzles, porous insulation, or open pipes</p> |
| Power | <p>Source and availability of power (usually electric, but sometimes hydraulic or pneumatic) and their connection interfaces</p> <p>Identification of all users of power (solenoids, instruments, TVC, igniter, sensors) and their duty cycles. Power distribution to the various users</p> <p>Conversion of power to needed voltages, DC/AC, frequencies, or power level</p> <p>Electric grounding connections of rocket motors, certain electric equipment or pyrotechnic devices, to minimize voltage buildup and prevent electrostatic discharges</p> <p>Shielding of high-voltage wires and/or components</p> <p>Telemetry and radio communications interface</p> <p>Command signal wires</p> |

TABLE 19–7. (*Continued*)

| Interface Category | Typical Detailed Interfaces |
|---|--|
| Propellants | <p>Heaters (e.g., to keep hydrazine from freezing or to prevent ice formation with cryogenic propellants)</p> <p>Interfaces with antennas, wiring, sensors, and electronics located in the propulsion section of the vehicle</p> <p>Thermal management of heat generated in electric components</p> <p>Sharing of propellants between two or more propulsion systems (main thrust chambers and control thrusters)</p> <p>Control of sloshing to prevent center of gravity (CG) excursions or to prevent gas from entering the liquid propellant tank outlet</p> <p>Design of solid propellant grain or liquid propellant tanks so as to limit CG travel</p> <p>Loading/unloading provisions for liquid propellants</p> <p>Access for X-ray inspection of grain for cracks or unbonded areas, while installed</p> <p>Visual access to inspect turbine blades for cracks and turbopump shaft for easy rotation</p> <p>Access to visually inspect grain cavity for cracks</p> <p>Access to inspect cleanliness of tanks, pipes, valves</p> <p>The properties of propellants will remain essentially unchanged between different batches of propellants</p> <p>Connection of drain pipes for turbopump seal leakage</p> <p>Command signals (start/stop/throttle, etc.) interface connections</p> |
| Vehicle flight control and communications | <p>Feedback signals (monitoring the status of the propulsion system, e.g., valve positions, thrust level, remaining propellant, pump speed, pressures, temperatures); telemetering devices</p> <p>Circumstances for activating the range safety destruct system</p> <p>Attitude control: command actuation in pitch, yaw, or roll; feedback of TVC angle position and slew rate, duty cycle, safety limits</p> <p>Division of control logic, computer capability, or data processing and databases between propulsion system controller, vehicle controller, test stand controller, or ground-based computer/controller system</p> <p>Number and type of fault detection devices and their connection methods</p> |
| Thermal | <p>Heat from rocket gas/exhaust plume, hot walls of propulsion system components, or aerodynamic airflow should not overheat critical exposed adjacent components</p> <p>Transfer of heat between propulsion system and the vehicle</p> <p>Provisions for venting cryogenic propellant tanks</p> <p>Radiators for heat rejection</p> |

(Continued)

TABLE 19–7. (*Continued*)

| Interface Category | Typical Detailed Interfaces |
|--------------------------|---|
| Plume | Radiative and convective heating of vehicle by plume Impingement (forces and heating) of plume from attitude control nozzle with vehicle components Noise effects on equipment and surrounding areas Avoiding contamination or condensation of plume species on vehicle or payload parts, such as solar panels, optical components of instruments, or radiation surfaces Attenuation of radio signals |
| Safety | Condition monitoring and sensing of potential imminent failure and automatic remedial actions to prevent or remedy impending failure (e.g., reduce thrust or shut off one of several redundant propulsion systems) Arming and disarming of igniter. Access to safe & arm device Safe disposal of hazardous liquid propellant leaking through pump shaft seal, valve stem seal, or vented from tanks Designed to avoid electrostatic buildup and discharge |
| Ground support equipment | Interface with standby power system Interfaces with heating/cooling devices on ground at launch or test site Supply and loading method for liquid propellant, pressurizing gases, and other fluids. Also, interface with method for unloading these Grounding wires to prevent electrostatic discharge with solid propellant rocket motors Electromechanical checkout Interface with ground systems for flushing, cleaning, drying the tanks and piping Transportation vehicles/boxes/vehicle erection devices Lifting devices and handling equipment Interface with fire extinguishing equipment on ground |

and compatibility between the propulsion system and the vehicle with its other subsystems under all likely operating conditions and mission options. Usually, an interface document or specification is prepared and it is useful to designers, operating personnel, or maintenance people.

Besides cold gas systems, a simple solid propellant rocket motor has the fewest and the least complex set of interfaces. A monopropellant liquid rocket engine also has relatively few and simple interfaces. A solid propellant motor with TVC and a thrust termination capability has additional interfaces, compared to a simple motor. Bipropellant rocket engines are more complex and the number and difficulty of interfaces increase if they have a turbopump feed system, throttling features, TVC, or pulsing capability. In electric propulsion systems the number and complexity of interfaces is highest for an electrostatic thruster with pulsing

capability, when compared to electrothermal systems. More complex electrical propulsion systems generally give higher values of specific impulse. If the mission includes the recovery and reuse of the propulsion system or a manned vehicle (where the crew can monitor and override the propulsion system commands), this will introduce additional interfaces, safety features, and requirements.

REFERENCES

- 19–1. W. J. Larson and J. R. Wertz (Eds.), *Space Mission Analysis and Design*, 2nd ed., Microcosm, Inc., and Kluver Academic Publishers, Boston, 1992.
- 19–2. J. C. Blair and R. S. Ryan, “Role of Criteria in Design and Management of Space Systems,” *Journal of Spacecraft and Rockets*, Vol. 31, No. 2, March–April 1994, pp. 323–329.
- 19–3. R. W. Humble, G. N. Henry, and W. J. Larson, *Space Propulsion Analysis and Design*, McGraw-Hill, New York, 1995.
- 19–4. D. K. Huzel and D. H. Huang, *Modern Engineering for Design of Liquid Propellant Rocket Engines*, rev. ed. *Progress in Astronautics and Aeronautics*, Vol. 147, AIAA, Washington, DC, 1992.
- 19–5. P. Fortescue, J. Stark, and G. Swinerd, *Spacecraft Systems Engineering*, 3rd ed., John Wiley & Sons, Hoboken, NJ, 2003.
- 19–6. Discussions with engineering personnel from Pratt & Whitney Rocketdyne, 2003 to 2008.
- 19–7. C. J. Meisl, “Life Cycle Cost Considerations for Launch Vehicle Liquid Propellant Engine,” *Journal of Propulsion and Power*, Vol. 4, No. 2, March–April 1988, pp. 117–119.
- 19–8. A. Norman, I. Cannon, and L. Asch, “The History and Future Safety Monitoring in Liquid Rocket Engines,” AIAA Paper 89-2410, presented at the 25th Joint Propulsion Conference, July 1989.

CHAPTER 20

ROCKET EXHAUST PLUMES

This chapter provides an introduction to the subject, general background, a description of various plume phenomena, their analysis and effects, and references for further study.

The plume is the moving formation of hot rocket exhaust gases (and often also with entrained small particles) outside the rocket nozzle. This gas formation is not uniform in structure, velocity, or composition. It contains several different flow regions and supersonic shock waves. It is usually visible as a brilliant flame, emits intense radiation energy in the infrared, visible, and ultraviolet segments of the spectrum, and is a strong source of noise. Many plumes leave a trail of smoke or vapor and they can discharge toxic exhaust gases. At higher altitudes the plume gases can spread over large distances, and a small portion of the plume gases can flow backward around the nozzle and reach components of the flight vehicle.

The plume characteristics (size, thrust level, shape, structure, emission intensity of photons or sound pressure waves, visibility, electrical interference, or smokiness) depend not only on the characteristics of the particular rocket propulsion system or its propellants, but also on the flight path, flight velocity, altitude, weather conditions, such as winds, humidity, or clouds, and the particular vehicle configuration. See Refs. 20–1 to 20–3. Progress has been steady in recent decades in gaining understanding of the complex, interacting physical, chemical, optical, aerodynamic, and combustion phenomena within plumes by means of laboratory experiments, computer simulation, measurements on plumes during static firing tests, flight tests, or simulated altitude tests in vacuum test chambers. Yet some is not fully understood or predictable. As shown in Table 20–1, there are many applications or situations where a prediction or a quantitative understanding of plume behavior is needed.

TABLE 20–1. Applications of Plume Technology

Design/Develop/Operate Flight Vehicles, Their Propulsion Systems, Launch Stands, or Launch Equipment

- For a given propulsion system and operating conditions (altitudes, weather, speed, afterburning with atmospheric oxygen, etc.) determine or predict the plume dimensions, its temperature profiles, emissions, or other plume parameters.
- Determine likely heat transfer to components of vehicle, test facility, propulsion system or launcher, and prevent damage by design changes. Include afterburning and recirculation.
- Estimate the ability of vehicle and test facilities to withstand intensive plume noise.
- Determine the aerodynamic interaction of the plume with the airflow around the vehicle, which can cause changes in drag and plume shape.
- Reduce impingement on vehicle components (e.g., plumes from attitude control thrusters hitting a solar panel); this can cause excessive heating or impingement forces that may turn the vehicle.
- Estimate and minimize erosion effects on vehicle or launcher components.
- Prevent deposits of condensed species on spacecraft windows, optical surfaces, solar panels, or radiating heat emission surfaces.
- Determine the backscatter of sunlight by plume particulates or condensed species, and minimize the scattered radiation that can reach into optical instruments on the vehicle, because this can give erroneous signals.
- Protect personnel using a shoulder-fired rocket launcher from heat, blast, noise, smoke, and toxic gas.
- Detect metal trace element vapors (Fe, Ni, Cu, Cr) as indicators of thrust chamber damage and potential failure.

Detect and Track Flight of Vehicles

- Analysis and/or measurement of plume emission spectrum or signature.
- Identify plumes of launch vehicles from a distance when observing from spacecraft, aircraft, or ground stations, using IR, UV, or visible radiations and/or radar reflections.
- Distinguish their emissions from background signals.
- Detect and identify smoke and vapor trails.
- Track plumes and predict the flight path or determine the launch location.
- Alter the propellant or the nozzle to minimize the plume signature, which means the radiation, radar signature, or primary smoke emissions.
- Estimate amount of secondary smoke under foul weather conditions.
- Reduce secondary smoke
- Provide an aim point on the body of an incoming missile by observing its plume radiance distribution using an infrared sensor aboard an interceptor of a boost phase missile defense system. (from Ref. 20–4).

Improve Understanding of Plume Behavior

- Improve theoretical approaches to plume phenomena.
- Improve or create novel or more realistic computer simulations.
- Provide further validation of theory by experimental results from flight tests, laboratory investigations, static tests, or tests in simulated altitude facilities.
- Understand and minimize the generation of high-energy noise.
- Understand the mechanisms of smoke, soot, or vapor formation, thus learning how to control them and minimize them.
- Provide a better understanding of emission, absorption, and scatter within plume.
- Provide a better prediction of chemiluminescence.
- Understand the effect of shock waves, combustion vibration, or flight maneuvers on plume phenomena.
- Understand the effects of plume gas remains on the stratosphere or ozone layer.
- Develop a better algorithm for simulating turbulence in different parts of the plume.

(Continued)

TABLE 20–1. (Continued)*Minimize Radio-Frequency Interference*

Determine the plume attenuation for specific antennas and antenna locations on the vehicle.
 Estimate and reduce the attenuation of radio signals that have to pass through the plume, typically between an antenna on the vehicle and an antenna on the ground or on another vehicle.
 Estimate and reduce radar reflections from plumes.
 Estimate and reduce the electron density and electron collision frequency in the plume; for example, by reducing certain impurities, such as sodium.

20.1. PLUME APPEARANCE AND FLOW BEHAVIOR

Figure 20–1 shows a simplified sketch of the front part of the nozzle exhaust plume of a large propulsion system operating at low altitude. The plume starts at the nozzle exit plane of the rocket propulsion system, where it has its smallest cross section. It expands in diameter as the plume gases move rapidly away from the vehicle. The flow at this nozzle exit is not uniform as explained in Chapter 3. The relative velocity between the exhaust gases of the plume (which have the same velocity as the vehicle) and the ambient air diminishes along the length of the plume, eventually approaching zero near the tail end of the plume. Small propulsion systems with low thrust have small plumes and thus emit much less radiation energy.

The inviscid core of the plume expands until the dynamic pressure of the external flow forces it to turn. The only way for a supersonic flow to turn is with an oblique shock wave, also called barrel shock, as will be explained later. This intercepting oblique shock wave curves toward the plume axis, where a strong normal shock wave, of a diameter smaller than the nozzle exit, has been formed.

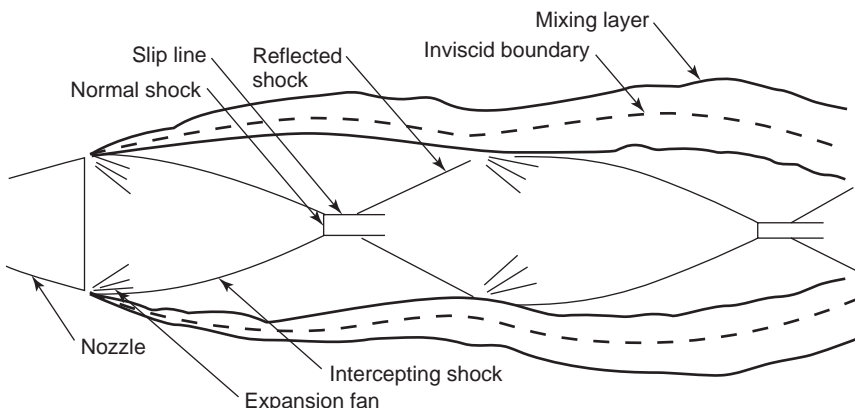


FIGURE 20–1. Simplified schematic diagram of the near-field section of the exhaust plume of a large rocket propulsion system operating at low altitude. (Used with permission from Ref. 20–1.) Similar figures also are in Refs. 20–2 and 20–3.

The inner flow is reflected at its boundary as an oblique expansion shock wave or as a reflection wave. The region immediately behind the normal shock wave is subsonic and very hot. In this normal shock wave the energy of the incoming supersonic flow velocity is converted into lower energy subsonic velocity and a major increase in thermal energy or local temperature. This normal wave and the hot subsonic region immediately downstream of it are clearly visible with many liquid propellants. Shock waves will be discussed later in this Chapter. After flowing through the hot subsonic zone, the gases in the plume flow are recompressed. This series of supersonic oblique and normal shock waves repeat themselves to form a characteristic pattern often called Mach diamonds, because of the diamond-shaped visible appearance. These Mach diamonds expand in scale with increasing altitude.

In the *mixing layer* (identified in Fig. 20-1) the hot gases from the plume (usually fuel rich with extra H₂ and CO) mix with the ambient air and burn with the oxygen of the air. This secondary combustion creates extra heat and causes the temperature in the mixing layer to rise by several hundred degrees. Therefore the mixing layer is usually a strong radiation emitter. With some propellants (LOX/LH₂ or LOX/alcohol) the mixing layer is transparent and the Mach diamonds in the core are clearly visible. With most solid propellants and with certain storable liquid propellants, this mixing layer is not transparent, in part because of the emission and absorption by suspended particles. Much of the infrared radiation from the inner plume core is obscure or absorbed by the bright outer mixing layer.

When axis of the plume is aligned with the vehicle axis, then a straight inner core and a symmetrical mixing layer are formed as seen in Fig. 20-1 and the sketches and information in Table 20-2. The plume shape and the mixing layer with air are geometrically very different, if the plume is at right angles to the vehicle axis, as is the case with target-homing upper stages of antimissile vehicles. In the case of a retrorocket the firing direction of the propulsion system is in a direction opposite to the vehicle's flight direction and the plume shape is again changed, but it is symmetrical (Ref. 20-4).

Table 20-2 shows three simple sketches of the change of plume configuration with altitude and lists their heat sources. In general the length and diameter of the plumes increase with altitude in the atmosphere, the temperatures and pressures within the plume become smaller along the length of the plume, and the plume typically becomes larger than the vehicle. All hot parts of a plume emit radiation. The first sketch is really a longer version of the plume in Fig. 20-1. It has a long inviscid core (exhaust gases that have not yet been mixed with air) with many Mach diamonds. At low altitude (under 5 km) when $p_2 \cong p_3$ the shape of the plume is nearly cylindrical and the mixing layer is also cylindrical or slightly conical. The second sketch identifies the three regions of a plume. In the transient region the shock waves and the radiation diminish with every Mach diamond and more of the exhaust gas is mixed with ambient air. At higher altitudes (10 to 25 km) the nozzle exit pressure p_2 exceeds the atmospheric pressure p_3 and the plume spreads out further and becomes larger. At even higher altitudes (above

TABLE 20-2. Altitude Characteristics of Large Plumes

| Plume Configuration (not to same scale) | 0–20 | 20–50 | 80 and above |
|--|------------------------------|--------------------------------|---|
| | | | |
| Altitude, km | 0–20 | 20–50 | 80 and above |
| <i>Heat transfer sources</i> | | | |
| 1. Shock waves | Minor source in central core | Major source | Major source |
| 2. Afterburning mantle | Major source | Minor source | Almost zero |
| 3. Base recirculation | Usually minor ^a | Major source ^a | Minor source |
| 4. Particulates (with solid propellants) | Can be major source | Major source | Minor source |
| Plume size | Longer than vehicle | Larger diameter and longer yet | Shock waves can be over 5 km wide |
| Plume shape | Near cylinder | Nearly conical | Core is small |
| Dimensions, m | 10–100 long | 200–1000 long | 1–15 km wide |
| Number of visible shock diamonds | 6 or more | 3–4 | Often only first inviscid region, sometimes $1\frac{1}{2}$ shock diamonds |

^aEven higher intensity with two or more nozzles firing

approximately 35 km) when $p_2 \gg p_3$, the atmospheric pressure is very low, the plume grows and can extend to several kilometers in diameter with only one or two Mach diamonds visible. Two relatively large diameter shock waves can be seen in the third sketch; one is in the thin air just ahead of the flight vehicle and is known as the bow shock wave. It occurs when the vehicle exceeds supersonic velocity. The other shock wave is attached to the tail end of the flight vehicle and is called the exhaust gas shock wave. A smaller version of this shock also appears at lower altitudes. In the far field (tail end of plume) the ambient air and the exhaust gases are fairly well mixed throughout a cross section of the plume and the local pressure is essentially that of the local ambient air.

As the supersonic exhaust gas flow emerges from the nozzle, it experiences Prandtl-Meyer type of expansion waves, which attach themselves to the nozzle exit lip. This expansion allows the outer streamlines just outside the nozzle to be bent and an increase in the Mach number of the gases in the outer layers of the plume. This expansion can, at higher altitudes, cause some small portion of the supersonic plume to be bent by more than 90° from the nozzle axis. The theoretical limit of a Prandtl-Meyer expansion is about 129° for gases with

$k = 1.4$ (air) and about 160° for gases with $k = 1.3$ (typical for a rocket exhaust mixture; see Ref. 20–5). This backward flow needs to be analyzed to estimate the heat and impingement effects and possible contamination of vehicle components (see Ref. 20–6).

The boundary layer next to the nozzle exit internal wall is a region of viscous flow, and the flow velocity is lower than in the main nozzle inviscid flow. The velocity decreases to zero right next to the wall. For large nozzles this boundary layer can be quite thick, say 2 cm or more. Figure 3–16 shows a subsonic and a supersonic region within the boundary layer inside the nozzle divergent section; it also shows a temperature and a velocity profile. While the supersonic flow layer is restricted in the angle through which it can be deflected, the subsonic boundary layer flow at the nozzle lip is in a continuum regime and may be deflected by up to 180° . Although the subsonic boundary layer represents only a small portion of the mass flow, it nevertheless lets its exhaust gases flow backward on the outside of the nozzle. This backflow has caused heating of and sometimes chemical damage to the vehicle and propulsion system parts.

The mass distribution or relative density is not uniform, as can be seen in Fig. 20–2, which is based on a calculated set of data for a high-altitude plume. Here 90% of the flow is within $\pm 44^\circ$ of the nozzle axis and only one hundred thousandth, or 10^{-5} , of the total mass flow is bent by more than 90° .

Figure 20–3 shows simplified sketches of the radiation intensity and the shape of the plumes for three propulsion systems, each driving one of three stages—all part of a single flight vehicle. The radiation is measured by a space-based sensor with a limited field of view, perhaps 1×1 km. Gaseous plumes radiate and absorb radiation only at specific narrow wave lengths or spectrum frequencies. Each chemical species in the exhaust (H_2 , H_2O , CO , N_2 , etc.) has its own characteristic emission wave lengths. These gases do not contain any particulates. The rise of the total emission intensity with altitude of the booster propulsion system curve is due to an increase in the plume diameter and a decrease in the atmospheric absorption between the booster and the space-based sensor. The subsequent decrease of its total intensity can be explained as the gradual decrease in afterburning as the vehicle gains altitude. The gap in the curves is due to stage separation (termination of booster thrust and subsequent start of the sustainer propulsion system). The sustainer has a lower thrust and a smaller plume and thus less total radiation intensity. The radiation intensity of the sustainer propulsion system rises as its plume expands and the radiating gas volume becomes larger. The decrease of the intensity shown in the figure is due to the limited field of view of the specific sensor, which can only see a piece of the large plume. The actual intensity increases somewhat, as seen by the dotted line in Fig. 20–3.

In the upper portion of Fig. 20–3 each sketch shows a key plume dimension, some shock waves, and the plume's shape. Each sketch is drawn to a different scale. The wiggly lines indicate effects of turbulence and wind on the mixing layer surrounding the core (afterburning). The lower part of the figure shows the plume radiation intensities of the various propulsion systems on a logarithmic scale as observed from a satellite. The field of view of the sustainer plume sensor

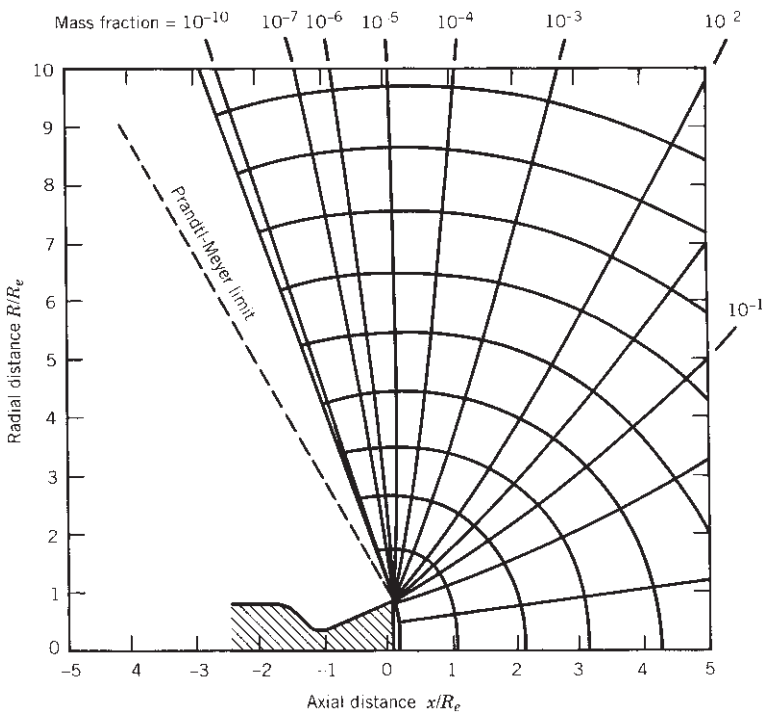


FIGURE 20–2. Density profile for vacuum plume expansion using a one-dimensional flow model for a small storable bipropellant thruster. The axial distance x and the plume radius R have been normalized with the nozzle exit radius R_e . Here $k = 1.25$, the Mach number of the nozzle exit is 4.0, and the nozzle cone half angle is 19° .

is limited (about 1 by 1 km). The dotted line is the estimated total radiation from the sustainer plume.

The sustainer or second stage almost always has a larger nozzle exit area ratio than the first or booster stage, and its plume gases at the nozzle exit have a substantially lower exit pressure. When the plume gas exit pressure is close to the ambient air pressure at altitude, the initial shape of the sustainer stage propulsion system plume will be nearly cylindrical and similar in shape to the initial booster plume shape, but smaller. The initial sustainer plume size and radiation intensity are small compared to the final booster plume, and this is in part responsible for the initial trough in the curve of the sustainer propulsion system in Fig. 20–3. As the mixing of air and plume diminishes with altitude, the emissions due to afterburning also diminish, and this is also partly responsible for the trough. As altitude increases further, the plume of the sustainer propulsion system spreads out and forms a larger body of radiating gas—hence more overall intensity of radiation.

At high altitude (above about 170 km) the plume expands further and eventually only the intrinsic core (one half or one and one half Mach diamonds) has a strong enough radiation to be measured by a remote sensor. (Ref. 20–4).

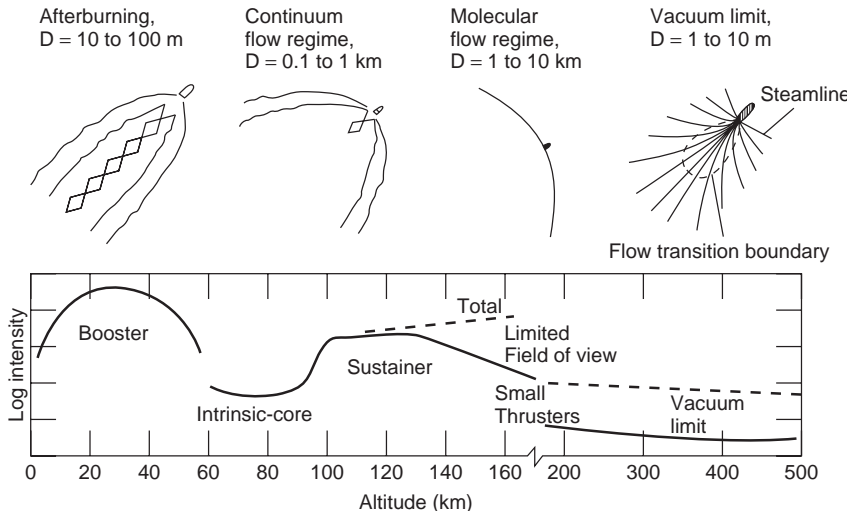


FIGURE 20–3. For a three-stage ascending rocket vehicle the plume radiation intensity from the three propulsion systems will vary with thrust level or mass flow, altitude, propellant combination, and gas temperatures within the plume. The four sketches are not drawn to the same scale. (Adapted with permission from Ref. 20–1.)

The multiple thrust chamber propulsion systems (typically 6 to 12 small thrusters) of the third stage (it could be a satellite or a multiple warhead upper stage) have much lower thrusts and even much smaller plumes than the other two stages, and thus their radiation intensities are the lowest. The only portion of the plumes hot enough to emit significant radiation is the inviscid core just downstream of the nozzle exit. Also radiation can come from the very hot gases in the small combustion chambers, but it can only be observed within a narrow angle through its nozzle. The radiations from these small thrusters are difficult to observe, because the intensity is small and often difficult to distinguish from the background radiation from the earth.

The booster and sustainer vehicles both operate in that part of the atmosphere where *continuum flow* prevails; that is, the mean free paths of the molecular motions are relatively small, frequent collisions between molecules occur, the gases follow the basic gas laws, and they can experience compression or expansion waves. As higher altitude is reached, the continuum regime changes into a *free molecular flow* regime, where there are fewer molecules per unit volume and the mean free path of the molecules between collisions becomes larger than the key dimension of the vehicle (e.g., length). Here the plume spreads out even more, some reaching diameters in excess of 10 km. Only the exhaust gases close to the nozzle exit experience continuum flow conditions, which allows the streamlines in the flow to spread out by means of successive Prandtl–Meyer expansion waves; once the gas reaches the boundary shown by the elliptical dashed line in the last sketch on the right in Fig. 20–3, the flow inside the dashed line will be in the

free molecular flow regime and molecules will continue to spread out in straight lines into space. The phenomenology of rocket exhaust plumes as seen from a space-based surveillance system is described in Ref. 20–1.

Spectral Distribution of Radiation

Gas species radiate specific narrow bands of the spectrum. The primary radiation emissions from most of the plume gases are usually in narrow bands of the infrared spectrum, to a lesser extent narrow bands in the ultraviolet spectrum, with relatively little energy in the visible spectrum. The emissions depend on the size, particular propellants, their mixture ratio, and their respective exhaust gas compositions. For example, the exhaust from the liquid hydrogen–liquid oxygen propellant combination contains mostly water vapor and hydrogen, and with a minor percentage of oxygen and dissociated species. Its radiation is strong in specific wavelength bands characteristic of the emissions from these hot gases (such as 2.7 and 6.3 μm , water—irradiated region) and 122 nanometers (hydrogen—ultraviolet region). As shown in Fig. 20–4, the hydrogen–oxygen plume is essentially transparent or colorless, since there are no strong emissions in the visible segment of the spectrum. The visible radiation from the white Mach diamonds are due to chemical reactions of the minor species O₂, OH, H, or O in the hot center region. The propellant combination of nitrogen tetroxide with methylhydrazine fuel gives strong emissions in the infrared region; in addition to the strong emissions for H₂O and hydrogen mentioned previously, there are strong emissions for CO₂ at 4.7 μm , CO at 4.3 μm , and weaker emission in the ultraviolet (UV) and visible ranges (due to bands of CN, CO, N₂, NH₃, and other intermediate and final gaseous reaction products). This gives it a pink orange–yellow color, but the plume is still partly transparent.

The exhausts of many solid propellants and some liquid propellants contain also *solid particles* and some contain also *condensed liquid droplets*. In this book the term “particulate” covers both types. In Tables 5–8 and 5–9 examples of solid propellant were given that had about 10% of small particles as aluminum oxide (Al₂O₃) in their incandescent white exhaust plumes; some kerosene-burning liquid propellants and many solid propellants have a small percentage of soot or small carbon particles in their exhaust. Receeding thermal insulation of solid propellant rocket motors can also contribute solid carbon particles to the exhausts. The radiation spectrum from hot solids is a continuous one, which peaks usually in the infrared (IR) region, but it also has strong emissions in the visible or UV region; this continuous spectrum is usually stronger in the visible range than the narrow-band emissions from the gaseous species in the plume. Afterburning in the mixing layer increases the temperature of the particles by several hundred degrees and intensifies their radiation emissions. Even with only 2 to 5% solid particles, the plumes radiate brilliantly and are therefore very visible to the eye. However, these particles in the outer layers of the plume obscure the central core and the shock wave patterns can no longer be observed.

The visible radiation of plumes from double-base propellant can be reduced or suppressed by adding a small amount (1 to 3%) of potassium compound. With

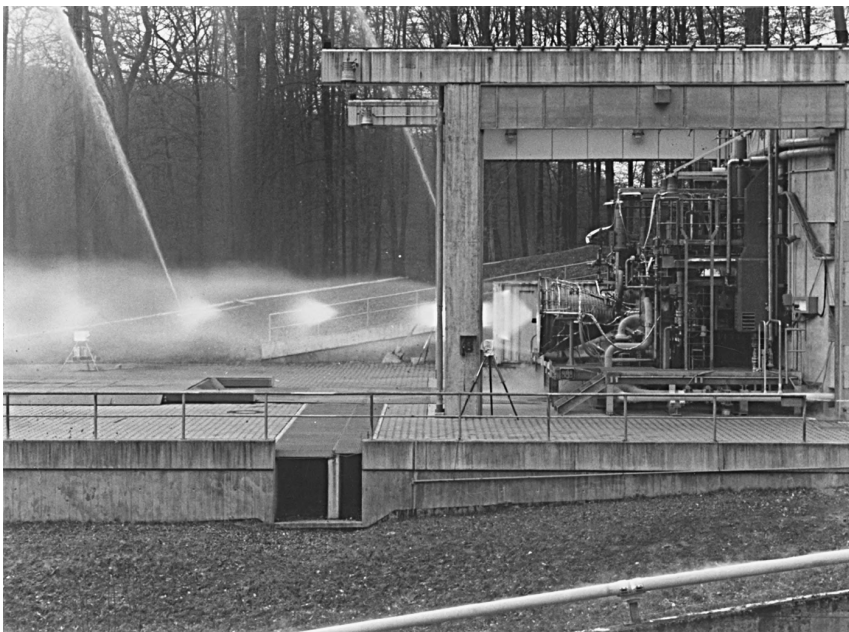


FIGURE 20–4. Visible plume created by the oxygen–hydrogen propellants of the Vulcain 60 thrust chamber, with a specific impulse of 439 sec at altitude, a nozzle expansion area ratio of 45, and a mixture ratio of 5.6. The upstream portions of the diamonds of the multiple shock wave patterns are visible in the core of the plume because of emissions from reacting minor species. (Courtesy of EADS Astrium, Germany.)

composite propellants the control of visible emissions by additives has not been as effective.

The distribution of solid small particles is far from uniform. Reaction products of many propellant combinations are not all gas, but contain *small solid particles* and/or *small condensed liquid droplets*. Figure 20–5 shows a simple sketch of two plumes one with solid particles shown in the lower half and another with condensed small liquid droplets in the upper half. The continuum radiation emissions energy from hot solid particles in the rocket exhaust is usually higher and often more visible than that of all the gaseous species in the exhaust. These small particulates (defined here as both condensed droplets and solid particles) cannot expand and they are accelerated or dragged along by the gas flow, but their velocities are always smaller than the higher velocity local gases. Large solid particles have more inertia than the smaller ones and it is difficult to change their direction. When the plume spreads out, a small portion of the gas can be turned to flow at more than a right angle to the plume axis, but the solid particles can only be turned through a small angle (perhaps 5° to 30°). They do not reach the outer boundary of the plume in Fig. 20–5. The central area of the plume contains essentially all the larger solid particles, and it is surrounded by an annular region with contains a few larger particles, but mostly medium sizes particles. Most of

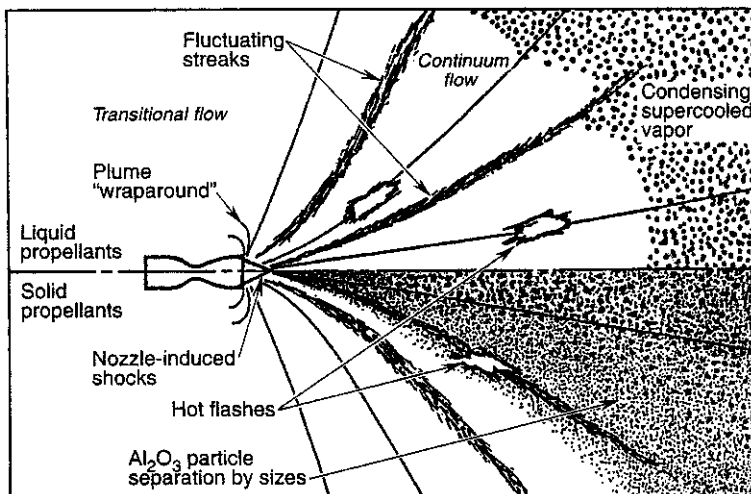


FIGURE 20–5. Simplified diagram of particulates in the plume flow at altitude. The upper half shows the condensation of gases into small liquid droplets and the lower half shows the plume from a solid motor with aluminum oxide solid small particles near the centerline of the plume. (Used with permission from Ref. 20–1.)

the smaller solid particles are in the next annular flow region. The outer region of the plume contains very few or no solid particles.

The mechanism with condensed liquid droplets is somewhat different. Certain gases condense to form liquid droplets at a particular liquefying temperature, irrespective of the location or the stream line within the plume. As the gases expand in the plume, they are cooled dramatically and they also absorb heat from the hot particulates. Therefore the distribution of condensed droplets is relatively uniform in the plume. A very small mass fraction of the gases deflect more than 90°, “wrap around” the nozzle exit flange, and flow forward.

In the upper half of Fig. 20–5 it can be seen that super-cooled water vapor can actually condense downstream from the nozzle exit into liquid droplets, presumably by homogeneous nucleation. The principal observable effect would be to scatter sunlight. The lower half of this figure shows solid alumina particles. Some of the larger particles can persist through the nozzle into the plume before solidifying by radiation cooling (Refs. 20–1 and 20–4).

Plumes with particulates remain visible by scattered sun light for a relatively long time even after the vehicle has gone. They can be shifted into different directions by local winds. The smoke or vapor trail marks the path of the vehicle that has just passed. Eventually the plume cools down, diffuses or mixes with more air, will no longer be visible, and is assimilated into the atmosphere.

Plumes frequently have some fluctuating visible hot streaks along the stream lines. They are hot moving flashes, pockets of more intense radiation, or locally hotter mixtures of gases as seen in Fig. 20–5. These hot local moving gas

anomalies originate in the unsteady combustion and injection processes in the combustion chamber and also are caused by turbulence. See Ref. 20–1.

The total radiation from the plume gases heats adjacent vehicle or propulsion system components. The prediction of radiative emission requires an understanding of the plume and the absorption of radiation by intervening atmospheric or plume gases (see Refs. 20–1 and 20–7). The heat transferred from the plume to vehicle components (by radiation and some by convection) will depend on the propellant combination, the nozzle configuration, the vehicle geometry, size, the number of nozzles, the trajectory, altitude, and the secondary turbulent flow around the nozzles and the tail section of the vehicle.

The observed or measured values of the radiation emissions have to be corrected. The signal strength diminishes as the square of the distance between the plume and the observation station, and its observed magnitude can change tremendously during a flight. The attenuation is a function of wavelength, rain, fog or clouds, the mass of air and gases between the hot part of the plume and the observing location, and depends on the flight vector direction relative to the line of sight. The total emission is a maximum when seen at right angles to the plume (see Refs. 20–1, 20–3, and 20–7). Radiation measurements can be biased by background radiations (important in satellite observation) or Doppler shift.

Multiple Nozzles

It is common to have more than one propulsion system operating at the same time, or more than one nozzle sending out hot exhaust gas plumes. For example, the Space Shuttle has three main engines and two solid rocket boosters running simultaneously. The interference and impingement of these plumes with one another will cause regions of high temperature in the combined plumes and therefore larger emissions, but the emissions will no longer be axisymmetrical. Also, the multiple nozzles can cause distortions in the airflow near the rear end of the vehicle and influence the vehicle drag and augment the hot backflow from the plume locally. With multiple propulsion systems the plumes impinge locally with each other and can create local hot spots. At high altitudes the plumes of multiple propulsion systems appear to merge into each other; analytically it can at times be approximated as that from an equivalent single nozzle providing the total flow, but with the properties and characteristics of the individual nozzles (Ref. 20–4).

Plume Signature

This is the term used for all the characteristics of the plume in the infrared, visible, and ultraviolet spectrum, its electron density, smoke or vapor, for a particular vehicle, mission, rocket propulsion system, and propellant (see Refs. 20–3, 20–9, and 20–10). In many military applications it is desirable to reduce the plume signature in order to minimize being detected or tracked. The initial stagnation temperature of the nozzle exit gas is perhaps the most significant factor influencing plume signature. As plume temperatures increase, higher levels of

radiation and radio-frequency interaction will occur. Emissions can be reduced if a propellant combination or mixture ratio with a lower combustion temperature is selected; unfortunately, this usually gives a lower performance. Ways to reduce smoke are described later in this Chapter. The plume signature is today often specified as a requirement for a new or modified rocket-propelled military flight vehicle, and it imposes limits on spectral emissions in certain regions of the spectrum and on the amount of acceptable smoke.

The atmosphere absorbs energy in certain regions of the spectrum. For example, the air contains some carbon dioxide and water vapor. These molecules absorb and attenuate the radiation in the frequency bands peculiar to these two species. Since many plume gases contain a lot of CO₂ or H₂O, the attenuation within the plume itself can be significant. The plume energy or intensity, as measured by spectrographic instruments, has to be corrected for the attenuation of the intervening air or plume gas.

Vehicle Base Geometry and Recirculation

The geometry of the nozzle exit(s) and the flight vehicle's tail or aft base have an influence on the plume. Figure 20–6 shows a single nozzle exit whose diameter is almost the same as the base or tail diameter of the vehicle body. If these two diameters are not close to each other, then a flat doughnut-shaped base or tail surface will exist. In this region the high-speed combustion gas velocity is usually larger than the air speed of the vehicle (which is about the same as the local air velocity relative to the vehicle) and an unsteady flow vortex-type recirculation will occur. This greatly augments the afterburning, the heat release to the base, and usually creates a low pressure on this base. This lower pressure in effect increases the vehicle's drag.

The airflow pattern at the vehicle tail can be different with different tail geometries, such as cylinder (straight), a diminishing diameter, or an increasing diameter conical shape, which helps to maintain the vehicle's aerodynamic stability. The airflow pattern and the mixing layer change dramatically with angle of attack, tail fins, or wings, causing an unsymmetrical plume shape. Flow separation of the airflow can also occur. In some cases the recirculation of fuel-rich exhaust gas mixed with air will ignite and burn; this dramatically increases the heat transfer to the base surfaces and causes some changes in plume characteristics.

Compression and Expansion Waves

A *shock wave* is a surface of discontinuity in a supersonic flow. In rocket plumes it is the very rapid change of kinetic energy to potential and thermal energy within that very thin wave surface. Fluid crossing a stationary shock wave rises suddenly and irreversibly in pressure and decreases in velocity. When it passes through a shock wave surface that is perpendicular or normal to the incoming

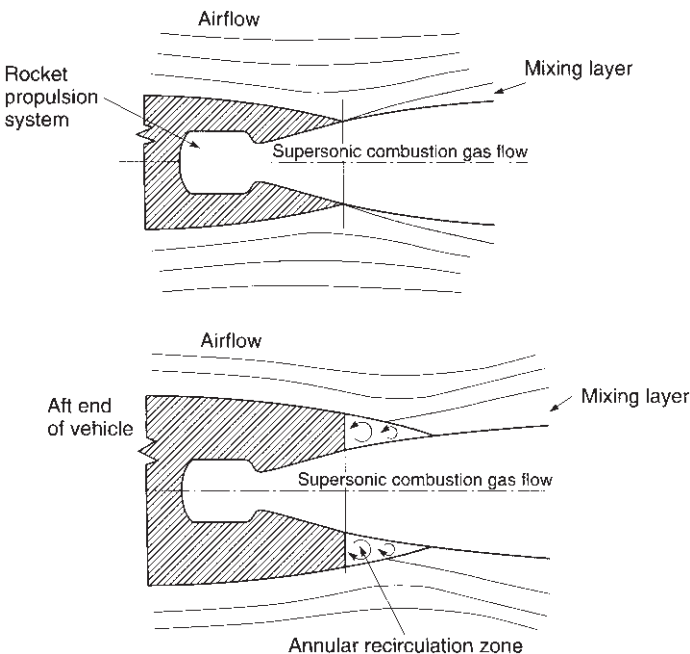


FIGURE 20–6. Diagrams of flow patterns around two different boat tails or vehicle aft configurations, with and without hot gas recirculation.

supersonic flow, then there is no change in flow direction. Such a normal shock produces the largest increase in pressure (and local downstream temperature) and is known as a *normal shock wave*. The flow velocity behind a normal shock wave is subsonic. When the incoming flow is at an angle less than 90° to the shock wave surface, it is known as a *weak compression wave* or as an *oblique shock wave*. Figure 20–7 illustrates the flow relationships and shows the angle of flow change. The temperature of the gas immediately behind a normal shock wave approaches the stagnation temperature of the combustion chamber. Here the radiation increases greatly. Also, here (and in other hot plume regions) dissociation of gas species and chemical luminescence (emission of visible light) can occur, as can be seen (downstream of strong shock waves) in Fig. 20–4.

The behavior of gas expansion in the supersonic flow has a fairly similar geometric relationship. It occurs at a surface where the flow undergoes a Prandtl–Meyer *expansion wave*, which is a surface where pressure is reduced and velocities are increased. Often there is a series of weak expansion waves next to each other; this occurs outside the lip of the diverging nozzle exit section when the nozzle exit gas pressure is higher than the ambient air pressure, as shown in Fig. 20–1.

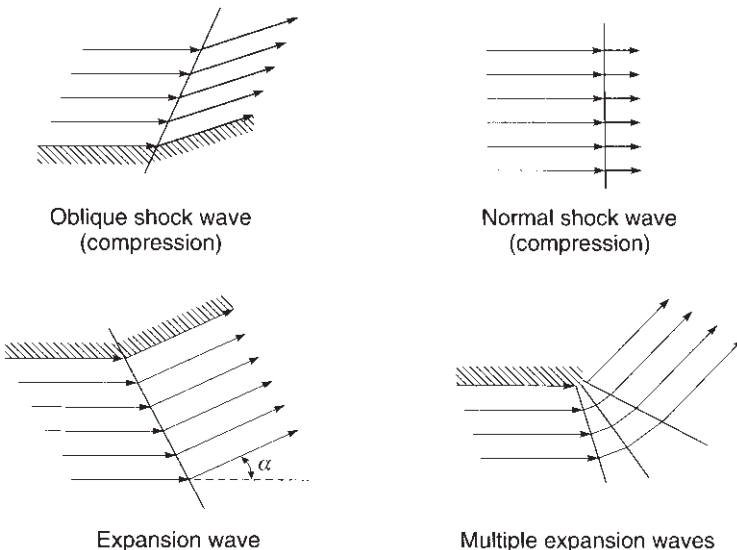


FIGURE 20–7. Simplified diagrams of oblique shock wave or compression wave, normal shock wave, and expansion wave. The change in the length of the arrows is an indication of the change in gas velocity as the flow crosses the wave front.

The plume from hydrogen–oxygen liquid propellant combustion consists mostly of superheated water vapor and hydrogen gas and is basically invisible. However, it is faintly visible because of the chemical reactions of minor species in the hot zones that are believed to be responsible for the pale pink orange and white skeletal wave pattern. The patterns are shown in Table 20–2 and Fig. 20–4.

The supersonic gas flow out of the nozzle exit is undisturbed until it changes direction in a wave front or goes through a normal shock. Diamond-shaped patterns are formed by compression and expansion wave surfaces. These patterns (shown in Table 20–2 and Fig. 20–4) then repeat themselves and are clearly visible in largely transparent plumes, such as those from hydrogen–oxygen or alcohol–oxygen propellant combinations. The pattern becomes weaker with each succeeding wave. The mixing layer acts as a reflector, because an expansion wave is reflected as a compression wave.

The interface surface between the rocket exhaust plume gas and the air flowing over the vehicle (or the air aspirated by the high-velocity plume) acts as a free boundary. Oblique shock waves are reflected at a free boundary as an opposite wave. For example, an oblique compression wave is reflected as an oblique expansion wave. This boundary is not usually a simple surface of revolution, but an annular layer, sometimes called a slip stream or mixing layer and it is distorted by turbulence.

20.2. PLUME EFFECTS

Smoke and Vapor Trails

Smoke is objectionable in a number of military missiles. It interferes with the transmission of optical signals, such as with a line-of-sight or electro-optical guidance system. Smoke would also hamper the vision of a soldier who guides a wire-controlled antitank weapon. Smoke, or a vapor trail, allows easy and rapid detection of a missile being fired, and visually tracking the flight path can reveal a covert launch site. Smoke is produced not only during rocket operation, but also by chuffing, the irregular combustion of solid propellant remainders after rocket cutoff. Chuffing, described in Chapter 14, produces small puffs of flame and smoke at frequencies of perhaps 2 to 100 Hz.

Primary smoke is a suspension of many very small solid particles in a gas, whereas secondary smoke is a set of condensed small liquid droplets suspended in a gas, such as condensed vapor trails, fog, or clouds. Secondary smoke can form in all-gas plumes and also in plumes that contain primary smoke. Many propellants leave visible trails of smoke and/or vapor from their plumes during powered rocket flight (see Refs. 20–3, 20–8, and 20–9). These trails are shifted by local winds after the vehicle has passed. They are most visible in the daytime, because they depend on reflected or scattered sunlight. The solid particles that form the primary smoke are mainly aluminum oxide (Al_2O_3 , typically 0.1 to 3 μm diameter) in composite solid propellants. Other solid particles in the exhaust of solid propellant are unburned aluminum, zirconium or zirconium oxide (from combustion stabilizer), or iron or lead oxides (in burn-rate catalyst). Carbon particles or soot can be formed from the thermal insulation of various solid propellants grains and some liquid propellants using hydrocarbon fuels.

During the external expansion of rocket exhaust plume gases the gas mixture is cooled by radiation, gas expansion, and convection with colder ambient air to below its dew-point temperature, where the water vapor condenses. Of course, this depends on local weather conditions. If the ambient temperature is low (e.g., at high altitude) and/or if the gas expands to low temperatures, the water droplets can freeze to form small ice crystals or snow. At high altitude, CO_2 , HCl , and other gases can also condense. Many rocket exhaust gases contain between 5 and 35% water, but the exhaust from the liquid hydrogen/liquid oxygen propellant combination can contain as much as 80%. If the exhaust contains tiny solid particles, these then act as nuclei upon which water vapor can condense, thus increasing the amount of nongaseous material in the plume, making the plume even more visible.

If reducing smoke in the plume is important to the mission, then a *reduced-smoke solid propellant* or a *minimum-smoke propellant* is often used. Alternatively a liquid propellant combination, known not to form small carbon particles, may be selected. They are described in Chapters 7 and 13. Even then, a secondary smoke trail can be formed under cold-weather and high-humidity conditions. However, under some weather conditions it will be difficult to see a trail containing vapor only.

Toxicity

The exhaust gases from many rocket propulsion systems contain toxic and/or corrosive gas species, which can cause severe health hazards and potential environmental damage near launch or test sites. Accidental spills of some liquid oxidizers, such as nitrogen tetroxide or red fuming nitric acid, can create toxic, corrosive gas clouds, which have higher density than air and will stay close to the ground. Exhaust gases such as CO or CO₂ present a health hazard if inhaled in concentrated doses. Gases such as hydrogen chloride (HCl) from solid propellants using a perchlorate oxidizer, nitrogen dioxide (NO₂), nitrogen tetroxide (N₂O₄), or vapors of nitric acid (HNO₃) have relatively low levels of allowable inhalation concentration before health damage can occur. Chapter 7 lists some of the safe exposure limits. The potential damage increases with the concentration of the toxic species in the exhaust, the mass flow or thrust level, and the duration of the rocket firing at or near the test/launch site.

Dispersion by wind and diffusion and dilution with air can reduce the concentrations of toxic materials to tolerable levels within a few minutes, but this depends on the quantity and the local weather conditions, as explained in Chapter 21. Careful attention is therefore given to scheduling the launch or test operations at times when the wind will carry these gases to nearby uninhabited areas. For very highly toxic exhaust gases (e.g., those containing beryllium oxide or certain fluorine compounds), and usually for relatively small thrust levels, the exhaust gases in static test facilities are captured, chemically treated, detoxified, and purified before release into the atmosphere.

Noise

Acoustical noise is an unavoidable by-product of thrust; it is particularly important in large launch vehicles with large propulsion systems. It is a primary design consideration in the vehicle and in much of the ground-support equipment, particularly electronic components. Besides being an operational hazard to personnel in and around rocket-propelled vehicles, it can be a severe annoyance to communities near rocket test sites. The acoustic power emitted by the Saturn V space flight vehicle at launch is about 2×10^8 W, enough to light up about 200,000 average homes if it were available as electricity.

Acoustic energy emission is mainly a function of exhaust velocity, mass of gas flow, exhaust gas density, and the velocity of sound in the quiescent medium. In these terms, the chemical rocket is the noisiest of all aircraft and missile propulsion devices. Sound intensity is highest near the nozzle exit and diminishes with the square of the distance from the source. Analytical models of noise from a rocket exhaust usually divide the plume into two primary areas, one being upstream of the shock waves and one being downstream (subsonic), with high-frequency sound coming from the first and low-frequency from the second. The shock wave itself is a generator of sound, as is the highly turbulent mixing of the high-velocity exhaust with its relatively quiescent surroundings. Sound emission is normally measured in terms of microbars (μbar) of *sound pressure*, but is also

expressed as *sound power* (W), *sound intensity* (W/ft^2), or *sound level* (decibels, dB). The relationship that exists among a decibel scale, the power, and intensity scales is difficult to estimate intuitively since the decibel is a logarithm of a ratio of two power quantities or two intensity quantities. Further, expression of a decibel quantity must also be accompanied by a decibel scale reference, for example, the quantity of watts corresponding to 0 dB. In the United States, the most common decibel scale references 10^{-13} W power, whereas the European scale references 10^{-12} W.

A large rocket can generate a sound level of about 200 dB (reference 10^{-13} W), corresponding to 10^7 W of sound power, compared to 140 dB for a 75-piece orchestra generating 10 W. Reducing the sound power by 50% reduces the value by only about 3 dB. In terms of human sensitivity, a 10-dB change usually doubles or halves the noise for the average person. Sound levels above 140 dB frequently introduce pain to the ear and levels above 160 become intolerable. In small propulsion systems the noise level is very much lower and often can be ignored. There is a remarkable similarity between the spectra of infrared and acoustic radiation (Ref. 20–4).

Spacecraft Surface Contamination

Contamination of sensitive surfaces of a spacecraft by rocket exhaust products can be a problem to vehicle designers and users. When deposited on a surface it can degrade the function of surfaces, such as solar cells, optical lenses, radiators, windows, thermal-control coatings, and mirrored surfaces. Propellants that have condensed liquids or solid particles in their exhaust appear to be more troublesome than propellants with mostly gaseous products, such as oxygen–hydrogen or monopropellant hydrazine. Plumes from most solid propellants contain contaminating species. Practically all the investigative work has been concerned with small storable liquid propellant attitude control pulse motors in the thrust range 1.0 to 500 N, the type commonly used for controlling vehicle attitude and orbit positioning over long periods of time. Deposits of hydrazinium nitrate and other materials have been found. The accumulation of exhaust products on surfaces is a function of many variables, including the propellants, combustion efficiency, combustion pressure, nozzle expansion ratio, surface temperature, and rocket–vehicle interface geometries. The prediction of exhaust contamination of spacecraft surfaces is only partly possible through analytical calculations. Reference 20–10 provides a comprehensive analytical model and computer program for liquid bipropellant rockets.

Another effect of clouds of condensed species (either tiny liquid droplets or solid particles) is to scatter sunlight and cause solar radiation to be diverted to optical instruments on the spacecraft, such as cameras, telescopes, IR trackers, or star trackers; this effect can cause erroneous instrument measurements. The scatter depends on the plume location relative to the instruments, the propellant, the density and size of particulates, the sensitive optical frequency, and the surface temperature of the instrument.

Radio Signal Attenuation

Rocket exhaust plumes generally interfere with the transmission of radio-frequency signals that must pass through the plume in the process of guiding the vehicle, radar detecting, or communicating with it. Solid propellant exhaust plumes usually cause more interference than liquid rocket engine plumes. Signal attenuation is a function of free electron density and electron collision frequency. Given these two parameters for the entire plume, the amount of attenuation a signal experiences in passing through the plume can be calculated. Figure 20–8 shows the minimum plume model sufficient for predicting signal attenuation that contains contours of constant electron density and electron collision frequency for momentum transfer. Free-electron density and activity in the exhaust plume are influenced by many factors, including the propellant formulation, propellant alkali impurities, exhaust temperature, motor size, chamber pressure, flight speed and altitude, and the distance downstream from the nozzle exit. Methods have been developed for analyzing (with computers) the physical and chemical composition, including electron density, and the attenuation characteristics of exhaust plumes (Refs. 20–11 to 20–13).

The relationship between several influential motor and vehicle design factors can be summarized from experience with typical solid propellant rockets as follows:

1. The presence of alkali metal impurities increases attenuation; changing the impurity level of potassium from 10 to 100 ppm increases the relative attenuation some 10-fold at low altitude. Both potassium (≈ 150 ppm) and sodium (≈ 50 ppm) are impurities in commercial-grade nitrocellulose and ammonium perchlorate.

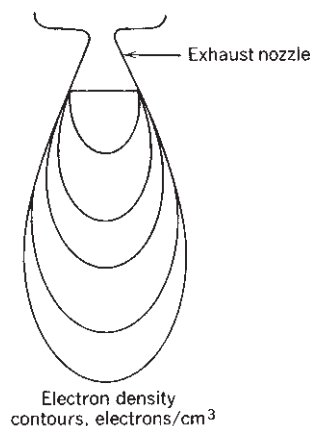


FIGURE 20–8. Exhaust plume model for predicting attenuation of radio communications signals. The contours shown are for either equal electron density or electron collision frequency; the highest values are near the nozzle exit.

2. The percentage of aluminum fuel is a major influence; increasing the percentage from 10 to 20% increases the attenuation fivefold at sea level and three- to fourfold at 7500 m altitude.
3. Increasing the chamber pressure for a given aluminized propellant from 100 to 2000 psi reduces the relative attenuation by about 50%.
4. Attenuation varies with the distance downstream from the nozzle exit plane and can be four to five times as great as at the nozzle exit plane, depending on the flight altitude, nozzle geometry, oxidizer-to-fuel ratio, flight velocity, altitude, and other parameters.

For many solid rocket applications, attenuation of radio or radar signal strength by the exhaust plume is no problem. When it is, attenuation can usually be kept at acceptable levels by controlling the level of alkali impurities in propellant ingredients and by using nonmetal fuels or a low percentage (< 5%) of aluminum. Motors with high expansion ratio nozzles help, since electrons combine with the positive ions as the exhaust temperature falls.

The electrons in the plume greatly increase its radar cross section, and hot plumes can readily be picked up with radar. The plume is usually a stronger radar reflector than the flight vehicle. A radar homing missile seeker would focus on the plume and not the vehicle. A reduction of the plume cross section is desirable (lower gas temperature, less sodium impurities).

Plume Impingement with Structures

In most reaction control systems there are several small thrusters and they are pointed in different directions. Although small thrusters have small plumes and the intensity of their radiation emissions is much lower, they have caused severe damage. There have been cases where the plumes of some of these thrusters have impinged upon a space vehicle surface, such as extended solar cell panels, radiation heat rejection surfaces, or aerodynamic control surfaces. This is more likely to happen at high altitude, where the plume diameters are large. This can lead to the overheating of these surfaces and to unexpected turning moments.

Also, during stage separation, there have been occasions where the plume of the upper stage impinges on the lower vehicle stage. This can cause overheating and impact damage not only to the lower stage (being separated), but by reflection also to the upper stage. Other examples are docking maneuvers or the launching of multiple rockets (nearly simultaneously) from a military barrage launcher. The plume of one of the rocket missiles impinges on another flying missile and causes it to experience a change in flight path, often not hitting the intended target.

20.3. ANALYSIS AND MATHEMATICAL SIMULATION

The complicated structure, the behavior, and many of the physical phenomena of plumes have been simulated by mathematical algorithms, and a number of

relatively complex computer programs exist (see Refs. 20–1 to 20–3 and 20–15 to 20–19). Although there has been remarkable progress in using mathematical simulations of plume phenomena, the results of such computer analyses are not always reliable or useful for making predictions of many of the plume characteristics; however, the models help in understanding the plumes and in extrapolating test results to different conditions within narrow limits. There are some physical phenomena in plumes that are not yet fully understood.

All simulations are really approximations, to various degrees; they require simplifying assumptions to make a reasonable mathematical solution possible, and their field of application is usually limited. They are aimed at predicting different plume parameters, such as temperature or velocity or pressure profiles, radar cross section, heat transfer, radiations, condensation, deposits on optical surfaces, impact forces, or chemical species. The analyses are usually limited to separate spatial segments of the plume (e.g., core, mantle, supersonic versus subsonic regions, continuum versus free molecular flow, near or far field), and many have different assumptions about the dynamics or steadiness of the flow (many neglect turbulence effects or the interaction between boundary layers and shock waves). Most are suitable only for steady-state conditions. The algorithms are also different in the treatment of chemical reactions, solids content, energy releases, composition changes within the plume, different flight and altitude regimes, the interactions with the airflow and the vehicle, or selected regions of the spectrum (e.g., IR only). Many require assumptions about particle sizes, their amounts, spatial and size distribution, gas velocity distribution, the geometry and boundaries of the mixing layer, or the turbulence behavior. The mathematical models are complex and can use one-, two-, or three-dimensional models. The analysis of a plume often requires using more than one model to solve for different predictions. Several models are given in Refs. 20–14 to 20–18. Many solutions are based in part on extrapolating measured data from actual plumes to guide the analyses. The specific analytical approaches are beyond the scope of this book and their mathematical resolutions are the domain of experts in this field. There are validated computer programs for a number of plume phenomena. Many are proprietary or limited in distribution.

The actual measurements on plumes during static and flight tests are used to verify the theories and they require highly specialized instrumentation, careful calibrations and characterization, skilled personnel, and an intelligent application of various correction factors. Extrapolating the computer programs to regions or parameters that have not been validated has often given poor results.

PROBLEMS

1. List at least two parameters that are likely to increase total radiation emission from plumes, and explain how they accomplish this. For example, increasing the thrust increases the radiating mass and size of the plume.
2. Look up the term *chemiluminescence* in a technical dictionary or chemical encyclopedia; provide a definition and explain how it can affect plume radiation.

3. If a high-altitude plume is seen from a high-altitude balloon, its apparent radiation intensity diminishes with the square of the distance between the plume and the observation platform and as the cosine of the angle of the flight path tangent with the line to the observation station. Establish your own trajectory and its relative location to the observation station. For a plume of an ascending launch vehicle, make a rough estimate of the change in the relative intensity received by the observing sensor during flight. Neglect atmospheric absorption of plume radiation and assume that the intensity of emitted radiation stays constant.

REFERENCES

- 20–1. F. S. Simmons, *Rocket Exhaust Plume Phenomenology*, Aerospace Press, The Aerospace Corporation, El Segundo 2000.
- 20–2. S. M. Dash, “Analysis of Exhaust Plumes and Their Interaction with Missile Airframes,” in M. J. Hemsch and J. N. Nielson (Eds.), *Tactical Missile Aerodynamics*, a book in the series of *Progress in Astronautics and Aeronautics*, Vol. 104, AIAA, Washington, DC, 1986.
- 20–3. A. C. Victor, “Solid Rocket Plumes,” Chapter 8 of: G. E. Jensen and D. W. Netzer (Eds.), *Tactical Missile Propulsion*, a book in the series of *Progress in Astronautics and Aeronautics*, Vol. 170, AIAA, 1996.
- 20–4. Personal communications from Frederick S. Simmons of The Aerospace Corporation, 2008
- 20–5. S. M. Yahya, *Fundamentals of Compressible Flow*, 2nd revised printing, Wiley Eastern Limited, New Delhi, 1986.
- 20–6. R. D. McGregor, P. D. Lohn, and D. E. Haflinger, “Plume Impingement Study for Reaction Control Systems of the Orbital Maneuvering Vehicle,” AIAA Paper 90-1708, June 1990.
- 20–7. R. B. Lyons, J. Wormhoudt, and C. E. Kolb, “Calculation of Visible Radiations from Missile Plumes,” in *Spacecraft Radiative Heat Transfer and Temperature Control*, a book in the series of *Progress in Astronautics and Aeronautics*, Vol. 83, AIAA, Washington, DC, June 1981, pp. 128–148.
- 20–8. *Rocket Motor Plume Technology*, AGARD Lecture Series 188, NATO, June 1993.
- 20–9. *Terminology and Assessment Methods of Solid Propellant Rocket Exhaust Signatures*, AGARD Advisory Report 287, NATO, February 1993.
- 20–10. R. J. Hoffman, W. D. English, R. G. Oeding, and W. T. Webber, “Plume Contamination Effects Prediction,” Air Force Rocket Propulsion Laboratory, December 1971.
- 20–11. L. D. Smoot and D. L. Underwood, “Prediction of Microwave Attenuation Characteristics of Rocket Exhausts,” *Journal of Spacecraft and Rockets*, Vol. 3, No. 3, March 1966, pp. 302–309.
- 20–12. W. A. Wood and J. R. De More, “Microwave Attenuation Characteristics of Solid Propellant Exhaust Products,” AIAA Paper 65-183, February 1965.
- 20–13. A. Mathor, “Rocket Plume Attenuation Model,” AIAA Paper 2006-5323, June 2006.
- 20–14. I. Boyd, Modeling of Satellite Control Thruster Plumes, PhD thesis, Southampton University, England, 1988.

- 20–15. S. M. Dash and D. E. Wolf, “Interactive Phenomena in Supersonic Jet Mixing Plumes, Part I: Phenomenology and Numerical Modeling Technique,” *AIAA Journal*, Vol. 22, No. 7, July 1984, pp. 905–913.
- 20–16. S. M. Dash, D. E. Wolf, R. A. Beddini, and H. S. Pergament, “Analysis of Two Phase Flow Processes in Rocket Exhaust Plumes,” *Journal of Spacecraft*, Vol. 22, No. 3, May–June 1985, pp. 367–380.
- 20–17. C. B. Ludwig, W. Malkmus, G. N. Freeman, M. Slack, and R. Reed, “A Theoretical Model for Absorbing, Emitting and Scattering Plume Radiations,” in *Spacecraft Radiative Transfer and Temperature Control*, a book of the series of *Progress in Astronautics and Aeronautics*, Vol. 83, AIAA, Washington, DC, 1981, pp. 111–127.
- 20–18. A. M. Kawasaki, D. F. Coats, and D. R. Berker, “A Two-Phase, Two-Dimensional, Reacting, Parabolized Navier-Stokes Solver for the Prediction of Solid Rocket Motor Flow Fields,” AIAA Paper 92–3600, July 1992.

CHAPTER 21

ROCKET TESTING

21.1. TYPES OF TESTS

Before rocket propulsion systems are put into operational use, they are subjected to several different types of tests, some of which are outlined below in the approximate sequence in which they are normally performed.

1. Manufacturing inspection and fabrication tests on individual parts (dimensional inspection, pressure tests, X rays, leak checks, electric continuity, electromechanical checks, etc.).
2. Component tests (functional and operational tests on igniters, nozzles, insulation, valves, thrusters, controls, injectors, structures, etc.).
3. Static rocket propulsion system tests (with complete propulsion system) on a test stand: (a) complete propulsion system tests (under rated conditions, off-design conditions, with intentional variations in environment or calibration); (b) with liquid propellants a partial or simulated rocket operation (for proper function, calibration, ignition, operation—often without establishing full thrust or operating for the full duration); for a reusable or restartable rocket propulsion system this can include many starts, long-duration endurance tests, and postoperational inspections and reconditioning.
4. Static vehicle tests (when rocket propulsion system is installed in a restrained, nonflying vehicle or stage) on a vehicle static test stand.

5. Flight tests: (a) with a specially instrumented or new propulsion system in a developmental flight test vehicle; (b) with a production vehicle.

Each of these five types of tests can be performed on at least three basic types of programs:

1. Research on and development or improvement of a new (or modified) rocket engine or rocket motor, their propellants, materials, or components.
2. Evaluation of the suitability of a new (or modified) rocket engine or novel rocket motor for a specified application or for flight readiness.
3. Production and quality assurance of a rocket propulsion system.

The first two types of programs are usually concerned with a novel or modified device and often involve the testing and measurement of new concepts or phenomena using experimental rockets. The testing of a new solid propellant grain, the development of a novel control valve assembly, and the measurement of the thermal expansion of a nozzle exhaust cone during firing operation are examples.

Production tests concern themselves with the measurement of a few basic parameters on production propulsion systems to assure that the performance, reliability, and operation are within specified tolerance limits. If the number of units is large, the test equipment and instrumentation used for these tests are usually partly or fully automated and designed to permit the testing, measurement, recording, and evaluation in a minimum amount of time.

During the early development phases of a program, many special and unusual tests are performed on components and complete rocket systems to prove specific design features and performance characteristics. Special facilities and instrumentation or modification of existing test equipment are used. Examples are large centrifuges to operate propulsion systems under acceleration or variable frequency vibration equipment for shaking complete systems and components. During the second type of program, some special tests are usually conducted to determine the statistical performance and reliability of a rocket system by operating a number of units of the same design. During this phase tests are also made to demonstrate the ability of the rocket system to withstand extreme limits of the operating conditions, such as high and low ambient temperature, variations in fuel composition, changes in the vibration environment, or exposure to moisture, rain, vacuum, or rough handling during storage. To demonstrate safety, sometimes, intentional malfunctions, spurious signals, or manufacturing flaws are introduced into the propulsion system, to determine the capability of the control system or the safety devices to handle and prevent a potential failure.

Before an experimental rocket system can be flown in a vehicle it usually has to pass a set of *preliminary flight rating tests* aimed at demonstrating its safety, reliability, and performance. It is not a single test, but a series of tests under various specified conditions operating limits, and performance tolerances, simulated environments, and intentional malfunctions. Thereafter the rocket system may be

used in experimental flights. However, before it can be put into production, it usually has to pass another specified series of tests under a variety of rigorous specified conditions, known as the *qualification test* or *preproduction test*. Once a particular propulsion system has been *qualified*, or passed a qualification test, it is usually forbidden to make any changes in design, fabrication processes, or materials without going through a careful review, extensive documentation, and often also a requalification test.

The amount and expense of testing of components and complete propulsion systems has decreased greatly in the last few decades. The reasons are more experience with prior similar systems, fewer development engines and fewer tests, better sensors, better analytical model simulations, use of health monitoring systems to identify incipient damage, which saves hardware, and more confidence in predicting a number of failure modes and their locations. Validated computer programs have removed many uncertainties and obviated needs for tests. In some applications the number of firing tests has decreased by a factor of 10 or more.

21.2. TEST FACILITIES AND SAFEGUARDS

For chemical rocket propulsion systems, each test facility usually has the following major systems or components:

1. A *test cell* or *test bay* where the article to be tested is mounted, usually in a special test fixture. If the test is hazardous, the test facility must have provisions to protect operating personnel and to limit damage in case of an accident.
2. An *instrumentation system* with associated computers for sensing, maintaining, measuring, analyzing, correcting, and recording various physical and chemical parameters. It usually includes calibration systems and timers to accurately synchronize the measurements.
3. A *control system* for starting, stopping, and changing the operating conditions.
4. Systems for handling heavy or awkward assemblies, supplying (or removing) liquid propellant, and providing maintenance, security, and safety.
5. For highly *toxic propellants* and *toxic plume gases* it has been required to capture the hazardous gas or vapor (firing inside a closed duct system), remove almost all of the hazardous ingredients (e.g., by wet scrubbing and/or chemical treatment), allow the release of the nontoxic portion of the cleaned gases, and safely dispose of any toxic solid or liquid residues from the chemical treatment. With an exhaust gas containing fluorine, for example, the removal of much of this toxic gas can be achieved by scrubbing it with water that contains dissolved calcium; it will then form calcium fluoride, which can be precipitated and removed.
6. In some tests specialized test equipment and unique facilities are needed to conduct static testing under different environmental conditions or under

simulated emergency conditions. For example, high and low ambient temperature tests of large motors may require a temperature-controlled enclosure around the motor; a rugged explosion-resistant facility is needed for bullet impact tests of propellant-loaded missile systems and also for cook-off tests, where gasoline or rocket fuel is burned with air below a stored missile. Similarly, special equipment is needed for vibration testing, measuring thrust vector forces and moments in three dimensions, or determining total impulse for very short pulse durations at low thrust.

Most rocket propulsion testing is now accomplished in sophisticated facilities under closely controlled conditions. Modern rocket test facilities are frequently located several miles from the nearest community to prevent or minimize effects of excessive noise, vibrations, explosions, and toxic exhaust clouds. Figure 21-1 shows one type of an open-air test stand for vertically down-firing large liquid propellant thrust chambers (100,000 to 2 million pounds thrust). It is best to fire the propulsion system in a direction (vertical or horizontal) similar to the actual flight condition. Figure 21-2 shows a simulated altitude test facility for rockets of about 10.5 metric tons thrust force (46,000 lbf). It requires a vacuum chamber in which to mount the engine, a set of steam ejectors to create a vacuum, water to reduce the gas temperature, and a cooled diffuser. With the flow of chemical rocket propellant combustion gases it is impossible to maintain a high vacuum in these kinds of facilities; typically, between 15 to 4 torr (20 to 35 km altitude) can be maintained. This type of test facility allows the operation of rocket propulsion systems with high-nozzle-area ratios that would normally experience flow separation at sea-level ambient pressures.

Prior to performing any test, it is common practice to train the test crew and go through repeated dry runs, to familiarize each person with his or her responsibilities and procedures, including the emergency procedures.

Typical personnel and plant security or safety provisions in a modern test facility include the following:

1. Concrete-walled blockhouse or control stations for the protection of personnel and instruments (see Fig. 21-3) remote from the actual rocket propulsion location.
2. Remote control, indication, and recording of all hazardous operations and measurements; isolation of propellants from the instrumentation and control room.
3. Automatic or manual emergency water deluge and fire-extinguishing systems.
4. Closed circuit television systems for remotely viewing the test.
5. Warning signals (siren, bells, horns, lights, speakers) to notify personnel to clear the test area prior to a test, and an all-clear signal when the conditions are no longer hazardous.

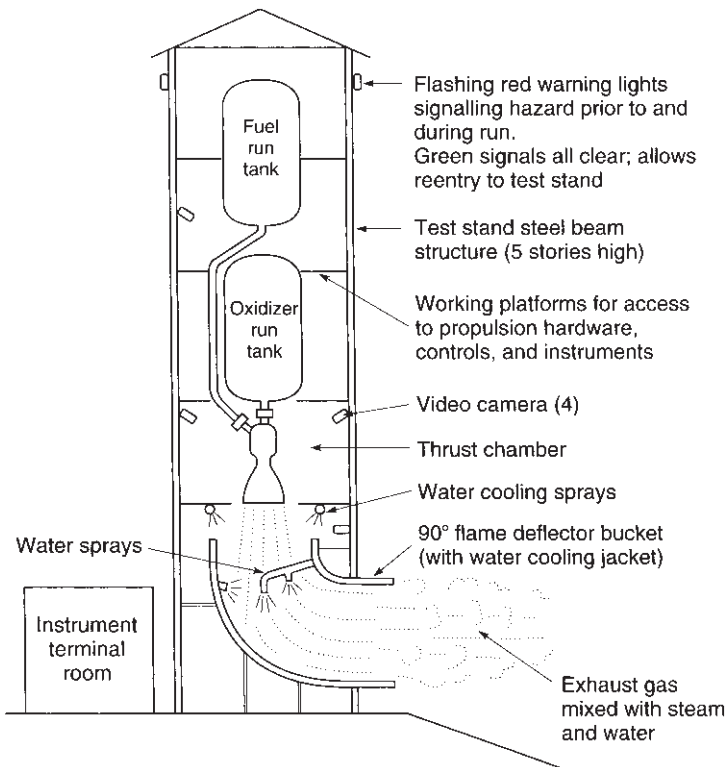


FIGURE 21–1. Simplified sketch of a typical static test stand for a large liquid propellant thrust chamber firing vertically downward. Only a small part of the exhaust plume (between the nozzle exit and flame bucket entrance) is visible. The flame bucket turns the exhaust gas plume by 90° (horizontal) and prevents the flame from digging a hole in the ground. Not shown here are cranes, equipment for installing or removing a thrust chamber, safety railings, high-pressure gas tank, the propellant tank pressurization system, separate storage tanks for fuel, oxidizer, or cooling water with their feed systems, or a small workshop.

6. Quantity and distance restrictions on the storage of liquid propellants, solid propellant ingredients, and solid propellants to minimize damage in the event of explosions; separation of fuels and oxidizers.
7. Barricades around hazardous test articles to reduce shrapnel damage in the event of a blast.
8. Explosion-proof electrical systems, spark-proof shoes, and nonspark hand tools to prevent ignition of flammable materials.
9. For certain hazardous propellants also safety clothing (see Fig. 21–4), including propellant- and fire-resistant suits, face masks and shields, gloves, special shoes, and hard hats.

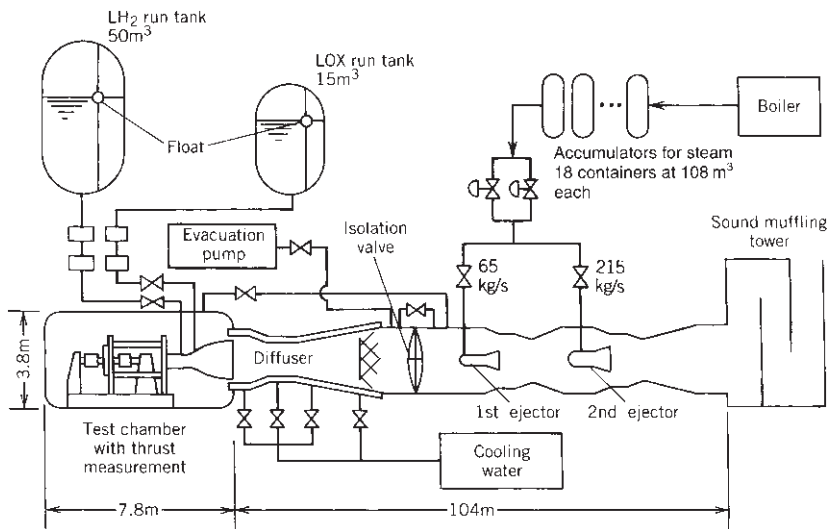


FIGURE 21–2. Simplified diagram of a simulated altitude, horizontal firing test facility for the LE-5 Japanese-designed thrust chamber (liquid oxygen–liquid hydrogen propellants) showing the method of creating a vacuum (6 torr during operation and 13 torr prior to start). The operating duration is limited to about 10 min by the capacity of the steam storage. (Reproduced from Ref. 21–1 with permission of the AIAA.)



FIGURE 21–3. Control room (inside a reinforced concrete blockhouse) for test operators, instrument recorders, and controls. Note the control console, closed-circuit television, radio and telephone, direct read-out meters, strip charts, high-speed tape recorders, oscilloscope, air-quality alarm, and emergency lights. (Courtesy of U.S. Air Force Phillips Laboratory.)



FIGURE 21-4. Plastic safety suit, gloves, boots, and hood used by test personnel in handling hazardous or corrosive liquid propellants. Safety shower, which starts automatically when a person steps onto the platform, washes away splashed or spilled propellant. (Official U.S. Air Force photograph.)

10. Rigid enforcement of rules governing area access, smoking, safety inspections, and so forth.
11. Limitations on the number of personnel that may be in a hazardous area at any time.

Monitoring the Environment and Controlling Toxic Materials

Open-air testing of chemical rocket propulsion systems frequently requires measurement and control of exhaust cloud concentrations and gas movement in the surrounding areas for safeguarding personnel, animals, and plants. Most test and launch facilities have several stations (both inside and outside the facilities) for collecting and measuring air samples before, during, and after a test. A toxic cloud of gas and particles can result from the exhaust gas of normal rocket operation, vapors or reaction gases from unintentional propellant spills, and gases

from fires, explosions, or from the intentional destruction of vehicles in flight or rockets on the launch stand. Environmental government regulations usually limit the maximum local concentration or the total quantity of toxic gas or particulates released to the atmosphere. The toxic nature of some of these liquids, vapors, and gases has been mentioned in Chapters 7 and 13. One method of control is for tests with discharges of moderately toxic gases or products to be postponed until favorable weather and wind conditions are present.

In the analysis of ground tests, the toxic cloud source is analysed as a *point source*, and in flight tests it is a *ribbon source*. The rate of exhaust cloud diffusion is influenced by many propulsion variables, including propellant, propulsion system size, exhaust temperature, and thrust duration; by many atmospheric variables, including wind velocity, direction, turbulence, humidity, and vertical stability or lapse rate, and by the surrounding terrain. Extensive analytical studies and measurements of the environmental exposure from explosions, industrial smoke, and gases, and exhausts from missile and space vehicle launchings give background useful for predicting the atmospheric diffusion and downwind concentrations of rocket exhaust clouds. Reference 21-2 describes hazards and toxic gas cloud dispersals and concentrations. Reference 21-3 evaluates the environmental impact of rocket exhausts from large units on the ozone in the stratosphere and on the ground weather near the test site; it concludes that the impacts are generally small and temporary. Reference 21-4 describes a test area atmospheric measuring network.

A widely used relationship for predicting atmospheric diffusion of gas clouds has been formulated by O. G. Sutton (Ref. 21-5). Many of the most modern equations and models relating to downwind concentrations of toxic clouds are extensions of Sutton's theory. Given below are the Sutton equations of primary interest to rocket and missile operators.

For instantaneous ground-level point-source nonisotropic conditions,

$$\chi_{(x,y,z,t)} = \frac{Q}{\pi^{3/2} C_x C_y C_z (\bar{u}t)^{3(2-n)/2}} \exp \left[-(\bar{u}t)^{n-2} \left(\frac{x^2}{C_x^2} + \frac{y^2}{C_y^2} + \frac{z^2}{C_z^2} \right) \right] \quad (21-1)$$

For continuous ground-level point-source nonisotropic conditions,

$$\chi = \frac{2Q}{\pi C_y C_z \bar{u} t^{2-n}} \exp \left[-x^{n-2} \left(\frac{y^2}{C_y^2} + \frac{z^2}{C_z^2} \right) \right] \quad (21-2)$$

where χ is the concentration in grams per cubic meter, Q is the source strength (grams for instantaneous, grams per second for continuous); $C_{x,y,z}$ are diffusion coefficients in the x , y , z planes, respectively; \bar{u} is the average wind velocity in meters per second, t is the time in seconds, and the coordinates x , y , z are in meters measured from the center of the moving cloud in the instantaneous case and from a ground point beneath the plume axis in the continuous case. The exponent n is a stability or turbulence coefficient, ranging from almost zero for

highly turbulent conditions to 1 as a limit for extremely stable conditions, and usually falling between 0.10 and 0.50.

A few definitions basic to the study of atmospheric diffusion of exhaust clouds are as follows:

1. *Micrometeorology*. Study and forecasting of atmospheric phenomena restricted to a region approximately 300 m above the earth's surface and a horizontal distance of approximately 5 miles.
2. *Lapse Rate*. The rate of decrease in temperature with increasing height above the earth's surface. The standard atmosphere (Appendix 2) has a lapse rate of about 6.4°C per 1000 m. Lapse rate is also affected by altitude, wind, and humidity.
3. *Inversion, or Inversion Layer*. Condition of negative lapse rate (temperature increases with increasing height). Usually formed near the ground at night.

The following are a few general rules and observations derived from experience with the atmospheric diffusion of rocket exhaust clouds:

1. Inversion presents a very stable layer and greatly reduces the vertical dispersion (the higher the lapse rate, the greater the vertical dispersion).
 2. A highly stable atmospheric condition tends to keep the exhaust plume or cloud intact and away from the earth's surface except when the exhaust products are much heavier than the surrounding air.
 3. High wind increases the rate of diffusion and reduces the thermal effects.
 4. For short firings (< 500 sec) the approximate dosages downwind are about the same as from an instantaneous point source.
 5. When the plume reaches about one-fourth the distance to a given point before emission is stopped, peak concentration will be about three-fourths of that from a continuous source of equal strength.
 6. The presence of an inversion layer significantly restricts the mixing or diffusion capacity of the propulsion system exhaust gases into the atmosphere; the effective air mass is that mass existing between the Earth's surface and the inversion layer.
 7. Penetration of the inversion layer due to the buoyancy force of the hot exhaust cloud seldom occurs.
 8. Earth surface dosage drops rapidly when missiles or space launch vehicles are destroyed in flight above a height of 1500 m as compared to lower altitudes of 600 to 1000 m.
- Interpretation of the hazard that exists once the concentration of the toxic agent is known also required knowledge of its effects on the human body, plants, and animals. Government tolerance limits for humans are given in Chapter 7 and in Ref. 7-5. There are usually three limits of interest: one for the short-time exposure of the general public, one for an 8-hr

exposure limit of workers, and an evacuation concentration. Depending on the toxic chemical, the 8-hr limit may vary from 5000 ppm for a gas such as carbon dioxide, to less than 1 ppm for an extremely toxic substance such as fluorine. Poisoning of the human body by exhaust products usually occurs from inhalation of the gases and fine solid particles, but the solid residuals that sometimes remain around a test facility for weeks or months following a test firing can enter the body through cuts and other avenues. Also, certain liquid propellants cause burns and skin rash or are poisonous when ingested, as explained in Chapter 7.

21.3. INSTRUMENTATION AND DATA MANAGEMENT

Considerable progress has been made. For further study the reader is referred to standard textbooks on instruments and computers used in testing, such as Ref. 21–6. Some of the physical quantities measured in rocket propulsion testing are:

1. Forces (thrust, thrust vector control side forces, short thrust pulses).
2. Flows (hot and cold gases, liquid fuel, liquid oxidizer, leakage).
3. Pressures (chamber, propellant, pump, tank, etc.).
4. Temperatures (chamber or case walls, propellant, structure, nozzle).
5. Timing and command sequencing of valves, switches, igniters, and so on.
6. Stresses, strains, and vibrations (combustion chamber, structures, solid propellants, liquid propellant lines, local accelerations of vibrating parts) (Ref. 21–7).
7. Time sequence of events (ignition, attainments of full pressure).
8. Movement and position of parts (valve stems, gimbal position, deflection of parts under load or heat).
9. Voltages, frequencies, and currents in electrical or control subsystems.
10. Visual observations (flame configuration, test article failures, explosions) using high-speed cameras or video cameras.
11. Special quantities such as turbopump shaft speed, liquid levels in propellant tanks, burning rates, flame luminosity, or exhaust gas composition.

Reference 21–8 gives a description of specialized diagnostic techniques used in propulsion systems, such as using nonintrusive optical methods, microwaves, and ultrasound for measurements of temperatures, velocities, particle sizes, or burn rates in solid propellant grains. Many of these sensors incorporate specialized technologies and, often, unique software. Each of the measured parameters can be obtained by different types of instruments, sensors, and analyzers, as indicated in Ref. 21–9.

Measurement System Terminology

Each measurement or each measuring system usually requires one or more *sensing elements* (often called transducers or pickups), a device for *recording*, *displaying*, and/or *indicating* the sensed information, and often also another device for *conditioning*, *amplifying*, *correcting*, or *transforming* the sensed signal into the form suitable for *recording*, *indicating*, *display*, or *analysis*. Recording of rocket propulsion test data has been performed in several ways, such as on *chart recorders* or in digital form on *memory devices*, such as on magnetic tapes or disks. Definitions of several significant terms are given below and in Ref. 21–6.

Range refers to the region extending from the minimum to the maximum rated value over which the measurement system will give a true and linear response. Usually an additional margin is provided to permit temporary overloads without damage to the instrument or need for recalibration.

Errors in measurements are usually of two types: (1) *human errors* of improperly reading or incorrectly adjusting the instrument, chart, or record and of improperly interpreting or correcting these data, and (2) *instrument or system errors*, which usually fall into four classifications: static errors, dynamic response errors, drift errors, and hysteresis errors (see Refs. 21–6 and 21–10). *Static errors* are usually fixed errors due to fabrication and installation variations; these errors can usually be detected by careful calibration, and an appropriate correction can then be applied to the reading. *Drift error* is the change in output over a period of time, usually caused by random wander and environmental conditions. To avoid drift error the measuring system has to be calibrated at frequent intervals at standard environmental conditions against known standard reference values over its whole range. *Dynamic response errors* occur when the measuring system fails to register the true value of the measured quantity while this quantity is changing, particularly when it is changing rapidly. For example, the thrust force has a dynamic component due to vibrations, combustion oscillations, interactions with the support structure, and the like. These dynamic changes can distort or amplify the thrust reading unless the test stand structure, the rocket mounting structure, and the thrust measuring and recording system are properly designed to avoid harmonic excitation or excessive energy damping. To obtain a good dynamic response requires a careful analysis and design of the total system.

A *maximum frequency response* refers to the maximum frequency (usually in cycles per second) at which the instrument system will measure true values. The natural frequency of the measuring system is usually above the limiting response frequency. Generally, a high-frequency response requires more complex and expensive instrumentation. Most of the instrument system (sensing elements, modulators, and recorders) must be capable of a fast response. Most of the measurements in rocket testing are made with one of two types of instruments: those made under nearly steady static conditions, where only relatively gradual changes in the quantities occur, and those made with fast transient conditions, such as rocket starting, stopping, or vibrations (see Ref. 21–11). This latter type of instrument has frequency responses above 200 Hz, sometimes as high as 20,000 Hz.

These fast measurements are necessary to evaluate the physical phenomena of rapid transients.

Linearity of the instrument refers to the ratio of the input (usually pressure, temperature, force, etc.) to the output (usually voltage, output display change, etc.) over the range of the instrument. Very often the static calibration error indicates a deviation from a truly linear response. A nonlinear response can cause appreciable errors in dynamic measurements. *Resolution* refers to the minimum change in the measured quantity that can be detected with a given instrument. *Dead zone* or *hysteresis* errors are often caused by energy absorption within the instrument system or play in the instrument mechanism; in part, they limit the resolution of the instrument.

Sensitivity refers to the change in response or reading caused by special influences. For example, the *temperature sensitivity* and the *acceleration sensitivity* refer to the change in measured value caused by temperature and acceleration. These are usually expressed in percent change of measured value per unit of temperature or acceleration. This information can serve to correct readings to reference or standard conditions.

Errors in measurement can arise from many sources. Reference 21–12 gives a standardized method, including mathematical models, for estimating the error, component by component, as well as the cumulative effect in the instrumentation and recording systems.

Electrical interference or “noise” within an instrumentation system, including the power supply, transmission lines, amplifiers, and recorders, can affect the accuracy of the recorded data, especially when low-output transducers are in use. Methods for measuring and eliminating objectionable electrical noise are given in Ref. 21–13.

Test Measurements

For every test of a rocket propulsion system or one of its components there should be one or more objectives, an identification of the article to be tested, a description of the test, an identification of the test facility, a list of specific measurements to be performed, instructions on storing, analyzing or displaying of the data, an interpretation of the results, and a conclusion.

In many tests, especially with large liquid propellant rocket engines, the data generated can be very large. Manual analysis of the data by skilled individuals was the original method, but it is too cumbersome. Today computers have become common place. They automatically correct the raw measured data, store it, analyze it, correct it, and display it. Some control systems can make decisions to control the engine and minimize test failure. This is really a version of a health monitoring system (HMS) described at the end of Section 11.5 and it is also discussed in the next section..

Often only a portion of the recorded data is actually analyzed or reviewed during or after the test. In complex rocket propulsion system development tests, sometimes between 100 and 400 different instrument measurements are made

and recorded. Some data need to be sampled frequently (e.g., some transients may be sampled at rates higher than 1000 times per second), whereas other data need to be taken at lower frequencies (e.g., temperature of mounting structure may be needed only every 1 to 5 sec). Multiplexing of data is commonly practiced to simplify data transmission. Most rocket test computer systems contain a configuration file to indicate data characteristics for each channel, such as range, gain, the references, the type of averaging, the parameter characteristics, or the data correction algorithms. Most of the data are not analyzed or printed out as hard copy; a detailed analysis occurs only if there is reason for understanding particular test events in more detail. This analysis may occur months after the actual tests and may not even be done on the same computer.

The proper *selection* of the type, number of measurements, or frequency of data collection is crucial in the sensing of the status of the health of the propulsion system to be tested. This selection is usually performed by the engineers working on the development of the particular propulsion system, who can identify the critical parameters which influence performance and likely impending failures.

The actual *test measurements* are performed with a variety of sensors, all modified to fit standard interfaces so they can be connected to a common computer or network. See Ref. 21–14. The measured outputs of each instrument or sensor are corrected for changes in the ambient temperatures, instrument calibration factors, nonlinear outputs, conversion of analog data into digital form, or filtering of data signals to eliminate signals outside the range of interest. *Recording* of data can be done by a computer in the engine, a computer on the ground, or in the flight vehicle. *Manipulation* of data includes changing of scale or providing a display (table, plots, or curves) of selected engine parameters in support of the data analysis of the test results.

Health Monitoring System (HMS)

The HMS relies on receiving the corrected data inputs from selected sensors, whose measurements were described in the prior paragraphs. HMSs are also discussed in Section 11.5. From the *simulated and validated analytical description of the propulsion system* it is possible to derive the nominal (desired) values for each of the parameters and they are entered into the HMS computer. This can include the nominal chamber pressure, thrust, nozzle wall temperature, voltage, and many others for both steady-state and transient conditions—all at various times of the engine operation. For each measured parameter and time this analytical model provides a nominal value, an upper limit value, and a lower limit value (also known as red line values), which identify the safe operating range of that parameter. The analytical model usually also includes the transient conditions (start/stop). The values of each parameter is often validated (and sometimes corrected) by actual test data from prior successful firing tests of this type of rocket engine.

Then an *automatic comparison* is made by the HMS computer between the *actual measured corrected data* and the same *data from the analytical simulation*.

It will show if the measured parameter is satisfactory (falls between the two limit lines) or unsatisfactory, if the measurement exceeds the safe limits. Since damage to a liquid propellant rocket engine can occur very quickly (in less than a second) an immediate action is necessary. In an impending failure one or more other measurements will usually also exceed their safe limits. For example, if the turbine inlet temperature becomes too hot, turbine blades may be damaged. If the turbine inlet gas temperature exceeds its safe limit, then usually the turbopump's shaft speed and the turbine inlet manifold temperature will also exceed their safe limits. By sensing an impending critical failure with more than one red line measurement, the likely incipient engine failure is confirmed and an occasional single sensor malfunction can be eliminated as a insufficient cause for starting a remedial action.

Decisions on possible remedial action can be done very quickly on a computer, certainly much faster than a decision by a human operator. If the computer receives three simultaneous related measurements that exceed their safe limit values, and if all three are related to the same potential failure, then a remedial action is allowed. Then the computer will automatically query a table of remedies, and a corrective action, which fits the three overlimit values, is quickly identified and selected and this remedy is automatically initiated. For the turbine inlet temperature example given above, this action may include throttling the total flow to the gas generator or changing the mixture ratio of the gas generator flow (provided the gas generator valves have a throttling capability) or to shut the engine down safely. This kind of fast action with decisions made by a computer has saved much engine hardware in development testing. It is a relatively new feature of rocket engine testing.

For some component tests programmable logic controllers are used to control the test operation instead of a computer, which usually requires some software development.

21.4. FLIGHT TESTING

Flight testing of rocket propulsion systems is always conducted in conjunction with tests of vehicles and other systems such as guidance, vehicle controls, or ground support. These flights usually occur along missile and space launch ranges, often over the ocean. If a flight test vehicle deviates from its intended path and appears to be headed for a populated area, a range safety official (or a computer) will have to either cause a destruction of the vehicle, abort the flight, or cause it to correct its course. Many propulsion systems therefore include devices that will either terminate the operation (shut off the rocket engine or open thrust termination openings into rocket motor cases as described in Section 14.3) or trigger explosive devices that will cause the vehicle (and therefore also the propulsion system) to disintegrate in flight.

Flight testing requires special launch support equipment, means for observing, monitoring, and recording data (cameras, radar, telemetering, etc.), equipment for

assuring range safety and for reducing data and evaluating flight test performance, and specially trained personnel. Different launch equipment is needed for different kinds of vehicles. This includes launch tubes for shoulder-held infantry support missile launchers, movable turret-type mounted multiple launchers installed on an army truck or a navy ship, a transporter for larger missiles, and a track-propelled launch platform or fixed complex launch pads for spacecraft launch vehicles. The launch equipment has to have provisions for loading or placing the vehicle into a launch position, for allowing access of various equipment and connections to launch support equipment (checkout, monitoring, fueling, etc.), for aligning or aiming the vehicle, or for withstanding the exposure to the hot rocket plume at launch.

During experimental flights extensive measurements are often made on the behavior of the various vehicle subsystems; for example, rocket propulsion parameters, such as chamber pressure, feed pressures, temperatures, and so on, are measured and the data are telemetered and transmitted to a ground receiving station for recording and monitoring. Some flight tests rely on salvaging and examining the test vehicle.

21.5. POSTACCIDENT PROCEDURES

In the testing of any rocket propulsion system there will invariably be failures, particularly when some of the operating parameters are close to their limit. With each failure comes an opportunity to learn more about the design, the materials, the propulsion performance, the fabrication methods, or the test procedures. A careful and thorough investigation of each failure is needed to learn the likely causes and identify the remedies or fixes to prevent a similar failure in the future. The lessons to be learned from these failures are perhaps the most important benefits of development testing. A formalized postaccident approach is often used, particularly if the failure had a major impact, such as high cost, major damage, or personnel injury. A major failure (e.g., the loss of a space launch vehicle or severe damage to a test facility) often causes the program to be stopped and further testing or flights put on hold until the cause of the failure is determined and remedial action has been taken to prevent a recurrence.

Of utmost concern immediately after a major failure are the steps that need to be taken to respond to the emergency. This includes giving first aid to injured personnel, bringing the propulsion system and/or the test facilities to a safe, stable condition, limiting further damage from chemical hazards to the facility or the environment, working with local fire departments, medical or emergency maintenance staff or ambulance personnel, and debris clearing crews, and quickly providing factual statements to the management, the employees, the news media, and the public. It also includes controlling access to the facility where the failure has occurred and preserving evidence for the subsequent investigation. All test personnel, particularly the supervisory people, need to be trained not only in preventing accidents and minimizing the impact of a potential failure, but also

how to best respond to the emergency. Reference 21–15 suggests postaccident procedures involving rocket propellants.

REFERENCES

- 21–1. K. Yanagawa, T. Fujita, H. Miyajima, and K. Kishimoto, “High Altitude Simulation Tests of LOX-LH₂ Engine LE-5,” *Journal of Propulsion and Power*, Vol. 1, No. 3, May–June 1985, pp. 180–186.
- 21–2. *Handbook for Estimating Toxic Fuel Hazards*, NASA Report CR-61326, April 1970.
- 21–3. R. R. Bennett and A. J. McDonald, “Recent Activities and Studies on the Environmental Impact of Rocket Effluents,” AIAA Paper 98-3850, July 1998.
- 21–4. R. J. Grosch, “Micro-Meteorological System,” Report TR-68-37, Air Force Rocket Propulsion Laboratory, November 1968 (AD 678856).
- 21–5. O. G. Sutton, *Micrometeorology*, Chapter 8, McGraw-Hill, New York, 1973.
- 21–6. D. Ramsey, *Principles of Engineering Instrumentation*, University of Michigan, Ann Arbor, MI, 1996.
- 21–7. K. G. McConnell and P. S. Varoto, *Vibration Testing: Theory and Practice*, 2nd ed., John Wiley & Sons, Hoboken, NJ, 2008.
- 21–8. Y. M. Timnat, *Diagnostic Techniques for Propulsion Systems*, Progress in Aerospace Sciences (Series), Vol. 26, No. 2, 1989, pp. 153–168.
- 21–9. R. S. Figliola and D. B. Beasley, *Theory and Design for Mechanical Measurements*, 4th ed., John Wiley & Sons, Hoboken, NJ, 2005.
- 21–10. R. Cerri, “Sources of Measurement Error in Instrumentation Systems,” Preprint 19-LA-61, Instrument Society of America, Research Triangle Park, NC .
- 21–11. P. M. J. Hughes and E. Cerny, “Measurement and Analysis of High-Frequency Pressure Oscillations in Solid Rocket Motors,” *Journal of Spacecraft and Rockets*, Vol. 21, No. 3, May–June 1984, pp. 261–265.
- 21–12. *Handbook for Estimating the Uncertainty in Measurements Made with Liquid Propellant Rocket Engine Systems*, Handbook 180, Chemical Propulsion Information Agency, April 30, 1969 (AD 855130).
- 21–13. “Grounding Techniques for the Minimization of Instrumentation Noise Problems,” Report TR-65-8, Air Force Rocket Propulsion Laboratory, January 1965 (AD 458129).
- 21–14. S. Schmalzel, F. Figuero, J. Morris, S. Mandayam, and R. Polikar, “An Architecture for Intelligent Systems Based on Smart Sensors,” *IEEE Transactions on Instrumentation and Measurement*, Vol. 34, No. 4, August 2005.
- 21–15. D. K. Shaver and R. L. Berkowitz, *Post-accident Procedures for Chemicals and Propellants*, Noyes Publications, Park Ridge, NJ, 1984.

APPENDIX 1

CONVERSION FACTORS AND CONSTANTS

Conversion Factors (arranged alphabetically)

Acceleration ($L t^{-2}$)^{*}

$$1 \text{ m/sec}^2 = 3.2808 \text{ ft/sec}^2 = 39.3701 \text{ in./sec}^2$$

$$1 \text{ ft/sec}^2 = 0.3048 \text{ m/sec}^2 = 12.0 \text{ in./sec}^2$$

$g_0 = 9.80665 \text{ m/sec}^2 = 32.174 \text{ ft/sec}^2$ (standard gravity pull at Earth's surface)

Area (L^2)

$$1 \text{ ft}^2 = 144.0 \text{ in.}^2 = 0.092903 \text{ m}^2$$

$$1 \text{ m}^2 = 1550.0 \text{ in.}^2 = 10.7639 \text{ ft}^2$$

$$1 \text{ in.}^2 = 6.4516 \times 10^{-4} \text{ m}^2$$

Density ($M L^3$)

Specific gravity is dimensionless, but has the same numerical value as *density* expressed in g/cm^3

$$1 \text{ kg/m}^3 = 6.24279 \times 10^{-2} \text{ lbm/ft}^3 = 3.61273 \times 10^{-5} \text{ lbm/in.}^3$$

$$1 \text{ lbm/ft}^3 = 16.0184 \text{ kg/m}^3$$

$$1 \text{ lbm/in.}^3 = 2.76799 \times 10^4 \text{ kg/m}^3$$

*The letters in parentheses after each heading indicate the dimensional parameters (L = length, M = mass, t = time, and T = temperature).

Energy, also Work or Heat (M L² t⁻²)

1.0 Btu = 1055.056 J (joule)

1.0 kW·hr = 3.600×10^6 J

1.0 ft-lbf = 1.355817 J

1.0 cal = 4.1868 J

1.0 kcal = 4186.8 J

Force (M L t⁻²)

1.0 lbf = 4.448221 N

1 dyne = 10^{-5} N

1.0 kg (force) [used in Europe] = 9.80665 N

1.0 ton (force) [used in Europe] = 1000 kg (force)

1.0 N = 0.2248089 lbf

1.0 millinewton (mN) = 10^{-3} N*Weight* is the *force* on a *mass* being accelerated by gravity (g_0 applies at the surface of the Earth)*Length (L)*

1 m = 3.2808 ft = 39.3701 in.

1 ft = 0.3048 m = 12.0 in.

1 in. = 2.540 cm = 0.0254 m

1 mile = 1.609344 km = 1609.344 m = 5280.0 ft

1 nautical mile = 1852.00 m

1 mil = 0.0000254 m = 1.00×10^{-3} in.1 micron (μm) = 10^{-6} m1 astronomical unit (au) = 1.49600×10^{11} m*Mass (M)*

1 slug = 32.174 lbm

1 kg = 2.205 lbm = 1000 g

1 lbm = 16 ounces = 0.4536 kg

Power (M L² t⁻³)

1 Btu/sec = 0.2924 W (watt)

1 J/sec = 1.0 W = 0.001 kW

1 cal/sec = 4.186 W

1 horsepower = 550 ft-lbf/sec = 745.6998 W

1 ft-lbf/sec = 1.35581 W

*Pressure (M L⁻¹ t⁻²)*1 bar = 10^5 N/m² = 0.10 MPa

1 atm = 0.101325 MPa = 14.696 psia

1 mm of mercury = 13.3322 N/m²

1 MPa = 10⁶ N/m²

1 psi or lbf/in.² = 6894.757 N/m²

Speed (or linear velocity) (L t⁻¹)

1 ft/sec = 0.3048 m/sec = 12.00 in./sec

1 m/sec = 3.2808 ft/sec = 39.3701 in./sec

1 knot = 0.5144 m/sec

1 mile/hr = 0.4770 m/sec

Specific Heat (L² t⁻² T⁻¹)

1 g-cal/g-°C = 1 kg-cal/kg-K = 1 Btu/lbm-°F = 4.186 J/g-°C =
 1.163×10^{-3} kW-hr/kg-K

Temperature (T)

1 K = (9/5)°R = 1.80°R

0°C = 273.15 K

0°F = 459.67°R

°C = (5/9)(°F - 32) °F = (9/5)°C + 32

Time (t)

1 mean solar day = 24 hr = 1440 min = 86,400 sec

1 calendar year = 365 days = 3.1536×10^7 sec

Viscosity (M L⁻¹ t⁻¹)

1 centistoke = 1.00×10^{-6} m²/sec

1 centipoise = 1.00×10^{-3} kg/m sec

1 lbf-sec/ft² = 47.88025 kg/m sec

Constants

J Mechanical equivalent of heat = 4.186 joule/cal = 777.9 ft-lbf/Btu
= 1055 joule/Btu

R' Universal gas constant = 8314.3 J/kg-mol-K = 1545 ft-lbf/lbm-mol-°R

V_{mole} Molecular volume of an ideal gas = 22.41 liter/kg-mol at standard conditions

e Electron charge = $1.6021176 \times 10^{-19}$ coulomb

ε₀ Permittivity of vacuum = 8.854187×10^{-12} farad/m

Gravitational constant = 6.673×10^{-11} m³/kg-sec

Boltzmann's constant $1.38065003 \times 10^{-23}$ J/K

Electron mass 9.109381×10^{-31} kg

Avogadro's number 6.022142×10^{26} /kg-mol

σ Stefan-Boltzman constant 5.6696×10^{-8} W/m²-K⁻⁴

APPENDIX 2

PROPERTIES OF THE EARTH'S STANDARD ATMOSPHERE

Sea-level pressure is 0.101325 MPa (or 14.696 psia or 1.000 atm).

| Altitude (m) | Temperature (K) | Pressure Ratio | Density (kg/m^3) |
|---------------|-----------------|--------------------------|-----------------------------|
| 0 (sea level) | 288.150 | 1.0000 | 1.2250 |
| 1,000 | 281.651 | 8.8700×10^{-1} | 1.1117 |
| 3,000 | 268.650 | 6.6919×10^{-1} | 9.0912×10^{-1} |
| 5,000 | 255.650 | 5.3313×10^{-1} | 7.6312×10^{-1} |
| 10,000 | 223.252 | 2.6151×10^{-1} | 4.1351×10^{-1} |
| 25,000 | 221.552 | 2.5158×10^{-2} | 4.0084×10^{-2} |
| 50,000 | 270.650 | 7.8735×10^{-4} | 1.0269×10^{-3} |
| 75,000 | 206.650 | 2.0408×10^{-5} | 3.4861×10^{-5} |
| 100,000 | 195.08 | 3.1593×10^{-7} | 5.604×10^{-7} |
| 130,000 | 469.27 | 1.2341×10^{-8} | 8.152×10^{-9} |
| 160,000 | 696.29 | 2.9997×10^{-9} | 1.233×10^{-9} |
| 200,000 | 845.56 | 8.3628×10^{-10} | 2.541×10^{-10} |
| 300,000 | 976.01 | 8.6557×10^{-11} | 1.916×10^{-11} |
| 400,000 | 995.83 | 1.4328×10^{-11} | 2.803×10^{-12} |
| 600,000 | 999.85 | 8.1056×10^{-13} | 2.137×10^{-13} |
| 1,000,000 | 1000.00 | 7.4155×10^{-14} | 3.561×10^{-15} |

Source: *U.S. Standard Atmosphere*, National Oceanic and Atmospheric Administration, National Aeronautics and Space Administration, and U.S. Air Force, Washington, DC, 1976 (NOAA-S/T-1562).

APPENDIX 3

SUMMARY OF KEY EQUATIONS FOR IDEAL CHEMICAL ROCKETS

| Parameter | Equations | Equation Numbers |
|--|--|--------------------------------------|
| Average exhaust velocity, v_2 (m/sec or ft/sec) (assume that $v_1 = 0$) | $v_2 = c - (p_2 - p_3)A_2/\dot{m}$ When $p_2 = p_3$, $v_2 = c$ $v_2 = \sqrt{[2k/(k-1)]RT_1[1 - (p_2/p_1)^{(k-1)/k}]}$ $= \sqrt{2(h_1 - h_2)}$ | 2-16 3-16 3-15 |
| Effective exhaust velocity, c (m/sec or ft/sec) | $c = c^* C_F = F/\dot{m} = I_s g_0$ | 3-32 |
| Thrust, F (N or lbf) | $c = v_2 + (p_2 - p_3)A_2/\dot{m}$ $F = c\dot{m} = cm_p/t_p$ $F = C_F p_1 A_t$ $F = \dot{m}v_2 + (p_2 - p_3)A_2$ $F = \dot{m}I_s g_0$ | 2-16 2-17 3-31 2-14 3-32 |
| Characteristic velocity, c^* (m/sec or ft/sec) | $c^* = c/C_F = p_1 A_t/\dot{m}$ $c^* = \frac{\sqrt{kRT_1}}{k\sqrt{[2/(k+1)]^{(k+1)/(k-1)}}}$ | 3-32 3-32 |
| Thrust coefficient, C_F (dimensionless) | $c^* = I_s g_0/C_F = F/(\dot{m}C_F)$ $C_F = c/c^* = F/(p_1 A_t)$ $C_F = \sqrt{\frac{2k^2}{k-1} \left(\frac{2}{k+1}\right)^{(k+1)/(k-1)} \left[1 - \left(\frac{p_2}{p_1}\right)^{(k-1)/k}\right]}$ $+ \frac{p_2 - p_3}{p_1} \frac{A_2}{A_t}$ | 3-32, 3-33 3-31, 3-32 3-30 |
| Total impulse | $I_t = \int F dt = Ft = I_s w$ | 2-1, 2-2, 2-5 |
| Specific impulse, I_s (sec) | $I_s = c/g_0 = c^* C_F/g_0$ $I_s = F/\dot{m}g_0 = F/\dot{w}$ $I_s = v_2/g_0 + (p_2 - p_3)A_2/(\dot{m}g_0)$ $I_s = I_t/(m_p g_0) = I_t/w$ | 2-5 2-16 2-4, 2-5 |

| Parameter | Equations | Equation Numbers |
|---|---|----------------------------|
| Propellant mass fraction, (dimensionless) | $\zeta = m_p/m_0 = \frac{m_0 - m_f}{m_0}$ $\zeta = 1 - \mathbf{MR}$ | 2-8, 2-9 4-4 |
| Mass ratio of vehicle or stage, \mathbf{MR} (dimensionless) | $\mathbf{MR} = \frac{m_f}{m_0} = \frac{m_0 - m_p}{m_0}$ $= m_f/(m_f + m_p)$ | 2-7 |
| Vehicle velocity increase in gravity-free vacuum, Δu (m/sec or ft/sec) (assume that $u_0 = 0$) | $m_0 = m_f + m_p$ $\Delta u = -c \ln \mathbf{MR} = c \ln \frac{m_0}{m_f}$ $= c \ln [m_0/(m_0 - m_p)]$ $= c \ln[(m_p + m_f)/m_f]$ | 2-10 4-6 4-5, 4-6 |
| Propellant mass flow rate, \dot{m} (kg/sec or lb/sec) | $\dot{m} = Av/V = A_1 v_1/V_1$ $= A_t v_t/V_t = A_2 v_2/V_2$ $\dot{m} = F/c = p_1 A_t / c^*$ $\dot{m} = p_1 A_t k \frac{[2/(k+1)]^{(k+1)/(k-1)}}{\sqrt{kRT_1}}$ $\dot{m} = m_p/t_p$ | 3-24 2-17, 3-32 3-24 |
| Mach number, M (dimensionless) | $M = v/a$ $= v/\sqrt{kRT}$ | 3-11 |
| Nozzle area rate, ϵ | At throat, $v = a$ and $M = 1.0$ $\epsilon = A_2/A_t$ $\epsilon = \frac{1}{M_2} \sqrt{\left[\frac{1 + \frac{k-1}{2} M_2^2}{1 + \frac{k-1}{2}} \right]^{(k+1)/(k-1)}}$ | 3-19 3-14 |
| Isentropic flow relationships for stagnation and free-stream conditions | $T_0/T = (p_0/p)^{(k-1)/k} = (V/V_0)^{(k-1)}$ | 3-7 |
| Satellite velocity, u_s , in circular orbit (m/sec or ft/sec) | $T_x/T_y = (p_x/p_y)^{(k-1)/k} = (V_y/V_x)^{k-1}$ $u_s = R_0 \sqrt{g_0/(R_0 + h)}$ | 4-26 |
| Escape velocity, u_e (m/sec or ft/sec) | $u_e = R_0 \sqrt{2g_0/(R_0 + h)}$ | 4-25 |
| Liquid propellant engine mixture ratio r and propellant flow \dot{m} | $r = \dot{m}_0/\dot{m}_f$ $\dot{m} = \dot{m}_0 + \dot{m}_f$ $m_f = \dot{m}/(r+1)$ $m_0 = r\dot{m}/(r+1)$ | 6-1 6-2 6-4 6-3 |
| Average density ρ_{av} for (or average specific gravity) | $\rho_{av} = \frac{\rho_0 \rho_f (r+1)}{r \rho_f + \rho_0}$ | 7-2 |
| Characteristic chamber length L^* | $L^* = V_c/A_t$ | 8-9 |
| Solid propellant mass flow rate \dot{m} | $\dot{m} = A_b r \rho_b$ | 12-1 |
| Solid propellant burning rate r | $r = ap_1^n$ | 12-5 |
| Ratio of burning area A_b to throat area A_t | $K = A_b/A_t$ | 12-4 |
| Temperature sensitivity of burning rate at constant pressure | $\sigma_p = \frac{1}{r} \left(\frac{\partial r}{\partial T} \right)_{p_1}$ | 12-8 |
| Temperature sensitivity of pressure at constant K | $\pi_K = \frac{1}{p_1} \left(\frac{\partial p}{\partial T} \right)_K$ | 12-9 |

INDEX

- Abbreviations and acronyms for chemical ingredients of solid propellants, 513–515
- Ablative cooling and materials, 275, 308, **573, 576–578**
- Acceleration of vehicle, terminal, 114
- Acoustic velocity, *see* Velocity of sound
- Acoustic absorbers, cavities, 362, 363
- Action time, *see* Burning time and action time
- Aerodynamic forces, *see* Drag; Lift
- Aerojet AJ-10–118I rocket engine, 274–275
- Aerospike engine or thrust chamber, 299–301; *see also* Nozzle
- Aging, *see* Solid propellant
- Air launched rocket, 148–152
- Altitude:
- test facilities, 738
 - variation of atmospheric air properties, 752 (Appendix 2)
 - variation of thrust, 34–36
- Aluminum or aluminum powder, 185, 187
188, 251, 304, 307, 442, 499, 501,
503, 514, **517**, 573, 606
- Ammonium nitrate (AN), 185, 500, 514,
515, 517, 524
- Ammonium perchlorate (AP), 185, 186,
448, 500, 501, 502, 503, **512–517**,
539; *see also* Particle size parameter
- Apogee, definition, 120
- Applications of plume technology, 712
- Applications of rockets, **14–26**, 196, 438
596–600, 625–627, 661–663,
700–701
- Apsidal drift, 125–126
- Arcjet, *see* Electric propulsion
- Area ratio of nozzle, *see* Nozzle
- Atlas space launch vehicle, 17, 18,
439
- Atmospheric properties, 752
(Appendix 2)
- Attitude control, *see* Reaction control
- Attitude control rockets or attitude control systems (ACS), *see* Auxiliary rockets
- Automatic engine controls, 409–410,
411–414; *see also* Liquid propellant rocket engines

Note: Boldface page numbers identify either a definition or the most pertinent or fundamental discussion of the listed item.

- Auxiliary rockets or auxiliary propulsion, 196–198, 229–232; *see also* Reaction control systems
- electric propulsion, 661–663
- liquid propellants, 232
- pulsing, 230, 292–293, 302, 661–663
- rotation maneuvers, 131–135
- solid propellant, 483–485
- station keeping, 127–128, 132, 663
- thrusters, 301–305
- Baffles, injector, 361
- Ballistic evaluation motors, 444
- Ballistic missile, 22, 123
- Ballistics, *see* Internal ballistics
- Battery, electric power, 664
- Bearings (of turbopump), 374–375
- Bell-shaped nozzle, *see* Nozzle
- Beryllium, 251, 517
- Binder, *see* Solid propellant(s); Grain
- Bipropellant, 198, 216, 231, 274–275
- Blast tube, *see* Nozzle
- Blow-down pressurized feed system, 210–217
- Bonding of solid propellant grains, *see* Grain, solid propellant
- Boron, 517
- Boundary layer, *see* Nozzle, boundary layer
- Burning rate, solid propellant, 437–458; *see also* Grain; Hybrid rocket; Solid propellant rocket motors
- burning surface contour, 444, 470
 - catalyst or burning rate modifier, 440, 518
 - effect of acceleration, 457, 458
 - erosive burning, 454–456, 590
 - exponent or pressure exponent, 446, 497
 - function of pressure, 446–449
 - modifier, 450–452
 - temperature sensitivity (coefficient), 450–452,
- Burning time and action time, 459, 464
- definition for solid propellant motor, 459, 464
- Burning surface, 444, 445, 451
- Buzzing combustion instability, 354
- c^* (cee star), *see* Characteristic velocity
- Carbon-carbon, 275, 288, 292, 310, 443, 573, 574, 680
- Carbon phenolic, 443, 569, 574, 575, 576
- Case or solid rocket motor case, 436, 439, 440, 443, 556–564, 587; *see also* Nozzle; Solid propellant rocket motor
- filament-wound reinforced plastic, 431, 441, 560–562
- loads, 557
- materials, 443, 462, 561–564
- metal, 441, 560–562
- stresses and elongation, 558–559
- Catalyst, 257, 263–265, 303, 634, 664
- Cathode, 636, 647, 648
- Cavitation, 368, 383–384
- Chamber (combustion), 198; *see also* Heat transfer; Thrust chamber
- gas composition, 177, 179, 187
- gas temperature, *see* Temperature, combustion gas
- geometry/volume, 75, 285–288
- pressure, *see* Nozzle pressure ratio
- pressure control, 419–421
- wall loads and stresses, 295–299
- Characteristic chamber length, 276, 287
- Characteristic speed (electric propulsion), 630–631
- Characteristic velocity or characteristic exhaust velocity or c^* , 36, 68, 184–185, 274, 442, 610
- c^* efficiency, 68
- Chemical equilibrium, 48, 162, 170–173
- Chemical reaction:
- in chamber or motor case, 165–168, 346–350
 - energy balance, 166
 - free energy or chemical potential, 164–165
 - mass balance, 167
 - in nozzle, 170–174
- Chemical rocket propellant performance analysis, 41, 42, 158–193
- Choked flow condition, 60
- Chugging combustion instability, 352, 613–616
- Classification of:
- electric thrusters, 622–623, 649
 - hazards, 441, 505–512

- liquid propellant feed systems, 208
 liquid propellant rocket engines,
 194–198
 rocket propulsion systems, **1–14**, 196
 solid propellants, 437–458
 thrust vector controls, 673–675
 turbines, 387–388
 solid propellant rocket motors, 441
 thrust vector controls, 673–675
 valves, 236–239
- Cold gas propellants and thrusters, 42, 198,
 233–236, **266–267**, 301–303
- Combustion; *see also* Temperature; Solid
 propellant rocket motors; Thrust
 chambers
 analysis and simulation, 165–169
 350–351
 control of instabilities, 360–363
 efficiency, 38–39, 346
 gas composition (of products), 177, 179,
 180, 183, 187, 188, 505
 hybrid propellant rockets, 600–604
 instability, 285, **352–363**, 545–552,
 613–615
 acoustic instability, 545–549
 rating techniques, 359–360
 remedy and design, 360–363,
 550–552
- liquid propellants, 254–255, **346–352**,
 422
 process, 160, 346–350, 537–541; *see
 also* Stay time
 solid propellants, 537–554
 stability assessment or rating technique,
 359–360, 550–552
 vibration, longitudinal, radial or
 tangential, 356–357
 vibration frequency, 352–353, 356,
 358–359, 548, 615–616
- Communication signal attenuation, 255
 Composite propellant, *see* Solid
 propellant(s)
 Computers programs:
 combustion analysis, 175–176, 350–351,
 549–550
 exhaust plume analysis, 729–730
 flow analysis, 569–570
 grain strain analysis, 478
 heat transfer, 312, 318
- ignition, 324
 nozzle contour, 571–572
 performance analysis, 408
 rocket engine control, 421–423
 Conical nozzle, 76–80; *see also* Nozzle
 Continuum flow regime, 717
 Controls for rocket engines, 213, 409–410
 411–423, 703
 Controls for rocket testing, 735, 746
 Conversion factors and constants, 749–750
 (Appendix 1)
- Cooling with liquid propellant; *see also*
 Radiation cooling; Regenerative
 cooling; Thrust chamber
 in cooling jackets, 289–290
 heat transfer, 311–323
 hydraulic losses in cooling jacket, 295
- Copper, 305–311
 Cost, 702
 Cracks in grain, *see* Failure modes
 Criteria for selection of optimum
 propulsion system, 699–705
 Cryogenic propellants, 199, 202–203,
 247–250
 Cumulative damage of solid propellants,
 481–483
 Curing agents for solid propellant, 514, **519**
 Current density, 637, 644
 Cut-off, *see* Thrust termination
- Dalton's law, 160
 Deep space flight, 123–124, 135
 Deflagration, 464, 508–509
 Delivered performance, 95
 Delta space launch vehicle, 16, 18
 Density, 752; *see also* Specific gravity of
 atmosphere
 average, for bipropellants, 253
 Density specific impulse, 253, 460, 594;
 see also Specific impulse
 Design calculation examples for:
 hybrid propellant rocket, 609–613
 liquid propellant thrust chamber,
 328–339
 solid propellant motor, 587–590
 Detonation, *see* Solid propellant, detonation
 Discharge:
 coefficients for injectors, 281–283
 correction factor for propulsion system,
 90–93

- Double-base propellant, *see* Solid propellant
- Drag:
- coefficient, 108
 - force, 107–109, 126, 129, 138
- Ducted rocket, 2
- Duct propulsion, 1–4, 9
- Duty cycle (pulsing), 137, 651–652
- Earth's rotation, 119, 139
- Effective exhaust velocity, *see* Exhaust velocity
- Electric propulsion, 11–12, 32, 42, **622–671**
- applications and missions, 625, 661–663
 - arcjet, 12, 32, 42, 624, **636–639**, 653, 658
 - electromagnetic or magnetoplasmadynamic, 32, 42, 624, **649–656**, 658, 660
 - electrostatic or ion thruster, 12, 32, 42, 623, 624–626, **642–648**, 658, 660
 - ionization schemes, 646–648
 - electrothermal, 622, **633–639**
 - flight performance, 628–631, 656–660
 - Hall effects thrusters, 32, 626, 649, **652–656**, 658, 660
 - performance data 32, 42, 626, 635, 658
 - power (magnitude), 32, 38–39, 624, 627–628, 644, 655, 658
 - power conditioning/conversion, **663–666**
 - power supply and power sources, 626, **663–666**
 - pulsed plasma, 11, 13, 32, 42, 626, **651–652**
 - resistojet, 32, 42, 626, **633–636**, 658
 - thruster efficiency, 624, 628, 644, 655, 658
 - thruster types, 622–623, 626, 658
 - typical propellants, 633, 639, 646, 652, 656, 658
- Electrostatic discharge, 506
- Elliptical orbit, 120–122
- Energy, 38–40, 118
- balance, 39
 - conservation, 49–50, 166
 - conversion efficiency, 38–40
- orbiting satellite, 118
- release efficiency, 168
- Engine, *see* Liquid propellant rocket engine
- Engine cycles, 221–228
- Enthalpy, chemical reaction, 49, 159, 166–168, 186, 458
- Entropy in nozzle expansion, 47, 163–165, 172, 186
- Environment, 267–268, 705; *see also* Hazards; Rocket exhaust plumes
- Equation summary, 753–754 (Appendix 3)
- Equivalent diameter (hydraulic radius), 320
- Erosive burning, *see* Burning rate
- Escape from solar system, 124
- Escape velocity from earth, 118–119
- Exhaust gas, exhaust jet, flame, *see* Rocket exhaust plume
- Exhaust nozzle, *see* Nozzle
- Exhaust velocity, *see* Nozzle, effective
- exhaust velocity; Nozzle, exit or exhaust velocity
- Expander cycle, 225
- Expansion-deflection nozzle, 77, 85
- Explosive ingredients of solid propellants, 519–520; *see also* HMX; Nitrocellulose: Nitroglycerine
- Expulsion efficiency, 201–202
- Extendible nozzle, 82–83, 311, 439
- Failure modes of solid rocket motors (cracks and debonding), 472–473
- Failure sensing, 746
- Failures, postaccident procedures, 747–748
- Feed system, liquid propellants, 198, **208–210**, 213; *see also* Tanks
- electric propulsion, 633–634
 - gas pressurized, 6, 214–216, 217–221, 274, 331; *see also* Blow-down feed system; Pressure regulator
 - with turbopump, 7, 197, **221–228**, 274, 331
- Filaments used for cases, 564–565
- Filament winding machines, 562–564
- Film coefficient (heat transfer):
- gas, 311–315
 - liquid, 311, 312
- Film cooling with liquid propellants, 294–295
- Finite element analysis 311, 478

- Flame, *see* Combustion; Rocket exhaust plume
- Flap in liner (also called boot), 480; *see also* Grain, Solid propellant rocket motors
- Flexible nozzle bearing, *see* Thrust vector control
- Flexible pipe joint, 237
- Flight, 103–158; *see also* Application; Drag; Lift; Spacecraft; Vehicle velocity
- ballistic missiles, 123
- forces acting on the vehicle, 107–110
- interplanetary, 121–122, 124
- maneuvers, 131–137
- motions, 110–114
- performance, chemical propulsion, 103–157
- performance, electrical propulsion, 628–631
- perturbations to space flight path, 124–128
- rotation maneuvers, 131, 133, 134–137
- in space, **116–131**
- stability, 152–153
- testing, 733, 746–748
- vehicles, 139–148
- velocity and acceleration at burn-out, 105, **110–114**, 118, 121, 630–631.
- Flow diagram or flow sheet:
- feed system, 216
 - manufacturing process, 530
 - preliminary design, 585
 - propulsion system selection, 694
- Flow (gas); *see also* Nozzle
- isentropic, 50, **53–75**
 - fuel mass flow (hybrid), 605–609
 - mass (or weight) flow, 29, 34, 50, **60**, 199, 274, 332, 409, 445, 448, 607–608, 643
 - multiphase flow (gas with liquid drops and/or solid particles), 88–89
 - supersonic, sonic and subsonic, 52, 60
- Flow, liquid propellant, 200, 371, 409–410, 413
- Fluorine, 247–250, 188, 598
- Flywheels, 230
- Force; *see also* Thrust
- acting on flight vehicle, 107–114
 - measurement, 742
 - solar radiation pressure, 13
- Free energy or chemical potential, 162–164
- Free molecular flow, 717
- Frozen equilibrium, 170–172, 174
- Fuel:
- cells, 664–665
 - hybrid rocket, *see* Hybrid propellant rockets
 - liquid propellant, 259–263
 - pump, 369, 370, 373
 - solid propellant, 517–518
- Gas constant, 50, 54, 190
- Gaseous propellant rocket engine, 8, 42, 199, **266–267**
- Gas generator; *see also* Liquid propellant rocket engine; Solid propellant rocket motor
- engine cycle, 222–228
 - liquid propellant, 185, 190
 - solid propellant, 438, 522–524
- Gas pressurized feed system, *see* Feed system
- Gelled liquid propellants, 199, **265–266**
- Geosynchronous earth orbit (GEO), *see* Orbit
- Gibbs free energy, *see* Free energy
- Gimbal, 195, 274, **675–677**, 681.
- Grain, solid propellant, **463–472**, 588; *see also* Solid propellant rocket motor
- aging, 481, 500, 507
 - binder, 443, **518**
 - bond strength, 473, 483
 - burning surface to nozzle throat area ratio (K), 446, 448
 - cartridge loaded, 441, **463**, 482
 - case-bonded, 441, **463**, 480
 - configurations, 463–472
 - design, 468
 - end burning, 466, 470
 - hybrid, 604–609
 - inhibitor, 464
 - insulator, thermal, 465
 - liner, 465
 - multiple grain (restartable), 470
 - perforation, port, or internal cavity, 464, 467
 - regressive, neutral, or progressive burning, 441, 464

- Grain, solid propellant (*continued*)
 sliver, 464, 470, 472
 stress and strain, 472–483
 cumulative damage, 482
 stress relief flap or boot,
480–481
 tensile strength, 476
 surface cracks, 472
 thermal cycling, 477
 volumetric loading, 466
 Graphite, 573, 574
 Gravitational attraction, 108–109
 Gravity gradients, 127
- Hazards:
 classification, 441, **509**
 explosion, *see* Solid propellant,
 detonation
 fire, 251
 health, 252, 267–268
 insensitive munitions, 509–511
 liquid propellants and engines, 252
 solid propellant, 505–512
 toxic gas exposure limits, 741–742
 toxicity, 511
- Heat of formation, 162–163
- Heat of reaction, 162
- Heat transfer, **288–295**, 334–337; *see also*
 Film coefficient; Liquid propellant
 thrust chamber, cooling
 analysis, 311–323
 cooling techniques; 289–294, 335; *see*
 also Insulation, thermal; Radiation
 cooling; Regenerative cooling
 film cooling, 293–294
 from exhaust plume, 711
 heat absorbing capacity of coolant, 320
 to liquid propellants, 254
 steady state, 290–292
 transient, 292–293
- Helium, 217, 266–267
- HMX (Cyclotetramethylene tetrinitramine),
 493–497, 499–502, 513–515,
 519–520
- Hohmann transfer orbit, 121, 629
- HTPB (Hydroxyl terminated
 polybutadiene), 497, 499–502, 514,
 516, **518**, 595, 605–606; *see also*
 Polybutadiene
- Hybrid propellant rockets, 8–9, **594–621**;
see also HTPB; Nozzle
 advantages/disadvantages, 594–595
 applications and propellants, 596–600
 combustion instability, 613–617
 design example, 609–613
 fuel regression rate, 601–604, 605–607
 performance analysis and grain
 configuration, 604–609
 performance data, 598–650, 609–613
- Hydrazine, 184, 247, 248, 250, **262–263**,
 264–265, 274, 320–321, 631–635,
 658; *see also* Monomethylhydrazine;
 Unsymmetrical dimethylhydrazine
- Hydrocarbon fuels:
 liquid, 259–261; *see also* RP-1 fuel
 solid, *see* Solid propellant, binder;
 Plasticizer
- Hydrogen, 177, 183–184, 190, 247–250,
261–262, 267, 310, 320, 633, 658
- Hydrogen, peroxide, 168–170, 247–250,
257–258
- Hydroxyl terminated polybutadiene, *see*
 HTPB
- Hypergolic ignition, *see* Ignition
- Ideal rocket, 48–49
- Ignition/igniter:
 analysis and design, 338, **581–582**
 delay or time lag, 324–325, 443
 hardware, 272, 439–440, **578–582**
 hypergolic (spontaneous), 254–255, 326,
 595, 600
 inadvertent ignition, 506–507
 liquid propellants, **254–255**, 272,
 323–326
 propellants for igniter, 327, 525–526
 pyrotechnic, pyrogen, 325, 443, 578–582
 solid propellants, 435, 439–440, 443,
 506–507, **541–543**
- Impulse, *see* Specific impulse; Total
 impulse
- Impulse to weight ratio, 31, 461
- Inconel, 307
- Inducer (impeller), 385–386
- Ingredients of solid propellants, 513–515
- Inhibitor, 464, 528
- Injector, liquid propellants, 198, 272,
276–285, 338; *see also* Thrust
 chamber

- baffles, 360–361
 effect on heat transfer, 285
 platelet, 273, **281**
 pressure drop and flow, 274, 280–284
 structure, 285
 types, 275, 277, 409–410
- Insensitive munitions, 509–511
- Instability of combustion, *see* Combustion
- Instrumentation, 194, **743–747**
- Insulation, thermal, external, 443, 528
- Insulation, thermal, internal, 294–295, 443, **466**, 526–528, 573
- Interfaces between propulsion system and vehicle, 430, **705–709**
- Internal ballistics, 458
- International rocket effort, 14; *see also* LE-7; RD-120, RD-170, Vulcain
- Interplanetary missions, 123–124, 130, 627
 data on planets, 119
 velocity requirements, 130
- Ion propulsion or ion rocket, *see* Electric propulsion
- Isentropic flow through nozzles, 50, **53–75**; *see also* Flow
- IUS (Interim Upper Stage) rocket motor (UTC), 439, 680
- Jet, *see* Rocket exhaust plume
- Jetavator, *see* Thrust vector control
- Jet fuel, 260
- Jet power, 38
- Jet vane, *see* Thrust vector control
- Kerosene, 259–260, 329, 409; *see also* RP-1 fuel
- Kinetic energy rate of jet, 38, 624
- Lapse rate, 741
- Launch vehicle, *see* Space launch vehicle
- LE-7 and LE-5A rocket engines (Japan), 274–275, 371, 404
- Life of electric propulsion, 658
- Life in space, 197
- Life of solid grain, 500
- Lift, aerodynamic:
 coefficient, 108–109
 force, 108
- Liner, 443, **465**, 526–529
- Liquid oxygen, *see* Oxygen
- Liquid propellant, 197, **198–201, 245–270**;
see also Fuel; Hydrazine; Hydrogen; Kerosene; Methane; Nitric Acid; Nitrogen tetroxide, Oxidizer; Oxygen; RP-1
- budget, 399–401
- combustion, 346–365; *see also* Combustion
- cryogenic, 199, 247–250
- gelled, 199, **265–266**
- hazards, **251–252**, 267–268
- heat transfer, 254, 288–295, 311–328
- ignition/start, 254–255, **323–326**
- mixture ratio, 178–181, 184, 190, **199**, 215, 274, **282**, 332, 371, 404, 409, 414, 421
- monopropellant, 32, 199, **263–265**, 302–303
- performance of several combinations, 177, 178, **183**
- properties, 246–255
- storable propellant, 199
- Liquid propellant rocket engines, 5–7, **194–244**, 274–276, 399–401; *see also* Auxiliary rockets; Controls; Engine cycles; Feed systems; Heat transfer; Tanks, Thrust chambers; Turbopumps
- advantages/disadvantages, 696, 697
- boost propulsion, 196, 197
- calibration, **423–430**
- chamber pressure, 274, 404, 409
- control, 206, **411–423**
- engine cycles, 222–228, 404
- engine preliminary design, 403–411
- engine design optimization, 408
- engine systems, 40–41, 401–402
- engine support structure, 194, 239–240
- gas generators and preburners, 185, 190, 223, **394–395**
- inert mass, 407
- pressurized gas or pump feed, 194, 197, **208–228**
- shut down or termination, 416–419
- starting, ignition, and thrust build-up, **323–326**, 414–419
- system integration and engine optimization, 430–431

- Liquid propellant rocket engines (*continued*)
 system performance, 401–403
 thrust chamber or thrusters, 271–345
 variable thrust, 326–328
- Lorentz force, 640, 650, 654
- Low Earth orbit (LEO), 128
- Lunar flight, 123–124
- Mach number, 51–52
- Magnetic field flight perturbation, 127
- Maintainability, 704
- Mandrel for solid propellant grain, 531
- Maraging steel, 562
- Masses of vehicle, definitions, 104
- Mass flow, 42, **60**, 445, 449, 609, 643; *see also* Flow (gas); Flow, liquid propellant
- Mass fraction, *see* Propellant mass fraction
- Mass ratio, **30**, 104–106, 113, 630
- Materials and materials properties, 305–311, 443, 557, 573, 635
- metals, 444; *see also* Niobium; Rhenium; Stainless steel; Titanium
- reinforced plastics, 444; *see also* Carbon-carbon
- Measurement/sensing of data, 743–745
- Methane, 184, 247–250, 260–261, 267, 633
- Micrometeorology, 741
- Migration in solid propellant grain, 528
- Minimum smoke propellants, 524
- Minuteman rocket motor, 686
- Missiles, military, 24, 25, 135, **148–152**, 437, 438, 440
- Missions, 196, 661–663, 703; *see also* Applications; Requirements
- Mission velocity, 128–131
- Mixing of solid propellant, 530, 531
- Mixture ratio, *see* Liquid propellant rocket engine; Hybrid propellant rocket
- Molecular mass (or weight), 53, 55, 161, 177, 178, 184, 185, 186, 188, 247, 248, 249, 260, 264, 267, 502, 646
- Monomethyl hydrazine, 183, 248, **263**, 273, 274
- Monopropellant, 42, 232, **263–265**; *see also* Thrust chamber, monopropellant
- Motor, *see* Rocket motor
- Movable nozzle, *see* Nozzle, extendible or movable
- Multistage or multistep rocket vehicles, 16–17, 140–145
- Multiple propulsion systems, **40–41**, **401–403**
- Net positive suction head, 384
- Niobium, 198, 273, 302, 307–311
- Nitric acid, or inhibited red fuming nitric acid (IRFNA), 247–250, **258**
- Nitrocellulose, 513, 516, **520**
- Nitrogen tetroxide, 247–250, **259**, 273, 274, 321, 409
- Nitroglycerine, 499, 513, 516, **520**
- Noise of exhaust plume, **726–727**
- Nozzle; *see also* Flow; Mass flow; Liquid propellant rocket engine; Solid propellant rocket motor; Specific impulse
- aerospike, 77, 84–85, **299–301**
- alignment, 96–97
- analysis, thermochemical, 170–175
- area ratio, 52, 58, 60, 62, 63, 66–67, 72, 177, 186, 188, 274, 329–331, 404, 409, 442
- bell shaped or contoured, **79–82**, 195, 329–331, 567–570, 677
- blast tube, 438, 440, 566
- boundary layer, 48, **86–87**; *see also* Hybrid propellant rockets
- change in gas composition, 174, 179–180, 183, 187, 188
- cone angle correction factor, 76–79
- conical, 76–79
- contraction ratio, 86
- critical pressure, temperature or velocity, 59–60
- divergence or diverging exit section, 76, 78, 86
- effective exhaust velocity, **30**, **33**, **36**, 55, 56, 458, 628
- erosion, 570, 590
- exit cone, 310, 566, 573
- exit or exhaust velocity, 34, **36–37**, 54, 55, 200
- exit gas composition, 177, 180
- expansion-deflection nozzle, 77, 85
- extendible or movable, 288, 310, 439, 565–567, 677, 680

- flow with frozen or shifting equilibrium, 170–172
- gas expansion process, 159
- heat absorption, 571–578
- illustrations of nozzles 8, 195, 436, 439
561, 566, 568, 679, 680
- insert, 8, 443, 472
- losses, 85–92, 570
- materials, 301, 307, 308, 571–578; *see also* Ablative materials
- multiphase flow, 88–89
- multiple nozzles, 85–86
- optimum expansion, 33, 65, 66–67, 183, 185
- over-expanded, 69–73
- performance correction, 90–92
- performance parameters/specified conditions, 94–96, 274, 409, 436, 439, 442, 568
- effect of altitude, 36, 64, 71, 72
- plug nozzle, *see* Nozzle, aerospike
- pressure drop or pressure ratio, 35, 51–52, 54–55, 58, 59–64, 66–67
177, 181, 182, 186–188
- scarfed, 96–97
- separation of flow, 69–73
- shape, length, and configuration, 75–85, 287–288, 330–331
- solid propellant rocket motors, 436, 444, 458, 564–578, 589
- submerged, 566–567
- supersonic, sonic, and subsonic flow, 52, 60
- theory, 47–96
- throat condition or diameter, 57–62
- under-expanded, 69–75
- Nuclear power generation, 666
- Nuclear rocket propulsion, 10–11, 32
- Nucleate boiling heat transfer, 319
- Ohm's law, 637
- Optimum expansion, *see* Nozzle, optimum expansion
- Orbits of satellites and spacecraft:
- circular, 118
 - deorbit, 133, 135
 - elliptical, 120–121
 - energy, 118
 - geosynchronous (GEO), 127, 627, 663
- injection into orbit, orbit transfer, 121–122, 132, 135; *see also* Hohmann transfer orbit
- low earth orbit (LEO), 128, 627, 629, 663
- maintenance, station keeping, 128, 132, 135, 663
- payloads for different orbits, 145–148
- period of revolution, 118
- perturbations, 124–128
- raising orbit altitude, 701, 121, 135, 663
- synchronous orbit *see* Orbit, geosynchronous
- Oxidizer(s):
- liquid, 256–259
 - pump, 368, 370, 373, 380
 - solid, 512–517, 519–520
- Oxygen, 177, 183, 185–187, 247–250, 256–257, 274, 329, 404, 409, 595, 598
- performance data with RP-1, 178–184
- performance data with hydrogen, 177, 184
- Particles or particulates:
- size parameters, 520–522
 - suspended in exhaust gas, 718–720
 - vibration damping, 361
- Pegasus space launch vehicle, 147, 306
- Perfect gas law, 50
- Performance; *see also* Nozzle, effective exhaust velocity; Nozzle, exit or exhaust velocity; Propellant mass fraction; Specific impulse
- actual, standard, delivered, and guaranteed, 94–96
 - considerations for propulsion systems, 703–704
 - correction factors, 90–92
 - theoretical values, 94, 158–193
- Perigee, 120
- Perturbation of flight path, 124–128
- Pipes or flow conduits, 236–239
- Piston expulsion, 207
- Pitch maneuver, 135, 674
- Planets, data, 119
- Plasticizer, 513, 519
- Plug nozzle, *see* Nozzle, aerospike
- Plume, *see* Rocket exhaust plume

- Pogo pulsations or feed system instability, 353–355
- Polybutedaine (various), 497, 499, 514, 516, 596; *see also* HTPB
- Polyether, polyester, polyurethane, 514, 516
- Port area or cavity, *see* Grain
- Positive expulsion devices, 201–208
- Power conditioning/conversion, *see* Electric propulsion
- Power interfaces, 707
- Preburner, *see* Liquid propellant rocket engines, gas generators and preburners
- Pressure, atmosphere, 752
- Pressure balance, 376–378, 424–426
- Pressure exponent, *see* Burning rate
- Pressure oscillations, *see* Combustion instability
- Pressure regulators, 6, 216, 231, 237
- Pressurized feed system, 6, 210–216; 217–221; *see also* Feed system
- Producibility, 704
- Propellant, *see* Liquid propellant; Solid propellant; Ignition; Gaseous propellant
- Propellant budget, 399–401
- Propellant mass fraction, 31, 105–106, 143–145, 443, 460, 629–630, 668
- Propellant tanks, *see* Tanks
- Propellant utilization, 213, 420–421
- Propulsive efficiency, 59
- Pulse modulation of pulsing thruster, 328, 649–650
- Pulsing thruster operation, *see* Duty cycle; Electric propulsion, pulsed plasma
- Pump, 371, 378–385; *see also* Turbopump cavitation, 375, 383–384 desirable propellant properties, 246–255 efficiency, 380, 382, 385 head and suction head, 380, 383–384 inducer, 385 shrouded impeller, 379–381 specific speed, 381–382 type or configuration, 373, 382
- Pyrolytic graphite, 573, 574
- Qualification of rocket propulsion system: preliminary flight rating test, 734 qualification test, 735
- Radiation heat transfer and cooling, 273, 288, 291–292, 309, 322–323, 573
- Ramjet, 2–4, 9
- RD-4–15 Thruster and small RCS (Aerojet Propulsion Co.) 274, 309
- RD-120, RD170, RD 253 (Russia), 228, 409, 419
- Reaction control system (RCS), 134–137 229–232, 301–305; *see also* Auxiliary rocket engine
- Reduced smoke propellant, 524–525
- Rendezvous (in space), 136, 172, 133, 135
- Reentry and landing, 132–133
- Regenerative cooling, 274, 291, 293, 310, 311–320; *see also* Thrust chamber
- Reliability, 213, 662, 703–704
- Requirements and constraints for solid propellant rocket motors, 583
- Requirements for mission, 196, 329, 466, 661–663, 703
- Residual propellant: liquid, 202 solid (slivers), 464, 470, 472
- Resistojet, 32, 42, 624, 633–636, 658; *see also* Electric propulsion
- Reusability, 196, 213
- Rhenium, 308, 635
- RL 10–3A rocket engine (Pratt & Whitney, Div. of UTC), 225, 404
- RL 10B-2 rocket engine (Pratt & Whitney, Div. of UTC), 274, 404
- Rocket engine, *see* Liquid propellant rocket engine
- Rocket exhaust plume, 710–732; *see also* Nozzle; Shock waves aerodynamic effect, 713–722 color, luminosity, and spectral distribution, 254–255, 717–721 plume appearance and shape, 713–719 radio signal attenuation, 713, 728–729 smoke, 255, 494–495, 726
- Rocket motor, *see* Solid propellant rocket motor
- Rocket-assisted gun-launched projectiles, 152

- Rocket propulsion:
- applications, **14–26**, 196–198, 438, 596–600, 625–627, 661–663
 - definition, 1
 - exhaust gas or flame, *see* Rocket exhaust plume
 - systems for certain flight maneuvers, 135
 - testing, 733–748
 - types of, 4–14
- Roll or roll maneuver, 135, 674
- RP-1 fuel (kerosene), 184, 247–250, 259–261, 274, 336
- RS-27 rocket engine (Boeing/Rocketdyne), 36, 274, 370
- RS-68 rocket engine (Boeing/Rocketdyne), 225, 226, 404
- Safe and arm device, 580, 581
- Safety; *see also* Hazards
- hybrid propellants, 594
 - liquid propellants, 213, **267–268**, 413, 736–739
 - rating of solid propellant, 495
 - solid propellants, 505–512, 580, 581; *see also* Insensitive munitions
 - survivability, 703
 - testing, 733–748
- Satellite:
- orbits and payloads, 117–121
 - period of revolution, 118
 - perturbing forces, 124–128
 - velocity, 118
- SCAT (Secondary combustion augmented thruster; Northrop-Grummann), 232
- Selection of rocket propulsion systems, **330**, **691–709**; *see also* Interfaces criteria, 699–705
- selection process, 693–701
- Separation of nozzle flow, 69–73
- Shifting equilibrium, 170–172, 174
- Silica phenolic, 574
- Shock wave, 48, 69–70, 301, 712–718, **722–724**
- Single stage to orbit, 21, 300–302
- Sliver, residual solid propellant, 442, 464, **470**, **472**, 486
- Sloshing of liquid in tank, 204–205
- Smoke of plume, *see* Rocket exhaust plume
- Solar cells, 665–666
- Solar heating propulsion or solar thermal propulsion, 13, 32, 42
- Solar propulsion (by radiation pressure) or solar sail, 13
- Solid propellant(s), 7, 8, 435, 442, 466, **492–536**; *see also* Burning rate; Combustion; Cumulative damage; Grain; Ignition
- abbreviations and acronyms for ingredients, 513–515
- aging, 481, 500, **507**
- aluminum, 493–496
- binder, 499, 513, 514, **518–519**
- characteristics and behavior, 498–505
- chemical ingredients (chamber), 498–505
- chemical gas reaction products, 187, 188, 505
- comparison of different types, 495–496, 499–500
- composite, **441**, 442, 447, 493–494, 499, 501–503, 513, 516
- composite modified double base, 441, **447**, **493–494**, 499, 501–503, 513, 516
- detonation, 495, 508–509; *see also* Deflagration
- double base, 441, **493**, 499–502, **513**, 516
- gas generator, 438, **522–524**
- hazards, 505–512
- high energy propellant, 494
- ingredients or raw materials, 499, 501, **512–522**; *see also* Aluminum; Ammonium nitrate; Ammonium perchlorate; HMX; HTPB; Nitrocellulose; Nitroglycerine; Polybutadiene
- material characterization, 474–477
- migration, 528
- particle size parameters, 520–522
- performance data, 442, 495, 496, 497, 502–504
- plasticizer, 513–515, 519
- processing or manufacturing, 497, 500, **529–532**
- cast or extruded, 495–496
- representative formulations, 501

- Solid propellant(s) (*continued*)
 safety, 495, 511–512
 smoky, smokeless, or low smoke,
 494–495, **524–525**
 stress relaxation modulus, **479**,
 497
 testing, 733–748
 thermal cycling, 477, 481
 upper pressure limit, 511
- Solid propellant rocket motors, 7, 8
435–491; *see also* Burning rate; Case;
 Grain; Ignition; Insulation; Liner;
 Nozzle; Solid propellants
 action time and burn time, 442, **459**
 advantages and disadvantages, 696, 697
 basic performance relations and data,
 442, **437–458**
 booster, 14–15, 19, 438
 chamber pressure, 445–452
 combustion, 446, 545–553
 components, 28, 435–437
 design approach, 583–590
 extinction or thrust termination, **543–545**
 insulators, liners, and inhibitors, 443,
 464, 465, **526–529**
 loads and failure mode, 477, 557
 materials, 443, 558, 573
 nozzles, 8, 436, 439, 464
 requirements and constraints, 583, 585
 tactical missile motors, 438, 440
 temperature limits, 438
 two-pulse motor (restartable), 471
 weights/masses (typical), 442, 461–462
- Spacecraft, 21–22, 23, 146; *see also* Orbits;
 Flight; Satellite
 attitude control, *see* Reaction control
 system
 maneuvers, 131–134
 mission velocity, 128–131
 perturbing forces, 124–128
 surface contamination, 727
- Space flight, *see* Flight; Orbits
- Space launch vehicles, 14–22, 145–148
 boosters, 14–15, 135, 438
 upper stages, 135, 438
- Space Shuttle, 19–20
 flight velocity breakdown, 129
 main engine, 20, 195 227–228, 371, 404,
 416–418
- reaction control and orbit maneuver
 system, 19, 212–214
 solid rocket motor/nozzle, 561, 568–570
- Specifications:
 rocket propulsion system, 694, 699–705
 propellants, 255
- Specific gravity/density, 184, 247–249,
 253, 442, 497, 598
- Specific heat ratio, 50, 68, 184
- Specific impulse, 3, **29**, 32, 38, 55, 173,
 177, 181, 182, 184, 185, 274, 404,
 409, 442, 460, 497, 502, 625, 658
 density specific impulse, 253
 theoretical, actual, reference, and
 guaranteed values, **94–96**, 460
- Specific power, 32, 629–630
- Specific speed (pump), 381
- Stability:
 combustion, 352–363
 flight, 152–153
 liquid propellant (chemical stability),
 253–254, 352–363
- Staged combustion cycle, 225, 228
- Staging configurations of vehicles, 131,
140–146
- Stagnation pressure and temperature,
 51–52
- Stainless steel, 274, 305–311
- Standard atmosphere, 752
- Starting, 323–326, 414–418; *see also*
 Controls for rocket engines; Feed
 systems; Ignition; Thrust chamber
- Static rocket system tests, *see* Testing
- Station keeping, *see* Auxiliary rocket
 systems; Orbits
- Stay time or residence time, 287, 350
- Stoichiometric mixture, 161
- Stop operations, *see* Thrust termination
- Storable liquid propellants, 199
- Strand burner, 444
- Strap-on motor/engine, 135, 141
- Stresses and strains, 295–299, 477–481,
 557–560; *see also* Case; Grain;
 Liquid propellant rocket engine; Solid
 propellant rocket motor; Tanks
- Structure, 194; *see also* Interfaces, Liquid
 propellant engine support structure,
- Summary of key equations, 753–754

- Sun, data, 119
 Supersonic, sonic, and subsonic nozzles, 52, 60
 Surface contamination by exhaust plume, 728
 Surface tension screens, 207
 Sweat cooling, 293–294
 Synchronous satellite, 120, 128, 627, 628, 632
- Tactical missile rocket motor, 22, 24, 26, 438, 440
 Tank(s), 194, **201–208**, 334
 positive expulsion during zero g, 204–208
 pressurization, 217–221
 Tank head start, 416–418
 T-burner, 550–551
 Temperature, 50–51
 combustion (chamber temperature), 32, 54–55, 59, 68, 177, 178, 183–185, 190, 312, 409, 442, 458, 497
 limits for solid propellant grain storage, 442, 461
 sensitivity of solid propellant (coefficient), 450–454
 stagnation, 51
 variation effects, 254
 wall (of chamber), 298, 312–314
 Tensile tests on propellant specimen, 473–476
 Testing of rocket propulsion systems, 733–748
 facilities and safeguards, 733–742
 flight testing, **746–747**
 instrumentation and data management, 742–746
 postaccident procedures, 747–748
 types of tests, 733–735
 Thermochemical data for carbonmonoxide, 165
 Thermodynamic properties of chemical constituents, 163
 Thermodynamic relations and nozzle flow, 49–96
 Throttling, *see* Variable thrust
 Thrust, 3, 28–30, **33–36**, **64–68**, 107, 112, 274, 404, 409, 442, 624, 643–644, 658, 663
 acting on vehicle, 110–112
 aerospike, 299–301
 altitude variation, 36
 coefficient, **64–68**, 186
 correction factor, 90–92, 200
 equation, 35, 64, 65, 68, 643, 644, 651
 termination, *see* Solid propellant rocket motors, extinction
 thrust level control, 215, 409
 theoretical, actual, reference, and guaranteed values, 94–96
 variable thrust, 326–328, 409
 Thrust chamber (small ones are called thrusters), 6, 194–195, 196, **271–344**, 347; *see also* Combustion; Electric propulsion; Heat transfer; Injection
 contraction area ratio, 177, 274
 cooling, 271–276, **311–323**, 334–337; *see also* Film cooling; Regenerative cooling
 design, 328–339
 ideal, 48–49
 ignition and start up, 323–326
 life, 305
 low thrust (called thrusters), 229–233, 301–305; *see also* Auxiliary rockets; Electric propulsion
 materials and fabrication, 305–311
 monopropellant, 42, **263–265**, 302–304
 pulsed or intermittent operation, 137, 232; *see also* Duty cycle
 sample design analysis, 328–339, 609–613
 tubes or milled channels, 195, 272, 273, 291, 334–337
 volume and shape, 285–288, 332–334
 wall loads and stresses, 295–299
 Thrust vector control (TVC), **673–689**
 alignment accuracy, 680, 682
 flexible bearing, 569, 676, 677, 679, 680
 gimbal or hinge, 195, **675–685**, 681
 injection of secondary fluid, 676–678, **683–684**
 integration with vehicle, 687–688
 jet tabs, 677, 682–683

- Thrust vector control (TVC) (*continued*)
 jet vanes, 675–678
 with multiple thrust chambers or nozzles,
 685–686
- Thrust to weight ratio, 332, 461
- Time to target, 149–150
- Titanium, 307, 443, 680
- Total impulse, **28–29**, 442, 456
- Toxicity, 252, 267–268, **511**, 735, 745; *see also* Hazards, health
 monitoring and control, 739–740
 toxic gas exposure limits, 741–742
- Turbine(s), 370, 371; *see also* Turbopump
 373, **387–391**
- Turbojet, 2, 4
- Turbopump, 7, 195, 197, **367–376**
 392–393; *see also* Pumps; Turbines
 advanced turbopumps, 368–370
 booster pump, 374
 design configurations, 368–370
 feed system, 196, **221–228**, 409
- Two-phase flow, 88–89, 460
- Ullage, definition, 201
- Unsymmetrical dimethylhydrazine
 (UDMH), 247–250, **262–263**, 409
- Valves, 6, 7, 9, 12, 13, **236–239**, 623
- Variable thrust, **326–328**
- Vehicle; *see also* Missile; Satellite;
 Spacecraft; Space launch vehicle
 acceleration, 114
 base geometry and recirculation, 714,
 722
 flight performance, 103–157, 329
 forces, 107–110
 integration with thrust vector control,
 687–688
- masses, definition, 105
- multistage, 16, 17, 140–145
- power, 38
- velocity of flight, 38, 105–109,
 110, 113, 118, 122–123, 129,
 630, 650.
- Velocity (exhaust gas); *see also* Nozzle, exit
 and exhaust velocity; Characteristic
 velocity; Specific impulse
 correction factor, 91, 460
 electric propulsion, 628, 643, 650
 effective exhaust velocity, 30, 36, 55, 68,
 458
 at nozzle exist, 54–56
 ratio, 62, 63
 of sound or acoustic velocity, 51, 60
 throat velocity, 59
- Venturi, 238
- Vertical flight at 80 degrees (sounding
 rocket), 114–116
- Vibration energy absorption, 507
- Vibration frequency (of chamber gas), *see*
 Combustion
- Vibrations of turbopumps, 378
- Volume impulse, 461
- Volumetric loading fraction, 466, 469
- Vortexing of liquid propellants, 204
- Vulcain rocket engine (France), 223, 404
- Warm gas propellant, 8, 232, 302
- Water hammer, 238
- Web thickness and web fraction, 443, **466**,
 469
- Xenon, 624, 646, 648, 655, 658
- Yaw maneuver, 131, 674
- YF-73, YF-75 rocket engines (China), 404